# REPORT DOCUMENTATION PAGE

Form Approved
OMB NO. 0704-0188

Public Reporting burden for this collection of information is estimated to average 1 hour per response, including the time for reviewing instructions, searching existing data sources, gathering and maintaining the data needed, and completing and reviewing the collection of information. Send comment regarding this burden estimates or any other aspect of this collection of information, including suggestions for reducing this burden, to Washington Headquarters Services, Directorate for information Operations and Reports, 1215 Jefferson Davis Highway, Suite 1204, Arlington, VA 22202-4302, and to the Office of Management and Budget, Paperwork Reduction Project (0704-0188,) Washington, DC 20503.

| 1. AGENCY USE ONLY ( Leave Blank) | 2. REPORT DATE | 3. REPORT TYPE AND DATES COVERED |
|---|---|---|
| | 29 June, 1999 | Final Technical Report:4/1/96-3/31/99 |

4. TITLE AND SUBTITLE
Spread-Spectrum Communications Exploiting Chaos

5. FUNDING NUMBERS
N00014-96-1-0753

6. AUTHOR(S)
Leon Chua

7. PERFORMING ORGANIZATION NAME(S) AND ADDRESS(ES)
University of California, Berkeley, CA 94720

8. PERFORMING ORGANIZATION REPORT NUMBER
442427-23111

9. SPONSORING / MONITORING AGENCY NAME(S) AND ADDRESS(ES)
Office of Naval Research
Program Officer Rabinder N Madan ONR 313
Ballston Centre Tower One
800 North Quincy Street
Arlington, VA 22217-5660

10. SPONSORING / MONITORING AGENCY REPORT NUMBER

11. SUPPLEMENTARY NOTES
N/A

12 a. DISTRIBUTION / AVAILABILITY STATEMENT
Approved for public release; distribution unlimited.

12 b. DISTRIBUTION CODE

13. ABSTRACT (Maximum 200 words)

Our research into the uses of chaotic systems in spread-spectrum communications has resulted in many significant and important advances. These advances were made in categories critical to the successful future incorporation of chaos in communication systems, such as: carrier design, cryptographic security, synchronization schemes, robustness analysis, channel capacity, commercial application, and practical synchronization in real-world wireless environments. Both theoretical and practical aspects were considered, for example: An integrated circuit capable of producing chaotic and hyperchaotic signals was fabricated; An important theory of generalized synchronization between different chaotic systems was developed; a new, improved synchronization scheme call Impulsive synchronization was invented, which has lead to the filing of a patent; and a method based on adaptive control theory was developed to efficiently cope with parameter drift in practical chaotic circuits and time-varying channel distortion.

| 14. SUBJECT TERMS | 15. NUMBER OF PAGES |
|---|---|
| Impulsive synchronization, hyperchaotic signals, chaotic signals, | 7 |
| | 16. PRICE CODE |

| 17. SECURITY CLASSIFICATION OR REPORT | 18. SECURITY CLASSIFICATION ON THIS PAGE | 19. SECURITY CLASSIFICATION OF ABSTRACT | 20. LIMITATION OF ABSTRACT |
|---|---|---|---|
| UNCLASSIFIED | UNCLASSIFIED | UNCLASSIFIED | UL |

NSN 7540-01-280-5500
**Form 298 (Rev.2-89)**
Prescribed by ANSI Std. 239-18

**Standard**

DTIC QUALITY INSPECTED 4

19990630 073

# Final Report
# ONR Contact No. N000149610753
# "Spread Spectrum Communication Exploiting Chaos"

Leon O. Chua
Electronics Research Laboratory,
Department of Electrical Engineering and Computer Sciences,
University of California at Berkeley, Berkeley, CA 94720, USA

June 28, 1999

## Abstract

Our research into the uses of chaotic systems in spread-spectrum communications has resulted in many significant and important advances, which have been documented in 39 published papers. These advances were made in categories critical to the successful future incorporation of chaos in communication systems, such as: carrier design, cryptographic security, synchronization schemes, robustness analysis, channel capacity, commercial applications, and practical sychronization in real-world wireless environments. Both theoretical and practical aspects were considered, for example: An intergrated circuit capable of producing chaotic and hyperchaotic signals was fabricated; An important theory of generalized synchronization between different chaotic systems was developed; a new, improved synchronization scheme called *impulsive synchronization* was invented, which has lead to the filing of a patent; and a method based on adaptive control theory was developed to efficiently cope with parameter drift in practical chaotic circuits and time-varying channel distortion.

Copies Furnished to DTIC
Reproduced From
Bound Original

# Progress Summary

We have made significant and important advances in the uses of chaotic systems for spread-spectrum communications under this funding. Many lasting contributions to this field of global research have resulted from our proposed and executed efforts, being published in 39 papers, including those in the following major categories: 1) carrier design for chaotic spread spectrum communication systems, 2) high-security systems combining chaotic spread spectrum communications and chaotic cryptography, 3) advanced chaotic synchronization schemes for chaotic digital code-division multiple access (CDMA) communication systems, 4) robustness of chaotic synchronization schemes based on $H_\infty$ robust control theory, 5) improvement of the channel capacity of chaotic spread-spectrum communication systems, 6) potential commercial applications of chaotic spread-spectrum communication systems, and 7) establishment of practical chaotic synchronization methods in wireless environment.

The research covered by this grant emphasized both the theoretical and hardware implementation aspects of chaotic spread-spectrum communications.

On the hardware front, we have successfully fabricated an IC chip containing four (4) chaotic circuit units, which can be used to generate hyperchaotic carriers or subcarriers for chaotic digital CDMA systems. This chaotic IC chip allows the flexibility of either functioning as multiple chaotic units or hyperchaotic units. We have also performed hardware experiments on the key technology of chaotic spread-spectrum communication systems — namely, chaotic impulsive synchronization — on both the chaotic circuits and hyperchaotic circuits. After a series of theoretical and experimental studies, the statistical properties of chaotic carriers generated by different kinds of chaotic and hyperchaotic systems were evaluated for choosing good chaotic carrier waveforms. Key technologies for exploiting these chaotic carriers were also carefully studied, including: synchronization of non-autonomous chaotic carrier generator without phase-locking, channel independent chaotic synchronization, generalized chaotic synchronization, and impulsive chaotic synchronization.

On the theoretical front, we have proved that two chaotic systems can be synchronized in a generalized sense which is very robust to nonlinear distortions and noise introduced by channels. Since the theoretical results guarantee that we can find the transformation of the synchronizing manifold associated with two synchronized chaotic systems in a generalized sense, two apparently different chaotic systems can be in fact synchronized to each other via a transformation called the generalized transformation. By taking advantage of this generalized synchronization, we found a chaotic spread-spectrum system can work under much more channel distortion and noise than those based on identical chaotic synchronization. Another advantage is that the huge number of available choices of generalized synchronization transformations makes chaotic spread-spectrum systems more secure. In the area of robustness of chaotic synchronization schemes, we have developed a rigorous theory of $H_\infty$ robustness for

the chaotic synchronization of two chaotic systems. This theory is indispensable for designing robust transmitters and receivers for chaotic spread-spectrum communications.

A significant advance made under the support of this grant which deserves special notice was the theoretical and experimental development of a revolutionary chaotic synchronization scheme called *impulsive synchronization.* Based on the theory of impulsive differential equations and impulsive control, we developed a solid theory to guide the design of an impulsive synchronization scheme. This new method overcomes many disadvantages of its predecessors and enhances the channel efficiency and degree of the security to an entirely new level, which makes potential commercial and military applications of chaotic digital CDMA possible. And, this method led to a brand new technology called "Chaotic Digital Code-Division Multiple Access for Wireless Communication Systems." A patent based on this invention has recently been filed by the University of California, Office of Technology Licensing, under Case No. B-97-080. Further experimental results on impulsive synchronization based on both chaotic and hyperchaotic systems show that the impulsive synchronization is much stable and robust than the continuous ones and provides much more flexibility in its implementation and its combination with digital communication standards. This is very promising for developing chaotic spread-spectrum communication systems which are compatible with the existing conventional spread-spectrum communication systems.

Finally, some other significant results are mentioned. To enhance the security of chaotic spread-spectrum communications systems, the conventional cryptographic methods based on discrete mathematics were embedded into our system structure. By doing so, we have a conventional cryptographic core and a chaotic spread-spectrum communication shell. Our study also concentrated on parameter mismatch and some other channel uncertainties. A method based on adaptive control theory was developed to efficiently cope with the parameter drift of practical chaotic circuits. Experimental results successfully demonstrated that this adaptive method can compensate for both channel distortion and parameter mismatch. Based on practical stability criteria, we also established a framework for the practical stability of impulsive synchronization. The result can be used to improve the robustness of chaotic digital CDMA systems.

# Research Progress Report

The period 4/1/96-3/31/99 covered by this grant was extremely productive for us, having made very good progress on most aspects of our research proposal. In particular, we have published 39 papers on topics from this research grant, which we now list and present.

1. Tao Yang; Chua, L.O. Generalized synchronization of chaos via linear transformations. International Journal of Bifurcation and Chaos in Applied Sciences and Engineering,

Jan. 1999, vol.9, (no.1):215-219.

2. Moiola, J.L.; Chua, L.O. Hopf bifurcations and degeneracies in Chua's circuit-a perspective from a frequency domain approach. International Journal of Bifurcation and Chaos in Applied Sciences and Engineering, Jan. 1999, vol.9, (no.1):295-303.

3. Tao Yang; Chua, L.O. Control of chaos using sampled-data feedback control. International Journal of Bifurcation and Chaos in Applied Sciences and Engineering, Dec. 1998, vol.8, (no.12):2433-8.

4. Chua, L.O.; Wu, C.W.; Zhong, G.-O.; Liu, L.F. Synthesizing arbitrary driving-point and transfer characteristics. IEEE Transactions on Circuits and Systems I: Fundamental Theory and Applications, Dec. 1998, vol.45, (no.12):1225-32.

5. Kolumban, G.; Kennedy, M.P.; Chua, L.O. The role of synchronization in digital communications using chaos. II. Chaotic modulation and chaotic synchronization. IEEE Transactions on Circuits and Systems I: Fundamental Theory and Applications, Nov. 1998, vol.45, (no.11):1129-40.

6. Tao Yang; Chua, L.O. Error performance of chaotic digital code-division multiple access (CDMA) systems. International Journal of Bifurcation and Chaos in Applied Sciences and Engineering, Oct. 1998, vol.8, (no.10):2047-59.

7. Tao Yang; Chua, L.O. Applications of chaotic digital code-division multiple access (CDMA) to cable communication systems. International Journal of Bifurcation and Chaos in Applied Sciences and Engineering, Aug. 1998, vol.8, (no.8):1657-69.

8. Tao Yang; Suykens, J.A.K.; Chua, L.O. Impulsive control of nonautonomous chaotic systems using practical stabilization. International Journal of Bifurcation and Chaos in Applied Sciences and Engineering, July 1998, vol.8, (no.7):1557-64.

9. Suykens, J.A.K.; Yang, T.; Chua, L.O. Impulsive synchronization of chaotic Lur'e systems by measurement feedback. International Journal of Bifurcation and Chaos in Applied Sciences and Engineering, June 1998, vol.8, (no.6):1371-81.

10. Panas, A.I.; Tao Yang; Chua, L.O. Experimental results of impulsive synchronization between two Chua's circuits. International Journal of Bifurcation and Chaos in Applied Sciences and Engineering, March 1998, vol.8, (no.3):639-44.

11. Guo-Qun Zhong; Chai Wah Wu; Chua, L.O. Torus-doubling bifurcations in four mutually coupled Chua's circuits. IEEE Transactions on Circuits and Systems I: Fundamental Theory and Applications, Feb. 1998, vol.45, (no.2):186-93.

12. Brown, R.; Chua, L.O. Clarifying chaos. II. Bernoulli chaos, zero Lyapunov exponents and strange attractors. International Journal of Bifurcation and Chaos in Applied Sciences and Engineering, Jan. 1998, vol.8, (no.1):1-32.

13. Tao Yang; Chua, L.O. Chaotic digital code-division multiple access (CDMA) communication systems. International Journal of Bifurcation and Chaos in Applied Sciences and Engineering, Dec. 1997, vol.7, (no.12):2789-805.

14. Curran, P.F.; Suykens, J.A.K.; Chua, L.O. Absolute stability theory and master-slave synchronization. International Journal of Bifurcation and Chaos in Applied Sciences and Engineering, Dec. 1997, vol.7, (no.12):2891-6.

15. Suykens, J.A.K.; Curran, P.F.; Tao Yang; Vandewalle, J.; and others. Nonlinear $H_\infty$ synchronization of Lur'e systems: dynamic output feedback case. IEEE Transactions on Circuits and Systems I: Fundamental Theory and Applications, Nov. 1997, vol.44, (no.11):1089-92.

16. Suykens, J.A.K.; Curran, P.F.; Vandewalle, J.; Chua, L.O. Robust nonlinear $H_\infty$ synchronization of chaotic Lur'e systems. IEEE Transactions on Circuits and Systems I: Fundamental Theory and Applications, Oct. 1997, vol.44, (no.10):891-904.

17. Kolumban, G.; Kennedy, M.P.; Chua, L.O. The role of synchronization in digital communications using chaos. I . Fundamentals of digital communications. IEEE Transactions on Circuits and Systems I: Fundamental Theory and Applications, Oct. 1997, vol.44, (no.10):927-36.

18. Tao Yang; Chua, L.O. Impulsive stabilization for control and synchronization of chaotic systems: theory and application to secure communication. IEEE Transactions on Circuits and Systems I: Fundamental Theory and Applications, Oct. 1997, vol.44, (no.10):976-88.

19. Volkovskii, A. Synchronization of chaotic systems using phase control. IEEE Transactions on Circuits and Systems I: Fundamental Theory and Applications, Oct. 1997, vol.44, (no.10):913-17.

20. Osipov, G.V.; Sushchik, M.M. The effect of natural frequency distribution on cluster synchronization in oscillator arrays. IEEE Transactions on Circuits and Systems I: Fundamental Theory and Applications, Oct. 1997, vol.44, (no.10):1006-10.

21. Suykens, J.A.K.; Chua, L.O. n-double scroll hypercubes in 1-D CNNs. International Journal of Bifurcation and Chaos in Applied Sciences and Engineering, Aug. 1997, vol.7, (no.8):1873-85.

22. Suykens, J.A.K.; Vandewalle, J.; Chua, L.O. Nonlinear $H_\infty$ synchronization of chaotic Lur'e systems. International Journal of Bifurcation and Chaos in Applied Sciences and Engineering, June 1997, vol.7, (no.6):1323-35.

23. Curran, P.F.; Chua, L.O. Absolute stability theory and the synchronization problem. International Journal of Bifurcation and Chaos in Applied Sciences and Engineering, June 1997, vol.7, (no.6):1375-82.

24. Tao Yang; Chai Wah Wu; Chua, L.O. Cryptography based on chaotic systems. IEEE Transactions on Circuits and Systems I: Fundamental Theory and Applications, May 1997, vol.44, (no.5):469-72.

25. Suykens, J.A.K.; Huang, A.; Chua, L.O. A family of n-scroll attractors from a generalized Chua's circuit. AEU-International Journal of Electronics and Communications, May 1997, vol.51, (no.3):131-8.

26. Yang, T.; Chua, L.O. Impulsive control and synchronization of nonlinear dynamical systems and application to secure communication. International Journal of Bifurcation and Chaos in Applied Sciences and Engineering, March 1997, vol.7, (no.3):645-64.

27. Suykens, J.A.K.; Curran, P.F.; Chua, L.O. Master-slave synchronization using dynamic output feedback. International Journal of Bifurcation and Chaos in Applied Sciences and Engineering, March 1997, vol.7, (no.3):671-9.

28. Suykens, J.A.K.; Vandewalle, J. Master-slave synchronization of Lur'e systems. International Journal of Bifurcation and Chaos in Applied Sciences and Engineering, March 1997, vol.7, (no.3):665-669.

29. Itoh, M.; Wu, C.W.; Chua, L.O. Communication systems via chaotic signals from a reconstruction viewpoint. International Journal of Bifurcation and Chaos in Applied Sciences and Engineering, Feb. 1997, vol.7, (no.2):275-86.

30. Kapitaniak, T.; Chua, L.O. Strange nonchaotic trajectories on torus. International Journal of Bifurcation and Chaos in Applied Sciences and Engineering, Feb. 1997, vol.7, (no.2):423-9.

31. Tao Yang; Chua, L.O. Channel-independent chaotic secure communication. International Journal of Bifurcation and Chaos in Applied Sciences and Engineering, Dec. 1996, vol.6, (no.12B):2653-60.

32. Gligoroski, D.; Dimovski, D.; Kocarev, L.; Urumov, V.; and L. O. Chua. A method for encoding messages by time targeting of the trajectories of chaotic systems. International

Journal of Bifurcation and Chaos in Applied Sciences and Engineering, Nov. 1996, vol.6, (no.11):2119-25.

33. Chua, L.O.; Tao Yang; Guo-Qun Zhong; Chai Wah Wu. Synchronization of Chua's circuits with time-varying channels and parameters. IEEE Transactions on Circuits and Systems I: Fundamental Theory and Applications, Oct. 1996, vol.43, (no.10):862-8.

34. Guo-Qun Zhong; Chua, L.O.; Brown, R. Experimental Poincare maps from the twist-and-flip circuit. IEEE Transactions on Circuits and Systems I: Fundamental Theory and Applications, Oct. 1996, vol.43, (no.10):874-9.

35. Tao Yang; Chua, L.O. Secure communication via chaotic parameter modulation. IEEE Transactions on Circuits and Systems I: Fundamental Theory and Applications, Sept. 1996, vol.43, (no.9):817-19.

36. Chai Wah Wu; Chua, L.O. On a variation of the Huberman-Lumer adaptive scheme. International Journal of Bifurcation and Chaos in Applied Sciences and Engineering, July 1996, vol.6, (no.7):1397-1407.

37. Brown, R.; Chua, L.O. From almost periodic to chaotic: the fundamental map. International Journal of Bifurcation and Chaos in Applied Sciences and Engineering, June 1996, vol.6, (no.6):1111-25.

38. Chai Wah Wu; Guo-Qun Zhong; Chua, L.O. Synchronizing nonautonomous chaotic systems without phase-locking. Journal of Circuits, Systems and Computers, June 1996, vol.6, (no.3):227-41.

39. Chai Wah Wu; Chua, L.O. On the generality of the unfolded Chua's circuit. International Journal of Bifurcation and Chaos in Applied Sciences and Engineering, May 1996, vol.6, (no.5):801-32.

International Journal of Bifurcation and Chaos, Vol. 9, No. 1 (1999) 215–219
© World Scientific Publishing Company

# GENERALIZED SYNCHRONIZATION OF CHAOS VIA LINEAR TRANSFORMATIONS

TAO YANG and LEON O. CHUA
*Department of Electrical Engineering and Computer Sciences,*
*University of California at Berkeley,*
*Berkeley, CA 94720, USA*

Received April 18, 1998; Revised July 13, 1998

Generalized synchronization (GS) of two chaotic systems is a generalization of identical synchronization. Usually, the manifold of GS is much more complex than the driven system and the driving system. In this paper, we study a special case of GS in which the synchronization manifold is linear (linear GS for short). In a theorem, we present the necessary and sufficient conditions under which a linear GS can be achieved between two chaotic systems. In particular, we study the linear GS of two Chua's circuits.

## 1. Introduction

In view of the potential applications of chaotic synchronization [Yang & Chua, 1996a, 1996b; Yang *et al.*, 1997], many different chaotic synchronization methods have been developed recently. Among them are: Identical synchronization (synchronization in the usual sense) [Carroll & Pecora, 1991] impulsive synchronization [Yang & Chua, 1997a, 1997b; Yang *et al.*, 1998] and general synchronization (GS) [Yang & Chua, 1996b; Hunt *et al.*, 1997]. The so-called generalized synchronization can give much richer dynamics than identical ones. Even some desynchronized cases (in the usual sense) due to the parameter mismatches [Wu *et al.*, 1996], distortions in transmitting channels [Chua *et al.*, 1996] and some other distortions can be regarded as GS. Applications of GS may be wider or more practical than those of identical synchronization because there always exist parameter mismatches and distortions in the physical world. For example, one recent application of GS is the design of a channel-independent chaotic secure communication system [Yang & Chua, 1996b]. In this paper, we present the theoretical results which give the conditions for a specific kind of GS whose synchronizing manifold is linear (we call it linear GS for short). We use a standard chaotic system, Chua's circuit, to demonstrate the validity of our theoretical results.

## 2. Linear Generalized Synchronization

Consider two dynamical systems

$$\begin{cases} \dot{\mathbf{x}} = f(\mathbf{x}) & \leftarrow \text{ driving system} \\ \dot{\mathbf{y}} = g(\mathbf{y}, h(\mathbf{x})) & \leftarrow \text{ driven system} \end{cases} \quad (1)$$

where $\mathbf{x} \in \mathbf{R}^n$, $\mathbf{y} \in \mathbf{R}^m$, $h : \mathbf{R}^n \mapsto \mathbf{R}^m$ is an arbitrary function.

**Definition 1.** Generalized synchronization (GS) [Yang & Chua, 1996b]

The two systems in (1) are said to be in a state of generalized synchronization, henceforth referred to as GS, if there exist a transformation $H : \mathbf{R}^n \mapsto \mathbf{R}^m$, a manifold $M = \{(\mathbf{x}, \mathbf{y}) | \mathbf{y} = H(\mathbf{x})\}$, and a set $B \subset \mathbf{R}^n \times \mathbf{R}^m$ with $M \subset B$ such that all trajectories of (1) with initial conditions in $B$ approach $M$ as $t \to \infty$.

*Remark.* Synchronization in the normal sense (identical synchronization) is a special case of GS with $m = n$, and $H(\mathbf{x}) = \mathbf{x}$.

Assume that a chaotic system can be decomposed into two parts[1]

$$\dot{\mathbf{x}} = A\mathbf{x} + \psi(\mathbf{x}) \tag{2}$$

where $A$ is an $n \times n$ constant matrix and $\psi : \mathbf{R}^n \mapsto \mathbf{R}^n$. Assume that we transmit the signal $\psi(\mathbf{x})$ to the driven system and consider the following unidirectional synchronization scheme:

$$\begin{cases} \dot{\mathbf{x}} = A\mathbf{x} + \psi(\mathbf{x}) & \leftarrow \text{ driving system} \\ \dot{\mathbf{y}} = A\mathbf{y} + \Lambda\psi(\mathbf{x}) & \leftarrow \text{ driven system} \end{cases} . \tag{3}$$

**Theorem 1.** *If the matrix $\Lambda$ commutes with $A$, then the two dynamic systems in Eq. (3) are in a state of GS via the following GS transformation*

$$\mathbf{y}(\infty) = H(\mathbf{x}) = \Lambda\mathbf{x} \tag{4}$$

*if and only if $A$ is negative definite.*

*Proof.* Let $\mathbf{z} = \mathbf{y} - \Lambda\mathbf{x}$, then the stability of the GS between the two dynamical systems in Eq. (3) via the GS transformation $\mathbf{y} = H(\mathbf{x}) = \Lambda\mathbf{x}$ is equivalent to that of the origin of the following system:

$$\begin{aligned} \dot{\mathbf{z}} &= [A\mathbf{y} + \Lambda\psi(\mathbf{x})] - [\Lambda A\mathbf{x} + \Lambda\psi(\mathbf{x})] \\ &= A\mathbf{y} - \Lambda A\mathbf{x} \\ &= A(\mathbf{y} - \Lambda\mathbf{x}) \text{ (since } \Lambda \text{ commutes with } A) \\ &= A\mathbf{z} . \end{aligned} \tag{5}$$

$\mathbf{z} = \mathbf{0}$ is asymptotically stable if and only if $A$ is negative definite. ■

*Remark.* When the GS is achieved, the state variables of the driving system and the driven system are connected by a linear transformation. This is why we call this kind of GS as linear GS.

The matrices which commute with an $n \times n$ matrix $A$ are solutions of the following matrix equation:

$$A\mathbf{X} = \mathbf{X}A \tag{6}$$

where $\mathbf{X}$ is an $n \times n$ matrix variable. Since the above equation has an infinite number of solutions, this provides us with several methods to construct linear GS between two chaotic systems. In the following sections, we present some results to demonstrate this fact.

## 3. Linear Generalized Synchronization of Two Chua's Circuits

In this section we study the linear GS of two Chua's circuits. A Chua's circuit [Madan, 1993; Chua, 1994], which consists of two linear capacitors $C_1$ and $C_2$, a linear inductor $L$, two linear resistors $R$ and $R_0$, and a piecewise-linear negative resistor called a Chua's diode, is described by the following state equation:

$$\begin{cases} \dfrac{dv_1}{dt} = \dfrac{1}{C_1}[G(v_2 - v_1) - f(v_1)] \\ \dfrac{dv_2}{dt} = \dfrac{1}{C_2}[G(v_1 - v_2) + i_3] \\ \dfrac{di_3}{dt} = -\dfrac{1}{L}[v_2 + R_0 i_3] \end{cases} \tag{7}$$

where $G = 1/R$ and $f(\cdot)$ is the piecewise-linear characteristics defined by

$$f(v_1) = G_b v_1 + \frac{1}{2}(G_a - G_b)(|v_1 + E| - |v_1 - E|) \tag{8}$$

where $E$ is the breakpoint voltage of the Chua's diode. The corresponding circuit is shown in Fig. 1. The block diagram of the circuit implementation of Chua's circuit and the parameters can be found in [Kennedy, 1992].

Let $\mathbf{x} = (v_1\ v_2\ i_3)^T$, then Chua's circuit can be decomposed as

$$A = \begin{pmatrix} -\dfrac{G}{C_1} & -\dfrac{G}{C_1} & 0 \\ \dfrac{G}{C_2} & -\dfrac{G}{C_2} & \dfrac{1}{C_2} \\ 0 & -\dfrac{1}{L} & -\dfrac{R_0}{L} \end{pmatrix} , \tag{9}$$

$$\Psi(\mathbf{x}) = \begin{pmatrix} \psi_1(\mathbf{x}) \\ \psi_2(\mathbf{x}) \\ \psi_3(\mathbf{x}) \end{pmatrix} = \begin{pmatrix} -\dfrac{1}{C_1} f(v_1) \\ 0 \\ 0 \end{pmatrix} .$$

[1]It should be noticed that this decomposition is very general in the sense that for a given chaotic system $\dot{\mathbf{x}} = f(\mathbf{x})$ and a prescribed matrix $A$, we can always have: $\dot{\mathbf{x}} = A\mathbf{x} + (f(\mathbf{x}) - A\mathbf{x})$. If we let $\psi(\mathbf{x}) = (f(\mathbf{x}) - A\mathbf{x})$ we then get this kind of decomposition.

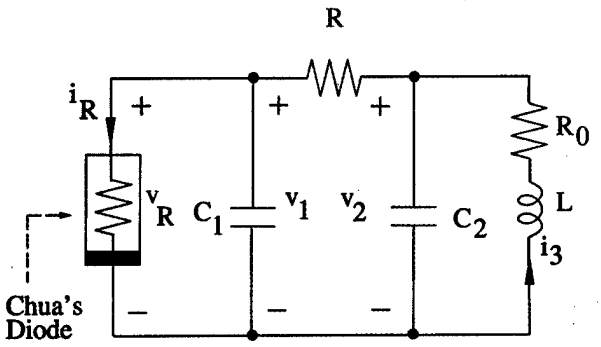


(a)

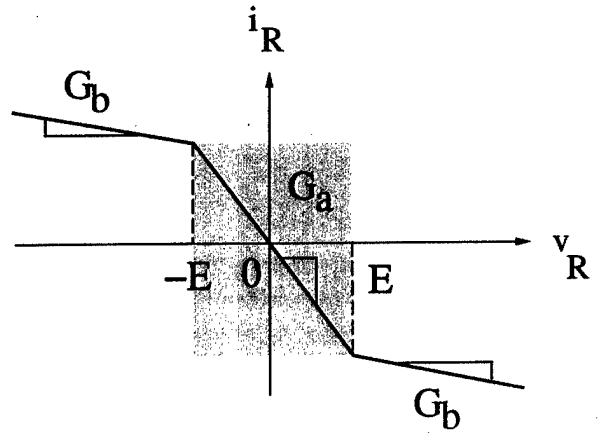


(b)

Fig. 1. (a) Block diagram of Chua's circuit. (b) Piecewise-linear characteristic of Chua's diode.

Since $\psi_2(\mathbf{x}) = \psi_3(\mathbf{x}) = 0$ it is not necessary to assign them to the driven system. What we needed to send is the signal $\psi_1(\mathbf{x}) = -1/C_1 f(v_1)$. Since $C_1$ in our simulations is considered as a constant, we only need to send the signal $f(v_1)$, which is the current through the Chua's diode in the driving system.

In this section, we present two simulation results. The parameters of Chua's circuits are chosen as follows: $C_1 = 5.56$ nF, $C_2 = 50$ nF, $G = 0.7$ mS, $L = 7.14$ mH, $G_a = -0.8$ mS, $G_b = -0.5$ mS, $E = 1$ and $R_0 = 0$. Under these conditions, the eigenvalues of $A$ are all located in the open left-hand plane. The fourth-order Runge–Kutta method with 5 $\mu$s fixed step size is used. The initial conditions for the driving Chua's circuit and the driven Chua's circuit are given respectively by $(v_1(0), v_2(0), i_3(0)) = (-0.2\text{ V}, -0.2\text{ V}, -1\text{ mA})$, and $(\tilde{v}_1(0), \tilde{v}_2(0), \tilde{i}_3(0)) = (-0.2\text{ V}, -0.2\text{ V}, 1\text{ mA})$.

### 3.1. *Simulation 1*

In this simulation, we let

$$\Lambda = \begin{pmatrix} \lambda & 0 & 0 \\ 0 & \lambda & 0 \\ 0 & 0 & \lambda \end{pmatrix} \tag{10}$$

where $\lambda \neq 0$. Observe that $\Lambda A = A\Lambda$. This is a very simple case that had been used in [Yang & Chua, 1996b] for building a channel independent chaotic secure communication system. The driven Chua's circuit is given by

$$\begin{cases} \dfrac{d\tilde{v}_1}{dt} = \dfrac{1}{C_1}[G(\tilde{v}_2 - \tilde{v}_1) - \lambda f(v_1)] \\ \dfrac{d\tilde{v}_2}{dt} = \dfrac{1}{C_2}[G(\tilde{v}_1 - \tilde{v}_2) + \tilde{i}_3] \\ \dfrac{d\tilde{i}_3}{dt} = -\dfrac{1}{L}[\tilde{v}_2 + R_0\tilde{i}_3] \end{cases} . \tag{11}$$

The simulation result is shown in Fig. 2(a). We choose $\lambda = 0.5$. Observer that the attractor of the driven system is a scaled version of that of the driving system with a scale factor 0.5.

### 3.2. *Simulation 2*

In this simulation, we choose

$$\Lambda = A = \begin{pmatrix} -\dfrac{G}{C_1} & -\dfrac{G}{C_1} & 0 \\ \dfrac{G}{C_2} & -\dfrac{G}{C_2} & \dfrac{1}{C_2} \\ 0 & -\dfrac{1}{L} & -\dfrac{R_0}{L} \end{pmatrix} . \tag{12}$$

Observe that $\Lambda A = A\Lambda = A^2$. In this case, the driven Chua's circuit is given by

$$\begin{cases} \dfrac{d\tilde{v}_1}{dt} = \dfrac{1}{C_1}[G(\tilde{v}_2 - \tilde{v}_1)] + \dfrac{G}{C_1^2} f(v_1) \\ \dfrac{d\tilde{v}_2}{dt} = \dfrac{1}{C_2}[G(\tilde{v}_1 - \tilde{v}_2) + \tilde{i}_3] - \dfrac{G}{C_1 C_2} f(v_1) \\ \dfrac{d\tilde{i}_3}{dt} = -\dfrac{1}{L}[\tilde{v}_2 + R_0\tilde{i}_3] \end{cases} . \tag{13}$$

If the GS between the driving and the driven Chua's circuits is achieved, the following relations should be satisfied.

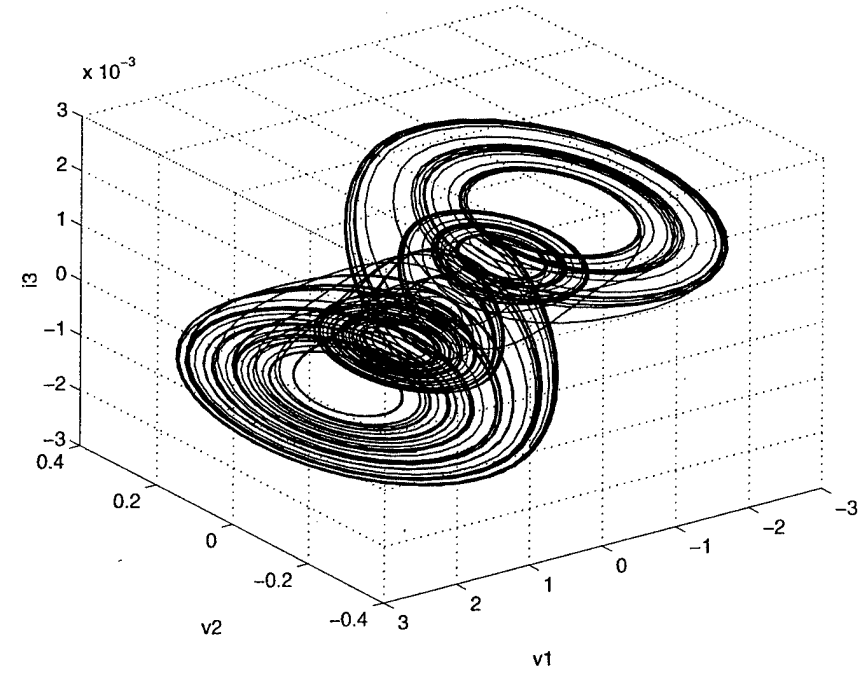


(a)

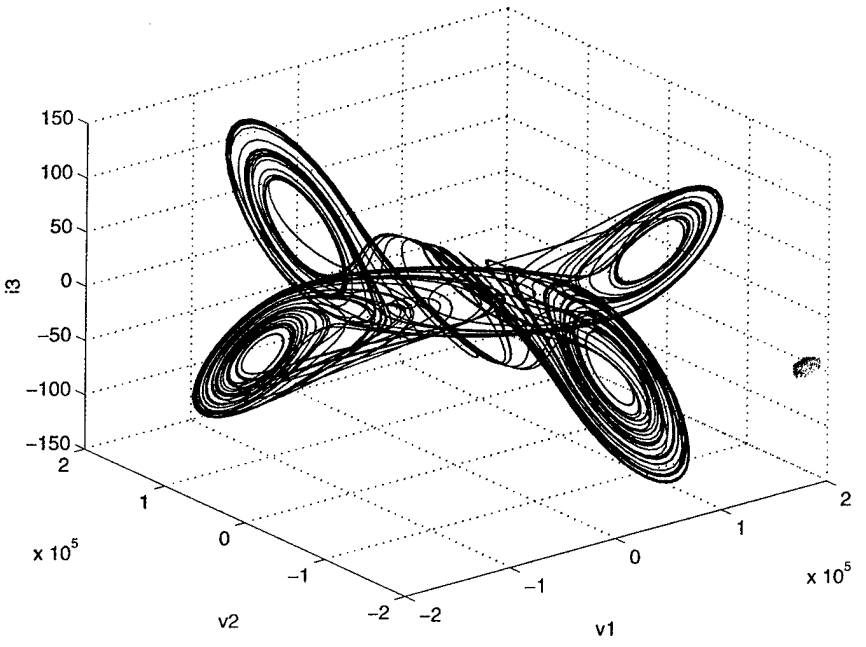


(b)

Fig. 2. Linear GS of two Chua's circuits. The attractor of the driving system is shown in red and that of the driven system is shown in blue. (a) Result of simulation 1. (b) Result of simulation 2.

$$\begin{aligned} \tilde{v}_1 &= -\frac{G}{C_1}v_1 + \frac{G}{C_1}v_2 \\ \tilde{v}_2 &= \frac{G}{C_2}v_1 - \frac{G}{C_2}v_2 + \frac{1}{C_2}i_3 \qquad \tilde{i}_3 = i_3/L \end{aligned} \tag{14}$$

The simulation result is shown in Fig. 2(b). The attractor of the driving system is scaled by a constant vector ($10^5$, $10^4$, $10^5$). Although the shapes of these two attractors are different, the linear transformation of the GS in Eq. (14) is satisfied.

## 4. Conclusions

In this paper, we present the theoretical results on linear GS between two chaotic systems. We also develop a method for decomposing chaotic systems in a special manner such that the linear GS can be achieved. Especially, we use Chua's circuits to demonstrate the validity of the theoretical results. The theoretical results can be used to design proper linear GS between two chaotic systems. They can also be used to interpret the behavior of the driven system. We observed that GS is a very robust phenomenon to parameter mismatch and noise. The potential application of GS to channel-independent chaotic secure communication was presented in [Yang & Chua, 1996b].

## Acknowledgment

This work is supported in part by the Office of Naval Research under grant numbers N00014-97-1-0463 and N00014-96-1-0753.

## References

Carroll, T. L. & Pecora, L. M. [1991] "Synchronizing chaotic circuits," *IEEE Trans. Circuits Syst.* **38**, 453–456.

Chua, L. O. [1994] "Chua's circuit — An overview ten years later," *J. Circuit Syst. Comput.* **4**(2), 117–159.

Chua, L.O., Yang, T., Zhong, G. Q. & Wu, C. W. [1996] "Synchronization of chua's circuits with time-varying channels and parameters," *IEEE Trans. Circuits Syst. I. Fundamental Theor. Appl.* **43**(10), 862–868.

Hunt, B. R., Ott, E. & Yorke, J. A. [1997] "Differentiable generalized synchronization of chaos," *Phys. Rev.* **E55**(4), 4029–4034.

Kennedy, M. P. [1992] "Robust OP AMP realization of Chua's circuit," *Frequenz* **46**(3,4), 66–80.

Madan, R. N. [1993] *Chua's Circuit: A Paradigm for Chaos* (World Scientific, Singapore).

Wu, C. W., Yang, T. & Chua, L. O. [1996] "On adaptive synchronization and control of nonlinear dynamical systems," *Int. J. Bifurcation and Chaos* **6**(3), 455–471.

Yang, T. & Chua, L. O. [1996] "Secure communication via chaotic parameter modulation," *IEEE Trans. Circuits Syst. I. Fundamental Theor. Appl.* **43**(9), 817–819.

Yang, T. & Chua, L. O. [1996] "Channel-independent chaotic secure communication," *Int. J. Bifurcation and Chaos* **6**(12B), 2653–2660.

Yang, T., Wu, C. W. & Chua, L. O. [1997] "Cryptography based on chaotic systems," *IEEE Trans. Circuits Syst. I. Fundamental Theor. Appl.* **44**(5), 469–472.

Yang, T. & Chua, L. O. [1997] "Impulsive control and synchronization of nonlinear dynamical systems and application to secure communication," *Int. J. Bifurcation and Chaos* **7**(3), 645–664.

Yang, T. & Chua, L. O. [1997] "Impulsive stabilization for control and synchronization of chaotic systems: Theory and application to secure communication," *IEEE Trans. Circuits Syst. I: Fundamental Theor. Appl.* **44**(10), 976–988.

Yang, T., Suykens, J. A. K. & Chua, L. O. [1998] "Impulsive control of nonautonomous chaotic systems using practical stabilization," *Int. J. Bifurcation and Chaos* **8**(7), 1557–1564.

International Journal of Bifurcation and Chaos, Vol. 9, No. 1 (1999) 295–303
© World Scientific Publishing Company

# HOPF BIFURCATIONS AND DEGENERACIES IN CHUA'S CIRCUIT — A PERSPECTIVE FROM A FREQUENCY DOMAIN APPROACH

JORGE L. MOIOLA* and LEON O. CHUA
*Department of Electrical Engineering and Computer Sciences,*
*Electronics Research Laboratory,*
*University of California at Berkeley,*
*Berkeley, CA 94720, USA*

Received March 1, 1998; Revised May 1, 1998

In the present work explicit formulas for analyzing the birth of limit cycles arising in the Chua's circuit through a Hopf bifurcation is provided. A local amplitude equation is derived using a frequency domain approach and harmonic balance approximations. Furthermore, the first Lyapunov index used to detect degenerate Hopf bifurcations is derived in terms of the parameters of the nonlinear circuit. A perspective for analyzing other bifurcations using this frequency domain approach is discussed.

## 1. Introduction

Chua's circuit has become a paradigm for complex oscillatory dynamics and chaos arising in simple electronic nonlinear circuits [Madan, 1993; Chua, 1994; Shil'nikov, 1994]. The bulk of papers regarding the complex dynamics in this circuit has focused on chaotic attractors, period-doubling bifurcations, period-adding bifurcations, and so on. In this paper, on the contrary, a study of Hopf bifurcation is performed using a frequency domain approach in a way reminiscent of the classical describing function method. The procedure consists of applying the harmonic balance method to provide the (local) amplitude solution for the emerging limit cycles. Moreover, the first Lyapunov index or curvature coefficient is obtained in terms of the relevant parameters of the circuit. The vanishing of the curvature coefficients allows us to study the birth of multiple periodic solutions in the unfoldings of the so-called degenerate Hopf bifurcation [Golubitsky & Langford, 1981].

This work follows the lines initiated in [Altman, 1993] regarding the dynamics of Hopf bifurcation in Chua's circuit. However, the procedure used here for approximating the amplitude of limit cycles does not use the center manifold theory or coordinate transformations. A frequency domain approach, closely related to control theory and the harmonic balance method are used to obtain the main results [Mees & Chua, 1979].

The motivation of this study comes from recent results obtained in [Khibnik *et al.*, 1993b] concerning the existence of multiple limit cycles around the symmetrical equilibria of Chua's circuit, as well as large amplitude cycles surrounding the three singular points. As we have used a smooth (third-order polynomial) nonlinearity to approximate the piecewise linear characteristics, this work shares similarities with continuous efforts made by other researchers in finding the maximum number

*On leave from Universidad Nacional del Sur, Avda. Alem 1253; 8000 Bahía Blanca, Argentina.
E-mail: jmoiola@fred.eecs.berkeley.edu

of limit cycles in planar cubic systems [Lloyd *et al.*, 1988; Lloyd & Pearson, 1990; Zoladek, 1995]. Since Chua's equations consists of three first-order ODEs, its dynamics are more complicated than those arising from two first-order ODEs (also called planar systems). In particular, it is a challenge to plot the successive curvature coefficients to determine regions of multiple periodic solutions in the parameter space. This letter is the first attempt in this direction. Moreover, a discussion is presented concerning the extension of this method to detect other bifurcations using a higher-order harmonic balance.

## 2. Main Results

The smooth model of Chua's circuit [Altman, 1993; Khibnik *et al.*, 1993b] is given by

$$\begin{aligned} \dot{x} &= \alpha[y - \varphi(x)]\,, \\ \dot{y} &= x - y + z\,, \\ \dot{z} &= -\beta y\,, \end{aligned} \tag{1}$$

where $\varphi(x) = c_1x^3 + c_3x$, is a cubic polynomial nonlinearity, $\alpha$, $\beta$, $c_1$, and $c_3$ are system parameters. The parameters $\alpha$ and $\beta$ will be used as the main bifurcation parameters in the following, for the sake of clarity. After making the following change of coordinates to simplify the structure of the linear part

$$\begin{bmatrix} x_1 \\ x_2 \\ x_3 \end{bmatrix} = \begin{bmatrix} 1 & 0 & 0 \\ 0 & 0 & -1 \\ 0 & 1 & 0 \end{bmatrix} \begin{bmatrix} x \\ y \\ z \end{bmatrix},$$

system (1) can be recast as follow:

$$\begin{aligned} \dot{x}_1 &= -\frac{1}{2}\alpha c_3 x_1 + \alpha x_3 - \frac{1}{2}\alpha c_3 x_1 - \alpha c_1 x_1^3\,, \\ \dot{x}_2 &= \beta x_3\,, \\ \dot{x}_3 &= x_1 - x_2 - x_3\,. \end{aligned} \tag{2}$$

Choosing the following equivalent representation of Eq. (2) (see [Moiola & Chen, 1996] for more details about the methodology):

$$\begin{aligned} \dot{x} &= A(\alpha, \beta)x + Bg(Cx; \alpha, \beta)\,, \\ y &= C(\alpha, \beta)x\,, \end{aligned}$$

where

$$A = \begin{bmatrix} -\alpha c_3/2 & 0 & \alpha \\ 0 & 0 & \beta \\ 1 & -1 & -1 \end{bmatrix}, \quad B = \begin{bmatrix} 1 \\ 0 \\ 0 \end{bmatrix},$$

$$C = [1 \quad 0 \quad 0]\,,$$

$$g(x;\, \alpha,\, \beta) = -\alpha\left(\frac{1}{2}c_3x_1 + c_1x_1^3\right),$$

we end up with a simple form for the linear transfer function $G(s;\, \alpha,\, \beta) = C[sI - A]^{-1}B$, where "$s$" is the variable of the Laplace transform,

$$\begin{aligned} &G(s;.,.) \\ &= \frac{s^2 + s + \beta}{s^3 + s^2\left(1 + \frac{1}{2}\alpha c_3\right) + s\left(\beta + \frac{1}{2}\alpha c_3 - \alpha\right) + \frac{1}{2}\alpha\beta c_3} \\ &= \frac{N(s)}{D(s)}\,. \end{aligned}$$

The Jacobian matrix to be used in the frequency domain formulation is

$$J = \frac{1}{2}\alpha c_3 + 3\alpha c_1 \hat{e}_1^2\,,$$

where $x_1 = -e_1$, $g(x_1) := f(e_1)$ and $\hat{e}_1$ is the equilibrium point obtained from

$$G(0;.,.)f(e_1) = \frac{2\beta}{\alpha\beta c_3}\left(\frac{1}{2}\alpha c_3 e_1 + \alpha c_1 e_1^3\right) = -e_1\,,$$

$$\Rightarrow \hat{e}_1^{(1)} = 0, \quad \text{and} \quad \hat{e}_1^{(2,3)} = \hat{e}_1^{(\pm)} = \pm\sqrt{\frac{-c_3}{c_1}}\,.$$

Notice that our selection of a unique representative variable $e_1$ simplifies the computation of the Hopf bifurcation formulas given in [Moiola & Chen, 1996] since the eigenvectors $v$ and $w^T$ are both equal to 1. However, explicit expressions for the original three variables can also be obtained, and in this case the expressions of the eigenvectors are slightly more complicated.

The following eigenlocus $G(s)J$ is then calculated about the symmetrical equilibrium points $\hat{e}_1^{(\pm)} = \pm\sqrt{-c_3/c_1}$ (called $P^{\pm}$ in the literature on Chua's circuit[1]) which give birth to a Hopf bifurcation under appropriate values of the system parameters:

$$\hat{\lambda} = G(s)J = \frac{-\frac{5}{2}\alpha c_3 N(s)}{D(s)}\,. \tag{3}$$

[1]Since $x_1 = -e_1$, then $P^+ = \hat{x}_1^{(+)} = -\sqrt{-c_3/c_1} = \hat{e}_1^{(-)} = -\hat{e}_1^{(+)}$

The Hopf bifurcation condition is obtained from Eq. (3) when $\hat{\lambda} = -1$ and $s = i\omega_0$, $\omega_0 \neq 0$ giving the following pair of equations

$$\omega_0^2 = \beta - 2\alpha c_3 - \alpha = \frac{-2\alpha c_3 \beta}{1 - 2\alpha c_3}. \tag{4}$$

Thus, a simple expression of the starting frequency of oscillations through the Hopf bifurcation mechanism at the symmetrical equilibrium points can be easily obtained from Eq. (4) as follows

$$\omega_0^2 = -2\alpha^2 c_3(1 + 2c_3). \tag{5}$$

Notice that to change (control) the frequency of emerging limit cycles the relevant parameters are $\alpha$ and $c_3$.

The following closed-loop transfer function is useful in the computation of the Hopf bifurcation formulas:

$$H(s;\, \alpha,\, \beta) = \frac{G(s;\, \alpha,\, \beta)}{[1 + G(s;\, \alpha,\, \beta)J]} = \frac{N(s)}{N(s)(s - 2\alpha c_3) - \alpha s}.$$

The Hopf bifurcation formulas needed for the computation of the amplitude equation and the first Lyapunov index are as follows:

$$V_{02} = -\frac{1}{4}H(0;.,.)D_2 v \otimes \overline{v}, = \frac{3}{4\hat{e}_1^{(\pm)}}; \tag{6}$$

$$V_{22}(\omega) = -\frac{1}{4}H(i2\omega;.,.)D_2 v \otimes v, = -\frac{6\alpha c_1 \hat{e}_1^{(\pm)}}{4}H(i2\omega); \tag{7}$$

$$p1(\omega) = D_2\left[\frac{1}{2}\overline{v} \otimes V_{22} + v \otimes V_{02}\right] + \frac{1}{8}D_3 v \otimes v \otimes \overline{v}, = 6\alpha c_1\left[\frac{1}{2}e_1^{(\pm)}V_{22}(\omega) + \frac{7}{8}\right], \tag{8}$$

where $D_2$ and $D_3$ are the second and third order partial derivatives of $f(e_1)$ evaluated at the equilibrium point $\hat{e}_1^{(\pm)}$, $\otimes$ is the tensorial product (in this case, the scalar product), and the bar denotes the complex conjugate operation. The amplitude equation is obtained from the following approximation

$$\hat{\lambda} = -1 + \theta^2\xi_1 = -1 - \theta^2 G(i\omega)p_1(\omega), \tag{9}$$

where $\theta$ is a measure of the amplitude of the first harmonic and $\xi_1$ is a complex number. Then, from Eq. (9) a measure of the amplitudes of the emerging limit cycles from Hopf bifurcations can be written as follows:

$$\theta = \sqrt{-\frac{\hat{\lambda} + 1}{G(i\omega)p_1(\omega)}}. \tag{10}$$

The computation of the first Lyapunov index requires the evaluation of Eqs. (6)–(8) at criticality [$s = i\omega_0$, $\omega_0 \neq 0$ given by Eq. (4)]. Several simplifications yield the following expressions:

$$V_{02} = -\frac{1}{4}H(0;.,.)D_2 v \otimes \overline{v}, = \frac{3}{4\hat{e}_1^{(\pm)}}, \tag{11}$$

$$V_{22}(\omega_0) = -\frac{1}{4}H(i2\omega_0;.,.)D_2 v \otimes v, = \frac{3}{4\omega_0\hat{e}_1^{(\pm)}}\left\{\frac{-(1 + 6\alpha c_3)\omega_0 + i4\alpha c_3}{3(1 - 2\alpha c_3) + i6\omega_0}\right\}, = \frac{3}{4\omega_0\hat{e}_1^{(\pm)}}v_2(\omega_0), \tag{12}$$

$$p_1(\omega_0) = D_2\left[\frac{1}{2}\overline{v} \otimes V_{22} + v \otimes V_{02}\right] + \frac{1}{8}D_3 v \otimes v \otimes \overline{v}, = 6\alpha c_1\left[\frac{3}{8}\frac{v_2(\omega_0)}{\omega_0} + \frac{7}{8}\right]. \tag{13}$$

Finally, the *curvature coefficient* (or the first Lyapunov index) can be expressed by

$$\sigma_1(\omega_0) = -\Re\left\{\frac{w^T G(i\omega_0)p_1(\omega_0)}{w^T G' J v}\right\} = -\Re\left\{\frac{[\alpha(1 + 2\alpha c_3) + i\omega_0]p_1(\omega_0)}{-2\omega_0^2 - \frac{5}{2}\alpha c_3 + i2\omega_0\left(1 - \frac{9}{2}\alpha c_3\right)}\right\}, \tag{14}$$

where $\Re\{.\}$ denotes the real part of a complex number. Equating expression (14) to zero gives the degenerate Hopf bifurcations points whose unfoldings

contain multiple limit cycles. This degenerate Hopf bifurcation curve can be continued in the parameter space $\alpha - \beta - c_3$ to search for other more complicated singularities as organizing centers of the dynamics. For this parameter set: $\alpha = 1.106691504$, $\beta = 1.09950956$, $c_1 = 1$ and $c_3 = -0.06934372403$ there is a Hopf bifurcation in the symmetrical equilibria $P^{\pm}$ with a frequency $\omega_0 = 0.3824948062$ having the first and second Lyapunov indexes equal to zero. According to the theory of degenerate Hopf bifurcations a structure of three nested limit cycles can be encountered for a suitable perturbation in the parameters $\alpha - \beta - c_3$.

Some simulations using LOCBIF [Khibnik *et al.*, 1993a] are presented below for illustration of the main results near the above mentioned singularity by fixing $c_1 = 1$ in all the cases considered. In Fig. 1, a stable limit cycle encircling $P^-$ is shown for $\alpha = 1.106691$, $\beta = 1.0991$, and $c_3 = -0.06934372$. The limit cycle is separated from the origin in the phase-plane (the left-top corner in Fig. 1).

Varying appropriately the parameters $\alpha$ and $\beta$ the stable limit cycle is deformed such that one of its extremes is near the origin (close to a saddle-loop separatrix bifurcation). This situation is depicted in Fig. 2 for $\alpha = 1.22043$, $\beta = 1.22$, and $c_3 = -0.06934372$.

Figures 3–5 show one large amplitude stable limit cycle surrounding the three equilibria and two unstable limit cycles surrounding $P^+$ and $P^-$. The simulations were obtained using different initial conditions in order to give an idea of the basins of attractions of the stable solutions.

In Fig. 6, a degenerate Hopf bifurcation curve (Hopf curve plus first Lyapunov index equal to zero, i.e. codimension 1 bifurcation) is depicted. Notice that the degenerate Hopf bifurcation of codimension 2 (regular Hopf plus the first and second Lyapunov indexes set equal to zero) is very close to the parameter setting depicted here. Also, it is very interesting to note that the Hopf degeneracy curve of codimension 1 has a turning point close to the limiting point in which $c_3 \to 0$. This type of bending of this Hopf degeneracy has been observed before in other systems (see [Planeaux, 1993; Moiola & Chen, 1996] for more details) in connection with the appearance of degenerate Hopf bifurcations of codimension 2 regarding multiple cycles.

In Figs. 7 and 8 similar structures of stable and unstable limit cycles are depicted. After

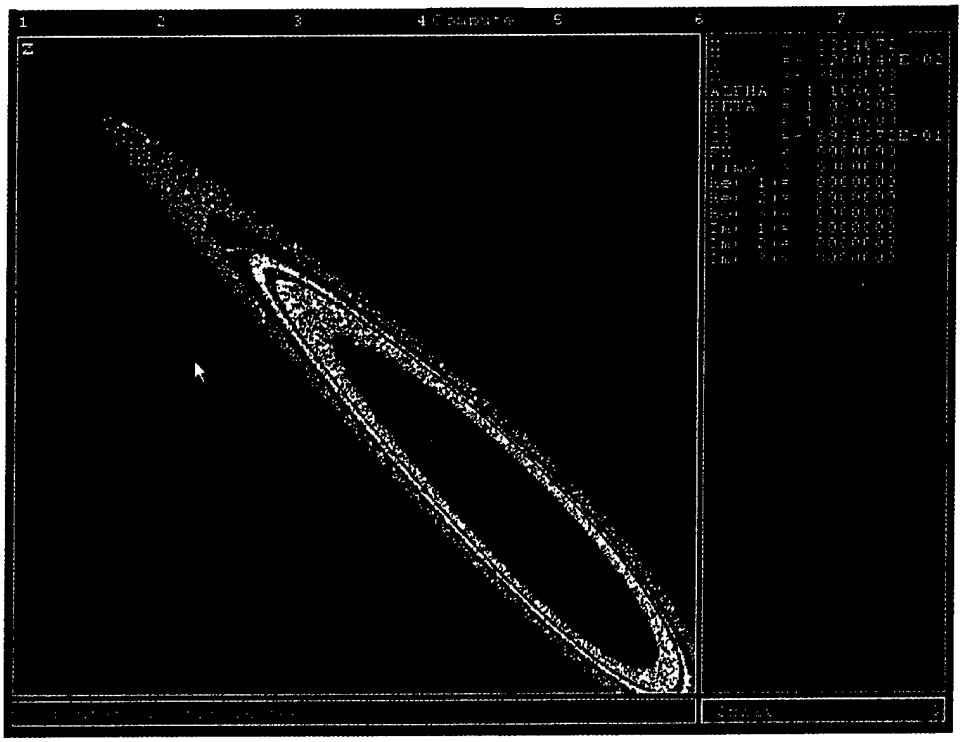

Fig. 1. Stable limit cycle (in red for color picture) surrounding the equilibrium point $P^-$ for $\alpha = 1.106691$, $\beta = 1.0991$, and $c_3 = -0.06934372$. (The limits of the axes are: $x_{\min} = 0$, $x_{\max} = 0.35$; $z_{\min} = -0.35$, $z_{\max} = 0$.)

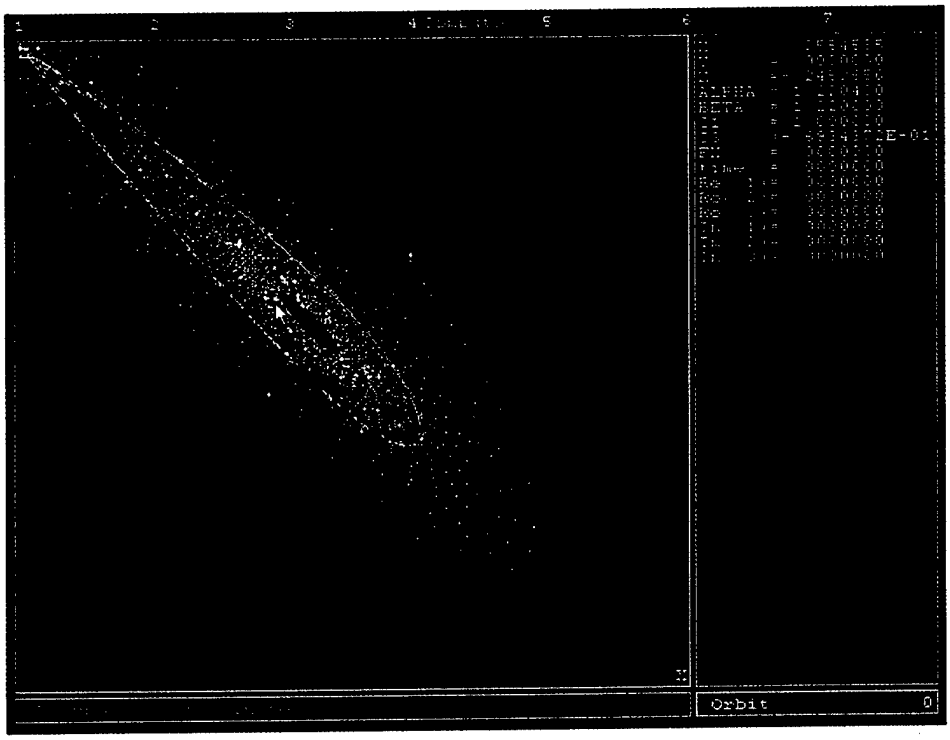


Fig. 2. Stable limit cycle (in red for color picture) surrounding the equilibrium point $P^-$ for $\alpha = 1.22043$, $\beta = 1.22$, and $c_3 = -0.06934372$. (The limits of the axes are: $x_{\min} = 0$, $x_{\max} = 0.60$; $z_{\min} = -0.60$, $z_{\max} = 0$.)

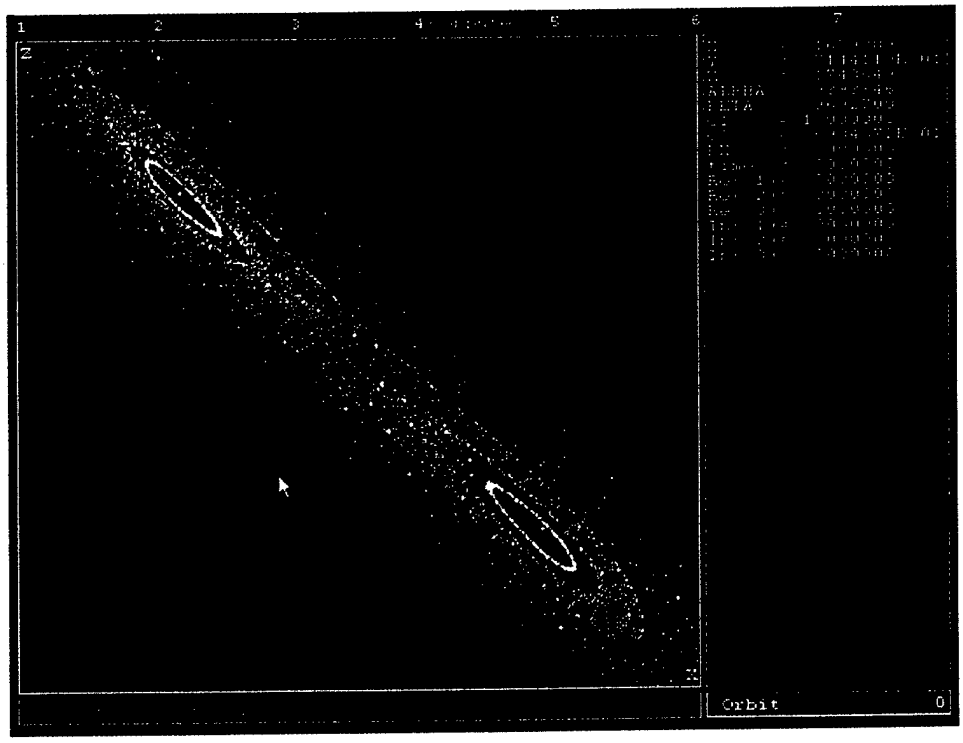


Fig. 3. Stable limit cycle (one trajectory in red for color picture) surrounding the three equilibria for $\alpha = 0.9893846$, $\beta = 0.96927$, and $c_3 = -0.06934372$. The unstable limit cycles — denoted by white continuous circles — surrounds the equilibria $P^{\pm}$. (The limits of the axes are: $x_{\min} = -0.5$, $x_{\max} = 0.5$; $z_{\min} = -0.5$, $z_{\max} = 0.5$.)

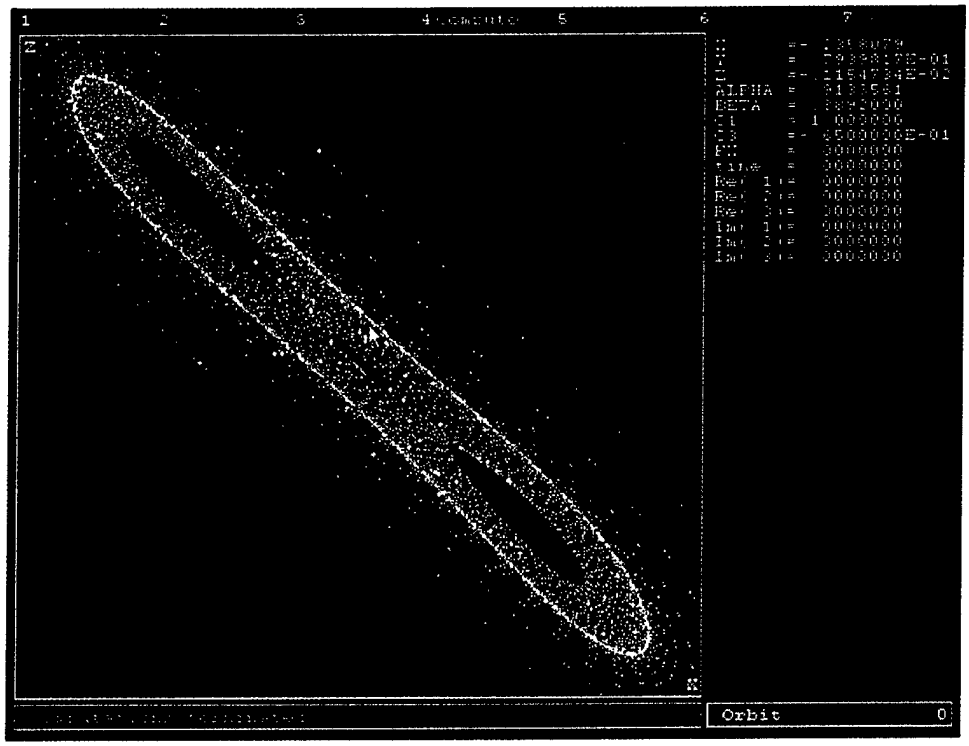


Fig. 4. Stable limit cycle (one trajectory in yellow for color picture) surrounding the three equilibria for $\alpha = 0.9133561$, $\beta = 0.88920$, and $c_3 = -0.065$. The unstable limit cycles are not shown in the figure. (The limits of the axes are: $x_{\min} = -0.5$, $x_{\max} = 0.5$; $z_{\min} = -0.5$, $z_{\max} = 0.5$.)

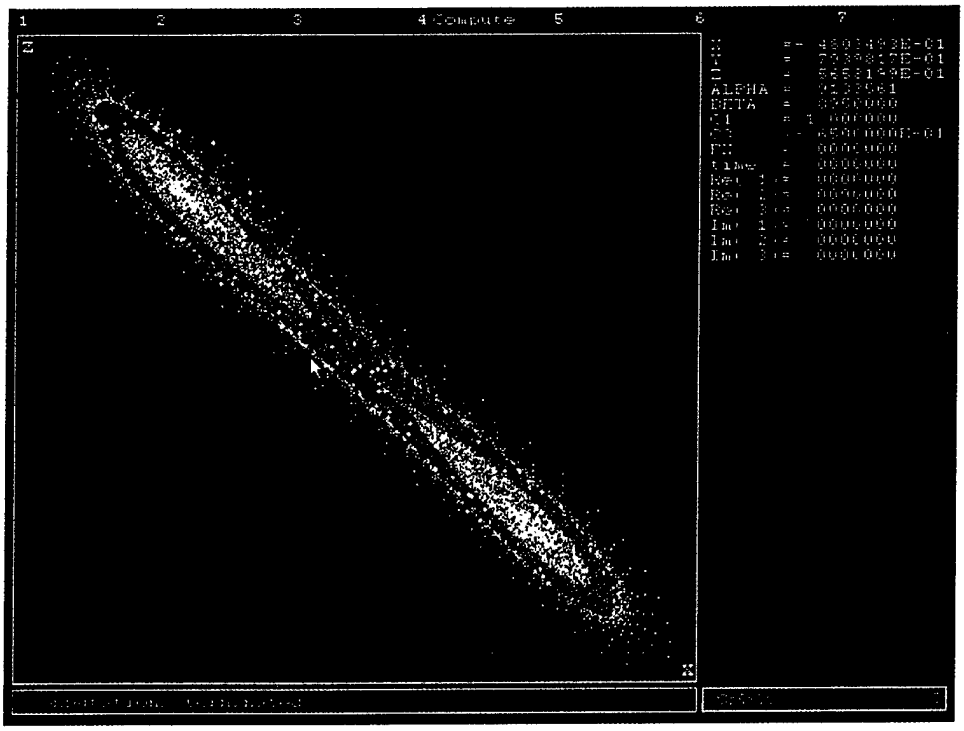


Fig. 5. Stable limit cycle surrounding the three equilibria for $\alpha = 0.9133561$, $\beta = 0.8950$, and $c_3 = -0.065$. The unstable limit cycles are not shown in the figure but they are closer to the stable limit cycle compared to the situation shown in Fig. 4. (The limits of the axes are: $x_{\min} = -0.5$, $x_{\max} = 0.5$; $z_{\min} = -0.5$, $z_{\max} = 0.5$.) (For color picture: yellow and white dots indicate contracting trajectories; red dots indicate expanding trajectories.)

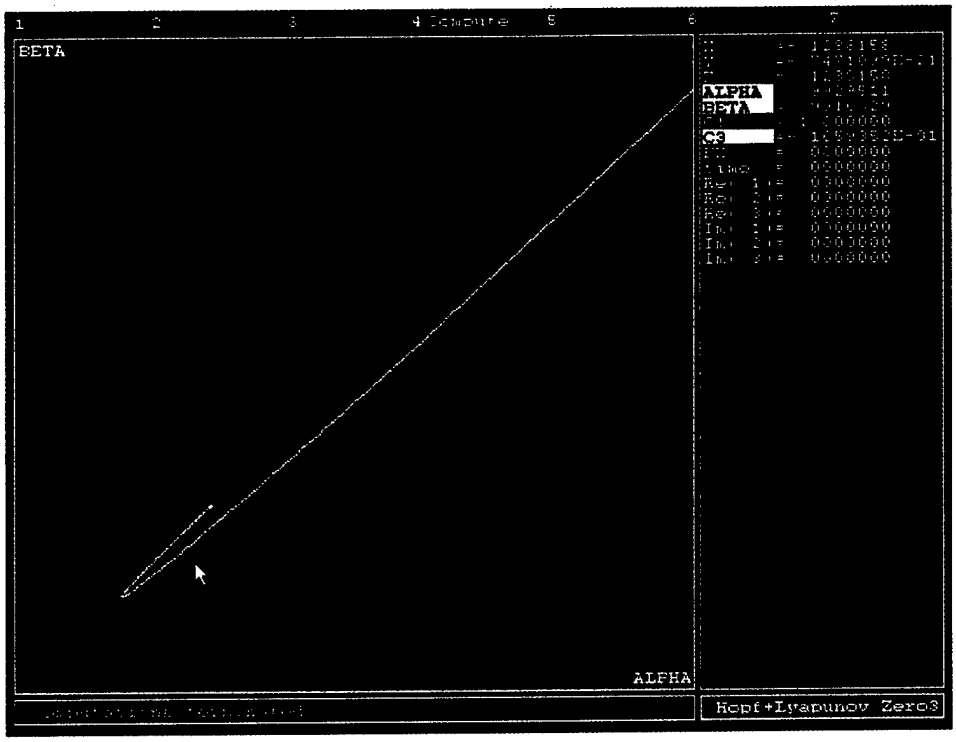


Fig. 6. Degenerate Hopf bifurcation curve (Hopf plus first Lyapunov index equal to zero). On this curve, on its top right there is a point having an extra condition: The second Lyapunov index is also equal to zero (not shown in the figure). (The limits of the axes are: $\alpha_{\min} = 0.98$, $\alpha_{\max} = 1.05$; $\beta_{\min} = 0.98$, $\beta_{\max} = 1.05$.)

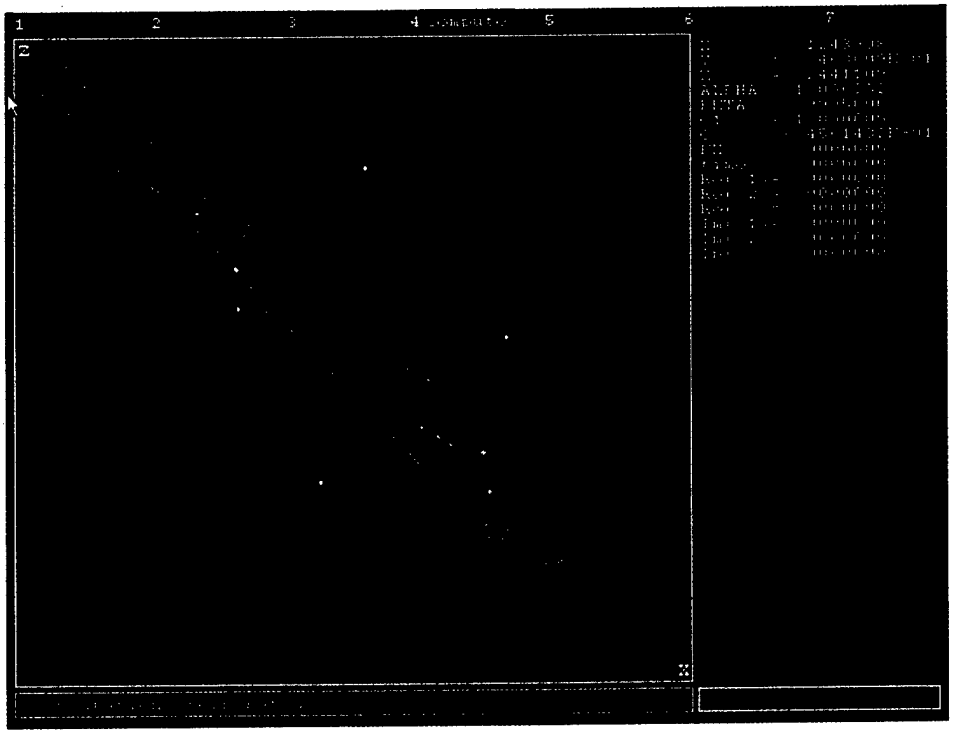

Fig. 7. Stable limit cycle surrounding the three equilibria for $\alpha = 1.006382$, $\beta = 0.9995$, and $c_3 = -0.04561432$ (in black for color picture). The unstable limit cycles surround the symmetrical equilibria. (The limits of the axes are: $x_{\min} = -0.1$, $x_{\max} = 0.4$; $z_{\min} = -0.4$, $z_{\max} = 0.1$.)

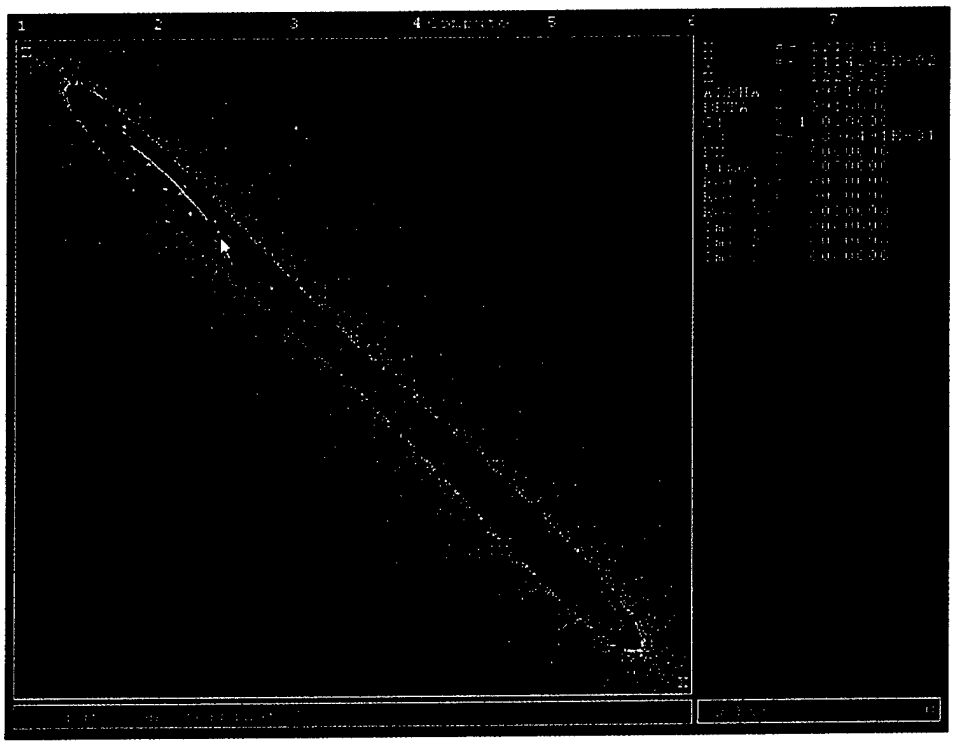

Fig. 8. Stable limit cycle surrounding the three equilibria for $\alpha = 0.99515$, $\beta = 0.9916$, and $c_3 = -0.02896491$ (in black for color picture). The unstable limit cycles surround the symmetrical equilibria (in red for color picture). (The limits of the axes are: $x_{\min} = -0.3$, $x_{\max} = 0.3$; $z_{\min} = -0.3$, $z_{\max} = 0.3$.)

looking for more complex structures of multiple limit cycles (excluding period-doubling bifurcations and chaotic attractors), we observed that the multiple cycles (more than two nested cycles) belong to a narrow band in the parameter setting, as it was observed before in other systems [Planeaux, 1993; Moiola & Chen, 1996], using AUTO [Doedel, 1986]. Since the accuracy of computer simulations using LOCBIF is limited, AUTO software should be used for this task.

## 3. Discussions and Concluding Remarks

The formulas for the amplitude equations of the limit cycles arising in Chua's circuit are obtained using a frequency domain approach. Moreover, an expression of the first Lyapunov index, which determines the stability of the emerging periodic solutions, is computed in terms of the system parameters. This preliminary step is important in order to study multiple limit cycles arising from degenerate Hopf bifurcations in this circuit. This frequency domain approach (also called Graphical Hopf Theorem, GHT for short) for analyzing periodic solutions has provided very useful results in dealing with degenerate Hopf bifurcations [Moiola & Chen, 1996]. Very recently, this approach has been adapted to handle approximate detection of the first period-doubling bifurcation [Berns *et al.*, 1998] in the time-delayed version of Chua's circuit, by considering a higher-order expansion of the periodic solutions. Other related research using a unified formulation for both Hopf and period-doubling bifurcations were given by Rand [1989] and Belhaq and Houssni [1995] for a specific system, and Tesi *et al.* [1996] and Basso *et al.* [1997] for a broader class of nonlinear systems. Continuous efforts and progress made by some researchers from mechanical engineering [Szemplinksa-Stupnicka & Rudowski, 1993; Donescu & Virgin, 1996; Janicki & Szemplinksa-Stupnicka, 1997] in characterizing accurately the birth of period-doubling bifurcations (subharmonic resonances in forced systems) using similar methods, had encouraged us to pursue a simple methodology to handle several types of periodic solutions and their bifurcations. Since the GHT provides also a useful graphical interpretation, it seems natural to continue this effort in order to give better accurate results using higher-order harmonic balance approximations and a type of convergence test for the accuracy of the solutions. A

unified approach to treat both Hopf bifurcations and period-doubling bifurcations as well as indication of symmetry-breaking would be very useful. In such studies, Chua's circuit dynamics offers an excellent vehicle and paradigm for testing any future development in this area.

## Acknowledgments

J. L. Moiola acknowledges the partial support of a Fulbright-Antorchas grant as well as CONICET and UNS. He also acknowledges the hospitalitiy of the Department of Electrical Engineering and Computer Sciences at UCB. The authors would like to thank D. W. Berns for the computation of the critical point having the vanishing of the first and second Lyapunov indexes. Additional support is provided by ONR grant number N00014-97-1-0463.

## References

Altman, E. J. [1993] "Normal form analysis of Chua's circuit with applications for trajectory recognition," *IEEE Trans. Circuits Syst.-II: Anal. Dig. Sign. Process.***40**, 675–682.

Basso, M., Genesio, R. & Tesi, A. [1997] "A frequency method for predicting limit cycle bifurcations," *Nonlin. Dyn.* **13**, 339–360.

Belhaq, M. & Houssni, M. [1995] "Symmetry-breaking and first-period-doubling following a Hopf bifurcation in a three dimensional system," *Mech. Res. Commun.* **22**(3), 221–231.

Berns, D. W., Moiola, J. L. & Chen G. [1998] "Predicting period-doubling bifurcations in nonlinear time-delayed feedback systems," *Proc. IEEE Int. Symp. Circuits and Systems (ISCAS'98)* Vol. III, Monterey California, USA, pp. 619–622.

Chua, L. O. [1994] "Chua's circuit. An overview ten years later," *J. Circuits Syst. Comput.* **4**, 117–159.

Doedel, E. J. [1986] *AUTO: Software for Continuation and Bifurcation Problems in Ordinary Differential Equations* (CIT Press, Pasadena, CA).

Donescu, P. & Virgin, L. N. [1996] "Efficient determination of higher-order periodic solution using $n$-mode harmonic balance," *IMA J. Appl. Math.* **56**, 21–32.

Golubitsky, M. & Langford, W. F. [1981] "Classification and unfoldings of degenerate Hopf bifurcations," *J. Diff. Eq.* **41**, 375–415.

Janicki K. L. & Szemplinska-Stupnicka, W. [1997] "Subharmonic resonances in a driven oscillator: Bifurcation structures and transitions to chaos," *European J. Mech. A/Solids* **16**, 671–694.

Khibnik, A. I., Kuznetsov, Yu. A., Levitin, V. V. & Nikolaev, E. V. [1993a] "Continuation techniques and interactive software for bifurcation analysis of ODE's and iterated maps," *Physica* **D62**, 360–371.

Khibnik, A. I., Roose, D. & Chua, L. O. [1993b] "On periodic orbits and homoclinic bifurcations in Chua's circuit with a smooth nonlinearity," *Int. J. Bifurcation and Chaos* **3**, 363–384.

Lloyd, N. G., Blows, T. R. & Kalenge, M. C. [1988] "Some cubic systems with several limit cycles," *Nonlinearity* **1**, 653–669.

Lloyd, N. G. & Pearson, J. M. [1990] "Conditions for a center and the bifurcation of limit cycles in a class of cubic systems," *Bifurcations of Planar Vector Fields*, eds. Françoise, J. P. & Roussarie, R., Lecture Notes in Mathematics, Vol. 1455 (Springer-Verlag), pp. 230–242.

Madan, R. N. [1993] *Chua's Circuit: A Paradigm for Chaos* (World Scientific, Singapore).

Mees, A. I. & Chua, L. O. [1979] "The Hopf bifurcation theorem and its applications to nonlinear oscillations in circuits and systems," *IEEE Trans. Circuits Syst.* **CAS-26**, 235–254.

Moiola, J. L. & Chen, G. [1996] *Hopf Bifurcation Analysis — A Frequency Domain Approach*, ed. Chua, L. O., Series on Nonlinear Science, Series A, Vol. 21 (World Scientific, Singapore).

Planeaux, J. B. [1993] *Bifurcation Phenomena in CSTR Dynamics*, PhD thesis, University of Minnesota.

Rand, R. H. [1989] "Analytical approximation for period-doubling following a Hopf bifurcation," *Mech. Res. Commun.* **16**(2), 117–123.

Shil'nikov, L. P. [1994] "Chua's circuit: Rigorous results and further problems," *Int. J. Bifurcation and Chaos* **4**, 489–519.

Szemplinska-Stupnicka, W. & Rudowski, J. [1993] "Bifurcation phenomena in a nonlinear oscillator: Approximate analytical studies versus computer simulation results," *Physica* **D66**, 368–380.

Tesi, A., Abed, E. H., Genesio, R. & Wang, H. O. [1996] "Harmonic balance analysis of period-doubling bifurcations with implications for control of nonlinear dynamics," *Automatica* **32**, 1255–1271.

Zoladek, H. [1995] "Eleven small limit cycles in a cubic vector field," *Nonlinearity* **8**, 843–860.

# SUBSCRIPTION INFORMATION

Home Page: **http://www.worldscientific.com/**

*Please send orders to your regular book supplier or directly to your nearest World Scientific office:*

***USA*** **World Scientific Publishing Co. Inc.**
1060 Main Street, River Edge, NJ 07661, USA
Toll-free fax: 1-888-977-2665 **Toll-free: 1-800-227-7562** E-mail: sales@wspc.com

***UK*** **World Scientific Publishing (UK) Ltd.**
57 Shelton Street, Covent Garden, London WC2H 9HE, UK
**Fax: 44-171-836-2020** Tel: 44-171-836-0888 E-mail: sales@wspc2.demon.co.uk

***SINGAPORE*** **World Scientific Publishing Co. Pte. Ltd.**
Farrer Road, P O Box 128, SINGAPORE 912805 Cable: "COSPUB"
**Fax: 65-467-7667** Tel: 65-466-5775 E-mail:sales@wspc.com.sg

***HONG KONG*** **World Scientific Publishing (HK) Co. Ltd.**
P O Box 72482, Kowloon Central Post Office, HONG KONG
**Fax: 852-2-771-8155** Tel: 852-2-771-8791 E-mail: wsped@hk.super.net

***NDIA*** **World Scientific Publishing Co. Pte Ltd.**
4911, 9th Floor, High Point IV, 45 Palace Road, Bangalore 560 001, India
Tix: 00845-2900 PCO IN **Fax: 91-80-220-5972** Tel: 91-80-220-5972

***TAIWAN*** **World Scientific Publishing Co. Pte. Ltd.**
4F-5, No. 88, Sec 3, Hsin-Sheng S Road, Taipei, TAIWAN, ROC
Tel: 886-2-2369 1366 **Fax: 886-2-2366-0460** E-mail: wsptw@ms13.hinet.net

❑ Please enter my subscription:

| IJBC (ISSN: 0218-1274) | Vol. 9/1999 (12 issues) | |
|---|---|---|
| Institutions/libraries (Print) | ❑ US$1406 | ❑ S$2179 |
| Institutions/libraries (Print + Electronic) | ❑ US$1547 | ❑ S$2397 |
| **SPECIAL RATES** | | |
| Institutions/libraries from developing countries (Print) | ❑ US$844 | ❑ S$1308 |
| Institutions/libraries from developing countries (Print + Electronic) | ❑ US$928 | ❑ S$1439 |
| Individuals | ❑ US$562 | ❑ S$872 |
| For airmail, please add | ❑ US$96 | ❑ S$149 |
| For surface mail, please add | ❑ US$55 | ❑ S$85 |

- Customers from Asia Pacific and Australasia (except Hong Kong and China), please pay in Singapore Dollars (S$).
- Customers from the rest of the world (including Hong Kong and China), please pay in US$.

❑ **Please send me a complimentary copy of *International Journal of Bifurcation and Chaos in Applied Sciences and Engineering***

Name:_____ Organization/institution:_____

Address:_____ E-mail:_____

City:_____ State:_____ Zip:_____ Country:_____

**METHODS OF PAYMENT**

- For cheque payment in USA, please make cheque payable to "World Scientific Publishing Co. Inc."
- For cheque payment from the rest of the world, please make cheque payable to "World Scientific Publishing Co. Pte. Ltd."
- **Please enclose your personal cheque or details of your credit card for INDIVIDUAL subscription.**

❑ Cheque/bank draft enclosed for the amount of _____

❑ Charge my ❑ Visa ❑ MasterCard ❑ Amex ❑ Diners Club

Card No:_____ Expiry date:_____

Signature:_____ Tel:_____

❑ Bill my company/institution:_____ (Please attach purchase order.)

Please add my name to your mailing list. My field of interest is_____

**RUSH ORDERS**
In USA and Canada,
☎call toll-free:
**1-800-227-7562**
In Europe, fax:
**44-171-836-2020**
In other countries, fax:
**65-466-7667**

*SINGAPORE • NEW JERSEY • LONDON • HONG KONG • BANGALORE • TAIPEI*

International Journal of Bifurcation and Chaos, Vol. 8, No. 12 (1998) 2433–2438
© World Scientific Publishing Company

# CONTROL OF CHAOS USING SAMPLED-DATA FEEDBACK CONTROL

TAO YANG and LEON O. CHUA
*Electronics Research Laboratory and*
*Department of Electrical Engineering and Computer Sciences,*
*University of California at Berkeley,*
*Berkeley, CA 94720, USA*

Received June 14, 1998; Revised August 5, 1998

In this paper we present a theory for control of chaotic systems using sampled data. The output of the chaotic system is sampled at a given sampling rate and the sampled output is used by a feedback subsystem to construct a control signal, which is held constant by a holding subsystem. Hence, during each control iteration, the control input remains unchanged. Theoretical results on the asymptotic stability of the resulting controlled chaotic systems are presented. Numerical experimental results via Chua's circuit are used to verify the theoretical results.

## 1. Introduction

The control of chaos by *sampled* data has been studied and observed in experiments [Yang & Chua, 1997a, 1997b; Panas *et al.*, 1998; Dedieu & Ogorzalek, 1994]. Previous results used the sampled data to change the state variables of the chaotic system "impulsively". In this paper, we redesign the controller such that the control signal, which is constructed from the sampling sequence of the output of the chaotic system, is fed into the chaotic system as a control input. In this sampled-data feedback control scheme, the state variables of the chaotic system are subject to continuous changes instead of "impulsive" changes. Unlike most of the previous results where the control input is constructed by the continuous observations of the output of the chaotic system, the controller presented in this paper uses the samples of the output of the chaotic system to construct control signals.

The main motivation for controlling chaos using sampled data is to exploit well-developed digital control techniques. In a digital controller, the output of the chaotic system is sampled and the sampled data is used to construct the appropriate control signals. Assuming that a finite time duration is needed by a digital processor to calculate the control signals, then the sampling frequency is limited by this time duration. On the other hand, a fast sampling device is usually more expensive than a slow one. It is important therefore to develop a theory to predict the performance of the controlled chaotic system with a given sampling rate.

The authors of [Dedieu & Ogorzalek, 1994] had presented some experimental results for controlling chaotic systems to referenced trajectories by using only sampled values. Although it is widely believed that the control of continuous chaotic systems by using digital controllers is possible, so far, there exists no theoretical results to guarantee the asymptotic stability of such controlled chaotic systems. In this paper, we present theoretical results which guarantee the asymptotic stability of sampled-data feedback control of chaotic systems.

The organization of this paper is as follows. In Sec. 2, the structure and theory of the sampled-data feedback controller are presented. In Sec. 3, the sampled-data feedback control of a typical chaotic

system (Chua's circuit) is given. In Sec. 4, some concluding remarks are given.

## 2. Control of Chaos Using Sampled Data

In this section we present the structure and the theory of a sampled-data feedback controller.

### 2.1. *Structure of control system*

The proposed structure of a chaotic control system with sampled data is shown in Fig. 1. The state variables of the chaotic system are observed (measured) by transducers and the result is used to construct the output signal $\mathbf{y}(t) = D\mathbf{x}(t)$ where $D$ is a constant matrix to be defined below. The output $\mathbf{y}(t)$ is then sampled by the sampling block to obtain $\mathbf{y}(k) = D\mathbf{x}(k)$ at discrete moments $k\Delta$, where $k = 0, 1, 2, \ldots$, and $\Delta$ is the sampling duration. Then $D\mathbf{x}(k)$ is used by the controller to calculate the control signal $\mathbf{u}(k)$. During the time interval $[k\Delta, (k+1)\Delta)$, the output of the holding block is $\mathbf{u}(k)$, which is fed back into the chaotic system as a *fixed* control input during the entire time slot $[k\Delta, (k+1)\Delta)$.

### 2.2. *Theory of stability*

Consider a chaotic dynamic system modeled by the state equation

$$\dot{\mathbf{x}} = \mathbf{f}(\mathbf{x}) \tag{1}$$

where $\mathbf{x} \in \Re^n$ is the state variable, $\mathbf{f}$: $\Re^n \mapsto \Re^n$ is a nonlinear function and $\mathbf{f}(\mathbf{0}) = \mathbf{0}$.

The controlled chaotic system is defined by

$$\begin{cases} \dot{\mathbf{x}}(t) = \mathbf{f}(\mathbf{x}(t)) + B\mathbf{u}(k), \; t \in [k\Delta, (k+1)\Delta) \\ \mathbf{u}(k+1) = C\mathbf{u}(k) + D\mathbf{x}(k), \; k = 0, 1, 2, \ldots \end{cases} \tag{2}$$

where $\mathbf{u} \in \Re^m$, $B \in \Re^n \times \Re^m$, $C \in \Re^m \times \Re^m$, $D \in \Re^m \times \Re^n$, and $t \in \Re_+$; $\mathbf{x}(k)$ is the sampled value of $\mathbf{x}(t)$ at $t = k\Delta$; $\Delta$ is the sampling duration. Observe that since $\mathbf{f}(\mathbf{0}) = \mathbf{0}$, $\begin{pmatrix} \mathbf{x} \\ \mathbf{u} \end{pmatrix} = \begin{pmatrix} \mathbf{0} \\ \mathbf{0} \end{pmatrix}$ is an *equilibrium point* of the system in Eq. (2). The asymptotic stability of this equilibrium point can be determined from that of the trivial solution of the associated linearized system:

$$\begin{cases} \dot{\mathbf{x}} = A\mathbf{x} + B\mathbf{u}(k), \; t \in [k\Delta, (k+1)\Delta) \\ \mathbf{u}(k+1) = C\mathbf{u}(k) + D\mathbf{x}(k), \; k = 0, 1, 2, \ldots \end{cases} \tag{3}$$

where $A \in \Re^n \times \Re^n$ is given by

$$A \triangleq \frac{\partial \mathbf{f}(0)}{\partial \mathbf{x}}. \tag{4}$$

**Definition 1.** An $n \times n$ matrix $\Gamma$ is said *Schur stable* if, and only if, all eigenvalues of $\Gamma$ lie in the unit disc centered at the origin.

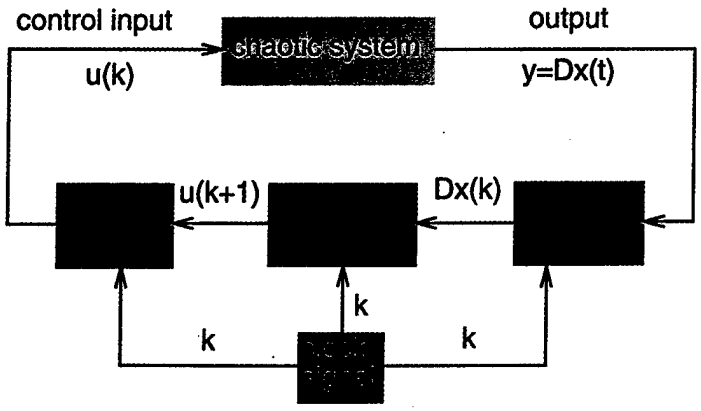


Fig. 1. Structure of a proposed sampled-data chaotic control system.

**Lemma 1.** *Suppose* $\mathbf{f} \in C^1[\Re^n, \Re^n]$, *then the equilibrium point* $(\mathbf{x}, \mathbf{u}) = (\mathbf{0}, \mathbf{0})$ *of the controlled chaotic system* (2) *is uniformly asymptotically stable if the associated matrix*

$$H \triangleq \begin{pmatrix} e^{A\Delta} & \left(\int_0^\Delta A^{\Delta-\tau} d\tau\right) B \\ D & C \end{pmatrix} \tag{5}$$

*is Schur stable.*

*Proof.* The proof follows directly from Theorem 5.1 of [Ye *et al.*, 1998], which assumes that $\Delta = 1$. The generalization for arbitrary $\Delta$, hence, follows easily. ■

Lemma 1 is not practical because it involves integration of matrices. The following theorem gives a more explicit criterion for the stability of the controlled chaotic system.

**Theorem 1.** *Suppose* $\mathbf{f} \in C^1[\Re^n, \Re^n]$ *and* $A$ *is nonsingular, then the equilibrium point* $(\mathbf{x}, \mathbf{u}) = (\mathbf{0}, \mathbf{0})$ *of the controlled chaotic system* (2) *is uniformly asymptotically stable if the spectral radius* $\rho(T)$ *of the matrix*

$$T \triangleq \begin{pmatrix} e^{A\Delta} & A^{-1}e^{A\Delta}B - A^{-1}B \\ D & C \end{pmatrix} \tag{6}$$

*is less than unity; i.e.* $\rho(T) < 1$.

*Proof.* Observe that

$$\begin{aligned} \left(\int_0^\Delta A^{\Delta-\tau} d\tau\right) B &= \left(-\int_0^\Delta A^{\Delta-\tau} d(\Delta-\tau)\right) B \\ &= \left(\int_0^\Delta A^t dt\right) B \\ &= \left(A^{-1}e^{At}|_0^\Delta\right) B \\ &= A^{-1}(e^{A\Delta} - I)B \end{aligned} \tag{7}$$

where $t = \Delta - \tau$ and $I \in \Re^n \times \Re^n$ is the identity matrix. Substituting (7) into (5), obtain $T = H$. Since the spectral radius $\rho(T) < 1$, we know that $T$ is Schur stable, and the theorem therefore follows from Lemma 1. ■

## 3. Control of Chua's Circuit with Sampled Data

In this example, we use Chua's oscillator [Madan, 1993], which is shown in Fig. 2(a), as the chaotic system. The state equation of the Chua's oscillator is given by

$$\begin{cases} \dfrac{dv_1}{dt} = \dfrac{1}{C_1}[G(v_2 - v_1) - f(v_1)] \\ \dfrac{dv_2}{dt} = \dfrac{1}{C_2}[G(v_1 - v_2) + i_3] \\ \dfrac{di_3}{dt} = \dfrac{1}{L}[-v_2 - R_0 i_3] \end{cases} \tag{8}$$

where $G = 1/R$ and $f(v_1)$ is the piecewise linear $v$–$i$ characteristic of Chua's diode, as shown in Fig. 2(b) and can be expressed explicitly by

$$f(v_1) = G_b v_1 + \frac{1}{2}(G_a - G_b)(|v_1 + E| - |v_1 - E|) \tag{9}$$

where $E$ is the breakpoint voltage of Chua's diode.

In this example, let us assume $R_0 = 0$ in (8). The dimensionless version of the resulting Chua's circuit is given by

$$\begin{cases} \dot{x} = \alpha(y - x - f(x)) \\ \dot{y} = x - y + z \\ \dot{z} = -\beta y \end{cases} \tag{10}$$

where $x = v_1/E$, $y = v_2/E$, $z = i_3/(EG)$, $\alpha = C_2/C_1$, $\beta = C_2R^2/L$, and

$$f(x) = bx + \frac{1}{2}(a - b)(|x + 1| - |x - 1|) \tag{11}$$

where $a = RG_a$ and $b = RG_b$. To control Chua's circuit to the origin, let us calculate

$$A = \left.\frac{\partial \mathbf{f}}{\partial \mathbf{x}}\right|_{\mathbf{x}=\mathbf{0}} = \begin{pmatrix} -\alpha(1+a) & \alpha & 0 \\ 1 & -1 & 1 \\ 0 & -\beta & 0 \end{pmatrix}. \tag{12}$$

Let us choose the parameters as follows: $\alpha = 10$, $\beta = 14.87$, $a = -1.27$ and $b = -0.68$, and

$$\begin{aligned} B &= \begin{pmatrix} 1 & 0 & 0 \\ 0 & 0 & 0 \\ 0 & 0 & 0 \end{pmatrix}, \quad C = \begin{pmatrix} 0.8 & 0 & 0 \\ 0 & 0 & 0 \\ 0 & 0 & 0 \end{pmatrix}, \\ D &= \begin{pmatrix} -0.6 & 0 & 0 \\ 0 & 0 & 0 \\ 0 & 0 & 0 \end{pmatrix}, \quad \Delta = 5 \times 10^{-3}. \end{aligned} \tag{13}$$

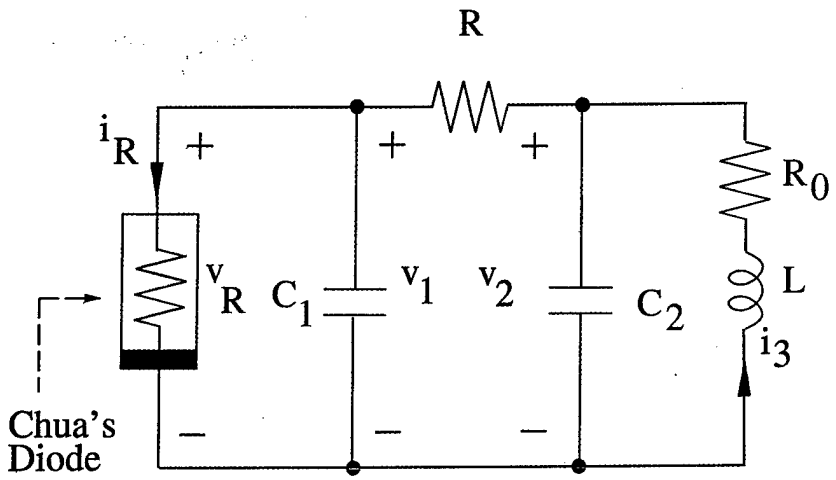


(a)

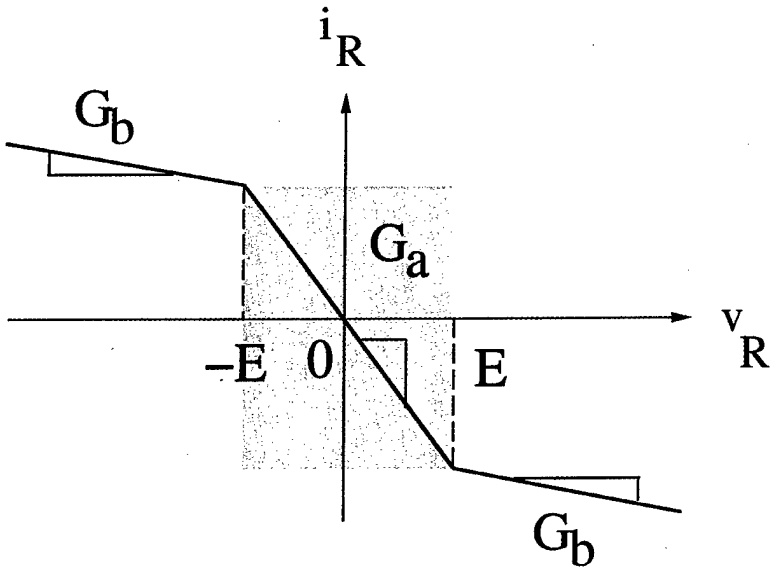


(b)

Fig. 2. (a) Chua's circuit. (b) Nonlinear $v$–$i$ characteristic of Chua's diode.

Using the above parameters, the controlled chaotic system is given by

$$\begin{cases} \dot{x} = \alpha(y - x - f(x)) + u_1(k) \\ \dot{y} = x - y + z \\ \dot{z} = -\beta y \end{cases}$$

$$u_1(k+1) = 0.8u_1(k) - 0.6x(k),\ k = 0,\ 1,\ 2, \ldots \tag{14}$$

The corresponding matrix $T$ in (6) is given by

$$T = \begin{pmatrix} 1.0137 & -0.0502 & 0.0001 & 0.0050 & 0 & 0 \\ 0.0050 & -0.9950 & 0.0050 & 0.0000 & 0 & 0 \\ -0.0002 & -0.0742 & 0.9998 & 0.0000 & 0 & 0 \\ -0.6000 & 0 & 0 & 0.8000 & 0 & 0 \\ 0 & 0 & 0 & 0 & 0 & 0 \\ 0 & 0 & 0 & 0 & 0 & 0 \end{pmatrix}. \tag{15}$$

The eigenvalues and their norms of the above matrix $T$ are listed in Table 1.

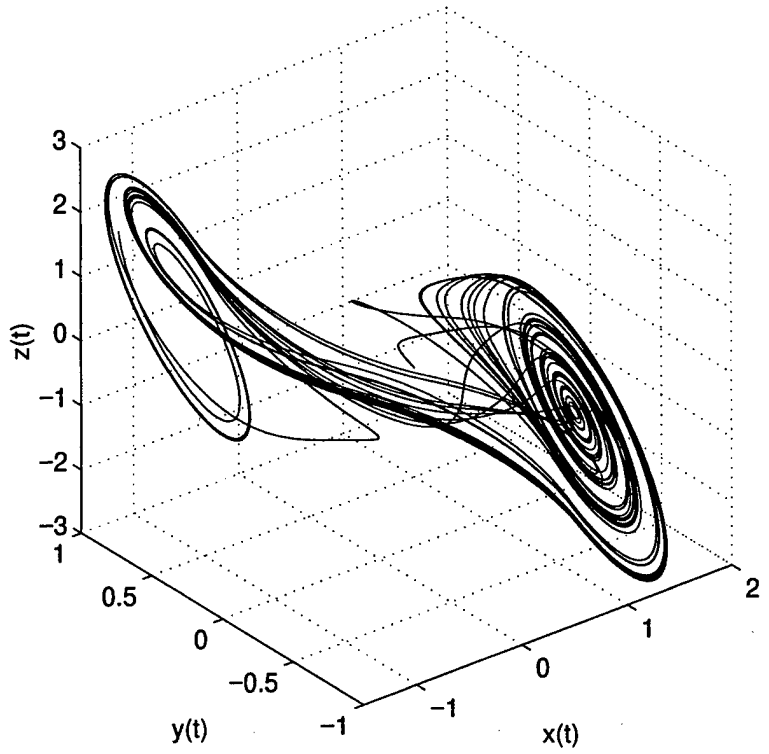


(a)

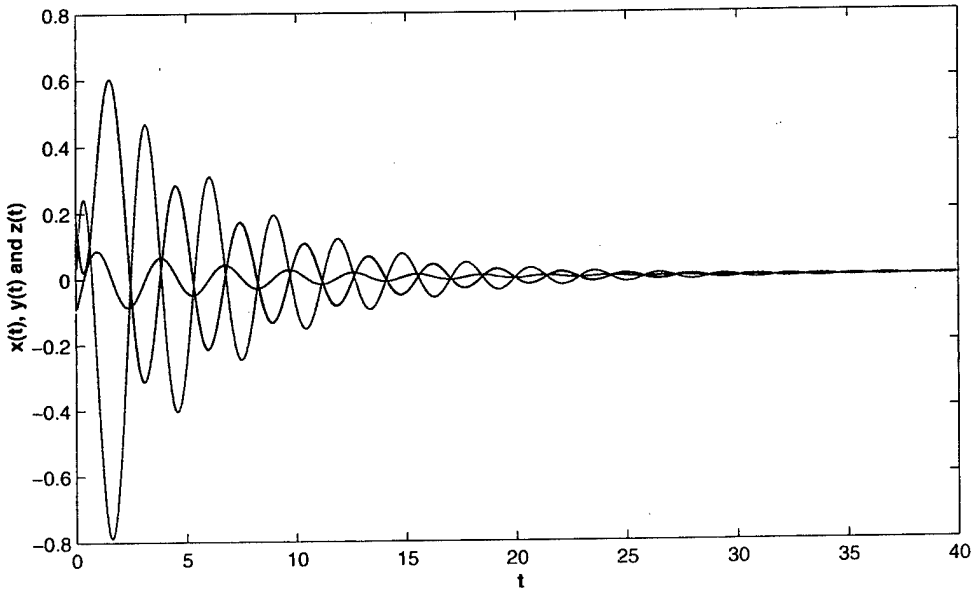


(b)

Fig. 3. Controlling Chua's circuit to the origin using sampled control signal. (a) The trajectory of Chua's circuit without control. (b) The controlled state variables of Chua's circuit: $x(t)$(blue), $y(t)$(red) and $z(t)$(green). (c) Control signal $u_1(k)$.

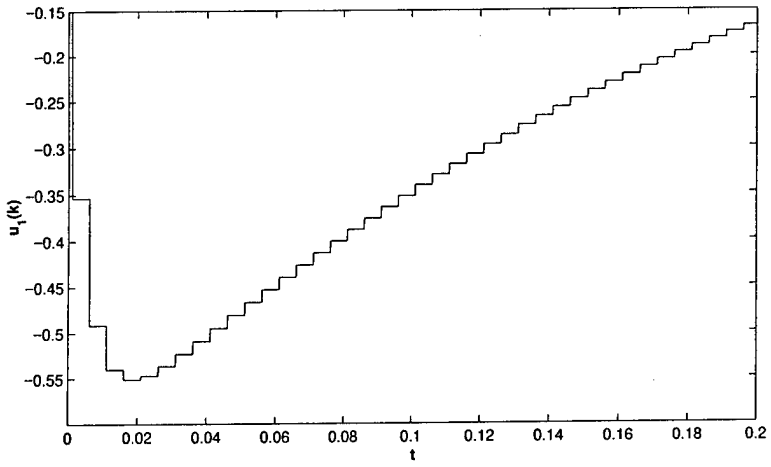


(c)

Fig. 3. (*Continued*)

Table 1. The eigenvalues and their norms of matrix $T$.

| Real Part | Imaginary Part | Norm |
|---|---|---|
| −0.994689 | 0.000000 | 0.994689 |
| 0.815117 | 0.000000 | 0.815117 |
| 0.998448 | 0.000000 | 0.998448 |
| 0.999623 | 0.000000 | 0.999623 |
| 0.000000 | 0.000000 | 0.000000 |
| 0.000000 | 0.000000 | 0.000000 |

Since $\rho(T) = 0.999623 < 1$, the controlled system is uniformly asymptotically stable at the origin. The simulation results are shown in Fig. 3. The initial condition for Chua's circuit is $(x(0), y(0), z(0)) = (0.2, -0.1, -0.01)$. The initial condition for the controller is $(u_1(0), u_2(0), u_3(0)) = (0, 0, 0)$. The sampling rate is 200 Hz. Figure 3(a) shows the trajectory of Chua's circuit without control. Figure 3(b) shows the controlled trajectory, which tends to the origin asymptotically. Figure 3(c) shows the details of the control signal $u_1(k)$.

## 4. Concluding Remarks

In the chaotic control community, it has been known for a long time that to control a chaotic system, the sampled data of the output is enough for constructing the control signals. This paper provides the theory of the stability of this method and also provides some constructive guidelines on the design of the controller. Since digital controllers are much more flexible than analog controllers, digital controllers had been widely used in industry. The results presented in this paper give a theoretical basis for designing digital controllers for controlling chaotic systems.

## Acknowledgment

This work is supported in part by the Office of Naval Research under grant numbers N00014-97-1-0463 and N00014-96-1-0753.

## References

Dedieu, H. & Ogorzalek, M. [1994] "Controlling chaos in Chua's circuit via sampled inputs," *Int. J. Bifurcation and Chaos* **4**(2), 447–456.

Madan, R. N. (ed.) [1993] *Chua's Circuit: A Paradigm for Chaos*, World Scientific Series on Nonlinear Science. Series B, Special Theme Issues and Proceedings Vol. 1 (World Scientific, Singapore).

Panas, A. I., Yang, T. & Chua, L. O. [1998] "Experimental results of impulsive synchronization between two Chua's oscillators," *Int. J. Bifurcation and Chaos* **8**(3), 639–644.

Yang, T. & Chua, L. O. [1997] "Impulsive control and synchronization of nonlinear dynamical systems and application to secure communication," *Int. J. Bifurcation and Chaos* **7**(3), 645–664.

Yang, T. & Chua, L. O. [1997] "Impulsive stabilization for control and synchronization of chaotic systems: Theory and application to secure communication," *IEEE Trans. Circuits Syst. I: Fundamental Theor. Appl.* **44**(10), 976–988.

Ye, H., Michel, A. N. & Hou, L. [1998] "Stability theory for hybrid dynamical systems," *IEEE Trans. Automatic Control* **43**(4), 461–474.

# Synthesizing Arbitrary Driving-Point and Transfer Characteristics

Leon O. Chua, *Fellow, IEEE*, Chai Wah Wu, Guo-Qun Zhong, and Luis Franscisco Liu

***Abstract*—The property of any two-terminal resistive device is characterized by its driving-point (DP) characteristic, and any two-port resistive device with zero input current and a load-independent output voltage is described by its transfer characteristic (TC). Synthesizing a two-port device with a prescribed transfer characteristic is usually easier than synthesizing a two-terminal device with a prescribed driving-point characteristic. In this paper we propose an approach to synthesize a driving-point characteristic of a two-terminal device from the transfer characteristic of a two-port device, so that the resulting DP plot of the two-terminal device is exactly the same as the TC plot of the two-port device. We also illustrate the use of digital circuitry to synthesize arbitrary transfer characteristics. This technique will benefit the design and analysis of complex nonlinear electronic circuits and systems. A variety of characteristics synthesized using this approach are presented.**

***Index Terms*—Driving-point characteristics, nonlinear circuit synthesis, transfer characteristics.**

## I. Introduction

TWO-TERMINAL, or one-port, devices play a major role in electrical circuits and systems. A two-terminal resistive device is characterized by a relation between the branch voltage and the branch current, so-called $v$–$i$ characteristic, or by its *driving-point (DP) characteristic* relating its port voltage and its port current [1], a fundamental concept in the study of electrical circuits. The DP characteristics of commercially available devices can usually be found in data books. However, there are other applications where a specific DP characteristic must be used. For example, in the synthesis of a nonlinear network which realizes a prescribed dynamical behavior the optimal $v$–$i$ characteristics of the synthesized nonlinear resistors are seldom available from existing commercial devices. Several approaches for synthesizing, in particular non-monotonic characteristic, have been reported in the literatures [2]–[6]. Unfortunately, synthesizing a device with an arbitrary $v$–$i$ characteristic is cumbersome, or even not applicable using these techniques.

Manuscript received August 27, 1996. This work was supported in part by the Office of Naval Research under Grant N00014-97-1-0463 and Grant N00014-96-1-0753, by the National Science Foundation under Grant MIP 86-14000, and by the Joint Services Electronics Program under Contract F49620-94-C-0038. This paper was recommended by Associated Editor A. Reibiger.

L. O. Chua, C. W. Wu, and L. F. Liu are with the Electronics Research Laboratory and the Department of Electrical Engineering and Computer Sciences, University of California at Berkeley, Berkeley, CA 94720 USA.

G.-Q. Zhong is with the Electronics Research Laboratory and the Department of Electrical Engineering and Computer Sciences, University of California at Berkeley, Berkeley, CA 94720 USA, on leave from Guangzhou Institute of Electronic Technology, Academia Sinica, Guangzhou 510070, China.

Publisher Item Identifier S 1057-7122(98)08612-7.

The class of two-port resistive devices with zero input current and a load-independent output voltage is characterized by their *transfer characteristic (TC)* between the input voltage $v_1$ and the response (output) voltage $v_2$ [1].[1] Usually synthesizing a two-port device with a prescribed transfer characteristic is easier than synthesizing a one-port device with a prescribed DP characteristic.

In this paper we propose an approach for synthesizing a prescribed DP characteristic of a nonlinear resistor from the TC of a two-port resistive element. The implementation of the TC-to-DP characteristic converter is described in Section II. A digital technique for synthesizing a two-port resistive element with an arbitrary TC is presented in Section III. In Section IV we demonstrate a variety of DP characteristics synthesized using the method proposed in this paper.

## II. Implementation of the TC-to-DP Characteristic Converter

The block diagram of the TC-to-DP characteristic converter is shown in Fig. 1. The TC-to-DP characteristic converter is a three-port device that when connected as in Fig. 1 would have a DP characteristic in the input port equal to the TC of the two-port under consideration. There are two realizations for the proposed conversion as described below.

### *Realization I*

The block diagram of realization I is shown in Fig. 2. This realization simply consists of a linear $R$ connected across the two-port. Assume that the TC of the two-port device is

$$v_2 = f(v_1). \tag{1}$$

According to the Kirchhoff's laws, we have

$$i = \frac{v_1 - v_2}{R} = \frac{v_1 - f(v_1)}{R}. \tag{2}$$

Defining

$$g(v_1) = \frac{v_1 - f(v_1)}{R} \tag{3}$$

we obtain

$$i = g(v_1). \tag{4}$$

[1]The concept of a *transfer characteristic* (TC) plot is well defined even if the input current is not zero [1]. However, the synthesis procedure is easier if $i_1 = 0$.

1057–7122/98$10.00 © 1998 IEEE

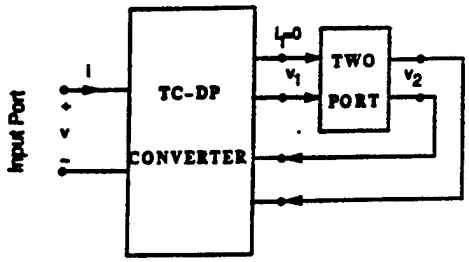


Fig. 1. Block diagram of TC-to-DP characteristic converter connected to a two-port. The TC-to-DP characteristic converter is a three-port device which when connected as shown would generate a DP characteristic in the input port equal to the TC of the two-port under consideration.

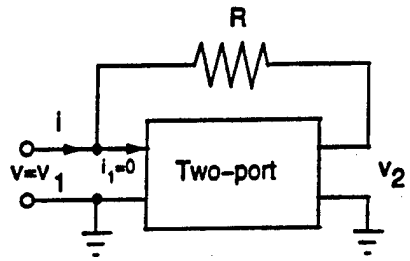


Fig. 2. Block diagram of *realization I* for the converter.

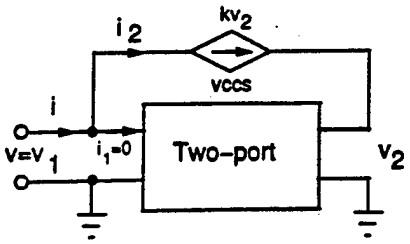


(a)

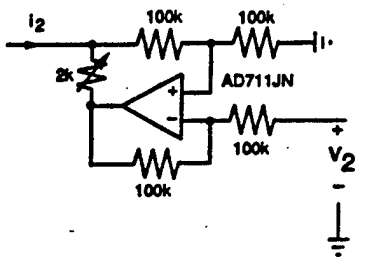


(b)

Fig. 3. (a) Block diagram of *realization II* for the converter. (b) Physical implementation of the voltage controlled current source (VCCS).

The only difference between the TC and the resulting DP characteristic is the linear term $v_1/R$ in (2) corresponding to a straight line with the slope $1/R$ in the $v$–$i$ plane. This needs to be taken into account in the design of the TC characteristic to obtain the correct DP characteristic.

*Realization II*

The block diagram of realization II is shown in Fig. 3(a). In the converter circuit we use a voltage-controlled current source (VCCS) instead of the linear resistor $R$ in Fig. 2. The implementation of the VCCS is shown in Fig. 3(b).

Assume also that the TC of the two-port device is defined by (1). The defining equation for the voltage controlled current source (VCCS) implies that

$$i_2 = kv_2 \tag{5}$$

where $k$ is the scale factor of the VCCS, thus we obtain

$$i = i_2 = kv_2. \tag{6}$$

Obviously, the resulting DP characteristic is

$$i = kf(v_1). \tag{7}$$

Thus the DP characteristic is a scaled version of the TC.

## III. A Digital Technique for Synthesizing Prescribed TC's of Two-Port Devices

In this section we describe an implementation of arbitrary transfer characteristics using digital hardware. The use of digital hardware allows for more flexibility and precision in synthesizing transfer characteristics, although operating at lower frequencies than analog hardware. This system, coupled with the TC-to-DP converter in the last section, results in a flexible platform for synthesizing arbitrary DP's, which are useful in prototyping complex nonlinear circuits.

In particular, we construct a two-port with an arbitrary transfer function between the port voltages, with zero current into the input port.

The voltage-to-voltage (V–V) transfer function generator is built using digital hardware coupled between necessary A/D and D/A converters, so that it appears as an analog device. The analog V–V mapping is performed in three distinct steps. First, the input analog voltage is sampled by the A/D converter and converted into a digital representation. Then, the digital representation is used by the digital hardware to map to the correct digital output. The conversion of the digital output into an analog output voltage completes the analog V–V mapping. Beyond selecting which D/A and A/D converters to use, most of the design work centers on how the digital output is chosen or calculated based on the digital input and the desired transfer characteristic.

We implemented two versions of the V–V transfer function generators, a two-port representation and a four-port representation. Different methods are utilized for these two versions to yield the correct output digital number given some input digital number. The two-port version finds the correct output using a table lookup with the inputs as the indexes. Since no actual calculations are done, for any desired transfer function, the output values will have to be precalculated and loaded into some type of digital memory, in this case EPROM's, prior to the operation of the circuit. This limits the flexibility of the one-port V–V function generator somewhat since each new function requires a new set of data. The four-port version manages to get around this limitation by using a DSP chip for the real-time calculation of the proper output values. This approach offers greater flexibility since new functions can be implemented by simply reprogramming the DSP chip. Furthermore, the amount of data required for a table lookup of a four-port TC will be too large to be practical. On the

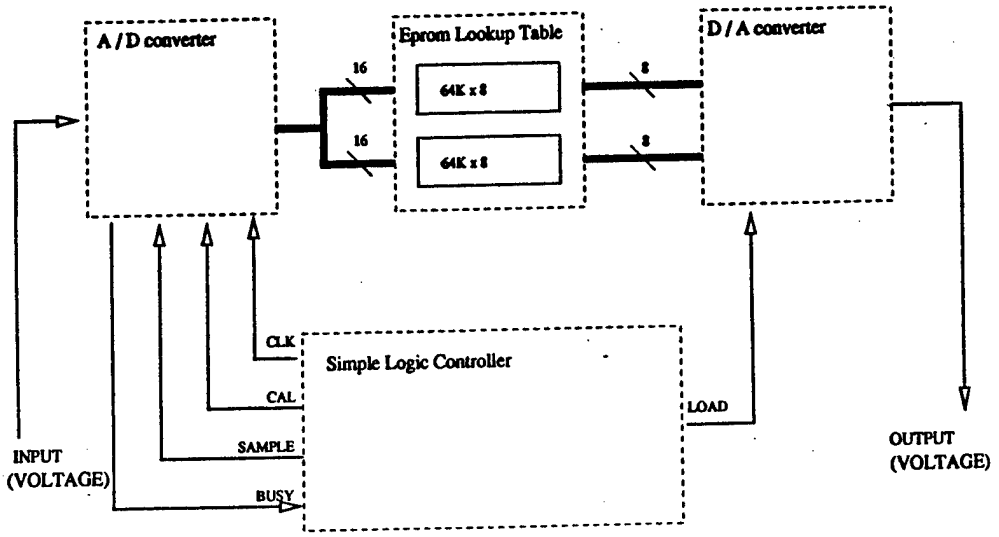


(a)

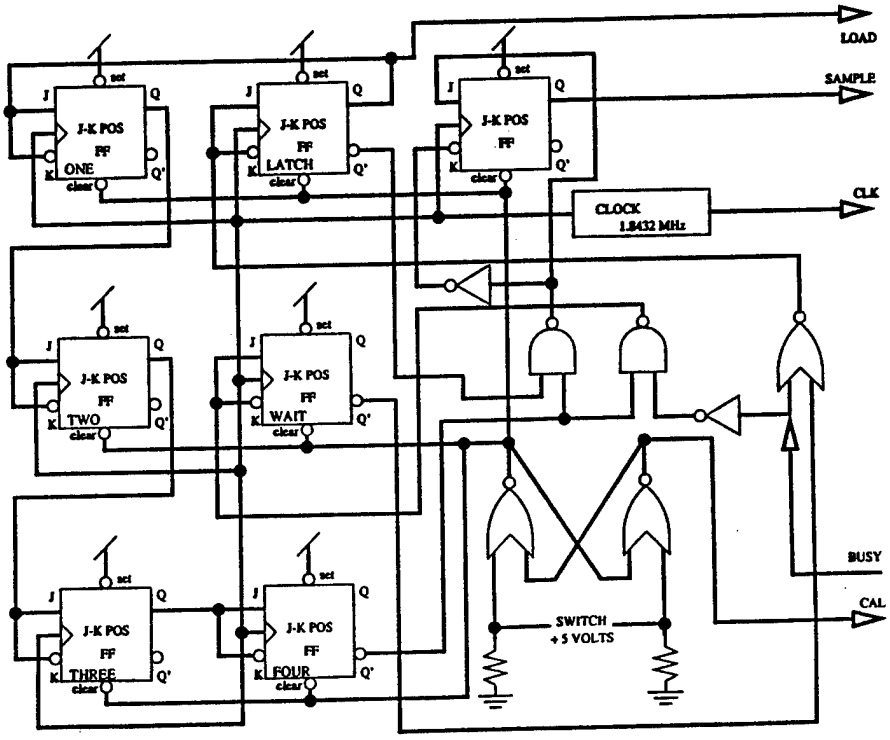


(b)

Fig. 4. (a) Top level block diagram of one-port arbitrary V–V transfer function generator. (b) Component level schematic of logic controller. A DSP chip is used to compute the corresponding output voltages given two input voltages.

other hand, in a table lookup approach, the time required to compute the output is independent of the complexity of the transfer characteristic, whereas this time can vary in a DSP implementation.

### A. Two-Port V–V Transfer function Generator

Fig. 4(a) depicts the top-level block diagram of the two-port V-V transfer function circuit. A small logic controller regulates input sampling, EPROM table lookup, and conversion into analog output. Any desired V–V transfer function can be achieved by simply loading the EPROM's with the correct data. All digital representations in this circuit have 16 bits of precision.

*Logic Design:* The logic controller is built as a finite state machine using one-hot encoding (one state per flip-flop) in order to simplify debugging. The controller provides a timing mechanism for the A/D and D/A converters. The specifics of this design are dependent on the actual A/D and D/A converters employed, and Fig. 4(b) gives a component level schematic of the logic controller. Fig. 4(c) shows the corresponding state transition diagram.

*EPROM Programming:* Data for the EPROM's are calculated using a simple C program implementing the transfer

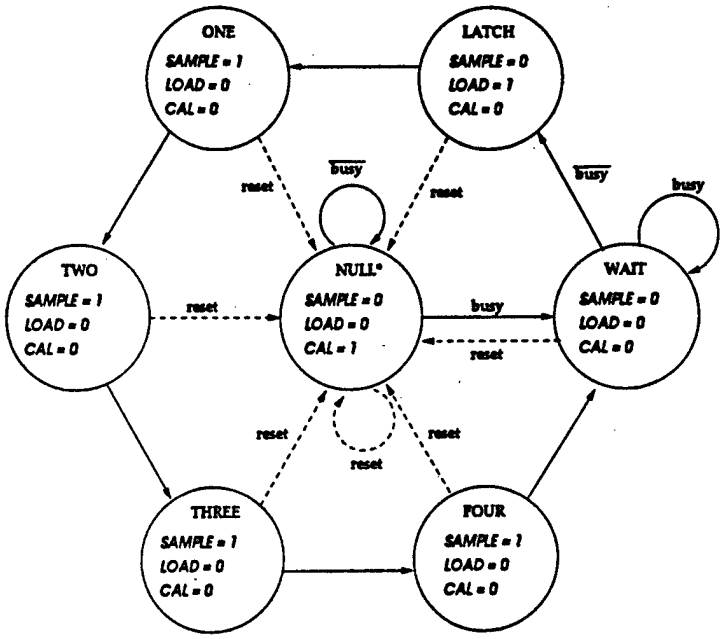


Solid lines indicate a synchronous state transition.
Dotted lines idicate an asynchronous state transition (global reset).

Corresponding outputs to each state are labeled inside the circles.

NOTE:
Even though one-hot encoding was utilized, for the sake of simplicity, the NULL state was encoded as all state elements being zero.

The SAMPLE output signal is actually derived from a toggle flip flop. This insures that SAMPLE is continuously asserted for a total of four clock cycles.

(c)

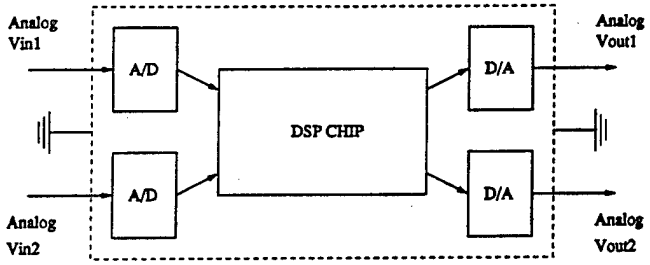


(d)

Fig. 4. *(Continued.)* (c) State transition diagram. (d) Block diagram of the four-port V–V transfer function generation. A DSP chip is used to compute the corresponding output voltages given two input voltages.

function. The program takes all possible input digital values and finds all respective output digital values depending on what transfer function is desired. This data is stored in a file so that an EPROM programmer can be used to load the information into the actual EPROM chips.

*Circuit Performance:* The resulting implementation runs at an overall sampling rate of 80.14 ksamples/s (kilosamples per second). The delay between the correct analog voltage being output after latching an analog voltage on to the analog input is 18 ms. Input and output voltage ranges have 16 bits of resolution.

*4) Analysis:* There are some issues associated with this design of the two-port V–V arbitrary function generator that require further investigation. Due to the digital nature of this realization, further study is required to study how aliasing, distortion, quantization error, and overall delay affect the behavior of nonlinear circuits utilizing this system.

### *B. Four-Port V–V Transfer Function Generator*

A DSP board is at the heart of the physical implementation of the four-port V–V arbitrary function generator, replacing the EPROM table lookup in the two-port version. We use a commercially available DSP board with two sets of A/D and D/A converters, which provides the ideal hardware for four-port representations. In a manner similar to the two-port design, input analog voltages from both ports are latched by the A/D converters. The proper corresponding output values are computed in real-time by the DSP chip and the D/A converters then output the analog voltages [Fig. 4(d)].

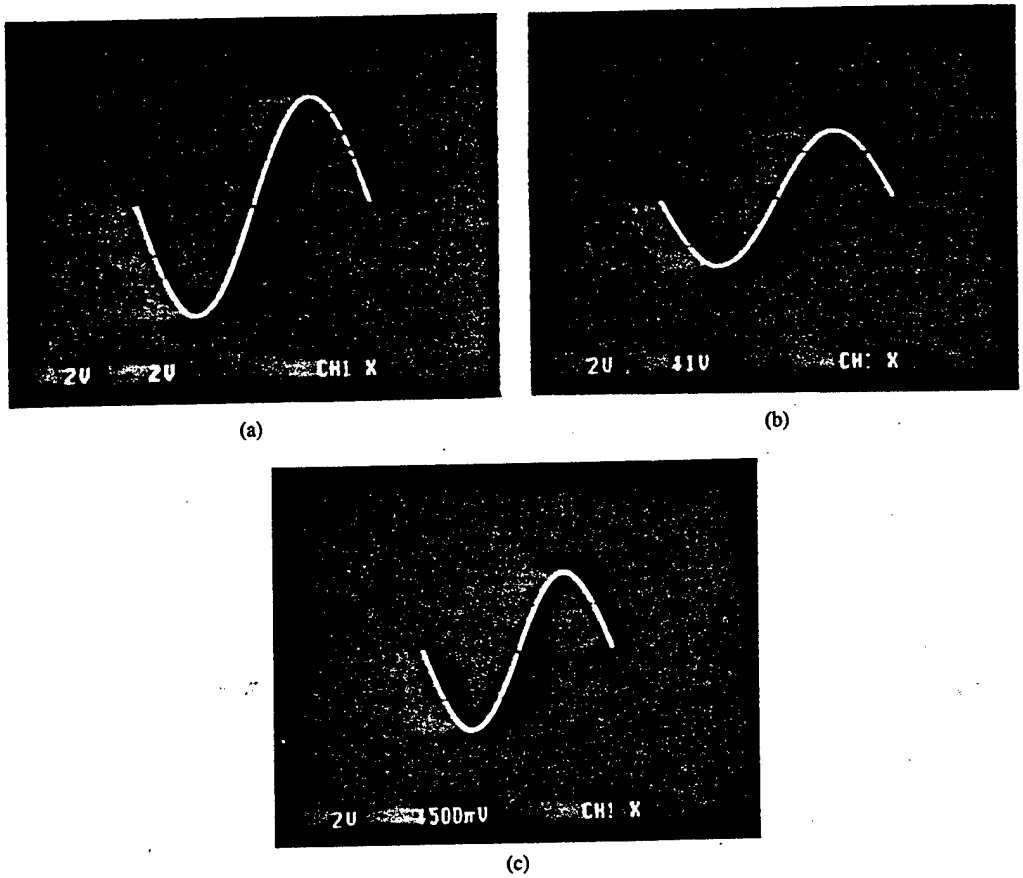


Fig. 5. (a) TC of a two-port device described by a sinusoidal function $v_2 = a\sin(v_1)$. (b), (c) DP characteristics $i = k\sin(v_1)$ converted by *Realizations I* and *II*, respectively.

*DSP Board:* The heart of the DSP board consists of a TMS320C30 floating point DSP chip. The board also provides low-pass filters for the inputs and outputs along with 16-bit D/A/D converters. All digital representation and calculations are performed in 16 bits precision and the maximum rate of sampling is 200 kHz.

*Real-Time Calculation of Output Values:* The DSP chip is programmed using either C or Assembly. The desired transfer function is written in the chosen language. The program is compiled and downloaded to the DSP chip, and the DSP chip will perform the necessary calculations by running the compiled programs. When the desired transfer characteristic is so complicated that it takes the DSP chip longer than a sample period to finish the computation, some samples will be discarded. The use of DSP's is more flexible than the use of lookup tables since a different transfer function can be realized by simply altering the program. Furthermore, with 16 bits of precision, the V–V transfer characteristics for a four-port will require too much memory for a practical table look-up approach.

*Performance:* The circuit runs at the maximum rate of 200 kHz with 16 bits of resolution for input and output voltages given simple transfer functions. Delay between the desired analog output voltage after a given input analog voltage is much less than the two port version if the circuit is run at this high sampling rate. The operation and reprogramming of the circuit is achieved interactively by running a TMS320 interface application on a personal computer.

*4) Analysis:* The four-port representation of the V–V transfer function generator has many of the same limitations associated with the two-port version discussed earlier, due to its inherent digital nature. The most important issue here is speed of operation, which is less than what can be achieved with analog parts.

## IV. Examples of DP Characteristics Synthesized from TC's

By using the approach proposed in this paper, a variety of DP characteristics of two-terminal, or one-port, devices synthesized from TC's of two-port devices are shown in Figs. 5–9. A TC of a two-port device, described by a sinusoidal function $v_2 = a\sin(v_1)$ shown in Fig. 5(a), is synthesized using the digital technique presented in Section III. Fig. 5(b) and (c) shows the DP characteristics $i = k\sin(v_1)$ converted by *realization I* shown in Fig. 2 (after compensation of the linear term) and *realization II* shown in Fig. 3(a), respectively, from the TC shown in Fig. 5(a). Next we choose a two-port device with a square function $v_2 = av_1^2$ TC. The circuit implementation using an analog multiplier and its TC described by a square function $v_2 = av_1^2$ are shown in Fig. 6(a) and (b), respectively. The DP characteristic $i = kv_1^2$ converted by *realization II* from the TC in Fig. 6(b) is shown in Fig. 6(c). Figs. 7(a) and 8(a) show two-port devices, which are operational amplifiers operating in a saturation region (Fig. 7) and a linear region (Fig. 8), respectively. The TC's,

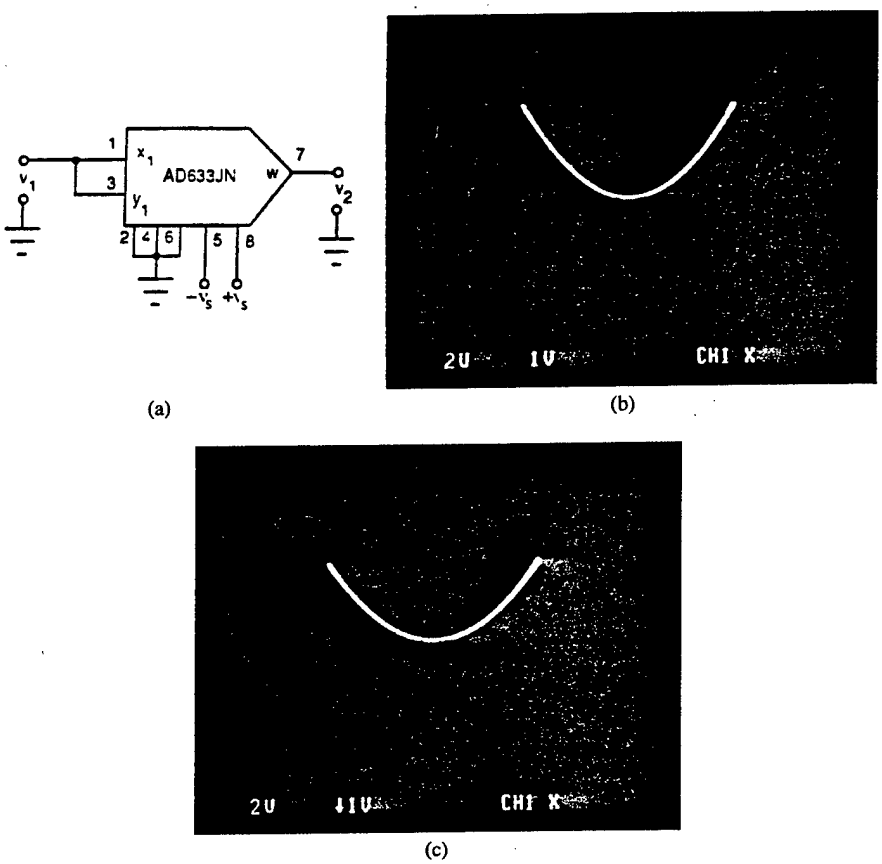


(a) (b) (c)

Fig. 6. (a) Circuit diagram of an analog square multiplier. (b) TC described by a square function $v_2 = av_1^2$. (c) DP characteristic $i = kv_1^2$ converted by *Realization II* from the TC in (b).

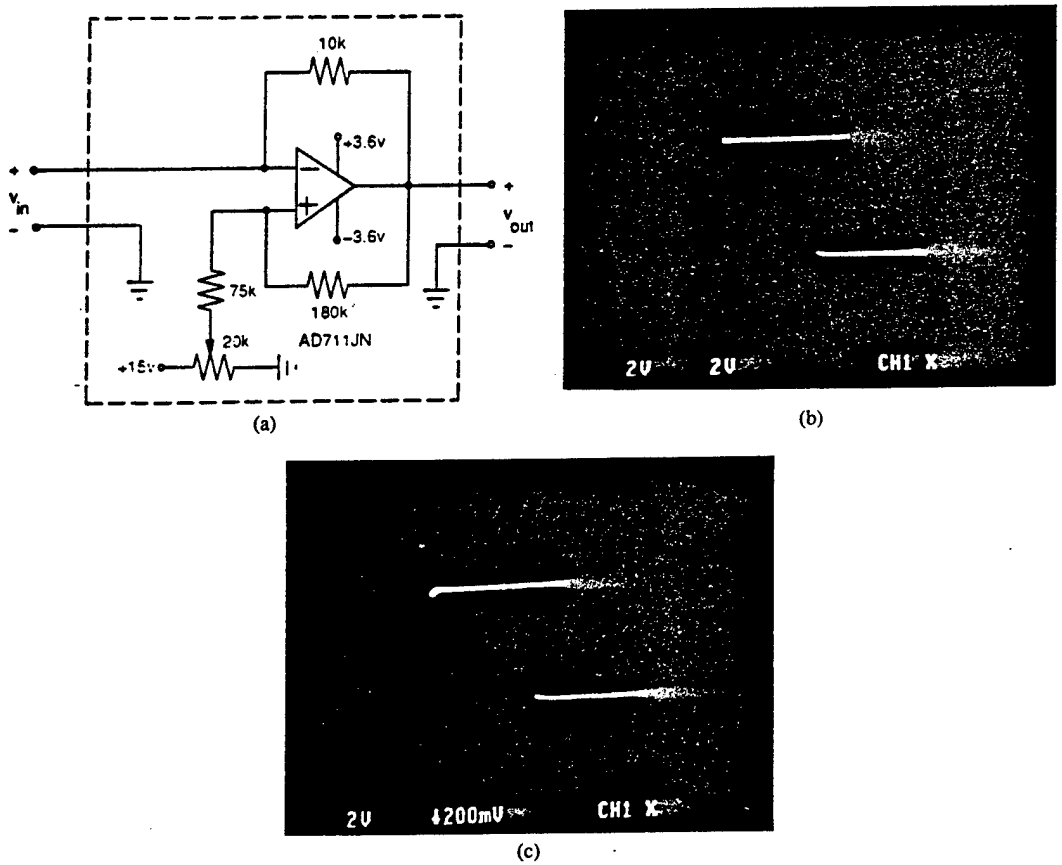


(a) (b) (c)

Fig. 7. (a) Circuit diagram of an amplifier operating in a saturation region. (b) TC of the two-port device shown in (a). (c) DP characteristic converted by *Realization II* from the TC in (b).

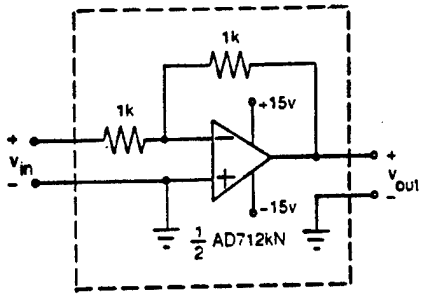


(a)

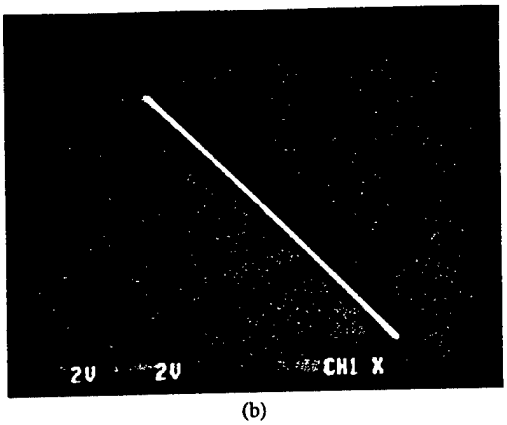


(b)

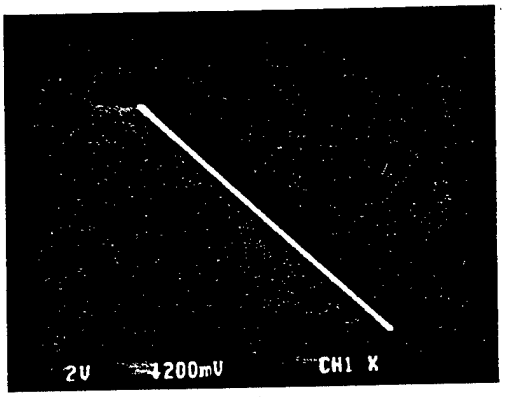


(c)

Fig. 8. (a) Circuit diagram of an amplifier operating in a linear region. (b) TC of the two-port device shown in (a). (c) DP characteristic converted by *Realization II* from the TC in (b).

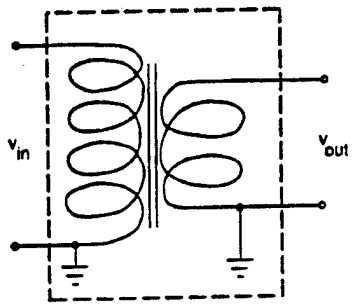


(a)

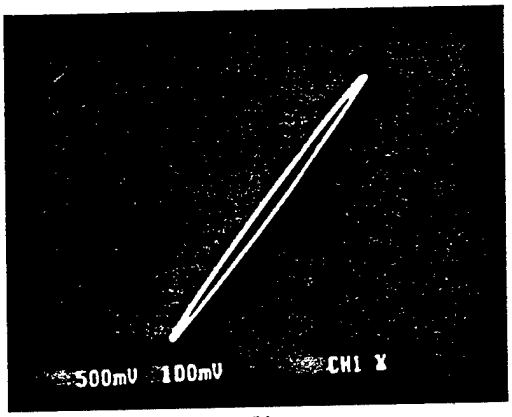


(b)

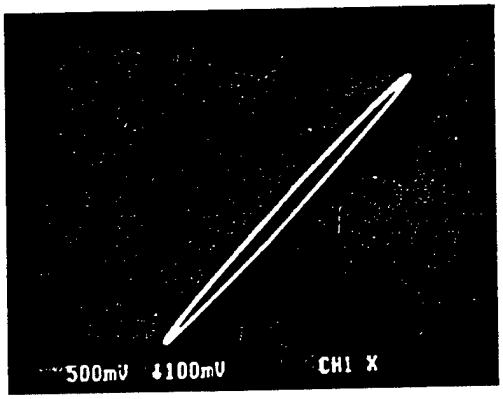


(c)

Fig. 9. (a) A low-power transformer driven by the outlet voltage 110 V, $f = 60$ Hz. (b) TC with a hysteresis of the two-port device shown in (a). (c) DP characteristic converted by *Realization II* from the TC in (b).

and the DP characteristics converted by *Realization II* from the TC's shown in Figs. 7(b) and 8(b) and Figs. 7(c) and 8(c), respectively. To validate the robustness of the converter presented in this paper, a low-power transformer is chosen as a two-port device, as shown in Fig. 9(a). Its TC with hysteresis and the resulting DP characteristic converted by *realization II* are shown in Fig. 9(b) and (c), respectively.

## V. Concluding Remarks

In this paper we propose an approach to synthesize prescribed DP characteristics of two-terminal, or one-port, devices from the transfer characteristics of two-port devices. A variety of the resulting DP characteristics experimentally measured validate the robustness of the method.

Using the *mutator* nonlinear network element reported in [7], an inductor with any prescribed $\phi$–$i$ characteristic, or a capacitor with any prescribed $q$–$v$ characteristic can be realized by connecting a nonlinear resistor with an appropriate $v$–$i$ characteristic across one port of the mutator, and the problem of realizing a nonlinear inductor, or capacitor, reduces to that of realizing a nonlinear resistor with an appropriate $v$–$i$ characteristic. Therefore, the approach proposed in this paper will benefit the synthesis not only of resistors, but also of inductors and capacitors with prescribed characteristics.

The proposed implementation of arbitrary one-ports, two-ports, and four-ports allows us to design hybrid analog–digital circuits, where the digital part is responsible for synthesizing the complex nonlinear part, whereas the analog part is responsible for synthesizing the linear part.[2] This results in a system which is faster than simulating the entire system in digital hardware, yet offers a degree of flexibility and complexity due to the digital hardware. Thus the system exploits the advantages of both analog and digital circuits.

[2] Or simple nonlinear parts which can be readily synthesized using available analog components.

## References

[1] L. O. Chua, *Introduction to Nonlinear Network Theory*. New York: McGraw-Hill, 1969.
[2] L. O. Chua, J. Yu, and Y. Yu, "Negative resistance devices," *Int. J. Circuit Theory Appl.*, vol. 11, no. 2, pp. 161–186, Apr. 1983.
[3] L. A. Chua and A.-C. Deng, "Negative resistance devices: Part II," *Int. J. Circuit Theory Appl.*, vol. 12, no. 4, pp. 337–373, Oct. 1984.
[4] L. O. Chua, J.-B. Yu, and Y.-Y. Yu, "Bipolar-MOSFET negative resistance devices," *IEEE Trans. Circuits Syst.*, vol. CAS-32, pp. 46–61, Jan. 1985.
[5] L. A. Chua and G.-Q. Zhong, "Negative resistance curve tracer," *IEEE Trans. Circuits Syst.*, vol. CAS-32, pp. 569–582, June 1985.
[6] E. Sanchez-Sinencio, J. Ramirez-Angulo, B. Lineares-Barranco, and A. Rodriguez-Vazquez, "Operational transconductance amplifier-based nonlinear function synthesis," *IEEE J. Solid-State Circuits*, vol. 24, pp. 1576–1586, Dec. 1989.
[7] L. O. Chua, "Synthesis of new nonlinear network elements," *Proc. IEEE*, vol. 56, pp. 1325–1340, Aug. 1968.

**Leon O. Chua** (S'60–M'62–SM'70–F'74), for biography, see p. 463 of the April 1998 issue of this TRANSACTIONS.

**Chai Wah Wu** (S'88–M'96), for photograph and biography, see p. 463 of the April 1998 issue of this TRANSACTIONS.

**Guo-Qun Zhong**, photograph and biography not available at the time of publication.

**Luis Franscisco Liu**, photograph and biography not available at the time of publication.

# The Role of Synchronization in Digital Communications Using Chaos—Part II: Chaotic Modulation and Chaotic Synchronization

Géza Kolumbán, *Senior Member, IEEE*, Michael Peter Kennedy, *Fellow, IEEE*, and Leon O. Chua, *Fellow, IEEE*

***Abstract*—In a digital communications system, data are transmitted from one location to another by mapping bit sequences to symbols, and symbols to sample functions of analog waveforms. The analog waveform passes through a bandlimited (possibly time-varying) analog channel, where the signal is distorted and noise is added. In a conventional system the analog sample functions sent through the channel are weighted sums of one or more sinusoids; in a chaotic communications system the sample functions are segments of chaotic waveforms. At the receiver, the symbol may be recovered by means of coherent detection, where all possible sample functions are known, or by noncoherent detection, where one or more characteristics of the sample functions are estimated. In a coherent receiver, synchronization is the most commonly used technique for recovering the sample functions from the received waveform. These sample functions are then used as reference signals for a correlator. Synchronization-based coherent receivers have advantages over noncoherent receivers in terms of noise performance, bandwidth efficiency (in narrow-band systems) and/or data rate (in chaotic systems). These advantages are lost if synchronization cannot be maintained, for example, under poor propagation conditions. In these circumstances, communication without synchronization may be preferable. In Part I, the theory and operation of conventional communications systems were surveyed and possible fields of application of chaotic communications were identified. In Part II, the theory of conventional telecommunications is extended to chaotic communications, chaotic modulation techniques and receiver configurations are surveyed, and chaotic synchronization schemes are described. In Part III, examples will be given of chaotic communications schemes with and without synchronization, and the performance of these schemes is evaluated in the context of noisy, bandlimited channels.**

***Index Terms*—Chaos, communication systems, digital communication, digital modulation, spread spectrum communication.**

## I. Introduction

RESEARCH into applications of chaos in communications has been motivated by the observation that chaotic systems can be synchronized. The basic idea is that information can be conveyed to a remote receiver by means of a wideband chaotic signal. Since 1992, a number of chaotic synchronization and modulation schemes have been proposed, most of which have been developed using heuristic arguments, without reference to conventional communications measures [1].

The objectives of this work are threefold:

1) to provide a theoretical context in which the performance of modulation schemes based on chaotic synchronization can be evaluated;
2) to develop a unified framework for discussing and comparing conventional and chaotic communication systems;
3) to highlight the special problems that arise when chaotic basis functions are used.

In Part I of this three-part paper [2], we described the major components of a digital communications system, identified the role of synchronization in coherent receivers, and motivated the use of chaotic rather than periodic basis functions.

In Section II of this part, we describe two digital chaotic modulation schemes—chaos shift keying (CSK) and differential chaos shift keying (DCSK)—and identify appropriate coherent, noncoherent, and differentially coherent receiver architectures.

The theoretical performance of chaotic communications receivers with and without synchronization is examined in Section III. We conclude that the synchronization-based recovery of chaotic basis functions from noisy received sample functions offers a potential advantage over noncoherent detection in terms of noise performance and data rate, but only if synchronization can be maintained. Under poor propagation conditions, where synchronization cannot be maintained, the advantages of coherent detection are lost. In such circumstances, a noncoherent receiver offers a more robust and less complex solution.

In Section IV, we consider the state of the art in synchronization of chaotic systems in the context of digital communications and highlight the weaknesses of current chaotic synchronization techniques.

In Part III of the paper [34], the performance of representative coherent and noncoherent chaotic communication schemes is evaluated in the context of a noisy and bandlimited channel.

## II. Survey of Chaotic Modulation and Demodulation Techniques

The basic idea of digital communication using a chaotic carrier is that the bits (binary modulation) or symbols ($M$-ary modulation) are mapped to sample functions of chaotic

Manuscript received August 1997. This work has been supported in part by the National Scientific Research Foundation of Hungary (OTKA) under Grant T-020522, by the Information Technologies RTD Programme of the European Commission (Esprit Project 21103 INSPECT), and by the Office of Naval Research under Grant N00014-96-1-0753.

G. Kolumbán is with the Department of Measurement and Information Systems, Technical University of Budapest, H-1521 Budapest, Hungary.

M. P. Kennedy is with the Department of Electronic and Electrical Engineering, University College Dublin, Dublin 4, Ireland.

L. O. Chua is with the Department of Electrical Engineering and Computer Sciences, University of California at Berkeley, Berkeley, CA 94720, USA.

Publisher Item Identifier S 1057-7122(98)07718-6.

1057–7122/98$10.00 © 1998 IEEE

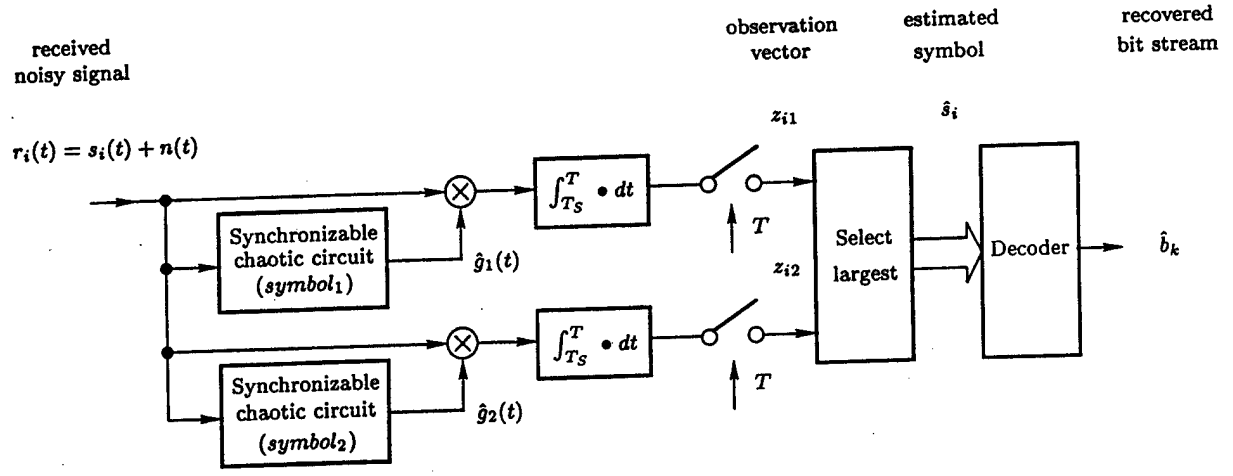


Fig. 1. Block diagram of coherent correlation CSK receiver for $M = 2$.

signals emanating from one or more chaotic attractors. In order to avoid periodicity, the symbols are mapped to the actual nonperiodic outputs of chaotic circuits and not to parameters of certain known sample functions.

The principal difference between a chaotic carrier and a conventional periodic carrier is that the sample function for a given symbol is nonperiodic and is different from one symbol interval to the next. Thus, the transmitted waveform is never periodic, even if the same symbol is transmitted repeatedly.

As in the case of conventional digital communications, we consider four categories of modulation techniques:

1) coherent correlation receiver with chaotic synchronization;
2) coherent matched filter receiver;
3) noncoherent detection techniques;
4) differentially coherent reception.

### A. Coherent Correlation Receiver with Chaotic Synchronization

*1) Coherent Detection of CSK: Chaos shift keying* (CSK) [3], [4] is a digital modulation scheme where each symbol is mapped to a different chaotic attractor. The number of attractors is equal to the size of the signal set in this case. The attractors may be produced by the same dynamical system for different values of a bifurcation parameter or by completely different dynamical systems.

Note that the information to be transmitted is carried not by the shape of the sample function but by the attractor which produces the sample function. The objective of the demodulator is to decide, on the basis of a received noisy and distorted sample function, which attractor is most likely to have produced this waveform.

Using the notation introduced in Part I [2], assume that each attractor produces a basis function $g_j(t)$ and that the elements of the signal set

$$s_i(t) = \sum_{j=1}^{N} s_{ij} g_j(t), \qquad j = 1, 2, \cdots, N$$

are given by $s_i(t) = g_i(t)$ for all $i$.

In terms of the components of the signal vector, this corresponds to the case $s_{ij} = 0$ if $i \neq j$ and $s_{ij} = 1$ if $i = j$. Furthermore, assume that the autocorrelation of each $g_j(t)$ with itself in each symbol interval $T$ is larger than the cross correlation with any of the other basis functions. In this case, a correlation receiver may be used to identify the attractor which is most likely to have produced the received signal [2].

As in the case of a conventional correlation receiver based on synchronization, a local synchronized copy of each basis function $g_j(t)$ *has to be produced* in the receiver using appropriate synchronization circuitry[1]. In the case of chaotic basis functions, this topic is called *chaotic synchronization*. We will deal with chaotic synchronization in more detail in Section IV, but first let us consider the conceptual process.

Synchronizable counterparts of the circuits which produce the basis functions $g_j(t)$ in the transmitter are used to recover the basis functions in a coherent correlation receiver, as shown in Fig. 1. Here, the received signal $r_i(t)$ tries simultaneously to synchronize all of the "synchronizable chaotic circuits" in the receiver.

For example, assume that the signal $s_i(t) = g_1(t)$ is transmitted. After a synchronization time $T_S$, which is analogous to the pull-in time in a phase-locked loop (PLL), the output $\hat{g}_1(t)$ converges to $g_1(t)$. By contrast, $\hat{g}_2(t)$ fails to synchronize with $g_1(t)$. The decision as to which symbol was transmitted is made on the basis of the "goodness" of synchronization. In the ideal case, $\hat{g}_1(t)$ is more strongly correlated with $r_i(t)$ than $\hat{g}_2(t)$ during the interval $[T_S, T]$. Hence, $z_{i1} > z_{i2}$ and the decision circuit decides that symbol 1 was transmitted.

In any realistic situation, the received signal is always corrupted by noise $n(t)$. Even in the case of perfect synchronization, the instantaneous value of the received signal may differ considerably from the recovered chaotic signal. This is why correlators *must* be used for the detection, i.e., to determine the "goodness" of synchronization. Because of the time-averaging involved in correlation, the use of correlators also tolerates loss of synchronization for short periods of time.

In any practical communications system, not only an isolated single symbol, but a sequence of symbols, has to be transmitted.

[1]Recall that the weights $s_{ij}$ are recovered by computing $\hat{s}_{ij} = \int_0^T r_i(t) g_j(t)\, dt$ for $j = 1, 2, \cdots, N$ [2].

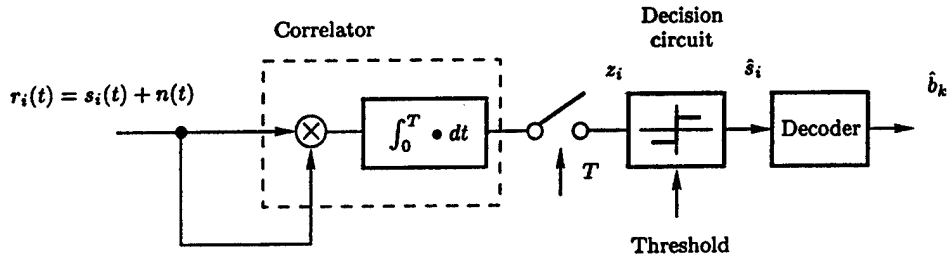


Fig. 2. Block diagram of a noncoherent receiver for COOK or CSK.

Even in a linear channel, interference among the successive symbols may appear, i.e., *intersymbol interference* (ISI) [5] may occur. One source of ISI can be the integrator used in the correlator. If the initial value of the integrator is reset to zero at the beginning of each observation period, by means of an *integrate-and-dump* circuit [5], for example, then this kind of ISI can be avoided.

We assume in the following that the timing information is available in the receiver. The initial value of the integrator(s) is reset to zero at the beginning of every observation period and the observation vector is generated at the end of each symbol interval. In Figs. 1–4, the start and end of each observation period are indicated by the limits of integration and the decision time instants are represented schematically by sampling switches.

*2) Data Rate of a Coherent Correlation Receiver with Chaotic Synchronization for CSK:* The disadvantage of a coherent correlation CSK receiver is that synchronization is lost and recovered every time the transmitted symbol is changed [4]. The symbol duration is therefore equal to the sum of the synchronization time $T_S$ *plus* the estimation time of the observation vector. The synchronization time puts an upper bound on the symbol rate and thus the data rate.

To maximize the data rate in conventional digital systems, synchronization is always maintained. If the transmitted signal does not contain a signal that can be used as a reference for synchronization (in the case of suppressed carrier modulation schemes, for example) then a nonlinear operation is used to regenerate the reference signal in the receiver [5], [6]. This idea could also be exploited in chaotic communications if a synchronization technique could be found which was sufficiently insensitive to some parameter of the chaotic basis functions. In that case, a selected parameter could be varied according to the modulation and synchronization could be maintained continuously. The symbols to be transmitted would then be mapped to the selected parameter of the chaotic sample function and only one attractor would be necessary; this is analogous to a conventional modulation technique where the attractor is a periodic trajectory whose amplitude, frequency, or phase might be controlled by the modulation.

If synchronization of a chaotic circuit could be maintained in the presence of other chaotic signals, then it would be possible to increase the size of the signal set by generating $s_i(t)$ as a weighted sum of basis functions with more than one nonzero weight, as discussed in Part I of this paper (see [2, Section III-B.1]). To our knowledge, none of the chaotic synchronization techniques which exist in the literature is sufficiently robust to permit augmentation of the signal set in this way [7].

### B. Coherent Matched Filter Receiver for CSK

Matched filters can be used only if the waveforms corresponding to each symbol are known in advance and preprogrammed as the impulse responses of filters. In the case of CSK modulation, the symbols are mapped to chaotic attractors and a different sample function is generated each time a symbol is transmitted[2]. Therefore, coherent matched filter receivers simply cannot be used in chaotic communications.

### C. Noncoherent Detection

*1) Noncoherent Detection of COOK: Chaotic on-off-keying* (COOK) offers the simplest solution to chaotic communication. In COOK, the chaotic signal is multiplied directly by the bit sequence to be transmitted, i.e. radiation of a chaotic signal is disabled for bit 0 and enabled for bit 1 [8].

The COOK receiver shown in Fig. 2 estimates the signal energy per bit $E_b$ carried by the transmitted signal and performs the decision by means of a level comparator.

*2) Noncoherent Detection of CSK:* Signals generated by different chaotic attractors generally have different statistical attributes, such as the mean of the absolute value, variance, and standard deviation. This observation suggests that CSK signals can also be demodulated by noncoherent receivers [9].

Let us consider chaotic sample functions generated by the same attractor but originating from different initial conditions as a *chaotic stochastic process* (for a more precise definition, see Part III of this paper). Let the binary information to be transmitted be mapped to the variances of chaotic stochastic processes. Chaotic stochastic processes with different variances may be obtained by using two different chaotic attractors or by multiplying the sample functions of one attractor by distinct weights.

The block diagram of a noncoherent CSK receiver is shown in Fig. 2. For the sake of simplicity, let us assume that the mean of the received signal is zero. In this case, the receiver can estimate the variance of the received signal using a correlator. The decision is made by a simple level comparator. If a parameter of the chaotic attractor other than its variance is to be evaluated in the demodulation process, the appropriate operation may be substituted for the multiplier in Fig. 2.

Not just statistical attributes but any robust characteristic of a chaotic signal may be exploited in order to implement a noncoherent CSK communication system. For example, in [10], the basis functions are two chaotic signals which have different average frequencies; these may be distinguished at the

[2]Because a chaotic waveform is not periodic, each sample function of length $T$ is different.

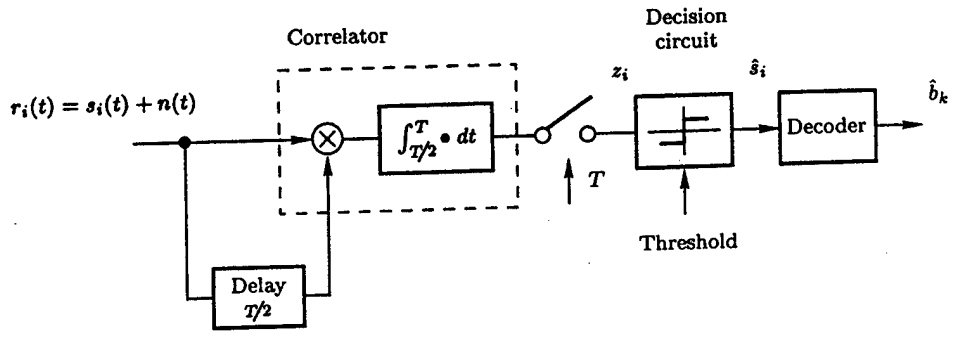


Fig. 3. Block diagram of a DCSK receiver.

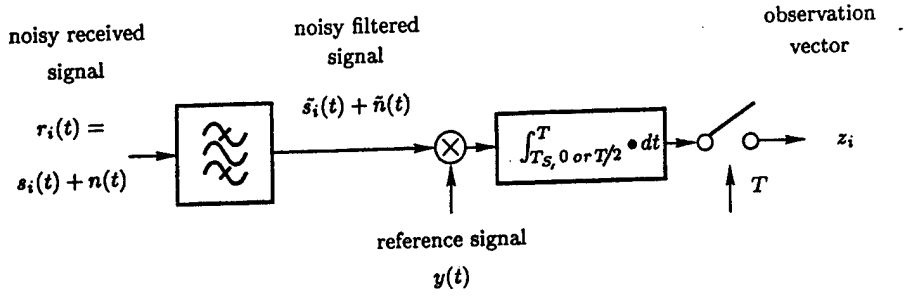


Fig. 4. General block diagram of a CSK receiver.

receiver by measuring the average value of the zero-crossing rate of the received signal.

Other modulation techniques have also been proposed. In [11], the autocorrelation function of a chaotic signal is modified according to the symbols to be transmitted. By measuring the autocorrelation function of the received signal, the transmitted symbol can be identified.

### D. Differentially Coherent Reception

One or more chaotic basis functions $g_j(t)$ must be recovered in order to implement a coherent correlation receiver. When propagation conditions are so poor that it is impossible to recover basis functions by chaotic synchronization, a differential modulation scheme (*differential chaos shift keying* (DCSK) [9]) and a differentially coherent correlation receiver may be used [12].

In DCSK, every symbol to be transmitted is represented by two sample functions. The first sample function serves as a *reference* while the second one carries the information. In the case of binary transmission, bit 1 is sent by transmitting a reference signal provided by the chaos generator twice in succession. For bit 0, the reference chaotic signal is transmitted, followed by an inverted copy of the same signal. The two sample functions are correlated in the receiver and the decision is made by a level comparator, as shown in Fig. 3[3].

## III. Theoretical Comparison of Chaotic Modulation Techniques

Noise performance is the most important characteristic of a modulation scheme and receiver. Since all of the chaotic modulation techniques discussed in this paper can be considered as variants of CSK modulation, we consider only the noise performance of CSK.

In the previous section, we saw that CSK transmissions can be demodulated in one of three ways:

1) a coherent correlation receiver, where the elements of the signal set are recovered by synchronization;
2) a noncoherent receiver (in this section, we assume that the demodulation is performed by estimating the *variance* of the received chaotic signal or the COOK technique is used); or
3) a differentially coherent receiver.

Note that similar circuitry is used to estimate the observation vector in Figs. 1–3. Each receiver configuration contains one or more correlators; the difference between the schemes is in the manner in which the reference signals are generated. Therefore, we will analyze all three receiver configurations using the common block diagram shown in Fig. 4. Because the channel (selection) filter plays an important role in the DCSK receiver, it is also included explicitly in this figure.

For simplicity, let the elements $s_i(t)$ of signal set be the basis functions $g_j(t)$. We denote by $y(t)$ and $\tilde{s}_i(t) + \tilde{n}(t)$ respectively, the reference signal and the filtered version of the noisy received signal which emerges from the channel filter. The decision is performed based on the observation vector. The probability of wrong decisions, and therefore the BER, depends on the mean value and variance of the observation vector [6].

### A. Coherent Correlation Receiver with Chaotic Synchronization

In a coherent correlation receiver, the elements of the signal set are recovered by synchronization from the noisy filtered received signal. The chaotic synchronization techniques which

[3]Note that a DCSK receiver differs fundamentally from a conventional DPSK receiver [6]. Because a reference signal is transmitted in *every* symbol period, the data rate is halved and the required energy per bit is doubled in DCSK compared to DPSK. However, the error propagation problem associated with differential encoding does not arise.

have been published to date are sensitive to both noise and distortion in the channel (see Section IV). In particular, the signal $s_i(t)$ cannot be recovered exactly when $r_i(t) \neq s_i(t)$.

Therefore, let $\hat{s}_i(t)$ denote the recovered chaotic signal, where $\hat{s}_i(t) \approx \tilde{s}_i(t)$ if $t > T_S$[4]. This corresponds to our reference signal $y(t)$ in Fig. 4.

As explained in Section II-A.1, we assume that synchronization is lost and recovered at the beginning of every new symbol. Since the synchronization transient cannot be used to transmit information, the observation vector must be estimated during the interval $T_S < t \leq T$. Let $s_i(t)$ and $s_j(t)$ denote the elements of the signal set for binary CSK modulation. Then the elements of the observation vector are given by

$$z_{i1} = \int_{T_S}^{T} [\tilde{s}_i(t) + \tilde{n}(t)]\hat{s}_i(t)\, dt = \int_{T_S}^{T} \tilde{s}_i(t)\hat{s}_i(t)\, dt + \int_{T_S}^{T} \tilde{n}(t)\hat{s}_i(t)\, dt \quad (1)$$

$$z_{i2} = \int_{T_S}^{T} \tilde{s}_i(t)\hat{s}_j(t)\, dt + \int_{T_S}^{T} \tilde{n}(t)\hat{s}_j(t)\, dt \quad (2)$$

where $\hat{s}_i(t)$ and $\hat{s}_j(t)$ correspond to $\hat{g}_1(t)$ and $\hat{g}_2(t)$, respectively, in Fig. 1.

Note that $z_{i1}$ and $z_{i2}$ are *random variables*, whose mean value depends on the bit energy of the chaotic signal and the "goodness" of synchronization [see the first term in (1)].

The variance of the estimation is determined by the chaotic signal[5] and the filtered noise. Note that the noise has no *direct* influence on the variance of estimation. As shown by the second terms of (1) and (2), the variance of estimation is influenced only by the cross correlation of noise and the recovered chaotic signal.

For a given chaotic signal and bandwidth of the channel filter, the variance of estimation is inversely proportional to the observation time $(T - T_S)$. The mean value of estimation does not depend on the noise; thus, the receiver is an *unbiased estimator*. In particular, this means that the threshold level required by the level comparator does not depend on the channel noise.

As in the case of a conventional receiver and periodic basis functions, the noise performance of a coherent correlation receiver using chaotic basis functions is theoretically excellent. However, the BER also depends on the "goodness" of synchronization [equivalently, the closeness of the reference signal $y(t)$ to the desired chaotic basis function $g_j(t)$]. Any synchronization error, especially loss of synchronization, results in a large degradation in the noise performance of a correlation receiver.

Loss of synchronization causes the bit error rate (BER) to rise significantly. Recall that a digital communications link is automatically severed at the system level if the BER increases above a predetermined threshold. Therefore, synchronization-based receivers are not suitable for noisy propagation environments.

Let us consider next a noncoherent receiver.

### B. Noncoherent Correlation Receiver

Here, we assume that decisions in the noncoherent receiver are made by estimating the variance of the received signal. The reference signal $y(t)$ is equal to the noisy filtered signal $\tilde{s}_i(t) + \tilde{n}(t)$ in this case, and the observation variable can be expressed as

$$z_i = \int_0^T [\tilde{s}_i(t) + \tilde{n}(t)]^2\, dt = \int_0^T \tilde{s}_i^2(t)\, dt + 2\int_0^T \tilde{s}_i(t)\tilde{n}(t)\, dt + \int_0^T \tilde{n}^2(t)\, dt \quad (3)$$

where a new term, which depends only on the filtered noise, appears.

The mean value of estimation depends on both the bit energy of the chaotic signal and the filtered noise (see the first and third terms in (3), respectively). In this case the receiver is a *biased estimator*; the threshold level of the comparator used as a decision circuit now depends on the noise level. In addition, the variance of estimation becomes much greater than in the previous case due to the third term in (3).

Imagine that a histogram of the observed values of $z_i$ is plotted for a large number of transmitted symbols. Because binary modulation is used, the histogram will have two distinct peaks. For a given noise level, channel filter and chaotic signal, the best noise performance can be achieved if the distance between the two peaks is a maximum. The separation of the peaks is determined by the distance between the elements of the signal set. For the case of noncoherent CSK, COOK ensures the maximum distance. In this case, the distance between the elements of the signal set is equal to twice the mean value of the energy per bit.

Is there a way to produce an unbiased estimator with antipodal signals [12] which ensures the maximum distance between the elements of a binary signal set? The answer is yes; DCSK offers a potential solution.

### C. Differentially Coherent Reception

In a DCSK receiver, the reference signal $y(t)$ is a delayed version of the filtered noisy signal. Note that different sample functions of filtered noise corrupt the inputs of the correlator. If the time-varying channel varies slowly compared to the symbol rate, then the observable element is

$$z_i = \int_{T/2}^{T} [\tilde{s}_i(t) + \tilde{n}_1(t)][\pm\tilde{s}_i(t) + \tilde{n}(t - T/2)]\, dt = \pm\int_{T/2}^{T} \tilde{s}_i^2(t)\, dt \pm \int_{T/2}^{T} \tilde{s}_i(t)\tilde{n}(t)\, dt + \int_{T/2}^{T} \tilde{s}_i(t)\tilde{n}(t - T/2)\, dt + \int_{T/2}^{T} \tilde{n}(t)\tilde{n}(t - T/2)\, dt \quad (4)$$

[4] Recall that $T_S$ is the synchronization time.

[5] The parameter required for demodulation must be *estimated* from sample functions of finite length. In the case of periodic sample functions, this estimation has zero variance if the observation interval is an integral number of periods. When chaotic basis functions are used, the estimation has a nonzero variance which results from the nonperiodicity of the underlying signals; this increases the overall variance of the observation vector [13]. This problem will be discussed in detail in Part III.

where the sign of the first and second terms depends on the binary modulation. The signals $\tilde{n}_1(t)$ and $\tilde{n}(t - T/2)$ denote the sample functions of filtered noise that corrupt the reference and information-bearing parts of the received signal, respectively.

By proper design of the channel filter[6], the two sample functions of the noise become uncorrelated and (4) can be simplified as follows

$$z_i = \pm \int_{T/2}^{T} \tilde{s}_i^2(t)\, dt \pm \int_{T/2}^{T} \tilde{s}_i(t)\tilde{n}(t)\, dt + \int_{T/2}^{T} \tilde{s}_i(t)\tilde{n}(t - T/2)\, dt. \quad (5)$$

Note that the receiver is an *unbiased estimator* in this case. This means that the threshold level of the decision circuit is zero and is independent of the noise level.

The mean value of the estimation depends on the bit energy of the chaotic signal; the variance of estimation is determined by the chaotic signal and the filtered noise. The application of antipodal signals ensures the maximum distance between the elements of the signal set for DCSK [see the first term in (5)]. As in the case of a coherent correlation receiver with synchronization, the noise has no direct influence on the variance of estimation. However, in contrast with (1), two cross-correlation terms appear in (5). For correct operation, we need to ensure that the first term, corresponding to the bit energy, dominates the two cross-correlation terms contributed by the noise.

### D. Coherent CSK versus DCSK

The main advantage of DCSK over CSK is that both the reference and information-bearing components of the transmitted signal pass through the *same* channel so they undergo the same transformation. This transformation does not change the correlation that carries the information, provided that the time-varying channel remains almost constant for the symbol duration.

Because there is no need for synchronization, the DCSK technique can be used even under poor propagation conditions. However, the symbol rate is halved compared with a synchronization-based receiver in which synchronization is maintained.

Recall, however, that the synchronization time $T_S$ of a coherent receiver is wasted—no information can be carried during this interval. If each symbol must be synchronized independently and the synchronization time $T_S$ is comparable to the correlation time $(T - T_S)$, then a DCSK system can in principle operate at the *same symbol rate* as a synchronization-based coherent receiver, with the added advantage of superior performance under poor propagation conditions.

Thus, synchronization-based recovery of chaotic basis functions from a noisy received signal offers superior performance to DCSK in terms of data rate only if synchronization can be maintained. This advantage is lost if the modulation technique requires the loss and recovery of synchronization at the beginning of every new symbol or if poor propagation conditions make it impossible to maintain synchronization.

[6]Let the channel filter be an ideal bandpass filter with bandwidth $BW_{RF}$. The cross-correlation of $\tilde{n}_1(t)$ and $\tilde{n}(t - T/2)$ becomes zero if $BW_{RF}T = n, n = 1, 2, 3, \cdots$ [6].

## IV. Synchronization in Chaotic Communications Systems

As explained in Part I of this paper, the primary use of synchronization in digital communications systems is for recovering basis function(s) in coherent correlation receivers, as illustrated for binary CSK in Fig. 1. In a real system, the signal which is received differs from that which was transmitted. At the very minimum, the signal is corrupted by additive noise as it passes through the channel; usually, it is also bandpass filtered. The transformation may be more severe if the channel is nonlinear, time-varying, or suffers from multipath effects.

Thus, the objective of the synchronization process is to recover basis functions from the noisy received signal in order to maximize the probability of correctly identifying the transmitted symbols. In this section, we examine chaotic synchronization techniques from this perspective.

### A. Chaotic Synchronization Schemes

Chaotic steady-state solutions are characterized by sensitive dependence on initial conditions: trajectories of two identical autonomous continuous-time dynamical systems started from slightly different initial conditions quickly become uncorrelated [14]. Surprisingly perhaps, it is nevertheless possible to synchronize these systems in the sense that a trajectory of one asymptotically approaches that of the other.

Several notions of synchronization have been proposed for chaotic systems, the strongest and most widely-used of which is *identical synchronization*, where the state of the receiver system converges asymptotically to that of the transmitter [14]. More recently, two weaker notions of synchronization, called *generalized synchronization* [15], [16] and *phase synchronization* [17], [18] have been introduced.

*1) Identical Synchronization:* Two continuous-time dynamical systems

$$\dot{\boldsymbol{x}} = \boldsymbol{f}(\boldsymbol{x}) \quad (6)$$

and

$$\dot{\boldsymbol{x}}' = \boldsymbol{f}'(\boldsymbol{x}') \quad (7)$$

are said to *synchronize identically* if

$$\lim_{t\to\infty} \|\boldsymbol{x}'(t) - \boldsymbol{x}(t)\| = 0$$

for any combination of initial states $\boldsymbol{x}(0)$ and $\boldsymbol{x}'(0)$.

From a communications perspective, we may think of system (6) as the transmitter and (7) as the receiver. The signal $s_i(t)$ which is transmitted is a linear combination of basis functions $g_j(t)$. For simplicity, we consider the case where only one basis function $g(t)$ is used and we assume that $s_i(t) \equiv g(t)$. At the receiver, we must recover the scalar basis function $g(t) = h(\boldsymbol{x}(t))$ which has been derived from the state of the transmitter (6). By synchronizing the state of the receiver

identically with that of the transmitter, and applying the same readout function $h(\cdot)$, the basis function can be recovered. In particular, if $\boldsymbol{x}'(t)$ can be made to converge to $\boldsymbol{x}(t)$ then the estimate $\hat{g}(t) = h(\boldsymbol{x}'(t))$ will converge to $g(t)$.

*2) Generalized Synchronization:* Systems (6) and (7) are said to exhibit *generalized synchronization* if there exists a transformation $\boldsymbol{M}$ such that

$$\lim_{t\to\infty} \|\boldsymbol{x}'(t) - \boldsymbol{M}(\boldsymbol{x}(t))\| = 0$$

where the properties of the transformation are independent of the initial conditions $\boldsymbol{x}(0)$ and $\boldsymbol{x}'(0)$.

Generalized synchronization occurs, for example, in unidirectionally-coupled chaotic systems where the driven system (the "synchronizable chaotic circuit" block in Fig. 1) is asymptotically stable [21].

If the transformation $\boldsymbol{M}$ is invertible, then

$$\hat{g}(t) = h(\boldsymbol{M}^{-1}(\boldsymbol{x}'(t)))$$

approaches $g(t)$. However, the transformation $\boldsymbol{M}$ is not necessarily invertible, so recovering the state $\boldsymbol{x}'(t)$ in a coherent receiver does not necessarily permit one to recover the required basis function.

*3) Phase Synchronization:* Phase synchronization of two coupled systems occurs if the difference $|\phi'(t) - \phi(t)|$ between the "phases" of the two systems is bounded by a constant [19], where the "phase" $\phi(t)$ is some suitably chosen monotonically increasing function of time. For example, in the case of a spiral Chua attractor [22], the angle of rotation about the unstable equilibrium point in a two-dimensional projection of the attractor would be a suitable choice.

In this work, we are concerned with recovering basis functions *exactly*, so we focus exclusively on *identical synchronization*. Since we are dealing with one-way communication between a transmitter (the drive system) and a receiver (the response system), we consider only unidirectional coupling between two systems. This is called a "drive-response" or "master-slave" configuration. In the following subsections, we present two classical approaches to identical drive-response synchronization of unidirectionally-coupled systems: Pecora-Carroll synchronization and error-feedback synchronization. In the language of control theory, Pecora-Carroll synchronization corresponds to open-loop state estimation, and error-feedback synchronization corresponds to asymptotic state estimation.

### *B. Pecora-Carroll Synchronization*

In the drive-response synchronization scheme proposed by Pecora and Carroll [23], a chaotic dynamical system

$$\dot{\boldsymbol{x}} = \boldsymbol{f}(\boldsymbol{x}) \tag{8}$$

with scalar output $g(t) = h(\boldsymbol{x})$, as shown in Fig. 5, is decomposed into two subsystems with states $\boldsymbol{x}_1$ and $\boldsymbol{x}_2$, respectively:

$$\dot{\boldsymbol{x}}_1 = \boldsymbol{f}_1(\boldsymbol{x}_1, \boldsymbol{x}_2) \tag{9}$$

$$\dot{\boldsymbol{x}}_2 = \boldsymbol{f}_2(\boldsymbol{x}_2, g(t)) \tag{10}$$

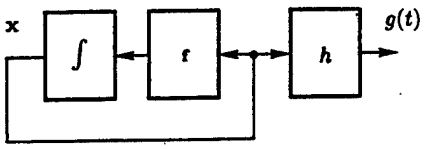


Fig. 5. Block diagram of drive system described by (8).

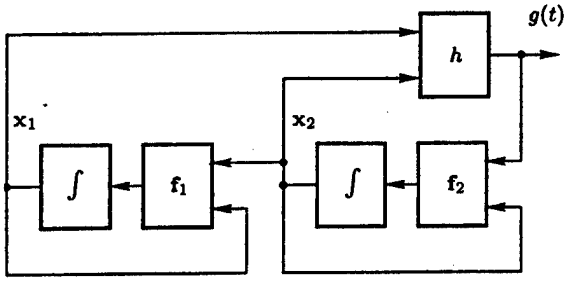


Fig. 6. Pecora-Carroll decomposition of (8) into two subsystems described by (9) and (10).

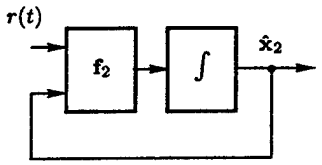


Fig. 7. Pecora-Carroll drive-response synchronization. The response system is a copy of the second subsystem in the drive system shown in Fig. 6.

where $\boldsymbol{x} = (\boldsymbol{x}_1, \boldsymbol{x}_2)$, and

$$g(t) = h(\boldsymbol{x}_1(t), \boldsymbol{x}_2(t))$$

is the scalar output signal, as before; this is illustrated in Fig. 6.

The system is partitioned in such a way that the conditional Lyapunov exponents[7] (CLE's) [23] of the second subsystem (10) are negative.

Qualitatively, the CLE's characterize the stability of the second subsystem (10) when driven by $g(t)$. If all CLE's are negative, the trajectory $\boldsymbol{x}_2(t)$ is asymptotically stable [23]. This means that the states of two or more copies of the second subsystem will synchronize identically when driven by the *same input* $g(t)$. This is the basis of Pecora-Carroll drive-response synchronization.

In particular, consider "Subsystem $\hat{2}$" in Fig. 7. This system is described by

$$\dot{\hat{\boldsymbol{x}}}_2 = \boldsymbol{f}_2(\hat{\boldsymbol{x}}_2, r(t)). \tag{11}$$

If the CLE's of this subsystem (called the "response system") are all negative and $\hat{\boldsymbol{x}}_2(0)$ is sufficiently close to $\boldsymbol{x}_2(0)$,

[7]Lyapunov exponents (LE's) [24] quantify the average exponential rate of separation of trajectories in a dynamical system under steady-state conditions. If one or more LE's is positive, then there is a "direction" in the system along which trajectories are stretched apart exponentially. In this case, the system is said to be chaotic. Conditional Lyapunov exponents (CLE's) are a measure of the average local exponential rate of separation of trajectories in a dynamical system along a reference trajectory which is defined by a prescribed input.

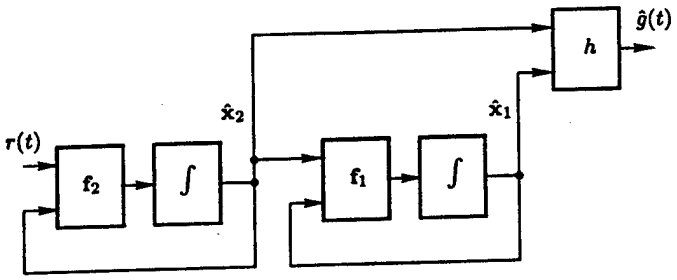


Fig. 8. Basis function recovery using cascaded Pecora-Carroll drive-response synchronization.

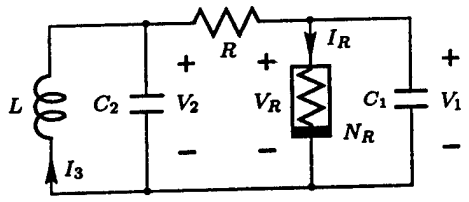


Fig. 9. Chua's circuit consists of a linear inductor $L$, two linear capacitors $(C_2, C_1)$, a linear resistor $R$, and a voltage-controlled nonlinear resistor $N_R$.

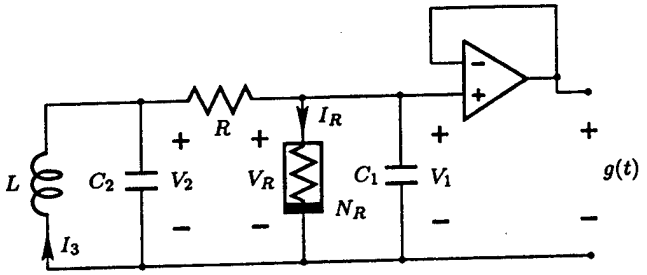


Fig. 10. Drive system using Chua's circuit to produce chaotic basis function $g(t)$.

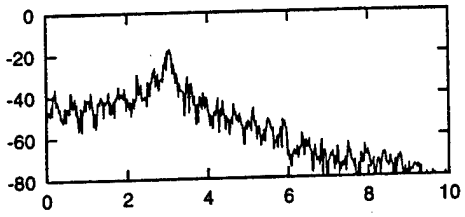


Fig. 11. Power spectrum of chaotic basis function $g(t)$ from Chua's circuit. Horizontal axis: $f$ (kHz); vertical axis $P(f)$ (dB).

and $r(t) = g(t)$, then the state $\hat{\boldsymbol{x}}_2$ of the response system converges asymptotically to $\boldsymbol{x}_2$, i.e.

$$\lim_{t\to\infty} \|\hat{\boldsymbol{x}}_2(t) - \boldsymbol{x}_2(t)\| = 0.$$

In terms of a communications system, the drive system (8) produces a chaotic basis function $g(t)$ which we assume, for simplicity, is transmitted directly through the channel and received, noisy and distorted, as $r(t)$.

Recall that the objective of synchronization in a coherent receiver is to estimate $g(t)$, given $r(t) \neq g(t)$. Therefore the response system must play the role of basis function recovery. It is not sufficient to recover $\boldsymbol{x}_2$; we need to recover both $\boldsymbol{x}_1$ and $\boldsymbol{x}_2$. This can be accomplished using cascaded drive-response synchronization. A second subsystem is added which is driven by the first, as shown in Fig. 8. Here,

$$\dot{\hat{\boldsymbol{x}}}_2 = \boldsymbol{f}_2(\hat{\boldsymbol{x}}_2, r(t)) \tag{12}$$

$$\dot{\hat{\boldsymbol{x}}}_1 = \boldsymbol{f}_1(\hat{\boldsymbol{x}}_1, \hat{\boldsymbol{x}}_2). \tag{13}$$

If the CLE's of (12) are all negative, and $\hat{\boldsymbol{x}}_2(0)$ is sufficiently close to $\boldsymbol{x}_2(0)$, and $r(t) = g(t)$, then $\hat{\boldsymbol{x}}_2(t)$ converges asymptotically to $\boldsymbol{x}_2(t)$. If, in addition, the CLE's of (13) are negative, then $\hat{\boldsymbol{x}}_1$ converges asymptotically to $\boldsymbol{x}_1$, i.e.

$$\lim_{t\to\infty} \|\hat{\boldsymbol{x}}_1(t) - \boldsymbol{x}_1(t)\| = 0,$$

and the output $\hat{g}(t) = h(\hat{\boldsymbol{x}}_1(t), \hat{\boldsymbol{x}}_2(t))$ converges asymptotically to $g(t)$. In this way, a basis function $g(t)$ may in principle be recovered from the received signal $r(t)$.

*1) Example: Pecora-Carroll Synchronization in Chua's Circuit:* We illustrate basis function recovery using Pecora-Carroll cascaded drive response synchronization in Chua's circuit [25]. This widely-studied circuit, shown in Fig. 9, consists of a linear inductor, a linear resistor, two linear capacitors, and a single nonlinear resistor $N_R$.

The dynamical behavior of the circuit is described by three ordinary differential equations:

$$\dot{V}_1 = \frac{G}{C_1}(V_2 - V_1) - \frac{1}{C_1} f(V_1), \tag{14}$$

$$\dot{V}_2 = \frac{G}{C_2}(V_1 - V_2) + \frac{1}{C_2} I_3, \tag{15}$$

$$\dot{I}_3 = -\frac{1}{L} V_2 \tag{16}$$

where $G = 1/R$ and $f(V_R) = G_b V_R + \frac{1}{2}(G_a - G_b)(|V_R + E| - |V_R - E|)$ is the piecewise-linear driving-point characteristic of the nonlinear resistor $N_R$.

This system may be partitioned into two subsystems in a number of different ways. Since the subcircuit consisting of $R$, $L$, and $C_2$ [described by (15) and (16)] is passive, and therefore has negative CLE's, we choose this as "Subsystem 2." "Subsystem 1" is described by (14) and the drive signal $g(t)$ is $V_1(t)$.

When $L = 18$ mH, $C_1 = 10$ nF, $C_2 = 100$ nF, $R \approx 1800\ \Omega$, $G_a = -50/66$ mS, $G_b = -9/22$ mS, and $E = 1$ V, the circuit shown in Fig. 10 produces a chaotic basis function $g(t)$ whose power spectrum is shown in Fig. 11; this is our drive system.

The response system contains a cascaded drive-response configuration. The first section, denoted "Subsystem $\hat{2}$," and described by

$$\dot{\hat{V}}_2 = \frac{G}{C_2}(r(t) - \hat{V}_2) + \frac{1}{C_2}\hat{I}_3 \tag{17}$$

$$\dot{\hat{I}}_3 = -\frac{1}{L}\hat{V}_2 \tag{18}$$

is a copy of Subsystem 2. As shown in Fig. 12, this circuit is followed by a copy of subsystem 1, which we label "Subsystem $\hat{1}$:"

$$\dot{\hat{V}}_1 = \frac{G}{C_1}(\hat{V}_2 - \hat{V}_1) - \frac{1}{C_1} f(\hat{V}_1) \tag{19}$$

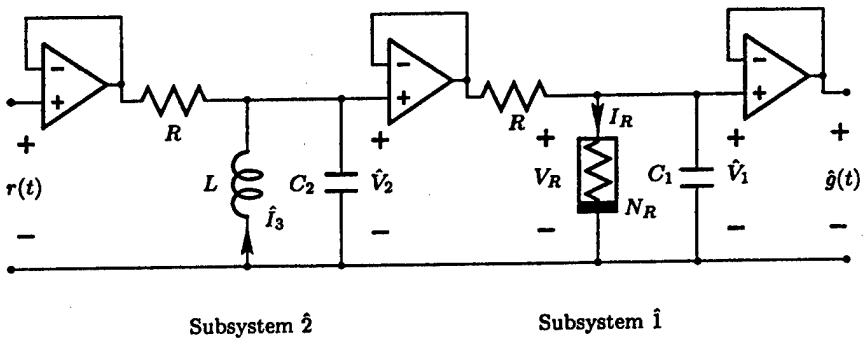


Fig. 12. Recovery of $g(t)$ from $r(t)$ using Chua's circuit in a Pecora-Carroll cascaded drive-response configuration.

If $r(t) \approx g(t)$, then $\hat{V}_2$ approaches $V_2$ asymptotically. If $\hat{V}_2 \approx V_2$ and, in addition, $\hat{V}_1(0)$ is sufficiently close to $V_1(0)$ and the CLE's of "Subsystem $\hat{1}$" are negative, then $\hat{V}_1$ approaches $V_1$ asymptotically and $\hat{g}(t) \approx g(t)$.

In this way, a basis function can be recovered from the received signal if $r(t) \approx g(t)$ and the parameters of the drive and response system are matched.

### C. Robustness of Pecora-Carroll Synchronization

In the discussion above, we have assumed that the parameters of the drive and response systems are identical, that a single basis function $g(t)$ is transmitted, that $r(t) \approx g(t)$, that the CLE's of the response subsystems are negative, and that the initial conditions of the systems are close; this rather extensive set of assumptions allows us to recover $g(t)$.

However, we pointed out in Part I of this paper that the minimum channel nonidealities which must be considered in a practical communications system are additive white Gaussian noise and linear bandpass filtering. Therefore, we must consider carefully the robustness of the modulation/demodulation scheme. How well can we recover $g(t)$ using synchronization from the noisy distorted version $r(t)$?

In every practical implementation of a telecommunications system, the transmitter and receiver circuits operate under different conditions, so it is necessary to consider the case of a mismatch between the parameters of the transmitter and receiver. The parameter mismatch also depends on temperature, aging, etc. The effect of parameter mismatch on the recovery of $g(t)$ has not been widely studied; further research is required in this area.

Pecora-Carroll drive-response synchronization is fundamentally an open-loop state estimation technique, the objective of which is to reconstruct the state $\boldsymbol{x}$ of the transmitter, given a noisy observation $r(t)$ of a basis function $g(t)$. Open-loop state estimators are sensitive to noise and parameter mismatch. Consequently, identical synchronization using the Pecora-Carroll technique is not robust, as we shall demonstrate by example in Part III of the paper.

CLE's are a local concept which characterize the behavior of a system close to a prescribed reference trajectory. If a driven system is nonlinear, then different inputs may drive the system through different regions of its state space and produce different CLE's. If a synchronization scheme relies on negative CLE's to recover $g(t)$, then the CLE's should be negative for all possible inputs under expected operating conditions.

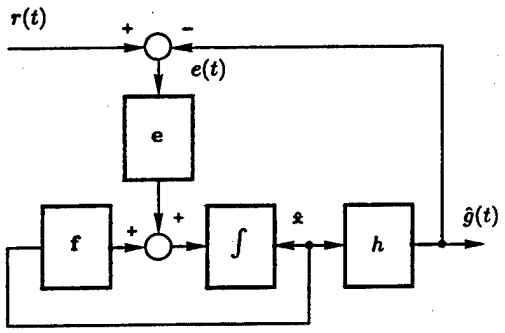


Fig. 13. Error-feedback synchronization.

One way to guarantee that the CLE's of the response subsystem are negative is to make that subsystem passive, as we did in our Chua's circuit example above. In this case, generalized synchronization always occurs, even if the parameters of the drive and response subsystems are mismatched. In this sense, generalized synchronization is a robust phenomenon. However, *identical synchronization*, which is required for recovering chaotic basis functions, occurs only if the parameters are matched.

Here, we have discussed a continuous-time state estimator. Variations on this theme which estimate the state by means of Takens-type delay reconstructions [26] are also possible.

The performance of the receiver in a drive-response configuration may be improved significantly by adding feedback in the state estimator. This technique, which we discuss in the next section, is called error-feedback synchronization.

### D. Error-Feedback Synchronization

The goal of the "synchronizable chaotic circuit" block in a receiver (see Fig. 1) is to estimate the basis function $g(t)$, given a noisy observation $r(t)$ of the signal. Error-feedback synchronization is a technique whereby the instantaneous difference between the estimate $\hat{g}(t)$ and the received signal $r(t)$ produces a scalar error signal $e(t)$ which modifies the state of the receiver so as to minimize the error.

Assuming that the basis function $g(t)$ has been generated by the system shown in Fig. 5, then the corresponding error-feedback synchronizable system has the structure given in Fig. 13.

Here,

$$\dot{\hat{\boldsymbol{x}}} = \boldsymbol{f}(\hat{\boldsymbol{x}}) + \boldsymbol{e}(e(t)), \tag{20}$$

where $e(t) = r(t) - \hat{g}(t)$ and $\hat{g}(t) = h(\hat{\boldsymbol{x}})$, as before.

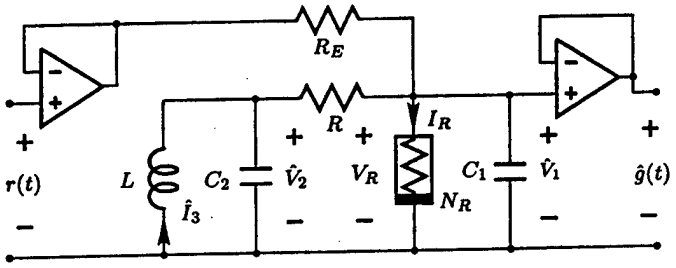


Fig. 14. Error-feedback synchronization in Chua's circuit.

With appropriate choices for $h(\cdot)$ and $\boldsymbol{e}(\cdot)$,

$$\lim_{t\to\infty} \|\hat{\boldsymbol{x}}(t) - \boldsymbol{x}(t)\| = 0.$$

If $\hat{\boldsymbol{x}}$, converges to $\boldsymbol{x}$, then $\hat{g}(t)$ converges to $g(t)$.

*1) Example: Error-Feedback Synchronization in Chua's Circuit:* Consider again the drive system formed by a Chua's circuit shown in Fig. 10 which produces a chaotic basis function $g(t)$. Error-feedback synchronization using linear feedback may be implemented by the circuit configuration given in Fig. 14.

Here,

$$\dot{\hat{V}}_1 = \frac{G}{C_1}(\hat{V}_2 - \hat{V}_1) - \frac{1}{C_1}F(\hat{V}_1) + \frac{G_E}{C_1}e \tag{21}$$

$$\dot{\hat{V}}_2 = \frac{G}{C_2}(r(t) - \hat{V}_2) + \frac{1}{C_2}\hat{I}_3 \tag{22}$$

$$\dot{\hat{I}}_3 = -\frac{1}{L}\hat{V}_2 \tag{23}$$

where $G_E = 1/R_E$ and $e(t) = r(t) - \hat{V}_1(t)$.

For a sufficiently small value of the coupling resistor $R_E$, $\hat{V}_1$ synchronizes with $V_1$ and $\hat{g}(t) \approx g(t)$.

### E. Proof of Synchronization

Synchronization in Pecora-Carroll drive-response systems may be established by numerically calculating the CLE's of the system. This approach is unsatisfactory in two respects: extensive simulation is required to calculate the CLE's. Moreover, the synchronization theorem is valid only for trajectories in the receiver which come sufficiently close to the reference trajectory in the transmitter.

Although one may justifiably argue that because the basis function $g(t)$ belongs to an attractor and that ergodicity on this attractor ensures that the trajectory $\hat{\boldsymbol{x}}_2(t)$ will eventually come close to $\boldsymbol{x}_2$ and "pull-in," there is no *a priori* upper bound on the pull-in time [4]. For a practical communications system, this is unacceptable. Worse still, *local* stability of the reference trajectory $\boldsymbol{x}_2(t)$ is not sufficient to guarantee that $\hat{\boldsymbol{x}}_2(t)$ will remain close to $\boldsymbol{x}_2(t)$ when random perturbations are added to the drive signal, as happens in a realistic channel model.

Recent work has highlighted the qualitative difference between "weak" and "strong" forms of chaotic synchronization in systems which have identical transversal Lyapunov exponents [27]. In the case of strong synchronization, additive noise produces a small synchronization error which is related to the noise level. Weak synchronization is characterized by intermittent desynchronization bursts of large amplitude when noise or parameter mismatches are present. Consequently, weak synchronization is not suitable for chaotic communications.

By contrast, several examples exist in the literature where *global* stability can be proven for the case $r(t) = g(t)$ when strong error-feedback synchronization is used [28]–[30]. This can be accomplished by using Lyapunov's direct method [31] to prove that the error system $(\hat{\boldsymbol{x}}(t) - \boldsymbol{x}(t))$ has a globally asymptotically stable equilibrium point at the origin.

In the case of error-feedback synchronization, design of the feedback and analysis of the stability of the error system reduces to a nonlinear observer design problem [32]. Synchronization performance in the presence of noise can also be improved by filtering the error signal $e(t)$ before applying it to the summing node in Fig. 13 [33].

## V. Concluding Remarks

Much of the recent research in chaotic communications has focused on synchronization. Our objectives in this work have been:

1) To provide a theoretical context in which the performance of modulation schemes based on chaotic synchronization can be evaluated,
2) To develop a unified framework for discussing and comparing conventional and chaotic communications systems, and
3) To highlight the special problems that arise when chaotic basis functions are used.

In Part I, we surveyed the theory and operation of the conventional digital communications systems and identified the minimum requirement for a realistic channel model. The use of chaotic carrier signals was motivated by highlighting the limitations of narrowband communications.

In Section II of Part II, we described the CSK, COOK, and DCSK modulation techniques.

We compared the theoretical performance of a coherent correlation receiver with synchronization, a noncoherent correlation receiver, and a DCSK correlation receiver in Section III.

We concluded that synchronization-based recovery of chaotic basis functions from noisy received sample functions offers potential advantages in terms of data rate and noise performance, but only if synchronization can be maintained. If synchronization cannot be maintained, then noncoherent detection represents a better choice.

In Section IV we surveyed the state-of-the-art in synchronization of chaotic systems in the context of digital communications.

In Part III, performance targets for chaotic communications techniques are summarized and examples (CSK with synchronization, noncoherent CSK and COOK, and DCSK correlation receiver) are given. We evaluate the performance of these systems in the context of a noisy and bandlimited channel. We also highlight a fundamental problem in chaotic communications of minimizing the variance of the estimation in the correlator.

## ACKNOWLEDGMENT

The authors have benefited significantly from extensive interaction with their colleagues in the Chaos Communications Collective, particularly during the "First Little Workshop on Spread Spectrum Communication and Chaos" at the EPFL, Lausanne, on 2 April 1996, and the "Second Little Workshop on Spread Spectrum Communication and Chaos" at University of California at Berkeley on 7 August 1996. Finally, the authors wish to thank the reviewers for their constructive criticism of this work.

## REFERENCES

[1] M. Hasler, "Engineering chaos for secure communication systems," *Phil. Trans. R. Soc. London A*, no. 1701, p. 353, Oct. 1995.

[2] G. Kolumbán, M. P. Kennedy, and L. O. Chua, "The role of synchronization in digital communication using chaos—Part I: Fundamentals of digital communications," *IEEE Trans. Circuits Syst. I, (Special Issue on Chaos Synchronization and Control: Theory and Applications)*, vol. 44, pp. 927–936, Oct. 1997.

[3] M. P. Kennedy and H. Dedieu, "Experimental demonstration of binary chaos shift keying using self-synchronizing Chua's circuits," in *Proc. IEEE Int. Specialist Workshop on Nonlinear Dynamics of Electronic Systems*, Dresden, germany, July 23–24, 1993, pp. 67–72.

[4] H. Dedieu, M. P. Kennedy, and M. Hasler, "Chaos shift keying: Modulation and demodulation of a chaotic carrier using self-synchronizing Chua's circuits," *IEEE Trans. Circuits Syst. II, (Special Issue on Chaos in Nonlinear Electronic Circuits—Part C: Applications)*, vol. 40, pp. 634–642, Oct. 1993.

[5] I. Frigyes, Z. Szabó, and P. Ványai, *Digital Microwave Transmission*. Amsterdam, The Netherlands: Elsevier Science, 1989.

[6] S. S. Haykin, *Communication Systems*, 3rd ed. New York: Wiley, 1994.

[7] G. Kolumbán, H. Dedieu, J. Schweizer, J. Ennitis, and B. Vizvári, "Performance evaluation and comparison of chaos communication systems," in *Proc. 4th Int. Workshop on Nonlinear Dynamics of Electronic Systems*, Sevilla, Spain, June 1996, pp. 105–110.

[8] G. Kolumbán, M. P. Kennedy, and G. Kis, "Performance improvement of chaotic communications systems," in *Proc. European Conf. on Circuit Theory and Design*, Budapest, Hungary, Aug. 30–Sept. 3, 1997, pp. 284–289.

[9] G. Kolumbán, B. Vizvári, W. Schwarz, and A. Abel, "Differential chaos shift keying: A robust coding for chaotic communication," in *Proc. 4th Int. Workshop on Nonlinear Dynamics of Electronic Systems*, Sevilla, Spain, June 27–28, 1996, pp. 87–92.

[10] T. Yang, "Recovery of digital signals from chaotic switching," *Int. J. Circuit Theory Appl.*, vol. 23, pp. 611–615, 1995.

[11] J. Schweizer, "A stochastic approach to spread spectrum communication using chaos," in *Proc. SPIE Chaotic Circuits for Communication*, Philadelphia, PA, Oct. 1995, pp. 115–125.

[12] A. J. Viterbi, *Principles of Coherent Communication*. New York: McGraw-Hill, 1966.

[13] G. Kolumbán, M. P. Kennedy, and G. Kis, "Determination of symbol duration in chaos-based communications," in *Proc. 5th Int. Workshop on Nonlinear Dynamics of Electronic Systems*, Moscow, June 26, 1997, pp. 217–222.

[14] M. P. Kennedy, "Three steps to chaos part I: Evolution," *IEEE Trans. Circuits Syst. I, (Special Issue on Chaos in Nonlinear Electronic Circuits—Part A: Tutorial and Reviews)*, vol. 40, pp. 640–656, Oct. 1993.

[15] H. Fujisaka and T. Yamada, "Stability theory of synchronized motion in coupled oscillator systems," *Prog. Theor. Phys.*, vol. 69, pp. 32–47, 1983.

[16] L. M. Pecora and T. L. Carroll, "Synchronization in chaotic systems," *Phys. Rev. Lett.*, vol. 64, no. 8, pp. 821–824, 1990.

[17] N. F. Rulkov, M. M. Sushchik, L. S. Tsimring, and H. D. Abarbanel, "Generalized synchronization of chaos in directionally coupled chaotic systems," *Phys. Rev. E*, vol. 51, no. 2, pp. 980–994, Feb. 1995.

[18] L. Kocarev, U. Parlitz, and T. Stojanovski, "Generalized synchronization of chaotic signals," in *Proc. NOLTA'95*, Las Vegas, NV, Dec. 10–14, 1995, pp. 953–956.

[19] M. G. Rosenblum, A. S. Pikovsky, and J. Kurths, "Phase synchronization of chaotic oscillators," *Phys. Rev. Lett.*, vol. 76, no. 11, pp. 1804–1807, Mar. 11, 1996.

[20] U. Parlitz, L. Junge, W. Lauterborn, and L. Kocarev, "Experimental observation of phase synchronization," *Phys. Rev. E*, vol. 54, no. 2, pp. 2115–2117, Aug. 1996.

[21] L. Kocarev and U. Parlitz, "Generalized synchronization, predictability, and equivalence of unidirectionaly coupled dynamical systems," *Phys. Rev. Lett.*, vol. 76, no. 11, pp. 1816–1819, Mar. 1996.

[22] M. P. Kennedy, "Three steps to chaos part II: A Chua's circuit primer," *IEEE Trans. Circuits Syst. I, (Special Issue on Chaos in Nonlinear Electronic Circuits—Part A: Tutorial and Reviews)*, vol. 40, pp. 657–674, Oct. 1993.

[23] L. M. Pecora and T. L. Carroll, "Driving systems with chaotic signals," *Phys. Rev. A*, vol. 44, no. 4, pp. 2374–2383, 1991.

[24] M. P. Kennedy, "Bifurcation and chaos," in W. K. Chen, Ed., *The Circuits and Filters Handbook*. Boca Raton, FL: CRC Press, 1995, pp. 1089–1164.

[25] R. N. Madan, Ed., *Chua's Circuit: A Paradigm for Chaos*. Singapore: World Scientific, 1993.

[26] T. S. Parker and L. O. Chua, *Practical Numerical Algorithms for Chaotic Systems*. New York: Springer-Verlag, 1989.

[27] M. Hasler, "Strong and weak forms of synchronization of chaotic systems," in *Proc. 5th Int. Workshop on Nonlinear Dynamics of Electronic Systems*, Moscow, Russia, June 26, 1997, pp. 2–7.

[28] R. He and P. G. Vaidya, "Analysis and synthesis of synchronous periodic and chaotic systems," *Phys. Rev. A*, vol. 46, no. 12, pp. 7387–7392, Dec. 1992.

[29] C. W. Wu and L. O. Chua, "A unified framework for synchronization and control of dynamical systems," *Int. J. Bifurc. Chaos*, vol. 4, no. 4, pp. 979–998, 1994.

[30] J. Schweizer, M. P. Kennedy, M. Hasler, and H. Dedieu, "Synchronization theorem for a chaotic system," *Int. J. Bifurc. Chaos*, vol. 5, no. 1, pp. 297–302, Feb. 1995.

[31] M. Vidyasagar, *Nonlinear Systems Analysis*. Englewood Cliffs, NJ: Prentice-Hall, 1978.

[32] H. Nijmeijer and I. Mareels, "An observer looks at synchronization," *IEEE Trans. Circuits and Syst. I, (Special Issue on Chaos Synchronization and Control: Theory and Applications)*, vol. 44, pp. 882–890, Oct. 1997.

[33] T. L. Carroll and L. M. Pecora, "Synchronizing nonautonomous chaotic circuits," *IEEE Trans. Circuits Syst. II, (Special Issue on Chaos in Nonlinear Electronic Circuits—Part C: Applications)*, vol. 40, pp. 646–650, Oct. 1993.

[34] G. Kolumbán, M. P. Kennedy, and L. O. Chua, "The role of synchronization in digital communication using chaos—Part III: Performance evaluation," *IEEE Trans. Circuits Syst. I*, submitted for publication.

**Géza Kolumbán** (M'92–SM'98) received the M.S. and Ph.D. degrees from the Technical University of Budapest and the C.Sc. degree from the Hungarian Academy of Sciences in 1976, 1990, and 1990 respectively.

After his graduation, he was employed as a research engineer by the Fine Mechanical Enterprise, Hungary, where he developed local generators, microwave transistor power amplifiers and VCO circuits for high-capacity microwave analog radio relay systems. He joined the Research Institute for Telecommunications, Hungary, in 1980, where he was involved in many system engineering projects like SCPC-type satellite telecommunications system, microwave satellite up- and down-converters, low-capacity microwave digital radio system, etc. He led a group of engineers whose duty was to develop frequency synthesizers and local generators for satellite and frequency hopping spread spectrum systems. He spent one year with Bilkent University in Turkey (1991–1992) and another year with the Eastern Mediterranean University in Cyprus (1992–1993) as an associate professor. He returned to the Technical University of Budapest in 1993, where he is employed as an associate professor at the Department of Instrument and Measurement Engineering. His current research interests are in nonlinear dynamics of different-type phase-locked loops, frequency synthesis by sampling phase-locked loop, chaotic communications, and applications of chaotic signals in measurement engineering.

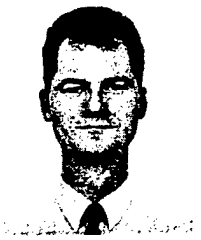

**Michael Peter Kennedy** (S'84–M'92–SM'95–F'98) received the B.E. (electronics) degree from the National University of Ireland in 1984, and was awarded the M.S. and Ph.D. degrees by the University of California at Berkeley in 1987 and 1991, respectively, for his contributions to the study of Neural Networks and Nonlinear Dynamics.

He worked as a Design Engineer with Philips Electronics, a Postdoctoral Research Engineer at the Electronics Research Laboratory, UC Berkeley, and as a Professeur Invité at the EPFL, Switzerland. He returned to University College Dublin (UCD) in 1992 as a College Lecturer in the Department of Electronic and Electrical Engineering, where he teaches Electronic Circuits and Computer-Aided Circuit Analysis, and directs the undergraduate Electronics laboratory. He was appointed Statutory Lecturer in UCD in 1996. He has published extensively in the area of nonlinear circuits and has taught courses on nonlinear dynamics and chaos in England, Switzerland, Italy, and Hungary.

Dr. Kennedy received the 1991 Best Paper Award from the International Journal of Circuit Theory and Applications for his paper with Leon Chua entitled "Hysteresis in Electronic Circuits: A Circuit Theorist's Perspective." He served as an Associate Editor of the IEEE TRANSACTIONS ON CIRCUITS AND SYSTEMS from 1993 to 1995 and is currently Chair of the IEEE Nonlinear Circuits and Systems Technical Committee. He has held visiting research positions at the EPFL, AGH Kraków, TU Budapest, and UC Berkeley. His research interests are in the simulation, design, analysis, synchronization, and control of nonlinear dynamical systems for applications in communications and signal processing.

**Leon O. Chua** (S'60–M'62–SM'70–F'74) received the S.M. and Ph.D. degrees from MIT and the University of Illinois in 1961 and 1964, respectively.

After seven years on the Faculty at Purdue University he moved to the University of California at Berkeley, where he is currently Professor of Electrical Engineering and Computer Sciences. He has been conferred with Honorary Doctorates by the EPFL, University of Tokushima, Technical University of Dresden, Technical University of Budapest, the University of Santiago de Compostela, and the University of Frankfurt. Professor Chua's research interests are in the areas of general nonlinear network and system theory. He has been a consultant to various electronic industries in the areas of nonlinear network analysis, modeling, and computer-aided design. He is the author of four books and has published extensively in the area of nonlinear networks and systems.

Professor Chua was elected a Fellow of the IEEE in 1974. He is currently a member of the Technical Committee on Nonlinear Circuits and Systems of the IEEE Circuits and Systems Society. He served as Editor of the *IEEE Transactions on Circuits and Systems* from 1973 to 1975 and as President of the *IEEE Circuits and Systems Society* in 1976. He is presently the editor of the *International Journal of Bifurcation and Chaos* and a deputy editor of the *International Journal of Circuit Theory and Applications*. Professor Chua is the holder of five U.S. patents. He is also the recipient of several awards and prizes, including the 1967 IEEE Browder J. Thompson Memorial Prize Award, the 1973 IEEE W.R.G. Baker Prize Award, the 1974 Frederick Emmons Terman Award, the 1976 Miller Research Professorship from the Miller Institute, the 1982 Senior Visiting Fellowship at Cambridge University, England, the 1982/1983 Alexander von Humboldt Senior U.S. Scientist Award at the Technical University of Munich, Germany, the 1983/1984 Visiting U.S. Scientist Award at Waseda University, Tokyo, from the Japan Society for Promotion of Science, the IEEE Centennial Medal in 1985, the 1985 Myril B. Reed Best Paper Prize, both the 1985 and 1989 IEEE Guillemin–Cauer Prizes, the Professor Invité International Award at the University of Paris-Sud from the French Ministry of Education in the fall of 1986, the 1993 Technical Achievement Award by the IEEE Circuits and Systems Society, and the 1995 M. E. Van Valkenburg Prize from the IEEE Circuits and Systems Society.

International Journal of Bifurcation and Chaos, Vol. 8, No. 10 (1998) 2047–2059
© World Scientific Publishing Company

# ERROR PERFORMANCE OF CHAOTIC DIGITAL CODE-DIVISION MULTIPLE ACCESS(CDMA) SYSTEMS

TAO YANG and LEON O. CHUA
*Electronics Research Laboratory and*
*Department of Electrical Engineering and Computer Sciences,*
*University of California, Berkeley, CA 94720, USA*

Received May 26, 1998; Revised June 30, 1998

Chaotic digital code-division multiple access ((CD)$^2$MA) systems are new types of communication systems using chaotic carriers. (CD)$^2$MA had found applications in both wireless and other communication systems. In this paper we study the error performance of chaotic digital code-division multiple access ((CD)$^2$MA) systems used in both wireless environment and cable networks. We present first the details of the interleave mode of the (CD)$^2$MA. When a (CD)$^2$MA system works in the interleave mode, each of its transmitters only transmits signals during a portion of the bit duration of the message signal. The total interference level is thus reduced which in turn increases the channel capacity. The relationship between the bit error rate (BER) and the interleave rate is studied in both the synchronous (CD)$^2$MA system used in cable systems, and the asynchronous (CD)$^2$MA system used in wireless environments. Our simulation results show that in a cable system the synchronous (CD)$^2$MA system can support 1.5 times more channel capacity than synchronous CDMA systems, and double the channel capacity of CDMA systems in wireless environments.

## 1. Introduction

A *digital information source* produces a finite set of possible messages while an *analog information source* produces messages that are defined on a continuum. A *digital communication system* transfers information from a digital source to a sink while an *analog communication system* transfers information from an analog source to a sink. A *digital waveform* is defined as a function of time that can have only a discrete set of values while an *analog waveform* is a function of time that has a continuous range of values. An electronic digital communication system usually has voltages and currents that have digital waveforms. In some cases, the digital information is transmitted to a sink by use of analog waveforms. In such cases, the system is still called a digital communication system. If the analog waveforms used are chaotic, we call it a *chaotic communication system.* A chaotic digital communication system has therefore a digital information source, and a chaotic carrier. The classical communication systems use sinusoidal carriers, which are not chaotic.

In view of the wide and continuous spectrum of chaotic carriers, a chaotic digital communication system is a spread spectrum system in nature. Before spread spectrum communication systems become widely used in commercial wireless markets, there is little motivation to use chaotic carriers in view of their low efficiency in sending narrow band information sources. An examination of previous chaotic communication systems [Yang & Chua, 1996a, 1996b; Wu *et al.*, 1996] will show that the chaotic carrier has a much wider bandwidth than that of the message signal. This low channel efficiency of chaotic communication system in narrow band communication settings may pose a serious disadvantage in commercial applications. This weakness was partially the reason why the study of past chaotic communication systems has focused on security issues rather than on commercial issues

[Yang *et al.*, 1997; Yang & Chua, 1997b]. In a secure communication system, the most important issue is security rather than the channel efficiency. However, in commercial applications, where chaotic communication systems could have a large potential market, channel efficiency is always the first consideration.

When we consider the application of chaotic carriers in spread spectrum communication systems, the situation is quite different. There are at least three reasons for studying chaotic communication systems from a theoretical point of view. Firstly, the success of nonlinear sciences, nonlinear mathematics and nonlinear engineering since the 1980's had set a solid basis for chaotic communication systems. Secondly, the development of the digital communication technology had made the efficiency of the spectrum resource the first priority over the price of the system. Besides these two reasons note also the rapid development of micro-electronics had followed the so called *Moore's Law* [Schaller, 1997], thereby offering a very high performance to price ratio to IC chips. So far, GaAs and silicon bipolar and BiCMOS technologies have contributed a major portion of the RF market. As a promising contender, the RF CMOS may also contribute to this market in the near future. Thirdly, the commercial spread spectrum communication systems had made use of chaotic carriers which occupy much more bandwidth than that of linear carriers.

So far, there are at least two approaches for applying chaos to spread spectrum communication systems, especially CDMA systems. The first approach uses a chaotic sequence to serve as chip sequences [Mazzini *et al.*, 1997]. Since the chip sequences used in the classical CDMA systems are designed in a theoretically orthogonal way, the improvement that chaotic chip sequences can achieve is very limited if the orthogonality of the chaotic chip sequences can not be guaranteed. Instead of fitting into the old framework, our chaotic digital code-decision multiple access ((CD)$^2$MA) systems [Yang & Chua, 1997a, 1997c] introduced revolutionary changes to the old communication framework, which is based on linear carriers,[1] by using *chaotic* (*nonlinear*) carriers.[2]

The relation between the carrier and the message signal in linear and chaotic communication systems is depicted in Fig. 1 in the frequency space (spectrum). Figure 1(a) shows the case where the linear carrier is a single sinusoidal tune while the message signal has a given bandwidth. Then, a modulation process spreads the bandwidth around the center frequency of the carrier. This method was originally designed for narrow-band communication systems. It has recently been used in commercial spread spectrum communication systems. The advantage of this method is the simplicity of the carrier, which can be generated by a limit cycle in a dynamic system, such as an electronic oscillator. Figure 1(b) shows the case where the nonlinear carrier is already a wide-band signal, such as a chaotic signal. We can see that in this case the message signal has a much smaller bandwidth than the nonlinear carrier. This implies that chaotic communication system should be a spread spectrum communication system. In other word, chaotic communication systems are specially designed for spread spectrum applications.

The main challenge in chaotic communication systems is the design of nonlinear carriers, which are (hyper-)chaotic signals. One disadvantage of a chaotic carrier is the lack of study of

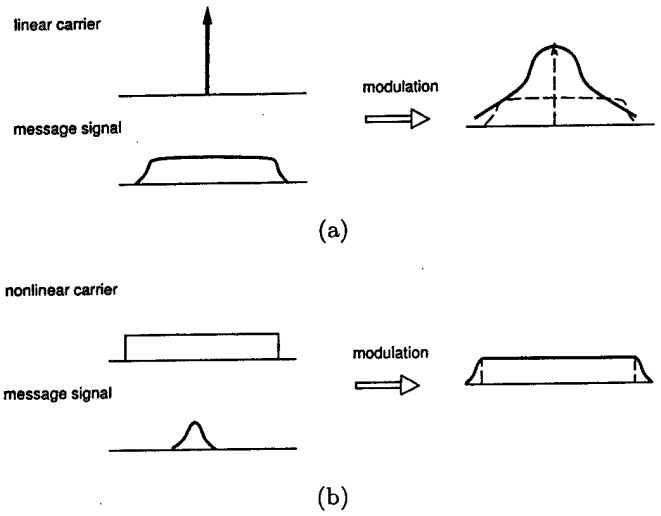


Fig. 1. Difference between the relations of carriers and message signals in linear and chaotic communication systems. (a) Linear communication system. (b) Chaotic communication system.

[1]Sometimes we can view the chip sequence used in CDMA as a *nonlinear* sub-carrier. However, since the chip sequence is finally transmitted by a linear carrier to the sink, we can not lump CDMA into nonlinear communication framework.

[2]Strictly speaking, the concept of a nonlinear carrier is wider than the concept of a chaotic carrier. For example, the solitons used in optical fiber communication systems is a kind of nonlinear carrier but not a chaotic one.

RF chaotic circuits in electrical engineering because nonlinearities were always suppressed as "undesirable" properties in previous RF circuit designs [Lee, 1998]. For example, a very common nonlinearity in RF circuits called *gain compression*, can cause desensitization and blocking when a weak, desired signal along with a strong interference is processed. However, in chaotic communication systems, we usually use gain compression to restrict the energy growth rate of chaotic trajectories and reshape chaotic attractors. This simple example shows the difference between the standpoints of linear communication systems and chaotic communication systems. The former tries to avoid the unavoidable nonlinearity while the latter exploits the benefits of nonlinearities.

The organization of this paper is as follows. In Sec. 2, theoretical results for evaluating bit-error-rate (BER) performance of $(CD)^2MA$ systems are given. In Sec. 3, details of interleave mode of $(CD)^2MA$ systems are presented. In Sec. 4, the BER performance of synchronous $(CD)^2MA$ in cable communication systems is presented. In Section 5, the BER performance of asynchronous $(CD)^2MA$ in wireless environment is presented. Finally, some concluding remarks are given in Sec. 6.

## 2. BER Performance of $(CD)^2MA$ Systems

To compare the performance of CDMA and $(CD)^2MA$ systems, which modulate binary signals using linear and chaotic carriers, respectively, we must analyze their bit-error-rate (BER) performances. This section is restricted to the coherent detection of binary phase shift keying (BPSK) modulation because BPSK is used to modulate the subcarrier (chip sequence) in CDMA systems [Viterbi, 1995], and the chaotic carrier in $(CD)^2MA$ systems [Yang & Chua, 1997c], respectively. We assume that when a signal $s_{i1}(t)$ (resp., $s_{i2}(t)$) is transmitted, the received signal, $r_i(t)$, is equal to $s_{i1}(t) + n(t) + I_i(t)$ (resp. $s_{i2}(t) + n(t) + I_i(t)$). While the noise $n(t)$ is always modeled as an additive white Gaussian noise (AWGN),[3] which gives us a mathematically tractable model, the interferences $I_i(t)$ from the other users in the same base station in wireless systems (or, from the same fiber node and headend in hybrid optical-coax cable networks) cannot be modeled by AWGN because they are simply not AWGN. Based on this consideration, we use simulation to model the interferences which are in fact "man-made" noises and model the channel noise as AWGN processes.

The "opposite-sign" signals, $s_{i1}(t)$ and $s_{i2}(t)$ can be defined by

$$s_{i1}(t) = \sqrt{E}c_i(t),\ s_{i2}(t) = -\sqrt{E}c_i(t),\ 0 \le t \le T \tag{1}$$

By using a $[0, T]$ *correlator* as the matched filter, the decision state of the detector will choose the $s_{ij}(t), j = 1, 2$ with the largest correlator output $z_iT$, or in the case of equal-energy opposite-sign signals, the detector's decision is based on the following criterion:

$$\begin{array}{ll} s_{i1}(t) & \text{if } z_i(T) > 0 \\ s_{i2}(t) & \text{otherwise} \end{array} \tag{2}$$

As shown in Fig. 2, two kinds of errors can be output by the detector: the first one takes place if $s_{i1}(t)$ is transmitted but the noise and interference is such that the detector measures a negative value of $z_i(T)$ and chooses $H_{i2}$ (the hypothesis that $s_{i2}(t)$ was sent). The second one takes place if $s_{i2}(t)$ is transmitted but the noise and interference is such that the detector measures a positive value of $z_i(T)$ and chooses $H_{i1}$ (the hypothesis that $s_{i1}(t)$ was sent). These two types of errors are shown as shadowed regions in Fig. 2.

The BER is then given by

$$\text{BER} = P(H_2|s_1)P(s_1) + P(H_1|s_2)P(s_2) \tag{3}$$

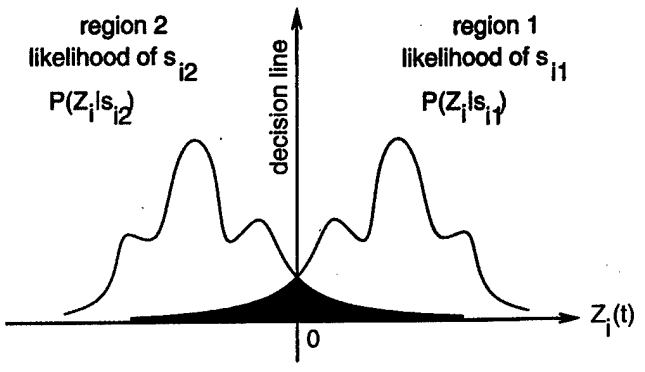


Fig. 2. Schematic plot of the probability of misclassification in the outputs of the decision rule of the detector.

[3]It should also be noted that in some channels noises cannot be modeled as AWGN. For example, in the 5–40 MHz band of cable TV systems, the channel noises are impulses picked up from home electronic devices and from narrow-band interferences picked up by the cable networks from other RF broadcast sources.

For a message signal, we can suppose that $P(s_1) = P(s_2) = 0.5$, and we have

$$\text{BER} = 0.5P(H_2|s_1) + 0.5P(H_1|s_2) \qquad (4)$$

In view of the complexities of the chaotic carriers, $P(Z_i|s_{i1})$ and $P(Z_i|s_{i2})$ are two very complex functions, which depends on the type of chaotic carrier, the interleave rate (see Sec. 3), and the channels. Instead of trying to model them by formulas, in this paper, we use well-designed simulations to determine these two functions.

## 3. Details of Interleave Technology used in (CD)$^2$MA Systems

Just as CDMA systems, (CD)$^2$MA systems are interference-limited but not dimension-limited as TDMA and FDMA. The main error source is not the channel noise but the interference from the other (CD)$^2$MA users. There are many tricks such as power control and speech active rate, which have been used to reduce global interference energy in a cell in CDMA systems. Besides these tricks, the (CD)$^2$MA can play one more trick to reduce global interference dramatically; namely, interleave technology.

We use the following example to demonstrate the interleave technology of (CD)$^2$MA systems. Suppose each user in a 6 MHz band uses a 32 kbps modem,[4] so that the processing gain is given by $G_p = 60000/32 \approx 188$. In a CDMA system, since a chip sequence around 6 MHz is used, the transmitter must send a continuous waveform to allow the receiver to recover the chip sequence. However, in a (CD)$^2$MA system, it is not necessary to keep a transmitter working all the time during a symbol duration because the redundancy in transmitting 1 bit can generate much interference energy. It is indeed remarkable that a (CD)$^2$MA system directly modulates the rather slow symbol sequence in its chaotic carrier instead of modulating a very fast chip sequence in a linear carrier as in the CDMA systems. This enables the (CD)$^2$MA system to work under a so-called *interleave mode.*

The block diagram of the interleave mode of (CD)$^2$MA is shown in Fig. 3. In this figure only the duration of one symbol bit $T_b$ is shown. Observe that this time interval is divided into small time fragments of length $T_a$ called an *active duration.* For sending a message bit in the bit duration

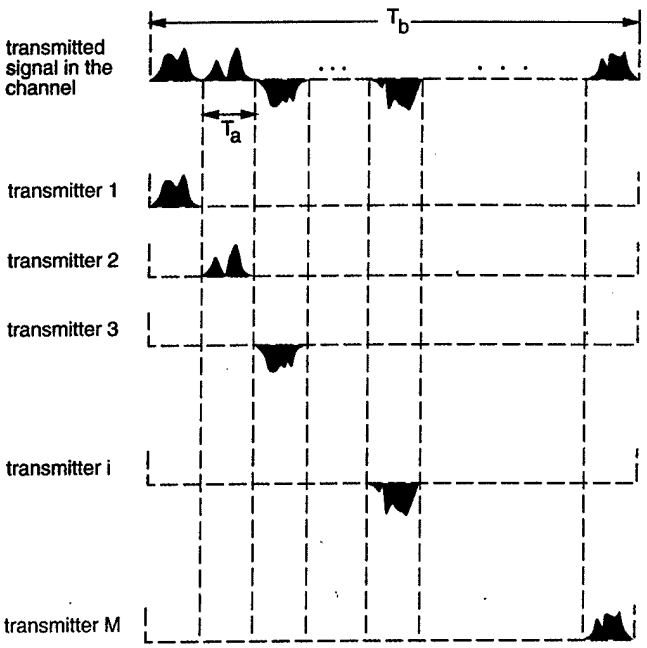


Fig. 3. Block diagram of the interleave mode in (CD)$^2$MA systems.

$(kT_b, (k+1)T_b]$, each transmitter only becomes active during a *prescribed* active duration located randomly within $(kT_b, (k+1)T_b]$. The ratio $R_I \triangleq T_b/T_a$ is called the *interleave rate,* which is a very important parameter for designing a good (CD)$^2$MA system. Since exploiting the interleave mode in (CD)$^2$MA systems is a new concept, the main purpose of this paper is to analyze how the interleave rate affects the BER performance of a (CD)$^2$MA system.

The principle of assigning an active duration to a certain active user is to reduce the overall interference level within a cell in wireless systems, or a headend controller in cable systems. The assignment of active duration is made at the base station, or at the headend controller by checking the number of active users, the data-link load of each user, and the total data-link load. At least two typical cases must be considered.

1. All users have the same data-link load.
This is the typical case in today's cellular phone systems, where each cellular phone has a 9.6 kbps data-link load. In this case, the active durations are distributed uniformly over the entire $T_b$. If the user number is less than $R_I$, then the active duration

[4]This example provides a typical setting of a coaxial cable TV systems designed for accessing the Internet [Yang & Chua, 1998].

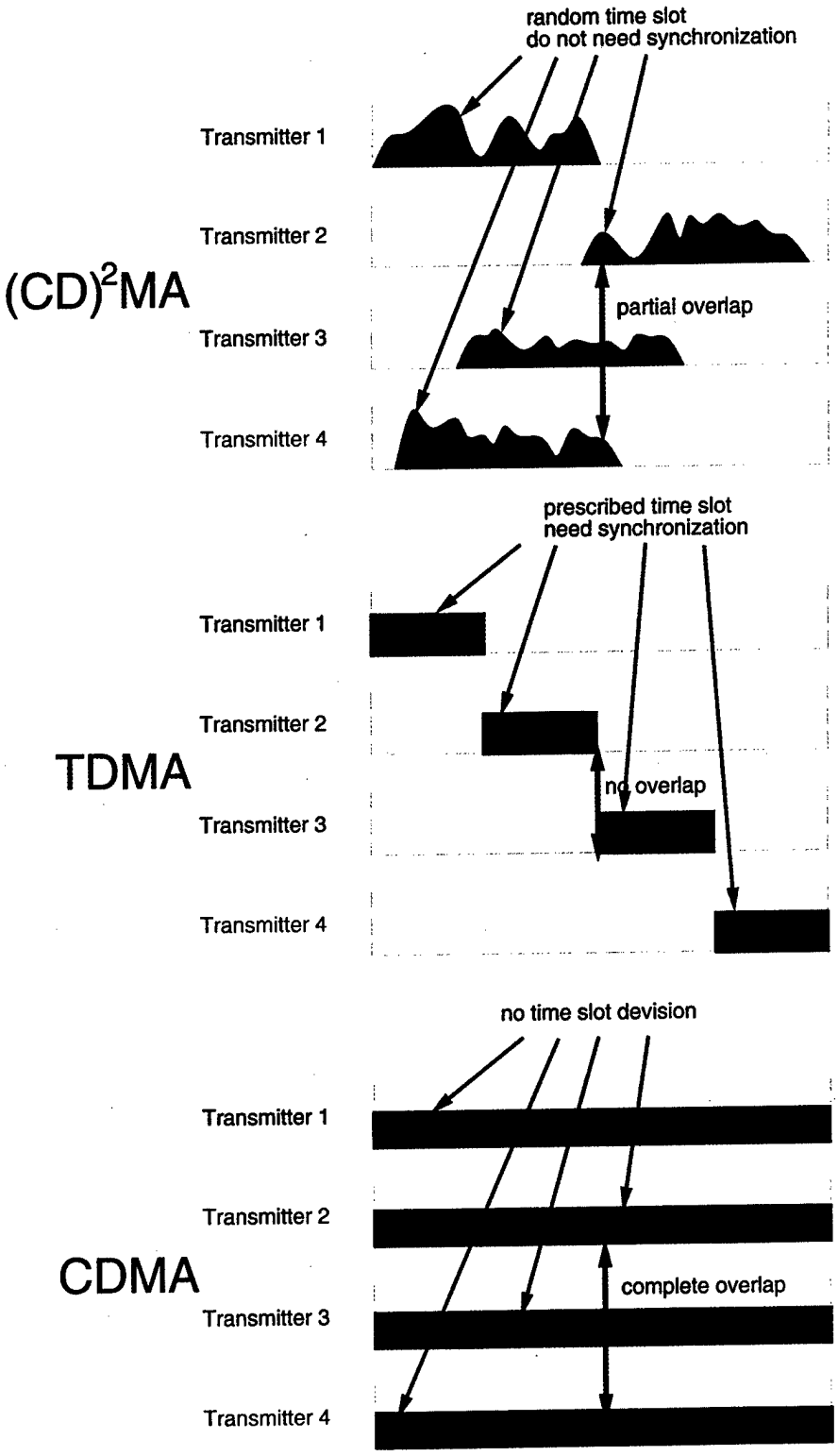


Fig. 4. Comparison of $(CD)^2MA$ interleave mode, TDMA and CDMA.

can be either separated from each other by empty time slots,[5] or enlarged to support a bigger data-link speed. If the user number is around $R_I$ then the active durations should be arranged consecutively one after the other to avoid overlaps. If the user number is much bigger than $R_I$, the overlap between different active durations is unavoidable. Our strategy in this case is to let the overlaps distribute uniformly over the duration $T_b$. In this case, two possible actions may be taken. The first is to keep $R_I$ unchanged while allowing the BER performance to degrade to some degree; namely, a soft degradation which is tolerable in speech communication. The second is to increase $R_I$ thereby resulting in a decrease of the maximum data-link load for each user but keeping the BER performance unchanged. This is important in the Internet applications. However, in both cases, the quality of service (QoS) is unavoidably degraded.

2. Users have different data-link loads.
In future Internet or other Information Superhighway frameworks, the QoS is closely linked to the user subscribing fee. In each framework, different QoS levels (of course, different fee rates) will be supported to exploit the spectrum resources more efficiently. Both high-speed data-links (such as high-resolution real-time images in telesurgery, teleconference and tele-robotic) and low-speed data-links (such as normal Internet users and cellular phone users) will coexist in the same local base station. The difference between different QoS levels is very large. For example, a 10-second delay to a tele-surgery system is much more critical than a 30-second delay to a casual Internet user. The dynamical range of the data-link speed may vary from 1 Mbps to 9.6 kbps. The current CDMA systems cannot support this big dynamical range because step switches are used to change the bit-rate. On the other hand, by assigning active durations, a $(CD)^2MA$ system can support *any* dynamical range that a bandwidth can support. This can easily be achieved by assigning different active durations to different QoS levels. For high-speed data-links, long active durations are assigned. For low-speed data-links, short active durations are assigned. Since different active durations and bit-rates are used in the same bandwidth, the overall assignment of durations should distribute the overlaps uniformly with respect to time. In this case, the active duration assigning process is not a trivial one because some dynamical algorithms must be used to monitor the overall interference level. However, since this happens at the base station, this technical complexity can be solved without modifying the mobile stations.

Although at first sight the interleave mode appears somewhat similar to TDMA, they are in fact quite different. The main distinction of $(CD)^2MA$ from TDMA and CDMA is shown in Fig. 4 where only four transmitters and $R_I = 2$ are shown for clarity. Observe that in a TDMA system, the "active duration" for each user is fixed. Once a TDMA system is set up a prescribed "active duration" will always be reserved for a certain user even if this user transmits nothing during this time slot.[6] In $(CD)^2MA$ systems, the active duration for a certain user is dynamically assigned at any location within the symbol bit duration to achieve a minimum peak interference at all times. This dynamical assignment results in a maximum usage efficiency of the spectrum resources. For example, if an *active* user is detected to be silent in a symbol bit duration, the base station will reassign the active durations such that the total overlap will be reduced. A $(CD)^2MA$ system is also different from a CDMA system because each CDMA user must transmit a modulated carrier continuously.

The reader should also note that synchronization in the interleave mode is the same as that presented before [Yang & Chua, 1997c]. This means that in the interleave mode the synchronization of the chaotic carrier is *continuous*.

## 4. Synchronous $(CD)^2MA$ for Cable Networks

Application of $(CD)^2MA$ to cable networks is very promising because cable networks can provide much a larger bandwidth than telephone lines. Figure 5(a) shows the outline of a typical current cable communication system. The central node of a cable TV system is the *headend*. Signals from different sources, such as satellite and terrestrial broadcast, Internet, as well as locally originating

[5]An empty time slot is defined as a time duration within which no user is active in *this* local central cell. However, the interference from other cells and noise still exists.
[6]This is one of the drawbacks of TDMA systems where resources are wasted by idle users.

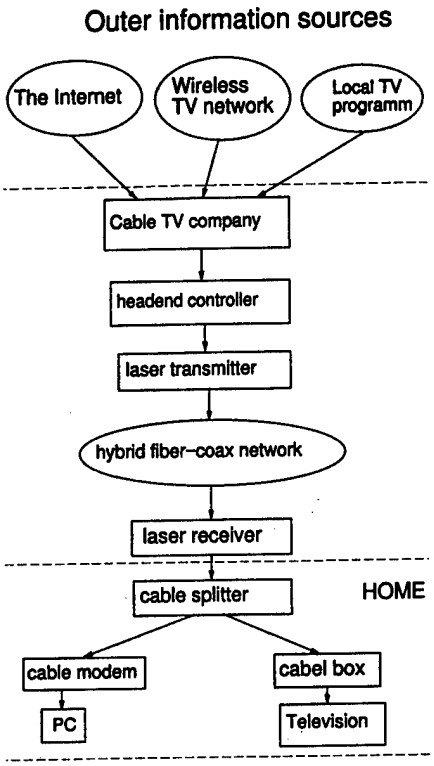


(a)

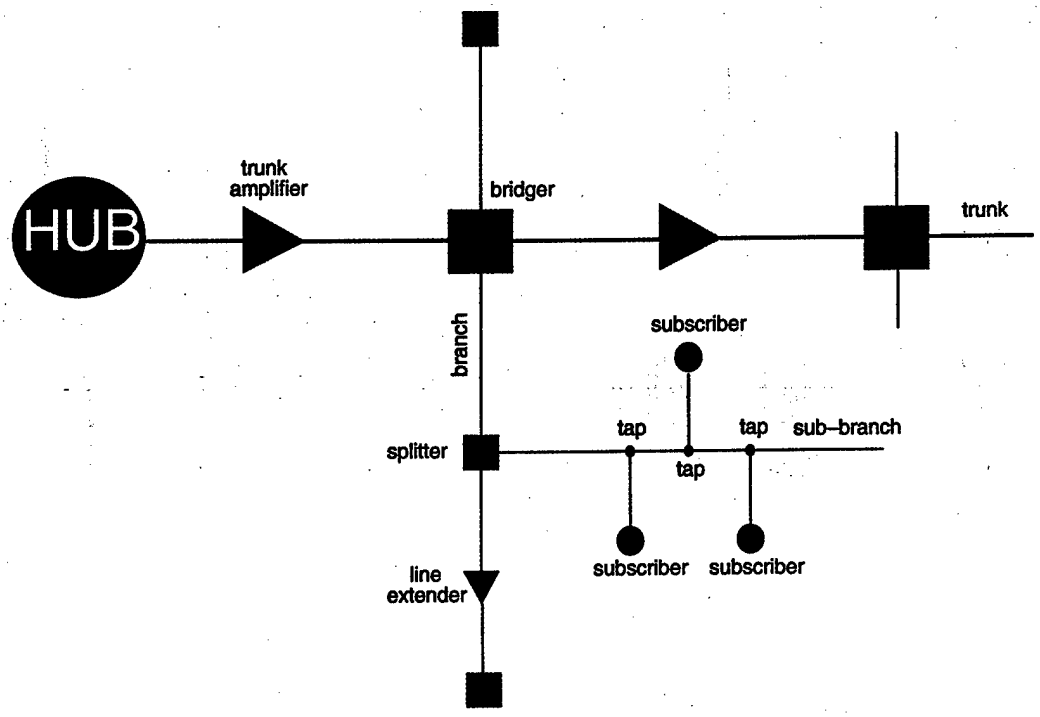


(b)

Fig. 5. Outline of typical current cable communication systems. (a) Block diagram of a typical cable communication system. (b) Block diagram of a single trunk.

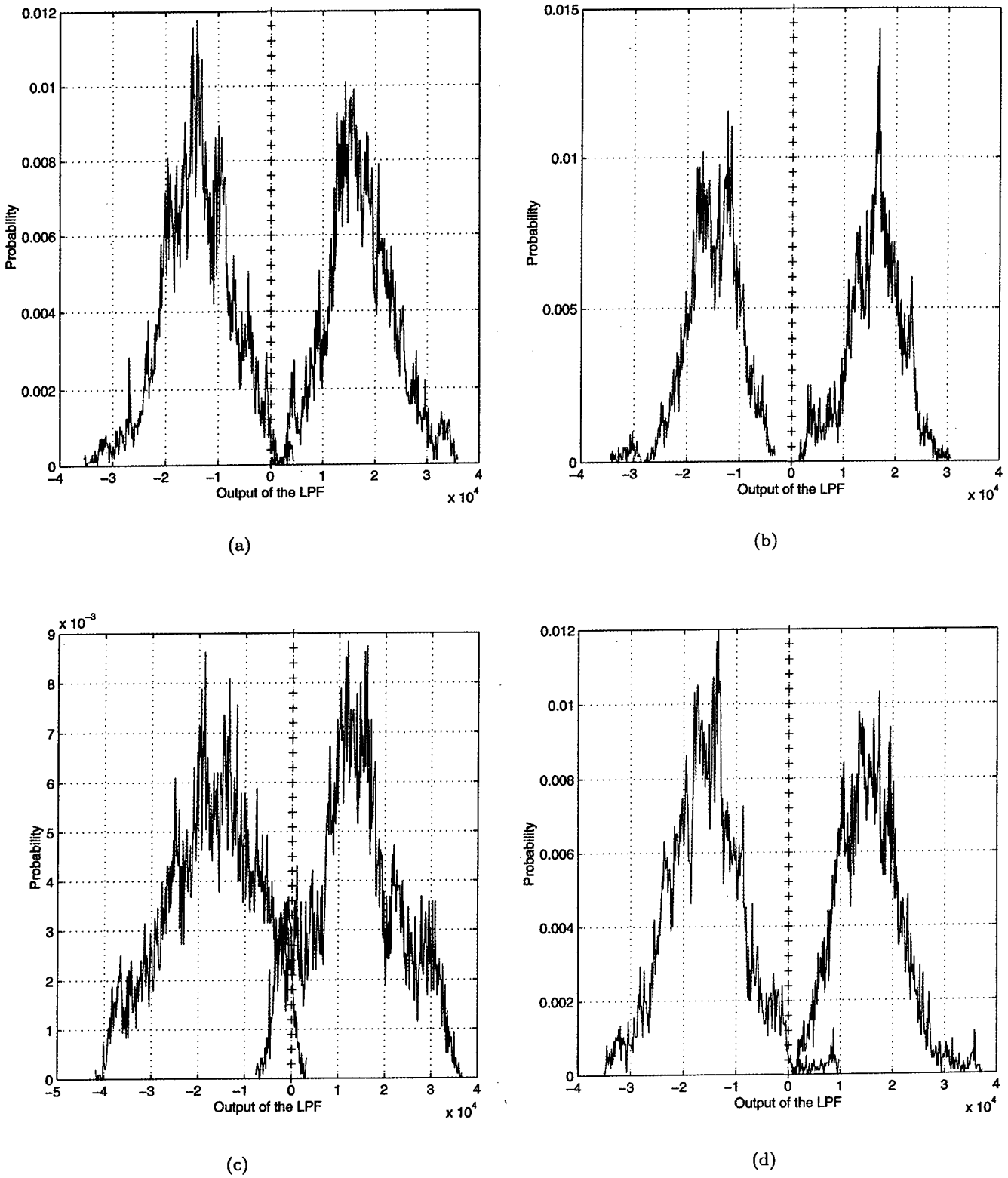


Fig. 6. Different probability density functions of the output of the LPF at the upstream receiver end. Conditions: each user uses a 32 kbps modem in a 6 MHz channel. (a) 470 users with interleave rate $R_I = 10$. (b) 300 users with interleave rate $R_I = 10$. (c) 470 users with interleave rate $R_I = 5$. (d) 300 users with interleave rate $R_I = 5$.

programming, are modulated onto radio frequency carriers and combined together for distribution over the cable system. Supertrunks (high-quality microwave, fiber optic, or cable links) connect the head-end to local distribution centers, known as *hubs*. Several trunks may originate from a hub to provide coverage over a large contiguous area. Figure 5(b) shows a single trunk of a typical cable TV system. Trunk amplifiers are installed along the trunk to maintain the signal level and compensate for cable transmission characteristics. The bridge amplifier serves as a high-quality tap, providing connection between the main trunk and multiple high-level branches. The line extender is a type of amplifier that maintains the signal level along the branch. The splitter connects a subbranch to a branch. Subscriber drops are connected to passive taps along the subbranch.

In a cable system, $(CD)^2MA$ can be synchronous. In this case, perfect power control is assumed and the delay from each path can be measured and compensated at the headend controller. In this section, the BER of a synchronous $(CD)^2MA$ system is given under different conditions, such as different modem speed, or different number of users.

The chaotic carrier for the $i$th user is modeled as

$$c_i(t) = \sum_{n=1}^{N} a_{i,n}(t)\cos(\omega_{i,n}t + \theta_{i,n})$$
$$= \mathrm{Re}\left\{\sum_{n=1}^{N} a_{i,n}(t)\exp(j\omega_{i,n}t + j\theta_{i,n})\right\}, N \to \infty \quad (5)$$

where $a_{i,n}(t) \in \Re$, $\omega_{i,n} \in$ [prescribed spectral band], and $\theta_{i,n} \in (-\pi, \pi]$ are, respectively, the amplitude, frequency and phase of the $n$th component of the chaotic carrier. In the simulations, $\omega_{i,n}$ is not necessarily equal to $\omega_{j,n}$ for $i \neq j$. In our model $\omega_{i,n}$ is chosen randomly in a small sub-band of the prescribed spectrum band.

### 4.1. *Performance with low-speed data links*

Let us investigate first the BER performance of $(CD)^2MA$ systems with low-speed modems. 100 subcarriers are used to model the chaotic carrier and we suppose that each user uses a 32 kbps modem. The bandwidth is 6 MHz. The interleave rate is $R_I = 10$. Figure 6(a) shows the case when 470 users are active in the network under a headend controller. In this figure, the blue curve and the green curve are the probability density functions of the outputs of the LPFs for bit-1 and bit-0, respectively. The red vertical line denotes the decision line. The overlap between the blue curve and the green one results in a 0.0089 BER. Figure 6(b) shows the case when 300 users are active. Observe that the blue and the green curves do not overlap each other. In this case the BER is 0.[7]

The interleave rate can affect the BER performance significantly. To show this we also give the simulation results for an interleave rate of $R_I = 5$. Figure 6(c) shows the case of 470 users. Comparing the results in Figs. 6(a) and (c) we find that the overlap is much larger in the latter. This results in a very big BER of 0.1072. Figure 6(d) shows the case of 300 users. Similarly, a decrease in the interleave rate increases the overlap and in turn the BER significantly. In this case, the BER is 0.0178, which is still larger than the case of 470 users with an interleave rate of 10.

The results of the BER performances with different interleave rates are shown in Fig. 7. The blue curve and the red curve show the BER performances with $R_I = 10$ and 5, respectively. Observe that by using only a low interleave rate the BER performance is already comparable to traditional S-CDMA systems [Yang & Chua, 1998]. With larger interleave rates the BER performance of $(CD)^2MA$ systems is much better than that of the traditional S-CDMA systems. The technical restriction on increasing the interleave rate is that the outskirts of the switching processes may be bigger than the active duration itself. In this case, strong interferences are introduced by the transient processes, rather than by the active duration. This in turn decreases the usage efficiency of the spectrum. The impulsive noises in cable TV systems also imposes a restriction on the decrease of $T_a$. The active duration $T_a$ should be large enough compared to the largest duration of impulsive noises.

[7]In fact, theoretically the BER cannot be zero. Our observation of zero value in Fig. 6(b) is due to the short length of our samples. However, the actual BER can be guaranteed to be less than $10^{-6}$ whenever a zero BER is observed in the simulations.

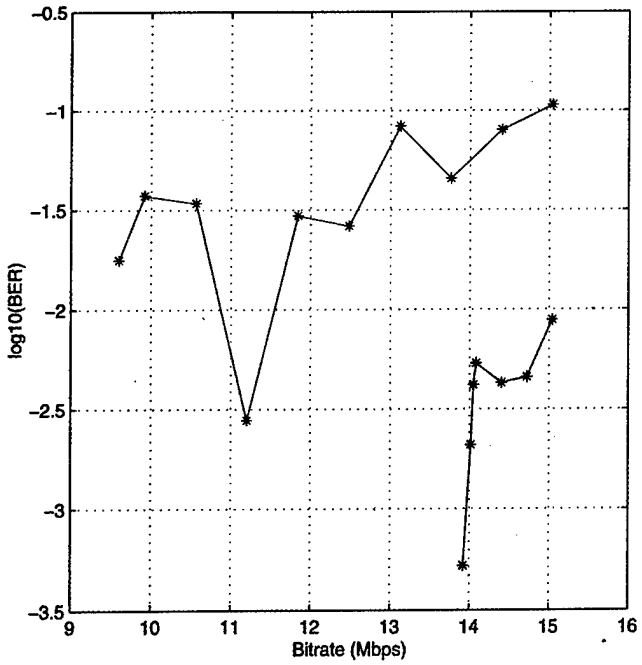


Fig. 7. The BER performance of synchronous $(CD)^2MA$ systems with different interleave rates in the low-speed modes of cable systems.

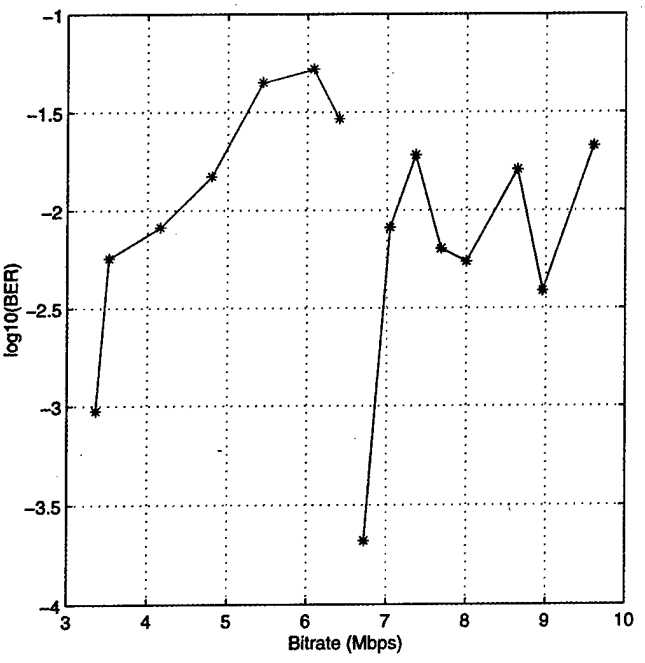


Fig. 8. The BER performance of synchronous $(CD)^2MA$ systems with different interleave rates in the high-speed modes of cable systems.

### 4.2. *Performance with high-speed data links*

Next let us study the case where each user uses a high-speed modem. The shapes of the probability density functions are qualitatively the same as those in the low-speed cases. The results of the BER performances with different interleave rates are shown in Fig. 8. The blue curve and the red curve show the BER performances with $R_I = 10$ and 5, respectively. Comparing the results in Figs. 7 and 8 we can see that the capacity that the $(CD)^2MA$ can provide for high-speed links is smaller than that for low-speed links. This result shows that in cable networks, a synchronous $(CD)^2MA$ system can efficiently support a large number of distributed low-speed links. This is just the case of digital personal communication systems (PCS). Since the channel capacity that can be provided under the low-speed condition is almost twice of that under the high-speed condition, another method to exploit the channel capacity is to subdivide the high-speed data streams into low-speed data sub-streams and then transmit the sub-streams.

## 5. $(CD)^2MA$ for Wireless Communication Systems

The outline of a $(CD)^2MA$ system in a wireless environment is shown in Fig. 9. A service region is usually divided into small regions called *cells*. In the downtown of a big city the radius of a cell may be as small as 2 km. The core of a cell is called a *base station*, which controls and monitors all users called *mobile stations*. A mobile station may be a cellular phone, or a mobile lap-top personal computer (PC).

In wireless applications of $(CD)^2MA$ systems, the channels are much more complicated than those in cable systems. The most significant difference is the multipath fading, which is depicted in Fig. 10. Observe that different buildings at different distances and directions can introduce different propagating paths between the mobile station and the base station.

The multipath channel is characterized by a set of equivalent complex-valued low-pass impulse responses

$$\left\{ h_k(t) = \sum_{l=1}^{L} \beta_{kl}\delta(t-\tau_{kl})\exp(-j\phi_{kl}) \right\}_{k=1}^{K} \qquad (6)$$

where $K$ denotes the number of active users. Here we assume that every link has a fixed number, $L$, of resolvable paths. The path gains $\{\beta_{kl}\}_{l=1}^{L}$, path delays $\{\tau_{kl}\}_{l=1}^{L}$, and path phases $\{\phi_{kl}\}_{l=1}^{L}$ are

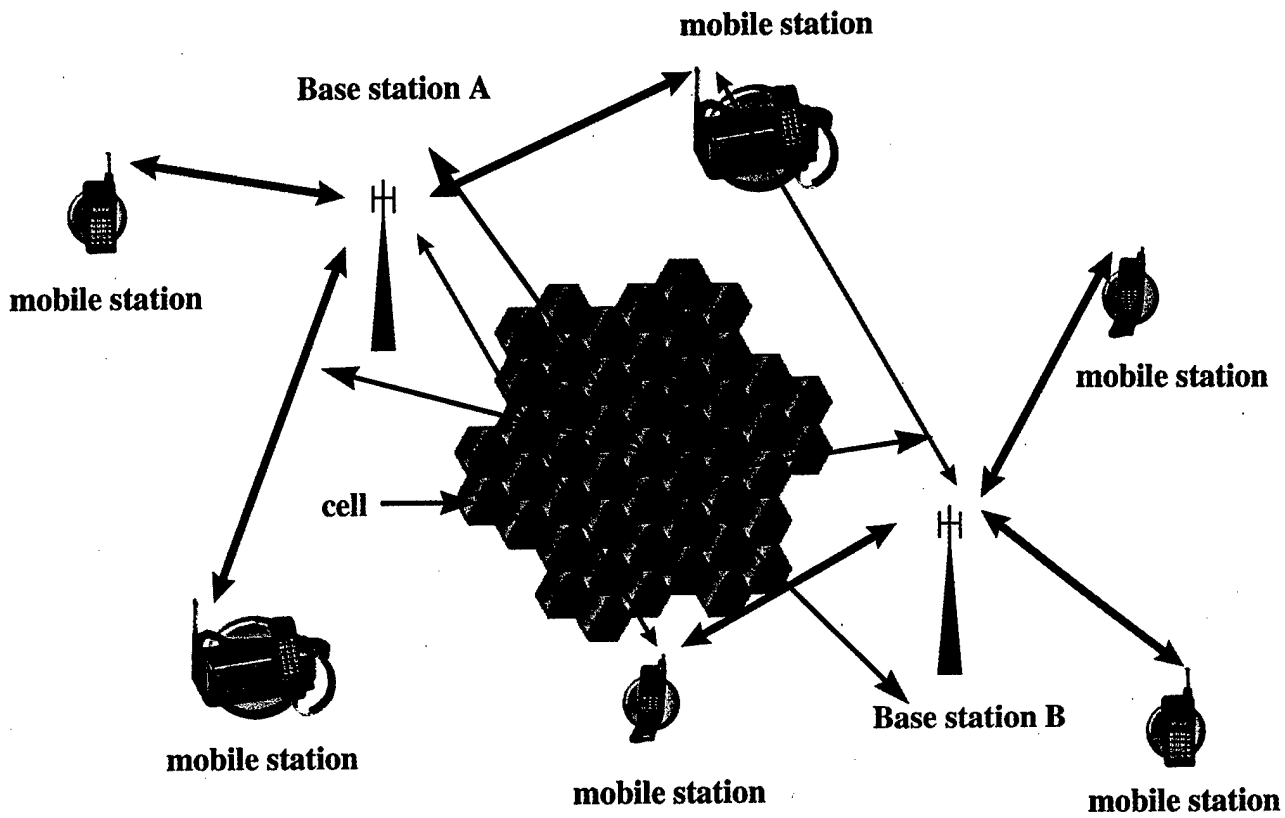


Fig. 9. Outline of a $(CD)^2MA$ system in a wireless environment.

three random variables. For a given $k$, $\{\beta_{kl}\}_{l=1}^{L}$ is modeled as a set of independent Rayleigh random variables whose probability density functions are given by

$$p(\alpha_k) = \frac{2\alpha_k e^{-\alpha_k^2/\sigma_{kr}^2}}{\sigma_{kr}^2}, \qquad \alpha_k > 0, \quad k = 1, 2, \ldots, L \tag{7}$$

We assume that the $L$ multi-path components are Rayleigh random variables of equal average strength, so that

$$\sigma_{kr}^2 = \sigma_r^2, \quad \text{for all } k = 1, 2, \ldots, L \tag{8}$$

Following [Wu *et al.*, 1995], we choose $\sigma_r = 4$ dB. The set $\{\tau_{kl}\}_{l=1}^{L}$ of random variables are mutually independent and uniformly distributed over $[0, \Delta]$, where $\Delta$ has an average value of 0.5 $\mu$s in suburban areas and 3 $\mu$s in urban areas. In certain mountain areas, $\Delta$ can be up to 100 $\mu$s [Lee, 1989, 1991]. The set $\{\phi_{kl}\}_{l=1}^{L}$ of random variables are independent uniform random variables over $[0, 2\pi)$, all of which are also statistically independent from each other.

To simulate the Rayleigh random variable $\alpha_k$, we first calculate the corresponding cumulative distribution function as

$$F(\alpha_k) = 1 - e^{-\alpha_k^2/\sigma_r^2} \tag{9}$$

and obtain

$$F^{-1}(x) = \sqrt{-\sigma_r^2 \log(1-x)} \tag{10}$$

If $x$ has the uniform distribution on $[0, 1]$, then $F^{-1}(x)$ has the probability density function as in Eq. (7). This is the basis for simulating Rayleigh random variables in our simulations, whose validity is guaranteed by Theorem 4.6.1 on page 148 of [Groeneveld, 1979].

With the above model, the received composite signal at the central node is given by

$$\begin{aligned} r(t) &= \mathrm{Re}\left\{\sum_{k=1}^{K}\sum_{l=1}^{L}\beta_{kl}c_k(t-\tau_{kl})\exp(-j\phi_{kl}) + \mu(t)\right\} \\ &= \mathrm{Re}\left\{\sum_{k=1}^{K}\sum_{l=1}^{L}\sum_{n=1}^{N}\beta_{kl}a_{k,n}(t-\tau_{kl})\exp[j\omega_{k,n}(t-\tau_{kl}) \right. \\ &\quad \left. + j\theta_{k,n} - j\phi_{kl}] + \mu(t)\right\} \end{aligned} \tag{11}$$

where $\mu(t)$ is a complex-valued white Gaussian noise with one-sided power spectral density $2N_0$.

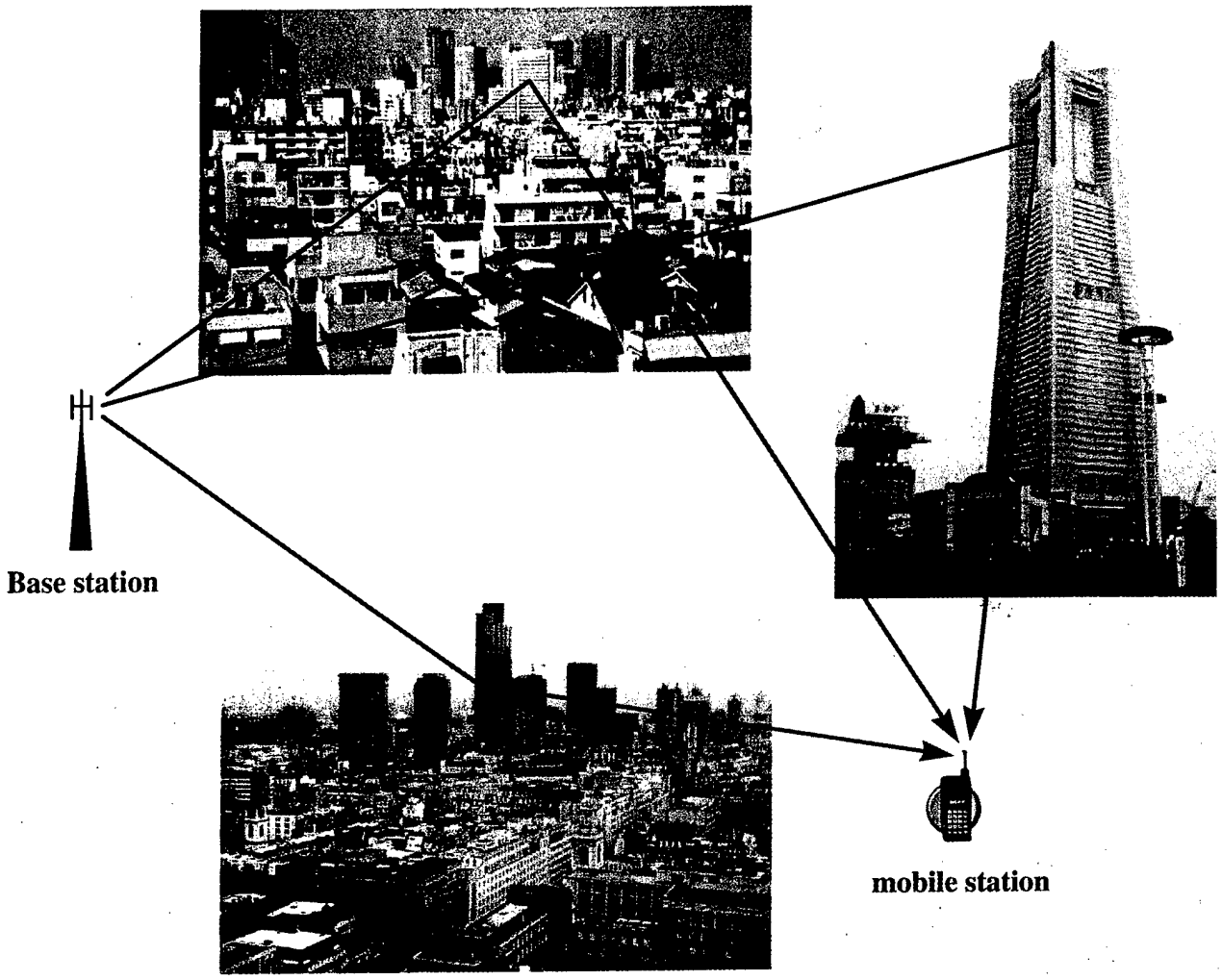


Fig. 10. Multipath fading in wireless $(CD)^2MA$ systems.

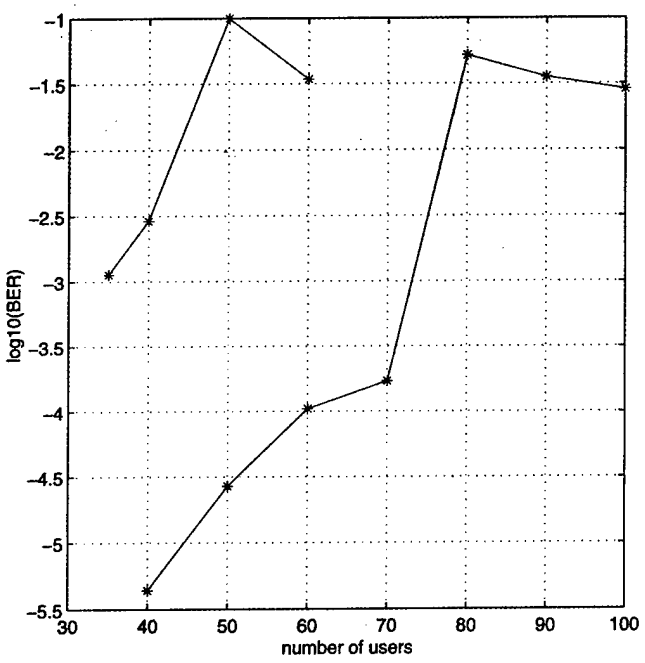


The conditions for our simulation are the same as those of the industrial standard IS-95: the bandwidth is 1.25 MHz, the message signal bit-rate is 9.6 kbps. Since the message bit duration $T_b$ is much bigger than that used in cable systems, $R_I$ can also be increased.

The results of the BER performance with different interleave rates are shown in Fig. 11. The blue curve and the red curve show the results of $R_I = 30$ and $R_I = 20$, respectively.

## 6. Concluding Remarks

The $(CD)^2MA$ system can work under the interleave mode, in which the transmitter needs only

Fig. 11. The BER performance for different interleave rates of $(CD)^2MA$ systems.

to be active for a small portion of the message bit duration. To ensure that the activity duration of each user is distributed uniformly over each symbol bit duration, the base station needs to send a control signal whenever a mobile station is activated in the cell.

Since a big interleave rate can only support many users with low speed data links, a $(CD)^2MA$ system may work in a hybrid mode under which some users use small interleave rates to support high speed data-links, while others use big interleave rates to support a large number of low speed data-links. This provides the $(CD)^2MA$ system with a very good property: in each base station, we can achieve high speed data access, such as downloading images to a mobile computer, and low speed data links, such as cellular phone or text transmission can be included without changing the link prototype. This kind of dynamical load redistribution can distribute the spectrum resource efficiently in a hybrid region such as the downtown of a big city.

In the interleave mode, the transmitted energy from each $(CD)^2MA$ user is much smaller than that used in CDMA systems. This contributes another big advantage for mobile $(CD)^2MA$ users by providing a longer battery life.

## Acknowledgment

This work is supported by the Office of Naval Research under grant No. N00014-96-1-0753.

## References

Groeneveld, R. A. [1979] *An Introduction to Probability and Statistics Using BASIC*, Vol. 26 of Statistics, Textbooks and Monographs (M. Dekker, NY).

Lee, T. H. [1998] *The Design of CMOS Radio-Frequency Integrated Circuits* (Cambridge University Press, Cambridge).

Lee, W. C. Y [1989] *Mobile Cellular Telecommunications Systems* (McGraw-Hill, NY).

Lee, W. C. Y. [1991] "Overview of cellular CDMA," *IEEE Trans. Vehicular Tech.* **40**(2), 291–302.

Mazzini, G., Setti, G. & Rovatti, R. [1997] "Chaotic complex spreading sequences for asynchronous DS-CDMA(I): System modeling and results," *IEEE Trans. Circuits Syst. I: Fundamental Theor. Appl.* **44**(10), 937–947.

Schaller, R. R. [1997] "Moore's law: Past, present and future," *IEEE Spectrum* **34**(6), 52–59.

Viterbi, A. J. [1995] *CDMA: Principles of Spread Spectrum Communication*, Addison-Wesley Wireless Communications Series (Addison-Wesley, Reading, MA).

Wu, C. W., Yang, T. & Chua, L. O. [1996] "On adaptive synchronization and control of nonlinear dynamical systems," *Int. J. Bifurcation and Chaos* **6**(3), 455–471.

Wu, G., Jalali, A. & Mermelstein, P. [1995] "On channel model parameters for microcellular CDMA systems," *IEEE Trans. Vehicular Tech.* **44**(3), 706–711.

Yang, T. & Chua, L. O. [1996] "Secure communication via chaotic parameter modulation," *IEEE Trans. Circuits Syst. I: Fundamental Theor. Appl.* **43**(9), 817–819.

Yang, T. & Chua, L. O. [1996] "Channel-independent chaotic secure communication," *Int. J. Bifurcation and Chaos* **6**(12B), 2653–2660.

Yang, T. & Chua, L. O. [1997] "Chaotic digital code-division multiple access (CDMA) systems," Technical Report memorandum No. UCB/ERL M97/58, Electronics Research Laboratory, College of Engineering, University of California, Berkeley, CA 94720, 3 June 1997.

Yang, T. & Chua, L. O. [1997] "Impulsive stabilization for control and synchronization of chaotic systems: Theory and application to secure communication," *IEEE Trans. Circuits Syst. I: Fundamental Theor. Appl.* **44**(10), 976–988.

Yang, T. & Chua, L. O. [1997] "Chaotic digital code-division multiple access (CDMA) systems," *Int. J. Bifurcation and Chaos* **7**(12), 2789–2805.

Yang, T. & Chua, L. O. [1998] "Applications of chaotic digital code-division multiple access (CDMA) to cable communication systems," *Int. J. Bifurcation and Chaos* **8**(8), 1657–1669.

Yang, T., Wu, C. W. & Chua, L. O. [1997] "Cryptography based on chaotic systems," *IEEE Trans. Circuits Syst. I: Fundamental Theor. Appl.* **44**(5), 469–472.

International Journal of Bifurcation and Chaos, Vol. 8, No. 8 (1998) 1657–1669
© World Scientific Publishing Company

# APPLICATIONS OF CHAOTIC DIGITAL CODE-DIVISION MULTIPLE ACCESS (CDMA) TO CABLE COMMUNICATION SYSTEMS

TAO YANG and LEON O. CHUA
*Electronics Research Laboratory and*
*Department of Electrical Engineering and Computer Sciences,*
*University of California at Berkeley,*
*Berkeley, CA 94720, USA*

Received December 15, 1997; Revised February 24, 1998

In this paper the technical details of chaotic digital code-division multiple access ($(CD)^2MA$) communication systems used in cable communication systems are presented. The cable communication system may be a pure coaxial RF cable network, a hybrid fiber-coax network, or a pure optical fiber network for high-capacity data link. As an example of its many potential applications in cable communication systems, $(CD)^2MA$ is used to support the upstream digital data communications in cable TV systems occupying the very noisy 5–40 MHz portion of spectrum. Although the $(CD)^2MA$ proposed in this paper is only used to support current Internet services via cable TV networks, it can also be used to support the high-speed data-link provided in the 550–750 MHz band in hybrid fiber-coax networks.

$(CD)^2MA$ is a new communication framework which uses band-limited chaotic carriers instead of linear ones. For the purpose of generality, in this paper the band-limited chaotic carriers are approximated by groups of linear sub-carriers, which distribute within the same bandwidth with a fixed amplitude, random phases and uniformly distributed frequencies. The theoretical result of the performance of $(CD)^2MA$ is given. We also provide the simulation results of the bit-error-rate (BER) performances of a synchronous $(CD)^2MA$ used in cable communication systems. The results show that the $(CD)^2MA$ system has a better performance than the synchronous CDMA system proposed for the same cable communication system. Technical details of $(CD)^2MA$ are also presented for the future design of prototype systems. We present the framework of the whole $(CD)^2MA$ system including carrier synchronization, timing recovery and the details of nonlinear carrier generators.

## 1. Introduction

Currently, the main networks connecting American homes to the Internet are telephone lines. However, the twisted pair copper telephone wire cannot provide much more bandwidth than 56 to 64 kbps. For this reason, many American families have to install separate telephone lines for their PCs.

Cable television system is a kind of communication system which was originally designed to broadcast television signals via coaxial RF cables rather than through the air [Baer, 1974]. More than 50 years older, the cable television system has covered almost every corner of North America and Europe. Today, cable TV companies have direct access to more than 63 million U.S. homes. Recently, due to the rapid growth of the Internet market, the functions of cable television systems have been changed from sending only analog television signals to sending both analog television signals *and* digital Internet information. In view of this conceptual change of usage of the cable television system, a brand new television set called *WebTV* (shown in Fig. 1) will

Fig. 1. The outline of a WebTV system.

usher in a new era of television [Tomari *et al.*, 1997], where entertainment and information services are combined into single devices. The main advantage of a cable TV network is its ability to transmit high-bandwidth video, voice and data. Furthermore, a cable TV network integrated with digital information sources can also create new Internet services such as interactive TV programs, high-speed on-line services and videophone services.

Being a mature technical and widespread commercial service, it has become very expensive to upgrade the existing cable TV system. For example, by using optical fibers, the bandwidth of a cable TV system can be enlarged by 50%, from 40–550 MHz to 40–750 MHz. In addition, the optical fiber is more reliable than a coaxial cable. However, even for a small city, it would cost $20 million to upgrade its cable system to fiber-optic lines.

A less costly approach is to keep the hardware framework of the cable TV systems unchanged but exploit optimally the channel capacity of existing networks. One of these methods is *synchronous*

*code division multiple access* (S-CDMA) proposed by Terayon Communication Systems.[1] Terayon's S-CDMA can provide a very robust transmission with a full 10 Mbps per 6 MHz channel upstream and downstream over a fiber-coax cable system. So far, since only a very small portion of the bandwidth, namely 5–40 MHz, can be used to provide two-way, high-speed data links between a subscriber and the Internet, the channel capacity of this portion of spectrum becomes very critical to the service quality for cable subscribers to access the Internet via cable TV networks.

Besides upgrading the cable TV network, a cable modem for converting the data stream to radio frequency should be plugged into a PC. The current price of a cable modem is about \$250 to \$600 [Huffaker, 1995]. Since today's PCs usually include pre-installed modems for accessing the Internet via telephone lines, a user may object to the extra cost of installing the cable modem. To overcome this objection, a cable modem should be cheap enough for the cable TV company to provide each user with a free cable modem at the outset. In designing the application of $(CD)^2MA$ to cable TV Internet services, we must always bear this consideration in mind such that all costly and sophisticated devices are concentrated at the fiber node, or at the head-end, to reduce the expense of the overall network.

We have shown in [Yang & Chua, 1997] that an asynchronous $(CD)^2MA$ technology can double the channel capacity of an asynchronous CDMA system in a wireless communication environment. In this paper, we propose a synchronous $(CD)^2MA$ technology and show that better performance than the S-CDMA can be achieved. Instead of employing a linear carrier, a $(CD)^2MA$ system uses a chaotic carrier. Whenever a chaotic carrier is used the nonlinearity of the channel can be exploited to make the carriers more distinguishable from each other by reducing the correlation of the different chaotic carriers generated by the same chaotic generator structure in different transmitters. For linear communication systems, however, any nonlinearity will change the waveforms of the linear carriers such that it is more difficult to recover the modulated information because the current design principle is to maintain the waveform unchanged all along the channel. Although beautiful theoretical analysis can be formulated in view of the simplicity of linearity, the price a linear communication system must pay is to ensure that *all* devices along the channel are operating only in linear regions. This makes the whole communication system expensive because nonlinearity is wasted as useless excess baggage.

The organization of this paper is as follows. In Sec. 2, the layout of today's cable TV system with Internet service is presented. In Sec. 3, The layout of the $(CD)^2MA$ system used in upstream and downstream cable TV systems is presented. In Sec. 4, the theoretical model of our proposed $(CD)^2MA$ scheme for cable TV systems is given. In Sec. 5, theoretical results on the performance of our $(CD)^2MA$ system are presented. In Sec. 6, a comparison between the performance of the S-CDMA system and the $(CD)^2MA$ system for the 5–40 MHz band in the same cable TV system is presented. Finally, some concluding remarks are given in Sec. 7.

## 2. Cable TV Systems

Figure 2(a) shows the outline of a typical current cable communication system, which is not only a two-way analogue TV broadcast system but a two-way information network. However, unlike telephone networks, a cable TV network is very asymmetric, with over 90% capacity used for downstream and the rest for the upstream. The functional change of cable communication systems from one-way to two-way is driven by the rapid growth of the demand for bandwidth on the Internet. The central node of a cable TV system is the *headend.* Signals from different sources, such as satellite and terrestrial broadcast, Internet, as well as local originating programming, are modulated onto radio frequency carriers and combined together for distribution over the cable system. Supertrunks (high-quality microwave, fiber optic, or cable links) connect the head-end to local distribution centers, known as *hubs.* Several trunks may originate from a hub to provide coverage over a large contiguous area. Figure 2(b) shows a single trunk of a typical cable TV system. Trunk amplifiers are installed along the trunk to maintain the signal level and compensate for cable transmission characteristics. The bridge amplifier serves as a high-quality tap, providing connection between the main trunk and multiple high-level branches. The line extender is a type of amplifier that maintains the signal level along the branch.

[1]At the URL: http://www.terayon.com

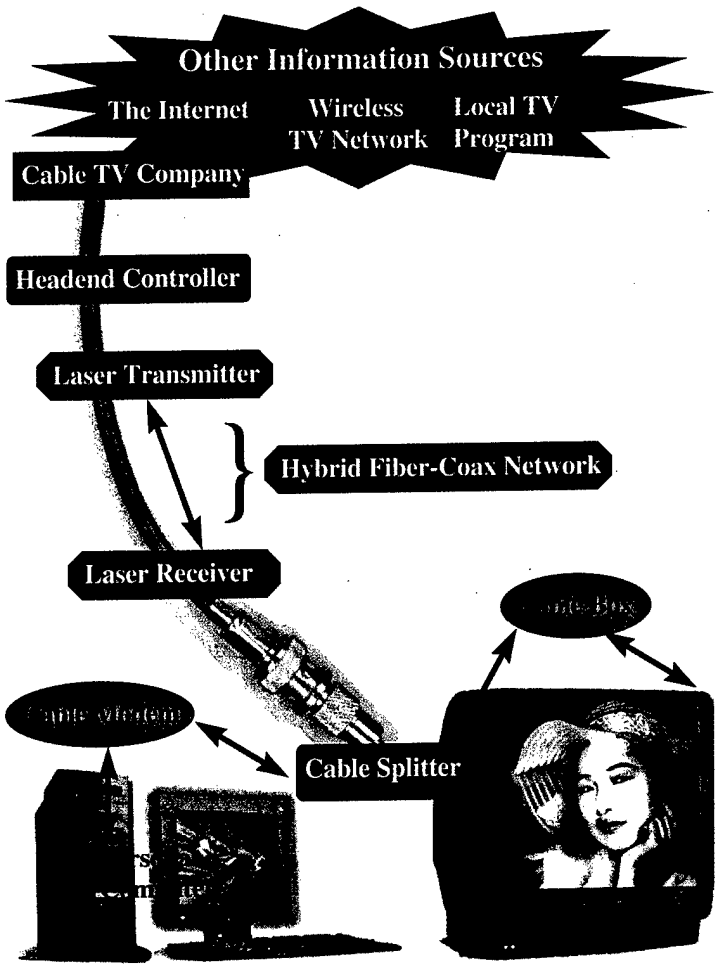


(a)

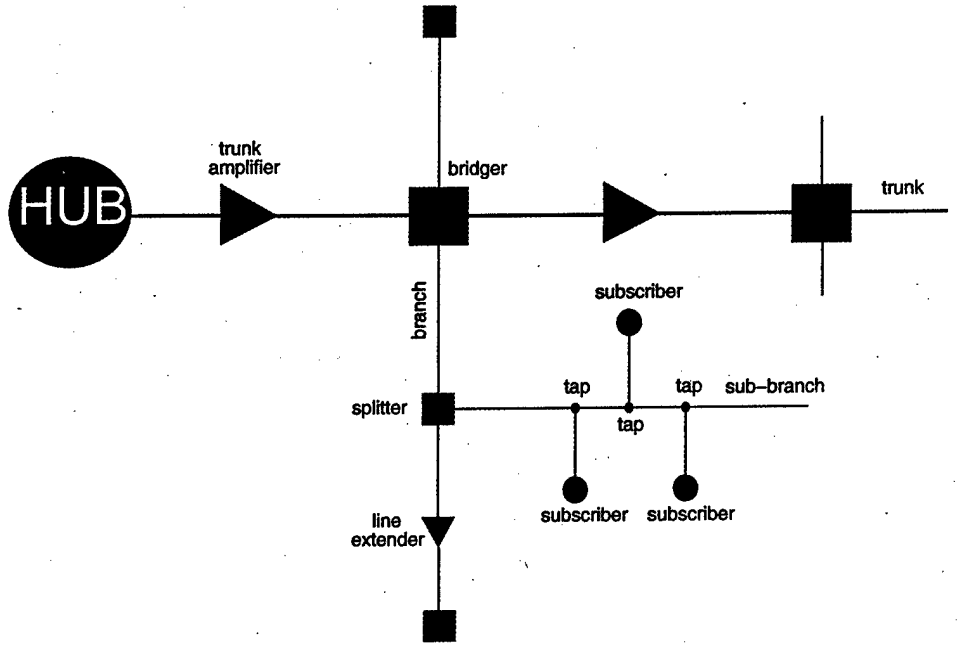


(b)

Fig. 2. The outline of typical current cable communication systems. (a) Block diagram of a typical cable communication system. (b) The block diagram of a single trunk.

The splitter connects a subbranch to a branch. Subscriber drops are connected to passive taps along the subbranch. Many cable TV companies support 500 subscribers per fiber node in hybrid fiber-coax networks [Huffaker, 1995]. If each subscriber has a 64 kbps modem for its PC, then a 32 Mbps per fiber node should be designed for peak hours. However, the available bandwidth is always swamped by more advanced Internet services such as teleconference where real time audio and video data streams are sent.

Technical limitations on channel capacity are set principally by cable amplifiers. The coaxial cable service occupies the 40–550 MHz portion of the spectrum, while the hybrid fiber-coax cable service occupies the 40–750 MHz portion of the spectrum. Since each commercial analog TV channel occupies a 6 MHz bandwidth, a cable TV system may provide up to 100 TV channels. In the future, a fully upgraded hybrid optical-coax cable network may use the 550–750 MHz band to provide digital video, high-speed data and telephone services. In this spectrum band, $(CD)^2MA$ can also find applications. For a two-way cable TV system, the spectrum slot located at 5–40 MHz provides subscribers with an upstream data-link to the outside world through the fiber-coax cable system. Formally, this upstream link can only provide a low speed data-link due to two main noise sources in this spectral slot (shown in Fig. 3). The first is impulsive noise from the electrical devices in PCs, TV sets, hair dryers, vacuum cleaner and etc., as well as vehicle emission systems. The second is narrowband interference picked up by the cable network itself such as Ham radio and Voice of America broadcasts.

In the Terayon S-CDMA system, it was reported that a total capacity of 10 Mbps per 6 MHz channel can be achieved in the 5–40 MHz band. While this represents a big advance in technology, this channel capacity may be too small to match the rapid future growth of demand of the Internet service, accompanied by the occupation of PCs and WebTVs in subscriber homes. Although the soft-degradation of the service quality of current CDMA systems can provide a barely satisfactory

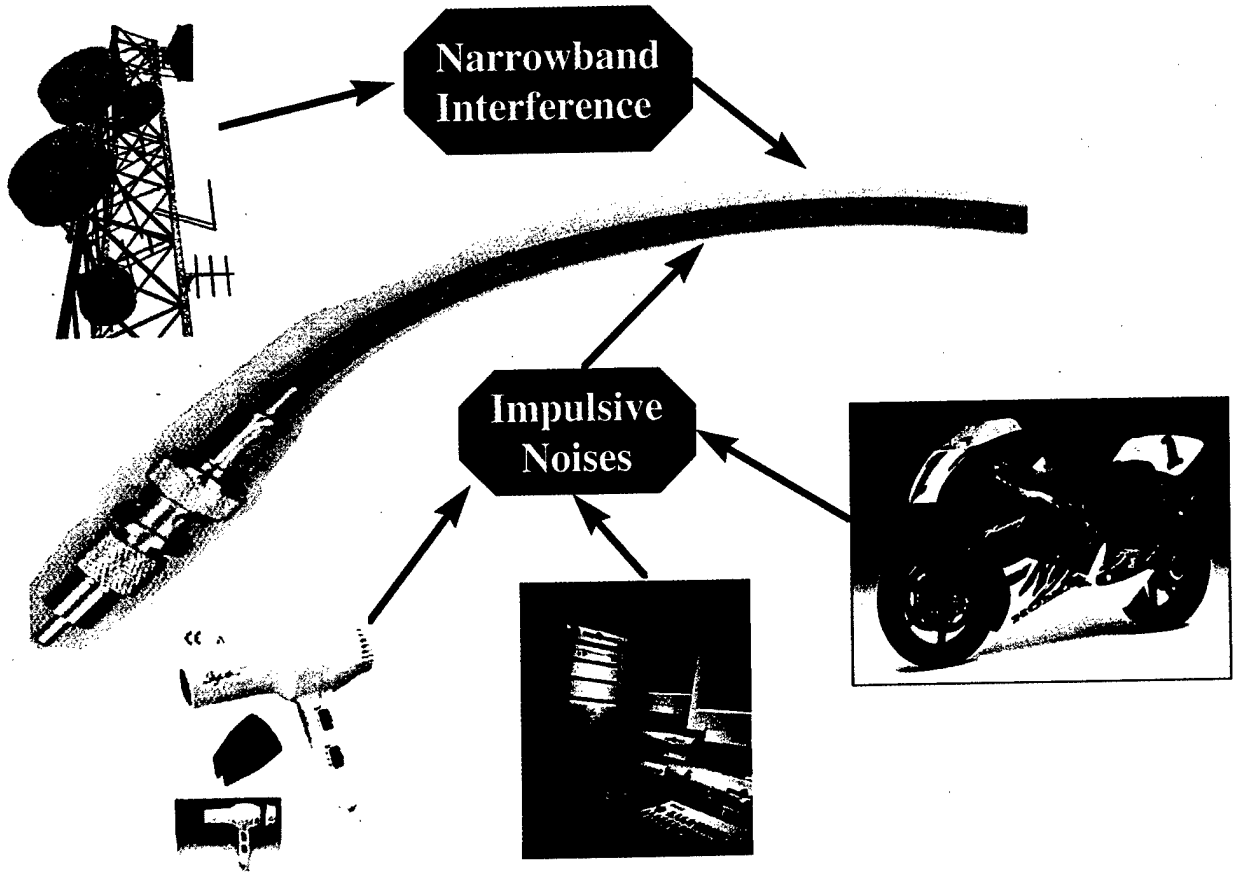


Fig. 3. Two main noise sources in the 5–40 MHz band of a cable TV system.

service to each subscriber during peak periods, such degradation of service can still be felt by subscribers if they are in the process of downloading image files, or some other data-intensive services, such as teleconferencing.

## 3. (CD)²MA for Cable Communication System

The main problems in using the 5–40 MHz band in cable TV systems are impulsive and narrowband noises. The multipath fading problem in wireless environments [Viterbi, 1995] does not occur in cable systems and the delay from each link can be measured *a priori*. Since the price that a subscriber is willing to pay for updating his cable service is relatively low, the transmitter and the receiver of the (CD)²MA system at the subscriber's end should be as simple as possible. The layout of the (CD)²MA transmitter for upstream communication is shown in Fig. 4. Since the hardware structure of a cable communication system is fixed during its operation, each head-end controller can broadcast a local clock signal to synchronize the local clocks of all subscribers under the same headend. The timing recovery in a cable communication system is thus solved.

The chaotic carrier used in the (CD)²MA system can be generated by an array of chaotic digital circuits, such as a "chaotic" (pseudo-chaotic) cellular automata [Toffoli, 1987], or a reversible cellular neural network [Crounse *et al.*, 1996; Yang *et al.*, 1996]. For manufacturing convenience, the hardware for each chaotic digital circuit is chosen to be the same in every transmitter. To ensure that at every moment the chaotic carriers in the same channel are orthogonal to each other, the headend controller must dynamically assign each transmitter a user ID number as the initial states of the digital chaotic generator whenever a subscriber begins sending information. Then, the output of the digital chaotic generator (which may be 8 or 12 bits) is fed into a D/A converter, whose output is sent to a frequency step-up for transferring the chaotic carrier to a different spectral band. Since the D/A converter may work at a clock speed of 1 MHz, we may have to shift this output to some prescribed 6 MHz channel within the 5–40 MHz band.

A frequency step-up is used to transfer the nonlinear carrier to an appropriate spectral band. This is accomplished by a *frequency multiplier*, which consists of a nonlinear circuit followed by a bandpass filter, as shown in Fig. 5(a). While there are many choices for the nonlinear device, the simplest one is a transistor biased in the nonlinear region. The frequency multiplier based on a transistor is shown in Fig. 5(b). If a bandpass signal $v_{\text{in}}(t)$ is fed into a frequency multiplier, the output $v_{\text{out}}(t)$ will appear in a frequency band at the $n$th harmonic of the input frequency(range). However, the multiplication factor $n$ that can be provided by this circuit is usually small with a typical value of 3 or 5 because the nonlinearity of a transistor is too "smooth". To get a large gain, we need to find some device which has much more irregular nonlinearities such as breakpoints.

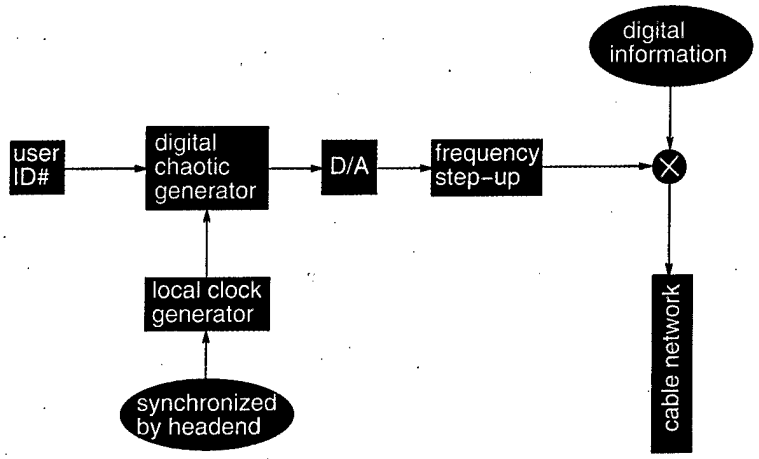


Fig. 4. The block diagram of the upstream transmitter at subscriber's end.

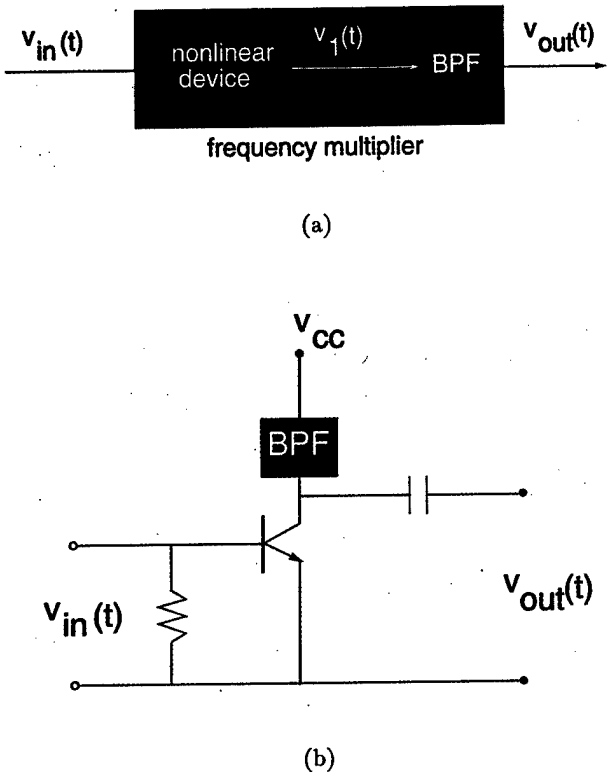


Fig. 5. A frequency multiplier used for the frequency step-up. (a) The block diagram of a frequency multiplier. (b) The circuit implementation of a frequency multiplier.

The block diagram of the receiver at the head-end controller for retrieving the digital signal from the $i$th user is shown in Fig. 6. Since the delay of the $i$th subscriber has been previously measured, the receiver in the headend controller can find the pre-measured time delay from a lookup table and generate the corresponding chaotic carrier with the corresponding delay. The signal received by the cable network is a mixture of noises and interferences from the other subscribers. The received signal is then multiplied by the regenerated carrier at the receiver. The result is low-pass filtered by a $[0, T]$ integrator and then thresholded and sampled to give the recovered digital signal. The timing signal used in sampling is provided by the local clock signal at the head-end controller. This recovered signal is then sent out to the Internet from the headend controller.

The downstream communication is almost the same as that of the upstream except that before the headend sends a chaotic carrier to user $i$, a time delay is compensated at the transmitter end. By doing this, the receiver at the subscriber's end is almost the same as its transmitter except for an additional $[0, T]$ integrator, a thresholding and a sampling circuit. The block digram of the receiver at the

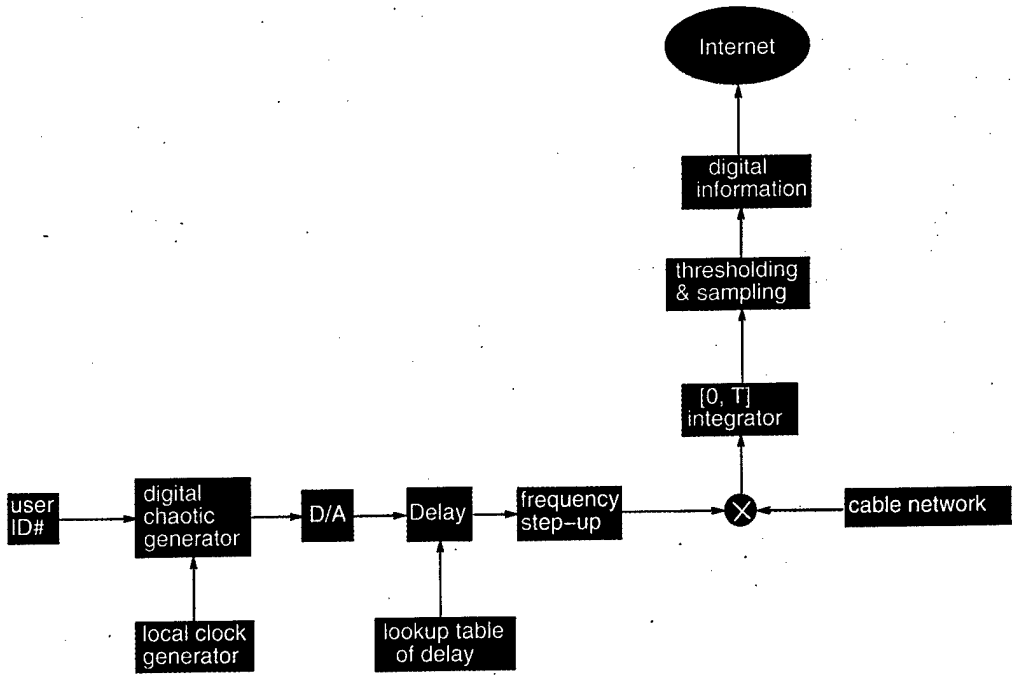


Fig. 6. The block diagram of the receiver at the headend controller for upstream communication.

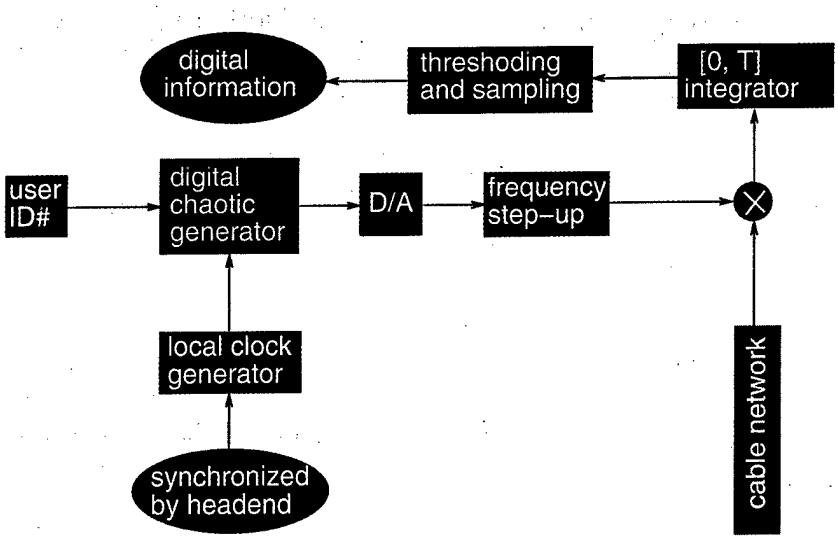


Fig. 7. The block diagram of the receiver at the subscriber's end for downstream communication.

subscriber's end is shown in Fig. 7. Observe that the main part of the transmitter is shared by the receiver. Since the synchronization signal is broadcast through the whole network, the expensive synchronization circuit is not installed in the subscriber's transmitter/receiver. Hence, the additional equipment in the subscriber's home is relatively inexpensive.

Under ideal conditions, the power levels of the chaotic carriers from different users at the fiber node (or the headend) should be the same. This is the power control problem, which had been extensively studied in wireless CDMA systems [Lee, 1989]. However, in view of the fixed hardware structures of cable TV networks, amplifiers can be designed to satisfy this condition. In this paper, perfect power control is assumed.

## 4. Model of Chaotic Digital CDMA Communication Systems

The difference between classical CDMA and $(CD)^2MA$ is that the former uses a pseudo-random digital NRZ signal as a nonlinear sub-carrier and this carrier is then used to modulate a linear carrier for central frequency shift. The latter uses chaotic carriers directly in the desired spectral band. To clarify the difference between them, in this section we present examples to show the different principles used in these two schemes.

Since in $(CD)^2MA$ systems many candidates of chaotic RF waveforms can be used as chaotic carriers, we give a theoretical model for a chaotic carrier which has a flat enough spectrum in the bandwidth we are interested in. The chaotic carrier for the $i$th user is given by

$$c_i(t) = \sum_{n=1}^{N} a_{i,n}(t)\cos(\omega_n t + \theta_{i,n}) = \mathrm{Re}\left\{\sum_{n=1}^{N} a_{i,n}(t)\exp(j\omega_n t + j\theta_{i,n})\right\},\ N \to \infty \tag{1}$$

where $j \triangleq \sqrt{-1}$, and $a_{i,n}(t) \in \Re$, $\omega_n \in$ [prescribed spectral band] and $\theta_{i,n} \in (-\pi, \pi]$ are respectively the amplitude, frequency and phase of the $n$th component of the chaotic carrier. Since $c_i(t)$ is a nonlinear wave, at least one of $a_{i,n}$, $n = 1, \ldots, N$, must be time-varying. Observe that the single tune carrier is a special case of $c_i(t)$ with $a_{il} \neq 0$ and $a_{ij} = 0$ if $j \neq l$ for a given $l$.

Similarly, the carrier for the $j$th user is modeled by

$$c_j(t) = \sum_{n=1}^{N} a_{j,n}(t)\cos(\omega_n t + \theta_{j,n}) = \mathrm{Re}\left\{\sum_{n=1}^{N} a_{j,n}(t)\exp(j\omega_n t + j\theta_{j,n})\right\},\ N \to \infty \tag{2}$$

Since in $(CD)^2MA$ systems, we usually use a $[0, T]$ integrator as the low-pass filter (LPF), the moving

average of the cross-correlation between $c_i(t)$ and $c_j(t)$, $i \neq j$ with time window $T$ is given by

$$
\begin{aligned}
r_{ij}(t) &= \frac{1}{T}\int_{t-T}^{t} c_i(t)c_j(t)dt \\
&= \frac{1}{T}\int_{t-T}^{t} \sum_{n=1}^{N} a_{i,n}(t)\cos(\omega_n t+\theta_{i,n}) \sum_{n=1}^{N} a_{j,n}(t)\cos(\omega_n t+\theta_{j,n})dt \\
&= \frac{1}{T}\int_{t-T}^{t} \sum_{n=1}^{N} a_{i,n}(t)\cos(\omega_n t+\theta_{i,n})a_{j,n}(t)\cos(\omega_n t+\theta_{j,n})dt \\
&\quad + \frac{1}{T}\int_{t-T}^{t} \sum_{n=1}^{N} a_{i,n}(t)\cos(\omega_n t+\theta_{i,n}) \sum_{m=1,\, m\neq n}^{N} a_{j,m}(t)\cos(\omega_m t+\theta_{j,m})dt \\
&= \frac{1}{2T}\int_{t-T}^{t} \sum_{n=1}^{N} a_{i,n}(t)a_{j,n}(t)\cos(\theta_{i,n}-\theta_{j,n})dt + \frac{1}{2T}\int_{t-T}^{t} \sum_{n=1}^{N} a_{i,n}(t)a_{j,n}(t)\cos(2\omega_n t+\theta_{i,n}+\theta_{j,n})dt \\
&\quad + \frac{1}{T}\int_{t-T}^{t} \sum_{n=1}^{N} a_{i,n}(t)\cos(\omega_n t+\theta_{i,n}) \sum_{m=1,\, m\neq n}^{N} a_{j,m}(t)\cos(\omega_m t+\theta_{j,m})dt\,, N\to\infty
\end{aligned}
\tag{3}
$$

Assuming that the phase of each subcomponent of a chaotic carrier is a random variable distributed uniformly over the interval $(-\pi, \pi]$, then $\theta_{i,n}-\theta_{j,n}$ distributes over $(-2\pi, 2\pi)$. Hence, we can choose $T$ large enough so that $r_{ij}(t)$ will be small enough.

In CDMA systems, binary pseudo-random sequences (chip sequences) are used to spread the bandwidth of the modulated signals over the larger transmission bandwidth, *and* to distinguish the different user signals by using the same transmission bandwidth. Then the chip sequence is modulated by a linear sinusoidal waveform using different modulation methods. The most commonly used method is QPSK modulation [Viterbi, 1995]. However, for simplicity and without loss of generality, let us choose the simplest "phase shift" method ("bit 1" shifts the 0 phase of the linear carrier while "bit 0" shifts the $\pi$ phase) for demonstration purposes. The $i$th carrier in a CDMA system is given by

$$
c_i(t) = a_i \cos\left(\omega t + \theta_i + \sum_{k=0}^{[t/T_c]} \psi_i(k)\right) \tag{4}
$$

where the two constants $a_i$ and $\omega$ are respectively the amplitude and frequency of the $i$th carrier; $T_c$ is the chip bit duration defined as the time span of a bit in the chip sequence; $[x]$ denotes the biggest integer less than $x$; and $\psi_i(k)$ is the phase shift caused by the $k$th chip value $p_k$; namely,

$$
\psi_i(k) = \begin{cases} 0, & p_k = 1 \\ \pi, & p_k = 0 \end{cases} \tag{5}
$$

Similarly, the carrier for the $j$th user is given by

$$
c_j(t) = a_j \cos\left(\omega t + \theta_j + \sum_{k=0}^{[t/T_c]} \psi_j(k)\right) \tag{6}
$$

The moving average of the cross-correlation between $c_i(t)$ and $c_j(t)$ with time window $T$ is given by

$$
\begin{aligned}
&r_{ij}(t) \\
&= \frac{1}{T}\int_{t-T}^{t} c_i(t)c_j(t)dt \\
&= \frac{1}{T}\int_{t-T}^{t} a_i \cos\left(\omega t+\theta_i+\sum_{k=0}^{[t/T_c]}\psi_i(k)\right) a_j \\
&\quad \times \cos\left(\omega t+\theta_j+\sum_{k=0}^{[t/T_c]}\psi_j(k)\right) dt \\
&= \frac{1}{2T}\int_{t-T}^{t} a_i a_j \cos\left(\theta_i-\theta_j+\sum_{k=0}^{[t/T_c]}\psi_i(k)-\psi_j(k)\right) dt \\
&\quad + \frac{1}{2T}\int_{t-T}^{t} a_i a_j \cos\left(2\omega t+\theta_i+\theta_j+\sum_{k=0}^{[t/T_c]}\psi_i(k)+\psi_j(k)\right) dt
\end{aligned}
\tag{7}
$$

For both chaotic CDMA and linear CDMA systems, the main goal is to make $r_{ij}(t) \to 0$ whenever $i \neq j$. Comparing Eqs. (3) and (7) we can see that the chaotic CDMA and the linear CDMA achieve this goal by using different strategies. In chaotic CDMA, the goal is to make the term

$$\frac{1}{2T}\int_{t-T}^{t}\sum_{n=1}^{N} a_{i,n}(t)a_{j,n}(t)\cos\left(\theta_{i,n}-\theta_{j,n}\right)dt \qquad (8)$$

as small as possible, but in linear CDMA the goal is to make the term

$$\frac{1}{2T}\int_{t-T}^{t} a_i a_j \cos\left(\theta_i-\theta_j+\sum_{k=0}^{[t/T_c]}\psi_i(k)-\psi_j(k)\right)dt \qquad (9)$$

as small as possible. To reduce the value of Eq. (9) we can reduce the transmitting energy of each carrier (restricted by the noise level), increase $T$ (restricted by the bit-rate of the message signal), increase the bit-rate of the chip sequence (restricted by bandwidth) and make $\psi_i(k) - \psi_j(k)$ as random as possible (restricted by the pseudo-random algorithm for generating the chip sequence).

To reduce the value of Eq. (8) we can also reduce the transmitting energy of each carrier and increase $T$. However, instead of increasing the bit-rate of the chip sequence, we need to use as many sub-carrier components as possible; instead of making $\psi_i(k) - \psi_j(k)$ random, we need to make $\theta_{i,n} - \theta_{j,n}$ random enough. We can then conclude that the main difference between a linear CDMA and a chaotic CDMA is that the former explores the spectrum resource from the time-domain, while the latter does it in the frequency-domain.

## 5. The BER Performance of (CD)²MA

In this section we study the bit-error-rate (BER) performance of (CD)²MA. This is a very important benchmark for measuring service performance. Throughout this section we assume that all signals are at constant power throughout the transmission period.

Suppose $y_i(t)$ is the output of the demodulator of the $i$th user and $x_{i,n}(t)$ is the $n$th bit of the message signal of the $i$th user. As with any digital communication system, spread spectrum or not, there are four components in the demodulator output:

- the desired output, which depends only on $x_{i,n}(t)$;
- the inter-symbol interference components, which depend only on $x_{i,n+m}(t)$, $m \neq 0$;
- the component due to background noise, which we assume to be white with a one-side density equal to $N_0$ watts/Hz;
- the other-user interference components, which depend on $x_{j,n+m}(t)$ for all $i \neq j$ and all $m$.

Let $T_b$ be the bit duration of the message signal, and choose a $[0, T_b]$ integrator as the LPF. Thus,

$$\Gamma = \int_0^{T_b} y_i(t)dt \qquad (10)$$

The sign of this measurement is used to decide whether the message bit is $+1$ or $-1$. The mean of $\Gamma$ is given by

$$\begin{aligned} E[\Gamma] &= \int_0^{T_b} E[y_i(t)|x_{i,n}(t)]dt \\ &= \sqrt{P_i}\int_0^{T_b} x_{i,n}(t)dt \\ &= \pm T_b\sqrt{P_i} \end{aligned} \qquad (11)$$

where $P_i$ is the power of $i$th chaotic carrier. The second equality is satisfied because we have assumed that every signal has constant power throughout the transmission period. Here, the sign depends on the sign of $x_{i,n}(t)$, which is constant over $[0, T_b]$.

Since the noise components are essentially uncorrelated,

$$\begin{aligned} \mathrm{Var}[\Gamma] &= \int_0^{T_b} \mathrm{Var}[y_i(t)|x_{i,n}(t)]dt \\ &= T_b(V_I + V_N + V_O) \end{aligned} \qquad (12)$$

where $V_I$, $V_N$ and $V_O$ are the variances of the inter-symbol interference, background noise and interference from all the other users, respectively.

Then the bit-error-rate (BER) is given by

$$\begin{aligned} \mathrm{BER} &= \Psi\left(\sqrt{\frac{(E[\Gamma])^2}{\mathrm{Var}[\Gamma]}}\right) \\ &= \Psi\left(\sqrt{\frac{T_b P_i}{V_I + V_N + V_O}}\right) \end{aligned} \qquad (13)$$

where

$$\Psi(x) \triangleq \frac{1}{\sqrt{2\pi}}\int_x^{\infty} e^{-s^2/2}ds\,. \qquad (14)$$

Assuming the inter-symbol interference to be negligible or zero, and since the other two components (background white noise and other-user interference) are independent of $x_{i,n}(t)$ for all $i$, it follows that the variance due to background noise is just the effect of a white noise with one-sided density $N_0$ on the receiver filter whose transfer function is $H^*(f)$, and must therefore contribute

$$V_N = (N_0/2)\int_{-\infty}^{\infty} |H(f)|^2 df = N_0/2\,. \quad (15)$$

This is because the filter gain is normalized, so that

$$\int_{-\infty}^{\infty} |H(f)|^2 df = 1\,. \quad (16)$$

To the user $i$ any other user $j$ has a constant carrier power $P_j$ modulated as $c_j(t)x_{j,n}(t)$ which is independent of and generally unsynchronized with that of user $i$. In addition, the carrier phase of the $j$th user's modulator will differ from that of the $i$th user. Hence, the effect of the $j$th user's signal on the $k$th user's demodulator will be that of a white noise with a two-sided density $P_j$ passing through the tandem combination of two filters in the transmitter and the receiver with a combined transfer function $|H(f)|^2$. Hence,

$$V_O = \sum_{j\neq i} \frac{P_j}{2}\int_{-\infty}^{\infty} |H(f)|^4 df\,. \quad (17)$$

It follows from Eqs. (13), (15) and (17) that

$$\mathrm{BER} = \Psi\left(\sqrt{\frac{2T_bP_i}{N_0 + \sum_{j\neq i} P_j\int_{-\infty}^{\infty}|H(f)|^4 df}}\right) \quad (18)$$

The numerator is just twice the bit energy, $E_b$, and the denominator is the effective interference density. Thus,

$$\mathrm{BER} = \Psi\left(\sqrt{\frac{2E_b}{I_0}}\right) \quad (19)$$

where

$$\frac{E_b}{I_0} = \frac{T_bP_i}{N_0 + \sum_{j\neq i} P_j\int_{-\infty}^{\infty}|H(f)|^4 df} \quad (20)$$

Since $(CD)^2MA$ systems are interference limited rather than noise limited, let us ignore the background noise (i.e. $N_0 = 0$) and assume that because of perfect power control, all users are received by the base station (headend or fiber node) receiver at the same power $P_i = P_j = P_c$ for any $i$ and $j$. Then for a given $E_b/I_0$ level, determined from Eq. (19) for the required BER, the maximum number of users, $K_{\max}$, obtained from Eq. (20), is given by

$$K_{\max} - 1 = \frac{1}{E_b/I_0}\frac{T_b}{\int_{-\infty}^{\infty}|H(f)|^4 df} = \frac{1}{E_b/I_0}\frac{W/R}{W\int_{-\infty}^{\infty}|H(f)|^4 df} \quad (21)$$

where $W$ is the bandwidth, $R$ is the bit rate and the integral in the denominator is lower-bounded by unity. Consequently,

$$K_{\max} - 1 \leq \frac{W/R}{E_b/I_0} \quad (22)$$

and the maximum bit-rate, $R_{\max}$, that this channel can support is given by

$$R_{\max} \leq \frac{W}{E_b/I_0} + R \quad (23)$$

For a given BER, the actual $E_b/I_0$ depends on the system design and error-correction code. It may approach but is never equal to the theoretical calculations. In the next section, we use simulation results to find the performance of $(CD)^2MA$ systems.

## 6. Comparison of BER Between S-CDMA and $(CD)^2MA$ Systems

In the upstream, the headend receives all the chaotic carriers from active subscribers, additive impulsive noises and narrowband noises from the cable network. The channel model of the upstream data-link located at the 5–40 MHz band in cable TV systems is only a noisy channel with narrowband interference and random impulsive noise with duration up to 100 $\mu$s. Since multipath fadings usually encountered in wireless mobile communication systems [Lee, 1989] do not occur here, a

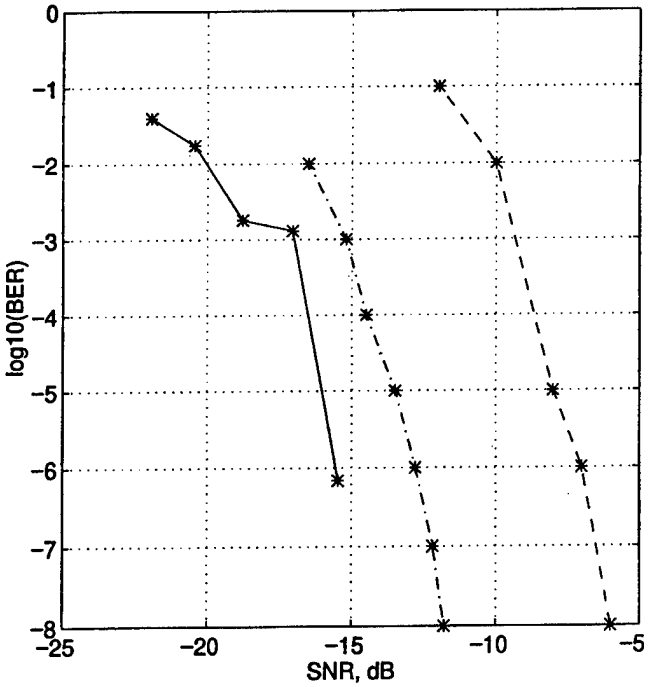


Fig. 8. The BER performance of the $(CD)^2MA$ system used in a cable communication system. The dashed line and the dash-dotted line are the corresponding results of the S-CDMA system under "normal mode" (dashed line) and "fall back mode" (dashdotted line), respectively.

spread spectrum communication system can be used much more easily in this channel than in a wireless communication channel. Furthermore, since the delay in a cable system is a fixed characteristic which can be measured, it is possible to use synchronous spread spectrum communication schemes, such as S-CDMA and synchronous $(CD)^2MA$.

Our simulation results of the $(CD)^2MA$ system are shown in Fig. 8. The solid line shows the BER performance when $N = 200$ sub-carriers are used to model the chaotic carrier of each subscriber. The parameters for the $[0, T]$ integrator at the receivers are chosen as $T = T_b = 1/64$ ms. One should note that the interference from the other users in the same 6 MHz channel is also considered as noise here. For comparison, the results of the Terayon's S-CDMA system in both normal mode and fall back mode are also shown in the same figure. We can see that the performance of $(CD)^2MA$ systems is much better than the S-CDMA scheme in its "fall back mode", which is the best operating mode that the Terayon's S-CDMA scheme can provide.

The quantitative comparison of the channel capacities of the S-CDMA in its fall back mode and the $(CD)^2MA$ is shown in Table 1. From Table 1 we

Table 1. The relationship between the channel capacities of the $(CD)^2MA$ system and the S-CDMA system in its fall back mode.

| BER | $10^{-6}$ | $10^{-5}$ | $10^{-4}$ | $10^{-3}$ | $10^{-2}$ |
|---|---|---|---|---|---|
| Capacity rate: $\frac{(CD)^2MA}{CDMA}$ | 1.50 | 1.50 | 1.40 | 1.35 | 1.41 |

can see that $(CD)^2MA$ can support a much higher bit-rate than S-CDMA when the BER is smaller than $10^{-5}$. A 1.5 times higher bit-rate in this case means that a $(CD)^2MA$ system can support a capacity of 15 Mbps per 6 MHz upstream.

## 7. Conclusions

In this paper, we apply $(CD)^2MA$ to cable communication systems by using the 5–40 MHz band which is very noisy for other narrow band communication schemes, such as the QPSK method. Time division multiple access (TDMA) and frequency division multiple access (FDMA) also cannot be used efficiently in this noisy portion of the spectrum because narrowband interference and long duration impulsive noises can introduce many errors in TDMA and FDMA systems. We also compare our $(CD)^2MA$ system to Terayon's S-CDMA system and found that the $(CD)^2MA$ system can perform much better than the S-CDMA system by increasing the channel capacity 1.5 times more than the best performance by an S-CDMA system.

In this paper, we emphasize the application of our $(CD)^2MA$ on the almost "useless" spectrum band in today's cable TV networks because its potential commercial benefit can easily be realized even without upgrading existing cable TV networks. However, readers should not form the wrong impression that $(CD)^2MA$ can only be used in coaxial networks. In fact, the $(CD)^2MA$ principle can also be used in future high-capacity digital data links based on pure optical fibers to enable a high bandwidth efficiency. On the other hand, since $(CD)^2MA$ systems are interference limited but not dimension-limited, it can provide more flexible performance choices for different services.

## Acknowledgment

This work is supported by the Office of Naval Research under grant No. N00014-97-1-0463.

## References


Baer, W. S. [1974] *Cable Television: Franchising Considerations* (Crane, Russak, NY).

Crounse, K. R., Yang, T. & Chua, L. O. [1996] "Pseudorandom sequence generation using the CNN universal machine with applications to cryptography," in *Proc. Fourth IEEE Int. Workshop on Cellular Neural Networks and Their Applications*, June 24–26, IEEE Catalog Number 96TH8180 and ISBN 0-7803-3261, pp. 433-438.

Huffaker, M. [1995] "Take the coax route [internet access through cable modems]," *Telephony* **229**(22), 44, 46, 48, 50–1, 27.

Lee, W. C. Y. [1989] *Mobile Cellular Telecommunications Systems* (McGraw-Hill, NY).

Toffoli, T. [1987] *Cellular Automata Machines: A New Environment for Modeling* (MIT Press, Cambridge).

Tomari, Y., Saito, M., Okada, N. & Yoshida, R. [1997] "Design and implementation of Internet-TV," *IEEE Trans. Consumer Electron.* **43**(3), 953–960.

Viterbi, A. J. [1995] *CDMA: Principles of Spread Spectrum Communication*, Wireless Communications Series (Addison-Wesley, Reading, MA).

Yang, T. & Chua, L. O. [1997] "Chaotic digital code-division multiple access (CDMA) systems," *Int. J. Bifurcation and Chaos* **7**(12), 2789–2805.

Yang, T., Chua, L. O. & Crounse, K. R. [1996] "Application of discrete-time cellular neural networks to image copyright labeling," in *Proc. Fourth IEEE Int. Workshop on Cellular Neural Networks and Their Applications*, June 24–26, IEEE Catalog Number 96 TH8180 and ISBN 0-7803-3261, pp. 19–24.

International Journal of Bifurcation and Chaos, Vol. 8, No. 7 (1998) 1557–1564
© World Scientific Publishing Company

# IMPULSIVE CONTROL OF NONAUTONOMOUS CHAOTIC SYSTEMS USING PRACTICAL STABILIZATION

TAO YANG
*Electronics Research Laboratory and Department of Electrical Engineering and Computer Sciences, University of California at Berkeley, Berkeley, CA 94720, USA*

JOHAN A. K. SUYKENS
*Katholieke Universiteit Leuven, Department of Electrical Engineering, ESAT-SISTA, Kardinaal Mercierlaan 94, B-3001 Leuven (Heverlee), Belgium*

LEON O. CHUA
*Electronics Research Laboratory and Department of Electrical Engineering and Computer Sciences, University of California at Berkeley, Berkeley, CA 94720, USA*

Received October 30, 1997; Revised March 1, 1998

In this paper, we use the concept of practical stabilization of impulsive differential equations for controlling nonautonomous chaotic systems. Instead of controlling a chaotic system to a point as in the case of asymptotic stabilization, the aim of practical control is to stabilize a chaotic system into a small region of phase space. This method is useful to control a chaotic system into a prescribed region. We present the theory of controlling a nonautonomous chaotic system into a small region around the origin and illustrate the method on Duffing's oscillator.

## 1. Introduction

Often, some well designed asymptotically stable control schemes do not work according to the designer's expectations. The domain of attraction may be very small, some physical parameters may not be included in the mathematical model or there are implementation errors of the controller. A method to overcome this problem is to use the concept of practical stability instead of asymptotic stability. In a practical control problem, one aims at controlling a system into a certain region of interest instead of an exact point. The reason is that measurement instruments for generating feedback signals only have a finite accuracy. If one wants to control a system to an exact point, the expense may be prohibitively high in some cases.

In the case of practical stability one stabilizes a system into a region of the phase space. From a practical point of view, the controlled system is considered to be stable if the fluctuation of states remains within some prescribed bounds. From a mathematical point of view, the equilibrium point may be unstable, but the performance on the other hand is acceptable.

The concept of impulsive control and synchronization of autonomous chaotic systems was first reported in [Amritkar & Gupte, 1993; Stojanovski *et al.*, 1996]. After that, this problem was found closely connected to the theory of impulsive differential equations [Yang *et al.*, 1997a, 1997b]. The rigorous theory of the asymptotic stability of impulsive control and synchronization of autonomous chaotic systems was presented in [Yang *et al.*, 1997a, 1997b; Yang & Chua, 1997a, 1997b, 1997c]. Applications of impulsive synchronization of chaotic systems to chaotic secure communication were

presented in [Stojanovski *et al.*, 1996; Yang & Chua, 1997a, 1997b, 1997c]. An important application of impulsive synchronization to chaotic digital code-division multiple access (CDMA) systems was presented in [Yang & Chua, 1997d, 1997e]. Impulsive control was also used to suppress chaos into periodic motions [Yang *et al.*, 1997c]. In this paper, we study impulsive control of nonautonomous chaotic systems by means of practical stability.

This paper is organized as follows. In Sec. 2 the basic theory of impulsive differential equation on nonautonomous chaotic system is presented. In Sec. 3, the theory of impulsive control of Duffing's Oscillator is presented. In Sec. 4, the simulation results are given and in Sec. 5 the conclusions are stated.

## 2. Basic Theory of Impulsive Differential Equations

Consider a general nonautonomous chaotic system

$$\dot{\mathbf{x}} = \mathbf{f}(t, \mathbf{x}, \mathbf{u}(t)) \tag{1}$$

where $\mathbf{f} : \Re_+ \times \Re^n \times \Re^m \mapsto \Re^n$ is continuous, $\mathbf{x} \in \Re^n$ is the state vector, $\dot{\mathbf{x}} \triangleq \frac{d\mathbf{x}}{dt}$ and $\mathbf{u}$: $\Re_+ \mapsto \Re^m$ is the external input. Consider a set $\{\tau_i\}$ with discrete time instants satisfying

$$0 < \tau_1 < \tau_2 < \cdots < \tau_i < \tau_{i+1} < \cdots,$$
$$\tau_i \to \infty \quad \text{as } i \to \infty.$$

Let

$$U(i, \mathbf{x}) = \Delta\mathbf{x}|_{t=\tau_i} \triangleq \mathbf{x}(\tau_i^+) - \mathbf{x}(\tau_i^-) \tag{2}$$

be a change of the state vector at time instant $\tau_i$, then an impulsively controlled chaotic system is given by

$$\begin{cases} \dot{\mathbf{x}} = \mathbf{f}(t, \mathbf{x}, \mathbf{u}(t)), & t \neq \tau_i \\ \Delta\mathbf{x} = U(i, \mathbf{x}), & t = \tau_i \\ \mathbf{x}(t_0^+) = \mathbf{x}_0, \quad t_0 \geq 0, & i = 1, 2, \ldots \end{cases} \tag{3}$$

which is called an impulsive differential equation in [Lakshmikantham *et al.*, 1989]. In order to study practical stability of the impulsive differential equation in Eq. (3) we use the following definitions [Lakshmikanthan *et al.*, 1989] and theorems.

Since Lyapunov's second method is a powerful tool for studying the stability of dynamic systems, it is also used to study the stability of impulsive differential equations. However, since the inner discontinuous properties of impulsive differential equations, we need a special kind of Lyapunov function which is described by the following definition.

**Definition 1.** Let $V$: $\Re_+ \times \Re^n \mapsto \Re_+$, then $V$ is said to belong to class $\mathcal{V}_0$ if

(1) $V$ is continuous in $(\tau_{i-1}, \tau_i] \times \Re^n$ and for each $\mathbf{x} \in \Re^n$, $i = 1, 2, \ldots$

$$\lim_{(t,\mathbf{y}) \to (\tau_i^+, \mathbf{x})} V(t, \mathbf{y}) = V(\tau_i^+, \mathbf{x}) \tag{4}$$

exists;

(2) $V$ is locally Lipschitzian in $\mathbf{x}$.

In Lyapunov's second method we need to check the derivative of a Lyapunov function along the solutions of the dynamic system. Since the solutions of an impulsive differential equation are discontinuous at $\tau_i$, we need to choose some special derivatives of a Lyapunov function along the solutions of an impulsive differential equation. One of these derivatives can be given by the following definition.

**Definition 2.** For $(t, \mathbf{x}) \in (\tau_{i-1}, \tau_i] \times \Re^n$, we define

$$D^+V(t, \mathbf{x}) \triangleq \lim_{h \to 0^+} \sup \frac{1}{h}[V(t + h, \mathbf{x} + h\mathbf{f}(t, \mathbf{x}, \mathbf{u}(t))) - V(t, \mathbf{x})]. \tag{5}$$

It is usually easy to study the stability of a first-order impulsive differential equation. However, the nonautonomous chaotic systems are at least two dimensional. To simplify the study of the stability of a high dimensional impulsive differential equation, one usually reduces the problem to that of a corresponding one dimensional impulsive differential equation called the comparison system, which is defined in the following way.

**Definition 3** (Comparison System). Let $V \in \mathcal{V}_0$ and assume that

$$\begin{cases} D^+V(t, \mathbf{x}) \leq g(t, V(t, \mathbf{x}), v(t)), & t \neq \tau_i \\ V(t, \mathbf{x} + U(i, \mathbf{x})) \leq \psi_i(V(t, \mathbf{x})), & t = \tau_i \end{cases} \tag{6}$$

where $g$: $\Re_+ \times \Re_+ \times \Re_+ \mapsto \Re$ is continuous and $\psi_i$: $\Re_+ \mapsto \Re_+$ is nondecreasing. Then the system

$$\begin{cases} \dot{w} = g(t, w, v(t)), & t \neq \tau_i \\ w(\tau_i^+) = \psi_i(w(\tau_i)), & i = 1, 2, \ldots \\ w(t_0^+) = w_0 \geq 0 \end{cases} \tag{7}$$

is the comparison system of Eq. (3).

Since the solutions of impulsive differential equations are piecewise continuous, the functions of these solutions are usually also piecewise continuous. We need the following definition to describe this kind of piecewise continuity.

**Definition 4.** $PC(\Re_+ \times \Re^n, \Re_+)$ denotes the set of functions $\chi$: $\Re_+ \times \Re^n \mapsto \Re_+$ which are continuous for $t \in \Re_+$, $t \neq \tau_k$ and are continuous from the left for $t \in \Re_+$. At points $\tau_k$, $\chi$ has a discontinuity of the first kind.

**Definition 5** (Practical Stability). The impulsively controlled system (3) is said to be practically stable if, given $(\lambda, A)$ with $\lambda > 0$ and $A > 0$ are real scalars, we have that $\|\mathbf{x}_0\| < \lambda$ implies $\|\mathbf{x}(t)\| < A$, $t \geq t_0$ for some $t_0 \in \Re_+$ and every $\mathbf{u} \in \Omega$.

*Remark.* Other practical stability notions can be defined based on this definition. See [Lakshmikantham *et al.*, 1990] for details of the standard practical stability notions.

We let

$$S(\rho) = \{\mathbf{x} \in \Re^n | \, \|\mathbf{x}\| < \rho\} \tag{8}$$

where $\|\cdot\|$ denotes Euclidean norm on $\Re^n$.

A function $\alpha$ is said to belong to class $\mathcal{K}$ if $\alpha \in C[\Re_+, \Re_+]$, $\alpha(0) = 0$ and $\alpha(x)$ is strictly increasing in $x$.

We let

$$\Omega = \{\mathbf{u} \in \Re^m | \Gamma(t, \mathbf{u}) \leq r(t), \, t \geq t_0\} \tag{9}$$

where $\Gamma \in C[\Re_+ \times \Re^m, \Re_+]$ and $r(t)$ is the maximal solution of the comparison system (7).

**Theorem 1** ([McRae, 1994] Theorem 3.1, p. 661). *Assume that*

(1) $g \in PC[\Re_+ \times \Re_+ \times \Re_+, \Re_+]$, $g(t, u, v)$ *is nondecreasing in* $u$ *for each* $(t, v)$ *and nondecreasing in* $v$ *for each* $(t, u)$;
(2) $\psi_i$ *is nondecreasing for each* $i$;
(3) $0 < \lambda < A$ (*respectively* $0 < A < \lambda$) *is given*;
(4) $V \in PC[\Re_+ \times \Re^n, \Re_+]$, $V(t, \mathbf{x})$ *is local Lipschitzian in* $\mathbf{x}$, *and there exists* $\alpha, \beta \in \mathcal{K}$ *such that*

$$\begin{aligned} &\beta(\|\mathbf{x}\|) \leq V(t, \mathbf{x}) \leq \alpha(\|\mathbf{x}\|), \\ &(t, \mathbf{x}) \in \Re_+ \times S(\rho), \, \rho > A; \end{aligned} \tag{10}$$

(5) *for* $(t, \mathbf{x}) \in (\tau_i, \tau_{i+1}] \times S(\rho)$ *and* $\mathbf{u}(t) \in \Omega$

$$D^+V(t, \mathbf{x}) \leq g(t, V(t, \mathbf{x}), \Gamma(t, \mathbf{u})); \tag{11}$$

(6) $\mathbf{x} \in S(A)$ *implies* $\mathbf{x} + U(i, \mathbf{x}) \in S(\rho)$ *and* $V(\tau_i^+, \mathbf{x} + U(i, \mathbf{x})) \leq \psi_i(V(t, \mathbf{x}))$, $\mathbf{x} \in S(\rho)$.
(7) $\alpha(\lambda) < \beta(A)$ (*respectively* $\alpha(\lambda) > \beta(A)$).

*Then, the practical stability properties of the comparison system* (7), *with respect to* $(\alpha(\lambda), \beta(A))$, *imply the corresponding practical stability properties of system* (3) *with respect to* $(\lambda, A)$ *for every* $\mathbf{u}(\mathbf{t}) \in \Omega$.

*Remark.* Theorem 1 is very powerful because it translates the stable problem of an $n$th-order impulsive differential equation into that of a first-order impulsive differential equation. In many cases, this translation provides us an easy way for studying stability of a high-order impulsive differential equation. In the next theorem, we present the stability criterion for a first-order impulsive differential equation, which is the general form of the comparison system of impulsively controlled chaotic systems that we study in this paper.

**Theorem 2.** *Suppose* $\Delta_{\max}$ *is the maximum interval between any two successive impulses, i.e.*

$$\Delta_{\max} \triangleq \max_{\forall i} \{\tau_i - \tau_{i-1}\} \tag{12}$$

*For given* $(\lambda, A)$, $(0 < \lambda < A)$ *or* $(0 < A < \lambda)$,

(1) *Let*

$$\begin{aligned} &g(t, w, v) = \phi w + \theta, \; \phi > 0, \; \theta > 0, \quad t \neq \tau_i \\ &\psi_i(w) = d_i w, \; d_i > 0, \quad t = \tau_i, \quad i = 1, 2, \ldots \\ &w(t_0^+) = w_0 \geq 0. \end{aligned} \tag{13}$$

(2)

$$\begin{aligned} &\lambda \prod_{i=1}^{\infty} d_i e^{\phi(t-t_0)} + \theta/\phi \sum_{j=1}^{\infty} \prod_{i=j}^{\infty} d_i |e^{\phi(t-\tau_j)} \\ &\quad - e^{\phi(t-\tau_{j-1})}| + |\theta/\phi(1 - e^{\phi\Delta_{\max}})| < A. \end{aligned} \tag{14}$$

*Then the system* (13) *is practically stable with respect to* $(\lambda, A)$ *for every* $v(t)$.

*Proof.* The solution of the comparison system (13)

is given in [Samoilenko & Perestyuk, 1995]

$$\begin{aligned} w(t, t_0, w_0) &= w_0 \prod_{i=1}^{k} d_i e^{\phi(t-t_0)} \\ &\quad + \theta/\phi \sum_{j=1}^{k} \prod_{i=j}^{k} d_i (e^{\phi(t-\tau_j)} - e^{\phi(t-\tau_{j-1})}) \\ &\quad + \theta/\phi (1 - e^{\phi(t-\tau_k)}) \\ &< w_0 \prod_{i=1}^{k} d_i e^{\phi(t-t_0)} \\ &\quad + \theta/\phi \sum_{j=1}^{k} \prod_{i=j}^{k} d_i |e^{\phi(t-\tau_j)} - e^{\phi(t-\tau_{j-1})}| \\ &\quad + |\theta/\phi (1 - e^{\phi(t-\tau_k)})|, \; t \in (\tau_k, \tau_{k+1}] . \end{aligned} \tag{15}$$

We have

$$|\theta/\phi (1 - e^{\phi(t-\tau_k)})| < |\theta/\phi (1 - e^{\phi \Delta_{\max}})|, \quad t \in (\tau_k, \tau_{k+1}] \tag{16}$$

Since $w_0 < \lambda$ we have $w(t, t_0, w_0) < A$. ■

## 3. Impulsive Control of Duffing's Oscillator

A Duffing's oscillator is given by

$$\begin{aligned} \dot{x} &= y \\ \dot{y} &= x - x^3 - \varepsilon y + \theta \cos(\omega t) . \end{aligned} \tag{17}$$

In this paper, we choose the parameters as: $\varepsilon = 0.25$, $\theta = 0.3$ and $\omega = 1$. The uncontrolled system is a chaotic system whose chaotic attractor is shown in Fig. 1.

The impulsively controlled Duffing's oscillator is given by

$$\left.\begin{aligned} \dot{x} &= y \\ \dot{y} &= x - x^3 - \varepsilon y + \theta \cos(\omega t) \end{aligned}\right\}, \quad t \neq \tau_i ,$$

$$\left.\begin{aligned} x(\tau_i^+) &= d_i x(\tau_i) \\ y(\tau_i^+) &= d_i y(\tau_i) \end{aligned}\right\}, \quad d_i > 0, t = \tau_i \tag{18}$$

To give conditions for practical stability of the impulsively controlled system in Eq. (18), we first construct a comparison system of (18). We then use Proposition 1 to show that the practical stability of the comparison system implies that of (18). Finally, we use Theorem 3 to show that the comparison system is practically stable.

**Proposition 1.** *The practical stability of impulsively controlled Duffing's oscillator in Eq. (18) with respect to* $(\lambda, A)$ *is implied by that of the following comparison system*

$$\begin{aligned} &g(t, w, v) = \phi w + \theta, \; \phi = \max\{1 - \varepsilon, 1 + x^2\}, \quad t \neq \tau_i \\ &\quad \psi_i(w) = d_i w, \; d_i > 0, \quad t = \tau_i, \quad i = 1, 2, \ldots \\ &\quad w(t_0^+) = w_0 \geq 0 \end{aligned} \tag{19}$$

*with respect to* $(\sqrt{2}\lambda, A)$.

*Proof.* Choose a Lyapunov function as [Yang & Yang, 1996]

$$V(t, \mathbf{x}) = |x| + |y| . \tag{20}$$

Then we have

$$\begin{aligned} D^+ V(t, \mathbf{x}) &= \dot{x} \operatorname{sgn}(x) + \dot{y} \operatorname{sgn}(y) \\ &= y \operatorname{sgn}(x) + x \operatorname{sgn}(y) - x^3 \operatorname{sgn}(y) \\ &\quad - \varepsilon |y| + \theta \sin(\omega t) \operatorname{sgn}(y) \\ &\leq (1 - \varepsilon)|y| + (1 + x^2)|x| + |\theta \sin(\omega t)| \\ &\leq \max(1 - \varepsilon, 1 + x^2) V(t, \mathbf{x}) + |\theta| . \end{aligned} \tag{21}$$

Hence

$$\begin{aligned} g(t, w, v) &= \max(1 - \varepsilon, 1 + x^2) w + |\theta| \\ &= \phi w + \theta \end{aligned} \tag{22}$$

where $\phi = \max(1 - \varepsilon, 1 + x^2)$.

Since

$$V(\tau_i^+, \mathbf{x}(\tau_i^+)) = d_i V(\tau_i, \mathbf{x}(\tau_i)) \tag{23}$$

we have $\psi_i(w) = d_i w$.

It is well known that $|x| + |y| \geq \sqrt{x^2 + y^2}$. Since

$$\begin{aligned} 2(x^2 + y^2) &= 2(|x|^2 + |y|^2) \geq |x|^2 + 2|x|\,|y| + |y|^2 \\ &= (|x| + |y|)^2 \end{aligned} \tag{24}$$

we have $|x| + |y| \leq \sqrt{2}\sqrt{x^2 + y^2}$. We then have $\alpha(\chi) = \sqrt{2}\chi$ and $\beta(\chi) = \chi$. We find that all conditions in Theorem 1 are satisfied. ■

**Theorem 3.** *Let* $d_i = d > 0$ *be constant for all* $i = 1, 2, \ldots,$ *the impulses are equidistant with a*

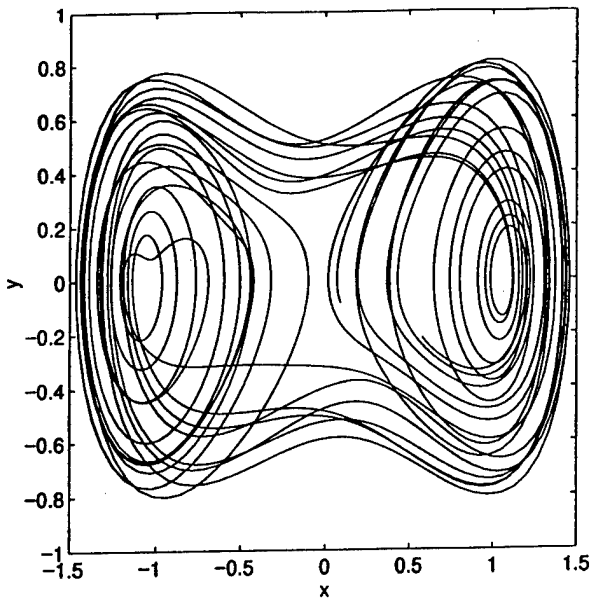


Fig. 1. The chaotic attractor of the uncontrolled Duffing's oscillator.

*fixed interval* $\delta = \tau_{i+1} - \tau_i$ *for all* $i = 1, 2, \ldots,$ *and*

(1)

$$\frac{1}{\delta}\ln(d) + \phi < 0\,, \tag{25}$$

(2)

$$\theta/\phi|1 - e^{\phi\delta}|de^{\phi\delta}\frac{1}{1 - de^{\phi\delta}} + \theta/\phi|1 - e^{\phi\delta}| < A\,,$$

*i.e.*

$$\theta/\phi\frac{|1 - e^{\phi\delta}|}{1 - de^{\phi\delta}} < A\,, \tag{26}$$

*then the impulsively controlled Duffing's oscillator is practically stable with respect to* $(\lambda, A)$ *for any* $\lambda < \infty$.

*Proof.* Let

$$\begin{aligned}\xi(t) &= \left[\frac{t - t_0}{\delta}\right]\ln(d) + \phi(t - t_0)\\ &= \left[\frac{t - t_0}{\delta}\right]\ln(d) + \phi\left\{\delta\left[\frac{t - t_0}{\delta}\right]\right\}\\ &\quad + \phi\left\{(t - t_0) - \delta\left[\frac{t - t_0}{\delta}\right]\right\}\\ &\le \left[\frac{t - t_0}{\delta}\right](\ln(d) + \delta\phi) + \delta\phi \end{aligned} \tag{27}$$

where $[\chi]$ denotes the largest integer less that $\chi$.

Since $1/\delta\ln(d) + \phi < 0$ one has

$$\lim_{t\to\infty}\xi(t) = -\infty \tag{28}$$

such that

$$\begin{aligned}\lim_{t\to\infty}\prod_{i=1}^{k} de^{\phi(t-t_0)} &= \lim_{t\to\infty} e^{\left[\frac{t-t_0}{\delta}\right]\ln(d)+\phi(t-t_0)}\\ &= \lim_{t\to\infty} e^{\xi(t)} = 0\,.\end{aligned} \tag{29}$$

From above, one sees that the first term in Eq. (14) becomes zero for any $\lambda < \infty$.

For $t \in (\tau_k, \tau_{k+1}]$ one has

$$\begin{aligned}&\lim_{k\to\infty}\theta/\phi\sum_{j=1}^{k}\prod_{i=j}^{k} d|e^{\phi(t-\tau_j)} - e^{\phi(t-\tau_{j-1})}|\\ &= \theta/\phi\lim_{k\to\infty}|1 - e^{\phi\delta}|\sum_{j=1}^{k}\prod_{i=j}^{k} de^{\phi(t-\tau_j)}\\ &= \theta/\phi\lim_{k\to\infty}|1 - e^{\phi\delta}|\sum_{j=1}^{k}\prod_{i=j}^{k} de^{\phi(\tau_{k+1}-\tau_j)}\\ &\le \theta/\phi|1 - e^{\phi\delta}|\lim_{k\to\infty}\sum_{j=1}^{k} d^j e^{j\phi\delta}\\ &= \theta/\phi|1 - e^{\phi\delta}|de^{\phi\delta}\frac{1}{1 - de^{\phi\delta}}\,.\end{aligned} \tag{30}$$

The last equation is satisfied if $de^{\phi\delta} < 1$, i.e. $1/\delta\ln(d) + \phi < 0$.

Since $w_0$ can be any finite value, it follows from Theorem 2 that the comparison system is practically stable with respect to $(\sqrt{2}\lambda, A)$ for any $\lambda < \infty$. It follows from Proposition 1 that the impulsively controlled Duffing's oscillator (18) is practically stable with respect to $(\lambda, A)$ for any $\lambda < \infty$. ■

*Remark.* Since $\lambda$ is used to decide the range of initial conditions, Theorem 3 guarantees that no matter how far the initial condition is away from the origin, the impulsively controlled Duffing's oscillator can be practically stabilized around the origin.

## 4. Numerical Experiments

We first study the relation between time interval $\delta$ and $d$ for given values of $A$. If $\theta/\phi > 0$, the

conditions in Eqs. (25) and (26) are reduced to

$$d < e^{-\phi\delta} - \frac{\theta}{A\phi}|1 - e^{-\phi\delta}| \tag{31}$$

which specifies how an increasing value of $\delta$ decreases $d$. From Fig. 1 we see that $-1.5 < x < 1.5$ such that $\phi = 3.25$. By choosing $\theta = 0.3$, the boundaries of practical stability for different values of $A$ are shown in Fig. 2. In Fig. 2 we only show the cases of $A = 0.01$, 0.05, 0.1 and 0.5. The region below the corresponding line is the practically stable region. We see that the lines intersect at the point $(\delta, d) = (0, 1)$. This means that if $d < 1$ is satisfied, we can impulsively control the Duffing's oscillator into any prescribed small region around the origin by choosing $\delta$ small enough. When $A$ approaches 0, the curves approach the open interval on the vertical axis, i.e. $d \in (0, 1)$ and $\delta = 0$.

We then present simulation results to verify the conclusions shown in Fig. 2. The simulation results are show in Fig. 3. The fourth-order Runge–Kutta method with fixed time step 0.01 s is used. The initial condition is $(x(0), y(0)) = (2, -2)$.

In Fig. 3(a) the practically stable result with small objective region is shown. We choose $A = 0.05$. By checking the second curve in Fig. 2, we

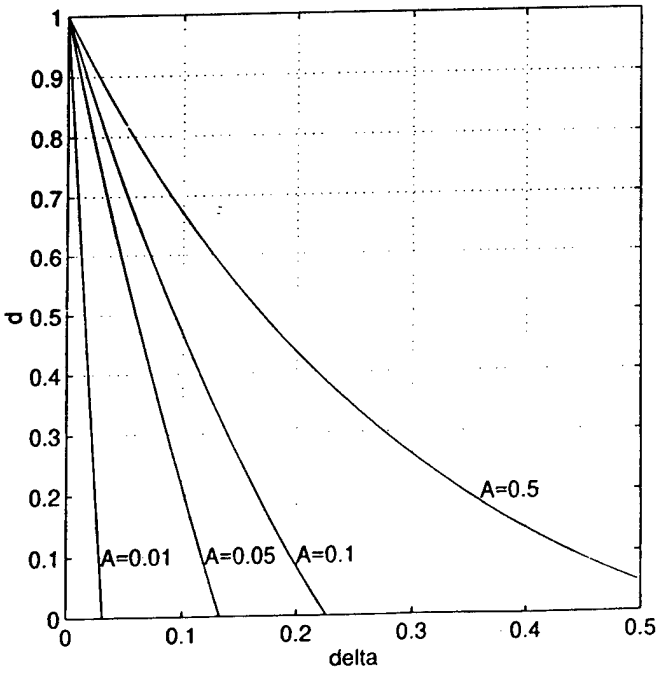


Fig. 2. The regions of practical stability under differ-ent $A$'s.

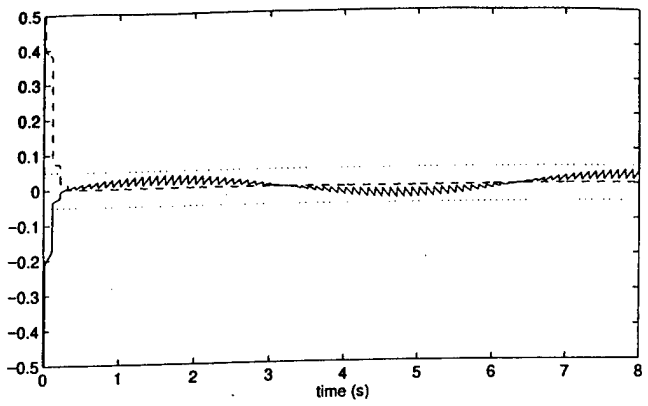


(a)

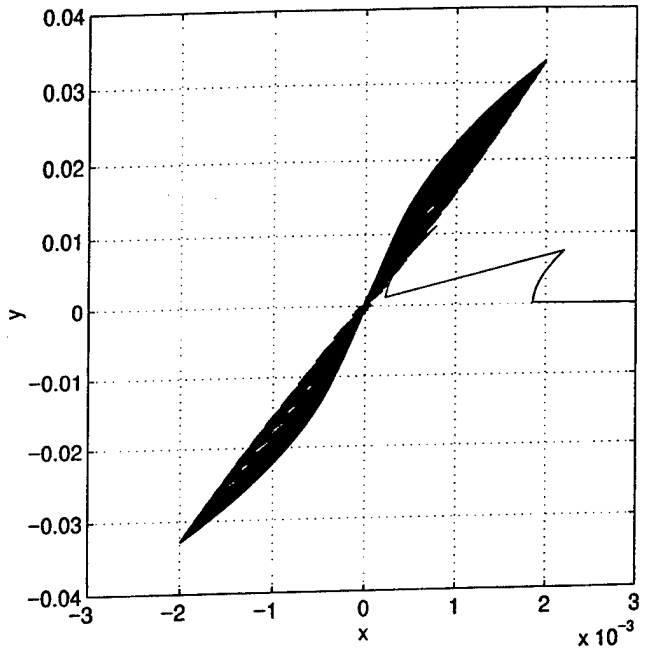


(b)

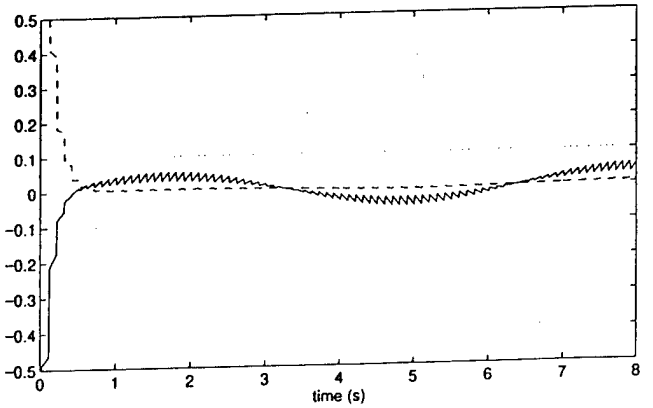


(c)

Fig. 3. The behaviors of the impulsively controlled Duffing's oscillator. (a) Practically stable result with small objective region. (b) $x$–$y$ plot of controlled trajectories. (c) Practically stable result with big objective region.

find the point $(\delta, d) = (0.1, 0.2)$ is in the practically stable region. It means that under this condition, the maximal amplitudes of $x$ and $y$ of the impulsively controlled system are less than 0.05. The dashed line and solid line show $x(t)$ and $y(t)$, respectively. We can see that $x(t)$ approaches 0 though $y(t)$ fluctuates around 0 with a small amplitude. The two horizontal dotted straight lines show the range of the states of the controlled system predicted by Fig. 2. We see that Theorem 3 gives a very good estimate for the range of the states of the controlled system.

Although Theorem 3 guarantees that the controlled trajectory will stay in the neighborhood of the origin, in order to give the reader an idea of the controlled attractor, in Fig. 3(b) we show the $x$–$y$ plot of the controlled trajectories. We find that after the trajectory enters the controlled attractor, it never escapes.

In Fig. 3(c) a practically stable result with large objective region is shown. We choose $A = 0.1$. By checking the third curve in Fig. 2, we find that the point $(\delta, d) = (0.1, 0.4663)$ is in the practically stable region. It means that under this condition, the maximal amplitude of $x$ and $y$ of the impulsive controlled system are smaller than 0.1. The dashed line and solid line show $x(t)$ and $y(t)$, respectively. In this case, we see that $x(t)$ fluctuates around 0 with a visible amplitude and $y(t)$ fluctuates around 0 with a small amplitude. The two horizontal dotted straight lines show the range of the states of the controlled system predicted by Theorem 3.

## 5. Conclusions

In this paper, we studied practical stability of impulsively controlled nonautonomous chaotic systems. Potential applications of the theory presented in this paper are impulsive synchronization and secure communication. There exist two different ways for practical stabilization of a nonautonomous chaotic system. One way is to reduce the interval between control impulses. Another way is to increase the intensity of each impulse. The theory presented in this paper may guide the design of both control schemes quantitatively.

## Acknowledgment

This work is supported by the Office of Naval Research under grant No. N00014-96-1-0753. J. Suykens is postdoctoral researcher with the National Fund for Scientific Research FWO — Flanders. His work is also supported by the Flemish Community in the framework of IUAP P4-02 and GOA-MIPS.

## References

Amritkar, R. E. & Gupte, N. [1993] "Synchronization of chaotic orbits: The effect of a finite time step," *Phys. Rev. E (Statistical Physics, Plasmas, Fluids, and Related Interdisciplinary Topics)*, **47**(6), 3889–3895.

Lakshmikantham, V., Bainov, D. D. & Simeonov, P. S. [1989] *Theory of Impulsive Differential Equations*, Series in Modern Applied Mathematics (World Scientific, Singapore).

Lakshmikantham, V., Leela, S. & Martynyuk, A. A. [1990] *Practical Stability of Nonlinear Systems* (World Scientific, Singapore).

McRae, F. A. [1994] "Practical stability of impulsive control systems," *J. Math. Anal. Appl.* **181**, 656–672.

Samoilenko, A. M. & Perestyuk, N. A. [1995] *Impulsive Differential Equations* (World Scientific, Singapore).

Stojanovski, T., Kocarev, L. & Parlitz, U. [1996] "Driving and synchronizing by chaotic impulses," *Phys. Rev.* **E54**(2), 2128–2131.

Yang, T., Yang, L.-B. & Yang, C.-M. [1997] "Impulsive synchronization of Lorenz systems," *Phys. Lett.* **A226**(6), 349–354.

Yang, T., Yang, L.-B. & Yang, C.-M. [1997] "Impulsive control of Lorenz system," *Physica* **D110**, 18–24.

Yang, T. & Chua, L. O. [1997] "Impulsive control and synchronization of chaotic systems and secure communication," Memorandum UCB/ERL M97/12, Electronics Research Laboratory, College of Engineering, University of California, Berkeley, CA 94720, 29 January.

Yang, T. & Chua, L. O. [1997] "Impulsive control and synchronization of nonlinear dynamical systems and application to secure communication," *Int. J. Bifurcation and Chaos* **7**(3), 645–664.

Yang, T. & Chua, L. O. [1997] "Impulsive stabilization for control and synchronization of chaotic systems: Theory and application to secure communication," *IEEE Trans. Circuits Syst. I: Fundamental Theor. Appl.* **44**(10), 976–988.

Yang, T. & Chua, L. O. [1997] "Chaotic digital code-division multiple access (CDMA) systems," *Int. J. Bifurcation and Chaos* **7**(12), 2789–2805.

Yang, T. & Chua, L. O. [1997] "Chaotic digital code-division multiple access (CDMA) systems," Memorandum UCB/ERL M97/58, Electronics

Research Laboratory, College of Engineering, University of California, Berkeley, CA 94720.

Yang, T., Yang, L.-B. & Yang, C.-M. [1997] "Control of Rössler system to periodic motions using impulsive control methods," *Phys. Lett.* **A232**(5), 356–361.

Yang, T. & Yang, L. B. [1996] "The global stability of fuzzy cellular neural network," *IEEE Trans. Circuits Syst. I: Fundamental Theor. Appl.* **43**(10), 880–883.

International Journal of Bifurcation and Chaos, Vol. 8, No. 6 (1998) 1371–1381
© World Scientific Publishing Company

# IMPULSIVE SYNCHRONIZATION OF CHAOTIC LUR'E SYSTEMS BY MEASUREMENT FEEDBACK

J. A. K. SUYKENS*
*Katholieke Universiteit Leuven,*
*Department of Electrical Engineering, ESAT-SISTA,*
*Kardinaal Mercierlaan 94, B-3001 Leuven (Heverlee), Belgium*

T. YANG† and L. O. CHUA‡
*Department of Electrical Engineering and Computer Sciences,*
*University of California at Berkeley, Berkeley, CA 94720, USA,*

Received October 30, 1997; Revised February 20, 1998

In this paper we consider impulsive control of master-slave synchronization schemes that consist of identical Lur'e systems. Impulsive control laws are investigated which make use of linear or nonlinear dynamic measurement feedback. A sufficient condition for global asymptotic stability is presented which is characterized by a set of matrix inequalities. Synchronization is proven for the error between the output signals. The method is illustrated on Chua's circuit and a hyperchaotic system with coupled Chua's circuits.

## 1. Introduction

Recently, methods for synchronization of nonlinear systems have been proposed which make use of impulsive control laws [Yang & Chua, 1997a, 1997b; Yang *et al.*, 1997; Stojanovski *et al.*, 1996, 1997]. In this way the error system of the synchronization scheme is stabilized using small control impulses. These methods are offering a direct method for modulating digital information onto a chaotic carrier signal for spread spectrum applications [Wu & Chua, 1997] and has been applied to chaotic digital code-division multiple access (CDMA) systems in [Yang & Chua, 1997c]. The method discussed in [Yang & Chua, 1997a, 1997b; Yang *et al.*, 1997] is based on a theory of impulsive differential equations described in [Lakshmikantham *et al.*, 1989]. At discrete time instants, jumps in the system's state are caused by a control input. Global asymptotic stability of the error system is proven by means of a Lyapunov function and is characterized by a set of conditions related to the time instants, the time intervals in between and a coupling condition between these.

However, so far the method has been applied ad hoc to the special cases of Chua's circuit [Yang & Chua, 1997a, 1997b] and the Lorenz system [Yang *et al.*, 1997]. Moreover full state information has been assumed, which means that knowledge of the full state vector of the system is needed in order to synchronize the systems by impulses. The aim of this paper is to present a general design procedure for master-slave synchronization schemes

*Author to whom correspondence should be addressed. E-mail: johan.suykens@esat.kuleuven.ac.be
†E-mail: taoyang@fred.eecs.berkeley.edu
‡E-mail: chua@fred.eecs.berkeley.edu

which consist of identical Lur'e systems [Khalil, 1992; Suykens *et al.*, 1996; Vidyasagar, 1993]. Examples of chaotic and hyperchaotic Lur'e systems are Chua's circuit [Chua *et al.*, 1986; Chua, 1994; Madan, 1993], generalized Chua's circuits that exhibit $n$-scroll attractors [Suykens *et al.*, 1997b] and arrays which consist of such chaotic cells [Kapitaniak & Chua, 1994; Suykens & Chua, 1997]. In practice the full state vector is often not available, not measurable or too expensive to measure. Therefore we investigate the case of measurement feedback for which we derive a sufficient condition of global asymptotic stability of the error system. This error is defined between the outputs (instead of states) of the master and slave system. For the sake of generality we study a nonlinear dynamic output feedback law where the state equation of the controller takes the form of a Lur'e system. This impulsive control law includes static output feedback and linear dynamic output feedback as special cases. The latter method has been discussed in [Suykens *et al.*, 1997a] for a continuous control law. The conditions for synchronization have been expressed as a matrix inequalities [Boyd *et al.*, 1994], which also occur in the context of nonlinear $H_\infty$ synchronization methods for secure communications applications [Suykens *et al.*, 1997c]. The design of the controller is done then by solving a nonlinear optimization problem which involves the matrix inequality. A similar approach is followed in this paper for the impulsive control case.

We illustrate the method on Chua's circuit and a hyperchaotic system with coupled Chua's circuits that exhibits the double–double scroll attractor [Kapitaniak & Chua, 1994]. Two identical Chua's circuits are impulsively synchronized by a linear dynamic output controller of first order where one state variable is measured on the circuits and one single control input is taken. While synchronization is theoretically proven for the difference between the measured state variables, the complete state vectors are synchronizing as well according to the simulation results. In another example it is shown how two double–double scroll attractors can be synchronized by measuring only one state variable and taking one single control input. In this case however, the synchronization is occurring for the output but not for the full state vector. Synchronization for the full state vector is obtained by a linear dynamic output feedback controller with two outputs and two control inputs (one for each of the two cells).

This paper is organized as follows. In Sec. 2 we present the master–slave synchronization scheme with impulsive control. In Sec. 3 the matrix inequalities are derived and controller design is discussed. In Sec. 4 examples are given.

## 2. Synchronization Scheme

We consider the following master–slave synchronization scheme

$$
\begin{aligned}
\mathcal{M}: &\begin{cases} \dot{x} = Ax + B\sigma(Cx) \\ p = Lx \end{cases} \\
\mathcal{S}: &\begin{cases} \dot{z} = Az + B\sigma(Cz), & t \neq \tau_i \\ q = Lz \end{cases} \\
\mathcal{C}: &\begin{cases} \dot{\xi} = E\xi + F(p-q) + W_F\sigma(V_{F_1}\xi + V_{F_2}(p-q)), & t \neq \tau_i \\ \Delta z = D_1 u, & t = \tau_i \\ \Delta\xi = D_2 v, & t = \tau_i \\ u = G_1\xi + H_1(p-q) \\ v = G_2\xi + H_2(p-q) \end{cases}
\end{aligned}
\tag{1}
$$

which consists of master system $\mathcal{M}$, slave system $\mathcal{S}$ and controller $\mathcal{C}$. $\mathcal{M}$ and $\mathcal{C}$ are identical Lur'e system with state vectors $x, z \in \mathbb{R}^n$ and matrices $A \in \mathbb{R}^{n\times n}$, $B \in \mathbb{R}^{n\times n_h}$, $C \in \mathbb{R}^{n_h\times n}$. A Lur'e system is a linear dynamical system, feedback interconnected to a static nonlinearity $\sigma(\cdot)$ that satisfies a sector condition [Khalil, 1992; Vidyasagar, 1993] (here it has been represented as a recurrent neural network with one hidden layer, activation function $\sigma(\cdot)$ and $n_h$ hidden units [Suykens *et al.*, 1996]). We assume that $\sigma(\cdot) : \mathbb{R}^{n_h} \mapsto \mathbb{R}^{n_h}$ is a diagonal

nonlinearity with $\sigma_i(\cdot)$ belonging to sector $[0, k]$ for $i = 1, \ldots, n_h$. The output (or measurement) vectors of $\mathcal{M}$ and $\mathcal{S}$ are $p, q \in \mathbb{R}^l$ with $l \leq n$ and $L \in \mathbb{R}^{l \times n}$.

For the impulsive control law $\mathcal{C}$, a set of discrete time instants $\tau_i$ is considered where $0 < \tau_1 < \tau_2 < \cdots < \tau_i < \tau_{i+1} < \cdots$ with $\tau_i \to \infty$ as $i \to \infty$ [Lakshmikantham *et al.*, 1989; Yang & Chua, 1997a, 1997b; Yang *et al.*, 1997]. For the sake of generality, a nonlinear dynamic output feedback controller of Lur'e form is taken here for the state equation with state vector $\xi \in \mathbb{R}^{n_\xi}$. At the time instants $\tau_i$, jumps in the state variables $z$ and $\xi$ are imposed

$$\begin{aligned} \Delta z|_{t=\tau_i} &= z(\tau_i^+) - z(\tau_i^-) \\ \Delta \xi|_{t=\tau_i} &= \xi(\tau_i^+) - \xi(\tau_i^-)\,. \end{aligned} \tag{2}$$

By means of the matrices $D_1$ and $D_2$, the state equations on which the impulsive controls $u \in \mathbb{R}^{m_z}$ and $v \in \mathbb{R}^{m_\xi}$ are applied, are decided upon. The output difference $p - q$ is taken as input of the controller $\mathcal{C}$. The matrices of the controller are of dimension $E \in \mathbb{R}^{n_\xi \times n_\xi}$, $F \in \mathbb{R}^{n_\xi \times l}$, $W_F \in \mathbb{R}^{n_\xi \times n_{h_\xi}}$, $V_{F_1} \in \mathbb{R}^{n_{h_\xi} \times n_\xi}$, $V_{F_2} \in \mathbb{R}^{n_{h_\xi} \times l}$, $D_1 \in \mathbb{R}^{n_z \times m_z}$, $D_2 \in \mathbb{R}^{n_\xi \times m_\xi}$, $G_1 \in \mathbb{R}^{m_z \times n_\xi}$, $G_2 \in \mathbb{R}^{m_\xi \times n_\xi}$, $H_1 \in \mathbb{R}^{m_z \times l}$, $H_2 \in \mathbb{R}^{m_\xi \times l}$ where $n_{h_\xi}$ is the number of hidden units in the Lur'e system of $\mathcal{C}$. Note that the control law also includes the cases of static output feedback ($G_1 = 0$, $G_2 = 0$) and linear dynamic output feedback ($W_F = 0$, $V_{F_1} = 0$, $V_{F_2} = 0$).

Given the synchronization scheme (1), the synchronization error is defined as $e = x - z$ for the state vectors and $e_L = p - q = Le$ for the outputs. The first case yields the error system

$$\mathcal{E}_1 : \begin{cases} \dot{e} &= Ae + B\eta(Ce; z), & t \neq \tau_i \\ \dot{\xi} &= E\xi + F(p-q) + W_F\sigma(V_{F_1}\xi + V_{F_2}(p-q)), & t \neq \tau_i \\ \Delta e &= -D_1 u, & t = \tau_i \\ \Delta \xi &= D_2 v, & t = \tau_i \\ u &= G_1\xi + H_1(p-q) \\ v &= G_2\xi + H_2(p-q) \end{cases} \tag{3}$$

where $\eta(Ce; z) = \sigma(Ce + Cz) - \sigma(Cz)$ and $\Delta e = \Delta x - \Delta z$ with $\Delta x = 0$ for the master system. The error system for $e_L$ becomes

$$\mathcal{E}_2 : \begin{cases} \dot{e}_L &= LAe + LB\eta(Ce; z), & t \neq \tau_i \\ \dot{\xi} &= E\xi + F(p-q) + W_F\sigma(V_{F_1}\xi + V_{F_2}(p-q)), & t \neq \tau_i \\ \Delta e_L &= -LD_1 u, & t = \tau_i \\ \Delta \xi &= D_2 v, & t = \tau_i \\ u &= G_1\xi + H_1(p-q) \\ v &= G_2\xi + H_2(p-q) \end{cases} \tag{4}$$

with $\Delta e_L = -L\Delta z$. This scheme will be studied in the sequel.

## 3. Stability, Matrix Inequalities and Controller Design

In order to derive a sufficient condition for global asymptotic stability of the error system $\mathcal{E}_2$, we take the Lyapunov function

$$V(e_L, \xi) = \zeta^T P \zeta = [e_L^T \quad \xi^T] \begin{bmatrix} P_{11} & P_{12} \\ P_{21} & P_{22} \end{bmatrix} \begin{bmatrix} e_L \\ \xi \end{bmatrix}, \quad P = P^T > 0\,. \tag{5}$$

According to Lakshmikantham *et al.* [1989], Yang and Chua [1997a, 1997b] and Yang *et al.* [1997] it is sufficient then to prove that

$$\begin{cases} \dot{V} \leq \alpha V, & \alpha > 0, \quad t \neq \tau_i & \text{(6a)} \\ V(\zeta + \Delta\zeta) < \beta V, & \beta > 0, \quad t = \tau_i & \text{(6b)} \\ \|\zeta + \Delta\zeta\|_2 < \|\zeta\|_2, & t = \tau_i & \text{(6c)} \\ \alpha(\tau_{i+1} - \tau_i) + \log\beta < 0\,. & & \text{(6d)} \end{cases}$$

From Eq. (6d) we find that $\beta < 1$ should be satisfied. We will express the conditions (6a)–(6c) now as matrix inequalities. In the derivation we exploit the inequalities

$$\begin{cases} \eta(Ce)^T \Lambda[\eta(Ce) - Ce] \leq 0, & \forall e \in \mathbb{R}^n \\ \sigma(\varphi)^T \Gamma[\sigma(\varphi) - V_{F_1}\xi - V_{F_2} Le] \leq 0, & \forall e \in \mathbb{R}^n,\ \xi \in \mathbb{R}^{n_\xi}\,. \end{cases} \tag{7}$$

These are related to the sector conditions on the nonlinearities $\eta(\cdot)$ and $\sigma(\cdot)$, which are assumed to belong to sector $[0, 1]$. $\Lambda$ and $\Gamma$ are diagonal matrices with positive diagonal elements and $\varphi = V_{F_1}\xi + V_{F_2} Le$. By employing (7) in an application of the $S$-procedure [Boyd *et al.*, 1994] a matrix inequality is obtained by writing

$$\dot{V} - \alpha V - 2\eta(Ce)^T \Lambda[\eta(Ce) - Ce] - 2\sigma(\varphi)^T \Gamma[\sigma(\varphi) - V_{F_1}\xi - V_{F_2} Le] \leq 0 \tag{8}$$

as a quadratic form $w^T Z w \leq 0$ in $w = [e;\ \xi;\ \eta;\ \sigma]$. Imposing this quadratic form to be negative semidefinite for all $w$, one obtains

$$Z = Z^T = \begin{bmatrix} Z_{11} & Z_{12} & Z_{13} & Z_{14} \\ \cdot & Z_{22} & Z_{23} & Z_{24} \\ \cdot & \cdot & Z_{33} & 0 \\ \cdot & \cdot & \cdot & Z_{44} \end{bmatrix} \leq 0 \tag{9}$$

with

$$\begin{aligned} Z_{11} &= A^T P_{11} L + L^T P_{11} A + L^T P_{12} F L \\ &\quad + L^T F^T P_{21} L - \alpha L^T P_{11} L \\ Z_{22} &= E^T P_{22} + P_{22} E - \alpha P_{22} \\ Z_{33} &= -2\Lambda \\ Z_{44} &= -2\Gamma \end{aligned} \qquad \begin{aligned} Z_{12} &= A^T P_{12} + L^T P_{12} E + L^T F^T P_{22} - \alpha L^T P_{12} \\ Z_{13} &= L^T P_{11} L B + C^T \Lambda \\ Z_{14} &= L^T P_{12} W_F + L^T V_{F_2}^T \Gamma \\ Z_{23} &= P_{21} L B \\ Z_{24} &= P_{22} W_F + V_{F_1}^T \Gamma\,. \end{aligned}$$

In order to express the other conditions (6b) and (6c) as matrix inequalities, we write

$$\zeta + \Delta\zeta = \begin{bmatrix} e_L \\ \xi \end{bmatrix} + \begin{bmatrix} \Delta e_L \\ \Delta\xi \end{bmatrix} = M \begin{bmatrix} e_L \\ \xi \end{bmatrix} \tag{10}$$

with

$$M = \begin{bmatrix} I - LD_1 H_1 & -LD_1 G_1 \\ D_2 H_2 & I + D_2 G_2 \end{bmatrix}.$$

This yields the matrix inequality

$$M^T P M < \beta P \tag{11}$$

for (6b) and

$$M^T M < I \tag{12}$$

for (6c). The latter matrix inequality is the underlying reason why we derived synchronization criteria for the error system $\mathcal{E}_2$ instead of $\mathcal{E}_1$, because it turns out that for $\mathcal{E}_1$ the condition (6c) leads to infeasibility.

The controller design is based then on the matrix inequalities (9), (11) and (12) by solving the feasibility problem

$$\text{Find} \quad \theta_c,\ Q,\ \Lambda,\ \Gamma,\ \alpha,\ \beta$$

$$\text{such that} \quad \begin{cases} Z \leq 0 \\ M^T P M < \beta P \\ M^T M < I \\ \alpha(\tau_{i+1} - \tau_i) + \log\beta < 0 \end{cases} \tag{13}$$

with $P = Q^T Q$ and the controller parameter vector $\theta_c$ containing the elements of the matrices $E$, $F, W_F, V_{F_1}, V_{F_2}, G_1, H_1, G_2, H_2$. This problem has to be solved for given matrices $A$, $B$, $C$, $L$, $D_1$, $D_2$ and a fixed choice of the time interval $\tau_{i+1} - \tau_i$.

## 4. Examples

In this section we illustrate the method on Chua's circuits and coupled Chua's circuits that exhibit the double–double scroll attractor.

### 4.1. *Chua's circuit*

We consider master–slave synchronization of two identical Chua's circuits by means of impulsive control. We take the following representation of Chua's circuit for the master system $\mathcal{M}$:

$$\begin{cases} \dot{x}_1 = a[x_2 - h(x_1)] \\ \dot{x}_2 = x_1 - x_2 + x_3 \\ \dot{x}_3 = -bx_2 \end{cases} \tag{14}$$

with nonlinear characteristic

$$h(x_1) = m_1 x_1 + \frac{1}{2}(m_0 - m_1)(|x_1 + c| - |x_1 - c|) \tag{15}$$

and parameters $a = 9$, $b = 14.286$, $m_0 = -1/7$, $m_1 = 2/7$ in order to obtain the double scroll

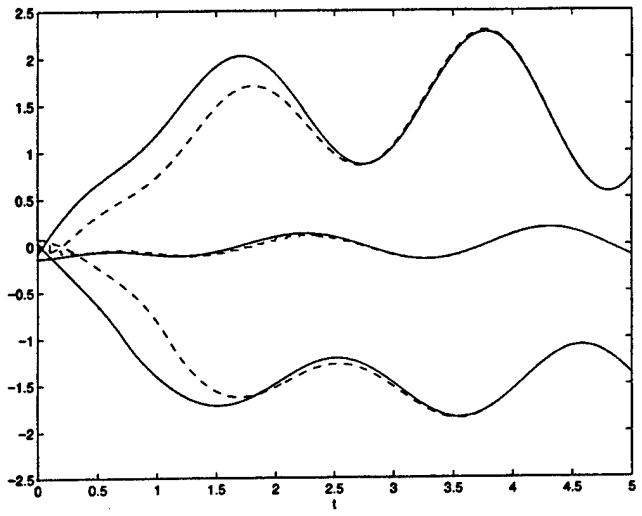


(a)

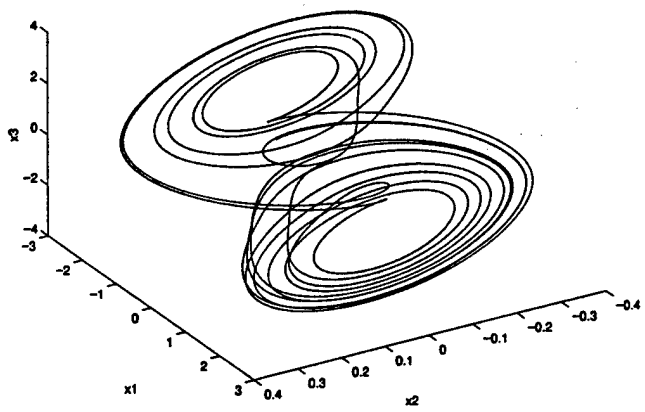


(b)

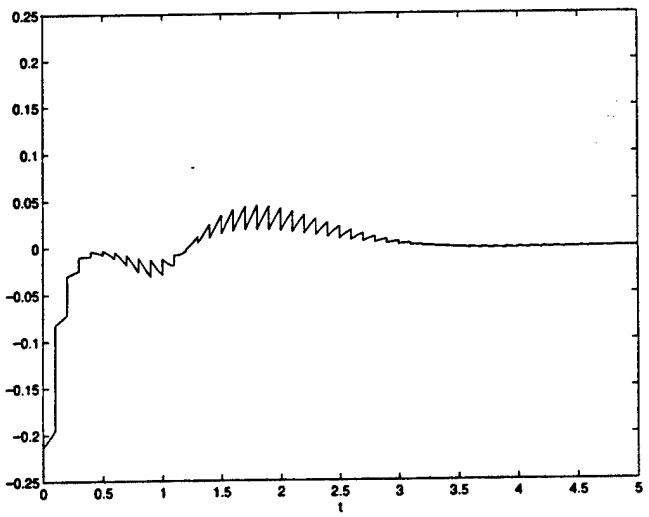


(c)

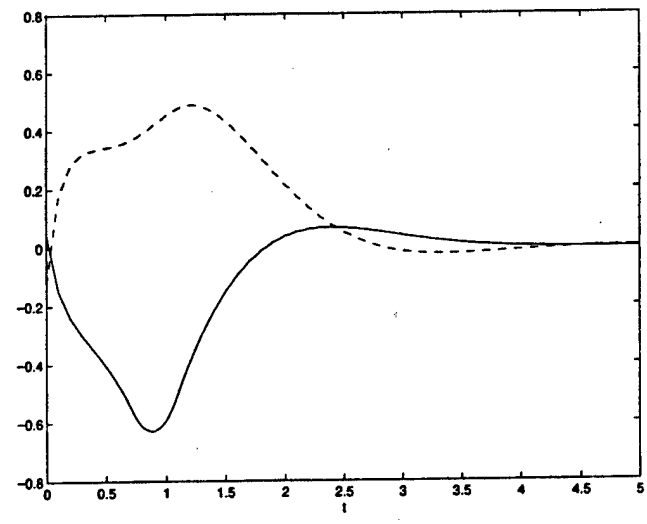


(d)

Fig. 1. Synchronization of two Chua's circuits by impulsive linear dynamic output feedback with one output and one control input: (a) $x(t)$ (solid line), $z(t)$ (dashed line); (b) three-dimensional view on the double scroll attractor generated at the master system; (c) output synchronization error $e_L(t) = e_2(t) = x_2 - z_2$; (d) $e_1(t)$ (solid line), $e_3(t)$ (dashed line); (e) impulsive control $D_1 u(t)$ applied to the slave system; (f) impulsive control $D_2 v(t)$ applied to the controller.

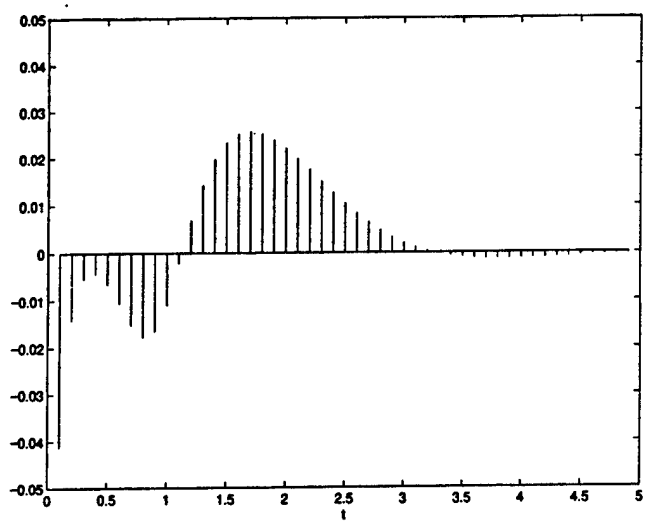

(e)

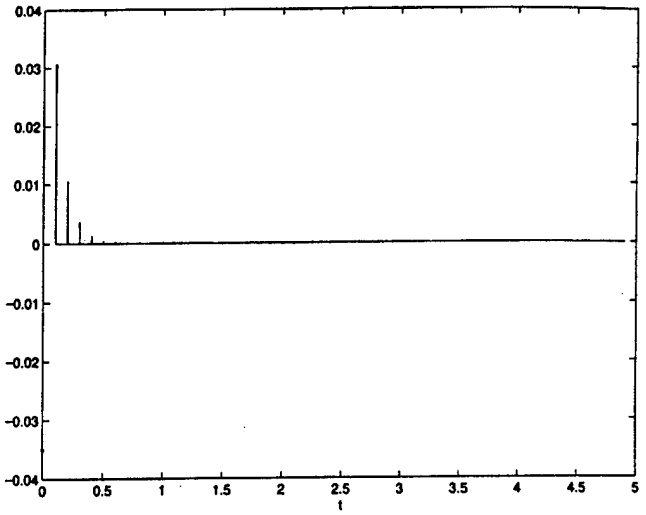

(f)

Fig. 1. (*Continued*)

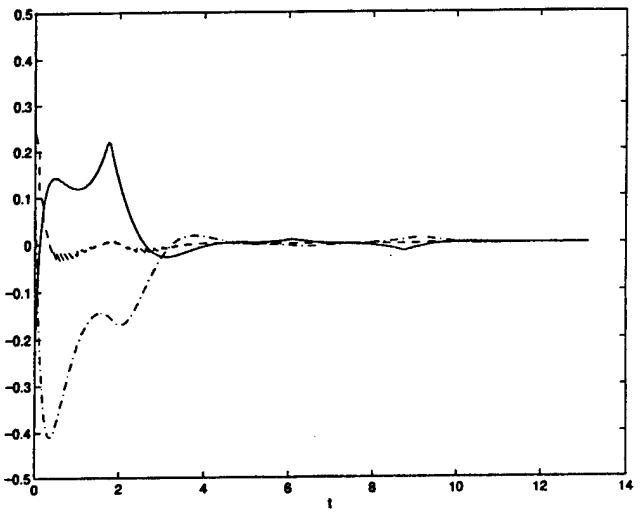

(a)

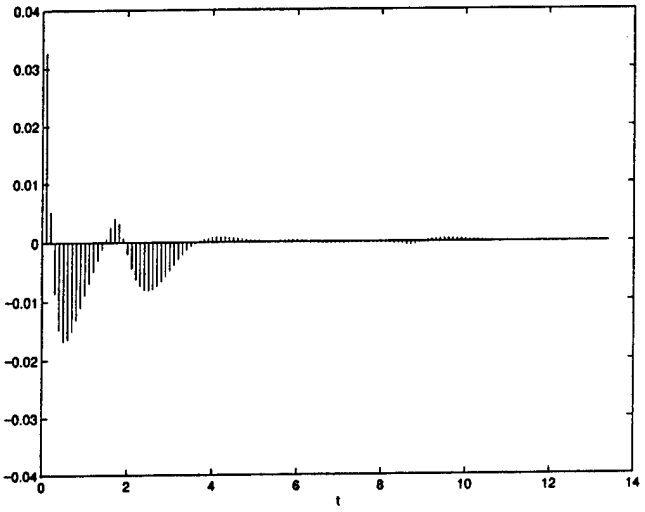

(b)

Fig. 2. Synchronization of two Chua's circuits by impulsive nonlinear dynamic output feedback with one output and one control input: (a) $e_L(t) = e_2(t)$ (dashed line), $e_1(t)$ (solid line), $e_3(t)$ (dash-dotted line); (b) impulsive control $D_1 u(t)$.

attractor [Chua *et al.*, 1986; Chua, 1994; Madan, 1993]. The nonlinearity $\phi(x_1) = (1/2)(|x_1 + c| - |x_1 - c|)$ (linear characteristic with saturation) belongs to sector $[0, 1]$. A Lur'e representation $\dot{x} = Ax + B\phi(Cx)$ of Chua's circuit is given then by

$$A = \begin{bmatrix} -am_1 & a & 0 \\ 1 & -1 & 1 \\ 0 & -b & 0 \end{bmatrix}, \quad B = \begin{bmatrix} -a(m_0 - m_1) \\ 0 \\ 0 \end{bmatrix}, \quad C = [1 \quad 0 \quad 0]. \tag{16}$$

Defining the outputs $p = x_2$, $q = z_2$ (hence $L = [0 \quad 1 \quad 0]$, $l = 1$) and impulsive control with $D_1 = \text{diag}\{0, 1, 0\}$, $D_2 = I$, $n_\xi = 1$, $m_\xi = 1$, $W_{EF} = 0$, $V_{F_1} = 0$, $V_{F_2} = 0$ (linear dynamic output feedback controller) the optimization problem (13) has been solved. Sequential quadratic programming [Fletcher, 1987] by means of the function constr of Matlab has been applied. The first constraint in (13)

was used as objective function $\lambda_{\max}(Z)$ (where $\lambda_{\max}(\cdot)$ denotes the maximal eigenvalue of a symmetric matrix) while the remaining three constraints have been imposed as hard constraints. The following starting points have been chosen for the optimization: $\theta_c$ random according to a Gaussian distribution with zero mean and standard deviation 0.1; $Q = I$; $\Lambda = I$; $\alpha = 10$; $\beta = 0.1$. The time interval $\tau_{i+1} - \tau_i$ was chosen fixed and equal to 0.1. Instead of $\beta$, the parameter $1/[1+\exp(-\beta)]$ (which belongs to $(0,1)$) was taken as unknown of the optimization problem. A feasible point which satisfies the constraints and brings the objective function close to zero is shown in Fig. 1. While synchronization is only proven for $x_2 - z_2$ by the Lyapunov function (5), the synchronization error $x - z$ for the complete state vector is also tending to zero. Small control impulses have to be applied to the slave system and to the linear dynamic output feedback controller. Simulations have been done on a SUN Ultra 2 workstation with a Runge–Kutta integration rule (*ode23* in Matlab) with tolerance $1.0e-10$.

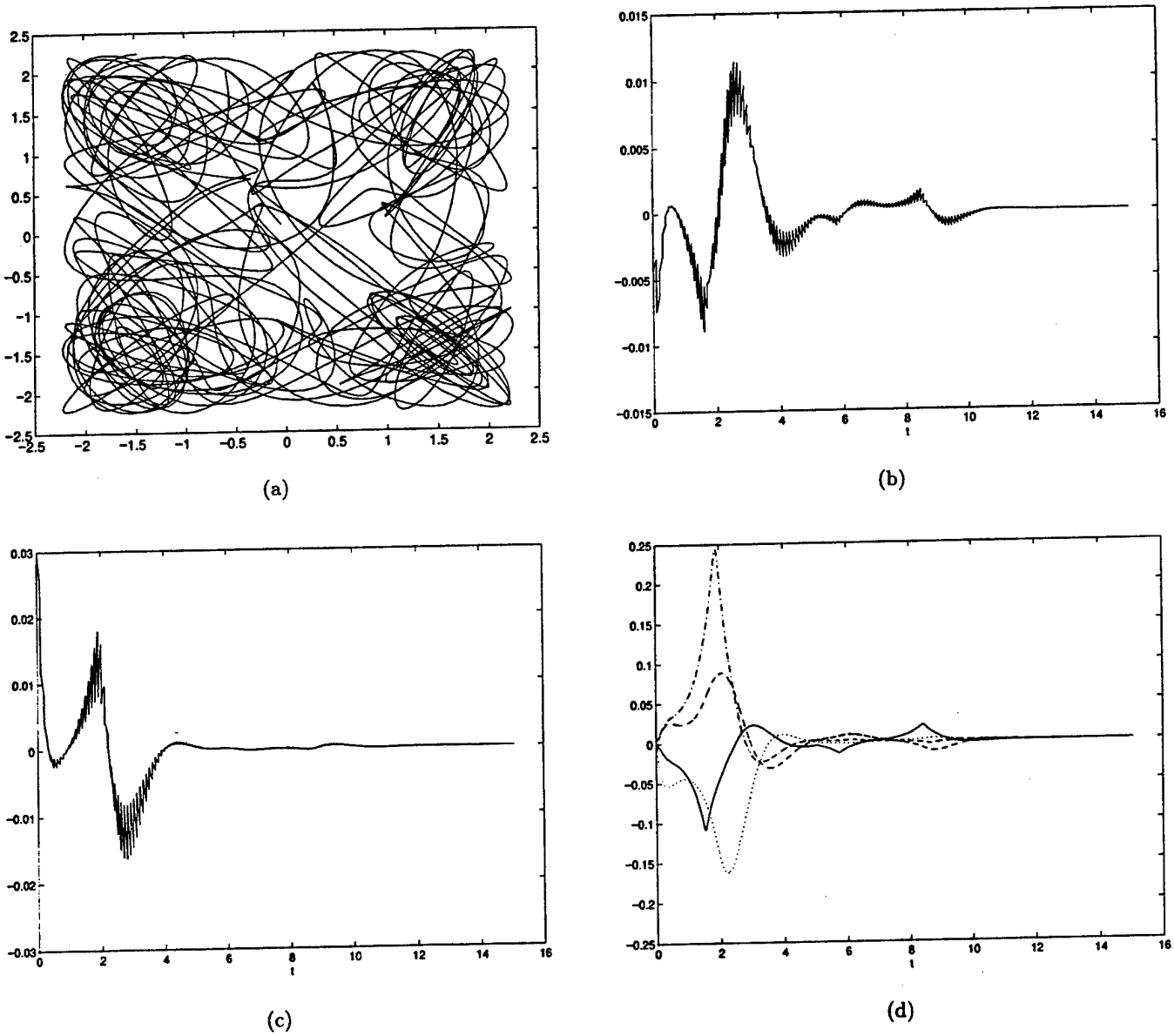


Fig. 3. Synchronization of two hyperchaotic systems (coupled Chua's circuits) by impulsive linear dynamic output feedback with two outputs and two control inputs: (a) double–double scroll attractor according to Kapitaniak & Chua, shown is $(x_1, x_4)$ for this hyperchaotic system with six state variables; (b) output synchronization error $e_2(t) = x_2 - z_2$; (c) output synchronization error $e_5(t) = x_5 - z_5$; (d) $e_1(t)$ (solid line), $e_3(t)$ (dashed line), $e_4(t)$ (dash-dotted line), $e_6(t)$ (dotted line); (e) impulsive control $u_2(t)$ applied to the slave system; (f) impulsive control $u_5(t)$ applied to the slave system; (g) impulsive control $v_1(t)$ applied to the controller; (h) impulsive control $v_2(t)$ applied to the controller.

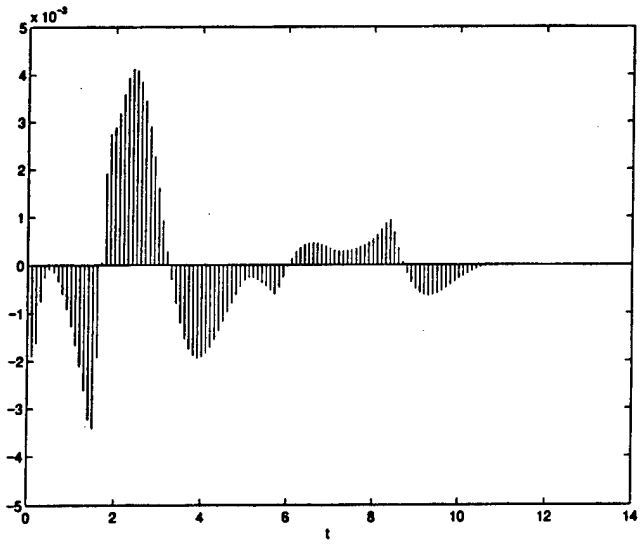


(e)

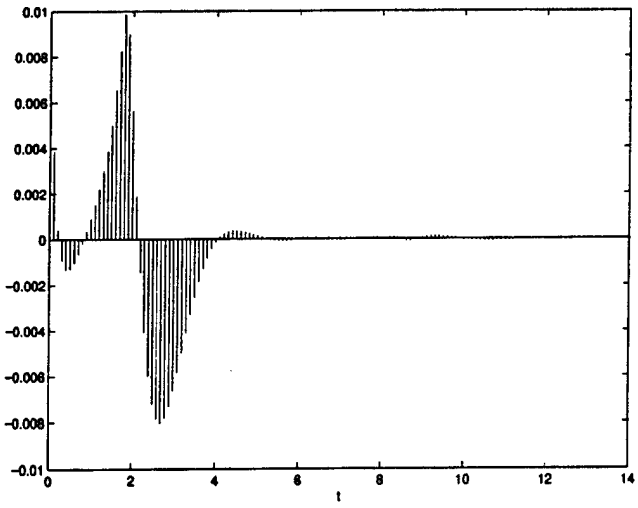


(f)

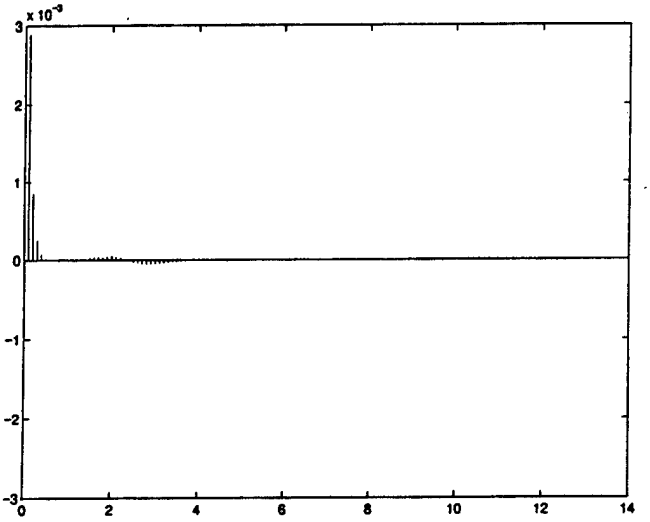


(g)

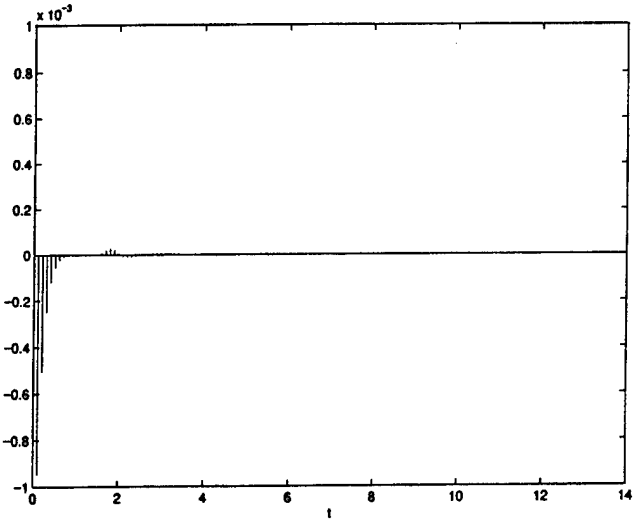


(h)

Fig. 3. (*Continued*)

A nonlinear dynamic output feedback law (1) has been studied for the same outputs and control input with $D_1 = \text{diag}\{0, 1, 0\}$, $D_2 = I$, $n_\xi = 3$, $m_\xi = 3$, $n_{h_\xi} = 1$ (controller with the same dimensions for $A$, $B$, $C$ as Chua's circuit but different values for the matrices). The same parameters were taken as before for the initialization of sequential quadratic programming, together with $\Gamma = I$. Simulation results are shown on Fig. 2. As for the linear feedback case the synchronization error between the full state vectors is tending to zero, while this is theoretically proven only for the measured variables.

### 4.2. *Coupled Chua's circuits*

We consider the following master system which consists of two unidirectionally coupled Chua circuits [Kapitaniak & Chua, 1994]

$$\begin{cases} \dot{x}_1 = a[x_2 - h(x_1)] \\ \dot{x}_2 = x_1 - x_2 + x_3 \\ \dot{x}_3 = -bx_2 \\ \dot{x}_4 = a[x_5 - h(x_4)] + K(x_4 - x_1) \\ \dot{x}_5 = x_4 - x_5 + x_6 \\ \dot{x}_6 = -bx_5 \end{cases} \tag{17}$$

with $h(x_i) = m_1 x_i + (1/2)(m_0 - m_1)(|x_i + c| - |x_i - c|)$ $(i = 1, 4)$. For $m_0 = -1/7$, $m_1 = 2/7$, $a = 9$, $b = 14.286$, $c = 1$, $K = 0.01$ the system exhibits hyperchaotic behavior with a double-double scroll attractor. The system can be represented in Lur'e form with $n = 6$, $n_h = 2$ and

$$A = \left[\begin{array}{ccc|ccc} -am_1 & a & 0 & 0 & 0 & 0 \\ 1 & -1 & 1 & 0 & 0 & 0 \\ 0 & -b & 0 & 0 & 0 & 0 \\ \hline 0 & 0 & 0 & -am_1 & a & 0 \\ 0 & -K & 0 & 1 & -1+K & 1 \\ 0 & 0 & 0 & 0 & -b & 0 \end{array}\right],$$

$$B = \left[\begin{array}{c|c} -a(m_0 - m_1) & 0 \\ 0 & 0 \\ 0 & 0 \\ \hline 0 & -a(m_0 - m_1) \\ 0 & 0 \\ 0 & 0 \end{array}\right],$$

$$C = \left[\begin{array}{ccc|ccc} 1 & 0 & 0 & 0 & 0 & 0 \\ \hline 0 & 0 & 0 & 1 & 0 & 0 \end{array}\right]. \tag{18}$$

We investigate the case of linear dynamic output feedback. First we define two outputs for the system ($p = [x_2; x_5]$, $q = [z_2; z_5]$) and two controls inputs ($D_1 = \text{diag}\{0, 1, 0, 0, 1, 0\}$). Furthermore we choose $n_\xi = 2$, $m_\xi = 2$, $W_{EF} = 0$, $V_{F_1} = 0$, $V_{F_2} = 0$. The initialization is done in the same way as in the previous examples. Simulation results show (Fig. 3) that the synchronization is obtained for the full state vector of the hyperchaotic system, while it is theoretically only shown for the outputs.

Next we study the case of linear dynamic output feedback with one output ($p = x_2$, $q = z_2$) and one control input ($D_1 = \text{diag}\{0, 1, 0, 0, 0, 0\}$). The other parameters and initialization were chosen in the same way as in the previous case. Simulation results are shown in Fig. 4. The synchronization error is tending to zero for the difference between the measurements, but not for the full state vector.

## 5. Conclusions

We discussed a systematic procedure for designing impulsive control laws in order to synchronize Lur'e systems. Examples of chaotic Lur'e systems are (generalized) Chua's circuits and arrays that contain such chaotic cells. The method makes use of measurement feedback instead of full state feedback. For the sake of generality, nonlinear dynamic output feedback controllers have been investigated which include the special cases of static

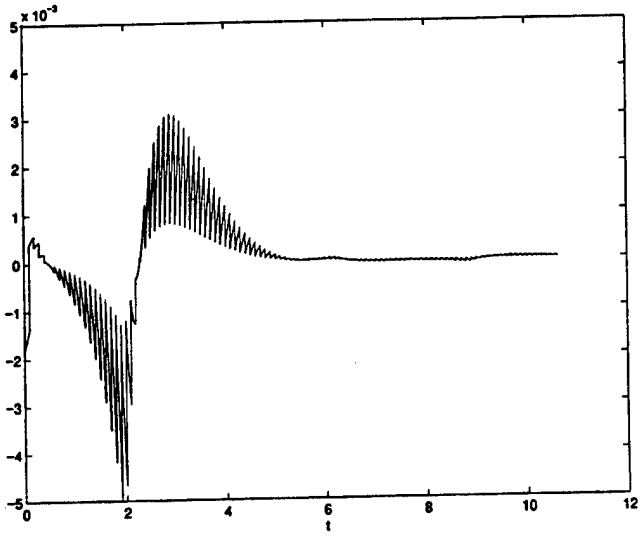


(a)

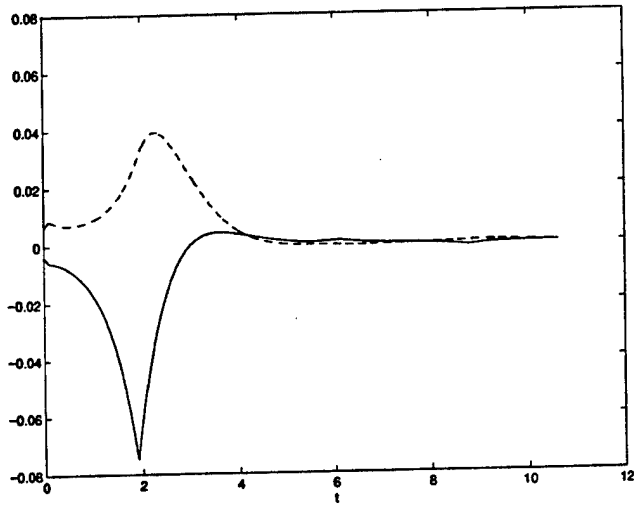


(b)

Fig. 4. Synchronization of the two hyperchaotic systems of Fig. 3 but with one output and one control input: (a) output synchronization error $e_L(t) = e_2(t) = x_2 - z_2$; (b) $e_1(t)$ (solid line), $e_3(t)$ (dashed line) (first cell); (c) $e_4(t)$ (solid line), $e_5(t)$ (dashed line), $e_6(t)$ (dotted line) (second cell); (d) impulsive control $D_1 u(t)$ applied to the slave system; (f) impulsive control $v_1(t)$ applied to the controller; (g) impulsive control $v_2(t)$ applied to the controller.

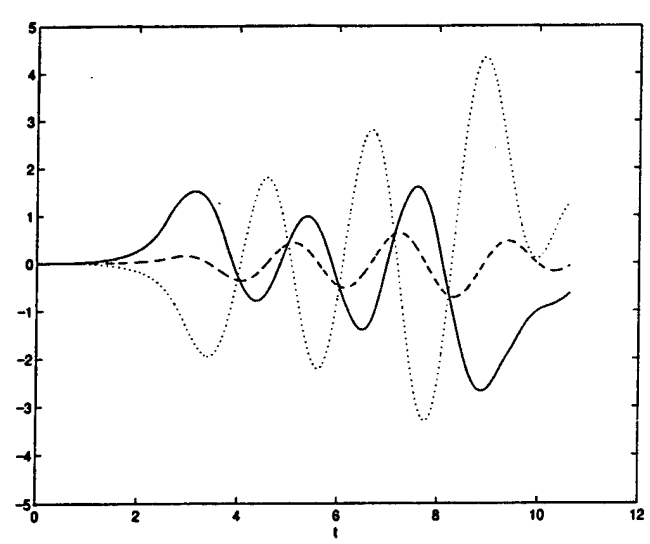


(c)

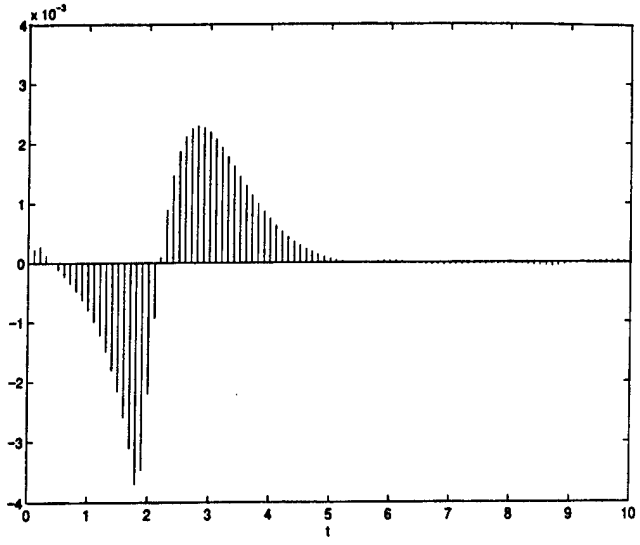


(d)

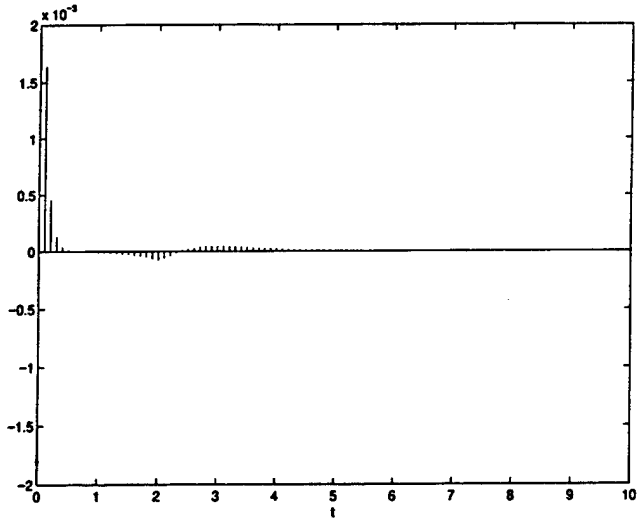


(e)

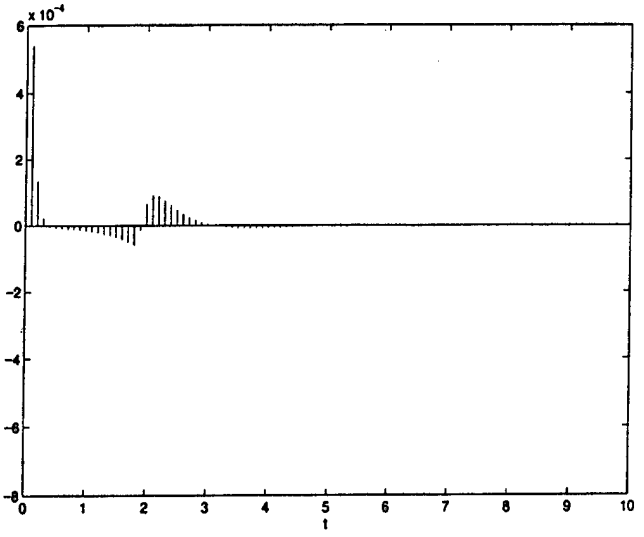


(f)

Fig. 4. (*Continued*)

output feedback and linear dynamic output feedback. Conditions for global asymptotic stability of the output error system are expressed as matrix inequalities. Simulation examples have been presented for Chua's circuit and coupled Chua's circuits that exhibit the double–double scroll attractor. In the latter case it was sufficient to measure one single variable and take one control input in order to obtain synchronization in the output. Often synchronization is also obtained for the full state vectors in addition to the theoretically guaranteed synchronization for the output vectors.

## Acknowledgment

This research work was carried out at the ESAT laboratory and the Interdisciplinary Center of Neural Networks ICNN of the Katholieke Universiteit Leuven, in the framework of the Belgian Programme on Interuniversity Poles of Attraction, initiated by the Belgian State, Prime Minister's Office for Science, Technology and Culture (IUAP P4-02) and in the framework of a Concerted Action Project MIPS (Modelbased Information Processing Systems) of the Flemish Community. J. Suykens is postdoctoral

researcher with the National Fund for Scientific Research FWO, Flanders. T. Yang and L. O. Chua were supported by the Office of Naval Research under grant No. N00014-96-1-0753.

## References

Boyd, S., El Ghaoui, L., Feron, E. & Balakrishnan, V. [1994] *Linear Matrix Inequalities in System and Control Theory*, SIAM (Studies in Applied Mathematics), Vol. 15.

Chua, L. O., Komuro, M. & Matsumoto, T. [1986] "The double scroll family," *IEEE Trans. Circuits Syst. I* **33**(11), 1072–1118.

Chua, L. O. [1994] "Chua's circuit 10 years later," *Int. J. Circuit Theor. Appl.* **22**, 279–305.

Fletcher, R. [1987] *Practical Methods of Optimization* (John Wiley, Chichester and New York).

Kapitaniak, T. & Chua, L. O. [1994] "Hyperchaotic attractors of unidirectionally-coupled Chua's circuits," *Int. J. Bifurcation and Chaos* **4**(2), 477–482.

Khalil, H. K. [1992] *Nonlinear Systems* (Macmillan Publishing Company, New York).

Lakshmikantham, V., Bainov, D. D. & Simeonov, P. S. [1989] *Theory of Impulsive Differential Equations* (World Scientific, Singapore).

Madan, R. N. (guest ed.) [1993] *Chua's Circuit: A Paradigm for Chaos* (World Scientific, Singapore).

Stojanovski, T., Kocarev, L. & Parlitz, U. [1996] "Driving and synchronizing by chaotic impulses," *Phys. Rev.* **E54**(2), 2128–2138.

Stojanovski, T., Kocarev, L. & Parlitz, U. [1997] "Digital coding via chaotic systems," *IEEE Trans. Circuits Syst. I* **44**(6), 562–565.

Suykens, J. A. K., Vandewalle, J. P. L. & De Moor, B. L. R. [1996] *Artificial Neural Networks for Modelling and Control of Non-Linear Systems* (Kluwer Academic Publishers, Boston).

Suykens, J. A. K., Curran, P. F. & Chua, L. O. [1997a] "Master–slave synchronization using dynamic output feedback," *Int. J. Bifurcation and Chaos* **7**(3), 671–679.

Suykens, J. A. K., Huang, A. & Chua, L. O. [1997b] "A family of $n$-scroll attractors from a generalized Chua's circuit," *Archiv für Elektronik und Ubertragungstechnik* **51**(3), 131-138.

Suykens, J. A. K., Curran, P. F., Yang, T., Vandewalle, J. & Chua, L. O. [1997c] "Nonlinear $H_\infty$ synchronization of Lur'e systems: Dynamic output feedback case," *IEEE Trans. Circuits Syst. I* **44**(11), 1089–1092.

Suykens, J. A. K. & Chua, L. O. [1997] "$n$-Double scroll hypercubes in 1D-CNNs," *Int. J. Bifurcation and Chaos* **7**(8), 1873–1885.

Vidyasagar, M. [1993] *Nonlinear Systems Analysis* (Prentice-Hall).

Wu, C. W. & Chua, L. O. [1994] "A unified framework for synchronization and control of dynamical systems," *Int. J. Bifurcation and Chaos* **4**(4), 979–989.

Yang, T. & Chua, L. O. [1997a] "Impulsive stabilization for control and synchronization of chaotic systems: Theory and application to secure communication," *IEEE Trans. Circuits Syst. I (Special Issue on Chaos Synchronization, Control and Applications)* **44**(10), 976–988.

Yang, T. & Chua, L. O. [1997b] "Impulsive control and synchronization of nonlinear dynamical systems and application to secure communication," *Int. J. Bifurcation and Chaos* **7**(3), 645–664.

Yang, T. & Chua, L. O. [1997c] "Chaotic digital code-division multiple access (CDMA) systems," *Int. J. Bifurcation and Chaos* **7**(12), 2789–2805.

Yang, T., Yang, L.-B. & Yang, C.-M. [1997] "Impulsive synchronization of Lorenz systems," *Phys. Lett.* **A226**, 349–354.

International Journal of Bifurcation and Chaos, Vol. 8, No. 3 (1998) 639–644
© World Scientific Publishing Company

# EXPERIMENTAL RESULTS OF IMPULSIVE SYNCHRONIZATION BETWEEN TWO CHUA'S CIRCUITS

ANDREY I. PANAS,* TAO YANG and LEON O. CHUA
*Electronics Research Laboratory and*
*Department of Electrical Engineering and Computer Sciences,*
*University of California at Berkeley,*
*Berkeley, CA 94720, USA*

Received October 30, 1997; Revised December 31, 1997

Impulsive synchronization of chaotic dynamic systems has some important applications to chaotic secure communication and chaotic spread-spectrum communication systems. In this paper we present some experimental results on impulsive synchronization between two Chua's circuits. In our experiments, only one synchronizing impulse sequence is transmitted. The robustness of impulsive synchronization with respect to variations in the frequency and the width of impulses is studied. Experimental results show that robust impulsive synchronization can be achieved under noisy conditions and a 2% parameter mismatch between the driving system and the driven system. We also found that an amplified impulse sequence with a gain greater than unity can make the impulsive synchronization more robust. Moreover, we found that impulsive synchronization can be achieved with very narrow impulses.

## 1. Introduction

The concept of impulsive control and synchronization of chaotic systems was first reported in [Amritkar & Gupte, 1993; Stojanovski *et al.*, 1996]. After that, this problem was found closely connected to the theory of impulsive differential equations [Yang & Chua, 1997c]. A rigorous theory of the asymptotic stability of impulsive control and synchronization of autonomous chaotic systems was presented in [Yang & Chua, 1997b, 1997c]. Some applications of impulsive synchronization of chaotic systems to chaotic secure communication, and to chaotic digital code-division multiple access (CDMA) systems were presented in [Stojanovski *et al.*, 1996; Yang & Chua, 1997b, 1997c] and in [Yang & Chua, 1997a], respectively.

All of the above results are theoretical. Since impulsive control and synchronization involves changing the state variables of continuous dynamic systems rapidly, it is necessary to investigate the problems that may arise in the *practical* implementation of impulsive synchronization. In this letter, we present some experimental results of impulsive synchronization between two Chua's circuits [Chua, 1994].

## 2. Experimental Configurations

In this letter, we choose Chua's circuit [Chua, 1994] as the chaotic system which is defined by

$$\begin{cases} \dfrac{dv_1}{dt} = \dfrac{1}{C_1}[G(v_2 - v_1) - f(v_1)] \\ \dfrac{dv_2}{dt} = \dfrac{1}{C_2}[G(v_1 - v_2) + i_3] \\ \dfrac{di_3}{dt} = -\dfrac{1}{L}v_2 \end{cases} \tag{1}$$

*On leave from the Institute of Radio Engineering and Electronics of the Russian Academy of Sciences, Mokhovaya St. 11, 103907 Moscow, Russia.

where $f(\cdot)$ is the nonlinear characteristic of Chua's diode, defined by

$$f(v_1) = G_b v_1 + \frac{1}{2}(G_a - G_b)(|v_1 + E| - |v_1 - E|) \quad (2)$$

and $E$ is the breakpoint voltage of Chua's diode. The corresponding circuit is shown in Fig. 1.

Although [Kennedy, 1992] had provided a physical implementation of Chua's circuit, for our present application, we have opted to use the circuit realization presented in [Dmitriev *et al.*, 1995], which we have found to be more robust for this application than the scheme given in [Kennedy, 1992].

The parameters chosen for this implementation are $C_1 = 5100$ pF, $C_2 = 47$ nF, $L = 18$ mH and $R = 1.65$ kΩ. The parameters for implementing Chua's diode are given by $E = 1.56$ V, $G_a = -0.757$ mS, and $G_b = -0.459$ mS. The Op Amps chosen in our implementation are type KR1401UD2A. With these parameters we obtain the Chua's double scroll strange attractor shown in the $v_1$–$v_2$ plane in Fig. 2, where the scale of the horizontal and the vertical axes is 0.2 V/div and 50 mV/div, respectively.

The block diagram of our impulsive synchronization using a single synchronizing impulse sequence is given in Fig. 3. Figure 3(a) shows the block diagram of impulsive synchronization via $v_1$ between two Chua's circuits. The switching signal $s(t)$ shown in Fig. 3(c) is used to switch on/off an electronic switching device (AD6 212 AKN). Whenever $s(t)$ assumes a high voltage level, the switch is on and a synchronizing impulse is transmitted from the driving system to the driven system. We call the width of the high voltage peaks as the *impulse width* $w_i$. The high voltage level of $s(t)$ is chosen to be greater than $5V$. The time interval between two consecutive impulses is called the *impulse period* $1/f_i$. Whenever $s(t)$ assumes a low voltage level, the switch is turned off and the two Chua's circuits are separated electronically. The low voltage level of $s(t)$ is chosen to be $0V$. Whenever $s(t)$ assumes a high voltage level, the two voltages $v_1(t)$ and $\tilde{v}_1(t)$ are connected by two voltage buffers, which force their output voltages to be equal to their input voltages, and hence $\tilde{v}_1(t)$ must tend rapidly to $v_1(t)$.

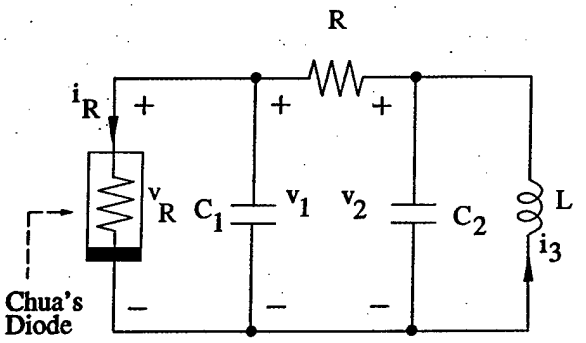


(a)

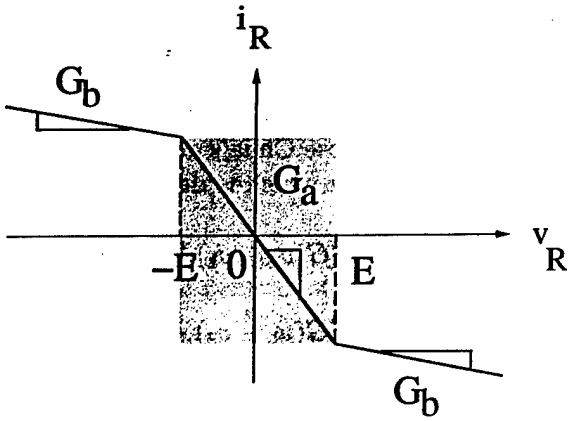


(b)

Fig. 1. (a) Chua's circuit. (b) Voltage-current characteristic of Chua's diode.

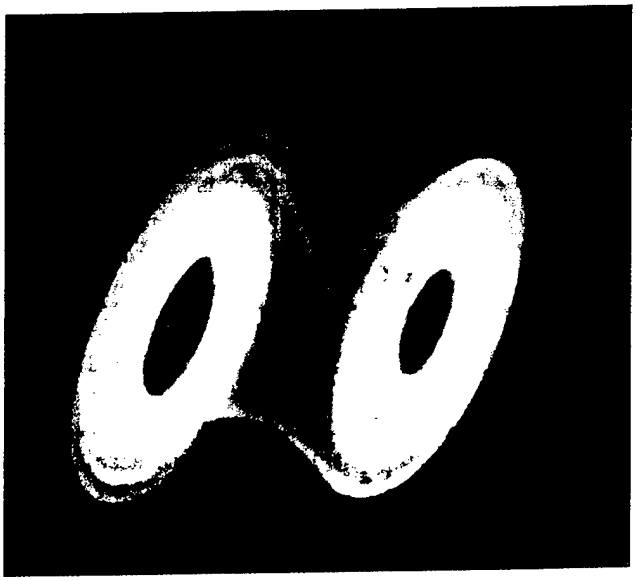

Fig. 2. The Chua's double scroll strange attractor observed from the Chua's circuit used in our experiments.

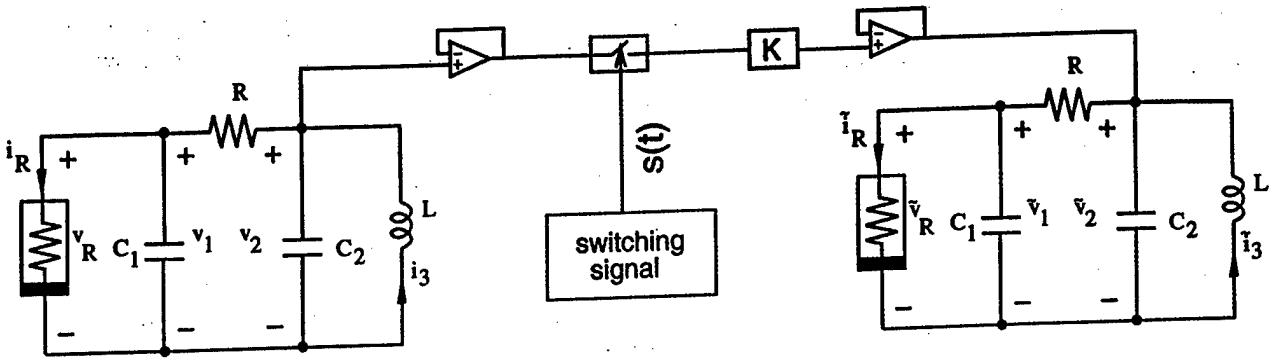


(a)

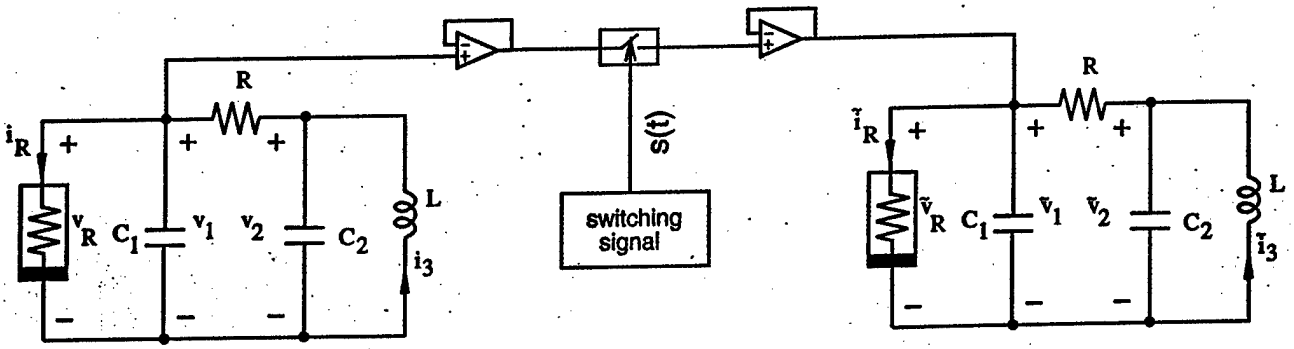


(b)

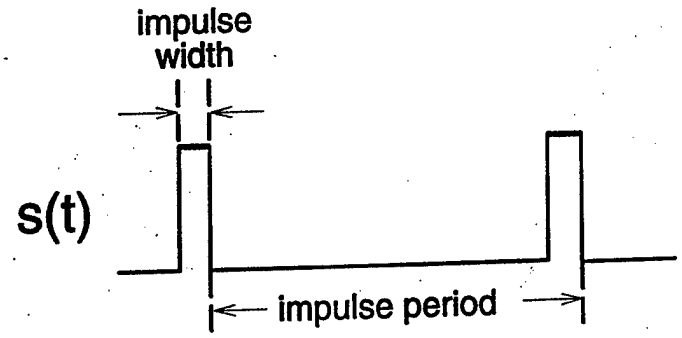


(c)

Fig. 3. The block diagram of impulsive synchronization between two Chua's circuits. (a) Impulsive synchronization via $v_1(t)$. (b) Impulsive synchronization via $v_2(t)$. (c) Illustration of switching signal $s(t)$.

Figure 3(b) shows the block diagram for impulsive synchronization via $v_2$ between two Chua's circuits. In this case, the voltages of capacitors $C_2$ in both Chua's circuits are connected impulsively by two voltage buffers and an electronic switch. It is the same structure as that in Fig. 3(a) except that a channel gain $K$ is introduced for increased generality.

## 3. Experimental Results

In this section, we present our experimental results of the configuration presented in Sec. 2. All pictures are taken directly from the screen of an oscilloscope.

### 3.1. $v_2$ *is the transmitted signal*

We first study the cases when the voltage $v_2$ is the transmitted signal as shown in Fig. 3(b). The experimental results are shown in Fig. 4. Figure 4(a) shows, in the $v_1$–$\tilde{v}_1$ plane, that the two Chua's circuits are originally desynchronized if impulsive coupling is not applied. Figure 4(b) shows, in the $v_1$–$\tilde{v}_1$ plane, that the two Chua's circuits are synchronized if the impulsive coupling is applied. The parameters for the synchronization impulses are: Frequency of impulses is $f_i = 18$ kHz, width of impulses is $w_i = 32$ $\mu$s. Figure 4(c) shows, in the $v_1$–$\tilde{v}_1$ plane, that the two Chua's circuits

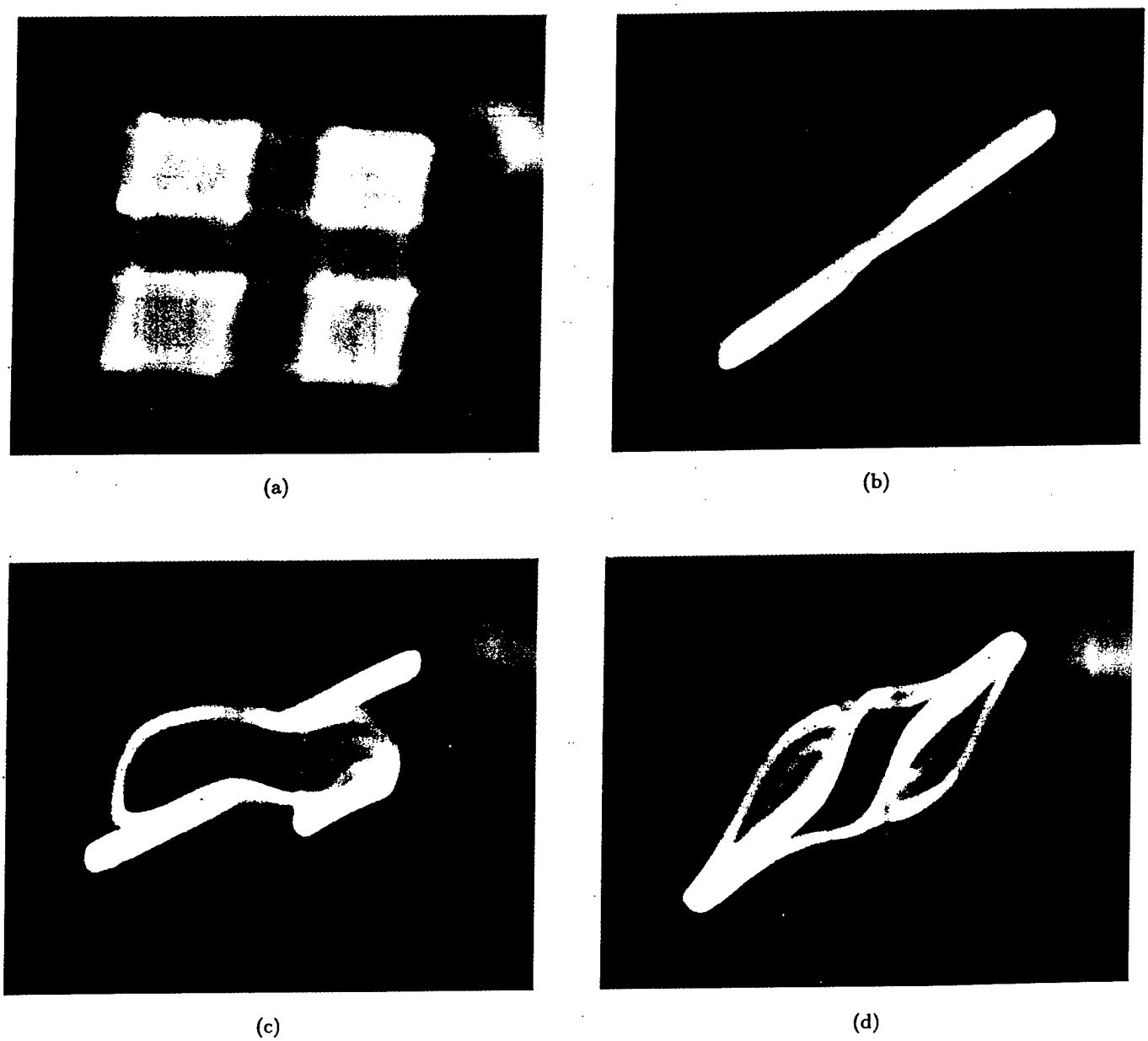


Fig. 4. The experimental results of impulsive synchronization when $v_2$ is sampled as the synchronizing impulse sequence. In this figure, the scale of the oscilloscope is 0.2 V/div for both horizontal and vertical axes. (a) The driving system and the driven system are originally desynchronized. (b) Impulsive synchronization ($K = 1$). (c) Desynchronization due to narrow impulses ($K = 1$). (d) Desynchronization due to wide impulses ($K = 1$). (e) Impulsive synchronization with $K > 1$ and narrow impulses.

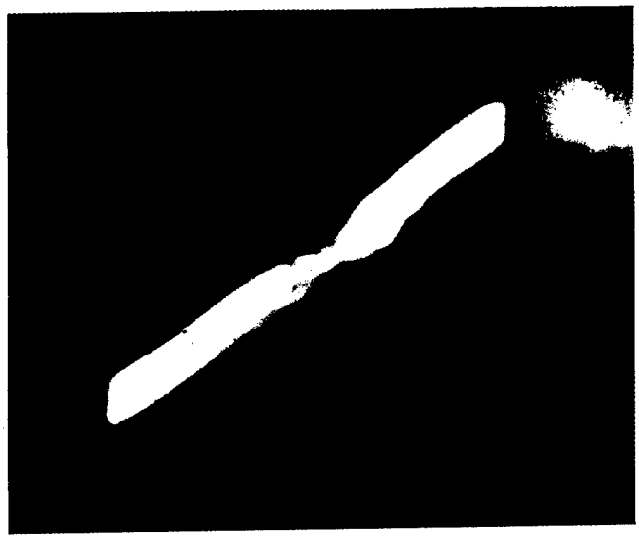

(e)

Fig. 4. (*Continued*)

become desynchronized if we decrease the width of the impulse beyond a certain limit. The parameters for the synchronization impulses are: $f_i = 18$ kHz and $w_i = 24$ $\mu$s. Figure 4(d) shows, in the $v_1$–$\tilde{v}_1$ plane, that the two Chua's circuits become desynchronized if we increase the width of the impulse beyond a certain limit. The parameters for the synchronization impulses are: $f_i = 18$ kHz and $w_i = 46$ $\mu$s. Figure 4(e) shows, in the $v_2$–$\tilde{v}_2$ plane, that impulsive synchronization between two Chua's circuits can be maintained with narrow impulses if the amplitude of the impulses is amplified by a gain $K > 1$. In this case, the parameters for the synchronization impulses are: $f_i = 18$ kHz, $w_i = 12$ $\mu$s and $K = 2.67$.

### 3.2. $v_1$ *is the transmitted signal*

We study next the cases when the voltage $v_1$ is the transmitted signal. The experimental results are shown in Fig. 5. Figure 5(a) shows, in the $v_2$–$\tilde{v}_2$ plane, that the two Chua's circuits are originally desynchronized if impulsive coupling is not applied. Figure 5(b) shows, in the $v_2$–$\tilde{v}_2$ plane, that the two Chua's systems are synchronized if impulsive coupling is applied. The parameters for the synchronization impulses are: $f_i = 20$ kHz and $w_i = 32$ $\mu$s. Figure 5(c) shows, in the $v_2$–$\tilde{v}_2$ plane, that impulsive synchronization in this case is very robust using only *narrow* impulses, where the parameters of the synchronization impulses are: $f_i = 20$ kHz and $w_i = 8$ $\mu$s. Figure 5(d) shows the switching signal $s(t)$ used in Fig. 5(c).

## 4. Conclusions

In this letter we present two different schemes for implementing impulsive synchronization between two chaotic electronic circuits, namely, Chua's circuits, via a single synchronizing impulse sequence. We observed that the impulsive synchronization is robust in the presence of a 2% parameter mismatch between the driving and the driven systems under noisy conditions. However, the impulsive synchronization between two Chua's circuits via a

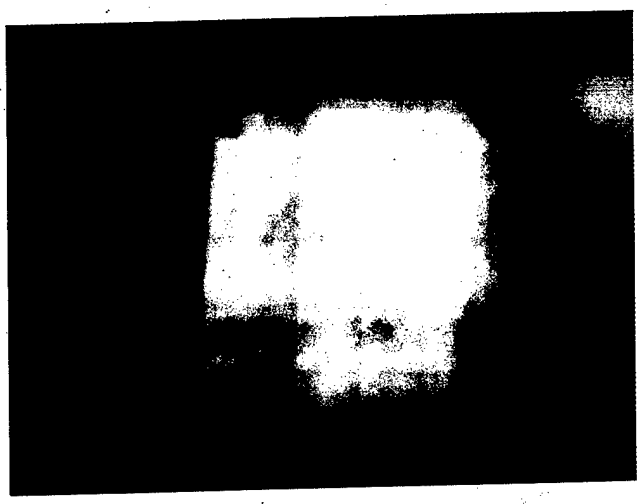

(a)

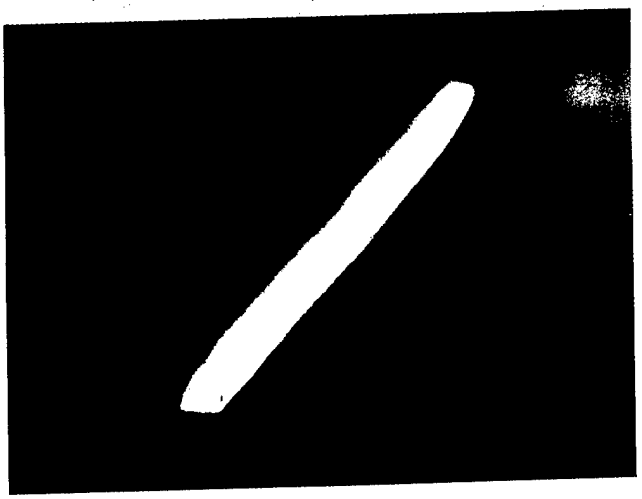

(b)

Fig. 5. The experimental results of impulsive synchronization when $v_1$ is sampled as the synchronizing impulse sequence. In this figure, the scale of the oscilloscope is 50 mV/div for both horizontal and vertical axes. (a) The driving system and the driven system are originally desynchronized. (b) Impulsive synchronization. (c) Impulsive synchronization with narrow impulses. (d) The switching signal $s(t)$ used in (c).

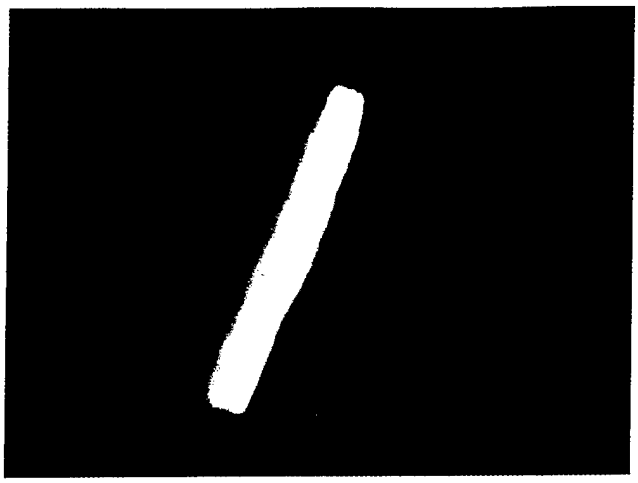

(c)

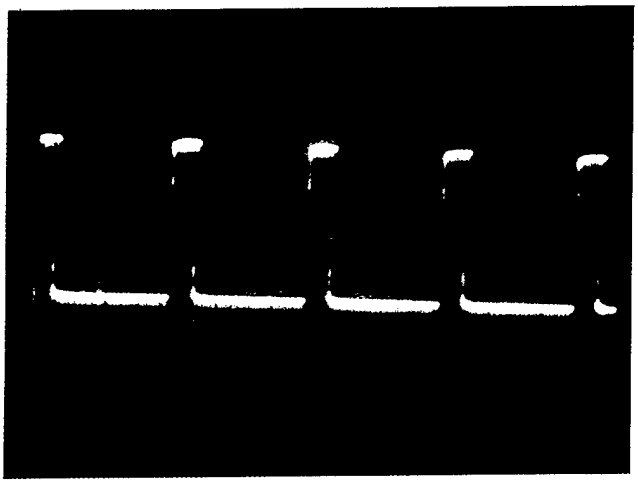

(d)

Fig. 5. (*Continued*)

single synchronizing impulse sequence is not asymptotically stable from a theoretical point of view. This is the reason why the frequency of the synchronizing impulse was chosen to around 10 kHz in our experiments.

Our experimental results show that the $v_1$-driving scheme is more robust than the $v_2$-driving scheme. This is because $v_1$ is directly connected to Chua's diode, which is the only nonlinearity in Chua's circuit.

## Acknowledgment

This work is supported in part by a NATO Linkage grant No. OUTR.LG 960578, and by the Office of Naval Research under grant No. N00014-96-1-0753.

## References

Amritkar, R. E. & Gupte, N. [1993] "Synchronization of chaotic orbits: The effect of a finite time step," *Phys. Rev.* **E47**(6), 3889–3895.

Dmitriev, A. S., Panas, A. I. & Starkov, S. O. [1995] "Experiments on speech and music signals transmission using chaos," *Int. J. Bifurcation and Chaos* **5**(4), 1249–54.

Kennedy, M. P. [1992] "Robust Op AMP realization of Chua's circuit," *Frequenz* **46**(3–4), 66–80.

Chua, L. O. [1994] "Chua's circuit — an overview ten years later," *J. Circuit Syst. Comput.* **4**(2), 117–159.

Stojanovski, T., Kocarev, L. & Parlitz, U. [1996] "Driving and synchronizing by chaotic impulses," *Phys. Rev.* **E54**(2), 2128–31.

Yang, T. & Chua, L. O. [1997a] "Chaotic digital code-division multiple access (CDMA) systems," *Int. J. Bifurcation and Chaos* **7**(12), 2789–2805.

Yang, T. & Chua, L. O. [1997b] "Impulsive control and synchronization of nonlinear dynamical systems and application to secure communication," *Int. J. Bifurcation and Chaos* **7**(3), 645–664.

Yang, T. & Chua, L. O. [1997c] "Impulsive stabilization for control and synchronization of chaotic systems: Theory and application to secure communication," *IEEE Trans. Circuits Syst. I: Fundamental Theor. Appl.* **44**(10), 976–988.

International Journal of Bifurcation and Chaos, Vol. 8, No. 1 (1998) 1–32
© World Scientific Publishing Company

# CLARIFYING CHAOS II: BERNOULLI CHAOS, ZERO LYAPUNOV EXPONENTS AND STRANGE ATTRACTORS

RAY BROWN
*Applied Chaos Technology Corporation,*
*3865 Wilson Boulevard, Suite 210, Arlington, VA 22203, USA*

LEON O. CHUA
*Department of Electrical Engineering and Computer Sciences,*
*University of California, Berkeley, CA 94720, USA*

Received March 31, 1997; Revised November 20, 1997

In this tutorial we continue the program initiated in "Clarifying Chaos: Examples and Counter Examples" by presenting examples that answer questions in five areas:

**Area 1. The Horseshoe/Bilateral Shifts/Bernoulli Systems**

Since the bilateral shift (which may also be called a Bernoulli shift) plays such an important role in some definitions of chaos we show that it is possible to construct a differential equation for an electronic circuit whose time-one map,[1] is exactly a bilateral shift, in particular the bakers transformation and the cat map [Arnold & Avez, 1989]. We insist on being able to build a circuit in order to be sure that our example is not just a mathematical abstraction. Also, in this set of examples we show that we may construct chaotic maps of any desired level of complexity.

**Area 2. Zero Lyapunov Exponents**

Since the existence of positive Lyapunov exponents is so often used as a definition of chaos we answer the question: Are there systems with zero Lyapunov exponents which are not considered chaotic by this definition, which have outputs which are more complex that some chaotic systems? The answer is yes, and for these systems, called skew translations and compound skew translations [Cornfeld *et al.*, 1982], all the eigenvalues are 1. Further, the skew translation may be linear, having only additions (no multiplication's). Skew translations exist in any number of dimensions and can be realized as the time-one maps of an electronic circuit. Skew translations can have sensitive dependence on initial conditions and zero autocorrelations. The significance of this example is that the Lyapunov exponent is less a measure of the level of complexity than one first imagined since a higher level of complexity can be obtained from a lower exponent.

**Area 3. Nonchaotic Strange Attractors**

This phenomenon is reported in [Grebogi *et al.*, 1984] and further developed by other researchers. Of note in this regard is the work of Ding *et al.* [1989] where the place of this phenomenon within nonlinear dynamics is discussed. We show here that the origin of this phenomenon is found in dynamical systems having orbits with low correlations regardless of their Lyapunov exponents. We present examples of skew translations having zero autocorrelations

[1]The terms "time-one map" and "Poincaré map" are, today, used interchangeably even within mathematical circles. While some differences in their precise definitions do exist, these differences do not affect the present-day usage of these terms.

and zero Lyapunov exponents that can be used to generate nonchaotic strange attractors. Further, we show that only minimal level of complexity is needed to obtain nonchaotic strange attractors by using a group rotation to produce one. The inverse of this idea is the chaotic nonstrange attractor which is also presented.

**Area 4. Nonlinearity**

Since nonlinearities are usually considered a key ingredient of chaotic dynamical systems we present examples to show that there are at least four distinct types of nonlinearities in ODEs leading to varying levels of chaos. All example ODEs have closed-form solutions in terms of elementary functions and thus give us direct insight into how the type of nonlinearity appears in the ODE and is manifested in its solution.

**Area 5. Relationship of Dissipation, Noninvertibility, Nonorientibility and Chaos**

There are many misconceptions about how these properties, especially dissipation, may contribute to chaos. We show that these properties are independent of chaos.

The overriding conclusion of this set of examples is that what we have traditionally called chaos is so varied in its level of complexity that it is almost a meaningless term when used by itself. In particular, the term "level of complexity" must be appealed to so often in order to clarify the varying degrees of chaos that the two terms "chaos" and "level of complexity" seem inseparable in any practical discussion of chaos. The key issue that gives rise to this confusion about the level of complexity of a chaotic dynamical system is its long- and short-term predictability. Chaotic dynamical systems may be quite predictable over very long but finite time scales, but unpredictable in infinite time. The need to consider system behavior over long, finite time scales is a practical matter and leads to the conclusion that the study of chaos must be concerned with both asymptotic and long, but finite, time dynamics.

## 1. Introduction

Poincaré–Birkhoff–Smale chaos, a term coined by J. Marsden, designates the family of chaotic dynamical systems for which the system is conjugate to a root of a shift[2] on a subset of its domain. This situation is often described by saying that the system has a horseshoe. While this definition cannot yet be proven to encompass all chaotic dynamical systems, it does represent a significant, if not the most significant, class of chaotic dynamical systems. Extensive literature exists which is devoted to showing systems which are chaotic by proving the presence of a horseshoe. There are, however, two quirks in this definition: (1) The horseshoe may exist on a set of measure zero; and (2) The system may be conjugate to such a small root of the shift that it has a very low order of complexity. This low level of complexity may result in the system having such a predictable nature over long but finite-time scales that the term "chaos" is misleading.

In Sec. 2, in order to convey an intuitive grasp of the meaning of the horseshoe in a useful formula, we construct an example of an ODE whose time-one map is exactly a horseshoe, not a root. Also, we show how routine it is to construct examples which illustrate how systems can be conjugate to a shift on a set of measure zero. Further, we examine numerous methods of altering a Bernoulli system so that enough of its level of complexity is retained to call the resulting system chaotic. This line of thought is motivated by the proof of Kalikow that one Bernoulli system may be used to modify another in such a way that the resulting system is a Kolomogrov system which is not Bernoulli [Walters, 1982]. In our recent paper *From Almost Periodic to Chaotic: The Fundamental Map* we demonstrated just how extraordinarily such modified Bernoulli systems may behave.

In Sec. 3 we construct examples of systems which meet some of the criteria of chaos, but which

[2]A mapping $f$ is a root of a shift, $S$, when, for some positive integer $n$, $f^n(x) = S(x)$. For example, $x \to 2x \bmod(1)$ is a root of $x \to 4x \bmod(1)$.

have zero Lyapunov exponents. These examples demonstrate the limitations of the most popular definition of chaos, positive Lyapunov exponents, and raise the question of how is a system's *level of complexity*, in a practical sense, best measured in dynamical systems.

In Sec. 4 we demonstrate the basic construction of nonchaotic strange attractors and show how they may arise from even linear skew translations on the two-dimensional torus.

In Sec. 5 we present examples to illustrate how four different features of dynamical systems may be modified to make it nonlinear. The point of this set of examples is to expand our insight into two-dimensional systems in a way not afforded by the traditional analysis of the Poincaré–Bendixson theory.

In Sec. 6 we clarify the relationships between dissipation, noninvertibility, nonorientation preserving, and chaos.

In Sec. 7, we summarize this paper and also summarize the combined results of our first paper and this paper.

In the following discussions we will use some abbreviations introduced in the first tutorial [Brown & Chua, 1996a], and include several more that will be used throughout this paper:

### Abbreviations

Sensitive dependence on initial conditions (SD), Zero Autocorrelation (ZA), Zero Lyapunov exponent (LZ), Positive Lyapunov Exponent (LP), Zero Entropy (ZE), Strange Attractor (SA), Ergodic (E), Weak Mixing (WX), Strong Mixing (SX), Kolomogrov (K), Bernoulli (B).

The formal definitions of the last five abbreviations are from ergodic theory and can be found in [Walters, 1982]. In short, they are measures of how well a transformation mixes up its domain when iterated over a infinite time span. Ergodic is the lowest form of mixing and Bernoulli the highest. Dynamical systems that have one of these forms of mixing have some level of complexity. Chaos is usually associated with B in some way.

### Algorithmic Complexity and Level of Complexity

The concept of algorithmic complexity developed by Chaiten, Kolomogrov, and others is used to distinguish two levels of complexity. In reference to infinite sequences of integers, a sequence has positive algorithmic complexity when the number of binary bits required to code the shortest computer program needed to produce the sequence is just about the same length as the number of binary bits required to write the sequence out explicitly. For infinite sequences, this number is defined in such a way that either it is positive or zero. A sequence of positive algorithmic complexity is, "essentially", random. Zero algorithmic complexity thus denotes sequences that are less than random. This encompasses all sequences which can be described by a finite algorithm. The square root of a prime number is such a sequence, as is the number $\pi$, and all other physical constants. This notion of complexity is too limiting for our use and so we introduce the notion of a *level of complexity* of a sequence. Entropy is a measure of a level of complexity, as is autocorrelation, and information. The Lyapunov exponent is a measure of a level of complexity as well. In the study of chaos, various researchers appeal to these measurements to characterize dynamical systems that have a degree of unpredictability or intractability. The complexity spectrum is a term introduced in [Brown & Chua, 1997] as a means of talking about all of these measurements of a dynamical systems collectively. No formal definition has yet been formulated.

## 2. Bernoulli Chaos

In our previous tutorial we presented numerous examples and counter-examples designed to sharpen our thinking about the definition of chaos. That paper served to show that the manifestations of chaos are varied and difficult to summarize in a single definition. In order to better understand the variety of ways in which chaos can arise, we begin with the Bernoulli systems, possibly the highest form of chaos, and carry out a program of systematic "dilution" of this form of chaos until chaos disappears altogether. The methods that we use to modify a Bernoulli system reveal how chaotic systems may arise. The most important motivating example is that of Kalikow of a Kolomogrov automorphism which is constructed by using one Bernoulli system to modify another in such a way that the resulting system is not Bernoulli, but is Bernoulli on a set of measure zero.

Once we have hit upon the idea of modifying Bernoulli systems as a means of creating chaos we may take off with this idea in all directions.

Among the ways to modify a Bernoulli system are:

(1) Form a cross-product between a Bernoulli and nonBernoulli;
(2) Form a partial product of Bernoulli with any other map, including Bernoulli ($K$-automorphisms);
(3) Compose Bernoulli and nonBernoulli;
(4) Form a function of a component of a Bernoulli (logistic map);
(5) Form the weighted average of a Bernoulli and nonBernoulli system (the fundamental map) [Brown & Chua, 1996].

This list is incomplete. The different ways a Bernoulli system may be modified to make a chaotic system are likely to be so numerous and varied that no single characterization would be possible.

## 2.1. *The Bernoulli map*

In our paper on the fundamental map [Brown & Chua, 1996b] we showed how to construct a function of a two-sided Bernoulli map. We repeat a portion of that construction as background to our derivation of the sequence of iterates of the cat map.

Before we repeat that construction we note that the map that is most easily proven to be a two-sided Bernoulli shift is the bakers transformation, [Arnold & Avez, 1968]. The most familiar formulation of this map is

$$\begin{pmatrix} x \\ y \end{pmatrix} \to \begin{pmatrix} 2x \\ y/2 \end{pmatrix} \bmod(1) \tag{1}$$

for $0 \le x \le 1/2$ and

$$\begin{pmatrix} x \\ y \end{pmatrix} \to \begin{pmatrix} 2x \\ (y+1)/2 \end{pmatrix} \bmod(1) \tag{2}$$

for $1/2 \le x \le 1$. This map formulation can be greatly simplified by the use of the notation $[x]$ which denotes the integer part of $x$. In this notation we have:

$$\begin{pmatrix} x \\ y \end{pmatrix} \to \begin{pmatrix} 2x \\ ([2x]+y)/2 \end{pmatrix} \bmod(1). \tag{3}$$

If we use $\{x\}$ for the fractional part of $x$ this simplifies to

$$\begin{pmatrix} x \\ y \end{pmatrix} \to \begin{pmatrix} \{2x\} \\ ([2x]+y)/2 \end{pmatrix}. \tag{4}$$

In this form, a closed-form solution for the $n$th term of this sequence is (note that this solution is not in terms of elementary functions):

$$\begin{pmatrix} \{2^n x\} \\ ([2^n x]+y)/2^n \end{pmatrix}. \tag{5}$$

Note that everything we have said about this map carries over to the case where 2 is replaced by any positive integer $k$. Thus

$$\begin{pmatrix} \{k^n x\} \\ ([k^n x]+y)/k^n \end{pmatrix} \tag{6}$$

is a formula for the $n$th iterate of a bi-lateral shift on $k$ symbols. While this sequence can be made the time-one map of an ODE representing an electronic circuit by our usual methods [Brown & Chua, 1992], we will direct our attention to the cat map instead. This is because the cat map is also a Bernoulli shift [Katznelson, 1971] and its solution can be expressed in terms of the elementary functions. Hence we will use the cat map as our basic example of a Bernoulli map, although the proof in case of the baker's transformation is easier to see [Arnold & Avez, 1968, Appendix 7].

As in [Brown & Chua, 1996b], let

$$\begin{pmatrix} u \\ v \\ w \\ z \end{pmatrix} = \begin{pmatrix} \cos(x) \\ \sin(x) \\ \cos(y) \\ \sin(y) \end{pmatrix}. \tag{7}$$

By direct substitution, application of the double-angle formulas for the sine and cosine, and simplification, we get the following four-dimensional system, $T$, on a two-dimensional space:

$$T\begin{pmatrix} u \\ v \\ w \\ z \end{pmatrix} = \begin{pmatrix} 0 & 0 & (u^2-v^2) & -2uv \\ 0 & 0 & 2uv & (u^2-v^2) \\ w & -z & 0 & 0 \\ z & w & 0 & 0 \end{pmatrix} \times \begin{pmatrix} u \\ v \\ w \\ z \end{pmatrix}. \tag{8}$$

In complex coordinates this map is given by:

$$T\begin{pmatrix} w \\ z \end{pmatrix} = \begin{pmatrix} w^2 z \\ wz \end{pmatrix} \tag{9}$$

where $|w| = |z| = 1$. A simple computation shows that this mapping is $1-1$, in particular:

$$T^{-1}\begin{pmatrix} w \\ z \end{pmatrix} = \begin{pmatrix} w\bar{z} \\ z^2\bar{w} \end{pmatrix}. \tag{10}$$

We now write the sequence of iterates of the cat map in closed form in terms of elementary functions. The key to doing this is the derivation of an expression for the $n$th power of the matrix used in the definition of the cat map. Let

$$A = \begin{pmatrix} 2 & 1 \\ 1 & 1 \end{pmatrix} \tag{11}$$

then

$$A^n = \frac{1}{(1-\lambda^2)\lambda^{n-1}} \begin{pmatrix} \lambda^{2n}(1-\lambda)+(2-\lambda) & 1-\lambda^{2n} \\ 1-\lambda^{2n} & (\lambda^{2n}(1-\lambda)+(1-2\lambda))/\lambda \end{pmatrix} \tag{12}$$

where $\lambda = 0.5(3+\sqrt{5})$, which is the largest eigenvalue of the matrix $A$. Using this we may write the $n$th term in the sequence of iterates of this map. For notational convenience let

$$\begin{pmatrix} a_n & b_n \\ c_n & d_n \end{pmatrix} = \frac{1}{(1-\lambda^2)\lambda^{n-1}} \begin{pmatrix} \lambda^{2n}(1-\lambda)+(2-\lambda) & 1-\lambda^{2n} \\ 1-\lambda^{2n} & (\lambda^{2n}(1-\lambda)+(1-2\lambda))/\lambda \end{pmatrix}$$

then

$$\begin{pmatrix} u_n \\ v_n \\ w_n \\ z_n \end{pmatrix} = \begin{pmatrix} \cos(a_n\phi_0 + b_n\theta_0) \\ \sin(a_n\phi_0 + b_n\theta_0) \\ \cos(c_n\phi_0 + d_n\theta_0) \\ \sin(c_n\phi_0 + d_n\theta_0) \end{pmatrix}. \tag{13}$$

Note that $b_n = c_n$.

This is the closed-form solution we seek for the chaotic mapping on the torus. By taking arctangents we obtain the Bernoulli iterates in terms of the elementary functions.

What we have done, as in our example of the logistic map, is not very complex. To obtain the solutions we sought, we needed only to find a method of getting around the use of the modulo(1) operation. The basic technique of doing this was explained in [Brown & Chua, 1996a]. The key idea to note, periodic functions perform the same operation as the modulo(1) function.

## 2.2. *The Bernoulli map as a Poincaré map*

By employing a two-phase gate we may construct the equations of a nonautonomous ODE whose Poincaré map is the Bernoulli map. This technique is explained in [Brown & Chua, 1993]. We have the following equation for which the Bernoulli map is the Poincaré map:

$$\begin{pmatrix} \dot{w} \\ \dot{z} \end{pmatrix} = \begin{pmatrix} (1-s(t))w\log(z) \\ s(t)z\log(w) \end{pmatrix} \tag{14}$$

where $s(t) = 0.5(1+\text{sgn}\,\sin(\omega t))$. Initial conditions must be taken to have absolute value 1.

The Bernoulli map can be written, as this equation suggests, as a composition of two maps:

$$T_1\begin{pmatrix} w \\ z \end{pmatrix} = \begin{pmatrix} w \\ zw \end{pmatrix} \tag{15}$$

$$T_2\begin{pmatrix} w \\ z \end{pmatrix} = \begin{pmatrix} wz \\ z \end{pmatrix} \tag{16}$$

which are time-one maps for autonomous ODEs. The Bernoulli map is $T_2 \circ T_1$. The component maps arise as time-one maps of the solutions of two systems of ODEs. The solutions are as follows:

$$\begin{pmatrix} w_1(t) \\ z_1(t) \end{pmatrix} = \begin{pmatrix} w_0 \\ z_0 w_0^t \end{pmatrix} \tag{17}$$

$$\begin{pmatrix} w_2(t) \\ z_2(t) \end{pmatrix} = \begin{pmatrix} w_0 z_0^t \\ z_0 \end{pmatrix} \tag{18}$$

which are the solutions of the separate component ODEs corresponding to the two phases of the function $s(t)$.

These equations are presented in complex form for convenience. The complex representation is not essential and no complex variable theory has been used in our analysis.

Now that we have a Bernoulli mapping in an algebraic formula we proceed to utilize this map to

construct examples of chaos which are less than Bernoulli.

### 2.3. *Cross products with Bernoulli systems*

The simplest way to obtain a map which is Bernoulli on a set of measure zero is to have at least one component of a cross product to be Bernoulli, and one that is not Bernoulli. Let,

$$T\begin{pmatrix} u \\ v \\ w \end{pmatrix} = \begin{pmatrix} u^2 v \\ uv \\ aw \end{pmatrix} \tag{19}$$

where the first two components are restricted to have modulus 1. If we choose $w_0 = 1$, and $0 < a < 1$, we form orbits for which the third coordinate converges to 0 but the first two are Bernoulli. By construction, $T$ is not Bernoulli but is Bernoulli on a set of measure zero. Further, the points of the first two components form a two-dimensional attractor which is Bernoulli.

The three-dimensional image of the orbits of the map defined by Eq. (19) is shown in Fig. 1. As seen there, the orbit converges to a two-dimensional square which is the attractor. Another way of looking at this figure is to think of the third coordinate as a time parameter. With this point of view, the time evolution of the Bernoulli map is portrayed by the third dimension. The uniformity of the points that lie above the attractor portray the randomness of the orbit. If the points that lie above the attractor formed a pattern, we would know that the Bernoulli system determined by the first two coordinates is less than random. This brings us to Fig. 2, another Bernoulli map. In this case, instead of our map being the analog of the one-dimensional map $2x \bmod(1)$, it is the analog of $1.032x \bmod(1)$. This map thus has a positive Lyapunov exponent, $\approx 0.032$, and is the root of a shift, a horseshoe. However, as seen in Fig. 2, it is less than random, having distinctive pattern features in its orbit. Figure 2 shows that having a positive Lyapunov exponent does not mean that there is a high degree of randomness, or chaos in the map, even though, by any definition, it is chaotic.

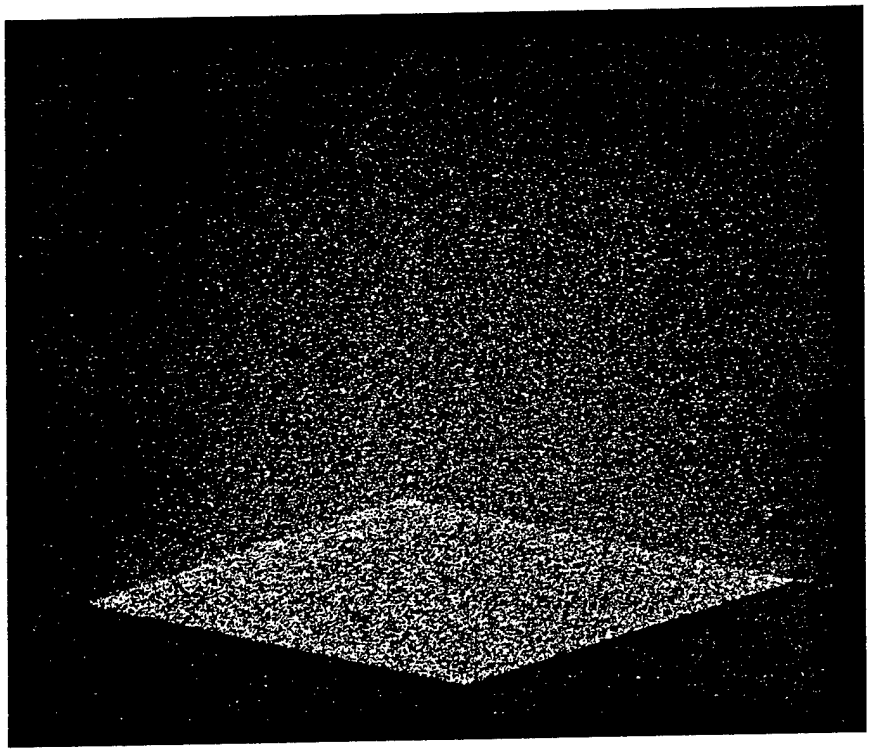

Fig. 1. In Fig. 1 we have made the domain, a square, of the cat map an attractor. The result is that, when the initial condition has a nonzero $z$ value the orbit is attracted to a square in the $x - y$ plane. The effect is reminiscent of mist rising from a body of water.

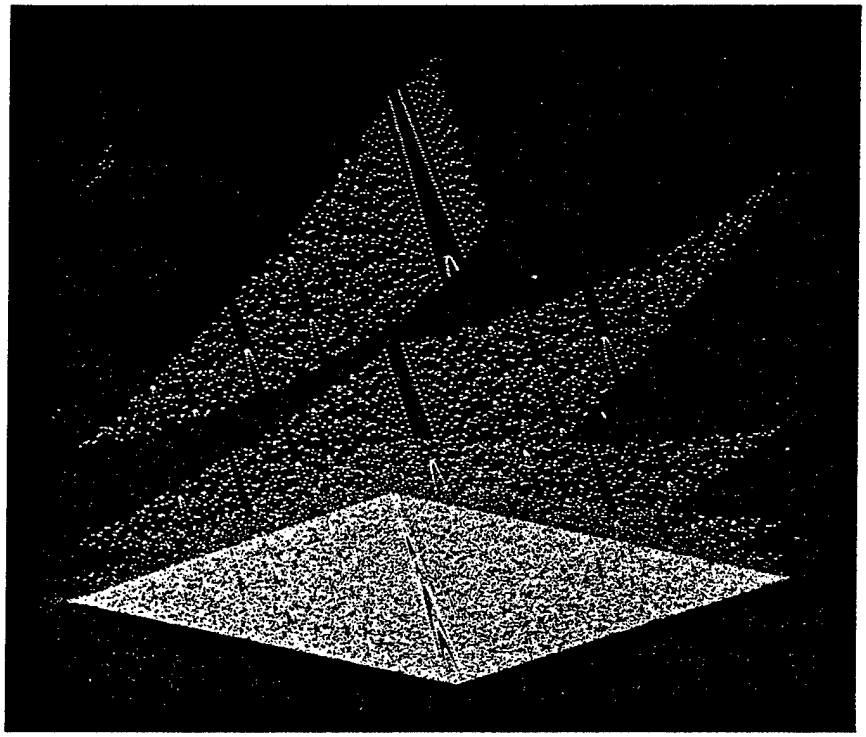

Fig. 2. In Fig. 2 we modified the cat map to have a Lyapunov exponent of $\approx 0.039$. The figure format is exactly the same as Fig. 1. The result is the development of nonchaotic graphical features. By making the range of the modified cat map an attractor, this breakdown in the level of complexity is clearly visible in the part of the orbit above the attractor.

## 2.4. *K-automorphisms*

Following an example of Kalikow from [Walters, 1982] we construct (without proof) a map which is a $K$-automorphism:

$$K\begin{pmatrix} u \\ v \\ w \\ z \end{pmatrix} = \begin{pmatrix} u^2 v \\ uv \\ \mathrm{sg}(u)(w^2 z) + (1 - \mathrm{sg}(u))(w\bar{z}) \\ \mathrm{sg}(u)(wz) + (1 - \mathrm{sg}(u))(z^2 \bar{w}) \end{pmatrix} \tag{20}$$

where $\mathrm{sg}(u) = 0.5(1 + \mathrm{sgn}(0.5 + \cos(\arg(u))$. We note that $K$ has a set of measure zero on which it is Bernoulli in analogy with the horseshoe of Smale. The construction is not a direct product, so we call it a partial product.

Figure 3 is a three-dimensional illustration of a modification of this map. The modification is to the first component where, for convenience, we have used the logistic map as a one-dimensional source of chaos to be used to switch between the cat map and its inverse. The exact equation for Fig. 3 is as follows:

$$K\begin{pmatrix} u \\ w \\ z \end{pmatrix} = \begin{pmatrix} 4u(1-u) \\ \mathrm{sg}(u)(2w + z) + (1 - \mathrm{sg}(u))(w - z)) \\ \mathrm{sg}(u)(w + z) + (1 - \mathrm{sg}(u))(2z - w) \end{pmatrix} \times \mathrm{mod}(1) \tag{21}$$

where $\mathrm{sg}(u) = 0.5(1 + \mathrm{sgn}(0.5 - u)$.

This example captures the essence of Eq. (21) while being simpler to implement on a computer. In the vertical dimension, $K$ is just the logistic map. In the $z$, $w$ dimension $K$ alternates between the cat map and its inverse. The Lyapunov exponent in the $z$, $w$ dimensions is the same as the cat map. However, the level of complexity of the orbit that cat map contributes is being constantly reversed by its inverse. The possibility of global chaos that comes from the cat map must always be compromised by the inverse, thus leaving only local, finite excursions of chaos that come from long runs by the logistic map having a value above 0.5. Thus the chaos of this map is actually being imparted by the logistic map. We will see in Sec. 3 that it is possible to construct an example of a three-dimensional map from Eq. (21) where we replace the first two components

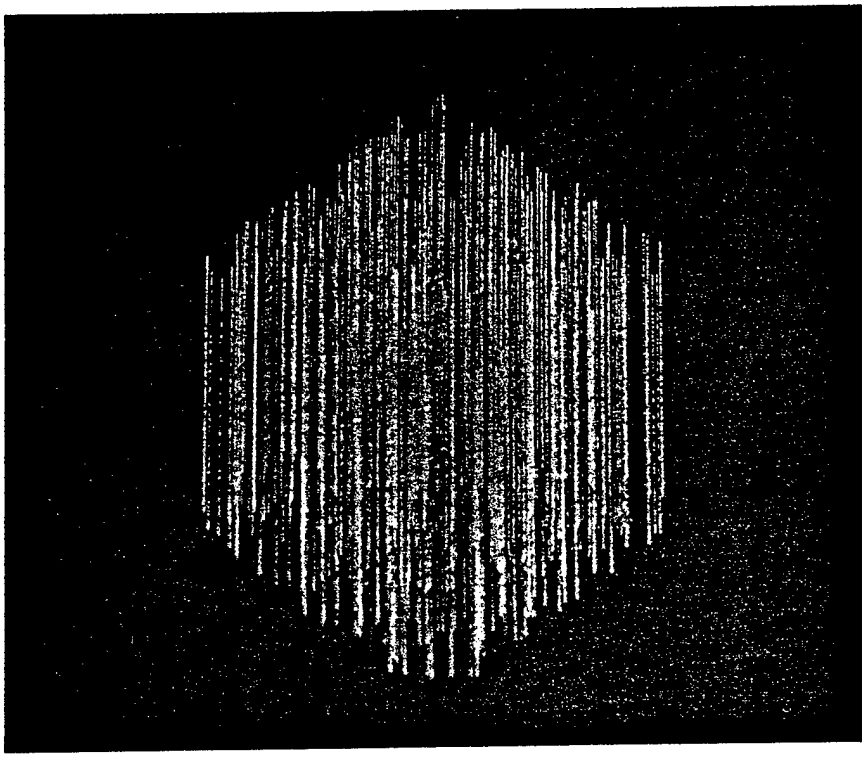

Fig. 3. The orbit of the $K$ map of Eq. (21) is presented with the same format as Figs. 1 and 2. While there are no orderly geometric features present as there are in Fig. 2, the orbit is clearly different from the cat map.

with a map which has a LZ, ZA, E, and hence it looks "random."

## 2.5. *Other partial products*

The following example is neither Bernoulli, $K$, nor almost periodic, but has a set of measure zero on which it is Bernoulli:

$$K\begin{pmatrix} u \\ v \\ w \\ z \end{pmatrix} = \begin{pmatrix} u^2 v \\ uv \\ \mathrm{sg}(u)(w^2 z) + (1 - \mathrm{sg}(u))(aw) \\ \mathrm{sg}(u)(wz) + (1 - \mathrm{sg}(u))(bz) \end{pmatrix} \tag{22}$$

since the third and fourth components of the map alternate "randomly" between Bernoulli and are almost periodic.

We note that by replacing the function $\mathrm{sgn}(u)$, which occurs in the definition of the function $\mathrm{sg}(u)$, in the above equations with a sigmoid function we make all examples infinitely differentiable.

## 2.6. *Gated compositions with Bernoulli systems*

We have shown how to use a two-phased gate to construct Poincaré maps from time-one maps of autonomous ODEs [Brown & Chua, 1993]. In those constructions we choose each phase of the gate to have equal time. Using a gate which does not have equal time gives us another construction. We explain this construction in two steps. First we describe the gate:

$$s_1(t) = 1 \quad \text{for} \quad 0 \le t < 1 \tag{23}$$

$$s_1(t) = 0 \quad \text{for} \quad 1 \le t < 3 \tag{24}$$

$$s_1(t+3) = s_1(t) \tag{25}$$

$$s_2(t) = 1 - s_1(t) \tag{26}$$

Note that $s_2(t)$ is nonzero twice as long as $s_1(t)$. Using this gate we define a general nonautonomous ODE:

$$\dot{x} = s_1(t)F_1(x) + s_2(t)F_2(x)\,. \tag{27}$$

The Poincaré map determined by sampling the map at times $t = 1, 2, 3, \ldots$, results in one point of the orbit being determined by $\dot{x} = F_1(x)$ and the next two points being determined by $\dot{x} = F_2(x)$, then back to the $F_1$ equation. The Poincaré map is not simply the composition of the maps determined by $F_1$ and $F_2$ because we must actually get one point

of the orbit from the $F_1$ equation and then get *two* points from the $F_2$ equation. A composition would omit the intermediate points, only recording the result of applying the $F_1$ equation and then the $F_2$ equation to the initial point. The presence of these intermediate points being included in the orbit is significant in that they alter the geometry and the level of complexity of the orbit.

The time difference between the two phases may be as long as we desire. In our example this ratio is 1:2. The greater the ratio between the phases the greater the difference in the contribution to the orbit by the two phases. In this way, we may combine a Bernoulli phase with an almost-periodic phase in such ratios (say, 1:1000000) that the Bernoulli contribution is as thin as we please and the resulting orbit must still be chaotic. This technique shows how to include a Bernoulli system at any desired level we choose to construct a chaotic orbit whose chaotic features are as "thin" as we choose. The mechanism illustrated by this example could easily be reflected in a real-world system in which complex forces alternated with periodic forces to shape some geological feature or biological feature of a life form.

Another technique we may use is to construct the time one-half map, i.e. sample the orbit at intervals of $t = 1/2$. In this way we get two Bernoulli points followed by four almost-periodic points. Doing this amounts to refining the gates into four phases, each gate being decomposed into two phases over its nonzero range. The technique of gate refinement corresponds to the mathematical technique of refining a partition of the real line, so often used in measure theory and ergodic theory. Using the refinement method we can now construct the ODE which is a gated composition of Bernoulli and almost periodic. After all the simplifications we get a three-phased gate as follows:

$$s_1(t) = 1 \text{ for } 0 \le t < 1 \tag{28}$$

$$s_1(t) = 0 \text{ for } 1 \le t < 6 \tag{29}$$

$$s_2(t) = 0 \text{ for } 0 \le t < 1 \tag{30}$$

$$s_2(t) = 1 \text{ for } 1 \le t < 2 \tag{31}$$

$$s_2(t) = 0 \text{ for } 2 \le t < 6 \tag{32}$$

$$s_3(t) = 0 \text{ for } 0 \le t < 2 \tag{33}$$

$$s_3(t) = 1 \text{ for } 2 \le t < 6 \tag{34}$$

We extend the functions to be periodic of period 6. Now we define our gated-circuit equation in complex variable notation:

$$\begin{pmatrix} \dot{w} \\ \dot{z} \end{pmatrix} = \begin{pmatrix} s_1(t)w\log(z) + s_3(t)z \\ s_2(t)z\log(w) - \lambda^2 s_3(t)w \end{pmatrix}. \tag{35}$$

By altering the ratios of the gate we obtain any level of chaos desired.

### Functions of Bernoulli Systems

In [Brown & Chua, 1996a], we showed how to compose periodic functions with exponential functions to get closed-form solutions to chaotic equations. The basic process can be extended to Bernoulli systems.

### Weighted Averages of Bernoulli and NonBernoulli Systems

In [Brown & Chua, 1996b], we illustrate how to combine Bernoulli with almost periodic to obtain a wide range of chaotic maps.

## 2.7. *Chaotic systems from Bernoulli time*

Since exponential stretching can generate chaos, any system that "circulates" through a region of exponential stretching an infinite number of times that is not offset by a equal amount of contracting may produce chaos. (Even if it circulates through an equal amount of contracting, it may still produce chaos.) Typically, circulation through a region of exponential stretching will depend on the initial conditions.

Bernoulli systems are an easy source of exponential stretching and, as we have shown earlier, may be decomposed into two maps which are each *nonexponentially* stretching. Hence we need only circulate through nonexponentially-stretching regions in some manner to generate chaos. An important question is whether we may circulate through a stretching region in an almost periodic manner and generate chaos. The answer is yes, since the unstable manifold of the Bernoulli system on the torus, the cat map, winds through the torus in an almost periodic manner. If this manifold were the orbit of a point moving with constant velocity the result would be almost periodic motion. This

comment leads to our next means of creating chaos from Bernoulli systems:

(6) Starting with a continuous-time system on a bounded manifold which is almost periodic and whose orbits have infinite arc length, we change the time parameter from $t$ to $\exp(t)$.

Having connected orbits of infinite arc length assures that the new system is invertible. If the arc length is finite, such as a circle, then the resulting system can be noninvertible. (For example, $x = \cos(\exp(t))$, $y = \sin(\exp(t))$.) By using the torus instead of a circle we have room to maneuver out of the way of previous points in the orbit. In particular, starting with any orbit on the torus inclined at an irrational angle from the vertical we obtain an orbit of infinite arc length on which we may move forward in exponential time to create chaos. This amounts to wrapping an orbit of $\dot{x} = x$, $\dot{y} = y$ around the torus inclined at an irrational angle. Generalizing this concept we have the following method of generating chaos from Bernoulli systems:

(7) Given any bounded manifold on which there is a vector field with integral curves having infinite arc length, we may change the time parameter to exponential time and obtain a chaotic system. It is only necessary to change the time to $a^t$ for $a > 1$ to obtain chaos.

As a variation on this idea we have the following method of generating chaos from Bernoulli systems:

(8) Given any sequence, we may intersperse an infinite number of points from a Bernoulli sequence by any rule and the resulting sequence becomes chaotic.

### 2.8. *Bernoulli space-time*

As we have noted, we may make almost periodic systems chaotic by changing the time scale. In general, a time scale which is accelerating cannot be distinguished from a uniform time scale in which spatial coordinates are accelerating. Thus, nonuniform Space-Time acceleration can give rise to chaos. Of course, this is "relative" to an imagined observer moving in a nonaccelerating frame. The nonuniform acceleration we are most interested in is the sort in which an object has some magnitude which is accelerating and decelerating, since no magnitude can increase indefinitely. An example is a planetary system consisting of three planets grouped as a unit (think of the earth having two large moons), orbiting around a star. Their mutual gravitational attractions can cause their orbits to be chaotic. The result is that there is no uniform time scale, since on each planet the sun rises at a different time during each revolution. The time scale is Bernoulli, and these life forms, if they could exist, live in Bernoulli Space-Time.

## 3. Complex Dynamics from Maps with Zero Lyapunov Exponents (LZ)

We now present examples to show that systems with zero Lyapunov exponents can produce a level of unpredictability greater than some chaotic systems.

The rationale for these examples is a theorem of Weyl [1916], and our observations in [Brown & Chua, 1996a] that the sequence $\sin(n^2)$ is uncorrelated and uniform. The example to be given is well known to ergodic theory but less known in the general scientific community. Also, we show how to make this map a Poincaré map for an electronic circuit. The map is:

$$T\begin{pmatrix} x \\ y \end{pmatrix} = \begin{pmatrix} x+y \\ y+\tau \end{pmatrix} \bmod(1) \tag{36}$$

If $\tau$ is irrational, this map is ergodic(E). Further, it is not a simple rotation, hence its obits are not almost periodic. The eigenvalues are 1, 1, hence the Lyapunov exponent (LZ) is 0. Further, it has zero entropy (ZE), see [Peterson, 1983] for all facts. This is a two-dimensional example of what is called in ergodic theory a *skew translation.* In complex coordinates it can be expressed as

$$T\begin{pmatrix} w \\ z \end{pmatrix} = \begin{pmatrix} wz \\ az \end{pmatrix} \tag{37}$$

where $|a| = |w| = |z| = 1$. We recall that a twist on the torus is written as

$$T\begin{pmatrix} w \\ z \end{pmatrix} = \begin{pmatrix} wz \\ z \end{pmatrix} \tag{38}$$

and so if $a = 1$ the twist and the skew translation are the same. Also, recall that a Bernoulli mapping on the torus is given by the composition of

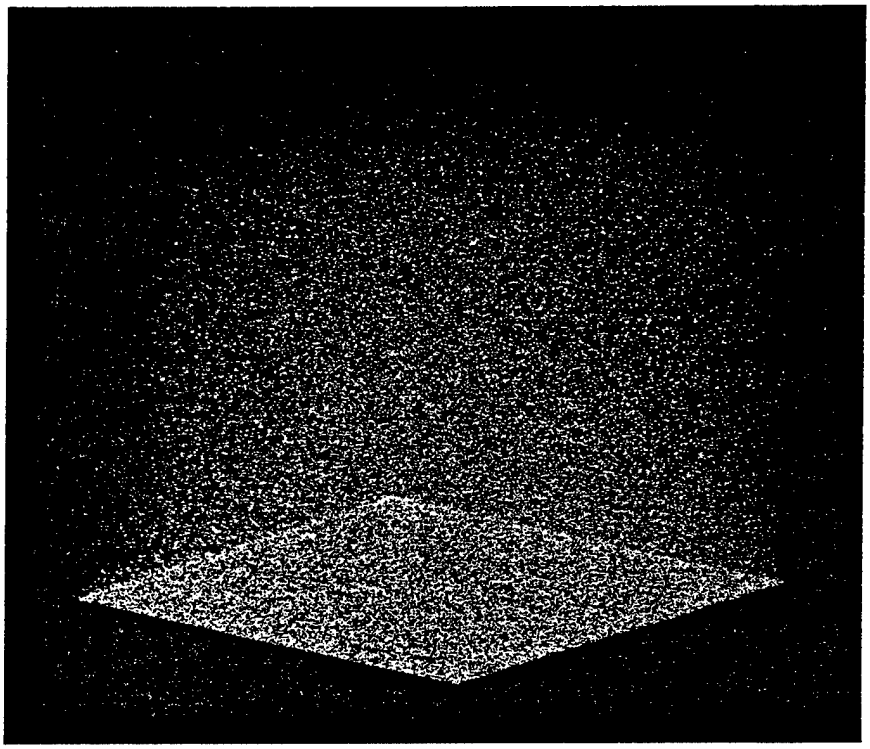

Fig. 4. The format of this orbit of a skew translation is the same as Fig. 1, the cat map. From a casual observation it is impossible to distinguish this orbit from the chaotic map in Fig. 1. However, the Lyapunov exponent is 0. In contrast to Fig. 2, a map with a positive Lyapunov exponent, this nonchaotic map more closely resembles chaos than the truly chaotic map of Fig. 2.

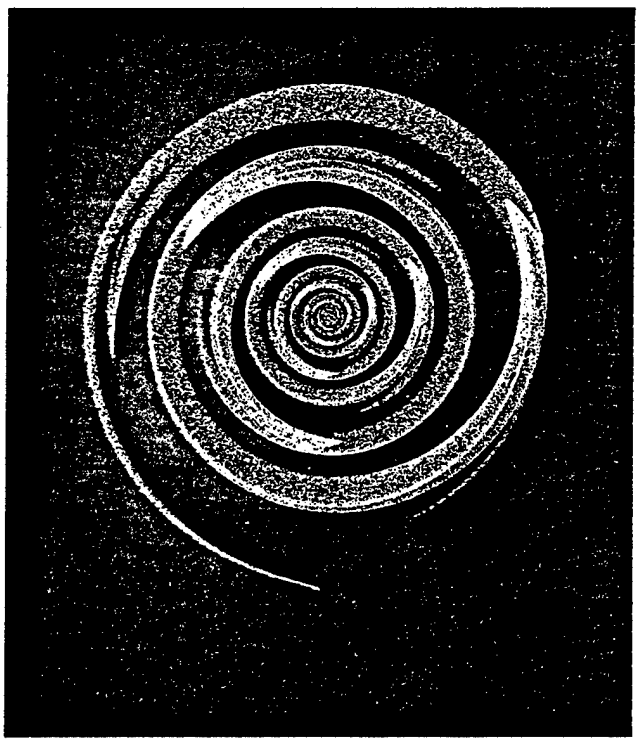

Fig. 5. In this figure we have transformed the orbit of Fig. 4 by a pair of twists. The result is an nonchaotic orbit that could be mistaken for a strange attractor.

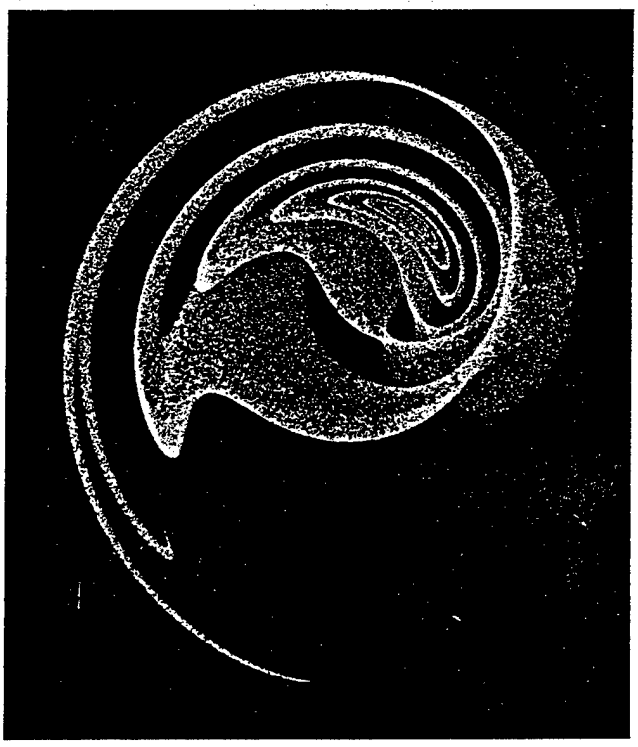

Fig. 6. In this figure we have transformed the orbit of Fig. 4 by another pair of twists, rendering a dramatic attractor which is nonchaotic.

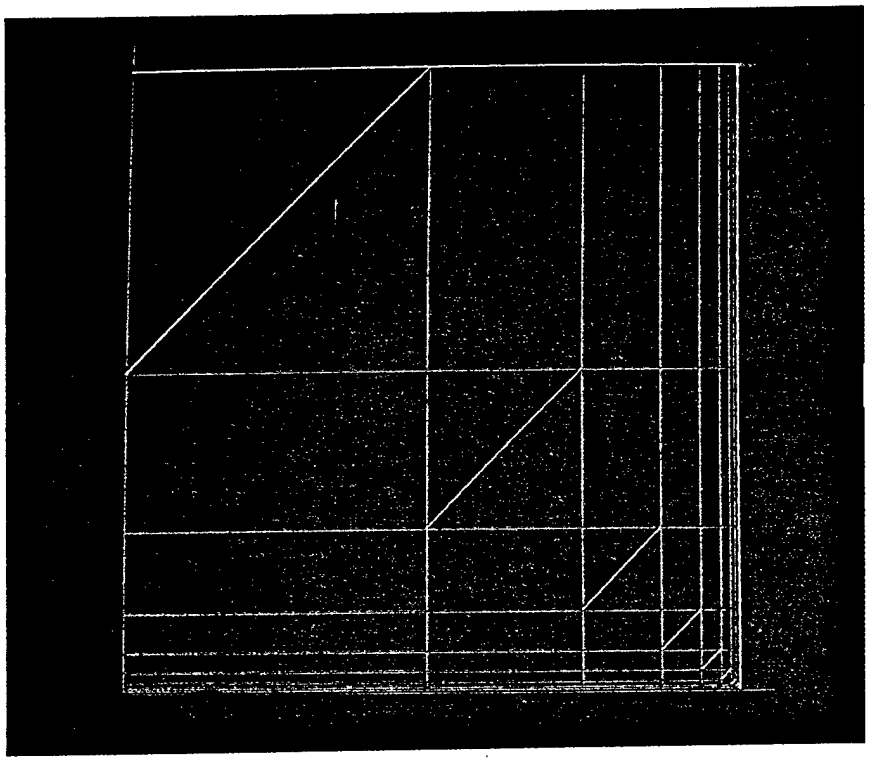

(a)

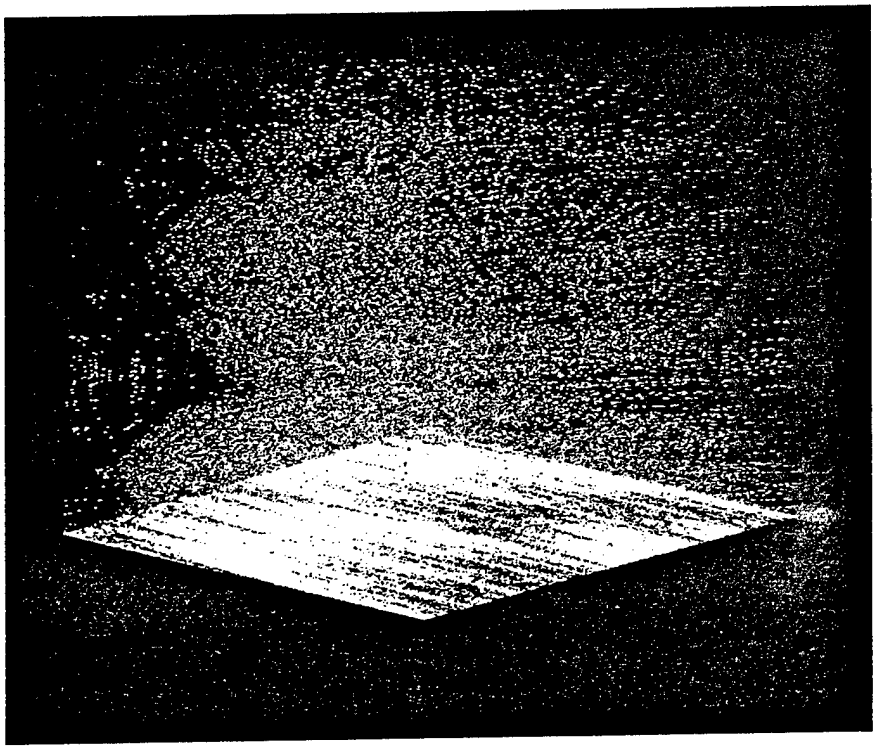

(b)

Fig. 7. (a) This figure is the graph of a simple ergodic map on the unit interval, an *interval exchange map* commonly encountered in ergodic theory. The $x$-axis partitions are at $(2^n - 1)/2^n$. The level of complexity here is minimal in that it is slightly more complicated than an irrational rotation. Except for the discontinuities, this map is made up of simple translations of intervals of the function $y = x$. (b) In this figure we have used the map of Fig. 7(a) to form a three-dimensional map in the format of Fig. 1. The orbit illustrated here shows just how complex this map can appear even though it is not chaotic.

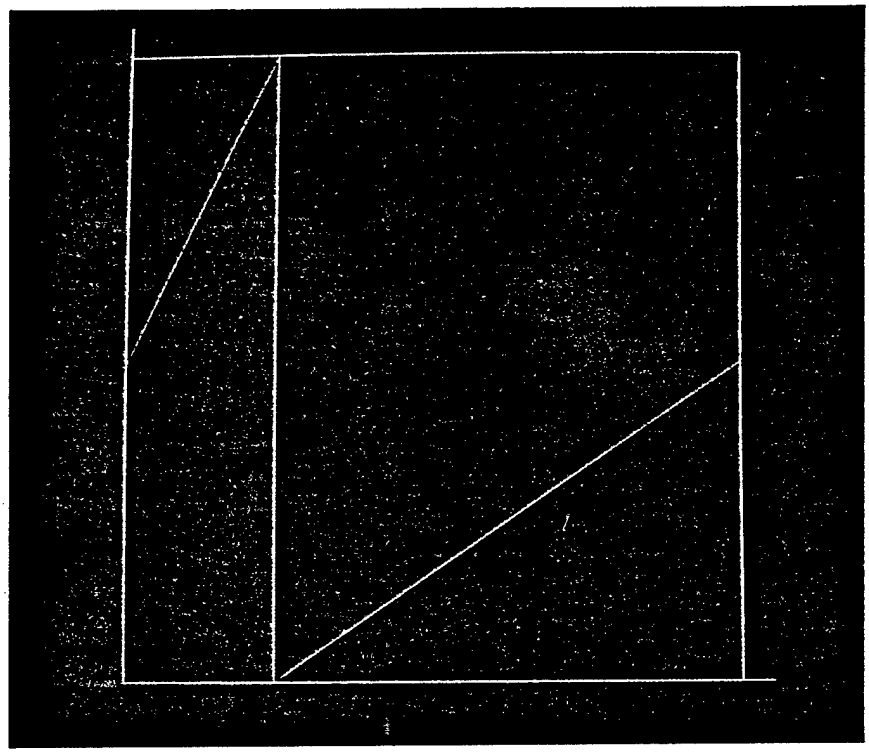

(a)

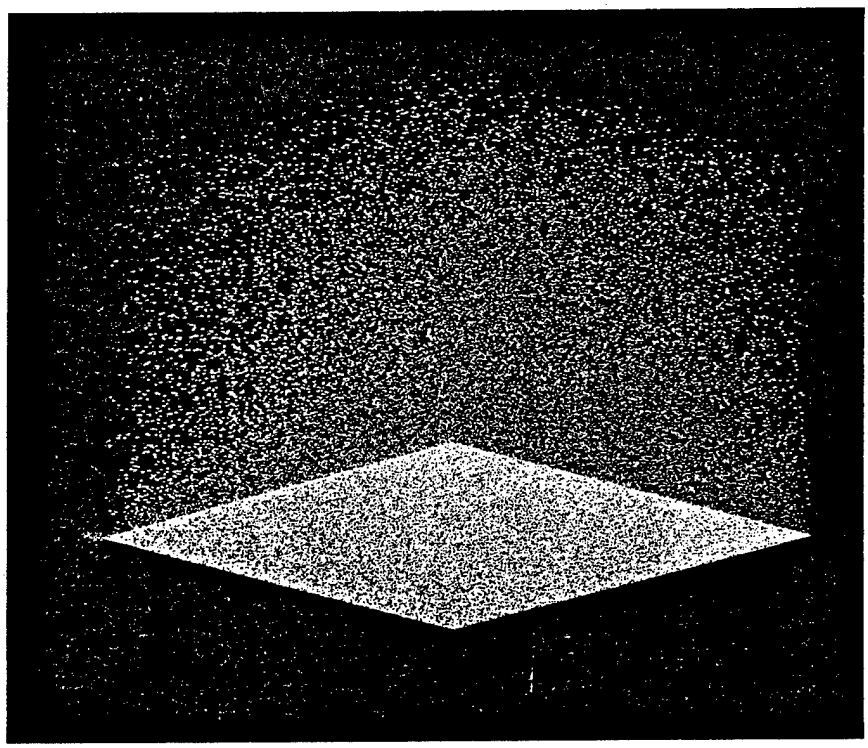

(b)

Fig. 8. In Fig. 8(a) we construct a map, $g(x)$, with LZ and E. As a result, the computation of the Lyapunov exponent is reduced to the fundamental theorem of calculus and we see that the total percentage of expansion must equal the total percentage of contraction so that the net is 0. Figure 8(b) reveals that this map produces a distribution of orbit points that is quite uniform. The map for Fig. 8(b) is the same as Eq. (44) where $f$ is replaced by $g$.

two twists:

$$T_1\begin{pmatrix} w \\ z \end{pmatrix} = \begin{pmatrix} wz \\ z \end{pmatrix} \tag{39}$$

$$T_2\begin{pmatrix} w \\ z \end{pmatrix} = \begin{pmatrix} w \\ zw \end{pmatrix} \tag{40}$$

and so

$$B\begin{pmatrix} w \\ z \end{pmatrix} = \begin{pmatrix} w^2 z \\ zw \end{pmatrix} = T_2 \circ T_1 . \tag{41}$$

The algebraic form of these equations reveals their relationships and clearly the skew translation falls between the twist (all orbits are almost periodic) and the Bernoulli map. If the complex number $a$ has positive algorithmic complexity, the orbits of the skew translation are, relative to the twist, unpredictable and have sensitive dependence on initial conditions (SD). In fact, the real-valued coordinates of this skew translation have factors like $\sin(n^2)$, $\cos(n^2)$ which are uncorrelated. To see this we obtain the $n$th iterate of this map by a direct computation:

$$T^n\begin{pmatrix} x \\ y \end{pmatrix} = \begin{pmatrix} x + ny + n(n+1)a/2 \\ y + na \end{pmatrix} \bmod(1) \tag{42}$$

By considering $k$-dimensional skew translations we may obtain terms which behave like $\sin(n^k)$, while retaining E, ZA, SD, and LZ. Following this idea to its natural conclusion we can construct a map with LZ which has terms that behave like $\sin(p(n))$ where $p(n) \approx \exp(n)$.

Figures 4–6 illustrate some orbits of a skew translation. Figure 4 is the analog of Fig. 1 in Sec. 2 and is presented in the same way. The exact equation is

$$T\begin{pmatrix} w \\ z \\ u \end{pmatrix} = \begin{pmatrix} w + z \\ a + z \\ bu \end{pmatrix} \bmod(1) \tag{43}$$

where $0 < |a|, |w|, |z|, |b| < 1$. Note that using addition mod 1 is just a convenient way of coding this equation. We could use a five-dimensional equation in accordance with our developed techniques and obtain the same figure. The significance of this LZ, ZE map is that the spatial orbit structure in appearance is clearly more complex than that of Fig. 2 which was produced by a LP map.

Figure 5 is produced by using Eq. (43) with a coordinate transformation defined by a twisting map. This demonstrates that an attractor's geometry can be separated from its level of complexity. Figure 6 demonstrates that other coordinate transformations can give the attractor any geometry we like. The specific coordinate transformation is not important. What is relevant is that the attractor can appear "strange" in one coordinate system while "familiar" in another.

Figure 7(a) illustrates a one-dimensional LZ map, $f(x)$. This example is due to Kakutani, see [Parry, 1981]. This map is far from chaos by any definition in that the orbits are slightly more complex than almost periodic orbits. But by making it a component of a three-dimensional map we reveal that it can produce an attractor which appears to have a high level of complexity, Fig. 7(b). The exact equation for Fig. 7(b) is as follows:

$$T\begin{pmatrix} w \\ z \\ u \end{pmatrix} = \begin{pmatrix} f(w) \\ z + w \\ au \end{pmatrix} \bmod(1) \tag{44}$$

where $0 < |w|, |z|, |b| < 1$. The "holes" in the attractor in Fig. 7(b) are not repelling regions, but rather reflections of the orbit correlation of the function $f$. If we iterate long enough, the entire square will be covered with the points of the orbit.

Taking a different turn we may ask if we can construct an example which is globally LZ for which there are times it is locally not LZ. This amounts to seeking an example which, when the exponents are averaged over infinite time, the exponents are not positive, but for which over finite periods of the orbit they are positive. Clearly, if there are some runs of positive exponents there must be some runs of negative exponents to force the average to be zero.

It is possible to construct any number of such maps on the unit interval so long as we allow a countable number of discontinuities. The process requires that the interval be partitioned into subintervals and on each subinterval we define our function to be increasing and differentiable. Further, on the set of subintervals the functions must be chosen to be invertible. Figure 8 is an example.

In Fig. 8(a) we construct a map, $g(x)$, with LZ and E. As a result, the computation of the Lyapunov exponent is reduced to the fundamental theorem of calculus and we see that the total percentage of expansion must equal the total percentage of contraction so that the net is 0. Figure 8(b) reveals that this map produces a distribution of orbit points that is quite uniform. The

map for Fig. 8(b) is the same as Eq. (44) where $f$ is replaced by $g$.

Thus there are LZ maps which are WX, SD, and ZA, but are not $B$ or even $K$. It is not known whether the map of Eq. (36) is SX for the right choice of $a$. These maps can be made Poincaré maps for ODEs which can be implemented in useful electronic circuits by the techniques of Brown and Chua [1993].

## 4. Strange Attractors and Space-Time Chaos

### 4.1. *The phenomena of strange nonchaotic attractors*

Numerous researchers have reported on strange nonchaotic attractors. An early paper is that of Grebogi *et al.* [1984]. The paper of Ding *et al.* [1989] is an important development of the 1984 paper. The authors sought to bring attention to the fact that an attractor may have complex geometry without arising from LP maps. The 1989 work sought to show how this fits into the scheme of nonlinear dynamics. We show here that the matter of nonchaotic strange attractors can be traced to low-orbit correlation. But first we address the 1984 and 1989 examples.

The skew translation of Eq. (36) may be modified to be nonlinear as follows:

$$\begin{pmatrix} x \\ y \end{pmatrix} \to \begin{pmatrix} f(x,y) \\ y+a \end{pmatrix} \bmod(1) \qquad (45)$$

where $a$ is a constant. We remind the reader that the use of the mod(1) function is only a convenience and may be replaced by elementary functions by increasing the dimensions of our space. From this equation it is clear that the equations of Grebogi *et al.* [1984] are nonlinear skew translations as is also the case with the equations of Ding *et al.* [1989]:

$$\begin{pmatrix} x_{n+1} \\ \theta_{n+1} \end{pmatrix} = \begin{pmatrix} f(x_n,\theta_n) \\ (\theta_n + 2\pi\omega)\bmod(2\pi) \end{pmatrix}. \qquad (46)$$

As with proving that maps are chaotic by proving the existence of horseshoes, for this line of analysis to be complete it would be necessary to show that the time-one maps of the ODE that are analyzing

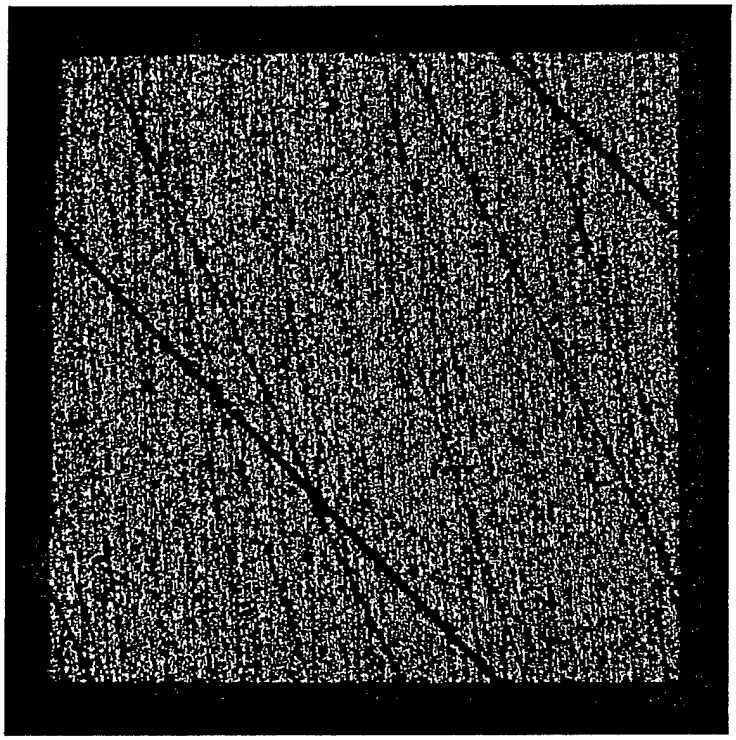

Fig. 9. Figure 9 demonstrates that the nonlinearities of the Grebogi, Ott, Pelikan and Yorke nonchaotic SA are not essential to obtain nonchaotic strange attractors. To obtain this attractor we have modified Eq. (36) to have an eigenvalue of 0.9999.

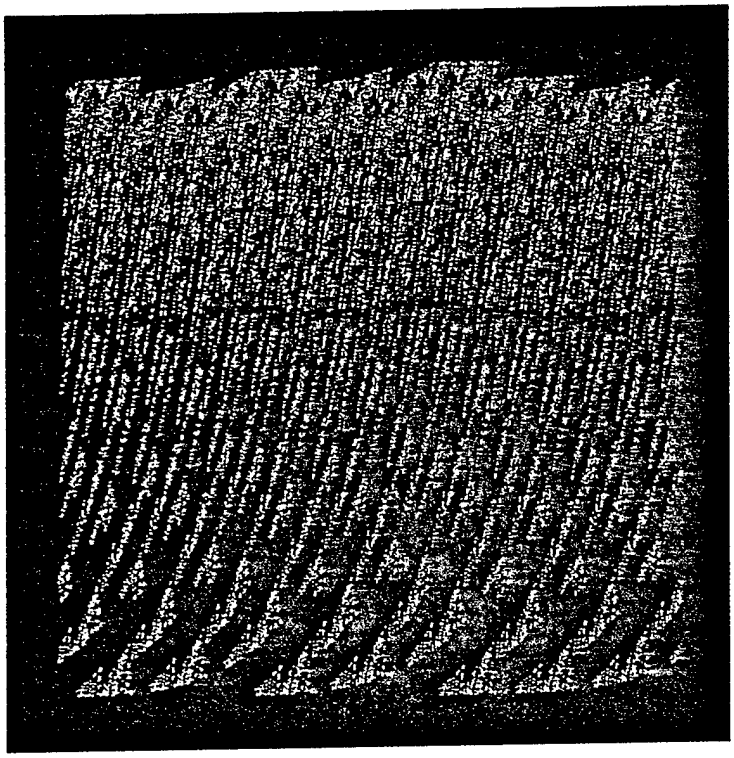

Fig. 10. Figure 10 is obtained by introducing a nonlinearity into the equation used to obtain Fig. 9. Introduction of the nonlinearity results in the formation of bending in the attractor.

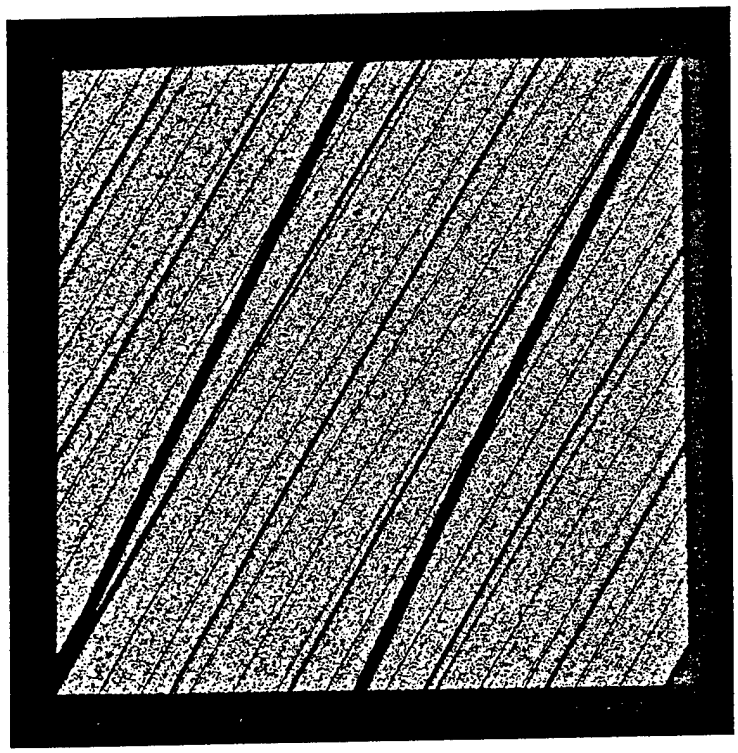

Fig. 11. In this figure we show that the process used to obtain a nonchaotic SA in Fig. 9 can also be used to produce a chaotic SA. Figures 9 and 11 demonstrate that the effect of damping is to reduce the level of complexity.

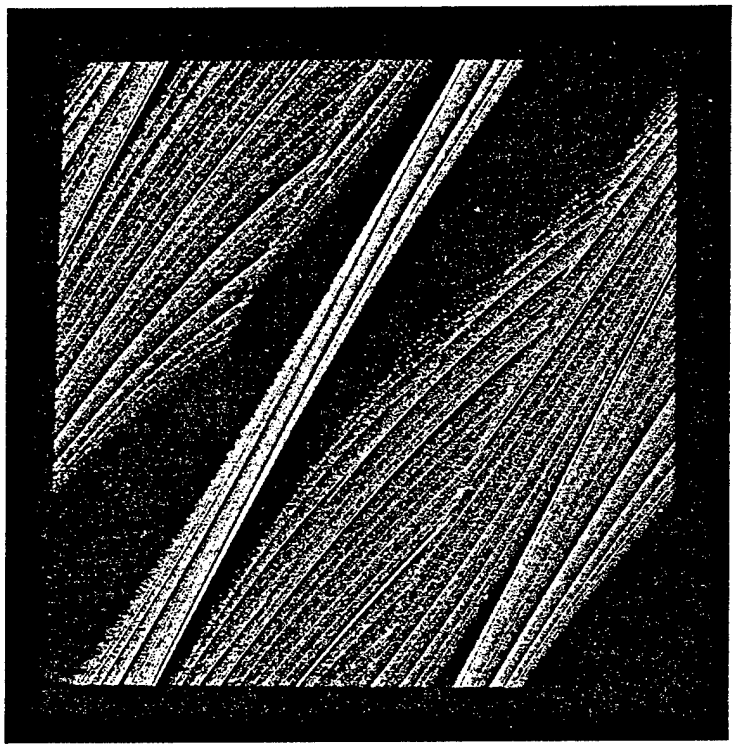

Fig. 12. This figure is made from Fig. 11 in the same way that Fig. 10 is made from Fig. 9, by introducing a nonlinearity. The result is the same: The nonlinearity introduces bending into the attractor.

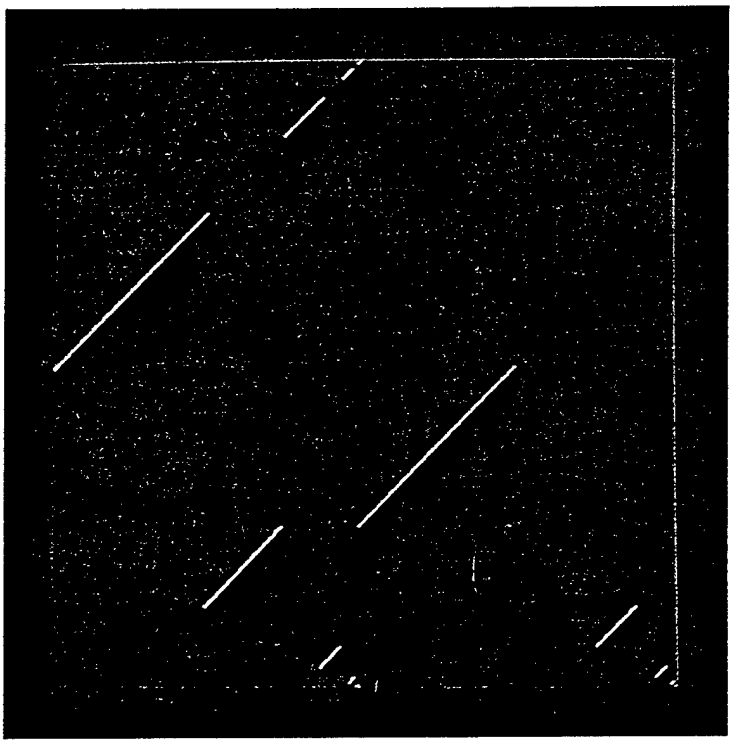

Fig. 13. This figure is a graph of a WX mapping, $x \to f(x)$, which is not SX constructed by Kakutani. It is LZ. All eigenvalues are 1, hence this map does no stretching.

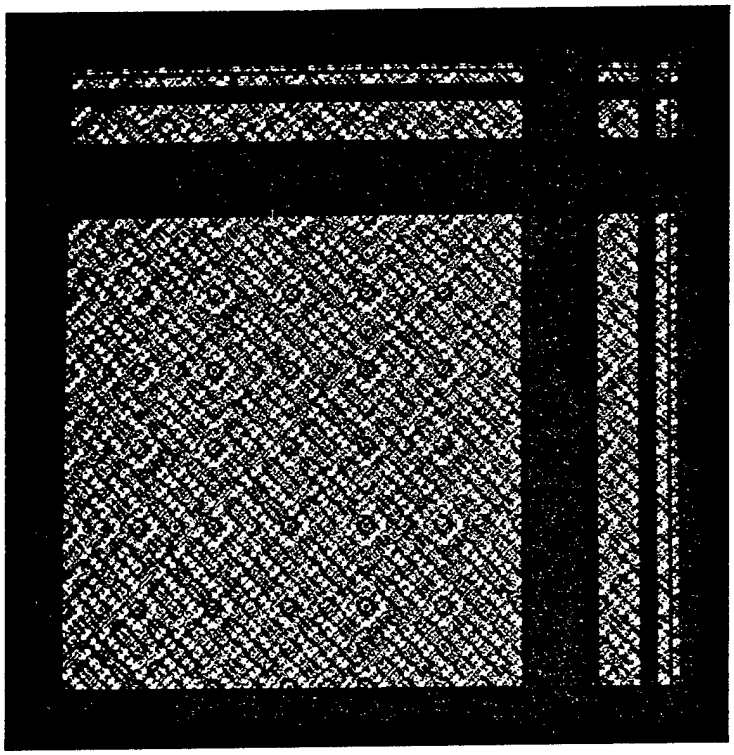

Fig. 14. In this figure we show an orbit of a map constructed from the map of Fig. 13. To get a two-dimensional image, we have formed the cross product of this mapping with itself, $(x, y) \to (f(x), f(y))$. The resulting mapping is also WX and LZ. The orbit shows a high degree of structure. A microscopic examination shows that the orbit has some level of complexity as well.

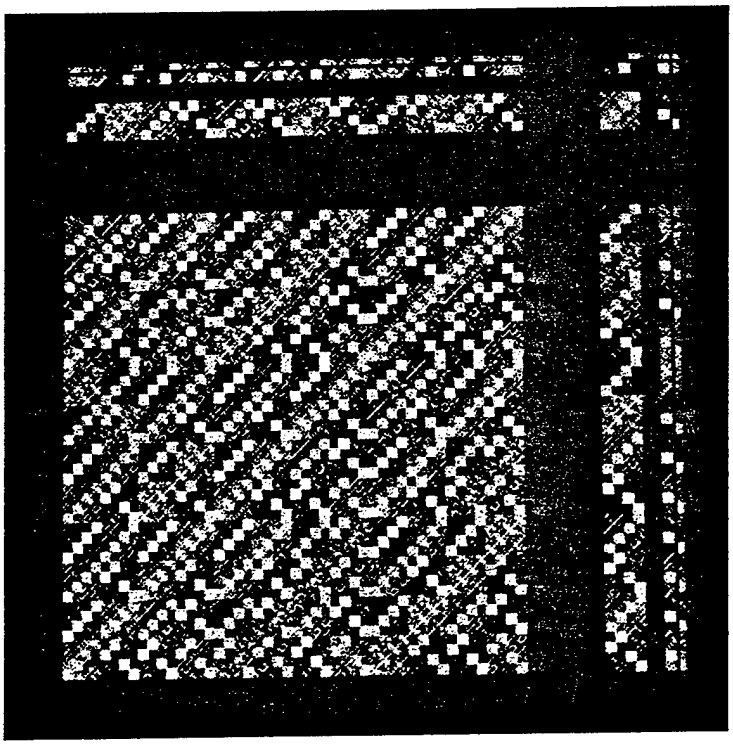

Fig. 15. In this figure we add a small measure of damping to the map in Fig. 14. The resulting map is $(x, y) \to (f(x), 0.999999\ f(y))$. Several orbits are shown, distinguished by different colors. Since the orbits are not standard curves, they are nonchaotic strange attractors.

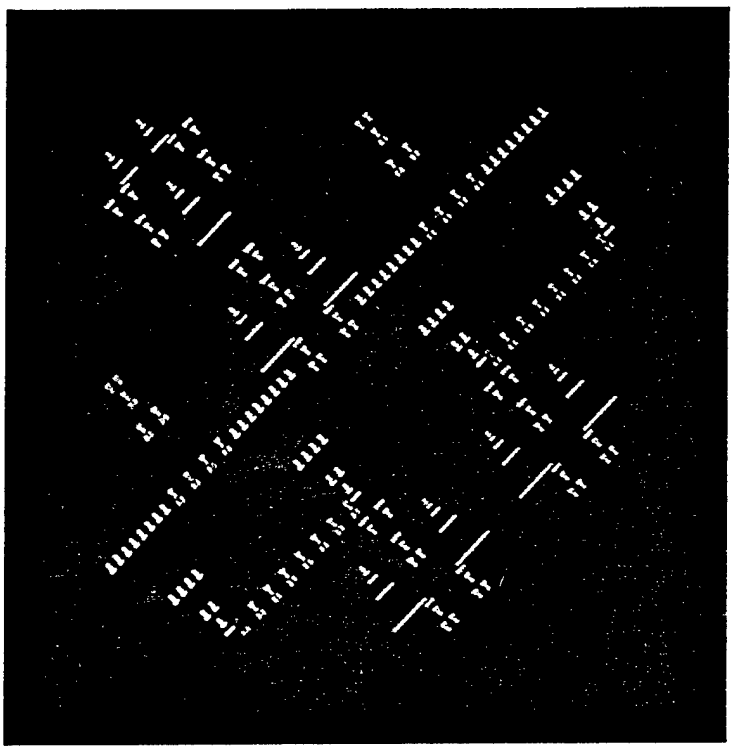

Fig. 16. This figure is constructed from the map in Fig. 7(a) by forming the direct product as we did in constructing Fig. 14 from Fig. 13. Four orbits are shown as indicated by the four colors. The presents of multiple distinct orbits shows that the map is not E.

are conjugate to a skew translation on some subset of its domain.

We now demonstrate that the nonlinearities of their maps are irrelevant to the existence of nonchaotic strange attractors. We modify Eq. (36) to have an eigenvalue less than 1:

$$\begin{pmatrix} x \\ y \end{pmatrix} \to \begin{pmatrix} \alpha x + y \\ y + a \end{pmatrix} \bmod(1) \qquad (47)$$

and obtain the attractor in Fig. 9.

By making the map nonlinear we can routinely introduce bending into the attractor [Fig. 10].

The explanation of the formation of nonchaotic strange attractors is that if the orbits of a map are uncorrelated in time, the geometry of the orbit can become uncorrelated in space. Skew translations can have ZA, and hence their dampened orbits can be made to look peculiar, depending on how the damping factor is included in the equation of the map.

In general, in the presence of damping, the correlation of the orbits of a map can vary from 0 to 1, depending on the size of the damping factor, and this level of correlation may be reflected in the spatial geometry of the orbits. But note that printed geometry, i.e. pictures, are a subjective element of human cognition, and what is peculiar is quite relative. It is possible to force the dampened uncorrelated orbits to take on familiar forms as well. Figure 4 demonstrates this. The attractor is a square. The effect on visual presentation of orbits is a function of *how* the damping is inserted in the equation. This distortion can happen for any map whose orbits lack some degree of correlation.

To further illustrate these ideas, if we modify the cat map to have damping, we may also get distorted attractor geometry as seen in Fig. 11.

The map for Fig. 11 is

$$\begin{pmatrix} x \\ y \end{pmatrix} \to \begin{pmatrix} 2x + y \\ x + (1 - 0.5\alpha)y \end{pmatrix} \bmod(1)\,. \qquad (48)$$

The parameter factor multiplying $y$ is chosen to make the determinant of this map $1-\alpha$. In Fig. 11, $\alpha = 0.02$.

By making the cat map nonlinear we cause the orbits to bend, as seen in Fig. 12.

The equation for Fig. 12 is

$$\begin{pmatrix} x \\ y \end{pmatrix} \to \begin{pmatrix} 2x + \sin(\beta y)^2 \\ x + (1 - 0.5\alpha)y \end{pmatrix} \bmod(1) \qquad (49)$$

where $\beta = 1.8$. Figure 12 bears resemblance to the figures in [Brown & Chua, 1996b] where the fundamental map is presented. By construction, the fundamental map provides an orderly evolution from periodic to chaotic that encompasses skew translations and nonchaotic strange attractors. For the inverse of this idea, Fig. 1 is an example of a nonstrange chaotic attractor in that the attractor is a square. It is possible to make a nonstrange chaotic attractor in the form a circle, straight line, or any simple geometric shape, except, possibly, a countable set of points.

Maps producing strange attractors have some level of complexity such as ZA, LP, or SD because the geometry is a reflection of orbit correlation. Thus the existence of strange attractors (SA) is a level of complexity we may add to our list of other measures. What we have seen is that the lower end of the level of complexity spectrum is periodic, and almost periodic dynamics. Next appears to be E, SD, WX, ZA, followed by LP. But this is not a totally ordered system, is it a partial order where SD is found in almost-periodic systems such as the twist on the two-dimensional torus. Of all the measures of complex dynamics, ZA and LP are the most general, but do not form a total ordering. Even by adding entropy we cannot obtain a single set of characteristics forming a total ordering. Either nature is being very capricious, or we just have not yet found the right measurements.

Relative to rotations, skew translations are quite complex, so we now ask the question *How low a level of complexity is needed to get SA?*. We present two examples. We begin with the WX map of Kakutani, see [Parry, 1981]. WX is mildly complex, but much less so than skew translations may be. Further, WX does not have to involve any stretching, contrary to what some authors have suggested. In fact the map of Kakutani is LZ [Fig. 13].

We present only the geometric form of this map due to its complicated definition found in [Parry, 1981]. Since this map is WX, its cross product is also WX and this is illustrated in Fig. 14. As can be seen, there is a large measure of global structure to an orbit, but on the detail level there is ample variation. If iterated long enough, the orbit will be dense, so the "empty" places in the figure do not indicate repelling regions.

By adding a small amount of damping, we get the attractor in Fig. 15, which may be termed strange.

Our last example of the phenomenon of nonchaotic SA demonstrates the considerable level of order that may be present and still obtain SA. We take the map of Fig. 7(a) to construct a strange attractor. This map, also constructed by Kakutani, is only E, and further, it has only discrete spectrum [Parry, 1981]. In simple language this means that among all E maps this type of E map is the simplest. For example, it is known that all E maps with discrete spectrum are group rotations. To obtain a two-dimensional illustration we form the cross product of this map with itself, and include a parameter, $\alpha$, we can vary:

$$\begin{pmatrix} x \\ y \end{pmatrix} \to \begin{pmatrix} f(x) \\ \alpha f(y) \end{pmatrix} . \tag{50}$$

In Fig. 16, $\alpha = 1.0$, we show typical orbits of this map, which is not E, hence orbits are not dense. The different orbits are indicated by different colors. The orbits of $f$ have a level of correlation ranging

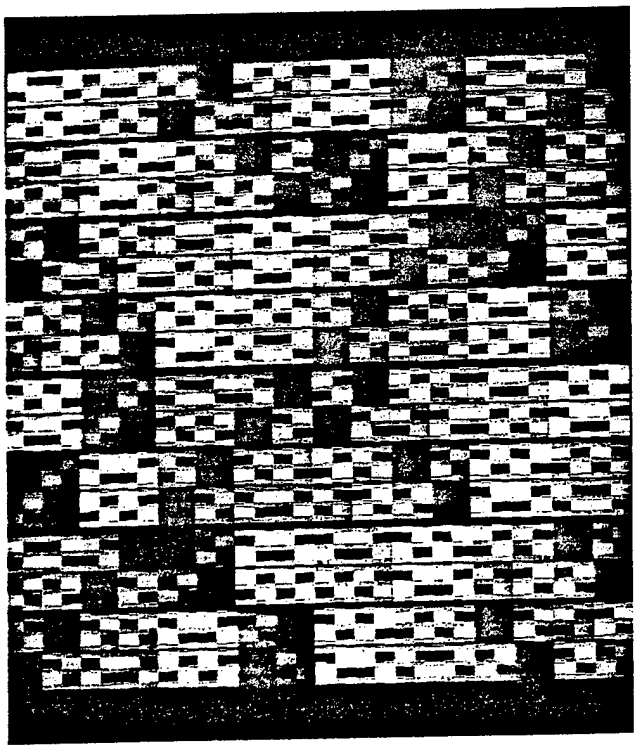

Fig. 17. This figure is obtained from Fig. 16 exactly as Fig. 15 was obtained from Fig. 14, by adding a small measure of damping to one coordinate, $\alpha = 0.999$. The result is the formation of nonchaotic strange attractors. Numerous orbits are shown as distinguished by the different colors. All orbits are strange in shape. This may be the weakest level of dynamics that can form nonchaotic strange attractors.

from about 0.55 to over 0.90, and the autocorrelation is nearly periodic.

In Fig. 17 we choose $\alpha = 0.999$, which is enough damping to form attractors. Figure 17 shows that the basins of attraction are in the shape of a block letter "S". There are multiple basins, as indicated by the numerous colors, but some colors have been used twice. This is not important, however, since the point is that the various attractors are peculiar in shape, all have about the same shape, and there are many basins of attraction.

We conclude that the strangeness of the geometry of an attractor plotted on a computer screen is a result of the amount of damping, how the damping occurs in the definition of the map, and most important, the correlation of orbits. The exact value of the initial conditions may be a factor also. Clearly, the association of SA with chaos is a coincidence of the orbit correlation found in chaos. The level of complexity found in chaos and even in skew translations is far more than needed to obtain this interesting phenomenon.

### 4.2. *Initial conditions versus algorithms*

The examples of the preceding sections have demonstrated the need to determine when two points are correlated. We may define correlation of two points as follows: We first discard their integer part and consider only the fractional part of the number. We now consider their fractional part as a sequence of integers between 0 and 9. As sequences, we may apply the usual formula for correlation of two sequences to obtain the desired definition.

Using this definition, we have the following observation whose proof poses no mathematical difficulties.

Let $x_0$ be any point in space, and let $U(x_0)$ be any neighborhood of $x_0$, however small. Then within $U(x_0)$ there are many points that are uncorrelated to $x_0$.

This means in simple terms that near any point are countless points that are uncorrelated with it and that the location of the uncorrelated points is in essence a random walk from $x_0$.

The significance of this fact is that any dynamical system that acts on two uncorrelated points in such a way as to move the insignificant, lower-level, digits up into a higher position of significance will be reflected in a complex relationship between the orbits of these two points. Hyperbolic systems are capable of doing this. The shift is defined to do precisely this and nothing more. Different algorithms have varying abilities to elevate the role of lower-level digits into significance, and this is reflected in our notions of E, WX, SX, etc. The significance of this reaches a maximum when applied to points having positive algorithmic complexity. These are points which cannot be described by a finite algorithm and hence, cannot be reached by finite iteration of a finite algorithm. Such points cannot be spatially correlated to points having zero algorithmic complexity. For example, any dynamical system which moves lower-level digits into significance has a level of complexity of its orbit solely as a result of the algorithmic complexity of its initial condition. We may think of this as the extreme of spatial complexity. The lack of correlation between two points each with zero algorithmic complexity is philosophically less extreme.

Any dissipative dynamical system that treats uncorrelated points differently and correlated points similarly can have many basins of attraction as well as very complex-looking attractors.

We have traditionally viewed distance, i.e. metrics, as our primary measure of significance. However, correlation between points appears to hold an equally significant role in science and is more responsible for the levels of complexity we see in the universe than anything except those dynamical systems that elevate the lower-levels of complexity of points into positions of significance.

As a result, at least two numbers are necessary when comparing two quantities: their distance apart and their correlation. Their distance is a measure of the present; their correlation is a measure of their potential future relationships. Of these two measurements, clearly correlation is the most illusive and accounts for much of the uncertainty of the future. When two quantities are uncorrelated, their future depends solely on the type of dynamics they undergo. In weather systems, dynamics can fluctuate drastically from almost periodic upward, and thus uncorrelated quantities can fluctuate from having an almost-periodic relationship to a near-random relationship.

We have talked of uncorrelated quantities without being specific about the level of *uncorrelation.* Consequently, we ask: *How is the level of correlation between quantities reflected in their future under given dynamical systems?*

A simple question that we can answer is whether a simple rational or integer-initial

condition can converge to something complex, but not having positive algorithmic complexity, under the action of a dynamical system. The answer is yes. Any algorithm for the computation of the digits of $\pi$ is an example. As noted in Part I of this tutorial, published last year, the Chudnovsky brothers have shown that the digits of $\pi$ are as complex as the outputs of typical random-number generators. Next we ask if we may construct an algorithm having multiple basins of attraction which converge to two different "complicated" irrational numbers. The answer is yes, and the number of attractors may be made as large as you like. A typical example is

$$x \to h_1(x)f(x) + h_2(x)g(x) \qquad (51)$$

where $f \to \sqrt{2}, g \to \sqrt{63}$ and $h_1(x)$ is 1 near $\sqrt{2}$ and 0 near $\sqrt{63}$, and $h_2(x)$ has the opposite specifications. If we start near either square root with a simple rational initial condition we converge to that square root, an irrational number. Hence it is a fact that we can use a finite algorithm to start at a simple initial condition and then, using this algorithm, be attracted to a complicated irrational number that tells us that dynamical systems can create some level of complexity, but not positive algorithmic complexity. We conclude that time can create a level of complexity and that space has an initial relative level of complexity. The spatial level of complexity is made more elusive by the mathematical fact that points exist with positive algorithmic complexity. The center of mass of a particle which is not initially located at a point of positive algorithmic complexity in a fixed-coordinate system can reach such a point — if the laws of nature have an expression as a finite algorithm — in only one of two ways: The algorithm involves a constant of positive algorithmic complexity, which contradicts its finite characterization; or it reaches the point at a moment in time of positive algorithmic complexity. However, particles having a center of mass with rational coordinates can converge to points having very complex coordinates in time under the action of a dynamical system that is expressible as a finite algorithm, regardless of the role of the time-coordinate.

We emphasize that the conclusions drawn are based on the relative spatial positions of points in a fixed-coordinate system. If the laws of nature are truly expressible as finite algorithms, then infinitely small particles located at some points can never reach other points within the same coordinate system in finite time. We repeat that this is significant only on a microscopic scale in which particles are vanishingly small. Hence, the *theory of chaos* implies a fine, complex structure of the fabric of the universe, if only in the abstract.

Our theory of chaos thus implies the existence of both a spatial and a temporal level of complexity. The spatial level of complexity is revealed by the degree of correlation between points and the absolute relative level of complexity of points within a fixed coordinate system. Temporal level of complexity is revealed by the action of finitely-describable dynamical systems on points located at perfectly simple coordinates such as rational or integer coordinates. The level of complexity of things thus emanates from these two sources through the myriad of dynamical systems that have varying abilities to move lower-level complexity of physical quantities into positions of significance for measurement and prediction purposes.

## 5. Sources of Nonlinearity

In [Brown & Chua, 1997] we described the complexity spectrum and noted that understanding this spectrum is prerequisite to understanding chaos. In order to fully understand the sources of levels of complexity in the complexity spectrum it is necessary to understand the sources of nonlinearity, a key feature in the production of a given level of complexity. Nonlinearity is not a necessary feature for the production of a level of complexity, as we saw in the previous section, but nonlinearities are among the most interesting sources of high levels of complexity.

The simplest venue within which to investigate the sources of nonlinearities is the two-dimensional autonomous ODEs. The only simpler venue could be one-dimensional ODEs, or maps, but we believe that this venue is harder to approach in a simple orderly manner than the two-dimensional systems because interesting one-dimensional maps are either not invertible or not continuous.

The Poincaré–Bendixon theory would appear to completely answer all questions about the class of two-dimensional autonomous ODEs; however, on closer examination we see that this theory provides no insight into the construction of equations with specific nonlinear features, nor does it even suggest an organization of this topic. It is the varying ways in which nonlinearities may occur in two-dimensional autonomous ODEs that will provide us

with the insight into the role that these systems play in the development of a level of complexity, not a classification of their periodic points as presented by Poincaré–Bendixon theory.

## 5.1. *The twist equation*

In Davis' *Introduction to Nonlinear Differential and Integral Equations* [1962] the dominant source of nonlinearities in ODEs is revealed as being the occurrence of nonlinear frequencies in the solutions of the ODEs. A simple example of this is the twist ODE

$$\begin{pmatrix} \dot{x} \\ \dot{y} \end{pmatrix} = r \begin{pmatrix} 0 & -1 \\ 1 & 0 \end{pmatrix} \begin{pmatrix} x \\ y \end{pmatrix} \tag{52}$$

where $r = \sqrt{x^2 + y^2}$. The time-one (or Poincaré) map is the simple twist map which was used to derive the twist-and-flip map, the first closed-form Poincaré map of an ODE having chaotic solutions. This equation was derived by asking the question: What is the simplest way in which a linear equation can be made nonlinear? Since, in the linear oscillator the initial conditions determine the amplitude of the system, a simple step would be to consider the family of curves given by

$$\begin{pmatrix} x(t) \\ y(t) \end{pmatrix} = \begin{pmatrix} r\cos(rt + \theta) \\ r\sin(rt + \theta) \end{pmatrix} \tag{53}$$

where $r$ is given above and is a function of the initial conditions. Since $r$ affects both amplitude and frequency, the ODE that this system solves must be nonlinear. The effect of multiplying $t$ by a function of the initial conditions is to cause neighboring orbits to separate, at different speeds. The orbits of the twist ODE in the phase plane are identical to those of the linear equation it was derived from. This procedure was shown to be very general in [Brown & Chua, 1993]: Given any linear autonomous ODE in any number of dimensions there is an infinite family of nonlinear autonomous ODE having the same set of orbits, fixed points, and types of fixed points.[3] The solutions differ only in that, in the nonlinear case, $t$ is multiplied by a function of the initial conditions that are constant along orbits.

## 5.2. *Example two: Nonlinear amplitude equation*

We now ask if it is possible to generate a nonlinear system in which $t$ is not multiplied by a function of the initial conditions but whose amplitude is a function of the initial conditions. The answer is yes, and the ODE is derived from the curves given by

$$\begin{pmatrix} x(t) \\ y(t) \end{pmatrix} = \begin{pmatrix} r\cos(t + \theta) \\ r^2\sin(t + \theta) \end{pmatrix} \tag{54}$$

where $r$ is a function of the initial conditions given by $r^2 = 0.5(x^2 + \sqrt{x^4 + 4y^2})$. By direct computations the following system of autonomous ODEs can be derived:

$$\begin{pmatrix} \dot{x} \\ \dot{y} \end{pmatrix} = \begin{pmatrix} 0 & -1/r \\ r & 0 \end{pmatrix} \begin{pmatrix} x \\ y \end{pmatrix} \tag{55}$$

where $r^2 = 0.5(x^2 + \sqrt{x^4 + 4y^2})$ is a constant along integral curves. This system has a feature in common with the ODE $\ddot{x} + x^3 = 0$ in that the shape of the integral curves varies with the initial conditions [Fig. 18]. The twist equations also have a feature in common with this second order ODE: The frequency varies with the initial conditions. However, in the twist equations, the solutions are all circles, thus the amplitude is essentially what we expect from a linear system. In the amplitude system, the frequencies are not a function of the initial conditions. Hence, the twist equations and the amplitude equations have completely separated two of the three features of nonlinear systems illustrated by $\ddot{x} + x^3 = 0$. The third feature, variable velocity along points of a single orbit, will be discussed in the next example.[4]

A natural question is whether the amplitude equation with periodic forcing produces chaos as well. The answer is yes.

By a direct computation a time-one or Poincaré map can be derived for the amplitude equation:

$$\mathbf{A}\begin{pmatrix} x \\ y \end{pmatrix} = \begin{pmatrix} \cos(\theta) & -\sin(\theta)/r \\ \sin(\theta)r & \cos(\theta) \end{pmatrix} \begin{pmatrix} x \\ y \end{pmatrix} \tag{56}$$

where $\theta$ is a fixed time interval. The orbits of this map are ellipses [Fig. 18]. For small initial

[3]This fact alone shows that the classification of periodic points and limit cycles is inadequate to describe the nonlinear dynamics of two-dimensional autonomous systems.

[4]As is known, when this later second order ODE is driven by a periodic force, it produces chaos. In fact $\ddot{x} + x^3 = a\cos(t)$ is Duffing's equation without the damping term.

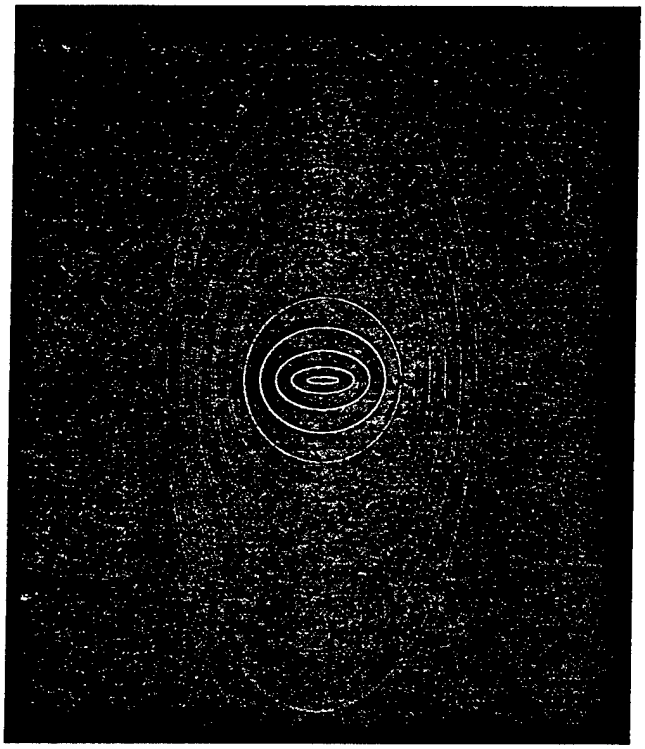

Fig. 18. In this figure we show the orbits of a nonlinear equation. Each orbit, considered by itself, is linear, varying from horizontal ellipses (yellow), to a circle (red), to vertical ellipses (dark blue). The relationship between the orbits is the source of the nonlinearity.

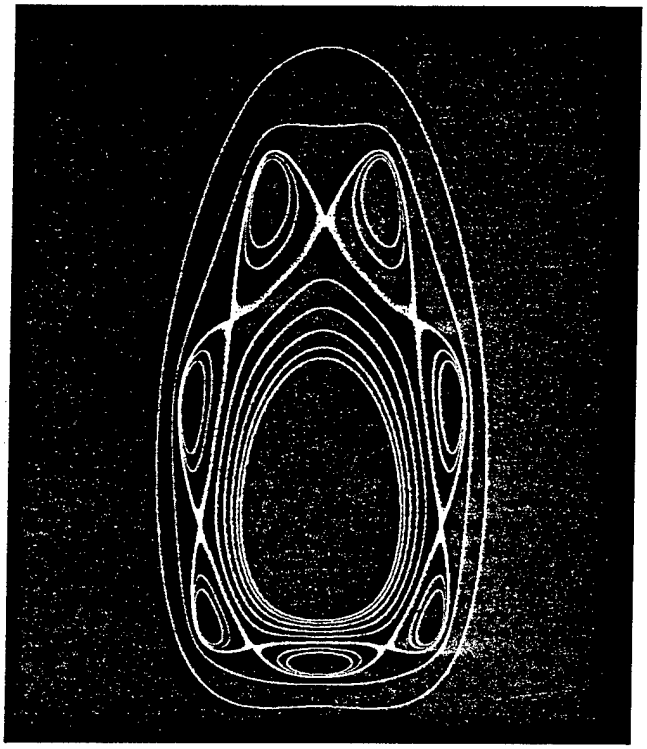

Fig. 19. In this figure, we demonstrate that by combining the map of Fig. 18 with a flip we obtain chaos, just as is done with the twist. As is shown in the figure, the full array of island chains (dark blue) and homoclinic tangles (light blue) are formed.

conditions the semi-major axis is horizontal (yellow orbits); for large initial conditions it is vertical (dark-blue orbits). Therefore one orbit is circular and, as seen in Fig. 18, red.

To obtain chaos using this nonlinear effect we must add forcing to the ODE, and this is done exactly as we did for the twist-and-flip equations. Doing this we can obtain a Poincaré map and have the analog of the twist-and-flip map which we will call FA. As with the twist-and-flip map we must offset the center of the integral curves by an amount $a$. After this is done our resulting map is

$$\mathbf{FA}\begin{pmatrix} x \\ y \end{pmatrix} = -\left[\begin{pmatrix} \cos(\theta) & -\sin(\theta)/r \\ \sin(\theta)r & \cos(\theta) \end{pmatrix}\begin{pmatrix} x-a \\ y \end{pmatrix} + \begin{pmatrix} a \\ 0 \end{pmatrix}\right] \tag{57}$$

and the orbits are seen in Fig. 19.

This map has no hyperbolic fixed points but does have high-order hyperbolic periodic points. For $\theta = 2.0$, $a = 0.5$ a period-six hyperbolic point is found at approximately $(1.0433, 1.1997)$. By direct inspection this point is found to have a horseshoe. This example illustrates the contribution of the geometry of the orbits to producing chaos.

## 5.3. *Example three: The Jacobi equation*

All two-dimensional vector fields can be put into the form:

$$\begin{pmatrix} \dot{x} \\ \dot{y} \end{pmatrix} = \left(\frac{\dot{r}}{r}\mathbf{I} + \dot{\theta}\mathbf{B}\right)\begin{pmatrix} x \\ y \end{pmatrix} \tag{58}$$

where $\mathbf{I}$ is the identity matrix and $\mathbf{B}$ is the matrix

$$\begin{pmatrix} 0 & -1 \\ 1 & 0 \end{pmatrix}. \tag{59}$$

When $\dot{r} = 0$ we get the equation:

$$\begin{pmatrix} \dot{x} \\ \dot{y} \end{pmatrix} = \left(\dot{\theta}\mathbf{B}\right)\begin{pmatrix} x \\ y \end{pmatrix} \tag{60}$$

the orbits must be circles, the same as the simple harmonic oscillator and the twist equation. For $\dot{\theta} = 1$ we obtain the simple harmonic oscillator. For $\dot{\theta} = r$ we obtain the twist. However, if

$$\frac{\partial \dot{\theta}}{\partial r} = 0 \tag{61}$$

we are still in a position to obtain closed-form solutions. If $\dot{\theta} = \sqrt{1 - k^2 \sin^2(\theta)}$ we obtain the closed-form solution

$$\begin{pmatrix} x(t) \\ y(t) \end{pmatrix} = \begin{pmatrix} r\,\mathrm{cn}(t+C) \\ r\,\mathrm{sn}(t+C) \end{pmatrix} \tag{62}$$

where sn, cn are the Jacobi elliptic functions. We call this the Jacobi Equation. These functions are the inverses of elliptic integrals and are derived in the classical problem of rectifying the ellipse.

Since $\dot{\theta}$ is not a function of $r$, the angular velocity does not change from orbit to orbit as was the case with the twist system. In fact, this system preserves lines through the origin and through any complete revolution a line or a region is mapped onto itself. The source of the nonlinearity is that along an orbit, the arc length is expanded and contracted in a periodic manner. In this system, matter is neither created, as happens in systems having a source, nor destroyed, as happens with systems having a sink, but rather is alternately compressed and stretched.

This system can be used to obtain chaos by the standard two-phase gate method: If we translate the system to $(a, 0)$ and compose it with the flip we obtain a Poincaré map that produces chaos while having only periodic hyperbolic points and no hyperbolic fixed points. The origin of chaos in this system is solely from the nonlinear acceleration taking place around circles.

A limitation of the Jacobi Equation is that the Jacobi elliptic functions, $\mathrm{sn}(t)$, $\mathrm{cn}(t)$ are not elementary functions. However, the time-one map determined by these equations can be constructed from elementary functions. For anyone wanting to proceed by constructing an example which avoids the use of the Jacobi Equation, we offer the following digression:

We may construct an example having these exact same properties which is solvable in terms of elementary functions. In place of $\dot{\theta} = \sqrt{1 - k^2 \sin^2(\theta)}$ we simply choose $\dot{\theta} = 2 - \sin^2(\theta)$, which is integrable in terms of elementary functions. Specifically, we have

$$\sin(\theta) = \frac{\sqrt{2}\sin(\psi)}{\sqrt{1 + \sin^2(\psi)}} \tag{63}$$

and

$$\cos(\theta) = \frac{\cos(\psi)}{\sqrt{1 + \sin^2(\psi)}} \tag{64}$$

where $\psi = \sqrt{2}(t + C)$, $C$ being the arbitrary constant of integration determined by the initial conditions. Since $\dot{r} = 0$, we can write the solution in rectangular coordinates from the above information and the initial conditions. Specifically,

$$\begin{pmatrix} \sin(\psi) \\ \cos(\psi) \end{pmatrix} = \begin{pmatrix} C_1 \cos(\sqrt{2}t) - C_2 \sin(\sqrt{2}t) \\ C_1 \sin(\sqrt{2}t) - C_2 \cos(\sqrt{2}t) \end{pmatrix} \tag{65}$$

with

$$C_1 = \frac{\sqrt{2}x_0}{\sqrt{2x_0^2 + y_0}}, \quad C_2 = \frac{y_0}{\sqrt{2x_0^2 + y_0}}. \tag{66}$$

The significance of these systems as a building-block of a level of complexity is twofold. First, the nonlinear acceleration around orbits of these two equations, when composed with simple linear factors, gives rise to chaos even though the nonlinearity is of the simplest conceivable form, far simpler than the twist map in that it has no shearing. Second, two observers traveling on nearby orbits lying on the same radial line will not experience relative motion. Further, observers riding on separate orbits will never separate by more than a fixed but small distance. It is nearly the opposite of sensitive dependence on initial conditions. Two observers riding on the same orbit will oscillate relative to each other while still remaining is circular motion. This stretching and compressing of arc length around the orbit means that the vector field has a nonzero divergence while having no sources or sinks. Matter is never created or destroyed as when there are attractors or repellers involved; it is only compressed and stretched. The result of this feature is that when it is composed with simple components such as the flip, chaos is created by a subtle process. In addition, a very unexpected result appears: Local attracting periodic points are mixed in with periodic, quasi-periodic and chaotic orbits [Fig. 20]. This is due to the nonzero divergence of this system. If the divergence were a result of sinks or sources, we would expect to obtain global attractors or repellers. But this is not what is found. The existence of local attracting fixed points also depends on the magnitude of the flip component used to compose these maps. Only certain flips combined with the right initial conditions can give rise to this unusual phenomena. Figure 20 illustrates beautifully the kinds of orbits possible with the Jacobi map as a factor. The presence of measure-preserving chaotic and elliptic

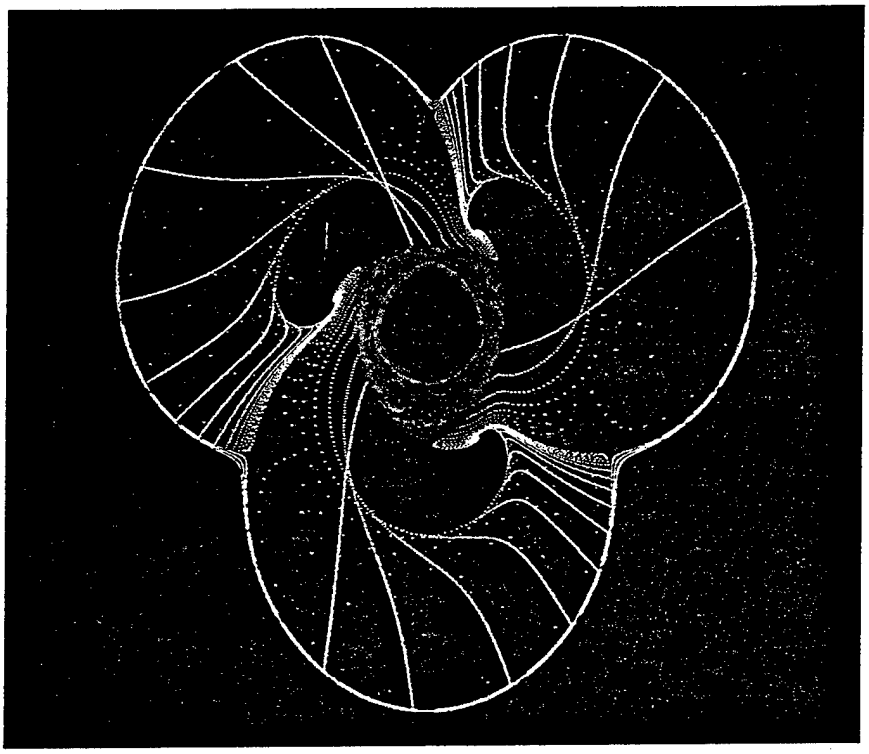

Fig. 20. Figure 20 is an example of a remarkable phenomena, the coexistence of local attracting periodic points (light blue orbits converge to period-three points) with nonattracting regions. A chaotic region having a homoclinic tangle is shown in red. This phenomena results from the nonzero divergence of the Jacobi equation.

orbits combined with period three attractors suggests the possibility of such systems existing in nature. The work of Freeman [1996] on the attractors of the brain combined with the nonattractor nature of common brain waves suggests that the brain is a system with these properties. This system may one day also explain how complex structures such as the spinal column can form from dynamical systems composed of simple components.

Three sources of autonomous, integrable nonlinearity in two dimensions are thus illustrated by these three equations: the twist equation, the amplitude equation and the Jacobi Equation. The twist equation is the most readily available source of chaos and it has zero divergence. The second of the two equations provides a source of asymmetry and subtlety not found in the twist equations and also has zero divergence. Two of these equations are induced by linear equations; all three have only linear orbits. In particular, the orbits are either ellipses or circles.

### 5.4. *Example four: Nonlinear orbits*

In the preceding three examples we imposed a constraint that the individual orbits of the ODE be linear and observed that nonlinearity could arise from three different sources: nonlinear frequencies, nonlinear relationships between neighboring orbits, and nonlinear divergence. Another source of nonlinearity must be nonlinear orbits.

We now illustrate how to obtain a nonlinear system that: (1) can be solved in closed form; (2) is not induced by a linear system; (3) whose orbits are not linear; (4) which preserves lines through the origin; and (5) which has zero divergence. We use the form of a vector field mentioned above:

$$\begin{pmatrix} \dot{x} \\ \dot{y} \end{pmatrix} = \left( \frac{\dot{r}}{r}\mathbf{I} + \dot{\theta}\mathbf{B} \right) \begin{pmatrix} x \\ y \end{pmatrix} \tag{67}$$

and make two assumptions. The first is that its underling group is measure preserving or, what is the same thing, the vector field is divergence-free. The second is that the system preserves lines through the origin. Using these two assumptions we derive the following partial differential equation for $\dot{r}$:

$$\frac{1}{r}\langle X, \nabla\dot{r}\rangle + \frac{\dot{r}}{r} + \langle \mathbf{B}X, \nabla\dot{\theta}\rangle = 0\,. \tag{68}$$

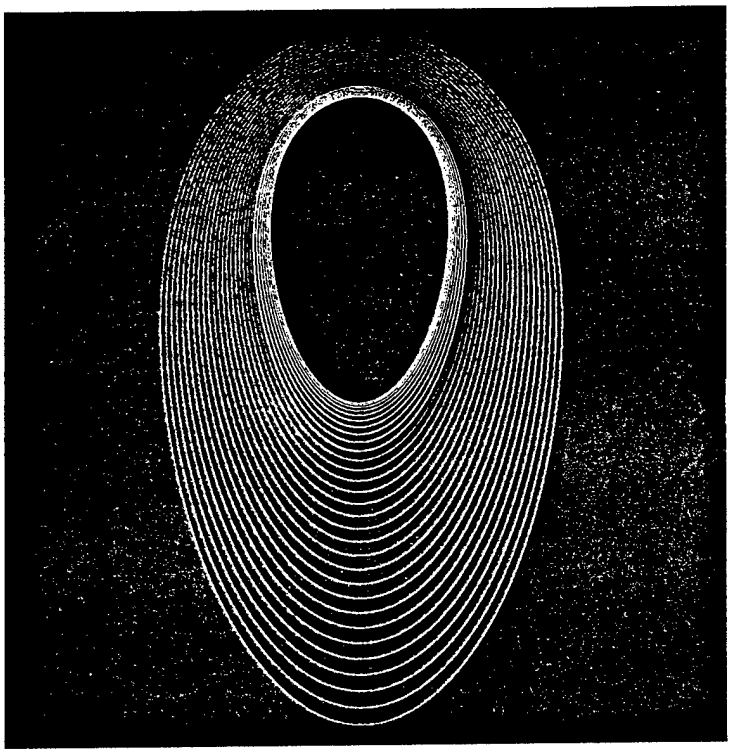

Fig. 21. Figure 21 illustrates the orbits of a nonlinear system that: (1) can be solved in closed form; (2) is not induced by a linear system; (3) whose orbits are not linear; (4) which preserves lines through the origin; and (5) which has zero divergence.

With the following notational convention we obtain the PDE in standard form. Let

$$\begin{pmatrix} \dot{r} \\ \dot{\theta} \end{pmatrix} = \begin{pmatrix} g(x, y) \\ f(\theta) \end{pmatrix} \tag{69}$$

Now the PDE becomes

$$xp + yq = -(z + rf'(\theta)) \tag{70}$$

where $p = z_x\, q = z_y$, $z = \dot{r} = g(x, y)$. The general solution is given by

$$z = h(x, y)F(x/y) \tag{71}$$

where $h$ is dependent on $f'(\theta)$. If we assume that $cz = rf'(\theta)$ is the form of the solution, then we obtain the following consistency equation to check:

$$xp + yq = -(c+1)z\,. \tag{72}$$

All of these assumptions would be fine if the solution of the resulting equation is consistent with these assumptions. By an application of standard methods for solving first-order partial differential equations we get

$$z = \frac{y}{-(c+1)}F(x/y)\,. \tag{73}$$

The consistency check we must make is to see whether

$$rf'(\theta) = \frac{y}{-(c+1)}F(x/y) \tag{74}$$

is possible. Since $y = r\sin(\theta)$, $x = r\cos(\theta)$ we see that if we choose $f(\theta) = a + b\sin(\theta)$, everything is consistent. In particular, we have

$$r = r_0\left(\frac{f(\theta_0)}{f(\theta)}\right)^{1/c} \tag{75}$$

and the first part of the solution is done. Now, if we choose $a > b$, the equation $\dot{\theta} = a + b\sin(\theta)$ is solvable in closed form for $\sin(\theta)$. Using a standard table of integrals we get

$$\frac{b + a\sin(\theta)}{a + b\sin(\theta)} = \sin(kt + C_0) \tag{76}$$

where $k = \sqrt{a^2 - b^2}$, and $C_0$ is a constant of integration to be determined from the initial conditions. From this relation we obtain $\sin(\theta)$, $\cos(\theta)$ and we are done.

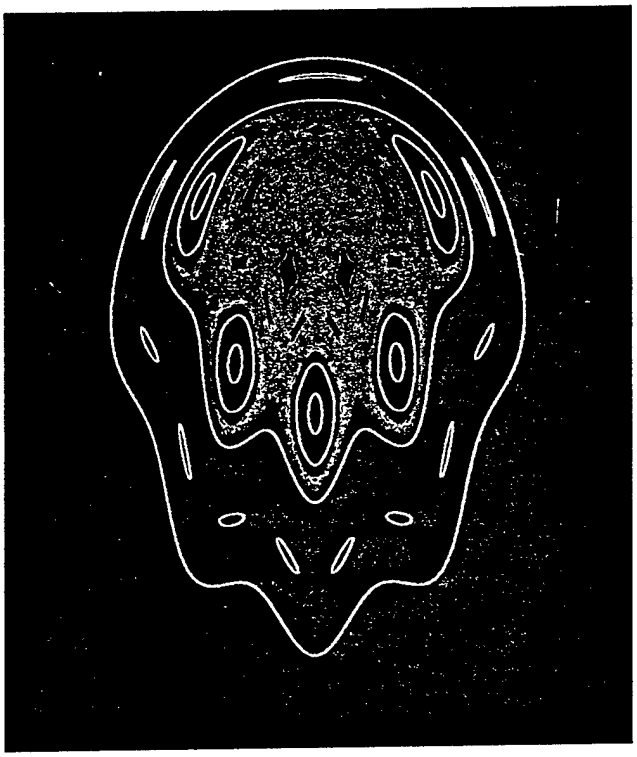

Fig. 22. In this figure we combine the map of Fig. 21 with a flip to obtain chaos. Familiar island-chains (red) and chaotic regions (blue) are formed.

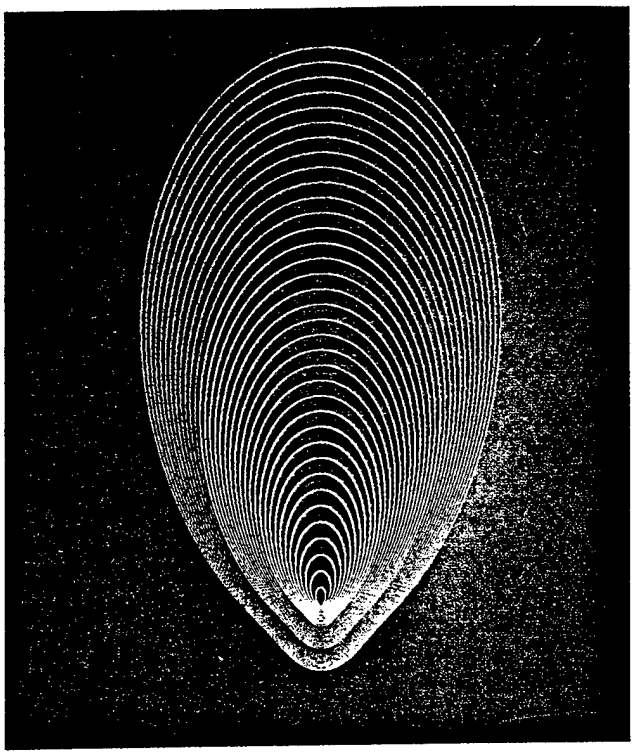

Fig. 23. Figure 23 illustrates the orbits of a nonlinear system that is the analog of Fig. 21, but which has nonzero divergence.

The general solution in rectangular coordinates is given by:

$$\begin{pmatrix} x(t) \\ y(t) \end{pmatrix} = r_0 \left( \frac{f(\theta_0)}{f(\theta)} \right)^{1/c} \begin{pmatrix} \cos(\theta) \\ \sin(\theta) \end{pmatrix} \qquad (77)$$

where we must have $c > 1$. Note that the root factor is not a constant since $f(\theta)$ is a function of time. The orbits cannot be linear, see Fig. 21, and, by construction, the system is divergence-free. Using the two-phase gate method, we may make this map a component of a Poincaré map which produces chaos [Fig. 22].

## 5.5. *Example five: Nonzero divergence, with nonlinear orbits*

It is possible to obtain nonzero divergence equations that are just as useful. One option is to solve the PDE $xp + yq = z$ and the choice

$$\dot{r} = -rf'(\theta) \qquad (78)$$

with $\dot{\theta} = f(\theta) \neq$ constant gives the closed-form solutions in rectangular coordinates:

$$\begin{pmatrix} x(t) \\ y(t) \end{pmatrix} = r_0 \frac{f(\theta_0)}{f(\theta)} \begin{pmatrix} \cos(\theta) \\ \sin(\theta) \end{pmatrix}. \qquad (79)$$

Note that if $\dot{\theta} = -1$ and $\dot{r} \neq 0$ we also get nonzero divergence.

This process can be greatly generalized. If $\dot{\theta} = f(\theta)$ and $r = C_0 G(\theta)$ we get an autonomous ODE:

$$\dot{r} = C_0 G''(\theta) f(\theta) \qquad (80)$$

where $C_0$ is eliminated from this equation by noting that $C_0 = r/G(\theta)$. So long as $\dot{\theta} = f(\theta)$ is solvable in closed form, we are done! For example, choose $f(\theta) = 2 - \sin^2(\theta)$. By use of a table of integrals we find that we can solve this equation for $\sin(\theta)$, which is all that is necessary to express the solution in rectangular coordinates. By choosing $G(\theta) = \sqrt{f(\theta)}(1 - 0.95\sin(\sin(\theta))$ we get the orbits of Fig. 23.

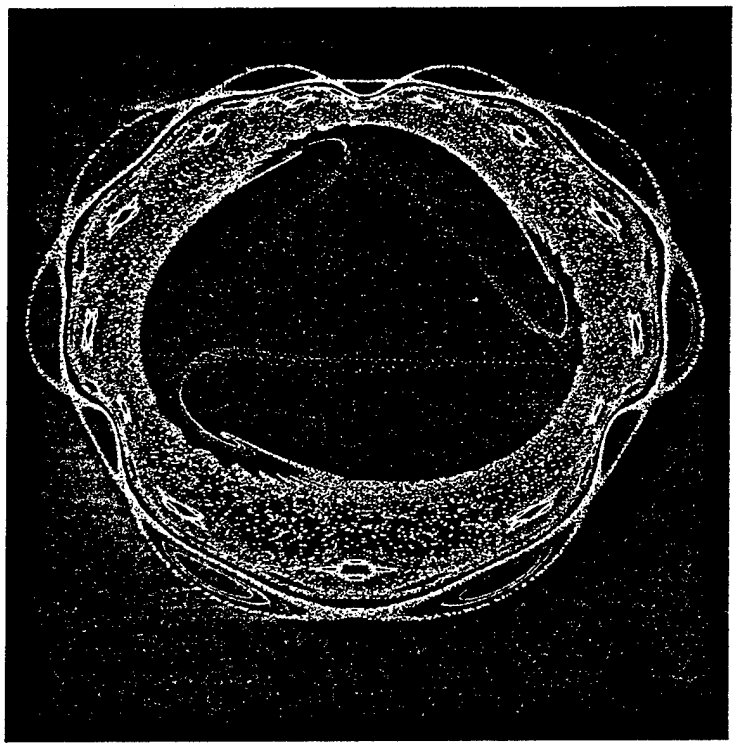

Fig. 24. In this figure, we compose the time-one map of Fig. 23 with a linear translation to get the Poincaré map for an electronic circuit using a two-phased gate. Just as in Fig. 20, local attracting periodic points form with nonattracting regions to produce a remarkable combination of dynamics: In dark blue are elliptic regions; in light blue and yellow are chaotic regions containing homoclinic tangles; in red are orbits that converge to a set of period-three points.

By composing this autonomous time-one map with a shift, we get the chaotic orbits of Fig. 24.

This system, like the Jacobi Equation, when composed with linear maps by the method of two-phase gates can generate local attracting fixed points alongside periodic, quasi-periodic, and chaotic orbits which are not attracting. The yellow orbits are chaos, the red are orbits being attracted to the period-three points. The light-blue are orbits of transient chaos that also converge to the period-three points. The dark-blue orbits are elliptic, hence represent almost periodic solutions of the ODE. Near the small yellow orbits we find chaotic, almost-periodic, and transient-chaotic solutions coexisting.

## 5.6. *Summary of nonlinear effects*

In this section we have given five examples to illustrate four ways that nonlinearities may arise in autonomous two-dimensional ODEs: (1) nonlinear frequencies along linear orbits; (2) nonlinear relationship between linear orbits; (3) nonlinear divergence along linear orbits; (4) nonlinear orbits. These *nonlinear effects* may be combined as seen in Examples 4 and 5 to increase the level of complexity of an orbit. These effects present a different approach to autonomous systems than that provided by an analysis of its fixed points (Poincaré–Bendixon theory) because the nature of these effects contribute directly to the development of a level of complexity in nonlinear nonautonomous equations such as the Duffing equation. As shown in [Brown, 1992], any of these autonomous systems may be used in a construction that leads to autonomous three-dimensional equations that is the analog of the two-phase gate method. In this way, it is possible to construct ever increasingly complex examples of autonomous or nonautonomous systems with any predetermined level of complexity. The practical aspect of this lies in the applications of chaos to diverse areas of the mathematical and life sciences. The theoretical importance lies in the fact that the development of a theory of levels of complexity will have as its foundation a rich set of examples and counterexamples that can be used to guide the formulation and proof of the mathematical and physical theories.

## 6. Relationships Between Attractors, Noninvertiblity, and Nondissipative Maps

Preliminary to this section we present some comments on dissipation, noninvertibility, and nonorientation-preserving properties of dynamical systems and their relationship to chaos.

### 6.1. *Chaos and attractors*

Many scientists associate chaos only with strange attractors or dissipative systems. For example, the Lorenz, Chua and Rossler equations are all dissipative. Historically, however, chaos was first mentioned[5] as a nondissipative system. Chaos and attractors are independent concepts, and the most complex forms of chaos occur in nondissipative systems. In fact, the presence of dissipation reduces the level of complexity and thus reduces the "level" of chaos.

### 6.2. *Chaos and noninvertibility*

Noninvertible systems are inherently more complex than invertible systems. This is best illustrated by the fact that noninvertibility is a sufficient condition for a system to have positive entropy. Noninvertible systems do not directly arise from solutions of differential equations. This suggests that noninvertibility is a source of a level of complexity.

### 6.3. *Nonorientation preserving and chaos*

Orientation-preserving maps are those for which the Jacobian determinant is positive. The significance of this is that nonorientation-preserving maps cannot arise from the solutions of differential equations whose Jacobian is positive. There are many chaotic maps which are not orientation preserving; most notably, there are parameter values for which the Jacobian derivative of the Hénon map is negative. Hence, nonorientation-preserving maps are a source of some level of complexity. In this section we clarify some important relationships between dynamical systems having these three properties to give a perspective of how they contribute to the development of a level of complexity and to remove any confusion about their contribution to the production of chaos.

We summarize the relationships in a series of informal statements which can be rigorously proven.

**Statement 1.**

Any dissipative system that arises from an ODE can be converted to a nondissipative system without altering the fundamental level of complexity. Specifically, for any dissipative system we may increase the dimension of the system by one and make it, essentially, nondissipative. The construction is simple. Let $T(\mathbf{X})$ be any $n$-dimensional dissipative system. Since it arises from an ODE, the Jacobian determinant, $\det(DT(\mathbf{X}))$, must be positive. The following mapping "contains" $T$ in an obvious sense and is nondissipative:

$$\begin{pmatrix} \mathbf{X} \\ z \end{pmatrix} \to \begin{pmatrix} T(\mathbf{X}) \\ z/(\det(DT(\mathbf{X}))) \end{pmatrix}. \qquad (81)$$

This map expands in the direction of the added coordinate $z$ by exactly the amount needed to keep the combined map nondissipative. Also, in this map $T$ remains "intact." The Jacobian determinant of the combined map is 1.

**Statement 2.**

Any noninvertible mapping can be made essentially invertible by doubling the number of coordinates. This was proven in [Brown & Chua, 1996b, Theorem 1] and is restated here for completeness.

**Statement 3.**

Any nondissipative map can be made dissipative in such a way that the original map is an attractor. Theorem 1 mentioned above also proves this statement.

**Statement 4.**

Any nonorientation-preserving mapping can be made orientation-preserving by increasing the dimension by one. A simplification of the construction of Statement 1 will do this: Add the coordinate $z \to -z$.

**Statement 5.**

Any mapping that can be written as a formula can be made the Poincaré map for some ODE for

[5]Poincaré in volume three, item 397, of his memoirs in reference to the level of complexity of the three-body problem. Poincaré never used the term *chaos* which was coined by Jim Yorke at the University of Maryland.

which an electronic circuit can be built. This result is a consequence of the above statements and the $n$-phase gate construction in [Brown & Chua, 1993]. As a result, we now expand Statement 1 as follows:

**Statement 6.**

Any dissipative system that can be written as a formula, regardless of whether it arises from an ODE, can be converted to a nondissipative system that does arise from an ODE without altering its level of complexity.

## 7. Summary

In this tutorial we have illustrated that there are degrees of chaos and that there are very interesting maps which are not considered chaotic but are more complex than much of what we call *chaos*. We conclude that it is impossible to talk of chaos in a meaningful way without also talking about the level of complexity of the chaotic system. From a practical point of view, there are nonchaotic systems that are just as useful in producing a high level of complexity as are many chaotic systems. Their use in spread-spectrum communications is a good practical example. Low-level encryption systems which are also low cost are another example. However, our philosophical wanderings have led us to suggest that there is a *theory of chaos* and that this theory in concerned with determining the ways in which complex outputs can arise from the action of dynamical systems, and with quantifying this level of complexity in a useful manner.

We have shown how nonlinearities can be formed in a variety of ways. The significance of this is that an application needing chaotic effects will be optimal if the construction assures that the chaos arises from the right processes. There are at least four different nonlinear processes in two dimensions that can be used to generate chaotic effects which have very different properties.

We have also shown that the features of dissipation, noninvertibility, and orientation-preserving are completely independent of chaos and can be added or subtracted from any application, as desired.

This paper is the fourth in a series of papers whose purpose is to clarify a wide range of issues about chaos through the construction of examples and counterexamples, [Brown & Chua, 1996a, 1996b, 1997] are the other three. In [Brown & Chua, 1996a] we presented 29 examples that answered such questions as "Can chaotic dynamical systems be solved in closed form in terms of elementary functions?", "Does sensitive dependence on initial conditions ever define chaos?", "What is the relationship between popular definitions of chaos?", and several other questions. In [Brown & Chua, 1996b] we presented 26 examples that illustrated the spectrum of complexity that lies between Bernoulli chaos and periodic dynamics. In [Brown & Chua, 1997] we presented 6 examples to show that even the existence of positive Lyapunov exponents is not equivalent to chaos, that the shift paradigm is inadequate to account for all the features of chaos, and that highly complex orbits can be generated by chaotic dynamics without requiring that the initial conditions have positive algorithmic complexity. In this paper we presented 24 examples that: illustrated how subtle levels of chaos can be generated by combining a wide range of nonchaotic systems with chaotic systems; illustrated parts of the complexity spectrum that resemble chaos; and, how subtle nonlinear effects in autonomous two-dimensional systems can contribute to the formation of chaos. In total, we have constructed over 85 examples of dynamical systems in terms of elementary functions for which electronic circuits can be made that illuminate various aspects of chaos and the complexity spectrum and refute many popular notions about chaos. What we can conclude is that defining chaos is every bit as difficult as predicting chaos. Our examples suggest we conclude this paper with the following interesting line of thought.

Let us conceive of a $n$-dimensional space where one coordinate is entropy, another coordinate is correlation dimension, another coordinate is the Lyapunov exponent, and another the autocorrelation at some fixed time, and so on until we have exhausted all measures of levels of complexity found in a dynamical system. For each dynamical system, let us make all these measurements and plot its place in this space. We ask the question: Do the chaotic dynamical systems form a connected set, a compact set, or perhaps do they form a fractal? In short, just what is the nature of this set?

## Acknowledgment

This work of the first author was supported in part by ONR contract N00014-95-C-0153.

## References


Arnold, V. & Avez, A. [1989] *Ergodic Problems of Classical Mechanics* (Addison-Wesley, New York).

Brown, R. & Chua, L. O. [1996a] "Clarifying chaos: Examples and counterexamples," *Int. J. Bifurcation and Chaos* **6**(2), 219–249.

Brown, R. & Chua, L. O. [1996b] "From almost periodic to chaotic: The fundamental map," *Int. J. Bifurcation and Chaos* **6**(6), 1111–1125.

Brown, R. & Chua, L. [1993] "Dynamical synthesis of Poincaré maps," *Int. J. Bifurcation and Chaos* **3**(5), 1235–1267.

Cornfeld, I., Fomin, S. & Sinai, Y. [1982] *Ergodic Theory* (Springer-Verlag, Berlin).

Ding, M., Grebogi, C. & Ott, E. [1989] "Evolution of attractors in quasiperiodically-forced systems: From quasiperiodic to strange nonchaotic to chaotic," *Phys. Rev. A*, 2593–2598.

Freeman, W. J. [1995] *Societies of Brains* (Lawrence Erlbaum Associates, Hillsdale, N.J).

Grebogi, C., Ott, E., Pelikan, S. & Yorke, J. [1984] "Strange attractors that are not chaotic," *Physica* **D13**, 261–268.

Katznelson, Y. [1971] "Ergodic automorphisms of $T^n$ are Bernoulli shifts," *Israel J. Math.* **10**, 186–195.

Parry, W. [1981] *Topics in Ergodic Theory* (Cambridge University Press, Cambridge).

Peterson, K. [1983] *Ergodic Theory* (Cambridge University Press, Cambridge).

Walters, P. [1982] *Introduction to Ergodic Theory* (Springer-Verlag, New York).

International Journal of Bifurcation and Chaos, Vol. 7, No. 12 (1997) 2789–2805
© World Scientific Publishing Company

# CHAOTIC DIGITAL CODE-DIVISION MULTIPLE ACCESS (CDMA) COMMUNICATION SYSTEMS

TAO YANG and LEON O. CHUA
*Electronics Research Laboratory and*
*Department of Electrical Engineering and Computer Sciences,*
*University of California at Berkeley,*
*Berkeley, CA 94720, USA*

Received June 26, 1997; Revised August 18, 1997

In this paper, the structure, principle and framework of chaotic digital code-division multiple access ($(CD)^2$ MA) communication systems are presented. Unlike the existing CDMA systems, $(CD)^2$MA systems use continuous pseudo-random time series to spread the spectrum of message signal and the spread signal is then directly sent through a channel to the receiver. In this sense, the carrier used in $(CD)^2$MA is a continuous pseudo-random signal instead of a single tone as used in CDMA. We give the statistical properties of the noise-like carriers. In a $(CD)^2$MA system, every mobile station has the same structure and parameters, only different initial conditions are assigned to different mobile stations. Instead of synchronizing two binary pseudo-random sequences as in CDMA systems, we use an impulsive control scheme to synchronize two chaotic systems in $(CD)^2$MA. The simulation results show that the channel capacity of $(CD)^2$MA is twice as large than that of CDMA.

## 1. Introduction

In the 1980s, many analog cellular communication networks were implemented over the world. These networks are already reaching their capacity limits in several service areas. This wireless communication technology has evolved from simple first-generation analog systems for business applications to second-generation digital systems with rich features and services for residential and business environments. There are several reasons for the transition from wireless analog to digital technology: Increasing traffic, which requires greater cell capacity, speech privacy, new services and greater radio link robustness.

During the late 1980s and early 1990s, the rapid growth in mobile communications put a high demand on system capacity and the availability of the technology for low-cost implementation of cellular and personal communication services (PCS) [Gang *et al.*, 1997]. CDMA has a larger system capacity than the existing analog systems. The increased system capacity is due to the improved coding gain/modulation density, voice activity, three-sector sectorization, and the reuse of the same spectrum in every cell. CDMA is a cost-effective technology that requires fewer, less-expensive cells and no costly frequency reuse pattern. The average power transmitted by the CDMA mobile stations averages about 6–7 mW, which is less than one tenth of the average power typically required by FM and TDMA phones. Transmitting less power means longer battery life. CDMA can improve the quality-of-service by providing both robust operation in fading environments and transparent (soft) hand-off. CDMA takes advantage of multi-path fading to enhance communications and voice quality. In narrow-band systems, fading causes a substantial degradation of signal quality.

Since some new services, such as wide-band data and video, are much more spectrum-intensive

than voice service, even the channel capacity improvement provided by CDMA will be depleted in the near future. This motivates some advanced wireless communication schemes, which can provide a bigger capacity. In this paper, we present a chaotic digital CDMA scheme. Before we design a chaotic digital CDMA system, we should solve the following problems.

### 1.1. *Spreading carriers*

In CDMA systems, pseudo-random signals are used to

(1) spread the bandwidth of the modulated signal to the larger transmission bandwidth and
(2) distinguish among the different user signals which are using the same transmission bandwidth in the multiple-access scheme.

Ideally, these pseudo-random signals should be samples of a sequence of independent random variables, uniformly distributed on an available alphabet or range. In this case, the CDMA system is equivalent to a one-time pad used in cryptographic system requiring the highest level of security. Since the key signal in a one-time pad should be as long as the message signal, it is not feasible to use it in CDMA [Simon *et al.*, 1994].

We must figure out a way to store/generate good pseudo-random signals in both the transmitter and the receiver, despite the finite storage capacity/generating capacity of physical processing systems. It would be very expensive and energy efficient to generate such a sequence by using some chaotic circuits, e.g. Chua's circuits. In fact, some methods to generate good pseudo-random signals for cryptographic purposes by using Chua's circuits [Yang *et al.*, 1997] have been already developed.

### 1.2. *Orthogonal functions*

Orthogonal functions are used to improve the bandwidth efficiency of a spread spectrum system. In CDMA, each mobile station uses one set of orthogonal functions representing the set of symbols used for transmission. Usually, the Walsh and Hadamard sequences are used to generate this kind of orthogonal functions for CDMA. In $(CD)^2$MA, it is difficult to find a theory to guarantee that the spectrum-spreading carriers are orthogonal. However, from simulations we find that there exist many methods to generate signals, which have very small cross correlations, by using chaotic signals. We can therefore choose good spectrum-spreading carriers from several promising candidates.

In CDMA, there exist two different methods of modulating the orthogonal functions into the information stream of the CDMA signal. The orthogonal set of functions can be used as the spreading code or can be used to form modulation symbols that are orthogonal. In $(CD)^2$MA, however, the "orthogonal function" itself serves as the carrier.

### 1.3. *Synchronization considerations*

In a CDMA system, the heart of the receiver is its synchronization circuitry, and the heartbeats are the clock pulses which control almost every step in forming the desired output. There exist three levels of synchronization in a CDMA system: (1) correlation interval synchronization, (2) spread-spectrum generator synchronization and (3) carrier synchronization.

To correlate the Walsh codes at the receiver, the receiver is required to be synchronized with the transmitter. In the forward direction, the base station can transmit a pilot signal to enable the receiver to recover synchronization. Just as the designers of the IS-665 wide-band CDMA system believed, with a wider bandwidth the base station can also recover the pilot signal sent by mobile stations. In $(CD)^2$MA, we also use this symmetric system between the base station and the mobile station.

In the $(CD)^2$MA system, we need to synchronize two chaotic systems. If we use the continuous synchronization scheme, we need a channel to transmit the chaotic signal. Even though we can embed a message signal into a chaotic carrier [Halle *et al.*, 1993], we cannot achieve a chaotic CDMA system. A promising method to improve this is the framework of impulsive synchronization [Yang & Chua, 1997a, 1997b]. In this paper, we will show that the $(CD)^2$MA system does not need the correlation interval synchronization and carrier synchronization. This makes the receiver in $(CD)^2$MA simple and low-power.

The $(CD)^2$MA system can increase the capacity of a radio channel. For mobile subscribers, this increased capacity translates to better service at a lower price. On the other hand, $(CD)^2$MA is also a promising technology for low-cost implementation

of cellular and PCS. The organization of this paper is as follows. In Sec. 2, we present the structure of $(CD)^2$MA system. In Sec. 3, we study the randomness of spreading carriers. In Sec. 4, we give the concept of impulsive synchronization. In Sec. 5, we show that a $(CD)^2$MA system has a larger channel capacity than CDMA. Section 6 contains the conclusion.

## 2. Structures of CDMA and $(CD)^2MA$ Systems

Information can be modulated into the spread-spectrum signal by several methods. The most common method is to add the information into the spectrum-spreading code before it is used for modulating the carrier frequency. The corresponding CDMA system is shown in Fig. 1. In Fig. 1, $d(t)$ and $c(t)$ are respectively called "message signal" and "spreading signal". The signal $\cos(\omega t)$ is called the carrier, and $x(t)$ is the encoded signal. At the receiver end, $I(t)$ is the interference signal which consists of channel noise, interference and/or jamming, and $r(t)$ is the recovered signal. $d(t)$ is a low frequency digital message signal with a data rate 9.6 kbps for IS-95 CDMA system. $c(t)$ is a high frequency spreading signal with a chip rate 1.2288 Mcps for IS-95 CDMA system. We can see that the chip rate is much higher than the data rate. This is the method by which the bandwidth of the message signal is spread.

On the other hand, the message signal can also be used to modulate the carrier directly, given the carrier also functions as spectrum-spreading signal. In $(CD)^2$MA system, we use this kind of modulation scheme. The corresponding $(CD)^2$MA system is shown in Fig. 2.

Comparing the $(CD)^2$MA system in Fig. 2 with the CDMA system in Fig. 1, we can see that both schemes use the synchronization of two identical spreading carrier generators. Instead of modulating a single tone (an RF sinusoidal signal) as in the CDMA system, a $(CD)^2$MA system transmits a pseudo-random RF spreading carrier directly. We give the details of every block in Fig. 2. To enhance the security of the $(CD)^2$MA system, we can also use two key signals to scramble the spreading carrier. The key signal can be assigned to each transmitter and receiver pair by the base station (cell). Since each mobile station can function either as a transmitter or as a receiver, we suppose that the key signals are set by both the receiver and the transmitter and can be refreshed during conversations. The key signals may only be used in cases where a very high security should be taken into

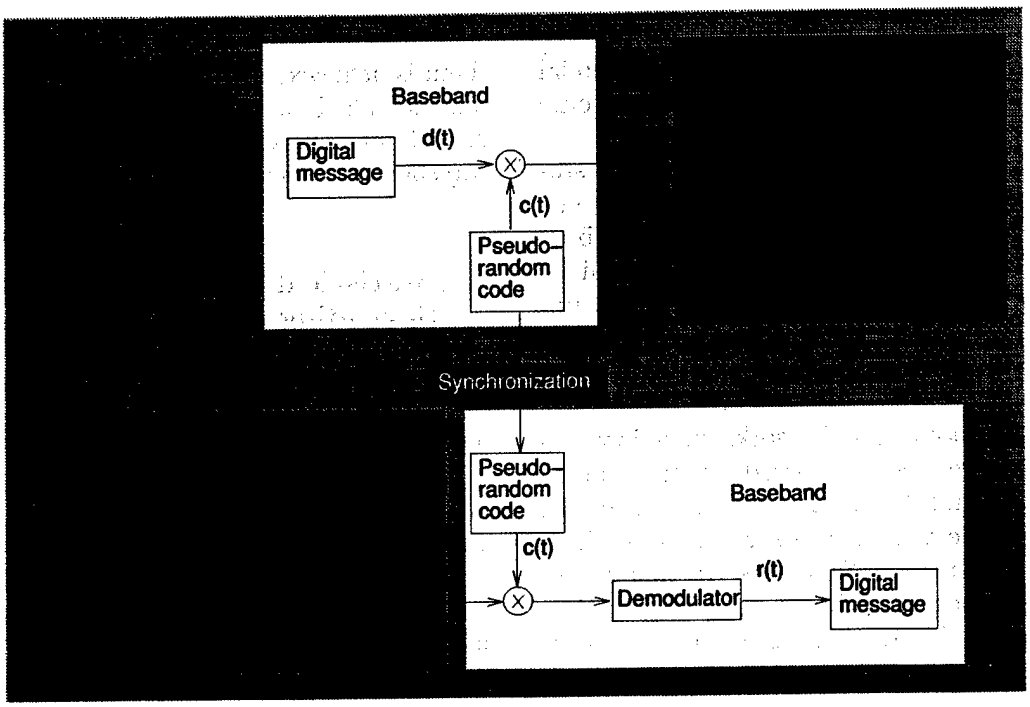


Fig. 1. The Block diagram of the CDMA system.

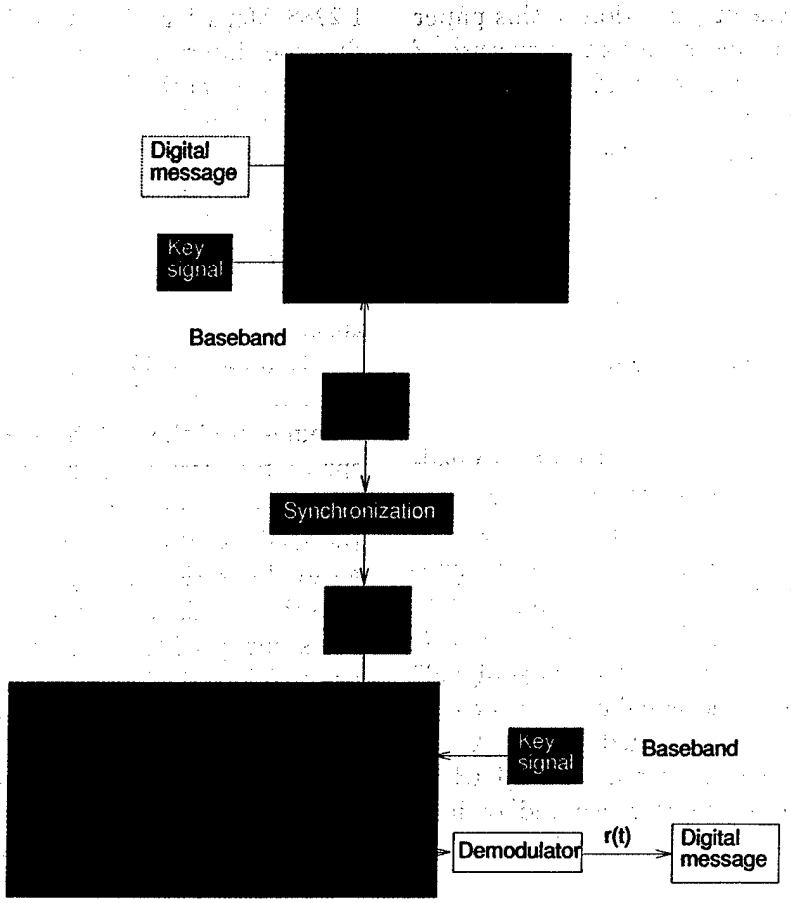


Fig. 2. The Block diagram of the $(CD)^2$MA system.

account (e.g. military applications). In commercial applications, the spreading signal is all along secure enough.

In the $(CD)^2$MA paradigm, every mobile station has the same chaotic circuit, e.g. Chua's circuit. Whenever two users are connected by the base station, they are assigned the same set of initial conditions to their chaotic circuits. Then, the impulsive synchronization scheme is used to maintain the synchronization between the two chaotic circuits.

Since the chaotic circuit works in a low frequency range, we need a spreading function to spread it into bandwidths in the MHz range. In principle, there are many nonlinear functions which can be used as spreading functions. In this paper, the spreading function is chosen according to that used in [Yang *et al.*, 1997]. That is, we use an $n$-shift scheme to spread the spectrum of the chaotic signal. The chaotic systems in both transmitter and receiver are identical and the synchronization between them is achieved by a new chaotic synchronization scheme called *impulsive synchronization*. The demodulator consists of some low-pass filtering and thresholding blocks.

## 3. Statistical Properties of Chaotic Spreading Carriers

We now study the properties of the spreading signal, which should have a narrow autocorrelation function for achieving a big channel capacity and small cross-relations. One of the ideal candidates for this kind of signal is white noise which has an autocorrelation function of a Dirac Delta function at the origin. Although from a deterministic model we cannot generate a true white noise signal, we still have the chance to generate its approximation which we call a pseudo-random signal. Since the cryptographic community has spent half a century trying to find a good binary pseudo-random

signal for the purpose of a high level of security of cryptographic algorithms, we borrow some methods used by them.

We first use a chaotic system to generate a good seed signal (low frequency in the range of KHz) and then use some spreading function to spread the spectrum into the range of MHz. In this paper, we choose the Chua's oscillator [Chua, 1994] as our chaotic system which has dynamics given by

$$\begin{cases} \dfrac{dv_1}{dt} = \dfrac{1}{C_1}[G(v_2 - v_1) - f(v_1)] \\ \dfrac{dv_2}{dt} = \dfrac{1}{C_2}[G(v_1 - v_2) + i_3] \\ \dfrac{di_3}{dt} = -\dfrac{1}{L}[v_2 + R_0 i_3] \end{cases} \tag{1}$$

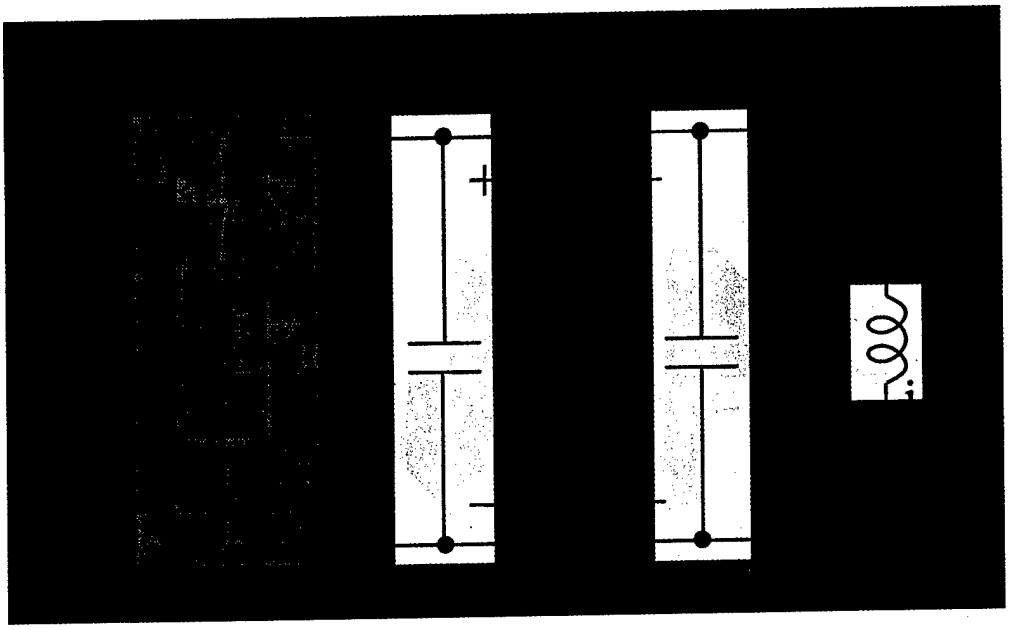

(a)

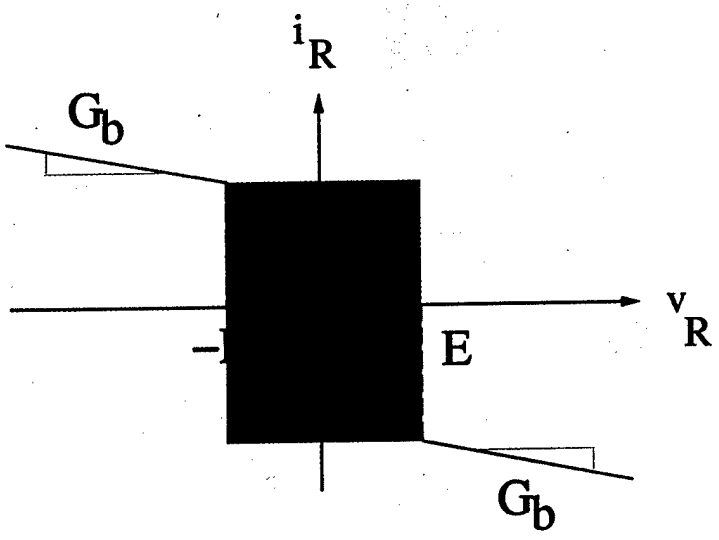


(b)

Fig. 3. (a) Chua's oscillator. (b) Chua's diode.

where $f(\cdot)$ is the nonlinear characteristics of Chua's diode given by

$$f(v_1) = G_b v_1 + \frac{1}{2}(G_a - G_b)(|v_1 + E| - |v_1 - E|) \tag{2}$$

and $E$ is the breakpoint voltage of Chua's diode. The corresponding circuit is shown in Fig. 3.

We use a continuous $n$-shift cipher to spread the chaotic signal generated by a Chua's circuit. The $n$-shift cipher is given by

$$\begin{aligned} x(t) &= e(p(t)) \\ &= \underbrace{f_1(\ldots f_1(f_1}_{n}(p(t), \underbrace{p(t)), p(t)), \ldots, p(t))}_{n} \end{aligned} \tag{3}$$

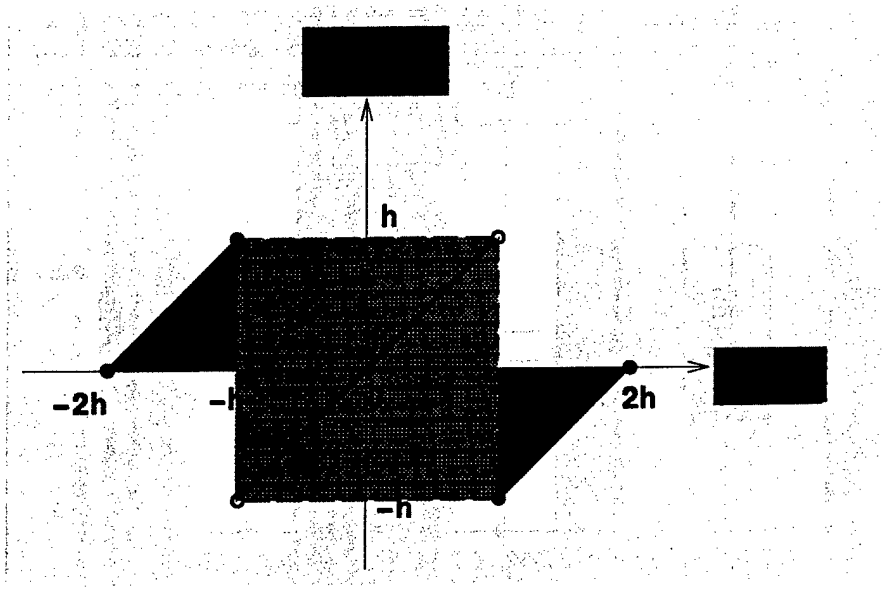


(a)

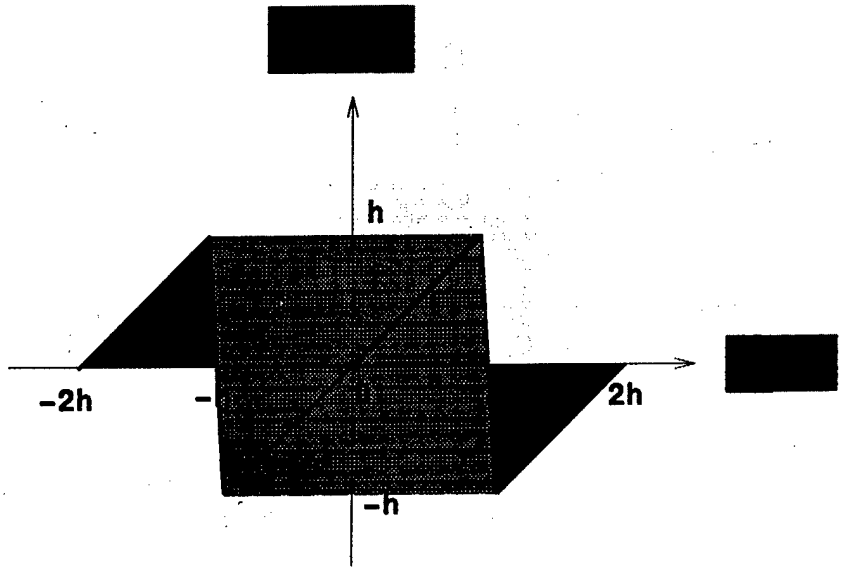


(b)

Fig. 4. Nonlinear function used in continuous shift cipher. (a) The ideal model. (b) The practical implementation.

where $h$ is chosen such that $p(t)$ lies within $(-h, h)$. $f_1(\cdot, \cdot)$ is a nonlinear function

$$f_1(x, k) = \begin{cases} (x+k) + 2h, & -2h \le (x+k) \le -h \\ (x+k), & -h < (x+k) < h \\ (x+k) - 2h, & h \le (x+k) \le 2h. \end{cases} \tag{4}$$

This function is shown in Fig. 4(a). Since the "jump-type" break points in Fig. 4(a) cannot be implemented in a practical circuit, what we need is the continuous version of this characteristics shown in Fig. 4(b). In this case, $f_1(\cdot, \cdot)$ is given by

$$f_1(x, k) = \begin{cases} \dfrac{h}{h-\Delta}(x+k) + 2h, & -2h \le (x+k) \le -h-\Delta \\ -\dfrac{h}{\Delta}(x+k+h), & -h-\Delta \le (x+k) < -h+\Delta \\ \dfrac{h}{h-\Delta}(x+k), & -h+\Delta \le (x+k) < h-\Delta \\ -\dfrac{h}{\Delta}(x+k-h), & h-\Delta \le (x+k) < h+\Delta \\ \dfrac{h}{h-\Delta}(x+k) - 2h, & h+\Delta \le (x+k) \le 2h. \end{cases} \tag{5}$$

In our $(CD)^2$MA systems, we choose the seed signal $p(t)$ as the voltage $v_1(t)$ of Chua's circuit. Since we choose $h = 1$ V, $p(t)$ is a normalized version of $v_1(t)$. Before we use the output of the $n$-shift function as the spreading carrier, we have to test its statistical properties. In our $(CD)^2$MA systems, the following parameters are used: $C_1 = 5.56$ nF, $C_2 = 50$ nF, $G = 0.7$ mS, $L = 7.14$ mH, $G_a = -0.8$ mS, $G_b = -0.5$ mS, $E = 1$ V, $R_0 = 0\ \Omega$ and $\Delta = 0.01$. Given this set of parameters, Chua's circuit has a double-scroll attractor.

There are many tests that can be used to help establish the random characteristics of a signal [Knuth, 1981]. In this paper, we use two frequency tests: The $\chi^2$ test and the Kolmogorov-Smirnoff (K-S) test. See [Knuth, 1981] for details about both the tests. They are used to verify that the signal is uniformly distributed.

For the $\chi^2$ test, the range of $x(t)$ is divided into 51 intervals. Our expectation is an equal number of observations in each interval. Thus the $\chi^2$ values computed on each sample will be expected to follow a $\chi^2$ distribution with 50 degrees of freedom.

For the K-S test, $K^+$ and $K^-$ are computed for each sample of $x(t)$. The values are expected to be $K_n$-distributed, where $n$ is the number of samples in the sampled $x(t)$. In our simulations, $n = 10^5$ and the sampling interval is $10^{-7}$ s.

The following tests which were based on $\chi^2$-tests are also used.

**Serial test:** In the sequences of sampled $x(t)$, we want pairs of successive numbers to be uniformly distributed in an independent manner. To carry out the serial test, we simply count the number of times that the sampled pair $(x(2j), x(2j+1))$ fall in different regions of the plane $[-1, 1] \times [-1, 1]$. We split the interval $[-1, 1]$ into $d$ subintervals and code each of them by an integer from 1 to $d$. When $x(2j)$ falls into a subinterval, we use the code of this subinterval, an integer $Y_{2j}$, to represent it. This kind of coding system is also used in the other tests. To carry out the serial test, we simply count the number of times that $(Y_{2j}, Y_{2j+1}) = (q, r)$ occurs, for $1 \le q, r \le d$. And the $\chi^2$-test is applied to these $k = d^2$ categories with probability $\frac{1}{d^2}$ for each category. We chose $d = 8$. The sequence of block should have a length $\ge 5d^2$.

**Gap test:** This test is used to test the length of "gaps" between occurrences of $Y_j$ in a certain range. If $\alpha$ and $\beta$ are two real numbers with $0 \le \alpha < \beta < d$, we want to consider the lengths of the consecutive subsequences $Y_j, Y_{j+1}, \ldots, Y_{j+r}$ in which $Y_{j+r}$ lies between $\alpha$ and $\beta$ but the other $Y$'s do not. In this test, we chose $d = 9$.

**Poker test:** The classical poker test considers $n$ group of five successive integers ($Y_{5j}$, $Y_{5j+1}$, $Y_{5j+2}$, $Y_{5j+3}$, $Y_{5j+4}$) for $0 \leq j < n$, and observes which of the following five categories is matched by each quintuple: 5 different, 4 different, 3 different, 2 different and 1 different.

In general we can consider $n$ groups of $k$ successive numbers, and we can count the number of $k$-tuples with $r$ different values. A $\chi^2$-test is then made, using the probability

$$p_r = \frac{d(d-1)\cdots(d-r+1)}{d^k} \left\{ \begin{matrix} k \\ r \end{matrix} \right\} \qquad (6)$$

that there are $r$ different. $\left\{ \begin{matrix} k \\ r \end{matrix} \right\}$ is a Stirling number [Halls *et al.*, 1993]. In this case, we chose $d = 9$.

Table 1 lists the test results of $x(t)$ with different initial conditions with 10-shift cipher function.

In Table 1, when a test result is between 0.01 and 0.99, it denotes that $x(t)$ can be viewed as a good pseudo-random sequence. The bold face numbers in Table 1 denote the test results which do not belong to good pseudo-random sequences. Since there are only two test results belonging to the "bad" pseudo-random cases, we conclude that the randomness of $x(t)$ is good enough for designing spreading carriers. And we can see that this randomness is independent of the initial condition. This initial condition independent property can be used to simplify the hardware of mobile stations because we only need to give different initial conditions to each mobile station for generating its spreading carrier. Since these tests are used in testing the randomness of sequences for cryptographic purposes, we can conclude that a good pseudo-random sequence should have a very narrow autocorrelation function.

## 4. Impulsive Synchronization of Chua's Circuits in $(CD)^2MA$

The idea of applying impulsive synchronization to $(CD)^2$MA is inspired by the fact that every mobile station of a CDMA system has a clock signal to make the receiver work autonomously once the clock signal is synchronized with that of the transmitter. The difference between impulsive synchronization and continuous synchronization is that, in the former, once the synchronization is achieved the receiver can work autonomously for a given time duration. This is achieved by sending synchronizing impulses to the receiver. We should send synchronizing impulses to the receiver at a given frequency because the noise and parameter mismatches between the chaotic systems in the transmitter and the receiver will soon desynchronize both. For this reason, in the $(CD)^2$MA system we need an overhead channel to transmit synchronizing impulses.

In this section, we study the impulsive synchronization of two Chua's oscillators. One of the Chua's oscillators is called the *driving system* and the other is called the *driven system.* In an impulsive synchronization configuration, the driving system is given by Eq. (1). Let $\mathbf{x}^T = (v_1\ v_2\ i_3)$, then we can rewrite the driving system in Eq. (1) into the form

$$\dot{\mathbf{x}} = A\mathbf{x} + \Phi(\mathbf{x}) \qquad (7)$$

Table 1. Results of different statistical tests of chaotic spreading carriers when different initial conditions are used.

| | $v_1(0) = -0.204$ V<br>$v_2(0) = 0.045$ V<br>$i_3(0) = 1.561$ mA | $v_1(0) = 1.568$ V<br>$v_2(0) = -0.741$ V<br>$i_3(0) = 2.301$ mA | $v_1(0) = 0.1$ V<br>$v_2(0) = 2.515$ V<br>$i_3(0) = -1.901$ mA | $v_1 = -2.56$ V<br>$v_2 = -1.349$ V<br>$i_3 = -2.002$ mA |
|---|---|---|---|---|
| $\chi^2$ Test | 0.021 | 0.013 | 0.054 | 0.07 |
| K-S Test, $K^+$ | 0.011 | 0.044 | 0.034 | **0.009** |
| K-S Test, $K^-$ | 0.034 | 0.025 | 0.029 | 0.012 |
| Serial Test | **0.008** | 0.067 | 0.045 | 0.074 |
| Gap Test | 0.055 | 0.054 | 0.082 | 0.03 |
| Poker Test | 0.063 | 0.019 | 0.018 | 0.06 |

where

$$A = \begin{pmatrix} -G/C_1 & G/C_1 & 0 \\ G/C_2 & -G/C_2 & 1/C_2 \\ 0 & -1/L & -R_0/L \end{pmatrix}, \quad \Phi(\mathbf{x}) = \begin{pmatrix} -f(v_1)/C_1 \\ 0 \\ 0 \end{pmatrix}. \tag{8}$$

Then the driven system is given by

$$\dot{\tilde{\mathbf{x}}} = A\tilde{\mathbf{x}} + \Phi(\tilde{\mathbf{x}}) \tag{9}$$

where $\tilde{\mathbf{x}}^T = (\tilde{v}_1, \tilde{v}_2, \tilde{i}_3)$ are the state variables of the driven system.

At discrete instants, $\tau_i$, $i = 1, 2, \ldots$, the state variables of the driving system are transmitted to the driven system and then the state variables of the driven system are subject to jumps at these instants. In this sense, the driven system is described by an impulsive differential equation

$$\begin{cases} \dot{\tilde{\mathbf{x}}} = A\tilde{\mathbf{x}} + \Phi(\tilde{\mathbf{x}}), & t \neq \tau_i \\ \Delta\tilde{\mathbf{x}}|_{t=\tau_i} = -B\mathbf{e}, & i = 1, 2, \ldots \end{cases} \tag{10}$$

where $B$ is a $3 \times 3$ matrix, and $\mathbf{e}^T = (e_1, e_2, e_3) = (v_1 - \tilde{v}_1, v_2 - \tilde{v}_2, i_3 - \tilde{i}_3)$ is the *synchronization error*. If we define

$$\Psi(\mathbf{x}, \tilde{\mathbf{x}}) = \Phi(\mathbf{x}) - \Phi(\tilde{\mathbf{x}}) = \begin{pmatrix} -f(v_1)/C_1 + f(\tilde{v}_1)/C_1 \\ 0 \\ 0 \end{pmatrix} \tag{11}$$

then the error system of the impulsive synchronization is given by

$$\begin{cases} \dot{\mathbf{e}} = A\mathbf{e} + \Psi(\mathbf{x}, \tilde{\mathbf{x}}), & t \neq \tau_i \\ \Delta\mathbf{e}|_{t=\tau_i} = B\mathbf{e}, & i = 1, 2, \ldots \end{cases}. \tag{12}$$

The conditions for the asymptotic stability of impulsive synchronization can be found in [Yang & Chua, 1997b]. The results in [Yang & Chua, 1997b] also show that the impulsive synchronization is robust enough to additive channel noise and the parameter mismatch between the driving and driven systems.

## 5. Considerations for Investigating the Capacities of CDMA and $(CD)^2MA$

Several approaches to estimate cellular CDMA capacity have been developed [Gilhousen *et al.*, 1991; Salmasi, 1991; Lee, 1991; Pickholtz, 1991]. In this paper, we use the method presented in [Gilhousen *et al.*, 1991] to estimate the capacity of $(CD)^2$MA. Due to the structural differences between CDMA and $(CD)^2$MA, we revise the method presented in [Gilhousen *et al.*, 1991], which was originally proposed for CDMA, to cope with our $(CD)^2$MA schemes.

As in CDMA, we focus on the reverse link capacity because the forward link uses coherent demodulation by the pilot carrier, which is being tracked, and since its multiple transmitted signals are synchronously combined, its performance will be superior to that of the reverse link.

The estimate of the capacity of a CDMA system depends on the model of the whole CDMA system. To model a CDMA system, the following factors should be considered.

### 5.1. *Interference*

We usually approximate the interference to a given user from all other multiple access users by a Gaussian process [Ulloa *et al.*, 1995]. As with any digital communication system, spread spectrum or not, there are four components of the demodulator output:

- the desired output,
- the inter-chip interference components, which is usually called inter-symbol interference for non-spread digital demodulation,
- the component due to background noise, and
- the other-user interference components,

In a CDMA system, the interference from the other users is much stronger than that from the noise.

### 5.2. *Power control*

It is well-known that one of the most serious problems faced by a DS CDMA system is the multi-user interference. Because all users are transmitting in the same frequency band and the cross-correlatons of the codes are rarely zero, the signal-to-inference ratio, and hence the performance, decreases as the number of users increases, which shows that DS

CDMA is an interference-limited, rather than a noise-limited, system.

An effect known as the "near-far" effect plays an especially important role when considering multi-user interference. The near-far effect can be explained by considering the reverse link. Due to the path-loss law (which implies that the received power decreases as the transmitter-receiver distance increases), a close user will dominate over a user located at the boundary. In order to overcome the near-far effect, power control can be used.

The propagating loss is generally modeled as the product of the $m$th power of distance $r$ and the log-normal component representing shadowing losses. This model represents slowly varying losses, even for users in motion, and applies to both reverse and forward links. The more rapidly varying Rayleigh fading losses are not included here. Thus, for a user at a distance $r$ from a base station, attenuation is proportional to

$$\alpha(r, \varepsilon) = r^m 10^{\varepsilon/10} \tag{13}$$

where $\varepsilon$ is the decibel attenuation due to shadowing, with zero mean and standard deviation $\sigma$. Experimental data [Lee, 1989] suggest the choices of $m = 4$ for the power law and $\sigma = 8\,\text{dB}$ for the standard deviation of $\varepsilon$.

Power control can be established by letting the base station continuously transmit a pilot signal that is monitored by all mobile stations. According to the power level detected by the mobile station, the mobile station adjusts its transmission power. In a practical power control system, power control errors occur [Jansen & Prasad, 1995], implying that the average received power at the base station may not be the same for each user signal.

### 5.3. *Multi-path propagation*

In terrestrial communication, the transmitted signal is reflected and refracted by different smooth or rough surfaces and different objects, so that it is replicated at the mobile station with different time delays. This is called *multi-path propagation.* It can be quite severe in urban areas or within a building. Different paths arrive at different amplitudes and carrier phases. The path amplitude depend on the relative propagation distances and the reflective or refractive properties of the terrain or buildings. In many cases, particularly in a confined area, each distinguishable multi-path component will be actually the linear combination of several indistinguishable paths of varying amplitudes. Since these will add as random vectors, the amplitude of each term will appear to be Rayleigh-distributed, and the phase uniformly distributed. This is the most commonly accepted model [Viterbi, 1995].

Since two code sequences with a relative delay of more than two chip durations usually have a low correlation value compared to the fully synchronized situation, DS CDMA offers the possibility to distinguish between paths with a relative delay of more than two chip durations. This is called *the inherent diversity* of DS CDMA, implying that it is possible to resolve a number of paths separately using only one receiver. This property makes DS CDMA suitable for applications in mobile radio environments, which are usually corrupted with severe multi-path effects.

The multi-path fading channel for the $k$th mobile station is characterized by a set of its low-pass equivalent complex-values impulse responses

$$\left\{ h_k(t) = \sum_{l=1}^{L} a_{kl}\delta(t - \tau_{kl}) \exp(-j\phi_{kl}) \right\}_{k=1}^{K} \tag{14}$$

where $K$ denotes the number of the active users. Here we assume that every link has a fixed number $L$ of resolvable paths. The path gains $\{a_{kl}\}_{l=1}^{L}$, path delays $\{\tau_{kl}\}_{l=1}^{L}$, and path phases $\{\phi_{kl}\}_{l=1}^{L}$ are three random variables. For a given $k$, $\{a_{kl}\}_{l=1}^{L}$ is modeled as the set of the independent Rayleigh random variables whose probability density functions are given by:

$$p(\alpha_k) = \frac{2\alpha_k e^{-\alpha_k^2/\sigma_{kr}^2}}{\sigma_{kr}^2}, \quad \alpha > 0, \quad k = 1, 2, \ldots, L. \tag{15}$$

We suppose that the $L$ multipath components are all Rayleigh of equal average strength, so that

$$\sigma_{kr}^2 = \sigma_r^2, \quad \text{for all } k = 1, 2, \ldots, L. \tag{16}$$

According to [Wu *et al.*, 1995], we choose $\sigma_r = 4$ dB. The $\{\tau_{kl}\}_{l=1}^{L}$ are mutually independent and uniformly distributed over $[\Delta_1, \Delta_2]$, and the $\{\phi_{kl}\}_{l=1}^{L}$ are independent uniform random variables over $[0, 2\pi)$, all of which are also statistically independent of each other. In this paper, we choose $L = 5$, and $\Delta_1$ and $\Delta_2$ are chosen in the corresponding simulation which will be presented later.

## 6. Channel Capacity of $(CD)^2MA$

For simplicity, in this paper we only study the unsectorized cases. For the sectorized cases all the arguments of the relations between CDMA and $(CD)^2$MA are also valid.

For the Shannon limit, the number of users that we can have in a cell is

$$M = \frac{G_p}{E_b/N_0} \leq 1.45 G_p \tag{17}$$

where $E_b$ is the energy per bit and $N_0$ is the noise power spectral density. $G_p$ is the *system processing gain* which is given by

$$G_p = \frac{B_w}{R} \tag{18}$$

where $B_w$ is the bandwidth of the channel and $R$ is the *information rate.*

In an actual system, the CDMA cell capacity is much lower than the theoretical upper-bound value given in Eq. (17). The CDMA cell capacity is affected by the receiver modulation performance, power control accuracy, interference from other non-CDMA system sharing the same frequency band, and other effects.

Every cell in a CDMA system shares the same bandwidth therefore causing the intercell interference, which we account for by introducing a factor $\beta$. The practical range of $\beta$ is $0.5 \sim 0.55$. The interference from users in other cells reduces the number of users in a cell. The power control accuracy is represented by a factor $\alpha$. The practical range for $\alpha$ is $0.5 \sim 0.9$. The reduction in the interference due to the voice activity is represented by $\nu$ which has a practical range of $0.45 \sim 1$. Then Eq. (17) becomes

$$M = \frac{G_p}{E_b/N_0} \times \frac{1}{1+\beta} \times \alpha \times \frac{1}{\nu}. \tag{19}$$

In the rest of this section, we give a design example to show how $(CD)^2$MA can have a larger capacity than CDMA. In CDMA we use phase-shift keying (BPSK) for the data modulation and quadrature phase-shift keying (QPSK) for the spreading modulation. However, just for the purpose of demonstrating the improvement of the $(CD)^2$MA to the channel capacity, we suppose that the coherent BPSK is employed for both data modulation and spreading modulation. Then the encoded signal in CDMA system is given by

$$x(t) = c(t)d(t)\cos\omega t \tag{20}$$

and for $(CD)^2$MA, it is given by

$$x(t) = c(t)d(t). \tag{21}$$

The CDMA receiver multiplies $x(t)$ by the PN waveform to obtain the signal

$$\begin{aligned} r_1(t) = c(t)(x(t)+I(t)) &= c^2(t)d(t)\cos\omega t + c(t)I(t) \\ &= d(t)\cos\omega t + c(t)I(t) \end{aligned} \tag{22}$$

where $I(t)$ denotes the sum of noise and interference. For the $(CD)^2$MA receiver, we have

$$r_2(t) = c(t)(x(t)+I(t)) = d(t) + c(t)I(t). \tag{23}$$

Since the frequency of $d(t)$ is much less than $c(t)I(t)$, from Eq. (23) we know that the SNR of $r_2(t)$ can be significantly enhanced by using a low-pass filter before we do any further processing. This is not the case when we inspect Eq. (22), in which $d(t)\cos\omega t$ and $c(t)I(t)$ have similar frequency range. We only need a small $E_b/N_0$ in $(CD)^2$MA. Furthermore, the interference from other users is also reduced.

We then used simulation results to show that $(CD)^2$MA has a bigger capacity than CDMA. The following conditions are used. The RF bandwidth $B_w = 1.25$ MHz. The chip rate is 1.2288 Mcps, and the data rate is $R = 9.6$ Kbps. For a CDMA system, assume that $E_b/E_0 = 6$ dB, the interference from the neighboring cells $\beta = 60\%$, the voice activity factor $\nu = 50\%$, and the power control accuracy factor $\alpha = 0.8$. Then for a CDMA system, the channel capacity is 33 mobile users per cell[1].

The most important benchmark for evaluating the service quality of a digital communication system is the bit-error-rate (BER). In this paper, the desired performance of the $(CD)^2$MA system is chosen to be $BER \leq 10^{-3}$, which is the same as that used for a CDMA systems. The condition for the evaluation is as follows. Suppose that every mobile station has a perfect power control performance then the base station receives equal power from each mobile station. We suppose that the delays

[1]Notice that we only study the unsectorized cell here.

due to the multi-paths are distributed uniformly in (0.4 $\mu s$, 1.2 $\mu s$), i.e. $\Delta_1 = 0.4\ \mu s$ and $\Delta_2 = 1.2\ \mu s$, which corresponds to the range from 0.5 chip duration to 1.5 chip duration used in CDMA. The simulation results for 60, 90 and 110 users/cell are summarized in Tables 2–4 respectively.

From Table 2 we find that for $(CD)^2$MA system, $E_b/N_0 = 4$dB is enough to give a good result under the condition of 60 users/cell. We use simulation to show this result. In our simulation, the RF bandwidth $B_w = 1.25$ MHz. A 10-shift cipher is used to generate the spread carriers. The data rate is $R = 9.6$ Kbps. An overhead channel is used to transmit synchronizing impulses for all users. The synchronizing impulses are digitalized into 32-bit floating point numbers. Every user needs to refresh their synchronizing impulses once every second. The bit rate of the overhead channel should be greater than 5.76 Kbps for all 60 users.

The simulation results are shown in Fig. 5. Figure 5(a) shows the mixed signal in the channel which is a mixture of 60 spreading carriers. Figures 5(b)–5(d) show the spreading carriers of the users A, B and C, respectively. Figures 5(e)–5(g) show the message signals (green waveforms) and the recovered signals (red waveforms) for the users A, B and C, respectively. We can see that the digital signals are recovered from the $(CD)^2$MA schemes.

Table 2. The relation between BER and $E_b/N_0$ with 60 users/cell.

| $E_b/N_0$ | 3 dB | 4 dB | 5 dB | 6 dB |
|---|---|---|---|---|
| $BER$ | $3.4 \times 10^{-3}$ | $6.8 \times 10^{-4}$ | $1.3 \times 10^{-4}$ | $3.7 \times 10^{-5}$ |

Table 3. The relation between BER and $E_b/N_0$ with 90 users/cell.

| $E_b/N_0$ | 3 dB | 4 dB | 5 dB | 6 dB |
|---|---|---|---|---|
| $BER$ | $7.5 \times 10^{-3}$ | $2.3 \times 10^{-3}$ | $7.3 \times 10^{-4}$ | $2.9 \times 10^{-4}$ |

Table 4. The relation between BER and $E_b/N_0$ with 110 users/cell.

| $E_b/N_0$ | 3 dB | 4 dB | 5 dB | 6 dB |
|---|---|---|---|---|
| $BER$ | $4.4 \times 10^{-2}$ | $3.8 \times 10^{-2}$ | $3.1 \times 10^{-2}$ | $2.7 \times 10^{-2}$ |

For comparison, we also show the case of $E_b/N_0 = 4$dB and 110 users/cell. From Table 4 we can see that the interference become so strong that the increase of $E_b/N_0$ cannot decrease the BER significantly. The simulation results are shown in Fig. 6. Figures 6(a)–6(c) show the recovered signals and the message signals of users A, B and C, respectively. We can see that for user C, there exist

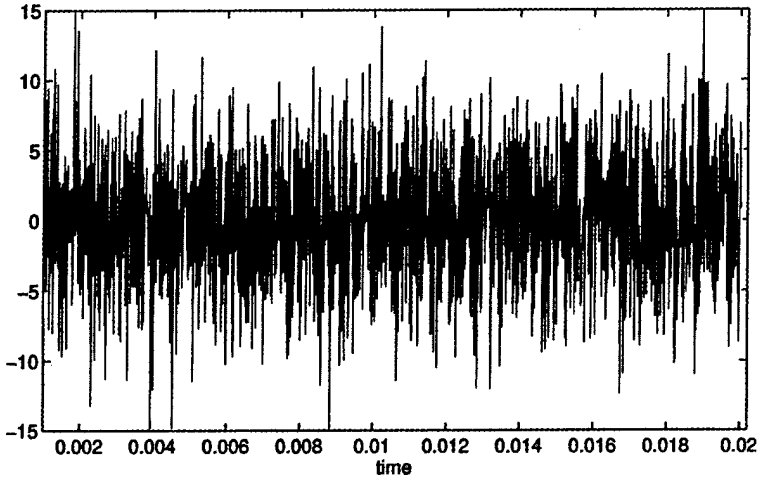


(a)

Fig. 5. Simulation results of the $(CD)^2$MA system with 60 users/cell and $E_b/N_0 = 4$dB. (a) The mixture of the spreading carriers in the channel. (b) The spread carrier for the user A. (c) The spread carrier for the user B. (d) The spread carrier for the user C. (e) The message signal (green) and the recovered signal (red) for the user A. (f) The message signal (green) and the recovered signal (red) for the user B. (g) The message signal (green) and the recovered signal (red) for the user C.

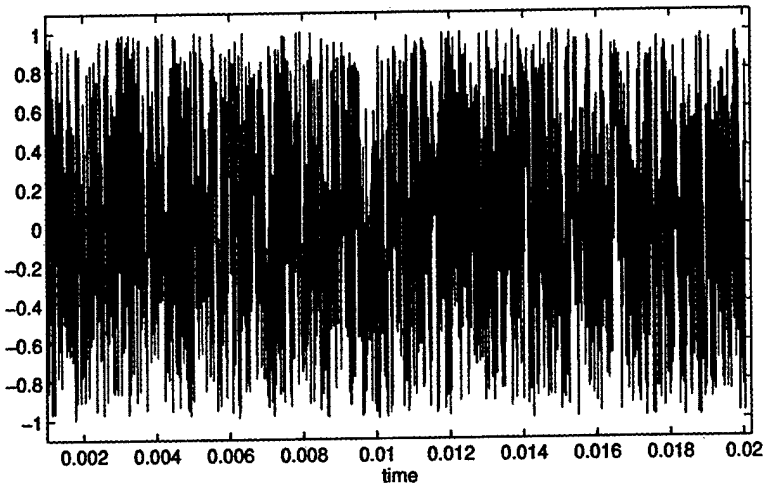


(b)

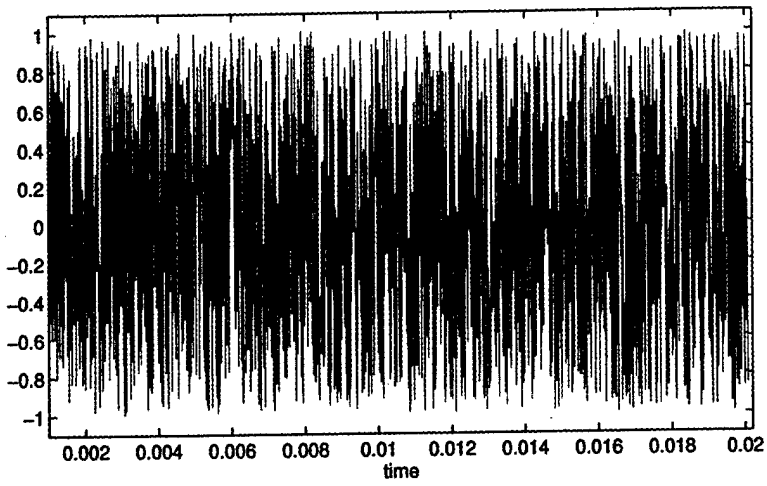


(c)

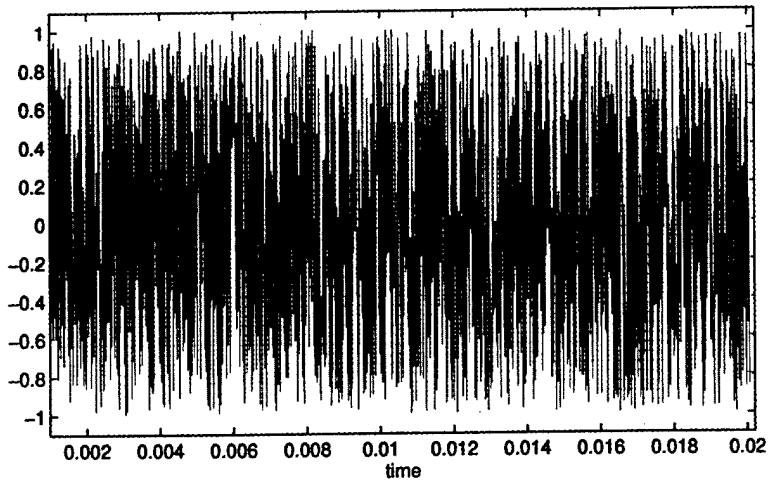


(d)

Fig. 5. *(Continued)*

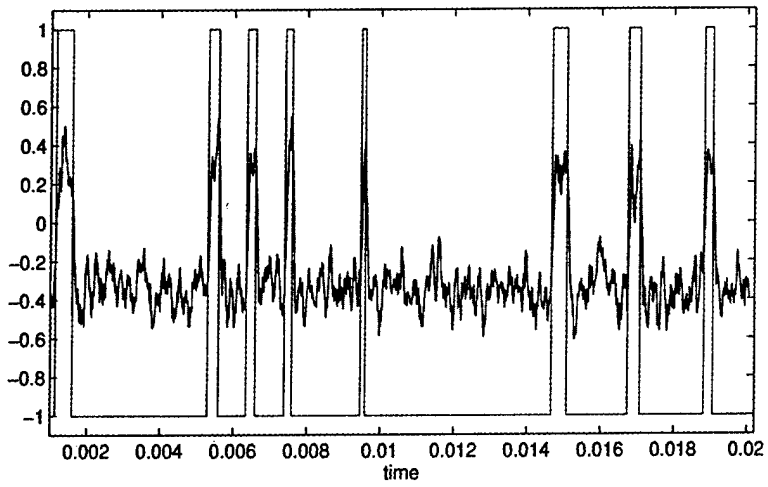


(e)

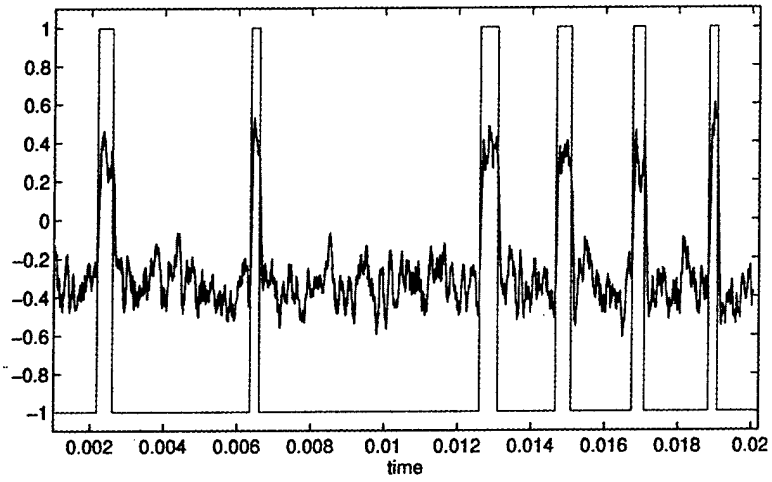


(f)

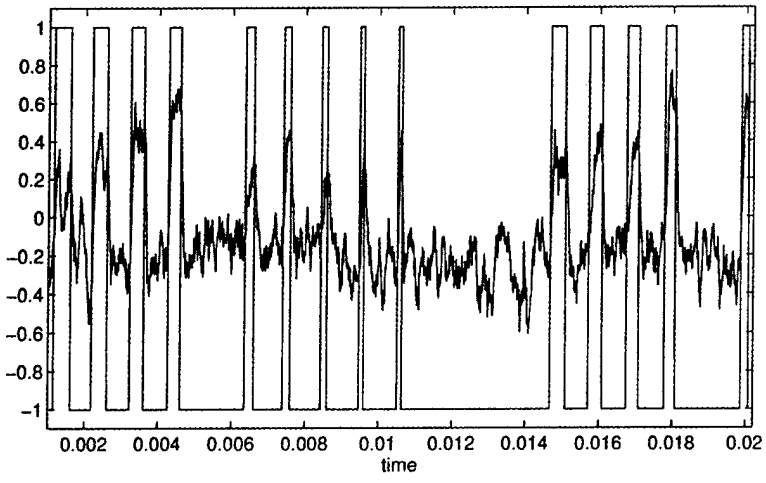


(g)

Fig. 5. *(Continued)*

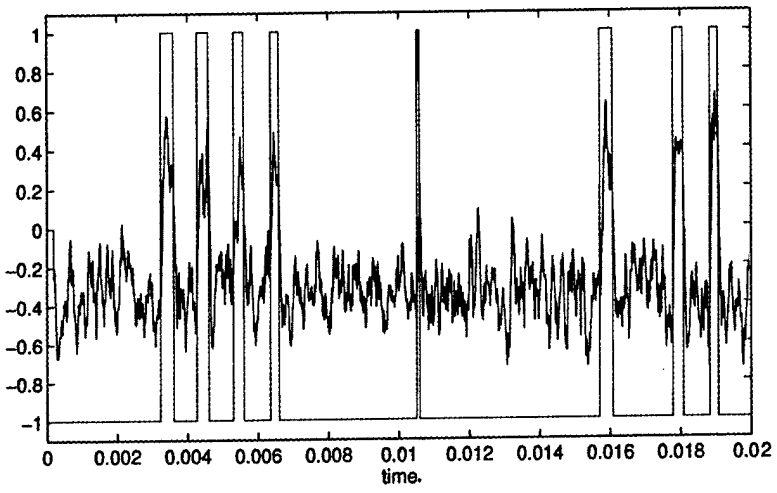


(a)

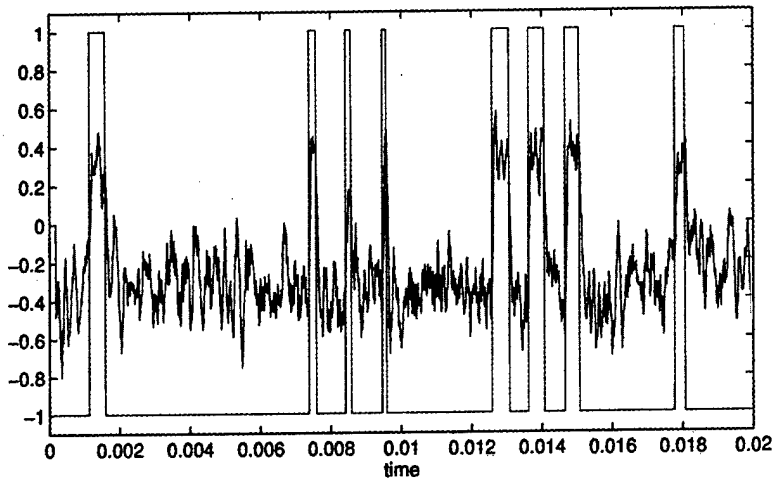


(b)

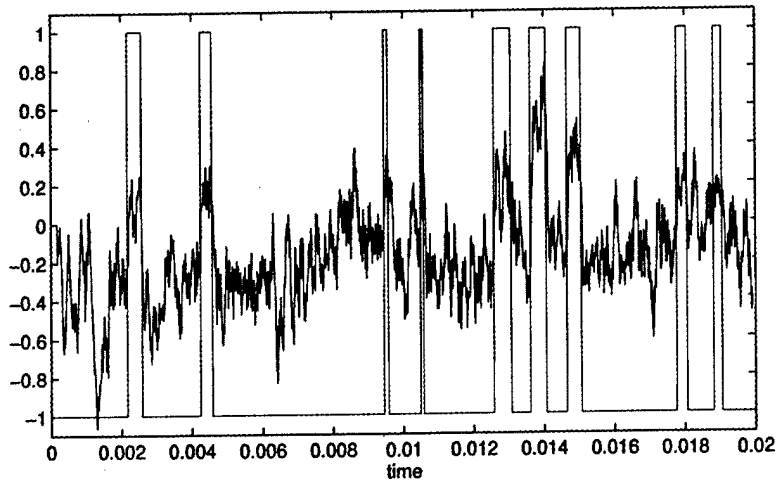


(c)

Fig. 6. Simulation results of the $(CD)^2$MA system with 110 users/cell and $E_b/N_0 = 4\,\text{dB}$. (a) The message signal (green) and the recovered signal (red) for the user A. (b) The message signal (green) and the recovered signal (red) for the user B. (c) The message signal (green) and the recovered signal (red) for the user C.

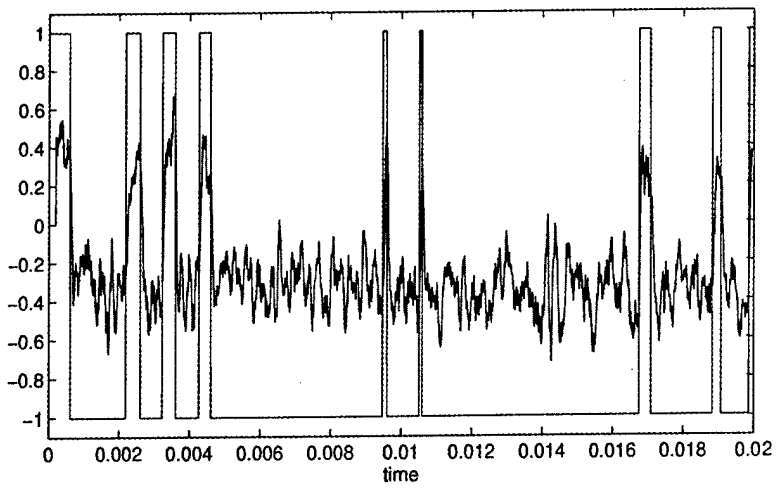


(a)

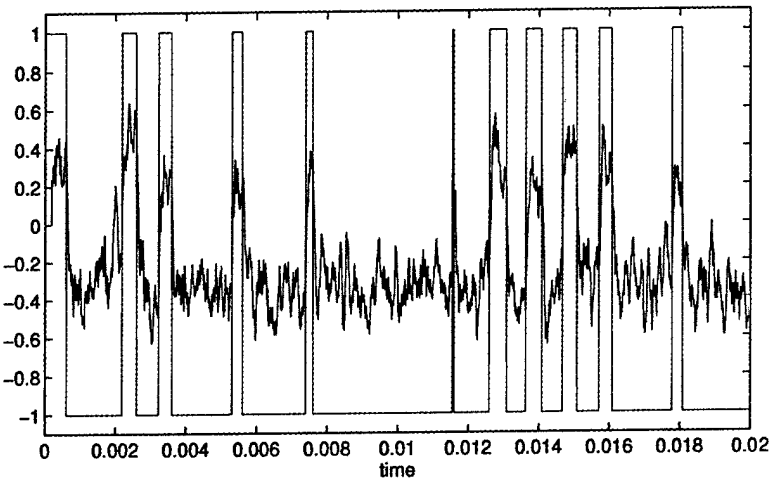


(b)

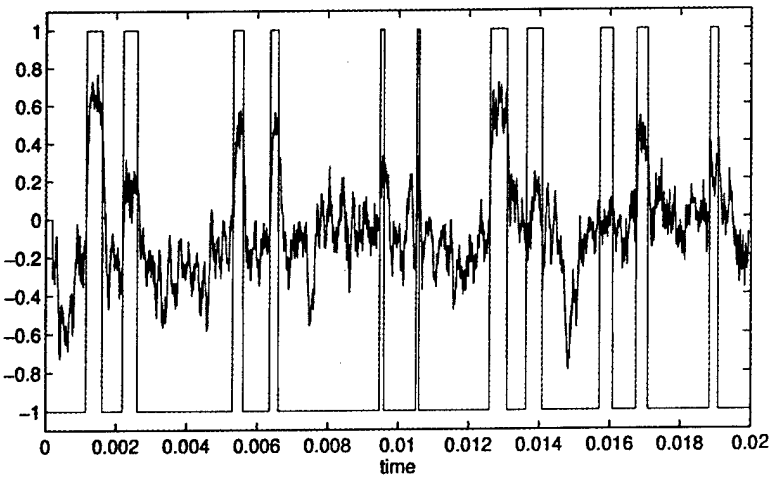


(c)

Fig. 7. Simulation results of the $(CD)^2$MA system with 90 users/cell and $E_b/N_0 = 4\,\text{dB}$. (a) The message signal (green) and the recovered signal (red) for the user A. (b) The message signal (green) and the recovered signal (red) for the user B. (c) The message signal (green) and the recovered signal(red) for the user C.

very serious bit errors. This is a big bit error probability which may degrade the speech quality very much.

Between 60 users/cell and 110 users/cell, we show the case $E_b/N_0 = 4\,\text{dB}$ and 90 users/cell. From Table 3 we can see that the service quality is decreased but is still usable. We also presented the simulation results in Fig. 7. Figures 7(a)–7(c) shows the recovered signals and the message signals of users A, B and C, respectively. We can see that for user C, there exist a few bit errors.

## 7. Conclusions

In this paper, we present a high capacity chaotic digital CDMA scheme which has twice the channel capacity[2] of CDMA. The improvement makes us use almost one-third of the Shannon limit of an ideal channel. We find that $(CD)^2$MA is a very promising scheme to reduce the subscriber fee of PCS by half, compared to the CDMA system. One of the critical problems in a chaotic CDMA scheme is to maintain the synchronization between two chaotic systems, since the synchronization signals would take a bandwidth of the order of the date rate if the continuous synchronization scheme is used. To overcome this problem we use an impulsive synchronization scheme to synchronize the two chaotic circuits in the linked pair. Thus, we only need a very small bandwidth for transmitting synchronization impulses.

## Acknowledgment

This work is supported by the Office of Naval Research under grant No. N00014-96-1-0753.

## References

Garg, V. K., Smolik, K. F. & Wilkes, J. E. [1997] *Applications of CDMA in wireless/personal communications* Feher/Prentice Hall digital and wireless communication series (Prentice Hall PTR, Upper Saddle River, NJ).

Gilhousen, K. S., Jacobs, I. M., Padovani, R., Viterbi, A. J. & Wheatley, C. E. [1991] "On the capacity of a cellular CDMA system," *IEEE Trans. Vehicular Technol.* **40**(2), 303–312.

Halle, K. S., Wu, C. W., Itoh, M. & Chua, L. O. [1993] "Spread spectrum communication through modulation of chaos," *Int. J. Bifurcation and Chaos* **3**(2), 469–477.

Jansen, M. G. & Prasad, R. [1995] "Capacity, throughput, and delay analysis of a cellular DS CDMA system with imperfect power control and imperfect sectorization," *IEEE Trans. Vehicular Technol.* **44**(1), 67–75.

Knuth, D. Z. [1981] *The Art of Computer Programming Vol. 2* (Addison-Wesley, Canada).

Lee, W. C. Y. [1989] *Mobile Cellular Telecommunications Systems* (McGraw-Hill, New York).

Lee, W. C. Y. [1991] "Overview of cellular CDMA," *IEEE Trans. Vehicular Technol.* **40**(2), 291–302.

Chua, L. O. [1994] "Chua's circuit — an overview ten years later," *J. Circuit Syst. Comput.* **4**(2), 117–159.

Pickholtz, R. L., Milstein, L. B. & Schilling, D. L. [1991] "Spread spectrum for mobile communication," *IEEE Trans. Vehicular Technol.* **40**(2), 313–322.

Salmasi, A. [1991] "Cellular and personal communication networks based on the application of code division multiple acess (CDMA)," In *Proc. Virginia Tech's 1st Symp. Wireless Personal Commun.* pp. 10.1–10.9.

Simon, M. K., Omura, J. K., Scholtz, R. A. & Levitt, B. K. [1994] *Spread Spectrum Communications Handbook* (McGraw-Hill, New York).

Ulloa, J. A., Taylor, D. P. & Poehlman, W. F. S. [1995] "An expert system approach for cellular CDMA," *IEEE Trans. Vehicular Technol.* **44**(1), 146–154.

Viterbi, A. J. [1995] *CDMA: Principles of Spread Spectrum Communication* Addison-Wesley Wireless Communications Series (Addison-Wesley, Reading, Mass.).

Wu, G., Jalali, A. & Mermelstein, P. [1995] "On channel model parameters for microcellular CDMA systems," *IEEE Trans. Vehicular Technol.* **44**(3), 706–711.

Yang, T. & Chua, L. O. [1997a] "Impulsive control and synchronization of chaotic systems and secure communication," Memorandum UCB/ERL M97/12, Electronics Research Laboratory, College of Engineering, Univ. California, Berkeley, CA 94720.

Yang, T. & Chua, L. O. [1997b] "Impulsive control and synchronization of nonlinear dynamical systems and application to secure communication," *Int. J. Bifurcation and Chaos* **7**(3), 645–664.

Yang, T., Wu, C. W. & Chua, L. O. [1997] "Cryptography based on chaotic systems," *IEEE Trans. Circuits Syst. — I: Fundamental Theory and Applications* **44**(5), 469–472.

[2]If the $E_b/N_0$ is increased to 6 dB as that used in CDMA systems, the $(CD)^2$MA system may even triple the channel capacity as shown in Table 3.

International Journal of Bifurcation and Chaos, Vol. 7, No. 12 (1997) 2891–2896
© World Scientific Publishing Company

# ABSOLUTE STABILITY THEORY AND MASTER-SLAVE SYNCHRONIZATION

P. F. CURRAN*
*Department of Electronic and Electrical Engineering*
*University College, Belfield, Donnybrook, Dublin 4, Ireland*

J. A. K. SUYKENS†
*Katholieke Universiteit Leuven,*
*Department of Electronic and Engineering, ESAT-SISTA,*
*Kardinaal Mercierlaan 94, B-3001 Leuven (Heverlee), Belgium*

L. O. CHUA‡
*Department of Electrical Engineering and Computer Sciences,*
*University of California, Berkeley, CA 94720, USA*

Received November 8, 1996; Revised December 5, 1996

In this note we indicate the manner in which synchronization criteria may be developed for master-slave connected Lur'e systems. For flexibility we incorporate linear, static state feedback. The criteria presented are based on the generation of Lur'e–Postnikov type Lyapunov functions for the error system.

## 1. Introduction

Recently much attention has been paid to the problem of synchronization [Pecora & Carroll, 1991; Wu & Chua, 1994; Hasler, 1994]. Chaotic systems in particular have been investigated with a view to the development of secure communication systems [Kocarev *et al.*, 1992; Parlitz *et al.*, 1992; Cuomo & Oppenheim, 1993]. A system which has received a great deal of attention in chaotic communication systems is the Chua oscillator [Chua *et al.*, 1993; Wu & Chua, 1994]. This system is a member of the more general class of Lur'e systems [Khalil, 1992].

The principal aim of this note is to extend the work of Curran and Chua [1997] on identifying the relationship which exists between the approach to the synchronization problem via the study of the *error system* [Wu & Chua, 1994; Suykens & Vandewalle, 1996], and the problem of classical absolute stability theory. While in the previous work [Curran & Chua, 1997] only quadratic Lyapunov functions were employed for the purpose of demonstrating global asymptotic stability of the error system (and hence synchronization), in the present work the more general Lur'e–Postnikov Lyapunov function is employed. As observed by Curran and Chua [1997] much of the existing work on the problem of synchronization employs quadratic Lyapunov functions. An exception is the paper by Suykens and Vandewalle [1996] where Lur'e–Postnikov Lyapunov functions (of a different type to those of the present note) are used. In effect the present note amounts to a discussion of this earlier paper [Suykens & Vandewalle, 1996]. A simplification of this earlier work is also achieved by selecting a

*E-mail: PCurran@Acadamh.UCD.ie
†E-mail: johan.suykens@esat.kuleuven.ac.be
‡E-mail: Chua@fred.EECS.Berkeley.EDU

different type of Lur'e–Postnikov Lyapunov function which avoids problems arising from the implicit dependence of the Lyapunov function on time. The discussion of the note also paves the way towards the application of the full choice of standard Lyapunov functions employed in the general theory of absolute stability.

This note is organized as follows. In Sec. 2 we present a number of equivalent sufficient conditions for synchronization of master-slave connected Lur'e systems with static, linear state feedback. In Sec. 3 we specialize these results for the case of Lur'e systems containing a single nonlinearity. On the basis of this specialization we offer a discussion of the success of the method used by Suykens and Vandewalle [1996] for the design of feedback matrices to achieve synchronization.

## 2. Synchronization of Lur'e Systems

Consider the multivariable Lur'e system [Vidyasagar, 1978; Khalil, 1992], which has the form

$$\dot{x} = Ax + Bf(C^T x), \quad f(0) = 0 \tag{1}$$

$A \in \mathbf{R}^{n\times n}$; $B$ and $C \in \mathbf{R}^{n\times r}$. After the fashion of Suykens and Vandewalle [1996] consider the synchronization scheme

$$\begin{cases} (\mathcal{M}) & \dot{x} = Ax + Bf(C^T x) \\ (\mathcal{S}) & \dot{y} = Ay + Bf(C^T y) + F(x - y) \end{cases} \tag{2}$$

where $F \in \mathbf{R}^{n\times n}$ is the feedback matrix to be designed. Assume

$$C^T = \begin{bmatrix} c_1^T \\ \vdots \\ c_r^T \end{bmatrix}, \quad f(\sigma) = \begin{bmatrix} f_1(\sigma_1) \\ \vdots \\ f_r(\sigma_r) \end{bmatrix}, \quad \sigma = \begin{bmatrix} \sigma_1 \\ \vdots \\ \sigma_r \end{bmatrix} \tag{3}$$

where $c_i \in \mathbf{R}^n$ and $f_i$ is a scalar function for each $i$. Such a nonlinearity is said to be of the diagonal type.

Defining the error signal $e = x - y$ one obtains the error system

$$(\mathcal{E})\ \dot{e} = (A - F)e + B[f(C^T e + C^T y) - f(C^T y)] \tag{4}$$

As usual [Curran & Chua, 1997] error system $(\mathcal{E})$ represents a class of systems. One seeks conditions under which this entire *class* is globally asymptotically stable (GAS) [Khalil, 1992; Vidyasagar, 1978]. To convert this problem into a standard problem of absolute stability theory we impose the following restriction on nonlinearity $f$

$$[f_i(\sigma_i + \zeta_i) - f_i(\zeta_i)][f_i(\sigma_i + \zeta_i) - f_i(\zeta_i) - k_i\sigma_i] \le 0 \quad \forall \sigma_i, \zeta_i \in \mathbf{R}, \quad \forall i. \tag{5}$$

This is a minor generalization of the restriction imposed by Suykens and Vandewalle [1996] and is standard in absolute stability theory [Khalil, 1992]. For the particular choice of $\zeta_i = 0$, restriction (5) leads to

$$f_i(\sigma_i)[f_i(\sigma_i) - k_i\sigma_i] \le 0 \quad \forall \sigma_i \in \mathbf{R}, \quad \forall i \tag{6}$$

which is the well-known sector $[0, k_i]$ constraint [Khalil, 1992; Vidyasagar, 1978].

Curran and Chua [1997] discuss the problem of the absolute stability of class (4) and (5) by employing a quadratic Lyapunov function. This approach is taken by Wu and Chua [1994] and numerous other authors. In general absolute stability theory one often employs more complicated Lyapunov functions, such as Lur'e–Postnikov functions [Khalil, 1992]. In employing such functions one is generally forced to impose more stringent conditions on the nonlinearity. In return the resulting stability criterion imposes fewer restrictions on the linear part of the Lur'e system. The conditions which must be imposed on the nonlinearity in order to allow the application of a variety of standard Lyapunov functions more complex than quadratic, effectively include the assumption of time-invariance of the class of differential equations under investigation. Although certain time-dependence is allowed, it is of a very weak type (effectively transient dependence, i.e. asymptotic convergence towards time-independent equations). These assumptions fail to hold for the class (4) and (5) when master system $(\mathcal{M})$ is chaotic. The strong time-dependence of (4) and (5) notwithstanding, it *is* possible to employ more general Lyapunov functions (such as Lur'e–Postnikov functions) by virtue of the fact that (4) is a subsystem of time-invariant system (2).

Select a Lur'e–Postnikov Lyapunov function

$$V(e) = e^T P e + \sum_{i=1}^{r} 2\gamma_i k_i \int_0^{c_i^T e} f_i(\rho)\, d\rho \tag{7}$$

$P = P^T > 0$, $P \in \mathbf{R}^{n\times n}$; $\gamma_i \ge 0 \forall i$. By construction $V(e)$ is positive definite and radially unbounded

[Khalil, 1992]. Taking the time derivative of (7) and applying the Lur'e S-procedure [Boyd *et al.*, 1994] one obtains

$$\begin{aligned}\dot{V}(e) &= \dot{e}^T P e + e^T P \dot{e} + \sum_{i=1}^{r} 2\gamma_i k_i f_i(c_i^T e)[c_i^T \dot{e}] \\ &\le e^T[(A-F)^T P + P(A-F)]e \\ &+ e^T P B\eta + \eta^T B^T P e \\ &+ \sum_{i=1}^{r} 2\gamma_i k_i f_i(c_i^T e)[c_i^T (A-F)e] \\ &+ \sum_{i=1}^{r} 2\gamma_i k_i f_i(c_i^T e) c_i^T B\eta \\ &- \sum_{i=1}^{r} 2\tau_i \eta_i(\eta_i - k_i c_i^T e) \\ &- \sum_{i=1}^{r} 2\beta_i f_i(c_i^T e)[f_i(c_i^T e) - k_i c_i^T e] \end{aligned} \tag{8}$$

where for notational convenience we have introduced

$$\eta_i = f_i(c_i^T e + c_i^T y) - f_i(c_i^T y)\,,$$
$$\eta = \begin{bmatrix} \eta_1 \\ \vdots \\ \eta_r \end{bmatrix} = f(C^T e + C^T y) - f(C^T y) \tag{9}$$

and where $\tau_i$ and $\beta_i$ are non-negative scalars for each $i$. The last two terms in (8) reflect inequalities (5) and (6). One may express the right-hand side of (8) as a quadratic in $e$, $f(C^T e)$, $\eta$ yielding

**Theorem 1.** *The derivative, $\dot{V}$, of the Lur'e–Postnikov function $V$ of Eq. (8) relative to differential class (4), (5) satisfies*

$$\dot{V}(e) \le [e^T,\, f^T(C^T e),\, \eta^T] W \begin{bmatrix} e \\ f(C^T e) \\ \eta \end{bmatrix} \tag{10}$$

*where*

$$W = \begin{bmatrix} (A-F)^T P + P(A-F) & ((A-F)^T C\Lambda K + CT_1 K) & (PB + CT_2 K) \\ ((A-F)^T C\Lambda K + CT_1 K)^T & -2T_1 & (K\Lambda C^T B) \\ (PB + CT_2 K)^T & (K\Lambda C^T B)^T & -2T_2 \end{bmatrix} \tag{11}$$

$$\Lambda = \text{diag.}[\gamma_i], \quad T_1 = \text{diag.}[\beta_i], \quad T_2 = \text{diag.}[\tau_i], \quad K = \text{diag.}[k_i]\,.$$

Theorem 1 (which is a standard application of the Lur'e S-procedure) suggests one sufficient condition for synchronization of (2), namely that the linear matrix inequality [Boyd *et al.*, 1994] $W < 0$ should permit a positive definite solution $P$ for some $\Lambda$, $T_1$ and $T_2$ diagonal, positive semi-definite matrices. Such a criterion may be tested numerically in the manner of Suykens and Vandewalle [1996]. However, the condition $W < 0$ is unnecessarily strong as it ignores the relationship which exists between $f$ and $\eta$. Assuming that $f_i(\sigma_i)$ does not equal zero for $\sigma_i$ nonzero, it follows that $f_i$ is zero only if $\eta_i$ is zero. In consequence one may define a function $q_i$ (which in general depends on $\sigma_i$ and $\zeta_i$) such that

$$f_i(\sigma_i) = q_i\eta_i = q_i[f_i(\sigma_i + \zeta_i) - f_i(\zeta_i)] \quad \forall\sigma_i, \quad \zeta_i \in \mathbf{R}\,. \tag{12}$$

Furthermore, assume

$$0 \le q_i(\sigma_i, \zeta_i) \le \hat{q}_i \quad \forall\sigma_i, \quad \zeta_i \in \mathbf{R}, \quad \hat{q}_i > 0 \tag{13}$$

$\hat{q}_i$ being a constant. Note that if restriction (5) is replaced by the slightly stronger restriction

$$\begin{aligned}&[f_i(\sigma_i + \zeta_i) - f_i(\zeta_i) - \varepsilon_i\sigma_i] \\ &[f_i(\sigma_i + \zeta_i) - f_i(\zeta_i - k_i\sigma_i] \le 0 \\ &\forall\sigma_i, \quad \zeta_i \in \mathbf{R}, \quad \forall i\end{aligned} \tag{14}$$

for some $\varepsilon_i \in (0, k_i)$, then it follows (by selecting $\zeta_i = 0$) that $f_i$ is sector $[\varepsilon_i, k_i]$. In consequence the condition $f_i(\sigma_i)$ nonzero for $\sigma_i$ nonzero is assured. Furthermore condition (13) holds with $\hat{q}_i \le k_i/\varepsilon_i$. Hence restrictions (12) and (13) do not amount to much more of a restriction on $f$ than restriction

(5). Subject to these restrictions one obtains from Eq. (10)

$$\dot{V}(e) \leq [e^T, \eta^T] Y_Q \begin{bmatrix} e \\ \eta \end{bmatrix} \tag{15}$$

where

$$Y_Q = \begin{bmatrix} (A-F)^T P + P(A-F) & PB + CT_2K + (A-F)^T C\Lambda KQ + CT_1KQ \\ (PB + CT_2K + (A-F)^T C\Lambda KQ + CT_1KQ)^T & -2QT_1Q + Q(B^T C\Lambda K)^T + (B^T C\Lambda K)Q - 2T_2 \end{bmatrix}$$

$$Q = \text{diag.}[q_i]\,. \tag{16}$$

In consequence $\dot{V}(e)$ will be less than a negative definite time-invariant function if

$$Y_Q < 0 \quad \forall Q \text{ s.t. } 0 \leq Q \leq \hat{Q} \tag{17}$$

where

$$\hat{Q} = \text{diag.}[\hat{q}_i]\,. \tag{18}$$

Note that $\hat{Q}$ is the constant diagonal matrix defined by the upper bounds on $q_i$ hypothesized in Eq. (13). It is therefore uniquely determined by the structure of nonlinearity $f$.

**Lemma 1.** *If $T_1 = 0$ then $Y_Q < 0 \forall Q$ such that $0 \leq Q \leq \hat{Q}$ if and only if $Y_{\tilde{Q}} < 0 \forall \tilde{Q}$ diagonal with ith diagonal term being either 0 or $\hat{q}_i$.*

*Proof.* Necessity is trivial. For sufficiency see Theorem 10.4, Khalil [1992]. The proof relies on the fact that matrix $Y_Q$ is a linear function of the parameters $q_i$. ■

## 3. Lur'e Systems with Single Nonlinearity

Specializing the results of the previous section to the case $r = 1$, one obtains

$$Y_q = \begin{bmatrix} (A-F)^T P + P(A-F) & Pb + (\tau + \beta q)kc + q\gamma k(A-F)^T c \\ (Pb + (\tau + \beta q)kc + q\gamma k(A-F)^T c)^T & -2(\beta q^2 - (c^T b)\gamma kq + \tau) \end{bmatrix} \tag{19}$$

where the substitutions

$$\begin{aligned} B \to b, \quad C \to c, \quad Q \to q, \quad \hat{Q} \to \hat{q} \\ \Lambda \to \gamma, \quad T_1 \to \beta, \quad T_2 \to \tau, \quad K \to k \end{aligned} \tag{20}$$

have been made. Note that $b$ and $c$ are $n \times 1$ vectors and all other newly introduced terms are scalars. The results of the previous section assert that synchronization of the single nonlinearity master-slave Lur'e system will occur if matrices $Y_q$ are negative definite for all $q$ in interval $[0, \hat{q}]$, and that this in turn occurs if and only if matrices $Y_0$ and $Y_{\hat{q}}$ are both negative definite, assuming $\beta = 0$.

**Lemma 2.** *If $\beta = 0$, then there exist non-negative scalars $\tau$ and $\gamma$ such that $Y_0 < 0$ and $Y_{\hat{q}} < 0$ if and only if there exist non-negative definite scalars $\tau$ and $\gamma$ such that $Y_0 < 0$ and $Y_1 < 0$.*

*Proof.* The proof follows readily from the observation that in the case of $\beta = 0$, $Y_{\hat{q}}$ evaluated at $\tau$, $\gamma$ is identical to $Y_1$ evaluated at $\tau$, $\hat{q}\gamma$. ■

**Lemma 3.** *Synchronization of the single nonlinearity master-slave Lur'e system occurs, subject to restrictions (5), (12) and (13) on f, if there exist non-negative parameters $\tau$ and $\gamma$ such that the linear matrix inequality*

$$\begin{bmatrix} (A-F)^T P + P(A-F) & Pb + \tau kc + \gamma k(A-F)^T c \\ (Pb + \tau kc + \gamma k(A-F)^T c)^T & -2\tau + 2(c^T b)\gamma k \end{bmatrix} < 0 \tag{21}$$

*permits a positive definite solution P which satisfies the residual scalar inequality*

$$\det \begin{bmatrix} -[(A-F)^T P + P(A-F)] & -[Pb + \tau kc] \\ -[Pb + \tau kc]^T & 2\tau \end{bmatrix} > 0. \tag{22}$$

*Proof.* From Lemmas 1 and 2 we need only show that the conditions of the present lemma imply that matrices $Y_0$ and $Y_1$ are negative definite for the particular choice of parameter $\beta = 0$. Linear matrix inequality (21) is precisely the condition $Y_1 < 0$. From this inequality it follows that $(A-F)^T + (A-F) < 0$. Hence $Y_0 < 0$ holds if $\det[-Y_0] > 0$, and this is precisely the residual scalar inequality (22). ■

Specializing the results of [Suykens & Vandewalle, 1996] to the case of Lur'e systems containing a single nonlinearity satisfying restrictions (5), (12) and (13), one notes that they address the problem of the synchronization of master-slave system (2) by employing the Lyapunov function

$$V(e) = e^T P e + 2\gamma k \int_0^{c^T e} [f(\rho + c^T y) - f(c^T y)] d\rho \tag{23}$$

to prove global asymptotic stability of error system (4). The dependency of this Lyapunov function on $y$ leads to extra terms in its derivative $\dot{V}(e)$ which are omitted in the earlier paper of Suykens and Vandewalle [1996]. This difficulty notwithstanding, the procedure of Suykens and Vandewalle [1996] for the selection of feedback matrix $F$ to achieve synchronization, succeeds in a number of important cases of Lur'e systems possessing a single nonlinearity. Synchronization occurs, according to [Suykens & Vandewalle, 1996], for any matrix $F$ chosen such that the linear matrix inequality (21) holds for some $P > 0$, $\tau \geq 0$, $\gamma \geq 0$. These conditions comprise $n+1$ of the $n+2$ determinental inequalities of (21) and (22) [obtained by applying Sylvester's conditions for negative definiteness of (21)]. A randomly generated solution $P$, $\tau$, $\gamma$ to the first $n+1$ of these inequalities appears to have a good chance of turning out to be a solution to the residual inequality also. Of course the conditions of [Suykens & Vandewalle, 1996], in effect the condition (21) of Lemma 3, may indeed represent sufficient conditions for synchronization of (2).

## 4. Conclusion

It has been shown how the more general, nonquadratic Lur'e–Postnikov Lyapunov function of absolute stability theory may be employed in the development of synchronization criteria for master-slave coupled Lur'e systems with static, linear feedback. This confirms the proposal of Suykens and Vandewalle [1996] that such Lyapunov functions do indeed have a role to play in the synchronization problem, notwithstanding the time dependence of the error system. The conditions of [Suykens & Vandewalle, 1996] have also been shown to be closely related to sufficient conditions for synchronization if not actually sufficient themselves.

It is clear that one chooses the Lur'e–Postnikov function appropriate to the master system ($\mathcal{M}$). This observation points the way towards the application of more general Lyapunov functions commonly employed in the absolute stability theory of Lur'e systems. The trade involved in the application of such functions is that one must impose tighter restrictions on the nonlinearities of the Lur'e system. The resulting criteria (synchronization criteria in this case) tend to possess more general *multipliers* or *free terms* [Vidyasagar, 1978], and consequently impose much weaker constraints on the linear part of the Lur'e systems. In short the synchronization criteria which emerge will prove synchronization for large classes of master-slave Lur'e systems for which synchronization cannot be proven by means of quadratic Lyapunov functions. In many practical systems (the Chua Oscillator, neural networks) the nonlinearities present satisfy much more stringent conditions than the elementary sector conditions most commonly employed in

the existing literature on synchronization of Lur'e systems. Indeed, the nonlinearities are often of diagonal type, time independent, sector type, monotone and odd [Vidyasagar, 1978]. The Lur'e–Postnikov Lyapunov function is probably the most general function which is *well-known* to be capable of taking account of the first three properties in this list. It is certainly the function of this type for which there exists the most complete theory (although there do exist more general functions of this type [Cao *et al.*, 1997]). In a subsequent note we propose to present an account of the application of functions capable of taking account of all five properties to the problem of synchronization of chaotic Lur'e systems.

## Acknowledgments

This work is supported by the University College Dublin and the Fulbright Fellowship Program. This research was undertaken at the University of California at Berkeley, partially within the framework of the Belgian Programme on Interuniversity Poles of Attraction, initiated by the Belgian State, Prime Minister's Office for Science, Technology and Culture (IUAP-17) and in the framework of a Concerted Action Project MIPS (Modelbased Information Processing Systems) of the Flemish Community. Work was also supported by Office of Naval Research under grant N00014-89-J-1402.

## References

Boyd, S., El Ghaoui, L., Feron, E. & Balakrishnan, V. [1994] *Linear Matrix Inequalities in System and Control theory* (SIAM: Studies in Applied Mathematics), Vol. 15.

Cao, Y. J., Wu, Q. H. & Cheng, S. J. [1997] "An improved Lyapunov function for power system stability analysis," *Int. J. Control*, in press.

Chua, L. O., Wu, C. W., Huang, A. & Zhong, G. Q. [1993] "A universal circuit for studying and generating chaos, part I: Routes to chaos," *IEEE Trans. Circuits Syst. I. Fundamental Theory and Applications* **10**(40), 732–744. Special Issue on Chaos in Electronic Circuits, Part A.

Cuomo, K. M. & Oppenheim, A. V. [1993] "Circuit implementation of synchronized chaos with applications to communications," *Phys. Rev. Lett.* **71**(1), 65–68.

Curran, P. F. & Chua, L. O. [1997] "Absolute stability theory and the synchronization problem," to be published.

Hasler, M. [1994] "Synchronization principles and applications," *Circuits Syst. Tutorials IEEE-ISCAS'94*, 314–326.

Khalil, H. K. [1992] *Nonlinear Systems* (MacMillan, New York).

Kocarev, L., Halle, K. S., Eckert, K., Chua, L. O. & Parlitz, U. [1992] "Experimental demonstration of secure communications via chaotic synchronization," *Int. J. Bifurcation and Chaos* **2**(3), 709–713.

Pecora, L. & Carroll, T. [1991] "Driving systems with chaotic signals," *Phys. Rev.* **A44**, 2374–2383.

Parlitz, U., Chua, L. O., Kocarev, L., Halle, K. S. & Shang, A. [1992] "Transmission of digital signals by chaotic synchronization," *Int. J. Bifurcation and Chaos* **2**(4), 973–977.

Suykens, J. A. K. & Vandewalle, J. [1996] "Master-Slave synchronization of Lur'e systems," *Int. J. Bifurcation and Chaos* **7**(3), 665–669.

Vidyasagar, M. [1978] *Nonlinear Systems Analysis* (Prentice Hall, New Jersey).

Wu, C. W. & Chua, L. O. [1994] "A unified framework for synchronization and control of dynamical systems," *Int. J. Bifurcation and Chaos* **4**(4), 979–998.

## REFERENCES

[1] L. Almeida, "A learning rule for asynchronous perceptrons with feedback in a combinatorial environment," in *Proc. First Int. Conf. Neural Networks*, 1987, pp. 609–618.

[2] K. Narendra and K. Parthasarathy, "Gradient methods for the optimization of dynamical systems containing neural networks," *IEEE Trans. Neural Networks*, vol. 2, pp. 252–262, 1991.

[3] B. Pearlmutter, "Learning state space trajectories in recurrent neural networks," *Neural Comput.*, vol. 1, pp. 263–269, 1989.

[4] F. Pineda, "Generalization of back-propagation to recurrent neural networks," *Phys. Rev. Lett.*, vol. 59, pp. 2229–2232, 1987.

[5] E. Sontag, *Mathematical Control Theory*. New York: Springer-Verlag, 1990.

[6] P. Werbos, "Backpropagation through time: What it does and how to do it," *Proc. IEEE*, vol. 78, pp. 1550–1560, 1990,

[7] R. Williams and D. Zipser, "A learning algorithm for continually running fully recurrent neural networks," *Neural Computat.*, vol. 1, pp. 270–280, 1989.


# Nonlinear $H_\infty$ Synchronization of Lur'e Systems: Dynamic Output Feedback Case

Johan A. K. Suykens, Paul F. Curran, Tao Yang, Joos Vandewalle, and Leon O. Chua

*Abstract*—**In this letter we introduce a new master–slave synchronization scheme for Lur'e systems, which makes use of vector field modulation and dynamic output feedback in order to recover a message signal. The synchronization scheme is represented in standard plant form according to modern control theory. I/O properties of the scheme are analyzed using a dissipativity approach with a quadratic storage function and a supply rate with finite $L_2$-gain. The method avoids transmission of the full state vector. The controller design is based on a matrix inequality, corresponding to nonlinear $H_\infty$ synchronization. The new scheme is illustrated on Chua's circuit.**

*Index Terms*—**Chua's circuit, dissipativity, dynamic output feedback, $L_2$-gain, Lur'e systems, master–slave synchronization, matrix inequality, nonlinear $H_\infty$ control.**

## I. INTRODUCTION

With respect to secure communication using chaotic systems [5], [17], a new method for master–slave synchronization of Lur'e systems has recently been proposed in [13] for recovery of the message signal. The problem has been approached from the viewpoint of control theory, by representing the synchronization scheme in standard plant form. I/O properties are analyzed using a dissipativity approach with a quadratic storage function and a supply rate with finite $L_2$-gain. A full static state feedback controller is designed based on a matrix inequality, which corresponds to nonlinear $H_\infty$ synchronization. Robustness against noise can be taken into account in the design. However the scheme requires the transmission of a number of signals equal to the number of state variables of the Lur'e system.

The aim of this letter is to present a new method for synchronizing the systems when fewer signals than the number of state variables are transmitted, which is an advantage with respect to implementation, particularly when the transmitted signals are voltages. Therefore we will apply a linear *dynamic output feedback* controller instead of a full static state feedback controller. This idea has been introduced in [14] and successfully applied to synchronization of chaotic and hyperchaotic Lur'e systems. While the scheme in [14] corresponds to the autonomous case, in this paper a message signal is introduced as external reference input.

This letter is organized as follows. In Section II we introduce the new synchronization scheme. In Section III we represent the scheme in standard plant form. In Section IV we derive a matrix inequality for dissipativity with finite $L_2$-gain and a quadratic storage function and formulate the corresponding nonlinear $H_\infty$ synchronization problem. In Section V we illustrate the method on Chua's circuit. For additional motivations on the nonlinear $H_\infty$ synchronization scheme we refer to [13].

## II. SYNCHRONIZATION SCHEME

Consider the following master–slave synchronization scheme

$$\begin{aligned}
\mathcal{R}&: \begin{cases} \dot{\mu} = R\mu + Sr \\ d = T\mu + Ur \end{cases} \\
\mathcal{M}&: \begin{cases} \dot{x} = Ax + B\sigma(Cx) + Dd \\ p = Hx \end{cases} \\
\mathcal{S}&: \begin{cases} \dot{z} = Az + B\sigma(Cz) + Fu \\ q = Hz \end{cases} \\
\mathcal{C}&: \begin{cases} \dot{\rho} = E\rho + G(p + \epsilon - q) \\ u = M\rho + N(p + \epsilon - q) \end{cases}
\end{aligned} \tag{1}$$

with master system $\mathcal{M}$, slave system $\mathcal{S}$, linear filter $\mathcal{R}$ and linear dynamic output feedback controller $\mathcal{C}$. The subsystems have state vectors $x, z \in R^n$, $\mu \in R^{n_r}$, $\rho \in R^{n_c}$ and output vectors $p, q \in R^l$, $u \in R^m$, $d \in R$, where $l, m \leq n$. The message signal is $r \in R$ and $\epsilon \in R^l$ is a disturbance input. At the transmitter $\mathcal{M}$, a linear transformation $H \in R^{l \times n}$ is applied to the state $x$. The resulting vector $p$ is transmitted along the channel. At the receiver $\mathcal{S}$, linear dynamic output feedback is applied by taking the difference between $p$ and $q$ as input to the controller with system matrices $E \in R^{n_c \times n_c}$, $G \in R^{n_c \times l}$, $M \in R^{m \times n_c}$, $N \in R^{m \times l}$. The transmitted signal $p$ is corrupted by the signal $\epsilon$. The identical master–slave Lur'e systems have system matrices $A \in R^{n \times n}$, $B \in R^{n \times n_h}$ and $C \in R^{n_h \times n}$ where $n_h$ corresponds to the number of hidden units (if one interprets the Lur'e system [8] as a class of recurrent neural networks [12]). The diagonal nonlinearity $\sigma(\cdot) : R^{n_h} \mapsto R^{n_h}$ is assumed to belong to sector $[0, k]$ (typically a linear characteristic with saturation or $\tanh(\cdot)$). At the master system the vector field is modulated by means of the term $Dd$. One has to ensure that the norm of this term is "small" compared to the norm of the other terms in the system dynamics. The low pass filter $\mathcal{R}$ has system matrices $R \in R^{n_r \times n_r}$, $S \in R^{n_r \times 1}$, $T \in R^{1 \times n_r}$, $U \in R$.

Manuscript received November 18, 1996; revised February 10, 1997. This work was supported in part by the Office of Naval Research under Grant N00014-96-1-0753 and the Fulbright Fellowship Program. This paper was recommended by Associate Editor U. Helmke.

J. A. K. Suykens and J. Vandewalle is with the Department of Electrical Engineering, Katholieke Universiteit Leuven, ESAT-SISTA, Kardinaal Mercierlaan 94, B-3001 Leuven (Heverlee), Belgium (e-mail: johan.suykens@esat.kuleuven.ac.be; joos.vandewalle@esat.kuleuven.ac.be).

P. F. Curran is with the Electronic and Electrical Engineering Department, University College, Belfield, Dublin 4, Ireland (e-mail: pcurran@acadamh.ucd.ie).

T. Yang and L. O. Chua are with the Department of Electrical Engineering and Computer Sciences, University of California, Berkeley, CA 94720 USA (e-mail: taoyang@fred.eecs.berkeley.edu; chua@fred.eecs.berkeley.edu).

Publisher Item Identifier S 1057-7122(97)06632-4.

1057–7122/97$10.00 © 1997 IEEE

$$\begin{cases} \begin{bmatrix} \dot{e} \\ \dot{\rho} \\ \dot{\mu} \end{bmatrix} = \begin{bmatrix} A - FNH & -FM & DT \\ GH & E & 0 \\ 0 & 0 & R \end{bmatrix} \begin{bmatrix} e \\ \rho \\ \mu \end{bmatrix} + \begin{bmatrix} B \\ 0 \\ 0 \end{bmatrix} \eta(Ce;z) + \begin{bmatrix} DU & -FN \\ 0 & G \\ S & 0 \end{bmatrix} \begin{bmatrix} r \\ \epsilon \end{bmatrix} \\ \nu = \begin{bmatrix} -\beta^T & 0 & T \end{bmatrix} \begin{bmatrix} e \\ \rho \\ \mu \end{bmatrix} + \begin{bmatrix} U & 0 \end{bmatrix} \begin{bmatrix} r \\ \epsilon \end{bmatrix}. \end{cases} \tag{2}$$

## III. Standard Plant Representation

According to [13], by defining the signal $e = x - z$ and the tracking error $\nu = d - \beta^T e$, where $\beta = [1; 0; 0; \cdots; 0]$ selects the first component of $e$, one obtains the following standard plant representation for the synchronization scheme: (see (2) at the top of the next page). This scheme has state vector $\xi = [e; \rho; \mu]$, exogenous input $w = [r; \epsilon]$ and regulated output $\nu$. The nonlinearity $\eta$ is given by $\eta(Ce;z) = \sigma(Ce + Cz) - \sigma(Cz)$.

## IV. Dissipativity with Finite $L_2$-Gain and Nonlinear $H_\infty$ Synchronization

In order to analyze I/O properties of the synchronization scheme in standard plant form (2), we consider a quadratic storage function [6], [7], [16]

$$\phi(\xi) = \xi^T P \xi = [e^T \quad \rho^T \quad \mu^T] \begin{bmatrix} P_{11} & P_{12} & P_{13} \\ P_{21} & P_{22} & P_{23} \\ P_{31} & P_{32} & P_{33} \end{bmatrix} \begin{bmatrix} e \\ \rho \\ \mu \end{bmatrix} \tag{3}$$

$$P = P^T > 0$$

and a supply rate with finite $L_2$-gain $s(r, \epsilon, \nu) = \gamma^2 (r^T r + \alpha^2 \epsilon^T \epsilon) - \nu^T \nu$, where $\alpha$ is a positive real constant. The system (2) is said to be dissipative [6], [7], [16] with respect to supply rate and the storage function if $\dot{\phi} \leq s(r, \epsilon, \nu)$, $\forall r, \epsilon, \nu$. Assume that the nonlinearity $\eta(Ce;z)$ belongs to sector $[0, k]$ [3]: $0 \leq \frac{\eta_i(c_i^T e; z)}{c_i^T e} = \frac{\sigma_i(c_i^T e + c_i^T z) - \sigma(c_i^T z)}{c_i^T e} \leq k, \forall e, z; \ (i = 1, \cdots, n_h; \ c_i^T e \neq 0)$. The inequality $\eta_i(c_i^T e; z)\,[\eta_i(c_i^T e; z) - k c_i^T e] \leq 0, \forall e, z; (i = 1, \cdots, n_h)$ holds then [8]. It follows from the mean value theorem that for differentiable $\sigma(\cdot)$ the sector $[0, k]$ condition on $\eta(\cdot)$ corresponds to $0 \leq \frac{d}{d\varphi}\sigma_i(\varphi) \leq k, \ \forall \varphi \ (i = 1, \cdots, n_h)$ [3].

*Observation:* Let $\Lambda = \mathrm{diag}\{\lambda_i\}$ be a diagonal matrix with $\lambda_i \geq 0$ for $i = 1, \cdots, n_h$. Then a sufficient condition for dissipativity of the synchronization scheme (2) with respect to the quadratic storage function (3) and the supply rate $s(r, \epsilon, \nu) = \gamma^2 (r^T r + \alpha^2 \epsilon^T \epsilon) - \nu^T \nu$ with finite $L_2$-gain $\gamma$ is given by the matrix inequality:

$$Z = Z^T = \begin{bmatrix} Z_{11} & Z_{12} & Z_{13} & Z_{14} & Z_{15} & Z_{16} \\ \cdot & Z_{22} & Z_{23} & Z_{24} & Z_{25} & Z_{26} \\ \cdot & \cdot & Z_{33} & Z_{34} & Z_{35} & Z_{36} \\ \cdot & \cdot & \cdot & Z_{44} & 0 & 0 \\ \cdot & \cdot & \cdot & \cdot & Z_{55} & 0 \\ \cdot & \cdot & \cdot & \cdot & \cdot & Z_{66} \end{bmatrix} < 0 \tag{4}$$

with

$$\begin{aligned} Z_{11} &= (A - FNH)^T P_{11} + P_{11}(A - FNH) \\ &\quad + H^T G^T P_{21} + P_{12} G H + \beta \beta^T \\ Z_{12} &= (A - FNH)^T P_{12} + H^T G^T P_{22} - P_{11} F M + P_{12} E \\ Z_{13} &= (A - FNH)^T P_{13} + H^T G^T P_{23} \\ &\quad + P_{11} D T + P_{13} R - \beta T \\ Z_{14} &= P_{11} B + k C^T \Lambda \\ Z_{15} &= P_{11} D U + P_{13} S - \beta U \\ Z_{16} &= P_{12} G - P_{11} F N \\ Z_{22} &= E^T P_{22} + P_{22} E - M^T F^T P_{12} - P_{21} F M \\ Z_{23} &= E^T P_{23} - M^T F^T P_{13} + P_{21} D T + P_{23} R \\ Z_{24} &= P_{21} B \\ Z_{25} &= P_{21} D U + P_{23} S \\ Z_{26} &= P_{22} G - P_{21} F N \\ Z_{33} &= R^T P_{33} + P_{33} R + T^T D^T P_{13} + P_{31} D T + T^T T \\ Z_{34} &= P_{31} B \\ Z_{35} &= P_{31} D U + P_{33} S + T^T U \\ Z_{36} &= P_{32} G - P_{31} F N \\ Z_{44} &= -2\Lambda \\ Z_{55} &= -\gamma^2 I + U^T U \\ Z_{66} &= -\alpha^2 \gamma^2 I. \end{aligned}$$

*Proof:* One checks the condition $\dot{\phi} - s \leq 0$ and applies the $\mathcal{S}$-procedure [1] using the sector condition on $\eta$, which gives $\dot{\phi} - s \leq \dot{\xi}^T P \xi + \xi^T P \dot{\xi} - 2\eta^T \Lambda (\eta - kCe) - s = \zeta^T Z \zeta < 0$. The quadratic form $\zeta^T Z \zeta$ is negative for all nonzero $\zeta = [e; \rho; \mu; \eta; r; \epsilon]$, provided $Z$ is negative definite. □

According to [13], the nonlinear $H_\infty$ synchronization problem seeks to find the linear dynamic output feedback controller $\mathcal{C}$ which minimizes the $L_2$-gain $\gamma$ [15] with respect to the matrix inequality (4):

$$\min_{E,G,M,N,P,\Lambda,\gamma} \gamma \quad \text{such that} \quad Z(E, G, M, N, P, \Lambda, \gamma) < 0. \tag{5}$$

According to [13] we will consider binary valued continuous time reference inputs. For this class of signals perfect recovery of the message signal is obtained by implementing the operation $\mathrm{sign}(\beta^T e)$ [13]. The advantage with respect to the method described in [13] for secure communication applications is that the design based on (4) allows nonlinear $H_\infty$ synchronization with transmission of one single signal.

## V. Example: Chua's Circuit

For Chua's circuit [2], [9] we take the Lur'e representation $\dot{x} = Ax + B\varphi(Cx)$ [13] with

$$A = \begin{bmatrix} -2.5714 & 9 & 0 \\ 1 & -1 & 1 \\ 0 & -14.2860 & 0 \end{bmatrix}, \quad B = \begin{bmatrix} 3.8571 \\ 0 \\ 0 \end{bmatrix}, \quad C = [1 \quad 0 \quad 0] \tag{6}$$

and $\varphi(x_1) = \frac{1}{2}(|x_1 + 1| - |x_1 - 1|)$ a linear characteristic with saturation that belongs to sector $[0, 1]$. Possible keys for cryptographical purposes are the parameters of Chua's circuit and the matrix $H$, which linearly combines the state variables. The key scheme is different from previous work in [18]. In [18] a second state variable and the parameter set are used as keys. Here the usage of the linear transformation is twofold. First, it is well-known that a mixture

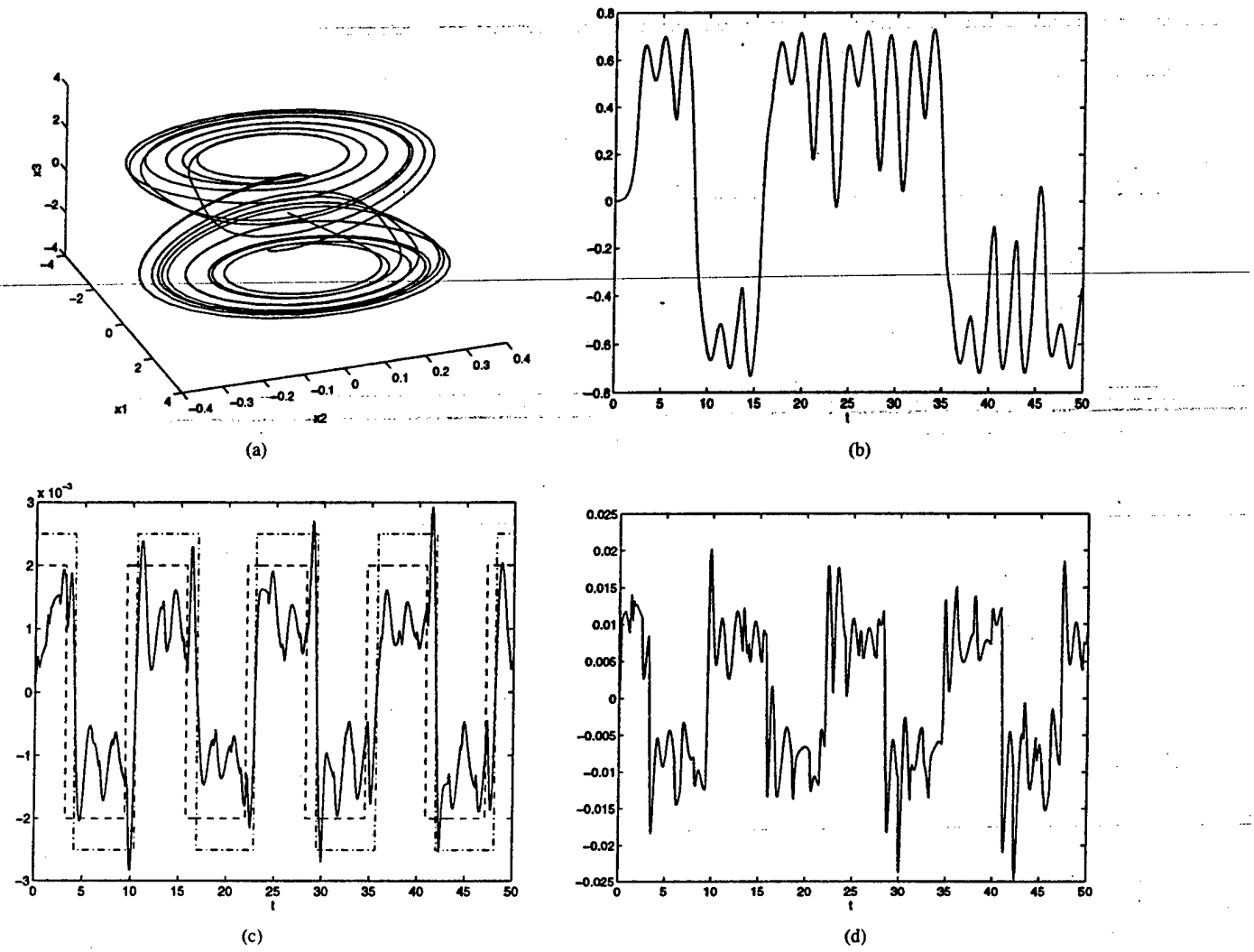


Fig. 1. Nonlinear $H_\infty$ synchronization of Chua's circuit using linear dynamic output feedback: (a) Double scroll attractor generated at the master system.The vector field of the master system is modulated by means of the linearly filtered message signal sign(cos(0.5t)). (b) Transmitted signal, which is a linear combination of the state variables of the master Chua's circuit. The message signal is invisible on this transmitted signal. (c) $\beta^T e$ (-), reference input sign(cos(0.5t)) (- -), recovered message sign($\beta^T e$) (--). (d) control signal $u(t)$, applied to the slave system.

of more than one chaotic signal can provide a higher security to overcome the identification based attack as presented in [10], [11] and the characteristics based attack as presented in [19]. Second, the key $H$ could be changed in order to avoid usage of the same key for a long time period. The security of the system is thereby improved.

In this example we take one-dimensional outputs $p, q$ ($l = 1$) with $H = [0.5; -0.5; 0.1]$ and a one-dimensional control signal $u$ ($m = 1$) with $F = [1:0:0]$. Furthermore $D = \beta = [1;0;0]$. For $\mathcal{R}$ a first order Butterworth filter is chosen with cut-off frequency 10 Hz. The nonlinear $H_\infty$ synchronization problem (5) was solved by means of sequential quadratic programming [4] (*constr* in Matlab). The positive definite matrix $P$ has been parameterized as $P = Q^T Q$ and

$$\min_{E,G,M,N,Q,\Lambda,\gamma} \gamma \quad \text{such that}$$
$$\lambda_{\max}[Z(E,G,M,N,Q,\Lambda,\gamma)] + \delta < 0 \qquad (7)$$

with $\delta = 0.01$ has been solved instead. In the supply rate $\alpha = 10$ is taken. We report the results here for a third order SISO controller. As starting point for the nonlinear optimization, random matrices were chosen for the controller according to a normal distribution with zero mean and standard variation 0.1, $Q = I_{n+n_c+n_r}$, $\Lambda = 0.1 I_{n_h}$, $\gamma = 100$. Suboptimal solutions to the nonconvex optimization problem yield satisfactory results. Fig. 1 shows simulation results obtained with this controller for a reference input $r = \text{sign}(\cos(0.5t))$. The message signal is invisible on the transmitted signal. The original message is recovered by taking sign($\beta^T e$). Simulations with zero mean white Gaussian noise for $\epsilon$ show that a standard deviation up to $1e{-}04$ for the noise is allowed in order to maintain perfect recovery. The robustness can be considerably improved by taking a smaller value for $\alpha$ in the supply rate. For $\alpha = 2$ a standard deviation of 0.1 is allowed for the noise.

## VI. Conclusion

In this letter a new method for master–slave synchronization of Lur'e systems has been introduced. It combines two recently introduced ideas, nonlinear $H_\infty$ synchronization [13] and synchronization by means of dynamic output feedback [14], in order to recover a class of message signals.

## Acknowledgment

This research was conducted at the University of California, Berkeley, in the framework of the Belgian Programme on Interuniversity Poles of Attraction, initiated by the Belgian State, Prime

Minister's Office for Science, Technology and Culture (IUAP-17) and in the framework of a Concerted Action Project MIPS (Modelbased Information Processing Systems) of the Flemish Community.

## REFERENCES


[1] S. Boyd, L. El Ghaoui, E. Feron, and V. Balakrishnan, *Linear Matrix Inequalities in System and Control Theory*, SIAM (Studies in Appl. Math.), vol. 15, 1994.

[2] L. O. Chua, "Global unfolding of Chua's circuit," *IEICE Trans. Fundament.*, vol. E76-A, no. 5, pp. 704–734, 1993.

[3] P. F. Curran and L. O. Chua, "Absolute stability theory and the synchronization problem," *Int. J. Bifurc. Chaos*, 1997, to be published.

[4] R. Fletcher, *Practical Methods of Optimization*. Chichester, U.K.: Wiley, 1987.

[5] M. Hasler, "Synchronization principles and applications," in *Circuits Syst. Tutorials IEEE-ISCAS'94*, pp. 314–326.

[6] D. J. Hill and P. J. Moylan, "The stability of nonlinear dissipative systems," *IEEE Trans. Automat. Contr.*, vol. AC-21, pp. 708–711, 1976.

[7] ——, "Connections between finite-gain and asymptotic stability," *IEEE Trans. Automat. Contr.*, vol. AC-25, pp. 931–936, 1980.

[8] H. K. Khalil, *Nonlinear Systems*. New York: Macmillan, 1992.

[9] R. N. Madan, Guest Ed., *Chua's Circuit: A Paradigm for Chaos*. Signapore: World Scientific, 1993.

[10] K. M. Short, "Steps toward unmasking secure communications," *Int. J. Bifurc. Chaos*, vol. 4, no. 4, pp. 957–977, 1994.

[11] ——, "Unmasking a modulated chaotic communications scheme," *Int. J. Bifurc. Chaos*, vol. 6, no. 2, pp. 367–375, 1996.

[12] J. A. K. Suykens, J. P. L. Vandewalle, and B. L. R. De Moor, *Artificial Neural Networks for Modeling and Control of Non-Linear Systems*. Boston, MA: Kluwer Academic, 1996.

[13] J. A. K. Suykens, J. Vandewalle, and L. O. Chua, "Nonlinear $H_\infty$ synchronization of chaotic Lur'e systems," *Int. J. Bifurc. Chaos*, vol. 7, no. 6, 1997.

[14] J. A. K. Suykens, P. F. Curran, and L. O. Chua, "Master-slave synchronization using dynamic output feedback," *Int. J. Bifurc. Chaos*, vol. 7, no. 3, pp. 671–679, 1997.

[15] A. van der Schaft, *$L_2$-Gain and Passivity Techniques in Nonlinear Control* (Lecture Notes in Control and Information Sciences 218.) New York: Springer-Verlag, 1996.

[16] J. C. Willems, "Dissipative dynamical systems I: General theory. II: Linear systems with quadratic supply rates," *Archive for Rational Mechan. Anal.*, vol. 45, pp. 321–343, 1972.

[17] C. W. Wu and L. O. Chua, "A unified framework for synchronization and control of dynamical systems," *Int. J. Bifurc. Chaos*, vol. 4, no. 4, pp. 979–989, 1994.

[18] T. Yang, C. W. Wu, and L. O. Chua, "Cryptography based on chaotic systems," *IEEE Trans. Circuits Syst. I*, vol. 44, no. 5, pp. 469–472, May 1997.

[19] T. Yang, "Recovery of digital signal from chaotic switching," *Int. J. Circuit Theory Applicat.*, vol. 33, no. 6, pp. 611–615, 1995.


# A New Sufficient Condition for Nonsymmetric CNN's to Have a Stable Equilibrium Point

Norikazu Takahashi and Leon O. Chua

***Abstract*—This letter gives a new sufficient condition for nonsymmetric CNN's to have at least one stable equilibrium point. Existence of a stable equilibrium point is important for nonsymmetric CNN's because it is a necessary condition for complete stability. It is shown that our sufficient condition is a generalization of a previous result concerning the existence of a stable equilibrium point, and that it can easily be applied to space-invariant CNN's with a 3 × 3 neighborhood.**

***Index Terms*—Cellular neural networks, complete stability, stable equilibrium points.**

## I. INTRODUCTION

A cellular neural network (CNN) is a dynamic nonlinear circuit which has many applications in the field of image processing [3]. For proper operation in such applications a CNN must be completely stable in the sense that every trajectory tends to an equilibrium point. For symmetric CNN's it was proved in [2] and [13] that they are completely stable. On the other hand, for nonsymmetric CNN's only a few sufficient conditions for complete stability were given so far [4]–[6] in spite of the existence of some useful nonsymmetric feedback templates, such as the connected component detector [11].

The existence of a stable equilibrium point is an important criterion for complete stability because in order for nonsymmetric CNN's to be completely stable there must be at least one stable equilibrium point. Some sufficient conditions for the existence of a stable equilibrium point were given so far [1], [7], [8]. In [7] a sufficient condition for a two-dimensional infinite CNN to have at least one of four equilibrium configurations was given. In [8] the necessary and sufficient condition for a CNN to have equilibrium points in every region was given.

In this letter, we first give a new sufficient condition for nonsymmetric CNN's to have at least one stable equilibrium point. It is remarkable that our sufficient condition does not depend on the value of the constant input vector. Secondly, we show that our sufficient condition is a generalization of that given in [1]. Finally we apply it to the feedback template of space-invariant CNN's with a 3 × 3 neighborhood.

## II. MAIN RESULTS

We deal with CNN's which can be defined by the following state equation:

$$\dot{x} = -x + Ay(x) + u \tag{1}$$

where $x = [x_1, x_2, \cdots, x_n]^T$ is the state vector, $A = [a_{ij}]$ is an $n \times n$ real matrix of which all diagonal elements are greater than 1, $u = [u_1, u_2, \cdots, u_n]^T$ is a constant input vector

Manuscript received December 9, 1996. This work was supported by Grant-In-Aid from Kyushu Industrial Technology Center. This paper was recommended by Associate Editor J. Pineda de Gyvez.

N. Takahashi is with the Electronics Research Laboratory, Department of Electrical Engineering and Computer Sciences, University of California, Berkeley, CA 94720 USA on leave from the Department of Computer Science and Communication Engineering, Kyushu University, Fukuoka 812 Japan.

L. O. Chua is with the Electronics Research Laboratory, Department of Electrical Engineering and Computer Sciences, University of California, Berkeley, CA 94720 USA.

Publisher Item Identifier S 1057-7122(97)06577-X.

1057–7122/97$10.00 © 1997 IEEE

# Robust Nonlinear $H_\infty$ Synchronization of Chaotic Lur'e Systems

Johan A. K. Suykens, Paul F. Curran, *Member, IEEE*, Joos Vandewalle, *Fellow, IEEE*, and Leon O. Chua, *Fellow, IEEE*

***Abstract*— In this paper, we propose a method of robust nonlinear $H_\infty$ master–slave synchronization for chaotic Lur'e systems with applications to secure communication. The scheme makes use of vector field modulation and either full static state or linear dynamic output error feedback control. The master–slave systems are assumed to be nonidentical and channel noise is taken into account. Binary valued continuous time message signals are recovered by minimizing the $L_2$-gain from the exogenous input to the tracking error for the standard plant representation of the scheme. The exogenous input takes into account the message signal, channel noise and parameter mismatch. Matrix inequality conditions for dissipativity with finite $L_2$-gain of the standard plant form are derived based on a quadratic storage function. The controllers are designed by solving a nonlinear optimization problem which takes into account both channel noise and parameter mismatch. The method is illustrated on Chua's circuit.**

***Index Terms*—Chua's circuit, Lur'e systems, matrix inequalities, parametric uncertainty, synchronization.**

## I. Introduction

SECURE communication [3], [11] is an important field for the application of synchronization theory. The link between absolute stability theory and synchronization of nonlinear systems has been investigated in a series of papers [7], [8], [24], [33], in particular for Lur'e systems and master–slave synchronization schemes. From a control theoretic point of view, this corresponds to the autonomous case without an external input (or message signal). Among the methods that consider a message signal in the synchronization scheme, one basically makes a distinction between chaotic masking and vector field modulation (see Kennedy in [3]). With respect to vector field modulation, we have proposed a new method of nonlinear $H_\infty$ synchronization [25], [26] which applies to binary valued continuous time message signals. The synchronization schemes are interpreted within the framework of modern control theory by taking standard plant representations. A new notion of synchronization error has been introduced which is based on the tracking error of the scheme. The aim of the nonlinear $H_\infty$ synchronization scheme is to minimize the influence of the exogenous input on the regulated output. The exogenous input contains the message signal and channel noise. The design has been based on matrix inequalities which follow from conditions of dissipativity with finite $L_2$-gain of the synchronization scheme. Dissipativity of nonlinear systems is a well-known and fundamental system theoretical concept which dates back to the work of Willems and Hill and Moylan [12], [13], [32]. A difference between the method proposed in [25], [26] and methods of nonlinear $H_\infty$ control theory such as [14], [30] is that in the former a quadratic storage function is chosen, while in the latter a general continuously differentiable nonlinear storage function is employed. In this way, matrix inequalities are obtained instead of a Hamilton–Jacobi inequality. The design of the controller has been achieved by solving a nonlinear optimization problem based on the matrix inequalities.

This previous work [25], [26] can be considered as a first step toward a *robust* synchronization theory. In this paper, we treat the problem of *parameter mismatch*, in addition to the problem of channel noise and take both into account in the controller design (adaptive control approaches to cope with parameter mismatch have been investigated, e.g., in [34]). We discuss the case of full static state error feedback and linear dynamic output error feedback. For identical master–slave systems this has been studied in [25], [26]. The class of nonlinear systems considered is in Lur'e form [16], [31]. Many systems of common interest such as Chua's circuit [4], [5], generalized Chua's circuits [28], arrays of such cells or cellular neural networks [6], [10], [15], [29] can be represented in Lur'e form. Chaotic or hyperchaotic behavior is obtained from these systems for the double scroll, $n$-scrolls, double-double scroll, and $n$-double scroll hypercube. For the autonomous case, i.e., without a message signal, parameter mismatch between the Lur'e systems has been investigated in [27]. One unexpected result of that study is that it is possible to allow a large parameter mismatch such that the systems remain master–slave synchronized up to a relatively small error. It has been illustrated on Chua's circuit in [27] that

Manuscript received January 15, 1997; revised May 27, 1997. This work was supported in part by the Office of Naval Research under Grant N00014-96-1-0753 and the Fulbright Fellowship Program. This paper was recommended by Guest Editor M. P. Kennedy.

J. A. K. Suykens and J. Vandewalle are with the Department of Electrical Engineering, ESAT-SISTA, Katholieke Universiteit Leuven, B-3001 Leuven (Heverlee), Belgium (e-mail: johan.suykens@esat.kuleuven.ac.be; joos.vandewalle@esat.kuleuven.ac.be).

P. F. Curran is with the Department of Electronic and Electrical Engineering, University College, Belfield, Dublin 4, Ireland (e-mail: pcurran@acadamh.ucd.ie).

L. O. Chua is with the Department of Electrical Engineering and Computer Sciences, University of California, Berkeley, CA 94720 USA (e-mail: chua@fred.eecs.berkeley.edu).

Publisher Item Identifier S 1057-7122(97)07329-7.

1057–7122/97$10.00 © 1997 IEEE

the chaotic slave system can be synchronized in this sense to a master system which behaves chaotically, shows limit cycle behavior or shows stable equilibrium behavior. Another example along this direction has been presented in [18], where full state error feedback has been used to synchronize two systems which are different (such as Chua's circuit and the Lorenz attractor). In this paper, we extend the ideas from the autonomous case to the case where there exists an external input. From the example of Chua's circuit it will follow that the allowed parameter mismatch is much smaller than for the autonomous case. By using a single transmission signal, the dynamic output feedback case leads to a simpler implementation of the synchronization than the full static state feedback scheme, but the latter has higher performance and a better flexibility for defining keys in a cryptographical scheme [25], [26].

This paper is organized as follows. In Section II, we present master–slave synchronization schemes with full static state error feedback and linear dynamic output error feedback. In Section III, we approach the synchronization problem from the viewpoint of modern control theory, by deriving standard plant representations. We take into account parameter mismatch between the Lur'e systems. In Section IV, we derive Theorems for dissipativity with finite $L_2$-gain of the synchronization schemes, these conditions being expressed as matrix inequalities. In Section V, we formulate the robust nonlinear $H_\infty$ synchronization problem, based on the Theorems of Section IV. In Section VI, we present an example on Chua's circuit. Both static state and dynamic output feedback are applied and a comparison is made. Channel noise and parameter mismatch are taken into account in the design.

## II. Synchronization Scheme

In this section, we consider the master–slave synchronization schemes with vector field modulation proposed in [25] and [26], but with parameter mismatch between the systems.

### A. Full Static State Error Feedback

Consider the master–slave synchronization scheme with full static state error feedback for nonidentical master–slave Lur'e systems:

$$\begin{aligned}
\mathcal{R}&: \begin{cases} \dot{\mu} = R\mu + Sr \\ d = T\mu + Ur \end{cases} \\
\mathcal{M}_s&: \begin{cases} \dot{x} = A_1 x + B_1 \sigma(C_1 x) + Dd \\ p = H_s x \end{cases} \\
\mathcal{S}_s&: \begin{cases} \dot{z} = A_2 z + B_2 \sigma(C_2 z) + u_s \\ q = H_s z \end{cases} \\
\mathcal{C}_s&: u_s = F(p + \epsilon - q)
\end{aligned} \tag{1}$$

with master system $\mathcal{M}_s$, slave system $\mathcal{S}_s$, full static state error feedback controller $\mathcal{C}_s$, and linear filter $\mathcal{R}$ (Fig. 1). The index $s$ refers to the *static* feedback case. The subsystems have state vectors $x, z \in \mathbb{R}^n$, $\mu \in \mathbb{R}^{n_r}$ and output vectors $p, q \in \mathbb{R}^n$, $u_s \in \mathbb{R}^n$, $d \in \mathbb{R}$. The message signal is $r \in \mathbb{R}$. At the transmitter $\mathcal{M}_s$, a linear transformation $H_s \in \mathbb{R}^{n\times n}$ is applied to the state vector $x$. The resulting vector $p$ is sent along the channel and is corrupted by the disturbance signal or channel noise $\epsilon \in \mathbb{R}^n$. At the receiver, full static state error feedback between the output $q$ of $\mathcal{S}_s$ and $p$ is applied with feedback matrix $F \in \mathbb{R}^{n\times n}$. The nonidentical master–slave Lur'e systems have system matrices $A_1, A_2 \in \mathbb{R}^{n\times n}$, $B_1, B_2 \in \mathbb{R}^{n\times n_h}$, and $C_1, C_2 \in \mathbb{R}^{n_h\times n}$, where $n_h$ corresponds to the number of hidden units (if one interprets the Lur'e system as a class of recurrent neural networks [16], [23], [31]). The diagonal nonlinearity $\sigma(.)$: $\mathbb{R}^{n_h} \mapsto \mathbb{R}^{n_h}$ is assumed to belong to sector $[0, k]$ [16], [31]. At the master system the vector field is modulated by means of the term $Dd$ with $D \in \mathbb{R}^{n\times 1}$. We choose message signals $r$ which satisfy $\|r\|_\infty = \sup_{t\geq 0} |r(t)| \leq 1$ and are binary valued. As a typical test signal for the synchronization scheme, signals of the form sign $(\cos \omega t)$ will be employed. When taking a chaotic Lur'e system, the norm of $D$ is chosen "small" (compared to the norm of the other terms in the system dynamics) in order to hide the message signal in the strange attractor. Furthermore, we assume that the master system possesses an initial state such that it is input to state stable for the considered class of message signals (see Assumption 2 in the sequel). The low pass filter $\mathcal{R}$ has system matrices $R \in \mathbb{R}^{n_r\times n_r}$, $S \in \mathbb{R}^{n_r\times 1}$, $T \in \mathbb{R}^{1\times n_r}$, $U \in \mathbb{R}$. In the synchronization scheme, the original message will be recovered from one of the components of the signal $p - q$.

### B. Dynamic Output Error Feedback

Consider now the master–slave synchronization scheme with dynamic output error feedback and nonidentical master–slave Lur'e systems:

$$\begin{aligned}
\mathcal{R}&: \begin{cases} \dot{\mu} = R\mu + Sr \\ d = T\mu + Ur \end{cases} \\
\mathcal{M}_d&: \begin{cases} \dot{x} = A_1 x + B_1 \sigma(C_1 x) + Dd \\ p = H_d x \end{cases} \\
\mathcal{S}_d&: \begin{cases} \dot{z} = A_2 z + B_2 \sigma(C_2 z) + F u_d \\ q = H_d z \end{cases} \\
\mathcal{C}_d&: \begin{cases} \dot{\rho} = E\rho + G(p + \epsilon - q) \\ u_d = M\rho + N(p + \epsilon - q) \end{cases}
\end{aligned} \tag{2}$$

with master system $\mathcal{M}_d$, slave system $\mathcal{S}_d$, linear dynamic output feedback controller $\mathcal{C}_d$, and linear filter $\mathcal{R}$ (Fig. 1). The index $d$ refers to the *dynamic* feedback case. The subsystems have state vectors $x, z \in \mathbb{R}^n$, $\mu \in \mathbb{R}^{n_r}$, $\rho \in \mathbb{R}^{n_c}$, and output vectors $p, q \in \mathbb{R}^l$, $u_d \in \mathbb{R}^m$, $d \in \mathbb{R}$, where $l, m \leq n$. The message signal is $r \in \mathbb{R}$ and $\epsilon \in \mathbb{R}^l$ is a disturbance input. At the transmitter $\mathcal{M}_d$, a linear transformation $H_d \in \mathbb{R}^{l\times n}$ is applied to the state vector $x$. The resulting vector $p$ is transmitted along the channel. At the receiver $\mathcal{S}_d$, linear dynamic output error feedback is applied by taking the difference between $p$ and $q$ as input to the

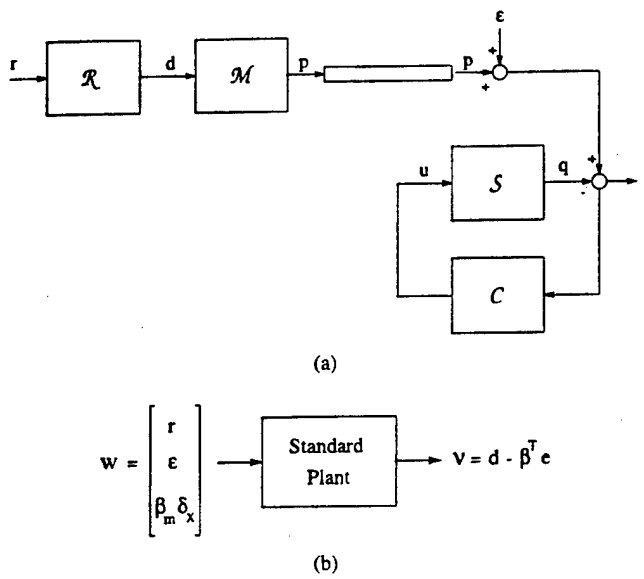


Fig. 1. (a) Synchronization scheme with master system $\mathcal{M}$ and slave system $\mathcal{S}$. Vector field modulation is applied to $\mathcal{M}$ by means of the signal $d$, which is the output of the low pass filter $\mathcal{R}$ with as input the message signal $r$. For $\mathcal{M}$ and $\mathcal{S}$ we consider Lur'e systems with parameter mismatch between the systems. The outputs of $\mathcal{M}$ and $\mathcal{S}$ are $p$ and $q$, which are linear transformations of the state variables $x$ and $z$, respectively. The signal $p$ is sent along the channel and is corrupted by means of the signal $\epsilon$. A binary valued continuous time message signal is considered which is recovered by defining a tracking error for the overall system and applying a controller $\mathcal{C}$ to the slave system. We consider the cases of full static state error feedback and linear dynamic output feedback for this controller, leading to the schemes $\{\mathcal{R}, \mathcal{M}_s, \mathcal{S}_s, \mathcal{C}_s\}$ and $\{\mathcal{R}, \mathcal{M}_d, \mathcal{S}_d, \mathcal{C}_d\}$, respectively. (b) Control theoretic interpretation of the synchronization scheme by means of its standard plant representation with exogenous input $w$ and regulated output $\nu$. The aim of *robust nonlinear* $H_\infty$ *synchronization* is to minimize the influence from the exogenous input on the regulated output. The exogenous input contains the message signal, the disturbance signal $\epsilon$ and the parameter $\beta_m \delta_x$ related to the parameter mismatch between the master–slave systems.

controller with system matrices $E \in \mathbb{R}^{n_c \times n_c}$, $G \in \mathbb{R}^{n_c \times l}$, $M \in \mathbb{R}^{m \times n_c}$, $N \in \mathbb{R}^{m \times l}$. Furthermore, $F \in \mathbb{R}^{n \times m}$. The transmitted signal $p$ is corrupted by the signal $\epsilon$. The system matrices of the master–slave Lur'e systems, the nonlinearity $\sigma(.)$, the vector field modulation and the low-pass filter $\mathcal{R}$ are the same as for the scheme (1). The same class of message signals is considered as in the state feedback case, but will be recovered from one of the components of the signal $x - z$.

## III. Standard Plant Representations

In this section, we derive standard plant representations for the synchronization schemes (1) and (2), taking into account the parameter mismatch between the master–slave systems.

### A. Full Static State Error Feedback

Defining $e_s = p - q$ and denoting the state equation of synchronization scheme (1) as

$$\begin{cases} \dot{x} = f_s(x, \mu, r) \\ \dot{z} = g_s(z, x, \epsilon) \end{cases} \tag{3}$$

with continuous nonlinear mappings $f_s(.,.,.)$: $\mathbb{R}^n \times \mathbb{R}^{n_r} \times \mathbb{R} \mapsto \mathbb{R}^n$ and $g_s(.,.,.)$: $\mathbb{R}^n \times \mathbb{R}^n \times \mathbb{R}^n \mapsto \mathbb{R}^n$, one obtains

$$\dot{e}_s = H_s[f_s(x, \mu, r) - g_s(z, x, \epsilon)]. \tag{4}$$

According to the proof of Theorem 14 in [27] and [33], we decompose this as

$$\dot{e}_s = H_s[v_s(x, z, \epsilon) + w_s(x, \mu, \epsilon)] \tag{5}$$

with

$$\begin{cases} v_s(x, z, \epsilon) = g_s(x, x, \epsilon) - g_s(z, x, \epsilon) \\ \qquad = (A_2 H_s^{-1} - F)e_s + B_2\eta(C_2 H_s^{-1} e_s; z) \\ w_s(x, \mu, \epsilon) = f_s(x, \mu, r) - g_s(x, x, \epsilon) \\ \qquad = DT\mu + DUr - F\epsilon + \varphi(x) \end{cases}$$

with $\varphi(x) = (A_1 - A_2)x + B_1\sigma(C_1 x) - B_2\sigma(C_2 x)$ and $\eta(C_2 H_s^{-1} e_s; z) = \sigma(C_2 H_s^{-1} e_s + C_2 z) - \sigma(C_2 z)$. According to [25], we define the tracking error $\nu = d - \beta^T e_s$, where $\beta = [1; 0; 0; \cdots; 0]$ selects the first component of $e_s$. The main motivation for defining this tracking error is that the signal $e_s$ cannot converge to zero when an external input is applied to the master system. For the synchronization scheme, we obtain then the standard plant representation [1], [19] (Fig. 1)

$$\begin{cases} \begin{bmatrix} \dot{e}_s \\ \dot{\mu} \end{bmatrix} = \begin{bmatrix} A_{2.} & H_s DT \\ 0 & R \end{bmatrix} \begin{bmatrix} e_s \\ \mu \end{bmatrix} + \begin{bmatrix} B_{2.} \\ 0 \end{bmatrix} \eta(C_{2.} e_s; z) \\ \qquad + \begin{bmatrix} H_s DU & -H_s F & H_s \\ S & 0 & 0 \end{bmatrix} \begin{bmatrix} r \\ \epsilon \\ \varphi(x) \end{bmatrix} \\ \nu = [-\beta^T \quad T] \begin{bmatrix} e_s \\ \mu \end{bmatrix} + [U \quad 0 \quad 0] \begin{bmatrix} r \\ \epsilon \\ \varphi(x) \end{bmatrix} \end{cases} \tag{6}$$

with state vector $\xi_s = [e_s; \mu]$ and regulated output $\nu$. The interpretation for the exogenous input will be given in Section IV. By definition, one has $A_{2.} = H_s A_2 H_s^{-1} - H_s F$, $B_{2.} = H_s B_2$, $C_{2.} = C_2 H_s^{-1}$. Note that the system matrices of the standard plant representation do not depend on $A_1$, $B_1$, $C_1$. The influence of the parameter mismatch is contained in $\varphi(x)$.

### B. Dynamic Output Error Feedback

Defining $e_d = x - z$ and denoting the state equation of synchronization scheme (2) as

$$\begin{cases} \dot{x} = f_d(x, \mu, r) \\ \dot{z} = g_d(z, x, \rho, \epsilon) \\ \dot{\rho} = h_d(\rho, x, z, \epsilon) \end{cases} \tag{7}$$

with continuous nonlinear mappings $f_d(.,.,.)$: $\mathbb{R}^n \times \mathbb{R}^{n_r} \times \mathbb{R} \mapsto \mathbb{R}^n$, $g_d(.,.,.,.)$: $\mathbb{R}^n \times \mathbb{R}^n \times \mathbb{R}^{n_c} \times \mathbb{R}^l \mapsto \mathbb{R}^n$, and $h_d(.,.,.,.)$: $\mathbb{R}^{n_c} \times \mathbb{R}^n \times \mathbb{R}^n \times \mathbb{R}^l \mapsto \mathbb{R}^{n_c}$, one obtains

$$\dot{e}_d = f_d(x, \mu, r) - g_d(z, x, \rho, \epsilon). \tag{8}$$

Like in the state feedback case, we decompose this as

$$\dot{e}_d = v_d(x, z, \rho, \epsilon) + w_d(x, \mu, \rho, \epsilon) \tag{9}$$

where

$$\begin{cases} v_d(x, z, \rho, \epsilon) = g_d(x, x, \rho, \epsilon) - g_d(z, x, \rho, \epsilon) \\ \qquad = (A_2 - FNH_d)e_d + B_2\eta(C_2e_d; z) \\ w_d(x, \mu, \rho, \epsilon) = f_d(x, \mu, r) - g_d(x, x, \rho, \epsilon) \\ \qquad = DT\mu - FM\rho + DUr - FN\epsilon + \varphi(x) \end{cases}$$

with $\eta(C_2e_d; z) = \sigma(C_2e_d + C_2z) - \sigma(C_2z)$ and $\varphi(x)$ as defined in the state error feedback case. Defining the tracking error $\nu = d - \beta^T e_d$, the following standard plant representation is obtained (Fig. 1):

$$\begin{cases} \begin{bmatrix} \dot{e}_d \\ \dot{\rho} \\ \dot{\mu} \end{bmatrix} = \begin{bmatrix} A_2 - FNH_d & -FM & DT \\ GH_d & E & 0 \\ 0 & 0 & R \end{bmatrix} \begin{bmatrix} e_d \\ \rho \\ \mu \end{bmatrix} \\ \qquad + \begin{bmatrix} B_2 \\ 0 \\ 0 \end{bmatrix} \eta(C_2e_d; z) + \begin{bmatrix} DU & -FN & I \\ 0 & G & 0 \\ S & 0 & 0 \end{bmatrix} \\ \qquad \cdot \begin{bmatrix} r \\ \epsilon \\ \varphi(x) \end{bmatrix} \\ \nu = [-\beta^T \quad 0 \quad T] \begin{bmatrix} e_d \\ \rho \\ \mu \end{bmatrix} + [U \quad 0 \quad 0] \begin{bmatrix} r \\ \epsilon \\ \varphi(x) \end{bmatrix} \end{cases} \tag{10}$$

with state vector $\xi_d = [e_d; \rho; \mu]$ and regulated output $\nu$. For the interpretation of the exogenous input we refer again to Section IV.

## IV. Dissipativity With Finite $L_2$-Gain

In this section, we first formulate assumptions on the nonlinearity and the boundedness of the trajectories of the master system. An interpretation for the exogenous input of the standard plant representations is given. Then conditions for dissipativity with finite $L_2$-gain and a quadratic storage function are derived for the synchronization schemes. These conditions are expressed as matrix inequalities.

We make the following two assumptions.

*Assumption 1:* The nonlinearity $\eta(C_2e_d; z)$ in (10) belongs to sector $[0, k]$:

$$0 \le \frac{\eta_i(c_{2_i}^T e_d; z)}{c_{2_i}^T e_d} = \frac{\sigma_i(c_{2_i}^T e_d + c_{2_i}^T z) - \sigma_i(c_{2_i}^T z)}{c_{2_i}^T e_d} \le k, \qquad \forall e_d, z;\ i = 1, \cdots, n_h\ (c_{2_i}^T e_d \neq 0) \tag{11}$$

where $c_{2_i}^T$ denotes the $i$th row vector of $C_2$. The same assumption is made for $\eta(C_{2_s}e_s; z)$ in (6).

The following inequalities hold [2], [16], [31]:

$$\begin{aligned} &\eta_i(c_{2*_i}^T e_s; z)\,[\eta_i(c_{2*_i}^T e_s; z) - kc_{2*_i}^T e_s] \le 0, \qquad \forall e_s, z; \qquad i = 1, \cdots, n_h \\ &\eta_i(c_{2_i}^T e_d; z)\,[\eta_i(c_{2_i}^T e_d; z) - kc_{2_i}^T e_d] \le 0, \qquad \forall e_d, z; \qquad i = 1, \cdots, n_h. \end{aligned} \tag{12}$$

It follows from the mean value theorem that for differentiable $\sigma(.)$ the sector condition $[0, k]$ on $\eta(.)$ corresponds to [7]

$$0 \le \frac{d}{d\rho}\sigma_i(\rho; z) \le k, \qquad \forall \rho, z; \qquad i = 1, \cdots, n_h. \tag{13}$$

*Assumption 2:* The master systems $\mathcal{M}_s$ and $\mathcal{M}_d$ are input to state stable in the sense that there exist initial states $x_0$ and a positive real constant $\delta_x$ such that

$$\|x(t)\|_2 \le \delta_x, \qquad \forall t \in [0, \infty) \tag{14}$$

for all continuous time reference inputs $r$ which satisfy $\|r\|_\infty = \sup_{t\ge 0}|r(t)| \le 1$.

The viewpoint that we take here is pragmatic in the sense that in practice one is not interested in employing a master system that possesses unbounded trajectories. Note that for a zero external input $d$ the upper bound $\delta_x$ is a measure for the "size" of the attractor of the chaotic master system [7]. The Lur'e systems, matrix $D$ and initial states are chosen such that the master system satisfies Assumption 2. Using the expression for $\varphi(x)$ one obtains $\|\varphi(x)\|_2 \le \beta_m\|x\|_2\ \forall x$ with $\beta_m = \|\Delta A\|_2 + k\|B_1\|_2\|C_1\|_2 + k\|B_2\|_2\|C_2\|_2$ and $\Delta A = A_1 - A_2$. In case $C_1 = C_2$ one obtains $\beta_m = \|\Delta A|_2 + k\|\Delta B\|_2\|C_2\|_2$ where $\Delta B = B_1 - B_2$. From Assumption 2, one has $\|\varphi(x)\|_2 < \beta_m\delta_x,\ \forall x$. Note that this upper bound might be conservative. On the other hand, this approach has led to useful criteria for robust synchronization of the autonomous synchronization scheme, discussed in [27]. For the upper bound we will consider a positive constant scaling factor $\alpha$

$$\|\varphi(x)\|_2 \le \alpha\beta_m\delta_x. \tag{15}$$

In order to analyze the I/O properties of the standard plant representation of the synchronization scheme with static state feedback (6), we consider the quadratic storage function [12], [13], [32]:

$$\phi(\xi_s) = \xi_s^T P \xi_s = [e_s^T \quad \mu^T] \begin{bmatrix} P_{11} & P_{12} \\ P_{21} & P_{22} \end{bmatrix} \begin{bmatrix} e_s \\ \mu \end{bmatrix}, \qquad P = P^T > 0 \tag{16}$$

and a supply rate with finite $L_2$-gain $\gamma$:

$$s(w, \nu) = \gamma^2 w^T w - \nu^T \nu \tag{17}$$

with regulated output $\nu$ and exogenous input $w$. As exogenous input we take $w = [r; \epsilon; \beta_m\delta_x]$, which consists of the reference input, disturbance signals and a constant signal related to the parameter mismatch between the master–slave systems. The system (6) is said to be dissipative [12], [13], [32] with respect to supply rate (17) and the storage function (16) if $\dot{\phi} \le s(w, \nu),\ \forall w, \nu$. The following Theorem holds.

*Theorem 1:* Let $\Lambda = \text{diag}\ \{\lambda_i\}$ be a diagonal matrix with $\lambda_i \ge 0$ for $i = 1, \cdots, n_h$. A sufficient condition for dissipativity of the synchronization scheme with full static state feedback (6) with respect to the storage function (16) and the supply rate with $L_2$-gain $\gamma$ (17) is given by the matrix inequality

$$Z = Z^T = \left[\begin{array}{ccccc|c} Z_{11} & Z_{12} & Z_{13} & Z_{14} & Z_{15} & P_{11}H \\ \cdot & Z_{22} & Z_{23} & Z_{24} & Z_{25} & P_{21}H \\ \cdot & \cdot & Z_{33} & 0 & 0 & 0 \\ \cdot & \cdot & \cdot & Z_{44} & 0 & 0 \\ \cdot & \cdot & \cdot & \cdot & Z_{55} & 0 \\ \hline \cdot & \cdot & \cdot & \cdot & \cdot & -\frac{\gamma^2 I}{\alpha^2} \end{array}\right] < 0 \quad (18)$$

with

$$\begin{aligned} Z_{11} &= A_{2.}^T P_{11} + P_{11}A_{2.} + \beta\beta^T \\ Z_{12} &= A_{2.}^T P_{12} + P_{11}H_s DT + P_{12}R - \beta T \\ Z_{13} &= P_{11}B_{2.} + kC_{2.}^T \Lambda \\ Z_{14} &= P_{11}H_s DU + P_{12}S - \beta U \\ Z_{15} &= -P_{11}H_s F \\ Z_{22} &= P_{21}H_s DT + T^T D^T H_s^T P_{12} \\ &\quad + P_{22}R + R^T P_{22} + T^T T \\ Z_{23} &= P_{21}B_{2.} \\ Z_{24} &= P_{21}H_s DU + P_{22}S + T^T U \\ Z_{25} &= -P_{21}H_s F \\ Z_{33} &= -2\Lambda, \\ Z_{44} &= -\gamma^2 I + U^T U, \\ Z_{55} &= -\gamma^2 I. \end{aligned}$$

*Proof:* The condition (15) is expressed as $\beta_m^2\delta_x^2 - \varphi^T\varphi/\alpha^2 \geq 0$. Together with the sector condition on $\eta$ (11), this condition is employed in an application of the $\mathcal{S}$-procedure ([2, p. 23]) in checking the condition $\dot{\phi} - s \leq 0$. This means that positive real constants $\lambda_i$ and $\tau$ are introduced such that

$$\dot{\phi} - s - 2\sum_i \lambda_i\eta_i(\eta_i - kc_{2.}^T e_s) + \tau\left(\beta_m^2\delta_x^2 - \frac{\varphi^T\varphi}{\alpha^2}\right) < 0$$

and by defining $\Lambda = \mathrm{diag}\{\lambda_i\}$:

$$\dot{\phi} - s - 2\eta^T\Lambda(\eta - kC_{2.}e_s) + \tau\left(\beta_m^2\delta_x^2 - \frac{\varphi^T\varphi}{\alpha^2}\right) < 0.$$

Using the expression for the supply rate $s = \gamma^2(r^T r + \epsilon^T\epsilon + \beta_m^2\delta_x^2) - \nu^T\nu$ and choosing $\tau = \gamma^2$ this condition becomes

$$\dot{\phi} - \gamma^2(r^T r + \epsilon^T\epsilon) + \nu^T\nu - 2\eta^T\Lambda(\eta - kC_{2.}e_s) - \frac{\gamma^2\varphi^T\varphi}{\alpha^2} < 0.$$

Using $\dot{\phi} = \dot{\xi}_s^T P\xi_s + \xi_s^T P\dot{\xi}_s$ and the equation of the standard plant representation (6), this can be written as the quadratic form $\zeta^T Z\zeta < 0$ with $\zeta = [e_s; \mu; \eta; r; \epsilon; \varphi]$. This expression is negative for all nonzero $\zeta$ if $Z$ is negative definite. □

In order to analyze the I/O properties of the standard plant representation of the synchronization scheme with dynamic output feedback (10), we consider the quadratic storage function

$$\phi(\xi_d) = \xi_d^T P\xi_d = [e_d^T \quad \rho^T \quad \mu^T]\begin{bmatrix} P_{11} & P_{12} & P_{13} \\ P_{21} & P_{22} & P_{23} \\ P_{31} & P_{32} & P_{33} \end{bmatrix}\begin{bmatrix} e_d \\ \rho \\ \mu \end{bmatrix}$$

$$P = P^T > 0 \quad (19)$$

and the supply rate with finite $L_2$-gain $\gamma$ (17) and exogenous input $w = [r; \epsilon; \beta\delta_x]$.

*Theorem 2:* Let $\Lambda = \mathrm{diag}\{\lambda_i\}$ be a diagonal matrix with $\lambda_i \geq 0$ for $i = 1, \cdots, n_h$. A sufficient condition for dissipativity of the synchronization scheme with dynamic output feedback (10) with respect to the storage function (19) and the supply rate with $L_2$-gain $\gamma$ (17) is given by the matrix inequality

$$Z = Z^T = \left[\begin{array}{cccccc|c} Z_{11} & Z_{12} & Z_{13} & Z_{14} & Z_{15} & Z_{16} & P_{11} \\ \cdot & Z_{22} & Z_{23} & Z_{24} & Z_{25} & Z_{26} & P_{21} \\ \cdot & \cdot & Z_{33} & Z_{34} & Z_{35} & Z_{36} & P_{31} \\ \cdot & \cdot & \cdot & Z_{44} & 0 & 0 & 0 \\ \cdot & \cdot & \cdot & \cdot & Z_{55} & 0 & 0 \\ \cdot & \cdot & \cdot & \cdot & \cdot & Z_{66} & 0 \\ \hline \cdot & \cdot & \cdot & \cdot & \cdot & \cdot & \frac{-\gamma^2 I}{\alpha^2} \end{array}\right] < 0 \quad (20)$$

with

$$\begin{aligned} Z_{11} &= (A_2 - FNH_d)^T P_{11} + P_{11}(A_2 - FNH_d) \\ &\quad + H_d^T G^T P_{21} + P_{12}GH_d + \beta\beta^T \\ Z_{12} &= (A_2 - FNH_d)^T P_{12} + H_d^T G^T P_{22} - P_{11}FM + P_{12}E \\ Z_{13} &= (A_2 - FNH_d)^T P_{13} + H_d^T G^T P_{23} \\ &\quad + P_{11}DT + P_{13}R - \beta T \\ Z_{14} &= P_{11}B_2 + kC_2^T\Lambda \\ Z_{15} &= P_{11}DU + P_{13}S - \beta U \\ Z_{16} &= P_{12}G - P_{11}FN \\ Z_{22} &= E^T P_{22} + P_{22}E - M^T F^T P_{12} - P_{21}FM \\ Z_{23} &= E^T P_{23} - M^T F^T P_{13} + P_{21}DT + P_{23}R \\ Z_{24} &= P_{21}B_2 \\ Z_{25} &= P_{21}DU + P_{23}S \\ Z_{26} &= P_{22}G - P_{21}FN \\ Z_{33} &= R^T P_{33} + P_{33}R + T^T D^T P_{13} + P_{31}DT + T^T T \\ Z_{34} &= P_{31}B_2 \\ Z_{35} &= P_{31}DU + P_{33}S + T^T U \\ Z_{36} &= P_{32}G - P_{31}FN \\ Z_{44} &= -2\Lambda \\ Z_{55} &= -\gamma^2 I + U^T U \\ Z_{66} &= -\gamma^2 I. \end{aligned}$$

*Proof:* According to the proof of Theorem 1, we use the inequality $\beta_m^2\delta_x^2 - \varphi^T\varphi/\alpha^2 \geq 0$ and the inequality from the sector condition on $\eta$. By employing these inequalities in the $\mathcal{S}$-procedure, one obtains

$$\dot{\phi} - \gamma^2(r^T r + \epsilon^T\epsilon) + \nu^T\nu - 2\sum_i \lambda_i\eta_i(\eta_i - kc_2^T e_d) - \frac{\gamma^2\varphi^T\varphi}{\alpha^2} < 0$$

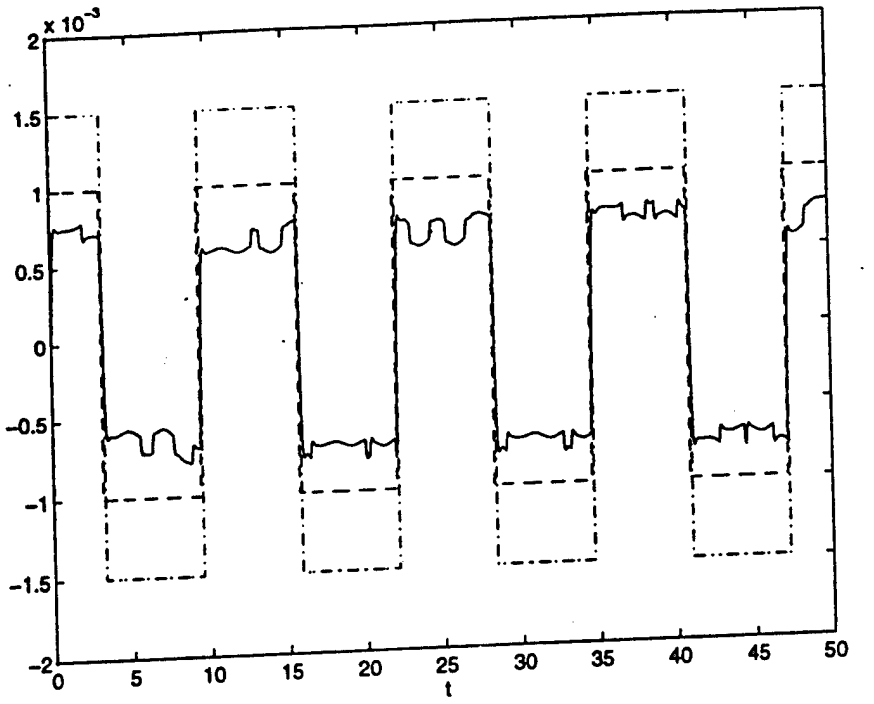


(a)

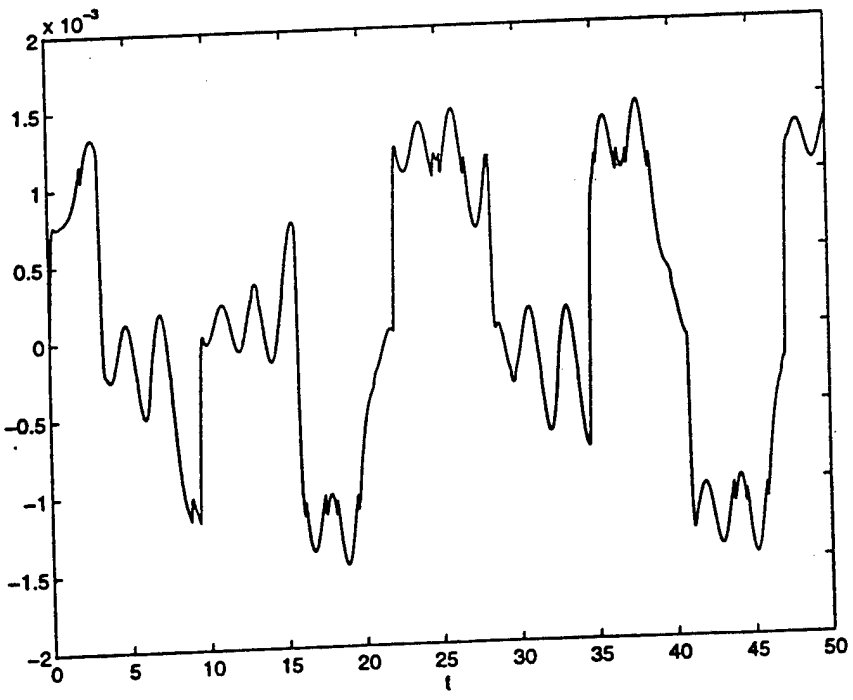


(b)

Fig. 2. Robust nonlinear $H_\infty$ synchronization of Chua's circuit using full static state error feedback. (a) $\beta^T e_s$ (-), scaled version of message signal sign $[\cos(0.5t)]$ (- -) and scaled version of recovered message signal $\text{sign}(\beta^T e_s)$ (-.). The parameter mismatch of the master with respect to the slave system is $\delta a_{11} = 0.001$. (b) $\beta^T e_s$ for a too large parameter mismatch $\delta a_{11} = 0.01$. The original message is not recovered in this case.

and by defining $\Lambda = \text{diag}\{\lambda_i\}$:

$$\dot{\phi} - \gamma^2(r^T r + \epsilon^T \epsilon) + \nu^T \nu - 2\eta^T \Lambda(\eta - kC_2 e_d) - \frac{\gamma^2 \varphi^T \varphi}{\alpha^2} < 0.$$

Using $\dot{\phi} = \dot{\xi}_d^T P \xi_d + \xi_d^T P \dot{\xi}_d$ and the equation of the standard representation (10) this can be written as the quadratic form $\zeta^T Z \zeta < 0$, with $\zeta = [e_d; \rho; \mu; \eta; r; \epsilon; \varphi]$. This expression is negative for all nonzero $\zeta$ if $Z$ is negative definite. □

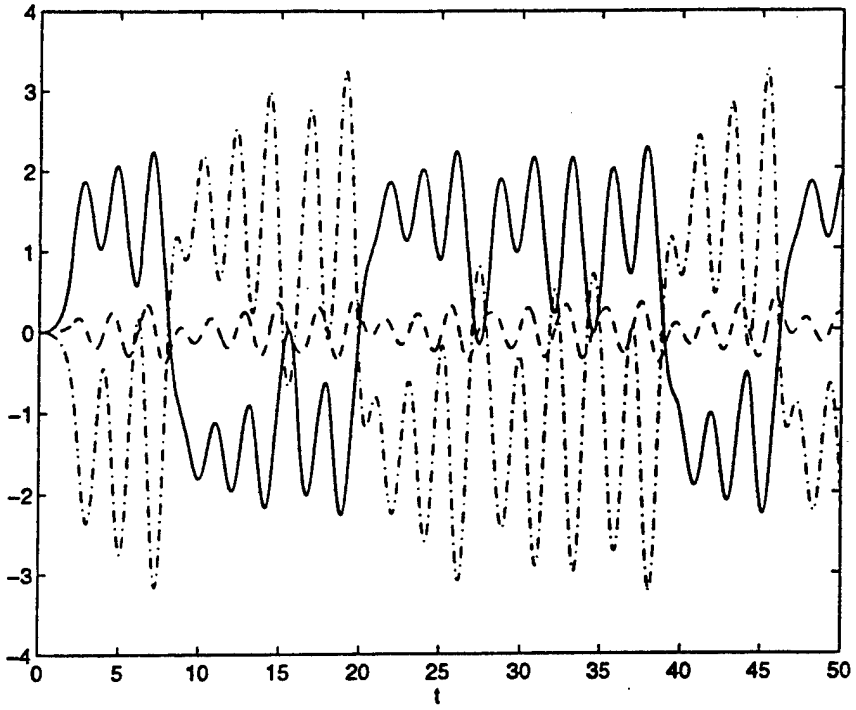


(a)

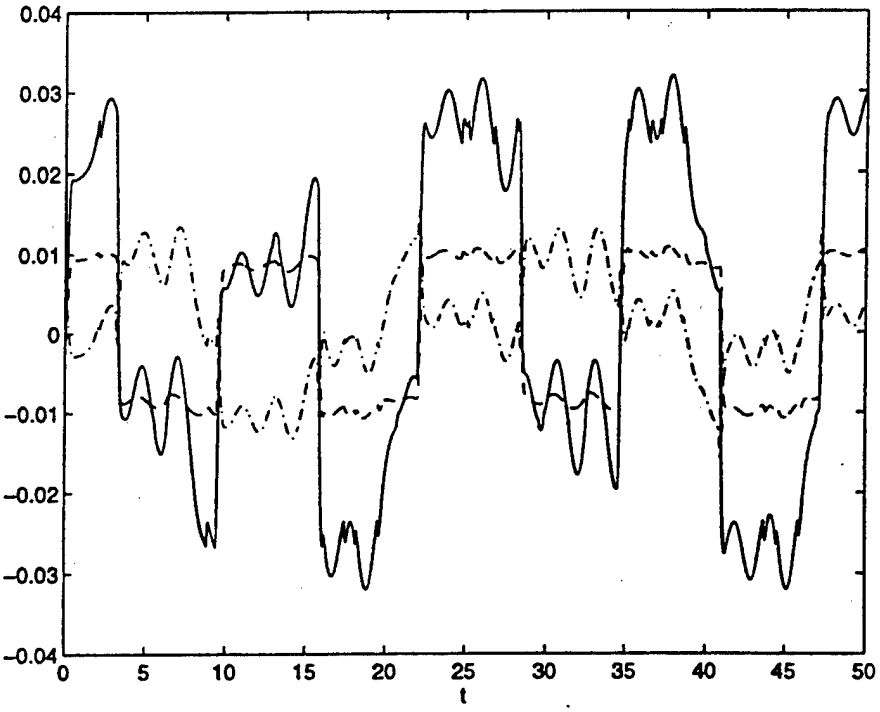


(b)

Fig. 3. Static state error feedback (continued). (a) Transmitted signals $p$ which are a linear transformation of the state variables $x$ of the master system, with $p_1$ (-), $p_2$ (- -), $p_3$ (-.). Applying vector field modulation, the message signal is invisible on the chaotic carrier signal. (b) Control signal $u$ applied to the slave system using full static state error feedback, with $u_1$ (-), $u_2$ (- -), $u_3$ (-.).

## V. Robust Nonlinear $H_\infty$ Synchronization

In this section, we explain how to design the controllers $C_s$ and $C_d$ based on the matrix inequalities (18) and (20). In nonlinear $H_\infty$ control theory (see e.g., [14], [30]) a controller for a given nonlinear plant is designed by considering a supply rate with finite $L_2$-gain. The optimal nonlinear $H_\infty$ control law corresponds to the minimal achievable $L_2$-gain which makes the closed-loop system dissipative. The optimal solution is characterized by means of a Hamilton–Jacobi inequality with respect to a general continuously differentiable nonlinear

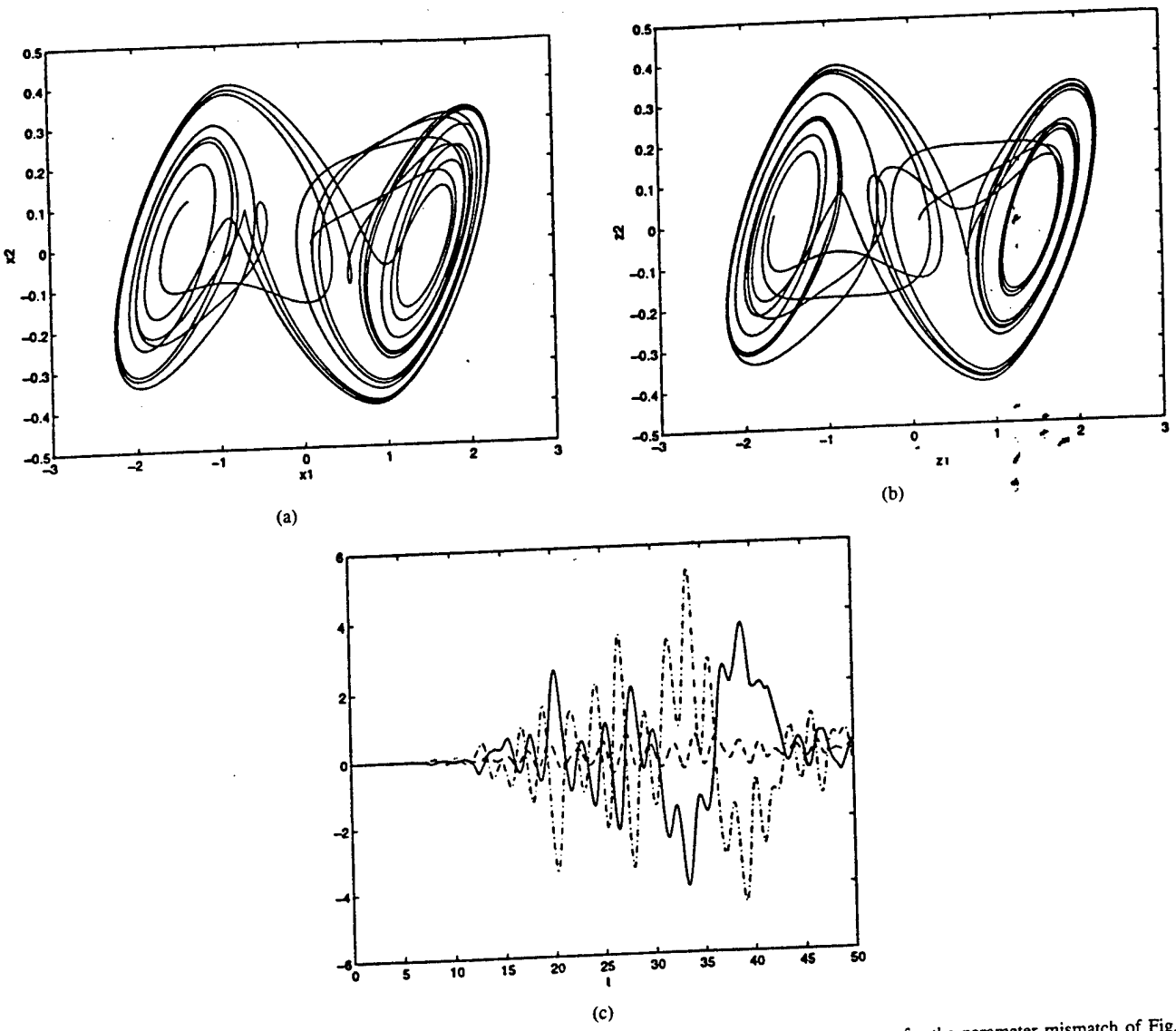


Fig. 4. Static state error feedback (continued). Behavior of the master and slave systems in the autonomous case, for the parameter mismatch of Fig. 2(a) and initial condition $x(0) = z(0) = [0.1; 0; 0]$. (a) $(x_1, x_2)$ of the master system. (b) $(z_1, z_2)$ of the slave system. (c) $x - z$ with respect to time.

storage function. On the other hand, in our previous work on nonlinear $H_\infty$ synchronization and in the present paper, we consider a quadratic storage function which leads to matrix inequalities. The nonlinear $H_\infty$ synchronization problem, as defined in [25], [26], corresponds to

$$\min_{\theta_c, P, \Lambda, \gamma} \gamma \text{ such that } \begin{cases} Z(\theta_c, P, \Lambda, \gamma, \alpha) < 0 \\ P = P^T > 0, \Lambda \geq 0 \text{ and diagonal} \end{cases} \quad (21)$$

where $\theta_c$ denotes the parameter vector of the controller $C_s$ or $C_d$, i.e., $\theta_c = F(:)$ or $\theta_c = [E(:); G(:); M(:); N(:)]$, respectively, where "(:)" denotes a columnwise scan of a matrix. In the *robust* nonlinear $H_\infty$ synchronization problem, the parameter $\alpha$ is maximized, in order to achieve maximal robustness with respect to parameter mismatch between the master–slave systems, as follows from (15). Using a penalty method [9] the problem can be formulated as follows:

$$\min_{\theta_c, P, \Lambda, \gamma, \alpha} \gamma + c\frac{1}{\alpha} \text{ such that } \begin{cases} Z(\theta_c, P, \Lambda, \gamma, \alpha) < 0 \\ P = P^T > 0, \Lambda \geq 0 \end{cases} \quad (22)$$

where $c$ is a positive real constant. In this way, the influence from the exogenous input on the regulated output is minimized, taking into account the reference input (message signal), the disturbance signal $\epsilon$ and the parameter mismatch. Because it is well-known from control theory that perfect tracking is impossible for all possible reference input signal, binary valued continuous time reference inputs $r$ are considered such that the message signal can be recovered from sign $(\beta^T e_{s,d})$ [25], [26]. The constraint $P > 0$ can be eliminated by taking the parametrization $P = Q^T Q$. The same applies to $\Lambda$. In practice, one solves

$$\min_{\theta_c, Q, \Lambda, \gamma, \alpha} \gamma + c\frac{1}{\alpha} \text{ such that } \lambda_{\max}[Z(\theta_c, Q, \Lambda, \gamma, \alpha)] + \delta < 0 \quad (23)$$

where $\lambda_{\max}[.]$ denotes the maximal eigenvalue of a symmetric matrix and $\delta$ a small positive constant. The constraint is differentiable as long as the two largest eigenvalues of $Z$ do not coincide. Otherwise a generalized gradient can be defined [22].

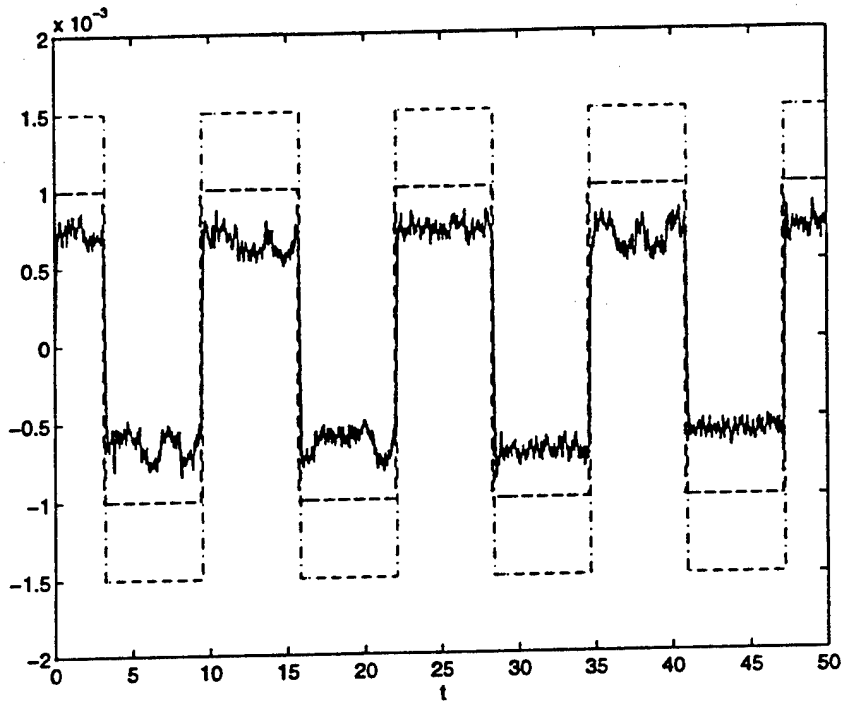


Fig. 5. Static state error feedback (continued). Simulation of the synchronization scheme for the same case as Fig. 2(a) but with zero mean white Gaussian channel noise $\epsilon$ with standard deviation 0.0001.

The optimization problem is nonconvex. However, suboptimal solutions yield satisfactory results as we will show by an example in the following section.

## VI. Example: Chua's Circuit

In this section, we illustrate the robust nonlinear $H_\infty$ synchronization method on Chua's circuit:

$$\begin{cases} \dot{x}_1 = a[x_2 - h(x_1)] \\ \dot{x}_2 = x_1 - x_2 + x_3 \\ \dot{x}_3 = -bx_2 \end{cases} \tag{24}$$

with nonlinear characteristic

$$h(x_1) = m_1 x_1 + \tfrac{1}{2}(m_0 - m_1)(|x_1 + 1| - |x_1 - 1|)$$

and parameters $a = 9$, $b = 14.286$, $m_0 = -\frac{1}{7}$, $m_1 = \frac{2}{7}$ in order to obtain the double scroll attractor [4], [5], [20]. The nonlinearity $\sigma(x_1) = \frac{1}{2}(|x_1 + 1| - |x_1 - 1|)$ (linear characteristic with saturation) belongs to sector [0, 1]. Hence, Chua's circuit can be interpreted as a Lur'e system $\dot{x} = Ax + B\sigma(Cx)$ where

$$A = \begin{bmatrix} -am_1 & a & 0 \\ 1 & -1 & 1 \\ 0 & -b & 0 \end{bmatrix}, B = \begin{bmatrix} -a(m_0 - m_1) \\ 0 \\ 0 \end{bmatrix}$$
$$C = [1 \quad 0 \quad 0]. \tag{25}$$

We assign the double scroll behavior to the slave system by taking $A_2 = A$, $B_2 = B$, $C_2 = C$. The parameter mismatch is considered with respect to this nominal slave system.

We first consider the synchronization scheme with full static state error feedback (1). Cryptographical aspects of this scheme are discussed in [25], where $H_s$ or an additional multilayer perceptron with square and full rank interconnection matrices may be used for the definition of a secret key, used by sender and receiver for enciphering and deciphering. We illustrate the working of the scheme here for $D = [1; 1; 1]$, $H_s = I$ and $\beta = [1; 0; 0]$. For the reference model $\mathcal{R}$ a first order Butterworth filter is chosen with cut-off frequency 10 Hz. For robust nonlinear $H_\infty$ synchronization, the nonlinear optimization problem (23) has been solved with $c = 1$, $\delta = 0.01$. In order to limit the control energy, an additional constraint $\|\theta_c\|_2 \leq 20$ has been taken into account. The optimization problem has been solved using sequential quadratic programming [9] (*constr* in Matlab). As starting point for the optimization problem a random matrix $F$, generated according to a normal distribution with zero mean and variance 0.1, was chosen. Further we select $Q = I$, $\Lambda = 0.1$, $\gamma = 100$, $\alpha = 1$. In Figs. 2–5, a resulting controller, corresponding to $\gamma = 1.47$ and $\alpha = 6.84$, is shown. The scheme has previously been investigated in [25] for identical master–slave systems. Fig. 2 shows the recovery for binary valued continuous time reference inputs or message signals, for nonidentical master-slave system. A perturbation of the element $a_{11}$ of the $A$ matrix $\delta a_{11} = 0.001$ is taken for the master system with respect to the nominal slave system with $A_2 = A$, $B_2 = B$, $C_2 = C$. For $\delta a_{11} = 0.01$ the original message cannot be recovered. This illustrates a difference between the synchronization scheme with reference input (1) and its autonomous case, i.e., without a message signal, considered in [27]. In the autonomous case a large parameter mismatch can be allowed such that the systems

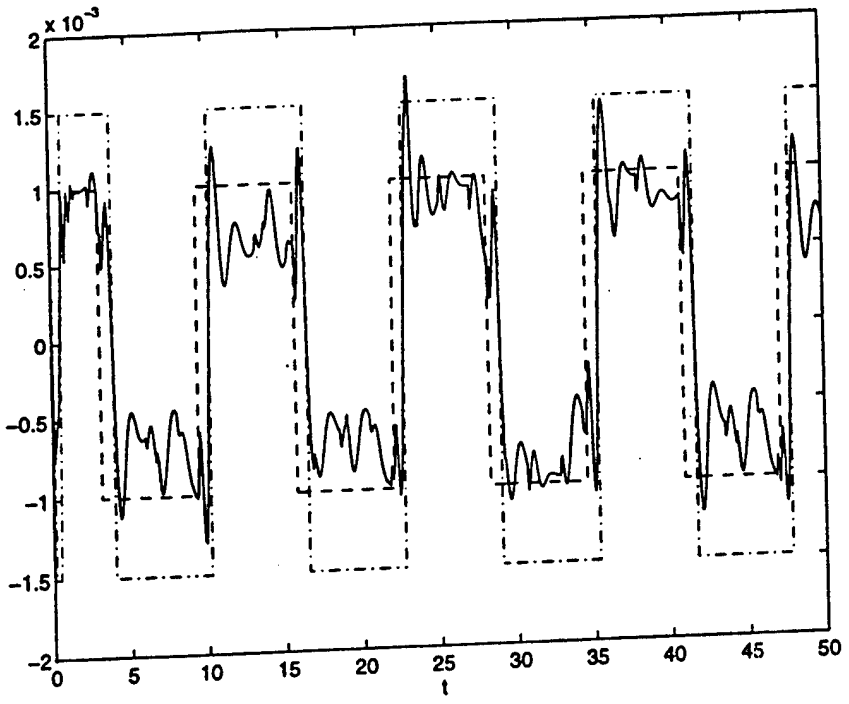


(a)

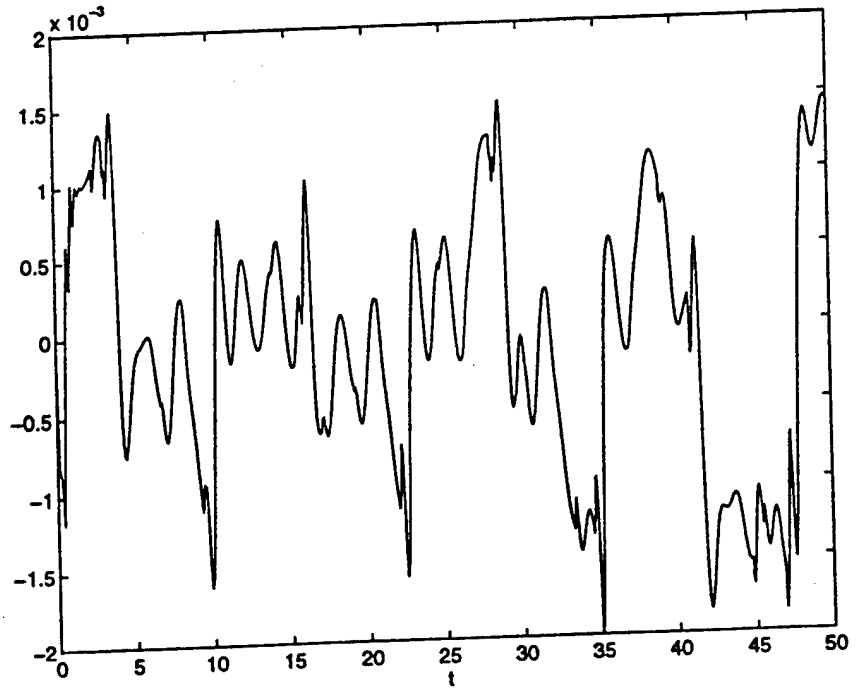


(b)

Fig. 6. Robust nonlinear $H_\infty$ synchronization of Chua's circuit using dynamic output feedback. (a) $\mathcal{B}^T e_d$ (-), scaled version of message signal sign $[\cos(0.5t)]$ (- -) and scaled version of recovered message signal sign ($\mathcal{B}^T e_d$) (-.). The parameter mismatch of the master with respect to the slave system is $\delta a_{11} = 0.001$. (b) $\mathcal{B}^T e_d$ for a too large parameter mismatch $\delta a_{11} = 0.005$. The original message is not recovered in this case.

remain synchronized up to a relatively small synchronization error, even when a master system with periodic behavior or stable points is considered for a chaotic slave system. The latter is different for the nonautonomous case, as is illustrated on Fig. 4. The transmitted signals and control signals are shown on Fig. 3. Fig. 5 shows the synchronization scheme for the parameter mismatch $\delta a_{11} = 0.001$ and zero mean Gaussian channel noise with standard deviation 0.0001. The amount of noise that can be tolerated is smaller than for the case without parameter mismatch [25]. The simulations for the deterministic

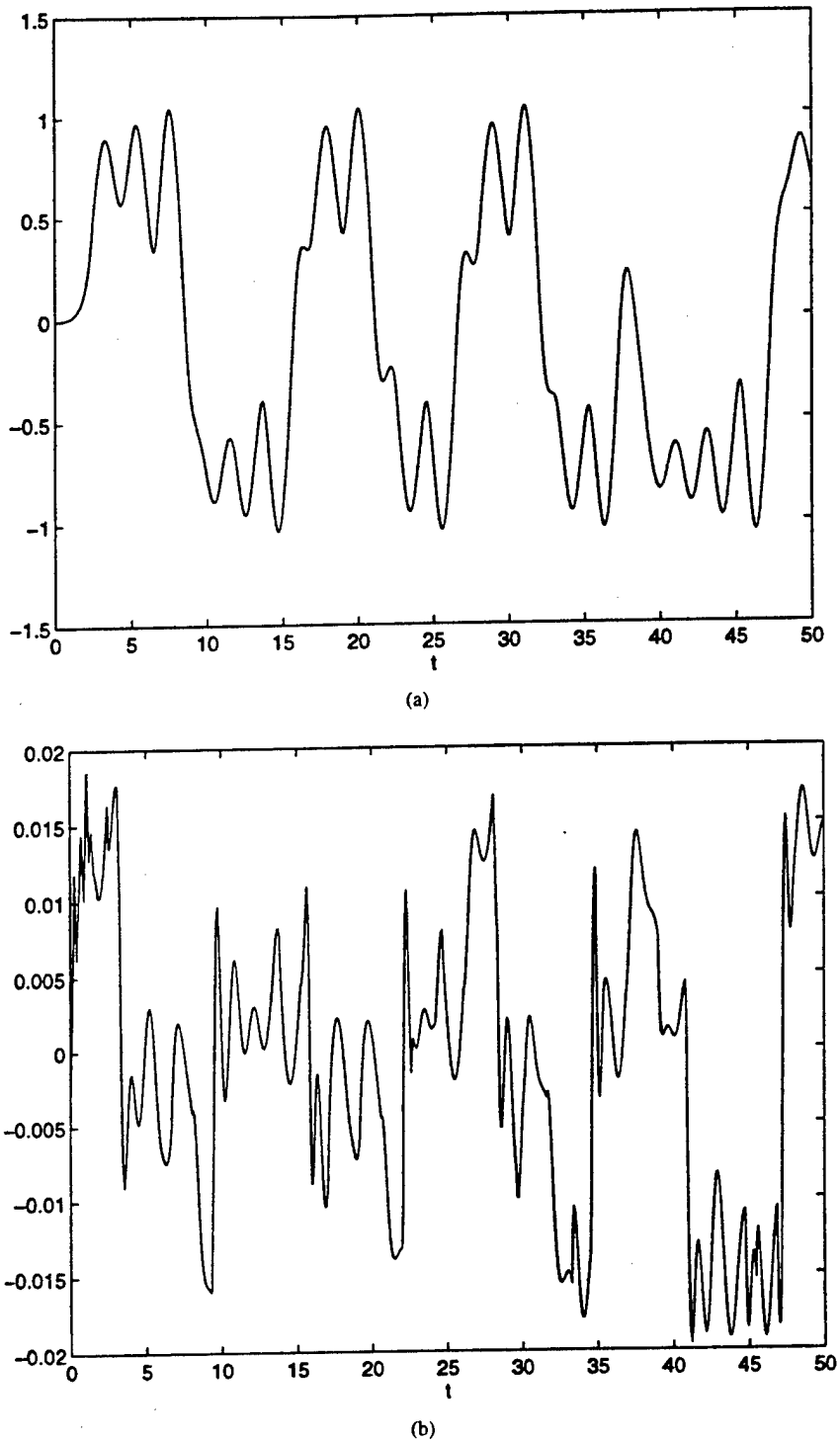


Fig. 7. Dynamic output feedback (continued). (a) Transmitted signal $p$ which is a linear combination of the state variables $x_1$, $x_2$ of the master system. Applying vector field modulation, the message signal is invisible on the chaotic carrier signal. (b) Control signal $u$ applied to the slave system.

case were done using a Runge–Kutta integration rule [21] (*ode23* in Matlab). Stochastic systems have been simulated using an Euler integration rule [17].

The case of robust nonlinear $H_\infty$ synchronization of Chua's circuit using dynamic output error feedback is shown on Figs. 6–8. Cryptographical issues of this scheme are discussed in [26]. The matrix $H_d$, together with parameters of Chua's circuit, can be chosen as a key. In the example here we take one-dimensional outputs $p$, $q(l = 1)$ with $H_d = [0.5; -0.5; 0]$, a one-dimensional control signal $u(m = 1)$ with $F = \beta = [1; 0; 0]$ and $D = \beta = [1; 0; 0]$. The same low pass filter $\mathcal{R}$ was chosen as for the static feedback case. The optimization problem (23) has been solved for $c = 5$, $\delta = 0.01$. An additional constraint $\|\theta_c\|_2 \leq 60$ is taken into account. A third-order SISO controller has been selected, which turned out to be the minimal order

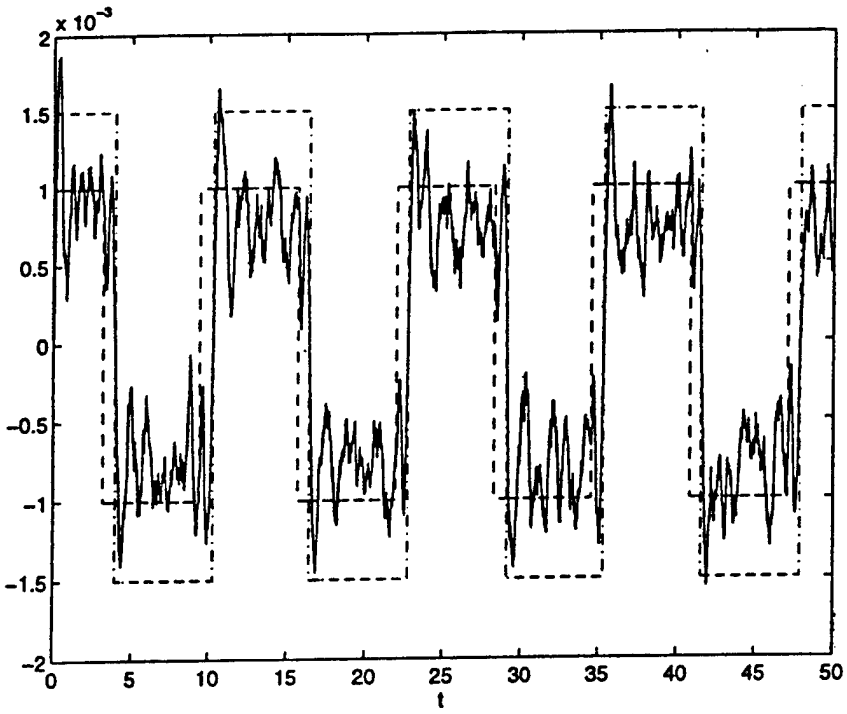


Fig. 8. Dynamic output feedback (continued). Simulation of the synchronization scheme with parameter mismatch $\delta a_{11} = 0.0001$ and zero mean white Gaussian channel noise $\epsilon$ with standard deviation 0.0001.

for achieving a good performance. As starting point for the optimization problem, random matrices were chosen for the controller according to a normal distribution with zero mean and standard deviation 0.1, $Q = I$, $\Lambda = 0.1$, $\gamma = 100$, and $\alpha = 1$. In Figs. 6–8, a resulting controller with $\gamma = 26.63$ and $\alpha = 1.59$ is shown. This scheme has been investigated for identical master–slave systems in [26]. In Fig. 6, a perturbation $\delta a_{11} = 0.001$ is considered for the master system with respect to the slave system. Perfect recovery is obtained for binary valued continuous time reference inputs, but not for a larger parameter mismatch $\delta a_{11} = 0.005$. The transmitted signal and control signal are shown on Fig. 7. Simulations with zero mean white Gaussian channel noise with standard deviation 0.0001 and parameter mismatch $\delta a_{11} = 0.0001$ are shown on Fig. 8. Hence, the performance of the full static state error feedback controller is better than for the dynamic output feedback controller, while the latter may lead to a simpler implementation of the synchronization scheme.

## VII. Conclusion

The influence of parameter mismatch between master–slave Lur'e systems has been studied with respect to the method of nonlinear $H_\infty$ synchronization. By representing the synchronization schemes in standard plant form and deriving conditions for dissipativity with finite $L_2$-gain, matrix inequalities have been derived. Controller design based on these matrix inequalities involves the solution of an optimization problem. The controller is rendered robust with respect to channel noise and parameter mismatch between the master–slave systems. The method further offers the possibility for incorporating channel models in the scheme. Both full static state error feedback and dynamic output error feedback have been investigated. For the latter method one can transmit a single signal, which may lead to a simpler implementation of the synchronization scheme. The full static state feedback method on the other hand has a higher performance. This has been illustrated on Chua's circuit. While in previous work we have shown that for the autonomous case a large parameter mismatch is tolerated for master–slave synchronization of the scheme up to a relatively small synchronization error, a smaller parameter mismatch is required for adequate performance of the scheme with message input.

## Acknowledgment

This work was conducted at the Katholieke Universiteit Leuven and the University of California at Berkeley, in the framework of the Belgian Programme on Interuniversity Poles of Attraction, initiated by the Belgian State, Prime Minister's Office for Science, Technology and Culture (IUAP-17) and in the framework of a Concerted Action Project MIPS (Modelbased Information Processing Systems) of the Flemish Community.

## References

[1] S. Boyd and C. Barratt, *Linear Controller Design, Limits of Performance*. Englewood Cliffs, NJ: Prentice-Hall, 1991.

[2] S. Boyd, L. El Ghaoui, E. Feron, and V. Balakrishnan, "Linear matrix inequalities in system and control theory," *SIAM (Studies in Applied Mathematics)*, vol. 15, 1994.

[3] W.-K. Chen, Ed., *The Circuits and Filters Handbook.* Boca Raton, FL: CRC, 1995.
[4] L. O. Chua, M. Komuro, and T. Matsumoto, "The double scroll family," *IEEE Trans. Circuits Syst. I*, vol. 33, pp. 1072–1118, Nov. 1986.
[5] L. O. Chua, "Chua's circuit 10 years later," *Int. J. Circuit Theory Applicat.*, vol. 22, pp. 279–305, 1994.
[6] L. O. Chua and T. Roska, "The CNN paradigm," *IEEE Trans. Circuits Syst. I*, vol. 40, pp. 147–156, Mar. 1993.
[7] P. F. Curran and L. O. Chua, "Absolute stability theory and the synchronization problem," *Int. J. Bifurc. Chaos*, 1997, to be published.
[8] P. F. Curran, J. A. K. Suykens, and L. O. Chua, "Absolute stability theory and master-slave synchronization," *Int. J. Bifurc. Chaos*, 1997, to be published.
[9] R. Fletcher, *Practical Methods of Optimization.* Chichester, U.K. and New York: Wiley, 1987.
[10] C. Guzelis and L. O. Chua, "Stability analysis of generalized cellular neural networks," *Int. J. Circuit Theory Applicat.*, vol. 21, pp. 1–33, 1993.
[11] M. Hasler, "Synchronization principles and applications," in *Circuits and Systems: Tutorials IEEE-ISCAS'94*, pp. 314–326.
[12] D. J. Hill and P. J. Moylan, "The stability of nonlinear dissipative systems," *IEEE Trans. Automat. Contr.*, vol. AC-21, pp. 708–711, 1976.
[13] ——, "Connections between finite-gain and asymptotic stability," *IEEE Trans. Automat. Contr.*, vol. AC-25, pp. 931–936, Apr. 1980.
[14] A. Isidori and A. Astolfi, "Disturbance attenuation and $H_\infty$ control via measurement feedback in nonlinear systems," *IEEE Trans. Automat. Contr.*, vol. 37, pp. 1283–1293, 1992.
[15] T. Kapitaniak and L. O. Chua, "Hyperchaotic attractors of unidirectionally-coupled Chua's circuits," *Int. J. Bifurc. Chaos*, vol. 4, no. 2, pp. 477–482, 1994.
[16] H. K. Khalil, *Nonlinear Systems.* New York: Macmillan, 1992.
[17] P. E. Kloeden, E. Platen, and H. Schurz, "The numerical solution of nonlinear stochastic dynamical systems: A brief introduction," *Int. J. Bifurc. Chaos*, vol. 1, no. 2, pp. 277–286, 1991.
[18] L. Kocarev, A. Shang, and L. O. Chua, "Transitions in dynamical regimes by driving: A unified method of control and synchronization of chaos," *Int. J. Bifurc. Chaos*, vol. 3, no. 2, pp. 479–483, 1993.
[19] J. M. Maciejowski, *Multivariable Feedback Design.* Reading, MA: Addison-Wesley, 1989.
[20] R. N. Madan, Guest Ed., *Chua's Circuit: A Paradigm for Chaos.* Signapore: World Scientific, 1993.
[21] T. S. Parker and L. O. Chua, *Practical Numerical Algorithms for Chaotic Systems.* New York: Springer-Verlag, 1989.
[22] E. Polak and Y. Wardi, "Nondifferentiable optimization algorithm for designing control systems having singular value inequalities," *Automatica*, vol. 18, no. 3, pp. 267–283, 1982.
[23] J. A. K. Suykens, J. P. L. Vandewalle, and B. L. R. De Moor, *Artificial Neural Networks for Modeling and Control of Non-Linear Systems.* Boston, MA: Kluwer Academic, 1996.
[24] J. A. K. Suykens, P. F. Curran, and L. O. Chua, "Master-slave synchronization using dynamic output feedback," *Int. J. Bifurc. Chaos*, vol. 7, no. 3, pp. 671–679, 1997.
[25] J. A. K. Suykens, J. Vandewalle, and L. O. Chua, "Nonlinear $H_\infty$ synchronization of chaotic Lur'e systems," *Int. J. Bifurc. Chaos*, vol. 7, no. 6, 1997, to be published.
[26] J. A. K. Suykens, P. F. Curran, T. Yang, J. Vandewalle, and L. O. Chua, "Nonlinear $H_\infty$ synchronization of Lur'e systems: Dynamic output feedback case," *IEEE Trans. Circuits Syst. I*, to be published.
[27] J. A. K. Suykens, P. F. Curran, and L. O. Chua, "Robust synthesis for master-slave synchronization of Lur'e systems," submitted for publication.
[28] J. A. K. Suykens, A. Huang, and L. O. Chua, "A family of $n$-scroll attractors from a generalized Chua's circuit," *Int. J. Electron. Commun. Special Issue at the Occasion of Prof. Lueder's 65th Birthday*, vol. 51, no. 3, pp. 131–138, 1997.
[29] J. A. K. Suykens and L. O. Chua, "$n$-Double scroll hypercubes in 1D-CNN's," *Int. J. Bifurc. Chaos*, vol. 7, no. 6, 1997.
[30] A. van der Schaft, "$L_2$-gain and passivity techniques in nonlinear control," *Lecture Notes in Control and Information Sciences 218.* New York: Springer-Verlag, 1996.
[31] M. Vidyasagar, *Nonlinear Systems Analysis.* Englewood Cliffs, NJ: Prentice-Hall, 1993.
[32] J. C. Willems, "Dissipative dynamical systems I: General theory. II: Linear systems with quadratic supply rates," *Archive Rational Mechan. Anal.*, vol. 45, pp. 321–343, 1972.
[33] C. W. Wu and L. O. Chua, "A unified framework for synchronization and control of dynamical systems," *Int. J. Bifurc. Chaos*, vol. 4, no. 4, pp. 979–989, 1994.
[34] C. W. Wu, T. Yang, and L. O. Chua, "On adaptive synchronization and control of nonlinear dynamical systems," *Int. J. Bifurc. Chaos*, vol. 6, no. 3, pp. 455–471, 1996.

**Johan A. K. Suykens** was born in Willebroek, Belgium, May 18, 1966. He received the degree in electromechanical engineering in 1989 and the Ph.D. degree in applied sciences in 1995, both from the Katholieke Universiteit Leuven, (K.U. Leuven) Belgium.

He is currently a post-Doctoral researcher with the ESAT-SISTA group of the K.U. Leuven. His research interests are mainly in nonlinear systems and neural networks, both theory and applications. He is author of the book *Artificial Neural Networks for Modeling and Control of Non-Linear Systems*, (Boston, MA: Kluwer Academic, 1996). He was a visiting post-Doctoral researcher with the University of California, Berkeley, in 1996.

**Paul F. Curran** (M'97) was born in Cork, Ireland, in 1965. He received the B.E. and Ph.D. degrees from University College, Dublin, Ireland, in 1987 and 1991, respectively.

In 1992, he joined the Department of Electronic and Electrical Engineering, University College. He is currently conducting research with the Nonlinear Electronics Laboratory, University of California, Berkeley, under the Fulbright Fellowship program.

**Joos Vandewalle** (F'92) was born in Kortrijk, Belgium, in August 1948. He received the electrical engineering degree and a doctorate in applied sciences, both from the Katholieke Universiteit Leuven (K.U. Leuven), Belgium, in 1971 and 1976, respectively.

From 1976 to 1978, he was Research Associate and from July 1978 to July 1979, he was a Visiting Assistant Professor both at the University of California, Berkeley. Since July 1979, he has been with the the ESAT Laboratory, K.U. Leuven, where he has been a Full Professor since 1986. In 1984, he became an Academic Consultant with the VSDM Group of IMEC (Interuniversity Microelectronics Center, Leuven). Since August 1996, he has been Chairman of the Department of Electrical Engineering, K.U. Leuven. He teaches courses in linear algebra, linear, and nonlinear system and circuit theory, signal processing, and neural networks. His research interests are mainly in mathematical system theory and its applications in circuit theory, control, signal processing, cryptography, and neural networks. He has authored or coauthored more than 200 papers in these areas. He is the coauthor (with S. Van Huffel) of the book *The Total Least Squares Problem* (Philadelphia, PA: SIAM, 1991) and the coeditor (with T. Roska) of the book *Cellular Neural Networks* (New York: Wiley, 1993).

Dr. Vandewalle is a member of the editorial board of *Journal A, a Quarterly Journal of Automatic Control* and of the *International Journal of Circuit Theory and its Applications*, and the *Journal of Circuits Systems and Computers*. From 1989 to 1991, he was an Associate Editor of the IEEE TRANSACTIONS ON CIRCUITS AND SYSTEMS in the area of nonlinear and neural networks. From 1991 to 1992, he held the Francqui chair on Artificial Neural Networks at the University of Liège, Belgium. He is one of the three coordinators of the Interdisciplinary Center for Neural Networks ICNN that was set up in 1993 in order to stimulate the interaction and cooperation among about 50 researchers on neural networks at the K.U. Leuven.

**Leon O. Chua** (S'60–M'62–SM'70–F'74) received the S.M. and Ph.D. degrees from the Massachusetts Institute of Technology, Cambridge, and the University of Illinois, Urbana, in 1961 and 1964, respectively.

After seven years on the Faculty of Purdue University, West Lafayette, IN, he moved to the University of California, Berkeley, where he is currently Professor of electrical engineering and computer sciences. He has been conferred with Honorary Doctorates by the EPFL, University of Tokushima, Technical University of Dresden, Technical University of Budapest, the University of Santiago de Compostela, and the University of Frankfurt. His research interests are in the areas of general nonlinear network and system theory. He has been a consultant to various electronic industries in the areas of nonlinear network analysis, modeling, and computer-aided design. He is the author of four books and has published extensively in the area of nonlinear networks and systems.

Professor Chua is currently a member of the Technical Committee on Nonlinear Circuits and Systems of the IEEE Circuits and Systems Society. He served as Editor of the IEEE TRANSACTIONS ON CIRCUITS AND SYSTEMS from 1973 to 1975, and as President of the IEEE Circuits and Systems Society in 1976. He is presently the Editor of the *International Journal of Bifurcation and Chaos* and a deputy Editor of the *International Journal of Circuit Theory and Applications*. He holds five U.S. patents. He is also the recipient of several awards and prizes, including the 1967 IEEE Browder J. Thompson Memorial Prize Award, the 1973 IEEE W. R. G. Baker Prize Award, the 1974 Frederick Emmons Terman Award, the 1976 Miller Research Professorship from the Miller Institute, the 1982 Senior Visiting Fellowship at Cambridge University, England, the 1982/1983 Alexander von Humboldt Senior U.S. Scientist Award at the Technical University of Munich, Germany, the 1983/1984 Visiting U.S. Scientist Award at Waseda University, Tokyo, from the Japan Society for Promotion of Science, the IEEE Centennial Medal in 1985, the 1985 Myril B. Reed Best Paper Prize, both the 1985 and 1989 IEEE Guillemin–Cauer Prizes, the Professor Invité International Award at the University of Paris-Sud from the French Ministry of Education in the fall of 1986, the 1993 Technical Achievement Award by the IEEE Circuits and Systems Society, and the 1995 M. E. Van Valkenburg Prize from the IEEE Circuits and Systems Society.

# The Role of Synchronization in Digital Communications Using Chaos—Part I: Fundamentals of Digital Communications

Géza Kolumbán, *Member, IEEE,* Michael Peter Kennedy, *Senior Member, IEEE,* and Leon O. Chua, *Fellow, IEEE*

***Abstract*— In a digital communications system, data is transmitted from one location to another by mapping bit sequences to symbols, and symbols to sample functions of analog waveforms. The analog waveform passes through a bandlimited (possibly time-varying) analog channel, where the signal is distorted and noise is added. In a conventional system the analog sample functions sent through the channel are weighted sums of one or more sinusoids; in a chaotic communications system, the sample functions are segments of chaotic waveforms. At the receiver, the symbol may be recovered by means of coherent detection, where all possible sample functions are known, or by noncoherent detection, where one or more characteristics of the sample functions are estimated. In a coherent receiver, synchronization is the most commonly used technique for recovering the sample functions from the received waveform. These sample functions are then used as reference signals for a correlator. Synchronization-based receivers have advantages over noncoherent ones in terms of noise performance and bandwidth efficiency. These advantages are lost if synchronization cannot be maintained, for example, under poor propagation conditions. In these circumstances, communication without synchronization may be preferable. The main aim of this paper is to provide a unified approach for the analysis and comparison of conventional and chaotic communications systems. In Part I, the operation of sinusoidal communications techniques is surveyed in order to clarify the role of synchronization and to classify possible demodulation methods for chaotic communications. In Part II, chaotic synchronization schemes are described in detail and proposed chaotic communications techniques are summarized. In Part III, examples of chaotic communications schemes with and without synchronization are given, and the performance of these schemes is evaluated in the context of noisy, bandlimited channels.**

***Index Terms*— Chaos, chaotic communications, chaotic synchronization.**

Manuscript received February 10, 1997; revised June 18, 1997. This work was supported in part by the National Scientific Research Foundation of Hungary (OTKA) under Grant T-020522, by the Information Technologies RTD Programme of the European Commission (Esprit Project 21103 INSPECT), and by the U.S. Office of Naval Research under Grant N00014-96-1-0753. This paper was recommended by Guest Editor M. J. Ogorzalek.

G. Kolumbán is with the Department of Measurement and Instrument Engineering, Technical University of Budapest, H-1521 Budapest, Hungary (e-mail: kolumban@mmt.bme.hu).

M. P. Kennedy is with the Department of Electronic and Electrical Engineering, University College Dublin, Dublin 4, Ireland (e-mail: Peter.Kennedy@ucd.ie).

L. O. Chua is with the Department of Electrical Engineering and Computer Sciences, University of California, Berkeley, CA 94720 USA (e-mail: chua@diva.eecs.berkeley.edu).

Publisher Item Identifier S 1057-7122(97)07316-9.

## I. Introduction

THE observation by Pecora and Carroll [1] that two chaotic systems can be synchronized has generated tremendous interest in transmitting information from one location to another using a wideband chaotic signal.

Many modern communications applications, such as mobile or indoor radio, are susceptible to multipath propagation effects arising from interaction between signals at the receiver which travel along different propagation paths. By contrast with a conventional digital modulation scheme, where the transmitted symbols are mapped to a finite set of periodic waveform segments for transmission, every transmitted symbol in a chaotic modulation scheme produces a different nonperiodic waveform segment. Because the cross correlations between segments of a chaotic waveform are lower than between pieces of periodic waveforms, chaotic modulation ought to offer better performance under multipath propagation conditions. Thus, chaotic modulation offers a potentially simple solution for robust wideband communications.

The chaotic communication schemes which have been proposed to date have been developed using heuristic arguments that make it impossible to compare them with conventional communications systems. Using the language of communications theory, this paper extends the basis function approach to proposed chaotic communications systems in order to provide a unified framework in which to compare and contrast conventional and chaotic communications techniques.

The principal difference between conventional and chaotic systems is that segments of chaotic waveforms, rather than sinusoids, are used as basis functions in chaotic communications. Because of the nonperiodic property of chaotic signals, there is a fundamental difference between conventional and chaotic systems. The parameters of the received chaotic waveform that are required in order to recover the transmitted information must be estimated from sample functions of finite length. Even in the noise-free case, this estimation has a nonzero variance; therefore, the symbol duration cannot be reduced below a certain lower bound.

Most of the research in the field of chaotic communications to date has assumed that the transmitter is connected to the receiver by an ideal channel [2]. Since the principal source

1057–7122/97$10.00 © 1997 IEEE

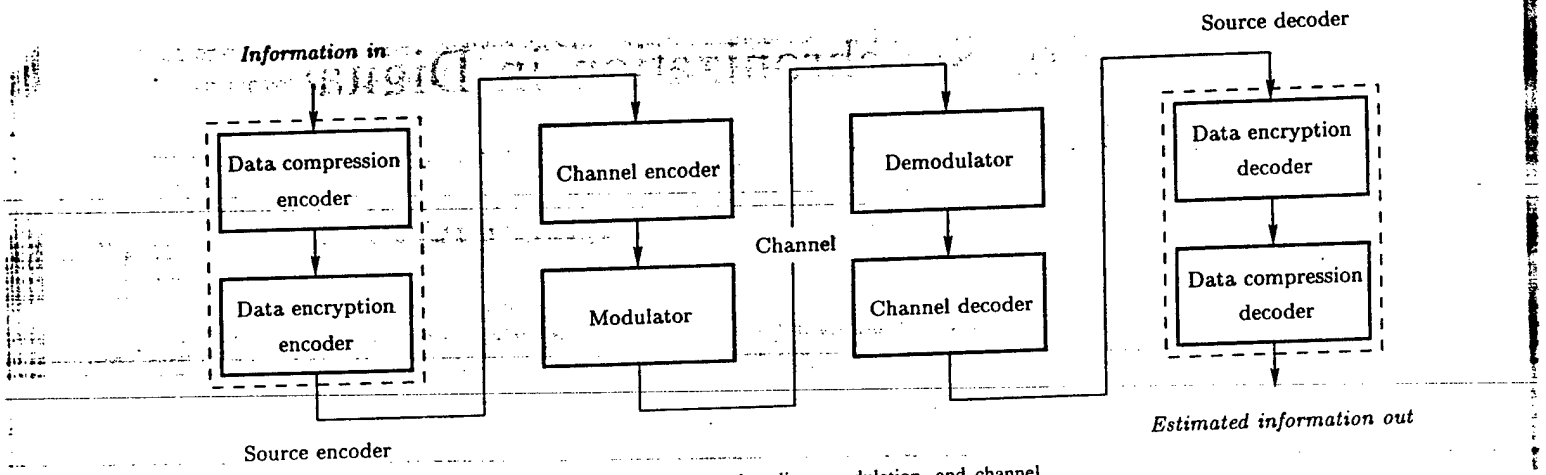


Fig. 1. Digital communications system showing source and channel coding, modulation, and channel.

of errors in a digital communications system is the channel, it is impossible to quantify the performance of a chaotic modulation technique by assuming an ideal channel. A realistic channel model must at least include additive noise and linear filtering.

Recent studies of chaotic synchronization, where significant noise and filtering are introduced in the channel, suggest that synchronization of chaos is not yet sufficiently robust for practical applications in communications [3].

In this three-part tutorial paper, we explain the role of synchronization in a digital communications system and evaluate the performance of chaotic modulation schemes.

In Section II of this part, we describe the major components of a digital communications system and show that the primary source of errors is the analog channel. We explain why a realistic channel model must include at least additive white Gaussian noise and band-limiting. We review the notion of bit error rate as a way of comparing digital modulation schemes.

In Section III, we show how a signal set may be constructed from a limited set of orthonormal basis functions and explain the advantages of this choice.

In Section IV, we show that the primary motivation for carrier synchronization is to permit coherent detection, the benefits of which are improved noise performance and bandwidth efficiency.

Under poor propagation conditions, where synchronization cannot be maintained, the advantages of coherent detection are lost. In such circumstances, a noncoherent receiver offers a more robust and less complex solution, as shown in Section V.

The potential advantages of using a chaotic carrier signal are explained in Section VI by highlighting the disadvantages of narrowband (sinusoidal) communications when propagation conditions are poor.

In Part II of the paper, we consider the state-of-the-art in synchronization of chaotic systems in the context of digital communications; in addition, proposed chaotic communications techniques are surveyed.

In Part III, performance targets for chaotic communications techniques are summarized and examples (CSK with synchronization, noncoherent CSK and DCSK correlation receiver) are given. Finally, the performance of these systems is evaluated in the context of a noisy and bandlimited channel.

## II. Overview of Digital Communications

### A. Basic Structure of a Digital Communications System

Communication system theory is concerned with the transmission of information from a source to a receiver through a channel [4], [5].

The goal of a digital communications system, shown schematically in Fig. 1, is to convey information from a digital information source (such as a computer, digitized speech or video, etc.) to a receiver as effectively as possible. This is accomplished by mapping the digital information to a sequence of symbols which vary some properties of an analog electromagnetic wave called the carrier. This process is called *modulation*. Modulation is always necessary because all practical telecommunications channels are bandlimited analog systems which cannot transmit digital signals directly.

At the receiver, the signal to be received is selected by a channel filter, demodulated, interpreted, and the information is recovered.

Conversion of the digital information stream to an analog signal for transmission may be accompanied by encryption and coding to add end-to-end security, data compression, and error-correction capability.

Built-in error-correction capability is required because real channels distort analog signals by a variety of linear and nonlinear mechanisms: attenuation, dispersion, intersymbol interference, intermodulation, PM/AM and AM/PM conversions, noise, interference, multipath effects, etc.

A *channel encoder* introduces algorithmic redundancy into the transmitted symbol sequence that can be used to reduce the probability of incorrect decisions at the receiver.

*Modulation* is the process by which a symbol is transformed into an analog waveform that is suitable for transmission. Common digital modulation schemes include *amplitude shift keying* (ASK), *phase shift keying* (PSK), *frequency shift keying* (FSK), *continuous phase modulation* (CPM), and *amplitude phase keying* (APK), where a one-to-one correspondence is

established between amplitudes, phases, frequencies, phase and phase transitions, and amplitudes and phases, respectively, of a sinusoidal carrier and the symbols.

The *channel* is the physical medium through which the information-carrying analog waveform passes as it travels between the transmitter and receiver.

The transmitted signal is invariably corrupted in the channel. Hence, the receiver never receives exactly what was transmitted. The role of the *demodulator* in the receiver is to produce from the received corrupted analog signal an estimate of the transmitted symbol sequence. The role of the *channel decoder* is to reconstruct the original bit stream, i.e., the information, from the estimated symbol sequence. Because of disturbances in real communications channels, error-free transmission is never possible.

Nonlinear dynamics has potential applications in several of the building blocks of a digital communications system: data compression, encryption, and modulation [6]. Data compression and encryption are potentially reversible, error-free digital processes. By contrast, the transmission of an analog signal through a channel and its subsequent interpretation as a stream of digital data are inherently error-prone.

In this paper, we focus on the application of chaos as a modulation scheme. In order to compare the use of a chaotic carrier signal with that of a conventional sinusoidal carrier, we must consider a realistic channel model and quantify the performance of each chaotic modulation scheme using this channel.

In this section, we introduce the minimum requirements for a realistic channel model and the performance measures by which we will compare conventional and chaotic modulation schemes.

### *B. Minimum Requirements for a Channel Model*

The definition of the telecommunications channel depends on the goal of the analysis performed. In the strict sense, the channel is the physical medium that carries the signal from the transmitter to the receiver. If the performance of a modulation scheme has to be evaluated, then the channel model should contain everything from the modulator output to the demodulator input. Even if the physical medium can be modeled by a constant attenuation, the following effects have to be taken into account:

1) In order to get maximum power transfer, the input and output impedances of the circuits of a telecommunications system are matched. This is why thermal noise modeled as *additive white Gaussian noise* (AWGN)[1] is *always present* at the input to an RF receiver.
2) The bandwidth of the channel has to be limited by a so-called channel (selection) filter in order to suppress the unwanted input signals that are always present at the input of a radio receiver and that cause interference due to the nonlinearities of the receiver.

[1]The definition for the Gaussian process is given in [4] and [7]. The autocorrelation of white noise is a Dirac delta function multiplied by $N_0/2$ and located at $\tau = 0$, where $N_0$ is the power spectral density of the noise.

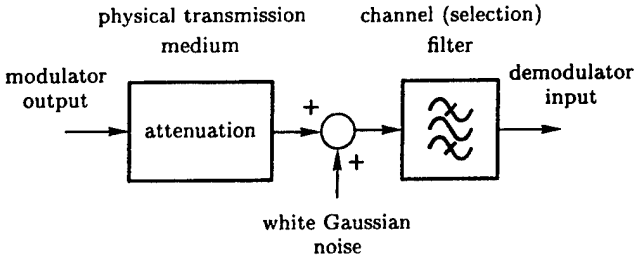


Fig. 2. Model of an additive-white-Gaussian-noise channel including the frequency selectivity of the receiver.

The simplest channel model that can be justified when evaluating the performance of a modulation scheme is shown in Fig. 2. Note that the channel filter is used only to select the desired transmission frequency band at the receiver and not to model any frequency dependence of the physical transmission medium. If, in addition to noise and attenuation, other nonidealities of the physical transmission medium (such as frequency dependence, selective fading, interferences, etc.) are to be taken into account, then these should be included in the first block in Fig. 2.

In the model shown in Fig. 2, we have assumed that the received signal is corrupted by AWGN. In a real telecommunications system, the noise may not be exactly white or Gaussian. The reasons for assuming AWGN are that

1) it makes calculations tractable;
2) thermal noise, which is of this form, is dominant in many practical communications systems; and
3) experience has shown that the relative performance of different modulation schemes determined using the AWGN channel model remains valid under real channel conditions, i.e., a scheme showing better results than another for the AWGN model also performs better under real conditions [4], [5].

### *C. Performance Measures*

The primary source of errors in a digital communications system is the analog channel. The fundamental problem of digital communications is to maximize the effectiveness of transmission through this channel.

The performance of a digital communications system is measured in terms of the *bit error rate* (BER) at the receiver. In general, this depends on the coding scheme, the type of waveform used, transmitter power, channel characteristics, and demodulation scheme. The conventional graphical representation of performance in a linear channel with AWGN, depicted in Fig. 3, shows BER versus $E_b/N_0$, where $E_b$ is the energy per bit and $N_0$ is the power spectral density of the noise introduced in the channel.

For a given background noise level, the BER may be reduced by increasing the energy associated with each bit, either by transmitting with higher power or for a longer period per bit. The challenge in digital communications is to achieve a specified BER with *minimum energy per bit*. A further consideration is *bandwidth efficiency*, defined as the ratio of data rate to channel bandwidth [4].

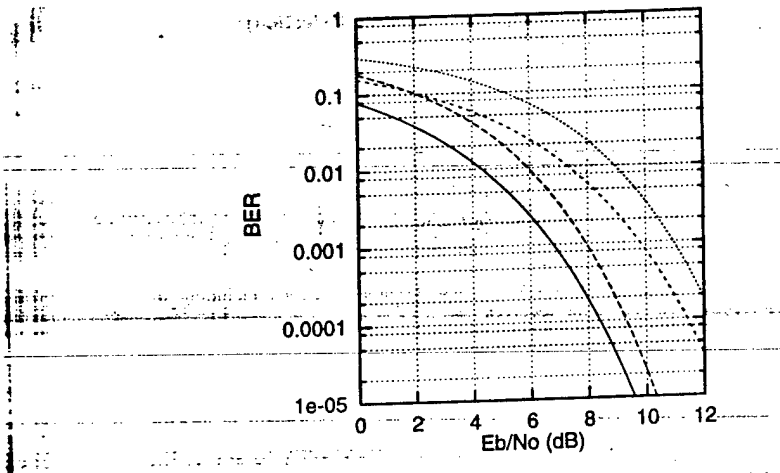


Fig. 3. Comparison of the noise performances of digital modulation schemes. From left to right: coherent binary phase shift keying (solid), differential phase shift keying (long dash), coherent (short dash) and noncoherent (dot) binary orthogonal frequency shift keying.

## III. Factors Affecting the Choice of Modulation Scheme

For a given BER and background noise level, the main goal in the design of a digital communications system is to minimize the energy required for the transmission of each bit. The second goal is the efficient utilization of channel bandwidth. These design requirements affect the choice of the modulation scheme to be used.

While modulation is a relatively straightforward process of mapping symbols to analog waveforms (elements of the so-called "signal set") in a deterministic manner, demodulation, which is concerned with mapping samples of a corrupted stochastic analog signal back to symbols, is a more difficult and error-prone task.

In this section, we consider ways of designing the signal set to maximize the bandwidth efficiency and minimize the probability of making incorrect decisions at the receiver.

### A. M-ary Modulation Schemes for Bandwidth Efficiency

In binary modulation schemes, where the bit stream is mapped to two possible signals, bandwidth efficiency is poor since the required channel bandwidth is proportional to the bit rate.

The bandwidth efficiency can be improved by using $M$-ary modulation schemes, where the signal set contains $M$ possible signals. In almost all applications, the number of possible signals $M$ is $2^n$, where $n$ is an integer. The symbol duration is given by $T = nT_b$, where $T_b$ is the bit duration.

In conventional digital communications systems, the elements of the signal set are sinusoids, where, for example, the amplitude, phase or frequency of the transmitted signal is varied among $M$ discrete values in the case of $M$-ary ASK (MASK), $M$-ary PSK (MPSK) and $M$-ary FSK (MFSK), respectively. In $M$-ary APK (MAPK), of which $M$-ary *quadrature amplitude modulation* (QAM) [8] is an example, both the amplitude and the phase of the reference sinusoid are varied.

In $M$-ary modulation schemes, one *symbol* is transmitted for every $n$ bits in the data stream. In particular, the incoming bit stream is transformed into a sequence of symbols and every symbol is mapped to an element of the signal set. Since symbols are transmitted once per $n$ bits, instead of once per bit, the required channel bandwidth is proportional to the *symbol rate* rather than the *bit rate* (except in the case of MFSK [4]), and the bandwidth efficiency is improved considerably.

### B. Orthonormal Basis Functions and Correlation Receivers

A coherent receiver performs demodulation by comparing the incoming signal with *all* elements of the signal set. If a linear AWGN channel model is assumed, the most effective way to accomplish this is by correlating the received signal with every element of the signal set and selecting the one with the largest correlation.

Therefore, a coherent receiver must in principle know all $M$ elements of the signal set. Since $M$ can be as large as 256 in modern modulation schemes, this seems like a difficult task. However, the large number of signals which must be known at the receiver can be reduced by introducing the idea of orthonormal basis functions.

*1) Orthonormal Basis Functions:* Let $s_i(t), i = 1, 2, \cdots, M$ denote the elements of the signal set. Our goal is to minimize the number of special signals, called *basis functions*, that have to be known at the receiver. Let the elements of the signal set be represented as a linear combination of $N$ real-valued orthonormal basis functions

$$g_j(t), \quad j = 1, 2, \cdots, N,$$

where

$$\int_0^T g_i(t)\, g_j(t)\, dt = \begin{cases} 1, & \text{if } i = j \\ 0, & \text{elsewhere.} \end{cases}$$

Then the elements of the signal set can be expressed as a linear combination of basis functions

$$s_i(t) = \sum_{j=1}^{N} s_{ij} g_j(t), \quad \begin{cases} 0 \le t \le T \\ i = 1, 2, \cdots, M \end{cases} \tag{1}$$

where $N \le M$. In conventional digital telecommunications systems, sinusoidal basis functions are used; the most common situation involves a quadrature pair of sinusoids.

*2) Signal Set Generation:* The coefficient $s_{ij}$ in (1) may be thought of as the $j$th element of an $N$-dimensional *signal vector* $\boldsymbol{s}_i$. The incoming bit stream is first transformed into a symbol sequence; the elements of the signal vector are then determined from the symbols. The signals $s_i(t)$ to be transmitted are generated as a weighted sum of basis functions, as given by (1).

*3) Recovery of the Signal Vector by Correlation:* Because the basis functions are orthonormal, the elements of the signal vector can be recovered from the elements of the signal set, i.e., from the received signal, if every basis function is known in the receiver. In particular

$$s_{ij} = \int_0^T s_i(t)\, g_j(t)\, dt, \quad \begin{cases} i = 1, 2, \cdots, M \\ j = 1, 2, \cdots, N. \end{cases} \tag{2}$$

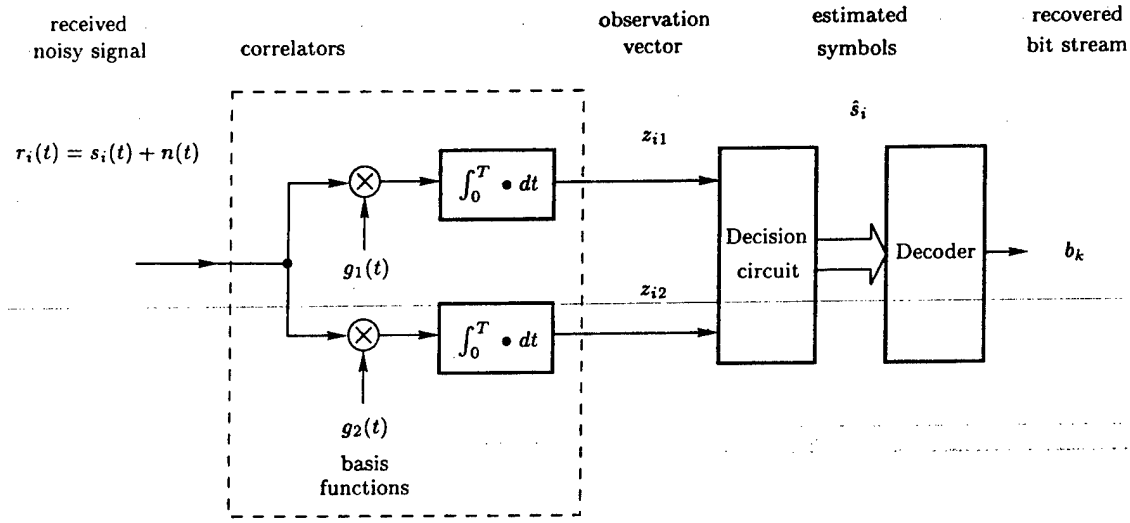


Fig. 4. Block diagram of correlation receiver for $N = 2$.

Thus, a demodulator consists of a bank of $N$ correlators, each of which recovers the weight $s_{ij}$ of basis function $g_j(t)$. Since there exists a one-to-one mapping between signal vectors and symbols, the transmitted symbols can be recovered by post-processing the outputs of the correlators, and the demodulated bit stream can thus be regenerated.

### C. Orthonormal Basis Functions for Bandwidth Efficiency

The main advantage of using orthonormal basis functions is that a huge signal set can be generated from a small number of basis functions. Typically, a pair of quadrature sinusoidal signals (a cosine and a sine) is used as the set of basis functions. Since quadrature sinusoidal signals can be generated using a simple phase shifter, it is sufficient to know (or recover) only one sinusoidal signal in the receiver.

An example showing modulator and demodulator circuits for binary PSK (BPSK) is given in Section V-A.

## IV. Detection of a Single Symbol in Noise: The Basic Receiver Configurations

The receiver must recognize the symbols sent via the channel in order to recover the information which has been transmitted. For the sake of simplicity, only the detection of a single isolated symbol is considered in this section, the effect of *intersymbol interference* (ISI), i.e., the interference between successive symbols is neglected [9].

Our goal is to minimize the average probability of symbol errors, i.e., to develop an optimum receiver configuration. For an AWGN channel and for the case when all symbols to be transmitted are equally likely, *maximum likelihood* (ML) detection has to be used in order to get an optimum receiver [8]. The ML detection method can be implemented by either correlation or matched filter receivers [4].

In this section, we demonstrate the connection between correlation and matched filter receivers, and consider the relative merits of coherent and noncoherent detection.

### A. Correlation and Matched Filter Receivers

*1) Correlation Receiver:* Equation (2) shows how the signal vector can be recovered from a received signal by correlators if the basis functions $g_j(t)$ are orthonormal and are known at the receiver. Note that, in addition to the basis functions, both the symbol duration $T$ and the initial time instant of symbol transmission have to be known at the receiver. The latter data are called *timing information*. The idea suggested by (2) is exploited in the correlation receiver shown in Fig. 4.

In any practical telecommunications system, the received signal is corrupted by noise, i.e., the input to each of the correlators is the sum of the transmitted signal $s_i(t)$ and a sample function $n(t)$ of a zero-mean, stationary, white, Gaussian noise process. The elements of the signal vector can still be estimated using correlators, although the estimates may differ from their nominal values, due to corruption in the channel.

The outputs of the correlators, called the *observation vector*, are the inputs of a decision circuit. The decision circuit applies the ML detection method, i.e., it chooses the signal vector from among all the possibilities that is the closest to the observation vector. Estimates of the symbols are determined from the signal vector and finally the demodulated bit stream is recovered from the estimated symbol sequence.

Note that in a correlation receiver *all the basis functions* and *the timing information* are required; these must be recovered from the (noisy) received signal.

*2) Matched Filter Receiver:* The observation vector can be also generated by a set of *matched filters* [4]. In a matched filter receiver a bank of matched filters is substituted for the correlators in Fig. 4. In this case the basis functions are stored locally as the impulse responses of the matched filters, i.e., only the timing information must be recovered from the received signal.

### B. Coherent and Noncoherent Receivers

*1) Coherent Receivers:* Receivers in which exact copies of all the basis functions are known are called *coherent receivers.*

In practice, coherent correlation receivers are used almost exclusively to demodulate ASK, PSK, and its special case of *quadrature phase shift keying* (QPSK), MPSK, and $M$-ary QAM (MQAM) signals.

The required impulse response of a matched filter can at best be approximated by a physically realizable analog filter. Any deviation from the ideal impulse response results in a large degradation of performance. Therefore, coherent matched filter receivers are not used in radio communications.

*2) Noncoherent Receivers:* In applications where the propagation conditions are poor, the basis functions $g_j(t)$ cannot be recovered from the received signal. In these cases, the conventional solution is to use MFSK ($M \geq 2$) modulation and a noncoherent receiver.

The basis functions $g_j(t)$ or the elements $s_i(t)$ of the signal set are not known in a noncoherent receiver, but one or more robust characteristics of $s_i(t)$, $i = 1, 2, \cdots, M$ can be determined. Demodulation is performed by evaluating one or more selected characteristics of the received signal.

For example, $M$ different *signaling frequencies* are used in MFSK. In a noncoherent FSK receiver, a bank of bandpass filters is applied to recognize the different signaling frequencies. The observation vector is generated by envelope detectors and the decision circuit simply selects the "largest" element of the observation vector [4].

### C. Relative Merits of Coherent and Noncoherent Receivers

It is often claimed that the main advantage of coherent receivers over noncoherent ones is that their performance in the presence of additive noise in the channel is better than that of their noncoherent counterparts. Let us estimate the size of this advantage for the selected application domain: digital communications.

In a practical digital communications system, communication is not possible if the BER becomes worse than $10^{-3}$ or $10^{-2}$, so we only consider operation below this range. For example, the average value of "raw" BER for terrestrial microwave radio systems varies from $10^{-7}$ to $10^{-6}$; with error correction, this can be reduced to below $10^{-9}$ [9].

The noise performance of coherent and noncoherent binary FSK receivers is shown in Fig. 3. At $E_b/N_0 = 10^{-2}$, the $E_b/N_0$ required by the noncoherent FSK receiver is only 1.6 dB greater than the corresponding value for the coherent one. Moreover, at high values of $E_b/N_0$, noncoherent FSK receivers perform almost as well as coherent ones for the same $E_b/N_0$.

The real advantage of the coherent technique is that huge signal sets can be generated by means of very few orthonormal basis functions. For example, in terrestrial digital microwave radio systems, 256 signals are typically generated using a pair of quadrature sinusoidal signals. This huge signal set results in excellent *bandwidth efficiency*. Moreover, the receiver must recover *just one* sinusoidal signal from the incoming signal.

For their part, noncoherent techniques offer two advantages over coherent detection:

1) When *propagation conditions are poor*, the basis functions cannot be recovered from the received signal because $r_i(t)$ differs too much from $s_i(t)$. In this case, a noncoherent receiver is the only possible solution.
2) Noncoherent receivers can, in principle, be implemented with *very simple circuitry*, because the basis functions do not need to be recovered.

## V. The Role of Synchronization in Digital Communications

In this section, we consider two fundamental synchronization problems: *timing recovery*, which is an essential part of digital communications, and *carrier recovery*, which is necessary only for coherent detection. We illustrate these issues in the context of BPSK.

### A. Example: Coherent Detection of BPSK

The block diagram of a coherent BPSK transceiver can be developed from (1) and Fig. 4. As shown in Fig. 5, the most important operations performed in the receiver are

1) recovery of the basis function $\hat{g}_1(t)$ and timing information;
2) determination of the elements $z_{ij}$ of the observation vector; and
3) decision making.

In the case of BPSK, two symbols are used to transmit the bit stream $b_k$. Thus, the signal set contains two sinusoidal signals $s_1(t)$ and $s_2(t)$. The binary symbols 0 and 1 are mapped to the signals

$$s_1(t) = \sqrt{\frac{2E_b}{T}} \cos(\omega_c t)$$

and

$$s_2(t) = -\sqrt{\frac{2E_b}{T}} \cos(\omega_c t)$$

respectively, where $0 \leq t \leq T$, $T = T_b$ and $E_b$ is the transmitted energy per bit.

To simplify the recovery of the basis function, each transmitted symbol is designed to contain an integral number of cycles of the sinusoidal carrier wave. Given that there is just one basis function of unit energy

$$g_1(t) = \sqrt{\frac{2}{T_b}} \cos(\omega_c t), \quad 0 \leq t < T$$

we recover the elements of the signal vector from (2) as

$$s_{11} = +\sqrt{E_b}$$

and

$$s_{21} = -\sqrt{E_b}.$$

Let us assume equally likely symbols; then ML detection yields an optimum receiver [8]. The decision rule is simply to make the decision in favor of symbol 0 if the received signal is "closer" to $s_1(t)$, i.e., if the output of the correlator is greater

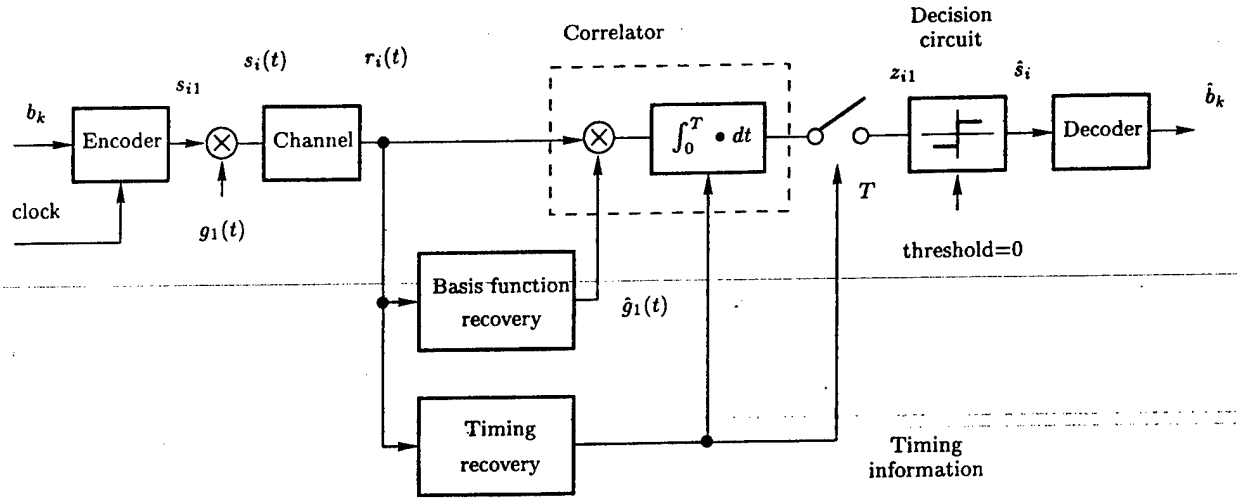


Fig. 5. Block diagram of a coherent BPSK receiver.

than zero at the decision time instant. If the observation signal $z_{i1}$ is less than zero, then the receiver decides that a symbol 1 has been transmitted. The decision circuit is simply a level comparator with zero threshold.

### B. Carrier Recovery and Timing Recovery

*1) Carrier Recovery and the Need for Synchronization in Coherent Detection:* In general, coherent reception requires knowledge of the basis functions at the receiver. Because matched filter receivers cannot be implemented in the analog signal domain, only correlation receivers can be used for coherent detection, and synchronization must be used to recover the basis functions.

In the special case of sinusoidal basis functions, knowledge of both the frequency and phase of a carrier is required. The basis functions are typically recovered from the received noisy signal by means of a suppressed carrier *phase-locked loop* (PLL). In conventional systems, estimation of the frequency and phase of the carrier is called *carrier recovery* [9].

*2) Timing Recovery and the Need for Symbol Synchronization in Digital Communications:* A second and more important type of synchronization also arises in digital communications. In any practical system, not only an isolated single symbol, but a sequence of symbols, has to be transmitted. To perform demodulation, the receiver has to know precisely the time instants at which the modulation can change its state. That is, it has to know the start and stop times of the individual symbols in order to assign the decision time instants and to determine the time instants when the initial conditions of the correlators have to be reset to zero in the receiver. Determination of these time instants is called *timing recovery* or *symbol synchronization.*

In contrast with carrier recovery, which is an optional step that is required only by coherent receivers, timing recovery is a *necessary* function in digital communications. The decision times at the receiver must be aligned in time (synchronized) with those corresponding to the ends of symbol intervals $T$ at the transmitter. Symbol synchronization must be achieved as soon as possible after transmission begins, and must be maintained throughout the transmission.

This paper is aimed at providing a clear exposition of the important issues in both conventional and chaotic modulation/demodulation techniques. Although symbol synchronization has to be solved in every digital communications system, it belongs to the decision circuit and not to the demodulation process. Therefore, the details of the timing recovery problem are not discussed in this paper. The interested reader can find excellent expositions of timing recovery in [8] and [11], for example.

In the next section, we discuss the advantages and disadvantages of synchronization for basis function recovery in coherent receivers.

### C. Advantages and Disadvantages of Synchronization

The main advantage of synchronization is that it makes the implementation of coherent receivers possible. As mentioned in Section IV-C, the most significant feature of a coherent receiver when used with a sinusoidal carrier is that by recovering just one signal, the carrier, (and regenerating the quadrature basis function by means of a simple phase-shifter) a pair of orthonormal basis functions can be generated and therefore a huge signal set can be used (256-QAM, for example). In addition, a coherent receiver has marginally better noise performance than its noncoherent counterpart.

However, there are significant costs associated with synchronization, in terms of synchronization time, circuit complexity, and severe penalties associated with loss of synchronization. In this section, we discuss these issues.

*1) Costs Associated with Achieving Synchronization in a Coherent Receiver:* In conventional digital communications systems, various types of PLL's are used to perform synchronization [10].

Two basic operation modes have to be distinguished for a PLL. Under normal operating conditions, the phase-locked condition has been achieved and is maintained. The PLL

simply follows the phase of an incoming signal; this is called the *tracking mode*.

Before the phase-locked condition is achieved, the PLL operates in a highly nonlinear *capture mode*. The time required for the PLL to achieve the phase-locked condition is called the *pull-in time*. The *transient time*, which is associated with the tracking mode, is always significantly shorter than the pull-in time.

In a digital communications system where the synchronization is lost at the beginning of every new symbol, the received symbol can be estimated from the noisy received signal only after the basis functions have been recovered, i.e., only after the phase-locked condition has been achieved. In this case, the total detection time associated with each bit is the sum of the pull-in time and the estimation time. In particular, a long pull-in time results in a very low symbol rate. This is why *synchronization is always maintained* in the carrier recovery circuits of conventional digital communications systems.

*2) Penalties for Failing to Achieve Synchronization in a Coherent Receiver:* The block diagram of a coherent correlation receiver is shown in Fig. 4. The received signal is always a stochastic process due to additive channel noise. The observation vector, i.e., the output of the correlators, is an estimation, where the mean value of estimation depends on the bit energy and the "goodness" of recovery of the basis functions. In conventional receivers, the variance of this estimation is determined by the noise spectral density $N_0$ [4]. The probability of error, i.e., the probability of making wrong decisions, depends on the mean value and variance of estimation. The main disadvantage of synchronization follows from the sensitivity of noise performance to the "goodness" of recovery of the basis functions.

The most serious problem is caused by the cycle slips in PLL's used for recovering a suppressed carrier. Due to the noise, the phase error is a random process in the PLL. If the variance of the phase error is large, cycle slips appear with high probability due to the periodic characteristic of the phase detector [12]. This means that the VCO phase, i.e., the phase of the recovered carrier, slips one or several cycles with respect to the reference phase. Every cycle slip results in a symbol error. For high *signal-to-noise ratio* (SNR), the probability of cycle slips is low, but it increases steeply with increasing noise power. This phenomenon results in a large degradation in noise performance.

Even if the physical transmission medium can be characterized by a pure attenuation, a small error in the phase of the recovered carrier may be present due to nonideal properties of the synchronization circuit. This error generally causes a large degradation in the noise performance of a coherent receiver [5], [13].

A real telecommunications channel always causes some transformation of the basis functions. This problem is especially hard to overcome in coherent receivers if the transmission medium is time-varying. The time-dependent channel transformation requires adaptive control of the recovered basis functions. This can be accomplished only by means of a wideband PLL circuit. However, in this case the recovered basis functions are corrupted by the channel noise passed by the PLL transfer function. This also results in a large degradation in the system's noise performance.

Disturbances and interferences passed by the channel filter may cause a transient in the carrier recovery circuit. The result of this transient is that the recovered basis functions deviate from their ideal values. This also results in performance degradation.

Synchronization can also be lost from time to time due to deep and/or selective fading [14]. Loss of synchronization automatically initiates a pull-in process which means that all symbols received during the pull-in time are lost. Once again, the result is a degradation in BER.

The conclusion is that coherent receivers exploiting synchronization offers the best system performance *if synchronization can be maintained.* However, they do not offer optimum performance if the SNR is low, the propagation conditions are poor, the properties of the channel are time-varying, or if the probability of deep fading is relatively high. In these cases, a more robust modulation scheme such as FSK with a noncoherent receiver must be used.

A further disadvantage of a coherent receiver from an implementation point of view is that it generally requires more complicated circuitry than its noncoherent counterpart.

## VI. Why Use a Chaotic Carrier?

In the previous sections, we have shown that the use of sinusoidal signals as basis functions in conventional digital modulation techniques offers excellent bandwidth efficiency. Moreover, these basis functions can be reconstructed easily by recovering a single sinusoidal carrier at the receiver. Why, then, is it necessary even to consider a modulation scheme which uses anything other than a sinusoidal carrier?

When a sinusoidal carrier is used, the transmitted power is concentrated in a narrow band, thereby resulting in high power spectral density. This has a number of serious drawbacks.

1) Multipath propagation is always present in many important radio applications such as mobile telephony and wireless LAN. It results in very high attenuation over narrow frequency bands. This means that the SNR may become very low or even a dropout may occur in a narrowband communications system. Low SNR results in symbol errors due to the cycle slips in the carrier recovery circuit. The extremely high attenuation causes not only a dropout in reception, but also loss of synchronization. Recall that when synchronization is lost in a coherent receiver, all symbols transmitted during the pull-in time of the receiver's synchronization circuitry are also lost.
2) Due to the high transmitted power spectral density narrowband communications cause *high levels of interference* with other users. Therefore, they are not suitable for unlicensed radio applications.
3) Narrowband signals are sensitive to narrowband interference.

4) Because of the high transmitted power spectral density, the probability of interception of narrowband communications is high.
5) The reception of messages by an unauthorized receiver is very simple because limited *a priori* knowledge is required for demodulation.

The difficulties summarized above can be overcome by using *spread-spectrum* (SS) techniques, where, in addition to a conventional digital modulation scheme, a pseudorandom spreading sequence is used to spread the spectrum of the transmitted signal [14]. The benefits of spreading can be achieved only if the pseudorandom sequences in the transmitter and receiver are *synchronized*.

Spread-spectrum communications using spreading sequences has two major disadvantages: it is not possible to achieve and maintain synchronization under poor propagation conditions, and the spreading and despreading processes require additional circuitry.

Chaotic signals are wideband signals that can be generated using very simple circuitry. A potentially cost-effective solution for wideband communications is to use a wideband chaotic carrier. In this approach, sample functions of chaotic waveforms are used as basis functions or as the elements of the signal set.

## VII. Concluding Remarks

Much of the recent research in chaotic communications has focused on synchronization. Our objectives in this paper are

1) to provide a theoretical context in which the performance of modulation schemes based on chaotic synchronization can be evaluated;
2) to develop a unified framework for discussing and comparing conventional and chaotic communications systems; and
3) to highlight the special problems that arise when chaotic basis functions are used.

In Section II, we described the major components of a digital communications system and emphasized that the primary source of errors is the analog channel. We identified the minimum requirements for a realistic channel model (additive white Gaussian noise and band-limiting) and illustrated the performance measures by which modulation schemes are judged.

The signal set in a conventional digital communications system is constructed from orthonormal sinusoidal basis functions. In Section III, we explained the advantages of this choice in terms of bandwidth efficiency and easy recovery of basis functions.

In Section IV, we demonstrated the equivalence of correlation and matched filter receivers and explained the ideas of coherent and noncoherent detection. The primary motivation for carrier synchronization is to permit coherent detection. Coherent detection, in turn, offers greater potential bandwidth efficiency.

Under poor propagation conditions, where synchronization cannot be maintained, the advantages of coherent detection are lost. In such circumstances, a noncoherent receiver offers a more robust and less complex solution.

Synchronization can be exploited in two ways in a digital communications system. Synchronization is required for timing recovery to establish the starts and ends of symbols in the transmitted sequence. If coherent detection is used, synchronization is also required to recover the carrier, typically by means of a PLL. In Section V, we showed when and how coherent detection fails.

We motivated the use of a chaotic carrier signal in Section VI by highlighting the disadvantages of narrowband communications when propagation conditions are poor.

In Part II of the paper, we consider the state-of-the-art in synchronization of chaotic systems in the context of digital communications, and current chaotic communications techniques are surveyed.

In Part III, performance targets for chaotic communications techniques are summarized and examples (CSK with synchronization, noncoherent CSK and DCSK correlation receiver) are given. Finally, the performance of these systems is evaluated in the context of a noisy and bandlimited channel.

## Acknowledgment

The authors have benefited significantly from extensive interaction with their colleagues in the Chaos Communications Collective, particularly during the "First Little Workshop on Spread Spectrum Communication and Chaos" at the EPFL, Lausanne, on April 2, 1996, and the "Second Little Workshop on Spread Spectrum Communication and Chaos" at UC Berkeley on August 7, 1996. Last, but not least, the authors wish to thank the reviewers for their constructive criticism of this paper.

## References

[1] L. M. Pecora and T. L. Carroll, "Synchronization in chaotic systems," *Phys. Rev. Lett.*, vol. 64, no. 8, pp. 821–824, 1990.
[2] M. Hasler, "Engineering chaos for secure communication systems," *Phil. Trans. R. Soc. Lond. A*, vol. 353, no. 1701, Oct. 16, 1995, pp. 115–126.
[3] G. Kolumbán, H. Dedieu, J. Schweizer, J. Ennitis, and B. Vizvári, "Performance evaluation and comparison of chaos communications systems," in *Proc. 4th Int. Workshop in Nonlinear Dynam. Electron. Syst.*, Seville, Spain, June 27–28, 1996, pp. 105–110.
[4] S. S. Haykin, *Communication Systems*, 3rd ed. New York: Wiley, 1994.
[5] J. G. Proakis, *Digital Communications*. Singapore: McGraw-Hill, 1983.
[6] M. P. Kennedy, "Communicating with chaos: State of the art and engineering challenges," in *Proc. 4th Int. Workshop in Nonlinear Dynam. Electron. Syst.*, Seville, Spain, June 27–28, 1996, pp. 1–8.
[7] J. S. Bendat and A. G. Piersol, *Measurement and Analysis of Random Data*, 2nd ed. New York: Wiley, 1996.
[8] E. A. Lee and D. G. Messerschmitt, *Digital Communications*, 2nd ed. Boston, MA: Kluwer Academic, 1993.
[9] I. Frigyes, Z. Szabó, and P. Ványai, *Digital Microwave Transmission*. Amsterdam, The Netherlands: Elsevier Science, 1989.
[10] F. M. Gardner, *Phaselock Techniques*, 2nd ed. New York: Wiley, 1979.
[11] M. K. Simon, S. M. Hinedi, and W. C. Lindsey, *Digital Communication Techniques: Signal Design and Detection*. Englewood Cliffs, NJ: PTR Prentice-Hall, 1995
[12] G. Ascheid and H. Meyr, "Cycle slips in phase-locked loops: A tutorial survey," *IEEE Trans. Commun.*, vol. COM-30, pp. 2228–2241, Oct. 1982.
[13] R. W. Lucky, J. Salz, and E. J. Weldon, *Principles of Data Communication*. New York: McGraw-Hill, 1968.
[14] R. C. Dixon, *Spread Spectrum Communication Systems with Commercial Applications*, 3rd ed. New York: Wiley, 1994.

**Géza Kolumbán** (M'92) received the M.S. and Ph.D. degrees from the Technical University of Budapest, Hungary, and the C.Sc. degree from the Hungarian Academy of Sciences in 1976, 1990, and 1990, respectively.

After graduation, he was with Fine Mechanical Enterprise, Hungary, as a research engineer where he developed local generators, microwave transistor power amplifiers and VCO circuits for high-capacity microwave analog radio relay systems. He joined the Research Institute for Telecommunications, Hungary, in 1980, where he was involved in many system engineering projects like SCPC-type satellite telecommunication system, microwave satellite up- and down-converter, low-capacity microwave digital radio system, etc. There, he headed a group of engineers, whose duty was to develop frequency synthesizers and local generators for satellite and frequency hopping spread spectrum systems. He spent one year with the Bilkent University, Turkey (1991–1992), and another year with the Eastern Mediterranean University, Cyprus (1992–1993) as an Associate Professor. He returned to the Technical University of Budapest in 1993, where he has been an Associate Professor with the Department of Instrument and Measurement Engineering. His current research interests are in nonlinear dynamics of different-type phase-locked loops, frequency synthesis by sampling phase-locked loop, chaotic communications, and application of chaotic signals in measurement engineering.

**Michael Peter Kennedy** (S'84–M'91–SM'95), for a photograph and biography, see this issue, p. 854.

**Leon O. Chua** (S'60–M'62–SM'70–F'74), for a biography, see this issue, p. 904.

# Synchronization of Chaotic Systems Using Phase Control

Alexander Volkovskii

*Abstract*—**Synchronization of chaotic systems by control using a phase feedback loop is investigated. Suggested algorithm of synchronization can be used both for discrete time and for continuous time systems. Due to similarity to the usual phase lock loop, this method allows to generalize the majority of applications of phase lock-in for chaotic systems.**

*Index Terms*—**Chaos, control, phase lock-in, synchronization.**

## I. Introduction

SYNCHRONIZATION OF chaotic systems has become an attractive field for research activities in recent years. Spread spectrum communications [1]–[4] nondestructive testing, failure monitoring, and system identification [5], have been proposed as potential applications of chaotic synchronization and motivate further studies. Many methods suggested for synchronization and repeatedly tested on various dynamical systems can be divided in two groups. Passive ones, based on coupling [6], [7], threshold lock-in [8], and synchronous chaotic response [9], are simple and robust, but unable to track an inevitable in experiments drift of parameters. From this point of view, the active synchronization using control of systems parameters [3], [10]–[14] seems to be preferable.

In most of these studies, the concept of synchronization of two $m$-dimensional chaotic systems

$$\dot{x}_k = F_k^x(x_1, \cdots, x_m),$$
$$\dot{y}_k = F_k^y(y_1, \cdots, y_m), \qquad k = 1, 2, \cdots, m$$

is based on the existence of the identical solutions: $x_i(t) \equiv y_i(t)$, however a few attempts to describe synchronization of nonidentical chaotic systems have also been undertaken [15]–[17]. Another kind of chaotic oscillations that should be naturally considered as synchronous can be achieved if the systems outputs are shifted in time: $x_i(t - t_0) \equiv y_i(t)$, $t_0 = \text{const}$. This situation is quite usual for periodic systems synchronized by phase lock loops (PLL). The main feature of synchronization in periodic case is that a control parameter (period) is just a time scaling factor, and variations of it do not change the dynamics of the adjusting oscillator. In this paper, we show that the same principle can be used for synchronization of chaotic systems and demonstrate by computer simulation that a broad versatility of applications of PLL (in-phase and anti-phase synchronization, frequency, phase and phase shift key-in modulation and demodulation, etc.) can be generalized on chaotic signals.

Manuscript received February 24, 1997; revised June 10, 1997. This work was supported by the International Association for the Promotion of Cooperation With Scientists from the Independent States of the FSU, Grant INTAS-94-2899, the U.S. Office of Naval Research, Grant N00014-96-1-0753, and the Russian Foundation for Basic Research, Project 96-02-18041. This paper was recommended by Guest Editor M. P. Kennedy.

The author is with the Radiophysics Department, Nizhny Novgorod State University, Nizhny Novgorod 603600, Russia (e-mail: volkovsk@hale.appl.sci-nnov.ru).

Publisher Item Identifier S 1057-7122(97)07327-3.

## II. Synchronization by Phase Control

The basic idea of phase synchronization is to control a time scale parameter $\tau^a$ of adjusting system (we use upper "$l$" and upper "$a$" indexes for leading and adjusting systems correspondently) in order to keep a constant value of the phase (time) shift between the oscillations, but suppose first that the time scale parameters are identical: $\tau^l = \tau^a$. In this case synchronization can be achieved by control of other parameters $p_i^a$ using error signals detected on $(m-1)$-dimensional Poincare cross sections $\Gamma^l$ and $\Gamma^a$ in the phase subspaces of leading and adjusting systems. One of the most general method of this synchronization is based on the Ott, Grebogi, Yorke "controlling chaos" (OGY) [18] and has been applied for synchronization of 2-$d$ maps [10]. Two other methods of controlling chaos—occasional proportional feedback [19] and adaptive parametric control [20], can be also used here. As a result of control, the trajectories of leading and adjusting systems (on $\Gamma^l$ and $\Gamma^a$ surfaces) converge to become identical. However, this synchronism is extremely sensitive to perturbations of the time scale parameters. Any (even small) detunings $\Delta\tau = \tau^l - \tau^a$ will result in a difference of the time moments $t^l(n)$ and $t^a(n)$ when trajectories cross the $\Gamma^l$ and $\Gamma^a$ surfaces. Thus, two identical in the phase subspaces trajectories will diverge in time. This seems to be the reason why synchronization using OGY control has not been realized in experiments with autonomous continuous time chaotic systems. Experimental results presented in [11], [12] have been achieved on two nonlinear resonators externally driven by *synchronous* sinusoidal signals. In this case, time scale parameters are determined by the period of the driving signal and can be exactly the same: $\tau^l \equiv \tau^a$.

To realize synchronization by "controlling chaos" in a more general case, the time dependence of parameters should be taken into account, and the phase space should be augmented by time coordinate. From a variety of possibilities to choose

1057–7122/97$10.00 © 1997 IEEE

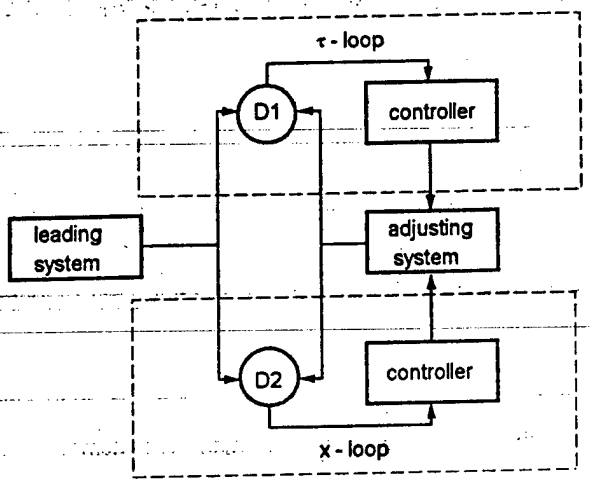


Fig. 1. Schematic illustration of the $x$–$\tau$ control scheme.

cross sections in this $(2m+1)$-dimensional phase space two can be specified. The first one is $t = t_0 + \Delta n$, $\Delta > 0$, $n = 0, 1, 2, \cdots$ (shift mapping). A control strategy on this map can be described as "to bring together trajectories at the same time moments." The limit $\Delta \to 0$ leads to the continuous feedback control. The second is the Poincare cross sections $\Gamma^l$ and $\Gamma^a$ in the phase subspaces of leading and adjusting systems supplemented by time. The feature of this choice is that it requires to measure only $2(m-1)$ values of phase variables (instead of $2m$) and time moments when trajectories cross $\Gamma^l$ and $\Gamma^a$. This can be essential if some phase variables are not accessible and time-delayed coordinates (in application to control see [18], [21]) can not be used due to computation-time and storage limitations. The time associated coordinates usually can be measured in an experiment and directly controlled by variation of parameter $\tau^a$. Due to the advantages of this method we have concentrated on it.

The control scheme is illustrated in Fig. 1. It includes two almost independent feedback loops: $\tau$-loop to control the time scale by adjusting parameter $\tau^a$ and $x$-loop to control phase variables on $\Gamma^l$ and $\Gamma^a$ by adjusting parameters $p_i^a$. The $x$-loop can be based on the OGY or any other control strategy that leads to elimination of the differences $|\tilde{x}_i^l(n) - \tilde{x}_i^a(n)|$, where $\tilde{x}_i(n)$ are trajectories of the Poincare maps. The $\tau$-loop can be constructed in the same manner as the ordinary phase or astatic frequency control loop. We have accented on the former because the latter seems hardly possible to be used in potential applications due to unpredictable (but constant) time shift between the chaotic oscillations in synchronous regime. The control equation for phase lock loop can be written as

$$\Delta\tau(n) = \Delta\tau(0) - \phi[\Delta t(n)] \tag{1}$$

where $\Delta\tau(n) = \tau^a(n) - \tau^l$ is the current detuning of the time scale parameters; $\Delta t(n) = t^a(n) - t^l(n)$ is the phase shift between the oscillations; $\phi(\Delta t)$—characteristic of the phase discriminator. It is assumed to be a smooth function, defined in some interval $\Delta t \in [t_{\min}, t_{\max}]$.

Suppose the time intervals between two intersections of $\Gamma^l$ and $\Gamma^a$ surfaces $t^l(n) - t^l(n-1)$ and $t^a(n) - t^a(n-1)$ are functions of phase variables and systems parameters

$$t^l(n) - t^l(n-1) = \tau^l T[\tilde{x}_k^l(n-1), p_i^l]$$
$$t^a(n) - t^a(n-1) = \tau^a(n-1) T[\tilde{x}_k^a(n-1), p_i^a(n-1)].$$

Then taking into account (1), we obtain the following linearized evolution equation for the time shift $\Delta t(n)$:

$$\begin{aligned}\Delta t(n) = \Delta t(n-1) &+ T[\tilde{x}_k^l(n-1), p_i^l] \\ &\cdot \{\Delta\tau(0) - \phi[\Delta t(n-1)]\} \\ &+ \tau^l(T_x'\Delta X + T_p'\Delta P)\end{aligned} \tag{2}$$

where

$$|\tilde{x}_k^l - \tilde{x}_k^a| \ll 1,\ |p_i^a - p_i^l| \ll 1,$$
$$T_x'\Delta X = \sum_{k=1}^{m} \frac{dT}{d\tilde{X}_k}[\tilde{X}_k^a(n-1) - \tilde{X}_k^l(n-1)],$$
$$T_p'\Delta P = \sum_{i=1}^{m1} \frac{dT}{dp_i}[p_i^a(n-1) - p_i^l].$$

As it has been mentioned above the time scale parameter does not have an effect on the system dynamics so the $x$-loop performs independently. Suppose that it is designed to be stable in accordance with one of known methods of controlling chaos and converges under $n \to \infty$ to $\tilde{x}_k^a = \tilde{x}_k^l$ and $p_i^a = p_i^l$ that leads to vanishing $\Delta X$ and $\Delta p$ in (2). The evolution equation for the time shift between the oscillations (2) has, therefore, the stationary solution

$$\Delta t^* = \phi^{-1}[\Delta\tau(0)] = \text{const} \tag{3}$$

that determines the phase shift $\Delta t^*$ in synchronous regime. This regime is stable (provided that $x$-loop is stable) if

$$\left|1 - T[\tilde{x}_k^l(n-1), p_i^l]\left.\frac{d\phi}{d\Delta t}\right|_{\Delta t^*}\right| < 1. \tag{4}$$

Equations (2)–(4) are very similar to those for periodic PLL [for periodic oscillations $T(\tilde{x}_k(n), p_i) = \text{const}$], and the main properties of synchronous regime are common for periodic and chaotic cases: 1) the synchronous regime exists in the interval of initial detunings $\phi_{\min} \le \Delta\tau(0) \le \phi_{\max}$, where $\phi_{\min}$ and $\phi_{\max}$ are the maximum and minimum output signals of the phase discriminator, and 2) the residual phase shift $\Delta t^*$ in the synchronous regime is determined by the initial detuning $\Delta\tau(0)$. By analogy with the periodic PLL, $x-\tau$ loop can be used for transmitting the information by chaotic signals. Modulation of the time scale parameter $\tau^l$ (frequency modulation) leads to the modulation of $\Delta\tau(0)$. In synchronous regime output of the phase discriminator $D_1$ is a function of $\Delta\tau(0)$ and, therefore, the information can be recovered.

## III. Computer Simulations

Chaotic synchronization by phase control loop has been tested in computer simulation with rink oscillators [22] used

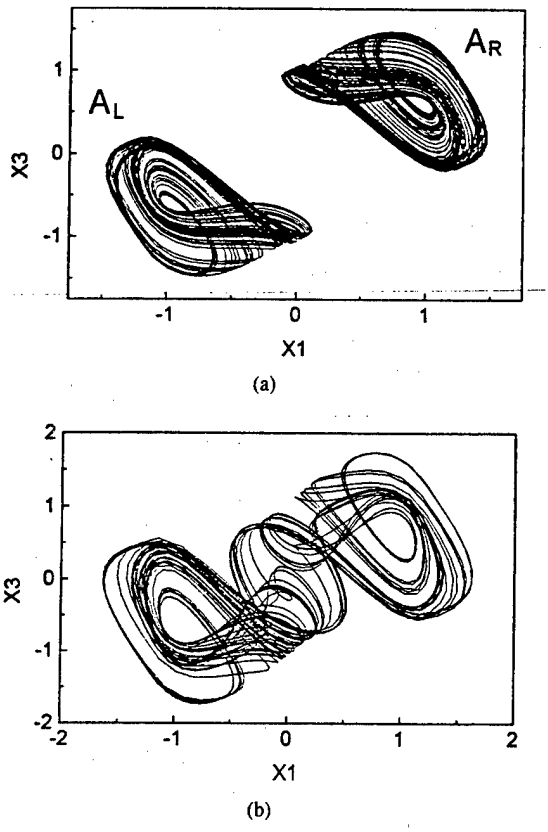


Fig. 2. The $(x_1, x_3)$ projections of the typical chaotic attractors for (a) $\delta = 0.43$, $\sigma = 0.72$, $\gamma = 0.1$, $\alpha = 16$ and (b) $\alpha = 22$.

as chaotic systems. Mathematical model for a single circuit (see [23] for circuit implementation) is the following:

$$\begin{aligned} \tau\dot{x}_1 &= x_2 \\ \tau\dot{x}_2 &= -x_1 - \delta x_2 + x_3 \\ \tau\dot{x}_3 &= \gamma[F(x_1) - x_3] - \sigma x_2 \end{aligned} \tag{5}$$

where

$$F(x) = \begin{cases} 0.528, & x \le 1.2 \\ \alpha x(1 - x^2), & -1.2 < x < 1.2 \\ -0.528, & x \ge 1.2 \end{cases}$$

$\tau$-time scale parameter.

The system (5) demonstrates a variety of chaotic behavior. The synchronization algorithm has been tested on two types of attractors shown in Fig. 2(a) and (b).

We have simulated as phase discriminator $D_1$ in $\tau$-loop a simple bistable flip-flop circuit. It can be set to a high output level at time moments $t^l(n)$ when the trajectory of leading system crosses the Poincare surface $\Gamma^l$ and reset at $t^a(n)$ corresponding to the adjusting systems intersection of $\Gamma^a$. In this case, function $\phi(\Delta t)$ is proportional to $\Delta t$ inside the interval $\Delta t \in [0, t_{\min}]$, where $t_{\min} = \min\{t_n^l - t_{n-1}^l, t_n^a - t_{n-1}^a\}$, $n = 1, 2, 3, \cdots$. Outside this interval, $\phi(\Delta t) = \phi(\Delta t, n)$ is a chaotic function. The adaptive parametric control [20] was used in the $x$-loop. To apply the original method to synchronization it was transformed in the following way. The

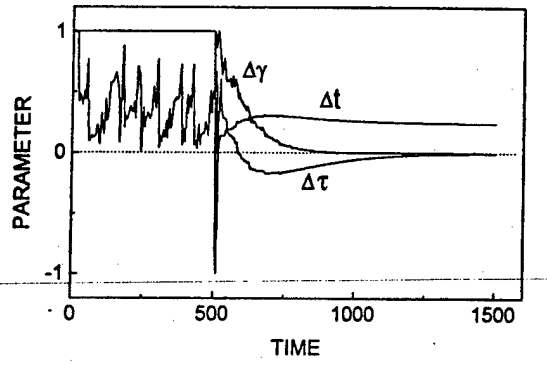


Fig. 3. The transient processes of the normalized time shift between the oscillations $\Delta t_{nr} = \Delta t/\Delta t_{\max}$ and the adjusted parameters: $\Delta\tau_{nr} = [\tau^a(n) - \tau^l]/\Delta\tau_{\max}$, $\Delta\gamma_{nr} = [\gamma^a(n) - \gamma^l]/\Delta\gamma_{\max}$ for $\alpha^l = \alpha^a = 16$, $\delta^l = \delta^a = 0.43$, $\sigma^l = \sigma^a = 0.72$, $\gamma^l = 0.1$, $\gamma^a(0) = 0.11$.

leading oscillator was considered as the *SYSTEM*, the adjusting oscillator as the *MODEL*. Parameters of the *MODEL* were controlled instead of the *SYSTEM* ones. It was proposed that only $x_1^l$ variable is received by the adjusting system. As the Poincare cross sections we used the planes $\dot{x}_1^a = 0$ and $\dot{x}_1^l = 0$. Parameter $\gamma^a$ was used as the control parameter. Perturbations were made in accordance with equation

$$\gamma^a(n+1) = \gamma^a(n) + \mu[x_1^a(n) - x_1^l(n)] \tag{6}$$

where $\mu$ is the constant parameter of the adaptive control.

As far as the adaptive parametric control [20] assumes coupling between the *MODEL* and the *SYSTEM*, the $x_1^a$ variable was adjusted after calculation $\gamma^a(n+1)$ so that $x_1^a(n) = x_1^l(n)$.

The results of simulations are shown in Figs. 3–5. In-phase synchronization of oscillations corresponding to attractors $A_R$ [Fig. 2 (a)] is illustrated in Fig. 3. In this computer experiment both the time scale parameter $\tau^a$ and the essential for the system dynamics parameter $\gamma^a$ was disturbed at the starting point $t = 0$. Available for control ranges of parameters were restricted as

$$0.5 \le \tau^a \le 1.5 \qquad 0.09 \le \gamma^a \le 0.11.$$

At the time moment $t = 500$ the control was turned on and the systems converged to the stationary synchronous regime. In spite of the constant phase shift the oscillations can be considered as synchronous chaotic oscillations and values of parameters of leading and adjusting systems are equal.

In practice, however, some parameters could be inaccessible for control. Detunings of these parameters destroy the stationary solution (3). In this case, the behavior of the phase shift became chaotic. Fig. 4 shows the transient process for the case of uncontrollable detuning of $\alpha^a$, while parameters $\gamma^a$ and $\tau^a$ were controlled. Uncontrollable detunings lead to appearance of chaotic fluctuations of the phase shift. Increasing of detunings leads to increasing of the amplitude of the fluctuations, and when the fluctuations leave the interval $[0, t_{\min}]$, synchronization is lost.

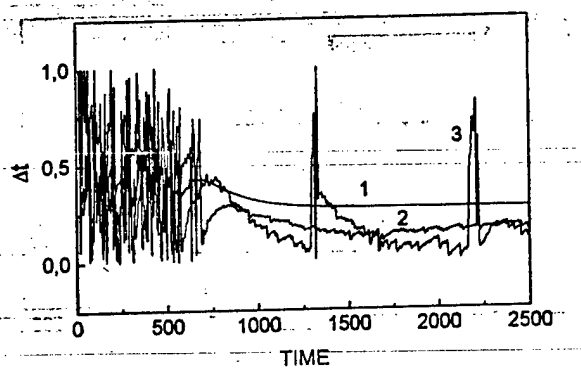


Fig. 4. The influence of the detunings of the uncontrollable parameter $\alpha^l$ on the amplitude of fluctuations of the phase shift in synchronous regime: $\delta^l = \delta^a = 0.43$, $\sigma^l = \sigma^a = 0.72$, $\gamma^l = 0.1$, $\gamma^a(0) = 0.11$, $\alpha^a = 16$, and 1) $\alpha^l = 16$; 2) 16.7; 3) 16.9

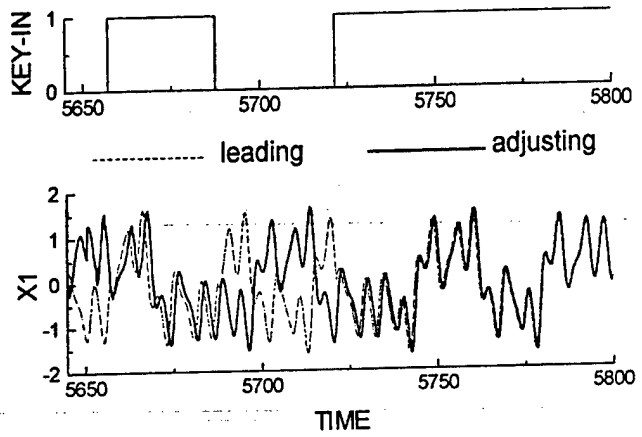


Fig. 5. The key-in modulation of chaotic signals.

It is known that PLL can be used for synchronization in both anti-phase and in-phase modes. The control scheme providing in-phase and antiphase synchronization is the same as shown in Fig. 1, but discriminators $D_1$ and $D_2$ are working with the absolute values of signals. Since $\dot{x}_1^a = 0$ and $\dot{x}_1^l = 0$ surfaces were taken as Poincare cross sections the $\tau$-loop is equivalent to that shown in Fig. 1, whereas, the control equation for the $x$-loop (6) is changed

$$\gamma^a(n+1) = \gamma^a(n) + \mu \operatorname{sign}\left[x_1^a(n)\right]\left[|x_1^a(n)| - |x_1^l(n)|\right].$$

As it is easy to see this control scheme is invariant with respect to the substitution $x_1^l \to -x_1^l$ and can be used to achieve in-phase and anti-phase synchronization. As far as switchings of the input variable $x_1^l \to -x_1^l$ do not break synchronization, this control scheme can be used for communicating with chaotic signals. Fig. 5 demonstrates the possibility of phase shift key-in modulation and demodulation of chaotic signals. It should be mentioned that phase shift key-in modulation is of great importance for high speed communication systems, because each bit of information is transmitted during half of the period of the carrier signal with relatively narrow frequency band of a channel. The graphs in Fig. 5 was plotted for parameters of the systems corresponding to the attractors shown in Fig. 2(b). In accordance with some message phase shift key-in $x_1^l \to -x_1^l$ was made at time moments when $x_1^l = 0$. As far as the phase of oscillations in the receiver (adjusting system) is not changed the message can be recovered by comparing the phases of the signals $x_1^l$ and $x_1^a$.

## IV. Conclusion

Synchronization by $x$-$\tau$ loops is a generalization of phase lock-in for chaotic systems. The independent control of a time scale parameter allows to reduce a dimension of calculations required for synchronization of continuous time autonomous chaotic systems by OGY method of controlling chaos. The main properties of synchronization scheme presented here are very similar to those of the ordinary PLL and the majority of applications of PLL can be directly transformed to the chaotic case. In particular, frequency and phase shift key-in modulation can be used with chaotic signals on the analogy of periodic ones.

## Acknowledgment

The author wishes to express his gratitude to M. Levinsen and N. Berntsen for stimulating discussions. Simulations have been performed on computer facilities of the CATS Center, Niels Bohr Institute, University of Copenhagen, Denmark.

## References

[1] L. Kocarev, K. S. Halle, L. O. Chua, and U. Parlitz, "Experimental demonstration of secure communication via chaotic synchronization," *Int. J. Bifurc. Chaos*, vol. 2, no. 3, pp. 709–713, 1992.

[2] K. M. Cuomo and A. V. Oppenheim, "Circuit implementation of synchronized chaos with applications to communications," *Phys. Rev. Lett.*, vol. 71, no. 1, pp. 65–68, 1993.

[3] T. L. Carroll and L. M. Pecora, "Cascading synchronized chaotic systems," *Physica D*, vol. 67, pp. 126–140, 1993.

[4] A. R. Volkovskii and N. F. Rul'kov, "Synchronous chaotic response of a nonlinear oscillating system as a principle for the detection of the information component of chaos," *Tech. Phys. Lett.*, vol. 19, no. 2, pp. 97–99, 1993.

[5] R. Brown, N. F. Rul'kov, and N. B. Tufillaro, "The effects of additive noise and drift in the dynamics of the driving on chaotic synchronization," *Phys. Lett. A*, vol. 196, pp. 201–205, 1994.

[6] H. Fujisaca and T. Yamada, "Stability theory of synchronized motion in coupled oscillator systems ," *Prog. Theor. Phys.*, vol. 69, pp. 32–47, 1983.

[7] V. S. Afraimovich, N. N. Verichev, and M. I. Rabinovich, "Stochastic synchronization of oscillations in dissipative systems," *Izv.VUZ. Radiofiz. RPQAE*, vol. 29, pp. 795–803, 1986.

[8] N. F. Rul'kov and A. R. Volkovskii, "Threshold synchronization of chaotic relaxation oscillations," *Phys. Lett. A*, vol. 179, pp. 332–336, 1993.

[9] L. M. Pecora and T. L. Carroll, "Driving systems with chaotic signals," *Phys. Rev. A*, vol. 44, no. 4, pp. 2374–2383, 1991.

[10] Y. C. Lai and C. Grebogi, "Synchronization of chaotic trajectories using control," *Phys. Rev. E*, vol. 47, no. 4, pp. 2357–2359, 1993.

[11] T. C. Newell, P. M. Alsing, A. Gavrielides, and V. Kovanis, "Synchronization of chaos using proportional feedback," *Phys. Rev. E*, vol. 49, no. 1, pp. 313–317, 1994.

[12] ——, "Synchronization of chaotic diode resonators by occasional proportional feedback," *Phys. Rev. Lett.*, vol. 72, no. 11, pp. 1647–1650, 1994.

[13] A. R. Volkovskii, "Phase lock-in of chaotic relaxation oscillators," in *Proc. 3-D Experiment. Chaos Conf.*, Edinburgh, Scotland, Aug. 21–23, 1995, pp. 289–298.

[14] U. Parlitz and L. Kocarev, "Multichannel communication using autosynchronization," *Int. J. Bifurc. Chaos*, vol. 6, no. 3, pp. 581–588, 1996.
[15] N. F. Rul'kov, A. R. Volkovskii, A. Rodriguez-Lozano, E. Del Rio, and M. G. Velarde, "Synchronous chaotic behavior of a response oscillator with chaotic driving," *Chaos, Solitons Fractals*, vol. 4, no. 2, pp. 201–211, 1994.
[16] N. F. Rulkov, M. M. Sushchik, and L. S. Tsimring, "Generalized synchronization of chaos in directionally coupled systems," *Phys. Rev. E*, vol. 51, no. 2, pp. 980–994, 1995.
[17] H. D. Abarbanel, N. F. Rulkov, and M. M. Sushchik, "Generalized synchronization of chaos: The auxiliary system approach," *Phys. Rev. E*, vol. 53, no. 5, pp. 4528–4535, 1996.
[18] E. Ott, C. Grebogi, and J. A. Yorke, "Controlling chaos," *Phys. Rev. Lett.*, vol. 64, no. 11, pp. 1196–1199, 1990.
[19] E. R. Hunt, "Stabilizing high-period orbits in a chaotic system: The diode resonator," *Phys. Rev. Lett.*, vol. 67, no. 15, pp. 1953–1955, 1991.
[20] D. Vassiliadis, "Parametric adaptive control and parameter identification of low-dimensional chaotic systems," *Physica D*, vol. 71, pp. 319–341, 1994.
[21] M. Ye, D. W. Peterman, and P. E. Wigen, "Controlling chaos in thin YIG films with a time-delayed method," *Phys. Lett. A*, vol. 203, pp. 23–28, 1995.
[22] A. S. Dmitriev, Y. V. Kislov, and S. O. Starkov, "Experimental study of appearance and interaction of strange attractors in the circle type self-oscillator," *Sov. Phys. Tech. Lett.*, vol. 30, pp. 1439–1441, 1985.
[23] N. F. Rul'kov, A. R. Volkovskii, A. Rodriguez-Lozano, E. Del Rio, and M. G. Velarde, "Mutual synchronization of chaotic self-oscillators with dissipative coupling," *Int. J. Bifurc. Chaos*, vol. 2, no. 3, pp. 669–676, 1992.

**Alexander Volkovskii** was born in Nizhny-Novgorod, Russia, in 1961. In 1983, he graduated from Lobachevskii State University, Nizhny Novgorod. He received the Ph.D. degree in radiophysics in 1994 from Lobachevskii State University, Nizhny Novgorod.

He has been with the Radiophysics Department, Lobachevskii State University, since 1994 as a Research Scientist and Assistant Professor. His scientific interests include nonlinear dynamics and chaos in electronic circuits, and computer simulations.

# Transactions Briefs

## The Effect of Natural Frequency Distribution on Cluster Synchronization in Oscillator Arrays

Grigori V. Osipov and Mikhail M. Sushchik

*Abstract*—**The synchronization in an array of oscillators is investigated numerically for different spatial distributions of natural frequencies along the array. Principal attention is focused on the natural frequency distribution when the total range of frequency values is constant but particular forms of distribution are changed. Under these condition, the synchronization increases significantly at the transition from the frequencies varying monotonically along the array to completely irregular distribution.**

*Index Terms*—**Control, lattice of nonlinear oscillators, synchronization.**

### I. Introduction

The relationship between the changes in space and time in extended systems and their array analogs has recently been attracting attention of the researchers in terms of both diagnostics [1], [2] and feasibility of different regimes [3]–[5]. It was found, and it may seem surprising at first sight, that under certain conditions time-periodic behavior is realized only in the presence of spatial disorder generated either by the system itself [3] or introduced from the outside, for example, by the dispersion of parameters of the elements in the array [4], [5]. In particular, a periodic regime may be realized in an array of identical nonlinear pendulums with harmonic forcing behaving chaotically, if there is a dispersion in their parameters [4]. In an analogous mathematical system but without external periodic forcing, that models a parallel array of current-biased Josephson junctions coupled via inductors, a small dispersion in the currents gives rise to enhanced mutual synchronization of oscillations in these junctions [5]. In the present brief, we also analyze the problem of the effect of disorder on synchronization but in a slightly different formulation. Specifically: How does the change of parameter (natural frequencies in the case of interest) distribution along the array influence synchronization, if the range of their values remains unchanged? We take as an example a one-dimensional array of oscillators described by a discrete analog of the Ginzburg–Landau equations to take into consideration the following frequency distribution:

$$\omega_j = \omega_0 + \frac{\Delta\omega^*}{2} + \frac{(j-1)(\Delta\omega - \Delta\omega^*)}{N} + \Delta\omega^*\xi_j \qquad (j = 1, \cdots, N) \tag{1}$$

where $\xi_j$ are uniformly distributed random numbers in the interval $[-0.5; +0.5]$, $N$ is the number of elements in the array, and $\Delta\omega$ is the interval of frequency dispersion. As $\Delta\omega^*$ is changing from 0 to $\Delta\omega$, the distribution changes from monotonic, completely regular to a completely irregular one. Such a choice of regular distribution in the form of the frequency variation that is linear along the array is explained by the fact that this consideration may be of independent interest.

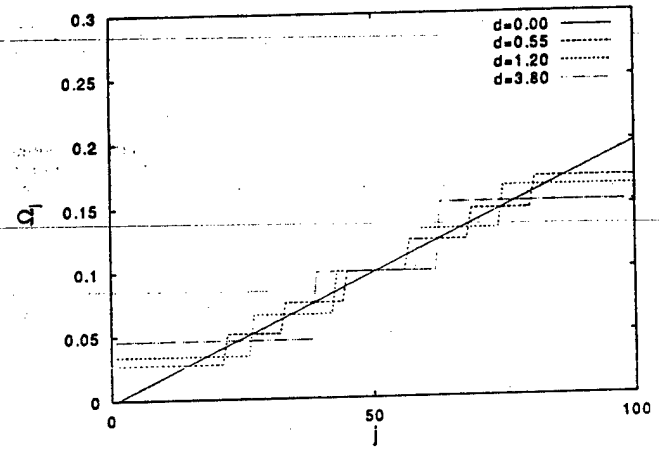


Fig. 1. Averaged frequencies $\Omega_j$ at different values of coupling coefficients $d$ for $\Delta = 2 \cdot 10^{-3}$.

### II. Synchronization Clusters and Multistability at Linear Variation of Natural Frequencies Along the Array

Arrays of oscillators with the natural frequencies varying linearly along them are interesting both conceptually and because they are encountered in a natural fashion in various situations. The presence of a sufficiently strong coupling between oscillators leads to local frequencies of excited collective oscillations that strongly differ from the natural frequencies. Besides, steps in the form of well pronounced and rather extended plateaus intermitting with relatively narrow transition region appear in their dependence on spatial coordinate. We briefly characterize this effect as cluster synchronization, where under a cluster we understand a coupled set of oscillators having the same average period $T$ or the corresponding mean frequency $\Omega \sim T^{-1}$, with no demand for constant phase difference between the elements and with allowance for limited variations in time.

Theoretical investigations of cluster synchronization in arrays with linear frequency variations have been carried out for a long time (see [6] and references cited therein). The formulation and analysis of the problem in the general context were attempted in [6] in the frame of the phase equation. Although that research enabled its authors to explain in a natural fashion a number of the peculiarities observed and to correlate them with the general properties of the array, the investigations performed almost at the same time [7] (see also [8]) revealed some effects in which amplitude variations are significant. A vivid manifestation is formation of clusters of oscillators with infinitesimal amplitude, even if the conditions of self-excitation in the absence of coupling are fulfilled for each of them (this effect is known as "oscillator death" [9]–[11]). The amplitude effects are also essential for the formation and restructuring of cluster structures, therefore, here we employ equations for slow complex amplitudes.

Manuscript received February 10, 1997; revised June 7, 1997. This work was supported in part by the International Association for the Promotion of Cooperation with Scientists from the Independent States of the FSU Grant INTAS-94-2899, by the U.S. Office of Naval Research under Grant N00014-96-1-0753, and by the Russian Foundation for Basic Research under Grant 96-02-18041 and Grant 96-02-16559. This paper was recommended by Guest Editor M. P. Kennedy.

G. V. Osipov is with the University of Nizhny Novgorod, Nizhny Novgorod, Russia (e-mail: osipov@hale.appl.sci-nnov.ru).

M. M. Sushchik is with the Institute of Applied Physics, Russian Academy of Science, Nizhny Novgorod, Russia (e-mail: sushch@euler.appl.sci-nnov.ru).

Publisher Item Identifier S 1057-7122(97)07318-2.

1057–7122/97$10.00 © 1997 IEEE

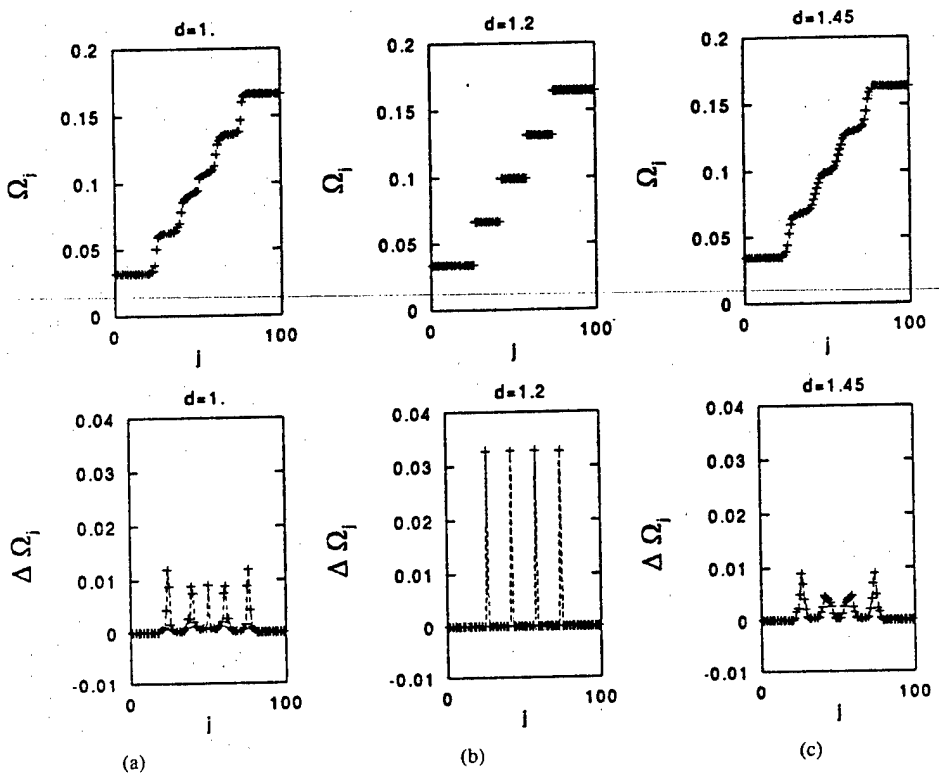


Fig. 2. Averaged frequencies $\Omega_j$ and their difference $\Delta\Omega_j = \Omega_{j+1} - \Omega_j$ for intermediate (a), (c) and perfect (b) cluster structures for $\Delta = 2 \cdot 10^{-3}$.

Their solution is more complicated than analysis of phase equations. Consequently, we have to use partial solutions obtained numerically.

### A. Model

We take as a model a one-dimensional array of oscillators having different natural frequencies. Each oscillator is coupled diffusively with its two nearest neighbors. The consideration is carried out in a quasiharmonic approximation in its traditional interpretation. The model equations may be written in the form

$$\dot{z} = i\hat{\Delta}z + p(\hat{I} - \hat{Z})z + d\hat{A}z \tag{2}$$

$$Z_{ij} = \begin{Bmatrix} z_j^2 & j = i \\ 0 & j \neq i \end{Bmatrix} \tag{3}$$

$$I_{ij} = \begin{Bmatrix} 1 & j = i \\ 0 & j \neq i \end{Bmatrix} \tag{4}$$

that is a discrete analog of the Ginzburg–Landau equation. Here, the vector–column $z$ and the diagonal matrix $\hat{Z}$ are made up of the $N$ functions $z_1, \cdots, z_N$ ($z_j = x_j + iy_j$) characterizing self-oscillations of $N$ oscillators, the elements of the diagonal matrix $\hat{\Delta}(\Delta_1, \cdots, \Delta_N)$ are equal to the frequency mismatch of the oscillators relative to the frequency of the first oscillator, and $d$ is the coefficient of coupling between the oscillators. The elements of matrix $\hat{A}$ are equal to $a_{11} = a_{NN} = -1$; $a_{jj} = -2$; $a_{j,j+1} = a_{j+1,j} = 1$ ($j = 1, \cdots, N-1$), while all the rest $a_{ij} = 0$. We take as the synchronization conditions the coincidence of averaged partial frequencies estimated from the relation

$$\Omega_j = \langle \omega_j \rangle = \frac{n_j(T)}{T}$$

where $n_j(T)$ is the number of the typical features of the time series $z_j = x_j + iy_j$ (e.g., the maximal $x_j$ exceeds certain values); $T = 2 \cdot 10^5$ is averaging time. A qualitative picture of the spatio-temporal structure of oscillations was obtained by plotting shadowgraphs of $z_j(t)$ on the $(j, t)$-plane. Arrays of 100 elements were investigated in all experiments.

### B. Regimes of Cluster Synchronization

The averaged frequencies of slow motions, $\Omega_j$, typical of the cases of small frequency gradients ($\Delta = \Delta_{j+1} - \Delta_j \leq 2 \cdot 10^{-3}$) are plotted in Fig. 1 for different values of coupling coefficients $d$ and the same initial conditions: $x_j(0) = -2$ for even $j$ and $x_j(0) = -2$ for odd $j$ [$y_j(0) = 0$ for all $j$]. Given sufficiently large coupling coefficients, the oscillators are synchronized all through the array, i.e., global synchronization occurs. As the coupling is decreased, smaller clusters are formed (Fig. 1) but with perfect clusters analogous to those shown in Fig. 2(b) observed only in a definite interval of parameters optimal for the formation of the given number of clusters. Deviation from perfectness outside this interval [Fig. 2(a) and (c)] may be attributed to competition of the effects of intracluster and intercluster interaction. The values of frequency for each cluster (except the edge ones) are close to those obtained by averaging natural frequencies over all the elements forming the cluster. In the considered case of linear dependence of phase mismatch on $j$ in Fig. 1, this corresponds to the intersection of the lines $\Omega_j = \Omega(j)$ and $\Omega_j = j\Delta$ exactly in the middle of the cluster.

The size of the almost perfect clusters $\Delta N_n$ shown in Fig. 1 satisfies, to an accuracy of $\pm 1$ element, the relations for the middle clusters:

$$\Delta N_n = \frac{N - 2N_0}{n} \tag{5}$$

and for the edge clusters:

$$\Delta N_n = \frac{N - 2N_0}{n} + N_0. \tag{6}$$

Here, $N(= 100)$ is the number of elements, $n(= 2, \cdots)$ is the number of clusters, and $N_0(= 8)$ is the correction allowing for nonuniformity due to edge effects. The difference between the edge and middle clusters grows with decreasing $\Delta$ and diminishes as $\Delta$ is increased.

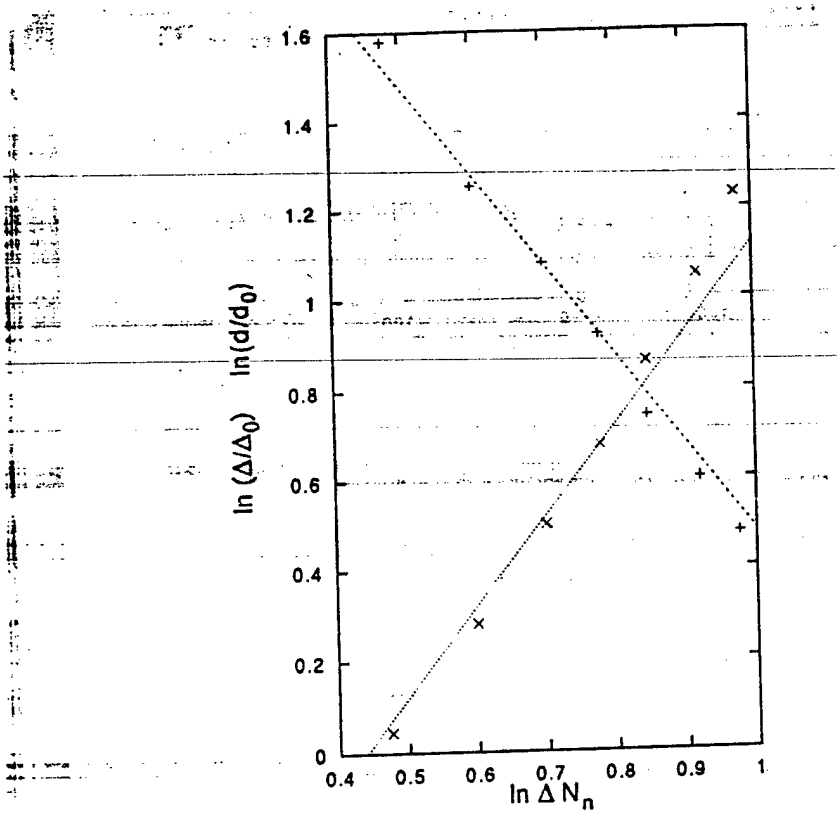


Fig. 3. Critical values of frequency gradient "×" in the range $\Delta \approx (0.5\text{–}17) \cdot 10^{-3}$ for $d = 1$ and of coupling coefficient "+" in the range $d \approx 0.3\text{–}3.8$ for $\Delta = 2 \cdot 10^{-3}$ at which the n-cluster structure breaks at the transition from $n$- to $(n+1)$-cluster depending on the size of the middle cluster $\Delta N_n$. The scale is logarithmic to an accuracy of arbitrarily chosen coordinate origin; the straight lines correspond to the dependence (5).

It is clear from Fig. 3 that the size of such clusters at the instant they break is scaled by the parameters $\Delta$ and $d$:

$$\Delta N \sim \left(\frac{d}{\Delta}\right)^{1/2}. \tag{7}$$

It is interesting that a similar scaling (see, e.g., [8])

$$(\Delta N + 2) \sim \left(\frac{d}{\Delta}\right)^{1/2} \tag{8}$$

specifies, in the phase equation approximation ($|z_j| = |z_0| = \text{const}$), the limiting size of the array with free ends in which global synchronization may occur. However, one should not exaggerate the significance of such a similarity because, as will be clear below, the coupling of clusters yields more complicated effects. Of the greatest significance is their manifestation at large coupling coefficients and mismatching, since amplitude variations and multistability are of principal importance in this case.

### C. Multistability

Investigations into transition processes revealed multistability that is manifested in formation of structures containing a different number of clusters depending on initial conditions for the same values of the parameters. For determination of the regions of the parameters at which different cluster patterns (Fig. 4) may be formed we investigated the solutions obtained at small variations of frequency mismatch $\Delta$ and simultaneous "adaptation" of initial conditions. Specifically, the "adaptation" procedure was the following. For the given values of $d$, the mismatch $\Delta$ was varied successively by $+5 \cdot 10^{-4}$ or by $-5 \cdot 10^{-4}$. The values from the steady-state solution obtained in the previous variant were taken as the initial conditions for (2) in each subsequent variant. Although the procedure described does not guarantee that all possible regimes will be found, it enables us to reveal qualitatively different transitions between the states possessing a different number of clusters. In the parameter regions where bistability (multistability) is observed, i.e., there exist two (several) states with different number of clusters, the transition between them occurs, as the parameters are changed, in a stepwise fashion—"hard" transition. Such states in the space of the parameters in the absence of multistability are divided by a finite interval, so that the transition occurs in a "soft" way, through a sequence of unsynchronized states transforming one into another. These two transition types may be identified by the corresponding spatial distributions of averaged values of the local frequencies. An example of a "hard" transition without intermediate structures from the state with four clusters to the state with five clusters is given in Fig. 5(a) when $\Delta \leq 5 \cdot 10^{-4}$. Fig. 5(b) shows a "soft" transition that occurs at a much greater interval of variations $\Delta \approx 2.2 \cdot 10^{-3}$ with a smooth transition of intermediate dependences $\Omega_j = \Omega(j)$ one into another.

Another manifestation of multistability, besides the "hard" transitions, is the absence of simple dependence on parameters of the number of clusters formed under the same initial conditions. In particular, Fig. 4 (see the points "○") demonstrates that, for monotonic variation of the gradient of frequency mismatch $\Delta$, the transition may occur both toward increasing and decreasing the number of clusters. This suggests that pattern formation may be controlled by relatively weak perturbation of parameters chosen at random.

## III. The Effect of Nonuniformity of Frequency Mismatch Gradient on Formation of Synchronized Clusters

### A. Controlling Structures by Regular Nonuniformities

We can distinguish at least two mechanisms of controlling the spatial structure of the system of interest when additional inhomogeneities of mismatch gradient $\Delta_j$ periodic along the array are introduced. One of them is associated with destruction of an attractor (or attractors), the other one is attributed to changes only of attraction basins (see, e.g., [4], [5]). It can be expected that the second mechanism is readily realized in the case of nontrivial dependence of the number of clusters on the magnitude of frequency mismatch gradient. Indeed, for the parameter values and initial conditions like in Section II-B (point "*" in Fig. 4 for $d = 5$), a relatively small, periodic along $j$ correction to the natural frequencies:

$$\omega_j = \Delta(j-1) + \varepsilon \sin\left[\frac{2\pi \cdot n^*(j-1)}{N}\right] \tag{9}$$

leads to formation of $n^*$ instead of $n$ clusters observed at $\varepsilon = 0$. Particularly, $\varepsilon = 10^{-4}$ for $n = 6$, $n^* = 5$, $\Delta = 0.9 \cdot 10^{-2}$.

By introducing a perturbation with a much larger amplitude $\varepsilon \geq 2 \cdot 10^{-3}$, one can influence not only the process of cluster formation in the regime of transition but also the structures that have already been formed. For example, the transition from 6 to 5 clusters occurs for $\varepsilon = 2 \cdot 10^{-3}$; $\Delta = 0.9 \cdot 10^{-2}$. This case corresponds to the first mechanism of forcing, namely, destruction of one of multistable states, in this case, the structure of 6 clusters. Another possible manifestation of this mechanism is formation of synchronization clusters from a nonsynchronized state, when the transition from a chaotic state in space and time to a state with $n^*$ clusters takes place.

Note that (9) does not give a clear picture of the relationship between the magnitudes of uniform and nonuniform component of frequency mismatch. Only comparison either of their gradient or of their changes over the modulation period along the array i

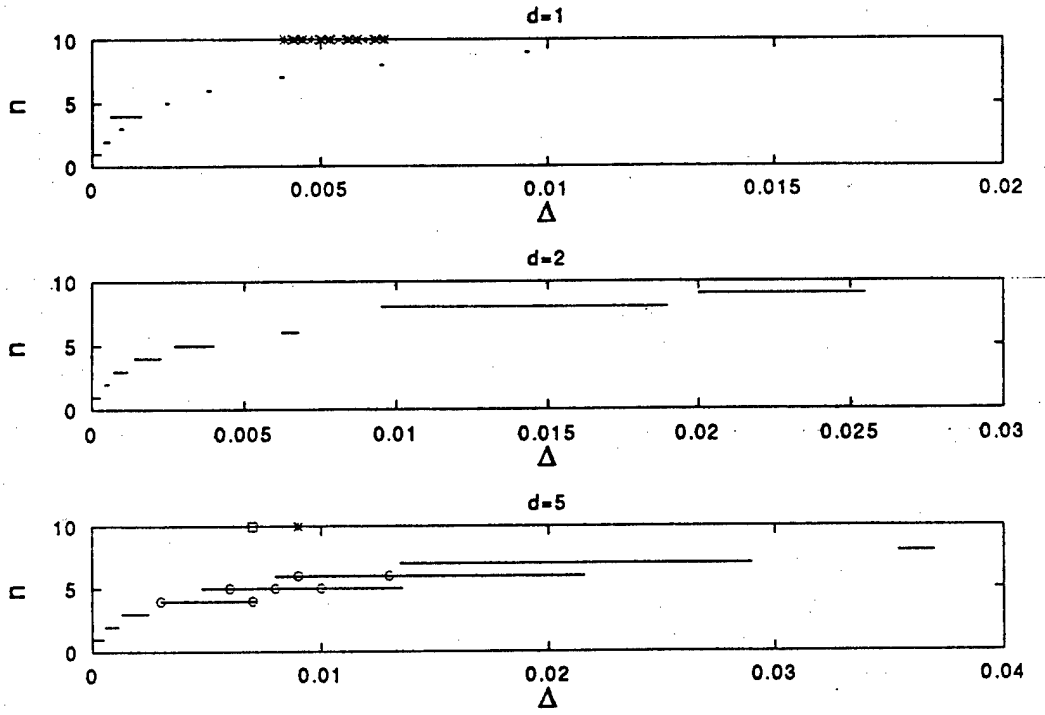


Fig. 4. Ranges of values of frequency gradients at which structures of $n$ perfect clusters like those shown in Fig. 2(b) for $d = 1; 2; 5$ are observed.

physically meaningful. By comparing these quantities one can see that the perturbation is determined by the parameter $(\varepsilon/\Delta)(2\pi n/N)$ that did not exceed 0.3 in all the cases considered.

### *B. The Effect of Random Dispersion of Natural Frequencies on Cluster Synchronization*

We restrict our consideration to one aspect of the effect exerted by spatially irregular parameter variations on the formation of synchronized structures. Namely, we investigate the dependence of spatial structures on the magnitude of random distribution of mismatch relative to some mean at a constant complete range of frequency variations. According to (1), the difference between natural frequencies of the neighboring elements is

$$\Delta_j = \omega_{j+1} - \omega_j = \frac{\Delta\omega - \Delta\omega^*}{N} + \Delta\omega^*\xi_j \qquad (10)$$

where $\xi_j$ are the random numbers distributed in the interval $[-0.5; +0.5]$. In the case of interest, it is reasonable to speak about averaged characteristics because, unlike the case considered above, for the same number of clusters their size and location in space differ greatly in different samples of random numbers.

The critical values of $d$ averaged over 20 samples of random numbers, at which the transition between cluster structures occurs, are presented in Fig. 6 for different dispersions of natural frequencies, $\Delta\omega^*$. The increase in dispersion leads, on the average, to a more regular spatial pattern. Simultaneously, the properties of time coherence of oscillations are improved. These effects are the most pronounced for global synchronization, and their manifestation is less distinct in shorter clusters. In particular, it is clear from Fig. 6 that, in the transition from a completely regular distribution ($\Delta\omega^* = 0$) to a completely random one ($\Delta\omega^* = \Delta\omega$), the critical value of coupling coefficient, $d_{cr}$, at which global synchronization occurs decreases by more than 20 times. This has the following qualitative explanation. In the case of linear frequency distribution, the left neighbor of an element has a phase lag relative to it on the average, while the right neighbor a phase advance, respectively. In other words, they "pull" the oscillator in opposite directions and their actions are compensated in this sense. For random frequency distribution, both the neighbors may either have a phase lag or a phase advance relative to a certain oscillator, i.e., they "pull" it in one direction. As a result, average frequencies of all the three elements are getting close, which leads to the formation of a synchronization cluster. Evidently, such clusters may arise at an arbitrary site of the array.

## IV. Conclusion

In this brief, the synchronization in an array of oscillators has been investigated numerically for different spatial distributions of natural frequencies along the array. We have found two scenarios: "soft" and "hard" of the transition between clusters of the synchronization. In the first one, a gradual adjustment of frequencies is observed, while in the other one the transition from the state with $n$ clusters to the state with $n + 1$ clusters occurs without intermediate structures, that is the consequence of multistability. Principal attention is focused on the natural frequency distribution when the total range of frequency values is constant but particular forms of distribution are changed. Under these conditions, the synchronization increases significantly at the transition from the frequencies varying monotonically along the array to completely irregular distribution.

The discrete Ginzburg–Landau equation considered above may be regarded as a model of an arbitrary discrete nonequilibrium medium near a critical point. Consequently, the results presented may be extended to a broad class of discrete media from different fields. The analysis of the synchronization processes in Ginzburg–Landau equation presented here agrees with the similar results obtained for a chain of coupled Van der Pol generators [12]. Moreover, many of the effects observed in the chain of coupled periodic oscillators were also revealed in analysis of the regimes of chaotic phase synchronization in a chain of coupled Rössler oscillators [13].

We believe that the results obtained may find practical applications to electronic circuits. For example, for designing high power

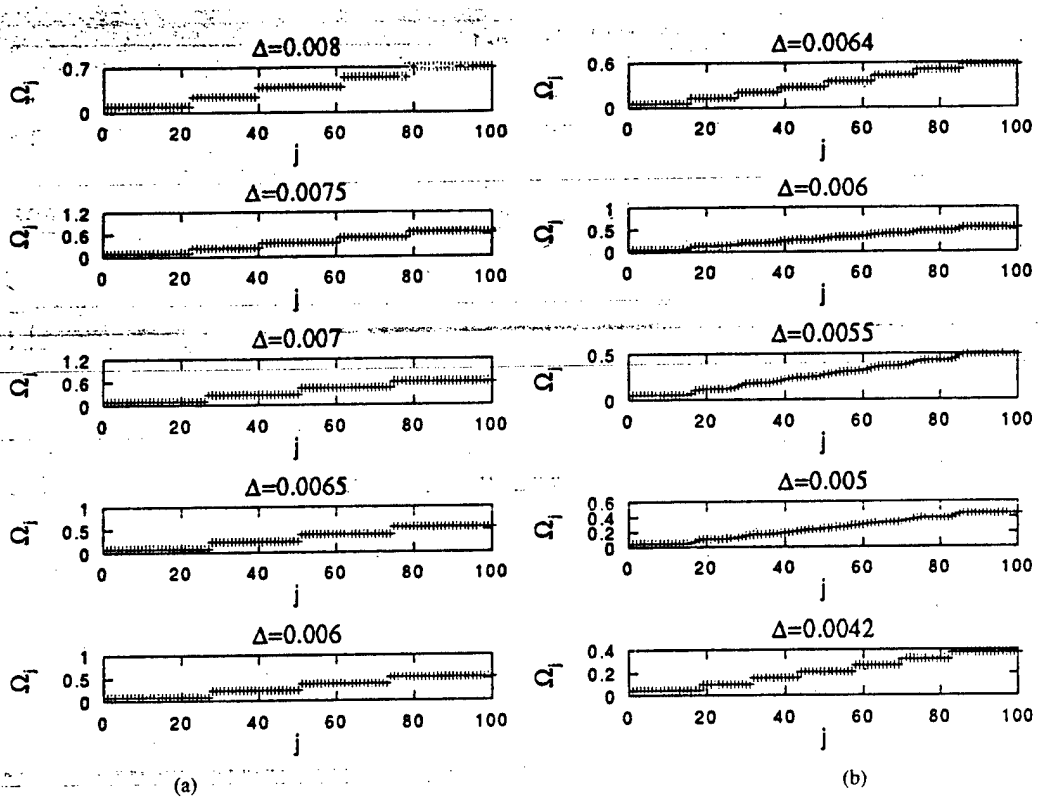


Fig. 5. Averaged frequencies $\Omega_j$ in the transitions from $n$-to $(n+1)$-clusters. (a) "Hard" transition for $d = 5$. (b) "Soft" transition for $d = 1$. The corresponding regions of the parameters are shown in Fig. 4 for $d = 1$ by "$*$" and for $d = 5$ by "□."

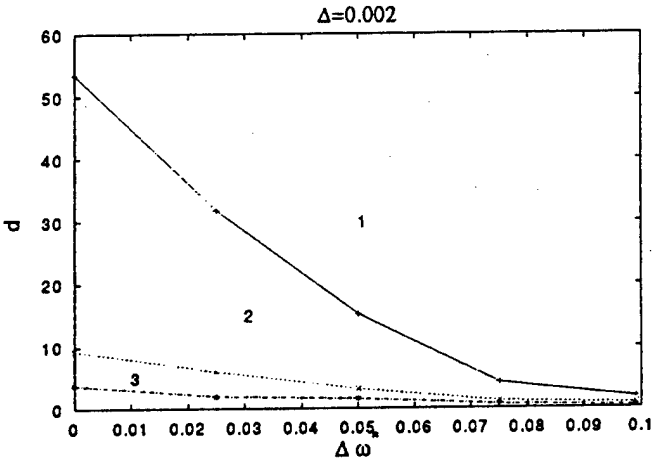


Fig. 6. Critical values of coupling coefficient $d$ averaged over 20 sample random frequency distributions. Region "1" corresponds to the global synchronization; there are two and three clusters in regions "2" and "3," accordingly.

generators consisting of a large number of devices, for analysis of Josephson junction arrays [14], coupled lasers [15], etc.

## REFERENCES

[1] L. Sh. Tsimring, "Nested strange attractors and universality of spatio-temporal chaos," *Phys. Rev. E*, vol. 18, pp. 3446–3454, 1993.
[2] L. N. Korzinov and M. I. Rabinovich, "Diagnostics of spatio-temporal disorder," *Izv. VUZov, Applied Nonlin. Dynam.*, vol. 2, pp. 59–70, 1994, in Russian.
[3] M. Bazhenov, M. Rabinovich, and L. Rubchinsky, "Time-periodic spatial chaos in the complex Ginzburg–Landau equation," *J. Stat. Phys.*, vol. 83, pp. 1165–1181, 1996.
[4] Y. Braiman, J. F. Lindner, and W. L. Ditto, "Taming spatiotemporal chaos with disorder," *Nature*, vol. 378, pp. 465–467, 1995.
[5] Y. Braiman, W. L. Ditto, K. Wiesenfeld, and M. L. Spano, "Disorder-enhanced synchronization," *Phys. Lett. A*, vol. 206, pp. 54–60, 1995.
[6] G. B. Ermentrout and N. Koppel, "Frequency plateaus in an array of weakly coupled oscillators," *SIAM J. Math. Anal.*, vol. 15, pp. 215–237, 1984.
[7] S. D. Drendel, N. P. Hors, and V. A. Vasiliev, "Regime of synchronization in cells of smooth-muscular tissues," *Dynamics of Cell Populations*, Collected Papers. Nizhny Novgorod, Russia: Nizhny Novgorod Univ. Press, 1984, p. 108.
[8] V. A. Vasiliev, Yu. M. Romanovsky, and V. G. Yakhno, *Autowave Processes*. Moscow, Russia: Nauka, 1987, in Russian.
[9] Y. Yamaguchi and H. Shimizu, "Theory of self-synchronization in the presence of native frequency distribution and external noises," *Physica D*, vol. 11, pp. 212–226, 1984.
[10] K. Bar-Eli, "On the stability of coupled chemical oscillators," *Physica D*, vol. 14, pp. 242–255, 1985.
[11] G. B. Ermentrout, "Oscillator death in populations of 'all to all' coupled nonlinear oscillators," *Physica D*, vol. 41, pp. 219–231, 1990.
[12] G. V. Osipov and M. M. Sushchik, "Cluster synchronization and control in a lattice of coupled oscillators," *Phys. Rev. E*, to be published.
[13] G. V. Osipov, A. S. Pikovsky, M. G. Rosenblum, and J. Kurths, "Phase synchronization effects in a lattice of nonidentical Rössler oscillators," *Phys. Rev. E*, vol. 55, pp. 2353–2361, 1997.
[14] S. Watanabe and S. H. Strogatz, "Constants of motion for superconducting Josephson arrays," *Physica D*, vol. 74, pp. 197–253, 1994.
[15] H. G. Winful and S. S. Wang, "Stability of phase locking in coupled semiconductor laser arrays," *Appl. Phys. Lett.*, vol. 53, pp. 1894–1896, 1988.

International Journal of Bifurcation and Chaos, Vol. 7, No. 8 (1997) 1873–1885
© World Scientific Publishing Company

# $n$-DOUBLE SCROLL HYPERCUBES IN 1-D CNNs

J. A. K. SUYKENS*
*Katholieke Universiteit Leuven, Department of Electrical Engineering, ESAT-SISTA, Kardinaal Mercierlaan 94, B-3001 Leuven (Heverlee), Belgium*

L. O. CHUA†
*Department of Electrical Engineering and Computer Science University of California at Berkeley, Berkeley, CA 94720, USA*

Received October 7, 1996; Revised October 26, 1996

Unidirectional and diffusive coupling of identical $n$-double scroll cells in a one-dimensional cellular neural network is studied. Weak coupling between the cells leads to hyperchaos, with $n$-double scroll hypercube attractors observed in the common state subspace of the cells. Individually the cells remain behaving as $n$-double scrolls. The $n$-double scroll hypercubes are filled with multiple scrolls. Their birth goes through the mechanism of intermittency.

## 1. Introduction

Among the many generalizations proposed to Chua's circuit (see e.g. [Chua, 1994; Madan, 1993]), the one introduced by Suykens and Vandewalle [1993] considers additional breakpoints in the nonlinear characteristic in order to generate multiple scrolls, resulting into so-called $n$-double scroll attractors, where $n$ is a natural number. The well-known double scroll corresponds to a 1-double scroll within this framework. An electrical circuit implementation has been made by Arena *et al.* [1996] which confirms the existence of $n$-double scrolls. Moreover this implementation makes use of a piecewise linear representation of the nonlinear characteristic.

On the other hand many interesting phenomena have been observed by taking Chua's circuits as cells in Cellular Neural Networks (CNNs) (see e.g. [Chua & Roska, 1993; Chua *et al.*, 1995]), with, for example, unidirectional or diffusive coupling between the cells. One-dimensional CNNs with diffusive coupling have been investigated in [Zheleznyak & Chua, 1994; Pivka, 1995; Nekorkin & Chua, 1993] with phenomena occurring such as spatiotemporal chaos, spatial disorder and traveling waves. In two-dimensional CNNs phenomena such as traveling waves, spiral waves, trigger and target waves and Turing patterns have been observed [Pérez–Muñuzuri *et al.*, 1993; Pivka, 1995; Chua & Goraş, 1995]. Scroll waves and scroll rings can be generated in three-dimensional CNNs with diffusive coupling [Pivka *et al.*, 1995]. Unidirectional coupling in one-dimensional CNNs has been studied in [Kapitaniak *et al.*, 1994; Kapitaniak & Chua, 1994].

In the latter work of Kapitaniak & Chua, hyperchaotic behavior has been generated by coupling identical Chua's circuits that behave individually as double scrolls. In the common state subspace of the cells the birth of a so-called double–double scroll attractor has been observed. The work reported in our paper is very much related to this result. Taking a 1D–CNN consisting of $n$-double scroll cells

*E-mail: johan.suykens@esat.kuleuven.ac.be
†E-mail: chua@fred.eecs.berkeley.edu

with weak unidirectional or diffusive coupling between the cells, an $n$-double scroll hypercube is obtained in the common state subspace of the cells. The dimension of this hypercube is equal to the number of cells in the array. The number of scrolls within the hypercube increases with the number $n$ of the $n$-double scroll cell. For the arrays that have been simulated, the number of positive Lyapunov exponents is equal to the number of cells, which has been stated also in [Kapitaniak & Chua, 1994]. The birth of the double–double scroll attractor in [Kapitaniak & Chua, 1994] goes by means of classical intermittency, with occasional bursts from a three-dimensional manifold to higher dimensions. A similar mechanism is at the basis of the birth of the $n$-double scroll hypercube.

An engineering motivation for studying higher dimensional hyperchaotic arrays is in, for instance, their use for secure communication applications (see e.g. [Wu & Chua, 1994]). CNNs consisting of $n$-double scroll circuits can be represented as Lur'e systems for which a condition of master–slave synchronization is given in [Suykens & Vandewalle, 1996]. The latter condition is based on a Lur'e–Postnikov Lyapunov function for the error system and is expressed as a matrix inequality.

This paper is organized as follows. In Sec. 2 we review the equations of $n$-double scroll circuits. In Sec. 3 1-D CNNs with unidirectional and diffusive coupling of $n$-double scroll cells are described. In Sec. 4 the existence of $n$-double scroll hypercubes for weak coupling is reported. In Sec. 5 the route from synchronization to hypercubes is discussed.

## 2. $n$-Double Scroll Circuits

The electrical circuit for obtaining $n$-double scrolls, according to the implementation of Arena *et al.* [1996], is given by

$$\begin{cases} \dot{x} = \alpha[y - h(x)] \\ \dot{y} = x - y + z \\ \dot{z} = -\beta y \end{cases} \tag{1}$$

with as nonlinear function the piecewise linear characteristic

$$h(x) = m_{2n-1}x + \frac{1}{2}\sum_{i=1}^{2n-1}(m_{i-1} - m_i)(|x + c_i| - |x - c_i|), \tag{2}$$

consisting of $2(2n-1)$ breakpoints, where $n$ is a natural number. In order to generate $n$-double scrolls one takes $\alpha = 9$ and $\beta = 14.286$. Some special cases are:

- 1-*double scroll*:

$$m_0 = -1/7 \quad m_1 = 2/7$$
$$c_1 = 1$$

corresponding to the well-known double scroll (see e.g. [Chua *et al.* 1986; Chua, 1994; Madan, 1993]).

- 2-*double scroll*:

$$m_0 = -1/7 \quad m_1 = 2/7 \quad m_2 = -4/7 \quad m_3 = m_1$$
$$c_1 = 1 \quad c_2 = 2.15 \quad c_3 = 3.6$$

- 3-*double scroll*:

$$m_0 = -1/7 \quad m_1 = 2/7 \quad m_2 = -4/7$$
$$m_3 = m_1 \quad m_4 = m_2 \quad m_5 = m_3$$
$$c_1 = 1 \quad c_2 = 2.15 \quad c_3 = 3.6 \quad c_4 = 8.2 \quad c_5 = 13.$$

The 2-double scroll and 3-double scroll are shown in Fig. 1. For more details about $n$-double scrolls we refer to [Suykens & Vandewalle, 1993; Arena *et al.* 1996].

## 3. One-Dimensional CNNs with $n$-Double Scroll Cells

Let us now consider the following one-dimensional cellular neural network (CNN) consisting of identical $n$-double scroll cells, with either unidirectional coupling between the cells

$$\begin{cases} \dot{x}^{(j)} = \alpha[y^{(j)} - h(x^{(j)})] \\ \dot{y}^{(j)} = x^{(j)} - y^{(j)} + z^{(j)} + K_{j-1}(y^{(j)} - y^{(j-1)}) \\ \dot{z}^{(j)} = -\beta y^{(j)}, \quad j = 1, 2, \ldots, L \end{cases} \tag{3}$$

or diffusive coupling as

$$\begin{cases} \dot{x}^{(j)} = \alpha[y^{(j)} - h(x^{(j)})] \\ \qquad + D_x(x^{(j-1)} - 2x^{(j)} + x^{(j+1)}) \\ \dot{y}^{(j)} = x^{(j)} - y^{(j)} + z^{(j)} \\ \dot{z}^{(j)} = -\beta y^{(j)}, \quad j = 1, 2, \ldots, L \end{cases} \tag{4}$$

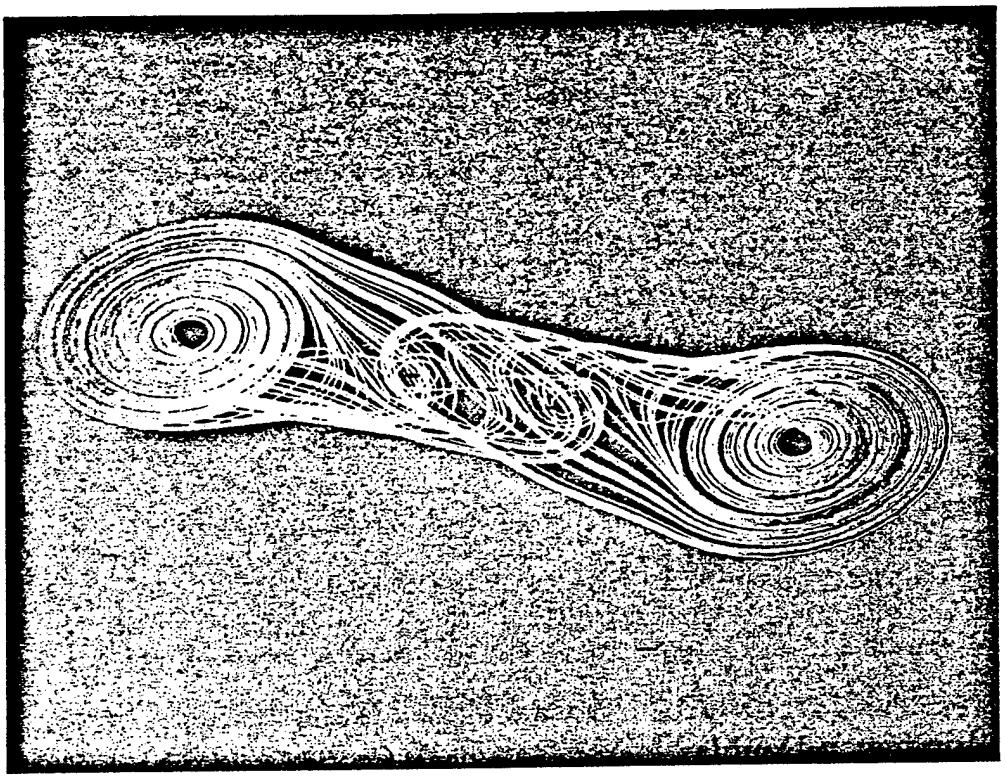

(a)

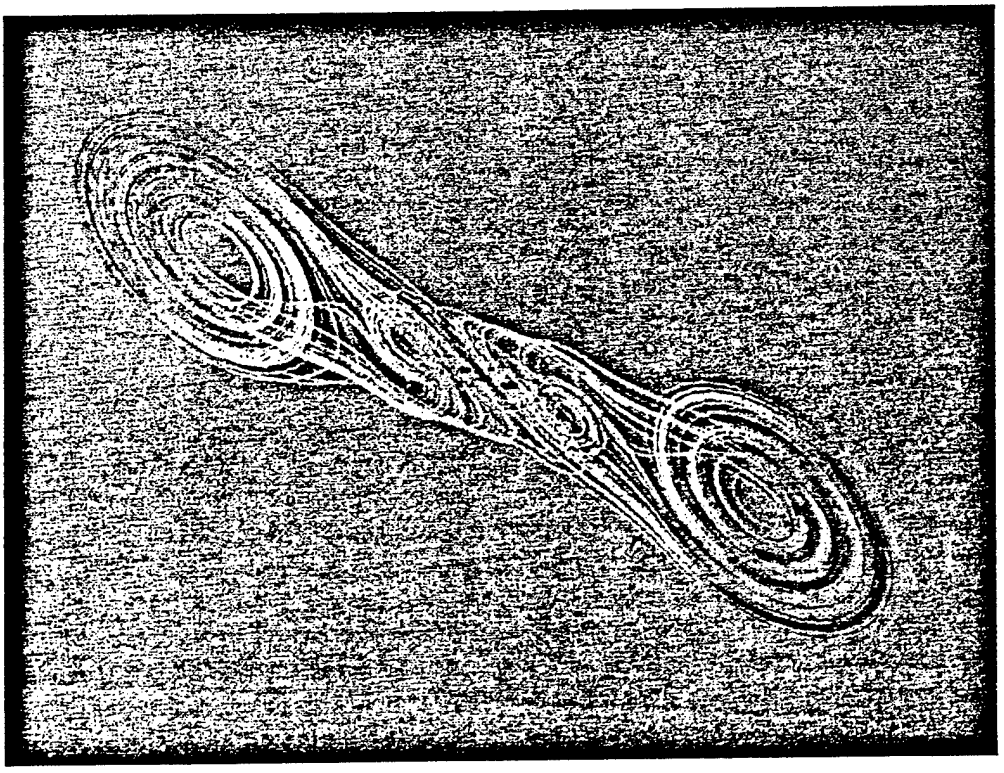

(b)

Fig. 1. (a) Three-dimensional view on the 2-double scroll attractor; (b) three-dimensional view on the 3-double scroll attractor.

or as

$$\begin{cases} \dot{x}^{(j)} = \alpha[y^{(j)} - h(x^{(j)})] \\ \dot{y}^{(j)} = x^{(j)} - y^{(j)} + z^{(j)} \\ \qquad + D_y(x^{(j-1)} - 2x^{(j)} + x^{(j+1)}) \\ \dot{z}^{(j)} = -\beta y^{(j)}, \quad j = 1, 2, \ldots, L \end{cases} \tag{5}$$

where $L$ denotes the number of cells. We impose the conditions $y^{(0)} = y^{(L)}$ for Eq. (3) and $x^{(0)} = x^{(L)}$, $x^{(L+1)} = x^{(1)}$ for Eqs. (4) and (5). For the coupling constants, $K_0 = 0$, $K_j = K$ $(j = 1, \ldots, L-1)$ and positive diffusion coefficients $D_x$, $D_y$ are chosen.

The scheme Eq. (3) with unidirectional coupling has been studied by Kapitaniak & Chua [1994] for the case $n = 1$ with Chua's circuits as cells. The other schemes of 1-D reaction–diffusion CNNs has been described in [Chua *et al.* 1995; Pivka, 1995; Zheleznyak & Chua, 1994].

## 4. Weak Coupling: $n$-Double Scroll Hypercubes

Let us consider first the case $n = 2$ with 2-double scroll circuits in the CNNs [Eqs. (3) and (5)]. Both for weak unidirectional and diffusive coupling one obtains a 2-double scroll hypercube in the common state subspace of the cells, i.e. in $(x^{(1)}, x^{(2)})$ for $L = 2$; $(x^{(1)}, x^{(2)}, x^{(3)})$ for $L = 3$; $(x^{(1)}, x^{(2)}, x^{(3)}, x^{(4)})$ for $L = 4$, etc. The dimension of the hypercube is equal to the number of cells $L$. So one obtains for $L = 2$, 3, 4 a 2-double scroll square, cube and hypercube, respectively (see Figs. 2 and 3). This phenomenon is typically obtained for 'small' values of $K$, $D_x$ or $D_y$, such as 0.01 or 0.001. For this weak coupling, the individual cells remain behaving as 2-double scrolls while the hypercube is formed in the common cell-space (Fig. 4). Simulation results for 10 cells with the formation of a ten-dimensional hypercube are shown in Fig. 5. The initial states were chosen 'close' to the origin (according to [Kapitaniak & Chua, 1994]): $x^{(j)} = 0.01 + (j-1)0.001$, $y^{(j)} = 0$, $z^{(j)} = 0$ for $j = 1, 2, \ldots, L$ and $L = 2$, 3, 4, 10. Similar phenomena were obtained for other choices of the initial state.

For the case $n = 3$ with 3-double scroll cells in the CNNs [Eqs. (3) and (4)], similar phenomena occur. 3-Double scroll squares, cubes and hypercubes, obtained for $L = 2$, 3, 4, respectively are shown in Figs. 6 and 7. The larger the number of $n$ the more scrolls the $L$-dimensional hypercube contains. The same initial states were chosen as for the corresponding $n = 2$ cases.

For the simulation results of weak coupling, described in this section, the number of positive Lyapunov exponents is equal to the number of cells, which means hyperchaos is obtained for $L \geq 2$. This confirms the conjecture on the number of positive Lyapunov exponents made in [Kapitaniak & Chua, 1994]. The estimated Lyapunov exponents are shown in Table 1. The algorithm with Gram–Schmidt orthonormalization described in [Parker & Chua, 1989] has been implemented in Matlab with joint simulation of the system equation and its variational equation using a Runge–Kutta integration rule (*ode23* in Matlab). The variational equations were analytically derived from Eq. (1). A Matlab to C compiler (*mcc* in Matlab) has been used. All simulations were done on a SUN Ultra1–140 workstation. The estimated values of the negative Lyapunov exponents much depend on the choice of the time horizon $T$ on which the system and its variational equation are simulated. Choosing a larger $T$ (but still making sure that no overflow occurs in the variational equation) results in a larger estimate for the Lyapunov dimension of the system. Indeed, according to Kaplan and Yorke the Lyapunov dimension is defined as $\mathcal{D}_l = j + (\lambda_1 + \cdots + \lambda_j)/|\lambda_{j+1}|$ where $j$ is the largest integer such that $\lambda_1 + \cdots + \lambda_j \geq 0$, provided the Lyapunov exponents are ordered as $\lambda_1 \geq \cdots \geq \lambda_d$, with $d$ being the dimension of the state space [Parker & Chua, 1989].

## 5. Route from Synchronization to the Hypercube

For the case $n = 2$ and 2 cells with unidirectional coupling one obtains synchronization for $K < -1.3$ and instability for $K > 0.38$. The route from synchronization to the hypercube goes through intermittency with occasional bursts to higher dimensions, as shown on Fig. 8 for the case of diffusive coupling with 3 cells. This phenomenon has been reported in [Kapitaniak & Chua, 1994] as well. For the case of diffusive coupling and 3 cells, the array synchronizes approximately for $D_y > 0.1$. For $D_y = 0.1$ and $D_y = 0.09$ the system behaves 'close' to synchronization, with the formation of additional scrolls in the common cell-space, but the array is not able to develop the full hypercube. For the simulations, the same initial states were taken as in the previous section.

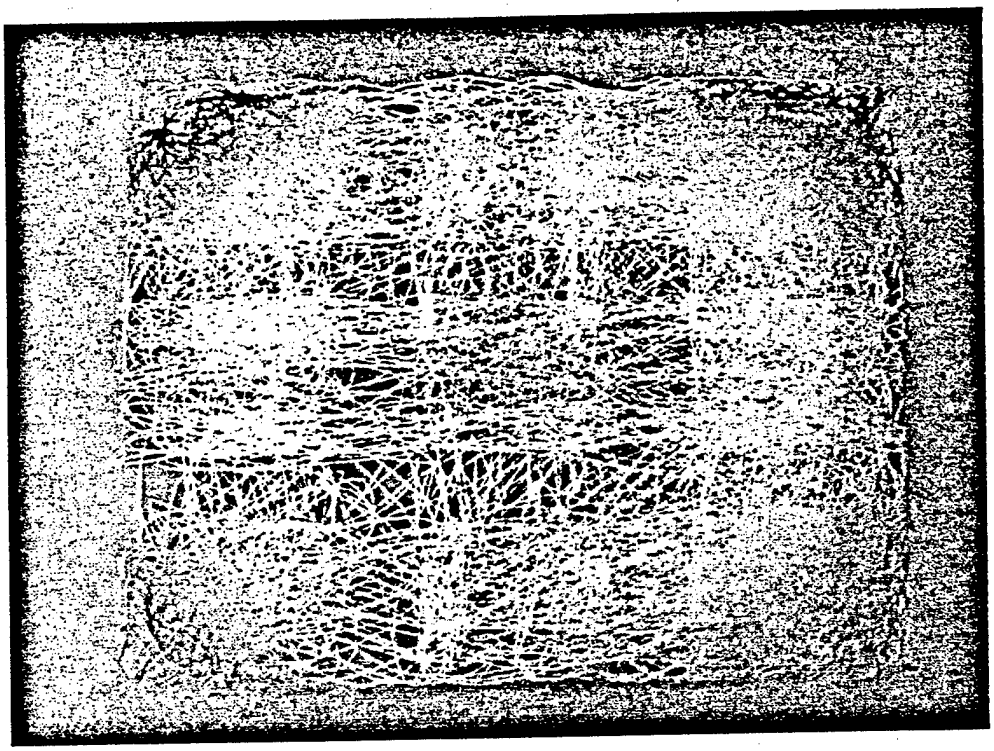

(a)

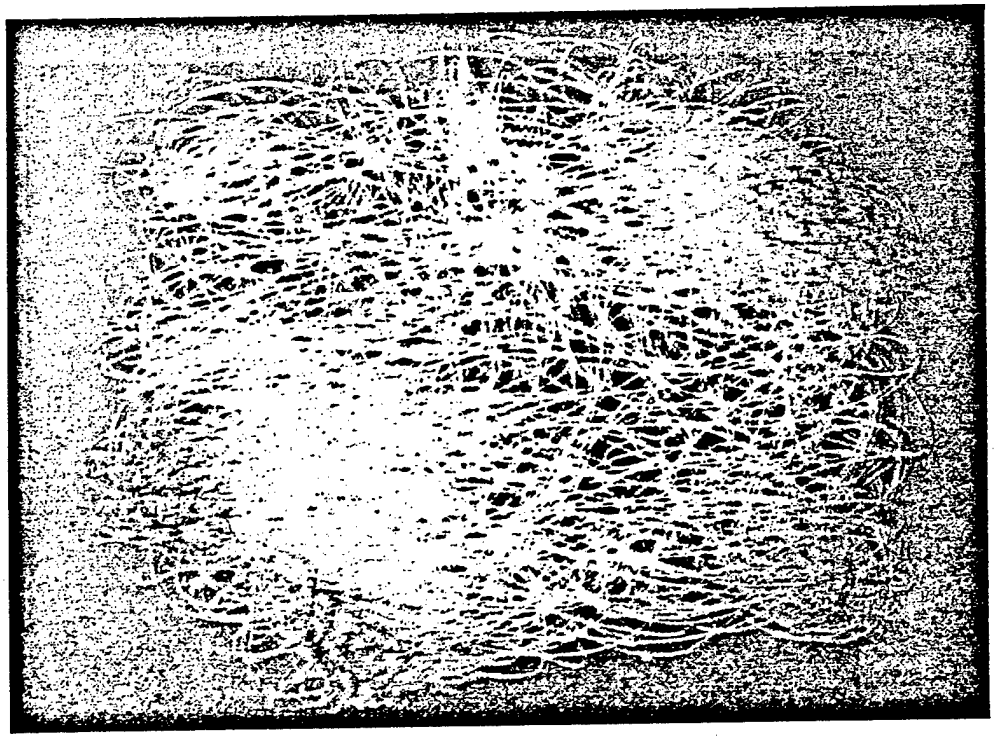

(b)

Fig. 2. (a) 2-double scroll square from a 1D–CNN with 2 cells of 2-double scroll circuits and unidirectional coupling between the cells ($K = 0.001$). Note the resemblance and difference with Fig. 2 in [Kapitaniak & Chua, 1994]. Shown is the plane $(x^{(1)}, x^{(2)})$. (b) 2-double scroll cube from a 1D–CNN with 3 cells of 2-double scroll circuits and unidirectional coupling between the cells ($K = 0.001$). The subspace $(x^{(1)}, x^{(2)}, x^{(3)})$ is shown.

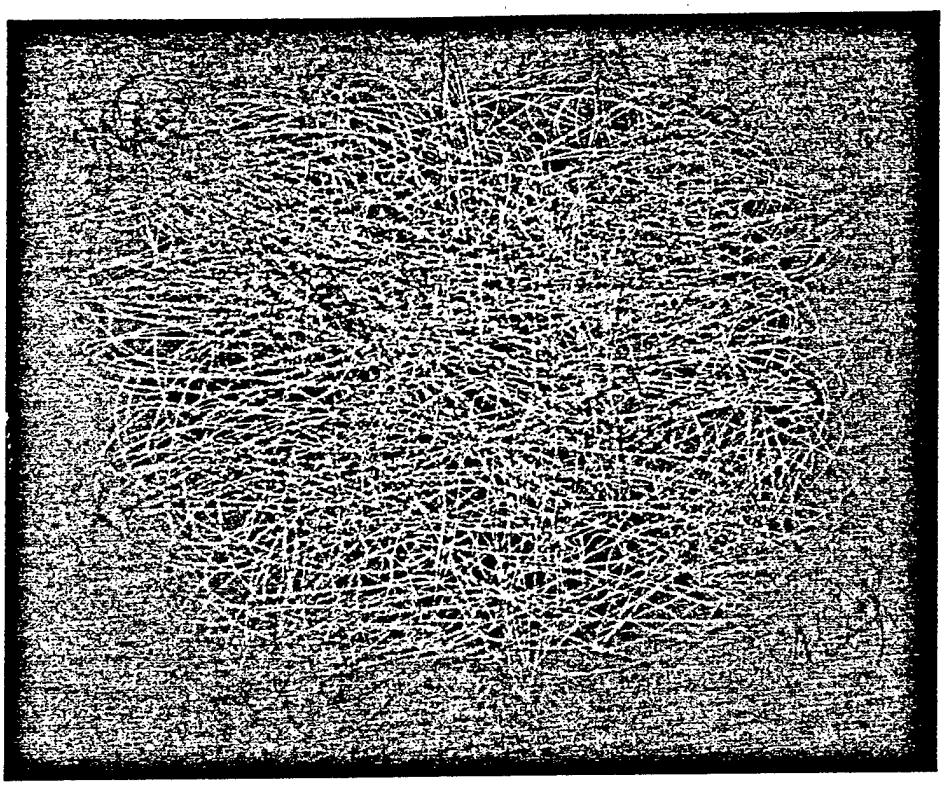

(a)

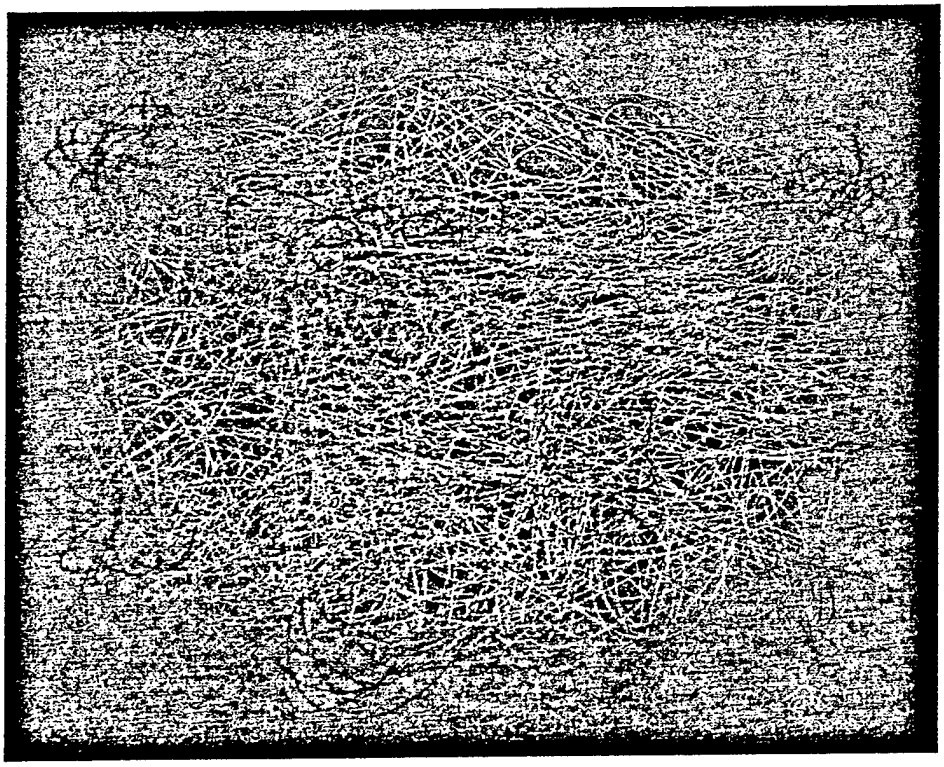

(b)

Fig. 3. 2-double scroll hypercube from a 1D–CNN with 4 cells of 2-double scroll circuits and diffusive coupling between the cells ($D_y = 0.01$). Two views are shown on this four-dimensional hypercube: (a) $(x^{(1)}, x^{(2)}, x^{(3)})$; (b) $(x^{(2)}, x^{(3)}, x^{(4)})$.

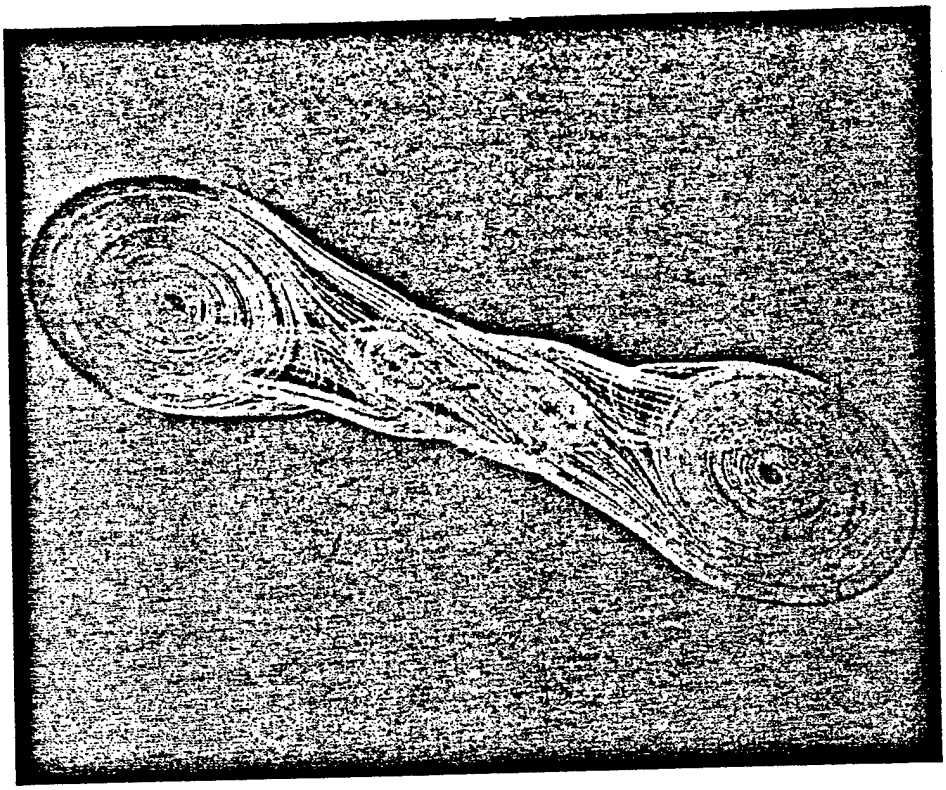

(a)

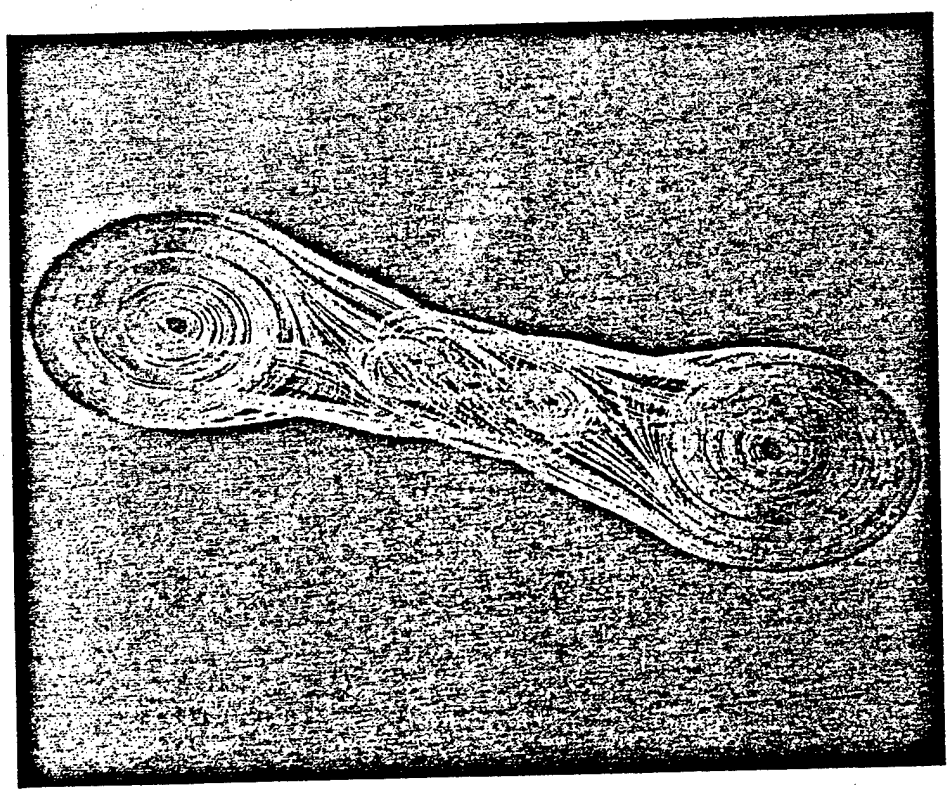

(b)

Fig. 4. While the 2-double scroll circuits reveal in their common cell state subspace a four-dimensional 2-double scroll hypercube (Fig. 3), the individual cells remain behaving as 2-double scrolls. In this figure this is illustrated for two of the four cells (cell 1 and 3): (a) $(x^{(1)}, y^{(1)}, z^{(1)})$, (b) $(x^{(3)}, y^{(3)}, z^{(3)})$.

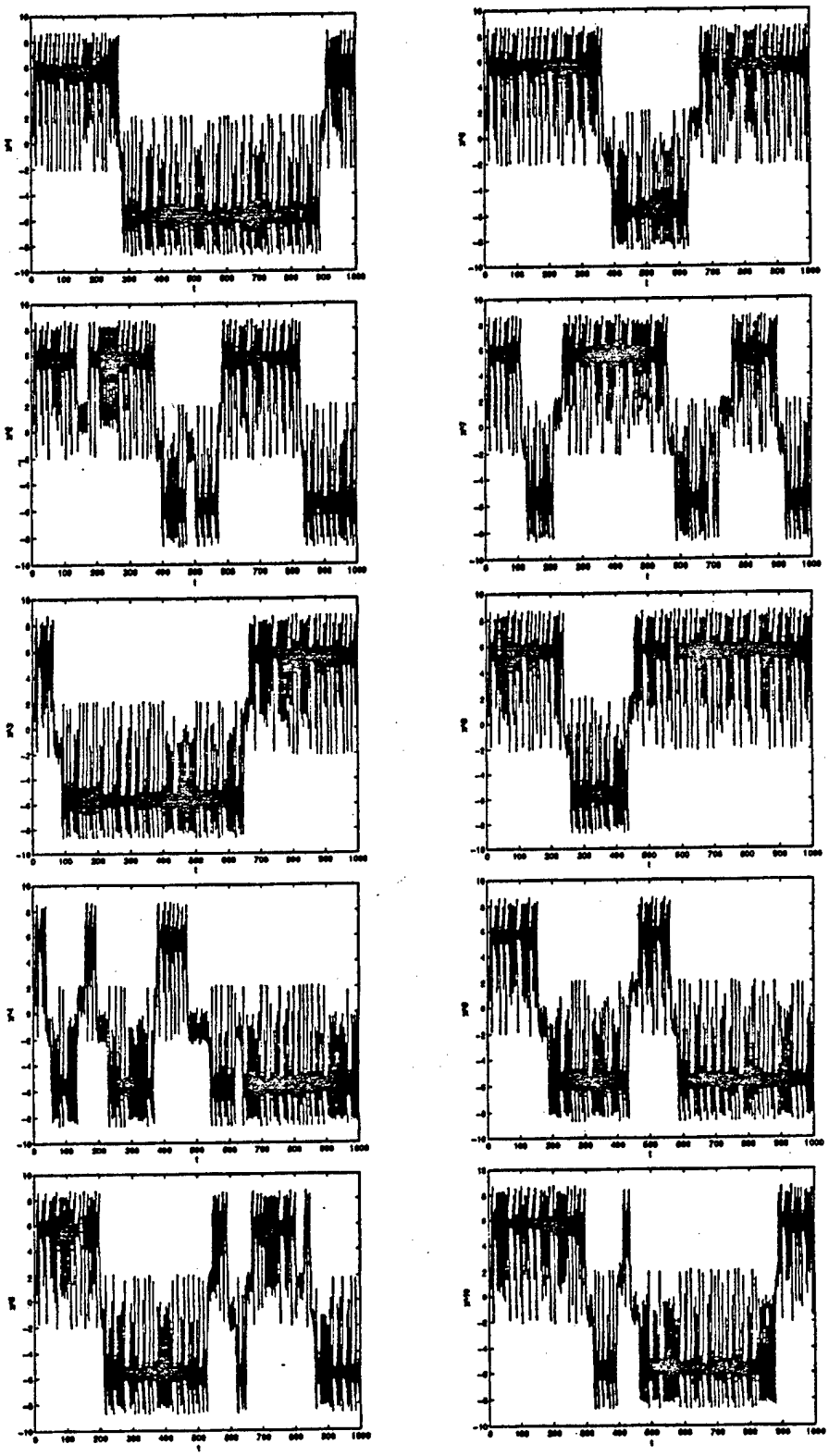

Fig. 5. Diffusive coupling ($D_y = 0.001$) between 10 cells of 2-double scroll circuits in a 1D–CNN, resulting into a ten-dimensional 2-double scroll hypercube. Shown are the variables $x^{(j)}$ for $j = 1, 2, \ldots, 10$ with respect to time for a certain initial state.

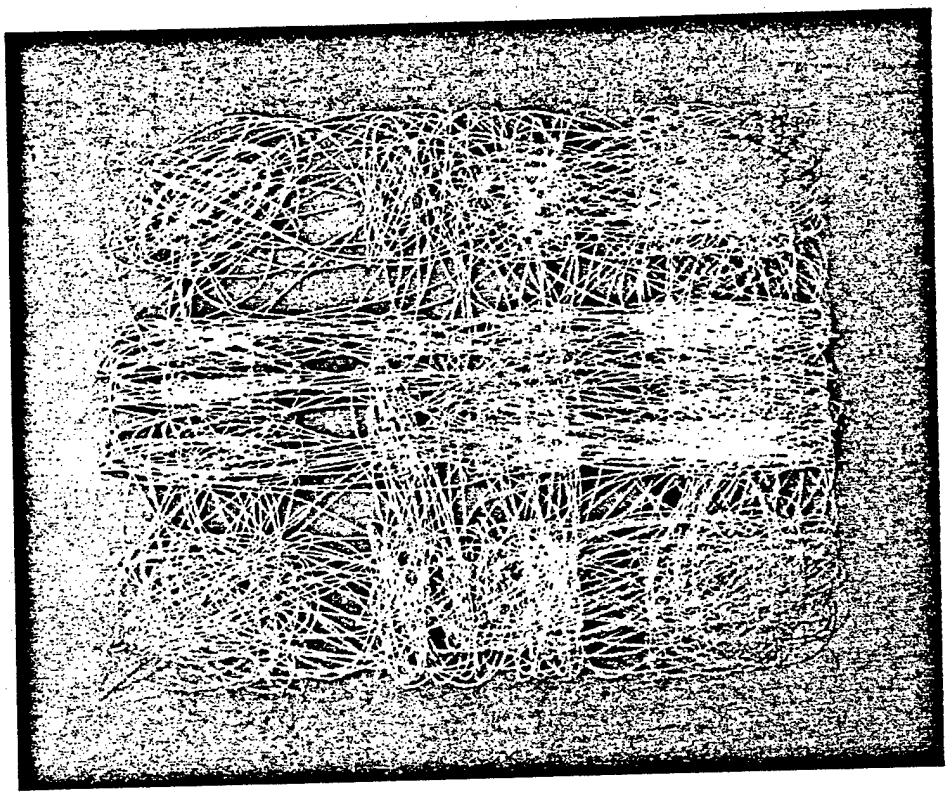

(a)

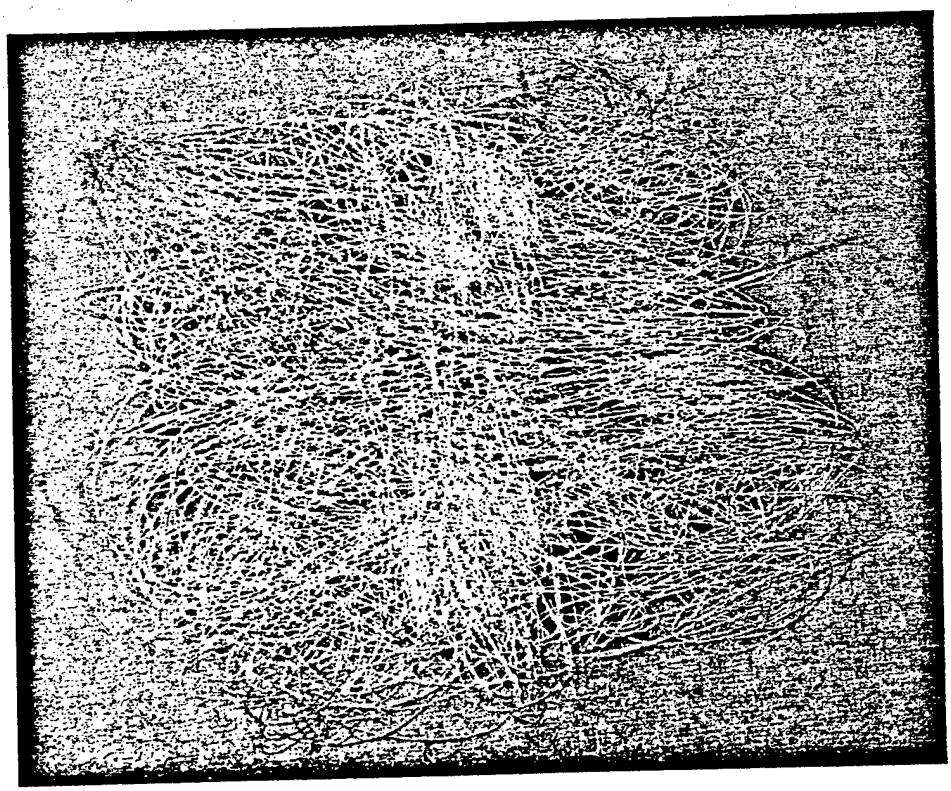

(b)

Fig. 6. (a) 3-double scroll square from a 1D–CNN with 2 cells of 3-double scroll circuits and unidirectional coupling between the cells ($K = 0.01$). Shown is the plane $(x^{(1)}, x^{(2)})$. (b) 3-double scroll cube from a 1D–CNN with 3 cells of 3-double scroll circuits and diffusive coupling between the cells ($D_x = 0.001$). Shown is the view $(x^{(1)}, x^{(2)}, x^{(3)})$.

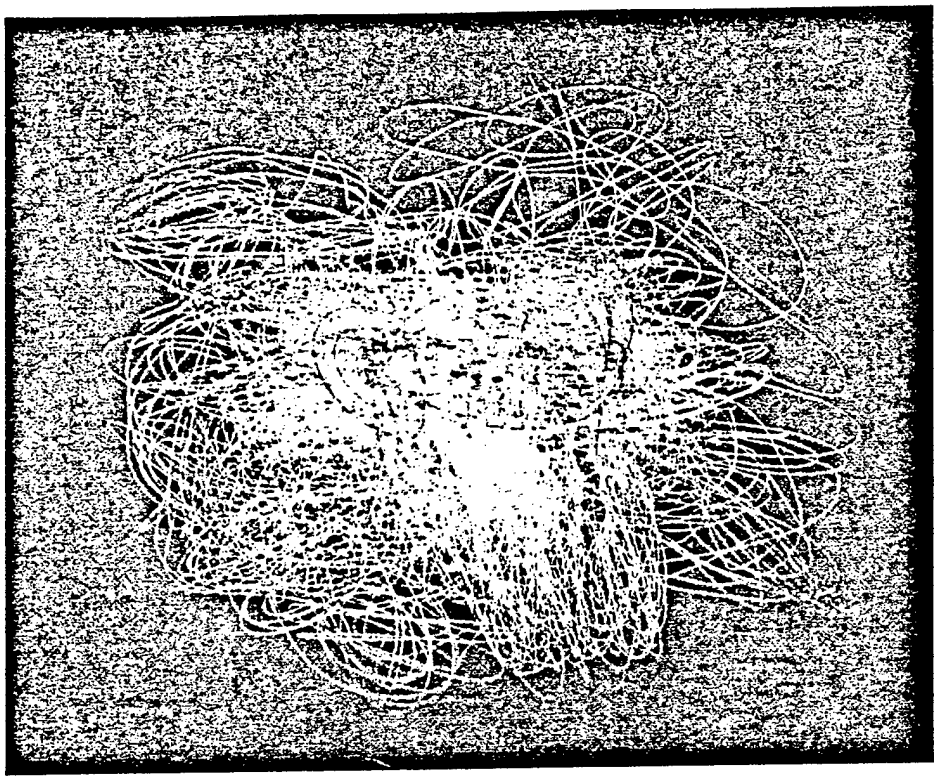

(a)

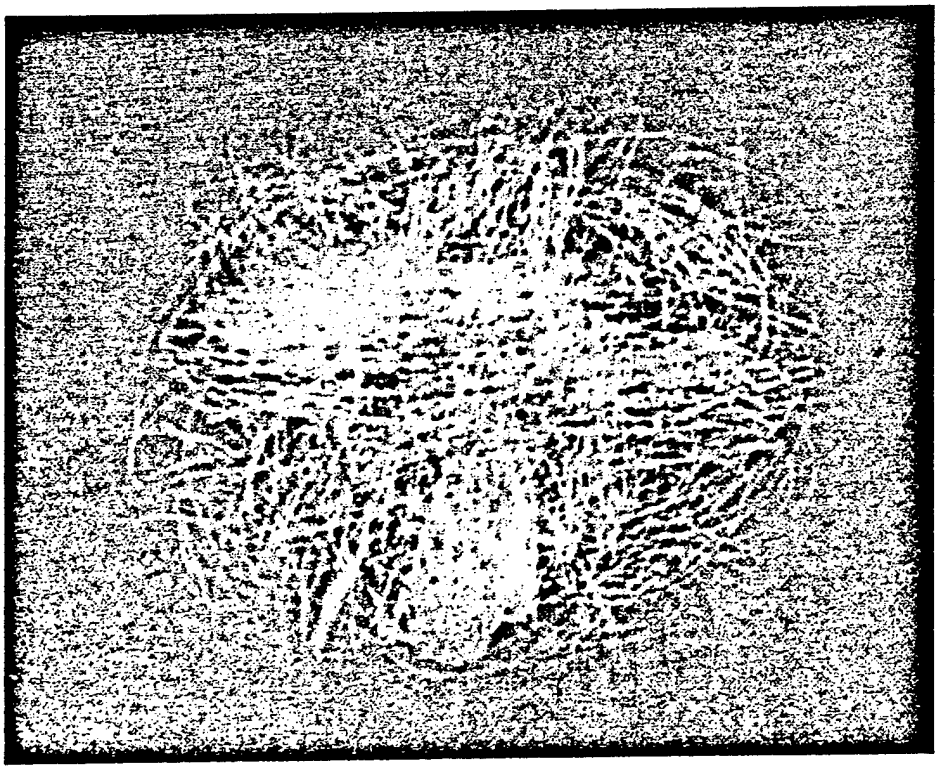

(b)

Fig. 7. 3-double scroll hypercube from a 1D–CNN with 4 cells of 3-double scroll circuits and diffusive coupling between the cells ($D = 0.001$). Two views are shown on this four-dimensional hypercube: (a) $(x^{(1)}, x^{(2)}, x^{(3)})$; (b) $(x^{(2)}, x^{(3)}, x^{(4)})$.

Table 1. In this Table estimations of Lyapunov exponents are made for 1D–CNNs with 2- and 3-double scroll cells and different numbers of cells. For weak coupling the array has a number of positive ($\lambda_+$), zero ($\lambda_0$) and negative ($\lambda_-$) Lyapunov exponents equal to the number of cells $L$. $\mathcal{D}_l$ is the estimated Lyapunov dimension and $T$ is the time horizon on which the array together with its variational equation have been simulated.

| Array | Coupling | $\lambda_+$ | $\lambda_0$ | $\lambda_-$ | $\mathcal{D}_l$ | $T$ |
|---|---|---|---|---|---|---|
| $n=2, L=2$ | $K=0.001$ | 0.30 | 0.00 | −0.87 | 4.6 | 30 |
| | | 0.28 | 0.00 | −0.90 | | |
| $n=2, L=4$ | $D_y=0.01$ | 0.34 | 0.00 | −1.41 | 8.7 | 20 |
| | | 0.28 | 0.00 | −1.43 | | |
| | | 0.23 | 0.00 | −1.46 | | |
| | | 0.17 | 0.00 | −1.48 | | |
| $n=2, L=10$ | $D_y=0.001$ | 0.34 | 0.00 | −2.62 | 21.1 | 10 |
| | | 0.32 | 0.00 | −2.77 | | |
| | | 0.31 | 0.00 | −2.86 | | |
| | | 0.31 | 0.00 | −2.92 | | |
| | | 0.29 | 0.00 | −2.96 | | |
| | | 0.28 | 0.00 | −2.99 | | |
| | | 0.27 | 0.00 | −3.02 | | |
| | | 0.26 | 0.00 | −3.04 | | |
| | | 0.26 | 0.00 | −3.07 | | |
| | | 0.23 | 0.00 | −3.10 | | |
| $n=3, L=2$ | $K=0.01$ | 0.28 | 0.00 | −0.88 | 4.6 | 30 |
| | | 0.27 | 0.00 | −0.91 | | |
| $n=3, L=4$ | $D_x=0.001$ | 0.33 | 0.00 | −1.42 | 8.8 | 20 |
| | | 0.29 | 0.00 | −1.43 | | |
| | | 0.25 | 0.00 | −1.47 | | |
| | | 0.23 | 0.00 | −1.49 | | |

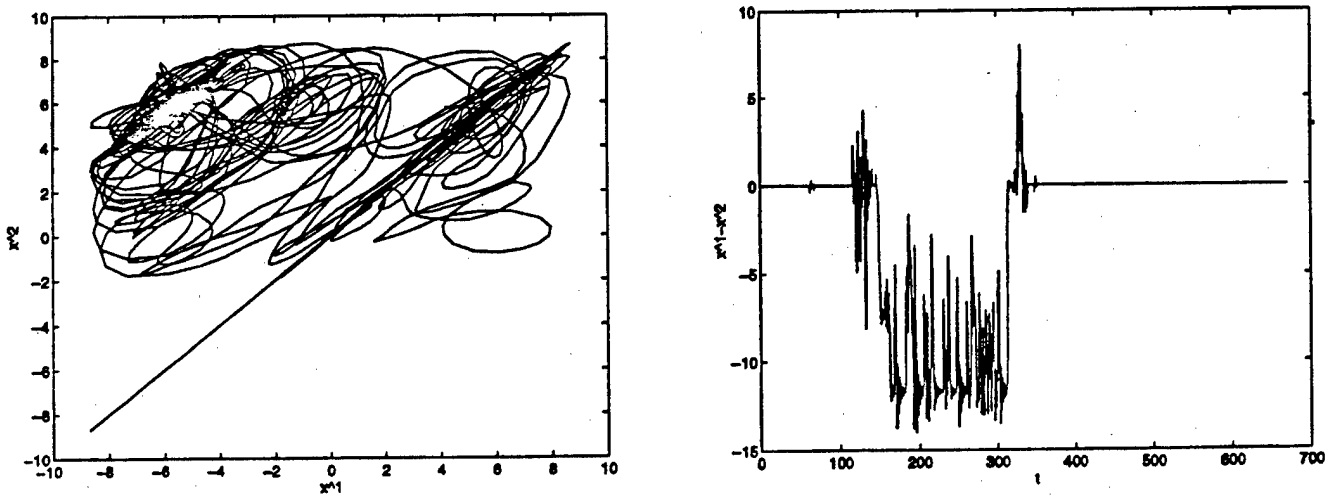


(a) (b)

Fig. 8. This figure shows unidirectional coupling between two 2-double scroll circuits for $K=-1.2$. Occasional synchronization between the two cells is clearly visible on (a) $(x^{(1)}, x^{(2)})$ and (b) $x^{(1)}(t)$–$x^{(2)}(t)$.

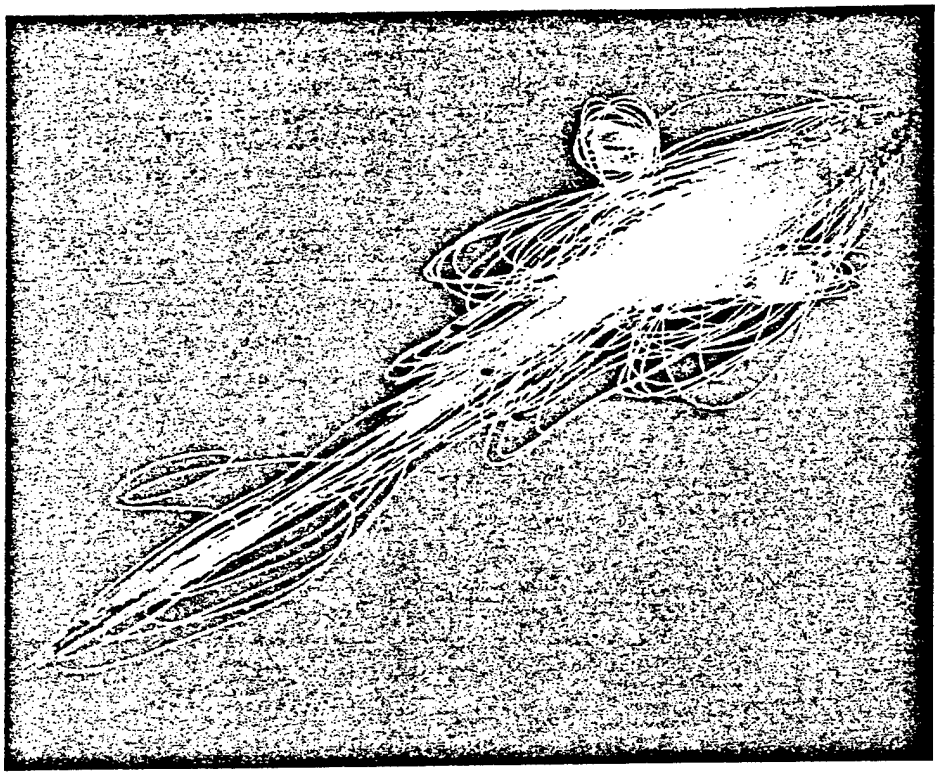

(a)

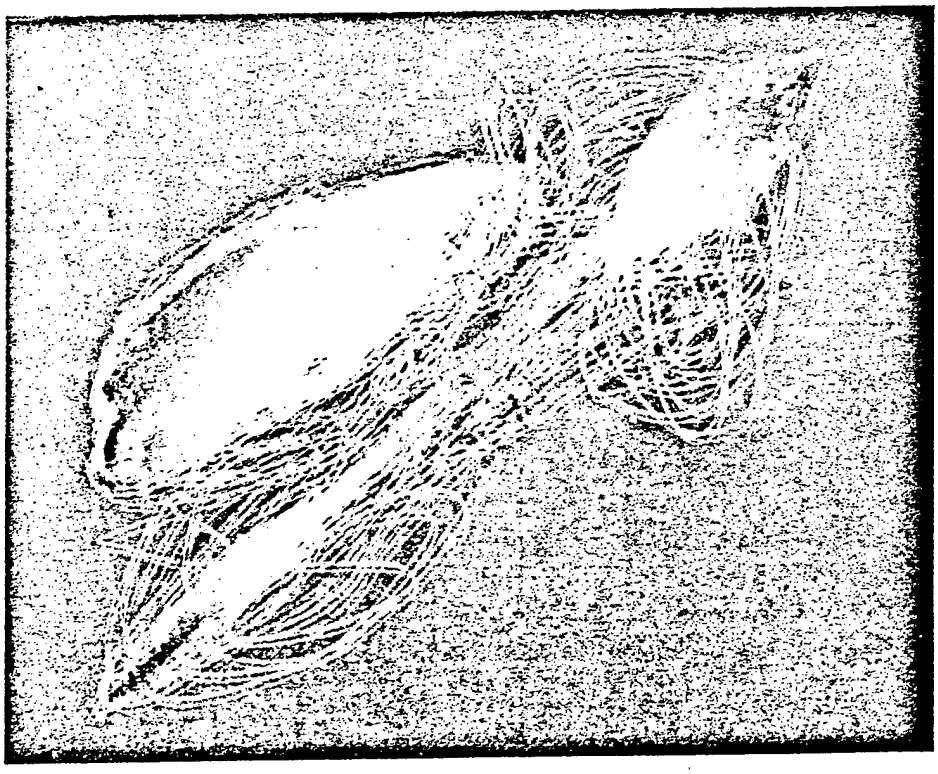

(b)

Fig. 9. Diffusive coupling between three 2-double scroll circuits for (a) $D_y = 0.1$ and (b) $D_y = 0.09$. For this choice of parameters the system is not able to develop the 2-double scroll cube. Shown is the view $(x^{(1)}, x^{(2)}, x^{(3)})$.

## 6. Conclusion

In this paper the new phenomenon of $n$-double scroll hypercubes has been described, which occurs in weak unidirectional or diffusive coupling of $n$-double scroll cells in one-dimensional CNNs. The dimension of the hypercube is equal to the number of cells in the array. The hypercube is filled with a number of multiple scrolls that increases with the number of $n$. For weak coupling the individual cells remain behaving as $n$-double scrolls, while the hypercube is formed in the common cell-space. For the simulations that have been done, the array behaves hyper-chaotically with a number of positive Lyapunov exponents equal to the number of cells. The route from synchronization to the hypercube in the array goes by means of intermittency, as earlier described by Kapitaniak and Chua for unidirectional coupling of Chua's circuits in 1-D CNNs. Potential applications of the $n$-double scroll hypercube CNN are in the use of high-dimensional chaos for secure communication applications and artificial neural information processing systems.

## Acknowledgments

This research work was carried out at the University of California at Berkeley, in the framework of the Belgian Programme on Interuniversity Poles of Attraction, initiated by the Belgian State, Prime Minister's Office for Science, Technology and Culture (IUAP-17) and in the framework of a Concerted Action Project MIPS (Modelbased Information Processing Systems) of the Flemish Community. The work is supported in part by the Office of Naval Research under grant N00014-96-1-0753. The authors would like to thank Tao Yang and Chai Wah Wu for helping to produce the color pictures.

## References

Arena, P., Baglio, P., Fortuna, F. & Manganaro, G. [1996] "Generation of $n$-double scrolls via cellular neural networks," *Int. J. Circuits Theory Appl.* **24**, 241–252.

Chua, L. O., Komuro, M. & Matsumoto, T. [1986] "The double scroll family," *IEEE Trans. Circuits Syst. – I* **33**(11), 1072–1118.

Chua, L. O. & Roska, T. [1993] "The CNN paradigm," *IEEE Trans. Circuits Syst. – I* **40**(3), 147–156.

Chua, L. O. [1994] "Chua's circuit 10 years later," *Int. J. Circuits Theory Appl.* **22**, 279–305.

Chua, L. O., Hasler, M., Moschytz, G. S. & Neirynck, J. [1995] "Autonomous cellular neural networks: A unified paradigm for pattern formation and active wave propagation," *IEEE Trans. Circuits Syst. – I* **42**(10), 559–577.

Chua, L. O. & Goraş, L. [1995] "Turing patterns in cellular neural networks," *Int. J. Electron.* **79**(6), 719–736.

Kapitaniak, T., Chua, L. O. & Zhong, G.-Q. [1994] "Experimental hyperchaos in coupled Chua's circuits," *IEEE Trans. Circuits Syst. – I* **41**(7), 499–503.

Kapitaniak, T. & Chua, L.O. [1994] "Hyperchaotic attractors of unidirectionally-coupled Chua's circuits," *Int. J. Bifurcation and Chaos* **4**(2), 477–482.

Madan, R. N. (Guest ed.) [1993] *Chua's Circuit: A Paradigm for Chaos* (World Scientific Publishing, Singapore).

Nekorkin, V. I. & Chua, L. O. [1993] "Spatial disorder and wave fronts in a chain of coupled Chua's circuits," *Int. J. Bifurcation and Chaos* **3**(5), 1281–1291.

Parker, T. S. & Chua, L. O. [1989] *Practical Numerical Algorithms for Chaotic Systems* (Springer-Verlag, New York).

Pérez–Muñuzuri, A., Pérez–Muñuzuri, V., Pérez–Villar, V. & Chua, L. O. [1993] "Spiral waves on a 2-D array of nonlinear circuits," *IEEE Trans. Circuits Syst. – I* **40**(11), 872–877.

Pivka, L. [1995] "Autowaves and spatio-temporal chaos in CNNs–Part I & Part II: A tutorial," *IEEE Trans. Circuits Syst. – I* **42**(10), 638–649 & 650–664.

Pivka, L., Zheleznyak, A. L., Wu, C. W. & Chua, L. O. [1995] "On the generation of scroll waves in a three-dimensional discrete active medium," *Int. J. Bifurcation and Chaos* **5**(1), 313–320.

Suykens, J. A. K. & Vandewalle, J. [1993] "Generation of $n$-double scrolls ($n = 1, 2, 3, 4, \ldots$)," *IEEE Trans. Circuits Syst. – I* **40**(11), 861–867.

Suykens, J. A. K. & Vandewalle, J. [1997] "Master–slave synchronization of Lur'e systems," *Int. J. Bifurcation and Chaos* **7**(3), 665–669.

Wu, C. W. & Chua, L. O. [1994] "A unified framework for synchronization and control of dynamical systems," *Int. J. Bifurcation and Chaos* **4**(4), 979–989.

Zheleznyak, A. L. & Chua, L. O. [1994] "Coexistence of low-and high-dimensional spatiotemporal chaos in a chain of dissipatively coupled Chua's circuits," *Int. J. Bifurcation and Chaos* **4**(3), 639–674.

International Journal of Bifurcation and Chaos, Vol. 7, No. 6 (1997) 1323–1335
© World Scientific Publishing Company

# NONLINEAR $H_\infty$ SYNCHRONIZATION OF CHAOTIC LUR'E SYSTEMS

J. A. K. SUYKENS* and J. VANDEWALLE†
*Katholieke Universiteit Leuven, Department of Electrical Engineering, ESAT-SISTA, Kardinaal Mercierlaan 94, B-3001 Leuven (Heverlee), Belgium*

L. O. CHUA‡
*Department of Electrical Engineering and Computer Science, University of California at Berkeley, Berkeley, CA 94720, USA*

Received October 25, 1996; Revised November 10, 1996

In this paper a master-slave synchronization scheme for Lur'e systems is investigated, which consists of vector field modulation by means of the message signal. Using a full state error feedback mechanism and formulating the synchronization problem within the standard plant framework of modern control theory, it is shown how the original message can be recovered for a class of binary-valued continuous time reference inputs or message signals. Input/output properties of the synchronization scheme are analyzed using the system-theoretical approach of dissipativity with a quadratic storage function and a supply rate of finite $L_2$-gain. The feedback matrix is designed such that the influence of the exogenous input on a tracking error is minimized, corresponding to a so-called nonlinear $H_\infty$ synchronization scheme. Channel noise is taken into account in the design. The method is illustrated on Chua's circuit and an $n$-double scroll circuit.

## 1. Introduction

From existing work on synchronization of nonlinear systems, it becomes clear that there is a close relationship between synchronization and control problems [Wu & Chua, 1994; Curran & Chua, 1996; Suykens & Vandewalle, 1996]. Conditions for synchronization of e.g. two identical chaotic systems, such as Chua's circuit, are often based on Lyapunov functions in order to prove global asymptotic stability of the error system. Especially for Lur'e systems, one can observe this link between the synchronization problem and absolute stabilization of the corresponding systems.

In this paper we consider synchronization problems of Lur'e systems, with respect to applications for secure communication. In secure communication an information bearing signal is hidden on a chaotic carrier signal (see [Hasler, 1994; Wu & Chua, 1994]). From the viewpoint of control theory, this message signal can be considered as the external "reference input" in the synchronization scheme. Generally speaking, in control theory one is interested in obtaining desirable properties for control schemes such as internal stability, optimal tracking, disturbance rejection [Boyd & Barratt, 1991; Maciejowski, 1989]. Often one starts by

*E-mail: johan.suykens@esat.kuleuven.ac.be
†E-mail: joos.vandewalle@esat.kuleuven.ac.be
‡E-mail: chua@fred.eecs.berkeley.edu

studying internal stability of the autonomous system (without external reference inputs). The next step is then to introduce the reference input in the control scheme and to study conditions for achieving optimal performance such as optimal tracking and disturbance attenuation. A similar approach could and partially has been followed already for synchronization problems, by first considering schemes without external input. Basically two schemes for introducing the information signal into the synchronization scheme have been proposed then in literature: Chaotic masking and vector field modulation (see [Kennedy, 1995]). Chaotic masking has the disadvantage that distortion and noise introduced by the channel are indistinguishable from the signal. We will investigate a type of vector field modulation which corresponds to a model reference control scheme.

One advantage of considering synchronization schemes from the viewpoint of control theory is that it offers a framework for taking noise and disturbances into account in the design. According to modern control theory (such as $H_\infty$ and $\mu$ robust control theory [Maciejowski, 1989] and $NL_q$ neural control theory [Suykens *et al.*, 1996]), we will represent the synchronization scheme in standard plant form, with as regulated output the tracking error and as exogenous input the message signal together with a disturbance input. The scheme consists of linear full static state error feedback. One is interested then in seeking a feedback matrix such that the influence from the exogenous input on the regulated output is minimized, according to a certain norm. The approach that we take in this paper is based on the fundamental system-theoretical concept of dissipativity [Willems, 1972; Hill & Moylan, 1976, 1990; Wyatt *et al.*, 1981]. We consider a quadratic storage function and a supply rate of finite $L_2$-gain and derive sufficient conditions for dissipativity of the synchronization scheme, expressed as matrix inequalities [Boyd *et al.*, 1994]. The feedback matrix is then designed by solving a constrained nonlinear optimization problem. Considering the feedback matrix of the synchronization scheme as the "controller", the design corresponds to nonlinear $H_\infty$ control [Isidori & Astolfi, 1992; van der Schaft, 1996], which leads us to the introduction of the new term *nonlinear $H_\infty$ synchronization*. Previous approaches to make synchronization schemes more flexible and robust have been studied (e.g. in [Chua *et al.*, 1996; Wu & Chua, 1993, 1994, 1996]) with investigations of parameter mismatch and coping with time-varying channels. The latter topics are not studied here, but also fit within frameworks of robust control theory, where parametric uncertainties, unmodeled dynamics, noise and disturbances are analyzed and could be taken into account in the controller synthesis [Maciejowski, 1989].

It is also clear from control theory that achieving perfect tracking for all possible reference inputs is impossible. In order to avoid this problem we consider binary valued continuous time reference inputs. Though perfect tracking cannot be achieved for this class of reference inputs, the original message is recovered by implementing a hard-limiting operation on the output. Furthermore, it is well-known that error feedback synchronization algorithms are among the best methods concerning tolerance of noise, which is confirmed here by computer simulations. The scheme however requires transmission of the full state vector of the master system.

The type of nonlinear systems that we consider in the synchronization scheme are of Lur'e form, which consist of a linear dynamical system interconnected by feedback to a static nonlinearity that satisfies a sector condition [Khalil, 1992; Vidyasagar, 1993]. Chua's circuits [Chua *et al.*, 1986; Chua, 1994; Madan, 1993] and piecewise linear implementations of $n$-double scroll circuits [Suykens & Vandewalle, 1993; Arena *et al.*, 1996] are examples of Lur'e systems and have been employed here to illustrate the nonlinear $H_\infty$ synchronization scheme. Also arrays with linear coupling of Lur'e cells are representable as Lur'e systems. Examples with Chua's circuits and $n$-double scroll circuits can be found in [Kapitaniak & Chua, 1994; Suykens & Chua, 1997] respectively.

This paper is organized as follows. In Sec. 2 we outline the synchronization scheme. In Sec. 3 we discuss the error system and its standard plant representation. In Sec. 4 we consider the autonomous case and derive a sufficient condition for global asymptotic stability of the error system, based on a quadratic Lyapunov function. In Sec. 5 the non-autonomous case is considered with the message signal as external input. A condition for dissipativity with finite $L_2$-gain is derived, based on a quadratic storage function. In Sec. 6 design of the feedback matrix in the nonlinear $H_\infty$ synchronization scheme is discussed. In Sec. 7 some cryptographical aspects of the synchronization scheme are discussed. Finally, in Sec. 8 examples are proposed for two

Lur'e systems: Chua's circuit and a 2-double scroll circuit.

## 2. Synchronization Scheme

Let us consider the following master-slave synchronization scheme

$$\mathcal{R}: \begin{cases} \dot{m} = Rm + Sr \\ d = Tm + Ur \end{cases}$$

$$\mathcal{M}: \begin{cases} \dot{x} = Ax + B\sigma(Cx) + Dd \\ p = Hx \end{cases} \quad (1)$$

$$\mathcal{S}: \begin{cases} \dot{z} = Az + B\sigma(Cz) + F(p + \varepsilon - q) \\ q = Hz \end{cases}$$

with master system $\mathcal{M}$, slave system $\mathcal{S}$, linear filter $\mathcal{R}$, state variables $x, z \in \mathbb{R}^n$ and $m \in \mathbb{R}^{n_r}$, outputs of the subsystems $p, q \in \mathbb{R}^n$ and $d \in \mathbb{R}$, message signal $r \in \mathbb{R}$ and disturbance input $\varepsilon \in \mathbb{R}^n$ (Fig. 1). At the transmitter $\mathcal{M}$, a linear transformation $H \in \mathbb{R}^{n \times n}$ is applied to the state $x$. The resulting vector $p$ is sent on the channel. At the receiver, error feedback (full static state feedback) between the output $q$ of $\mathcal{S}$ and the transmitted signal $p$, which is corrupted by $\varepsilon$, is applied with feedback matrix $F \in \mathbb{R}^{n \times n}$. In the autonomous case, the master and slave system (without feedback) are identical Lur'e systems [Khalil, 1992; Vidyasagar, 1993] with $A \in \mathbb{R}^{n \times n}$, $B \in \mathbb{R}^{n \times n_h}$ and $C \in \mathbb{R}^{n_h \times n}$ where $n_h$ corresponds to the number of hidden units (in case one interprets the Lur'e system as a class of recurrent neural networks [Suykens *et al.*, 1996]). The diagonal nonlinearity $\sigma(\cdot) : \mathbb{R}^{n_h} \mapsto \mathbb{R}^{n_h}$ is assumed to belong to sector $[0, k]$ (typically a linear characteristic with saturation or $\tanh(\cdot)$). At the master system the vector field is modulated by means of the term $Dd$. One has to ensure then that the norm of this term is "small" compared to the norm of the other terms in the system dynamics, by taking a small amplitude for the message $r$ and choosing the matrices $R \in \mathbb{R}^{n_r \times n_r}$, $S \in \mathbb{R}^{n_r \times 1}$, $T \in \mathbb{R}^{1 \times n_r}$, $U \in \mathbb{R}$ of the low pass filter $\mathcal{R}$ appropriately. The scheme Eq. (1) is different from chaotic masking, which simply adds the information bearing signal to the output of a chaotic system. The latter method suffers from the fact that channel noise is indistinguishable from the transmitted signal (see [Kennedy, 1995]). Finally, the method of recovering the message $r$ is based on a control theoretic interpretation of the scheme Eq. (1) and is explained in the next section.

## 3. Error System and Standard Plant Interpretation

Defining the signal $e = p - q$ one obtains the error system:

$$\mathcal{E}: \dot{e} = A_* e + B_* \eta(C_* e;\, z) + HDd - HF\varepsilon \quad (2)$$

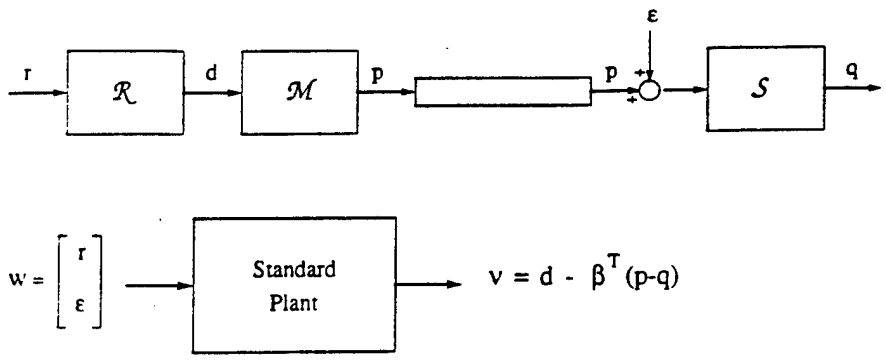


Fig. 1. (Top) Synchronization scheme with master system $\mathcal{M}$ and slave system $\mathcal{S}$. The vector field of the master system is modulated by means of the signal $d$, which is the output of a linear filter $\mathcal{R}$ with as input the message $r$. The state $x$ of $\mathcal{M}$ is linearly transformed into the transmitted signal $p$. The output of the channel is corrupted by the signal $\varepsilon$. The filtered message $d$ is recovered by means of a tracking mechanism, using full state error feedback between $p$ and $q$. The signal $q$ is the result of a linear state transformation (same as for $\mathcal{M}$) on the state $z$ of $\mathcal{S}$. (Bottom) Control theoretic interpretation of the synchronization scheme by its standard plant representation, with exogenous input $w$ and regulated output $\nu = d - \beta^T e$ with $e = p - q$. The exogenous input consists of the filtered message signal $d$ and the channel noise $\varepsilon$. The aim is to find a feedback matrix such that the influence of the exogenous input on the tracking error $\nu$ is minimized. This is done in the sense of a nonlinear $H_\infty$ control scheme, finding the minimal $L_2$-gain by solving a constrained nonlinear optimization problem that involves matrix inequalities. Considering binary valued continuous time reference inputs $r$, the original message is recovered from $\beta^T e$.

with $A_* = HAH^{-1} - HF$, $B_* = HB$, $C_* = CH^{-1}$ and nonlinearity $\eta(C_*e;\, z) = \sigma(C_*e + Cz) - \sigma(Cz)$. For the autonomous case (zero $d$ and $\varepsilon$) the signal $e$ is an error signal in the sense that one is interested in asymptotically synchronizing two chaotic Lur'e systems such that $\|e\| = \|p - q\| \to 0$ as $t \to \infty$. However, the non-autonomous case with non-zero external input $r$ requires another notion of "error", since $e$ is not tending towards the origin for non-zero external inputs. Therefore we will consider the system $\{\mathcal{R},\, \mathcal{M},\, \mathcal{S}\}$ as a model reference control scheme with reference model $\mathcal{R}$ where a feedback matrix $F$ has to be designed such that the *tracking error*:

$$\nu = d - \beta^T e \tag{3}$$

is minimized, where $\beta = [1;\, 0;\, 0;\, \ldots;\, 0]$ selects the first component of the signal $e$.

In modern control theory one considers so-called standard plant forms, with regulated and sensed output and exogenous and actuator input [Boyd & Barratt, 1991; Maciejowski, 1989; Suykens *et al.*, 1996]. The regulated output then consists of the tracking error and eventually also the control signal, in case one wants to minimize the control energy. The exogenous input includes the reference input, disturbance inputs and noise. For the synchronization scheme $\{\mathcal{E},\, \mathcal{R}\}$, the standard plant representation is of the form

$$\begin{cases} \dot{\xi} = f(\xi,\, w) \\ \nu = g(\xi,\, w) \end{cases} \tag{4}$$

with exogenous input $w = [r;\, \varepsilon]$, regulated output $\nu$ and state vector $\xi = [e;\, m]$. More specifically one obtains the equations:

$$\begin{cases} \begin{bmatrix} \dot{e} \\ \dot{m} \end{bmatrix} = \begin{bmatrix} A_* & HDT \\ 0 & R \end{bmatrix} \begin{bmatrix} e \\ m \end{bmatrix} + \begin{bmatrix} B_* \\ 0 \end{bmatrix} \eta(C_*e;\, z) \\ \qquad + \begin{bmatrix} HDU & -HF \\ S & 0 \end{bmatrix} \begin{bmatrix} r \\ \varepsilon \end{bmatrix} \\ \nu = [-\beta^T \quad T] \begin{bmatrix} e \\ m \end{bmatrix} + \begin{bmatrix} U & 0 \end{bmatrix} \begin{bmatrix} r \\ \varepsilon \end{bmatrix}; \end{cases} \tag{5}$$

One aims then at minimizing the influence of the exogenous input on the regulated output and tracking low pass filtered signals $d$, as specified by means of the filter $\mathcal{R}$. An additional filter could be specified for the disturbance input $\varepsilon$, when a noise model for the channel is available. On the other hand, it is clear from control theory that achieving a zero tracking error $\nu$ for all possible message signals $r$ is impossible. This problem is avoided by assuming binary valued continuous time reference inputs $r$ and recovering the message by doing a hard-limiting operation on the variable $\beta^T e$. This principle will be demonstrated in the examples of Sec. 8.

## 4. Autonomous Case: Internal Stability

Let us first consider the autonomous case for the standard plant form of the synchronization scheme, i.e. with zero exogenous input $w$, yielding

$$\begin{cases} \dot{e} = A_*e + HDTm + B_*\eta(C_*e;\, z) \\ \dot{m} = Rm\,. \end{cases} \tag{6}$$

Assume that the nonlinearity $\eta(C_*e;\, z)$ belongs to sector $[0,\, k]$ [Curran & Chua, 1996; Suykens & Vandewalle, 1996]:

$$0 \leq \frac{\eta_i(c_{*_i}^T e;\, z)}{c_{*_i}^T e} = \frac{\sigma_i(c_{*_i}^T e + c_{*_i}^T z) - \sigma(c_{*_i}^T z)}{c_{*_i}^T e} \leq k\,, \quad \forall e,\, z;\; i = 1, \ldots, n_h\,. \tag{7}$$

The following inequality holds then [Boyd *et al.*, 1994; Khalil, 1992; Vidyasagar, 1993]:

$$\eta_i(c_{*_i}^T e;\, z)[\eta_i(c_{*_i}^T e;\, z) - kc_{*_i}^T e] \leq 0\,, \quad \forall e,\, z;\; i = 1, \ldots, n_h\,. \tag{8}$$

It follows from the mean value theorem that for differentiable $\sigma(\cdot)$ the sector $[0,\, k]$ condition on $\eta(\cdot)$ corresponds to [Curran & Chua, 1996]:

$$0 \leq \frac{d}{d\rho}\sigma_i(\rho;\, z) \leq k\,, \quad \forall \rho,\, z;\; i = 1, \ldots, n_h\,. \tag{9}$$

Defining $\xi = [e;\, m]$ and taking a quadratic Lyapunov function

$$V(\xi) = \xi^T P \xi = [e^T \quad m^T] \begin{bmatrix} P_{11} & P_{12} \\ P_{21} & P_{22} \end{bmatrix} \begin{bmatrix} e \\ m \end{bmatrix}, \quad P = P^T > 0\,, \tag{10}$$

which is radially unbounded, it is straightforward then to find a sufficient condition for global asymptotic stability of Eq. (6).

**Theorem 1.** *Let $\Lambda = \mathrm{diag}\{\lambda_i\}$ be a diagonal matrix with $\lambda_i \geq 0$ for $i = 1, \ldots, n_h$. Then a sufficient condition for global asymptotic stability of Eq. (6),*

*based on the quadratic Lyapunov function Eq. (10), is given by the matrix inequality*

$$Y = Y^T = \begin{bmatrix} A_*^T P_{11} + P_{11} A_* & A_*^T P_{12} + P_{12} R & P_{11} B_* + k C_*^T \Lambda \\ \cdot & R^T P_{22} + P_{22} R + T^T D^T H^T P_{12} + P_{21} H D T & P_{21} B_* \\ \cdot & \cdot & -2\Lambda \end{bmatrix} < 0. \quad (11)$$

*Proof.* Taking the time-derivative of the Lyapunov function and applying the $S$-procedure [Boyd *et al.*, 1994], using the inequalities from the nonlinearities, one obtains:

$$\begin{aligned} \dot{V} &= \dot{\xi}^T P \xi + \xi^T P \dot{\xi} \\ &\le \dot{\xi}^T P \xi + \xi^T P \dot{\xi} - \sum_i 2\lambda_i \eta_i (\eta_i - k c_{*_i}^T e) \\ &\le (A_* e + H D T m + B_* \eta)^T (P_{11} e + P_{12} m) \\ &\quad + (Rm)^T (P_{21} e + P_{22} m) \\ &\quad + (e^T P_{11} + m^T P_{21})(A_* e + H D T m + B_* \eta) \\ &\quad + (e^T P_{12} + m^T P_{22}) R m - \sum_i 2\lambda_i \eta_i (\eta_i - k c_{*_i}^T e) \\ &\le \zeta^T Y \zeta < 0 \end{aligned}$$

where $\zeta = [e; m; \eta]$. The latter expression is negative $\forall$ nonzero $\zeta$ provided $Y$ is negative definite. ∎

## 5. Non-Autonomous Case: Dissipativity with Finite $L_2$-Gain

In order to study input/output properties of the synchronization scheme Eq. (1), we follow the dissipativity approach, introduced in system theory by Willems [1972] and further developed in [Hill & Moylan, 1976, 1980]. With respect to the standard plant form Eq. (5), we consider the *supply rate* with finite $L_2$-gain $\gamma$ (see [Hill & Moylan, 1976, 1980]):

$$s(w, \nu) = \gamma^2 w^T w - \nu^T \nu. \quad (12)$$

Another well-known type of supply rate takes the inner product between the input and output of the system, which corresponds to the well-known case of passivity. The system Eq. (5) with supply rate Eq. (12) is said to be *dissipative* if for all locally square integrable $w$ and all $t_f \ge 0$ one has

$$\int_0^{t_f} s(w(t), \nu(t)) dt \ge 0 \quad (13)$$

with $\xi(0) = 0$ and $s(w, \nu)$ integrated along the trajectory of Eq. (5) [Hill & Moylan, 1976, 1980]. Note that the assumption of locally square integrability of $w$ is not satisfied when the channel noise $\epsilon$ is a zero mean white Gaussian noise signal. Therefore, at the theoretical level, we will consider $\epsilon$ rather as a deterministic disturbance input than as a stochastic input and simulate the obtained results afterwards with noisy inputs (as is usually done in $H_\infty$ control theory). Furthermore the system Eq. (5) is dissipative with respect to supply rate Eq. (12) if there exists a storage function $\phi(\xi) : \mathbb{R}^n \mapsto \mathbb{R}$ satisfying $\phi(\xi) > 0$ for $\xi \neq 0$ and $\phi(0) = 0$ and [Hill & Moylan, 1976, 1980]

$$\dot{\phi}(\xi) \le s(w, \nu), \qquad \forall w, \nu. \quad (14)$$

The following theorem proves then dissipativity with finite $L_2$-gain of the synchronization scheme with respect to a quadratic storage function

$$\phi(\xi) = \xi^T P \xi, \qquad P = P^T > 0. \quad (15)$$

Note the resemblance between the use of the quadratic storage function for the non-autonomous case and the quadratic Lyapunov function for the autonomous case.

**Theorem 2.** *Let $\Lambda = \mathrm{diag}\{\lambda_i\}$ be a diagonal matrix with $\lambda_i \ge 0$ for $i = 1, \ldots, n_h$. Then a sufficient condition for dissipativity of the synchronization scheme Eq. (5) with respect to the quadratic storage function Eq. (15) and the supply rate with finite $L_2$-gain $\gamma$ Eq. (12) is given by the matrix inequality*

$$Z = Z^T = \begin{bmatrix} Z_{11} & Z_{12} & Z_{13} & Z_{14} & Z_{15} \\ \cdot & Z_{22} & Z_{23} & Z_{24} & Z_{25} \\ \cdot & \cdot & Z_{33} & 0 & 0 \\ \cdot & \cdot & \cdot & Z_{44} & 0 \\ \cdot & \cdot & \cdot & \cdot & Z_{55} \end{bmatrix} < 0 \quad (16)$$

*with*

$$Z_{11} = A_*^T P_{11} + P_{11} A_* + \beta\beta^T \qquad Z_{22} = P_{21} HDT + T^T D^T H^T P_{12} + P_{22} R + R^T P_{22} + T^T T$$
$$Z_{12} = A_*^T P_{12} + P_{11} HDT + P_{12} R - \beta T \qquad Z_{23} = P_{21} B_*$$
$$Z_{13} = P_{11} B_* + k C_*^T \Lambda \qquad Z_{24} = P_{21} HDU + P_{22} S + T^T U$$
$$Z_{14} = P_{11} HDU + P_{12} S - \beta U \qquad Z_{25} = -P_{21} HF$$
$$Z_{15} = -P_{11} HF \qquad Z_{33} = -2\Lambda,\ Z_{44} = -\gamma^2 I + U^T U,\ Z_{55} = -\gamma^2 I.$$

*Proof.* Writing the expression for $\dot{\phi} - s(w, \nu)$ and applying the $S$-procedure [Boyd *et al.*, 1994], using the inequalities for the nonlinearity, one obtains

$$\begin{aligned}
\dot{\phi} - s(w, \nu) &= \dot{\xi}^T P \xi + \xi^T P \dot{\xi} - s(w, \nu) \\
&\leq \dot{\xi}^T P \xi + \xi^T P \dot{\xi} - \sum_i 2\lambda_i \eta_i (\eta_i - k c_{*_i}^T e) - s(w, \nu) \\
&\leq (A_* e + B_* \eta + HDTm + HDUr - HF\varepsilon)^T (P_{11} e + P_{12} m) + (Rm + Sr)^T (P_{21} e + P_{22} m) \\
&\quad + (e^T P_{11} + m^T P_{21})(A_* e + B_* \eta + HDTm + HDUr - HF\varepsilon) + (e^T P_{12} + m^T P_{22})(Rm + Sr) \\
&\quad - \sum_i 2\lambda_i \eta_i (\eta_i - k c_{*_i}^T e) - \gamma^2 (r^2 + \varepsilon^T \varepsilon) + (Tm - \beta^T e + Ur)^T (Tm - \beta^T e + Ur) \\
&\leq \zeta Z \zeta < 0
\end{aligned}$$

where $\zeta = [e;\ m;\ \eta;\ r;\ \varepsilon]$. The latter expression is negative $\forall$ nonzero $\zeta$, if $Z$ is a negative definite matrix. ■

## 6. Nonlinear $H_\infty$ Synchronization

Given the matrix inequality of Theorem 2, the question arises as to how to design the feedback matrix $F$ for the given master–slave synchronization scheme. In nonlinear $H_\infty$ control theory (see e.g. [Isidori & Astolfi, 1992; van der Schaft, 1996]) one designs a controller for a given nonlinear plant by considering a supply rate with finite $L_2$-gain like Eq. (12). The optimal $H_\infty$ control law corresponds then to the minimal $L_2$-gain $\gamma$ that is achievable for the system such that the closed-loop system is dissipative. In nonlinear $H_\infty$ control theory, the optimal solution is characterized by a Hamilton–Jacobi inequality with respect to a continuously differentiable nonlinear storage function. For Lur'e systems and a quadratic storage function on the other hand, the optimal solution can be expressed in terms of matrix inequalities, as is shown in Theorem 2. The *nonlinear* $H_\infty$ *synchronization* problem is formulated then as:

$$\min_{F,P,\Lambda,\gamma} \gamma \quad \text{such that} \quad Z(F, P, \Lambda, \gamma) < 0. \qquad (17)$$

This problem-formulation itself suggests a way of solving it by means of constrained nonlinear optimization. The constraint is differentiable as long as the two largest eigenvalues of the matrix $Z$ do not coincide [Polak & Wardi, 1982]. Otherwise a generalized gradient can be defined according to the theory of non-differentiable optimization. A convergent algorithm has been described in [Polak & Wardi, 1982], including an analytic expression for the gradient of the constraint in Eq. (17). In general the problem Eq. (17) is non-convex. Hence one may need several starting points or a global search method, though suboptimal solutions often already yield satisfactory results, as will be demonstrated in the examples of Sec. 8.

## 7. Some Cryptographical Aspects

According to Kerckhoff's principle of cryptography, it is assumed in secret key algorithms that the algorithm is known in public and that the key, used by the sender and receiver, is secret and is used for enciphering and deciphering [Ford, 1994; Schneier, 1994]. An example is the widely used DES (Data Encryption Standard) algorithm, which makes use of a 64-bit input and a 56-bit key. For the

synchronization scheme this means that the Lur'e system and the model reference filter are known, i.e. the matrices $A$, $B$, $C$, $R$, $S$, $T$, $U$ are known in public. A possible key for the synchronization scheme is the matrix $H$. One may generate full rank random matrices $H$ using as key the seed of the random generator. Once $H$ is known by the receiver, $F$ can be calculated from the nonlinear optimization problem Eq. (17) and the message can be recovered. The security can be easily enhanced further by applying an additional static nonlinear transformation on the vector $p$, by means of a multilayer perceptron with $l$ layers:

$$p_* = W_1 \tanh(W_2 \tanh(W_3 \ldots \tanh(W_l p) \ldots)) \tag{18}$$

with full rank matrices $W_i \in \mathbb{R}^{n \times n}$ for $i = 1, \ldots, l$. One could generate the matrices $W_i$ in the same way as $H$. The activation function $\tanh(\cdot)$ is applied componentwise to the elements of the vectors (diagonal nonlinearity). Because the activation function $\tanh(\cdot)$ is invertible, the received signal $p_*$ is readily transformed back into $p$.

## 8. Examples

### 8.1. *Chua's circuit*

Let us take the following representation of Chua's circuit:

$$\begin{cases} \dot{x}_1 = \alpha[x_2 - h(x_1)] \\ \dot{x}_2 = x_1 - x_2 + x_3 \\ \dot{x}_3 = -\beta x_2 \end{cases} \tag{19}$$

with nonlinear characteristic

$$h(x_1) = m_1 x_1 + \frac{1}{2}(m_0 - m_1)(|x_1 + c| - |x_1 - c|) \tag{20}$$

and parameters $\alpha = 9$, $\beta = 14.286$, $m_0 = -1/7$, $m_1 = 2/7$ in order to obtain the double scroll attractor [Chua *et al.*, 1986; Chua, 1994; Madan, 1993]. The nonlinearity $\varphi(x_1) = \frac{1}{2}(|x_1 + c| - |x_1 - c|)$ (linear characteristic with saturation) belongs to sector $[0, 1]$. Hence Chua's circuit can be represented as the Lur'e system $\dot{x} = Ax + B\varphi(Cx)$ with

$$A = \begin{bmatrix} -\alpha m_1 & \alpha & 0 \\ 1 & -1 & 1 \\ 0 & -\beta & 0 \end{bmatrix}, \quad B = \begin{bmatrix} -\alpha(m_0 - m_1) \\ 0 \\ 0 \end{bmatrix},$$
$$C = [1 \quad 0 \quad 0]. \tag{21}$$

The nonlinear $H_\infty$ synchronization problem Eq. (17) was solved by means of sequential quadratic programming (*constr* in Matlab) [Fletcher, 1987], with numerical calculation of the gradients, in a slightly modified way than Eq. (17). The positive definite matrix $P$ has been parameterized as $P = Q^T Q$ and

$$\min_{F,Q,\Lambda,\gamma} \gamma \text{ such that } \lambda_{\max}[Z(F, Q, \Lambda, \gamma)] + \delta < 0 \tag{22}$$

with $\delta = 0.01$ has been solved instead, where $\lambda_{\max}[\cdot]$ denotes the maximal eigenvalue of a symmetric matrix. In the experiments $D = [1; 1; 1]$, $\beta = [1; 0; 0]$ and $H$ is a randomly generated matrix, according

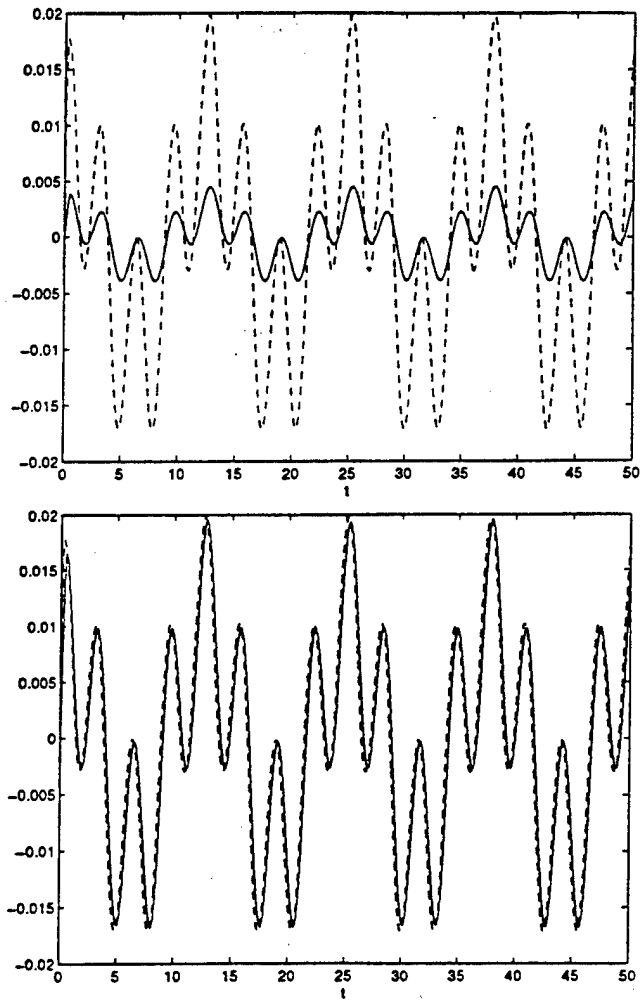


Fig. 2. Simulation results for Chua's circuit as master–slave Lur'e systems: (Top) signals $\beta^T e$ (-) and $d$ (--), corresponding to $r = 0.01(\cos(0.5t) + \cos(2t))$. Hence the tracking is not perfect, but the waveforms are basically the same up to a constant scaling. (Bottom) scaled signal $\beta^T e$ (-) such that the error with $d$ (--) is minimal.

to a normal distribution with zero mean and variance one. For the reference model, a first order Butterworth filter was chosen with cut-off frequency 10 Hz. As starting point for the nonlinear optimization a random matrix was taken for the feedback matrix $F$, generated according to a normal distribution with zero mean and variance 0.1, and $Q = I_{n+n_r}$, $\Lambda = 0.1 I_{n_h}$, $\gamma = 100$. For multistart local optimization with 10 such random starting points, the minimal obtained $L_2$-gain $\gamma$ was equal to 0.82.

Simulation results of the synchronization scheme with the obtained feedback matrix $F$ are shown on Figs. 2–6. On Fig. 2 a reference input

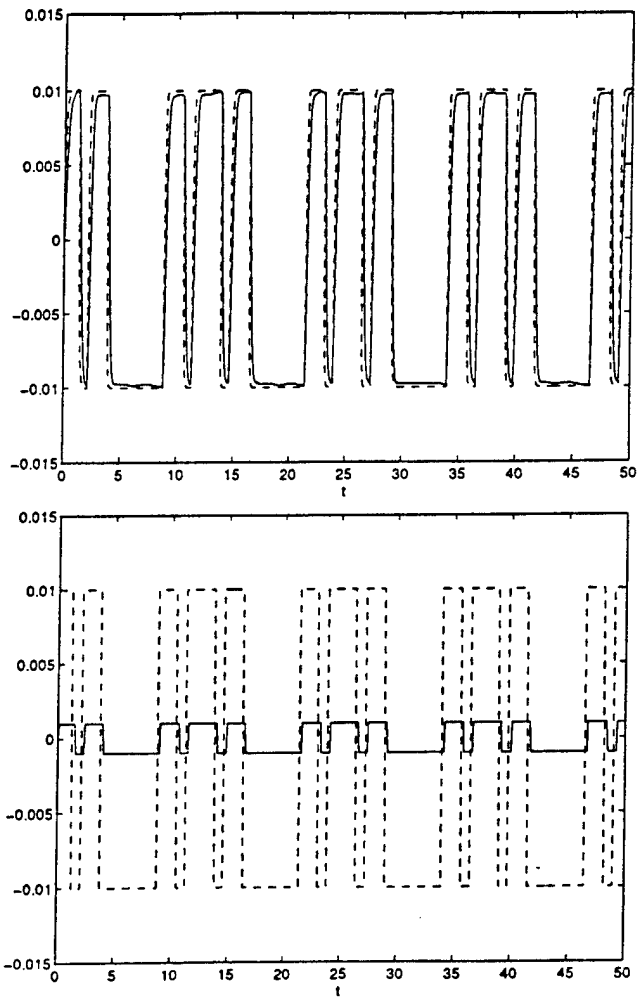


Fig. 3. Chua's circuit (continued). (Top) scaled signal $\beta^T e$ (-) and $r = 0.01\,\mathrm{sign}(\cos(0.5t) + \cos(2t))$ (--). (Bottom) scaled version of the hard-limited signal $\mathrm{sign}(\beta^T e)$ and $r = 0.01\,\mathrm{sign}(\cos(0.5t) + \cos(2t))$ (--) showing that the message can be recovered for a class of binary valued continuous time reference inputs.

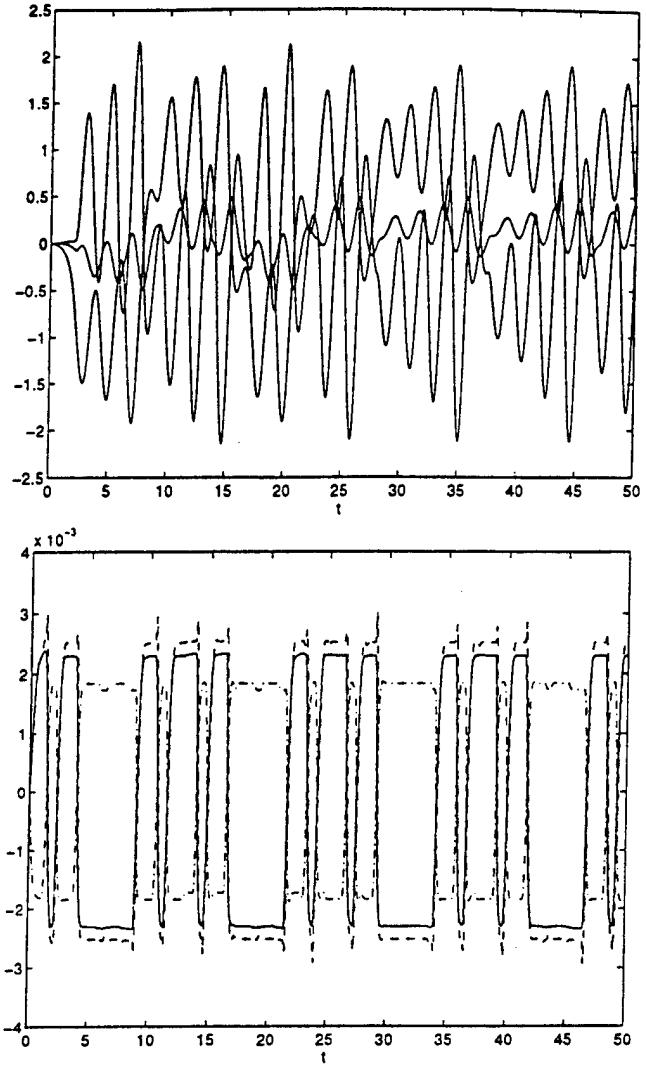


Fig. 4. Chua's circuit (continued). (Top) transmitted signals $p$. Because of the modulation of the vector field by the message signal $r(t)$ (corresponding to Fig. 3) with a small amplitude, the message signal is invisible on the chaotic waveform. (Bottom) 3 components of the signal $e$ of the error system: $e_1$ (-), $e_2$ (--), $e_3$ (-·), corresponding to Fig. 3.

$r = 0.01(\cos(0.5t) + \cos(2t))$ has been taken. The recovered signal $\beta^T e$ is approximately equal to the filtered message signal $d$, up to a constant scaling. This motivates the use of the synchronization scheme for binary valued continuous time reference inputs, as is shown on Fig. 3, where perfect recovery of the message is obtained, also in the case of channel noise (Fig. 6). The message signal is invisible on the transmitted signals (Fig. 4), because of the small amplitude of $r$ for the vector field modulation of the master system. The attractor for the $x$ and corresponding $p$ variables are shown on Fig. 5. The simulations of the deterministic systems

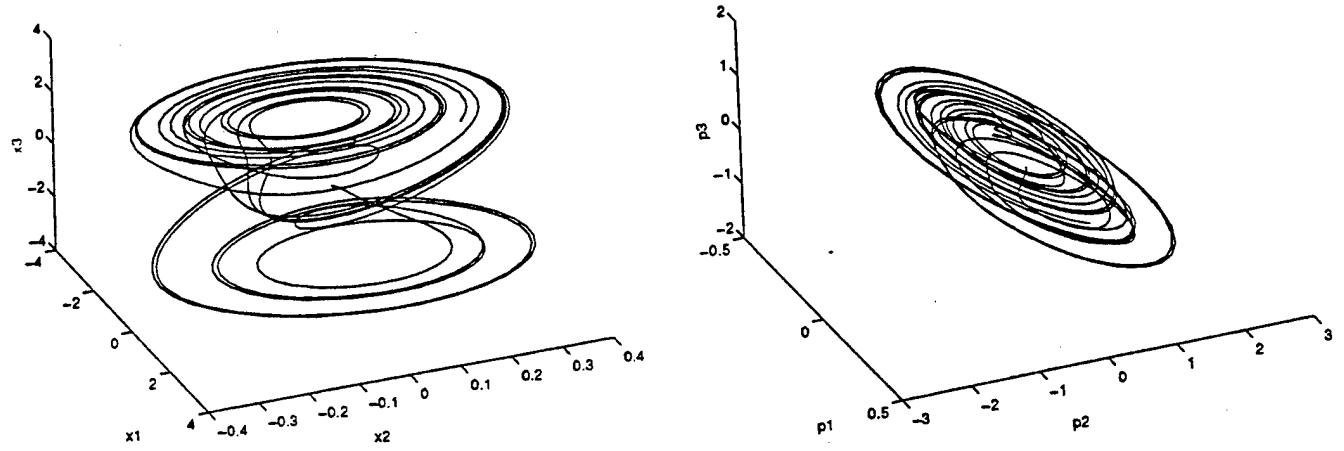


Fig. 5. Chua's circuit (continued). (Left) state variables $x$ of the double scroll at the master system, modulated by the signal $d$ corresponding to Fig. 3. (Right) transformed attractor $p = Hx$.

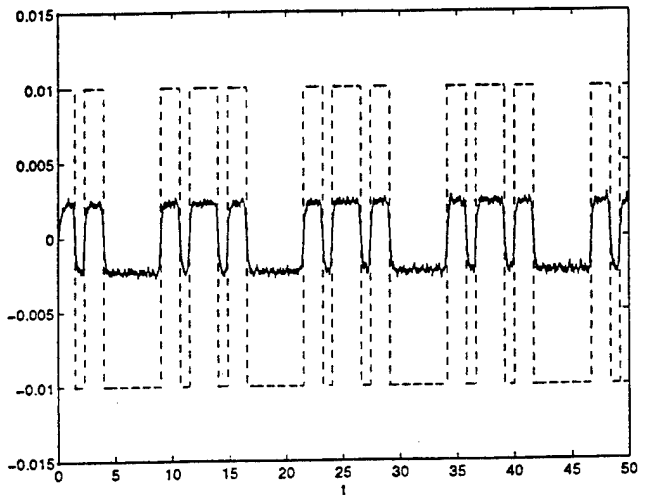


Fig. 6. Chua's circuit (continued). Simulations of the synchronization scheme, corresponding to Fig. 3 (Bottom), but with noise signal $\varepsilon$ (zero mean white Gaussian with zero mean and standard deviation 0.001). This amount of noise can be tolerated in the scheme. Note that the design of the feedback matrix takes into account the disturbance input $\varepsilon$ through the exogenous input $w$.

are done by means of a Runge–Kutta integration rule (*ode23* in Matlab) [Parker & Chua, 1989]. Stochastic systems were simulated using an euler integration rule [Kloeden, 1991].

## 8.2. *2-Double scroll*

In [Suykens & Vandewalle, 1993] a generalization of Chua's circuit has been proposed by introducing additional breakpoints in the nonlinear characteristic, in order to generate multiple scrolls, resulting

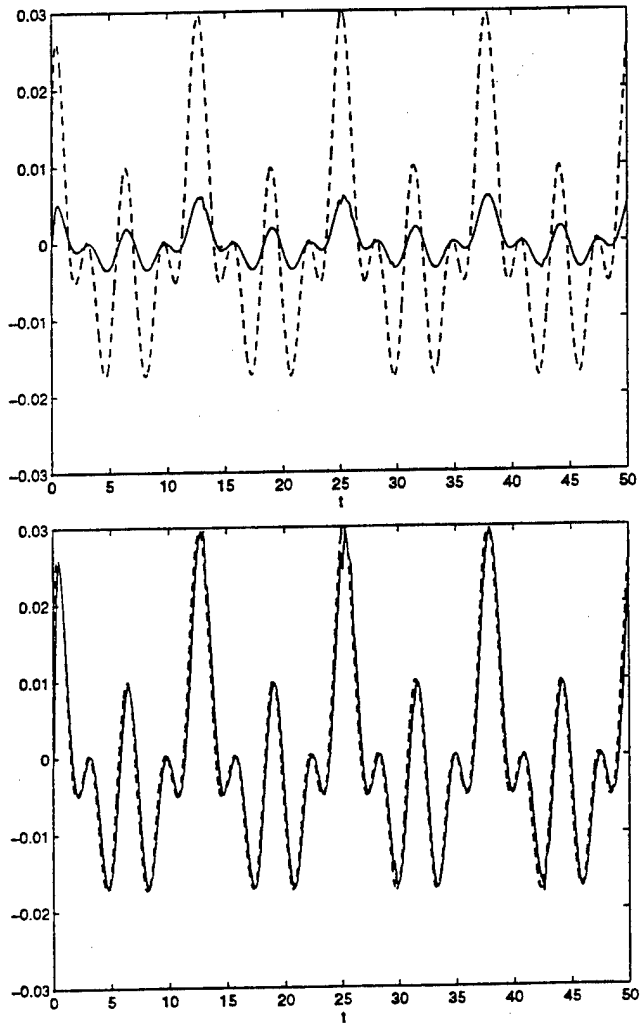


Fig. 7. Simulation results for 2-double scroll as master–slave Lur'e systems: (Top) signals $\beta^T e$ (-) and $d$ (--), corresponding to $r = 0.01(\cos(0.5t) + \cos(t) + \cos(2t))$. (Bottom) scaled signal $\beta^T e$ (-) such that the error with $d$ (--) is minimal.

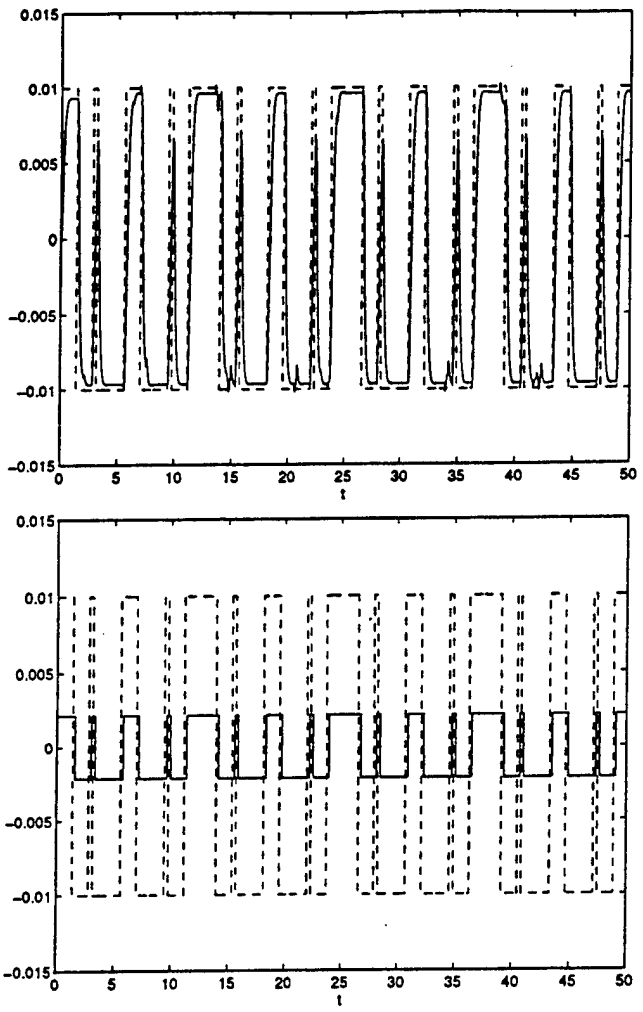

Fig. 8. 2-double scroll (continued). (Top) scaled signal $\beta^T e$ (-) and $r = 0.01\,\mathrm{sign}(\cos(0.5t) + \cos(t) + \cos(2t))$ (--). (Bottom) scaled version of the recovered hardlimited signal $\mathrm{sign}(\beta^T e)$ and $r = 0.01\,\mathrm{sign}(\cos(0.5t) + \cos(t) + \cos(2t))$ (--).

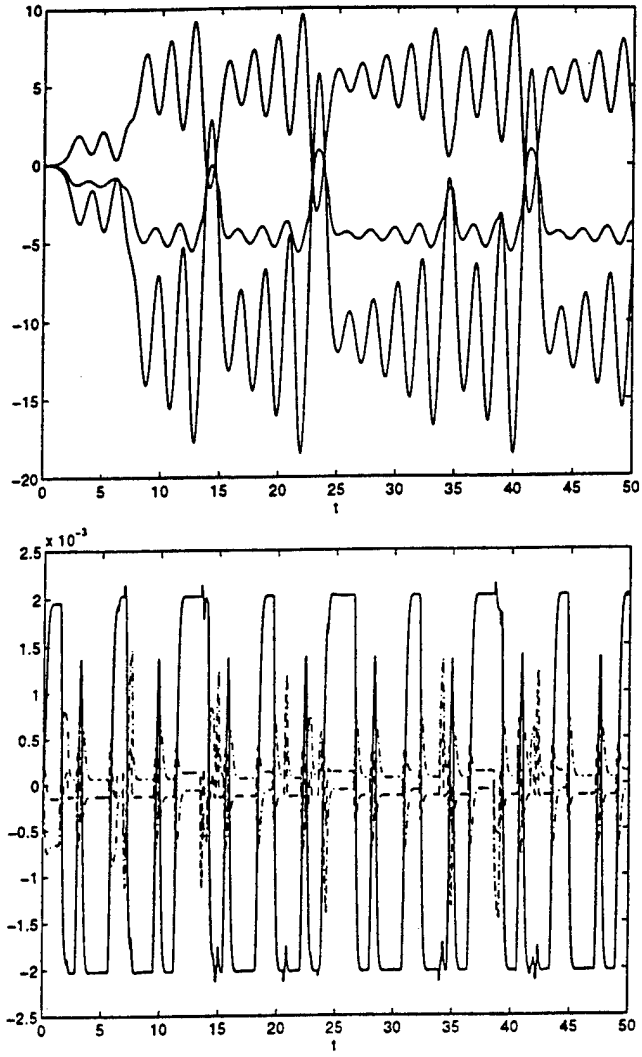

Fig. 9. 2-double scroll (continued). (Top) transmitted signals $p$. The message signal, corresponding to Fig. 8, is again invisible on the chaotic waveform. (Bottom) 3 components of the signal $e$ of the error system: $e_1$ (-), $e_2$ (--), $e_3$ (-·), corresponding to Fig. 8.

into so-called $n$-double scrolls attractors, where $n$ is a natural number. The well-known double scroll corresponds to a 1-double scroll within this framework. An electrical circuit implementation has been made by Arena *et al.* [1996], which makes use of a piecewise linear representation of the nonlinear characteristic. The latter $n$-double scroll circuit is described as:

$$\begin{cases} \dot{x}_1 = \alpha[x_2 - h(x_1)] \\ \dot{x}_2 = x_1 - x_2 + x_3 \\ \dot{x}_3 = -\beta x_2 \end{cases} \tag{23}$$

with as nonlinear function the piecewise linear characteristic:

$$h(x_1) = m_{2n-1}x_1 + \frac{1}{2}\sum_{i=1}^{2n-1}(m_{i-1} - m_i) \times (|x_1 + c_i| - |x_1 - c_i|), \tag{24}$$

consisting of $2(2n-1)$ breakpoints, where $n$ is a natural number. We will consider here the 2-double scroll attractor, which is obtained for $\alpha = 9$, $\beta = 14.286$, $m_0 = -1/7$, $m_1 = 2/7$, $m_2 = -4/7$, $m_3 = m_1$, $c_1 = 1$, $c_2 = 2.15$, $c_3 = 3.6$.

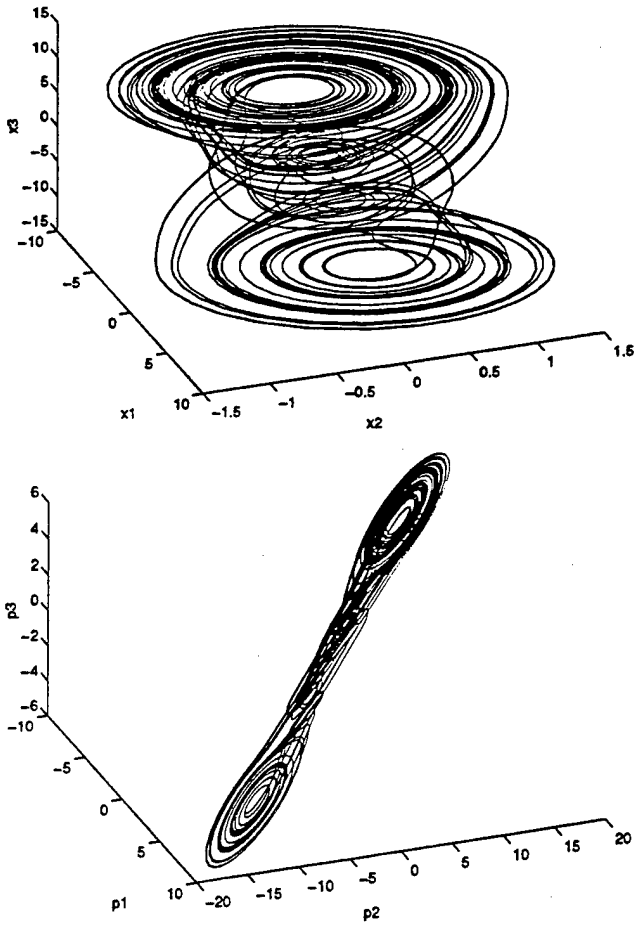


Fig. 10. 2-double scroll (continued). (Top) state variables $x$ of the double scroll at the master system, modulated by the signal $d$ corresponding to Fig. 8. (Bottom) transformed attractor $p = Hx$.

The 2-double scroll circuit can be represented as the Lur'e system $\dot{x} = Ax + B\varphi(Cx)$ with

$$A = \begin{bmatrix} -\alpha m_1 & \alpha & 0 \\ 1 & -1 & 1 \\ 0 & -\beta & 0 \end{bmatrix}, \quad B = \begin{bmatrix} b_{11} & b_{12} & b_{13} \\ 0 & 0 & 0 \\ 0 & 0 & 0 \end{bmatrix},$$

$$C = \begin{bmatrix} 1 & 0 & 0 \\ 1 & 0 & 0 \\ 1 & 0 & 0 \end{bmatrix} \tag{25}$$

with $b_{11} = -\alpha(m_0 - m_1)$, $b_{12} = -\alpha(m_1 - m_2)$, $b_{13} = -\alpha(m_2 - m_3)$. The nonlinearity $\varphi(\cdot)$ belongs to sector $[0, 1]$ with $\varphi_i(x_1) = \frac{1}{2}(|x_1 + c_i| - |x_1 - c_i|)$.

The nonlinear $H_\infty$ synchronization problem Eq. (22) was solved by means of sequential quadratic programming in the same way as for the example on the double scroll, with the same choice for $\delta$, $D$, $\beta$, $H$, the reference model and the number of starting points for the optimization problem. The minimal $L_2$-gain obtained for $\gamma$ was equal to 1.16. Simulation results of the synchronization scheme with the obtained feedback matrix $F$ are presented on Figs. 7–11. On Fig. 7 a reference input $r = 0.01(\cos(0.5t)+\cos(t)+\cos(2t))$ has been taken. Like for the double scroll, the recovered signal $\beta^T e$ is approximately equal to the filtered message signal $d$, up to a constant scaling. The application to a binary-valued continuous time reference input $r = 0.01\,\mathrm{sign}(\cos(0.5t) + \cos(t) + \cos(2t))$ is shown on Fig. 8, with perfect recovery of the message, also in the case of channel noise (Fig. 11). The message signal is invisible on the transmitted signals (Fig. 9). The attractor for the $x$ and corresponding $p$ variables are shown on Fig. 10.

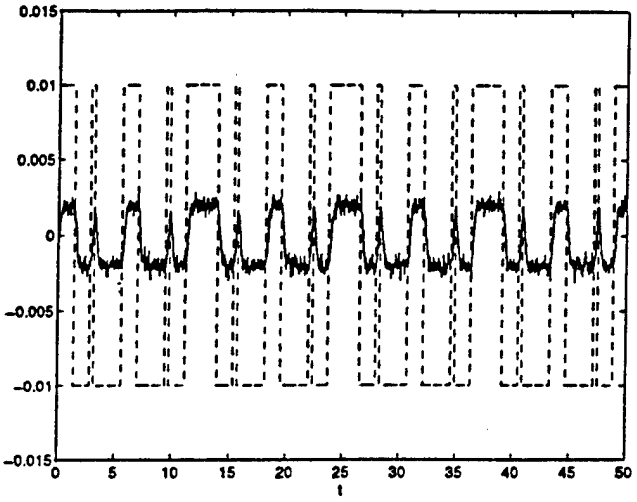


Fig. 11. 2-double scroll (continued). Simulations of the synchronization scheme, corresponding to Fig. 8 (Bottom), but with noise signal $\epsilon$ (zero mean white Gaussian with zero mean and standard deviation 0.001). This amount of noise can be tolerated in the synchronization scheme.

## 9. Conclusion

A master–slave synchronization scheme for Lur'e systems has been investigated with vector field modulation of the master system by the message signal. The scheme has been interpreted in a control theoretical sense by means of its standard plant representation. A method of nonlinear $H_\infty$ synchronization has been proposed for recovery of binary valued continuous time reference inputs. It involves the design of a state feedback matrix such that the influence from the exogenous input on the regulated output, characterized by its $L_2$-gain, is minimized.

Channel noise is taken into account in the design of the feedback matrix. The method could be modified to incorporate channel and noise models. The nonlinear $H_\infty$ synchronization scheme has been demonstrated on Chua's circuit and a 2-double scroll circuit. The method also applies to arrays that consist of Lur'e cells with linear coupling between the cells. However, the proposed scheme basically requires transmission of the full state vector of the master system. A suggestion for further research is to investigate output feedback mechanisms which would require fewer signals to be transmitted. Also, the influence of parameter mismatch between the Lur'e systems can be further studied. An extension of the present nonlinear $H_\infty$ synchronization scheme that takes into account these parametric uncertainties in addition to channel noise, may finally lead to a complete framework for robust synthesis of master-slave synchronization schemes.

## Acknowledgment

This research work was carried out at the University of California at Berkeley, in the framework of the Belgian Programme on Interuniversity Poles of Attraction, initiated by the Belgian State, Prime Minister's Office for Science, Technology and Culture (IUAP-17) and in the framework of a Concerted Action Project MIPS (Modelbased Information Processing Systems) of the Flemish Community. The work is supported in part by the Office of Naval Research under grant N00014-96-1-0753. The author would like to thank Paul Curran, Tao Yang and Peter Kennedy for having many stimulating discussions during his stay at U.C. Berkeley.

## References

Arena, P., Baglio, P., Fortuna, F. & Manganaro, G. [1996] "Generation of $n$-double scrolls via cellular neural networks," *Int. J. Circuit Theory and Appl.* **24**, 241–252.

Boyd, S. & Barratt, C. [1991] *Linear Controller Design, Limits of Performance* (Prentice-Hall).

Boyd, S., El Ghaoui, L., Feron, E. & Balakrishnan, V. [1994] *Linear Matrix Inequalities in System and Control Theory*, SIAM (Studies in Applied Mathematics), Vol. 15.

Chen, W.-K. (ed.) [1995] *The Circuits and Filters Handbook* (CRC Press).

Chua, L. O., Komuro, M. & Matsumoto, T. [1986] "The double scroll family," *IEEE Trans. Circuits Syst. I* **33**(11), 1072–1118.

Chua, L. O. [1994] "Chua's circuit 10 years later," *Int. J. Circuit Theory Appl.* **22**, 279–305.

Chua, L. O., Yang, T., Zhong, G.-Q. & Wu, C. W. [1996] "Adaptive synchronization of Chua's oscillators," *Int. J. Bifurcation and Chaos* **6**(1), 189–201.

Curran, P. F. & Chua, L. O. [1996] "Absolute stability theory and the synchronization problem," *Int. J. Bifurcation and Chaos*, this issue.

Fletcher, R. [1987] *Practical Methods of Optimization* (John Wiley and Sons, Chichester and New York).

Ford, W. [1994] *Computer Communications Security: Principles, Standard Protocols and Techniques* (Prentice Hall).

Hasler, M. [1994] "Synchronization principles and applications," *Circuits & Syst.: Tutorials IEEE-ISCAS '94*, 314–326.

Hill, D. J. & Moylan, P. J. [1976] "The stability of nonlinear dissipative systems," *IEEE Trans. Auto. Control* **AC-21**, 708–711.

Hill, D. J. & Moylan, P. J. [1980] "Connections between finite-gain and asymptotic stability," *IEEE Trans. Automatic Control* **AC-25**(5), 931–936.

Isidori, A. & Astolfi, A. [1992] "Disturbance attenuation and $H_\infty$ control via measurement feedback in nonlinear systems," *IEEE Trans. Auto. Control* **AC-37**, 1283–1293.

Kapitaniak, T. & Chua, L. O. [1994] "Hyperchaotic attractors of unidirectionally-coupled Chua's circuits," *Int. J. Bifurcation and Chaos* **4**(2), 477–482.

Kennedy, [1995] in *The Circuits and Filters Handbook* ed. Chen, W.-K. (CRC Press), pp. 1089–1163.

Khalil, H. K. [1992] *Nonlinear Systems* (Macmillan Publishing Company, New York).

Kloeden, P. E., Platen, E., & Schurz, H. [1991] "The numerical solution of nonlinear stochastic dynamical systems: A brief introduction," *Int. J. Bifurcation and Chaos* **1**(2), 277–286.

Maciejowski, J. M. [1989] *Multivariable Feedback Design* (Addison-Wesley).

Madan, R. N. (guest ed.) [1993] *Chua's Circuit: A Paradigm for Chaos* (World Scientific, Singapore).

Parker, T. S. & Chua, L. O. [1989] *Practical Numerical Algorithms for Chaotic Systems* (Springer-Verlag, New York).

Polak, E. & Wardi, Y. [1982] "Nondifferentiable optimization algorithm for designing control systems having singular value inequalities," *Automatica* **18**(3), 267–283.

Schneier, B. [1994] *Applied Cryptography: Protocols, Algorithms and Source Code in C* (John Wiley & Sons, New York).

Suykens, J. A. K. & Vandewalle, J. [1993] "Generation of $n$-double scrolls ($n = 1, 2, 3, 4, \ldots$)," *IEEE Trans. Circuits Syst. I* **40**(11), 861–867.

Suykens, J. A. K., Vandewalle, J. P. L. & De Moor, B. L. R. [1996] *Artificial Neural Networks for Modelling and Control of Non-Linear Systems* (Kluwer Academic Publishers, Boston).

Suykens, J. A. K. & Vandewalle, J. [1996] "Master–slave synchronization of Lur'e systems," *Int. J. Bifurcation and Chaos* **7**(3), 665–669.

Suykens, J. A. K. & Chua, L. O. [1997] "$n$-double scroll hypercubes in 1-D CNNs," *Int. J. Bifurcation and Chaos*, to appear.

van der Schaft, A. [1996] *$L_2$-gain and Passivity Techniques in Nonlinear Control*, Lecture Notes in Control and Information Sciences 218 (Springer-Verlag, New York).

Vidyasagar, M. [1993] *Nonlinear Systems Analysis* (Prentice-Hall).

Willems, J. C. [1972] "Dissipative dynamical systems I: General theory. II: Linear systems with quadratic supply rates," *Archive for Rational Mechanics and Analysis* **45**, 321–343.

Wu, C. W. & Chua, L. O. [1993] "A simple way to synchronize chaotic systems with applications to secure communications systems," *Int. J. Bifurcation and Chaos* **6**(3), 1619–1627.

Wu, C. W. & Chua, L. O. [1994] "A unified framework for synchronization and control of dynamical systems," *Int. J. Bifurcation and Chaos* **4**(4), 979–989.

Wu, C. W., Yang, T. & Chua, L. O. [1996] "On adaptive synchronization and control of nonlinear dynamical systems," *Int. J. Bifurcation and Chaos* **6**(3), 455–471.

Wyatt, J. L., Chua, L. O., Gannett, J. W., Göknar, I. C. & Green, D. N. [1981] "Energy concepts in state-space theory of nonlinear $n$-ports: Part I — Passivity," *IEEE Trans. Circuits Syst.*, **CAS-28**(1), 48–61.

International Journal of Bifurcation and Chaos, Vol. 7, No. 6 (1997) 1375–1382
© World Scientific Publishing Company

# ABSOLUTE STABILITY THEORY AND THE SYNCHRONIZATION PROBLEM

P. F. CURRAN*
*Department of Electronic and Electrical Engineering, University College, Belfield, Donnybrook, Dublin 4, Ireland*

L. O. CHUA†
*Department of Electrical Engineering and Computer Sciences, University of California, Berkeley, CA 94720, USA*

Received October 21, 1996; Revised December 12, 1996

Several results on synchronization by Pecora and Carroll [1991], Cuomo and Oppenheim [1993] and Wu and Chua [1994] are evaluated in the context of absolute stability theory, with significant generalizations being achieved. A robustness property of the resulting synchronization criteria is established.

## 1. Introduction

Recently there has been a great deal of interest in the problem of synchronization [Pecora & Carroll, 1991; Wu & Chua, 1994; Hasler, 1994]. Chaotic systems have received particular attention against the general background of a significant international research effort towards the development of secure communications based on chaotic systems [Kocarev *et al.*, 1992; Parlitz *et al.*, 1992; Cuomo & Oppenheim, 1993].

The principal aim of this paper is to show that certain synchronization results of Pecora and Carroll [1991], Cuomo and Oppenheim [1993] and Wu and Chua [1994], may be unified and generalized in the framework of absolute stability theory. Further, every synchronization criterion derived by constructing a quadratic Lyapunov function for the error system [Cuomo & Oppenheim, 1993; Wu & Chua, 1994], may be *systematically* derived in this framework. Whereas the majority of the Lyapunov functions actually developed (as distinct from development in principle) in the existing literature on synchronization have been of very low dimension (usually 3), or have consisted of elementary combinations of such functions in the case of large scale systems, absolute stability theory reduces the generation problem for $n$-dimensional systems to the problem of solving Linear Matrix Inequalities (LMIs) [Boyd *et al.*, 1994], or to the problem of determining when such solutions exist. There exist efficient numerical algorithms for the resolution of both of these problems [Boyd *et al.*, 1994].

Although applicable to only a restricted number of schemes of the Pecora–Carroll type the synchronization criteria obtained (being in the form of LMIs) are algebraic and do *not* require the calculation of conditional Lyapunov exponents [Pecora & Carroll, 1991].

This framework also permits the development of synchronization criteria for $n$-dimensional systems containing multiple nonlinearities. Once more,

*E-mail: PCurran@Acadamh.UCD.ie
†E-mail: Chua@fred.EECS.Berkeley.EDU

the synchronization problems for these systems are reduced to Linear Matrix Inequalities and are therefore rendered numerically tractable. Given the recent concensus that secure communication systems require high dimensional chaos (and consequently high dimensional chaotic synchronizing subsystems), this feature is of primary importance.

A synchronization criterion will be of little practical value if the synchronization it predicts is not robust to subsystem mismatch and channel noise, i.e. if synchronization, pertaining in the ideal system, fails entirely in the presence of arbitrarily small levels of these quantities. We prove that the synchronization criteria presented in this paper also imply robust synchronization and are therefore meaningful in practical synchronization problems.

## 2. Generalization of Result of Cuomo and Oppenheim

Consider a system having the form

$$\dot{x} = Ax + f(q_1^T x,\, q_2^T x, \ldots,\, q_r^T x,\, t)(bc^T - cb^T)x \quad (1)$$

$A \in \mathbb{R}^{n\times n}$, $q_1, \ldots, q_r$, $b$, $c \in \mathbb{R}^n$, $b$ and $c$ linearly independent. It is clear that the Lorenz equations provide an example of a system having this special form. This system may be viewed as a Lur'e system possessing two nonlinearities [Khalil, 1992], but with the special property that these nonlinearities are *identical*. This property permits one to generate an absolute stability criterion for such systems which is applicable under much broader conditions than any of the standard absolute stability criteria for general Lur'e systems. A special case of this criterion for the Lorenz equations appears in the work of Cuomo and Oppenheim [1993]. After the fashion of Cuomo and Oppenheim [1993], and employing the state feedback of Wu and Chua [1994], we propose the following synchronization scheme

$$\begin{aligned}\dot{x} &= Ax + f(q_1^T x, \ldots, q_r^T x,\, t)(bc^T - cb^T)x \\ \dot{y} &= Ay + f(q_1^T x, \ldots, q_r^T x,\, t)(bc^T - cb^T)y \\ &\quad -K(x-y)\end{aligned} \quad (2)$$

with $K \in \mathbb{R}^{n\times n}$. Defining the *error signal* $e = x - y$, one obtains the error system

$$\dot{e} = Ae + f(q_1^T x, \ldots, q_r^T x,\, t)(bc^T - cb^T)e + Ke\,. \quad (3)$$

A *sufficient* condition for synchronization of (2) is that (3) be globally asymptotically stable [Khalil, 1992]. Selecting a positive definite quadratic Lyapunov function (which is radially unbounded)

$$V(e) = e^T P e\,, \quad P = P^T > 0 \quad (4)$$

a sufficient condition for global asymptotic stability of (3) is presented in the following Theorem.

**Theorem 1.** *A sufficient condition for global asymptotic stability of error system (3) for any $f$ which is bounded when its arguments are bounded, is that*

$$\Lambda^T(sI - (A+K))^{-1}\Lambda \quad \text{be strictly positive real} \quad (5)$$

*where* $\Lambda = [b,\, c]$.

*Proof.* Using (3) one obtains for the derivative of $V$

$$\begin{aligned}\dot{V}(e) &= e^T[(A+K)^T P + P(A+K)]e \\ &\quad + f(q_1^T x, \ldots, q_r^T x,\, t)e^T(B^T P + PB)e\end{aligned} \quad (6)$$

where $B = bc^T - cb^T$. We require that $\dot{V}$ be less than a negative definite, time-invariant function for *any* $f$ which is bounded for bounded arguments. This requirement is satisfied if and only if

$$(A+K)^T P + P(A+K) < 0\,, \quad B^T P + PB = 0\,. \quad (7)$$

It is readily shown that when matrix $B$ has the special form $bc^T - cb^T$ then

$$B^T P + PB = 0 \quad \text{iff} \quad Pb = \gamma b,\, Pc = \gamma c \quad (8)$$

$\gamma \in \mathbb{R}$ with $\gamma > 0$ as $P > 0$. Equations (7) and (8) imply

$$\begin{aligned}P[b,\, c] &= \gamma[b,\, c]\,, \\ (A+K)^T P + P(A+K) &< 0\,.\end{aligned} \quad (9)$$

A necessary and sufficient condition for the existence of $P > 0$ such that (9) holds is that

$$\Lambda^T(sI - (A+K))^{-1}\Lambda \quad \text{be strictly positive real} \quad (10)$$

where $I$ is the $n \times n$ identity matrix and $\Lambda = [b,\, c]$. See Khalil [1992, lemma 5.1] for proof. ■

As previously noted, Theorem 1 significantly generalizes the result of Cuomo and Oppenheim

[1993]. The paucity of restrictions imposed on $f$ in this criterion is remarkable and reflects the special form of system (1). For general Lur'e systems one must impose more stringent restrictions on $f$ to obtain useful synchronization criteria.

Equation (9) is a Linear Matrix Inequality (LMI). It has been noted in recent years [Boyd *et al.*, 1994] that it is often easier to numerically test (9) directly, than to test (10). Hence, although (10) is (in the sense of being free of existentials) a more complete criterion, it is not (in the sense of numerical testability) the most useful criterion.

### 2.1. *Example: Cuomo and Oppenheim*

As an application of LMI (9) consider the system investigated by Cuomo and Oppenheim [1993]. For suitable choice of state vector this system has form (1) with

$$A = \begin{bmatrix} -\sigma & \sigma & 0 \\ 0 & -1 & 0 \\ 0 & 0 & -\beta \end{bmatrix}, \quad b = \begin{bmatrix} 0 \\ 0 \\ 1 \end{bmatrix},$$
$$c = \begin{bmatrix} 0 \\ 1 \\ 0 \end{bmatrix}, \quad f(\cdot, t) = 10u(t). \tag{11}$$

For (11) to possess (as required by Cuomo and Oppenheim) a quadratic Lyapunov function independent of any restriction (except boundedness) on $u(t)$, the above argument asserts that there must exist a $3 \times 3$ symmetric matrix $P > 0$ satisfying (9) with $K$ set to zero. One may assume $\gamma = 1$ without loss of generality. Hence

$$P = \begin{bmatrix} p_{11} & 0 & 0 \\ 0 & 1 & 0 \\ 0 & 0 & 1 \end{bmatrix} > 0,$$
$$A^T P + PA = \begin{bmatrix} -2p_{11}\sigma & p_{11}\sigma & 0 \\ p_{11}\sigma & -2 & 0 \\ 0 & 0 & -2\beta \end{bmatrix} < 0. \tag{12}$$

One may readily show that (12) permits a solution $p_{11}$ if and only if $\sigma > 0$, $\beta > 0$. Cuomo and Oppenheim [1993] offer the particular solution $p_{11} = \frac{1}{\sigma}$. The general theory yields the full range of solutions $0 < p_{11} < \frac{4}{\sigma}$.

## 3. Generalization of Result of Wu and Chua

Now consider the general Lur'e system [Vidyasagar, 1978]

$$\dot{x} = Ax - bf\left(c^T x, t\right) \tag{13}$$

$A \in \mathbb{R}^{n\times n}$; $b, c \in \mathbb{R}^n$. A system of this kind which frequently arises in the synchronization literature is the celebrated Chua oscillator [Chua *et al.*, 1993]. Consider the following synchronization scheme

$$\begin{aligned} \dot{x} &= Ax - bf(c^T x, t) \\ \dot{y} &= Ay - bf(c^T y, t) - K(x - y) \end{aligned} \tag{14}$$

where $K \in \mathbb{R}^{n\times n}$. Defining error signal $e = x - y$ one determines the error system

$$\begin{aligned} \dot{e} &= (A + K)e \\ &\quad - b[f(c^T e + c^T y, t) - f(c^T y, t)] \\ &= (A + K)e - b\eta(c^T e, t). \end{aligned} \tag{15}$$

Assume that nonlinearity $f$ satisfies restriction

$$\alpha \le \frac{[f(\sigma + \zeta, t) - f(\zeta, t)]}{\sigma} = \frac{\eta(\sigma, t)}{\sigma} \le \beta \; \forall \sigma \neq 0, \zeta, t \tag{16}$$

[Wu & Chua, 1994]. Synchronization of (14) occurs if system (15) is globally asymptotically stable. Several equivalent sufficient conditions for global asymptotic stability of (15) are presented in the following Theorem.

**Theorem 2.** *Assuming $\alpha$ finite, a sufficient condition for global asymptotic stability of error system (15) is given by*

**Case 1:** $\beta = \infty$

Form 1. Frequency Domain Criterion.

$$c^T(sI - (A + K - \alpha bc^T))^{-1}b \quad \text{strictly positive real.} \tag{17}$$

Form 2. Constrained Lyapunov Matrix Inequality.

$$\exists P = P^T > 0,$$
$$P \in \mathbb{R}^{n\times n} \quad \text{s.t. } (A + K - \alpha bc^T)^T P + P(A + K - \alpha bc^T) < 0$$
$$\text{and} \qquad Pb = c. \tag{18}$$

**Case 2:** $\beta < \infty$

Form 1. Frequency Domain Criterion.

$$\frac{1}{(\beta-\alpha)} + c^T(sI - (A + K - \alpha bc^T))^{-1}b \qquad \text{strictly positive real.} \tag{19}$$

Form 2. Simultaneous Lyapunov Matrix Equation.

$$\begin{gathered} \exists P = P^T > 0, \\ P \in \mathbb{R}^{n\times n} \quad \text{s.t. } (A + K - \alpha bc^T)^T P + P(A + K - \alpha bc^T) < 0 \\ \text{and} \qquad (A + K - \beta bc^T)^T P + P(A + K - \beta bc^T) < 0\,. \end{gathered} \tag{20}$$

Form 3. Linear Matrix Inequality.

$$\exists P > 0 \quad \text{s.t.} \begin{bmatrix} (A + K - \alpha bc^T)^T P + P(A + K - \alpha bc^T) & Pb - c \\ (Pb - c)^T & \dfrac{2}{(\beta-\alpha)} \end{bmatrix} < 0\,. \tag{21}$$

We omit the proof of Theorem 2 as it is merely a statement of the well-known circle criterion [Vidyasagar, 1978; Khalil, 1992]. We have omitted Form 3 for Case 1 as it is a trivial restatement of Form 2.

As noted above, efficient numerical algorithms exist for solving Linear Matrix Inequalities [Boyd *et al.*, 1994], and/or for determining when such solutions exist. The LMI forms 2 and 3 are therefore regarded as the most important for practical applications.

We note that the circle criterion is equivalent to the existence of a quadratic Lyapunov function $e^T Pe$ having negative derivative along the trajectories of error system (15) for *any* nonlinearity $f$ satisfying (16) [Curran, 1993]. Hence this result subsumes the synchronization criterion for Lur'e systems derived by Wu and Chua [Theorem 7, 1994]. The circle criterion explicitly uses parameters $\alpha$ and $\beta$ and therefore improves upon the result of Wu and Chua [Theorem 7, 1994] where only the fact that $\alpha > 0$ is actually employed. Finally, the criterion provides for a *systematic* procedure for generating quadratic Lyapunov functions which is numerically tractable.

## 4. The Pecora–Carroll Synchronization Scheme

We consider the following synchronization scheme which is an elementary example of the scheme due to Pecora and Carroll [1991]. Commencing with a system of form (1) (with $r \le n-2$ assumed), assume that one may select variables $q_1^T x, \ldots, q_{n-2}^T x$ such that $\{q_1, \ldots, q_{n-2}, b, c\}$ are orthogonal. Applying the Pecora–Carroll scheme, construct a copy of the dynamical equations for $q_{r+1}^T x, \ldots, q_{n-2}^T x$, $b^T x$, $c^T x$. After the change of variables $q_1^T x \mapsto x_1, \ldots, q_{n-2}^T x \mapsto x_{n-2}$, $b^T x \mapsto x_{n-1}$, $c^T x \mapsto x_n$, the scheme attains the canonical form

$$\begin{aligned} \dot{x} &= \begin{bmatrix} A_{11} & A_{12} \\ A_{21} & A_{22} \end{bmatrix} x \\ &\quad + f(\hat{x}_1, t)\left(\begin{bmatrix} 0 \\ b_2 \end{bmatrix}\left[0^T, c_2^T\right] - \begin{bmatrix} 0 \\ c_2 \end{bmatrix}\left[0, b_2^T\right]\right) x \\ \dot{y} &= [A_{21}, A_{22}]\begin{bmatrix} \hat{x}_1 \\ y \end{bmatrix} \\ &\quad + f(\hat{x}_1, t)\left(b_2\left[0, c_2^T\right] - c_2\left[0, b_2^T\right]\right)\begin{bmatrix} \hat{x}_1 \\ y \end{bmatrix} \end{aligned} \tag{22}$$

where $x^T = [\hat{x}_1^T, \hat{x}_2^T]$ with $\hat{x}_1 \in \mathbb{R}^r$. Pecora and Carroll require that state $y$ and *substate* $\hat{x}_2$ asymptotically converge. Defining the error signal $e = \hat{x}_2 - y$, one may determine the error system

$$\dot{e} = A_{22}e + f(\hat{x}_1, t)(b_2 c_2^T - c_2 b_2^T)e \tag{23}$$

which is once more a system of form (1). Global asymptotic stability of error system (23) for *any* $f$ (bounded for bounded arguments) comprises a sufficient condition for synchronization of the Pecora–Carroll form. This is precisely the problem which was discussed in Sec. 2. It follows that the synchronization criteria of Sec. 2 also comprise criteria for synchronization of Pecora–Carroll scheme (22). The resulting criterion is algebraic, permits efficient

numerical testing and does not involve the calculation of conditional Lyapunov exponents [Pecora & Carroll, 1991].

### 4.1. *Example: Pecora and Carroll*

Consider the $x$-driven copy of the Lorenz equations [Pecora & Carroll, 1991]

$$\begin{aligned} \dot{y}' &= -xz' + rx - y' \\ \dot{z}' &= xy' - \beta z' . \end{aligned} \tag{24}$$

Defining error signal $e_1 = y - y'$, $e_2 = z - z'$, the error system takes form (1) with

$$A = \begin{bmatrix} -1 & 0 \\ 0 & -\beta \end{bmatrix}, \quad b = \begin{bmatrix} 0 \\ 1 \end{bmatrix}, \quad c = \begin{bmatrix} 1 \\ 0 \end{bmatrix}, \quad f(\cdot, t) = x(t) . \tag{25}$$

Hence, by Theorem 1 this error system is globally asymptotically stable for any *bound* driving signal $x$ if there exists $P = I$ (the identity matrix) such that

$$A^T P + PA = \begin{bmatrix} -2 & 0 \\ 0 & -2\beta \end{bmatrix} < 0, \quad \text{i.e. if} \quad \beta > 0 . \tag{26}$$

### 4.2. *Further comments*

It is clear from the above discussion that the Pecora–Carroll synchronization scheme is strongly related to an absolute stability problem in the case where the drive system has form (1) and where the response system is driven by *all* of the arguments of the nonlinearity. Similar comments pertain when the drive system is of the general Lur'e type considered in Sec. 3 and again where the response system is driven by all of the arguments of the nonlinearity.

In certain cases where the response system is *not* driven by all of the arguments of the nonlinearity, absolute stability theory may still be employed to devise sufficient conditions for synchronization. For example, the error system associated with the $y$-driven copy of the Lorenz equations [Pecora & Carroll, 1991] has the form of Lur'e system (13) with

$$A = \begin{bmatrix} -\sigma & 0 \\ 0 & -\beta \end{bmatrix}, \quad b = c = \begin{bmatrix} 1 \\ 0 \end{bmatrix}, \quad f(\zeta, t) = -y(t)\zeta . \tag{27}$$

If one assumes $y$ to be bounded, then Theorem 2 provides sufficient conditions for this error system to be globally asymptotically stable.

## 5. Multivariable Criteria

Systems (1) and (13) possess a single nonlinearity but are of arbitrarily high dimension. By exploiting this freedom of dimension one may hope to establish synchronization of highly complex chaotic systems. A second means of ensuring this complexity is to select systems possessing a larger number of nonlinearities. As a generalization of the special system of Sec. 2, we propose the following multiple nonlinearity system

$$\begin{aligned} \dot{x} &= Ax + \sum_{i=1}^{m} f_i(q_1^T x, \ldots, q_r^T x, t)(b_i c_i^T - c_i b_i^T)x \\ \dot{y} &= Ay + \sum_{i=1}^{m} f_i(q_1^T x, \ldots, q_r^T x, t)(b_i c_i^T - c_i b_i^T)y \\ &\quad - K(x - y) \end{aligned} \tag{28}$$

where $K \in \mathbb{R}^{n \times n}$. Proceeding in the manner of Sec. 2, one constructs the error system for error $e = x - y$

$$\dot{e} = (A + K)e + \sum_{i=1}^{m} f_i(q_1^T x, \ldots, q_r^T x, t) B_i e \tag{29}$$

where $B_i = b_i c_i^T - c_i b_i^T$. Following the discussion of Sec. 2, one readily verifies the following Theorem.

**Theorem 3.** *A sufficient condition for global asymptotic stability of error system (29) for any nonlinearities $f_i$ bounded for bounded arguments, is that there exists $P = P^T > 0$, $P \in \mathbb{R}^{n \times n}$ such that*

$$\begin{aligned} A^T P + PA < 0 \quad \text{and} \quad Pb_i = \gamma_i b_i , \\ Pc_i = \gamma_i c_i , \quad \gamma_i \in \mathbb{R} \, \forall i . \end{aligned} \tag{30}$$

Once more, this is a constrained matrix inequality. One may employ the KYP lemma [Khalil, 1992] to determine an associated frequency domain condition which is both necessary and sufficient for the existence of a positive definite solution $P$ to (30). However, as previously noted, in practice one often tests (30) directly for a solution of the required form, because such a test may be implemented in a numerically efficient manner [Boyd *et al.*, 1994].

The form of the general multivariable Lur'e system is standard [Vidyasagar, 1978]. We take

$$\begin{aligned}\dot{x} &= Ax - Bf(C^T x, t)\\ \dot{y} &= Ay - Bf(C^T y, t) - K(x-y)\end{aligned} \tag{31}$$

where $B$, $C$, $\in \mathbb{R}^{n\times m}$, $K \in \mathbb{R}^{n\times n}$, $f$ is a vector function from $\mathbb{R}^{m+1}$ into $\mathbb{R}^m$. The error system for error $e = x - y$ becomes

$$\begin{aligned}\dot{e} &= (A+K)e\\ &\quad - B[f(C^T e + C^T y, t) - f(C^T y, t)].\end{aligned} \tag{32}$$

Assume $f$ to satisfy the constraint

$$\begin{aligned}&[K_2\sigma - f(\sigma+\zeta, t) + f(\zeta, t)]^T[f(\sigma+\zeta, t)\\ &\quad - f(\zeta, t) - K_1\sigma] \geq 0 \,\forall\sigma, \quad \zeta \in R^m, \quad \forall t\end{aligned} \tag{33}$$

where $K_1$, $K_2 \in \mathbb{R}^{m\times m}$. We select a quadratic Lyapunov function

$$V(e) = e^T P e, \quad P > 0 \tag{34}$$

and may prove the following Theorem.

**Theorem 4.** *A sufficient condition for global asymptotic stability of error system (32) is that there exists $P \in \mathbb{R}^{n\times n}$, $P = P^T > 0$ and scalar $\gamma \geq 0$ satisfying the Linear Matrix Inequality*

$$Y = Y^T = \begin{bmatrix} Y_{11} & Y_{12} \\ \cdot & Y_{22}\end{bmatrix} < 0 \tag{35}$$

*where*

$$\begin{aligned}Y_{11} &= (A+K)^T P + P(A+K)\\ &\quad - \frac{\gamma}{2}C(K_2^T K_1 + K_1^T K_2)C^T\\ Y_{12} &= -PB + \frac{\gamma}{2}C(K_1+K_2)^T\\ Y_{22} &= -\gamma I\,.\end{aligned}$$

*Proof.* Taking the time derivative of $V$, applying the $S$-procedure [Boyd *et al.*, 1994] and using (33), one obtains

$$\begin{aligned}\dot{V}(e) &\leq e^T[(A+K)^T P + P(A+K)]e - e^T PB\eta\\ &\quad - \eta^T B^T P e + \frac{\gamma}{2}[K_2 C^T e - \eta]^T[\eta - K_1 C^T e]\\ &\quad + \frac{\gamma}{2}[\eta - K_1 C^T e]^T[K_2 C^T e - \eta]\\ &\leq \zeta^T Y \zeta < 0\end{aligned} \tag{36}$$

where

$$\begin{aligned}\eta &= f(C^T e + C^T y, t) - f(C^T y, t)\,,\\ \zeta^T &= [e^T, \eta^T]\,.\end{aligned} \tag{37}$$

■

Restrictions other than (33) lead to different Linear Matrix Inequalities.

## 6. Robustness of Synchronization Criteria

In practical implementations of the synchronization schemes presented above, two non-ideal effects occur: (i) channel noise corrupts the transmitted components of state $x$, and (ii) subsystem mismatch is present. A synchronization criterion is of little use if the synchronization it predicts may be destroyed by arbitrarily low levels of channel noise and/or subsystem mismatch. In short, a synchronization criterion should imply robust synchronization. The purpose of this final section is to show that synchronization criteria based on absolute stability theory possess this property. We prove this result for the criterion of Theorem 1 only, as the proof for all other criteria is similar.

Consider system (1) subject to channel noise and mismatch

$$\begin{aligned}\dot{x} &= Ax + f(q_1^T x, \ldots, q_r^T x, t)(bc^T - cb^T)x\\ \dot{y} &= \hat{A}y + \hat{f}(q_1^T\hat{x}, \ldots, q_r^T\hat{x}, t)(bc^T - cb^T)y\\ &\quad - K(\hat{x} - y)\end{aligned} \tag{38}$$

where $\hat{x}$ is the received vector when $x$ is transmitted. As a measure of noise and mismatch, assume

$$\begin{aligned}&\|\hat{x} - x\|_2 < \delta_1\,, \quad \|\hat{A} - A\| < \delta_2\\ &|\hat{f}(\hat{z}, t) - f(z, t)| \leq \delta_3\|\hat{z} - z\|_2 \,\forall\hat{z}\,,\\ &z \in R^r \text{ such that } \|\hat{z} - z\|_2 < \delta_1\,, \forall t\,.\end{aligned} \tag{39}$$

Note: For simplicity we have assumed no mismatch in vectors $b$, $c$. This reflects the fact that in many important examples $b$ and $c$ may be selected as specific vectors and thus encode the *structure* and not the parameter values of the subsystems. As we assume no mismatch in structure, the assumption of matched $b$, $c$ is often justified. If a mismatch of these vectors does occur the robustness results

of the present section. may be rederived. Similar comments apply to the assumed match of vectors $q_1, \ldots, q_r$.

Defining error signal $e = y - x$ the error system becomes

$$\dot{e} = (\hat{A} + K)e + \hat{f}(\hat{z}_1, \ldots, \hat{z}_r, t)(bc^T - cb^T)e + u(t) \tag{40}$$

where

$$\begin{aligned} u(t) = (\hat{A} - A)x + [\hat{f}(\hat{z}_1, \ldots, \hat{z}_r, t) \\ - f(z_1, \ldots, z_r, t)](bc^T - cb^T)x \\ + K(x - \hat{x}) . \end{aligned} \tag{41}$$

Finally, we assume that substate $x$ of system (38) is bounded, i.e.

$$\|x(t)\|_2 < \Delta \forall t \tag{42}$$

for some constant $\Delta > 0$. In practice we will not employ a subsystem possessing unbounded trajectories and consequently assumption (42) is guaranteed. Equations (39), (41) and (42) imply that $\exists\, \mathcal{U}$ such that

$$\begin{aligned} &\|u(t)\|_2 < \mathcal{U} \ \forall t \quad \text{and} \\ &\lim_{(\delta_1, \delta_2, \delta_3) \to (0, 0, M)} \mathcal{U} = 0 \quad \text{for any } M \text{ finite} . \end{aligned} \tag{43}$$

For the purposes of the present paper, we define robust synchronization as follows:

**Definition 1.** System (38) *robustly synchronizes* if, given any $\varepsilon > 0$, there exist $\hat{\delta}_1 > 0$, $\hat{\delta}_2 > 0$ and $\hat{\delta}_3 > 0$ such that, in the presence of channel fidelity $\delta_1 < \hat{\delta}_1$, parameter mismatch $\delta_2 < \hat{\delta}_2$ and nonlinearity mismatch $\delta_3 < \hat{\delta}_3$, the norm of the error converges to less than $\epsilon$ for any norm-bounded initial conditions.

We may now state and prove a robustness property for the synchronization criterion of Theorem 1.

**Theorem 5.** *If the matched synchronization system (1) with nominal parameter values $\hat{A}$ and nonlinearity $\hat{f}$ satisfies synchronization criterion (5) then mismatched system (38) robustly synchronizes.*

*Proof.* By the assumption of the Theorem and Eq. (7) there exists $P$ such that $V(e) = e^T P e$ is positive definite, radially unbounded, and further that

$$\dot{V}(e) = e^T((\hat{A} + K)^T P + P(\hat{A} + K))e + 2e^T P u(t) \tag{44}$$

with $(\hat{A} + K)^T P + P(\hat{A} + K)$ real, symmetric, negative definite having least negative eigenvalue $-\lambda < 0$. As $P$ is positive definite we may denote its largest eigenvalue by $\mu > 0$. Applying Eq. (44) and standard matrix manipulation one obtains

$$\dot{V}(e) \leq -\lambda \|e\|_2^2 + 2\mu \|e\|_2 \mathcal{U} . \tag{45}$$

Hence $\dot{V} < 0$ if

$$\|e\|_2 > \frac{2\mu\mathcal{U}}{\lambda} . \tag{46}$$

It follows [LaSalle & Lefschetz, 1961] that every trajectory of the error system remains bounded and converges to the closed ball of radius $\frac{2\mu\mathcal{U}}{\lambda}$ centered at the origin. From Eq. (43), one may make $\frac{2\mu\mathcal{U}}{\lambda}$ arbitrarily small by selecting $\delta_1$, $\delta_2$ arbitrarily small and $\delta_3$ finite. Robust synchronization follows by definition. ■

Theorem 5 asserts that synchronization criterion (5) implies robust synchronization. In a similar way one may demonstrate that all of the synchronization criteria presented in this paper also imply robust synchronization in the sense of Definition 1.

## 7. Conclusion

In this paper we have presented an overview of several results in absolute stability theory and have established the relationship between these results and the error system approach to the determination of sufficient conditions for synchronization of identical, finite dimensional, systems of Lur'e type. In particular we have generalized synchronization results of Pecora and Carroll [1991], Cuomo and Oppenheim [1993] and Wu and Chua [1994]. Robustness of the resulting criteria has been proven.

All problems are shown to reduce to linear matrix inequalities which may be solved by means of efficient numerical algorithms. The results presented provide for the systematic exploitation of quadratic Lyapunov functions in the development of criteria for synchronization and for certain schemes of the Pecora–Carroll type. With regard to the latter, the synchronization criteria obtained do not involve the conditional Lyapunov exponents.

## Acknowledgments

This work is supported by University College Dublin and the Fulbright Fellowship Program.

## References

Boyd, S., El Ghaoui, L., Feron, E. & Balakrishnan, V. [1994] *Linear Matrix Inequalities in System and Control theory* (SIAM: Studies in Applied Mathematics), Vol. 15.

Chua, L. O., Wu, C. W., Huang, A. & Zhong, G. Q. [1993] "A universal circuit for studying and generating chaos, part I: Routes to chaos," *IEEE Trans. Circuits Syst. — I: Fundamental Theory and Applications* **10**(40), 732–744, Special Issue on Chaos in Electronic Circuits, Part A.

Cuomo, K. M. & Oppenheim, A. V. [1993] "Circuit implementation of synchronized chaos with applications to communications," *Phys. Rev. Lett.* **71**(1), 65–68.

Curran, P. F. [1993] "Proof of the circle criterion for state space systems via quadratic Lyapunov functions — Part 1," *Int. J. Control* **57**(4), 921–955.

Hasler, M. [1994] "Synchronization principles and applications," *Circuits and Systems: Tutorials IEEE–ISCAS'94*, 314–326.

Khalil, H. K. [1992] *Nonlinear Systems* (MacMillan, New York).

Kocarev, L., Halle, K. S., Eckert, K., Chua, L. O. & Parlitz, U. [1992] "Experimental demonstration of secure communications via chaotic synchronization," *Int. J. Bifurcation and Chaos* **2**(3), 709–713.

LaSalle, J. P. & Lefschetz, S. [1961] *Stability by Liapunov's Direct Method with Applications* (Academic Press, New York)

Pecora, L. & Carroll, T. [1991] "Driving systems with chaotic signals," *Phys. Rev.* **A44**, 2374–2383.

Parlitz, U., Chua, L. O., Kocarev, L., Halle, K. S. & Shang, A. [1992] "Transmission of digital signals by chaotic synchronization," *Int. J. Bifurcation and Chaos* **2**(4), 973–977.

Vidyasagar, M. [1978] *Nonlinear Systems Analysis* (Prentice Hall, New Jersey).

Wu, C. W. & Chua, L. O. [1994] "A Unified framework for synchronization and control of dynamical systems," *Int. J. Bifurcation and Chaos* **4**(4), 979–998.

# Express Letters

## Cryptography Based on Chaotic Systems

Tao Yang, Chai Wah Wu, and Leon O. Chua

*Abstract*— **In this letter, a new chaos-based secure communication scheme is proposed in an attempt to thwart the attacks proposed recently. Instead of encoding the message signal in a chaotic system directly, we use two chaotic signals in our scheme. One of the chaotic signals is used to synchronize the chaotic encrypter and the chaotic decrypter. The other is used to encrypt the plain signal by using a multishift cipher scheme. Thus the transmitted signal is not used to encrypt the message and a more complicated method of encryption is used.**

### I. Introduction

Recently, there has been much interest in the use of two synchronized chaotic systems for the purpose of secure communication. A chaotic signal has a spread-spectrum and can hide a small message signal in the spectral domain [6]. However, in the time domain, a chaotic system can be easily identified by using one of its state variables [1]–[5].

The authors of [2] and [7] found that the additive masking method and the chaotic switching method are not secure. Also, the parameter methods (either using message signal to modulate a parameter or change a state-variable) have a low security [8], [9].

All the attacks proposed in [2] and [7]–[9] are based on the fact that the chaos-based secure communication systems are not sensitive enough to the modeling error of the transmitter. So, an intruder can recover the message signal by using an approximate model with some errors which can be easily removed by standard filtering methods. To defend itself against these attacks, a chaos-based cryptosystem is proposed in this letter. Our method is much more sensitive to the recovering errors and the modeling errors, so the level of security is enhanced. Furthermore, state variables other than the transmitted variable is used in the encrypter (as was done in [13]), thereby thwarting attacks which reconstructs only the transmitted variable [2], [8].

### II. Chaotic Cryptosystem

A chaotic cryptosystem is shown in Fig. 1. In Fig. 1, the encrypter consists of a chaotic system and an encryption function $e()$. The key signal $k(t)$ is one of the state variables of the chaotic system. Another state variable $s(t)$ is the transmitted signal, which is transmitted through a public channel to the decrypter and used to synchronize the decrypter. $y(t)$ is the encrypted signal which is fed back into the chaotic system.

The decrypter consists of a chaotic system and a decryption function $d()$. The decrypter can find the key signal when the decrypter and the encrypter are synchronized. The encrypted signal is also recovered via synchronization. Then, $d()$ is used to decrypt the encrypted signal.

It should be noted that in the scheme shown in Fig. 1, both the key signal $k(t)$ and the encrypted signal $y(t)$ are not transmitted to the decrypter. It is different from the traditional discrete cryptosystem where both the key and the encrypted signal should be transmitted to the decrypter [12].

We use Chua's circuits, which exhibits double scroll chaotic attractors, to implement one such chaotic cryptosystem as shown in Fig. 2, where $v_R(t)$ is the transmitted signal, $v_2(t)$ is the key signal, and $p(t)$ denotes the plain text signal (the message signal). The state equations of this cryptosystem are described.

*Encrypter:*

$$\begin{cases} \dfrac{dv_1}{dt} = \dfrac{1}{C_1}[G(v_2 - v_1) - f(v_R)] \\ \dfrac{dv_2}{dt} = \dfrac{1}{C_2}[G(v_1 - v_2) + i_3] \\ \dfrac{di_3}{dt} = \dfrac{1}{L}[-v_2] \end{cases} \tag{1}$$

where $f()$ is the nonlinear characteristics of Chua's diode in Chua's circuit given by

$$f(v_1) = G_b v_1 + \frac{1}{2}(G_a - G_b)(|v_1 + E| - |v_1 - E|) \tag{2}$$

and $E$ is the breakpoint voltage of Chua's diode. The voltage $v_R$ is given by

$$v_R = v_1 - e(p(t)) \tag{3}$$

where $e(p(t))$ is the encrypted signal.

*Decrypter:*

$$\begin{cases} \dfrac{d\tilde{v}_1}{dt} = \dfrac{1}{C_1}[G(\tilde{v}_2 - \tilde{v}_1) - f(v_R)] \\ \dfrac{d\tilde{v}_2}{dt} = \dfrac{1}{C_2}[G(\tilde{v}_1 - \tilde{v}_2) + \tilde{i}_3] \\ \dfrac{d\tilde{i}_3}{dt} = \dfrac{1}{L}[-\tilde{v}_2] \end{cases} \tag{4}$$

$$\tilde{e}(p(t)) = \tilde{v}_1 - v_R \tag{5}$$

where $\tilde{e}(p(t))$ is the recovered encrypted signal. A set of sufficient conditions for synchronizing systems (1) and (4) are $C_1 > 0, C_2 > 0. G > 0. L > 0$ [10]. Since this synchronization configuration of two Chua's circuits is error-free, we have $\tilde{e}(p(t)) \to e(p(t))$ when the synchronization is achieved.

We use an $n$-shift cipher to encrypt the plain signal. The $n$-shift cipher is defined by

$$e(p(t)) = \underbrace{f_1(\cdots f_1(f_1}_{n}(p(t), \underbrace{v_2(t)). v_2(t)). \ldots . v_2(t))}_{n}) = y(t) \tag{6}$$

where $h$ is chosen such that $p(t)$ and $v_2(t)$ lie within $(-h. h)$. And $f_1(*. *)$ is the following nonlinear function

$$f_1(x. k) = \begin{cases} (x + k) + 2h. & -2h \le (x + k) \le -h \\ (x + k). & -h < (x + k) < h \\ (x + k) - 2h. & h \le (x + k) \le 2h \end{cases} \tag{7}$$

This function is shown in Fig. 3.

Manuscript received March 12, 1996; revised June 27, 1996. This work was supported in part by the Office of Naval Research under Grant N00014-96-1-0753. This paper was recommended by Associate Editor T. Endo.

T. Yang is with the Department of Electrical Engineering and Computer Sciences, University of California, Berkeley, CA 94720 USA, on leave from the Department of Automatic Control Engineering, Shanghai University of Technology, Shanghai 200072, P.R. China.

C. W. Wu and L. O. Chua are with the Electronics Research Laboratory and the Department of Electrical Engineering and Computer Sciences, University of California, Berkeley, CA 94720 USA.

Publisher Item Identifier S 1057-7122(97)02071-0.

1057–7122/97$10.00 © 1997 IEEE

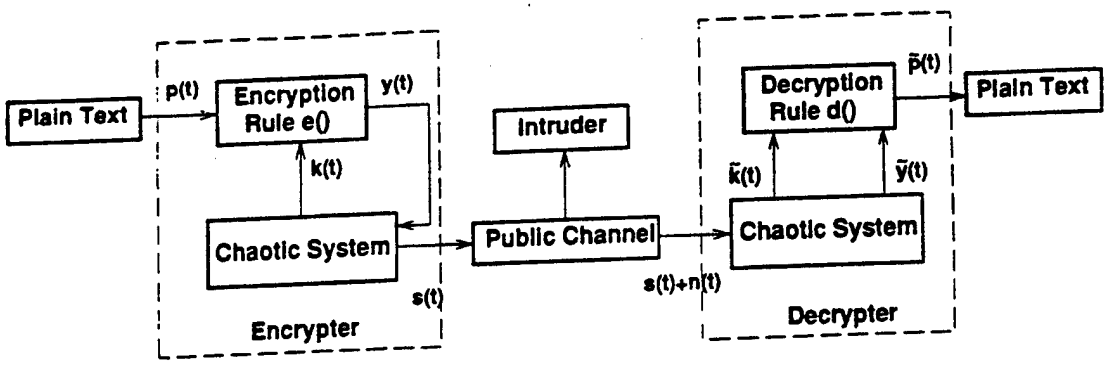


Fig. 1. Block diagram of the chaotic cryptosystem.

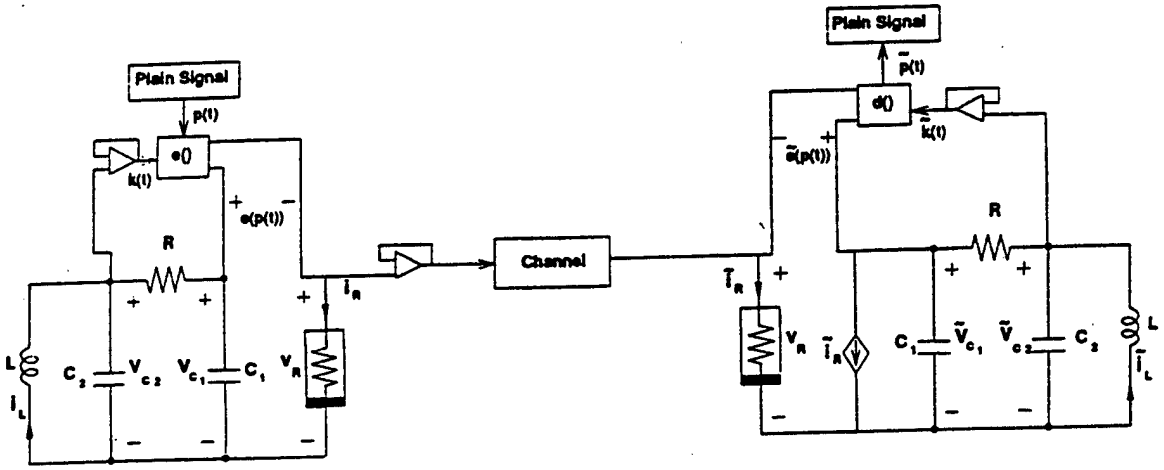


Fig. 2. Block diagram of the Chua's circuits based cryptosystem.

The corresponding decryption rule is the same as the encryption rule

$$p(t) = d(y(t)) = e(y(t)) = \underbrace{f_1(\cdots f_1(f_1}_{n}(y(t), \underbrace{-\tilde{v}_2(t)), -\tilde{v}_2(t)), \cdots, -\tilde{v}_2(t))}_{n} \quad (8)$$

where $\tilde{v}_2(t)$ is recovered in the receiver circuit and should approximate $v_2(t)$.

In the $n$-shift cipher, the key signal $v_2(t)$ is used $n$ times to encrypt the plain signal. Since the encrypted signal is a function of $v_2(t)$ and $p(t)$, and since the encrypted signal is used to drive the Chua's circuit, it hides both the dynamical and the statistical characteristics of both $v_2(t)$ and $p(t)$.

## III. Simulation Results

In this section, we study the performance of the attack proposed in [8] to the chaotic cryptosystem. In all of the following simulations, the following parameters are used: $C_1$ =5.56 nF, $C_2$ = 50 nF, $G$ = 0.7 mS, $L$ = 7.14 mH, $G_a = -0.8$ mS, $G_b = -0.5$ mS, $E$ = 1 V. The initial conditions are $(v_1(0), v_2(0), i_3(0)) = (-0.2$ V, $-0.02$ V, 0.1 mA) and $(\tilde{v}_1(0), \tilde{v}_2(0), \tilde{i}_3(0)) = (0.02$ V, $-0.12$ V, $-0.1$ mA), respectively. So, the encrypter and the decrypter are initially desynchronized. $h$ = 0.4 V. A 30-shift cipher is used ($n$ =30 and $h$ =0.4 V).

First, we show the performance of our cryptosystem. Fig. 4 shows the results when a sinusoidal signal is encrypted. Fig. 4(a) shows the transmitted signal $v_R(t)$. Fig. 4(b) shows the recovered and then decrypted signal. One can see that the plain signal is decrypted perfectly except for the first 8 ms, which is needed to synchronize both Chua's circuits.

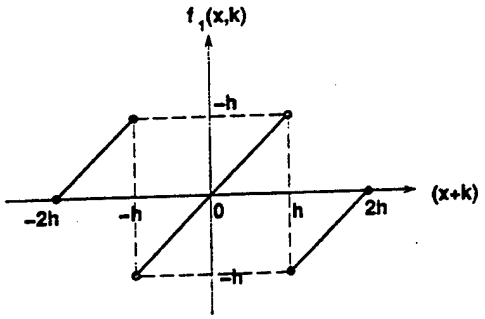


Fig. 3. Nonlinear function used in continuous shift cipher.

Suppose that an intruder can successfully reconstruct the dynamics of the transmitted signal. By repeating the method proposed in [8], we find the best recovered message signal has a SNR$\approx$ 20 dB. This SNR is high enough for an intruder to find the sinusoidal signal from the recovered result when the chaotic secure communication scheme proposed in [10] is used. But the following simulation shows that this SNR is too low to decrypt the recovered encrypted signal when the scheme shown in Fig. 2 is used. Fig. 4(c) shows the recovered encrypted signal using the method in [8]. Since the encrypted signal is a very good pseudorandom signal, which almost distributes uniformly in the full frequency range, no standard filtering method can be used to enhance the SNR of the encrypted signal. Next suppose that the intruder can successfully reconstruct $v_2(t)$ with a SNR = 20 dB. Then the decrypted signal is shown in Fig. 4(d), from which one can see that the intruder can not find the plain signal.

We then study the effects of parameter mismatch. We first consider the mismatch of parameter $h$. Fig. 5(a) shows the decrypted signal

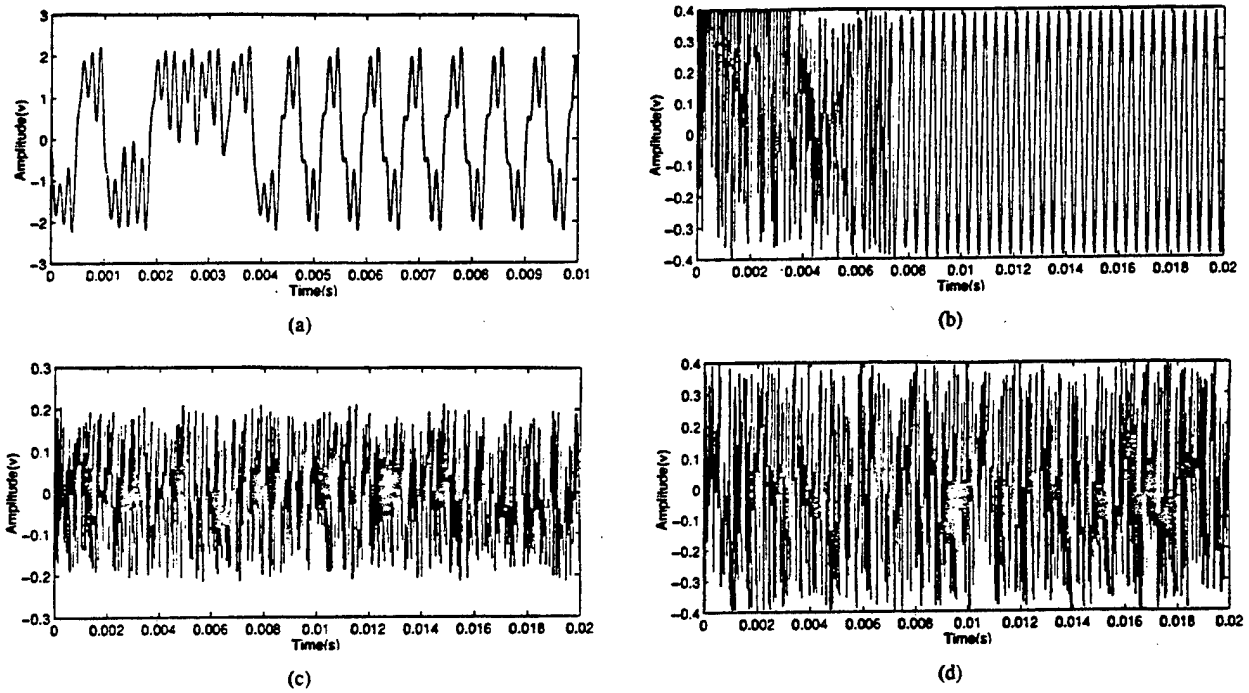


Fig. 4. (a) The transmitted signal. (b) The recovered and then decrypted signal. (c) The recovered encrypted signal using the method in [8]. (d) The decrypted result of that shown in Fig. 4(c).

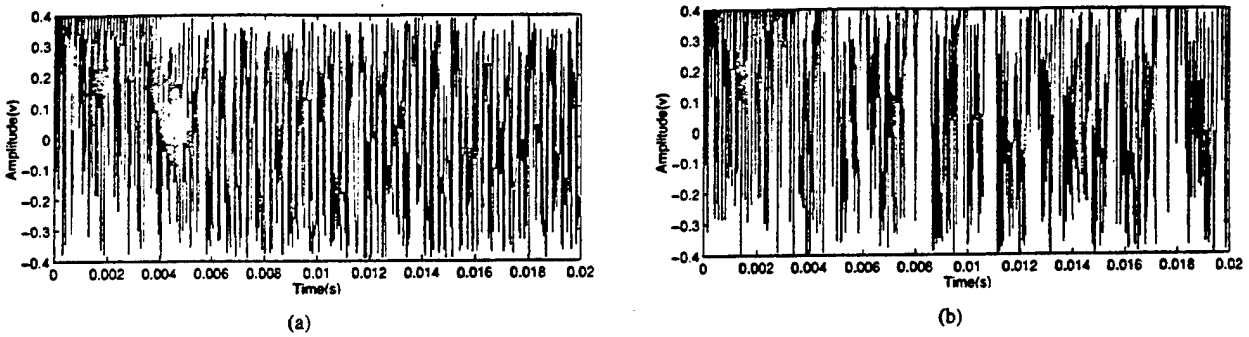


Fig. 5. (a) The decrypted signal when 0.01 V mismatch of $h$ exists. (b) The decrypted signal when 1% mismatch of $G$ exists.

when $h$ in the decrypter has a 0.01 V mismatch. One can see that the plain signal is hard to be recovered from this decrypted result. However, when $h$ has a mismatch smaller than 5 mV, the plain signal can be easily recovered from the decrypted signal. We then study the cases when $G$ is mismatched. Fig. 5(b) shows the decrypted signal when $G$ has a 1% mismatch, one can see that the plain signal is hard to be recovered from this result. When $G$ has a mismatch smaller than 0.05%, the plain signal can be recovered from the decrypted signal by using a low-passed filter. If $G$ has a mismatch between 0.05–0.1%, the plain signal can also be recovered by using some spectral analysis methods. When mismatch is above 1%, it is hard to recover the plain signal.

## IV. Conclusion

We present here a secure communication system which thwarts various attack schemes presented in the literature. In particular, we use an encryption rule which is very sensitive to the accuracy in the recovered signal. Furthermore, we use state variables other than the transmitted state variables for encryption. Using the current method, the intruder can only recover the encrypted signal with an accuracy which is too low to decrypt the recovered encrypted signal. Furthermore, the intruder also need to reconstruct the key signal which is different from the transmitted signal by using some reconstruction methods which have not been reported so far.

## References

[1] U. Parlitz, R. Zoller, J. Holzfuss, and W. Lauterborn, "Reconstructing physical variables and parameters from dynamical systems," *Int. J. Bifurc. Chaos*, vol. 4, no. 6, pp. 1715–1719, 1994.

[2] K. Short, "Steps toward unmasking secure communications," *Int. J. Bifurc. Chaos*, vol. 4, no. 4, pp. 959–977, 1994.

[3] L. Aguirre and S. Billings, "Retrieving dynamical invariants from chaotic data using NARMAX models," *Int. J. Bifurc. Chaos*, vol. 5, no. 2, pp. 449–474, 1995.

[4] S. Haykin and X. Li, "Detecting of signals in chaos," *Proc. IEEE*, vol. 83, pp. 95–122, Jan. 1995.

[5] J. Stark and B. Arumugam, "Extracting slowly varying signals for a chaotic background," *Int. J. Bifurc. Chaos*, vol. 2, no. 2, pp. 413–419, 1992.

[6] K. Halle, C. W. Wu, M. Itoh, and L. O. Chua, "Spread spectrum communication through modulation of chaos," *Int. J. Bifurc. Chaos*, vol. 3, no. 2, pp. 469–477, 1992.

[7] T. Yang, "Recovery of digital signals from chaotic switching," *Int. J. Circuit Theory Applicat.*, vol. 23, no. 6, pp. 611–615, Nov.–Dec. 1995.

[8] K. Short, "Unmasking a modulated chaotic communications scheme," *Int. J. Bifurc. Chaos*, vol. 6, no. 2, pp. 367–375, 1996.

[9] C. W. Wu, T. Yang, and L. O. Chua, "On adaptive synchronization and control of nonlinear dynamical systems," *Int. J. Bifurc. Chaos*, vol. 6, no. 3, pp. 455–471, 1996.
[10] C. W. Wu and L. O. Chua, "A simple way to synchronize chaotic system with applications to secure communication systems," *Int. J. Bifurc. Chaos*, vol. 3, no. 6, pp. 1619–1627, 1993.
[11] L. O. Chua, "Chua's circuit—An overview ten years later," *J. Circuit, Syst., Comput.*, vol. 4, no. 2, pp. 117–159, Jan. 1994.
[12] D. Stinson, *Cryptography: Theory and Practice*. Boca Raton, FL: CRC Press, 1995.
[13] C. W. Wu and L. O. Chua, "A unified framework for synchronization and control of dynamical systems," *Int. J. Bifurc. Chaos*, vol. 4, no. 4, pp. 979–998, 1994.

1057–7122/97$10.00 © 1997 IEEE

AEU Int. J. Electron. Commun.
51 (1997) No. 3, 131–138
© S. Hirzel Verlag
Stuttgart


# A Family of $n$-Scroll Attractors from a Generalized Chua's Circuit

Johan A. K. Suykens, Anshan Huang, and Leon O. Chua

*Dedicated to Professor Ernst Lüder on the occasion of his 65th birthday*

*Abstract* **Previously, $n$-double scroll attractors have been introduced by Suykens and Vandewalle. A generalized Chua's circuit was considered with additional breakpoints in the nonlinear characteristic. A piecewise-linear implementation and experimental confirmation has been given by Arena et al. In this paper we present a more complete family of $n$-scroll attractors generated from the latter circuit. The new family contains both an even and odd number of scrolls, while the previous work considered only an even number. A Lur'e representation of the generalized Chua's circuit is also given.**

*Keywords* **Chaos, generalized Chua's circuit, $n$-double scroll, piecewise-linear, Lur'e system.**

## 1. Introduction

Chua's circuit is well-known to be a paradigm for chaos [1], being a simple nonlinear electrical circuit that reveals a rich variety of phenomena [2]–[5]. It is the real life existing proof of chaos, as experimentally confirmed first in [6]. After its introduction around 1983, many generalizations have been proposed [5]. From a system theoretical point of view Chua's circuit can be considered as a particular case of a Lur'e system [7]–[10]. Lur'e systems consist of a linear dynamical system, interconnected by feedback to a static nonlinearity that satisfies a sector condition In this sense the generalizations that have been made are twofold. With respect to the linear part, higher dimensional Chua's circuits have been investigated in [10]–[12]. For the nonlinear part a cubic smooth nonlinearity instead of the piecewise linear characteristic has been studied in [1], [13]. Another generalization is related to the introduction of additional breakpoints in the nonlinearity, leading to the $n$-double scroll attractors, first proposed in 1991 by Suykens and Vandewalle [14], [15]. An experimental confirmation of $n$-double scrolls has been given by Arena et al. in 1996 [16], [17]. The latter work follows the ideas of [15] but implements a piecewise linear characteristic.

In this paper a more complete family of $n$-scroll attractors is presented, based on the work of Arena et al. The new family contains attractors with an even as well as an odd number of scrolls. The $n$-double scrolls ($2n$-scroll attractors in the new family) correspond to the even case with Chua's double scroll being a 2-scroll attractor. According to the CNN paradigm [18], [19], Chua's circuits can be taken as cells within a one- or two-dimensional cellular array. Using weak linear coupling between chaotic cells, hyperchaos is obtained in a CNN array. This has been demonstrated in [20] and [21] with the double-double scroll attractor and the $n$-double scroll hypercube CNN, using double scrolls and $n$-double scrolls as cells respectively. Other phenomena that have been obtained from CNNs with Chua's circuits as cells are travelling waves, spiral waves, trigger and target waves and Turing patterns [22]. New phenomena can be expected by taking the generalized Chua's circuit with multiple breakpoints as cells within CNNs. Furthermore Chua's circuit has been used for secure communication applications [23]. For Lur'e systems, master-slave synchronization schemes have been investigated in [24], [25], with illustrations on Chua's circuit, 2-double scroll circuits and coupled cells. A Lur'e representation of the generalized Chua's circuit will be given in this paper, such that the $n$-scroll attractors can be used for such applications.

In Section 2 we present the generalized Chua's circuit and the family of $n$-scroll attractors. In Section 3 we discuss the equilibrium points and Jacobian matrix. Finally, in Section 4 a Lur'e representation of the circuit is given.

## 2. Generalized Chua's Circuit and $n$-Scroll Attractors

Consider the following generalized Chua's circuit

$$\begin{aligned} \dot{x} &= \alpha[y - h(x)], \\ \dot{y} &= x - y + z, \\ \dot{z} &= -\beta y \end{aligned} \tag{1}$$

with piecewise linear characteristic

$$h(x) = m_{2q-1}x + \frac{1}{2}\sum_{i=1}^{2q-1}(m_{i-1} - m_i)(|x + c_i| - |x - c_i|) \tag{2}$$

where $q$ denotes a natural number. This circuit has been implemented by Arena et al. in [16], [17] in order to confirm the $n$-double scroll attractors, introduced by Suykens and Vandewalle in [14], [15]. Taking $q = n$ one obtains the $n$-double scroll attractors for the parameters $\alpha = 9$, $\beta = 14.286$ with the vectors $m = [m_0, m_1, \ldots, m_{2q-1}]$, $c = [c_1, c_2, \ldots, c_{2q-1}]$ chosen as:

- $q = 1$: double scroll (2-scroll) [1]–[5], [26]

$$\begin{aligned} m &= [-1/7, +2/7], \\ c &= 1. \end{aligned} \tag{3}$$

Received December 2, 1996.

Dr. ir. J. A. K. Suykens, Katholieke Universiteit Leuven, Department of Electrical Engineering, ESAT-SISTA, Kardinaal Mercierlaan 94, B-3001 Leuven (Heverlee), Belgium. Email: johan.suykens@esat.kuleuven.ac.be.

Eng. A. Huang, Prof. Dr. L. O. Chua, Department of Electrical Engineering and Computer Science, University of California at Berkeley, Berkeley, CA 94720, USA. Email: anshan, chua@fred.eecs.berkeley.edu.

AEÜ Int. J. Electron. Commun.
51 (1997) No. 3, 131–138

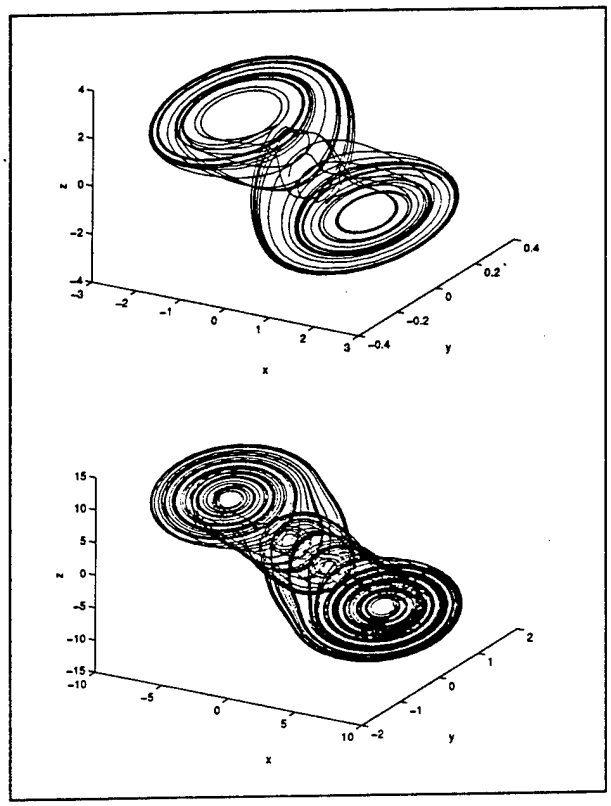

Fig. 1. Three dimensional view on the double scroll (top) and the 2-double scroll (bottom).

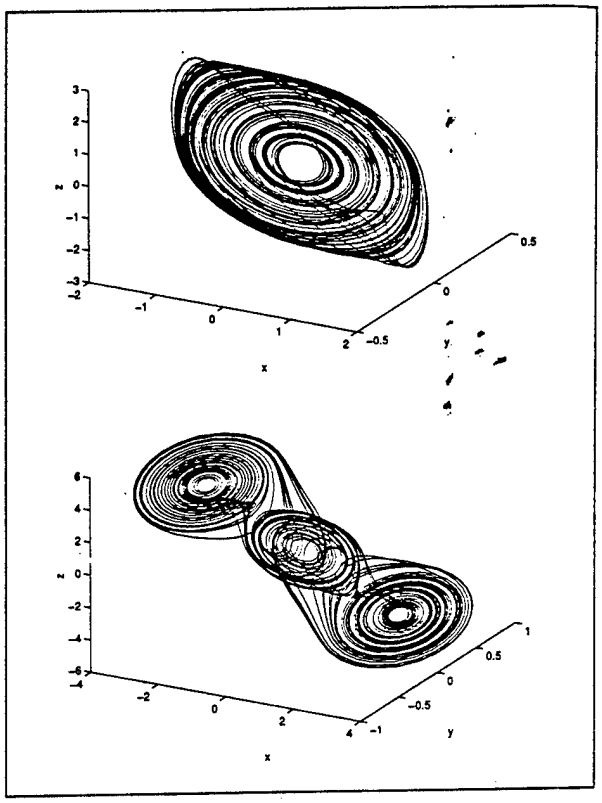

Fig. 2. Three dimensional view on the 1-scroll (top) and the 3-double scroll (bottom).

- $q = 2$: 2-double scroll (4-scroll) [16], [17]

$$m = [-1/7, +2/7, -4/7, +2/7], \quad c = [1, 2.15, 3.6]. \tag{4}$$

- $q = 3$: 3-double scroll (6-scroll) [16], [17]

$$m = [-1/7, +2/7, -4/7, +2/7, -4/7, +2/7], \quad c = [1, 2.15, 3.6, 8.2, 13]. \tag{5}$$

The components of vector $m$ have alternating signs and the sign of $m_0$ is negative in the case of $n$-double scrolls. Here we want to propose a more complete family of $n$-scroll attractors, that contains both an even and odd number of scrolls, with $n$ being a natural number. $n$-scroll attractors with an odd number of scrolls are generated from (1) by taking the same values for the $\alpha, \beta$ parameters but the opposite sign for the vector $m$ in the nonlinearity. For the resulting attractors shown on Figs. 1–6 the following nonlinearities have been taken:

- $q = 1$: 1-scroll

$$m = [+1/7, -2/7], \quad c = 1. \tag{6}$$

- $q = 2$: 3-scroll

$$m = [+0.9/7, -3/7, +3.5/7, -2.4/7], \quad c = [1, 2.15, 4]. \tag{7}$$

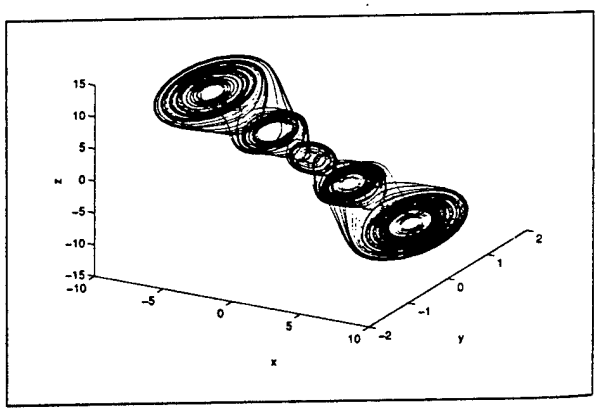

Fig. 3. Three dimensional view of 5-Scroll attractor.

- $q = 3$: 5-scroll

$$m = [+0.9/7, -3/7, +3.5/7, -2.7/7, +4/7, -2.4/7], \quad c = [1, 2.15, 3.6, 6.2, 9]. \tag{8}$$

- $q = 4$: 7-scroll

$$m = [+0.9/7, -3/7, +3.5/7, -2.4/7, +2.52/7, -1.68/7, +2.52/7, -1.68/7], \quad c = [1, 2.15, 3.6, 6.2, 9, 14, 25]. \tag{9}$$

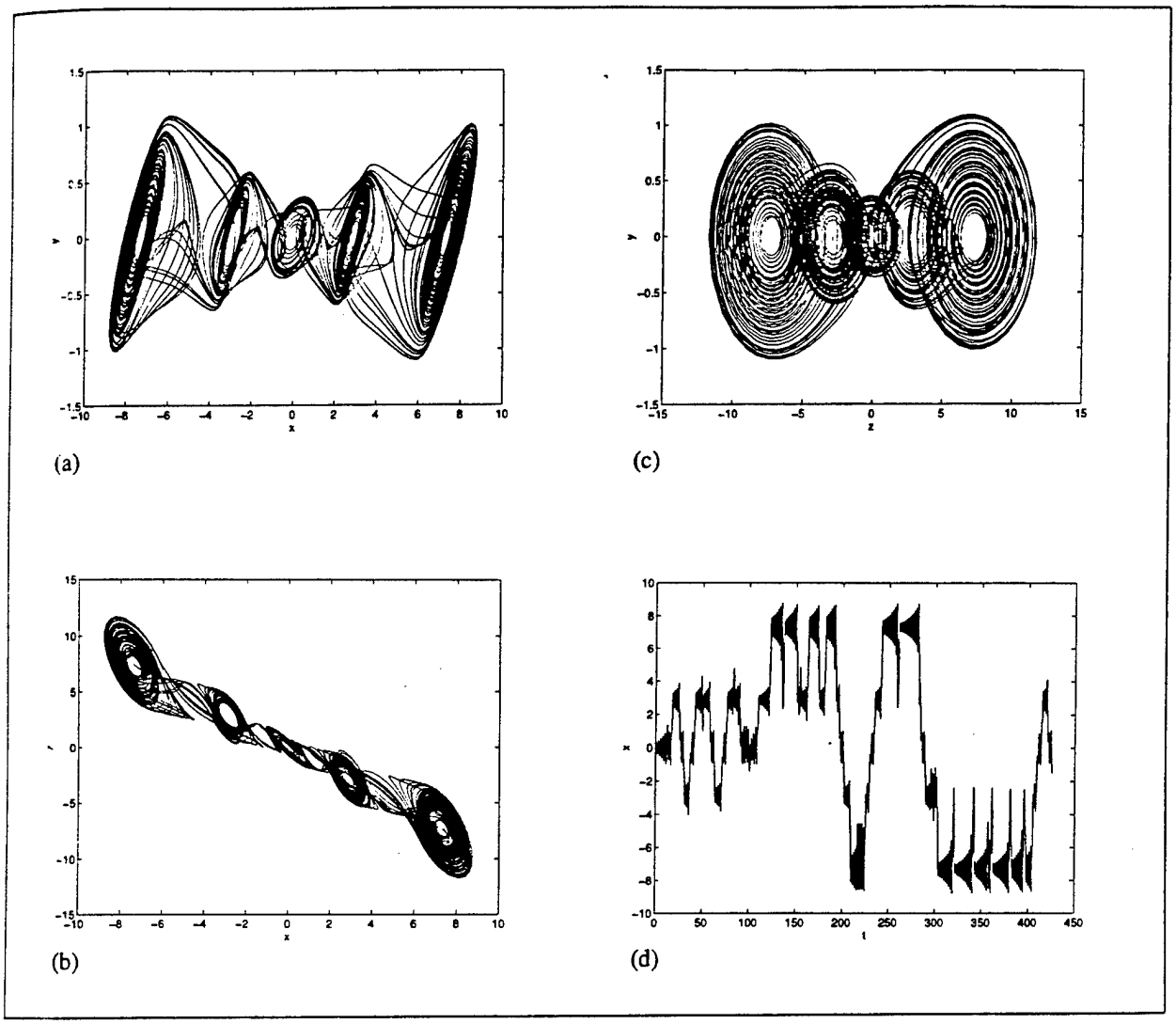


Fig. 4. 5-Scroll attractor shown in Fig. 3: (a) $(x, y)$, (b) $(x, z)$, (c) $(z, y)$, (d) $x(t)$.

Hence for a given value $q$, an even or odd number of scrolls can be obtained from the circuit (1)–(2), depending on the sign of the vector $m$. In the odd case a scroll is generated at the origin. The circuits were simulated by means of a Runge-Kutta integration rule with adaptive step size (ode23 in Matlab) on a Sun-Ultrasparc workstation. The Matlab to C compiler mcc has been used.

## 3. Equilibrium Points and Jacobians

The equilibrium points of the circuit (1)–(2) are given by:

$$\begin{cases} h(x) = 0 \\ x + z = 0 \\ y = 0. \end{cases} \tag{10}$$

Defining $w_{2q} = \alpha m_{2q-1}$ and $w_i = \alpha(m_{i-1} - m_i)$, $i = 1, 2, \ldots, 2q-1$ the condition $h(x) = 0$ corresponds to

$$w_{2q}x + \varphi(x) = 0 \tag{11}$$

where $\varphi(x) = (1/2)\sum_{i=1}^{2q-1} w_i(|x + c_i| - |x - c_i|)$. The nonlinearities and the corresponding equilibrium points for the circuit are shown on Figs. 7–8 for the case of an even and odd number of scrolls. The nonlinearity $\varphi(x)$ has $4q-2$ breakpoints, which yields $4q-1$ equilibrium points in the circuit. The origin is an equilibrium point. The other equilibrium points appear in pairs, which we denote here as $eq_j^{\pm} = [x_{eq_j^{\pm}}, 0, -x_{eq_j^{\pm}}]$, for $j = 1, 2, \ldots, 2q-1$ (the index $j$ orders the points in terms of increasing $x$ coordinates). In Table 1 an overview is given on the relation between the value of $q$, the number of scrolls, the number of breakpoints in the nonlinearity and the number of equilibrium points.

AEÜ Int. J. Electron. Commun.
51 (1997) No. 3, 131–138

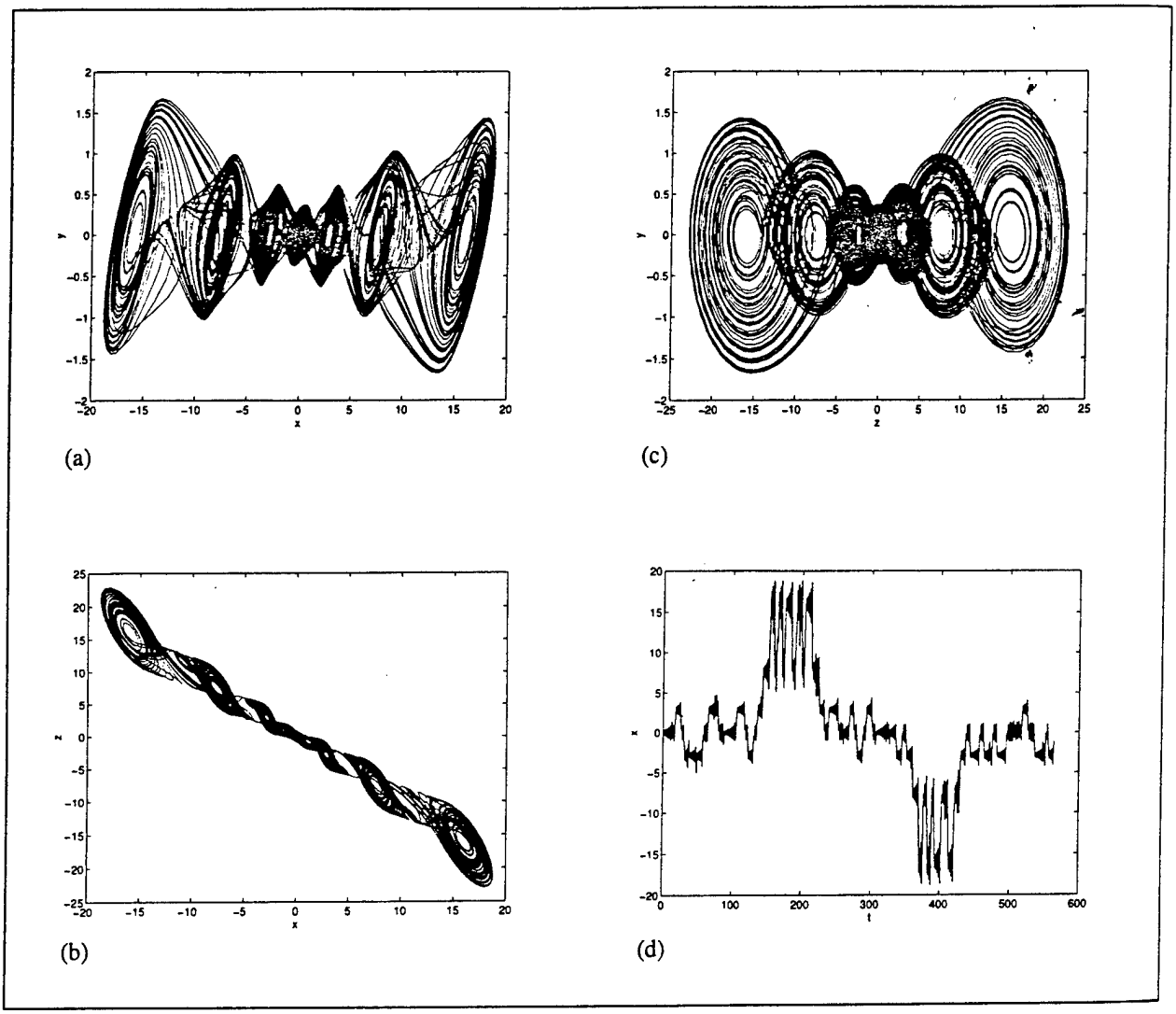


Fig. 5. 7-Scroll attractor shown in Fig. 6: (a) $(x, y)$, (b) $(x, z)$, (c) $(z, y)$, (d) $x(t)$.

Table 1. Overview of the relationship between the value of $q$ in the generalized Chua's circuit, the number of hidden units $n_h$ in the Lur'e representation, the number of scrolls for the even and odd case, the number of equilibrium points of the circuit and the number of breakpoints in the nonlinear characteristic. The even or odd case is determined by the sign of the vector $m$ in the nonlinearity.

| $q$ | $n_h$ | $n$ = # scrolls | | # eq. points | # breakpoints |
|---|---|---|---|---|---|
| | | even | odd | | |
| 1 | 1 | 2 | 1 | 3 | 2 |
| 2 | 3 | 4 | 3 | 7 | 6 |
| 3 | 5 | 6 | 5 | 11 | 10 |
| 4 | 7 | 8 | 7 | 15 | 14 |
| ⋮ | ⋮ | ⋮ | ⋮ | ⋮ | ⋮ |
| $q$ | $2q-1$ | $2q$ | $2q-1$ | $4q-1$ | $4q-2$ |

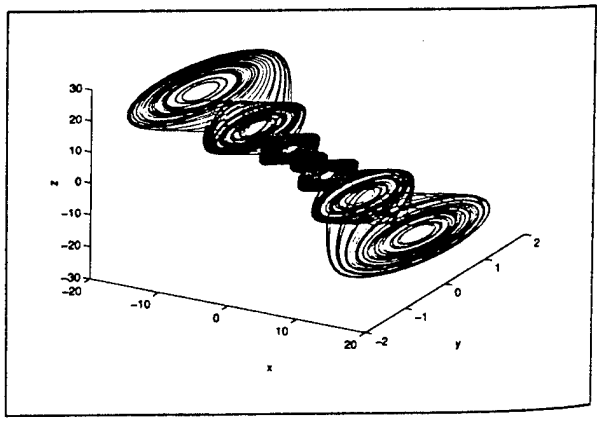

Fig. 6. Three dimensional view of 7-Scroll attractor.

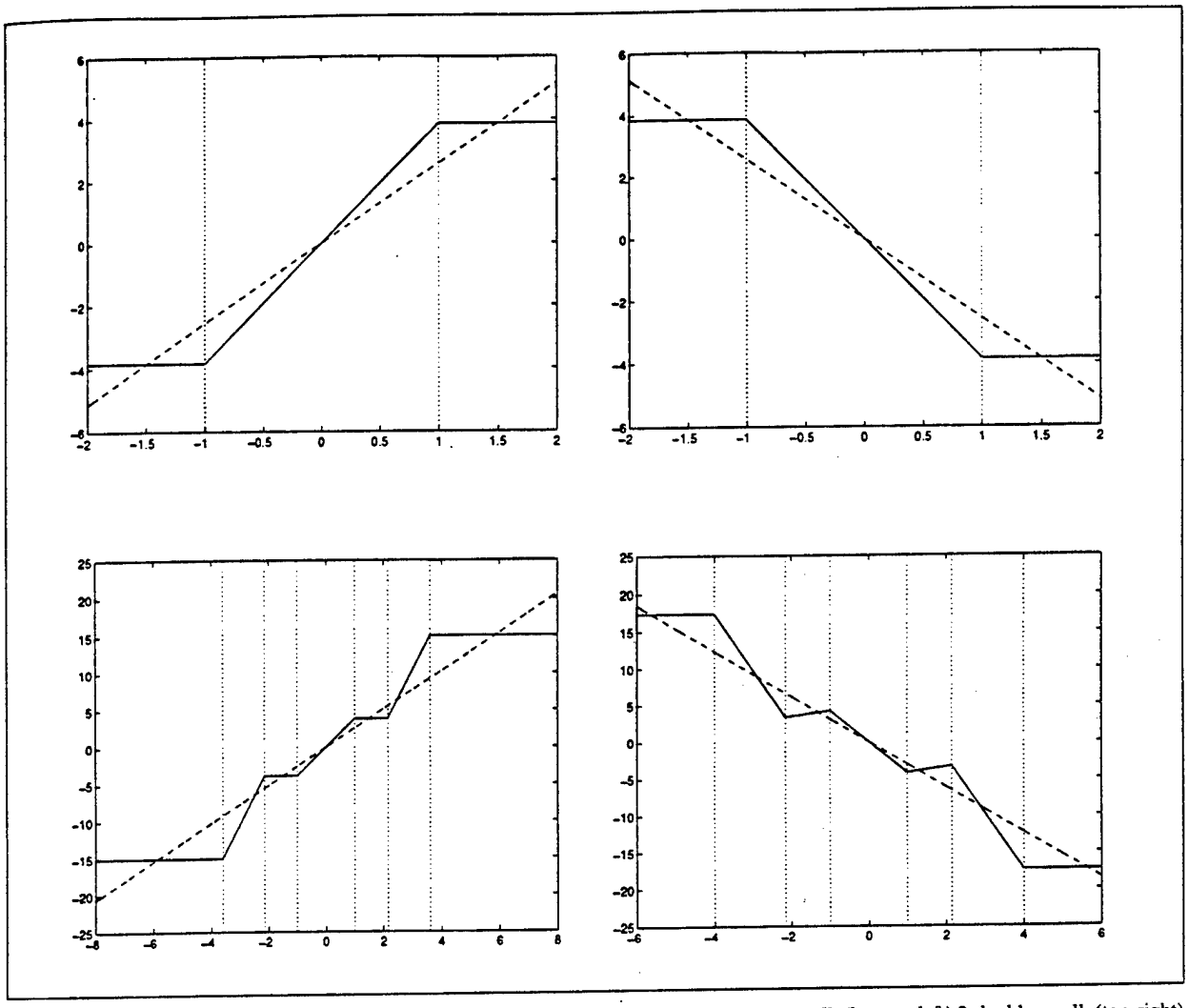

Fig. 7. Nonlinearities for the generalized Chua's circuit. (top-left) double scroll, (top-right) 1-scroll, (bottom-left) 2-double scroll, (top-right) 3-scroll. The equilibrium points of the circuits are located at the intersection between the curves in full lines ($-\varphi(x)$) and dashed lines ($w_{2q}x$). The dotted lines locate the breakpoints.

The Jacobian matrix of the circuit is given by

$$J(x) = \begin{bmatrix} -w_{2q} & \alpha & 0 \\ 1 & -1 & 1 \\ 0 & -\beta & 0 \end{bmatrix} + \sum_{i=1}^{2q-1} M_i \qquad (1)$$

where

$$M_i = \begin{cases} \begin{bmatrix} -w_i & 0 & 0 \\ 0 & 0 & 0 \\ 0 & 0 & 0 \end{bmatrix}, & -c_i < x < c_i \\ 0, & x < -c_i \text{ or } c_i < x. \end{cases}$$

Evaluated at the equilibrium points this becomes

$$J(0) = \begin{bmatrix} -\sum_{i=1}^{2q} w_i & \alpha & 0 \\ 1 & -1 & 1 \\ 0 & -\beta & 0 \end{bmatrix},$$

$$J(eq_j^{\pm}) = \begin{bmatrix} -\sum_{i=j+1}^{2q} w_i & \alpha & 0 \\ 1 & -1 & 1 \\ 0 & -\beta & 0 \end{bmatrix} \qquad (2)$$

for $j = 1, \ldots, 2q-1$. Denoting the element $J_{11}$ of the Jacobian matrices as $k$, the eigenvalue configurations of $J$ with respect to the parameter $k$ are shown on Fig. 9.

For $\alpha = 9, \beta = 14.286$ four regions can be defined with $k_1 = -7.2740, k_2 = -0.7267, k_3 = 0$ (see Fig. 9). For the design of $n$-scroll attractors, the vectors $m$ and $c$ are chosen such that the eigenvalue configurations belong to regions II-IV, i.e. $k_1 < k < k_2$ and $k_3 < k$, respectively. The nonlinearities (3)–(9) lead to the following eigenvalue configurations of the Jacobians, evaluated at the equilibrium points:

1. **Even case**:
   - $q = 1$: double scroll
     II - [IV] - II

AEÜ Int. J. Electron. Commun. 51 (1997) No. 3, 131–138

- $q = 2$: 2-double scroll
  II - IV - II - [IV] - II - IV - II
- $q = 3$: 3-double scroll
  II - IV - II - IV - II - [IV] - II - IV - II - IV - II

2. **Odd case:**
- $q = 1$: 1-scroll
  IV - [II] - IV
- $q = 2$: 3-scroll
  IV - II - IV - [II] - IV - II - IV
- $q = 3$: 5-scroll
  IV - II - IV - II - IV - [II] - IV - II - IV - II - IV
- $q = 4$: 7-scroll
  IV - II - IV - II - IV - II - IV - [II] - IV - II - IV - II - IV - II - IV

These structures for the eigenvalue configurations are a necessary condition in order to obtain $n$-scroll attractors, but are not sufficient due to the local stability analysis. Assuming an $n$-scroll attractor has been obtained for a certain value of $n$, a constructive but very qualitative approach to obtain an $(n+2)$-scroll attractor, is to create the possibility for having two additional scrolls by taking into account the structure of the eigenvalue configurations and modifying that part of the nonlinearity which is responsible for generating the outer scrolls, such that a transition can be made to the additional scrolls. In this way the vectors $m$ and $c$ have been determined in (3)–(9).

## 4. Lur'e Representation

In this section we give a Lur'e representation of the generalized Chua's circuit. Lur'e systems [7], [8] are of the form

$$\begin{aligned} \dot{\xi} &= A\xi + Bu, \\ y &= C\xi, \\ u &= \sigma(y) \end{aligned} \tag{3}$$

with $\xi \in \mathbb{R}^p$, $u, y \in \mathbb{R}^{n_h}$, $\sigma(\cdot) : \mathbb{R}^{n_h} \mapsto \mathbb{R}^{n_h}$ a diagonal nonlinearity belonging to sector $[0, K]$ and $A \in \mathbb{R}^{p \times p}$, $B \in \mathbb{R}^{p \times n_h}$, $C \in \mathbb{R}^{n_h \times p}$. Lur'e systems might be interpreted also as a class of recurrent neural networks of the form

$$\dot{\xi} = A\xi + B\sigma(C\xi) \tag{4}$$

with interconnection matrices $A, B, C$, having one hidden layer with a number of $n_h$ hidden neurons and zero bias terms [27].

The Lur'e representation for (1)–(2) is given by

$$\begin{aligned} A &= \begin{bmatrix} -\alpha w_{2q} & \alpha & 0 \\ 1 & -1 & 1 \\ 0 & -\beta & 0 \end{bmatrix}, \\ B &= \begin{bmatrix} -\alpha w_1 & -\alpha w_2 & \dots & -\alpha w_{2q-1} \\ 0 & 0 & \dots & 0 \\ 0 & 0 & \dots & 0 \end{bmatrix}, \\ C &= \begin{bmatrix} 1 & 0 & 0 \\ 1 & 0 & 0 \\ \vdots & \vdots & \vdots \\ 1 & 0 & 0 \end{bmatrix}. \end{aligned} \tag{5}$$

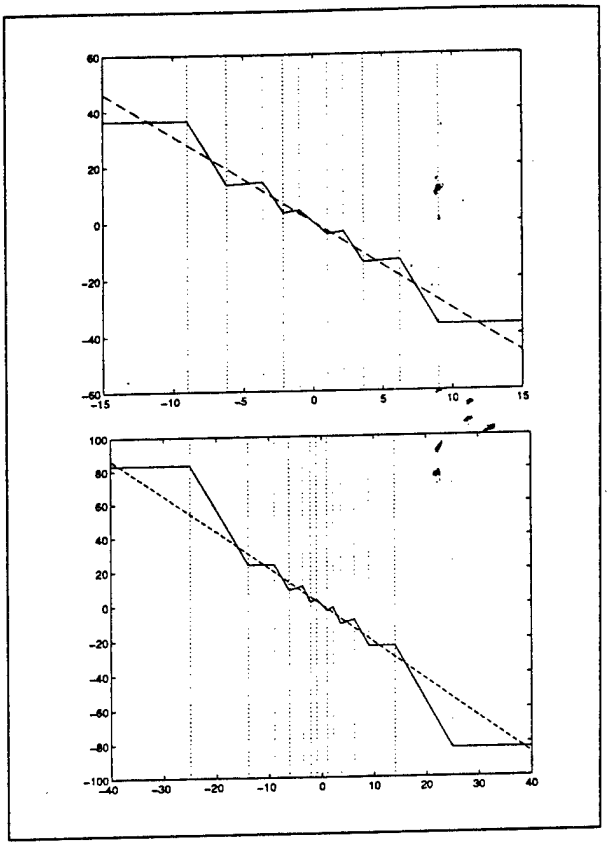

Fig. 8. Nonlinearity of the generalized Chua's circuit for the case of 5-scroll (top) and 7-scroll (bottom).

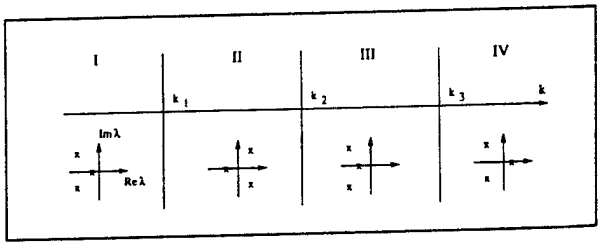


Fig. 9. Eigenvalue configurations of the Jacobian matrix, with respect to parameter $k$. In order to obtain $n$-scrolls, the nonlinearities are designed such that the eigenvalue configurations of the Jacobians, evaluated at the equilibrium points, belong alternating to the regions II and IV.

The vector valued nonlinearity $\sigma = [\sigma_1, \sigma_2, \dots, \sigma_{n_h}]$ with $n_h = 2q - 1$ consists of components $\sigma_i(x, c_i) = (1/2)(|x + c_i| - |x - c_i|)$, for $i = 1, 2, \dots, n_h$. Hence $\sigma(\cdot)$ belongs to sector $[0, 1]$. This representation is illustrated on Fig. 10 for a 3-scroll attractor.

## 5. Conclusion

In this paper we introduced a family of $n$-scroll attractors, which contains attractors both with an even and odd number of scrolls. The even case corresponds to $n$-double

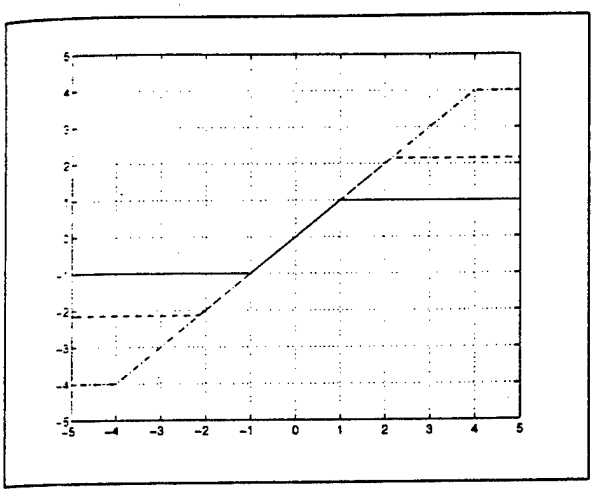

Fig. 10. Lur'e representation of the generalized Chua's circuit. The nonlinearities $\sigma_1(x, c_1)$ (——), $\sigma_2(x, c_2)$ (– – –), $\sigma_3(x, c_3)$ (—·— ), that belong to sector $[0, 1]$, are shown for a 3-scroll attractor.

scrolls. The $n$-scroll attractors are obtained from a generalized Chua's circuit, having a piecewise linear nonlinear characteristic with multiple breakpoints. The work is related to the implementation made by Arena et al. for $n$-double scrolls. The generalized Chua's circuit can be used as a new type of cell within cellular neural networks, in order to obtain and model new kinds of phenomena. Furthermore a Lur'e representation has been given, such that $n$-scrolls can be used for synchronization applications.

## Acknowledgement

This research work was carried out at the University of California at Berkeley, in the framework of the Belgian Programme on Interuniversity Poles of Attraction, initiated by the Belgian State, Prime Minister's Office for Science, Technology and Culture (IUAP-17) and in the framework of a Concerted Action Project MIPS (Modelbased Information Processing Systems) of the Flemish Community. The work is supported in part by the Office of Naval Research under grant N00014-96-1-0753.

## References

[1] Madan, R. N.: Chua's circuit: A paradigm for chaos. Singapore: World Scientific Publ., 1993.

[2] Chua, L. O.; Komuro, M.; Matsumoto, T.: The double scroll family. IEEE Trans. Circ. a. Syst. Pt. I CAS–33 (1986), 1072–1118.

[3] Chua, L. O.: Global unfolding of Chua's circuit. IEICE Trans. Fundamentals E76-A (1993), 704–734.

[4] Chua, L. O.; Wu, C. W.; Huang, A.; Zhong, G.-Q.: A universal circuit for studying and generating chaos, Part I: Routes to chaos, Part II: Strange attractors. IEEE Trans. Circ. a. Syst. Pt. I CAS– 40 (1993), 732–744, 745–761.

[5] Chua, L. O.: Chua's circuit: An overview ten years later. J. Circ., Syst., a. Comput. 4 (1994), 117–159.

[6] Zhong, G.-Q.; Ayrom, F.: Experimental confirmation of chaos from Chua's circuit. Int. J. Circ. Theory a. Appl. 13 (1985), 93–98.

[7] Khalil, H. K.: Nonlinear systems. New York: Macmillan, 1992.

[8] Vidyasagar, M.: Nonlinear systems analysis. Englewood Cliffs: Prentice-Hall, 1993.

[9] Guzelis, C.; Chua, L. O.: Stability analysis of generalized cellular neural networks. Int. J. Circ. Theory a. Appl. 21 (1993), 1–33.

[10] Wu, C. W.; Chua, L. O.: On the generality of the unfolded Chua's circuit. Int. J. Bifurc. a. Chaos 6 (1996), 801–832.

[11] Götz, M.; Feldmann, U.; Schwarz, W.: Synthesis of higher-dimensional Chua circuits. IEEE Trans. Circ. a. Syst. Pt. I CAS– 40 (1993), 854–860.

[12] Kocarev, L.; Karadzinov, L.; Chua, L. O.: $n$-dimensional canonical Chua's circuit. J. Circ., Syst., a. Comput. 3 (1993), 239–258.

[13] Huang, A.; Pivka, L.; Wu, C.-W.; Franz, M.: Chua's equation with cubic nonlinearity. Int. J. Bifurc. a. Chaos 6 (1996).

[14] Suykens, J. A. K.; Vandewalle, J.: Quasilinear approach to nonlinear systems and the design of $n$-double scroll ($n = 1, 2, 3, 4, \ldots$). IEE Proc. Pt. G 138 (1991), 595–603.

[15] Suykens, J. A. K.; Vandewalle, J.: Generation of $n$-double scrolls ($n = 1, 2, 3, 4, \ldots$). IEEE Trans. Circ. a. Syst. Pt. I CAS– 40 (1993), 861–867.

[16] Arena, P.; Baglio, S.; Fortuna, L.; Manganaro, G.: Generation of $n$-double scrolls via cellular neural networks. Int. J. Circ. Theory a. Appl. 24 (1996), 241–252.

[17] Arena, P.; Baglio, S.; Fortuna, L.; Manganaro, G.: State controlled CNN: A new strategy for generating high complex dynamics. IEICE Trans. Fundamentals E79-A (1996), 1647–1657.

[18] Chua, L. O.; Roska, T.: The CNN paradigm. IEEE Trans. Circ. a. Syst. Pt. I CAS– 40 (1993), 147–156.

[19] Chua, L. O.; Hasler, M.; Moschytz, G. S.; Neirynck, J.: Autonomous cellular neural networks: A unified paradigm for pattern formation and active wave propagation. IEEE Trans. Circ. a. Syst. Pt. I CAS– 42 (1995), 559–577.

[20] Kapitaniak, T.; Chua, L. O.: Hyperchaotic attractors of unidirectionally-coupled Chua's circuits. Int. J. Bifurc. a. Chaos 4 (1994), 477–482.

[21] Suykens, J. A. K.; Chua, L. O.: $n$-double scroll hypercubes in 1D-CNNs. Int. J. Bifurc. a. Chaos (1997). to appear.

[22] Muñuzuri, A. P.; Pérez-Muñuzuri, V.; Gómez-Gesteira, M.; Chua, L. O.; Pérez-Villar, V.: Spatiotemporal structures in discretely-coupled arrays of nonlinear circuits: A review. Int. J. Bifurc. a. Chaos 5 (1995), 17–50.

[23] Wu, C. W.; Chua, L. O.: A unified framework for synchronization and control of dynamical systems. Int. J. Bifurc. a. Chaos 4 (1994), 979–989.

[24] Suykens, J. A. K.; Vandewalle, J.; Chua, L. O.: Nonlinear $H_\infty$ synchronization of chaotic Lur'e systems. Int. J. Bifurc. a. Chaos (1997). to appear.

[25] Suykens, J. A. K.; Curran, P. F.; Chua, L. O.: Master-slave synchronization using dynamic output feedback. Int. J. Bifurc. a. Chaos 7 (1997).

[26] Chua, L. O.: The genesis of Chua's circuit. AEÜ 46 (1992), 250–257.

[27] Suykens, J. A. K.; Vandewalle, J. P. L.; De Moor, B. L. R.: Artificial neural networks for modelling and control of nonlinear systems. Boston: Kluwer Academic Publ., 1996.

AEÜ Int. J. Electron. Commun. 51 (1997) No. 3, 131–138

**Johan A. K. Suykens** was born in Willebroek Belgium, May 18, 1966. He obtained the degree in Electro-Mechanical Engineering in 1989 and the doctoral degree in Applied Sciences in 1995, both at the Katholieke Universiteit Leuven Belgium. He is currently a postdoctoral researcher at the ESAT-SISTA group of the K.U. Leuven. His research interests are mainly in nonlinear systems and neural networks, theory and applications. He is author of the book "Artificial Neural Networks for Modelling and Control of Non-Linear Systems", published by Kluwer Academic Publishers. He has been a visiting postdoctoral researcher at the University of California at Berkeley in 1996.

**Anshan Huang** was born in Jian Su province, People's Republic of China in 1941. He graduated from Harbin Polytechnic Institute, Harbin, in 1966. From 1970 to 1980 he was with the Shanghai Aircraft Research Institute (SARI). During 1980–1989 he was with the Shanghai Institute of Mechanical Engineering. From 1989–1992 he was with the SARI as a senior engineer. From May 18, 1992, he was with the Nonlinear Electronics Laboratory, University of California, Berkeley, as a visiting scholar. His research interests include linear and nonlinear circuit theory, especially chaotic circuits.

**Leon O. Chua** is currently a professor of electrical engineering and computer sciences at the University of California, Berkeley. He is the holder of six U.S. patents. He is also the recipient of several awards and prizes, including the 1967 IEEE Browder J. Thompson Memorial Prize Award, the 1973 IEEE W.R.G. Baker Prize Award, the 1974 Frederick Emmons Terman Award, the 1976 Miller Research Professorship, the 1982 Senior Visiting Fellowship at Cambridge University, the 1982/83 Alexander von Humboldt Senior U.S. Scientist Award at the Technical University of Munich, the 1983/84 Visiting U.S. Scientist Award at Waseda University, Tokyo, the IEEE Centennial Medal in 1985, the 1985 Myril B. Reed Best Paper Prize, the 1986 and 1989 IEEE Guillemin-Cauer Prizes and the 1995 M.E. Van Valkenburg Award. In 1986 he was awarded a *Professeur invité* International Award at the University of Paris-Sud from the French Ministry of Education. He was also awarded a *Doctor Honoris Causa* from the Ecole Polytechnique Fédérale, Lausanne, Switzerland, in 1983, an Honoray Doctorate from the University of Tokushima, Japan, in 1984, an Honorary Doctorate from the Technische Universität Dresden in 1992, a *Doctor Honoris Causa* from the Technical University of Budapest, Hungary, in 1994, a *Doctor Honoris Causa* from the University of Santiago de Compostela, Spain, in 1995, and a *Doctor Honoris Causa* from the University of Frankfurt, Germany, in 1996.

## Book-Reviews

**August W. Rihaczek, Stephen J. Hershkowitz: Radar Resolution and Complex Image Analysis**. ARTECH HOUSE, Boston/London, 1996, 524 pages, 404 Figures, 23 cm × 16 cm, bound, price $ 78, ISBN 0-89006-868-2.

Image processing and interpretation is nowadays a very important discipline for feature extraction, target classification and identification, with a lot a civilian and military applications. With the advent of modern SAR (synthetic aperture radar) a new generation of images which differs considerably from optical images requires new techniques and algorithms. Radar images are different from optical images in that 1. radar images are complex (although so far most of the image processing techniques are based on amplitude only); 2. radar has the potential of 3D interferometric images; 3. the geometry is different; 4. radar can produce polarimetric images; 5. the reflectivity for microwaves is different from optical waves. All these aspects have to be taken into account when doing radar image interpretation.

In addition to the third edition of the classical work "Principles of High-Resolution Radar" which appered recently here is a new book by A. W. Rihaczek and his co-worker, Stephen J. Hershkowitz. This book is mainly concerned with the analysis of *complex* images , with particular emphasis on the classification and identification of man-made targets. By "complex" the evaluation of amplitude and phase of backscattered echoes is meant, not the "complexity" of target structures (which however, plays an important role as well).

Well-known high resolution methods are usually based on a certain mathematical target model. For instance, the classical resolution theory based on Doppler and range, is based on the assumption of point targets. Such model is used for comparison with the actual measured data by correlation techniques. Superresolution techniques like the maximum entropy method (MEM) are also based on target models (in case of MEM an autoregressive signal model is assumed). The problem with man-made targets is that because of the complexity of their structure it is almost impossible to find a signal model which is characteristic of the target, however simple enough to be useful for practical applications. Solving the wave equation for such complicated boundary conditions like a man-made target is impossible because of the complexity of the problem.

The techniques used by the authors is briefly described as follows. First some image cuts are taken along straight lines through responses of interest, obtaining the amplitude and phase functions along each cut. By looking for amplitude maxima, minima, bulges, phase inflection points, and other changes of the phase a transform interval is defined that includes the response of interest and excludes interference. Taking the FFT over the interval amplitude and phase functions are obtained which is much easier to interpret than the original amplitude and phase history along the cut. This process has been automated to a certain point, however, as the authors state, improvement is always possible.

Since the techniques used in this book are not based on mathematical models the reader will not find many mathematical formulas, but, instead, a large number of figures. Most of these figures are amplitude/phase twin plots and so-called peak plots which contain strong amplitude values in the form of black spots. In the accompanying text the plots are interpreted extensively.

Chapter 1 is entitled "Modern Approaches to Modern Radar Problems". The history of radar resolution is briefly described.

(continued on page 177)

International Journal of Bifurcation and Chaos, Vol. 7, No. 3 (1997) 645–664
© World Scientific Publishing Company

# IMPULSIVE CONTROL AND SYNCHRONIZATION OF NONLINEAR DYNAMICAL SYSTEMS AND APPLICATION TO SECURE COMMUNICATION

TAO YANG and LEON O. CHUA
*Electronics Research Laboratory and*
*Department of Electrical Engineering and Computer Sciences,*
*University of California at Berkeley,*
*Berkeley, CA 94720, U.S.A.*

Received January 15, 1997; Revised February 10, 1997

Impulsive control is a newly developed control theory which is based on the theory of impulsive differential equations. In this paper, we stabilize nonlinear dynamical systems using impulsive control. Based on the theory of impulsive differential equations, we present several theorems on the stability of impulsive control systems. An estimation of the upper bound of the impulse interval is given for the purpose of asymptotically controlling the nonlinear dynamical system to the origin by using impulsive control laws. In this paper, impulsive synchronization of two nonlinear dynamical systems is reformulated as impulsive control of the synchronization error system. We then present a theorem on the asymptotic synchronization of two nonlinear systems by using synchronization impulses. The robustness of impulsive synchronization to additive channel noise and parameter mismatch is also studied. We conclude that impulsive synchronization is more robust than continuous synchronization. Combining both conventional cryptographic method and impulsive synchronization of chaotic systems, we propose a new chaotic communication scheme. Computer simulation results based on Chua's oscillators are given.

## 1. Introduction

Impulsive differential equations [Samoilenko & Perestyuk, 1995] describe evolution processes which at certain moments change their state by jumps. Processes of such character can be found in many fields, such as: physics, mechanics, population dynamics, chemical technology, economics, biology and electrical engineering.

Since the seminal paper of Ott, Grebogi and Yorke (OGY) [1990], several methods for control and stabilization of chaotic motions have recently been presented [Chen & Dong, 1993; Chua *et al.*, 1996; Wu *et al.*; 1996, Stojanovski *et al.*; 1996]. In view of the rich dynamics of chaotic systems, there exists a large variety of approaches for controlling such systems. Some of these approaches include adaptive control [Chua *et al.*, 1996; Wu *et al.*, 1996], error-feedback control [Pyragas, 1992], time-delay feedback control [Pyragas, 1992], OGY method [Ott *et al.*, 1990], predictive Poincaré control [Schweizer & Kennedy, 1995] occasional proportional feedback control [Hunt & Johnson, 1993] and impulsive control [Stojanovski *et al.*, 1996].

In fact, the predictive Poincaré control and the occasional proportional feedback control are two impulsive control schemes with varying impulse intervals. Impulsive control is attractive because it allows the stabilization of a chaotic system using only small control impulses, and it offers a direct method for modulating digital information onto a chaotic carrier signal for spread spectrum

applications. However, due to a lack of effective tools for analyzing impulsive differential equations [Lakshmikantham *et al.*, 1989], most impulse control schemes had been designed mainly by trial-and-error. The study of the stability of an impulsive differential equation is much more difficult than that of its "corresponding" differential equation [Samoilenko & Perestyuk, 1995]. For example, consider the impulsive system

$$\begin{cases} \dot{\mathbf{x}} = A\mathbf{x}, & t \neq \tau_i, \\ \Delta\mathbf{x}|_{t=\tau_i} = B\mathbf{x} \end{cases} \tag{1}$$

where $A$ and $B$ are two constant matrices, and $\Delta\mathbf{x}|_{t=\tau_i} \triangleq \mathbf{x}(\tau_i^+) - \mathbf{x}(\tau_i^-)$, $\mathbf{x}(\tau_i^-)$ and $\mathbf{x}(\tau_i^+)$ being the left and right limit of $\mathbf{x}(t)$ at $t = \tau_i$. The solution of the above system is given by

$$\mathbf{x}(t, \mathbf{x}_0) = \mathbf{X}(t, \mathbf{x}_0)\mathbf{x}_0 \tag{2}$$

where

$$\mathbf{X}(t, \mathbf{x}_0) = e^{A(t-\tau_i)} \prod_{t_0 < \tau_j < t} (I + B)e^{A(\tau_j - \tau_{j-1})}, \quad \tau_0 = t_0, \quad \tau_i < t \leq \tau_{i+1} \tag{3}$$

As can be seen from this formula, it is not possible in the general case to give necessary and sufficient conditions for stability of solutions of the above system in terms of the eigenvalues of the matrix of this system, which is possible for systems of ordinary differential equations with constant coefficients.

In this paper, we investigate the stability of impulsively controlled chaotic systems. First, the stability of the trivial solution of a kind of impulsive differential equation is studied. Then the theoretical results are used to study the conditions under which an impulsive control of Chua's oscillator is asymptotically stable. An estimate of the upper bound of the impulsive interval is also presented.

Then, an impulsive control theory is used to study the impulsive synchronization of two chaotic systems. We first show that the impulsive synchronization problem is an impulsive control problem. Then a theorem is given for guaranteeing the asymptotic stability of impulsive synchronization. Since only the synchronization impulses are sent to the driven system in an impulsive synchronization scheme, the information redundancy in the transmitted signal is reduced. In this sense, even low-dimensional chaotic systems can provide high security. In this paper, we will use impulsive synchronization to develop a new framework for chaotic secure communication.

The organization of this paper is as follows. In Sec. 2, a theory on the stability of impulsive differential equations is given. In Sec. 3, a stability criterion for impulsive control of Chua's oscillator is presented. In Sec. 4, simulation results on the impulsive control of Chua's oscillator are provided. In Sec. 5, the theory and simulation results of impulsive synchronization of Chua's oscillators are presented. In Sec. 6, application of impulsive synchronization to secure communication is presented. In Sec. 7, some concluding remarks are given.

## 2. Basic Theory of Impulsive Differential Equations

Consider the general nonlinear system

$$\dot{\mathbf{x}} = \mathbf{f}(t, \mathbf{x}) \tag{4}$$

where $\mathbf{f} : \mathbf{R}_+ \times \mathbf{R}^n \mapsto \mathbf{R}^n$ is continuous, $\mathbf{x} \in \mathbf{R}^n$ is the state variable, and

$$\dot{\mathbf{x}} \triangleq \frac{d\mathbf{x}}{dt}.$$

Consider a discrete set $\{\tau_i\}$ of time instants, where

$$0 < \tau_1 < \tau_2 < \cdots < \tau_i < \tau_{i+1} < \cdots,$$
$$\tau_i \to \infty \quad \text{as} \quad i \to \infty$$

Let

$$U(i, \mathbf{x}) = \Delta\mathbf{x}|_{t=\tau_i} \triangleq \mathbf{x}(\tau_i^+) - \mathbf{x}(\tau_i^-) \tag{5}$$

be the "jump" in the state variable at the time instant $\tau_i$. Then this impulsive system is described by

$$\begin{cases} \dot{\mathbf{x}} = \mathbf{f}(t, \mathbf{x}), & t \neq \tau_i \\ \Delta\mathbf{x} = U(i, \mathbf{x}), & t = \tau_i \\ \mathbf{x}(t_0^+) = \mathbf{x}_0, t_0 \geq 0, i = 1, 2, \ldots \end{cases} \tag{6}$$

This is called an impulsive differential equation [Lakshmikantham *et al.*, 1989]. To study the stability of the impulsive differential Eq. (6) we use the following definitions and theorems [Lakshmikantham *et al.*, 1989].

**Definition 1.** Let $V : \mathbf{R}_+ \times \mathbf{R}^n \mapsto \mathbf{R}_+$, then $V$ is said to belong to class $\mathcal{V}_0$ if

1. $V$ is continuous in $(\tau_{i-1}, \tau_i] \times \mathbf{R}^n$ and for each $\mathbf{x} \in \mathbf{R}^n$, $i = 1, 2, \ldots$,

$$\lim_{(t,\mathbf{y})\to(\tau_i^+,\mathbf{x})} V(t, \mathbf{y}) = V(\tau_i^+, \mathbf{x}) \tag{7}$$

exists;

2. $V$ is locally Lipschitzian in $\mathbf{x}$

**Definition 2.** For $(t, \mathbf{x}) \in (\tau_{i-1}, \tau_i] \times \mathbf{R}^n$, we define

$$D^+V(t, \mathbf{x}) \triangleq \lim_{h\to 0} \sup \frac{1}{h}[V(t+h, \mathbf{x} + hf(t, \mathbf{x})) - V(t, \mathbf{x})] \tag{8}$$

**Definition 3.** Comparison system. Let $V \in \mathcal{V}_0$ and assume that

$$\begin{cases} D^+V(t, \mathbf{x}) \le g(t, V(t, \mathbf{x})), & t \ne \tau_i \\ V(t, \mathbf{x} + U(i, \mathbf{x})) \le \psi_i(V(t, \mathbf{x})), & t = \tau_i \end{cases} \tag{9}$$

where $g : \mathbf{R}_+ \times \mathbf{R}_+ \mapsto \mathbf{R}$ is continuous and $\psi_i : \mathbf{R}_+ \mapsto \mathbf{R}_+$ is nondecreasing. Then the system

$$\begin{cases} \dot{w} = g(t, w), & t \ne \tau_i \\ w(\tau_i^+) = \psi_i(w(\tau_i)) \\ w(t_0^+) = w_0 \ge 0 \end{cases} \tag{10}$$

is called the comparison system of Eq. (6).

**Definition 4**

$$S_\rho = \{\mathbf{x} \in \mathbf{R}^n | \ ||\mathbf{x}|| < \rho\} \tag{11}$$

where $\|\cdot\|$ denotes the Euclidean norm on $\mathbf{R}^n$.

**Definition 5.** A function $\alpha$ is said to belong to class $\mathcal{K}$ if $\alpha \in C[R_+, R_+], \alpha(0) = 0$ and $\alpha(x)$ is strictly increasing in $x$.

**Assumptions.** $f(t, 0) = 0, U(i, 0) = 0$ and $g(t, 0) = 0$ for all $i$.

*Remark.* With the above assumptions we find that the trivial solutions of Eqs. (6) and (10) are identical for all times except at the discrete set $\{\tau_i\}$.

**Theorem 1** (Theorem 3.2.1, p. 139 [Lakshmikantham *et al.*, 1989]). *Assume that the following three conditions are satisfied:*

1. $V : \mathbf{R}_+ \times S_\rho \mapsto \mathbf{R}_+$, $\rho > 0, V \in \mathcal{V}_0, D^+V(t, \mathbf{x}) \le g(t, V(t, \mathbf{x})), t \ne \tau_i$.
2. *there exists a* $\rho_0 > 0$ *such that* $\mathbf{x} \in S_{\rho_0}$ *implies that* $\mathbf{x} + U(i, \mathbf{x}) \in S_{\rho_0}$ *for all* $i$ *and* $V(t, \mathbf{x} + U(i, \mathbf{x})) \le \psi_i(V(t, \mathbf{x})), t = \tau_i, \mathbf{x} \in S_{\rho_0}$.
3. $\beta(||\mathbf{x}||) \le V(t, \mathbf{x}) \le \alpha(||\mathbf{x}||)$ *on* $\mathbf{R}_+ \times S_\rho$, *where* $\alpha(\cdot), \beta(\cdot) \in \mathcal{K}$.

*Then the stability properties of the trivial solution of the comparison system (10) imply the corresponding stability properties of the trivial solution of (6).*

**Theorem 2** (Corollary 3.2.1., p. 142 [Lakshmikantham *et al.*, 1989]). *Let* $g(t, w) = \dot{\lambda}(t)w, \lambda \in C^1[\mathbf{R}_+, \mathbf{R}_+], \psi_i(w) = d_i w, d_i \ge 0$ *for all* $i$. *Then the origin of system (6) is asymptotically stable if the conditions*

$$\lambda(\tau_{i+1}) + \ln(\gamma d_i) \le \lambda(\tau_i), \quad \text{for all } i, \text{ where } \gamma > 1 \tag{12}$$

and

$$\dot{\lambda}(t) \ge 0 \tag{13}$$

are satisfied.

## 3. Impulsive control of Chua's oscillator

In this section, we study the impulsive control of Chua's oscillators [Chua, 1993] by applying the theory presented in the previous section. The dimensionless form of a Chua's oscillator is given by [Chua, 1993]

$$\begin{cases} \dot{x} = \alpha(y - x - f(x)) \\ \dot{y} = x - y + z \\ \dot{z} = -\beta y - \gamma z \end{cases} \tag{14}$$

where $f(x)$ is the piecewise-linear characteristics of the Chua's diode, which is given by

$$f(x) = bx + \frac{1}{2}(a - b)(|x + 1| - |x - 1|) \tag{15}$$

where $a < b < 0$ are two constants.

Let $\mathbf{x}^T = (x \ y \ z)$, then we can rewrite the Chua's oscillator equation into the form

$$\dot{\mathbf{x}} = A\mathbf{x} + \Phi(\mathbf{x}) \tag{16}$$

where

$$A = \begin{pmatrix} -\alpha & \alpha & 0 \\ 1 & -1 & 1 \\ 0 & -\beta & -\gamma \end{pmatrix}, \quad \Phi(\mathbf{x}) = \begin{pmatrix} -\alpha f(x) \\ 0 \\ 0 \end{pmatrix} \tag{17}$$

The impulsive control of a Chua's oscillator is then given by

$$\begin{cases} \dot{\mathbf{x}} = A\mathbf{x} + \Phi(\mathbf{x}), & t \neq \tau_i \\ \Delta\mathbf{x}|_{t=\tau_i} = B\mathbf{x} \end{cases} \tag{18}$$

We use the following theorem in order to guarantee the asymptotic stability of the origin of the controlled Chua's oscillator.

**Theorem 3.** *Let $d_1$ be the largest eigenvalue of $(I + B^T)(I + B)$, where $B$ is a symmetric matrix, $\rho(I+B) \leq 1$, where $\rho(\cdot)$ denotes the spectral radius of $I+B$. Let $q$ be the largest eigenvalue of $(A+A^T)$ and let the impulses be equidistant from each other and separated by interval $\Delta$. If*

$$0 \leq q + 2|\alpha a| \leq -\frac{1}{\Delta}\ln(\xi d_1), \quad \text{where } \xi > 1 \tag{19}$$

*then the origin of the impulsively controlled Chua's oscillator is asymptotically stable.*

*Proof.* Let us construct the Lyapunov function $V(t, \mathbf{x}) = \mathbf{x}^T\mathbf{x}$. For $t \neq \tau_i$, we have

$$\begin{aligned} D^+V(t, \mathbf{x}) &= \mathbf{x}^T A\mathbf{x} + \mathbf{x}^T A^T\mathbf{x} + \mathbf{x}^T\Phi(\mathbf{x}) + \Phi^T(\mathbf{x})\mathbf{x} \\ &\leq q\mathbf{x}^T\mathbf{x} + 2|\alpha a|\mathbf{x}^T\mathbf{x} \\ &= (q + 2|\alpha a|)V(t, \mathbf{x}) \end{aligned} \tag{20}$$

Hence, condition 1 of Theorem 1 is satisfied with $g(t, w) = (q + 2|\alpha a|)w$.

Since $B$ is symmetric we know $(I + B)$ is also symmetric. By using the Euclidean norm we have

$$\rho(I + B) = ||I + B|| \tag{21}$$

Given any $\rho_0 > 0$ and $\mathbf{x} \in S_{\rho_0}$, we have

$$||\mathbf{x} + B\mathbf{x}|| \leq ||I + B||||\mathbf{x}|| = \rho(I + B)||\mathbf{x}|| \leq ||\mathbf{x}|| \tag{22}$$

The last inequality follows from $\rho(I+B) \leq 1$. Consequently, $\mathbf{x} + B\mathbf{x} \in S_{\rho_0}$.

For $t = \tau_i$, we have

$$\begin{aligned} V(\tau_i, \mathbf{x} + B\mathbf{x}) &= (\mathbf{x} + B\mathbf{x})^T(\mathbf{x} + B\mathbf{x}) \\ &= \mathbf{x}^T(I + B^T)(I + B)\mathbf{x} \\ &\leq d_1 V(\tau_i, \mathbf{x}) \end{aligned} \tag{23}$$

Hence condition 2 of Theorem 1 is satisfied with $\psi_i(w) = d_1 w$. We can see that condition 3 of Theorem 1 is also satisfied. It follows from Theorem 1 that the asymptotic stability of the impulsively controlled Chua's oscillator in Eq. (18) is implied by that of the following comparison system

$$\begin{cases} \dot{\omega} = (q + 2|\alpha a|)\omega, & t \neq \tau_i \\ \omega(\tau_i) = d_1\omega(\tau_i) \\ \omega(t_0) = \omega_0 \geq 0 \end{cases} \tag{24}$$

From Eq. (19), we have

$$\int_{\tau_i}^{\tau_{i+1}} (q + 2|\alpha a|)dt + ln(\xi d_1) \leq 0, \quad \xi > 1 \tag{25}$$

and $\dot{\lambda}(t) = q+2|\alpha a| \geq 0$. It follows from Theorem 2 that the trivial solution of Eq. (18) is asymptotically stable. ■

Theorem 3 also gives an estimate for the upper bound $\Delta_{\max}$ of $\Delta$; namely,

$$\Delta_{\max} = \left|\frac{\ln(\xi d_1)}{q + 2|\alpha a|}\right|, \quad \xi \longrightarrow 1^+ \tag{26}$$

Observe that the upper bound given by Eq. (26) is sufficient but not necessary. Consequently, we can only say that we have a predicted stable region, which is usually smaller than the actual stable region because we cannot assert that all other regions are unstable.

## 4. Simulation results of impulsive control

In the following simulations, we choose the parameters of Chua's oscillator as $\alpha = 15, \beta = 20$, $\gamma = 0.5, a = -\frac{120}{7}, b = -\frac{75}{7}$. A fourth-order Runge–Kutta method with step size $10^{-5}$ is used. The initial condition is given by $(x(0), y(0), z(0)) = (-2.121304, -0.066170, 2.881090)$. The uncontrolled trajectories are shown in Fig. 1, which is the Chua's double scroll attractor.

### 4.1. *Simulation 1: strong control*

In this simulation, we choose the matrix $B$ as

$$B = \begin{pmatrix} k & 0 & 0 \\ 0 & -1 & 0 \\ 0 & 0 & -1 \end{pmatrix} \tag{27}$$

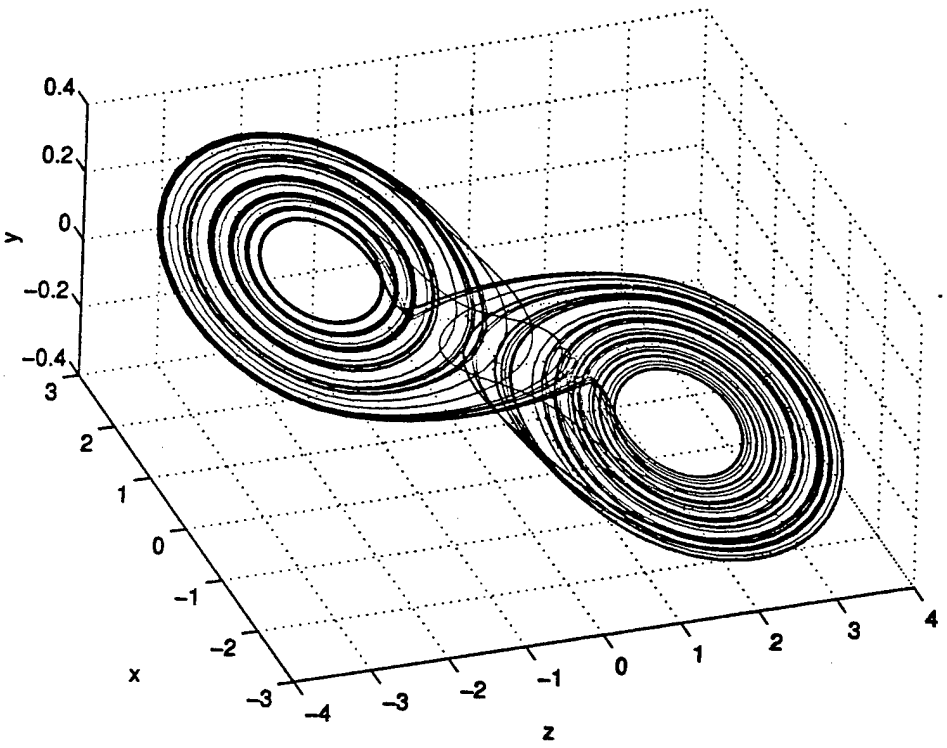


Fig. 1. The Chua's double scroll attractor.

where the impulsive control is "strong". It follows from Theorem 3 that $\rho(I+B) \leq 1$ should be satisfied, which implies that $-2 \leq k \leq 0$. By using this $B$ matrix, it is easy to see that

$$d_1 = (k+1)^2 \tag{28}$$

We have

$$A = \begin{pmatrix} -15 & 15 & 0 \\ 1 & -1 & 1 \\ 0 & -20 & -0.5 \end{pmatrix}, \qquad A + A^T = \begin{pmatrix} -30 & 16 & 0 \\ 16 & -2 & -19 \\ 0 & -19 & -1 \end{pmatrix} \tag{29}$$

from which we find $q = 20.162180$. Then an estimate of the boundaries of the stable region is given by

$$0 \leq \Delta \leq -\frac{(\ln \xi + \ln(k+1)^2)}{q + 2|\alpha a|}, \qquad -2 \leq k \leq 0 \tag{30}$$

Figure 2 shows the stable region for different $\xi$'s. The entire region below the curve corresponding to $\xi = 1$ is the predicted stable region. When $\xi \longrightarrow \infty$, the stable region shrinks to a line $k = -1$.

The simulation results are shown in Fig. 3. Figure 3(a) shows instability for $k = -1.5$ and $\Delta = 1$.

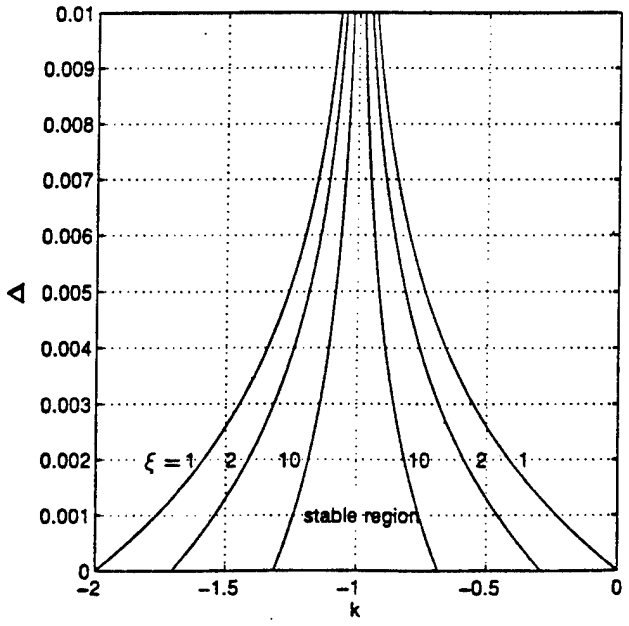


Fig. 2. Estimate of the boundaries of stable regions with different $\xi$'s used in simulation 1.

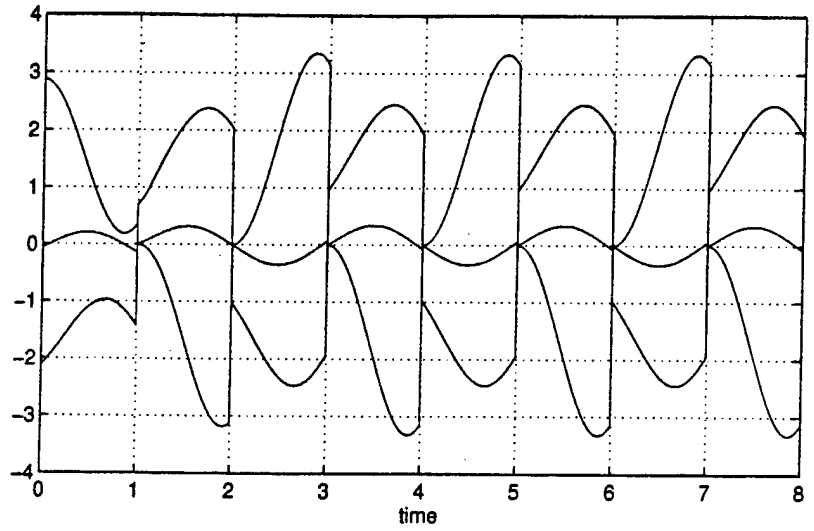


(a)

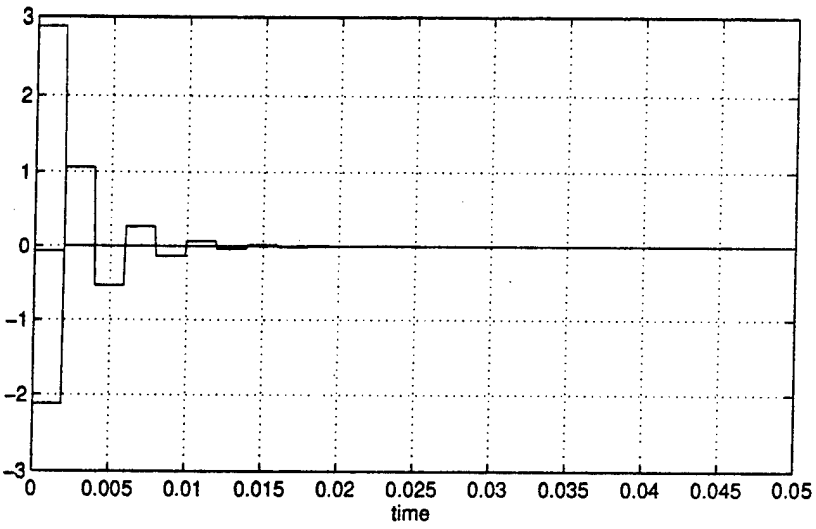


(b)

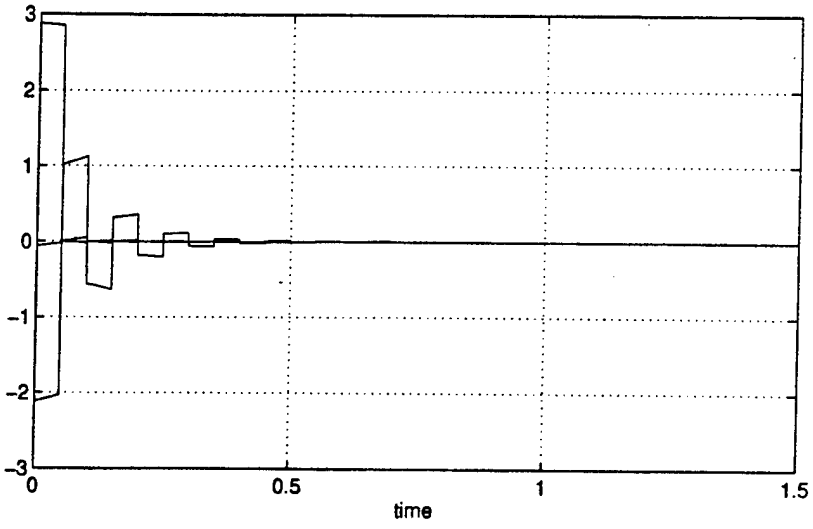


(c)

Fig. 3. Simulation results. (a) Unstable results outside the stable region. (b) Stable results inside the predicted stable region. (c) Stable results outside the predicted stable region.

The blue waveform, the red waveform and the green waveform correspond to $x(t), y(t)$ and $z(t)$, respectively. Figure 3(b) shows stable results within the stable region for $k = -1.5$ and $\Delta = 0.002$. One can see that the system asymptotically approaches the origin with a settling time of about 0.05. However, the true stable region is larger than that predicted in Fig. 2. In order to demonstrate this fact, we show in Fig. 3(c) the stable results for $k = -1.5$ and $\Delta = 0.05$. We can also see that the system asymptotically approaches the origin with a settling time of about 1.4 which is much larger than that shown in Fig. 3(b).

### 4.2. *Simulation 2: Weak control*

In this simulation, we choose the matrix $B$ as

$$B = \begin{pmatrix} k & 0 & 0 \\ 0 & -0.1 & 0 \\ 0 & 0 & -0.1 \end{pmatrix} \tag{31}$$

where the impulsive control is much weaker than that chosen in simulation 1.

It is easy to see that

$$d_1 = \begin{cases} (k+1)^2, & (k+1)^2 \geq 0.81 \\ 0.81, & \text{elsewhere} \end{cases} \tag{32}$$

An estimate of the boundaries of the stable region is given by

$$0 \leq \Delta \leq \begin{cases} -\dfrac{\ln\xi + \ln(k+1)^2}{q + 2|\alpha a|}, & (k+1)^2 \geq 0.81 \\ -\dfrac{\ln\xi + \ln(0.81)}{q + 2|\alpha a|}, & \text{elsewhere} \end{cases} \quad , \quad l - 2 \leq k \leq 0 \tag{33}$$

Figure 4 shows the stable region. The entire region below the curve corresponding to $\xi = 1$ is the predicted stable region. In this case, $\Delta$ is always bounded. It seems that we cannot control the system to the origin with an arbitrarily prescribed speed because $\xi$ has to satisfy $1 < \xi < \frac{100}{81}$. This is different from the case shown in Fig. 2, where any value of $\xi > 1$ is possible.

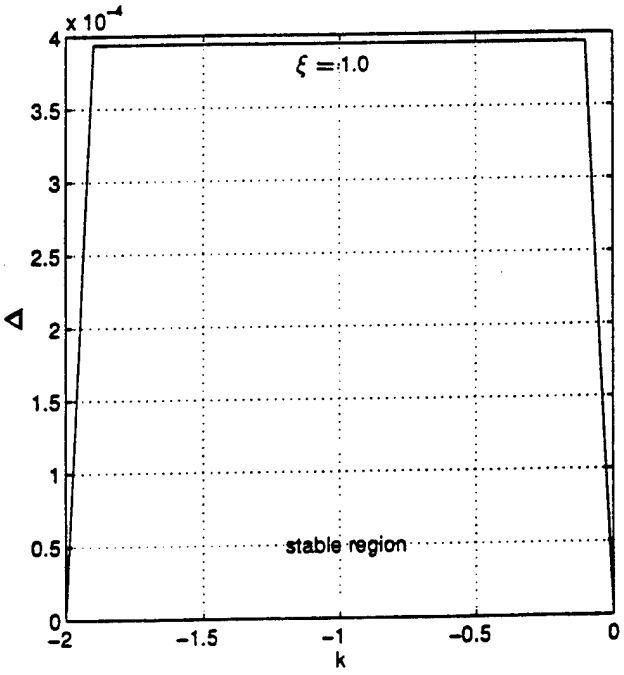


Fig. 4. Estimate of the boundaries of stable region used in simulation 2.

The simulation results are shown in Fig. 5. Again, the blue waveform, the red waveform and the green waveform correspond to $x(t), y(t)$ and $z(t)$, respectively. Figure 5(a) shows the instability results for $k = -1$ and $\Delta = 0.4$. Figure 5(b) shows the stable results in the stable region for $k = -1$ and $\Delta = 3 \times 10^{-4}$. The control system asymptotically approaches the origin with a settling time of about 0.05. Also, the true stable region is larger than that predicted in Fig. 4. To demonstrate this fact, we show in Fig. 5(c) the stable results for $k = -1$ and $\Delta = 0.01$. We can also see that the system asymptotically approaches the origin with a settling time equal approximately to 1, which is much larger than that shown in Fig. 5(b).

## 5. Impulsive synchronization of Chua's oscillators

In this section, we study the impulsive synchronization of two Chua's oscillators. One of the Chua's oscillators is called the *driving system* and the other is called the *driven system*. In an impulsive synchronization configuration, the driving system is given by Eq. (14). The driven system is given by

$$\dot{\tilde{\mathbf{x}}} = A\tilde{\mathbf{x}} + \Phi(\tilde{\mathbf{x}}) \tag{34}$$

where $\tilde{\mathbf{x}} = (\tilde{x}, \tilde{y}, \tilde{z})$ is the state variables of the driven system.

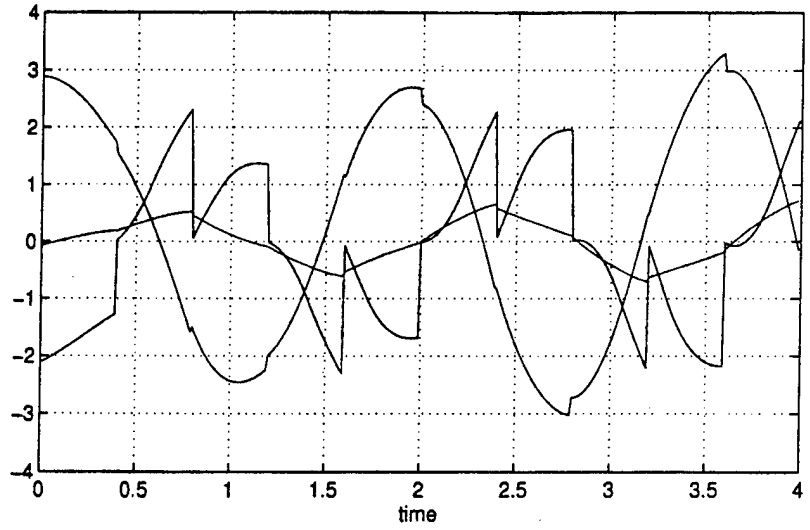


(a)

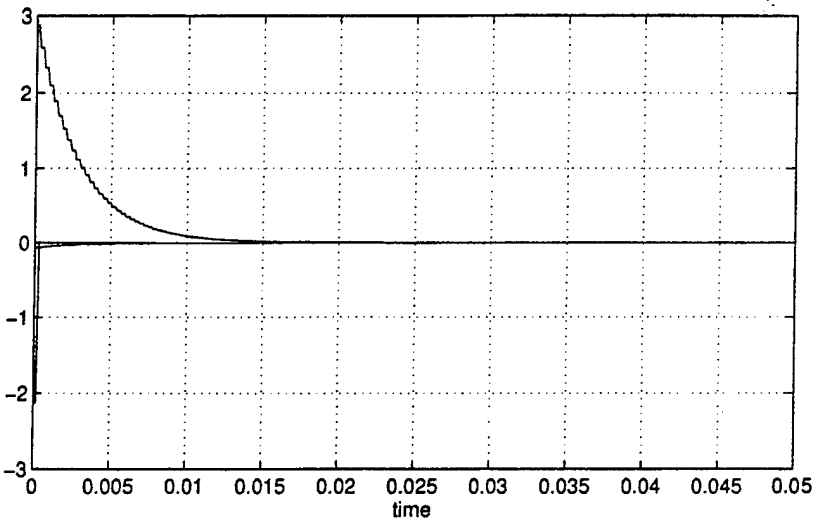


(b)

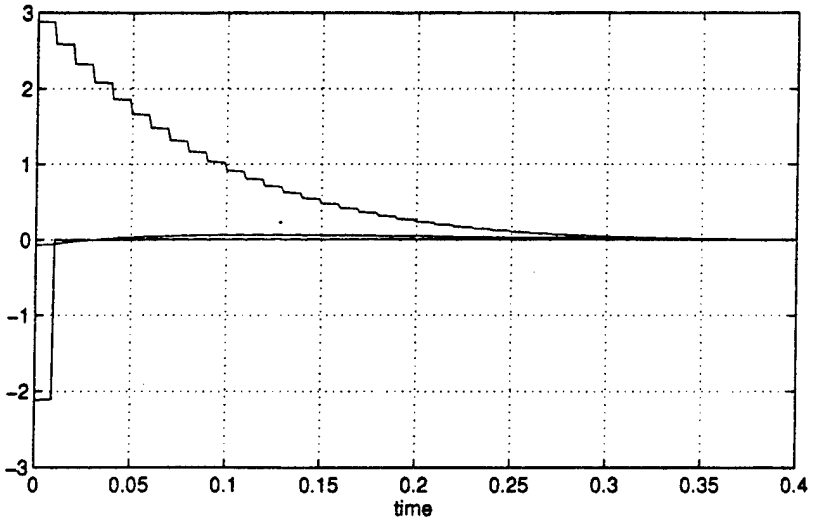


(c)

Fig. 5. Simulation results. (a) Unstable results outside the stable region. (b) Stable results in the stable region. (c) Stable results outside the stable region.

At discrete instants, $\tau_i$, $i = 1, 2, \ldots$, the state variables of the driving system are transmitted to the driven system and then the state variables of the driven system are subject to jumps at these instants. In this sense, the driven system is described by the impulsive differential equation

$$\begin{cases} \dot{\tilde{\mathbf{x}}} = A\tilde{\mathbf{x}} + \Psi(\tilde{\mathbf{x}}), & t \neq \tau_i \\ \Delta\tilde{\mathbf{x}}|_{t=\tau_i} = -B\mathbf{e}, & i = 1, 2, \ldots \end{cases} \tag{35}$$

where $B$ is a $3 \times 3$ matrix, and $\mathbf{e}^T = (e_x, e_y, e_z) = (x - \tilde{x}, y - \tilde{y}, z - \tilde{z})$ is the *synchronization error*. If we define

$$\Psi(\mathbf{x}, \tilde{\mathbf{x}}) = \Phi(\mathbf{x}) - \Phi(\tilde{\mathbf{x}}) = \begin{pmatrix} -\alpha f(x) + \alpha f(\tilde{x}) \\ 0 \\ 0 \end{pmatrix} \tag{36}$$

then the error system of the impulsive synchronization is given by

$$\begin{cases} \dot{\mathbf{e}} = A\mathbf{e} + \Psi(\mathbf{x}, \tilde{\mathbf{x}}), & t \neq \tau_i \\ \Delta\mathbf{e}|_{t=\tau_i} = B\mathbf{e}, & i = 1, 2, \ldots \end{cases} \tag{37}$$

We use the following theorem to guarantee that our impulsive synchronization is asymptotically stable.

**Theorem 4.** *Let $d_1$ be the largest eigenvalue of $(I + B^T)(I + B)$, where $B$ is a symmetric matrix. Assume the spectral radius $\rho$ of $I + B$ satisfies $\rho(I + B) \leq 1$. Let $q$ be the largest eigenvalue of $(A + A^T)$ and assume the impulses are equidistant from each other and separated by an interval $\Delta$. If*

$$0 \leq q + 2|\alpha a| \leq -\tfrac{1}{\Delta}\ln(\xi d_1), \quad \xi > 1 \tag{38}$$

*then the impulsive synchronization of two Chua's oscillators is asymptotically stable.*

*Proof.* Observe that the error system in Eq. (37) is almost the same as the system in Eq. (18) except for $\Psi(\mathbf{x}, \tilde{\mathbf{x}})$. Similarly, let us construct the Lyapunov function $V(t, \mathbf{e}) = \mathbf{e}^T\mathbf{e}$. For $t \neq \tau_i$, we have

$$\begin{aligned} D^+V(t, \mathbf{e}) &= \mathbf{e}^T A\mathbf{e} + \mathbf{e}^T A^T\mathbf{e} + \mathbf{e}^T\Psi(\mathbf{e}) + \Psi^T(\mathbf{e})\mathbf{e} \\ &\leq q\mathbf{e}^T\mathbf{e} + 2|\alpha||f(x) - f(\tilde{x})|e_x \\ &\leq q\mathbf{e}^T\mathbf{e} + 2|\alpha a|e_x^2 \\ &\leq (q + 2|\alpha a|)\mathbf{e}^T\mathbf{e} \\ &= (q + 2|\alpha a|)V(t, \mathbf{e}) \end{aligned} \tag{39}$$

Hence, condition 1 of Theorem 1 is satisfied with $g(t, w) = (q + 2|\alpha a|)w$. The rest of this proof is the same as that of Theorem 3. ■

For the rest of this section, we present our simulation results. We choose the matrix $B$ as

$$B = \begin{pmatrix} -1.5 & 0 & 0 \\ 0 & -1 & 0 \\ 0 & 0 & -1 \end{pmatrix} \tag{40}$$

The initial conditions are given by $(x(0), y(0), z(0)) = (-2.121304, -0.066170, 2.881090)$ and $(\tilde{x}(0), \tilde{y}(0), \tilde{z}(0)) = (0, 0, 0)$. The other parameters are the same as those used in Sec. 4. Since the stability boundary estimates are the same as those in Sec. 4, we do not repeat them here. Figure 6 shows our simulation results. Figure 6(a) shows the stable results within our predicted stable region with $k = -1.5$ and $\Delta = 0.002$. The blue waveform, the red waveform and the green waveform show $e_x(t), e_y(t)$ and $e_z(t)$, respectively. We can see that impulsive synchronization was achieved rapidly. Figure 6(b) shows that if $\Delta = 5$ then our impulsive synchronization is unstable.

### 5.1. *Effects of channel noise*

Let us study next the robustness of the impulsive synchronization to additive channel noise. In the following simulations, we choose the matrix $B$ as

$$B = \begin{pmatrix} -1 & 0 & 0 \\ 0 & -1 & 0 \\ 0 & 0 & -1 \end{pmatrix} \tag{41}$$

The initial conditions are given by $(x(0), y(0), z(0)) = (-2.121304, -0.066170, 2.881090)$ and $(\tilde{x}(0), \tilde{y}(0), \tilde{z}(0)) = (0, 0, 0)$. The other parameters are the same as those used in Sec. 4. Figure 7 shows the simulation results when the signal-to-noise ratio (SNR) and the time interval of the impulses are given respectively by SNR=20 dB and $\Delta = 0.1$. Figure 7(a) shows the noise (the red waveform) in impulses $x(\tau_i)$ and the synchronization error (the blue waveform) $x - \tilde{x}$. Figure 7(b) shows the noise (the red waveform) in impulses $y(\tau_i)$ and the synchronization error (the blue waveform) $y - \tilde{y}$. Figure 7(c) shows the noise (the red waveform) in impulses $z(\tau_i)$ and the synchronization error (the blue waveform) $z - \tilde{z}$. From the above simulation results we find that the synchronization errors are

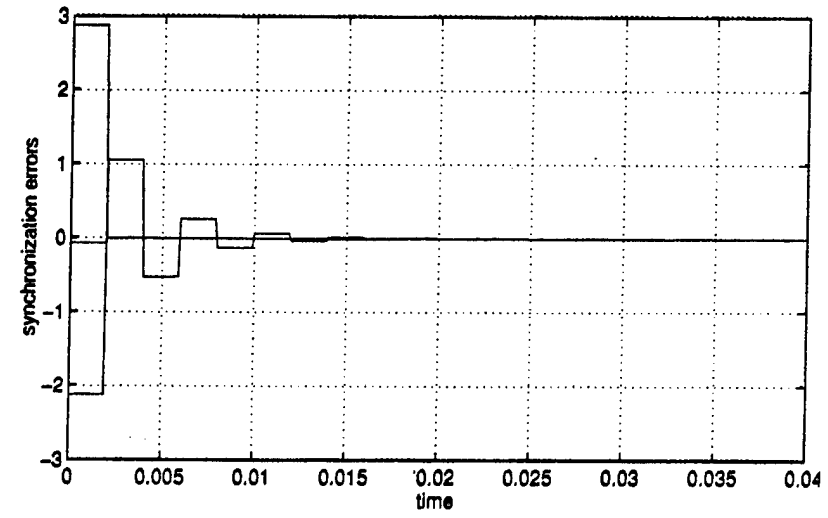


(a)

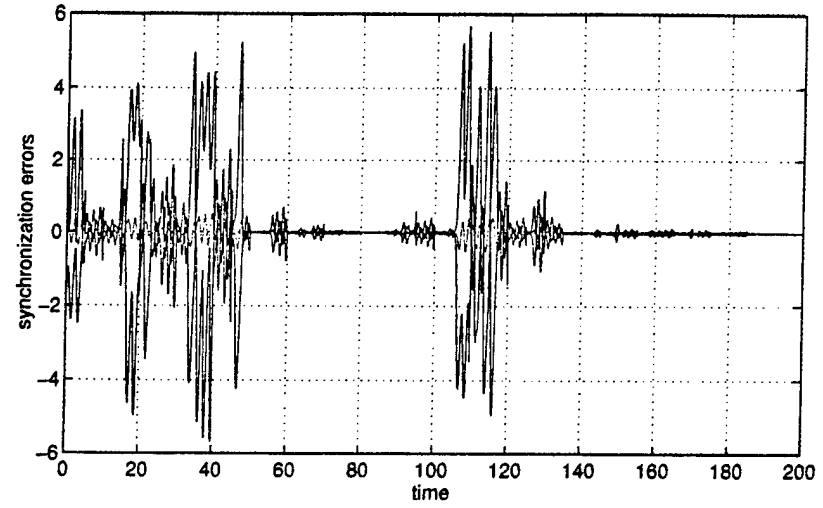


(b)

Fig. 6. Simulation results of impulsive synchronization. (a) Stable synchronization results inside our predicted stable region. (b) Synchronization cannot be achieved when $\Delta$ is too large.

comparable to the noise in the synchronization impulses.

For comparison, we also presented the corresponding results when a continuous synchronization is used. The driven system of the continuous synchronization is given by

$$\begin{cases} \dot{\tilde{x}} = \alpha(\tilde{y} - \tilde{x} - f(\tilde{x})) \\ \dot{\tilde{y}} = (x + n(t)) - \tilde{y} + \tilde{z} \\ \dot{\tilde{z}} = -\beta\tilde{y} - \gamma\tilde{z} \end{cases} \tag{42}$$

where $x$ is the first state variable of the driving system and $n(t)$ is the additive channel noise. When $n(t) = 0$, the driving system and the driven system can be synchronized. When the additive noise is added in the transmitted signal with SNR=20 dB, the synchronization errors are shown in Fig. 7(d). Observe that the synchronization error $x - \tilde{x}$ of the continuous scheme is bigger than that of the impulsive scheme.

Given a SNR level, the synchronization errors of the impulsive scheme become bigger if $\Delta$ increases. In our simulations we find if $\Delta = 1$ then

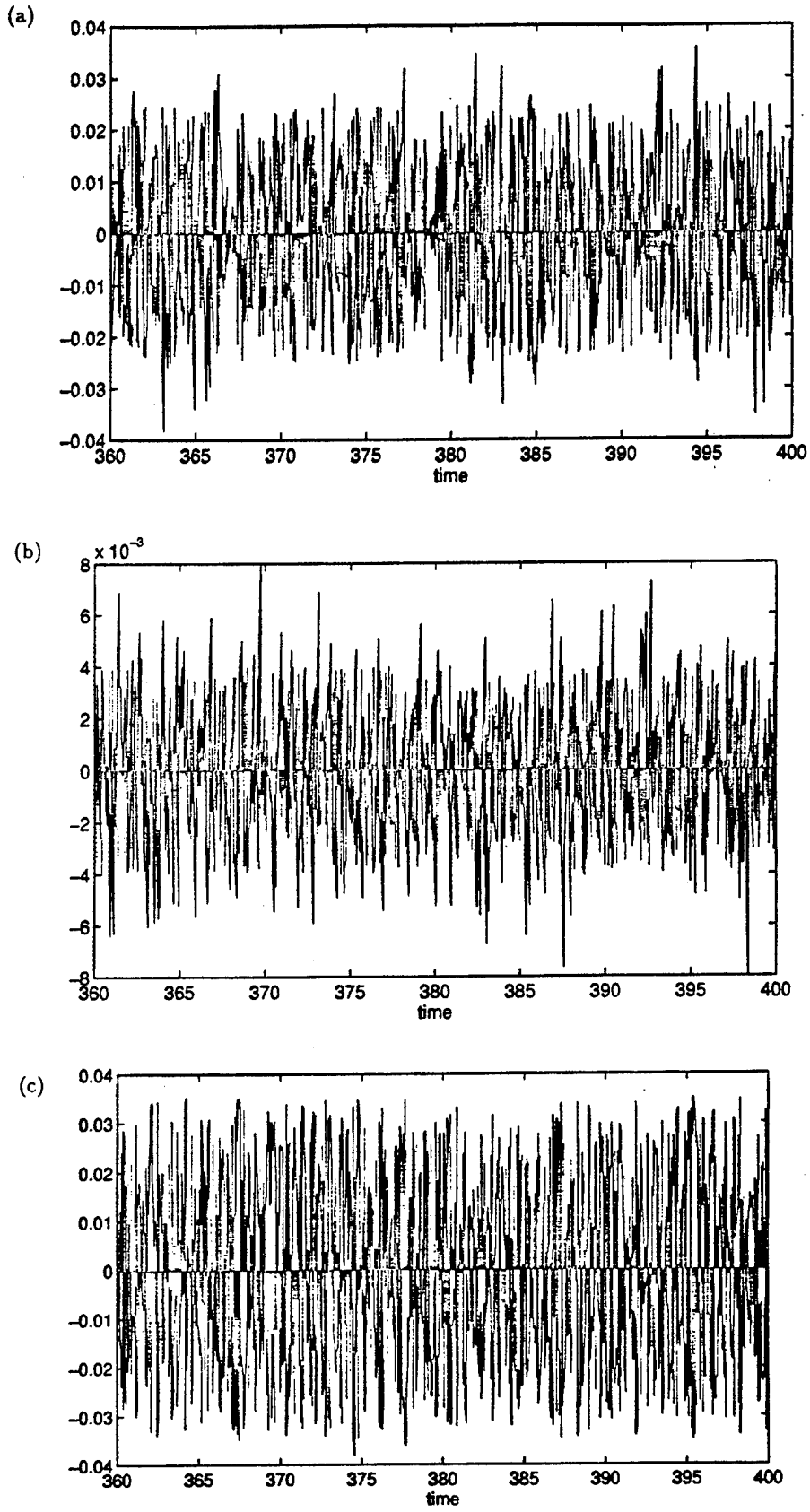


Fig. 7. Simulation results of the impulsive synchronization and the continuous synchronization when channel noise is added. (a) Noise in impulses $x(\tau_i)$(red) and the synchronization error $x-\tilde{x}$(blue) of the impulsive synchronization. (b) Noise in impulses $y(\tau_i)$(red) and the synchronization error $y-\tilde{y}$(blue) of the impulsive synchronization. (c) Noise in impulses $z(\tau_i)$(red) and the synchronization error $z-\tilde{z}$(blue) of the impulsive synchronization. (d) Synchronization errors $x-\tilde{x}$(blue), $y-\tilde{y}$(red) and $z-\tilde{z}$(green) of the continuous synchronization.

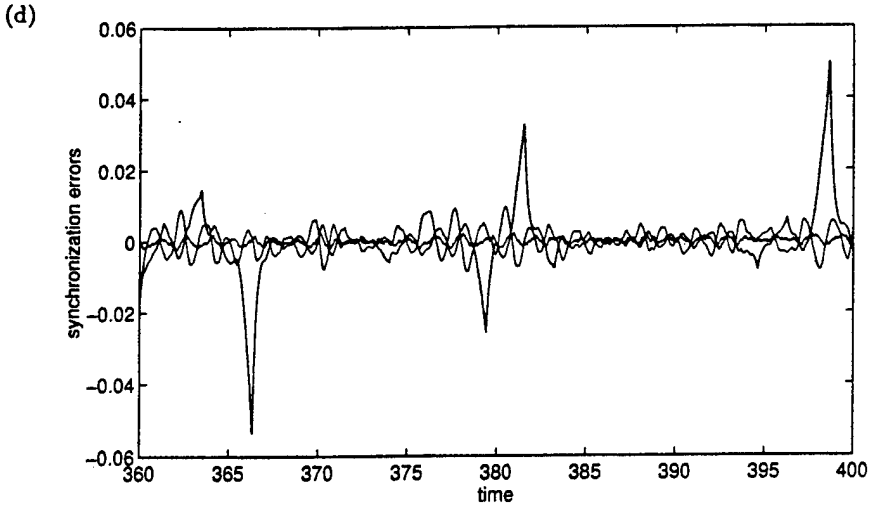


Fig. 7. (*Continued*)

there exist some big synchronization error peaks. The simulation results are shown in Fig. 8 with SNR= 20 dB. Figure 8(a) shows the noise (the red waveform) in the impulses $x(\tau_i)$ and the synchronization error (the blue waveform) $x-\tilde{x}$. Figure 8(b) shows the noise (the red waveform) in the impulses $y(\tau_i)$ and the synchronization error (the blue waveform) $y-\tilde{y}$. Figure 8(c) shows the noise (the red waveform) in the impulses $z(\tau_i)$ and the synchronization error (the blue waveform) $z-\tilde{z}$. From the simulation results we find that the synchronization errors are comparable to the noise most of the time. However, when the $\Delta$ becomes too big, e.g. $\Delta = 6$, then most of the time we observe that the synchronization errors are much bigger than the noise.

From the above simulation we can conclude that if $\Delta$ is small enough, e.g. $\Delta = 0.1$, then the impulsive synchronization is more robust than the continuous synchronization. This is because in continuous synchronization the synchronization error system is continuously disturbed by the continuous channel noise and more often pushed to some local instabilities than in impulsive synchronization. This in turn results in more frequent large peaks of synchronization errors in continuous synchronization.

### 5.2. *Effects of parameter mismatch*

The parameter mismatch is any parameter difference between the driving system and the driven system. The robustness of impulsive synchronization to parameter mismatch is studied in the following simulations. Figure 9 shows the synchronization errors when different parameter mismatches are used. Figure 9(a) shows the results when only 1% mismatch exists in parameter $\alpha$ with $\Delta = 0.1$. Figure 9(b) shows the results when 10% mismatch exists in the parameter $\alpha$ with $\Delta = 0.1$. Observe that the impulsive synchronization is robust enough against parameter mismatch. We also show the results when the continuous synchronization scheme is used. Figure 9(c) shows the results when a 1% mismatch exists in the parameter $\alpha$ and when continuous synchronization is used. Observe that there exist some very big synchronization errors in $x-\tilde{x}$. Figure 9(d) shows the results when a 10% mismatch exists in the parameter $\alpha$ and when continuous synchronization is used. Observe that there exist some very big synchronization errors in $x-\tilde{x}$. From the above we can see that impulsive synchronization is less sensitive to parameter mismatches than continuous synchronization.

## 6. A Secure Communication System

Since the publication of several chaotic cryptanalysis results in *low-dimensional chaos-based* secure communication systems [Yang, 1995; Short, 1994], there were concerns that such communication schemes may not be secure enough. To overcome this objection, one approach is to exploit hyper chaos-based secure communication systems, but such systems may introduce more difficulties to synchronization.

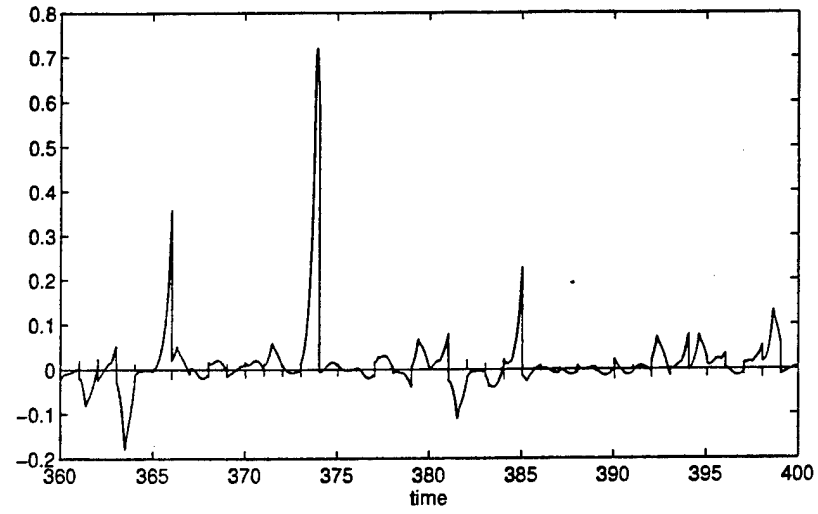


(a)

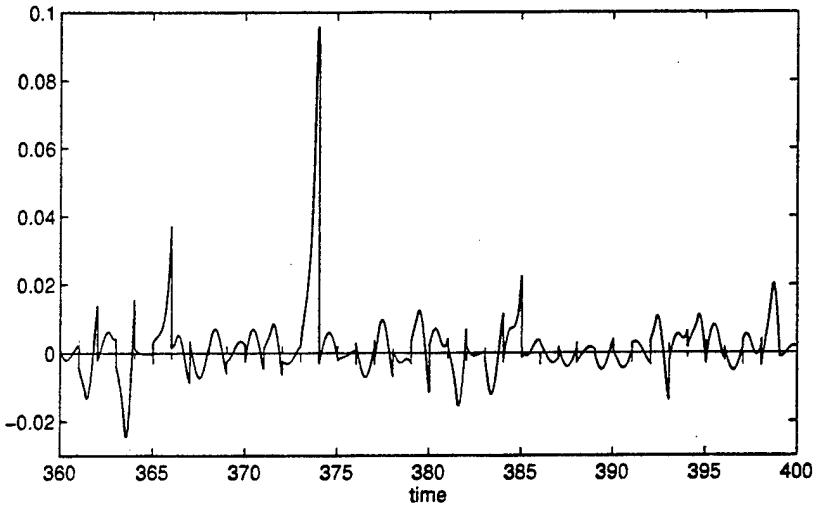


(b)

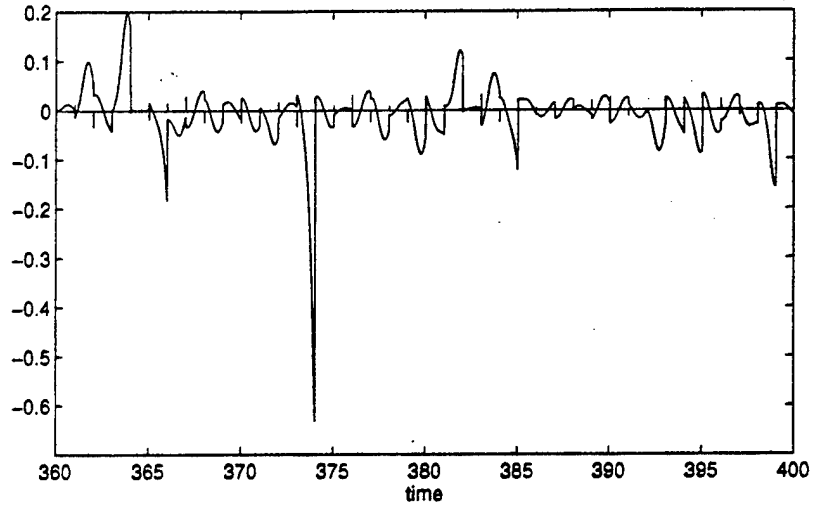


(c)

Fig. 8. Simulation results of the impulsive synchronization when channel noise is added and $\Delta$ is big. (a) Noise in impulses $x(\tau_i)$(red) and the synchronization error $x-\tilde{x}$(blue). (b) Noise in impulses $y(\tau_i)$(red) and the synchronization error $y-\tilde{y}$(blue). (c) Noise in impulses $z(\tau_i)$(red) and the synchronization error $z-\tilde{z}$(blue).

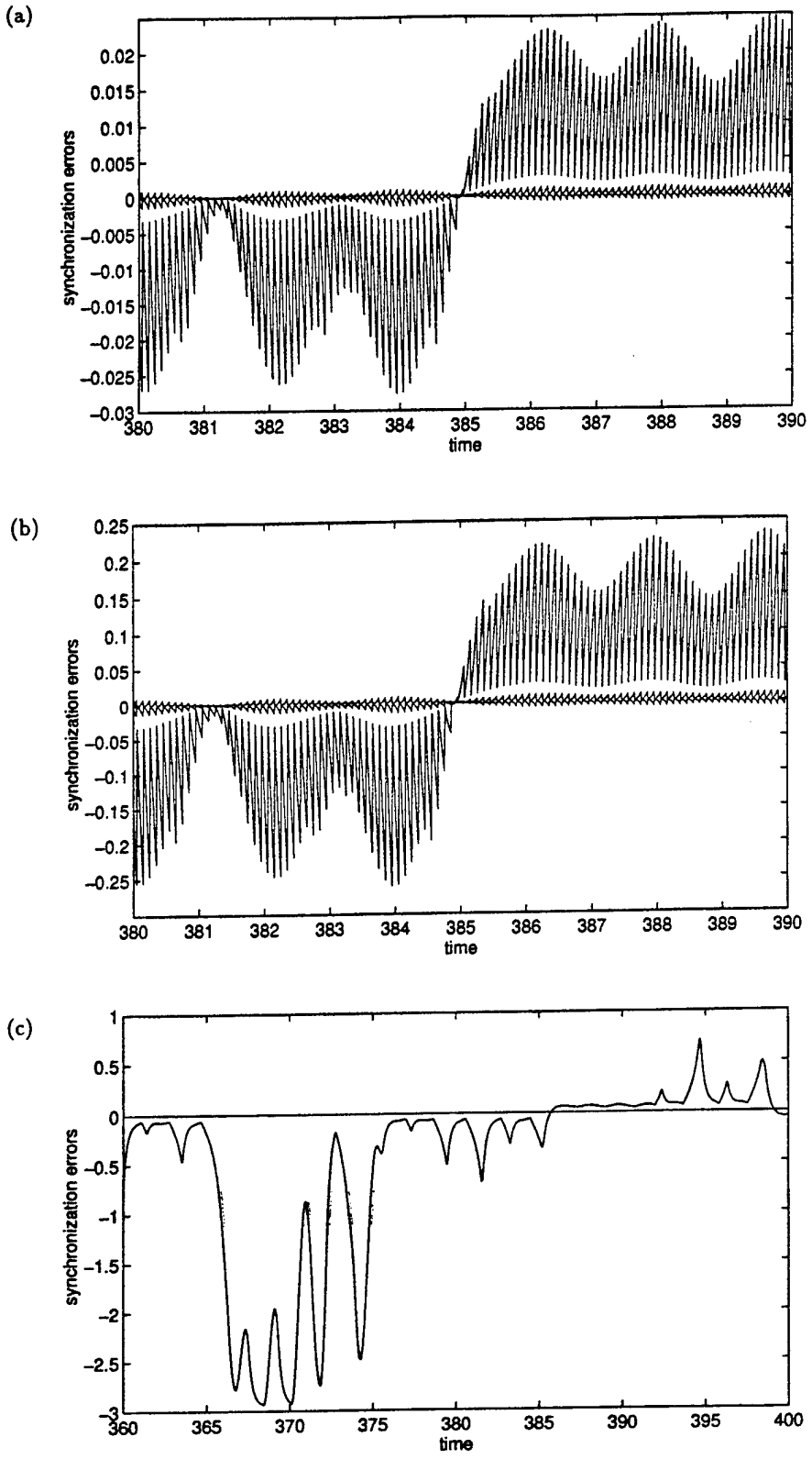


Fig. 9. Simulation results of the impulsive synchronization and the continuous synchronization when parameter mismatches exist. (a) A 1% mismatch exists in $\alpha$. The synchronization errors of the impulsive synchronization: $x - \tilde{x}$(blue), $y - \tilde{y}$(red) and $z - \tilde{z}$(green). (b) A 10% mismatch exists in $\alpha$. The synchronization errors of the impulsive synchronization: $x - \tilde{x}$(blue), $y - \tilde{y}$(red) and $z - \tilde{z}$(green). (c) A 1% mismatch exists in $\alpha$ when the continuous synchronization is used. The synchronization errors $x - \tilde{x}$(blue), $y - \tilde{y}$(red) and $z - \tilde{z}$(green). (d) A 10% mismatch exists in $\alpha$ when the continuous synchronization is used. The synchronization errors $x - \tilde{x}$(blue), $y - \tilde{y}$(red) and $z - \tilde{z}$(green).

(d)

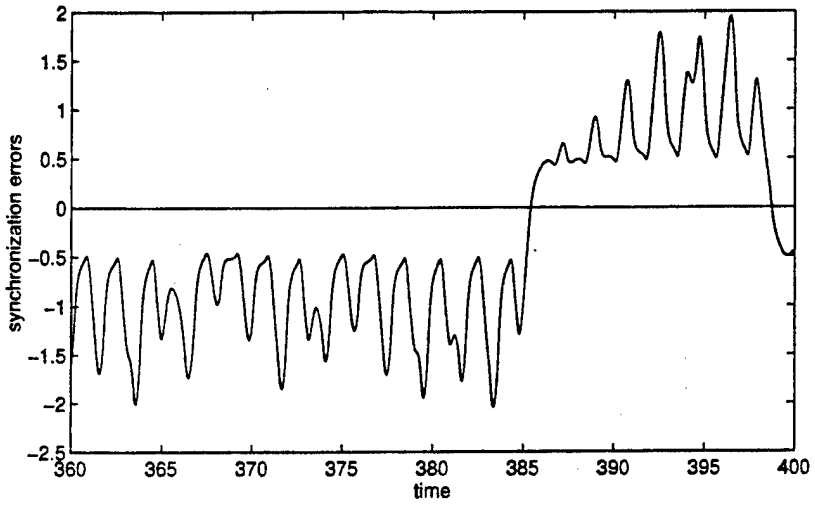


Fig. 9. (*Continued*)

On the other hand, we can enhance the security of low-dimensional chaos-based secure communication schemes by combining conventional cryptographic schemes with a chaotic system [Yang *et al.*, 1997]. To overcome the low security objections against low-dimensional continuous chaos-based schemes, we should overcome the following problems: (1) make the transmitted signal more complex, and (2) reduce the redundancy in the transmitted signal. To achieve the first goal, it is not necessary to use hyperchaos. In [Yang *et al.*, 1997] we have presented a method to combine a conventional cryptographic scheme with low-dimensional chaos to obtain a very complex transmitted signal. To achieve the second goal, impulsive synchronization offers a very promising approach.

In this section, we combine the results in [Yang *et al.*, 1997] and impulsive synchronization to give a new chaotic secure communication scheme. The block diagram of this scheme is shown in Fig. 10.

From Fig. 10 we can see that this chaotic secure communication system consists of a transmitter and a receiver. In both the transmitter and the receiver, there exist two identical chaotic systems. Also, two identical conventional cryptographic schemes are embedded in both the transmitter and the receiver. Let us now consider the details of each block in Fig. 10. The transmitted signal consists of a sequence of time frames. Every frame has a length of $T$ seconds and consists of two regions. In Fig. 11 we show the concept of a time frame and its components. The first region of the time frame is a synchronization region consisting of synchronization impulses. The synchronization impulses are used to impulsively synchronize the chaotic systems in both transmitter and receiver. The second region is the scrambled signal region where the scrambled signal is contained. To ensure synchronization, we have $T < \Delta_{\max}$. Within every time frame, the synchronization region has a length of $Q$ and the remaining time interval $T - Q$ is the scrambled signal region.

The composition block in Fig. 10 is used to combine the synchronization impulses and the scrambled signal into the time frame structure shown in Fig. 11. The simplest combination method is to substitute the beginning $Q$ seconds of every time frame with synchronization impulses. Since $Q$ is usually very small compared with $T$, the lost of time for packing a message signal is negligible. The decomposition block is used to separate the synchronization region and the scrambled signal region within each frame at the receiver end. Then the separated synchronization impulses are used to make the chaotic system in the receiver to synchronize with that in the transmitter. The stability of this impulsive synchronization is guaranteed by our results in Sec. 5.

In the transmitter and the receiver, we use the same cryptographic scheme block for purposes of bi-directional communication. In a bi-directional communication scheme, every cellular phone should function both as a receiver and a transmitter. Here, the key signal is generated by the chaotic system.

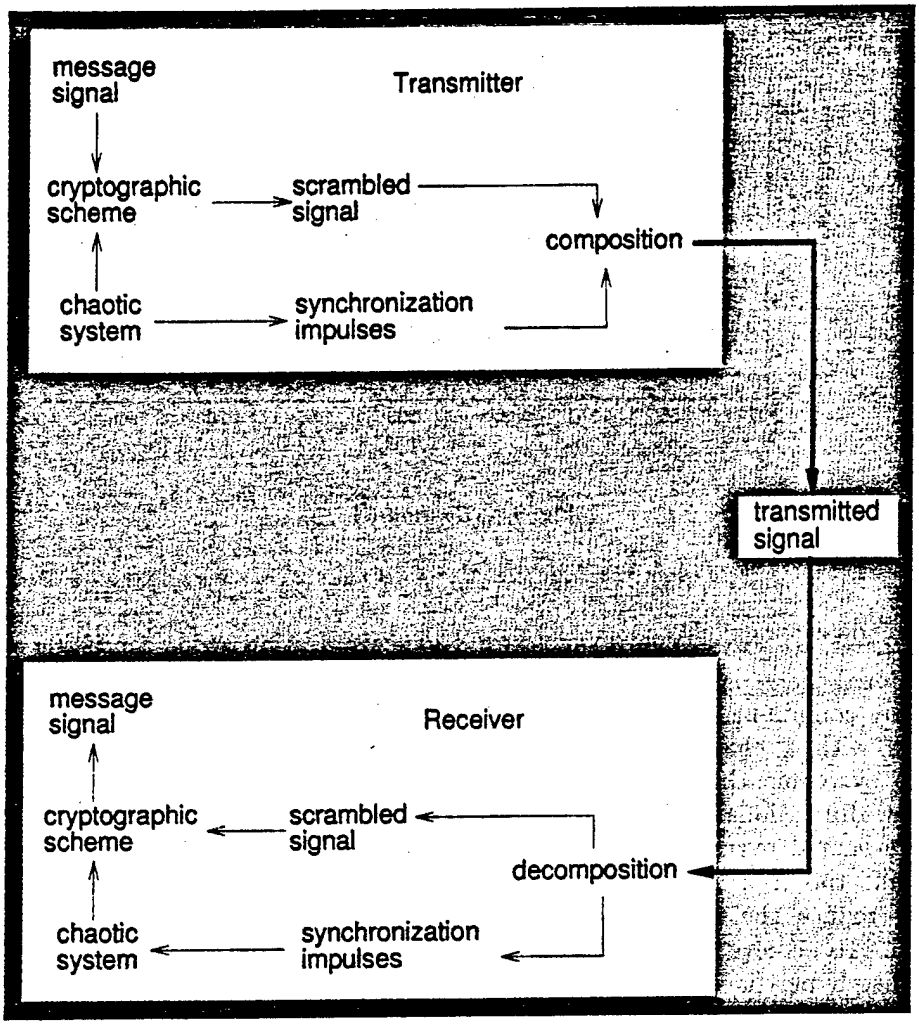


Fig. 10. Block diagram of the impulsive-synchronization based chaotic secure communication system.

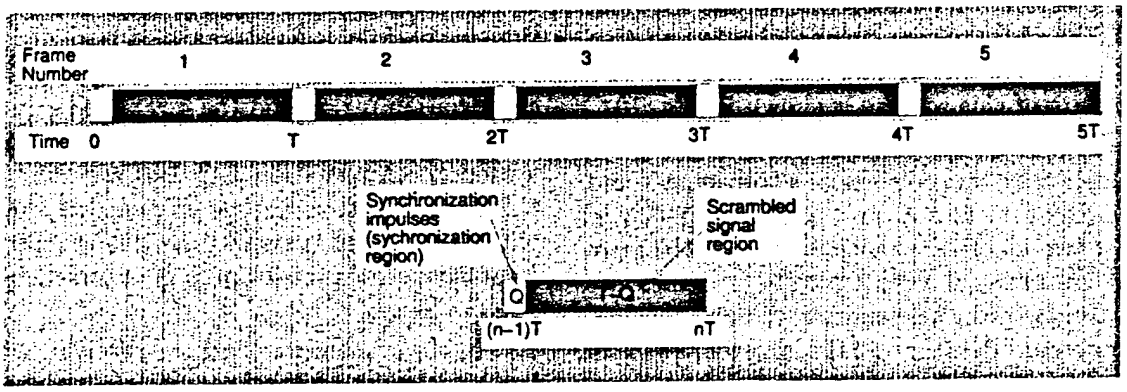


Fig. 11. Illustration of the concept of a time-frame and its components.

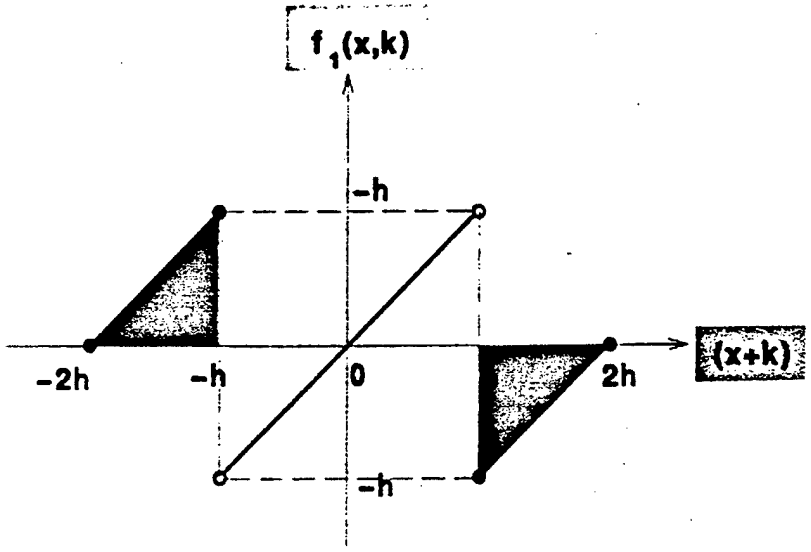


Fig. 12. Nonlinear function used in the continuous shift cipher.

The cryptographic scheme is as follows [Yang *et al.*, 1997]:

We use a continuous $n$-shift cipher to encrypt the plain signal(message signal). The $n$-shift cipher is given by

$$e(p(t)) = \underbrace{f_1\Big(\ldots f_1\Big(f_1}_{n}\Big(p(t), \underbrace{k(t)\Big), k(t)\Big), \ldots, k(t)\Big)}_{n}$$
$$= y(t) \tag{43}$$

where $h$ is chosen such that $p(t)$ and $k(t)$ lie within $(-h, h)$. Here, $p(t)$ and $k(t)$ denote the plain signal and the key signal, respectively, and $y(t)$ denotes the encrypted signal. The key signal $k(t)$ is chosen as a state variable of the chaotic system. The notation $f_1(\cdot, \cdot)$ denotes a scalar nonlinear function of two variables defined as follow:

$$f_1(x,k) = \begin{cases} (x+k) + 2h, & -2h \le (x+k) \le -h \\ (x+k), & -h < (x+k) < h \\ (x+k) - 2h, & h \le (x+k) \le 2h \end{cases} \tag{44}$$

This function is shown in Fig. 12.

The corresponding decryption rule is the same as the encryption rule

$$p(t) = d(y(t))$$
$$= e(y(t))$$
$$= \underbrace{f_1\Big(\ldots f_1\Big(f_1}_{n}\Big(y(t), \underbrace{-k(t)\Big), -k(t)\Big), \ldots, -k(t)\Big)}_{n} \tag{45}$$

To decode the encrypted signal, the same key signal should be used.

The simulation results are as follows. We use an FM scheme to modulate the synchronization impulses such that the synchronization region is located in the initial 1% of every time frame. We choose the frame length as $T = 1s$. In the synchronization region of every time frame, we transmit the impulses of the three state variables of the Chua's oscillators. The parameter of the encrypted signal is chosen as $h = 0.4$. A continuous 10-shift cipher was used. We choose $x$ and $\tilde{x}$ as the key signals and normalized them to fall within the amplitude range $[-0.4, 0.4]$.

Figure 13 shows the simulation results of the above proposed secure communication system for transmitting a speech signal. Figure 13(a) shows the waveforms of the sampled speech of four Chinese digits "NING"(zero) — "YI"(one) — "ER"(two) — "SANG"(three). The sampling rate is 8K. Figure 13(b) shows the spectrograms of the original

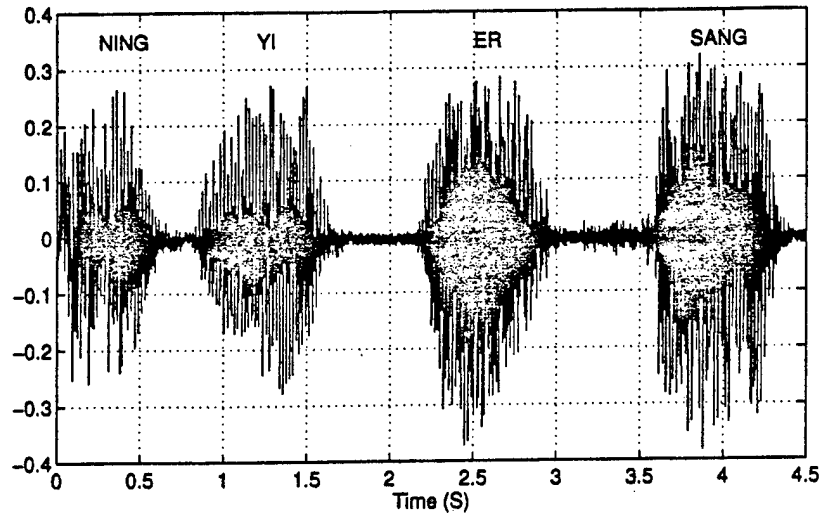


(a)

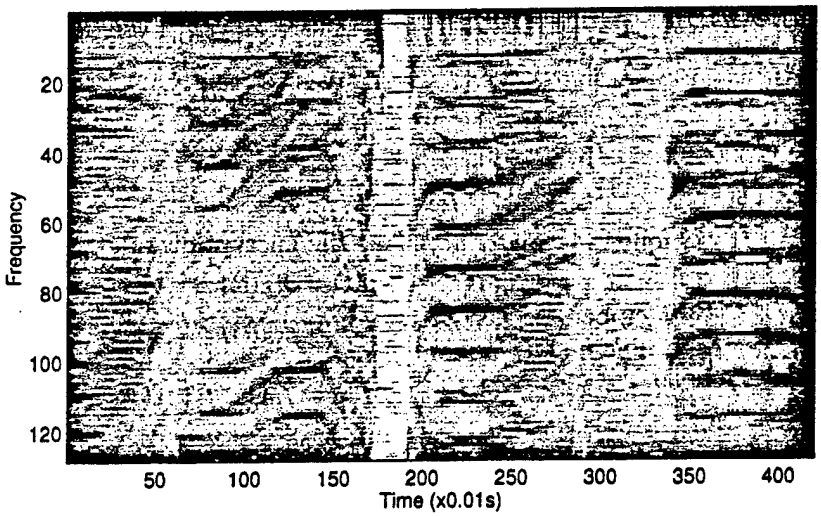


(b)

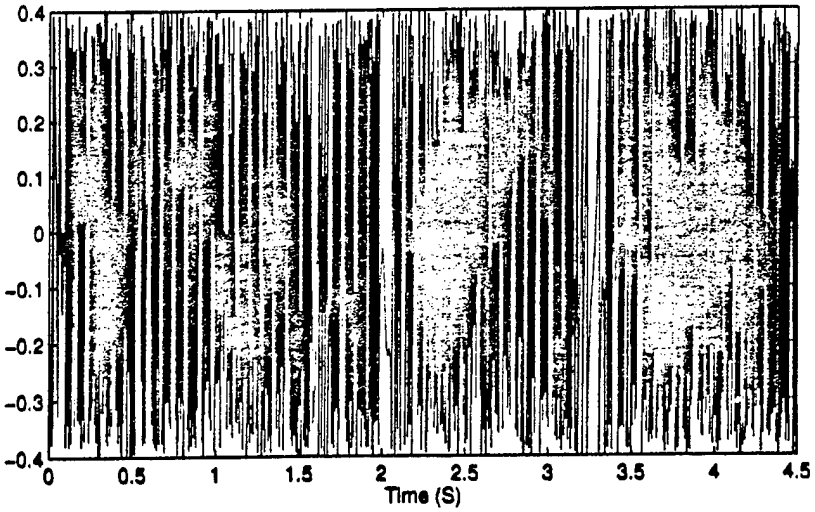


(c)

Fig. 13. The simulation results. (a) The time-domain waveform of the speech signal. (b) The spectrogram for the original speech signal. (c) The time-domain waveform of the scrambled speech signal. (d) The spectrogram of the scrambled speech signal. (e) The time-domain waveform of the descrambled speech signal. (f) The spectrogram of the descrambled speech signal.

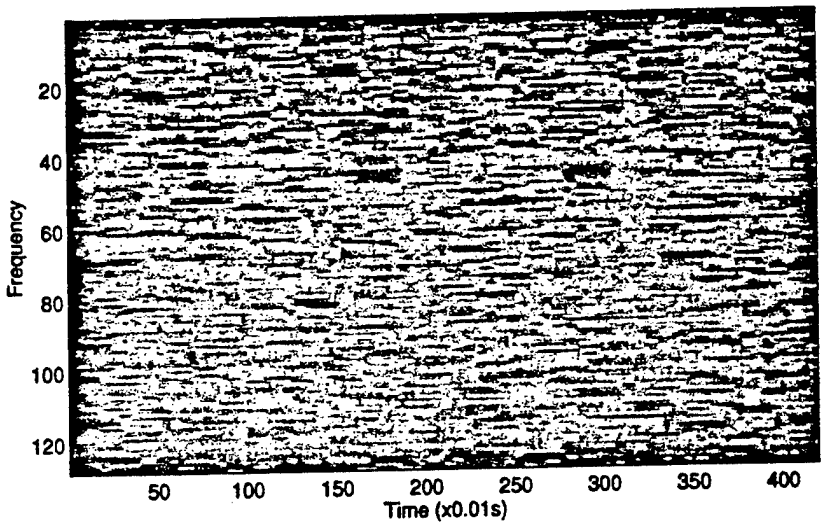


(d)

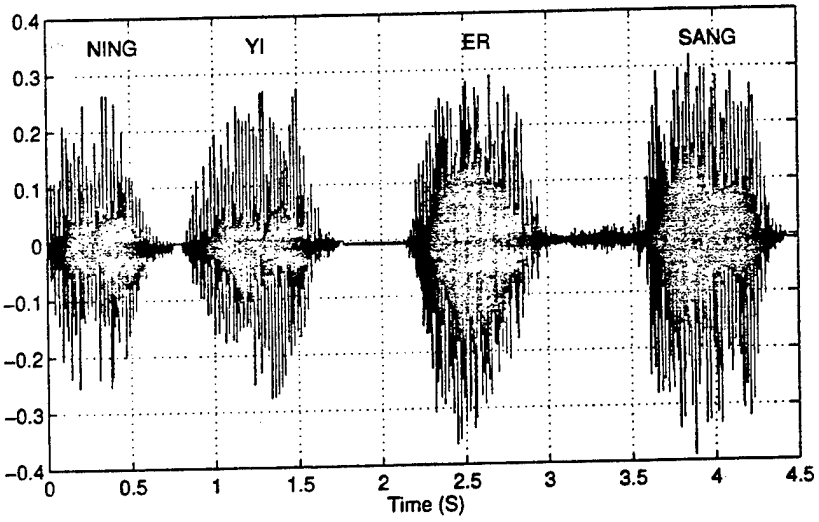


(e)

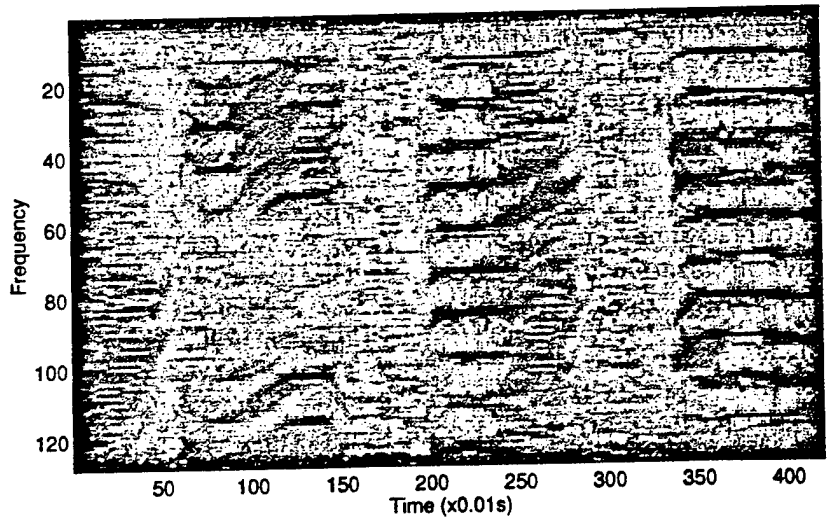


(f)

Fig. 13. (*Continued*)

speech signal in Fig. 13(a), from which we can see the structure of the speech signal. Figure 13(c) shows the waveforms of the received scrambled speech signal and the additive channel noise with SNR=16 dB. This additive noise cannot change the value of the synchronization impulses which are modulated by FM. Figure 13(d) shows the spectrograms for the scrambled speech signal and the additive channel noise. We can see that the structure of the signal in Fig. 13(b) was totally covered by an almost uniformly distributed noise-like spectrum. Figure 13(e) shows the waveforms of the descrambled speech signal. Figure 13(f) shows the spectrograms of the descrambled speech signal. We can see that some noises were introduced into the recovered results due to the channel noise, and that the spectrograms became a little blur. But the structure of the speech signal was perfectly recovered.

## 7. Concluding Remarks

In this paper we have presented a theory of impulsive control of chaotic dynamical systems. An estimate of the upper bound of the impulse interval $\Delta$ is also presented. Since all of our results are based on rigorous theoretical analysis and proofs, the results in this paper provide a framework and foundation for future works. We then use this theory to impulsively control and synchronize Chua's oscillators. An application of impulsive chaotic synchronization to secure communication is presented. The chaotic secure communication scheme presented here is a combination of a conventional cryptographic method and impulsive synchronization.

We present some simulation results to show the robustness of impulsive synchronization to additive channel noise and parameter mismatch. We find that the impulsive synchronization has the same degree of robustness to additive channel noise as that of continuous synchronization. Furthermore, we find that impulsive synchronization is much more robust to parameter mismatch than continuous synchronization.

## Acknowledgment

This work is supported by the Office of Naval Research under grant No. N00014-96-1-0753.

## References

Chen, G. & Dong, X. [1993] "From chaos to order — Perspectives and methodologies in controlling nonlinear dynamical systems," *Int. J. Bifurcation and Chaos* **3**(6), 1363–1409.

Chua, L. O., Yang, T., Zhong, G. Q. & Wu, C. W. [1996] "Adaptive synchronization of Chua's Oscillators," *Int. J. Bifurcation and Chaos* **6**(1), 189–201.

Chua, L. O. [1993] "Global unfolding of Chua's circuit," *IEICE Trans. Fundamentals* **E76-A**(5), 704–734.

Hunt, E. R. & Johnson, G. [1993] "Keeping chaos at bay," *IEEE Spectrum* **30**(11), 32–36.

Lakshmikantham, V., Bainov, D. D. & Simeonov, P. S. [1989] *Theory of Impulsive Differential Equations* (World Scientific, Singapore).

Ott, E., Grebogi, C. & Yorke, J. A. [1990] "Controlling chaos," *Phys. Rev. Lett.* **64**(11), 1196–1199.

Pyragas, K. [1992] "Continuous control of chaos by self-controlling feedback," *Phys. Lett.* **A170**(6), 421–428.

Samoilenko, A. M. & Perestyuk, N. A. [1995] *Impulsive Differential Equations* (World Scientific, Singapore).

Schweizer, J. & Kennedy, M. P. [1995] "Predictive Poincaré control: A control theory for chaotic systems," *Phys. Rev.* **E52**(5), 4865–4876.

Short, K. M. [1994] "Steps toward unmasking secure communications," *Int. J. Bifurcations and Chaos* **4**(4), 959–977.

Stojanovski, T., Kocarev, L. & Parlitz, U. [1996] "Driving and synchronizing by chaotic impulses," *Phys. Rev.* **E43**(9), 782–785.

Wu, C. W., Yang, T. & Chua, L. O. [1996] "On adaptive synchronization and control of nonlinear dynamical systems," *Int. J. Bifurcation and Chaos* **6**(3), 455–471.

Yang, T. [1995] "Recovery of digital signals from chaotic switching," *Int. J. Circ. Theor. Appl.* **23**(6), 611–615.

Yang, T., Wu, C. W. & Chua, L. O. [1997] "Cryptography based on chaotic systems," *IEEE Trans. Circ. Syst. I: Fundamental Theory and Applications* **44**(5) (in press).

International Journal of Bifurcation and Chaos, Vol. 7, No. 3 (1997) 671–679
© World Scientific Publishing Company

# MASTER-SLAVE SYNCHRONIZATION USING DYNAMIC OUTPUT FEEDBACK

J. A. K. SUYKENS*
*Katholieke Universiteit Leuven,*
*Department of Electrical Engineering, ESAT-SISTA,*
*Kardinaal Mercierlaan 94, B-3001 Leuven (Heverlee), Belgium*

P. F. CURRAN†
*145, Electronic and Electrical Engineering,*
*University College, Belfield, Dublin 4, Ireland*

L. O. CHUA‡
*Department of Electrical Engineering and Computer Science,*
*University of California at Berkeley, Berkeley, CA 94720, USA*

Received October 15, 1996; Revised November 8, 1996

A method of linear dynamic output feedback for master-slave synchronization of two identical Lur'e systems is introduced. In this scheme, synchronization is obtained using one or at least fewer measurement signals and control signals than the number of state variables of the Lur'e system. A sufficient condition for global asymptotic stability of the error system is derived from a quadratic Lyapunov function and is expressed as a matrix inequality. The dynamic controller is designed by solving a constrained nonlinear optimization problem. The method is demonstrated on Chua's circuit and a hyperchaotic circuit consisting of 2-double scroll cells.

## 1. Introduction

Present master-slave synchronization schemes for general classes of nonlinear systems, such as Lur'e systems, often assume full static state feedback, using the difference between the full state vectors as an error signal to synchronize the slave to the master system [Wu & Chua, 1994; Curran & Chua, 1997; Suykens & Vandewalle, 1997]. Only in more specific cases, such as Chua's circuit, has static state feedback been applied using fewer state variables [Kapitaniak *et al.*, 1994]. A natural question one may raise then is how synchronization could be obtained for a general class of nonlinear systems based on e.g. a single or fewer measurement signals and fewer control signals. In many practical situations, measuring all the state variables of the system is inconvenient or even impossible. A motivating application is in secure communication, where for implementational reasons the use of one single transmission signal is preferable over transmission of the full state vector of the system [Hasler, 1994; Wu & Chua, 1994].

It is well-known that there exists a close relationship between synchronization and control

*E-mail: johan.suykens@esat.kuleuven.ac.be
†E-mail: pcurran@acadamh.ucd.ie
‡E-mail: chua@fred.eecs.berkeley.edu

problems [Wu & Chua, 1994]. Therefore, in order to obtain synchronization based on fewer signals, we will adopt the idea of *dynamic output feedback* from control theory. When one is confronted with the problem of controlling some plant for which not all the state variables are measurable (lack of full state information), one either constructs an observer system to estimate the state of the plant, used in combination with state feedback, or one directly applies a dynamic output feedback law, from the measurable outputs to the actuator inputs. In *linear* control theory, these ideas are particularly well developed [Boyd & Barratt, 1991; Maciejowski, 1989]. An example is the LQG (Linear Quadratic Gaussian) regulator problem, which considers the optimal control of a linear system corrupted by process and measurement noise. The optimal solution by means of output feedback is given by a linear dynamic controller. For this controller the so-called separation principle holds, which means that one can split the controller into two parts: A dynamical observer system and a static state feedback applied to the observer estimated state [Boyd & Barratt, 1991; Maciejowski, 1989].

Although we are dealing in this paper with nonlinear rather than linear systems, we will investigate the application of a *linear* dynamic output feedback mechanism in order to synchronize two identical nonlinear systems. We consider a class of nonlinear systems which can be represented in Lur'e form [Khalil, 1992; Vidyasagar, 1993]. Examples of Lur'e systems are Chua's circuit [Chua *et al.*, 1986; Chua, 1994; Madan, 1993] and piecewise-linear versions of $n$-double scroll circuits [Suykens & Vandewalle, 1993; Arena *et al.*, 1996]. Arrays which consist of such circuits as cells with linear coupling between the cells can also be represented as Lur'e systems. Examples are the double-double scroll attractor [Kapitaniak & Chua, 1994] and the $n$-double scroll hypercube CNN [Suykens & Chua, 1997]. Furthermore, a Lur'e representation for generalized cellular neural networks has been derived in [Guzelis & Chua, 1993]. In this paper we derive a sufficient condition for synchronization of Lur'e systems based on a quadratic Lyapunov function. The condition is expressed as a matrix inequality (see [Boyd *et al.*, 1994] for an overview of linear matrix inequalities in systems and control theory) on which the design of the output feedback controller is based by solving a constrained nonlinear optimization problem. The controller design is illustrated both on a chaotic system (Chua's circuit) and a hyperchaotic system (coupled 2-double scroll cells). The dynamic control laws for achieving synchronization obtained are fairly simple and are of first and second order respectively.

This paper is organized as follows. In Sec. 2 we introduce the master-slave synchronization scheme with dynamic output feedback. In Sec. 3 we derive the error system and a sufficient condition for global asymptotic stability based on a quadratic Lyapunov function. In Sec. 4, design of the dynamic output feedback controller, based on the matrix inequality, is explained. Finally, in Sec. 5 the method is illustrated on a chaotic and a hyperchaotic Lur'e system, respectively Chua's circuit and a coupled system with 2-double scroll cells.

## 2. Synchronization Scheme

Let us introduce the following master-slave synchronization scheme

$$\mathcal{M}: \begin{cases} \dot{x} = Ax + B\sigma(Cx) \\ p = Hx \end{cases}$$

$$\mathcal{S}: \begin{cases} \dot{z} = Az + B\sigma(Cz) + Du \\ q = Hz \end{cases} \qquad (1)$$

$$\mathcal{C}: \begin{cases} \dot{\rho} = E\rho + G(p - q) \\ u = M\rho + N(p - q) \end{cases}$$

which consists of a master system $\mathcal{M}$, a slave system $\mathcal{S}$ and a controller $\mathcal{C}$ (Fig. 1). The master system is a Lur'e system with state vector $x \in \mathbb{R}^n$ and matrices $A \in \mathbb{R}^{n \times n}$, $B \in \mathbb{R}^{n \times n_h}$, $C \in \mathbb{R}^{n_h \times n}$. A Lur'e system is a linear dynamical system, feedback interconnected to a static nonlinearity $\sigma(\cdot)$ that satisfies a sector condition [Khalil, 1992; Vidyasagar, 1993] (here it has been represented as a recurrent neural network with one hidden layer, activation function $\sigma(\cdot)$ and $n_h$ hidden units [Suykens *et al.*, 1996]). We assume that $\sigma(\cdot)$: $\mathbb{R}^{n_h} \mapsto \mathbb{R}^{n_h}$ is a diagonal nonlinearity with $\sigma_i(\cdot)$ belonging to sector $[0, k]$ for $i = 1, \ldots, n_h$. The output vector of the master system is $p \in \mathbb{R}^l$, with $l \leq n$. The slave system consists of an identical Lur'e system with state vector $z \in \mathbb{R}^n$, but is controlled by means of the control vector $u \in \mathbb{R}^m$ through the matrix $D \in \mathbb{R}^{n \times m}$. The signal $u$ is the output of a linear dynamic output feedback controller. The input of this controller is the difference between the outputs of the master and the slave system, i.e. $p$ and $q$.

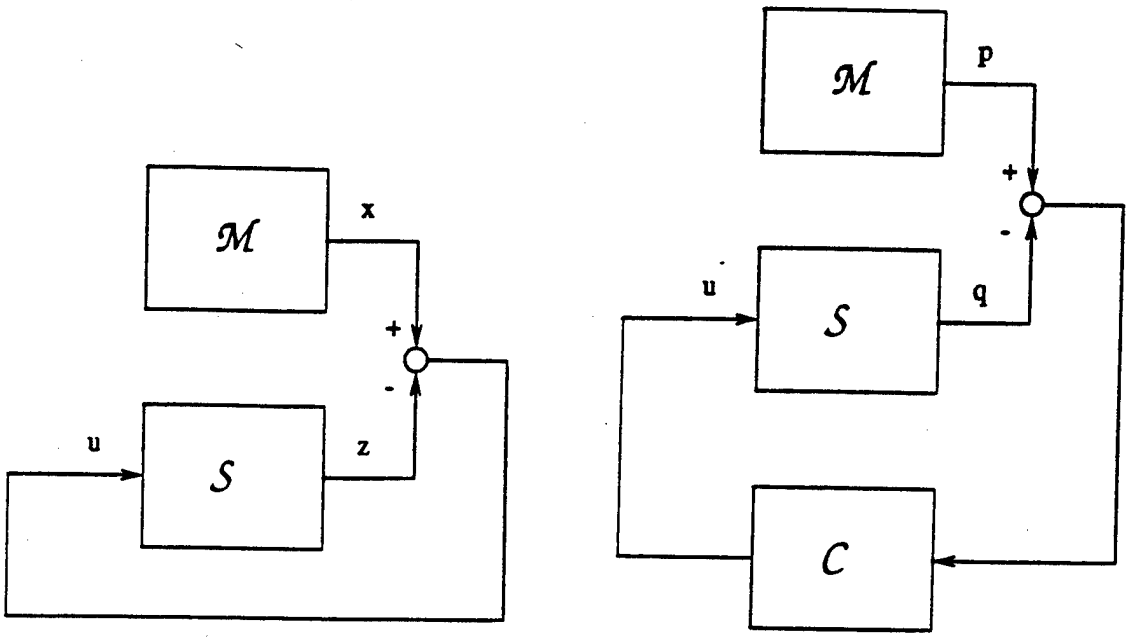


Fig. 1. This figure illustrates the difference between full static state feedback (a), and dynamic output feedback (b), for master-slave synchronization of Lur'e systems: (a) the slave system $\mathcal{S}$ is synchronized to the master system $\mathcal{M}$ by taking the difference between the state vectors $x$, $z \in \mathbf{R}^n$ and applying a feedback matrix. (b) output variables $p$, $q \in \mathbf{R}^l$ are defined with $l \leq n$. A linear dynamic output feedback controller is taken instead of a static feedback controller. For the control vector $u \in \mathbf{R}^m$ one has $m \leq n$.

The linear dynamic controller has the state vector $\rho \in \mathbb{R}^{n_c}$ and consists of the matrices $E \in \mathbb{R}^{n_c \times n_c}$, $G \in \mathbb{R}^{n_c \times l}$, $M \in \mathbb{R}^{m \times n_c}$, $N \in \mathbb{R}^{m \times l}$. In previous work on master-slave synchronization, only full static state error feedback $u = F_s(x - z)$ or static output feedback $u = F_o(p - q)$ have been considered with $F_s \in \mathbb{R}^{n \times n}$, $F_o \in \mathbb{R}^{m \times l}$ [Wu & Chua, 1994; Kapitaniak *et al.*, 1994; Curran & Chua, 1997; Suykens & Vandewalle, 1997].

## 3. Error System and Global Asymptotic Stability

We define the error signal $e = x - z$, which yields the error system:

$$\begin{bmatrix} \dot{e} \\ \dot{\rho} \end{bmatrix} = \begin{bmatrix} A - DNH & -DM \\ GH & E \end{bmatrix} \begin{bmatrix} e \\ \rho \end{bmatrix} + \begin{bmatrix} B \\ 0 \end{bmatrix} \eta(Ce; z) \tag{2}$$

with nonlinearity $\eta(Ce; z) = \sigma(Ce + Cz) - \sigma(Cz)$. Assume that the nonlinearity $\eta(Ce; z)$ belongs to sector $[0, k]$ [Curran & Chua, 1997; Suykens & Vandewalle, 1997]:

$$0 \leq \frac{\eta_i(c_i^T e; z)}{c_i^T e} = \frac{\sigma_i(c_i^T e + c_i^T z) - \sigma(c_i^T z)}{c_i^T e} \leq k\,, \quad \forall e, z; \quad i = 1, \ldots, n_h \quad (c_i^T e \neq 0)\,. \tag{3}$$

The following inequality then holds [Boyd *et al.*, 1994; Khalil, 1992; Vidyasagar, 1993]:

$$\eta_i(c_i^T e; z)[\eta_i(c_i^T e; z) - k c_i^T e] \leq 0\,, \quad \forall e, z; \quad i = 1, \ldots, n_h\,. \tag{4}$$

It follows from the mean value theorem that for differentiable $\sigma(\cdot)$ the sector condition $[0, k]$ on $\eta(\cdot)$ corresponds to [Curran & Chua, 1997]:

$$0 \leq \frac{d}{d\rho}\sigma_i(\rho; z) \leq k, \quad \forall \rho, z; \quad i = 1, \ldots, n_h\,. \tag{5}$$

We are interested to see under what condition the error system is globally asymptotically stable, which means that whatever the choice of the initial states $x(0)$, $z(0)$, $\rho(0)$, the error $\|[x - z; \rho]\|_2 \to 0$ as $t \to \infty$. Defining the state vector $\xi = [e; \rho]$ and taking a positive definite quadratic Lyapunov

function (which is radially unbounded)

$$V(\xi) = \xi^T P \xi = [e^T \rho^T] \begin{bmatrix} P_{11} & P_{12} \\ P_{21} & P_{22} \end{bmatrix} \begin{bmatrix} e \\ \rho \end{bmatrix}, \quad P = P^T > 0, \tag{6}$$

a sufficient condition for global asymptotic stability of Eq. (2) is derived in the following Theorem.

**Theorem.** *Let $\Lambda = \mathrm{diag}\{\lambda_i\}$ be a diagonal matrix with $\lambda_i \geq 0$ for $i = 1, \ldots, n_h$. Then a sufficient condition for global asymptotic stability of the error system of Eq. (2) is given by the matrix inequality*

$$Y = Y^T = \begin{bmatrix} Y_{11} & Y_{12} & Y_{13} \\ \cdot & Y_{22} & Y_{23} \\ \cdot & \cdot & Y_{33} \end{bmatrix} < 0 \tag{7}$$

*where*

$$\begin{aligned} Y_{11} &= (A - DNH)^T P_{11} + P_{11}(A - DNH) \\ &\quad + H^T G^T P_{21} + P_{12} GH \\ Y_{12} &= (A - DNH)^T P_{12} + H^T G^T P_{22} \\ &\quad - P_{11} DM + P_{12} E \\ Y_{13} &= P_{11} B + kC^T \Lambda \\ Y_{22} &= E^T P_{22} + P_{22} E - M^T D^T P_{12} - P_{21} DM \\ Y_{23} &= P_{21} B \\ Y_{33} &= -2\Lambda . \end{aligned}$$

*Proof.* Taking the time-derivative of the Lyapunov function, applying the $S$-procedure [Boyd *et al.*, 1994] and using the inequalities of Eq. (4), one obtains:

$$\begin{aligned} \dot{V} &= \dot{\xi}^T P \xi + \xi^T P \dot{\xi} \\ &\leq \dot{\xi}^T P \xi + \xi^T P \dot{\xi} - \sum_i 2\lambda_i \eta_i (\eta_i - k c_i^T e) \\ &\leq [(A - DNH)e - DM\rho + B\eta]^T (P_{11} e + P_{12} \rho) \\ &\quad + (E\rho + GHe)^T (P_{21} e + P_{22} \rho) \\ &\quad + (e^T P_{11} + \rho^T P_{21})[(A - DNH)e - DM\rho + B\eta] \\ &\quad + (e^T P_{12} + \rho^T P_{22})(E\rho + GHe) \\ &\quad - 2\eta^T \Lambda (\eta - kCe) \\ &\leq \zeta^T Y \zeta < 0 \end{aligned}$$

where $\zeta = [e; \rho; \eta]$. The latter expression is negative for all non-zero $\zeta$ provided $Y$ is negative definite. ■

## 4. Controller Design

The dynamic output feedback controller $\mathcal{C}$ can be designed on the basis of matrix inequality Eq. (7) by solving the following nonlinear optimization problem:

$$\min_{E,G,M,N,P,\Lambda} \lambda_{\max}[Y(E, G, M, N, P, \Lambda)], \quad \text{such that} \begin{cases} P = P^T > 0 \\ \Lambda \geq 0 \text{ and diagonal} \end{cases} \tag{8}$$

where $\lambda_{\max}[\cdot]$ denotes the maximal eigenvalue of a symmetric matrix. When the maximal eigenvalue of $Y$ is negative, a feasible point to the matrix inequality is obtained, resulting in a controller which synchronizes the Lur'e systems. However, the optimization problem of Eq. (8) is non-convex. It may also become non-differentiable when the two largest eigenvalues of the matrix $Y$ coincide. Convergent algorithms for this kind of non-differentiable optimization problem have been described e.g. in [Polak & Wardi, 1982]. The constraint $P > 0$ can be eliminated by considering the parameterization $P = Q^T Q$. A similar idea applies to $\Lambda$. The optimization problem becomes then

$$\min_{E,G,M,N,Q,\Lambda} \lambda_{\max}[Y(E, G, M, N, Q, \Lambda)]. \tag{9}$$

## 5. Examples

### 5.1. *Chua's circuit*

In this example we consider master-slave synchronization of two identical Chua's circuits using linear dynamic output feedback. We take the following representation of Chua's circuit:

$$\begin{cases} \dot{x}_1 = \alpha[x_2 - h(x_1)] \\ \dot{x}_2 = x_1 - x_2 + x_3 \\ \dot{x}_3 = -\beta x_2 \end{cases} \tag{10}$$

with nonlinear characteristic

$$h(x_1) = m_1 x_1 + \frac{1}{2}(m_0 - m_1)(|x_1 + c| - |x_1 - c|) \tag{11}$$

and parameters $\alpha = 9$, $\beta = 14.286$, $m_0 = -1/7$, $m_1 = 2/7$ in order to obtain the double scroll attractor [Chua *et al.*, 1986; Chua, 1994; Madan, 1993]. The nonlinearity $\varphi(x_1) = \frac{1}{2}(|x_1 + c| - |x_1 - c|)$ (linear characteristic with saturation) belongs to

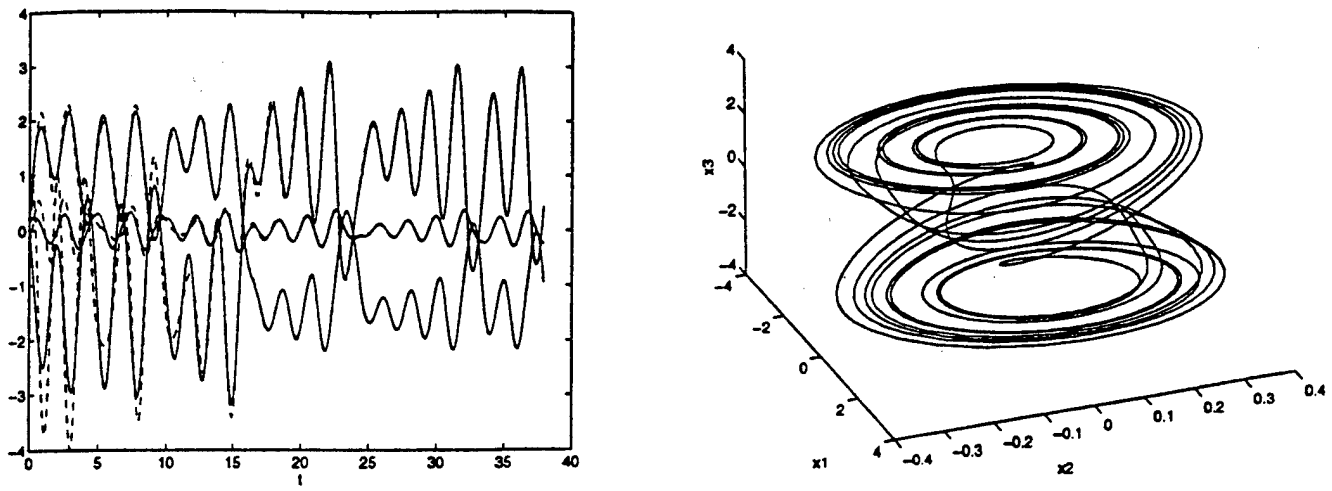


(a) (b)

Fig. 2. This figure shows master-slave synchronization of two identical Chua's circuits using a first order linear dynamic output feedback controller. One single output and control signal have been used. (a) Shown are the state variables of the Chua's circuits with respect to time for a randomly chosen initial condition: (-) master system, (- -) slave system. (b) three-dimensional view on the double scroll attractor generated at the master system.

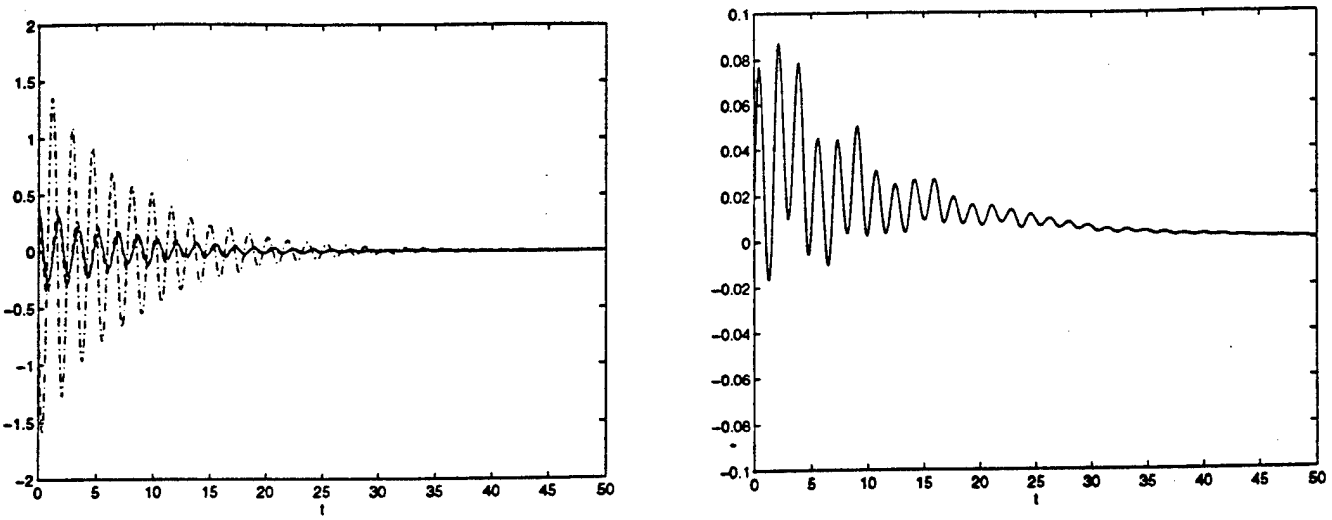


(a) (b)

Fig. 3. Chua's circuit (continued). (a) error signal $x - z$ with respect to time: (-) $x_1 - z_1$, (- -) $x_2 - z_2$, (-.) $x_3 - z_3$. (b) state variable $\rho$ of the controller with respect to time.

sector $[0, 1]$. Hence Chua's circuit can be interpreted as the Lur'e system $\dot{x} = Ax + B\varphi(Cx)$ where

$$A = \begin{bmatrix} -\alpha m_1 & \alpha & 0 \\ 1 & -1 & 1 \\ 0 & -\beta & 0 \end{bmatrix}, \quad B = \begin{bmatrix} -\alpha(m_0 - m_1) \\ 0 \\ 0 \end{bmatrix},$$

$$C = [1 \quad 0 \quad 0]. \tag{12}$$

Suppose now that we measure the first state variables $x_1$ and $z_1$ only in order to synchronize the circuits and that we take just one control signal to control the slave system. This corresponds to the choice $H = [1\ 0\ 0]$, $D = [1; 0; 0]$ $(l = m = 1)$. Controllers of order 1, 2 and 3 have been designed based on the optimization problem of Eq. (9). We report the results here for the simplest controller with

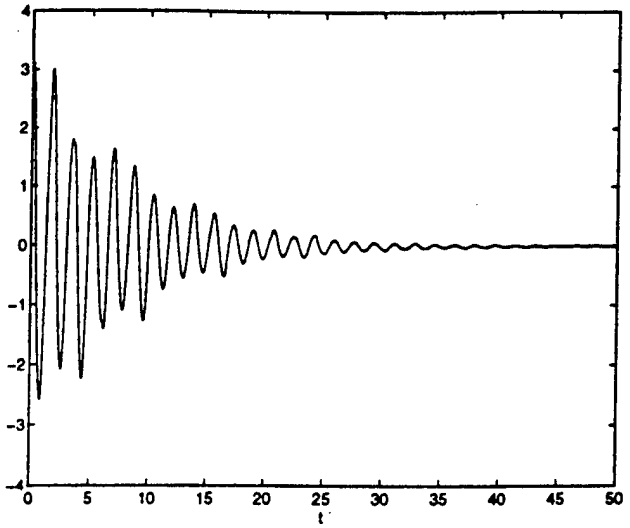


Fig. 4. Chua's circuit (continued). Control signal $u$ with respect to time, applied to the slave system using the first order linear dynamic output feedback controller.

$n_c = 1$. A 2-norm constraint on the controller parameter vector $[E(:); G(:); M(:); N(:)]$ $(< 10)$ has been used for Eq. (9), where ":" denotes a column-wise scanning of a matrix. Sequential quadratic programming [Fletcher, 1987] has been applied in order to optimize Eq. (9) using Matlab's optimization toolbox (function *constr*). As starting point for the iterative procedure, a random controller parameter vector has been chosen according to a normal distribution with zero mean and variance 0.1. For the matrix $Q$, a square random matrix was chosen according to the same distribution but with variance equal to 3. The matrix $\Lambda$ has been initialized as $100\,I$. Simulation results for master-slave synchronization of the Chua's circuits are shown in Figs. 2–4 for the resulting controller

$$\left[\begin{array}{c|c} E & G \\ \hline M & N \end{array}\right] = \left[\begin{array}{c|c} -0.1403 & 0.6492 \\ \hline -0.8758 & 9.9394 \end{array}\right].$$

The systems have been simulated using a Runge–Kutta integration rule with adaptive step size (*ode23* in Matlab) [Parker & Chua, 1989].

## 5.2. *Hyperchaotic system with 2-double scroll cells*

In this example we consider master-slave synchronization for a special case of the $n$-double scroll hypercube CNN, which consist of two 2-double scroll cells with unidirectional coupling between the cells [Suykens & Chua, 1997]. The system is described by

$$\begin{cases} \dot{x}_1 = \alpha[x_2 - h(x_1)] \\ \dot{x}_2 = x_1 - x_2 + x_3 \\ \dot{x}_3 = -\beta x_2 \\ \dot{x}_4 = \alpha[x_5 - h(x_4)] + K(x_4 - x_1) \\ \dot{x}_5 = x_4 - x_5 + x_6 \\ \dot{x}_6 = -\beta x_5 \end{cases} \tag{13}$$

with, as nonlinear function, the piecewise linear characteristic:

$$h(x_1) = m_{2n-1}x_1 + \frac{1}{2}\sum_{i=1}^{2n-1}(m_{i-1} - m_i) \times(|x_1 + c_i| - |x_1 - c_i|), \tag{14}$$

consisting of $2(2n-1)$ breakpoints, where $n$ is a natural number which determines the number of scrolls obtained. An isolated cell behaves as a 2-double scroll for $\alpha = 9$, $\beta = 14.286$, $m_0 = -1/7$, $m_1 = 2/7$, $m_2 = -4/7$, $m_3 = m_1$, $c_1 = 1$, $c_2 = 2.15$, $c_3 = 3.6$. For weak coupling between the two cells, hyperchaos is obtained with two positive Lyapunov exponents, as shown in [Suykens & Chua, 1997]. We choose $K = 0.01$ for the unidirectional coupling constant in Eq. (13).

A Lur'e representation $\dot{x} = Ax + B\varphi(Cx)$ for the system Eq. (13) is given by:

$$A = \left[\begin{array}{ccc|ccc} -\alpha m_1 & \alpha & 0 & 0 & 0 & 0 \\ 1 & -1 & 1 & 0 & 0 & 0 \\ 0 & -\beta & 0 & 0 & 0 & 0 \\ \hline 0 & 0 & 0 & -\alpha m_1 & \alpha & 0 \\ 0 & -K & 0 & 1 & -1+K & 1 \\ 0 & 0 & 0 & 0 & -\beta & 0 \end{array}\right],$$

$$B = \left[\begin{array}{ccc|ccc} b_{11} & b_{12} & b_{13} & 0 & 0 & 0 \\ 0 & 0 & 0 & 0 & 0 & 0 \\ 0 & 0 & 0 & 0 & 0 & 0 \\ \hline 0 & 0 & 0 & b_{11} & b_{12} & b_{13} \\ 0 & 0 & 0 & 0 & 0 & 0 \\ 0 & 0 & 0 & 0 & 0 & 0 \end{array}\right],$$

$$C = \left[\begin{array}{ccc|ccc} 1 & 0 & 0 & 0 & 0 & 0 \\ 1 & 0 & 0 & 0 & 0 & 0 \\ 1 & 0 & 0 & 0 & 0 & 0 \\ \hline 0 & 0 & 0 & 1 & 0 & 0 \\ 0 & 0 & 0 & 1 & 0 & 0 \\ 0 & 0 & 0 & 1 & 0 & 0 \end{array}\right] \tag{15}$$

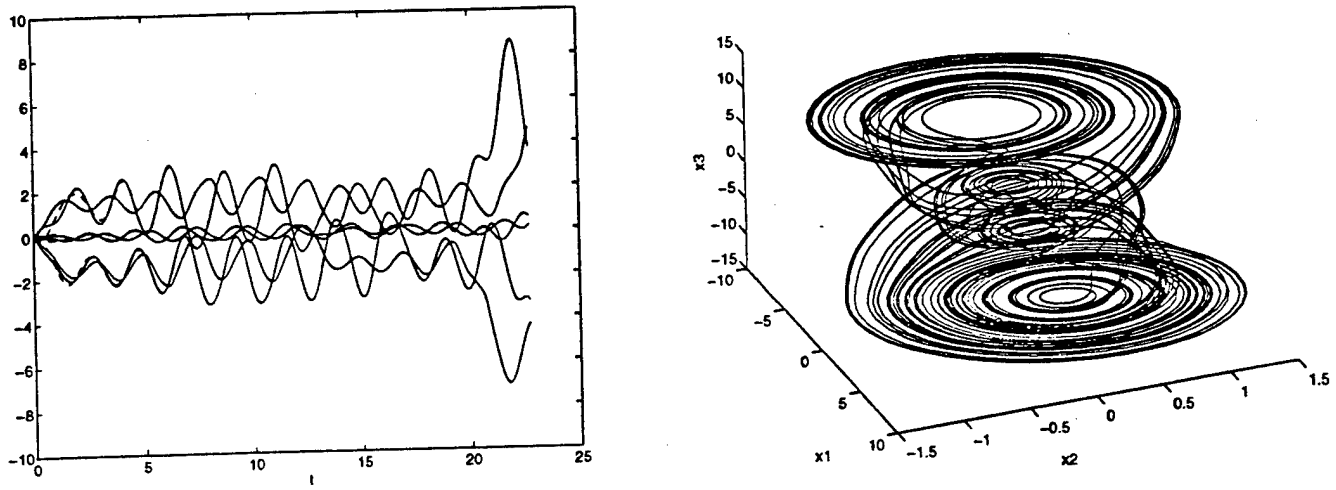


(a) (b)

Fig. 5. This figure shows master-slave synchronization between two identical hyperchaotic systems, that consist of two unidirectionally coupled 2-double scroll cells, using a second order dynamic output feedback controller. (a) Shown are the state variables of the 6-dimensional circuit with respect to time for a randomly chosen initial condition: (-) master system, (- -) slave system. (b) three-dimensional view on the 2-double scroll attractor generated at the first cell.

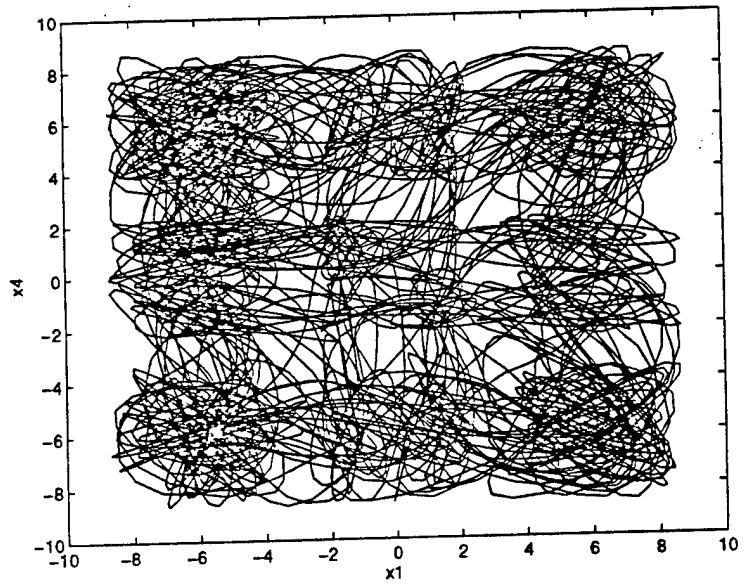


Fig. 6. 2-double scroll cells (continued). For weak coupling between the two 2-double scroll cells, a 2-double scroll square is obtained in the common cell space $(x_1, x_4)$ as a special case of the $n$-double scroll hypercube CNN [Suykens & Chua, 1997].

with $b_{11} = -\alpha(m_0 - m_1)$, $b_{12} = -\alpha(m_1 - m_2)$, $b_{13} = -\alpha(m_2 - m_3)$. The nonlinearity $\varphi(\cdot)$: $\mathbb{R}^6 \mapsto \mathbb{R}^6$ belongs to sector $[0, 1]$ with $\varphi_i(x_1) = \frac{1}{2}(|x_1 + c_i| - |x_1 - c_i|)$ $(i = 1, 2, 3)$ and $\varphi_i(x_4) = \frac{1}{2}(|x_4 + c_{i-3}| - |x_4 - c_{i-3}|)$ $(i = 4, 5, 6)$.

We consider two identical Lur'e systems Eq. (15) for the master and slave system. In order to synchronize the systems by means of linear dynamic output feedback, we define two outputs and two control signals $(l = m = 2)$ as:

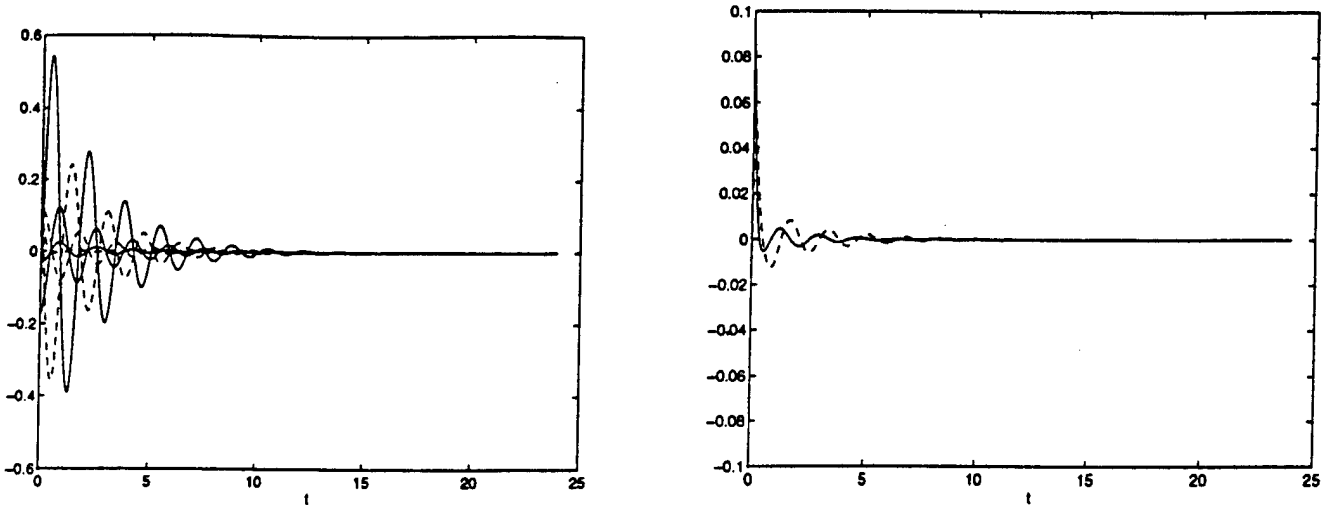


(a) (b)

Fig. 7. 2-double scroll cells (continued). (a) error signal $x - z$ with respect to time: (-) $x_i - z_i$ for $i = 1, 2, 3$, (- -) $x_i - z_i$ for $i = 4, 5, 6$. (b) state variables $\rho$ of the controller with respect to time.

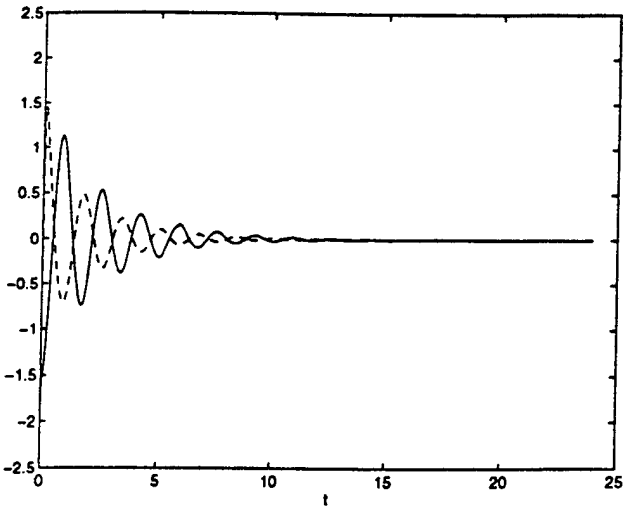


Fig. 8. 2-double scroll cells (continued). Control signals $u$ with respect to time, applied to the slave system using the linear dynamic output feedback controller.

$$H = \begin{bmatrix} 1 & 0 & 0 & 0 & 0 & 0 \\ 0 & 0 & 0 & 1 & 0 & 0 \end{bmatrix}, \quad D = \begin{bmatrix} 1 & 0 \\ 0 & 0 \\ 0 & 0 \\ 0 & 1 \\ 0 & 0 \\ 0 & 0 \end{bmatrix}. \tag{16}$$

We demonstrate the method for a second order controller ($n_c = 2$). A 2-norm constraint on the controller parameter vector $[E(:); G(:); M(:); N(:)]$ ($< 80$) has been taken into account for Eq. (9). As starting point for sequential quadratic programming in order to optimize Eq. (9), a random controller parameter vector has been chosen according to a normal distribution with zero mean and variance 0.1. For the matrix $Q$ a square random matrix was chosen according to the same distribution but with variance equal to 3. The matrix $\Lambda$ has been initialized as $1000\,I$. Simulation results are shown in Figs. 5–8 for the resulting controller

$$\left[\begin{array}{c|c} E & G \\ \hline M & N \end{array}\right] = \left[\begin{array}{cc|cc} 0.3729 & -4.7355 & -2.3533 & -4.1974 \\ 8.4883 & -19.5393 & -8.6672 & 6.3477 \\ \hline -7.2920 & -2.3984 & 45.4291 & 5.2582 \\ -38.8729 & 7.9657 & -16.7269 & 42.0817 \end{array}\right].$$

## 6. Conclusion

In this paper a linear dynamic output feedback mechanism has been introduced for master-slave synchronization of Lur'e systems. Rather than using the error between the full state vectors to synchronize the systems, the scheme enables one to use fewer measurement signals and fewer control signals than the number of state variables of the Lur'e systems. A sufficient condition for global asymptotic stability of the error system has been derived based

on a quadratic Lyapunov function. The controller design is achieved by solving a constrained nonlinear optimization problem, based on the derived matrix inequality. The method has been illustrated on Chua's circuit and a hyperchaotic system that consists of coupled 2-double scroll cells.

## Acknowledgment

This research work was carried out at the University of California at Berkeley, in the framework of the Belgian Programme on Interuniversity Poles of Attraction, initiated by the Belgian State, Prime Minister's Office for Science, Technology and Culture (IUAP-17) and in the framework of a Concerted Action Project MIPS (Model-based Information Processing Systems) of the Flemish Community. The work is supported in part by the Office of Naval Research under grant N00014-96-1-0753 and the Fulbright Fellowship Program.

## References

Arena, P., Baglio, P., Fortuna, F. & Manganaro, G. [1996] "Generation of $n$-double scrolls via cellular neural networks," *Int. J. Circ. Theor. Appl.* **24**, 241–252.

Boyd, S. & Barratt, C. [1991] *Linear Controller Design, Limits of Performance* (Prentice-Hall).

Boyd, S., El Ghaoui, L., Feron, E. & Balakrishnan, V. [1994] *Linear Matrix Inequalities in System and Control Theory* SIAM (Studies in Applied Mathematics), Vol. 15.

Chua, L. O., Komuro, M. & Matsumoto, T. [1986] "The double scroll family," *IEEE Trans. Circ. Syst. I* **33**(11), 1072–1118.

Chua, L. O. [1994] "Chua's circuit 10 years later," *Int. J. Circ. Theor. Appl.* **22**, 279–305.

Curran, P. F. & Chua, L. O. [1997] "Absolute stability theory and the synchronization problem," *Int. J. Bifurcation and Chaos*, to appear.

Fletcher, R. [1987] *Practical Methods of Optimization* (John Wiley and Sons, Chichester and New York).

Guzelis, C. & Chua, L. O. [1993]. "Stability analysis of generalized cellular neural networks," *Int. J. Circ. Theor. Appl.* **21**, 1–33.

Hasler, M. [1994] "Synchronization principles and applications," *Circ. Syst.: Tutorials IEEE-ISCAS '94*, 314–326.

Kapitaniak, T. & Chua, L. O. [1994] "Hyperchaotic attractors of unidirectionally-coupled Chua's Circuits," *Int. J. Bifurcation and Chaos* **4**(2), 477–482.

Kapitaniak, T., Chua, L. O. & Zhong, G.-Q. [1994] "Experimental synchronization of chaos using continuous controls," *Int. J. Bifurcation and Chaos* **4**(2), 483–488.

Khalil, H. K. [1992] *Nonlinear Systems* (Macmillan Publishing Company, New York).

Maciejowski, J. M. [1989] *Multivariable Feedback Design* (Addison-Wesley).

Madan, R. N. (Guest Editor) [1993] *Chua's Circuit: A Paradigm for Chaos* (World Scientific, Singapore).

Parker, T. S. & Chua, L. O. [1989] *Practical Numerical Algorithms for Chaotic Systems* (Springer-Verlag, New York).

Polak, E. & Wardi, Y. [1982] "Nondifferentiable optimization algorithm for designing control systems having singular value inequalities," *Automatica* **18**(3), 267–283.

Suykens, J. A. K. & Vandewalle, J. [1993] "Generation of $n$-double scrolls ($n = 1, 2, 3, 4, \ldots$)," *IEEE Trans. Circ. Syst. I* **40**(11), 861–867.

Suykens, J. A. K., Vandewalle, J. P. L. & De Moor, B. L. R. [1996] *Artificial Neural Networks for Modelling and Control of Non-Linear Systems* (Kluwer Academic Publishers, Boston).

Suykens, J. A. K. & Vandewalle, J. [1997] "Master-slave synchronization of Lur'e systems," *Int. J. Bifurcation and Chaos*, this issue.

Suykens, J. A. K. & Chua, L. O. [1997] "$n$-double scroll hypercubes in 1-D CNNs," *Int. J. Bifurcation and Chaos*, to appear.

Vidyasagar, M. [1993] *Nonlinear Systems Analysis* (Prentice-Hall).

Wu, C. W. & Chua, L. O. [1994] "A unified framework for synchronization and control of dynamical systems," *Int. J. Bifurcation and Chaos* **4**(4), 979–989.

Letters

International Journal of Bifurcation and Chaos, Vol. 7, No. 3 (1997) 665–669
© World Scientific Publishing Company

# MASTER-SLAVE SYNCHRONIZATION OF LUR'E SYSTEMS

J. A. K. SUYKENS* and J. VANDEWALLE†
*Katholieke Universiteit Leuven,*
*Department of Electrical Engineering, ESAT-SISTA,*
*Kardinaal Mercierlaan 94, B-3001 Leuven (Heverlee), Belgium*

Received July 2, 1996

In this paper we present a sufficient condition for master-slave synchronization of Lur'e systems. The scheme makes use of linear full static state feedback. The criterion is based on a Lur'e–Postnikov Lyapunov function for global asymptotic stability of the error system. The condition is basically the same as the one for global asymptotic stability of the Lur'e system, controlled with linear state feedback. The design of the feedback matrix is done by solving a constrained nonlinear optimization problem. The method is illustrated on the synchronization of Chua's circuit.

## 1. Introduction

Recently there is a lot of interest in the use of synchronization for secure communication applications. In [Hasler, 1994] an overview of methods for synchronization is presented, including decomposition into subsystems, linear feedback and an inverse system approach. In order to use synchronization in transmission systems, a useful information-carrying signal is transmitted, hidden in a chaotic signal. Methods for hiding the information are, e.g. chaotic masking, chaotic switching and direct chaotic modulation.

The work described in this paper is related to synchronization by linear feedback, which investigates the problem from the viewpoint of control theory. It has already been shown that there is a close relationship between the synchronization problem and the problem of controlling chaos by linear feedback [Chen, 1993; Hasler, 1994; Wu & Chua, 1994]. The same observation will be made here based upon a matrix inequality, that expresses a sufficient condition for global asymptotic stability of the error system. Conditions for synchronization of general nonlinear systems have been derived for quadratic Lyapunov functions [Wu & Chua, 1994, 1995]. The condition proved in this paper, is derived from a Lur'e–Postnikov Lyapunov function, which consists of a quadratic Lyapunov function plus integral term. We consider Lur'e systems which consist of a linear dynamical system, feedback interconnected to a static nonlinearity that satisfies a sector condition. Many nonlinear systems can be represented in this form, including e.g. Chua's circuit [Guzelis & Chua, 1993]. The fact that the nonlinearities satisfy a sector condition is exploited to derive the matrix inequality. It also yields a systematic procedure for designing the feedback matrix, by solving a constrained nonlinear optimization problem. Finally,

Author to whom correspondence should be addressed
*E-mail: Johan.Suykens@esat.kuleuven.ac.be
†E-mail: Joos.Vandewalle@esat.kuleuven.ac.be

in order to use this method for chaotic masking, Lur'e systems that reveal high dimensional chaos should be used in order to obtain secure communication schemes. Generalized cellular neural networks that generate high dimensional chaos are possible candidates for that purpose: they have been represented as Lur'e systems in [Guzelis & Chua, 1993].

This paper is organized as follows. In Sec. 2 we present the matrix inequality condition for synchronization of Lur'e systems. In Sec. 3 we illustrate the method on synchronizing Chua's circuit.

## 2. Matrix Inequality for Synchronization of Lur'e Systems

Let us consider a Lur'e system, which is of the form [Boyd *et al.*, 1994; Khalil, 1992; Narendra & Taylor, 1973]:

$$\begin{aligned} \dot{x} &= Ax + Bu \\ y &= Cx \\ u &= \sigma(y)\,, \end{aligned} \tag{1}$$

consisting of a linear dynamical system, feedback interconnected to static nonlinearities $\sigma_i(\cdot)$ that satisfy sector condition $[0,\ k]$ for all $i = 1, \ldots, n_h$; with state vector $x(t) \in \mathbb{R}^n$ and matrices $A \in \mathbb{R}^{n\times n}$, $B \in \mathbb{R}^{n\times n_h}$, $C \in \mathbb{R}^{n_h\times n}$. Using two identical Lur'e systems in a master-slave synchronization scheme with linear full static state feedback, one has:

$$\begin{cases} (\mathcal{M})\ \dot{x} = Ax + B\sigma(Cx) \\ (\mathcal{S})\ \dot{z} = Az + B\sigma(Cz) + F(x - z) \end{cases} \tag{2}$$

with master $\mathcal{M}$ and slave $\mathcal{S}$ and feedback matrix $F \in \mathbb{R}^{n\times n}$. The aim of synchronization is then to obtain $\|x(t) - z(t)\| \to 0$ for time $t \to \infty$. Defining the error signal $e = x - z$, one obtains the error system:

$$\dot{e} = (A - F)e + B\eta(Ce) \tag{3}$$

with $\eta(Ce) = \sigma(Ce + Cz) - \sigma(Cz)$. In the sequel we use the shorthand notation $\eta$ for $\eta(Ce)$. Assume a sector condition $[0,\ k]$ on $\eta(\cdot)$ which gives the following inequalities for $\eta$:

$$\eta_i[\eta_i - kc_i^T e] \leq 0, \quad i = 1, \ldots, n_h \ \ \forall x,\, z \in \mathbb{R}^n\,, \tag{4}$$

where $c_i^T$ denotes the $i$th row of $C$.

Now we investigate under what condition the error signal goes to zero, whatever the choice of the initial states $x(0)$, $z(0)$. Therefore we take the Lur'e–Postnikov Lyapunov function:

$$V(e) = e^T P e + \sum_{i=1}^{n_h} 2\gamma_i \int_0^{c_i^T e} \eta_i(\rho) k d\rho \tag{5}$$

with $P = P^T > 0$ and $\gamma_i \geq 0$ (assume $z$ is quasi constant with respect to error dynamics). This function is positive everywhere and radially unbounded and is used in order to show under which condition the error system is globally asymptotically stable with unique equilibrium point $e = 0$. The following Theorem is obtained:

**Theorem.** *Let $\Gamma = \mathrm{diag}\{\gamma_i\}$, $T = \mathrm{diag}\{\tau_i\}$ be diagonal matrices with $\gamma_i,\ \tau_i \geq 0$ for $i = 1, \ldots, n_h$. Then, if there exist $P = P^T > 0$, $\Gamma$, $T$ and a feedback matrix $F$ such that*

$$Y = Y^T = \begin{bmatrix} (A - F)^T P + P(A - F) & PB + kC^T T + k(A - F)^T C^T \Gamma \\ B^T P + kTC + k\Gamma C(A - F) & -2T + k\Gamma CB + kB^T C^T \Gamma \end{bmatrix} < 0 \tag{6}$$

*then based upon (5) the system (2) synchronizes, with error system (3) having a unique and globally asymptotically stable equilibrium point $e = 0$.*

*Proof.* Taking the time derivative of (5) and applying the $\mathcal{S}$-procedure [Boyd *et al.*, 1994] by using the inequalities (4), one obtains:

$$\dot{V} = \dot{e}^T P e + e^T P \dot{e} + \sum_i 2\gamma_i \eta_i (c_i^T e) k c_i^T \dot{e} \leq [(A - F)e + B\eta]^T P e + e^T P[(A - F)e + B\eta]$$

$$+ \sum_i 2\gamma_i \eta_i (c_i^T e) k c_i^T [(A - F)e + B\eta] - \sum_i 2\tau_i \eta_i [\eta_i - kc_i^T e]\,.$$

Writing this as a quadratic form in $[e;\ \eta]$ one obtains

$$\dot{V} \leq [e^T\ \eta^T] Y \begin{bmatrix} e \\ \eta \end{bmatrix} < 0\,.$$

This expression is negative $\forall$ nonzero $x,\ z \in \mathbb{R}^n$ if $Y$ is negative definite. ■

*Remarks*

- The condition for global asymptotic stability of a Lur'e system, stabilized by linear state feedback:

$$\dot{x} = Ax + B\sigma(Cx) + u, \quad u = Kx \qquad (7)$$

leads to the same condition as (6), if one takes the Lyapunov function

$$V(x) = x^T P x + \sum_i^{n_h} 2\gamma_i \int_0^{c_i^T x} \sigma_i(\rho) k d\rho \qquad (8)$$

with $P = P^T > 0$, $\gamma_i \geq 0$. The same observation of similarity between this stabilization problem and the synchronization problem has been made, e.g. in Wu & Chua [1994].

- For a given Lur'e system and feedback matrix $F$, one has a linear matrix inequality (LMI) in the unknown matrices $P$, $\Gamma$, $T$. Finding these unknown matrices corresponds to solving a convex optimization problem [Boyd *et al.*, 1994]. The overall design problem of finding a feedback matrix $F$ together with $P$, $\Gamma$, $T$ such that (6) is satisfied however leads to a nonconvex optimization problem.

## 3. Example: Synchronization of Chua's Circuit

In order to illustrate the previous Theorem, let us consider the master-slave synchronization problem for Chua's circuit:

$$\begin{cases} (\mathcal{M})\ \dot{x} = A_c x + B_c g(C_c x) \\ (\mathcal{S})\ \dot{z} = A_c z + B_c g(C_c z) + F(x - z) \end{cases} \qquad (9)$$

A Chua's circuit generates the double scroll attractor [Chua *et al.*, 1986] for

$$A_c = \begin{bmatrix} -6.3 & 6.3 & 0 \\ 0.7 & -0.7 & 1 \\ 0 & -7 & 0 \end{bmatrix},$$

$$B_c = \begin{bmatrix} -9 \\ 0 \\ 0 \end{bmatrix}, \quad C_c = [1\ \ 0\ \ 0]$$

and $g(\alpha) = -0.5\alpha - 0.15|\alpha + 1| + 0.15|\alpha - 1|$. Taking $A = A_c$, $B = B_c$, $C = -C_c$ [Guzelis & Chua, 1993] one obtains the representation (2), with $\sigma(\cdot)$ belonging to sector $[0;\ 0.8]$ and $k = 0.8$. In order to find a feedback matrix $F$ and matrices $P$, $\Gamma$ and $T$ such that (6) is satisfied and (9) synchronizes, the following constrained nonlinear optimization problem has been solved

$$\min_{F,R,\Gamma,T} \lambda_{\max}(Y) \quad \text{such that} \quad \|F\|_2 \leq c\,, \qquad (10)$$

where $\lambda_{\max}(\cdot)$ denotes the maximal eigenvalue and $P = R^T R$. The constraint $\|F\|_2 \leq c$ is used because otherwise the norm on $F$ becomes too large. In the simulations $c = 5$ was taken. Sequential quadratic programming (SQP) [Fletcher, 1987] with numerical calculation of the gradients was used in Matlab (function *constr* [The MathWorks Inc., 1994]) in order to minimize (10). The cost function is differentiable as long as the two largest eigenvalues of $Y$ do not coincide [Polak & Wardi, 1982]. Multistart local optimization was done with starting points $\Gamma = 0.1$, $T = 1$, $R = I_3$ and $F$ a random matrix with random elements normally distributed with zero mean and variance 1. Figure 1 shows the behavior of the circuits (9), corresponding to one of the feasible points to (6), for some initial states of $x$ and $z$.

## 4. Conclusion

In this paper we investigated the synchronization problem of Lur'e systems, that consist of a linear dynamical system with feedback interconnected to a static nonlinearity that satisfies a sector condition. Using a Lur'e–Postnikov Lyapunov function a matrix inequality is obtained that expresses a sufficient condition for global asymptotic stability of the error system. A systematic design procedure exists in order to find the feedback matrix by solving a constrained nonlinear optimization problem. The method has been demonstrated on Chua's circuit with the double scroll. For secure communication, Lur'e systems that produce high dimensional chaos are needed. Generalized cellular neural networks might be used for that purpose.

## Acknowledgments

This research work was carried out at the ESAT laboratory and the Interdisciplinary Center of Neural Networks ICNN of the Katholieke Universiteit

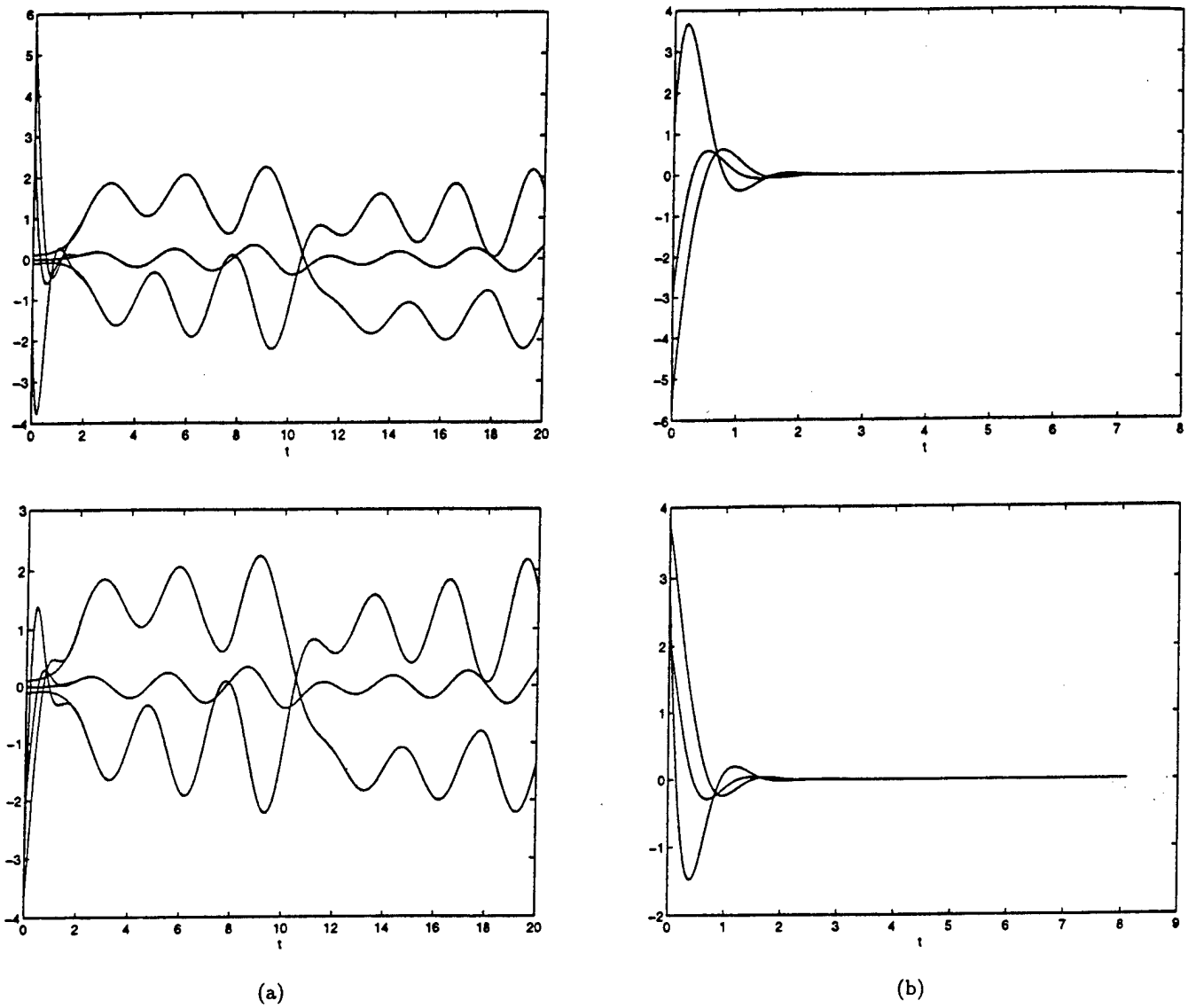


(a) (b)

Fig. 1. (a) The figure shows the 6 state variables through time of a master-slave synchronization system, where the master system behaves as Chua's double scroll for initial state [0.1; 0; −0.1]. For the slave system two randomly chosen initial states were taken, shown at the top and bottom. (b) Corresponding error signals through time.

Leuven, in the framework of the Belgian Programme on Interuniversity Poles of Attraction, initiated by the Belgian State, Prime Minister's Office for Science, Technology and Culture (IUAP-17) and in the framework of a Concerted Action Project MIPS (Modelbased Information Processing Systems) of the Flemish Community.

## References

Boyd, S., El Ghaoui, L., Feron, E. & Balakrishnan V. [1994] *Linear Matrix Inequalities in System and Control Theory*, SIAM (Studies in Applied Mathematics), Vol. **15**.

Chen, G. [1993] "Controlling Chua's global unfolding circuit family," *IEEE Trans. Circ. Syst. I* **40**(11), 829–832.

Chua, L. O., Komuro, M. & Matsumoto T. [1986] "The double scroll family," *IEEE Trans. Circ. Syst. I* **33**(11), 1072–1118.

Fletcher, R. [1987] *Practical Methods of Optimization*, Second Edition (John Wiley and Sons, Chichester and New York).

Guzelis, C. & Chua, L. O. [1993] "Stability analysis of generalized cellular neural networks," *Int. J. Circ. Theor. Appl.* **21**, 1–33.

Hasler, M. [1994], "Synchronization principles and applications," *Circ. Syst.: Tutorials IEEE-ISCAS'94* 314–326.

Khalil, H. K. [1992] *Nonlinear Systems* (Macmillan Publishing Company, New York).

Narendra, K. S. & Taylor, J. H. [1973] *Frequency Domain Criteria for Absolute Stability* (Academic Press, New York).

Polak, E. & Wardi, Y. [1982] "Nondifferentiable optimization algorithm for designing control systems having singular value inequalities," *Automatica* **18**(3), 267–283.

The MathWorks Inc. [1994] *Matlab Version 4.2, Optimization Toolbox.*

Wu, C. W. & Chua, L. O. [1994] "A unified framework for synchronization and control of dynamical systems," *Int. J. Bifurcation and Chaos* 4(4), 979–989.

Wu, C. W. & Chua, L. O. [1995] "Synchronization in an array of linearly coupled dynamical systems," *IEEE Trans. Circ. Syst. I* **42**(8), 430–447.

International Journal of Bifurcation and Chaos, Vol. 7, No. 2 (1997) 275–286
© World Scientific Publishing Company

# COMMUNICATION SYSTEMS VIA CHAOTIC SIGNALS FROM A RECONSTRUCTION VIEWPOINT

MAKOTO ITOH
*Department of Electrical Engineering and Computer Science, Nagasaki University, Nagasaki 852, Japan*

CHAI WAH WU
*IBM T. J. Watson Research Center, P.O. Box 218, Yorktown Heights, NY 10598, USA*

LEON O. CHUA
*Department of Electrical Engineering and Computer Sciences, University of California, Berkeley, CA 94720, USA*

Received August 23, 1996

In this paper, we study communication systems, modulators, and demodulators using chaotic systems from the perspective of reconstruction of attractors. We consider a two-step approach to the recovery of information signals from chaotic modulation. To recover the information signal modulated by a chaotic dynamical system, the first step is to reconstruct the chaotic attractor given a subset of the state variables. The second step is to reconstruct the information signal from the chaotic attractors. Two main techniques to accomplish this are the Takens reconstruction theorem and the chaotic synchronization theorem. In general, a combination of these two techniques are needed to recover the information signal. We show a systematic way to reconstruct an attractor and the injected signal exactly from a *scalar* observable for a subclass of Lur'e systems. We illustrate this approach using several examples. Extensions to discrete-time systems are also presented.

## 1. Introduction

There has been much interest in the implementation of communication systems using chaotic signals and systems. Recently, several approaches were proposed to give a uniform view on modulating and demodulating information using chaotic signals [Wu & Chua, 1994; Feldmann *et al.*, 1995; Wu *et al.*, 1996]. In general, a signal is modulated by applying it as an input to a chaotic system, and the modulated signal is tapped from the output of the chaotic system. Demodulation is possible if we can deduce the input to the system using only the information in the output signal. In the inverse system approach, an inverse system is constructed to accomplish this goal. The relative degree is used to determine the order of the inverse system. As the initial condition is not known to necessary precision, the determi nation of the input from the output needs to be (asymptotically) independent from the initial conditions of the chaotic system. Synchronization between the chaotic system (modulator) and the inverse system (demodulator) is used to accomplish this. In essence, the inverse system reconstructs the chaotic attractor from the output and constructs the input from the reconstructed attractor.

In this paper we illustrate how the general framework in [Wu & Chua, 1994; Feldmann *et al.*, 1995] can be used in practice for modulation and demodulation of signals using chaotic attractors by means of several examples. The main approach is

to reconstruct the chaotic attractor from a subset of state variables that was transmitted and recover the information signal from the reconstructed attractor. Most previous work concentrates on using chaotic synchronization for this reconstruction. In the inverse system approach, some of the state variables (as determined by the relative degree) can be reconstructed by taking the derivatives of the output. This is essentially Takens' method of reconstructing an attractor from observables. In this paper we illustrate how this version of the Takens reconstruction theorem can be used for the reconstruction and discuss differences between chaotic synchronization and Takens' method. We give examples where both methods are needed. In particular, we give examples where Takens' theorem is used to recover some variables which are then used to synchronize the transmitter and receiver to obtain the rest of the attractor. The recovered attractor is then used to recover the information signal by means of Takens' method.

We use lowercase, bold uppercase and bold lowercase letters for scalars (or scalar-valued functions), matrices and vectors respectively. The transpose of a matrix $\mathbf{A}$ is denoted $\mathbf{A}^T$. The vector $\mathbf{0}$ denotes the zero vector and $\mathbf{e}_i$ denotes the $i$th unit vector, i.e. $\mathbf{e}_1 = (1, 0, \ldots, 0)^T$. The integer $n$ is usually used to denote the size of matrices and vectors.

## 2. Reconstruction of Attractors

Consider the $n$-dimensional dynamical system (with a chaotic attractor):

$$\dot{\mathbf{x}} = \mathbf{f}(\mathbf{x}, t) \tag{1}$$

where $\mathbf{x} = (x_1, x_2, \ldots, x_n)^T \in R^n$ and $\mathbf{f}$ is a smooth ($C^\infty$) vector field on $R^n$.

The goal is to reconstruct the attractor using only a function of a subset of the state variables. We discuss two ways this can be done; the Takens reconstruction method and the chaotic synchronization method.

### 2.1. *Takens reconstruction theorem*

The Takens reconstruction theorem[1] [Takens, 1981] on the Euclidean space $\mathbb{R}^n$ is stated as follows: If a smooth function $y(t) = \phi(\mathbf{x}(t))$ is given, where $\phi$ is a scalar real-valued function, then *generically* we can reconstruct the chaotic attractor in Eq. (1) using $\tilde{\mathbf{y}} \equiv (y, \dot{y}, \ddot{y}, \ldots, y^{(m-1)})^T$ where $m > 2n$. Here, the symbols $\dot{y}$, $\ddot{y}$, and $y^{(m-1)}$ indicate $\frac{dy}{dt}$, $\frac{d^2y}{dt^2}$, and $\frac{d^{m-1}y}{dt^{m-1}}$, respectively. Thus there exists a continuous function $\mathbf{h}$ such that

$$\mathbf{x} = \mathbf{h}(\tilde{\mathbf{y}}, t) \tag{2}$$

or equivalently

$$(\mathbf{x}_1, \mathbf{x}_2, \ldots, \mathbf{x}_n) = (h_1(\tilde{\mathbf{y}}, t), h_2(\tilde{\mathbf{y}}, t), \ldots, h_n(\tilde{\mathbf{y}}, t)) \tag{3}$$

where $\mathbf{h} = (h_1, h_2, \ldots, h_n)^T$ and $h_i$ are continuous functions.

Note that $y = \phi(\mathbf{x}) \triangleq g_1(\mathbf{x}, t)$, $\dot{y} = \frac{d\phi(\mathbf{x})}{d\mathbf{x}} \cdot \mathbf{f}(\mathbf{x}, t) \triangleq g_2(\mathbf{x}, t)$ and $y^{(i)} = \frac{dy^{(i-1)}}{dt} = \frac{dg_i(\mathbf{x}, t)}{d\mathbf{x}} \cdot \mathbf{f}(\mathbf{x}, t) + \frac{dg_i(\mathbf{x}, t)}{dt} = g_{i+1}(\mathbf{x}, t)$, where $\frac{d\phi}{d\mathbf{x}}$ denotes the *gradient* of $\phi(\mathbf{x})$ and $\cdot$ denotes the vector (inner) dot product. Thus, we also have

$$\tilde{\mathbf{y}} = \mathbf{g}(\mathbf{x}, t)\,, \tag{4}$$

and

$$\begin{aligned}(y, \dot{y}, \ddot{y}, \ldots, y^{(m-1)}) \\ = (g_1(\mathbf{x}, t), g_2(\mathbf{x}, t), \ldots, g_m(\mathbf{x}, t))\end{aligned} \tag{5}$$

where $\mathbf{g} = (g_1, g_2, \ldots, g_m)^T$ and $g_i$ are smooth functions. Note that $\mathbf{g}$ is completely determined by $\phi$ and $\mathbf{f}$. Furthermore, $\mathbf{x} = \mathbf{h}(\mathbf{g}(\mathbf{x}, t), t)$.

By taking the derivative with respect to $t$ of $y^{(m-1)} = g_m(x, t)$ and using Eqs. (1)–(3) we obtain:

$$\begin{aligned} y^{(m)} &= \frac{\partial}{\partial \mathbf{x}} g_m(\mathbf{x}, t) \cdot \dot{\mathbf{x}} + \frac{\partial}{\partial t} g_m(\mathbf{x}, t) \\ &= \frac{\partial}{\partial \mathbf{x}} g_m(\mathbf{h}(\tilde{\mathbf{y}}, t), t) \cdot \mathbf{f}(\mathbf{h}(\tilde{\mathbf{y}}, t), t) \\ &\quad + \frac{\partial}{\partial t} g_m(\mathbf{h}(\tilde{\mathbf{y}}, t), t) \\ &\triangleq F(\tilde{\mathbf{y}}, t) \end{aligned} \tag{6}$$

Using the variables $y_1 = y$, $y_2 = \dot{y}$, $y_3 = \ddot{y}, \ldots$, $y_m = y^{(m-1)}$, we have another form of Eq. (1) (in a higher dimensional phase space):

$$\begin{aligned} \frac{dy_1}{dt} &= y_2\,, \\ \frac{dy_2}{dt} &= y_3, \ldots, \frac{dy_m}{dt} = F(y_1, y_2, \ldots, y_m, t)\,. \end{aligned} \tag{7}$$

[1]The version of Takens' theorem we use throughout this paper is different from the commonly used version where delay coordinates are used to reconstruct the attractor.

Suppose we do not know what $F$ is exactly. If we assume that $F$ is a polynomial which does not depend on $t$,[2] then we can determine the parameters of $F$. The function $F$ can be written as:

$$\begin{aligned} &F(y, \dot{y}, \ddot{y}, \ldots, y^{(m-1)}, t) \\ &\quad = \sum a_{k_1,k_2,k_3,\ldots,k_m} y^{k_1} (\dot{y})^{k_2} (\ddot{y})^{k_3} \cdots (y^{(m-1)})^{k_m} \\ &\quad = y^{(m)} \end{aligned} \tag{8}$$

The parameters $a_{k_1,k_2,k_3,\ldots,k_m}$ can be determined from $y(t)$ by finding $\tilde{\mathbf{y}}$ and $y^{(m)}$ at a finite number of time points and plugging into Eq. (8) to obtain a set of linear equations which we can solve if $y$ is not degenerate.

Thus it is generally possible to reconstruct the chaotic attractor from the given $y(t)$. It is also possible to estimate unknown parameters using the above method.

The requirement of $m > 2n$ is a sufficient condition on the dimension of the reconstructed phase space for this method to work. In certain cases the attractor can be reconstructed using a smaller $m$. In particular, $m$ can be taken to be $m > 2d$, where $d$ is the box-counting dimension of the chaotic attractor. For the class of bilinear systems, if the relative degree is $n$, then $m$ can be set to be equal to $n$. We illustrate this for a certain class of Lur'e systems which includes Chua's circuit and Chua's oscillator and give an explicit expression for the reconstruction.

**Definition 1.** The pair $(\mathbf{A}, \mathbf{w}^T)$ is observable if the matrix

$$\mathbf{K} = \mathbf{K}(\mathbf{A}, \mathbf{w}^T) = \begin{pmatrix} \mathbf{w}^T \\ \mathbf{w}^T\mathbf{A} \\ \mathbf{w}^T\mathbf{A}^2 \\ \vdots \\ \mathbf{w}^T\mathbf{A}^{n-1} \end{pmatrix} \tag{9}$$

is nonsingular, where $\mathbf{A}$ is an $n \times n$ matrix and $\mathbf{w}$ is an $n \times 1$ vector.

**Theorem 1.** *Consider the system:*

$$\dot{\mathbf{x}} = \mathbf{A}\mathbf{x} + \mathbf{e}_1 f_1(\mathbf{x}, t) \tag{10}$$

*where* $\mathbf{x} = (x_1, \ldots, x_n)^T$, $f_1$ *is a continuous real-valued function of* $n+1$ *variables and* $\mathbf{A}$ *is a matrix with nonzero elements only in the diagonal below the main diagonal and the entries above. Equivalently,* $\mathbf{A}$ *is the sum of a tridiagonal matrix and an upper triagonal matrix. Suppose that the pair* $(\mathbf{A}, \mathbf{e}_n^T)$ *is observable. Let* $\tilde{\mathbf{y}} \equiv (x_n, \dot{x}_n, \ddot{x}_n, \ldots, x_n^{(n-1)})^T$. *Then there exists functions* $\mathbf{g}$ *and* $\mathbf{h}$ *such that* $\mathbf{x} = \mathbf{h}(\tilde{\mathbf{y}})$ *and* $\tilde{\mathbf{y}} = \mathbf{g}(\mathbf{x})$. *Furthermore, if* $f_1$ *is an encoding function of the form* $f_1(\mathbf{x}, t) = e(\mathbf{x}, s(t))$ *with an inverse decoding function, i.e. there exists a function* $d(\cdot, \cdot)$ *such that* $d(e(\mathbf{x}, s(t)), \mathbf{x}) = s(t)$ *for all* $\mathbf{x}$, $s$, *then we can recover* $s(t)$ *from* $(x_n, \dot{x}_n, \ddot{x}_n, \ldots, x_n^{(n)})^T$.

*Proof.* Define $\mathbf{a}_i^j$ as the $i$th row of $\mathbf{A}^j$. Because of the locations of the nonzero elements of $\mathbf{A}$, it is easy to see that $\mathbf{a}_n^j\mathbf{e}_1 = \mathbf{0}$ for $j = 0, 1, \ldots, n-2$. Then $x_n = \mathbf{e}_n^T\mathbf{x} = \mathbf{a}_n^0\mathbf{x}$, $\dot{x}_n = \mathbf{a}_n^1\mathbf{x}$, and $\ddot{x}_n = \mathbf{a}_n^1\mathbf{A}\mathbf{x} + \mathbf{a}_n^1\mathbf{e}_1 f_1(\mathbf{x}, t) = \mathbf{a}_n^2\mathbf{x}$ etc., until $x_n^{(n-1)} = \mathbf{a}_n^{n-1}\mathbf{x}$. This means that

$$\tilde{\mathbf{y}} = (\mathbf{e}_n^T\mathbf{x}, \mathbf{a}_n^1\mathbf{x}, \ldots, \mathbf{a}_n^{n-1}\mathbf{x})^T = \mathbf{K}(\mathbf{A}, \mathbf{e}_n^T)\mathbf{x}$$

Since $\mathbf{K}(\mathbf{A}, \mathbf{e}_n^T)$ is invertible by hypothesis, there exists an invertible linear mapping between $\tilde{\mathbf{y}}$ and $\mathbf{x}$. We can find $\dot{x}_1$ as

$$\dot{x}_1 = \mathbf{e}_1^T\dot{\mathbf{x}} = \mathbf{e}_1^T\mathbf{K}(\mathbf{A}, \mathbf{e}_n^T)^{-1}\dot{\tilde{\mathbf{y}}}$$

If $f_1(\mathbf{x}, t) = e(\mathbf{x}, s(t))$, then from $\dot{x}_1 = \mathbf{e}_1^T\mathbf{A}\mathbf{x} + e(\mathbf{x}, s(t))$, we can recover $s(t)$ as

$$s(t) = d(\dot{x}_1 - \mathbf{e}_1^T\mathbf{A}\mathbf{K}(\mathbf{A}, \mathbf{e}_n^T)^{-1}\tilde{\mathbf{y}}, \mathbf{K}(\mathbf{A}, \mathbf{e}_n^T)^{-1}\tilde{\mathbf{y}})$$

■

An example of a pair of encoding-decoding functions are $e(\mathbf{x}, s) = p(\mathbf{x}) + s(t)$ and $d(\mathbf{y}, \mathbf{x}) = \mathbf{y} - p(\mathbf{x})$ for some function $p$. In linear system theory, the statement that $(\mathbf{A}, \mathbf{e}_n^T)$ is observable means that we can reconstruct the state vector $\mathbf{x}$ in the system $\dot{\mathbf{x}} = \mathbf{A}\mathbf{x}$ by observing only $x_n$ for some time. The above theorem says that the same can be done for the nonlinear Lur'e system (10). Note that a matrix in companion form [e.g. Eq. (13)] satisfies the conditions for $\mathbf{A}$ in this theorem.

**Corollary 1.** *Consider the system:*

$$\dot{\mathbf{x}} = \mathbf{A}\mathbf{x} + \mathbf{b} f_1(\mathbf{x}, t) \tag{11}$$

*where* $\mathbf{x} = (x_1, \ldots, x_n)^T$, *and* $f_1$ *is a continuous real-valued function of* $n+1$ *variables. Suppose* $(\mathbf{A}^T, \mathbf{b}^T)$ *is observable,*[3] *i.e.* $\mathbf{K} = \mathbf{K}(\mathbf{A}^T, \mathbf{b}^T)$ *is*

[2] $F$ does not depend on $t$ if Eq. (1) is autonomous.

[3] This is equivalent to saying that $(\mathbf{A}, \mathbf{b})$ is *controllable*.

*invertible. Let* $\mathbf{w} = \mathbf{K}^{-1}\mathbf{e}_n$, *i.e.* $\mathbf{w}$ *is the last column of* $\mathbf{K}^{-1}$. *Let* $\tilde{\mathbf{y}} \equiv (y, \dot{y}, \ddot{y}, \ldots, y^{(n-1)})^T$ *where* $y = \mathbf{w}^T\mathbf{x}$. *If* $(\mathbf{A}, \mathbf{w}^T)$ *is observable, then there exists functions* $\mathbf{g}$ *and* $\mathbf{h}$ *such that* $\mathbf{x} = \mathbf{h}(\tilde{\mathbf{y}})$ *and* $\tilde{\mathbf{y}} = \mathbf{g}(\mathbf{x})$. *Furthermore, if* $f_1$ *is an encoding function of the form* $f_1(\mathbf{x}, t) = e(\mathbf{x}, s(t))$ *with an inverse decoding function, i.e. there exists a function* $d(\cdot, \cdot)$ *such that* $d(e(\mathbf{x}, s(t)), \mathbf{x}) = s(t)$ *for all* $\mathbf{x}$, $s$, *then we can recover* $s(t)$ *from* $(y, \dot{y}, \ddot{y}, \ldots, y^{(n)})^T$.

*Proof.* Using the change of variables $\mathbf{x} = \mathbf{K}^T\mathbf{z}$, system (11) can be written as:

$$\dot{\mathbf{z}} = (\mathbf{K}^T)^{-1}\mathbf{A}\mathbf{K}^T\mathbf{z} + (\mathbf{K}^T)^{-1}\mathbf{b}f_1(\mathbf{K}^T\mathbf{z}, t) \quad (12)$$

The matrix $(\mathbf{K}^T)^{-1}\mathbf{A}\mathbf{K}^T$ is of the form [Wu & Chua, 1996a, 1996b]:

$$\begin{pmatrix} 0 & 0 & & -r_0 \\ 1 & 0 & \ddots & -r_1 \\ & \ddots & \ddots & \vdots \\ & & 1 & -r_{n-1} \end{pmatrix} \quad (13)$$

Since $(\mathbf{K}^T)^{-1}\mathbf{b} = \mathbf{e}_1$, and $(\mathbf{A}, \mathbf{w}^T)$ is observable, system (12) satisfies the hypotheses of Theorem 1. By Theorem 1, we can reconstruct $\mathbf{z}$ from $z_n$, $\dot{z}_n, \ldots, z_n^{(n-1)}$. From the definition of $\mathbf{w}$, $z_n = \mathbf{e}_n^T\mathbf{z} = \mathbf{e}_n^T(\mathbf{K}^T)^{-1}\mathbf{x} = \mathbf{w}^T\mathbf{x} = y$. From $\mathbf{z}$ we can find $\mathbf{x}$ since $\mathbf{K}$ is invertible. The rest of the proof is similar to the proof of Theorem 1. ■

*Remark.* Note that the conditions on the system imply that the system has relative degree $n$.

## 2.2. *Chaotic synchronization*

Pecora and Carroll [1991] showed that it is possible to synchronize two chaotic systems by driving the slave system with certain state variables of the master system. Thus the attractor is reconstructed in the slave system by using only a subset of the state variables. The basic synchronization theorem is stated as follows [Wu & Chua, 1994]:

Consider two systems in the following master-slave configuration

$$\dot{\mathbf{x}} = \mathbf{f}(\mathbf{x}, \phi(\mathbf{x}), t) \quad \leftarrow \text{Master system} \quad (14)$$

$$\dot{\tilde{\mathbf{x}}} = \mathbf{f}(\tilde{\mathbf{x}}, \phi(\mathbf{x}), t) \quad \leftarrow \text{Slave system} \quad (15)$$

If $\dot{\mathbf{x}} = \mathbf{f}(\mathbf{x}, \mathbf{e}(t), t)$ is globally asymptotically stable for all $\mathbf{e}(t)$, then $\tilde{\mathbf{x}} \to \mathbf{x}$ as $t \to \infty$. Thus $\phi(\mathbf{x})$ is used in the slave system to reconstruct the attractor $\mathbf{x}(t)$ via synchronization. Pecora and Carroll proposed the use of conditional Lyapunov exponents to determine the asymptotically stability of $\dot{\mathbf{x}} = \mathbf{f}(\mathbf{x}, \mathbf{e}(t), t)$, when $\mathbf{e}(t)$ is a trajectory of the master system, while the use of Lyapunov functions can also be effective in determining synchronization [Wu & Chua, 1994].

There are some differences between this method of reconstructing the attractor and Takens' method. When the state equation of Eq. (1) is known, in Takens' method we still cannot recover the original attractor in Eq. (1) unless we know $h_i$ explicity (as in the case of Theorem 1), while recovery of the original attractor is possible through chaotic synchronization. On the other hand, if the exact state equation of Eq. (1) is not known, we can still conclude by Takens' method that there is an embedding of the attractor into the reconstructed phase space. However, when the master and slave system are not identical, chaotic synchronization is not guaranteed, although for the case when the master and slave system are close to each other, generalized synchronization can occur [Kocarev *et al.*, 1995; Sushchik *et al.*, 1995]. The other difference between the two methods is that one method might work while the other fails. For example, for a nongeneric vector field in which Takens' method fails, synchronization can sometimes recover the state variables. We will given examples illustrating this in the next section. Concerning practical implementations, the use of differentiation in Takens' method can generate high frequency noise (especially in numerical implementations) which is absent in chaotic synchronization. On the other hand, differentiation can be implemented in analog circuitry via linear capacitors and inductors.

# 3. Reconstruction and Demodulation of Signals

Consider now the system

$$\frac{d\mathbf{x}}{dt} = \mathbf{f}(\mathbf{x}, \mathbf{s}(t)) \quad (16)$$

where $\mathbf{s}(t)$ is the information signal injected into the otherwise autonomous system. Given an observable measurement $y = \phi(\mathbf{x})$, the goal is to recover $\mathbf{s}$ from $y$. The transformation of $\mathbf{s}(t)$ into $y(t)$ is called *modulation* and is in general dependent on the initial condition of the system. Similarly the transformation of $y(t)$ into $\mathbf{s}(t)$ is called *demodulation*. We can

also think of this process of reconstructing $\mathbf{s}(t)$ from $y$ as a form of *nonlinear filtering.* Several synchronization schemes have been proposed to implement this transformation (asymptotically) [Cuomo, 1993; Dedieu *et al.*, 1993; Wu & Chua, 1993, 1994; Cuomo & Oppenheim, 1993; Feldmann *et al.*, 1995].

By rewriting the system (16) as

$$\begin{aligned} \frac{d\mathbf{x}}{dt} &= \mathbf{f}(\mathbf{x}, \mathbf{s}(t)) \\ \frac{d\mathbf{s}}{dt} &= \mathbf{s}'(t) \end{aligned} \tag{17}$$

and considering $(\mathbf{x}, \mathbf{s})$ as the state of this augmented system, we see that generically $\mathbf{s}$ can be recovered by using Takens' method if we know the corresponding $h_i$'s of the embedding. Note that whether the system is generic can depend on the choice of $\phi$. For example, suppose the system can be decomposed as:

$$\begin{aligned} \frac{d\mathbf{x}_1}{dt} &= \mathbf{f}_1(\mathbf{x}_1) \\ \frac{d\mathbf{x}_2}{dt} &= \mathbf{f}_2(\phi(\mathbf{x}_1), \mathbf{x}_2, \mathbf{s}(t)) \\ \frac{d\mathbf{s}}{dt} &= \mathbf{s}'(t) \end{aligned} \tag{18}$$

Then it is clear that given $y = \phi(\mathbf{x}_1)$, it is in general not possible to reconstruct $\mathbf{s}$ or $\mathbf{x}_2$. In other words, the system is *not* generic, and Takens' method fails.

On the other hand, if $\dot{\mathbf{x}}_2 = \mathbf{f}_2(y, \mathbf{x}_2, \mathbf{s}(t))$ is asymptotically stable when $y$ and $\mathbf{s}$ are considered external inputs, then we can recover $\mathbf{x}_2$ via chaotic synchronization from $x_1$ and $\mathbf{s}$.

Consider the system

$$\begin{aligned} \frac{d\mathbf{x}_1}{dt} &= \mathbf{f}_1(\mathbf{x}_1, \mathbf{s}(t)) \\ \frac{d\mathbf{x}_2}{dt} &= \mathbf{f}_2(\mathbf{x}_1, \mathbf{x}_2) \\ \frac{d\mathbf{s}}{dt} &= \mathbf{s}'(t) \end{aligned} \tag{19}$$

Given $y = \phi(\mathbf{x}_2)$, in general it is not possible to recover $x_1$ or $\mathbf{s}(t)$ via chaotic synchronization. But it is possible that Takens' method can be used here to reconstruct $\mathbf{x}_1$.

These examples show that given the differences between Takens' method and the chaotic synchronization method, the best approach is to combine the two methods in reconstructing $\mathbf{x}$ and $\mathbf{s}$ from $y$. Thus the general form of the algorithm for reconstructing the information signal $\mathbf{s}(t)$ from $y = \phi(\mathbf{x})$ is as follows. First use alternately Takens's method and the chaotic synchronization method to recover more and more of the state $\mathbf{x}$ until the entire state is recovered. Then $\mathbf{s}$ is recovered from $\mathbf{x}$ using Takens's method. The relative degree of a bilinear system is an indication of the maximum number of state variables which can be recovered by Takens' method.

## 4. Examples

In this section we apply the discussion above to some chaotic systems.

**Example 1** (Duffing's Equation).

(a) *Reconstruction of Chaotic Attractor* Consider the well-known Duffing's equation

$$\begin{aligned} \frac{dx}{dt} &= y\,, \\ \frac{dy}{dt} &= -\delta y + x - x^3 + \gamma\cos(t) \end{aligned} \tag{20}$$

where $\delta$ and $\gamma$ are some constant parameters. This equation is equivalent to the following scalar differential equation:

$$\ddot{x} + \delta\dot{x} - x + x^3 - \gamma\cos(t) = 0\,. \tag{21}$$

Therefore, if the signal $x(t)$ is given, we can easily reconstruct a chaotic attractor of (20) by using $(x(t), \dot{x}(t))$. This is because the following relation holds:

$$(x(t), \dot{x}(t)) = (x(t), y(t))\,. \tag{22}$$

In other words, the system satisfies the hypothesis of Theorem 1.

(b) *Estimation of Parameters* The parameters of (20) can be estimated from a given signal. Suppose $x(t)$ is given, then we can find the parameters $\delta$ and $\gamma$ from the following relations:

$$\begin{pmatrix} \dot{x}(t_0) & -\cos(t_0) \\ \dot{x}(t_1) & -\cos(t_1) \end{pmatrix} \begin{pmatrix} \delta \\ \gamma \end{pmatrix} = \begin{pmatrix} x(t_0) - x^3(t_0) - \ddot{x}(t_0) \\ x(t_1) - x^3(t_1) - \ddot{x}(t_1) \end{pmatrix} \tag{23}$$

Thus by finding $x$, $\dot{x}$ and $\ddot{x}$ at two suitable timepoints, we can estimate the values of $\delta$ and $\gamma$. By using many pairs of timepoints and averaging the estimates, we can get better estimates of the parameters.

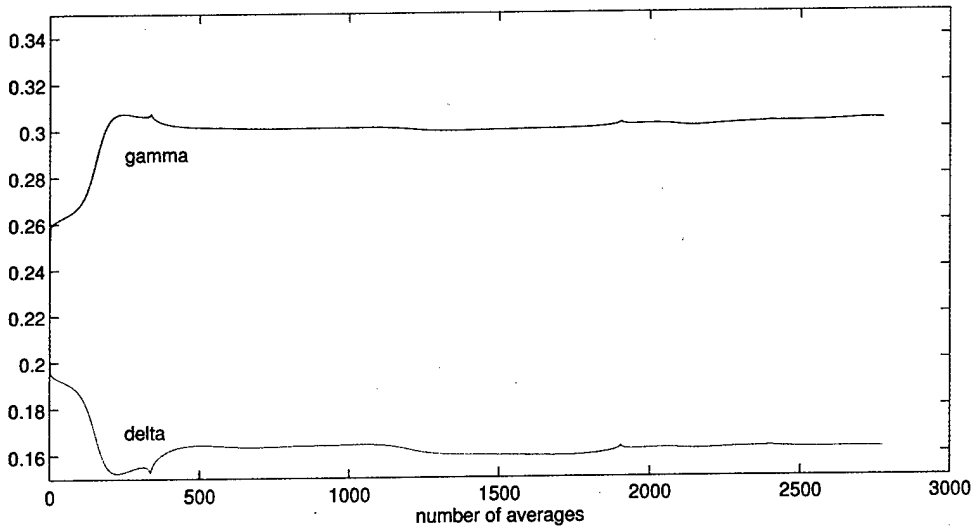


Fig. 1. Estimates of $\delta$ and $\gamma$ are shown on the vertical axis. The horizontal axis indicates the number of pairs of timesteps used. The observable is $x$ from Duffing's equation with $\delta = 0.15$ and $\gamma = 0.3$.

As mentioned before, a major problem with using Takens' method is the introduction of errors in evaluating the derivatives of the observable. We show here some computer simulations results illustrating this procedure of estimating the parameters. The derivatives are obtained via forward differences and the estimates of $\delta$ and $\gamma$ are averages over several pairs of timesteps. Figure 1 shows the estimates of $\delta$ and $\gamma$ versus the number of pairs of timesteps used. The observable is $x$ from Duffing's equation with $\delta = 0.15$ and $\gamma = 0.3$.

(c) *Construction of Communication Systems* We construct the communication system by injecting the information signal $s(t)$ into the Duffing's equation

$$\ddot{x} + \delta\dot{x} + x^3 - x - \gamma\cos(t) - s(t) = 0\,. \quad (24)$$

or equivalently

$$\begin{aligned} \frac{dx}{dt} &= y\,, \\ \frac{dy}{dt} &= -\delta y + x - x^3 + \gamma\cos(t) + s(t)\,. \end{aligned} \quad (25)$$

Then $s(t)$ is reconstructed from the signal $(x(t), \dot{x}(t), \ddot{x}(t))$:

$$s(t) = \ddot{x} + \delta\dot{x} + x^3 - x - \gamma\cos(t)\,. \quad (26)$$

In Fig. 2 we show the recovered $s(t)$ when $s(t)$ is a sine wave of frequency $\frac{1}{4\pi}$ and amplitude 0.1.

**Example 2** (Chua's Oscillator). The state equations of Chua's oscillator in a dimensionless form is given by

$$\begin{aligned} \frac{dx}{dt} &= \alpha(y - f(x))\,, \\ \frac{dy}{dt} &= x - y + z\,, \\ \frac{dz}{dt} &= -\beta y - \gamma z\,, \end{aligned} \quad (27)$$

where $\alpha$, $\beta$, $\gamma$ are parameters and $f(x)$ is a 3-segment piecewise-linear function.

(a) *Reconstruction of Chaotic Attractor* By Theorem 1, we can reconstruct the chaotic attractor by using $(z(t), \dot{z}(t), \ddot{z}(t))$ when $\beta \neq 0$. In fact, we have

$$\begin{aligned} \dot{z} &= -\beta y - \gamma z\,, \\ \ddot{z} &= \beta(\gamma + 1)y - \beta x + (\gamma^2 - \beta)z\,. \end{aligned} \quad (28)$$

Thus we obtain

$$\begin{aligned} x &= -\frac{\ddot{z} + (\gamma + 1)\dot{z} + (\gamma + \beta)z}{\beta} \\ y &= -\frac{\dot{z} + \gamma z}{\beta} \end{aligned} \quad (29)$$

(b) *Construction of Communication Systems* Using Eqs. (28) and (29), Eq. (27) can be written as:

$$\begin{aligned} &z^{(3)} + (\gamma + 1)\ddot{z} + (\beta + \gamma - \alpha)\dot{z} - \alpha\gamma z \\ &\quad = \alpha\beta f\left(-\frac{\ddot{z} + (\gamma + 1)\dot{z} + (\gamma + \beta)z}{\beta}\right). \end{aligned} \quad (30)$$

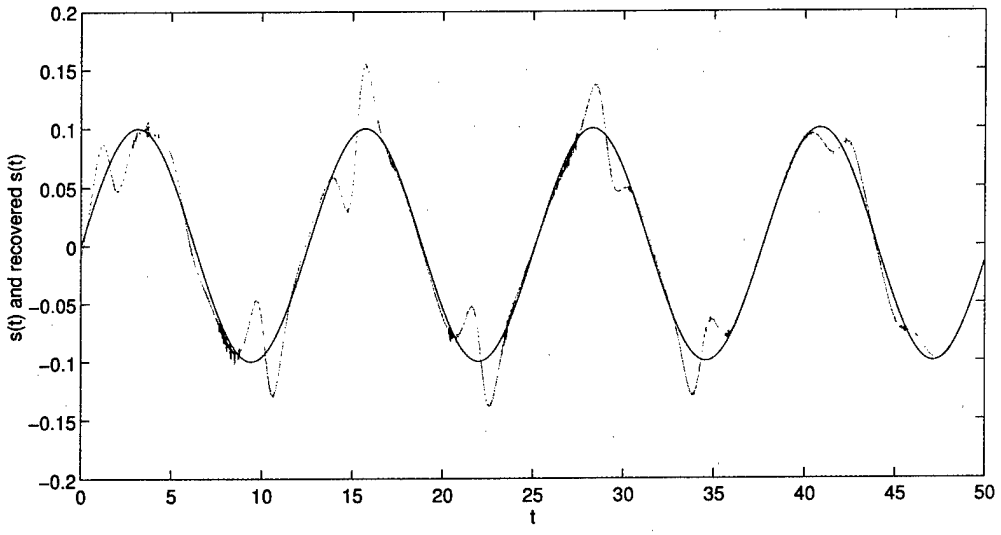


Fig. 2. Recovered information signal $s(t)$ (shown in red) when $s(t)$ is a sine wave of frequency $\frac{1}{4\pi}$ and amplitude 0.1 (shown in blue).

If $f$ is a cubic polynomial $f(x) = ax^3 + bx$ then we obtain

$$\begin{aligned}
&\beta^2 z^{(3)} + a\alpha(\dddot{z}^3 + 3(\gamma+1)\ddot{z}\dot{z}^2 + 6(\gamma+1)(\beta+\gamma)z\dot{z}\ddot{z} \\
&\quad + 3(\beta+\gamma)^2\ddot{z}z^2 + 3(\gamma+1)\ddot{z}^2 z \\
&\quad + 3(\beta+\gamma)\ddot{z}^2 z + (\gamma+1)^3\dot{z}^3 + 3(\gamma+1)^2(\beta+\gamma)\dot{z}^2 z \\
&\quad + 3(\gamma+1)(\beta+\gamma)^2\dot{z}z^2 + (\beta+\gamma)^3 z^3) \\
&\quad + \beta^2((\gamma+1+b\alpha)\ddot{z} + (\beta+\gamma-\alpha+b\alpha(\gamma+1))\dot{z} \\
&\quad + (b\alpha(\alpha+\beta) - \alpha\gamma)z) = 0\,. \qquad (31)
\end{aligned}$$

We can estimate the parameters in (27) from the given signal $z(t)$ by using $z(t_n)$, $\dot{z}(t_n)$, $\ddot{z}(t_n)$, $z^{(3)}(t_n)$ $(n = 1, 2, 3, \ldots)$.

Next we inject the informational signal $s(t)$ into the system [Halle *et al.*, 1993; Wu & Chua, 1993; Feldmann *et al.*, 1995]:

$$\begin{aligned}
&z^{(3)} + (\gamma+1)\ddot{z} + (\beta+\gamma-\alpha)\dot{z} - \alpha\gamma z \\
&\quad - \alpha\beta f\left(-\frac{\ddot{z} + (\gamma+1)\dot{z} + (\gamma+\beta)z}{\beta}\right) = -\beta s(t)\,, \qquad (32)
\end{aligned}$$

or equivalently

$$\begin{aligned}
\frac{dx}{dt} &= \alpha(y - f(x)) + s(t)\,, \\
\frac{dy}{dt} &= x - y + z\,, \qquad (33) \\
\frac{dz}{dt} &= -\beta y - \gamma z\,.
\end{aligned}$$

Then $s(t)$ is recovered from $(z(t), \dot{z}(t), \ddot{z}(t))$ as:

$$s(t) = \frac{z^{(3)} + (\gamma+1)\ddot{z} + (\beta+\gamma-\alpha)\dot{z} - \alpha\gamma z - \alpha\beta f\left(-\dfrac{\ddot{z} + (\gamma+1)\dot{z} + (\gamma+\beta)z}{\beta}\right)}{-\beta} \qquad (34)$$

For $\beta \neq 0$ this system satisfies Theorem 1 with $f_1(\mathbf{x}, t) = f(x) + s(t)$ and thus we can recover $(x, y, z)$ from $z(t)$ and then recover $s(t)$ from $(x(t), y(t), z(t))$. In other words, the chaotic attractor and $s(t)$ are reconstructed by

$$\begin{aligned}
(x(t), y(t), z(t)) &= \left(-\frac{\ddot{z} + (\gamma+1)\dot{z} + (\gamma+\beta)z}{\beta}, -\frac{\dot{z} + \gamma z}{\beta}, z\right), \\
s(t) &= \frac{dx}{dt} - \alpha(y - f(x))\,. \qquad (35)
\end{aligned}$$

(c) *The case where the signal $x(t)$ is given* Consider the case where the signal $x(t)$ is given. Since the first equation in (33) contains $s(t)$, we cannot reconstruct $(x, y, z)$ from $x(t)$. However, we can recover $y(t)$ and $z(t)$ by synchronization. Substituting $x(t)$ into (33), we get

$$\begin{aligned} \frac{dy'}{dt} &= x(t) - y' + z' \,, \\ \frac{dz'}{dt} &= -\beta y' - \gamma z' \,. \end{aligned} \tag{36}$$

Solving this equation, we can approximate the trajectory of the chaotic attractor and the signal $s(t)$ by

$$(x(t), y'(t), z'(t)) \,, \tag{37}$$

$$r(t) = \frac{dx(t)}{dt} - \alpha(y'(t) - f(x(t))) \,. \tag{38}$$

We know that $|y(t) - y'(t)|$, $|z(t) - z'(t)| \to 0$ for $t \to \infty$ [Chua *et al.*, 1993] and thus $r(t) \to s(t)$. In Fig. 3 we show the recovered signal $r(t)$ (shown in red) when $s(t)$ is a sinusoidal signal of amplitude 0.2 and frequency $\frac{5}{2\pi}$. In [Wu & Chua, 1994] another method of recovering $s(t)$ for this setup is presented.

**Example 3** (Chua's Oscillator with Two Information Signals). Consider Chua's oscillator with two injected signals $s(t)$ and $u(t)$.

$$\begin{aligned} \frac{dx}{dt} &= \alpha(y - f(x)) + s(t) \,, \\ \frac{dy}{dt} &= x - y + z + u(t) \,, \\ \frac{dz}{dt} &= -\beta y - \gamma z \,. \end{aligned} \tag{39}$$

Suppose that $z(t)$ is given. Then we have

$$\begin{aligned} \dot{z} &= -\beta y - \gamma z \,, \\ \ddot{z} &= -\beta \dot{y} - \gamma \dot{z} \\ &= -\beta x + \beta(1 + \gamma) y + (\gamma^2 - \beta) z - \beta u(t) \end{aligned} \tag{40}$$

From (40), we get

$$y = -\frac{\dot{z} + \gamma z}{\beta} \tag{41}$$

Substituting this into (39), we find

$$\frac{dx}{dt} = \alpha \left( -\frac{\dot{z}(t) + \gamma z(t)}{\beta} - f(x) \right) + s(t) \tag{42}$$

Since $s(t)$ is included in this equation, one more signal is needed to reconstruct a chaotic attractor. For example, we use the two signals $x(t)$ and $z(t)$. We can then reconstruct the attractor by $\left(x(t), -\frac{\dot{z}(t)+\gamma z(t)}{\beta}, z(t)\right)$. The signals $s(t)$ and $u(t)$ are reconstructed by:

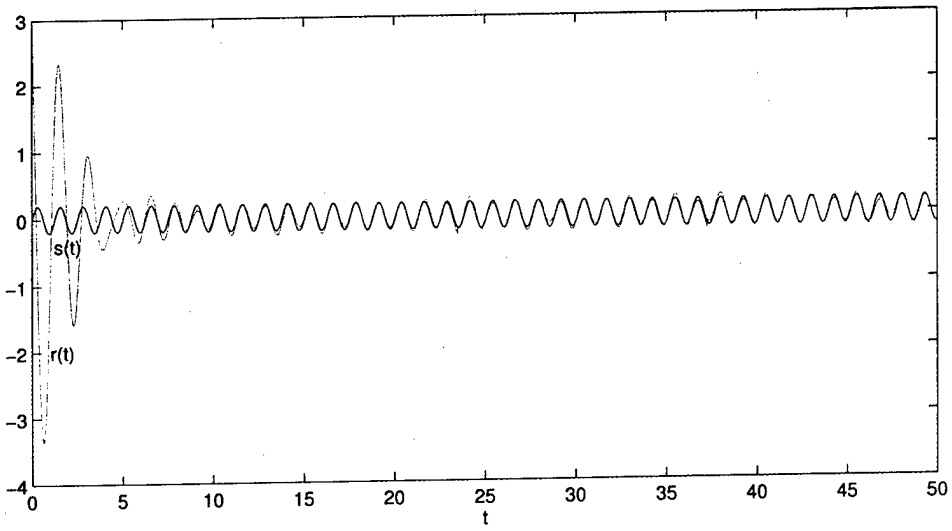


Fig. 3. Recovered information signal $r(t)$ (shown in red) when $s(t)$ (shown in blue) is a sinusoidal signal of amplitude 0.2 and frequency $\frac{5}{2\pi}$.

$$s(t) = \frac{dx(t)}{dt} + \alpha\left(\frac{\dot{z}(t) + \gamma z(t)}{\beta} + f(x(t))\right)$$

$$u(t) = -\frac{\ddot{z}(t) + (\gamma+1)\dot{z}(t) + (\gamma+\beta)z(t) + \beta x(t)}{\beta} \tag{43}$$

**Example 4.** Consider the case where the information signal $s(t)$ is injected at a different position of Eq. (27) [Wu & Chua, 1993]:

$$z^{(3)} + (\gamma+1)\ddot{z} + (\beta+\gamma-\alpha)\dot{z} - \alpha\gamma z - \alpha\beta f\left(-\frac{\ddot{z} + (\gamma+1)\dot{z} + (\gamma+\beta)z}{\beta} + s(t)\right) = 0\,, \tag{44}$$

equivalently

$$\begin{aligned} \frac{dx}{dt} &= \alpha(y - f(x + s(t)))\,, \\ \frac{dy}{dt} &= x - y + z\,, \\ \frac{dz}{dt} &= -\beta y - \gamma z\,. \end{aligned} \tag{45}$$

Suppose that signal $u(t) = x(t) + s(t)$ is given. Then, $\dot{u}(t)$ includes $\dot{s}(t)$, and therefore $(x(t), y(t), z(t))$ must be reconstructed via synchronization rather than Takens' method. Substituting $u(t) = x(t) + s(t)$ into the above equation, we have

$$\begin{aligned} \frac{dx'}{dt} &= \alpha(y' - f(u(t)))\,, \\ \frac{dy'}{dt} &= x' - y' + z'\,, \\ \frac{dz'}{dt} &= -\beta y' - \gamma z'\,. \end{aligned} \tag{46}$$

Therefore, we can approximate the chaotic attractor and signal $s(t)$ by

$$(x'(t), y'(t), z'(t))\,, \tag{47}$$

$$r(t) = u(t) - x'(t) \to s(t) \tag{48}$$

**Example 5** (Lorenz System Coupled with Linear System). Consider the linear feedback chaotic system [Cuomo, 1995]:

$$\begin{aligned} \frac{dx}{dt} &= \sigma(y - x) + \nu + s(t)\,, \\ \frac{dy}{dt} &= \gamma x - y - xz\,, \\ \frac{dz}{dt} &= xy - bz\,, \\ \frac{d\lambda}{dt} &= A\lambda + Bx\,, \\ \nu &= C\lambda + Dx\,. \end{aligned} \tag{49}$$

Here, $\sigma$, $\gamma$, and $b$ are some constants. $\lambda$ is a vector and $\nu$ is a scalar. The matrix $A$ is $N \times N$, $B$ is $N \times 1$, $C$ is $1 \times N$, and $D$ is $1 \times 1$. The first three state equations correspond to the *Lorenz system* and the last equation is the *constrained surface.* Under certain conditions, this system has a high dimensional chaotic attractor.

Suppose that $x(t)$ is given as the transmitted signal. Since $s(t)$ is included in the derivative of $x$, we have to create $y(t)$, $z(t)$, $\lambda(t)$ by synchronization. Substituting $x(t)$ into (81), we obtain:

$$\begin{aligned} \frac{dy'}{dt} &= \gamma x(t) - y' - x(t)z'\,, \\ \frac{dz'}{dt} &= x(t)y' - bz'\,, \\ \frac{d\lambda'}{dt} &= A\lambda' + Bx(t)\,, \\ \nu &= C\lambda + Dx\,. \end{aligned} \tag{50}$$

The chaotic attractor and the signal $s(t)$ are approximated by

$$(x(t), y'(t), z'(t), \lambda'(t)) \approx (x(t), y(t), z(t), \lambda(t)) \tag{51}$$

$$s(t) = \frac{dx(t)}{dt} - \sigma(y'(t) - x(t)) - C\lambda'(t) - Dx(t)\,. \tag{52}$$

If we know that $|y(t) - y'(t)|$, $|z(t) - z'(t)|$, $|\lambda(t) - \lambda'(t)| \to 0$ as $t \to \infty$ then $s(t)$ is recovered.

## 5. Discrete-Time Dynamical Systems

The reconstruction approach can be applied not only to continuous-time dynamical systems, but also to discrete-time dynamical systems. Only a slight change is needed to adapt it to discrete-time systems. The results obtained here are transformed

to those for discrete-time dynamical systems by replacing the derivatives with time-advanced states variables:

$$(x(t), \dot{x}(t), \ddot{x}(t), \ldots, x^{(m)}) \rightarrow (x(i), x(i+1), \ldots, x(i+m)) \quad (53)$$

The advantage of using discrete-time systems is that there are no errors introduced by numerical differentiation as in the continuous-time case.

An analog of Theorem 1 for discrete-time systems is the following:

**Theorem 2.** *Consider the system:*

$$\mathbf{x}(i+1) = \mathbf{A}\mathbf{x}(i) + \mathbf{e}_1 f_1(\mathbf{x}(i), i) \quad (54)$$

*where* $\mathbf{x} = (x_1, \ldots, x_n)^T$, $f_1$ *is a continuous real-valued function of* $n+1$ *variables and* $\mathbf{A}$ *is a matrix with nonzero elements only in the diagonal below the main diagonal and the entries above. Equivalently,* $\mathbf{A}$ *is the sum of a tridiagonal matrix and a upper triagonal matrix. Suppose that the pair* $(\mathbf{A}, \mathbf{e}_n^T)$ *is observable. Let* $\tilde{\mathbf{y}}(i) \equiv (x_n(i), x_n(i+1), \ldots, x_n(i+n-1))^T$. *Then there exists functions* $\mathbf{g}$ *and* $\mathbf{h}$ *such that* $\mathbf{x}(i) = \mathbf{h}(\tilde{\mathbf{y}}(i))$ *and* $\tilde{\mathbf{y}}(i) = \mathbf{g}(\mathbf{x}(i))$. *Furthermore, if* $f_1$ *is an encoding function of the form* $f_1(\mathbf{x}(i), i) = e(\mathbf{x}(i), s(i))$ *with an inverse decoding function, i.e. there exists a function* $d(\cdot, \cdot)$ *such that* $d(e(\mathbf{x}(i), s(i)), \mathbf{x}(i)) = s(i)$ *for all* $\mathbf{x}(i)$, $s(i)$, *then we can recover* $s(i)$ *from* $(x_n(i), x_n(i+1), \ldots, x_n(i+n))^T$.

*Proof.* Define $\mathbf{a}_i^j$ as the $i$th row of $\mathbf{A}^j$. As in Theorem 1, $\mathbf{a}_n^j \mathbf{e}_1 = \mathbf{0}$ for $j = 0, 1, \ldots, n-2$. Then $x_n(i) = \mathbf{e}_n^T \mathbf{x}(i) = \mathbf{a}_n^0 \mathbf{x}(i)$, $x_n(i+1) = \mathbf{a}_n^1 \mathbf{x}(i)$, and $x_n(i+2) = \mathbf{a}_n^1 \mathbf{x}(i+1) = \mathbf{a}_n^1 \mathbf{A}\mathbf{x}(i) + \mathbf{a}_n^1 \mathbf{e}_1 f_1(\mathbf{x}(i), i) = \mathbf{a}_n^2 \mathbf{x}(i)$ etc., until $x_n(i+n-1) = \mathbf{a}_n^{n-1}\mathbf{x}(i)$. This means that

$$\begin{aligned}\tilde{\mathbf{y}}(i) &= (\mathbf{e}_n^T \mathbf{x}(i), \mathbf{a}_n^1 \mathbf{x}(i), \ldots, \mathbf{a}_n^{n-1}\mathbf{x}(i))^T \\ &= \mathbf{K}(\mathbf{A}, \mathbf{e}_n^T)\mathbf{x}(i)\end{aligned}$$

Since $\mathbf{K}(\mathbf{A}, \mathbf{e}_n^T)$ is invertible by hypothesis, there exists an invertible linear mapping between $\tilde{\mathbf{y}}(i)$ and $\mathbf{x}(i)$. We can find $x_1(i+1)$ as

$$x_1(i+1) = \mathbf{e}_1^T \mathbf{x}(i+1) = \mathbf{e}_1^T \mathbf{K}(\mathbf{A}, \mathbf{e}_n^T)^{-1} \tilde{\mathbf{y}}(i+1)$$

If $f_1(\mathbf{x}(i), i) = e(\mathbf{x}(i), s(i))$, then from $x_1(i+1) = \mathbf{e}_1^T \mathbf{A}\mathbf{x}(i) + e(\mathbf{x}(i), s(i))$, we can recover $s(i)$ as

$$s(i) = d(x_1(i+1) - \mathbf{e}_1^T \mathbf{A}\mathbf{K}(\mathbf{A}, \mathbf{e}_n^T)^{-1}\tilde{\mathbf{y}}(i), \mathbf{K}(\mathbf{A}, \mathbf{e}_n^T)^{-1}\tilde{\mathbf{y}}(i)) \quad \blacksquare$$

*Remark.* A discrete-time version of Corollary 1 can also be derived.

**Example 6** (The Henon Map). The state equations for the Henon map are given by

$$x(i+1) = y(i) + 1 - ax(i)^2 \quad (55)$$

$$y(i+1) = bx(i) \quad (56)$$

(a) *Reconstruction of Chaotic Attractor* For $b \neq 0$, the system satisfies the condition of Theorem 2 and the attractor can be reconstructed from $y(i)$ and $y(i+1)$ as:

$$(x(i), y(i)) = \left(\frac{y(i+1)}{b}, y(i)\right)$$

(b) *Communication System* We can inject an information signal $s(i)$ as follows:

$$x(i+1) = y(i) + 1 - ax(i)^2 + s(i) \quad (57)$$

$$y(i+1) = bx(i) \quad (58)$$

or equivalently:

$$x(i+2) + ax(i+1)^2 - bx(i-1) - 1 - s(i+1) = 0 \quad (59)$$

Again, the system satisfies the condition of Theorem 2 when $b \neq 0$, and $s(i)$ can be recovered from $y(i)$, $y(i+1)$ and $y(i+2)$ as:

$$s(i) = \frac{y(i+2)}{b} + \frac{a}{b^2} y(i+1)^2 - y(i) - 1 \quad (60)$$

In Fig. 4 we show the attractor in the $x$ versus $y$ plane when $a = 1.4$ and $b = 0.3$ with $s(t)$ being a square wave of amplitude 0.001 and period 4. Figure 5 shows the recovered information signal $s(i)$ using Eq. (60) which is identical to the injected square wave.

**Example 7** (Chaotic Digital Encoding). [Frey, 1993] introduced the following chaotic modulator/demodulator pair:

$$x(i) = s(i-1) + x(i-1) + f(x(i-2)) \quad (61)$$

$$r(i-1) = x(i) - (x(i-1) + f(x(i-2))) \quad (62)$$

where $s(i)$ is the information signal, $x(i)$ is the chaotic modulated signal, $r(i)$ is the recovered signal which should be equal to $s(i)$, and $f$ is the nonlinear left circular bit shifting function.

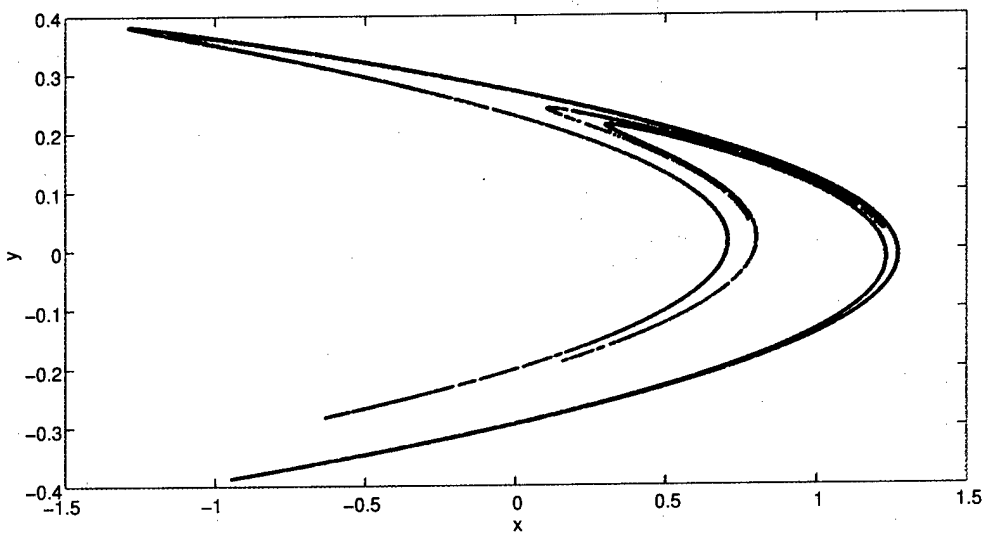


Fig. 4. Chaotic attractor of the Henon map when $a = 1.4$ and $b = 0.3$. The injected signal $s(t)$ is a square wave of amplitude 0.001 and period 4.

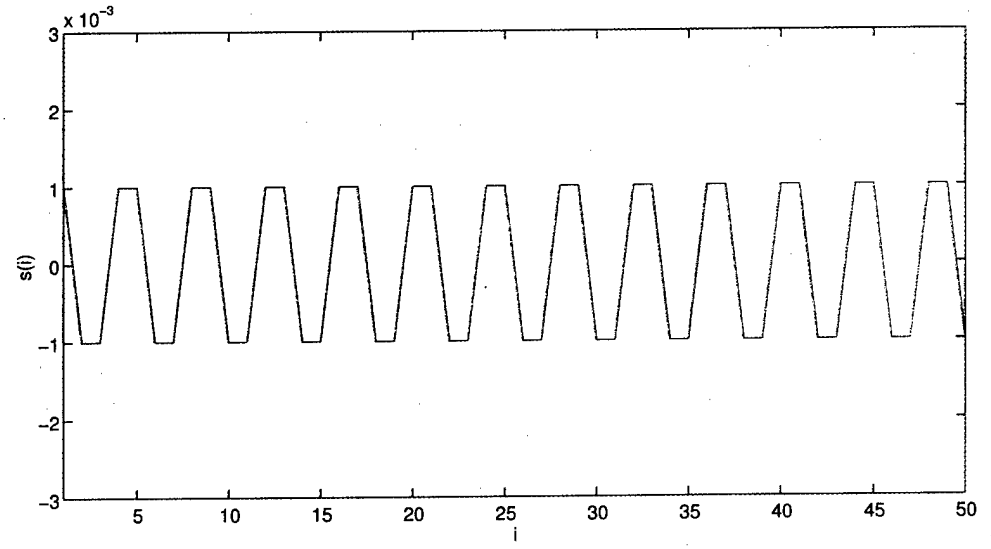


Fig. 5. Recovered signal $s(i)$ from the chaotic attractor of the Henon map in Fig. 4. The injected signal $s(t)$ is a square wave of amplitude 0.001 and period 4.

Equation (61) can be rewritten as

$$x(i+1) = x(i) + f(y(i)) + s(i)$$

$$y(i+1) = x(i)$$

The system satisfies the hypothesis of Theorem 2 and thus $s(i)$ can be recovered from $y(i)$, $y(i+1)$, and $y(i+2)$. Applying the algorithm in Theorem 2 we can recover $s(i)$ as

$$s(i) = r(i) = y(i+2) - y(i+1) - f(y(i))$$

which is equivalent to Eq. (62).

## Acknowledgments

C. W. Wu would like to thank Anshan Huang for helpful comments. This work was supported in part by the Japanese Ministry of Education, the Telecommunication Advancement Foundation, the Okawa Institute of Information and Telecommunication, the Office of Naval Research under grant N00014-89-J-1402, and the Joint Services Electronics Program under contract number F49620-94-C-0038. The United States Government is authorized

to reproduce and distribute reprints for governmental purposes not withstanding any copyright notation hereon.

## References

Chua, L. O., Itoh, M., Kocarev, L. & Eckert, K. [1993] "Chaos synchronization in Chua's circuit," *J. Circ. Syst. Comput.* **3**(1), 93–108.

Cuomo, K. M. & Oppenheim, A. V. [1993] "Circuit implementation of synchronized chaos with applications to communications," *Phys. Rev. Lett.* **71**(1), 65–68.

Cuomo, K. M. [1993] "Synthesizing self-synchronizing chaotic systems," *Int. J. Bifurcation and Chaos* **3**(5), 1327–1337.

Cuomo, K. M. [1995] "Systematic synthesis procedure for high-dimensional chaotic systems," in *Proc. 1995 Int. Symp. Circuits and Systems*, 1017–1020.

Dedieu, H., Kennedy, M. P. & Hasler, M. [1993] "Chaos shift keying: Modulation and demodulation of a chaotic carrier using self-synchronizing Chua's circuits," *IEEE Trans. Circ. Syst. II: Analog and Digital Signal Processing* **40**(10), 634–642.

Feldmann, U., Hasler, M. & Schwarz, W. [1995] "On the design of a synchronizing inverse of a chaotic system," in *Proc. ECCTD'95 Euro. Conf. Circuit Theory & Design*, 479–482.

Frey, D. R. [1993] "Chaotic digital encoding: An approach to secure communications," *IEEE Trans. Circ. Syst. II: Analog and Digital Signal Processing* **40**(10), 660–666.

Halle, K. S., Wu, C. W., Itoh, M. & Chua, L. O. [1993] "Spread spectrum communication through modulation of chaos," *Int. J. Bifurcation and Chaos* **3**(2), 469–477.

Kocarev, L., Parlitz, U. & Stojanovski, T. [1995] "Generalized synchronization of chaotic signals," in *1995 Int. Symp. Nonlinear Theory and Its Applications* (Las Vegas), 953–956.

Pecora, L. M. & Carroll, T. L. [1991] "Driving systems with chaotic signals," *Phys. Rev.* **A44**(4), 2374–2383.

Sushchik, M. M., Rulkov, N. F., Tsimring, L. S. & Abarbanel, H. [1995] "Generalized synchronization of chaos in directionally coupled chaotic systems," in *1995 Int. Symp. Nonlinear Theory and Its Applications* (Las Vegas), 949–952.

Takens, F. [1981] "Detecting strange attractors in turbulence," in *Lecture Notes in Mathematics 898*, (Springer-Verlag, Berlin), 366–381.

Wu, C. W. & Chua, L. O. [1993] "A simple way to synchronize chaotic systems with applications to secure communication systems," *Int. J. Bifurcation and Chaos* **3**(6), 1619–1627.

Wu, C. W. & Chua, L. O. [1994] "A unified framework for synchronization and control of dynamical systems," *Int. J. Bifurcation and Chaos* **4**(4), 979–998.

Wu, C. W. & Chua, L. O. [1996a] "On linear topological conjugacy of Lur'e systems," *IEEE Trans. Circ. Syst. I: Fundamental Theory and Applications* **43**(2), 158–161.

Wu, C. W. & Chua, L. O. [1996b] "On the generality of the unfolded Chua's circuit," *Int. J. Bifurcation and Chaos* **6**(6), 801–832.

Wu, C. W., Zhong, G. Q. & Chua, L. O. [1996] "Synchronizing nonautonomous chaotic systems without phase-locking," *J. Circ. Syst. Comput.* **6**(3), 227–241.

International Journal of Bifurcation and Chaos, Vol. 7, No. 2 (1997) 423–429
© World Scientific Publishing Company

# STRANGE NONCHAOTIC TRAJECTORIES ON TORUS*

T. KAPITANIAK
*Division of Dynamics, Technical University of Lodz, Stefanowskiego 1/15, 90-924 Lodz, Poland*

L. O. CHUA
*Department of Electrical Engineering and Computer Sciences, University of California, Berkeley, CA 94720, USA*

Received January 15, 1997

In this letter we have shown that aperiodic nonchaotic trajectories characteristic of strange nonchaotic attractors can occur on a two-frequency torus. We found that these trajectories are robust as they exist on a positive Lebesgue measure set in the parameter space.

## 1. Introduction

Strange nonchaotic attractors [Grebogi *et al.*, 1984; Bondeson *et al.*, 1985; Romeiras & Ott, 1987; Romeiras *et al.*, 1987; Ding *et al.*, 1989a, 1989b; Kapitaniak *et al.*, 1990; Brindley & Kapitaniak, 1991a, 1991b; Kapitaniak, 1991, Heagy & Hammel, 1998; Feudel *et al.*, 1995; Anishchenko *et al.*, 1996a, Zhu and Liu, 1997] are attractors which are strange in a geometrical sense, i.e. they have a fractal structure and contain an uncountably infinite number of points and they are not piecewise differentiable.

On the other hand, they are not chaotic because the necessary condition of the exponential divergence of the trajectories is absent, i.e. there are no positive Lyapunov exponents. This type of attractors was found to be characteristic of quasiperiodically forced systems [Romeiras & Ott, 1987; Romeiras *et al.*, 1987; Ding *et al.*, 1989a, 1989b; Kapitaniak *et al.*, 1990; Brindley & Kapitaniak, 1991a, 1991b; Kapitaniak, 1991; Anishchenko *et al.*, 1996a; Liu & Zhu, 1996] as it was shown that they exist on a set of positive Lebesgue measure in the parameter space.

Recently Anishchenko *et al.* [1996b] showed that strange nonchaotic attractors can occur not only in a quasiperiodically forced system but also in autonomous and periodically forced systems.

In order to establish that an attractor is a strange nonchaotic attractor one has: (1) to calculate the Lyapunov exponents and (2) check that the attractor is not differentiable. The first task is simple and the tools for the second one can be found in [Pikovsky & Feudel, 1995].

Although a typical trajectory on a strange nonchaotic attractor is characterized by a nonpositive, largest Lyapunov exponent, it was shown that there are time intervals in which the largest transient Lyapunov exponent is positive, i.e. there are parts of the attractor on which divergence of nearby trajectories is observed [Kapitaniak, 1993, 1995; Pikovsky & Feudel, 1995]. Trajectories on strange nonchaotic attractors have continuous power spectra which

*This work is supported in part by KBN (Poland) under project no. 7T07A 039 10 and by the Office of Naval Research grant N00014-96-I-0753.

share some similarities with the spectra of chaotic trajectories but also have some features which allow distinction between these two types of trajectories [Romeiras & Ott, 1987].

In this letter we show numerically that aperiodic (with continuous spectrum) trajectories similar to those which are characteristic of strange nonchaotic attractors can be observed on a two-frequency torus. Due to these similarities we call them strange nonchaotic trajectories on torus.

This letter is organized as follows. In Sec. 2 we describe the basic properties of the considered system (a quasi-periodically forced circuit). Section 3 is devoted to the numerical studies of the strange nonchaotic trajectories on torus. Finally we summarize our results in Sec. 4.

## 2. Quasi-Periodically Forced Circuit

We investigated the dynamics of the nonautonomous circuit shown in Fig. 1(a). This circuit is a classical configuration of a forced negative-resistance oscillator [Reich, 1961]. $N$ denotes a voltage-controlled resistor described by $i = g(v)$, which in our case was a Chua's diode [Kennedy, 1992; Cruz & Chua, 1992] shown in Fig. 1(b). The expression $g(v) = G_b v + 0.5(G_a - G_b)[|v + B_p| - |v - B_p|]$ is the mathematical representation of the characteristic curve of Chua's diode [Kennedy, 1992]. The actual values of $G_a$, $G_b$ and $B_p$ are $-0.76$ mS, $-0.41$ mS, and 1.0 V, respectively. External forcing $f(t)$ was taken as a quasi-periodic function $f(t) = F(\sin(\Omega_1 t) + \sin(\Omega_2 t))$, where $\Omega_1$ and $\Omega_2$ are

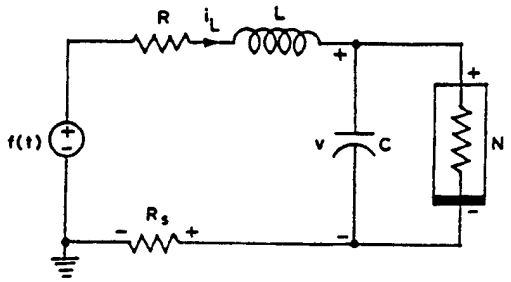


(a)

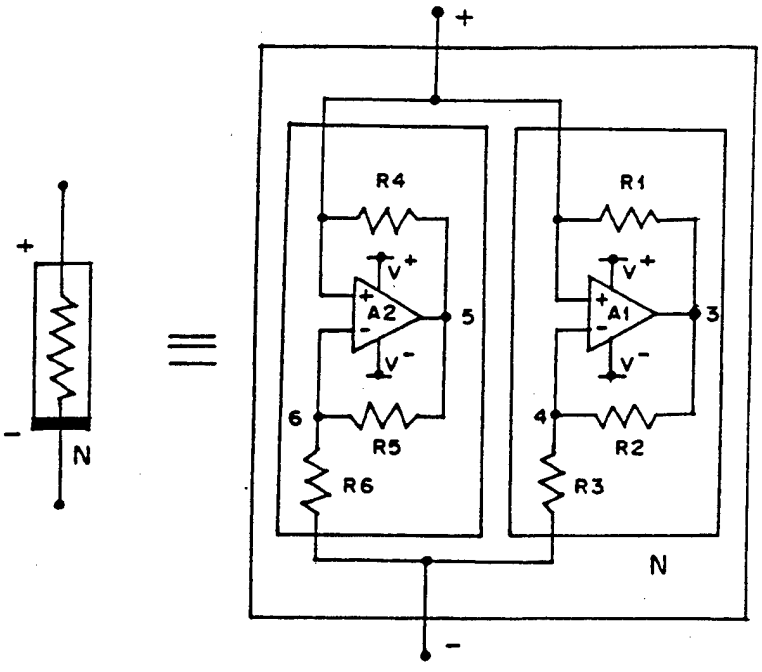


(b)

Fig. 1. (a) Experimental realization of the simple nonautonomous circuit; $N$ is the Chua's diode and $R_s$ is the current sensing resistor, (b) Circuit realization of Chua's diode $N$ using an 8 pin dual OP-Amp (AD712) [Kennedy, 1992]; $R_1 = R_2 = 220\ \Omega$, $R_3 = 2.2$ k$\Omega$, $R_4 = R_5 = 22$ k$\Omega$, $R_6 = 3.3$ k$\Omega$, $V^+ = +9$ V and $V^- = -9$ V.

incommensurate frequencies. The parameters of the circuit elements are fixed as $C = 10$ nF, $L = 18$ mH, $R = 1340\ \Omega$, $R_s = 20\ \Omega$ and the frequencies $(= \Omega_{1,2}/2\pi)$ of the external forcing sources are 8890 Hz and 16763 Hz, respectively. In the case of $\Omega_2 = 0$ our circuit reduces to the one considered by Murali *et al.* [1994].

The dynamics of the considered circuit is described by the following dimensionless equations

$$\begin{aligned} \dot{x} &= y - g(x) \\ \dot{y} &= -\beta y - v\beta y - \beta x + f(\sin\omega_1 t + \sin\omega_2 t) \end{aligned} \tag{1}$$

where $v = xB_p$, $i_L = GyB_p$, $G = 1/R$, $\omega_1 = \Omega_1 C/G$, $\omega_2 = \Omega_2 C/G$, $t = \tau C/G$, $\beta = (C/LG^2)$, $v = GR_s$, and $f = (F\beta/B_p)$. Obviously $g(x) = bx + 0.5(a-b)[|x+1| - |x-1|]$, where $a = G_a/G$ and $b = G_b/G$.

The dynamics of Eq. (1) depends on the parameters $v$, $\beta$, $a$, $b$, $\omega_1$, $\omega_2$ and $f$. The circuit parameters are rescaled as $\beta = 1$, $v = 0.015$, $a = -1.02$, $b = -0.55$, $\omega_1 = 0.75$ and $\omega_2 = \sqrt{2}$. The amplitude of the external quasi-periodic forcing $f$ was taken as a control parameter.

## 3. Route from Two-Frequency Quasi-Periodicity to Chaos

We considered the route to chaos starting from a two-frequency torus attractor obtained for $f = 0.08$ which is shown in Fig. 2(a). Typical trajectory on this attractor is quasi-periodic with two basic periods $T_1 = 4\pi/\omega_1$ and $T_2 = 2\pi/\omega_2$. With an increase of the forcing amplitude $f$ at $f = 0.086$, the $T^1$ torus undergoes bifurcation (band-merging crisis) in which it is destroyed and a new two-dimensional torus $T^2$ with a different shape is created. This new torus is shown in Fig. 2(b) ($f = 0.088$). With a further increase of $f$ we observe a breakdown of the $T^2$ torus at $f = 0.0918$ and the creation of a strange chaotic attractor. A typical chaotic attractor is shown in Fig. 2(c) for $f = 0.092$.

The plot of the Lyapunov exponent versus forcing amplitude $f$ is shown in Fig. 3 (except for the two trivial zero exponents the largest exponent $\lambda_{\max}$ was taken). From Figs. 2 and 3 we can depict the system behavior for different parameter settings as described in Fig. 3. Over the range $I$ the system exhibits a two-frequency quasi-periodic behavior, the corresponding Lyapunov exponent is negative and the trajectories evolve on a torus. Over the range $II$

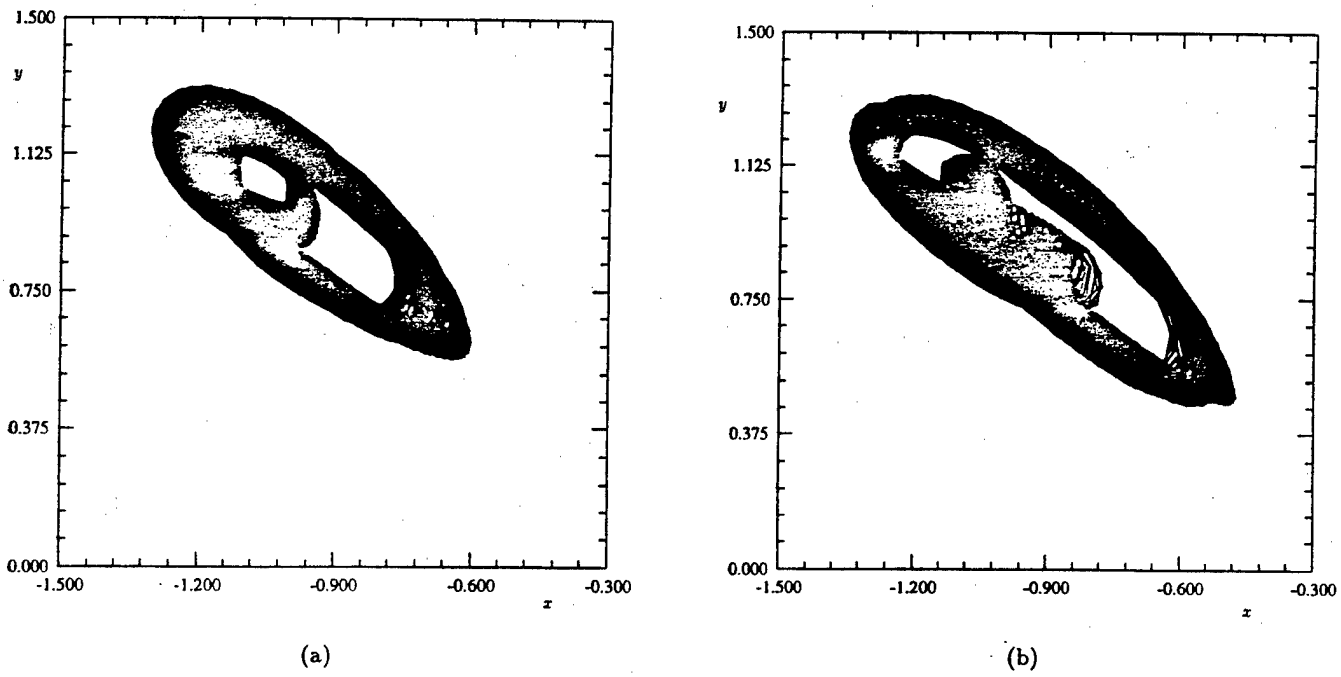


Fig. 2. Attractors for the system (1): $\beta = 1$, $v = 0.015$, $a = -1.02$, $b = -0.55$, $\omega_1 = 0.75$ and $\omega_2 = \sqrt{2}$; (a) two frequency torus for $f = 0.080$, (b) two frequency torus for $f = 0.088$, (c) strange chaotic attractor for $f = 0.092$.

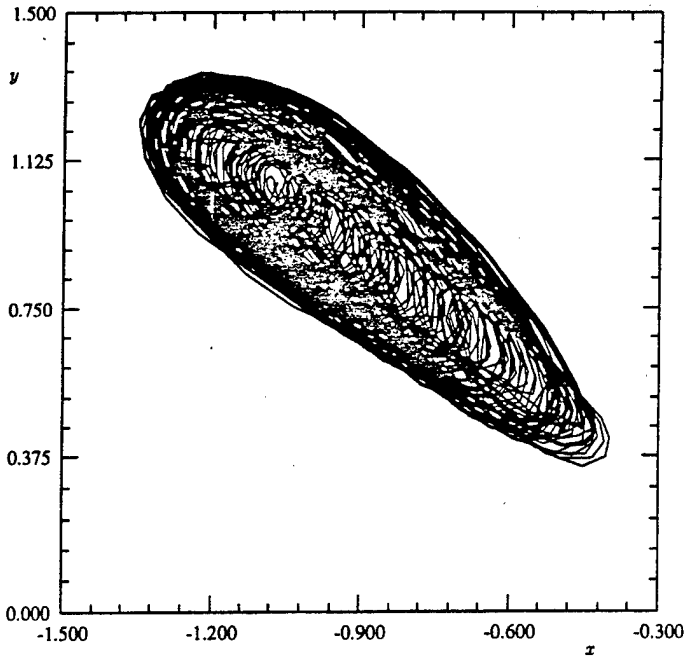


(c)

Fig. 2. (*Continued*)

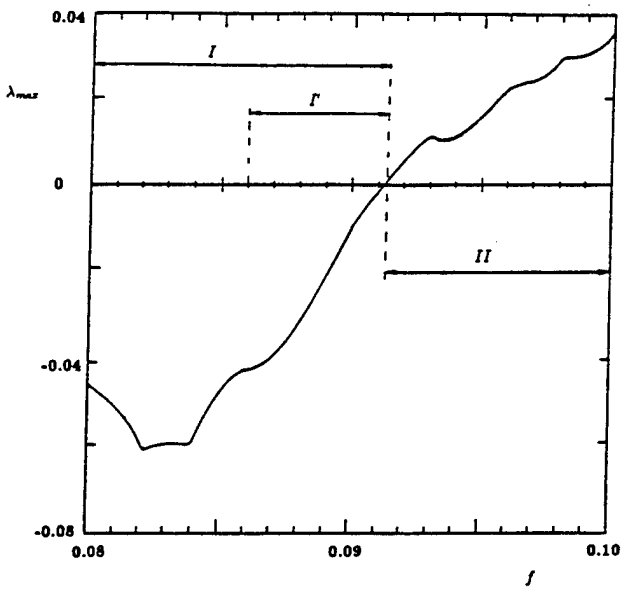


Fig. 3. The plot of the Lyapunov exponent versus forcing amplitude $f$ for the system (1) (the largest exponent $\lambda_{\max}$; except two trivial zero exponents was plotted): $\beta = 1$, $v = 0.015$, $a = -1.02$, $b = -0.55$, $\omega_1 = 0.75$ and $\omega_2 = \sqrt{2}$.

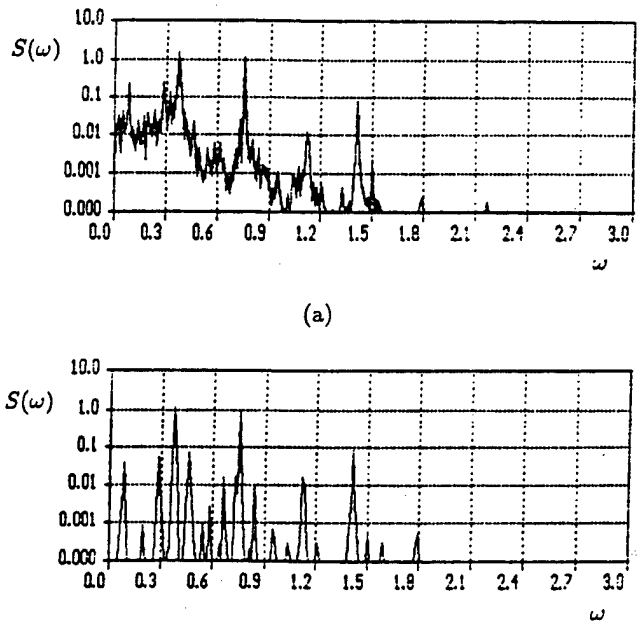


(a)

(b)

Fig. 4. Power spectra of the trajectories on two-frequency torus: $\beta = 1$, $v = 0.015$, $a = -1.02$, $b = -0.55$, $\omega_1 = 0.75$ and $\omega_2 = \sqrt{2}$; (a) $f = 0.088$, (b) $f = 0.080$.

the Lyapunov exponent is positive and we observe the evolution of a strange chaotic attractor.

The route to chaos exhibited in our system is different from other routes found to be typical for quasi-periodically forced systems [Ding *et al.*, 1989b; Kapitaniak *et al.*, 1990; Heagy & Hammel, 1994; Venkatesan & Lakshmanan, 1997] as we did not observe strange nonchaotic attractors.

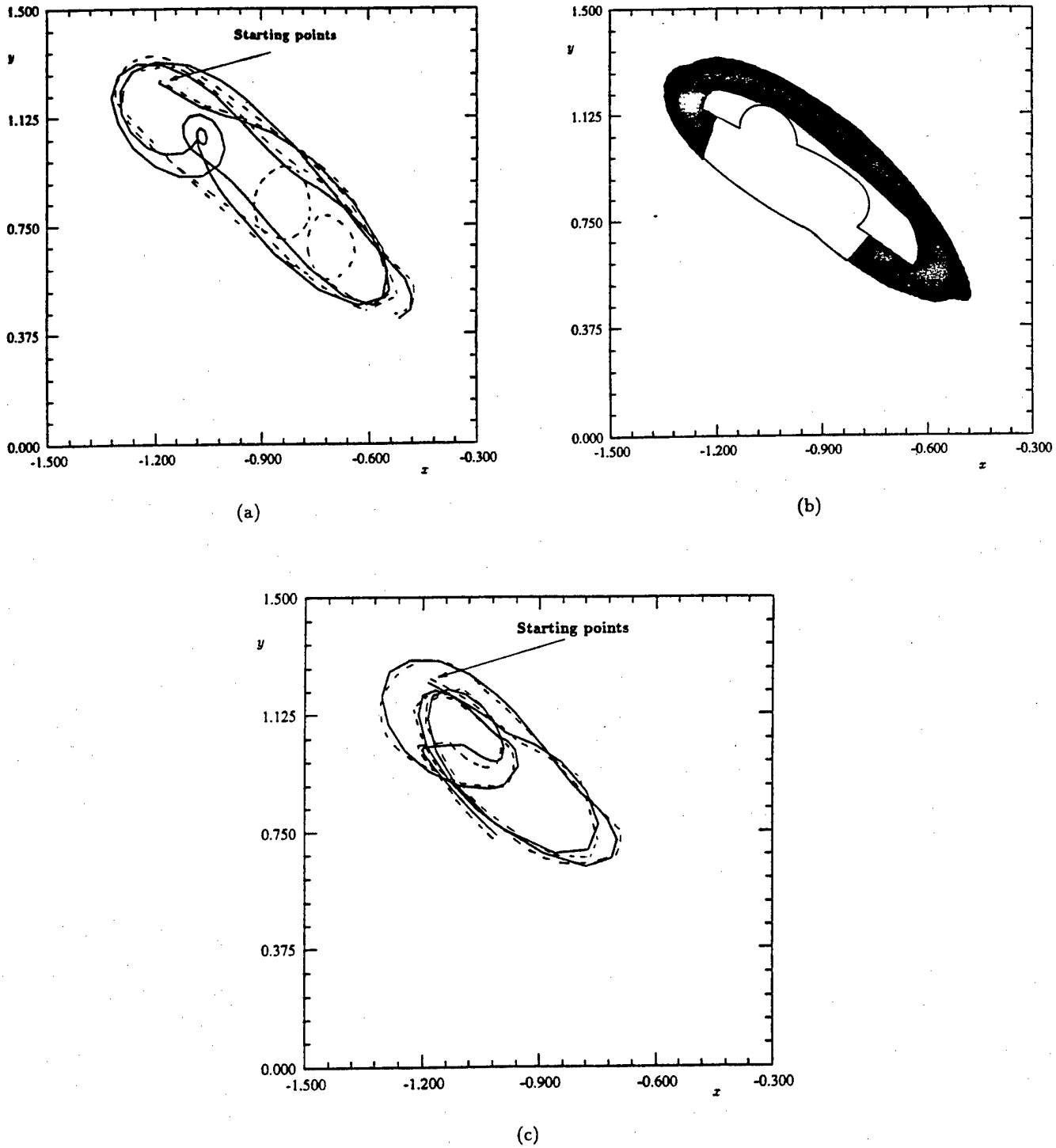


Fig. 5. (a) and (c) evolution of two nearby trajectories on two-frequency torus; (a) strange nonchaotic trajectories for $f = 0.088$, (c) two-frequency quasiperiodic trajectories for $f = 0.080$; (b) the regions on the attractor where two nearby strange nonchaotic trajectories stay close together is indicated in black and the region where these trajectories diverge is shown in white.

Closer investigation of the trajectiories on the torus in the neighborhood of its breakdown point $f = 0.0918$ allowed us to find trajectories with a continuous power spectra, like the one for $f = 0.088$ shown in Fig. 4(a) while the power spectra for the trajectories far from the breakdown point are discrete — Fig. 4(b) ($f = 0.080$). Aperiodic trajectories with a continuous power spectra are observed

in the range $I'$ of the forcing amplitude $f$. At $f = 0.086$ the $T^1$ torus undergoes a band-merging crisis bifurcation which allows the creation of such trajectories on the $T^2$ torus.

Now let us consider the evolutions of two nearby trajectories on the two-frequency torus $T^2$. Over the range $I'$ of $f$ parameter example of such evolution is shown in Fig. 5(a). It can be noticed that two trajectories (solid and broken lines) stay close together on most parts of the attractor indicated in black in Fig. 5(b), but there is a particular region on the attractor shown in white where nearby trajectories diverge. Transient Lyapunov exponent is negative in the black part but positive in the white portion. On the other hand, for $f \in I \setminus I'$, nearby trajectories stay close together on the entire attractor (transient largest Lyapunov exponent is always nonpositive) as shown in Fig. 5(c).

In Kapitaniak [1995] it was shown that the existence of attractor regions with local divergence of nearby trajectories is a property characteristic of strange nonchaotic attractors. This property as well as the continuous power spectrum of the aperiodic trajectories on the two-frequency torus led us to call such trajectories as strange nonchaotic.

In our numerical studies Eq. (1) was integrated by using a fourth-order Runge–Kutta method with 100 time steps per period $T_1$ of $\sin \omega_1 t$. The number of periods $T_1$ used for the calculations of Lyapunov exponents was $10^8$.

Strange nonchaotic trajectories were found to be robust in our system as they exist on a positive Lebesgue measure set in the parameter space, mainly for $f \in (0.0865, 0.0918)$.

## 4. Conclusions

We have found numerically that aperiodic nonchaotic trajectories, which are typical for strange nonchaotic attractors can exist on a two-frequency torus. As the power spectra and distributions of transient Lyapunov exponents of these trajectories have the same characteristic properties as in the case of trajectories on strange nonchaotic attractors, we called them strange nonchaotic trajectories on torus. We found that strange nonchaotic trajectories are robust as they exist on a positive Lebesgue measure set in the parameter space. The appearance of strange nonchaotic trajectories is connected with a new type of torus bifurcation where after band-merging crisis of the two-frequency torus $T^1$, another two-frequency torus $T^2$ with a different shape is created.

In quasiperiodically forced systems a typical route to chaos evolves from strange nonchaotic attractors. It was found that this route can be realized in four different ways

- two-frequency quasiperiodicity → three-frequency quasiperiodicity → strange nonchaotic attractors → chaos [Ding *et al.*, 1989b].
- two-frequency quasiperiodicity → strange nonchaotic attractors → chaos [Kapitaniak *et al.*, 1990].
- two-frequency quasiperiodicity → torus doubling → wrinkling → strange nonchaotic attractors → chaos [Heagy & Hammel, 1994].
- two-frequency quasiperiodicity → torus doubling → torus merging → strange nonchaotic attractors → chaos [Venkatesan & Lakshmanan, 1997].

Our study allows us to add a new route which seems to be typical: two-frequency quasiperiodicity (two-frequency torus $T^1$) → strange nonchaotic trajectories on a $T^2$ torus → chaos.

## References

Anishchenko, V. S., Vadivasova, T. E. & Sosnovtseva, O. [1996a] "Mechanisms of ergodic torus destruction and appearance of strange nonchaotic attractors," *Phys. Rev.* **E53**, 3231–3234.

Anishchenko, V. S., Vadivasova, T. E. & Sosnovtseva, O. [1996b] "Strange nonchaotic attractors in autonomous and periodically driven systems," *Phys. Rev.* **E54**, 3231–3234.

Bondeson, A., Ott, E. & Antonsen, T. M. [1985] "Quasiperiodicity forced damped pendula and Schrodinger equations with quasiperiodic potentials: Implications of their equivalence," *Phys. Rev. Lett.* **55**, 2103–2106.

Brindley, J. & Kapitaniak, T. [1991a] "Analytical predictors for strange nonchaotic attractors," *Phys. Lett.* **A155**, 361–364.

Brindley, J. & Kapitaniak, T. [1991b] "Existence and characterization of strange nonchaotic attractors in nonlinear systems," *Chaos, Solitons and Fractals* **1**, 323–337.

Cruz, J. M. & Chua, L. O. [1992] "A CMOS IC nonlinear resistor for Chua's circuit," *IEEE Trans. Circuits and Systems* **39**, 985–995.

Ding, M., Grebogi, C. & Ott, E. [1989a] "Evolution of attractors in quasiperiodically forced systems: From quasiperiodic to strange nonchaotic to chaotic," *Phys. Rev.* **A39**, 2593–2598.

Ding M., Grebogi, C. & Ott, E. [1989b] "Dimensions of strange nonchaotic attractors," *Phys. Lett.* **A137**, 167–172.

Feudel, U., Kurths, J. & Pikovsky, A. [1995] "Strange nonchaotic attractors in a quasi-periodically forced circle map," *Physica* **D88**, 176–186.

Grebogi, C., Ott, E. & Yorke, J. A. [1984] "Strange attractors that are not chaotic," *Physica* **D13**, 261–268.

Heagy, J. F. & Hammel, S. M. [1994] "The birth of strange nonchaotic attractors," *Physica* **D70**, 140–153.

Kapitaniak, T., Ponce, E. & Wojewoda, J. [1990] "Route to chaos via strange nonchaotic attractors," *J. Phys.* **A23**, L383–L387.

Kapitaniak, T. [1991] "On strange nonchaotic attractors and their dimensions," *Chaos, Solitons and Fractals* **1**, 67–77.

Kapitaniak, T. [1993] "Generating strange nonchaotic trajectories," *Phys. Rev.* **E47**, 4408–4410.

Kapitaniak, T. [1995] "Distribution of transient Lyapunov exponents of quasiperiodically forced systems," *Progr. Theoret. Phys.* **93**, 831–833.

Kennedy, M. P. [1992] "Robust op amp realization of Chua's circuit," *Frequenz* **46**, 66–80.

Liu, Z. & Zhu, Z., [1996] "Strange nonchaotic attractors from quasiperiodically forced Ueda's circuit," *Int. J Bifurcation and Chaos* **6**, 1383–1388.

Murali, K., Lakshmanan, M. & Chua, L. O. [1994] "Bifurcation and chaos in the simplest dissipative nonautonomous circuit," *Int. J Bifurcation and Chaos* **4**, 1511–1524.

Pikovsky, A. S. & Feudel, U. [1995] "Characterizing strange nonchaotic attractors," *Chaos* **5**, 253–255.

Reich, H. J. [1961] *Functional Circuits and Oscillators* (D. van Nostrad Co, Princeton, NJ), pp. 197.

Romeiras, F. J. & Ott, E. [1987] "Strange nonchaotic attractors of the damped pendulum with quasiperiodic forcing," *Phys. Rev.* **A35**, 4404–4413.

Romeiras, F. J., Bondeson, A., Ott, E., Antonsen, T. M. & Grebogi, C. [1987] "Quasiperiodically forced dynamical systems with strange nonchaotic attractors," *Physica* **D26**, 277–294.

Venkatesan, A. & Lakshmanan, M. [1997] "Nonlinear dynamics of damped and drived velocity-dependent systems," *Phys. Rev. E*, in press.

Zhu, Z. & Liu, Z. [1997] "Strange nonchaotic attractors of Chua's Circuit with quasiperiodic excitation," *Int. J. Bifurcation and Chaos* **7**, 227–238.

International Journal of Bifurcation and Chaos, Vol. 6, No. 12B (1996) 2653–2660
© World Scientific Publishing Company

# CHANNEL-INDEPENDENT CHAOTIC SECURE COMMUNICATION

TAO YANG and LEON O. CHUA
*Electronics Research Laboratory and*
*Department of Electrical Engineering and Computer Sciences,*
*University of California at Berkeley, Berkeley, CA 94720, USA*

Received September 2, 1996; Revised November 8, 1996

The generalized synchronization (GS) of two identical chaotic systems through an unknown channel is studied. First, some theoretical results of GS through an unknown channel are derived. Finally, an application of GS to channel-independent chaotic secure communication is presented.

## 1. Introduction

The basic setup in most chaos-based synchronization schemes for secure communication systems consists of a specially designed transmitter and a receiver. To enhance the degree of security, we always send a chaotic signal to the receiver. It is well-known, however, that if the transmitted signal is too "simple", then security cannot be guaranteed [Yang, 1995; Short, 1994]. On the other hand, if a more complex signal, e.g. a hyper-chaotic signal, is used as the transmitted signal, the robustness of the synchronization will be weakened. Moreover, it will be very difficult to design adaptive methods for compensating the inevitable parameter mismatch and channel distortions [Chua *et al.*, 1996a, 1996b; Wu *et al.*, 1996]. Recently, a new method had been proposed [Yang *et al.*, 1996] for enhancing the security of low-dimensional secure communication schemes so that it would be difficult to break them with current cryptanalysis techniques for chaotic systems [Yang, 1995; Short, 1994].

Non-ideal channels pose a serious problem in chaos-based secure communication schemes. The experimental results in [Chua *et al.*, 1996a, 1996b] have demonstrated that a time-varying or distorted channel can desynchronize the systems. In [Chua *et al.*, 1996a] and [Chua *et al.*, 1996b], the authors used an adaptive channel compensation method to overcome the non-ideal channel problem. Recently, Carroll [1996] presented an amplitude-independent synchronization scheme, which was very promising for overcoming the non-ideal channel problem. In this letter, we study the channel-independent synchronization problem in the more general framework of *generalized synchronization* (GS) [Kocarev & Parlitz, 1996; Rulkov *et al.*, 1996].

While most previous works would scramble the message signal with only one chaotic state variable, Yang *et al.* [1996] had presented a message scrambling scheme which used two chaotic state-variables. In this letter, we propose the possibility of utilizing the non-ideal channel property to scramble the message signal. This channel scrambling scheme is used to overcome the time series identification attack scheme presented in [Short, 1994], which is sensitive to the amplitude of the transmitted signal.

## 2. Generalized Synchronization Through Non-Ideal Channels

Consider two dynamical systems

$$\begin{cases} \dot{\mathbf{x}} = f(\mathbf{x}) & \leftarrow \text{driving system} \\ \dot{\mathbf{y}} = g(\mathbf{y},\, h(\mathbf{x})) & \leftarrow \text{driven system} \end{cases} \tag{1}$$

where $\mathbf{x} \in R^n$, $\mathbf{y} \in R^m$, $h : R^n \mapsto R^m$ is an arbitrary function.

**Definition 1.** Generalized synchronization (GS) [Kocarev & Parlitz, 1996; Rulkov *et al.*, 1996]. The two systems in (1) are said to be in a state of generalized synchronization, henceforth referred to as GS, if there exists a transformation $H : R^n \mapsto R^m$, a manifold $M = \{(\mathbf{x}, \mathbf{y})|\mathbf{y} = H(\mathbf{x})\}$, and a set $B \subset R^n \times R^m$ with $M \subset B$ such that all trajectories of (1) with initial conditions in $B$ approach $M$ as $t \to \infty$.

*Remark.* Synchronization in the normal sense is a special case of GS with $m = n$, and $H(\mathbf{x}) = \mathbf{x}$.

Assume that a chaotic system can be decomposed into two parts

$$\dot{\mathbf{x}} = \phi(\mathbf{x}) + \psi(\mathbf{x}) \tag{2}$$

where $\phi(\mathbf{x})$ satisfies the condition

$$\phi(\lambda\mathbf{x}) = \lambda\phi(\mathbf{x}) \tag{3}$$

where $\lambda \in R$ is a nonzero constant. Let the signal $\psi(\mathbf{x})$ be transmitted to the driven system and consider the unidirectional synchronization scheme

$$\begin{cases} \dot{\mathbf{x}} = \phi(\mathbf{x}) + \psi(\mathbf{x}) & \leftarrow \text{driving system} \\ \dot{\mathbf{y}} = \phi(\mathbf{y}) + \lambda\psi(\mathbf{x}) & \leftarrow \text{driven system} \end{cases} \tag{4}$$

where $\lambda \neq 0$ is the channel gain.

**Theorem 1.** *If $\phi(\mathbf{x})$ is decreasing in $D \in R^n$, $\mathbf{x}_0 \in D$ and $\frac{1}{\lambda}\mathbf{y}_0 \in D$, then the two dynamic systems in Eq. (4) are GS via the transformation*

$$H(\mathbf{x}) = \lambda\mathbf{x} \tag{5}$$

*Proof.* Since $\lambda \neq 0$, let $\mathbf{z} = \frac{1}{\lambda}\mathbf{y}$ and recast the driven system in Eq. (4) into

$$\begin{aligned} \dot{\mathbf{z}} &= \frac{1}{\lambda}\phi(\mathbf{y}) + \psi(\mathbf{x}) \\ &= \phi\left(\frac{1}{\lambda}\mathbf{y}\right) + \psi(\mathbf{x}) \\ &= \phi(\mathbf{z}) + \psi(\mathbf{x}) \end{aligned} \tag{6}$$

Let the error be $\mathbf{e} = \mathbf{x} - \mathbf{z}$ so that the error system is given by

$$\dot{\mathbf{e}} = \phi(\mathbf{x}) - \phi(\mathbf{z}) . \tag{7}$$

Since $\frac{1}{\lambda}\mathbf{y}_0 \in D$, we have $\mathbf{z}_0 \in D$. Construct the Lyapunov function

$$V = \frac{1}{2}\mathbf{e}^T\mathbf{e} \tag{8}$$

Observe that

$$\dot{V} = \mathbf{e}^T\dot{\mathbf{e}} = \mathbf{e}^T(\phi(\mathbf{x}) - \phi(\mathbf{z})) \leq 0 . \tag{9}$$

Since $\phi(.)$ is decreasing in $D$, by hypothesis, the last inequality is satisfied, and the $\mathbf{x}$-$\mathbf{z}$ system is identically synchronized (synchronization in the usual sense) as $t \to \infty$, i.e.

$$\lim_{t\to\infty} \mathbf{y}(t) = \lim_{t\to\infty} \lambda\mathbf{z}(t) = \lambda\mathbf{x}(t) . \tag{10}$$

It follows that $\mathbf{y} = H(\mathbf{x}) = \lambda\mathbf{x}$ is the associated GS transformation. ■

**Example.** Consider Chua's oscillator defined by [Chua, 1993]

$$\begin{cases} \dot{x} = \alpha[y - x - f(x)] \\ \dot{y} = x - y + z \\ \dot{z} = -\beta y - \gamma z \end{cases} \tag{11}$$

where

$$f(x) = bx + \frac{1}{2}(a - b)(|x + 1| - |x - 1|) . \tag{12}$$

Equation (11) can be decomposed as follow:

$$\underbrace{\begin{pmatrix} \dot{x} \\ \dot{y} \\ \dot{z} \end{pmatrix}}_{\dot{\mathbf{x}}} = \underbrace{\begin{pmatrix} -\alpha & \alpha & 0 \\ 1 & -1 & 1 \\ 0 & -\beta & -\gamma \end{pmatrix}\begin{pmatrix} x \\ y \\ z \end{pmatrix}}_{\phi(\mathbf{x})} + \underbrace{\begin{pmatrix} -\alpha f(x) \\ 0 \\ 0 \end{pmatrix}}_{\psi(\mathbf{x})} . \tag{13}$$

If $\phi(\mathbf{x})$ is decreasing globally,[1] we have $D = R^3$. It follows that we only need to transmit a scalar

[1] We can choose $\alpha$, $\beta$ and $\gamma$ such that the following matrix

$$\begin{pmatrix} -\alpha & \alpha & 0 \\ 1 & -1 & 1 \\ 0 & -\beta & -\gamma \end{pmatrix}$$

is negative definite. It follows from Theorem 4 in [Wu & Chua, 1994] that $\phi(\mathbf{x})$ is decreasing globally.

signal $f(x)$ for achieving GS. The receiver system is simply:

$$\underbrace{\begin{pmatrix}\dot{x}_1\\ \dot{y}_1\\ \dot{z}_1\end{pmatrix}}_{\dot{\mathbf{x}}_1} = \underbrace{\begin{pmatrix}-\alpha & \alpha & 0\\ 1 & -1 & 1\\ 0 & -\beta & -\gamma\end{pmatrix}\begin{pmatrix}x_1\\ y_1\\ z_1\end{pmatrix}}_{\phi(\mathbf{x}_1)} + \lambda \underbrace{\begin{pmatrix}-\alpha f(x)\\ 0\\ 0\end{pmatrix}}_{\psi(\mathbf{x})}. \tag{14}$$

Our simulation results are shown in Fig. 1. Figure 1(a) shows the attractor of the driving system, which resembles the lower branch of a Chua's spiral attractor. The Lissajous figures, henceforth called the GS plots between the three respective pairs of variables $x_1$ versus $x$, $y_1$ versus $y$, and $z_1$ versus $z$, are shown in Figs. 1(b), 1(c), and 1(d), respectively. Observe that the associated GS transformation function $H(\cdot)$ for these systems is *linear* in accordance with Eq. (5) of Theorem 1. Comparing the two attractors in Figs. 1(a) and 1(e) one can see that they have the same shape. Indeed, they are scaled versions of each other.

## 3. Secure Communication

In this section, we propose an application of the preceding channel-independent GS schemes to chaotic secure communication of *binary* signals. Our proposed scheme is significant because practical channels are always distorted. We will use a chaotic switching scheme to scramble the binary message signal. At the transmitter end, the binary signal is used to switch some parameter of the function $\psi(\mathbf{x})$ between two parameter sets, which correspond to bit-0 and bit-1, respectively. At the receiver end, our parameter change can be detected by comparing the received signal and a state-variable signal generated by the receiver. The block diagram of our proposed scheme is shown in Fig. 2. Observe that before the signal is transmitted to the channel, we use a *random* gain to scramble it. Observe also that a clock signal is used to ensure that during the time period of every bit, the adaptable gain is kept unchanged.

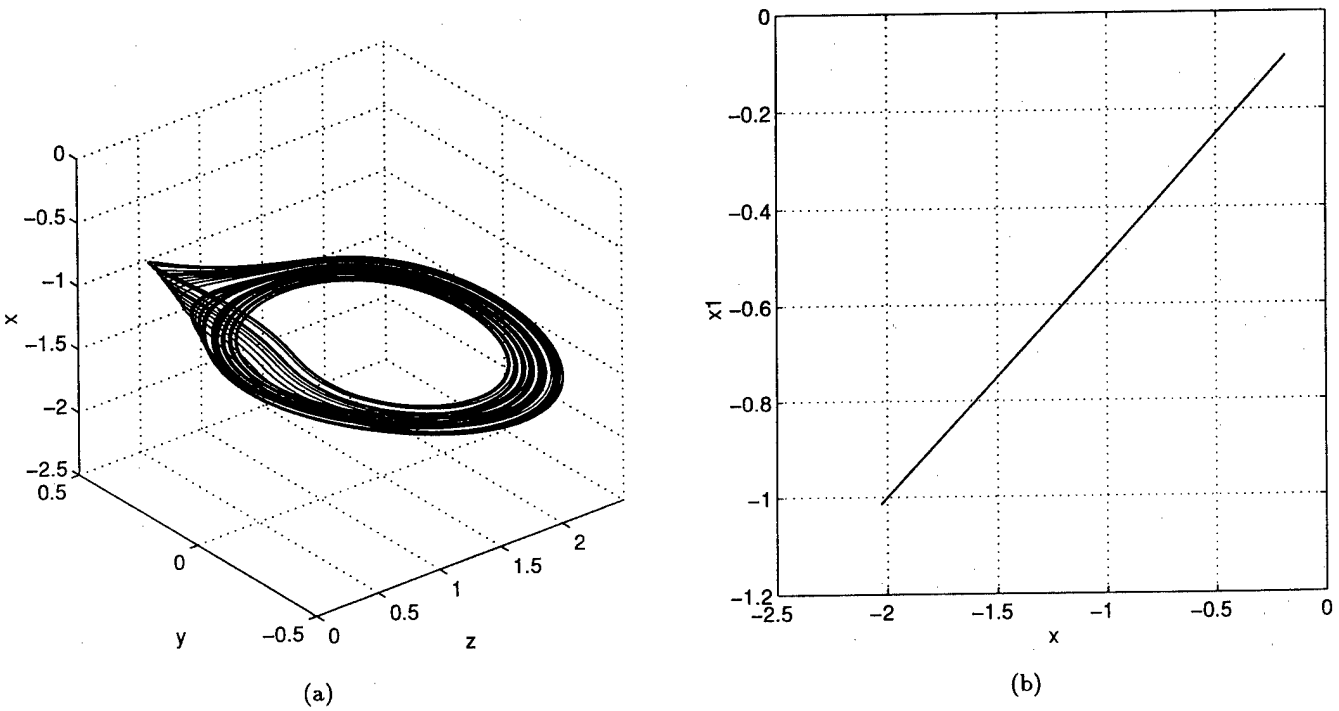


Fig. 1. Simulation results with a linear channel with unknown gain. (a) Attractor of the driving system. (b) the $x - x_1$ GS plot. (c) the $y - y_1$ GS plot. (d) the $z - z_1$ GS plot. (e) Corresponding attractor of the driven system.

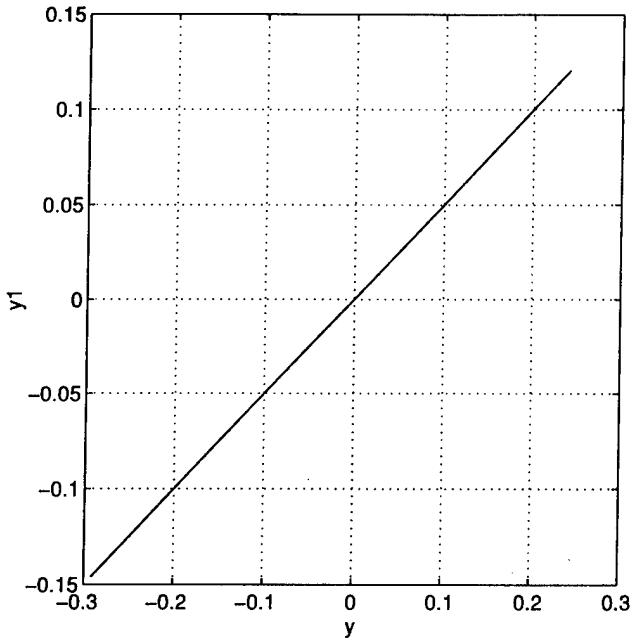


(c)

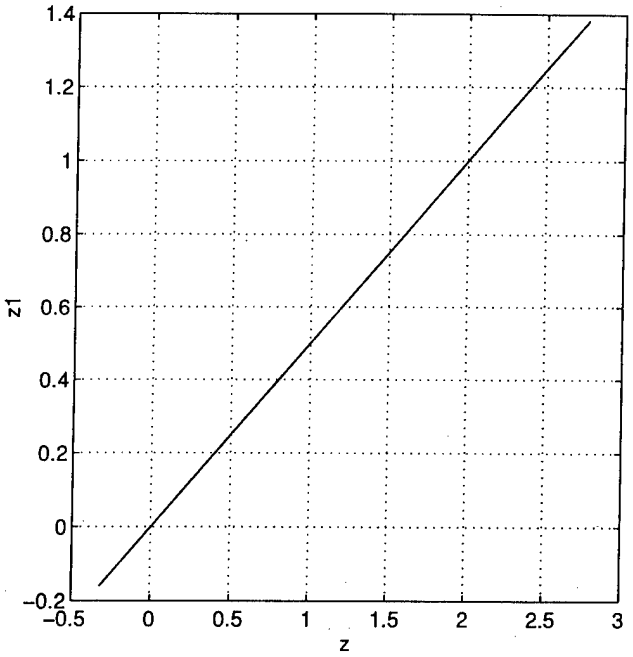


(d)

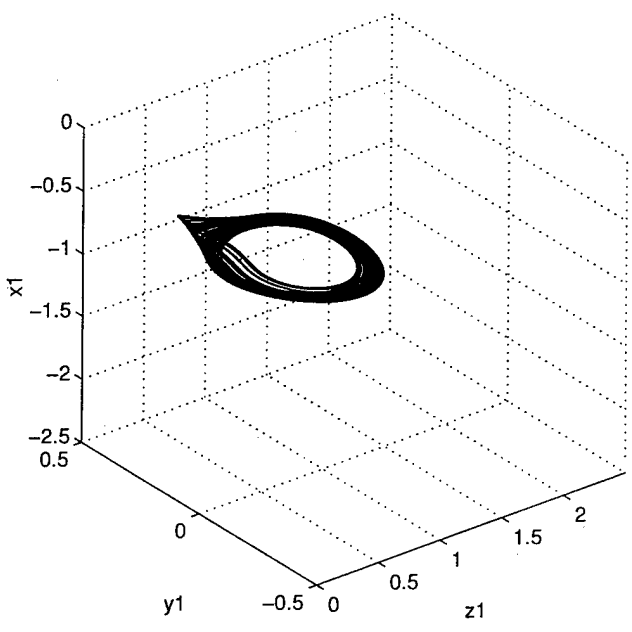


(e)

Fig. 1. (*Continued*)

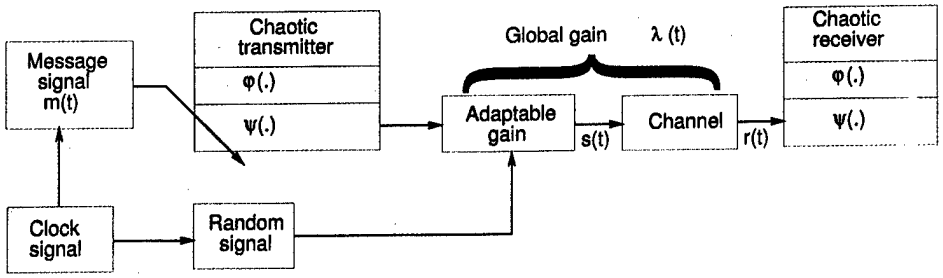


Fig. 2. Block diagram of a GS-based secure communication scheme.

Observe that our random signal can be a *truly random signal*[2] sampled from the real physical world and that both the transmitter and the receiver do not need to know anything about this random sequence. However, for an intruder trying to figure out the message signal from the transmitted signal by using standard identification methods, he has to figure out first what the random sequence is. This security improvement scheme can be efficiently used to protect our system from such possible eavesdropper *attack* as proposed in [Short, 1994].

In the following illustrations, we will use Chua's oscillators as the chaotic transmitter and receiver. For convenience of hardware implementation, we will use the following actual circuit equations of Chua's oscillator

$$\begin{cases} \dfrac{dv_1}{dt} = \dfrac{1}{C_1}\left[G(v_2 - v_1) - f(v_1)\right] \\ \dfrac{dv_2}{dt} = \dfrac{1}{C_2}\left[G(v_1 - v_2) + i_3\right] \\ \dfrac{di_3}{dt} = \dfrac{1}{L}\left[-v_2 - R_0 i_3\right] \end{cases} \tag{15}$$

where $G = \frac{1}{R}$ and $f(v_1)$, the piecewise linear $v - i$ characteristics of Chua's diode, is given by

$$f(v_1) = G_b v_1 + \frac{1}{2}(G_a - G_b)(|v_1 + E| - |v_1 - E|) \tag{16}$$

where $E$ is the breakpoint voltage of Chua's diode. We will choose $f(v_1)$ as our transmitted signal. The receiver is given by:

$$\begin{cases} \dfrac{d\hat{v}_1}{dt} = \dfrac{1}{C_1}\left[G(\hat{v}_2 - \hat{v}_1) - r(t)\right] \\ \dfrac{d\hat{v}_2}{dt} = \dfrac{1}{C_2}\left[G(\hat{v}_1 - \hat{v}_2) + \hat{i}_3\right] \\ \dfrac{d\hat{i}_3}{dt} = \dfrac{1}{L}\left[-\hat{v}_2 - R_0 \hat{i}_3\right] \end{cases} \tag{17}$$

where $r(t)$ is the received signal.

We modulate the digital signal by switching the value of the two parameters $G_a$ and $G_b$ in Eq. (16). At the receiver, we determine the value of

$$\hat{G} \triangleq \frac{r(t)}{\hat{v}_1(t)} \tag{18}$$

at the moments when both $\dot{\hat{v}}_1 = 0$ and $\mathrm{sgn}(\hat{v}_1)\ddot{\hat{v}}_1 < 0$, where $\hat{v}_1(t)$ is the voltage across capacitor $C_1$.

In the following simulation, the parameters for coding *bit-0* are: $C_1 = 17$ nF, $C_2 = 178$ nF, $G = 1$ mS, $L = 12$ mH, $G_a = -1.139$ mS, $G_b = -0.711$ mS, $E = 1$ V, $R_0 = 20\ \Omega$. The parameters for coding *bit-1* are the same except for $G_a = -1.189$ mS and $G_b = -0.611$ mS. A fourth-order Runge–Kutta method with fixed step-size $10^{-5}$ s is used in our simulation.

To recover the binary message signal at the receiver end, let us first study the difference between the $|\hat{v}_1|$-$\hat{G}$ maps when different parameter sets and channel gains are used. For each fixed parameter set, the values of $|\hat{v}_1|$ and $\hat{G}$ will vary as we change the channel gain parameter $\lambda$. Let us plot the values of $|\hat{v}_1|$ and $\hat{G}$ in the $|\hat{v}_1|$ versus $\hat{G}$ plane as $\lambda$ varies from 0.01 to 1, as shown in Fig. 3(a) in two colors: the "red" curve corresponding to *bit 0*, and the "blue" curve corresponding to *bit 1*. It should be noted that only those points corresponding to the moments when $\dot{\hat{v}}_1 = 0$ and $\mathrm{sgn}(\hat{v}_1)\ddot{\hat{v}}_1 < 0$ are plotted. The difference between these two "bit detection" plots are significant. In fact, it is the

[2]Here, a *truly random signal* means that even the transmitter cannot reproduce this random signal.

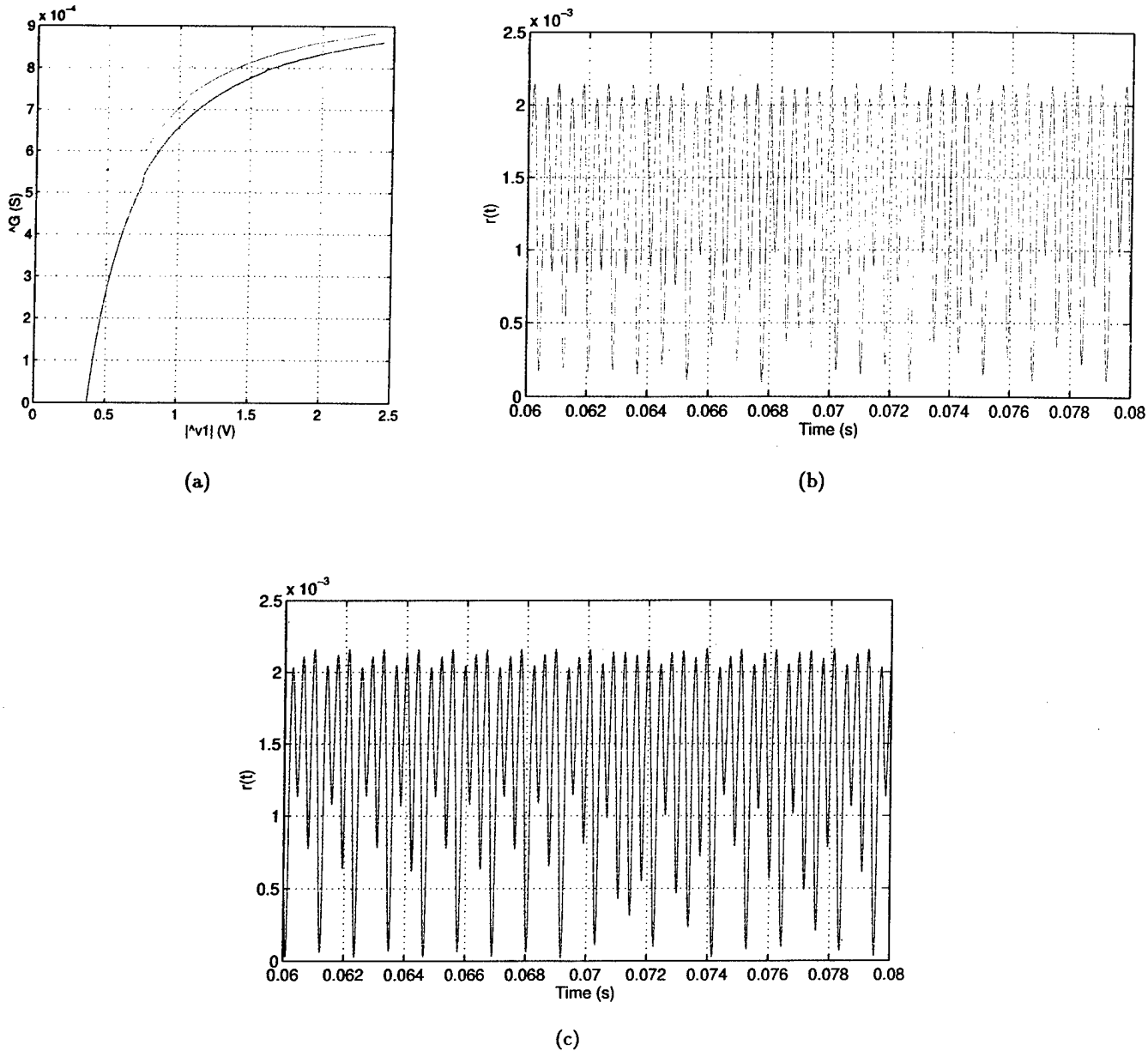


**Fig. 3. Bit detection maps corresponding to two qualitatively similar waveforms. (a) The difference between the two $|\hat{v}_1|$-$\hat{G}$ plots corresponding to the two parameter sets for coding bit-0 and bit-1. (b) Waveform of $r(t)$ for coding bit-0. (c) Waveform of $r(t)$ for coding bit-1.**

direct foundation for recovering the message signal from the received signal. When the transmitter parameters are switched between two parameter sets, the corresponding $|\hat{v}_1|$-$\hat{G}$ plot will switch between these two curves. Observe that the spacings between these two plots are essentially independent of the channel gain $\lambda$. Hence, to recover the binary message signal, we only have to measure the peaks of $|\hat{v}_1(t)|$ and the corresponding values of $\hat{G}$. The waveform of $r(t)$ (in red) for coding bit-0 with $\lambda = 1$ is shown in Fig. 3(b). The waveform of $r(t)$ (in blue) for coding bit-1 with $\lambda = 1$ is shown in Fig. 3(c). Observe that these two waveforms reveal no discernible qualitative differences between them and it is not obvious at all that they hide a binary message.

The message recovering process is as follows. First, we use the received signal to derive a $|\hat{v}_1|$-$\hat{G}$ "bit-detection" map. We can even fabricate this map together with the receiver to serve as

another hardware key. In practical applications, the receiver recovers the message signal by matching the GS results with the $|\hat{v}_1|$-$\hat{G}$ bit detection map.

In particular, it is very important for our chaotic switching method to work at a high bit-rate — both from security considerations [Yang, 1995], and for increasing transmission efficiency. To achieve this goal, we can set up a look-up table at the transmitter end. Whenever a bit change occurs (i.e. from bit-1 to bit-0 or from bit-0 to bit-1), the transmitter randomly selects a point in the stable attractor corresponding to the next bit. This point should satisfy the condition that $f(v_1)$ is the same as that of the last instant of the former bit. This can be easily implemented by finding $v_1$ from $f(v_1)$ and then using $v_1$ to locate the point. Our simulation results are shown in Fig. 4. Figure 4(a) shows the received signal. Figure 4(b) shows the randomly changed (or scrambled) global channel gain $\lambda(t)$ (in blue), the binary message signal (in green) and the

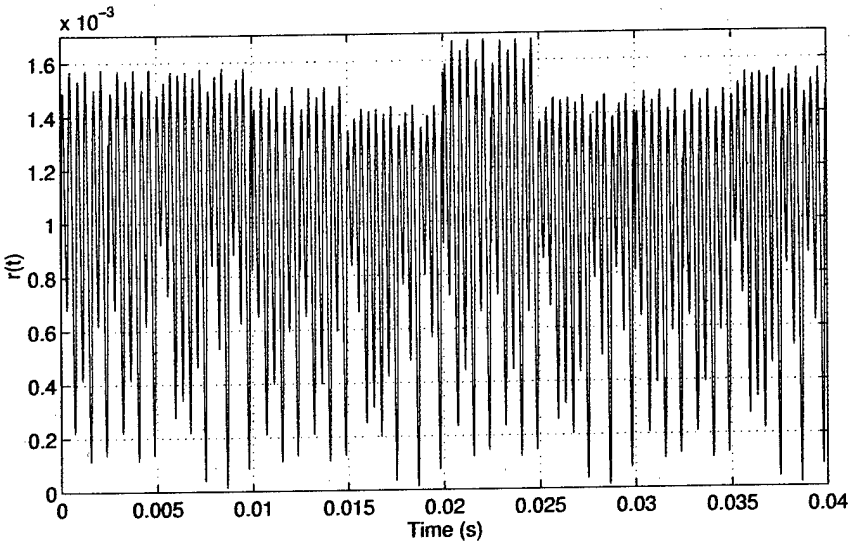


(a)

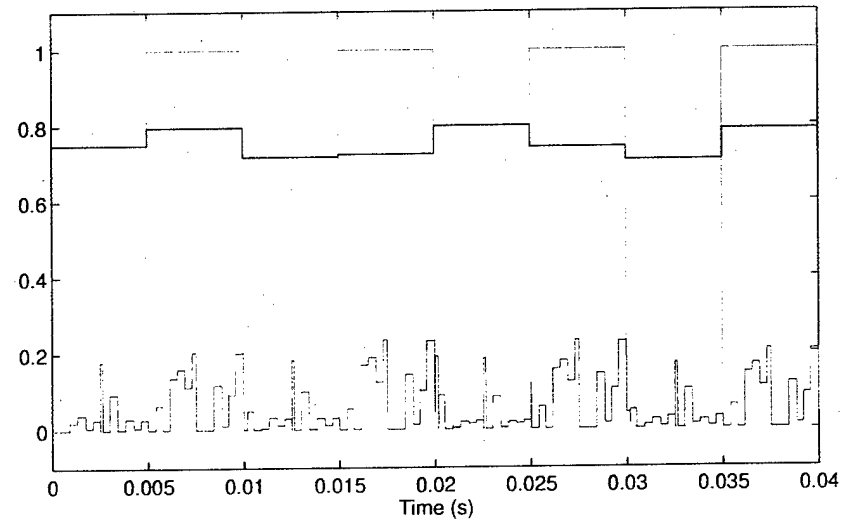


(b)

Fig. 4. Simulation results of channel-independent chaotic switching. (a) The received signal. (b) The message signal (green), recovered signal (red) and the global channel gain (blue).

recovered signal (in red). From Fig. 4(b), one can see that the digital signal can be easily recovered by using a moving average filter and thresholding.

## 4. Concluding Remarks

One disadvantage of a chaotic-synchronization based spread-spectrum communication is its sensitivity to variations in the channel gain. In this letter, we present a new scheme which is insensitive to channel distortions. Since the amplitude of our transmitted signal is scrambled by a randomly varying gain, it would be nearly impossible to apply any identification-based method to break the security of our proposed scheme.

## Acknowledgments

This work is supported by the Office of Naval Research under grant No. N00014-96-1-0753.

## References

Carroll, T. L. [1996] "Amplitude-independent chaotic synchronization," *Phys. Rev.* **E53**(4), 3117–3122.

Chua, L. O. [1993] "Global unfolding of Chua's circuit," *IEICE Trans. Fundamentals* **E76-A**(5), 704–734.

Chua, L. O., Yang, T., Zhong, G. Q. & Wu, C. W. [1996] "Adaptive synchronization of Chua's oscillators," *Int. J. Bifurcation and Chaos* **6**(1), 189–201.

Chua, L. O., Yang, T., Zhong, G. Q. & Wu, C. W. [1996] "Synchronization of Chua's circuits with time-varying channels and parameters," *IEEE Trans. Circ. Syst. — I: Fundamental Theory and Applications* **43**(10), 862–868.

Kocarev, L. & Parlitz, U. [1996] "Generalized synchronization, predictability, and equivalence of unidirectionally coupled dynamical systems," *Phys. Rev. Lett.* **76**(11), 1816–1819.

Rulkov, N. F., Sushchik, M. M. & Tsimring, L. S. [1996] "Generalized synchronization of chaos in directionally coupled chaotic systems," *Phys. Rev.* **E51**(2), 980–994.

Short, K. M. [1994] "Steps toward unmasking secure communications," *Int. J. Bifurcations and Chaos* **4**(4), 957–977.

Wu, C. W. & Chua, L. O. [1994] "A unified framework for synchronization and control of dynamical systems," *Int. J. Bifurcations and Chaos* **4**(4), 430–447.

Wu, C. W., Yang, T. & Chua, L. O. [1996] "On adaptive synchronization and control of nonlinear dynamical systems," *Int. J. Bifurcations and Chaos* **6**(3), 455–471.

Yang, T. [1995] "Recovery of digital signals from chaotic switching," *Int. J. Circ. Theor. Appl.* **23**(6), 611–615.

Yang, T., Wu, C. W. & Chua, L. O. [1997] "Cryptography based on chaotic systems," *IEEE Trans. Circ. Syst. — I: Fundamental Theory and Applications*, accepted for publication.

International Journal of Bifurcation and Chaos, Vol. 6, No. 11 (1996) 2119–2125
© World Scientific Publishing Company

# A METHOD FOR ENCODING MESSAGES BY TIME TARGETING OF THE TRAJECTORIES OF CHAOTIC SYSTEMS

D. GLIGOROSKI
*Institute of Informatics, Faculty of Natural Sciences, P.O. Box 162, Skopje, Macedonia*
D. DIMOVSKI
*Institute of Mathematics, Faculty of Natural Sciences, P.O. Box 162, Skopje, Macedonia*
L. KOCAREV
*Department of Electrical Engineering, P.O. Box 574, Skopje, Macedonia*
V. URUMOV
*Institute of Physics, Faculty of Natural Sciences, P.O. Box 162, Skopje, Macedonia*
L. O. CHUA
*Department of Electrical Engineering and Computer Sciences, University of California, Berkeley, CA 94720, USA*

Received March 30, 1996; Revised May 4, 1996

We suggest a method for encoding messages by chaotic dynamical systems. The main idea is that by targeting the trajectories of some chaotic dynamical system with time constraint, someone can send a information to the remote recipient. The concept is based on setting receptors in the phase space of the dynamical system, and then targeting the trajectory between them. We considered the time of arriving from one receptor to another as a carrier of information obtained by searching in the table of values for arriving times.

## 1. Introduction

Since 1990, when an inspiring article about controlling chaos appeared [Ott *et al.*, 1990], many possible applications arose from the concept of controlling chaos. One of the possible applications was first considered by Hayes, Grebogi and Ott in [Hayes *et al.*, 1993] relying on targeting techniques (see [Hayes *et al.*, 1993; Shinbrot *et al.*, 1990]). There they proposed to code some information by targeting a chaotic trajectory between two half-planes of a Poincaré section. Every hit of the trajectory at one of the half-planes was treated as sending a bit of information (0 or 1). Many researchers agreed that besides the fact that the idea was nice and it was experimentally verified in [Hayes *et al.*, 1994], the transmission of the data was too slow for any practical application. After that, a new refreshing idea came from Schweizer and Kennedy (see [Schweizer & Kennedy, 1995]), where Poincaré section was divided into regions whose number was between $2^4$ and $2^8$, so called subsectors, and the trajectory was controlled and targeted between those subsectors following a desired symbolic sequence (so called Predictive Poincaré Control (PPC)). The size of the alphabet they deal with, was equal to the number of the subsectors i.e. between $2^4$ and $2^8$.

In this paper we propose another approach, based on the fact that a huge amount of information is discarded when the time of arrival of the trajectory from one position to another is omitted. In

this case we will show that the size of the alphabet can be more than $2^{17}$.

## 2. The Method for Solution of Time Targeting Problem in Chaotic Systems

In [Gligoroski *et al.*, 1996] a method for the solution of the Time Targeting Problem was given. Here we briefly describe the method. Instead of the dynamical system given by

$$\dot{\mathbf{x}} = \mathbf{F}(\mathbf{x}, \mathbf{p}), \tag{1}$$

where $\mathbf{x} = (x_1, x_2, \ldots, x_n)$ is a point in the phase space we consider the system

$$\dot{\mathbf{x}} = \mathbf{F}(\mathbf{x}, \mathbf{p}) + \mathbf{g}(\mathbf{x}), \tag{2}$$

where $\mathbf{g}$ is a real $n$-component function of $\mathbf{x}$. In [Gligoroski *et al.*, 1996] this component was chosen to take small values, i.e. $|\mathbf{g}(\mathbf{x})| \leq \delta$, for $\delta$ relatively small fixed value (less than 0.1% of the size of the attractor), but as we will see further, for defining a method for digital communication by chaotic systems, there is no need for that restriction. First let us accept some common notions that will be used in the article. Let $\mathcal{A} \subset R^n$ be the attractor of the dynamical system described by (1) in $n$-dimensional phase space $R^n$, and let $\mathbf{r}_1 \in \mathcal{A}$ be a point, in the $\varepsilon$-neighborhood $O(\mathbf{r}_1, \varepsilon)$ of which we want to target the trajectory of the dynamical system, starting from a point $\mathbf{r}_2 \in \mathcal{A}$. Further, denote by $T(\mathbf{f}, \mathbf{x}_0)$ the trajectory obtained by (1), with some initial point $\mathbf{x}_0$ at $t = 0$, where $\mathbf{f}$ is a solution of (1). In [Gligoroski *et al.*, 1996] it was discussed that there exists a part of the trajectory $T(\mathbf{f}, \mathbf{x})$ with the property that $\mathbf{x} \in \mathcal{A}$ and $\mathbf{x} = \mathbf{f}(\mathbf{x}, 0)$ and there exists $t > 0$, such that $(\forall s)(0 \leq s < t)\mathbf{f}(\mathbf{x}, s) \notin O(\mathbf{r}_1, \varepsilon)$ and $\mathbf{f}(\mathbf{x}, t) \in \partial O(\mathbf{r}_1, \varepsilon)$, where $\partial O(\mathbf{r}_1, \varepsilon)$ is the boundary of the neighborhood $O(\mathbf{r}_1, \varepsilon)$. By $\hat{T}_{\mathbf{r}_1}$ we denote that part of the trajectory.

Further, for every $\hat{T}_{\mathbf{r}_1}$ ($\hat{T}_{\mathbf{r}_1} \subset R^n$), we define $\mathbf{h} : \hat{T}_{\mathbf{r}_1} \to R^{n+1}$ by:

$$\mathbf{h}(\mathbf{x}') = (\mathbf{f}(\mathbf{x}, \mathbf{s}), \mathbf{t} - \mathbf{s}), \quad \text{for every } \mathbf{x}' = \mathbf{f}(\mathbf{x}, s) \in \hat{T}_{\mathbf{r}_1}, \tag{3}$$

We denote $\mathbf{h}(\hat{T}_{\mathbf{r}_1})$ by $\hat{T}^t_{\mathbf{r}_1}$. So the points $\mathbf{x}'^t \in \hat{T}^t_{\mathbf{r}_1}$ are of the form $\mathbf{x}'^t = (x'_1, x'_2, \ldots, x'_n, t^{\mathbf{r}_1}_{\mathbf{x}}) \in R^{n+1}$ where $\mathbf{x}' = (x'_1, x'_2, \ldots, x'_n)$ and the $(n+1)$th coordinate $t^{\mathbf{r}_1}_{\mathbf{x}} = t - s$ (i.e. time coordinate) is the time needed for the system (1) to arrive at $O(\mathbf{r}_1, \varepsilon)$ starting from $\mathbf{x}'$ without perturbation.

Having all these definitions, we will now describe the algorithm for solving the Time Targeting Problem in chaotic systems. The notation is similar like in [Gligoroski *et al.*, 1996] but it is adopted for the purposes of this article.

### Preparatory Phase

***Step 1.*** Take a random point $\mathbf{r}_1 \in \mathcal{A}$ in whose neighborhood one wants to arrive, from some random point $\mathbf{r}_2 \in \mathcal{A}$, and specify the time *TargetTime* for reaching the $O(\mathbf{r}_1, \varepsilon)$ from $\mathbf{r}_2$.

***Step 2.*** Collect the data of the set $\{\hat{T}^t_{\mathbf{r}_{1j}}\}_{j=1,N}$ for the point $\mathbf{r}_1$.

### Controlling Phase

***Step 3.*** Set $\mathbf{x} \in O(\mathbf{r}_2, \varepsilon)$ and *CountDown* = *TargetTime*.

***Step 4.*** Integrate the system (1) starting from $\mathbf{x}$, for a small time step $\Delta\tau$, reaching some new point $\mathbf{x}$; Decrease *CountDown* by $\Delta\tau$, i.e. *CountDown* = *CountDown* $- \Delta\tau$.

***Step 5.*** Find the point $\hat{\mathbf{y}}^t_j \in \{\hat{T}^t_{\mathbf{r}_{1j}}\}_{j=1,N}$ which is at a "smallest distance" from the point $\mathbf{x}^t = (\mathbf{x}, \mathit{CountDown})$.

***Step 6.*** Push $\mathbf{x}$ to a new position $\mathbf{x}$, toward the point $\hat{\mathbf{y}}_j$ where $\hat{\mathbf{y}}^t_j = (\hat{\mathbf{y}}_j, t^{\mathbf{r}_1}_{\hat{\mathbf{y}}_j})$, with the restriction that the perturbation does not exceed $\delta$.

***Step 7.*** If $\mathbf{x} \notin O(\mathbf{r}_1, \varepsilon)$ and *CountDown* $> 0$ then go to Step 4.

In the Fig. 1 we are showing the results of applying the above algorithm on the double scroll attractor of the Chua's circuit [Parker & Chua, 1989] defined by the equations

$$\frac{dx}{dt} = \alpha(y - h(x)), \quad \frac{dy}{dt} = x - y + z, \quad \frac{dz}{dt} = -\beta y \tag{4}$$

where $h$ is the piecewise-linear function

$$h(x) = \begin{cases} m_1 x + (m_0 - m_1), & x \geq 1 \\ m_0 x, & |x| \leq 1 \\ m_1 x - (m_0 - m_1), & x \leq -1 \end{cases} \tag{5}$$

and where $\alpha = 9$, $\beta = 100/7$, $m_0 = -1/7$, $m_1 = 2/7$, and for the points $\mathbf{r}_1 = (1.845436494276013,$

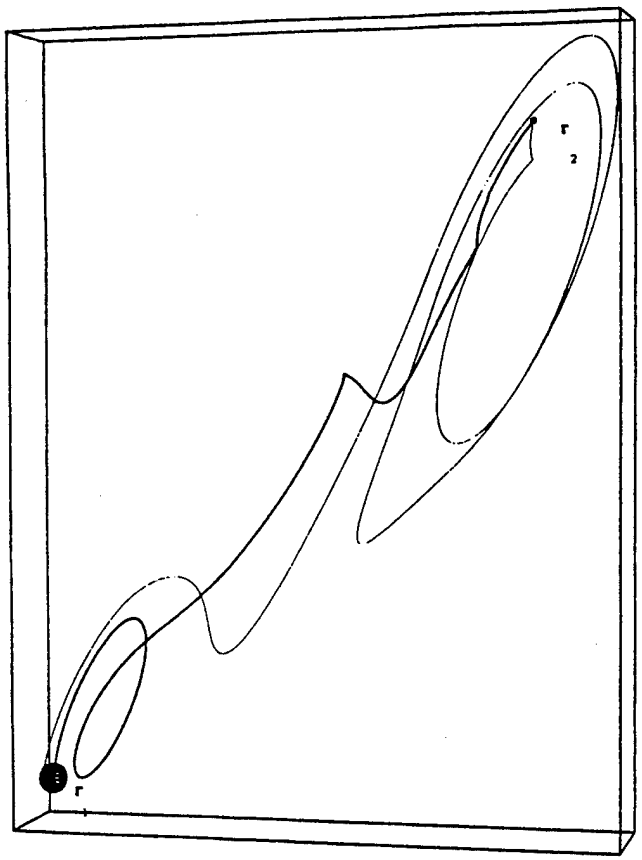


Fig. 1. Time Targeting on the double scroll attractor; Thin trajectory started at $\mathbf{r}_2$ reached $O(\mathbf{r}_1, \varepsilon)$ after *TargetTime*= 4.5; Thick trajectory started at $\mathbf{r}_2$ reached $O(\mathbf{r}_1, \varepsilon)$ after *TargetTime*= 7.0.

0.122463900650633, −2.010749234398700) and $\mathbf{r}_2$ = (−1.683256250478941, 0.141054046947965, 2.583098236358436), with $\Delta\tau = 0.001$, $\delta = 0.002$, $\varepsilon = 0.1$ and *TargetTime*=4.5 and *TargetTime*= 7.0.

As mentioned, if someone wants to control a chaotic system in some real physical system, he(she) will have to deal with perturbations which will be naturally constrained by some amount $\delta$. On the other hand if the above algorithm is going to be used in digital communications then, this constrain does not need to be considered. Exactly this case will be described in the following section.

## 3. A Method for Coding Information, by Time Targeting of the Chaotic Trajectories

To exploit the concept of targeting the trajectories for coding some information, we will define $M$ points in the phase space such that they will be as receptors and we will create a table of values describing what information was sent when the chaotic trajectory arrived from say receptor $\mathbf{r}_i$ to the receptor $\mathbf{r}_j$ (Table 1). So let us denote by $\mathbf{r}_i \in \mathcal{A}$, $i = 1, \ldots, M$ the points in which $\varepsilon$-neighborhood $O(\mathbf{r}_i, \varepsilon)$ we want to target the trajectory of the dynamical system. We will consider the transmission of the data as sending the sequence of letters $a_i \in \Sigma$, where $\Sigma = \{a_1, a_2, \ldots, a_m\}$ is an alphabet consisting of $m$ letters. We additionally want the position of the receptors and the value of $\varepsilon$ to be such that $(\forall i, j)(O(\mathbf{r}_i, \varepsilon) \cap O(\mathbf{r}_j, \varepsilon) = \emptyset)$.

Table 1. Table for definition of a finite automaton from the receptors $\mathbf{r}_i$.

| $\Omega$ | $\mathbf{r}_1$ | $\mathbf{r}_2$ | $\cdots$ | $\mathbf{r}_M$ |
|---|---|---|---|---|
| $\mathbf{r}_1$ | $U_{1,1}$ | $U_{1,2}$ | $\cdots$ | $U_{1,M}$ |
| $\mathbf{r}_2$ | $U_{2,1}$ | $U_{2,2}$ | $\cdots$ | $U_{2,M}$ |
| $\vdots$ | $\vdots$ | $\vdots$ | $\ddots$ | $\vdots$ |
| $\mathbf{r}_M$ | $U_{M,1}$ | $U_{M,2}$ | $\cdots$ | $U_{M,M}$ |

Now for every $i, j \in \{1, 2, \ldots, M\}$ we define $M^2$ subsets of the set $\Sigma$, $U_{i,j} = \{a_{\nu_1}, a_{\nu_2}, \ldots, a_{\nu_{ij}}\} \subseteq \Sigma$ such that:

$$(\forall i \in \{1, 2, \ldots, M\}) \left( \bigcup_{j=1}^{M} U_{i,j} = \Sigma \right) \qquad (6)$$

$$(\forall i, j_1, j_2 \in \{1, 2, \ldots, M\})(j_1 \neq j_2)(U_{i,j_1} \cap U_{i,j_2} = \emptyset) \qquad (7)$$

With Table 1, we can define deterministic finite automaton $A = (K, \Sigma, \Omega, s, F)$ where $K = \{\mathbf{r}_1, \mathbf{r}_2, \ldots, \mathbf{r}_M\}$ is a finite set of $M$ states, $\Sigma = \{a_1, a_2, \ldots, a_m\}$ is an alphabet consisting of $m$ letters, $s$ is the initial state, $F \subseteq K$ is the set of final states and $\Omega$ is the transition function from $K \times \Sigma$ to $K$ given by Table 1 (see [Lewis & Papadimitriu, 1981]). Note that conditions (6) and (7) guarantee that $\Omega$ is well defined. Now if we want the automaton $A$ to work in our dynamical system (1), then we will have to make the following assumptions and changes:

1. If $\mathbf{x} = f(\mathbf{x}_0, t) \in O(\mathbf{r}_i, \varepsilon)$ then we will say that the automaton is in the state $\mathbf{r}_i$;
2. For every $a_\nu \in U_{i,j}$ we will define unique time $T^i_{a_\nu}$ and that value will mean that if we are in the state $\mathbf{r}_i$ (i.e. in the $O(\mathbf{r}_i, \varepsilon)$) then if we want

to send the letter $a_\nu$ we will have to send some information to the receiver, such that chaotic trajectory will arrive from $\mathbf{r}_i$ to $\mathbf{r}_j$ for the time $T^i_{a_\nu}$.

3. We will slightly change the nature of the automaton, defining that the subset $F$ of the final states, will be dynamically determined during the work of the automaton. Namely from the set $\Sigma$ we will determine a letter $a_{STOP}$, that will determine the set $F$ in the following manner: If the letter $a_{STOP}$ was processed through the automaton, then the actual state $\mathbf{r}_\nu$ will become a member of $F$, i.e. the work of the automaton will stop. Formally this means that the automaton $A$ recognizes the language $(\Sigma \backslash \{a_{STOP}\})^* a_{STOP}$.

Now we give a description of the method for coding (decoding) the messages, i.e. the communication between two participants. Both sender and receiver will have to have these common information:

1. Definition of the dynamical system, which could be **private** or **public**.
2. Definition of the initial position $\mathbf{x}_0 \in R^n$ which will be **private**.
3. Definition for the integration time step $\Delta\tau$, which could be **public**.
4. Definition of the position of the $M$ receptors $\mathbf{r}_i \in \mathcal{A}$, $i = 1, \ldots, M$ which will be **private**.
5. Definition of the function $\Omega$ which could be **public**.
6. Definition of the corresponding values of times $T^i_{a_\nu}$ which could be **public**.

From all this it follows that the key for secure communication will be the $(M+1)$-tuple $(\mathbf{x}_0, \mathbf{r}_1, \mathbf{r}_2, \ldots, \mathbf{r}_M)$ or the $(M+2)$-tuple $(\mathbf{F}, \mathbf{x}_0, \mathbf{r}_1, \mathbf{r}_2, \ldots, \mathbf{r}_M)$.

Below, in the form of the algorithm we give the actions that will have to make both sender and receiver of the information.

## Preparatory Phase

***Step 1.*** For every receptor $\mathbf{r}_i$, $i = 1, \ldots, M$ define the sets of trajectories $\mathbf{T}_i = \{\hat{T}^t_{\mathbf{r}_{i,j}}\}_{j=1,N_i}$.

***Step 2.*** Take a word $\mathbf{w} = w_1 w_2 \cdots w_k \in \Sigma^*$ which is to be sent, and set $\mathbf{w}' = w_2 w_3 \cdots w_k$ where $w_l \in \Sigma$, $l = 1, \ldots, k$.

***Step 3.*** Set $\mathbf{x} = \mathbf{x}_0$.

***Step 4.*** Set $i = 1$, $R = \mathbf{r}_1$.

## Transmission Phase

***Step 4.*** In the table for $\Omega$, for the receptor $R$ find the column $j$ where the first letter of $\mathbf{w}$, i.e. $w_1 = a_\nu \in U_{i,j}$ is. For the $a_\nu$ set $TargetTime = T^i_{a_\nu}$.

***Step 5.*** From the set $\mathbf{T}_j$ find a point $\mathbf{y}^t = (\mathbf{y}, TargetTime)$ i.e. such that $\mathbf{f}(\mathbf{y}, TargetTime) \in O(\mathbf{r}_j, \varepsilon)$, and $\mathbf{f}(\mathbf{y}, s) \notin O(\mathbf{r}_j, \varepsilon)$ for $0 \leq s < TargetTime - \Delta\tau$.

***Step 6.*** Transmit the vector $\alpha = \mathbf{y} - \mathbf{x}$.

***Step 7.*** Set $\mathbf{x} = \mathbf{f}(\mathbf{y}, TargetTime)$.

***Step 8.*** Set $i = j$.

***Step 9.*** Set $R = \mathbf{r}_i$.

***Step 10.*** Set $\mathbf{w} = \mathbf{w}'$ and then set $\mathbf{w}' = w_2 w_3 \cdots w_{|\mathbf{w}|}$, where $|\mathbf{w}|$ is the length of the word $\mathbf{w}$.

***Step 11.*** If not ($|\mathbf{w}| = 0$ or $R \in F$) then GoTo Step 4.

Here we have to give a commentary about some of the steps. In the Step 1, while determining $\mathbf{T}_i$, $i = 1, \ldots, M$ one additional condition has to be satisfied:

$$(\forall i, j \in \{1, 2, \ldots, M\})(\forall l \in \{1, \ldots, N_i\}) \\ (i \neq j)(\hat{T}^t_{\mathbf{r}_{il}} \cap O(\mathbf{r}_j, \varepsilon) = \emptyset) \tag{8}$$

The condition (8) ensures that during the evolution in the dynamical system, the trajectory will not meet some other receptor except the wanted one. There is no necessity every time in the beginning of the communication for the sender to search for $\mathbf{T}_i$, $i = 1, \ldots, M$, but it would be practical if he(she) calculates them once prior the communication. The receiver does not have to have this information. The exchange of information is made in Step 6. In fact the receiver will receive a sequence of the $n$-dimensional vectors $(\alpha_l)$, $l = 1, \ldots, k$ which will translate the initial position in the phase space from where the receiver will integrate the dynamical system. Below the steps of the receiver are described.

## Preparatory Phase

***Step 1.*** Set $\mathbf{x} = \mathbf{x}_0$.

***Step 2.*** Set $i = 1$, $R = \mathbf{r}_1$.

## Decoding Phase

***Step 3.*** Receive the vector $\alpha$.

*Step 4.* Set $\mathbf{x} = \mathbf{x} + \alpha$.

*Step 5.* Integrate the system (1) until $\mathbf{x} \in O(\mathbf{r}_j, \varepsilon)$ for some $j = 1, 2, \ldots, M$, i.e. find the smallest *TargetTime* such that $\mathbf{f}(\mathbf{x}, TargetTime) \in O(\mathbf{r}_j, \varepsilon)$.

*Step 6.* In the $i$th row of the table for $\Omega$, find the letter $a_\nu \in U_{i,j}$ such that $TargetTime = T^i_{a_\nu}$.

*Step 7.* Set $i = j$.

*Step 8.* Set $R = \mathbf{r}_i$.

*Step 9.* If $R \notin F$ GoTo Step 3.

As a general note, for the above method, we have to say that both sender and receiver must have the same libraries for mathematical computing for ensuring that there will not occur minor numerical differences, that could evolve in considerable differences during the time evolution of the chaotic dynamical system. Namely, it is obvious that the above method is very sensitive (like the chaotic system it deals with) to small differences in initial conditions. It is possible that different computer architectures under the same or different operating systems, do not perform 100% exactly the same mathematical operations. So there is the danger of making those small differences in computing between two correspondents on different computer architectures. In practice, however, we tested numerically our algorithm in HP Apollo 700 with HP-UX, DEC with ULTRIX and PC486-Linux, and in all cases while working with 20 decimal digits accuracy, the results were identical. Of course in general, such a situation cannot be expected for every computer architecture, including the architectures mentioned above. One of the solutions that will increase the robustness of the algorithm but will decrease the capacity of the method for coding different letters of the alphabet $\Sigma$ is to change the strict condition for associating the real numbers $T^i_{a_\nu}$ for the letters $a_\nu$ in $U_{i,j}$ that represents the time. Instead of that if for every $a_\nu \in U_{i,j}$ we associate the interval of times $[T^i_{(a_\nu)_1}, T^i_{(a_\nu)_2}]$, then the method will gain more robustness on slight numerical discrepancies and possible noise in communication. Another solution is to define and use common numerical libraries for performing mathematical calculations. Actually it is done with ANSI/IEEE standards (ANSI/IEEE 1985; Miner 1995).

As a second note here, we want to stress the fact that if the sets $|U_{i,j}| = 1$ then it implies that the number of the letters in the alphabet $\Sigma$ is equal to $M$. That further implies that the transition function $\Omega$ represents some quasigroup transformation. In that case if someone wants to ensure that the method is still secure, one should keep the definition of $\Omega$ private. This case needs no chaotic system to be involved, and is investigated in [Markovski *et al.*, 1996]). However, if $|U_{i,j}| \geq 1$, i.e. $|U_{i,j}| \approx \frac{m}{M}$ and $m \gg M$, to eliminate ubiquity in the transition function $\Omega$, we use a nonlinear chaotic system and the algorithm for time targeting the trajectory. This gives sufficient time ensuring that the transition function $\Omega$ could be announced publicly. But, if someone decides to keep the function $\Omega$ private, it is natural that the security of the method will be increased further.

## 4. A Numerical Example

We give here a simple example that implements the proposed method. For representing real numbers in the numerical calculations we used standard *double* variables in the C programming language, and used standard ANSI mathematical libraries under the UNIX operating system. We chose a descriptive alphabet $\Sigma$ to be $\Sigma = \{$*happy, today, this, Saturday, is, we, are, STOP*$\}$. The reasons for this are given in the following section. Let the chaotic dynamical system be described by Eqs. (4). First we will pick three points from its attractor i.e. we will set the number of receptors to be $M = 3$. Let the three receptors be

$$\mathbf{r}_1 = (1.845436494276013,\ 0.122463900650633,\ -2.010749234398700),$$

$$\mathbf{r}_2 = (-1.683256250478941,\ 0.141054046947965,\ 2.583098236358436),$$

and

$$\mathbf{r}_3 = (-1.452028431812372,\ -0.225366862676237,\ 0.597956830041859).$$

Then we have to define the table for $\Omega$, as well as the corresponding times for every element of the $\Sigma$ for every row of the table. Such a table is defined by Table 2.

Let suppose that the secret initial condition is $\mathbf{x}_0 = (2.029371965283351,\ 0.057933549559485,\ -2.794092337408118)$, and that we want to send the sentence: "*we are happy*". According to the algorithm given above, the initial state of the automaton is $s = \mathbf{r}_1$. So to send "*we*" we will have

Table 2. Table for definition a finite automaton for coding.

| $\Omega$ | $\mathbf{r}_1$ | | | $\mathbf{r}_2$ | | | | $\mathbf{r}_3$ | | |
|---|---|---|---|---|---|---|---|---|---|---|
| $\mathbf{r}_1$ | *Saturday* | *are* | | *we* | *is* | *today* | *STOP* | *happy* | *this* | |
| | 0.911 | 1.370 | | 0.549 | 1.784 | 3.400 | 2.010 | 4.001 | 3.991 | |
| $\mathbf{r}_2$ | *Saturday* | *STOP* | *today* | *is* | *we* | *are* | *this* | *happy* | | |
| | 3.091 | 2.123 | 5.047 | 4.844 | 0.159 | 0.237 | 0.301 | 2.919 | | |
| $\mathbf{r}_3$ | *STOP* | | | *is* | *Saturday* | *we* | *happy* | *are* | *today* | *this* |
| | 4.077 | | | 1.348 | 2.000 | 0.091 | 1.111 | 2.064 | 1.455 | 2.210 |

to send a perturbation vector $\alpha$ such that starting from the initial position $\mathbf{x} = \mathbf{x}_0 + \alpha$ the dynamical system (4) will come to the $\epsilon$-neighborhood of the receptor $\mathbf{r}_2$ exactly after 0.549 time units. Indeed if $\alpha = (-3.954324138116263, -0.28359011560741, 4.626806197778236)$ then starting from the point $\mathbf{x} = \mathbf{x}_0 + \alpha = (-1.924952172832912, -0.225656566047925, 1.832713860370118)$ the chaotic trajectory of the system (4) will come in the $\epsilon$-neighborhood of the receptor $\mathbf{r}_2$, i.e. the trajectory will come in the position $\mathbf{x} = (-1.762665576253783, 0.088770903414361, 2.605385352837998)$. Then, looking at the table we conclude that for sending "*are*" we will have to send another perturbation vector $\alpha = (-0.209641631598652, -0.172502772344169, -0.07711156800614294)$, such that the trajectory from the new initial position $\mathbf{x} = \mathbf{x} + \alpha = (-1.972307207852435, -0.083731868929808, 2.528273784831855)$ will arrive again in the $\epsilon$-neighborhood of $\mathbf{r}_2$ after 0.237 time units. The position of the $\mathbf{x}$ in that moment will be $\mathbf{x} = (-1.746011264985092, 0.082867097899804, 2.534200977720516)$. Looking again in the $\mathbf{r}_2$-row we conclude that now the new perturbation $\alpha$ will be $\alpha = (1.048357637743255, -0.049699544821496, -1.441960951981411)$ and so the initial position $\mathbf{x} = \mathbf{x} + \alpha = (-0.697653627241837, 0.033167553078308, 1.092240025739105)$ will cause that trajectory to come in the $\epsilon$-neighborhood of $\mathbf{r}_3$ after 2.919 time units. The position of $\mathbf{x}$ in that moment will be $\mathbf{x} = (-1.388171378238194, -0.157326981953662, 0.569821842613611)$. Finally, we will send the perturbation vector $\alpha = (0.619234964397997, 0.3962522891898819, -0.04052289455508007)$ that will cause the trajectory starting from initial position $\mathbf{x} = (-0.768936413840197, 0.238925307236220, 0.529298948058531)$ to come in the $\epsilon$-neighborhood of $\mathbf{r}_1$ after 4.077 time units, meaning that we have send the element "*STOP*".

## 5. Practical Application of the Method and Further Directions

In the previous section we gave the numerical example, where we have chosen alphabet $\Sigma$ to be $\Sigma = \{$*happy, today, this, Saturday, is, we, are, STOP*$\}$. We did so because we want to stress that using the above method one can define an alphabet with more than $10^5$ elements, and for that alphabet can define the corresponding table for the function $\Omega$ having only ten receptors. This can easily be evaluated if someone calculated the average length of trajectories in the set $\mathbf{T}_i = \{\hat{T}^t_{\mathbf{r}_{ij}}\}_{j=1,N_i}$. In our experimental case it was more than 10. Bearing in mind that the integration step was $\Delta\tau = 0.001$ it follows that only with 10 receptors one can define an alphabet with more than $10^5$ elements. That number can be many, many times greater if we change the low-dimensional chaotic dynamical systems such as that of the equations (4) by high dimensional chaotic dynamical systems. So we expect that one can use the above method for encoding the entire natural languages. This fact also opens possibilities to apply the method in some kind of data compression, and this will be a matter for further research.

From the statistical point of view, we have not still investigated in detail how the statistical correlation between plain and encoded messages are. However, first impressions are that if someone wants to use a method for secure communication by the secret key, there will be a lot of possibilities for choosing the secret key. First, the initial position and the positions of receptors can be chosen theoretically from an unlimited set of possibilities in the phase space (in practical implementation the limit will depend on the number of accurate digits the computers deal with). Second the number of possibilities to choose a chaotic dynamical system is also theoretically and practically unlimited, and the coding and decoding is based on the use of

nonlinear and chaotic systems. Third, the working of the automaton $A$ implies that coding of the sentences is context dependent, so we assume that statistical attack on the key will be very hard. Fourth, because both sender and receiver may have their own database for the sets $\mathbf{T}_i$, $i = 1, \ldots, M$, the same sentence could be coded in different ways. Fifth, there is a possibility of the agreement between correspondents, that will change the initial position $\mathbf{x}_0$, every time the communication is done, so the method will simulate the one-time pad system for secure communication (see [Shannon, 1949]). Sixth, because of the very big number of letters in $\Sigma$ and the context dependent coding, a particular vector $\alpha$ that was sent, will practically never be sent again in a session of communication.

Here we also want to stress the fact that there are possibilities to apply the above method for pattern recognition (especially recognition of voice signals). Namely if we look at the activity of the recipient of the data, exchanged between two participants with the method described above, then we can say that the recipient has the knowledge to recognize the data he(she) receives from the sender. The knowledge is incorporated into Table 1, and the placement of the receptors $\mathbf{r}_i$. So the problem of recognition of the signals can be reformulated as the problem of finding appropriate receptors and the problem of filling the Table 1. Further research will head in that direction.

## References


ANSI/IEEE, [1985] "IEEE standard for binary floating-point arithmetic," *ANSI/IEEE Std 754*.

Gligoroski, D., Dimovski, D. & Urumov, V. [1996] "A solution of time targeting problem in multidimensional chaotic systems by small perturbations," preprint.

Hayes, S., Grebogi C. & Ott, E. [1993] "Communicating with chaos," *Phys. Rev. Lett.* **70**, 3031–3034.

Hayes, S., Grebogi, C., Ott, E. & Mark, A. [1994] "Experimental control of chaos for communication," *Phys. Rev. Lett.* **73**, 1781–1784.

Lewis, H. R. & Papadimitriu, C. H. [1981] *Elements of the Theory of Computation* (Prentice-Hall).

Markovski, S., Gligoroski, D. & Andova, S. [1996] "Using quasigroups for one-one secure encoding," preprint.

Miner, P. S. [1995] "Defining the IEEE-854 floating-point standard in PVS," NASA Technical Memorandum 110167, June 1995.

Ott, E., Grebogi C. & Yorke J. A. [1990] "Controlling chaos," *Phys. Rev. Lett.* **64**, 1196–1199.

Parker, T. S. & Chua, L. O. [1989] *Practical Numerical Algorithms for Chaotic Systems* (Springer-Verlag).

Schweizer, J. & Kennedy, M. P. [1995] "Predictive Poincaré control: A control theory for chaotic systems," *Phys. Rev.* **E52**, 4865-4876.

Shannon, C. E. [1949] "Communication theory of secrecy systems," *Bell Syst. Tech. J.* **28**, 656–715.

Shinbrot, T., Ott, E., Grebogi, C. & Yorke, J. A. [1990] "Using chaos to direct trajectories to targets," *Phys. Rev. Lett.* **65**, 3215–3218.

which represent the existence conditions for the PLC. Since $L(j\omega_0)$ is a complex number, (6) and (7) constitute three independent equations that can be solved with respect to $A$, $B$ and $\omega_0$. Plots of $A$ and $B$ versus $\theta$ are shown in Fig. 2.

The third step for chaos prediction is the evaluation of the distortion index $\Delta$, defined in (7) of [7] and reported as a function of $\theta$ in Fig. 3.

According to [7], chaos is expected in the parameter range such that the two conditions C1 and C2 reported above, are fulfilled. Condition C1 reduces to the inequality $B > A$; from Fig. 2 it is seen that C1 is satisfied if $\theta \leq 0.160$. Condition C2 can be expressed as $\delta^- < \Delta < \delta^+$, where $\delta^-$ is the upper bound corresponding to a true prediction, whereas $\delta^+$ is the lower bound corresponding to an unreliable prediction (see p. 155 of [7]). By assuming $\delta^- = 0.03$ and $\delta^+ = 0.1$, the corresponding $\theta$ interval becomes approximately $0.157 \leq \theta \leq 0.175$. Then by intersecting the two conditions, we expect chaos in the range $0.157 \leq \theta \leq 0.160$. The time simulation of the circuit, shown in Fig. 4, confirms the prediction; in fact it is seen from Fig. 4 that at $\theta = 0.19$ the system exhibits a period-1 limit cycle; then a period doubling bifurcation occurs for $\theta = 0.165$ and eventually a double-scroll like attractor is observed for $\theta = 0.158$ and $\theta = 0.160$.

## III. Conclusion

We have shown that the complex dynamics of the time-delayed Chua's circuit can be investigated through the spectral approach developed in [7], based upon the describing function technique and on the evaluation of the distortion index. In particular we have concentrated on a set of parameters which gives rise to a double-scroll like attractor and we have shown that its existence and characteristics can be easily predicted, via the spectral technique, without resorting to simulation. We remark that by following the same approach the dynamic behavior of the TDCC can be investigated in the whole of the parameter space. Moreover the above spectral technique allows to study the effects of the parasitics in those circuits described by difference equations, which have found applications in secure communications (see [1]).

## References


[1] B. Sheu, M. Ismail, E. Sanchez-Sinencio, and T. H. Wu, *Microsystems Technology for Multimedia Applications: An Introduction*. New Jersey: IEEE Press, 1995, pp. 245–349.

[2] R. Bellmann and K. L. Cooke, *Differential-Difference Equations*. New York, London: Academic, 1963.

[3] A. N. Sharkowsky, Yu. Maistrenko, P. Deregel, and L. O. Chua, "Dry turbolence from a time-delayed Chua's circuit," *J. Circuits, Syst. Comput.*, vol. 3, pp. 645–668, June 1993.

[4] M. Biey, F. Bonani, M. Gilli, and I. Maio, "On the effect of the capacitor on the delayed Chua's circuit," in *Int. Symp. Nonlinear Theory Its Applicat.*, Haway, Dec. 1993, pp. 803–806.

[5] M. Gilli, "A spectral approach for chaos prediction in delayed cellular neural networks," *Int. J. Bifurc. Chaos*, pp. 869–875, Aug. 1995.

[6] R. Genesio and A. Tesi, "A harmonic balance approach for chaos prediction: Chua's circuits," *Int. J. Bifurc. Chaos*, vol. 2, no. 1, pp. 61–79, 1992.

[7] ——, "Distortion control of chaotic systems: The Chua's circuit," *J. Circuits, Syst. Comput.*, vol. 3, no. 1, pp. 151–171, 1993.


# Experimental Poincaré Maps from the Twist-and-Flip Circuit

Guo-Qun Zhong, Leon O. Chua, and Ray Brown

*Abstract*—**In this letter, we present a physical implementation of the twist-and-flip circuit containing a nonlinear gyrator. Many *phase portraits* and their associated *Poincaré maps* are observed experimentally from this circuit and presented in this paper.**

## I. Introduction

Fractals are one of many manifestations of complicated chaotic dynamics. The fractal phenomenon can occur not only in autonomous systems typical of Chua's circuit [1]–[3], but also in nonautonomous systems driven by time-varying signals and therefore described by a nonautonomous system of ordinary differential equations

$$\dot{\mathbf{x}} = f(\mathbf{x}, t) \tag{1}$$

where $\mathbf{x}$ is a vector in an $n$-dimensional Euclidean space $\mathbf{R}^n$.

The twist-and-flip circuit offers one of the simplest paradigms for nonautonomous chaos. Indeed, the state equations associated with the twist-and-flip circuit are the only known nonautonomous system of ordinary differential equations whose Poincaré map can be derived in an *explicit analytic* form. Based on this property of the circuit an in-depth mathematical analysis of the twist-and-flip map has been carried out exhaustively and rigorously [4], [5]. The various fractals corresponding to several classes of nonlinear gyration conductance functions $g(v_1, v_2)$ from this map have been generated numerically [6].

In this letter we describe a physical implementation of the *twist-and-flip circuit* with a simple nonlinear gyration conductance function $g(v_1, v_2)$, driven by a square-wave voltage source. A variety of phase portraits and the corresponding Poincaré maps observed experimentally from this setup will be presented.

## II. Physical Implementation of the Twist-and-Flip Circuit

The twist-and-flip circuit contains simply two linear capacitors $C_1$ and $C_2$, a voltage source $s(t)$, and a *nonlinear* gyrator, as shown in Fig. 1(a). The voltage source $s(t)$ for driving the circuit is a square wave of amplitude $a$ and angular frequency $\omega$ (or period $P = \frac{2\pi}{\omega}$), as shown in Fig. 1(b). The gyrator, which is the only nonlinear element in the circuit, is described by the equations

$$\left.\begin{aligned} i_1 &= g(v_1, v_2)v_2 \\ i_2 &= -g(v_1, v_2)v_1 \end{aligned}\right\} \tag{2}$$

where $g(v_1, v_2)$ is the associated gyration conductance [7]. In this letter we assume that

$$g(v_1, v_2) > 0, \quad \text{for } -\infty < v_1, v_2 < \infty.$$

Manuscript received October 31, 1995. This work was supported in part by the Office of Naval Research under Grant N00014-89-J-1402 and by the National Science Foundation under Grant MIP 86-14000. This paper was recommended by Associate Editor B. Sheu.

G.-Q. Zhong is with the Department of EECS, Univeristy of California, Berkeley, CA 94720 USA on leave from the Guangzhou Institute of Electronic Technology, Academia Sinica, Guangzhou 510070, People's Republic of China.

L. O. Chua and R. Brown are with the Department of EECS, Univeristy of California, Berkeley, CA 94720 USA.

Publisher Item Identifier S 1057-7122(96)07620-9.

1057–7122/96$05.00 © 1996 IEEE

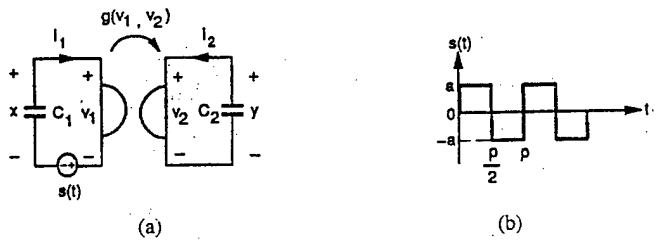


(a) (b)

Fig. 1. (a) Twist-and-flip circuit containing two linear capacitors and a gyrator characterized by a nonlinear gyration conductance function $g(v_1, v_2)$, driven by a voltage source $s(t)$. (b) Voltage source $s(t)$ in (a), a square wave with amplitude $a$ and angular frequency $\omega$.

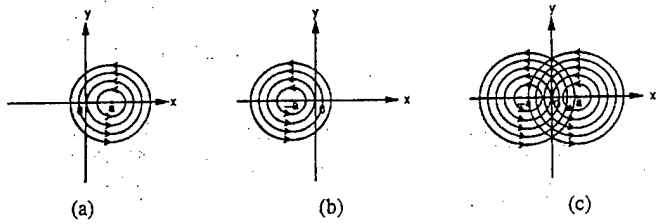


(a) (b) (c)

Fig. 2. (a) Phase portrait centered at $x = a$ over each positive-half cycle of $s(t)$. (b) Phase portrait centered at $x = -a$ over each negative-half cycle of $s(t)$. (c) Combined phase portrait over a full period of $s(t)$.

### A. State Equations of the Twist-and-Flip Circuit

Applying **KCL** and **KVL** to the circuit shown in Fig. 1(a), we obtain

$$\left.\begin{aligned} i_1 &= -C_1 \tfrac{dx}{dt} \\ i_2 &= -C_2 \tfrac{dy}{dt} \end{aligned}\right\} \tag{3}$$

where

$$\begin{aligned} v_1(t) &= x(t) - s(t), \\ v_2(t) &= y(t). \end{aligned}$$

Introducing (2) into (3) and normalizing $C_1 = C_2 = 1$, we obtain the following state equations governing the dynamics of the twist-and-flip circuit

$$\frac{dx}{dt} = -g(x - s(t), y)y \tag{4a}$$

$$\frac{dy}{dt} = g(x - s(t), y)(x - s(t)) \tag{4b}$$

where

$$s(t) = a, \quad t \in \left(n, n + \frac{1}{2}\right)P \text{ (positive-half cycle)}$$

$$s(t) = -a, \quad t \in \left(n + \frac{1}{2}, n + 1\right)P \text{ (negative-half cycle)}$$

$$n = 0, 1, 2, \cdots.$$

Dividing (4b) by (4a), we obtain

$$\frac{dy}{dx} = -\frac{(x - a)}{y} \tag{5a}$$

and

$$\frac{dy}{dx} = -\frac{(x + a)}{y} \tag{5b}$$

over each positive- and negative-half cycles, respectively. Obviously, (5) defines a phase portrait consisting of a family of concentric circles, centered at $x = a$ over each positive-half cycle $t \in (n, n + \frac{1}{2})P$, and at $x = -a$ over each negative-half cycle $t \in (n + \frac{1}{2}, n + 1)P, n = 0, 1, 2, \cdots$, as shown in Fig. 2(a) and (b). The phase portrait over a full period is shown in Fig. 2(c).

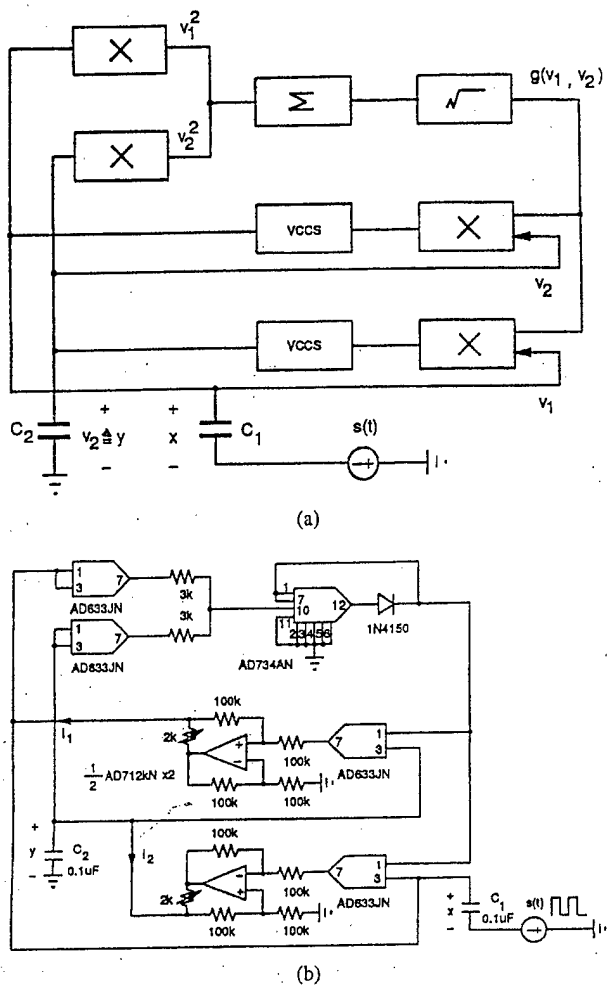


Fig. 3. (a) Block diagram of physical implementation for the twist-and-flip circuit. (b) Implemented circuit diagram of the twist-and-flip circuit.

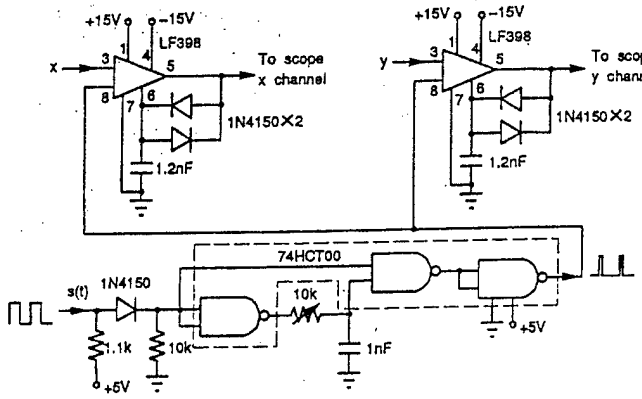


Fig. 4. Experimental setup for observing the Poincaré map.

### B. Implementation of the Twist-and-Flip Circuit

To implement the twist-and-flip circuit shown in Fig. 1(a), we must specify the nonlinear gyration conductance function $g(v_1, v_2)$ for the circuit. In this letter we choose

$$g(v_1, v_2) = \sqrt{v_1^2 + v_2^2}. \tag{6}$$

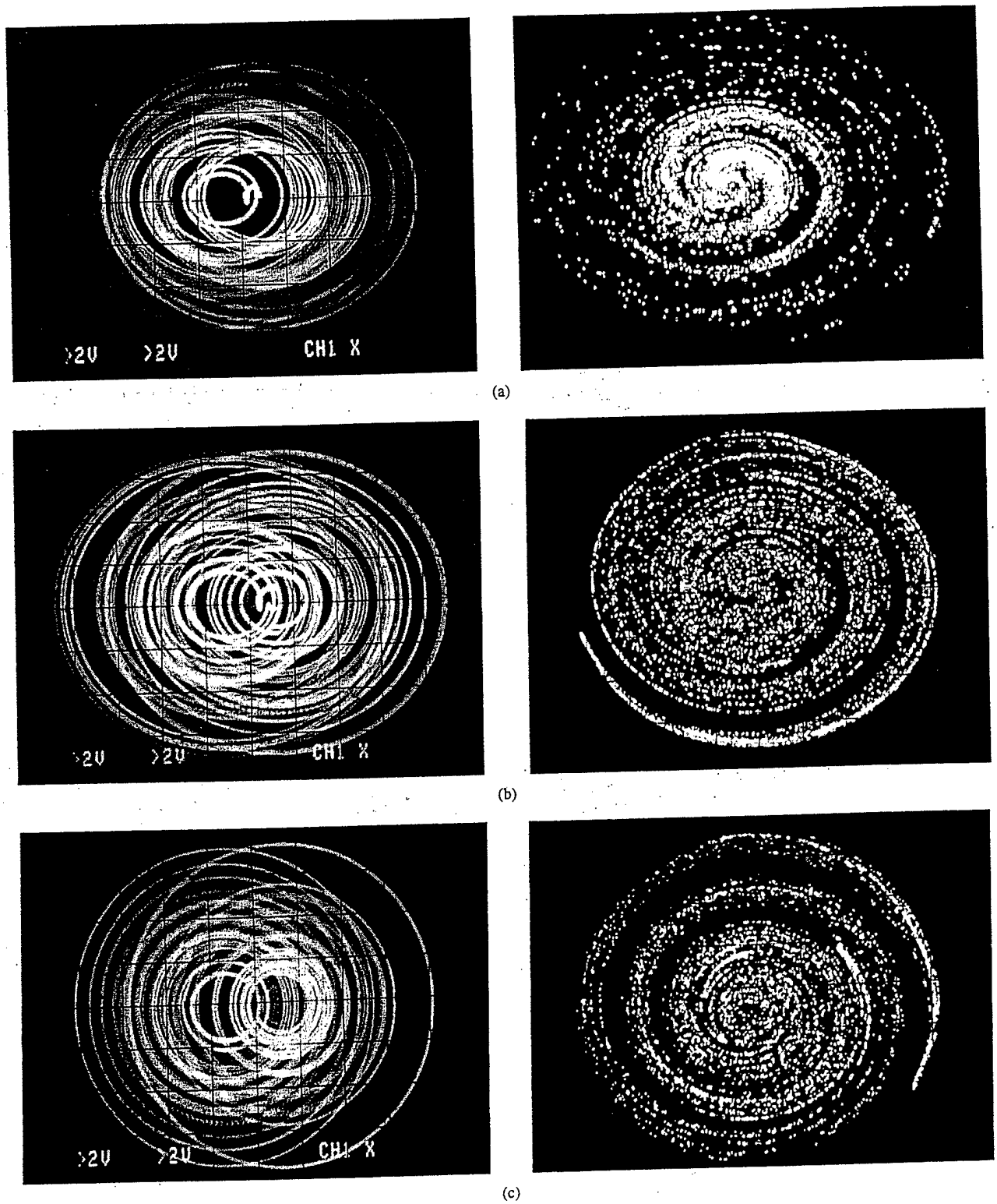


Fig. 5. Experimentally observed phase portrait (left) and its corresponding Poincaré map (right) of the twist-and-flip circuit, driven by a square-wave voltage source $s(t)$ with the circuit operating in a chaotic regime. Horizontal axis is $x$, vertical axis is $y$. Parameter values: (a) $a = 1.0$ V, $P = 1.8$ ms. (b) $a = 1.5$ V, $P = 2.4$ ms. (c) $a = 2.0$ V, $P = 1.35$ ms.

The block diagram of the physical implementation for the twist-and-flip circuit is shown in Fig. 3(a). It consists of two squaring functional blocks, two multipliers, two voltage-controlled current sources, one adder, one square-root functional block, two linear capacitors $C_1$ and $C_2$, and a square-wave voltage source $s(t)$. The two squaring functional blocks, the adder, and the square-root functional block together perform the task to realize the gyration conductance function (6). The two analog multipliers and voltage-controlled current sources together realize the (2). The capacitors $C_1$ and $C_2$ are connected across port 1 and port 2 of the gyrator, respectively. The input signal to the twist-and-flip circuit is $s(t)$, a square-wave voltage source with

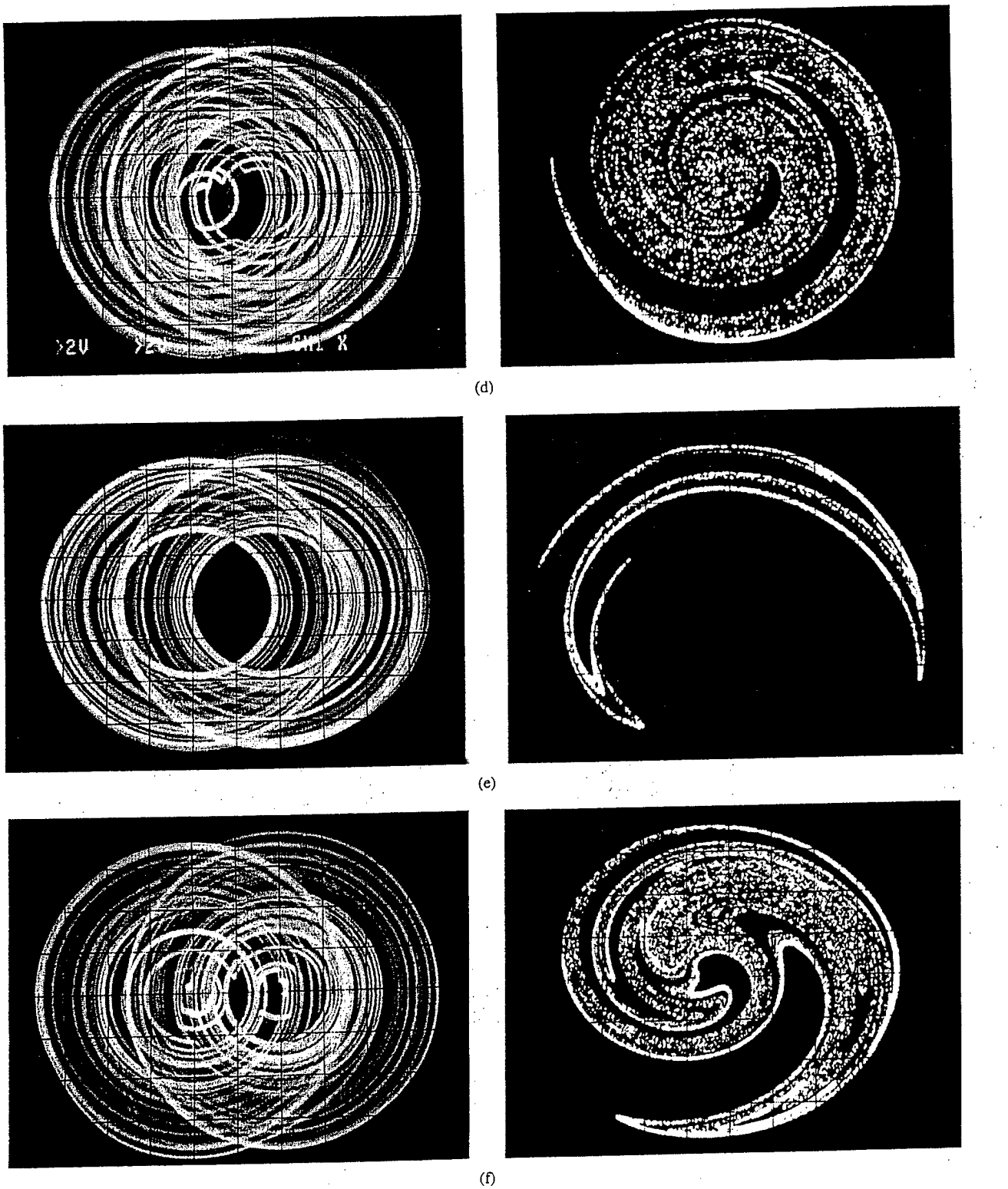

Fig. 5. *(Continued.)* Experimentally observed phase portrait (left) and its corresponding Poincaré map (right) of the twist-and-flip circuit, driven by a square-wave voltage source $s(t)$ with the circuit operating in a chaotic regime. Horizontal axis is $x$, vertical axis is $y$. (d) $a = 2.0$ V, $P = 1.7$ ms. (e) $a = 2.5$ V, $P = 1.3$ ms. (f) $a = 3.0$ V, $P = 0.81$ ms.

amplitude $a$ and angular frequency $\omega$. The analog multipliers AD633JN and AD734AN are respectively used to implement all multiplications, squaring, and square-rooting operations in Fig. 3(a). The complete circuit diagram of the twist-and-flip circuit is shown in Fig. 3(b).

## III. Experimental Observations of Poincaré Maps in the Twist-and-Flip Circuit

Though the twist-and-flip circuit has an explicit mathematical solution, its asymptotic behavior in the $x$-$y$ phase plane is nevertheless muddled by an infinite tangle of intersections of the trajectory upon

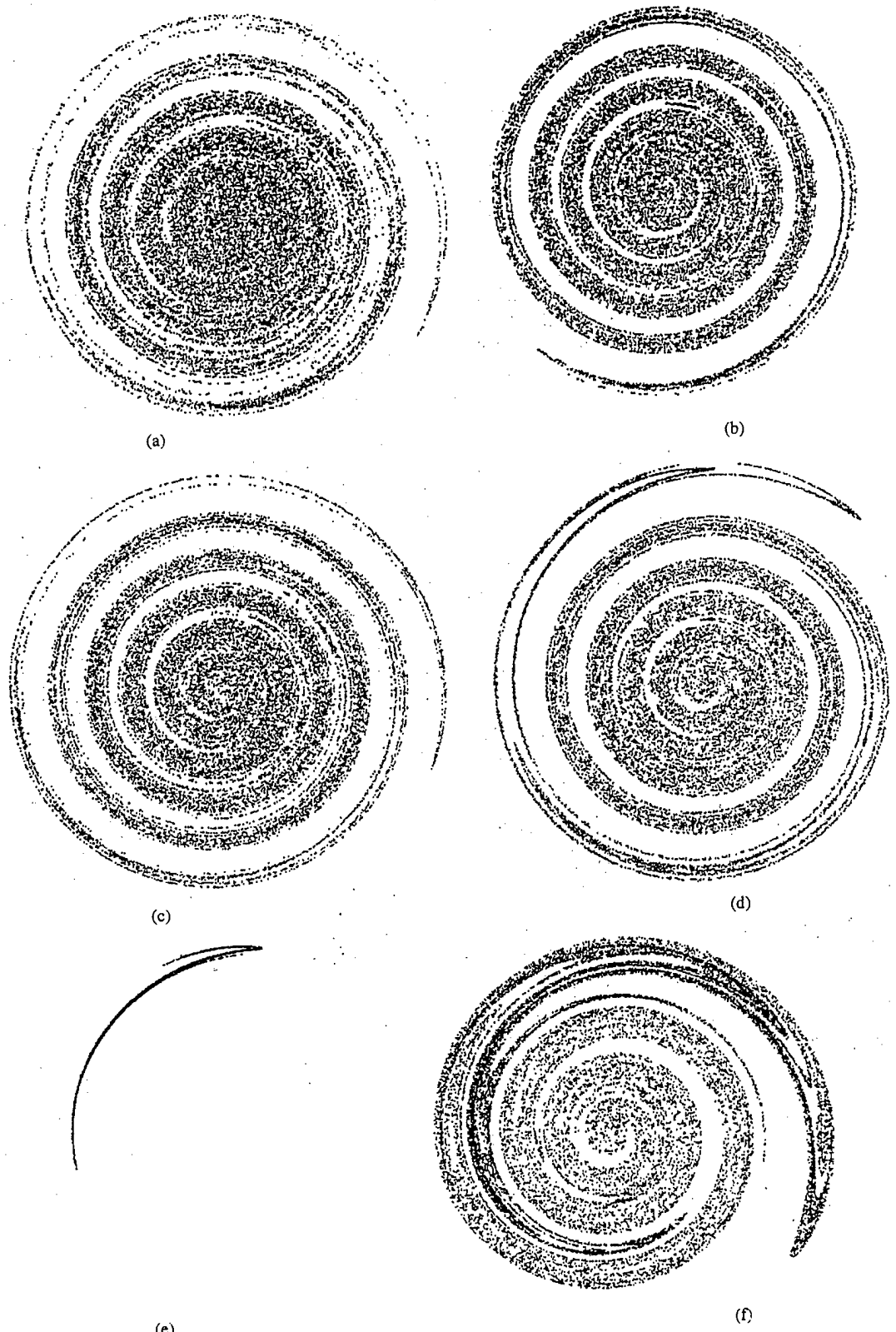


Fig. 6. Numerically simulated Poincaré map for the circuit operating in a chaotic regime. Horizontal axis is $x$, vertical axis is $y$. Parameter values: (a) $a = 1.0$ V, $P = 1.8$ ms, $\alpha = 0.013$, $\beta = 3$. (b) $a = 1.5$ V, $P = 2.4$ ms, $\alpha = 0.026$, $\beta = 2.3$. (c) $a = 2.0$ V, $P = 1.35$ ms, $\alpha = 0.02$, $\beta = 1.5$. (d) $a = 2.0$ V, $P = 1.7$ ms, $\alpha = 0.02$, $\beta = 2.5$. (e) $a = 2.5$V, $P = 1.3$ms, $\alpha = 0.020\,605$, $\beta = 2.2686$. (f) $a = 3.0$V, $P = 0.81$ ms, $\alpha = 0.006$, $\beta = 5.8$.

itself. The standard method to untangle such a mess of points and extract some useful asymptotic information is to analyze the dynamics of the associated Poincaré map defined as follows: Given any point $(x_0, y_0)$, the Poincaré map of $(x_0, y_0)$ for the circuit is a point $(x_1, y_1)$ that corresponds to the position of the trajectory (originating from $(x_0, y_0)$) at $t = P = \frac{2\pi}{\omega}$ [6].

Fig. 4 shows the circuit setup used in our experimental observations of the Poincaré map. The sampled-and-hold output signals

$x$ and $y$ of the circuit are connected respectively to the horizontal and vertical channels of an oscilloscope, operating in $X$-$Y$ mode. The sample-and-hold impulse is generated by the square-wave voltage source $s(t)$ used for driving the twist-and-flip circuit.

By changing the amplitude $a$ or the period $P$ of the square-wave voltage source $s(t)$, a rich variety of phase portraits, including chaotic and periodic behaviors, have been observed from the implemented twist-and-flip circuit. The experimentally constructed phase portrait, and its corresponding Poincaré map in the $x$-$y$ plane, are shown in Fig. 5(a)–(f). Note that the phase portrait in the $x$-$y$ plane is muddled by an infinite tangle of intersections of the trajectory upon itself, whereas the corresponding Poincaré map in the $x$-$y$ plane is a clearly defined set of points illustrating the chaotic attractor occurring in the twist-and-flip circuit. To compare with theoretic results, the Poincaré maps obtained by numerical simulation for the circuit operating in a chaotic regime are shown in Fig. 6(a)–(f). The simulation is based on (4a) and (4b), in which capacitances $C_1$ and $C_2$ are normalized to 1. The twist-and-flip circuit is theoretically lossless. However, the physical realization of this circuit must necessarily involve some losses, however small. These losses, or damping factors are nonlinear and very difficult to model exactly. Therefore, to construct a reasonable simulation requires some approximations to these losses. The way to include damping in the twist-and-flip mapping is suggested by the dissipative example in [4], and the derivations of dissipative Poincaré maps in [5]. Using these results we include two dissipative parameters in the simulations, $\alpha$, and $\beta$. The resulting simulations of the Poincaré maps shown in Fig. 6(a)–(f) have the same voltages and frequencies utilized in the circuit corresponding to Fig. 5(a)–(f). While the correspondences are not exact, the differences we believe are due to the difficulties of capturing the exact form of the nonlinear dissipative terms to be included in the twist-and-flip maps used to simulate the circuit. Given this qualification, several of the Poincaré maps occurring in Fig. 5 are in excellent geometric agreement to what is seen in typical dissipative twist-and-flip maps. From this we conclude that this circuit is a good electronic realization of the twist-and-flip paradigm of chaos.

The trajectory is stable when the circuit operates in a periodic regime. In this case, the phase portrait in the $x$-$y$ plane is stationary, and the Poincaré map is a set of periodic points. When a square wave of amplitude $a = 0$ over each negative-half cycle is used as the sample-and-hold voltage, we obtain the display shown in Fig. 7(a) and (b), in which the phase portrait and its Poincaré map over each positive-half cycle of the square-wave voltage source $s(t)$ appear simultaneously.

## IV. Concluding Remarks

The most remarkable property of the twist-and-flip circuit is that its associated nonautonomous state equations have an *explicit* and *simple* Poincaré map, making it mathematically tractable. This circuit is imbued with a full repertoire of complicated chaotic dynamics. In this letter, we have implemented the twist-and-flip circuit having a nonlinear *gyration conductance function* defined by $g(v_1, v_2) = \sqrt{v_1^2 + v_2^2}$, and presented numerically simulated observations utilizing the twist-and-flip map model with losses. Due to the complex nature of the actual model for the losses and the sensitivity of the dissipative Poincaré map to the nonlinear dissipative parameters, constructing the exact damping model is difficult and is an open question for further study. Utilizing the same circuit synthesis technique, a rich variety of Poincaré maps can be observed experimentally by synthesizing other twist-and-flip circuits having more complicated gyration conductance functions, such as those presented in [6].

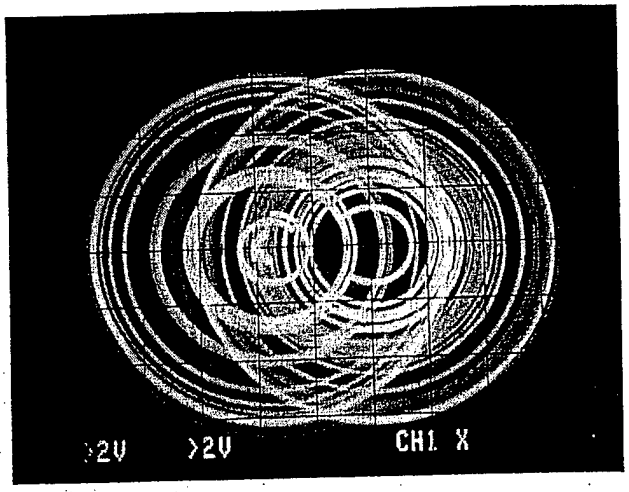


(a)

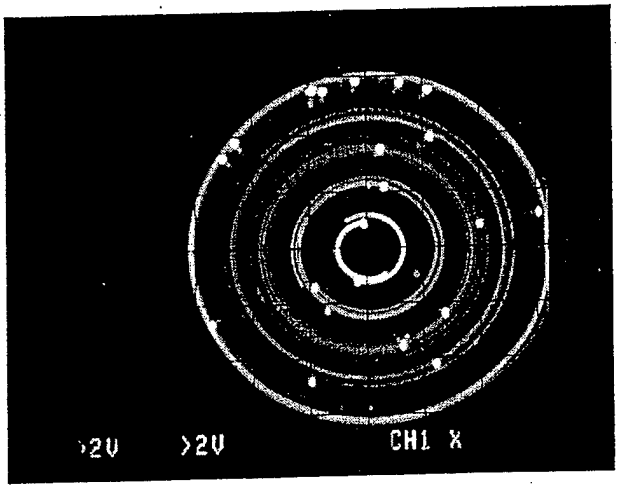


(b)

Fig. 7. Phase portrait and Poincaré map experimentally observed with the circuit operating in a chaotic regime. Horizontal axis is $x$, vertical axis is $y$. $a = 3.0$ V, $P = 2.4$ ms: (a) Phase portrait in $x$-$y$ plane. (b) Corresponding Poincaré map superimposed on the phase portrait over each positive-half cycle of $s(t)$.

## Acknowledgment

One of the authors (G. Q. Zhong) would like to thank C. W. Wu for helpful discussions.

## References

[1] L. O. Chua, "The genesis of Chua's circuit," *Archiv Elektronik Uebertragungstechnik*, vol. 46, no. 4, pp. 250–257, 1992.
[2] R. N. Madan, Guest Ed., Special Issue on "Chua's circuit: A paradigm for chaos," *J. Circuits, Syst. Comput.*, Part I: Mar. 1993; Part II: June 1993.
[3] G. Q. Zhong and F. Ayrom, "Experimental confirmation of chaos from Chua's circuit," *Int. J. Circuit Theory Applicat.* vol. 13, no. 1, pp. 93–98, 1985.
[4] R. Brown and L. O. Chua, "Horseshoes in the twist-and-flip map," *Int. J. Bifurc. Chaos*, vol. 1, no. 1, pp. 235–252, 1991.
[5] ——, "Generalizing the twist-and-flip paradigm," *Int. J. Bifurc. Chaos*, vol. 1, no. 2, pp. 385–416, 1991.
[6] L. O. Chua, R. Brown, and N. Hamilton, "Fractals in the twist-and-flip circuit," *Proc. IEEE*, vol. 81, pp. 1466–1491, Oct. 1993.
[7] L. O. Chua, *Introduction to Nonlinear Network Theory*. New York: McGraw-Hill, 1969.

# Secure Communication via Chaotic Parameter Modulation

Tao Yang and Leon O. Chua

*Abstract*—**In this letter, we extend chaotic switching to general chaotic parameter modulation. By using adaptive controller, synchronization between transmitter and receiver is maintained and message signal is recovered. Computer simulation results are given.**

## I. Introduction

Chaotic switching [1], [2] is the simplest form of chaotic parameter modulation. In this method, the message signal $s(t)$ is assumed to be binary, and is used to modulate one or more parameters of a chaotic switching transmitter by representing binary "one" for one set of parameters and binary "zero" for a different set. At the receiver, $s(t)$ is decoded by using the synchronization error to decide whether the received signal corresponds to one set of parameters, or the other.

Although chaotic switching is more robust against noise than chaotic masking, it suffers from a lower information transmission rate than those methods which transmit analog signals directly. This is because the receiver has to wait until synchronization and desynchronization have been achieved before the next bit is transmitted. On the other hand, Tao Yang [3] found that an intruder could use short-time zero-crossing rate (STZCR) to recover $s(t)$ from the transmitted chaotic signal. So, it has a low degree of security.

In this letter, we propose a more general chaotic parameter modulation scheme with applications to secure communication. In our method $s(t)$ may be analog or digital.

## II. Transmission of Signal by Chaotic Parameter Modulation

In this letter, all results are based on Chua's circuit [4], [5], which exhibits a family of chaotic attractors and can be easily implemented in hardware. As shown in Fig. 1(a), Chua's circuit consists of a linear inductor $L$, a linear resistor $R$, two linear capacitors $C_1$ and $C_2$ and a nonlinear resistor—the Chua's diode $N_R$. The state equations for Chua's circuit are given by

$$\begin{cases} \frac{dv_1}{dt} = \frac{1}{C_1}[G(v_2 - v_1) - f(v_1)] \\ \frac{dv_2}{dt} = \frac{1}{C_2}[G(v_1 - v_2) + i_3] \\ \frac{di_3}{dt} = \frac{1}{L}[-v_2 - R_0 i_3] \end{cases} \tag{1}$$

where $v_1$, $v_2$, and $i_3$ are the voltage across $C_1$, the voltage across $C_2$ and the current through $L$, respectively. We set $G = \frac{1}{R}$. The term $R_0 i_3$ is added to account for the small resistance of the inductor in the physical circuit. The piece-wise linear $v$-$i$ characteristic $f(v_1)$ of the Chua's diode, is given by

$$f(v_1) = G_b v_1 + \frac{1}{2}(G_a - G_b)(|v_1 + E| - |v_1 - E|) \tag{2}$$

where $E$ is the breakpoint voltage of the Chua's diode as shown in Fig. 1(b).

Manuscript received January 23, 1996. This paper was recommended by Associate Editor B. Sheu.

T. Yang is with the Electronics Research Laboratory and the Department of Electrical Engineering and Computer Sciences, University of California, Berkeley, CA 94720 USA on leave from the Department of Automatic Control Engineering, Shanghai University of Technology, Shanghai 200072, P. R. China.

L. O. Chua is with the Department of Electrical Engineering and Computer Sciences, University of California, Berkeley, CA 94720 USA.

Publisher Item Identifier S 1057-7122(96)06839-0.

To transmit $s(t)$ via our chaotic parameter modulation scheme, the receiver must chosen as follows:

$$\begin{cases} \frac{d\tilde{v}_1}{dt} = \frac{1}{C_1}[\tilde{G}(\tilde{v}_2 - \tilde{v}_1) - f(\tilde{v}_1) + K_1(v_1 - \tilde{v}_1)] \\ \frac{d\tilde{v}_2}{dt} = \frac{1}{C_2}[\tilde{G}(\tilde{v}_1 - \tilde{v}_2) + \tilde{i}_3 + K_1(v_1 - \tilde{v}_1)] \\ \frac{d\tilde{i}_3}{dt} = \frac{1}{L}[-\tilde{v}_2 - \tilde{R}_0\tilde{i}_3 + K_1(v_1 - \tilde{v}_1)] \end{cases} \tag{3}$$

We first use a "modulation rule" to modulate $s(t)$ in a parameter of the transmitter in (1). Then an adaptive controller is used at the receiver to maintain synchronization by continuously tracking the changes in the modulated parameter. So, $s(t)$ can be recovered by this adaptive controller. The parameter for the unmodulated Chua's circuit were chosen as follows: $C_1 = 5.56$ nF, $C_2 = 50$ nF, $G = 0.700\,28$ mS, $L = 7.14$ mH, $R_0 = 0\ \Omega$, $G_a = -0.8$ mS, $G_b = -0.5$ mS, $E = 1$ V, $K_1 = 0.01$. In this case, the Chua's circuit exhibits a double-scroll Chua's attractor as shown in Fig. 2. In this letter, we discuss the cases when only one parameter of the transmitter is modulated while the others remain constant. At the receiver, the corresponding parameter is changed by an adaptive controller while the others are fixed at the same values as in the transmitter.

### A. G-Modulation

In this case, the modulation rule is given by

$$G(t) = Gs(t), \tilde{G}(t) = G\tilde{s}(t) \tag{4}$$

where $\tilde{s}(t)$ is the recovered message signal.

The adaptive controller is given by

$$\begin{aligned} \dot{\tilde{s}}(t) &= k_1 \operatorname{sgn}\left(\frac{\partial \dot{\tilde{v}}_1}{\partial \tilde{s}(t)}\right)(v_1 - \tilde{v}_1) \\ &= k_1 \operatorname{sgn}\left(\frac{1}{C_1}G(\tilde{v}_2 - \tilde{v}_1)\right)(v_1 - \tilde{v}_1). \end{aligned} \tag{5}$$

Simulation result is shown in Fig. 3 with $k_1 = 10^6$. The signal $s(t)$(dashed line) is defined as follows:

$$s(t) = \begin{cases} 1.05, & 0 \le t < 20 \text{ ms} \\ 1.15, & 20 \text{ ms} \le t < 40 \text{ ms} \\ 1.1 - 0.05\sin\left(\frac{15\pi}{2}t\right), & 40 \text{ ms} \le t < 100 \text{ ms} \end{cases} \tag{6}$$

Observe that $\tilde{s}(t)$(solid line) tracks $s(t)$ continuously except for an interval from 40 ms to 66 ms when $\tilde{s}(t)$ is almost constant while $s(t)$ changes. This is because for the parameter range corresponding to the waveform of $s(t)$ in this interval, synchronization is maintained even though $\tilde{s}(t) \neq s(t)$.

### B. $C_1$-Modulation

In this case, the modulation rule is given by

$$\frac{1}{C_1(t)} = \frac{s(t)}{C_1}, \frac{1}{\tilde{C}_1(t)} = \frac{\tilde{s}(t)}{C_1}. \tag{7}$$

The adaptive controller is given by

$$\begin{aligned} \dot{\tilde{s}}(t) &= k_1 \operatorname{sgn}\left(\frac{\partial \dot{\tilde{v}}_1}{\partial \tilde{s}(t)}\right)(v_1 - \tilde{v}_1) \\ &= k_1 \operatorname{sgn}\left(\frac{1}{C_1}[G(\tilde{v}_2 - \tilde{v}_1) - f(\tilde{v}_1) + K_1(v_1 - \tilde{v}_1)]\right) \\ &\quad \times (v_1 - \tilde{v}_1). \end{aligned} \tag{8}$$

Simulation result is shown in Fig. 4 with $k_1 = 2 \times 10^6$. The signal $s(t)$ (dashed line) is defined by (6). Observe that $\tilde{s}(t)$ (solid line) tracks $s(t)$ continuously with a relatively big error.

1057–7122/96$05.00 © 1996 IEEE

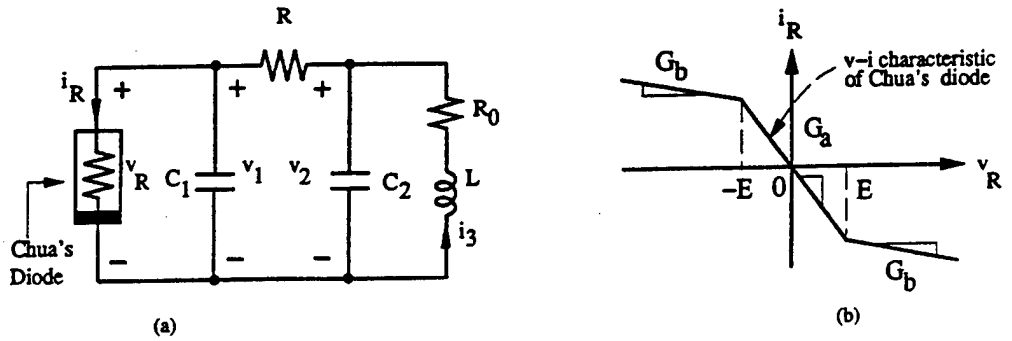


Fig. 1. (a) Chua's circuit. (b) Nonlinear $v$-$i$ characteristic of Chua's diode.

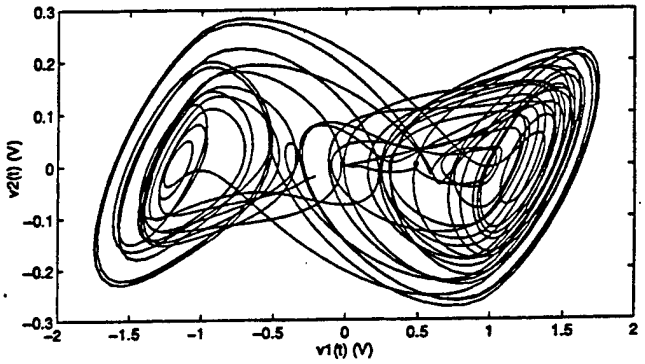


Fig. 2. Chaotic attractor of Chua's circuit used in simulations.

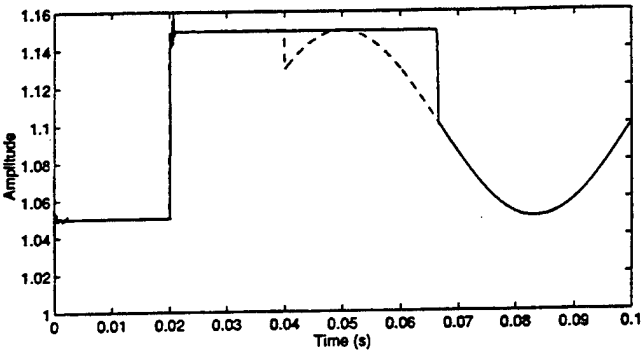


Fig. 3. Transmitted signal $s(t)$ (dashed line) and recovered signal $\tilde{s}(t)$ (solid line) obtained by modulating the parameter $G$.

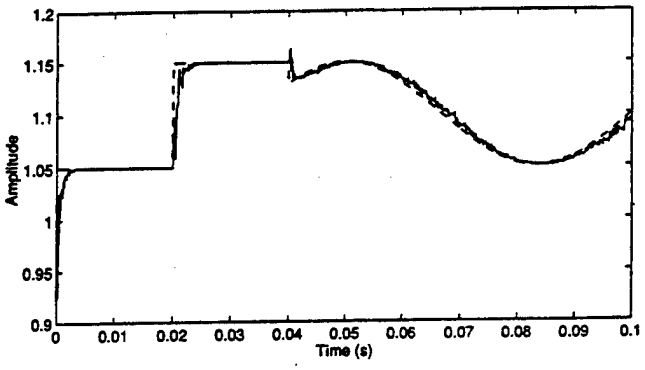


Fig. 4. Transmitted signal $s(t)$ (dashed line) and recovered signal $\tilde{s}(t)$ (solid line) obtained by modulating the parameter $C_1$.

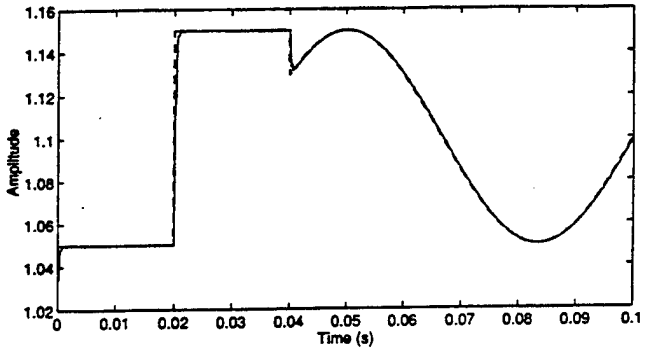


Fig. 5. Transmitted signal $s(t)$ (dashed line) and recovered signal $\tilde{s}(t)$ (solid line) obtained by modulating the parameter $C_2$.

### C. $C_2$-Modulation

In this case, the modulation rule is given by

$$\frac{1}{C_2(t)} = \frac{s(t)}{C_2}, \frac{1}{\tilde{C}_2(t)} = \frac{\tilde{s}(t)}{C_2}. \tag{9}$$

The adaptive controller is given by

$$\begin{aligned}\dot{\tilde{s}}(t) &= k_1 \operatorname{sgn}\left(\frac{\partial \dot{\tilde{v}}_2}{\partial \tilde{s}(t)}\right)(v_1 - \tilde{v}_1) \\ &= k_1 \operatorname{sgn}\left(\frac{1}{C_2}[G(\tilde{v}_1 - \tilde{v}_2) + \tilde{i}_3 + K_1(v_1 - \tilde{v}_1)]\right)(v_1 - \tilde{v}_1).\end{aligned} \tag{10}$$

Simulation result is shown in Fig. 5 with $k_1 = 10^6$. The signal $s(t)$ (dashed line) is defined by (6). Observe that $\tilde{s}(t)$ (solid line) tracks $s(t)$ continuously with a small error.

### D. L-Modulation

In this case, the modulation rule is given by

$$\frac{1}{L(t)} = \frac{s(t)}{L}, \frac{1}{\tilde{L}(t)} = \frac{\tilde{s}(t)}{L}. \tag{11}$$

The adaptive controller is given by

$$\begin{aligned}\dot{\tilde{s}}(t) &= k_1 \operatorname{sgn}\left(\frac{\partial \dot{\tilde{i}}_3}{\partial \tilde{s}(t)}\right)(v_1(t) - \tilde{v}_1) \\ &= k_1 \operatorname{sgn}\left(\frac{1}{L}[-\tilde{v}_2 - R_0\tilde{i}_3 + K_1(v_1 - \tilde{v}_1)]\right)(v_1 - \tilde{v}_1).\end{aligned} \tag{12}$$

Simulation result is shown in Fig. 6 with $k_1 = 10^6$. The signal $s(t)$(dashed line) is defined by (6). Observe that $\tilde{s}(t)$(solid line) tracks $s(t)$ continuously with very small error and big overshoot.

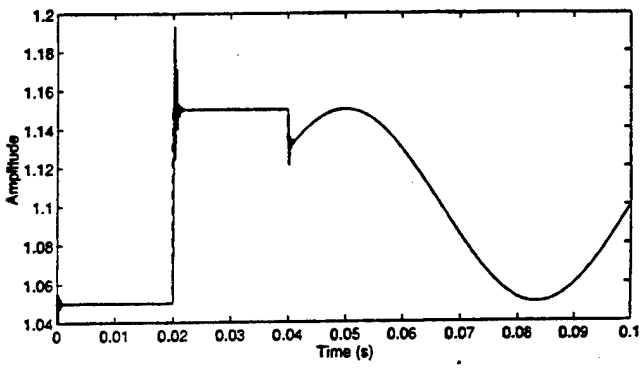


Fig. 6. Transmitted signal $s(t)$ (dashed line) and recovered signal $\tilde{s}(t)$ (solid line) obtained by modulating the parameter $L$.

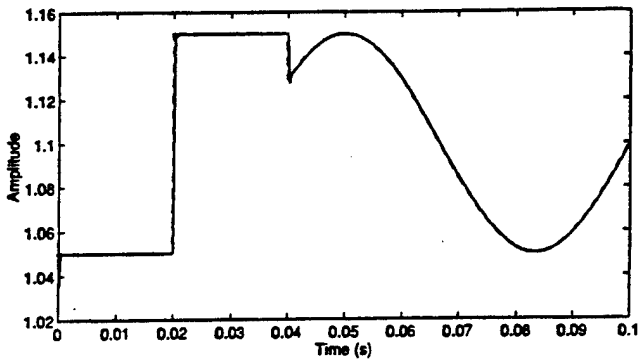


Fig. 7. Transmitted signal $s(t)$ (dashed line) and recovered signal $\tilde{s}(t)$ (solid line) obtained by modulating the parameter $R_0$.

### *E. $R_0$-Modulation*

In this case, the modulation rule is given by

$$R_0(t) = R_0 + s(t), \tilde{R}_0(t) = R_0 + \tilde{s}(t). \tag{13}$$

The adaptive controller is given by

$$\begin{aligned}\dot{\tilde{s}}(t) &= k_1 \operatorname{sgn}\left(\frac{\partial \dot{\tilde{i}}_3}{\partial \tilde{s}(t)}\right)(v_1(t) - \tilde{v}_1) \\ &= k_1 \operatorname{sgn}\left(-\frac{\tilde{i}_3}{L}\right)(v_1 - \tilde{v}_1).\end{aligned} \tag{14}$$

Simulation result is shown in Fig. 7 with $k_1 = 10^8$. The signal $s(t)$(dashed line) is defined by (6). Observe that $\tilde{s}(t)$(solid line) tracks $s(t)$ continuously with a small error.

## III. Conclusion

Different schemes of chaotic parameter modulation are presented. Their performances are shown by computer simulation results.

## References

[1] U. Parlitz, L. O. Chua, L. Kocarev, K. S. Halle, and A. Shang, "Transmission of digital signal by chaotic synchronization," *Int. J. Bifurcation Chaos*, vol. 2, no. 4, pp. 973–977, 1992.

[2] H. Dedieu, M. P. Kennedy, and M. Hasler, "Chaotic shift keying: Modulation and demodulation of a chaotic carrier using self-synchronization Chua's circuits," *IEEE Trans. Circuits Syst. II*, vol. 40, pp. 634–642, Oct. 1993.

[3] T. Yang, "Recovery of digital signals from chaotic switching," *Int. J. Circuit Theory Applicat.*, vol. 23, no. 6, pp. 611–615, Nov.–Dec. 1995.

[4] L. O. Chua, "Chua's circuit—An overview ten years later," *J. Circuits, Syst., Comput.*, vol. 4, no. 2, pp. 117–159, June 1994.

[5] J. M. Cruz and L. O. Chua, "An IC chip of Chua's circuit," *IEEE Trans. Circuits Syst. II*, vol. 40, pp. 614–625, Oct. 1993.

International Journal of Bifurcation and Chaos, Vol. 6, No. 7 (1996) 1397–1407
© World Scientific Publishing Company

# ON A VARIATION OF THE HUBERMAN–LUMER ADAPTIVE SCHEME

CHAI WAH WU and LEON O. CHUA
*Electronics Research Laboratory and*
*Department of Electrical Engineering and Computer Sciences,*
*University of California at Berkeley, Berkeley, CA 94720, USA*

Received March 1, 1996; Revised May 5, 1996

In this letter, we present a variation of the Huberman–Lumer scheme for adaptive systems. We show that this scheme has the advantage that for nonlinear systems with linear parameters, the synchronization error can be proven to approach zero. We also present an adaptive scheme for nonlinear systems with multiplicative parameters. Examples using Chua's oscillators are presented.

## 1. Introduction

Recently, there has been much work done in using adaptive controllers to synchronize two chaotic systems which are not identical [Sinha *et al.*, 1990; John & Amritkar, 1994; Celka, 1995; Chua *et al.*, 1996; Wu *et al.*, 1996].

The purpose of this letter is to continue the study of adaptive controllers which are used to enforce the synchronization, even though initially the two coupled systems are not identical. In particular, we present a variation of the Huberman–Lumer scheme [Huberman & Lumer, 1990] and show that it can be justified theoretically for nonlinear systems with linear parameters. In particular, using a Lyapunov approach we show that for nonlinear systems with linear parameters under certain conditions, this scheme will make the synchronization error approach zero. We also show a modification of this scheme for systems with multiplicative parameters. Finally, computer simulations using Chua's oscillator will be given.

We use lowercase, bold uppercase, and bold lowercase letters for scalars (or scalar-valued functions), matrices, and vectors, respectively.

## 2. An Adaptive Synchronization and Control Scheme

Consider two coupled continuous-time systems described by:

$$\left.\begin{aligned} \dot{x}_1 &= f_1(\mathbf{x}, a_{11}, \ldots, a_{1m}, \mathbf{x}, \tilde{\mathbf{x}}, t) \\ &\vdots \\ \dot{x}_n &= f_n(\mathbf{x}, a_{n1}, \ldots, a_{nm}, \mathbf{x}, \tilde{\mathbf{x}}, t) \end{aligned}\right\} \leftarrow \text{System 1} \tag{1}$$

$$\left.\begin{aligned} \dot{\tilde{x}}_1 &= f_1(\tilde{\mathbf{x}}, \tilde{a}_{11}, \ldots, \tilde{a}_{1m}, \mathbf{x}, \tilde{\mathbf{x}}, t) \\ &\vdots \\ \dot{\tilde{x}}_n &= f_n(\tilde{\mathbf{x}}, \tilde{a}_{n1}, \ldots, \tilde{a}_{nm}, \mathbf{x}, \tilde{\mathbf{x}}, t) \end{aligned}\right\} \leftarrow \text{System 2} \tag{2}$$

where $\mathbf{x} = (x_1, \ldots, x_n)^T$ and $\tilde{\mathbf{x}} = (\tilde{x}_1, \ldots, \tilde{x}_n)^T$ are the state vectors of the two systems, and $\{a_{ij}\}$ and $\{\tilde{a}_{ij}\}$ are the *parameters* of System 1 and System 2, respectively. A straightforward way to synchronize these two systems is the following two-step approach. First, make sure that the two systems are synchronized when the parameters in the two systems are identical, i.e., the two systems are

identical.[1] Second, adjust the parameters such that the corresponding parameters in the two systems approach each other. The reason $\mathbf{x}$ and $\tilde{\mathbf{x}}$ appear twice in the arguments of $f_i$ in Eqs. (1) and (2) is so that we can more easily state the following sufficient condition for when the two systems synchronize [Wu & Chua, 1994]:

**Theorem 1.** *If $a_{ij} = \tilde{a}_{ij}$ for all $i$, $j$ and*

$$\dot{x}_1 = f_1(\mathbf{x}, a_{11}, \ldots, a_{1m}, \mathbf{u}, \tilde{\mathbf{u}}, t)$$
$$\vdots$$
$$\dot{x}_n = f_n(\mathbf{x}, a_{n1}, \ldots, a_{nm}, \mathbf{u}, \tilde{\mathbf{u}}, t)$$

*is globally asymptotically stable for all external inputs $\mathbf{u}$ and $\tilde{\mathbf{u}}$, then the systems (1) and (2) will synchronize for arbitrary initial states $\mathbf{x}(0)$ and $\tilde{\mathbf{x}}(0)$.*

It is not always possible to implement this two-step approach. Fortunately, this two-step approach is not necessary for synchronization. Let us assume that the parameters in System 1 are fixed. Assume that the two systems synchronize when the parameters are identical, i.e., the first step is satisfied. When the parameters in the two systems are different, the goal in the second step is to adaptively change the parameters $\{\tilde{a}_{ij}\}$ in System 2 such that they approach the parameters $\{a_{ij}\}$ in System 1. However, if we want to change the parameters of System 2 without any information about the parameters in System 1, this might not be possible. If synchronization is our goal, what we want is to change $\{\tilde{a}_{ij}\}$ such that $\tilde{\mathbf{x}}$ approaches $\mathbf{x}$. For certain systems, it could be true that when $\tilde{\mathbf{x}}$ approaches $\mathbf{x}$, it is neccesary that $\tilde{a}_{ij} \to a_{ij}$. However, in Sec. 5, we show an example where although the synchronization errors are small, the parameters in the two systems are not matched (although they do oscillate near each other). This is an example of weak coupling where the first step in the above two-step approach is not satisfied, and thus the second step cannot be used to achieve synchronization, but synchronization is still possible.

Huberman and Lumer [1990] proposed a class of adaptive algorithms for $\tilde{a}_{ij}$ for discrete time systems. For continuous time systems such as (1) and (2), these algorithms are of the form:

$$\dot{\tilde{a}}_{ij} = -\delta_{ij} G\left(r_i, \frac{dr_i}{d\tilde{a}_{ij}}\right) \tag{3}$$

[1]Thus when $a_{ij} = \tilde{a}_{ij}$, we have $\tilde{\mathbf{x}} \to \mathbf{x}$ as $t \to \infty$.

where $r_i = x_i - \tilde{x}_i$ and $\delta_{ij} > 0$. In particular, Huberman and Lumer propose $G$ to be

$$G\left(r_i, \frac{dr_i}{d\tilde{a}_{ij}}\right) = r_i \cdot \mathrm{sgn}\left(\frac{dr_i}{d\tilde{a}_{ij}}\right) \tag{4}$$

which was also used successfully in [John & Amritkar, 1994].

## 2.1. *A variation of the Huberman–Lumer scheme*

**Definition 1.** A function $\mu : \mathbb{R} \to \mathbb{R}$ is *strictly passive* [Chua & Green, 1976] if it lies in the open first and third quadrants. Thus $\mu$ is strictly passive if and only if $\mu(0) = 0$ and $x\mu(x) > 0$ for all $x \neq 0$. A function $\mu : \mathbb{R} \to \mathbb{R}$ is in class $\mathcal{D}$ if it is strictly passive and there exists a strictly increasing function $\psi$ such that $\psi(0) = 0$ and $|\mu(x)| \geq |\psi(x)|$ for all $x$.

An example of a function $\mu$ in class $\mathcal{D}$ is shown in Fig. 1. Most strictly passive functions belong to class $\mathcal{D}$. An example of a strictly passive function which is not in class $\mathcal{D}$ is one which approaches the $x$-axis as $x \to \infty$ (Fig. 2).

The purpose of this letter is to propose the following function for $G$ instead of Eq. (4):

$$G\left(r_i, \frac{dr_i}{d\tilde{a}_{ij}}\right) = \mu(r_i)\left(\frac{dr_i}{d\tilde{a}_{ij}}\right)$$
$$= -\mu(r_i)\left(\frac{d\dot{\tilde{x}}_i}{d\tilde{a}_{ij}}\right) \tag{5}$$

where $\mu$ is a function of class $\mathcal{D}$ as defined in Definition 1.

Some candidates for $\mu$ include the signum function, $\mathrm{sgn}(x)$, the identity function, $\mathrm{sgn}(x)(e^{|x|} - 1)$, and $x^n$ for $n$ odd and positive. When $\mu$ is the signum function, the resulting $G$ becomes

$$G\left(r_i, \frac{dr_i}{d\tilde{a}_{ij}}\right) = \mathrm{sgn}(r_i)\left(\frac{dr_i}{d\tilde{a}_{ij}}\right). \tag{6}$$

Theoretical results for the case $\mu(x) = x$ have been presented in [Wu *et al.*, 1996].

There is an analogy between these schemes and the signed LMS schemes used in adaptive signal processing [Clarkson, 1993]. Equation (4) would correspond to the Clipped LMS or Signed Regressor algorithm, while Eq. (6) would correspond to the Pilot LMS or Signed Error algorithm.

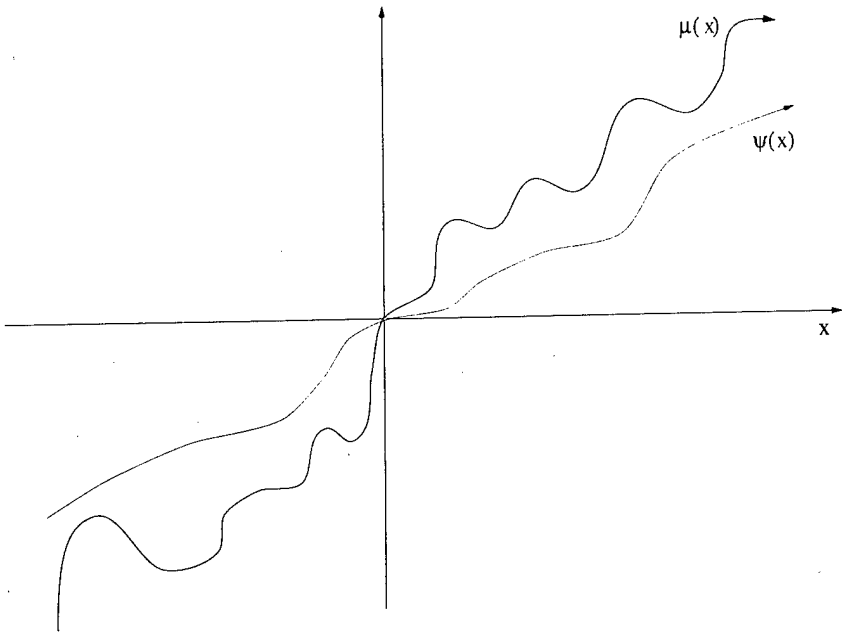


Fig. 1. Function $\mu$ belongs to class $\mathcal{D}$. Function $\psi$ is a strictly increasing function such that $|\mu(x)| \geq |\psi(x)|$ for all $x$.

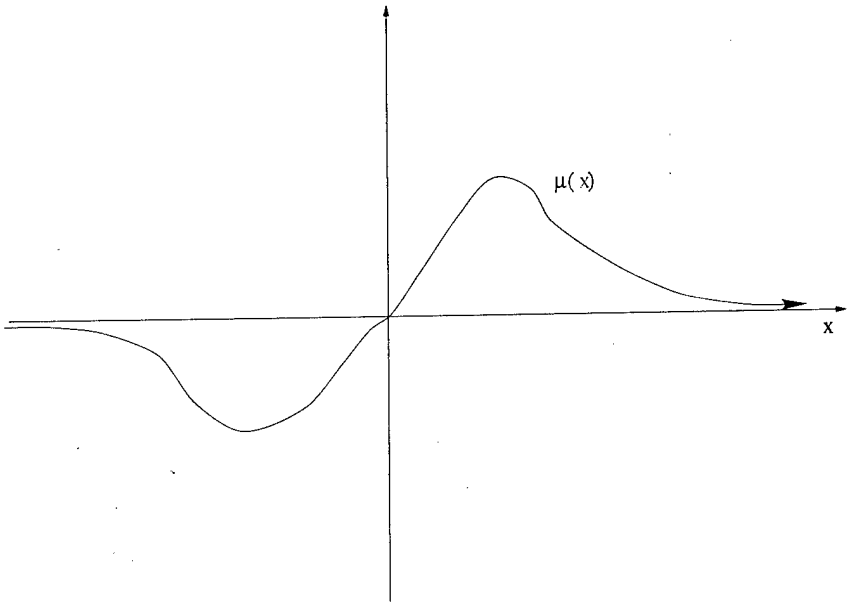


Fig. 2. The strictly passive function $\mu$ does not belong to class $\mathcal{D}$ since it approaches the $x$-axis as $x \to \pm\infty$.

## 3. Two Coupled Nonlinear Systems with Linear Parameters

One advantage of the proposed adaptation scheme is that under certain conditions theoretical results can be derived for the class of nonlinear systems with linear parameters. Many chaotic systems in the literature belong to this class (See [Wu & Chua, 1996] for several examples of such chaotic systems).

We consider the class of systems where the parameters in the system are linear factors. The state

equations for two such systems coupled together are given by:

$$\left.\begin{aligned} \dot{x}_1(t) &= d_1(\mathbf{x}) + \sum_{j=1}^{m} a_{1j} f_{1j}(\mathbf{x}) + u_1 + k_1(\mathbf{x}) - k_1(\tilde{\mathbf{x}}) \\ &\vdots \\ \dot{x}_n(t) &= d_n(\mathbf{x}) + \sum_{j=1}^{m} a_{nj} f_{nj}(\mathbf{x}) + u_n + k_n(\mathbf{x}) - k_n(\tilde{\mathbf{x}}) \end{aligned}\right\} \leftarrow \text{System 1} \tag{7}$$

$$\left.\begin{aligned} \dot{\tilde{x}}_1(t) &= d_1(\tilde{\mathbf{x}}) + \sum_{j=1}^{m} \tilde{a}_{1j} f_{1j}(\tilde{\mathbf{x}}) + u_1 + h_1(\tilde{\mathbf{x}}) - h_1(\mathbf{x}) \\ &\vdots \\ \dot{\tilde{x}}_n(t) &= d_n(\tilde{\mathbf{x}}) + \sum_{j=1}^{m} \tilde{a}_{nj} f_{nj}(\tilde{\mathbf{x}}) + u_n + h_n(\tilde{\mathbf{x}}) - h_n(\mathbf{x}) \end{aligned}\right\} \leftarrow \text{System 2} \tag{8}$$

where $\mathbf{x} = (x_1, \ldots, x_n)^T$ and $\tilde{\mathbf{x}} = (\tilde{x}_1, \ldots, \tilde{x}_n)^T$ are the state vectors of System 1 and System 2, respectively. We assume that $d_i$, $f_{ij}$ are nonlinear functions which are continuously differentiable. The vector $\mathbf{u} = (u_1, \ldots, u_n)^T$ constitutes the external inputs to the two systems. Thus both systems receive the same external input. The scalars $a_{ij}$ and $\tilde{a}_{ij}$ are the *parameters* of System 1 and System 2, respectively. The continuous functions $h_i$ and $k_i$ denote the additive coupling between the two systems. The functions $d_i$ denote the part of the system which is identical in the two systems. There is no need to adapt this part of the system. For example, this part can contain parameters which are identical in both systems.

We assume that the parameters $a_{ij}$ in System 1 are constant, and try to adjust $\tilde{a}_{ij}$ adaptively such that $\tilde{\mathbf{x}}$ approaches $\mathbf{x}$ as $t \to \infty$. Applying the adaptation rule (5) to this system results in

$$\dot{\tilde{a}}_{ij} = \delta_{ij} \mu(x_i - \tilde{x}_i) f_{ij}(\tilde{\mathbf{x}}) \tag{9}$$

for some constants $\delta_{ij} > 0$.

**Definition 2.** A function $\mu : \mathbb{R} \to \mathbb{R}$ is *odd-symmetric* if $\mu(x) = -\mu(-x)$ for all $x$, i.e., the graph of $\mu$ is point-symmetric with respect to the origin.

**Lemma 1.** *Let $\mu : \mathbb{R} \to \mathbb{R}$ be an odd-symmetric increasing function. Let $g_i$ be a set of arbitrary real-valued continuously differentiable functions. If the functions $g_i$ have bounded derivatives, then*

$$\left| \sum_i \mu(h_i)(g_i(\mathbf{x}) - g_i(\mathbf{x}+\mathbf{h})) \right| \le p \sum_i \mu(h_i) h_i$$

*for some $p > 0$ and for all $\mathbf{x}$, $\mathbf{h}$ where*

$$\mathbf{h} = (h_1, \ldots, h_n)^T .$$

*Proof.* By hypothesis, there exists $p > 0$ such that $|g_k(\mathbf{x}) - g_k(\mathbf{x}+\mathbf{h})| \le p \max_i |h_i|$ for all $k$, $\mathbf{x}$, $\mathbf{h}$. Let $j$ be the index such that $\max_i |h_i| = |h_j|$. Then

$$\begin{aligned} &|\mu(h_k)(g_k(\mathbf{x}) - g_k(\mathbf{x}+\mathbf{h}))| \\ &\quad \le |\mu(h_k)|\,|g_k(\mathbf{x}) - g_k(\mathbf{x}+\mathbf{h})| \\ &\quad \le p|\mu(h_k)|\,|h_j| \le p|\mu(h_j)|\,|h_j| \\ &\quad = p\mu(h_j)h_j \le p \sum_i \mu(h_i)h_i . \end{aligned}$$

Note that $|\mu(h_k)| \le |\mu(h_j)|$ since $\mu$ is odd-symmetric and increasing. By summing over all indices $k$ and redefining $p$ we obtain the desired result. ■

The main result in this section is the following theorem which gives theoretical justifications for the adaptive scheme in Eq. (5) when $\mu$ is a piecewise-continuous, odd-symmetric, and increasing function in class $\mathcal{D}$ such that $x\mu(x)$ is continuous:

**Theorem 2.** *Consider the adaptive controllers for $\tilde{a}_{ij}$ given by Eq. (9) where $\mu$ is a piecewise-continuous, odd-symmetric, and increasing function in class $\mathcal{D}$ such that $x\mu(x)$ is continuous. We also assume that $k_i$'s and $h_i$'s are linear functions of the form $k_i(\mathbf{x}) = k_i x_i$, $h_i(\mathbf{x}) = h_i x_i$ and adapt the*

*coefficients using the following controllers:*

$$\begin{aligned} \dot{k}_i &= -\kappa_i^k \mu(x_i - \tilde{x}_i)(x_i - \tilde{x}_i)\,, \\ \dot{h}_i &= -\kappa_i^h \mu(x_i - \tilde{x}_i)(x_i - \tilde{x}_i)\,, \end{aligned} \tag{10}$$

*where* $\kappa_i^k + \kappa_i^h > 0$.

*If the Jacobian matrix of*

$$\begin{pmatrix} d_1 + \sum_j a_{1j} f_{1j} \\ \vdots \\ d_n + \sum_j a_{nj} f_{nj} \end{pmatrix} \tag{11}$$

*is bounded, then* $\mathbf{x} - \tilde{\mathbf{x}} \to 0$ *as* $t \to \infty$.

*Proof.* Define $\Psi(x) = \int_0^x \mu(\tau)d\tau$. The function $x\Psi(x)$ is strictly increasing since $\mu$ belongs to class $\mathcal{D}$.

By Lemma 1

$$\left| \sum_i \mu(x_i - \tilde{x}_i) \left( \left( d_i + \sum_j a_{ij} f_{ij} \right)(\mathbf{x}) - \left( d_i + \sum_j a_{ij} f_{ij} \right)(\tilde{\mathbf{x}}) \right) \right|$$

is less than $p \sum_i \mu(x_i - \tilde{x}_i)(x_i - \tilde{x}_i)$ for some $p > 0$. Consider a set of positive constants $\{k_1^{\max}, \ldots, k_n^{\max}\}$ such that $k_i^{\max} > p$ for all $i$.

Construct the following Lyapunov function:

$$V = \sum_i \Psi(x_i - \tilde{x}_i) + \frac{1}{2} \sum_{ij} \frac{1}{\delta_{ij}} (a_{ij} - \tilde{a}_{ij})^2 + \frac{1}{2} \sum_i \frac{1}{\kappa_i^k + \kappa_i^h} (k_i^{\max} + k_i + h_i)^2 \,.$$

Since $x\Psi(x)$ is strictly increasing and $\Psi(0) = 0$, it follows that $\Psi(x) > 0$ for all $x \neq 0$. If we define $a(x) = \min(\Psi(x), \Psi(-x))$ and $b(x) = \max(\Psi(x), \Psi(-x))$, it follows that $a$ and $b$ are functions of class $K$ [Lakshmikantham & Liu, 1993] and $a(|x|) \leq \Psi(x) \leq b(|x|)$.

By differentiating $V$ along the trajectories, we obtain

$$\begin{aligned} \dot{V} &= \sum_i \mu(x_i - \tilde{x}_i)(\dot{x}_i - \dot{\tilde{x}}_i) \\ &\quad + \sum_{ij} \frac{1}{\delta_{ij}} (a_{ij} - \tilde{a}_{ij})(-\dot{\tilde{a}}_{ij}) \\ &\quad - \sum_i (k_i^{\max} + k_i + h_i)\mu(x_i - \tilde{x}_i)(x_i - \tilde{x}_i) \\ &= \sum_i \mu(x_i - \tilde{x}_i)(d_i(\mathbf{x}) - d_i(\tilde{\mathbf{x}}) \\ &\quad + (k_i + h_i)(x_i) - (k_i + h_i)(\tilde{x}_i)) \\ &\quad + \sum_{ij} \mu(x_i - \tilde{x}_i)(a_{ij} f_{ij}(\mathbf{x}) - \tilde{a}_{ij} f_{ij}(\tilde{\mathbf{x}})) \\ &\quad - \sum_{ij} (a_{ij} - \tilde{a}_{ij})(\mu(x_i - \tilde{x}_i) f_{ij}(\tilde{\mathbf{x}})) \\ &\quad - \sum_i (k_i^{\max} + k_i + h_i)\mu(x_i - \tilde{x}_i)(x_i - \tilde{x}_i) \\ &= \sum_i \mu(x_i - \tilde{x}_i)(d_i(\mathbf{x}) - d_i(\tilde{\mathbf{x}}) - k_i^{\max}(x_i - \tilde{x}_i)) \\ &\quad + \sum_{ij} \mu(x_i - \tilde{x}_i)(a_{ij} f_{ij}(\mathbf{x}) - a_{ij} f_{ij}(\tilde{\mathbf{x}})) \\ &\leq \sum_i (p - k_i^{\max})\mu(x_i - \tilde{x}_i)(x_i - \tilde{x}_i) \leq 0 \,. \end{aligned} \tag{12}$$

Note that $(p - k_i^{\max}) < 0$ and $\mu(x_i - \tilde{x}_i)(x_i - \tilde{x}_i) = 0$ if and only if $x_i = \tilde{x}_i$. The values of $\tilde{a}_{ij}$ and $k_i + h_i$ are bounded since otherwise $V$ will go to infinity. It can be shown that $k_i$ and $h_i$ are bounded [Wu *et al.*, 1996] and the theorem then follows from Theorem 1.2.3 of [Lakshmikantham & Liu, 1993]. ■

*Remark.* It is clear from the proof of Theorem 2 that this result also holds if instead of adapting the coupling coefficients $k_i$ and $h_i$ we keep them fixed at values such that $k_i + h_i < -p$ for all $i$.

## 4. Two Coupled Nonlinear Systems with Multiplicative Parameters

When the parameters are not linear, but multiplicative, a simple change of variables allow us to use Theorem 2 to design adaptive controllers for this case as well.

The state equations for two such systems coupled together are given by:

$$\left.\begin{aligned} \dot{x}_1(t) &= d_1(\mathbf{x}) + \sum_{j=1}^{m} g_{1j}(a_{1j}) f_{1j}(\mathbf{x}) + u_1 + k_1(x_1 - \tilde{x}_1) \\ &\vdots \\ \dot{x}_n(t) &= d_n(\mathbf{x}) + \sum_{j=1}^{m} g_{nj}(a_{nj}) f_{nj}(\mathbf{x}) + u_n + k_n(x_n - \tilde{x}_n) \end{aligned}\right\} \leftarrow \text{System 1} \tag{13}$$

$$\left.\begin{aligned} \dot{\tilde{x}}_1(t) &= d_1(\tilde{\mathbf{x}}) + \sum_{j=1}^{m} g_{1j}(\tilde{a}_{1j}) f_{1j}(\tilde{\mathbf{x}}) + u_1 + h_1(\tilde{x}_1 - x_1) \\ &\vdots \\ \dot{\tilde{x}}_n(t) &= d_n(\tilde{\mathbf{x}}) + \sum_{j=1}^{m} g_{nj}(\tilde{a}_{nj}) f_{nj}(\tilde{\mathbf{x}}) + u_n + h_n(\tilde{x}_n - x_n) \end{aligned}\right\} \leftarrow \text{System 2} \tag{14}$$

where $\mathbf{x} = (x_1, \ldots, x_n)^T$ and $\tilde{\mathbf{x}} = (\tilde{x}_1, \ldots, \tilde{x}_n)^T$ are the state vectors of System 1 and System 2, respectively. The scalars $a_{ij}$ and $\tilde{a}_{ij}$ are the parameters of the two systems, respectively. We assume that $g_{ij}$, $d_i$, $f_{ij}$ are nonlinear functions which are continuously differentiable. As in the statement of Theorem 2 the coupling is linear and connects only corresponding state variables.

We assume that the parameters $a_{ij}$ in System 1 are constant, and try to adjust $\tilde{a}_{ij}$, $k_i$, and $h_i$ adaptively such that $\tilde{\mathbf{x}}$ approaches $\mathbf{x}$ as $t \to \infty$.

**Corollary 1.** *Suppose that $g'_{ij}$ is never zero.*[2] *Consider the adaptive controllers for $\tilde{a}_{ij}$ given by*

$$\dot{\tilde{a}}_{ij} = \delta_{ij} \frac{\mu(x_i - \tilde{x}_i) f_{ij}(\tilde{\mathbf{x}})}{g'_{ij}(\tilde{a}_{ij})} \tag{15}$$

*for some constants $\delta_{ij} > 0$ where $\mu$ is a piecewise-continuous, odd-symmetric, and increasing function in class $\mathcal{D}$ such that $x\mu(x)$ is continuous. We adapt $k_i$ and $h_i$ using the adaptive controllers in Eq. (10).*

*If the Jacobian matrix of*

$$\begin{pmatrix} d_1 + \sum_j g_{1j}(a_{1j}) f_{1j} \\ \vdots \\ d_n + \sum_j g_{nj}(a_{nj}) f_{nj} \end{pmatrix} \tag{16}$$

*is bounded, then $\mathbf{x} - \tilde{\mathbf{x}} \to 0$ as $t \to \infty$.*

[2]This implies that $g_{ij}$ is one-to-one.

*Proof.* Using the change of variables $\tilde{g}_{ij} = g_{ij}(\tilde{a}_{ij})$ and applying Theorem 2, we see that the following controllers for $\tilde{g}_{ij}$ will imply the conclusions of the corollary:

$$\dot{\tilde{g}}_{ij} = \delta_{ij} \mu(x_i - \tilde{x}_i) f_{ij}(\tilde{\mathbf{x}}) . \tag{17}$$

Since $\dot{\tilde{g}}_{ij} = g'_{ij}(\tilde{a}_{ij}) \dot{\tilde{a}}_{ij}$, the corollary is proved. ■

Some examples for $g_{ij}$ include $g_{ij}(x) = \frac{1}{x}$ for $x > 0$ and $g_{ij}(x) = x$. For example, in the system $\dot{v} = -\frac{v^3}{R}$, the parameter $R$ is multiplicative with $g(R) = \frac{1}{R}$.

*Remark.* If we apply Eq. (5) to systems (13) and (14), we obtain the following adaptive controllers for $\tilde{a}_{ij}$:

$$\dot{\tilde{a}}_{ij} = \delta_{ij} \mu(x_i - \tilde{x}_i) g'_{ij}(\tilde{a}_{ij}) f_{ij}(\tilde{\mathbf{x}})$$

which differs from Eq. (15) by a (time-varying) positive factor of $(g'_{ij}(\tilde{a}_{ij}))^2$.

## 5. Simulation Results Using Chua's Oscillator

In this section, we illustrate the results in the previous sections via computer simulations using Chua's oscillator. In particular, we choose several candidates for $\mu$ from the class $\mathcal{D}$ and use them to synchronize two nonidentical Chua's oscillators.

In contrast to Theorem 2 we will not use adaptive coupling. In particular, we will use a fixed coupling between only the $x$ state variables in the two

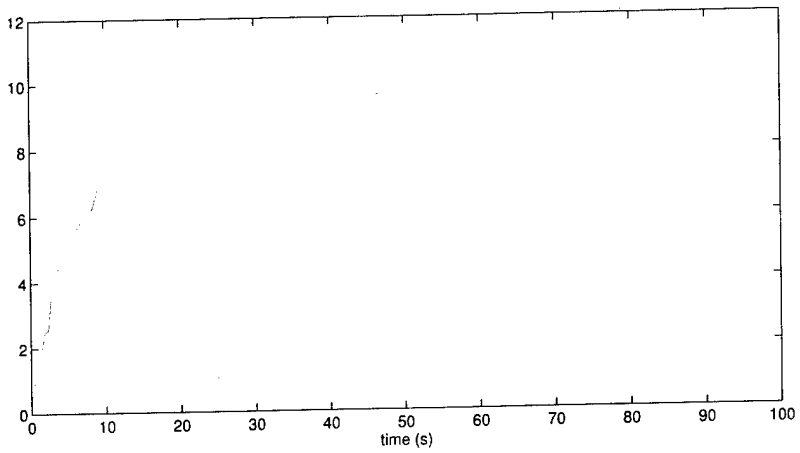


Fig. 3. $\tilde{\alpha}$ as a function of time, with $c = -20a$, $\delta = 100$, and $\mu(x) = x$.

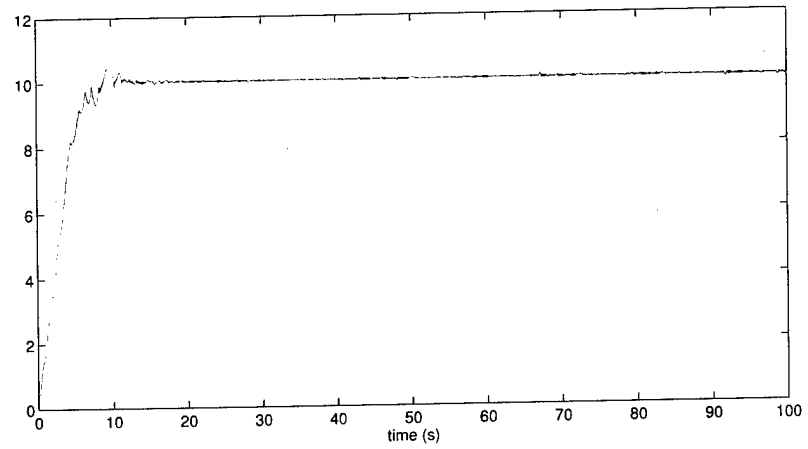


Fig. 4. $\tilde{\alpha}$ as a function of time, with $c = -20a$, $\delta = 10$, and $\mu(x) = \text{sgn}(x)$.

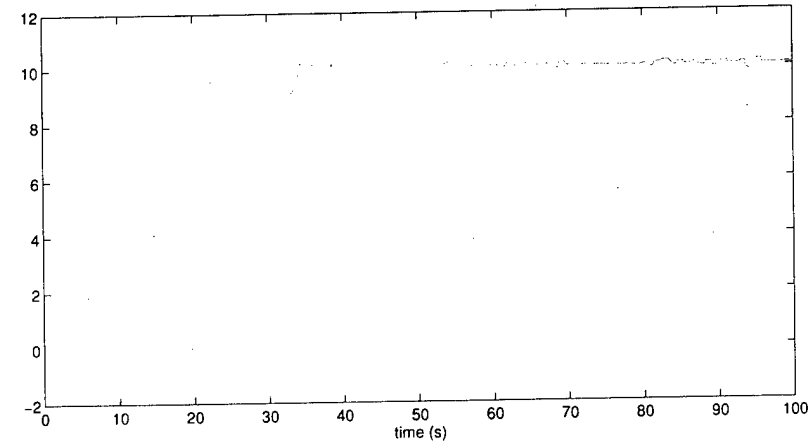


Fig. 5. $\tilde{\alpha}$ as a function of time, with $c = -20a$, $\delta = 1$, and $\mu(x) = \text{sgn}(x)(e^{|x|} - 1)$.

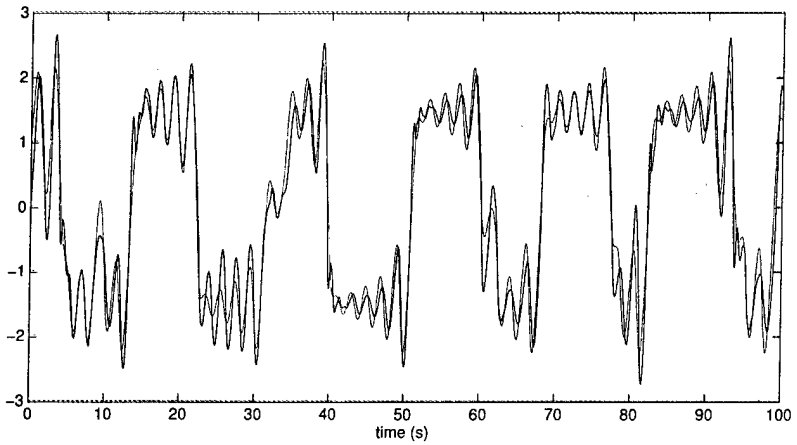


Fig. 6. $x$ and $\tilde{x}$ as functions of time. $c = -2a$, $\delta = 10$, $\mu(x) = \text{sgn}(x)$.

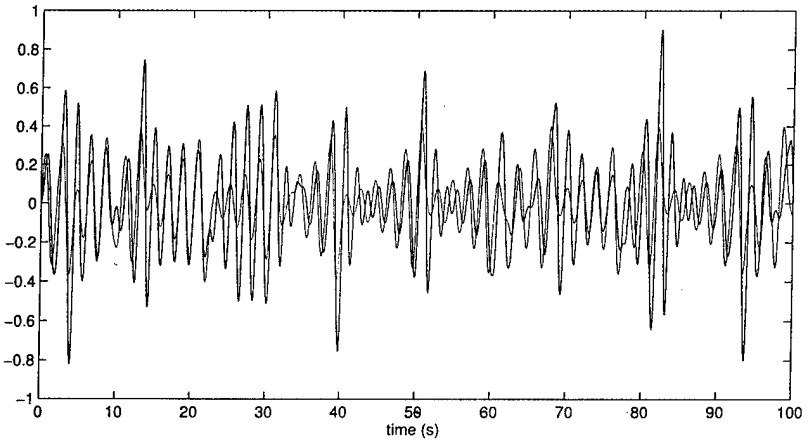


Fig. 7. $y$ and $\tilde{y}$ as functions of time. $c = -2a$, $\delta = 10$, $\mu(x) = \text{sgn}(x)$.

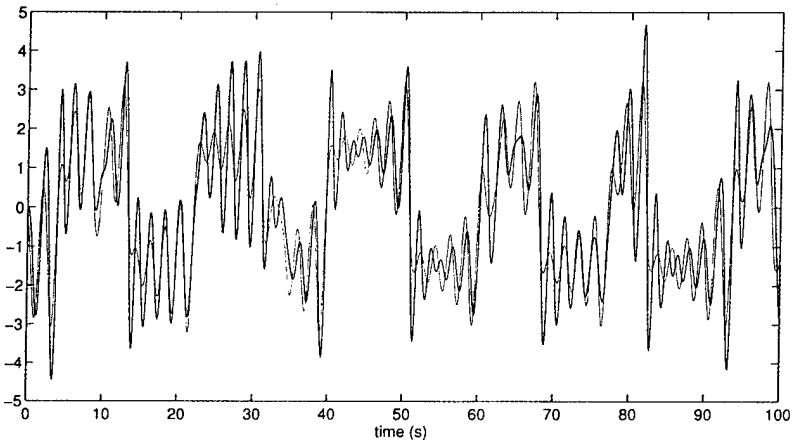


Fig. 8. $z$ and $\tilde{z}$ as functions of time. $c = -2a$, $\delta = 10$, $\mu(x) = \text{sgn}(x)$.

systems. In fact, we show that even when the coupling is not strong enough to synchronize the two systems when the parameters are identical, the use of adaptive controllers can still maintain the synchronization in some sense. In [Chua *et al.*, 1996] it was shown that an adaptive controller for channel gain compensation also exhibits this phenomenon.

The state equations used for synchronizing two Chua's oscillators are given by:

$$\begin{aligned}
\frac{dx}{dt} &= \alpha(y - x - f(x)), \\
\frac{dy}{dt} &= x - y + z, \\
\frac{dz}{dt} &= -\beta y - \gamma z, \\
\frac{d\tilde{x}}{dt} &= \tilde{\alpha}(\tilde{y} - \tilde{x} - f(\tilde{x})) + c(x - \tilde{x}), \qquad (18) \\
\frac{d\tilde{y}}{dt} &= \tilde{x} - \tilde{y} + \tilde{z}, \\
\frac{d\tilde{z}}{dt} &= -\beta\tilde{y} - \gamma\tilde{z}, \\
\frac{d\tilde{\alpha}}{dt} &= \delta\mu(x - \tilde{x})(\tilde{y} - \tilde{x} - f(\tilde{x})),
\end{aligned}$$

and

$$f(x) = bx + \frac{1}{2}(a - b)(|x + 1| - |x - 1|).$$

The fixed parameters are chosen as $\alpha = 10$, $\beta = 15.6$, $\gamma = 0.001$, $a = -1.14$, $b = -0.714$.

In Fig. 3 we show $\tilde{\alpha}$ when $\delta = 100$, $\mu(x) = x$, and $c = -20a$, where $a$ is a parameter defining $f$ and corresponds to the slope of the middle segment of the piecewise linear function $f$. $\tilde{\alpha}$ is initially chosen to be $10^{-5}$.

In Fig. 4 we show $\tilde{\alpha}$ when $c = -20a$, $\delta = 10$, and $\mu(x) = \text{sgn}(x)$. $\tilde{\alpha}$ is initially chosen to be $10^{-5}$.

In Fig. 5 we show $\tilde{\alpha}$ when $c = -20a$, $\delta = 1$, and $\mu(x) = \text{sgn}(x)(e^{|x|} - 1)$. $\tilde{\alpha}$ is initially chosen to be $10^{-5}$.

When we set $c = -2a$, the resulting coupling is not enough to synchronize the two systems even when $\alpha = \tilde{\alpha}$. In fact, simulations show that when $\alpha = \tilde{\alpha}$, $\tilde{x}$, $\tilde{y}$, and $\tilde{z}$ will diverge to infinity. However, when $\delta = 10$ and $\mu(x) = \text{sgn}(x)$, the adaptive controller for $\tilde{\alpha}$ will keep $\tilde{x}$ in "phase" to $x$. Figures 6–8 compare the state variables in the two systems. The state variables $x$, $y$, and $z$ are shown in red and the state variables $\tilde{x}$, $\tilde{y}$, and $\tilde{z}$ are shown in blue. We see that $y$ and $\tilde{y}$ (and also $z$ and $\tilde{z}$) are less in phase than $x$ and $\tilde{x}$.

In Fig. 9 we show $\tilde{\alpha}$ as a function of time. We see that $\tilde{\alpha}$ does not converge towards $\alpha$, but fluctuates around a value below $\alpha = 10$. This is an example where $\tilde{\alpha}$ cannot converge towards $\alpha$ for the system to synchronize, since the coupling is too weak. Thus the time-varying mismatch in parameters is used here to *reduce* the synchronization error rather than to increase it.

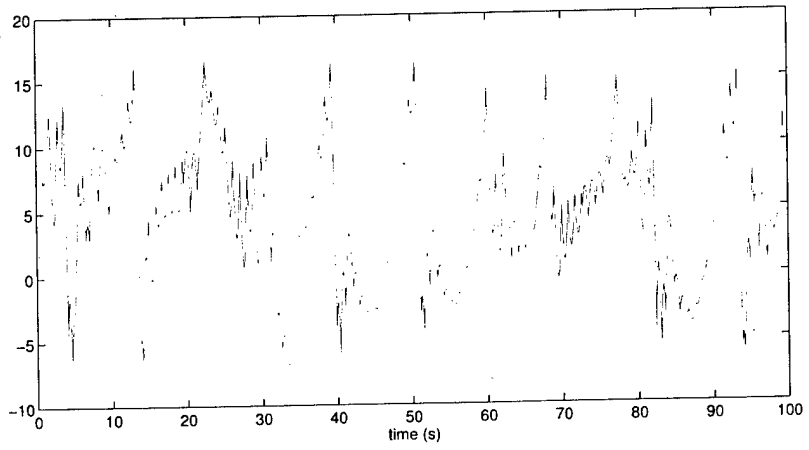


Fig. 9. $\tilde{\alpha}$ as a function of time. $c = -2a$, $\delta = 10$, $\mu(x) = \text{sgn}(x)$. We see that $\tilde{\alpha}$ fluctuates around a value below $\alpha = 10$.

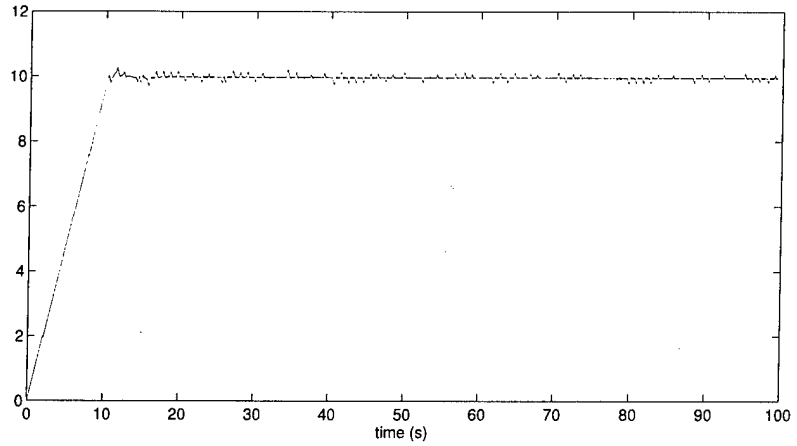


Fig. 10. $\tilde{\alpha}$ as a function of time with $c = -20a$ and $\dot{\tilde{\alpha}} = \text{sgn}(x - \tilde{x})\text{sgn}(\tilde{y} - \tilde{x} - f(\tilde{x}))$.

## 6. Generalizations

An obvious generalization of the scheme in Eq. (5) is to use the following $G$ in Eq. (3):

$$G\left(r_i, \frac{d\dot{r}_i}{d\tilde{a}_{ij}}\right) = \mu_1(r_i)\mu_2\left(\frac{d\dot{r}_i}{d\tilde{a}_{ij}}\right)$$

$$= -\mu_1(r_i)\mu_2\left(\frac{d\dot{\tilde{x}}_i}{d\tilde{a}_{ij}}\right)$$

where $\mu_1$ and $\mu_2$ are functions in class $\mathcal{D}$. Thus for the coupled systems (7) and (8) the controllers for $\tilde{a}_{ij}$ are:

$$\dot{\tilde{a}}_{ij} = \delta_{ij}\mu_1(x_i - \tilde{x}_i)\mu_2(f_{ij}(\tilde{\mathbf{x}}))\,.$$

Using the coupled Chua's oscillators in Sec. 5 with $c = -20a$ and $\dot{\tilde{\alpha}} = \text{sgn}(x - \tilde{x})\text{sgn}(\tilde{y} - \tilde{x} - f(\tilde{x}))$ we find that the two Chua's oscillators will still synchronize. Figure 10 shows $\tilde{\alpha}$ as a function of time.

## 7. Conclusions

In this letter, we present a variation of the adaptive scheme presented in [Huberman & Lumer, 1990]. We give theoretical justifications for this scheme when the system is nonlinear with linear parameters. This scheme also has the property that it can synchronize two systems even when the coupling is weak. Computer simulation results based on Chua's oscillator are presented and an extension to systems with multiplicative parameters is given.

## Acknowledgments

This work is supported in part by the Office of Naval Research under grant N00014-89-J-1402, and by the Joint Services Electronics Program under contract number F49620-94-C-0038. The United States Government is authorized to reproduce and distribute reprints for governmental purposes notwithstanding any copyright notation hereon.

## References

Celka, P. [1995] "Synchronization of chaotic systems through parameter adaptation," in *IEEE Int. Symp. Circ. Syst. Proc.* **1**, 692–695.

Chua, L. O. & Green, D. N. [1976] "A qualitative analysis of the behavior of dynamic nonlinear networks: Stability of autonomous networks," *IEEE Trans. Circ. Syst.*, **23**(6), 355–379.

Chua, L. O., Yang, T., Zhong, G.-Q. & Wu, C. W. [1996] "Adaptive synchronization of Chua's oscillators," *Int. J. Bifurcation and Chaos* **6**(1), 189–201.

Clarkson, P. M. [1993] *Optimal and Adaptive Signal Processing* (CRC Press).

Huberman, B. A. & Lumer, E. [1990] "Dynamics of adaptive systems," *IEEE Trans. Circ. Syst.* **37**(4), 547–550.

John, J. K. & Amritkar, R. E. [1994] "Synchronization by feedback and adaptive control," *Int. J. Bifurcation and Chaos* **4**(6), 1687–1695.

Lakshmikantham, V. & Liu, X. Z. [1993] *Stability Analysis In Terms of Two Measures* (World Scientific, Singapore).

Sinha, S., Ramaswamy, R. & Rao, J. S. [1990] "Adaptive control in nonlinear dynamics," *Physica* **D43**, 118–128.

Wu, C. W. & Chua, L. O. [1994] "A unified framework for synchronization and control of dynamical systems," *Int. J. Bifurcation and Chaos* **4**(4), 979–998.

Wu, C. W. & Chua, L. O. [1996] "On the generality of the unfolded Chua's circuit," *Int. J. Bifurcation and Chaos* **6**(5), 801–832.

Wu, C. W. Yang, T. & Chua, L. O. [1996] "On adaptive synchronization and control of nonlinear dynamical systems," *Int. J. Bifurcation and Chaos* **6**(3), 455–471.

International Journal of Bifurcation and Chaos, Vol. 6, No. 6 (1996) 1111–1125
Theme Issue (Part 2)
© World Scientific Publishing Company

# FROM ALMOST PERIODIC TO CHAOTIC: THE FUNDAMENTAL MAP

RAY BROWN
*Applied Chaos Technology Corporation,*
*P.O. Box 1608, Arlington, VA 22210, USA*

LEON O. CHUA
*Department of Electrical Engineering and Computer Sciences,*
*University of California, Berkeley, CA 94720, USA*

Received December 16, 1995; Revised April 7, 1996

In this paper we present a single map that displays an extraordinary range of dynamics that lies between the Bernoulli maps and almost periodic maps. Of central importance is the fact that this map illustrates how almost-periodic dynamics evolves into Bernoulli dynamics. Due to its continuous spectrum of dynamics between Bernoulli and almost periodic, we call this map the *fundamental map* in contrast to the better known standard map. The range of dynamics found in this map suggests that as order gives way to chaos, both the geometry of the orbit and the sequence of coordinates of the points of the orbit evolve from order to disorder. An interesting point brought out by this map is that the spatial and temporal properties of orbits near each end of the scale bear some striking similarities. Additionally, we show how to derive a Poincaré map from the fundamental map and derive the associated ODE, an equation for an electronic circuit.

## 1. Introduction

In this paper we describe a one-parameter family of maps that range from a shift on $n$-symbols to an almost-periodic map. This family illustrates the extraordinary range of dynamics that can occur between these two limits and suggests how the evolution from almost periodic to Bernoulli takes place. A significant question is "Where in this parameter space does chaos actually begin?" The figures obtained from different parameter values of this map illustrate interesting relationships between order and chaos, and how, as order begins to evolve into chaos, the spatial and temporal relationships of an orbit are transformed.

As a practical application, this map may be used to generate data that can be used for the evaluation of empirical tests of pseudo-random processes such as the empty box test [Lake, 1996]. Lastly, we observe that this map may be generalized to higher dimensions.

We begin by showing how to construct a useful formula for a Bernoulli map in two dimensions.

## 2. From Almost Periodic to Bernoulli

### 2.1. *A useful formula for a Bernoulli map*

In this section we show how to construct a function of a two-sided Bernoulli map which provides insight into how two-sided Bernoulli maps manifest themselves in algebraic forms. The algebraic representation of two-sided Bernoulli maps is essential to

recognizing when we are encountering chaos in our "everyday" equations. The construction extends the methods used for one-sided shifts found in our paper on examples and counterexamples [Brown & Chua, 1996]. Let

$$\begin{pmatrix} u \\ v \\ w \\ z \end{pmatrix} = \begin{pmatrix} \cos(\phi) \\ \sin(\phi) \\ \cos(\theta) \\ \sin(\theta) \end{pmatrix} \tag{1}$$

Note that while these coordinates are in four dimensions, they are identified by only $\phi$ and $\theta$, and hence represent only a two-dimensional space embedded in four dimensions.

Now we derive an algebraic representation of a Bernoulli map in terms of elementary functions using the Anosov dynamical system on the torus defined by

$$\mathrm{A}\begin{pmatrix} \phi \\ \theta \end{pmatrix} = \begin{pmatrix} 2\phi + \theta \\ \phi + \theta \end{pmatrix} \bmod (1) \tag{2}$$

This system is also known as the cat map and is known to be a bi-lateral Bernoulli map on the unit square. Note the occurrence of the addition modulo 1 function in this definition of the Anosov map. This must be removed in any algebraic representation we seek because this operation is not an elementary function and it does not occur explicitly in the laws of nature. In fact, the operation of addition mod 1 is a mathematical abstraction that is very useful for proving theorems while obscuring the relationship between the conclusion of a theorem and its connection to the physical world.

By direct substitution of the components of Eq. (2) into Eq. (1), and by an application of the double angle formulas for the sine and cosine, we get, after simplification, the four-dimensional system:

$$\mathrm{T}\begin{pmatrix} u \\ v \\ w \\ z \end{pmatrix} = \begin{pmatrix} 0 & 0 & (u^2 - v^2) & -2uv \\ 0 & 0 & 2uv & (u^2 - v^2) \\ w & -z & 0 & 0 \\ z & w & 0 & 0 \end{pmatrix} \begin{pmatrix} u \\ v \\ w \\ z \end{pmatrix}$$

What is revealed by this map is that the bi-lateral Bernoulli map is equivalent to a map defined by a two-component twist system: the upper right block of four entries is a twist as is the lower left block of four entries. The $u$, $v$ component of this map is acting as a twist on the $w$, $z$ component and vice versa.

Implementation of this map on a computer must be done carefully due to the rapid accumulation of round-off errors. By taking the arctangents/ $2\pi$ we obtain a map on the unit square which is a bi-lateral Bernoulli map. An implementation of this map in QuickBASIC is:

```
FOR i= 1 TO N
u1=(u^2-v^2)*w-2*u*v*z
v1=2*u*v*w+(u^2-v^2)*z
w1=u*w-v*z
z1=v*w+u*z
phi=arctangent(v1/u1)
theta=arctangent(z1/w1)
u=cos(phi)
v=sin(phi)
w=cos(theta)
z=sin(theta)
PSET (phi/(2*pi),theta/(2*pi)),10
NEXT i
```

The computation of the arctangents is included to compensate for round-off errors. Also, we plot the points in the angular coordinates to retain the uniformity of the Bernoulli distribution.

Following this example we may derive countless additional examples of functions of bilateral shifts on any number of symbols in terms of elementary functions.

## 2.2. *Combining Bernoulli with almost periodic*

The preceding map, if transformed to complex coordinates $w = \psi_1 + \eta_1 i$, $z = \psi_2 + \eta_2 i$, can be represented by:

$$\mathrm{B}\begin{pmatrix} w \\ z \end{pmatrix} = \begin{pmatrix} w^2 z \\ wz \end{pmatrix} \tag{3}$$

where the modulus of the complex numbers $|w| = |z| = 1$.

An almost-periodic map in complex coordinates can be written as

$$\mathrm{A}\begin{pmatrix} w \\ z \end{pmatrix} = \begin{pmatrix} aw \\ bz \end{pmatrix} \tag{4}$$

where $a$, $b$ are complex numbers satisfying $|w| = |z| = |a| = |b| = 1$. This is a pair of rotations on the cross product of two unit circles known as the complex torus in two dimensions.

We generalize the Bernoulli map to all two-dimensional complex space by redefining B as

follows:

$$\mathrm{B}\begin{pmatrix} w \\ z \end{pmatrix} = \begin{pmatrix} \dfrac{w^2 z}{|w^2 z|} \\ \dfrac{wz}{|wz|} \end{pmatrix} \tag{5}$$

B is now defined on the complex plane and projects every vector onto the complex torus. The torus is, in effect, an attractor, and B restricted to the torus is an invertible differentiable mapping. It is not necessary to similarly redefine A since A is bounded even when $|w|, |z| \neq 1$.

We form a typical linear combination of these two maps often used in vector computations to get the following map:

$$\mathrm{T}\begin{pmatrix} w \\ z \end{pmatrix} = (1-\lambda)\mathrm{B}\begin{pmatrix} w \\ z \end{pmatrix} + \lambda \mathrm{A}\begin{pmatrix} w \\ z \end{pmatrix} \tag{6}$$

where $0 \leq \lambda \leq 1$. To make this equation a mapping on the torus we need

$$K_1 = |(1-\lambda)w^2 z + \lambda(aw)| \tag{7}$$

and

$$K_2 = |(1-\lambda)wz + \lambda(bz)| \tag{8}$$

We now define the fundamental map as

$$B_\lambda(1, a, b)\begin{pmatrix} w \\ z \end{pmatrix} = \left[(1-\lambda)\begin{pmatrix} \dfrac{w^2 z}{K_1} \\ \dfrac{wz}{K_2} \end{pmatrix} + \lambda \begin{pmatrix} \dfrac{aw}{K_1} \\ \dfrac{bz}{K_2} \end{pmatrix}\right] \tag{9}$$

This is a mapping on the complex torus. When $\lambda = 0$, it is Bernoulli, and when $\lambda = 1$ it is almost periodic. For all other values of $\lambda$ it is somewhere in-between. Stated differently, it is a one-parameter family of maps, which, except at the origin, are $C^\infty$ (when considered as real valued maps) that continuously vary from an almost-periodic map to a Bernoulli map on two symbols.

We note that $B_\lambda$ is not an analytic map. This is of no significance since the use of complex coordinates here is only a notational convenience and the theory of complex variables is not used in any of the results. As real valued maps, $B_\lambda$ and the subsequence maps that we present are infinitely differentiable, except possibly at the origin.

If we generalize this map further we may obtain a set of maps that continuously vary from an almost-periodic map to a Bernoulli map on $n$-symbols. The generalization is.

$$B_\lambda(n, a, b)\begin{pmatrix} w \\ z \end{pmatrix} = \left[(1-\lambda)\begin{pmatrix} \dfrac{w^{n+1} z^n}{K_1} \\ \dfrac{wz}{K_2} \end{pmatrix} + \lambda \begin{pmatrix} \dfrac{aw}{K_1} \\ \dfrac{bz}{K_2} \end{pmatrix}\right] \tag{10}$$

and $K_i$ are the divisors needed to force the mapping to stay on the complex torus.

## 3. A Poincaré Map: The Second Fundamental Map

In this section we derive a Poincaré map for a circuit which is an arbitrarily small perturbation of the fundamental map and derive the associated circuit equations.

We note that the fundamental map is not always invertible, but by using the technique of Brown & Chua [1993], it can be embedded in an invertible map which is an arbitrarily small perturbation of the fundamental map. This new map, which is a four-dimensional complex map, will be called the second fundamental map. Its key properties are:

(1) it has the full range of dynamics of the fundamental map, ranging from Bernoulli to almost periodic;
(2) it contains period doubling bifurcations to chaos;
(3) it contains the full range of dynamics from attracting dynamics to measure preserving dynamics;
(4) it is invertible; and,
(5) it is a closed form Poincaré map for an electronic circuit.

### 3.1. *The second fundamental map*

The general method for embedding any map into a Poincaré map was suggested in Brown & Chua [1993] but was not explicitly stated. We now state this result formally:

**Theorem 1.** *Let $f : \mathbf{R}^n \to \mathbf{R}^n$ be any differentiable (not necessarily invertible) function on $\mathbf{R}^n$. Then $f$ can be embedded in a Poincaré map for an electronic circuit as follows:*

*Let* $\mathbf{x}, \mathbf{y} \in \mathbf{R}^n$ *be any two vectors in* $\mathbf{R}^n$ *and define* $T: \mathbf{R}^{2n} \to \mathbf{R}^{2n}$ *by the equation:*

$$\mathrm{T}\begin{pmatrix}\mathbf{x}\\ \mathbf{y}\end{pmatrix} = \begin{pmatrix} f(c\mathbf{y}+\mathbf{x}) - c\mathbf{y} \\ c\mathbf{y}+\mathbf{x}\end{pmatrix} \tag{11}$$

*where* $c$ *is any real number, then,*

(1) T *is* 1-1, *has the same number of derivatives as* $f$, *and* $\det(\mathrm{DT}) = c^n$;
(2) *for all* $c > 0$ T *is a Poincaré map for an ODE in* $\mathbf{R}^{2n}$;
(3) *for* $c = 0$, *the range of* T *is the graph of* $f$, *and the orbit of a point* $(\mathbf{x}, \mathbf{y})$ *under* T *is the orbit of* $\mathbf{x}$ *under* $f$, *i.e.* $(f^{n+1}(\mathbf{x}), f^n(\mathbf{x}))$;
(4) *for any* $\mathbf{x} \in \mathbf{R}^n$, *if* $|c| < 1$ *then* $(f^{n+1}(\mathbf{x}), f^n(\mathbf{x}))$, *is a subset an attractor*;
(5) *as* $c \to 0$, *the attractor of* T *converges to the orbit of* $\mathbf{x}$ *under* $f$.

*Proof.* All assertions are direct computations. ■

Using Theorem 1, we write down the second fundamental map:

$$F_\lambda\begin{pmatrix}\Theta\\ \Psi\end{pmatrix} = \begin{pmatrix} B_\lambda(n, c\Psi+\Theta) - c\Psi \\ c\Psi+\Theta\end{pmatrix} \tag{12}$$

From the above theorem we know that the second fundamental map preserves the dynamics of the fundamental map. The analogy is our example of a Poincaré map for a two-dimensional equation which was a small perturbation of the map $x \to 2x \bmod (1)$ in Brown & Chua [1993]. The second fundamental map is the composition of three invertible maps, all of which are time-one maps of complex ODEs. We now show how to construct the circuit using the fundamental map.

### 3.2. *The circuit*

In this section we use greek letters to represent four-dimensional complex vectors. Thus,

$$\Psi = \begin{pmatrix}u\\ v\end{pmatrix} \qquad \Theta = \begin{pmatrix}w\\ z\end{pmatrix}$$

where $u, v, w, z$ are complex variables. In this notation the fundamental map is written as $B_\lambda(n, \Psi)$. The three components of the second fundamental map are:

$$\mathrm{T}_1\begin{pmatrix}\Theta\\ \Psi\end{pmatrix} = \begin{pmatrix}\Theta\\ c\Psi\end{pmatrix} \tag{13}$$

$$\mathrm{T}_2\begin{pmatrix}\Theta\\ \Psi\end{pmatrix} = \begin{pmatrix}\Theta\\ \Psi+\Theta\end{pmatrix} \tag{14}$$

$$\mathrm{T}_3\begin{pmatrix}\Theta\\ \Psi\end{pmatrix} = \begin{pmatrix}\Theta - \Psi + B_\lambda(n, \Psi)\\ \Psi\end{pmatrix} \tag{15}$$

where $c$ is any real number. The second fundamental map is the composition of these three maps.

The second fundamental map is the Poincaré map for:

$$\begin{pmatrix}\dot\Theta\\ \dot\Psi\end{pmatrix} = \begin{pmatrix} s_3(t)(B_\lambda(n, \Psi) - \Psi)\\ s_2(t)\Theta - s_1(t)\Psi\end{pmatrix} \tag{16}$$

where $s_i(t)$ is a three-phase gate as shown in Fig. 1.

### 3.3. *Detailed circuit equations*

In this section we write down the eight-dimensional real-variable equations for the second fundamental map circuit. In order to do this we must change our notation, thus in this section we define:

$$\Psi = \begin{pmatrix}x\\ y\\ w\\ z\end{pmatrix} \qquad \Theta = \begin{pmatrix}\theta_1\\ \theta_2\\ \theta_3\\ \theta_4\end{pmatrix}$$

where $x, y, w, z, \theta_i$ are *real* variables. In this notation the eight-dimensional circuit equation is

$$\begin{pmatrix}\dot\theta_1\\ \dot\theta_2\\ \dot\theta_3\\ \dot\theta_4\end{pmatrix} = s_3(t)\begin{pmatrix} f_1(x, y, w, z) - c\theta_1\\ f_2(x, y, w, z) - c\theta_2\\ f_3(x, y, w, z) - c\theta_3\\ f_4(x, y, w, z) - c\theta_4\end{pmatrix} \tag{17}$$

$$\begin{pmatrix}\dot x\\ \dot y\\ \dot w\\ \dot z\end{pmatrix} = s_2(t)\begin{pmatrix}\theta_1\\ \theta_2\\ \theta_3\\ \theta_4\end{pmatrix} - s_1(t)\begin{pmatrix}x\\ y\\ w\\ z\end{pmatrix} \tag{18}$$

where we define the $f_i$ in the following equations. First we need to define $g_i$ and $K_i$ as a notational

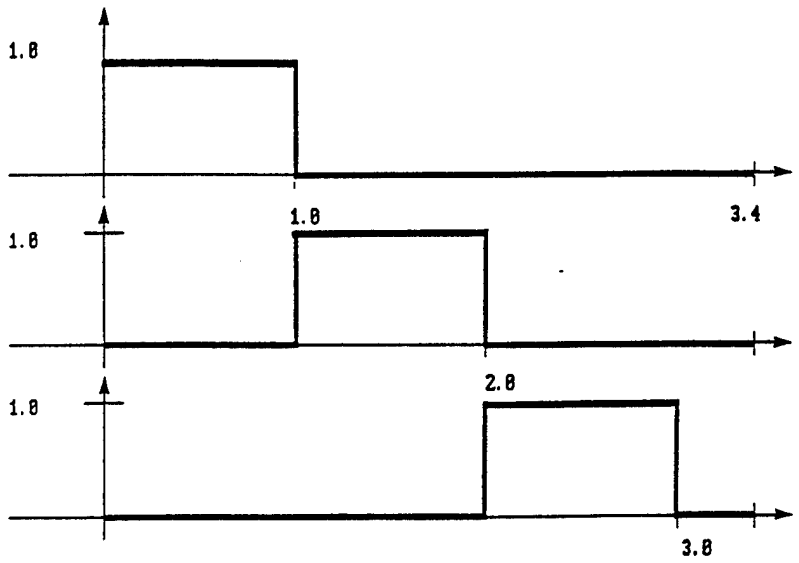


Fig. 1. The functions $s_i(t)$, $i = 1, 2, 3$, constitute a three-phase gate function. Each is periodic of the same period. $s_2(t)$ and $s_3(t)$ are phase shifts of the function $s_1(t)$.

convenience:

$$\begin{pmatrix} g_1(x, y, w, z) \\ g_2(x, y, w, z) \\ g_3(x, y, w, z) \\ g_4(x, y, w, z) \end{pmatrix} = (1-\lambda) \begin{pmatrix} (x^2-y^2)w - 2xyz \\ 2xyw + (x^2-y^2)z \\ xw - yz \\ xz + yw \end{pmatrix} + \lambda \begin{pmatrix} a_1x - a_2y \\ a_2x + a_1y \\ b_1w - b_2z \\ b_2w + b_1z \end{pmatrix} \tag{19}$$

$$K_{1a} = (1-\lambda)^2(x^2+y^2)(w^2+z^2) + \lambda^2(a_1^2+a_2^2) \tag{20}$$

$$K_{1b} = 2(1-\lambda)\lambda(a_1(xw+yz) + a_2(xz+yw)) \tag{21}$$

and $K_1 = \sqrt{x^2+y^2}\sqrt{K_{1a}+K_{1b}}$.

$$K_2 = \sqrt{(w^2+z^2)[(1-\lambda)^2(x^2+y^2) + \lambda^2(b_1^2+b_2^2) + 2\lambda(1-\lambda)(b_1w+b_2z)]} \tag{22}$$

We can now complete the definition of the functions $f_i$:

$$f_1 = \frac{g_1}{K_1} \qquad f_2 = \frac{g_2}{K_1} \qquad f_3 = \frac{g_3}{K_2} \qquad f_4 = \frac{g_4}{K_2} \tag{23}$$

### 3.4. *The attractors*

What is most useful about these maps is what they reveal about the transition between almost periodic and chaotic dynamics. While the second fundamental map is in eight dimensions, the essential dynamics occurs in only two dimensions: In addition to the two dimensions used to portray the dynamics, two more are needed to arrange for the map to operate on a two-dimensional manifold which is compact (the torus). The additional four dimensions are used to make the map invertible. Another way of seeing this is to note that, by inspection, the three component maps that make up the second fundamental map, only one carries the dynamics of the fundamental map, Eq. (18), and that map only uses four dimensions. Of the four dimensions used only two are really needed since the parameter $c$ may be chosen to be arbitrarily small. For example, we could choose $c = 10^{-10000}$.

### 3.4.1. *Figures 2–11*

In Figs. 2–11 we show how the variation of a single parameter in the second fundamental map produces a diverse array of dynamics which start at Bernoulli and end almost periodic. In Fig. 2, we choose $\lambda = 0$ to obtain a pure Bernoulli orbit. This orbit could be obtained by using the cat map. The orbit appears uniform yet irregular. The map is measure preserving on the attractor. Using the empty box test we would conclude that this orbit is pseudo-random.

In Fig. 3, we have chosen $\lambda = 1$ to obtain a pure almost periodic orbit. This orbit is dense in a closed curve. This orbit could be obtained by a rotation on the torus. Figures 2 and 3 demonstrate the two extremes of the second fundamental map.

In Fig. 4, we choose $\lambda = 0.2$ to obtain a small perturbation of the cat map. The measure preserving feature is apparently lost, but the pseudo-random feature is preserved. This is to be expected due to the "structural stability" of the cat map. We conclude that the map is still chaotic, though not strictly Bernoulli which requires that the map be measure preserving.

In Figs. 5 and 6, we increase $\lambda$ and the orbits become less uniform and twisted. These images are what we might expect to see if we were to twist the underlying space while leaving the orbit uniform. Another view might be that the two-dimensional orbit has buckled into higher dimensions in order to retain its invertibility.

In Fig. 7, $\lambda = 0.5$ and the orbit now is "half Bernoulli and half almost periodic". A bifurcation has taken place in that repelling regions have appeared as large empty spaces and the orbit is now clearly higher dimensional though we are only showing a two-dimensional projection. Though the map is half and half in the parameter space, it is still clearly chaotic, but not Bernoulli. What we can conclude is that the contribution from the Bernoulli component is still strong enough that the map is chaotic. It is worth recalling at this point that the second fundamental map is a closed form Poincaré map for an electronic circuit.

In Fig. 8, $\lambda = 0.65$ and is weighted toward almost periodic dynamics. The ripples represent the formation of order while the orbit is clearly disorderly to the eye. The Bernoulli component keeps this orbit chaotic. The ripples resemble wind swept sand dunes as seen from overhead. Does this suggest that the ripples in sand dunes are the result of a combined random and almost periodic process?

In Fig. 9, ($\lambda = 0.7$) the addition of 0.05 to the parameter value of Fig. 8 has pushed the orbit into almost-periodic motion. The orbit is an attractor which appears to have chaotic transients. While the dynamics appear almost-periodic, the closed orbits that formed are highly "nonlinear". Thus we have what we might call "geometric chaos" within almost-periodic motion.

In Fig. 10, $\lambda = 0.76$ and the "chaotic" geometry has vanished with another bifurcation. Now the orbit could be described as a uniform almost-periodic motion where we have twisted or wrinkled the underlying space. This apparent uniformity on a twisted space was seen as we perturbed the Bernoulli map in Figs. 4–6.

In Fig. 11, we have a nearly uniform almost-periodic orbit for $\lambda = 0.9$.

#### *Summary of Figs. 2–11*

By varying the parameter $\lambda$ from 0 to 1 we observed the transition from Bernoulli dynamics to almost periodic dynamics. From the initial conditions and rotation factors chosen, we never encountered period doubling bifurcations. By other choices of rotation factors we can obtain period doubling transitions to chaos. One striking feature of the transition is the appearance of the underlying space becoming twisted at each end of the parameter range suggesting that a loss of geometric uniformity may precede the loss of orbit uniformity. During the transition two bifurcations were observed. The first occurred when repelling regions first formed and the second occurred when the attractor became one-dimensional. Clearly, these features are related. In this series of examples, the influence of the Bernoulli term in the second fundamental map maintained the presence of chaos even when the map was weighted toward almost-periodic dynamics. The effect of combining Bernoulli dynamics with almost-periodic dynamics as done here will be more fully explored in *Clarifying Chaos II: Bernoulli Chaos*, to appear.

### 3.4.2. *Figures 12–27*

In Figs. 12–27 we display a wide range of dynamics that can be found in the second fundamental map. These figures are produced by changing the rotation factor in the almost-periodic term of the fundamental map.

In Fig. 12, $\phi_1 = 0.9$, $\phi_2 = 0$, $\lambda = 0.65$. The system is weighted toward AP, we obtain a one-dimensional attractor with a highly irregular shape.

In Fig. 13, $\phi_1 = 0.5$, $\phi_2 = 0.18$, $\lambda = 0.65$. The orbit is a spiral into a single attracting fixed point.

In Fig. 14, $\phi_1 = 2.5764$, $\phi_2 = 0.4$, $\lambda = 0.60$. The orbit geometry is very complex and the orbit itself appears to be AP. It is an attractor.

In Fig. 15, $\phi_1 = 0.5$, $\phi_2 = 0.5$, $\lambda = 0.80$. The dynamics are AP and if the orbit is sampled over infinite time it will fill out the plane. This is another example of how the orbit geometry begins to bend and twist before chaos sets in.

In Fig. 16, $\phi_1 = 0.5$, $\phi_2 = 0.5$, $\lambda = 0.70$. $\lambda$ has been shifted toward B and has now become twisted in a higher dimensional space. The nature of the dynamics is uncertain.

In Fig. 17, $\phi_1 = 0.1$, $\phi_2 = 0.1$, $\lambda = 0.64$. An attractor buckled in higher dimensional space appears. The dynamics appear to be chaotic.

In Fig. 18, $\phi_1 = 1.0$, $\phi_2 = 0.1$, $\lambda = 0.705$. This attractor is beyond strange, having both one- and two-dimensional features. The two-dimensional feature is not transient. There is an order to the orbit, but it does not appear to be AP. We might call this class of attractors, X-attractors.

In Fig. 19, $\phi_1 = 0.1$, $\phi_2 = 2.1$, $\lambda = 0.705$. This is another X-attractor having both one- and two-dimensional features. The webbing and the claws are separated by an area that will fill out as the orbit is continued.

In Fig. 20, $\phi_1 = 2.5$, $\phi_2 = 0.1$, $\lambda = 0.635$. Another X-attractor is shown with rope like features extending from the two-dimensional areas.

In Fig. 21, $\phi_1 = 2.6$, $\phi_2 = 0.0$, $\lambda = 0.58$. This attractor is only slightly weighted toward AP. It has folded into higher dimensions as can be seen by the apparent overlapping of the folds. The orbit is clearly chaotic.

In Fig. 22, $\phi_1 = 0.05$, $\phi_2 = 5.5$, $\lambda = 0.73$. This is an orbit that might be chaotic but it cannot be determined by observation. It has areas where points are concentrated. Considered in two dimensions only, it appears not to be an attractor but rather to have areas of nonuniform density.

In Fig. 23, $\phi_1 = 0.7$, $\phi_2 = 2.5$, $\lambda = 0.76$. This orbit is AP with twisted geometry. If the orbit is run out it will fill the plane.

In Fig. 24, $\phi_1 = 2.6$, $\phi_2 = 0.0725$, $\lambda = 0.72$. Another AP orbit with twisted geometry which will fill out the plane.

In Fig. 25, $\phi_1 = 1.0$, $\phi_2 = 0.9$, $\lambda = 0.73$. This AP orbit will fill out the plane and shows relatively moderate twisting.

In Fig. 26, $\phi_1 = 2.6$, $\phi_2 = 0.9$, $\lambda = 0.75$. This orbit has the appearance of being gently twisted. It is AP.

In Fig. 27, $\phi_1 = 0.1$, $\phi_2 = 2.1$, $\lambda = 0.0$. In this figure, we have $c = 0.999$, a value that makes the map nearly measure preserving. The dynamics is indeterminate by observation but the geometry of the orbit looks chaotic. There are areas that appear to be continuous, but this is an illusion. The orbit circulates in higher dimensions taking on the appearance of a ball of yarn that has unraveled in a random manner.

### *Summary of Figs. 12–27*

What is most apparent from these figures is that chaotic dynamics has a far greater diversity than we have supposed. It is clear that we may construct chaotic attractors having high dimensional characteristics and having geometry as bizarre as our imagination allows. It should be clear that chaos is not a low-dimensional phenomena in a measure theoretic sense but can be found in any dimension with any predetermined set of characteristics. The examples constructed here are not merely academic mathematical abstractions, but can be realized in electronic hardware. Additionally, the diversity of attractors constructed from a simple formula have shapes that are suggestive of natural phenomena. This raises the question: "Are many natural processes simple combinations of random and nonrandom processes?", if so, the fundamental map is a simple model for such processes.

## 3.5. *Figure data*

These figures, computed for $c = 10^{-10}$, are an accurate computer replication of an attractor of the second fundamental map. In only one figure do we allow $c$ to take on a larger value. The resulting figure, Fig. 27, illustrates just how complex the geometry of an orbit can be for the second fundamental map when it is *not* an approximation of the fundamental map.

In Figs. 2–27

$$a = (\cos(\phi_1), \sin(\phi_1)), \quad b = (\cos(\phi_2), \sin(\phi_2)),$$

and $\Psi_0 = \Theta_0$ where

$$\Theta_0 = (\cos(1.266), \sin(1.266), \cos(0.9273), \sin(0.9273))$$

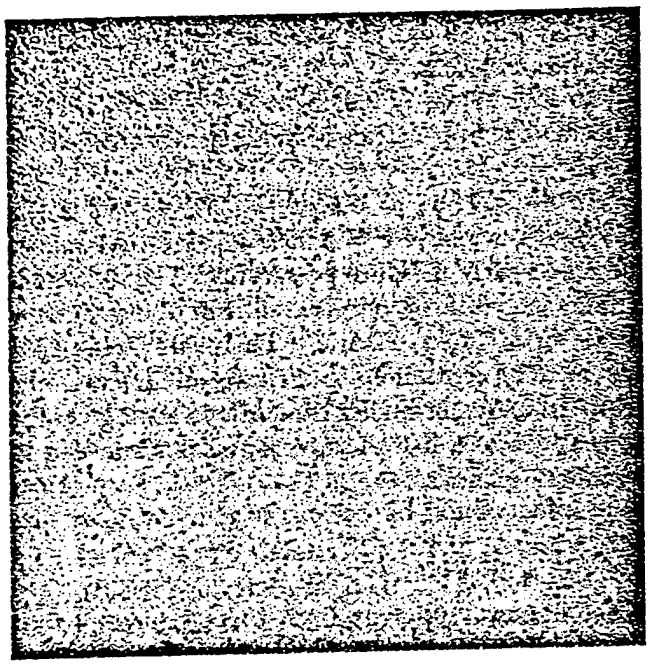

Fig. 2. Orbit of the map $F_0(1, a, b)(w_0, z_0)$ defined by Eq. (12). In this figure, $\phi_1 = 0.9$, $\phi_2 = 0.4$. The horizontal axis is the argument of $w$, and the vertical axis is the argument of $z$. This figure shows the upper limits of chaos, a Bernoulli orbit.

Fig. 3. Orbit of the map $F_1(1, a, b)(w_0, z_0)$ defined by Eq. (12). In this figure, $\phi_1 = 0.9$, $\phi_2 = 0.4$. This figure shows the lower limit of the map's complexity, an almost-periodic orbit that lies on a one-dimensional manifold.

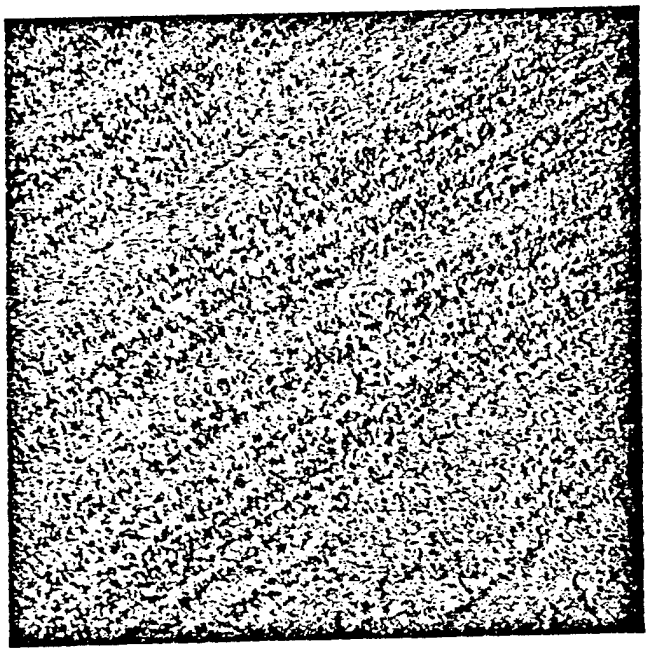

Fig. 4. Orbit of the map $F_{0.2}(1, a, b)(w_0, z_0)$ defined by Eq. (12). In this figure, $\phi_1 = 0.9$, $\phi_2 = 0.4$. We have added a small amount of almost-periodic dynamics to the Bernoulli map causing striations to appear in the previously uniform orbits. The dynamics are still chaotic though apparently not Bernoulli any longer.

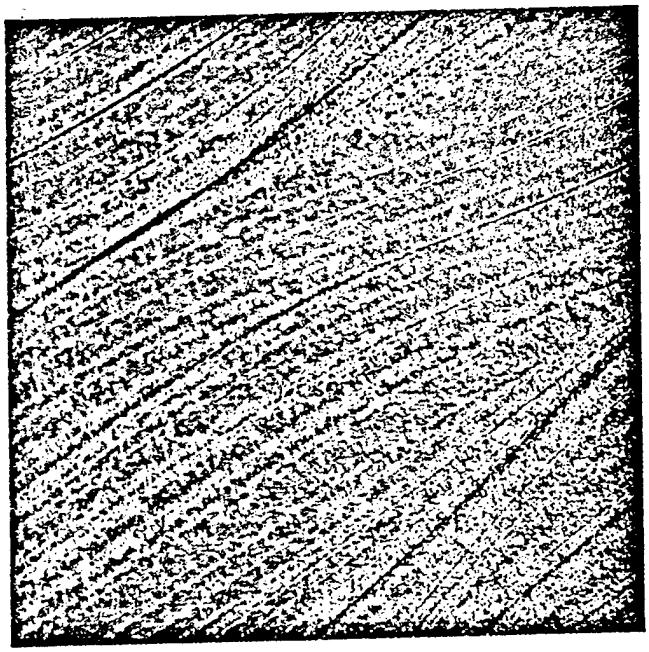

Fig. 5. Orbit of the map $F_{0.3}(1, a, b)(w_0, z_0)$ defined by Eq. (12). In this figure, $\phi_1 = 0.9$, $\phi_2 = 0.4$. By a further increase in almost-periodic dynamics the striations become more prominent. By inspection we determine that chaos is still present.

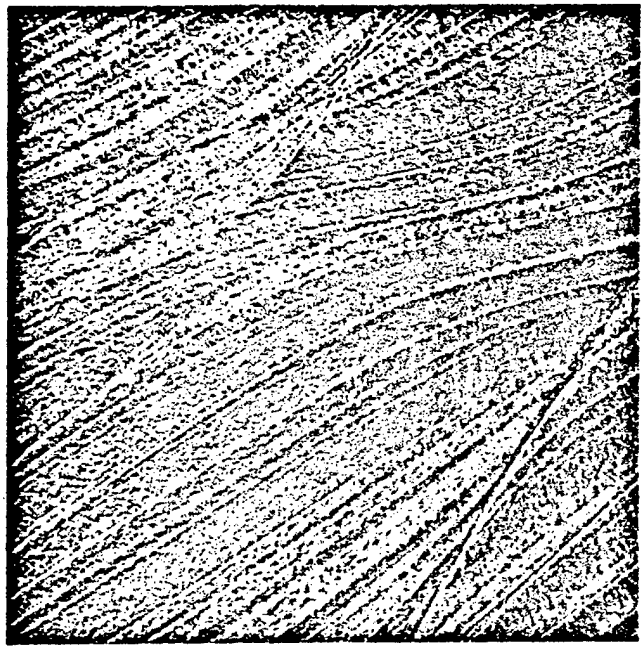

Fig. 6. Orbit of the map $F_{0.4}(1, a, b)(w_0, z_0)$ defined by Eq. (12). In this figure, $\phi_1 = 0.9$, $\phi_2 = 0.4$. Still further increases in almost-periodic dynamics cause the striations to become ever more prominent and by inspection we determine that chaos is still present.

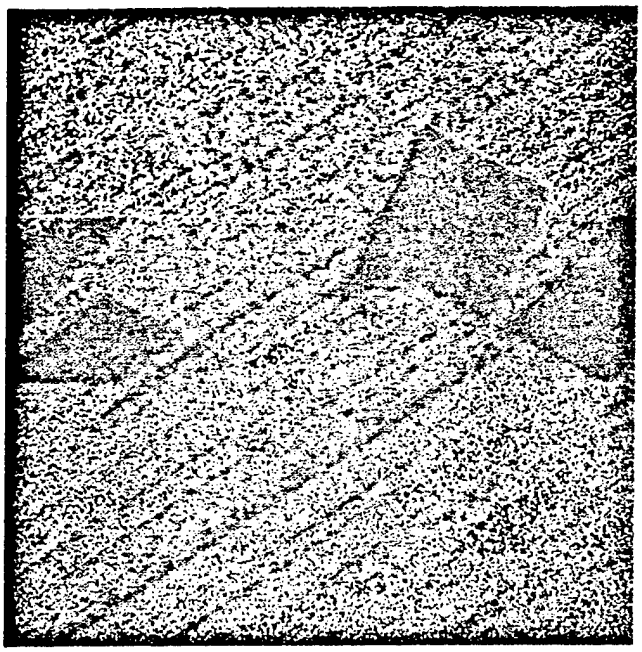

Fig. 7. Orbit of the map $F_{0.5}(1, a, b)(w_0, z_0)$ defined by Eq. (12). In this figure, $\phi_1 = 0.9$, $\phi_2 = 0.4$. Another increment of almost-periodic motion gives a map which is half Bernoulli and half almost-periodic. A bifurcation has taken place as indicated by the prominent empty spaces that have appeared and form repelling regions. The combined mapping remains chaotic.

Fig. 8. Orbit of the map $F_{0.65}(1, a, b)(w_0, z_0)$ defined by Eq. (12). In this figure, $\phi_1 = 0.9$, $\phi_2 = 0.4$. Another increment of almost-periodic motion brings about another bifurcation in that the prominent empty spaces have vanished. The orbit now displays ripples. Order seems to be appearing at this point. The almost-periodic component of the map is now higher than the Bernoulli component, but by inspection we determine that the map is neither Bernoulli nor almost periodic.

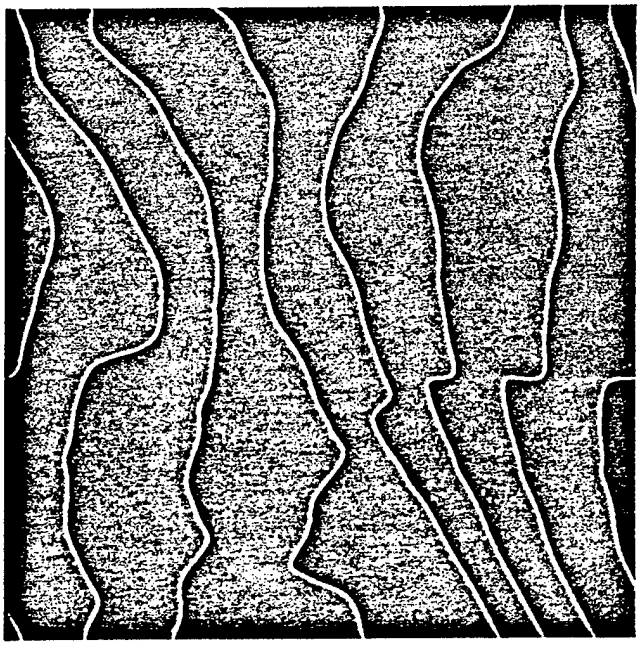

Fig. 9. Orbit of the map $F_{0.7}(1, a, b)(w_0, z_0)$ defined by Eq. (12). In this figure, $\phi_1 = 0.9$, $\phi_2 = 0.4$. A smaller increment of almost-periodic motion brings about another bifurcation: the orbits are one-dimensional attractors and are now clearly almost-periodic.

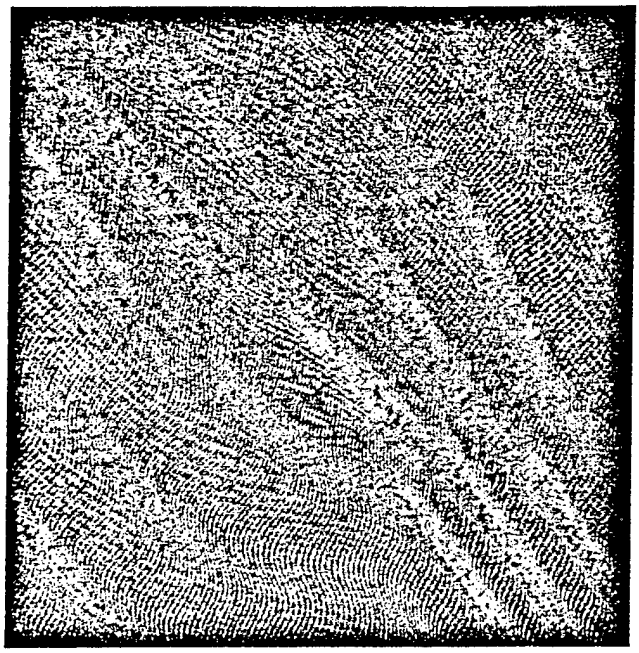

Fig. 10. Orbit of the map $F_{0.76}(1, a, b)(w_0, z_0)$ defined by Eq. (12). In this figure, $\phi_1 = 0.9$, $\phi_2 = 0.4$. Another small increment of almost-periodic motion brings about another bifurcation: the closure of the orbit is two-dimensional. Something similar to the striations that appeared in Fig. 4 now appear in a more orderly fashion in this figure.

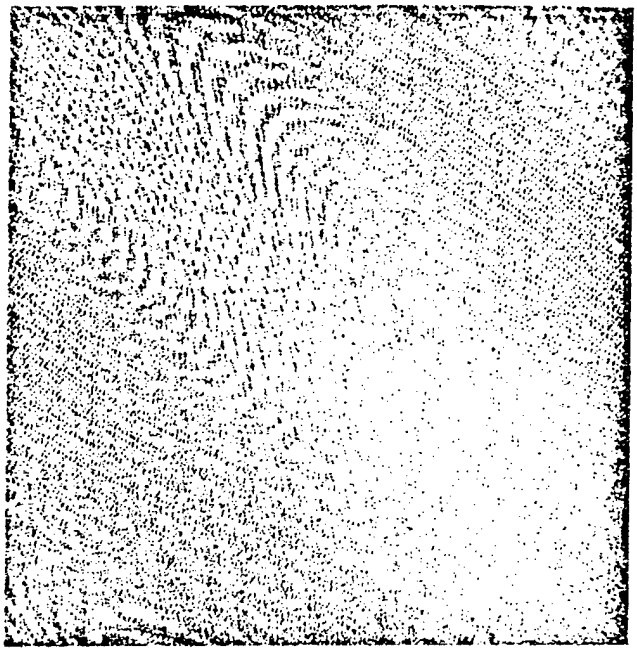

Fig. 11. Orbit of the map $F_{0.9}(1, a, b)(w_0, z_0)$ defined by Eq. (12). As before $\phi_1 = 0.9$, $\phi_2 = 0.4$. The combined map is 90 percent almost-periodic but the dynamics are totally almost-periodic. The striations are lost and the orbit now appears uniform. The closure of the orbit is two-dimensional. In some sense this uniformity is a slight variation of the uniform distribution of points that we associate with a Bernoulli map.

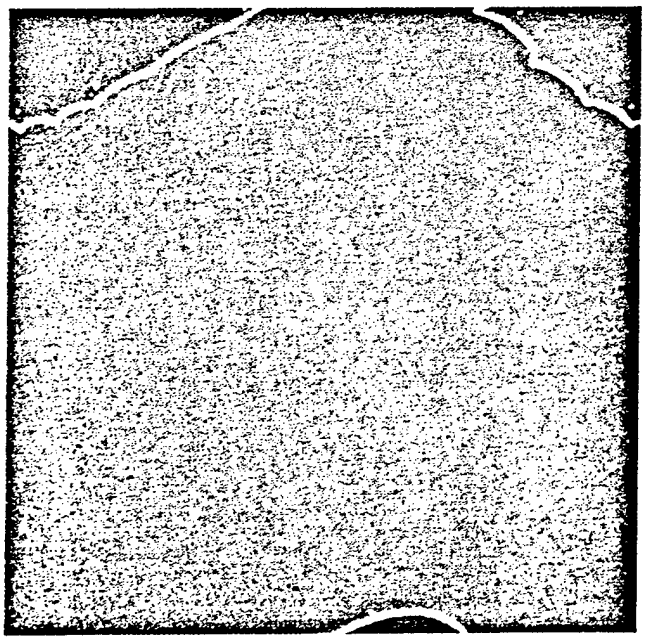

Fig. 12. Orbit of the map $F_{0.65}(1, a, b)(w_0, z_0)$ defined by Eq. (12). In this figure, we change the rotation factor. $\phi_1 = 0.9$, $\phi_2 = 0$. Also, we choose a value of $\lambda$ which weights the combined map toward almost-periodic dynamics. The dynamics appear almost-periodic but by inspection this is not easy to determine. The attractor is one-dimensional. The geometry of the orbit is becoming complex and is reminiscent of nonlinear dynamics in its curvature.

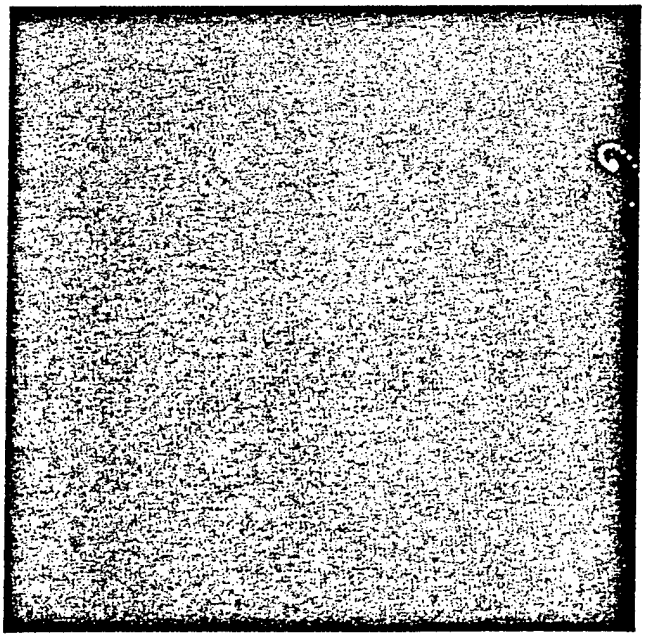

Fig. 13. Orbit of the map $F_{0.65}(1, a, b)(w_0, z_0)$ defined by Eq. (12). In this figure, the rotation factor is $\phi_1 = 0.5$, $\phi_2 = 0.18$. The dynamics are a simple point attractor.

Fig. 14. Orbit of the map $F_{0.6}(1, a, b)(w_0, z_0)$ defined by Eq. (12). In this figure, the rotation factor is $\phi_1 = 2.5764$, $\phi_2 = 0.4$. The dynamics are indeterminate by inspection and the orbit is another one-dimensional attractor. The geometry of the orbit is very complex.

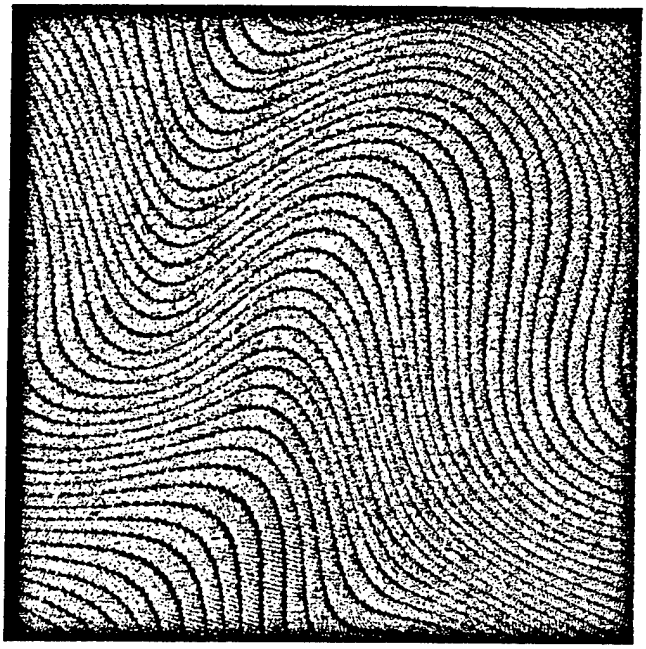

Fig. 15. Orbit of the map $F_{0.8}(1, a, b)(w_0, z_0)$ defined by Eq. (12). In this figure, the rotation factor is $\phi_1 = 0.5$, $\phi_2 = 0.5$. The dynamics are almost periodic. While the dynamics are simple, the orbit looks as complex as a fingerprint. The closure of the orbit is two-dimensional.

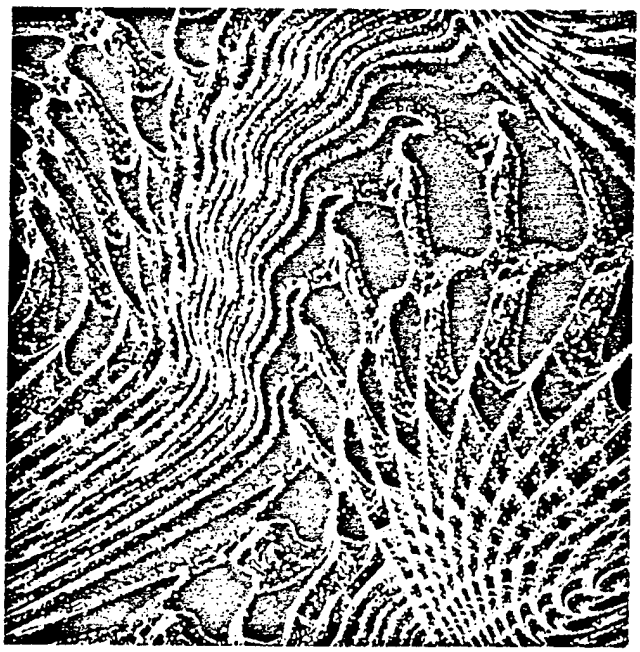

Fig. 16. Orbit of the map $F_{0.7}(1, a, b)(w_0, z_0)$ defined by Eq. (12). In this figure, the rotation factor is $\phi_1 = 0.5$, $\phi_2 = 0.5$. Portions of this attractor bears some resemblance to the top of a sea shell. The dynamics are uncertain but are presumed to be chaotic. The empty regions are repelling regions.

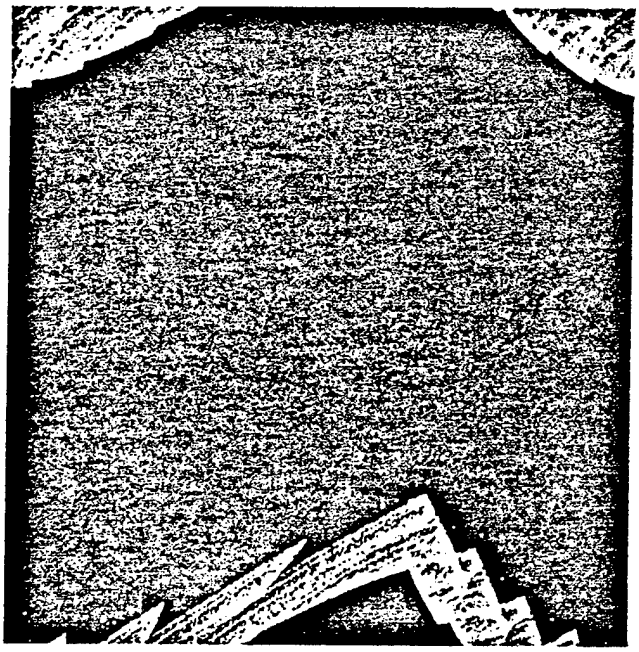

Fig. 17. Orbit of the map $F_{0.64}(1, a, b)(w_0, z_0)$ defined by Eq. (12). In this figure, the rotation factor is $\phi_1 = 0.1$, $\phi_2 = 0.1$. The dynamics are most certainly chaotic. The empty region is repelling.

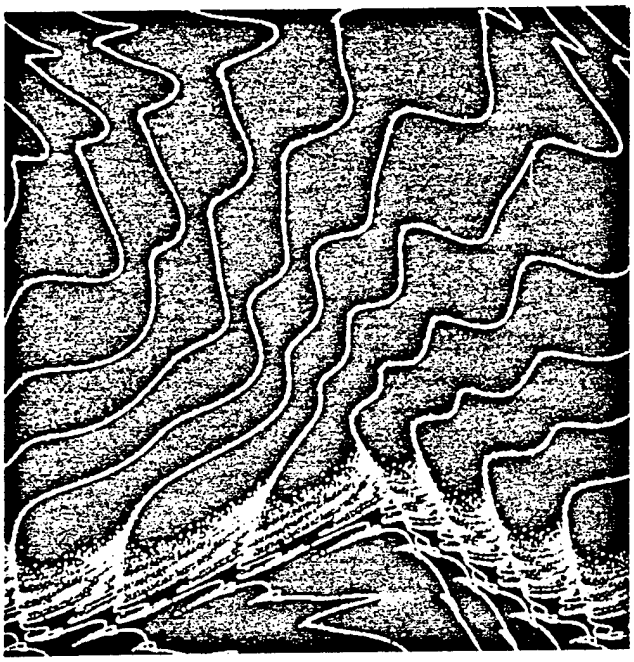

Fig. 18. Orbit of the map $F_{0.705}(1, a, b)(w_0, z_0)$ defined by Eq. (12). In this figure, the rotation factor is $\phi_1 = 0.1$, $\phi_2 = 0.1$, hence this attractor is a small perturbation of Fig. 17. The dynamics are most certainly chaotic with large empty repelling regions. This attractor seems to be transitioning between one- and two-dimensional dynamics in that neither the one-dimensional portion nor the two-dimensional portion are transients.

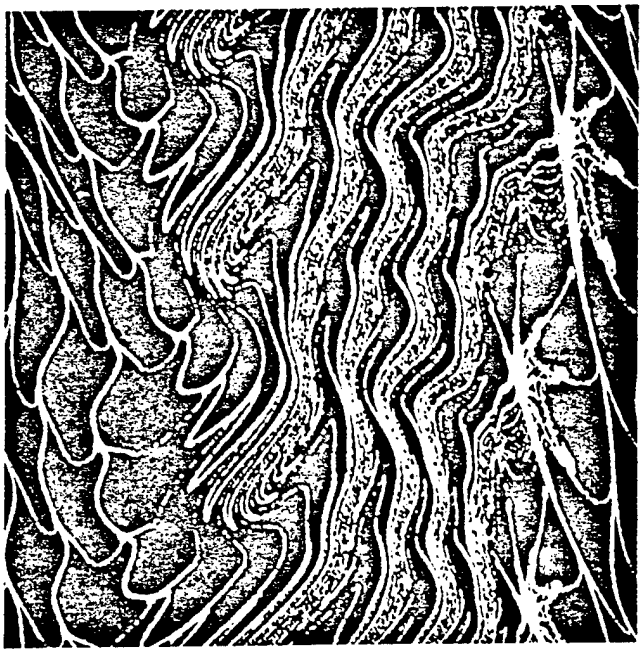

Fig. 19. Orbit of the map $F_{0.705}(1, a, b)(w_0, z_0)$ defined by Eq. (12). In this figure, the rotation factor is $\phi_1 = 0.1$, $\phi_2 = 2.1$. The dynamics are chaotic with large empty repelling regions. Some portions of this attractor resemble the unstable manifold of some two-dimensional twist-and-flip systems. The structures on the right-hand side of the attractor figure resemble cobwebs. They are not transients.

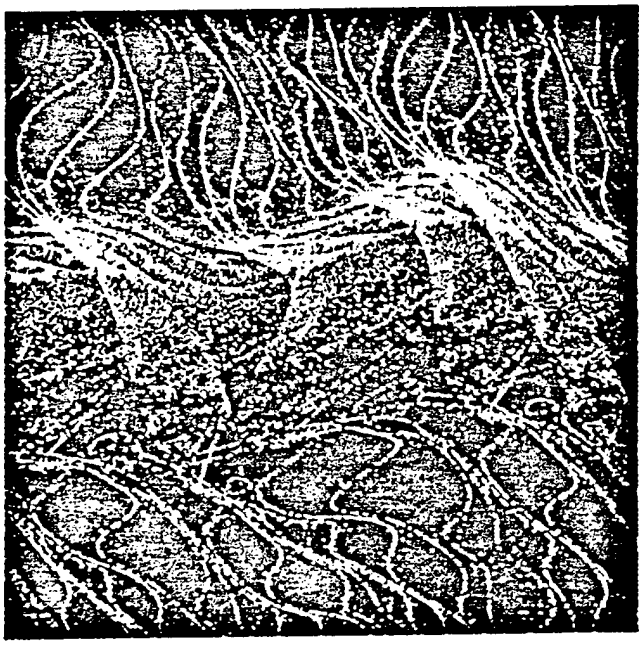

Fig. 20. Orbit of the map $F_{0.635}(1, a, b)(w_0, z_0)$ defined by Eq. (12). In this figure, the rotation factor is $\phi_1 = 2.5$, $\phi_2 = 0.1$. The dynamics are chaotic. Another example of transitioning between one-dimensional and two-dimensional dynamics.

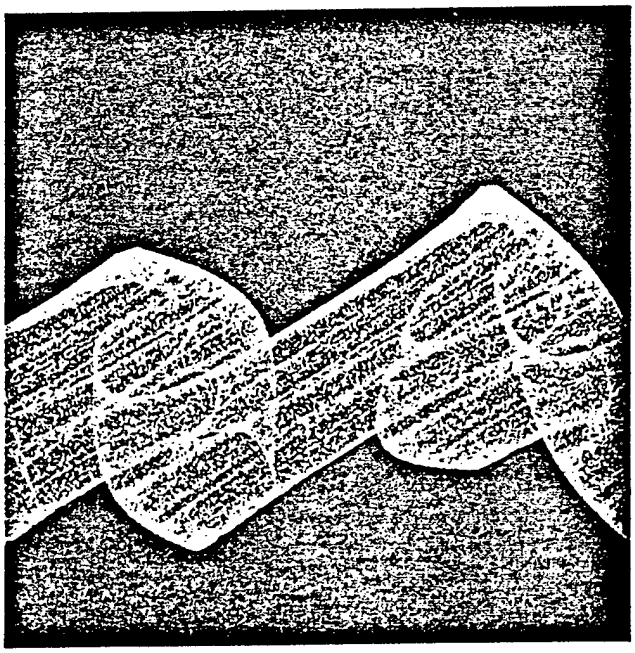

Fig. 21. Orbit of the map $F_{0.58}(1, a, b)(w_0, z_0)$ defined by Eq. (12). In this figure, the rotation factor is $\phi_1 = 2.6$, $\phi_2 = 0.0$. The dynamics are chaotic. This attractor is a small perturbation of Fig. 20 and has transitioned completely to two-dimensional dynamics.

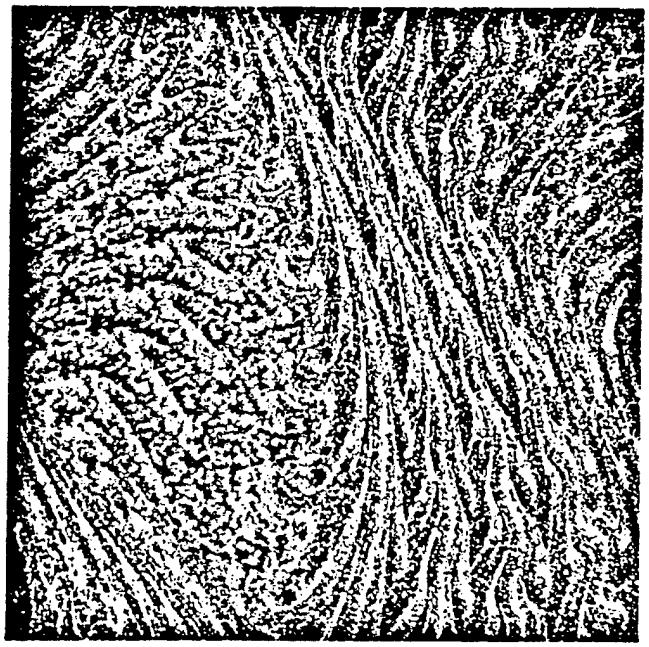

Fig. 22. Orbit of the map $F_{0.73}(1, a, b)(w_0, z_0)$ defined by Eq. (12). In this figure, the rotation factor is $\phi_1 = 0.5$, $\phi_2 = 5.5$. The dynamics are chaotic. The feathery texture of this attractor gives it the appearance of smoke.

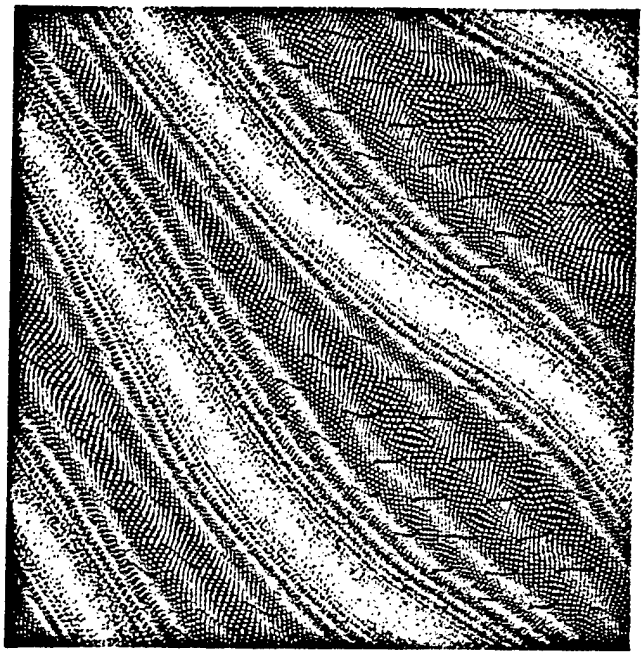

Fig. 23. Orbit of the map $F_{0.76}(1, a, b)(w_0, z_0)$ defined by Eq. (12). In this figure, the rotation factor is $\phi_1 = 0.7$, $\phi_2 = 2.5$. The dynamics are almost periodic. This attractor could also resemble some portions of a smoke trail.

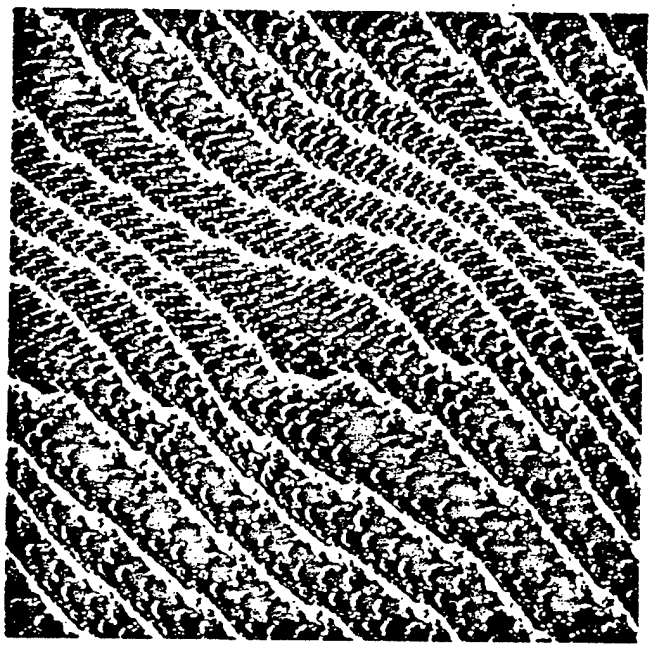

Fig. 24. Orbit of the map $F_{0.72}(1, a, b)(w_0, z_0)$ defined by Eq. (12). In this figure, the rotation factor is $\phi_1 = 0.0725$, $\phi_2 = 2.6$. The dynamics are uncertain. This attractor resembles the surface of a large body of water blown by a high wind as seen from above.

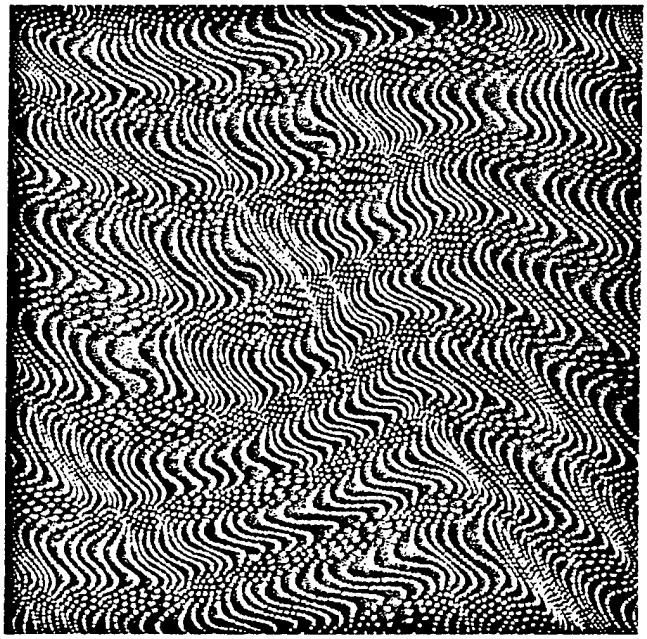

Fig. 25. Orbit of the map $F_{0.73}(1, a, b)(w_0, z_0)$ defined by Eq. (12). In this figure, the rotation factor is $\phi_1 = 1.0$, $\phi_2 = 0.9$. The dynamics are almost periodic. This attractor also resembles the surface of a large body of water blown by a high wind as seen from above.

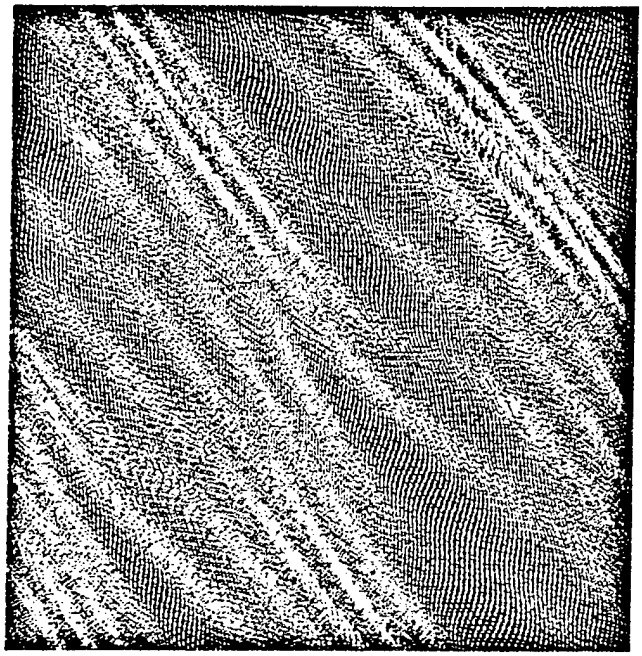

Fig. 26. Orbit of the map $F_{0.75}(1, a, b)(w_0, z_0)$ defined by Eq. (12). In this figure, the rotation factor is $\phi_1 = 2.6$, $\phi_2 = 0.9$. The dynamics are almost periodic. This attractor resembles the surface of a thick liquid or pliable solid such as taffy.

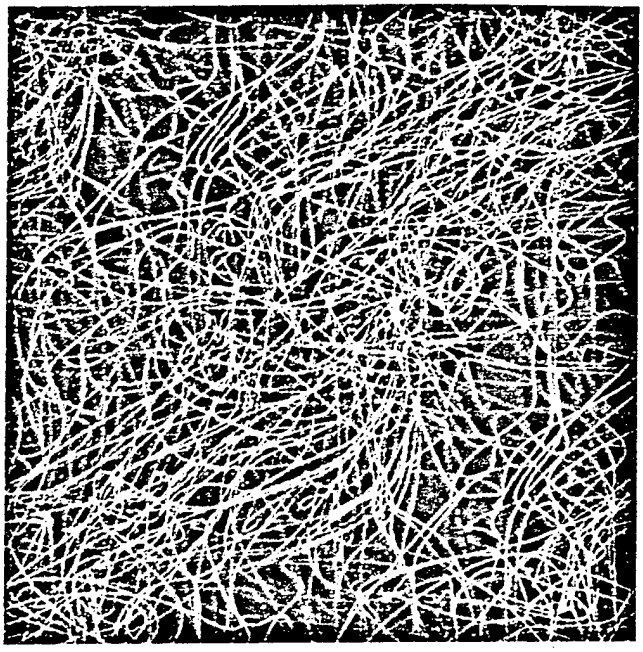

Fig. 27. Orbit of the map $F_{0.75}(1, a, b)(w_0, z_0)$ defined by Eq. (12) where $c = 0.999$. The dynamics are very nearly measure-preserving. In this figure, the rotation factor is $\phi_1 = 0.1$, $\phi_2 = 2.1$. The dynamics are uncertain. This attractor resembles a tangled ball of yarn.

The graph coordinates, $(x, y)$, are the argument of the first component of the complex vector $F_\lambda(1, a, b)(\Theta, \Psi)$, i.e., $\Theta$. The length of the $x$-axis and $y$-axis is 6.5. The orbits all lie in a square with sides of length $2\pi$.

## 4. Summary and Conclusions

The fundamental map describes an extraordinary range of two-dimensional dynamics. It is particularly useful in developing intuition into the evolution from almost-periodic dynamics to the highest end of chaotic dynamics, the Bernoulli maps. On each end of this dynamical spectrum analogous changes take place as we move toward the other end of the spectrum in that the orbit geometry first loses its uniformity. Further, as we proceed from almost-periodic dynamics toward Bernoulli the map becomes more nonlinear and this nonlinearity first appears as a change in the geometric appearance of the orbits. These changes can be used to better understand the transition into chaos and to discriminate between chaotic and non-chaotic processes. In particular, tests for randomness can be examined by the use of data generated by the fundamental map. The fundamental map may be useful in identifying the point of demarcation between chaos and order. Lastly, the fundamental map may be a simple model for how random and non-random processes combine to form complex and varied natural processes.

## Acknowledgments

The work of the first author was supported by ONR contract N00014-95-C-0153.

## References

Arnold, V. & Avez, A. [1989] *Ergodic Problems of Classical Mechanics* (Addison-Wesley, New York).

Beardon, A. [1991] *Iteration of Rational Functions* (Springer-Verlag, New York).

Brown, R. & Chua, L. [1993] "Dynamical synthesis of Poincaré maps," *Int. J. of Bifurcation and Chaos* **3**(5), 1235–1267.

Brown, R. & Chua, L. [1996] "Clarifying chaos: Examples and counterexamples," *Int. J. of Bifurcation and Chaos* **6**(2), 219–249.

Cornfeld, I., Fomin, S. & Sinai, Y. [1982] *Ergodic Theory* (Springer-Verlag, Berlin).

Katznelson, Y. [1976] *An Introduction to Harmonic Analysis* (Dover Publications, New York).

Lake, D. E. [1996], "Detecting regularity in minefields and chaotic signals using the empty box test," *Proceedings of the 8th IEEE Signal Processing Workshop on Statistical Signal and Array Processing* Corfu, Greece, June 24–26, 1996 (to appear).

Shil'nikov, L. [1994] "Chua's circuit: Rigorous results and future problems," *Int. J. of Bifurcation and Chaos* 4(3), 489–519.

Walters, P. [1982] *Introduction to Ergodic Theory* (Springer-Verlag, New York).

Wiggins, S. [1990] *Introduction to Applied Nonlinear Dynamical Systems and Chaos* (Springer-Verlag, New York).

Wiggins, S. [1992] *Chaotic Transport in Dynamical Systems* (Springer-Verlag, New York).

International Journal of Bifurcation and Chaos, Vol. 6, No. 5 (1996) 801–832
Theme Issue (Part 1)
© World Scientific Publishing Company

# ON THE GENERALITY OF THE UNFOLDED CHUA'S CIRCUIT

CHAI WAH WU and LEON O. CHUA
*Electronics Research Laboratory and*
*Department of Electrical Engineering and Computer Sciences,*
*University of California at Berkeley,*
*Berkeley, CA 94720, USA*

Received June 15, 1995; Revised October 10, 1995

In this paper, we study the generality of Chua's oscillator by deriving a class of vector fields that Chua's oscillator is equivalent to. For the class of vector fields with a *scalar* nonlinearity, we prove that under certain conditions, two such vector fields are *topologically conjugate* if the Jacobian matrices at each point have the same eigenvalues and the equilibrium points are matched up. We show how these conditions are related to the complete state observability of a corresponding linear system. These results are used to show that the $n$-dimensional Chua's oscillator is topologically conjugate to almost every vector field in this class. We comment on the special case when the vector field is piecewise-linear and in particular when the vector field is 2-segment piecewise-linear. These results are illustrated by transforming several systems studied in the literature into equivalent Chua's oscillators.

We also extend some of these results to the case of several scalar nonlinearities. As a corollary we prove that almost all piecewise-linear vector fields with parallel boundary planes are topologically conjugate if the boundary planes and equilibrium points are the same and the eigenvalues in corresponding regions are the same. We also give a dual result of topological conjugacy.

## 1. Introduction

It is known that the unfolded Chua's circuit, also known as Chua's oscillator [R. Madan, Guest Editor, 1993], with an odd-symmetric 3-segment piecewise-linear nonlinearity is *topologically conjugate* to almost all three-dimensional systems with a 3-segment odd-symmetric piecewise-linear continuous vector field [Chua, 1993; Shil'nikov, 1994]. The purpose of this paper is to extend this result to the case where the *nonlinearity* is no longer odd-symmetric or piecewise-linear but may be *any arbitrary continuous* function and the dimension of the system may also be arbitrary. We will do this in two steps. In the first step, we show that under certain conditions, nonlinear vector fields are topologically conjugate if the Jacobian matrices at each point have the same eigenvalues (Sec. 2). In the second step, we show that Chua's oscillator can synthesize almost any eigenvalue patterns of vector fields in our class (Sec. 3). These steps are combined in Sec. 4 to give the main result of this paper. Sections 5 and 6 are devoted to the special case of piecewise-linear vector fields. In Sec. 7 the results in Sec. 2 are extended to systems with several scalar nonlinearities. We show that almost all piecewise-linear vector fields with parallel boundary planes are determined, up to topological conjugacy, by the boundary planes, equilibrium points and the eigenvalues in each region. This generalizes previously known results on linear conjugacy of

piecewise-linear vector fields. Section 8 is devoted to a dual result of topological conjugacy.

We use lowercase, bold uppercase and bold lowercase letters for scalars (or scalar-valued functions), matrices and vectors, respectively. The transpose of a matrix $\mathbf{A}$ is denoted $\mathbf{A}^T$. The vector $\mathbf{0}$ denotes the zero vector and $\mathbf{e}_i$ denotes the $i$th unit vector, i.e., $\mathbf{e}_1 = (1, 0, \ldots, 0)^T$. Let $\chi(\mathbf{A}) = \det(\lambda\mathbf{I} - \mathbf{A})$ denote the characteristic polynomial of the matrix $\mathbf{A}$. The integer $n$ is usually used to denote the size of matrices and vectors.

## 2. Topological Conjugacy under Equivalence of Eigenvalues

We consider the following class of vector fields in *Lur'e* form:

**Definition 1.** The class $\mathcal{C}(\mathbf{w})$ consists of vector fields of the form:

$$\dot{\mathbf{x}} = \mathbf{A}\mathbf{x} + f(\mathbf{w}^T\mathbf{x})\mathbf{b} \tag{1}$$

where $\mathbf{A}$ is an $n \times n$ matrix, $\mathbf{w}$, $\mathbf{b}$ are $n \times 1$ vectors and $f(\cdot) : \mathbb{R} \to \mathbb{R}$ is a real-valued continuous function. The class $\mathcal{C}$ is defined as $\mathcal{C} = \bigcup_{\mathbf{w}} \mathcal{C}(\mathbf{w})$.

If $\mathbf{w} = \mathbf{0}$, $\mathcal{C}(\mathbf{w})$ reduces to the class of affine systems. When $\mathbf{w} \neq \mathbf{0}$, there exists a nonsingular matrix $\mathbf{M}$ such that $\mathbf{M}^T\mathbf{w} = \mathbf{e}_1$. Using the transformation $\mathbf{x} \to \mathbf{M}\mathbf{x}$, system (1) can be written as

$$\dot{\mathbf{x}} = \mathbf{A}\mathbf{x} + f(\mathbf{e}_1^T\mathbf{x})\mathbf{b} \tag{2}$$

where $\mathbf{A} \to \mathbf{M}^{-1}\mathbf{A}\mathbf{M}$ and $\mathbf{b} \to \mathbf{M}^{-1}\mathbf{b}$. Thus for $\mathbf{w} \neq 0$, vector fields in $\mathcal{C}(\mathbf{w})$ are topologically conjugate to vector fields in $\mathcal{C}(\mathbf{e}_1)$.

Vector fields in class $\mathcal{C}(\mathbf{w})$ can be considered to be nonlinear vector fields where the nonlinearity occurs only in the direction $\mathbf{w}$ and the changes in the Jacobian matrix are of a fixed form. In this paper, we will mainly be working with vector fields in class $\mathcal{C}$. By translating an equilibrium point to the origin, a seemingly larger class of vector fields can be shown to be reducible to class $\mathcal{C}$.

**Definition 2.** A point $\mathbf{x}^*$ is a virtual equilibrium point of the system $\dot{\mathbf{x}} = \mathbf{f}(\mathbf{x})$ if

- $\mathbf{x}^*$ is not an equilibrium point of the system; i.e., $\mathbf{f}(\mathbf{x}^*) \neq \mathbf{0}$.
- There exists a point $\hat{\mathbf{x}}$ where the Jacobian matrix exists and such that $\mathbf{x}^*$ is an equilibrium point of the system linearized at point $\hat{\mathbf{x}}$; i.e., $\hat{\mathbf{A}}\mathbf{x} + \hat{\mathbf{b}}$ is the linearized vector field at $\hat{\mathbf{x}}$ and $\hat{\mathbf{A}}\mathbf{x}^* + \hat{\mathbf{b}} = \mathbf{0}$, where $\hat{\mathbf{A}} = D\mathbf{f}(\mathbf{x})|_{\mathbf{x}=\hat{\mathbf{x}}}$ and $\hat{\mathbf{b}} = \mathbf{f}(\hat{\mathbf{x}}) - \hat{\mathbf{A}}\hat{\mathbf{x}}$.

The property of a system possessing a (real or virtual) equilibrium point is generic; a real or virtual equilibrium point exists whenever the Jacobian matrix at some point is nonsingular. In general, there are uncountably many equilibrium points in a system. For example, consider the simple first order circuit shown in Fig. 1(a). The virtual equilibrium points are found by linearizing the nonlinear resistor around some point and finding the intersection with the $v$-axis which corresponds to the equilibrium point of the linearized circuit. Some of the equilibrium points of this circuit are shown in Fig. 1(b), where the blue curve is the $v$-$i$ characteristic of the nonlinear resistor. The red tangent lines correspond to the affine $v$-$i$ characteristics of the resistor in the linearized circuit.

**Definition 3.** The class $\mathcal{C}'(\mathbf{w})$ consists of vector fields of the form:

$$\dot{\mathbf{x}} = \mathbf{A}\mathbf{x} + h(\mathbf{w}^T\mathbf{x})\mathbf{b} + \mathbf{c} \tag{3}$$

where $h(\cdot)$ is a continuous real-valued function such that the system has at least one equilibrium point which can be real or virtual. We define $\mathcal{C}' = \bigcup_{\mathbf{w}} \mathcal{C}'(\mathbf{w})$.

**Lemma 1.** *The vector fields in class $\mathcal{C}'$ is equivalent to a subset of the vector fields in class $\mathcal{C}$ in the sense that after a change of coordinates, Eq. (3) can be written as Eq. (1).*

*Proof.* Let $\mathbf{x}^*$ be an equilibrium point (which can be real or virtual) of system (3). $\mathbf{x}^*$ being an equilibrium point means that there exists a real number $d$ such that $\mathbf{A}\mathbf{x}^* + d\mathbf{b} + \mathbf{c} = \mathbf{0}$. Let $\mathbf{y} = \mathbf{x} - \mathbf{x}^*$. Then

$$\begin{aligned}\dot{\mathbf{y}} = \dot{\mathbf{x}} &= \mathbf{A}\mathbf{y} + \mathbf{A}\mathbf{x}^* + h(\mathbf{w}^T(\mathbf{y} + \mathbf{x}^*))\mathbf{b} + \mathbf{c} \\ &= \mathbf{A}\mathbf{y} + f(\mathbf{w}^T\mathbf{y})\mathbf{b}\end{aligned}$$

where $f(\mathbf{w}^T\mathbf{y}) = h(\mathbf{w}^T\mathbf{y} + \mathbf{w}^T\mathbf{x}^*) - d$. ■

Lemma 1 says that we can translate one of the equilibrium points to the origin, thereby obtaining a simpler form and reducing class $\mathcal{C}'$ to class $\mathcal{C}$.

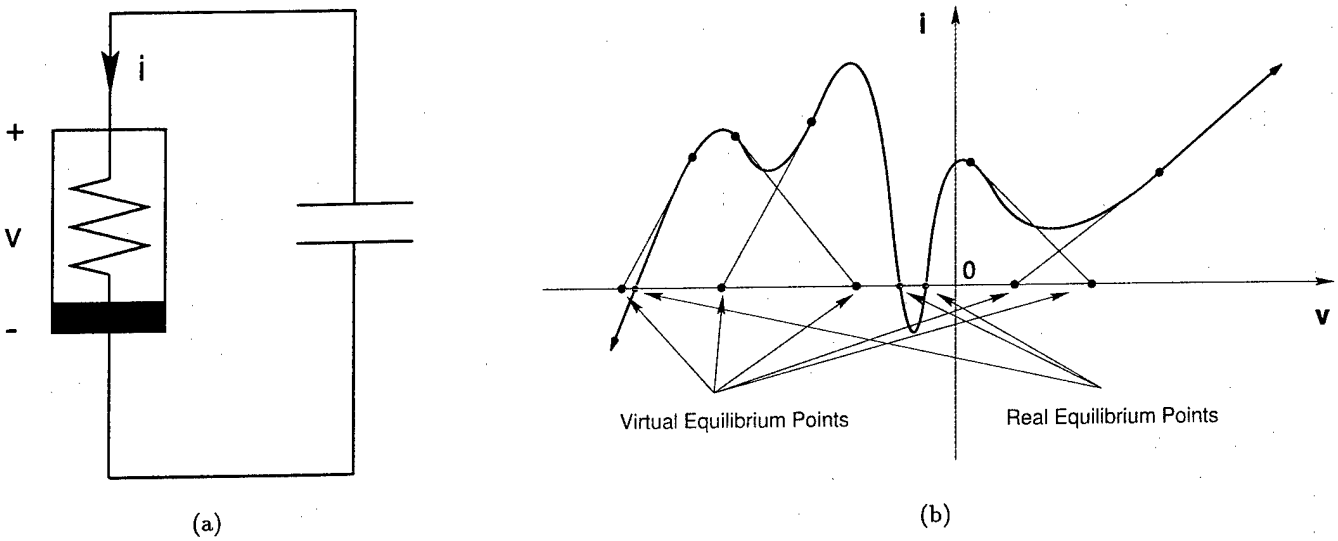


(a) (b)

Fig. 1. (a) First order nonlinear circuit consisting of a linear capacitor and a nonlinear resistor. (b) Some equilibrium points of the circuit in (a). The blue curve indicates the $v$-$i$ characteristic of the nonlinear resistor. The red tangent lines correspond to the affine $v$-$i$ characteristics of the resistor in the linearized circuit.

**Definition 4.** The pair $(\mathbf{A}, \mathbf{w})$ satisfies condition $K$ if the matrix

$$\mathbf{K} = \mathbf{K}(\mathbf{A}, \mathbf{w}) = \begin{pmatrix} \mathbf{w}^T \\ \mathbf{w}^T\mathbf{A} \\ \mathbf{w}^T\mathbf{A}^2 \\ \vdots \\ \mathbf{w}^T\mathbf{A}^{n-1} \end{pmatrix} \tag{4}$$

is nonsingular, where $\mathbf{A}$ is an $n \times n$ matrix and $\mathbf{w}$ is an $n \times 1$ vector.

Note that $\mathbf{w}^T[\mathbf{K}(\mathbf{A}, \mathbf{w})]^{-1} = \mathbf{e}_1^T$ when $\mathbf{K}(\mathbf{A}, \mathbf{w})$ is invertible. Also note that if $(\mathbf{A}, \mathbf{w})$ satisfy condition $K$, then $\mathbf{w} \neq \mathbf{0}$. The set of $(\mathbf{A}, \mathbf{w})$ which satisfy condition $K$ is of full measure. One of the consequences of $(\mathbf{A}, \mathbf{w})$ satisfying condition $K$ is that $\mathbf{A}$ is similar to a matrix in companion form.

**Lemma 2.** *If $(\mathbf{A}, \mathbf{w})$ satisfies condition $K$, then*

$$\mathbf{KAK}^{-1} = \begin{pmatrix} 0 & 1 & 0 & \\ 0 & 0 & 1 & \ddots \\ & & \ddots & \ddots \\ -r_0 & -r_1 & \cdots & -r_{n-1} \end{pmatrix} \triangleq \hat{\mathbf{A}} \tag{5}$$

*where $\chi(\mathbf{A}) = \lambda^n + r_{n-1}\lambda^{n-1} + \cdots + r_1\lambda + r_0$ and $\mathbf{K} = \mathbf{K}(\mathbf{A}, \mathbf{w})$ is as defined in Eq. (4).*

*Proof.* By the Cayley–Hamilton theorem, we have

$$\mathbf{KA} = \begin{pmatrix} \mathbf{w}^T\mathbf{A} \\ \mathbf{w}^T\mathbf{A}^2 \\ \mathbf{w}^T\mathbf{A}^3 \\ \vdots \\ \mathbf{w}^T\mathbf{A}^n \end{pmatrix} = \begin{pmatrix} \mathbf{w}^T\mathbf{A} \\ \mathbf{w}^T\mathbf{A}^2 \\ \mathbf{w}^T\mathbf{A}^3 \\ \vdots \\ \mathbf{w}^T(-r_{n-1}\mathbf{A}^{n-1} - \cdots - r_1\mathbf{A} - r_0\mathbf{I}) \end{pmatrix}$$

$$= \begin{pmatrix} 0 & 1 & 0 & \\ 0 & 0 & 1 & \ddots \\ & & \ddots & \ddots \\ -r_0 & -r_1 & \cdots & -r_{n-1} \end{pmatrix} \mathbf{K}. \quad \blacksquare$$

Note that any companion matrix in form (5) together with $\mathbf{e}_1$ satisfies condition $K$.

**Lemma 3.** *If $\mathbf{M}$ is nonsingular, then $\mathbf{K}(\mathbf{A}, \mathbf{w})\mathbf{M} = \mathbf{K}(\mathbf{M}^{-1}\mathbf{AM}, \mathbf{M}^T\mathbf{w})$. In particular, for all nonsingular $\mathbf{M}$,*

$(\mathbf{A}, \mathbf{w})$ satisfies condition $K$

$\iff (\mathbf{M}^{-1}\mathbf{AM}, \mathbf{M}^T\mathbf{w})$ satisfies condition $K$

*Proof*

$$\mathbf{K}(\mathbf{A}, \mathbf{w})\mathbf{M} = \begin{pmatrix} \mathbf{w}^T \\ \mathbf{w}^T\mathbf{A} \\ \mathbf{w}^T\mathbf{A}^2 \\ \vdots \\ \mathbf{w}^T\mathbf{A}^{n-1} \end{pmatrix} \mathbf{M} = \begin{pmatrix} \mathbf{w}^T\mathbf{M} \\ \mathbf{w}^T\mathbf{M}\mathbf{M}^{-1}\mathbf{AM} \\ \mathbf{w}^T\mathbf{M}\mathbf{M}^{-1}\mathbf{A}^2\mathbf{M} \\ \vdots \\ \mathbf{w}^T\mathbf{M}\mathbf{M}^{-1}\mathbf{A}^{n-1}\mathbf{M} \end{pmatrix}$$

$$= \mathbf{K}(\mathbf{M}^{-1}\mathbf{AM}, \mathbf{M}^T\mathbf{w})$$

Since $\mathbf{M}$ is nonsingular, the second part of the lemma follows. ■

**Lemma 4.** *For all matrices* $\mathbf{A}$ *and all vectors* $\mathbf{b}$, $\mathbf{w}$

$(\mathbf{A}, \mathbf{w})$ satisfies condition $K$

$$\Longleftrightarrow (\mathbf{A} + \mathbf{b}\mathbf{w}^T, \mathbf{w}) \text{ satisfies condition } K$$

*Proof.* The case $\mathbf{w} = \mathbf{0}$ is trivially true. Let $\mathbf{K} = \mathbf{K}(\mathbf{A}, \mathbf{w})$ be defined as in (4). First note that $\mathbf{w}^T = \mathbf{e}_1^T\mathbf{K}$. We claim that $\mathbf{w}^T(\mathbf{A} + \mathbf{b}\mathbf{w}^T)^i$ can be written as $\mathbf{c}_i^T\mathbf{K}$ for some vector $\mathbf{c}_i$. Thus $\mathbf{c}_0 = \mathbf{e}_1$.

$$\begin{aligned}\mathbf{w}^T(\mathbf{A} + \mathbf{b}\mathbf{w}^T)^{i+1} &= \mathbf{c}_i^T\mathbf{K}(\mathbf{A} + \mathbf{b}\mathbf{w}^T)\\ &= \mathbf{c}_i^T\hat{\mathbf{A}}\mathbf{K} + \mathbf{c}_i^T\mathbf{K}\mathbf{b}\mathbf{e}_1^T\mathbf{K}\\ &= \mathbf{c}_i^T(\hat{\mathbf{A}} + \mathbf{K}\mathbf{b}\mathbf{e}_1^T)\mathbf{K}\end{aligned}$$

Thus $\mathbf{c}_{i+1}^T = \mathbf{c}_i^T(\hat{\mathbf{A}} + \mathbf{K}\mathbf{b}\mathbf{e}_1^T)$. Since $\mathbf{c}_0 = (1, 0, \ldots)^T$ and $\mathbf{c}_1 = (\mathbf{e}_1^T\mathbf{K}\mathbf{b}, 1, 0, \ldots)^T$, etc, it is clear that the matrix

$$\begin{pmatrix} \mathbf{c}_0^T \\ \mathbf{c}_1^T \\ \vdots \\ \mathbf{c}_{n-1}^T \end{pmatrix}$$

is lower triangular with 1's on the diagonal, i.e. it is nonsingular.

Since

$$\begin{pmatrix} \mathbf{w}^T \\ \mathbf{w}^T(\mathbf{A} + \mathbf{b}\mathbf{w}^T) \\ \mathbf{w}^T(\mathbf{A} + \mathbf{b}\mathbf{w}^T)^2 \\ \vdots \\ \mathbf{w}^T(\mathbf{A} + \mathbf{b}\mathbf{w}^T)^{n-1} \end{pmatrix} = \begin{pmatrix} \mathbf{c}_0^T \\ \mathbf{c}_1^T \\ \vdots \\ \mathbf{c}_{n-1}^T \end{pmatrix} \mathbf{K}$$

the result follows. ■

**Lemma 5.** *Let* $\mathbf{A}$ *and* $\tilde{\mathbf{A}}$ *be matrices, and* $\mathbf{b}$, $\tilde{\mathbf{b}}$ *and* $\mathbf{w}$ *be vectors. For each real number* $\delta$, *define* $\mathbf{A}_\delta$ *and* $\tilde{\mathbf{A}}_\delta$ *as follows:*

$$\mathbf{A}_\delta = \mathbf{A} + \delta\mathbf{b}\mathbf{w}^T, \quad \tilde{\mathbf{A}}_\delta = \tilde{\mathbf{A}} + \delta\tilde{\mathbf{b}}\mathbf{w}^T$$

*Then* $\mathbf{A}_\delta$ *has the same eigenvalues as* $\tilde{\mathbf{A}}_\delta$ *for all* $\delta$ *if and only if* $\mathbf{A}_{\delta_1}$ *and* $\tilde{\mathbf{A}}_{\delta_1}$ *have the same eigenvalues and* $\mathbf{A}_{\delta_2}$ *and* $\tilde{\mathbf{A}}_{\delta_2}$ *have the same eigenvalues for some* $\delta_1 \neq \delta_2$.

*Proof.* One direction is clear. Without loss of generality we can assume that $\mathbf{w} = \mathbf{e}_1$. Let $b_i$ and $\tilde{b}_i$ denote the $i$th entry of $\mathbf{b}$ and $\tilde{\mathbf{b}}$, respectively and let $a_{ij}$ and $\tilde{a}_{ij}$ denote the $(i, j)$th entry of $\mathbf{A}$ and $\tilde{\mathbf{A}}$, respectively. Expanding along the first column, $\chi(\mathbf{A})$, $\chi(\tilde{\mathbf{A}})$, $\chi(\mathbf{A}_\delta)$, $\chi(\tilde{\mathbf{A}}_\delta)$ can be written as:

$$\chi(\mathbf{A}) = (\lambda - a_{11})p_1(\lambda) - a_{21}p_2(\lambda) - \cdots - a_{n1}p_n(\lambda)$$

$$\chi(\tilde{\mathbf{A}}) = (\lambda - \tilde{a}_{11})\tilde{p}_1(\lambda) - \tilde{a}_{21}\tilde{p}_2(\lambda) - \cdots - \tilde{a}_{n1}\tilde{p}_n(\lambda)$$

$$\chi(\mathbf{A}_\delta) = \chi(\mathbf{A}) - \delta b_1 p_1(\lambda) - \delta b_2 p_2(\lambda) - \cdots - \delta b_n p_n(\lambda)$$

$$\chi(\tilde{\mathbf{A}}_\delta) = \chi(\tilde{\mathbf{A}}) - \delta\tilde{b}_1\tilde{p}_1(\lambda) - \delta\tilde{b}_2\tilde{p}_2(\lambda) - \cdots - \delta\tilde{b}_n\tilde{p}_n(\lambda)$$

for some polynomials $p_i$ and $\tilde{p}_i$.

By the assumption $\chi(\mathbf{A}_{\delta_1}) - \chi(\mathbf{A}_{\delta_2}) = \chi(\tilde{\mathbf{A}}_{\delta_1}) - \chi(\tilde{\mathbf{A}}_{\delta_2})$, i.e.,

$$\begin{aligned}&(\delta_2 - \delta_1)(b_1p_1(\lambda) + b_2p_2(\lambda) + \cdots + b_np_n(\lambda))\\ &\quad = (\delta_2 - \delta_1)(\tilde{b}_1\tilde{p}_1(\lambda) + \tilde{b}_2\tilde{p}_2(\lambda) + \cdots + \tilde{b}_n\tilde{p}_n(\lambda))\end{aligned} \tag{6}$$

Since $\delta_2 - \delta_1 \neq 0$, we can multiply both sides of Eq. (6) by $\frac{\delta - \delta_1}{\delta_1 - \delta_2}$, add $\chi(\mathbf{A}_{\delta_1})$ to the left side, and add $\chi(\tilde{\mathbf{A}}_{\delta_1})$ to the right side to get $\chi(\mathbf{A}_\delta) = \chi(\tilde{\mathbf{A}}_\delta)$. ■

**Lemma 6.** *Let* $\mathbf{b}$ *be a vector and let* $(\mathbf{A}, \mathbf{w})$ *satisfy condition* $K$. *Then* $\mathbf{K}\mathbf{b}$ *is uniquely determined by the eigenvalues of* $\mathbf{A}$ *and* $\mathbf{A} + \mathbf{b}\mathbf{w}^T$, *where* $\mathbf{K} = \mathbf{K}(\mathbf{A}, \mathbf{w})$ *is defined in Eq.* (4). *Furthermore,* $\mathbf{b}$ *is uniquely determined by* $\mathbf{A}$, $\mathbf{w}$ *and the eigenvalues of* $\mathbf{A} + \mathbf{b}\mathbf{w}^T$.

*Proof.* Write the characteristic polynomials of $\mathbf{A}$ and $\mathbf{A} + \mathbf{b}\mathbf{w}^T$ as:

$$\begin{aligned}\chi(\mathbf{A}) &= \lambda^n + r_{n-1}\lambda^{n-1} + \cdots + r_1\lambda + r_0\\ \chi(\mathbf{A} + \mathbf{b}\mathbf{w}^T) &= \lambda^n + s_{n-1}\lambda^{n-1} + \cdots + s_1\lambda + s_0\end{aligned} \tag{7}$$

Let $\mathbf{K}\mathbf{b} = (\tilde{b}_1, \tilde{b}_2, \ldots, \tilde{b}_n)^T$. Then $\mathbf{K}\mathbf{A}\mathbf{K}^{-1}$ is in companion form by Lemma 2 and

$$\begin{aligned}\mathbf{K}(\mathbf{A} + \mathbf{b}\mathbf{w}^T)\mathbf{K}^{-1} &= \mathbf{K}\mathbf{A}\mathbf{K}^{-1} + \mathbf{K}\mathbf{b}\mathbf{e}_1^T\\ &= \begin{pmatrix} \tilde{b}_1 & 1 & 0 & \\ \tilde{b}_2 & 0 & 1 & \ddots \\ \vdots & & \ddots & \ddots \\ \tilde{b}_n - r_0 & -r_1 & \cdots & -r_{n-1} \end{pmatrix}\end{aligned} \tag{8}$$

By expanding along the first column, we see that the characteristic polynomial of $\mathbf{K}(\mathbf{A} + \mathbf{b}\mathbf{w}^T)\mathbf{K}^{-1}$ is:

$$\chi(\mathbf{K}(\mathbf{A}+\mathbf{b}\mathbf{w}^T)\mathbf{K}^{-1}) = \chi(\mathbf{K}\mathbf{A}\mathbf{K}^{-1}) - \tilde{b}_1(\lambda^{n-1}+r_{n-1}\lambda^{n-2}+\cdots+r_1) - \tilde{b}_2(\lambda^{n-2}+r_{n-1}\lambda^{n-3}+\cdots+r_2) - \cdots - \tilde{b}_{n-1}(\lambda+r_{n-1}) - \tilde{b}_n \quad (9)$$

which is equal to $\chi(\mathbf{A}+\mathbf{b}\mathbf{w}^T)$. Comparing Eq. (7) with Eq. (9) the following set of equations is obtained:

$$\begin{pmatrix} 1 & 0 & & 0 \\ r_{n-1} & 1 & \ddots & \\ r_{n-2} & r_{n-1} & \ddots & 0 \\ r_1 & r_2 & \cdots & 1 \end{pmatrix} \begin{pmatrix} \tilde{b}_1 \\ \tilde{b}_2 \\ \vdots \\ \tilde{b}_n \end{pmatrix} = \begin{pmatrix} r_{n-1}-s_{n-1} \\ r_{n-2}-s_{n-2} \\ \vdots \\ r_0-s_0 \end{pmatrix} \quad (10)$$

So $\mathbf{b}$ is determined by $\mathbf{K}\mathbf{b}$ which in turn is uniquely determined by $r_i$ and $s_i$ which is determined by the eigenvalues of $\mathbf{A}$ and $\mathbf{A}+\mathbf{b}\mathbf{w}^T$. ■

**Corollary 1.** *Let* $\mathbf{A}$ *be a matrix and* $\mathbf{w}$, $\mathbf{b}_1$ *and* $\mathbf{b}_2$ *be vectors. Suppose that* $(\mathbf{A}, \mathbf{w})$ *satisfies condition* $K$. *The matrices* $\mathbf{A}+\mathbf{b}_1\mathbf{w}^T$ *and* $\mathbf{A}+\mathbf{b}_2\mathbf{w}^T$ *have the same eigenvalues if and only if* $\mathbf{b}_1 = \mathbf{b}_2$.

*Proof.* One direction is clear. Now let $\mathbf{A}' = \mathbf{A}+\mathbf{b}_1\mathbf{w}^T$. Then $\mathbf{A}+\mathbf{b}_2\mathbf{w}^T = \mathbf{A}'+(\mathbf{b}_2-\mathbf{b}_1)\mathbf{w}^T$. Lemma 4 implies that $(\mathbf{A}', \mathbf{w})$ satisfies condition $K$. Applying Eq. (10) in Lemma 6 to $\mathbf{A}'$ and $\mathbf{A}'+(\mathbf{b}_2-\mathbf{b}_1)\mathbf{w}^T$ for the case where $r_i = s_i$ we see that $\mathbf{b}_2-\mathbf{b}_1 = \mathbf{0}$. ■

The following theorem gives some concepts which are equivalent to condition $K$.

**Theorem 1.** *Let* $\mathbf{A}$ *be a matrix and* $\mathbf{w}$, $\mathbf{b}_1$ *and* $\mathbf{b}_2$ *be vectors. The following statements are equivalent:*

(1) *The linear system*

$$\dot{\mathbf{x}} = \mathbf{A}\mathbf{x} \qquad y = \mathbf{w}^T\mathbf{x} \quad (11)$$

*is completely state observable.*[1]

(2) *The pair* $(\mathbf{A}, \mathbf{w})$ *satisfies condition* $K$.

(3) *No nontrivial subspace, which is invariant under* $\mathbf{A}$, *is orthogonal to* $\mathbf{w}$.

(4) *The matrices* $\mathbf{A}+\mathbf{b}_1\mathbf{w}^T$ *and* $\mathbf{A}+\mathbf{b}_2\mathbf{w}^T$ *have the same eigenvalues if and only if* $\mathbf{b}_1 = \mathbf{b}_2$.

*Proof.* The equivalence between the first two statements is a standard result in linear system theory [Chen, 1984]. The equivalence between statements 2 and 3 follows from the fact that $\mathbf{K}\mathbf{b} = \mathbf{0}$ if and only if $\mathbf{w}^T\mathbf{A}^i\mathbf{b} = 0$ for all nonnegative integers $i$. From Corollary 1 statement 2 implies statement 4. Suppose that $(\mathbf{A}, \mathbf{w})$ does not satisfy condition $K$. Without loss of generality we can assume $\mathbf{w} \neq \mathbf{0}$. Let $\mathbf{b} \neq \mathbf{0}$ be in the kernel of $\mathbf{K}(\mathbf{A}, \mathbf{w})$. This implies that $\mathbf{w}^T\mathbf{A}^i\mathbf{b} = 0$ for all nonnegative integers $i$. Now let $\lambda > |\mathbf{A}|$ be a real number and $\mathbf{M}^T\mathbf{w} = \mathbf{e}_1$ for $\mathbf{M}$ nonsingular. Since $\lambda$ is not in the spectrum of $\mathbf{A}$, the matrix $\lambda\mathbf{I}-\mathbf{A}$ is invertible. Then $(\lambda\mathbf{I}-\mathbf{A}-\mathbf{b}\mathbf{w}^T) = (\lambda\mathbf{I}-\mathbf{A})(\mathbf{I}-(\lambda\mathbf{I}-\mathbf{A})^{-1}\mathbf{b}\mathbf{w}^T)$. By expanding $(\lambda\mathbf{I}-\mathbf{A})^{-1}$ as a power series, we see that $\mathbf{w}^T(\lambda\mathbf{I}-\mathbf{A})^{-1}\mathbf{b} = \mathbf{e}_1^T\mathbf{M}^{-1}(\lambda\mathbf{I}-\mathbf{A})^{-1}\mathbf{b} = 0$, i.e., the first element of the vector $\mathbf{M}^{-1}(\lambda\mathbf{I}-\mathbf{A})^{-1}\mathbf{b}$ is 0. Therefore the first row and all columns except the first column of $\mathbf{M}^{-1}(\lambda\mathbf{I}-\mathbf{A})^{-1}\mathbf{b}\mathbf{e}_1^T$ consists of zero entries and thus $\det(\mathbf{I}-(\lambda\mathbf{I}-\mathbf{A})^{-1}\mathbf{b}\mathbf{w}^T) = \det(\mathbf{I}-\mathbf{M}^{-1}(\lambda\mathbf{I}-\mathbf{A})^{-1}\mathbf{b}\mathbf{e}_1^T) = 1$. Thus the characteristic polynomials of $\mathbf{A}$ and $\mathbf{A}+\mathbf{b}\mathbf{w}^T$ agree for all $\lambda > |\mathbf{A}|$. This implies that these polynomials are equal and thus $\mathbf{A}$ and $\mathbf{A}+\mathbf{b}\mathbf{w}^T$ have the same eigenvalues. This means that statement 4 is not satisfied. ■

*Remark 1.* In studying the absolute stability problem (or Lur'e problem) of a system in form (1), it is sometimes assumed that the linear system (11) is observable [Vidyasagar, 1978], and thus $(\mathbf{A}, \mathbf{w})$ satisfies condition $K$.

*Remark 2.* Piecewise-linear systems where the Jacobian $\mathbf{A}$ and the normal vectors to the boundary planes $\mathbf{w}$ satisfy statement 3 in the above theorem are called *proper* in Komuro [1988]. In light of Theorem 1, this coincides with the following definition of "proper":

**Definition 5.** A vector field in $\mathcal{C}$ written in the form (1) is called *proper* if $(\mathbf{A}, \mathbf{w})$ satisfy condition $K$.

*Remark 3.* Proper vector fields form a set of full measure in $\mathcal{C}$. Lemma 4 implies that Definition 5

[1] A (time-invariant) linear system

$$\dot{\mathbf{x}} = \mathbf{A}\mathbf{x} \qquad \mathbf{y} = \mathbf{C}\mathbf{x}$$

is said to be completely state observable if there exists a time $t > 0$ such that for any initial state $\mathbf{x}_0$ at time 0, the knowledge of the output $\mathbf{y}$ over the time interval $[0, t]$ suffices to determine $\mathbf{x}_0$ [Chen, 1984].

is well-defined for a vector field in $\mathcal{C}$. Furthermore, the matrix $\mathbf{A}$ in the definition can be replaced by the Jacobian matrix at any point.

*Remark 4.* Statement 4 in Theorem 1 provides a characterization for state observability of single-input single-output (SISO) systems. It says that an SISO system

$$\begin{aligned} \dot{\mathbf{x}} &= \mathbf{A}\mathbf{x} + \mathbf{b}u \\ y &= \mathbf{w}^T\mathbf{x} \end{aligned} \tag{12}$$

is state observable if and only if for all $\mathbf{b} \neq \mathbf{0}$, constant gain output feedback (i.e., $u = y$) moves the poles of the system.

Consider a linear system of the form $\dot{\mathbf{x}} = \mathbf{A}\mathbf{x}$. Two such linear systems are *linearly conjugate*, i.e. topologically conjugate via an affine mapping, if the Jacobian matrices are similar, i.e. have the same Jordan form matrix. If we restrict ourselves to matrices which are similar to a matrix in companion form, then all Jordan blocks must be of maximum order, and the eigenvalues uniquely determine the Jordan form matrix up to permutation. Thus if we assume that the Jacobian matrices are similar to some matrix in companion form, then two linear systems are linearly conjugate if the eigenvalues are the same. Lemma 2 says that matrices $\mathbf{A}$ which satisfy condition $K$ with some $\mathbf{w}$ are examples of such matrices. This result of topological conjugacy by matching of eigenvalues is generalized in the next theorem which is the main theorem in this section. It is a generalization of the global unfolding theorem in Chua [1993] and gives conditions under which vector fields in $\mathcal{C}$ are topologically conjugate whenever the eigenvalues of the Jacobian matrices are matched up at every point.

**Theorem 2.** *Consider the systems*

$$\dot{\mathbf{x}} = \mathbf{A}\mathbf{x} + f(\mathbf{w}^T\mathbf{x})\mathbf{b} \tag{13}$$

*and*

$$\dot{\tilde{\mathbf{x}}} = \tilde{\mathbf{A}}\tilde{\mathbf{x}} + f(\tilde{\mathbf{w}}^T\tilde{\mathbf{x}})\tilde{\mathbf{b}} \tag{14}$$

*Assume that both systems are proper. Then system (13) and system (14) are topologically conjugate if the eigenvalues of* $\mathbf{A}$ *and* $\tilde{\mathbf{A}}$ *are the same and the eigenvalues of* $\mathbf{A}+\mathbf{b}\mathbf{w}^T$ *and* $\tilde{\mathbf{A}}+\tilde{\mathbf{b}}\tilde{\mathbf{w}}^T$ *are the same.*

*Proof.* The proof follows the same steps as in Chua [1993]. By hypothesis, the matrices $\mathbf{K} = \mathbf{K}(\mathbf{A}, \mathbf{w})$ and $\tilde{\mathbf{K}} = \mathbf{K}(\tilde{\mathbf{A}}, \tilde{\mathbf{w}})$ are nonsingular. Note that $\mathbf{w}^T\mathbf{K}^{-1} = \tilde{\mathbf{w}}^T\tilde{\mathbf{K}}^{-1} = \mathbf{e}_1^T$. Let us denote

$$\begin{aligned} \chi(\mathbf{A}) &= \chi(\tilde{\mathbf{A}}) = \lambda^n + r_{n-1}\lambda^{n-1} + \cdots + r_1\lambda + r_0 \\ \chi(\mathbf{A}+\mathbf{b}\mathbf{w}^T) &= \chi(\tilde{\mathbf{A}}+\tilde{\mathbf{b}}\tilde{\mathbf{w}}^T) \\ &= \lambda^n + s_{n-1}\lambda^{n-1} + \cdots + s_1\lambda + s_0 \end{aligned} \tag{15}$$

Using the transformation $\mathbf{y} = \mathbf{K}\mathbf{x}$, we obtain a system of the form:

$$\begin{aligned} \dot{\mathbf{y}} &= \mathbf{K}\mathbf{A}\mathbf{K}^{-1}\mathbf{y} + f(\mathbf{w}^T\mathbf{K}^{-1}\mathbf{y})\mathbf{K}\mathbf{b} \\ &= \hat{\mathbf{A}}\mathbf{y} + f(\mathbf{e}_1^T\mathbf{y})\mathbf{K}\mathbf{b} \end{aligned}$$

where $\hat{\mathbf{A}}$ is defined in Eq. (5).

Similarly using $\tilde{\mathbf{y}} = \tilde{\mathbf{K}}\tilde{\mathbf{x}}$, we get

$$\begin{aligned} \dot{\tilde{\mathbf{y}}} &= \tilde{\mathbf{K}}\tilde{\mathbf{A}}\tilde{\mathbf{K}}^{-1}\tilde{\mathbf{y}} + f(\tilde{\mathbf{w}}^T\tilde{\mathbf{K}}^{-1}\tilde{\mathbf{y}})\tilde{\mathbf{K}}\tilde{\mathbf{b}} \\ &= \hat{\mathbf{A}}\tilde{\mathbf{y}} + f(\mathbf{e}_1^T\tilde{\mathbf{y}})\tilde{\mathbf{K}}\tilde{\mathbf{b}} \end{aligned}$$

By Lemma 6, the vectors $\mathbf{K}\mathbf{b}$ and $\tilde{\mathbf{K}}\tilde{\mathbf{b}}$ are uniquely determined by the coefficients $r_i$ and $s_i$ and are thus equal to each other. Thus the two systems above are identical, which means that systems (13) and (14) are topologically conjugate. ■

*Remark 5.* By Lemma 5, for differentiable $f$, e.g., the *smooth* version of Chua's equation [Huang *et al.*, 1996], the condition that the eigenvalues of $\mathbf{A}$ and $\tilde{\mathbf{A}}$ are the same and the eigenvalues of $\mathbf{A}+\mathbf{b}\mathbf{w}^T$ and $\tilde{\mathbf{A}}+\tilde{\mathbf{b}}\tilde{\mathbf{w}}^T$ are the same is equivalent to the condition that the Jacobian matrices of the two systems (13) and (14) (with the same nonlinear function $f$) have the same eigenvalues at every point.

Thus almost all systems in $\mathcal{C}$ are determined, up to topological conjugacy, by two sets of eigenvalues and the scalar nonlinearity $f$.

**Lemma 7.** *Suppose* $(\mathbf{A}, \mathbf{w})$ *and* $(\tilde{\mathbf{A}}, \tilde{\mathbf{w}})$ *satisfy condition K and* $\mathbf{A}$ *and* $\tilde{\mathbf{A}}$ *have the same eigenvalues. The transfer function* $g(s) = \mathbf{w}^T(s\mathbf{I}-\mathbf{A})^{-1}\mathbf{b}$ *is equal to the transfer function* $\tilde{g}(s) = \tilde{\mathbf{w}}^T(s\mathbf{I}-\tilde{\mathbf{A}})^{-1}\tilde{\mathbf{b}}$ *if and only if* $\mathbf{A}+\mathbf{b}\mathbf{w}^T$ *and* $\tilde{\mathbf{A}}+\tilde{\mathbf{b}}\tilde{\mathbf{w}}^T$ *have the same eigenvalues.*

*Proof.* By writing $(s\mathbf{I} - \mathbf{A})^{-1}$ and $(s\mathbf{I} - \tilde{\mathbf{A}})^{-1}$ as a power series, we see that $g(s) = \tilde{g}(s)$ if and only if $\mathbf{w}^T\mathbf{A}^i\mathbf{b} = \tilde{\mathbf{w}}^T\tilde{\mathbf{A}}^i\tilde{\mathbf{b}}$ for all nonnegative integers $i$. This is equivalent to $\mathbf{K}\mathbf{b} = \tilde{\mathbf{K}}\tilde{\mathbf{b}}$ where $\mathbf{K} = \mathbf{K}(\mathbf{A}, \mathbf{w})$ and $\tilde{\mathbf{K}} = \mathbf{K}(\tilde{\mathbf{A}}, \tilde{\mathbf{w}})$. The matrix $\mathbf{A}+\mathbf{b}\mathbf{w}^T$ is similar to $\mathbf{K}\mathbf{A}\mathbf{K}^{-1} + \mathbf{K}\mathbf{b}\mathbf{w}^T\mathbf{K}^{-1} = \hat{\mathbf{A}} + \mathbf{K}\mathbf{b}\mathbf{e}_1^T$. Similarly,

$\tilde{\mathbf{A}} + \tilde{\mathbf{b}}\tilde{\mathbf{w}}^T$ is similar to $\hat{\mathbf{A}} + \tilde{\mathbf{K}}\tilde{\mathbf{b}}\mathbf{e}_1^T$. By Theorem 1, $\mathbf{Kb} = \tilde{\mathbf{K}}\tilde{\mathbf{b}}$ is equivalent to $\hat{\mathbf{A}}+\mathbf{Kbe}_1^T$ and $\hat{\mathbf{A}}+\tilde{\mathbf{K}}\tilde{\mathbf{b}}\mathbf{e}_1^T$ having the same eigenvalues. ■

**Definition 6** ([Chen, 1984]). A linear time-invariant dynamical system is *irreducible* if and only if there does not exist a linear time-invariant dynamical system of lesser dimension that has the same transfer-function matrix.

The SISO system (12) is irreducible if and only if the pairs $(\mathbf{A}, \mathbf{w})$ and $(\mathbf{A}^T, \mathbf{b})$ both satisfy condition $K$ [Chen, 1984].

**Lemma 8.** *Suppose the two systems*

$$\dot{\mathbf{x}} = \mathbf{Ax} + \mathbf{b}u \qquad \dot{\tilde{\mathbf{x}}} = \tilde{\mathbf{A}}\tilde{\mathbf{x}} + \tilde{\mathbf{b}}\tilde{u}$$
$$y = \mathbf{w}^T\mathbf{x} \qquad \tilde{y} = \tilde{\mathbf{w}}^T\tilde{\mathbf{x}}$$

*are irreducible. Then* $\mathbf{w}^T(s\mathbf{I} - \mathbf{A})^{-1}\mathbf{b} = \tilde{\mathbf{w}}^T(s\mathbf{I} - \tilde{\mathbf{A}})^{-1}\tilde{\mathbf{b}}$ *if and only if* $\mathbf{A}$ *and* $\tilde{\mathbf{A}}$ *have the same eigenvalues and* $\mathbf{A} + \mathbf{bw}^T$ *and* $\tilde{\mathbf{A}} + \tilde{\mathbf{b}}\tilde{\mathbf{w}}^T$ *have the same eigenvalues.*

*Proof.* By Chen [1984, Theorem 5.20], if $\mathbf{w}^T(s\mathbf{I} - \mathbf{A})^{-1}\mathbf{b} = \tilde{\mathbf{w}}^T(s\mathbf{I}-\tilde{\mathbf{A}})^{-1}\tilde{\mathbf{b}}$, then $\mathbf{A}$ and $\tilde{\mathbf{A}}$ are similar matrices. The rest follows from Lemma 7. ■

From an input-output properties point of view, this has the following interpretation. The systems (13) and (14) can be decomposed into a linear and a nonlinear part as shown in Fig. 2(a). Suppose both linear parts have the same transfer function $g(s)$. Then both systems can be depicted as Fig. 2(b).

There is essentially only one irreducible state-space realization of $g(s)$, so if the linear parts are irreducible, then the two systems are linearly conjugate. This is what Lemma 8 and Theorem 2 say.

If the linear parts are observable but not controllable (i.e. $(\mathbf{A}, \mathbf{w})$ and $(\tilde{\mathbf{A}}, \tilde{\mathbf{w}})$ satisfy condition $K$, but $(\mathbf{A}^T, \mathbf{b})$ and $(\tilde{\mathbf{A}}^T, \tilde{\mathbf{b}})$ do not), then by Lemma 7 these 2 systems are still linearly conjugate if $\mathbf{A}$ and $\tilde{\mathbf{A}}$ have the same eigenvalues.

**Lemma 9.** *Let* $f$ *and* $g$ *be differentiable functions from* $\mathbb{R}$ *to* $\mathbb{R}$. *If* $f'(x) = g'(\mu x)$ *for some constant* $\mu \neq 0$ *and for all* $x$, *then* $\mu f(x) = g(\mu x) + e$ *for all* $x$ *and some constant* $e$.

*Proof.* Let $\tilde{g}(x) = g(\mu x)$. Then $\tilde{g}'(x) = \mu g'(\mu x)$. This implies that $\mu f'(x) = \tilde{g}'(x)$. Thus $\mu f = \tilde{g} + e$ for some constant $e$. ■

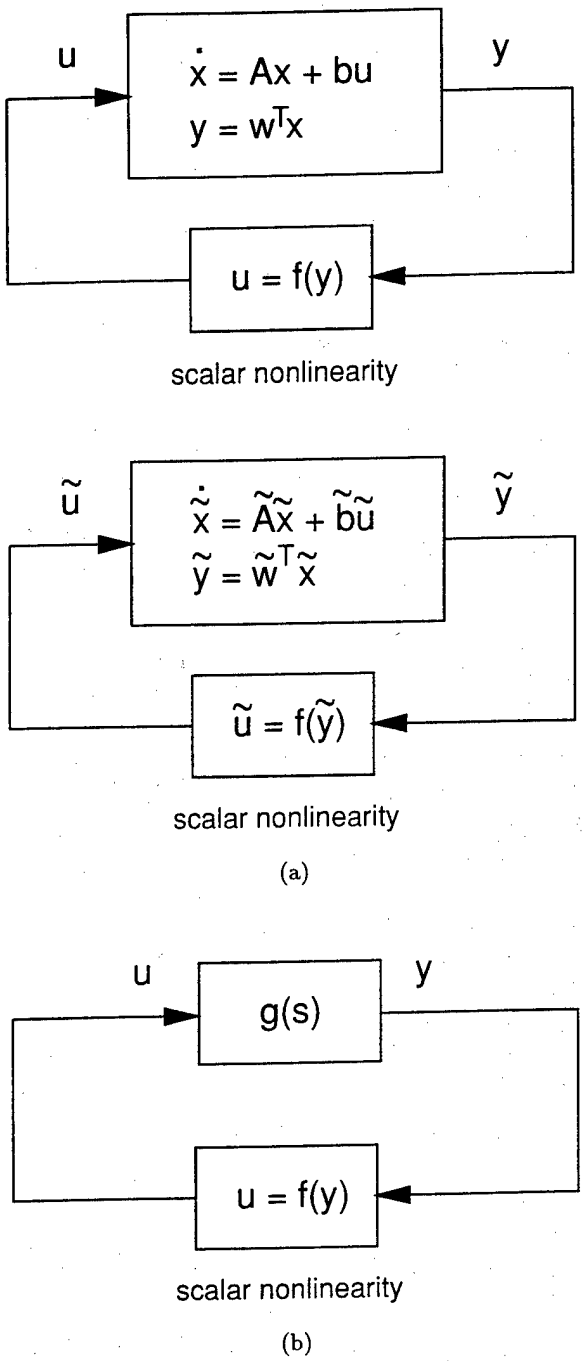


Fig. 2. (a) System (13) and system (14) each decomposed as a linear system with (scalar) nonlinear feedback. (b) By expressing the transfer function of the linear part as $g(s)$, the systems in (a) can be depicted as shown.

**Definition 7.** We say that a virtual equilibrium point $\mathbf{x}^*$ in system 1 and a virtual equilibrium point $\mathbf{y}^*$ in system 2 are *matched* if $\mathbf{x}^* = \mathbf{y}^*$ and the same point $\hat{\mathbf{x}}$ is used in both systems for the linearization (Definition 2). Two real equilibrium points are *matched* if they are the same.

The next theorem shows that matching the equilibrium points and the eigenvalues of the Jacobian matrices at every point are sufficient to guarantee topological conjugacy of vector fields in $\mathcal{C}(\mathbf{w})$.

**Theorem 3.** *Consider two systems in $\mathcal{C}$:*

$$\dot{\mathbf{x}} = \mathbf{A}\mathbf{x} + f(\mathbf{w}^T\mathbf{x})\mathbf{b} \tag{16}$$

*and*

$$\dot{\mathbf{x}} = \tilde{\mathbf{A}}\mathbf{x} + g(\tilde{\mathbf{w}}^T\mathbf{x})\tilde{\mathbf{b}} \tag{17}$$

*where $f$ and $g$ are differentiable functions. Suppose that these two systems are proper and have at least one matched (real or virtual) equilibrium point and their Jacobian matrices at each point have the same eigenvalues, then these systems are topologically conjugate.*

*Proof.* By Lemma 1 we can assume that both systems have an equilibrium point at the origin. Fix $\mathbf{x}_1$ and define $\mathbf{A}' = \mathbf{A} + f'(\mathbf{w}^T\mathbf{x}_1)\mathbf{b}\mathbf{w}^T$ and $\tilde{\mathbf{A}}' = \tilde{\mathbf{A}} + g'(\tilde{\mathbf{w}}^T\mathbf{x}_1)\tilde{\mathbf{b}}\tilde{\mathbf{w}}^T$. Then Eqs. (16)–(17) can be written as follows:

$$\dot{\mathbf{x}} = \mathbf{A}'\mathbf{x} + (f(\mathbf{w}^T\mathbf{x}) - f'(\mathbf{w}^T\mathbf{x}_1)\mathbf{w}^T\mathbf{x})\mathbf{b} \tag{18}$$

$$\dot{\mathbf{x}} = \tilde{\mathbf{A}}'\mathbf{x} + (g(\tilde{\mathbf{w}}^T\mathbf{x}) - g'(\tilde{\mathbf{w}}^T\mathbf{x}_1)\tilde{\mathbf{w}}^T\mathbf{x})\tilde{\mathbf{b}} \tag{19}$$

Then $(\mathbf{A}', \mathbf{w})$ and $(\tilde{\mathbf{A}}', \tilde{\mathbf{w}})$ both satisfy condition $K$ by Lemma 4 and $\mathbf{A}'$ and $\tilde{\mathbf{A}}'$ have the same eigenvalues. This implies that $\mathbf{w} \neq \mathbf{0}$ and $\tilde{\mathbf{w}} \neq \mathbf{0}$.

Without loss of generality we can assume that $\mathbf{A}$ and $\tilde{\mathbf{A}}$ have the same eigenvalues, as otherwise we can always perform the above transformation. We can also assume without loss of generality that $\mathbf{b} \neq \mathbf{0}$ and $f$ and $g$ are *not* affine functions. The Jacobian matrices of system (16) and system (17) at $\mathbf{x}$ are $\mathbf{A} + f'(\mathbf{w}^T\mathbf{x})\mathbf{b}\mathbf{w}^T$ and $\tilde{\mathbf{A}} + g'(\tilde{\mathbf{w}}^T\mathbf{x})\tilde{\mathbf{b}}\tilde{\mathbf{w}}^T$, respectively which are similar to $\hat{\mathbf{A}} + f'(\mathbf{w}^T\mathbf{x})\mathbf{K}\mathbf{b}\mathbf{e}_1^T$ and $\hat{\mathbf{A}} + g'(\tilde{\mathbf{w}}^T\mathbf{x})\tilde{\mathbf{K}}\tilde{\mathbf{b}}\mathbf{e}_1^T$. From Corollary 1 it follows that $f'(\mathbf{w}^T\mathbf{x})\mathbf{K}\mathbf{b} = g'(\tilde{\mathbf{w}}^T\mathbf{x})\tilde{\mathbf{K}}\tilde{\mathbf{b}}$ for all $\mathbf{x}$. Since $\mathbf{K}\mathbf{b} \neq 0$, we must have $f'(\mathbf{w}^T\mathbf{x}) = cg'(\tilde{\mathbf{w}}^T\mathbf{x})$ for all $\mathbf{x}$ for some constant $c$. Let $\mathbf{x} = \frac{\alpha}{\mathbf{w}^T\mathbf{w}}\mathbf{w}$ for some $\alpha \in \mathbb{R}$ and $\mu = \frac{\tilde{\mathbf{w}}^T\mathbf{w}}{\mathbf{w}^T\mathbf{w}}$. Then $f'(\alpha) = cg'(\mu\alpha)$ for all real $\alpha$. $\mu \neq 0$ since otherwise $f$ is affine. By Lemma 9 this implies that $\mu f(\alpha) = cg(\mu\alpha) + e$ for some constant $e$. Since $g$ is not affine, i.e., $g'(\tilde{\mathbf{w}}^T\mathbf{x}) \neq 0$ for some $\mathbf{x}$, it follows that $c\mathbf{K}\mathbf{b} = \tilde{\mathbf{K}}\tilde{\mathbf{b}}$.

Similar to the proof of Theorem 2, by using the transformations $\mathbf{y} = \mathbf{K}\mathbf{x}$ and $\mathbf{y} = \frac{1}{\mu}\tilde{\mathbf{K}}\mathbf{x}$ for the two systems, respectively, we get

$$\dot{\mathbf{y}} = \hat{\mathbf{A}}\mathbf{y} + f(\mathbf{e}_1^T\mathbf{y})\mathbf{K}\mathbf{b}$$

$$\dot{\mathbf{y}} = \hat{\mathbf{A}}\mathbf{y} + \frac{1}{\mu}g(\mu\mathbf{e}_1^T\mathbf{y})\tilde{\mathbf{K}}\tilde{\mathbf{b}}$$

By using $\mu f(\alpha) = cg(\mu\alpha) + e$ these two systems simplify to

$$\dot{\mathbf{y}} = \hat{\mathbf{A}}\mathbf{y} + \frac{1}{\mu}g(\mu\mathbf{e}_1^T\mathbf{y})\tilde{\mathbf{K}}\tilde{\mathbf{b}} + \frac{e}{\mu}\mathbf{K}\mathbf{b}$$

and

$$\dot{\mathbf{y}} = \hat{\mathbf{A}}\mathbf{y} + \frac{1}{\mu}g(\mu\mathbf{e}_1^T\mathbf{y})\tilde{\mathbf{K}}\tilde{\mathbf{b}}$$

Now if they share an equilibrium point $\mathbf{y}^* = \mathbf{0}$, then $\hat{\mathbf{A}}\mathbf{y}^* + \frac{d}{\mu}\tilde{\mathbf{K}}\tilde{\mathbf{b}} + \frac{e}{\mu}\mathbf{K}\mathbf{b} = \mathbf{0}$ for the first system, and $\hat{\mathbf{A}}\mathbf{y}^* + \frac{d}{\mu}\tilde{\mathbf{K}}\tilde{\mathbf{b}} = \mathbf{0}$ for the second system, where $d = g(\mu\mathbf{e}_1^T\mathbf{y}^*)$ if the equilibrium point is real, and $d = \mu g'(\mu\mathbf{e}_1^T\hat{\mathbf{y}})\mathbf{e}_1^T(\mathbf{y}^* - \hat{\mathbf{y}}) + g(\mu\mathbf{e}_1^T\hat{\mathbf{y}})$ if the equilibrium point is virtual due to linearization around $\hat{\mathbf{y}}$. In either case, we see that $\frac{e}{\mu}\mathbf{K}\mathbf{b} = \mathbf{0}$, thus the two systems are topologically conjugate. ■

Since topological conjugacy is preserved under an affine change of coordinates, Theorem 3 can be stated with more generality.

**Theorem 4.** *Consider two systems in $\mathcal{C}$*

$$\dot{\mathbf{x}} = \mathbf{A}_1\mathbf{x} + f(\mathbf{w}_1^T\mathbf{x})\mathbf{b}_1 = \mathbf{h}_1(\mathbf{x}) \tag{20}$$

*and*

$$\dot{\mathbf{y}} = \mathbf{A}_2\mathbf{y} + g(\mathbf{w}_2^T\mathbf{y})\mathbf{b}_2 = \mathbf{h}_2(\mathbf{y}) \tag{21}$$

*where $f$ and $g$ are differentiable functions and $\mathbf{A}_1$ and $\mathbf{A}_2$ are $n \times n$ matrices. Suppose that these two systems are proper. Suppose further that $\mathbf{T}$ is a nonsingular matrix and $\mathbf{t}$ is a vector such that $\tilde{\mathbf{x}}$ and $\tilde{\mathbf{y}} = \mathbf{T}\tilde{\mathbf{x}} + \mathbf{t}$ are real equilibrium points of (20) and (21), respectively and $D\mathbf{h}_1(\mathbf{x})$ shares the same eigenvalues as $D\mathbf{h}_2(\mathbf{T}\mathbf{x} + \mathbf{t})$ for all $\mathbf{x}$, then the two systems (20) and (21) are topologically conjugate.*

*Proof.* Without loss of generality we can assume that $\mathbf{b}_1$ and $\mathbf{b}_2$ are nonzero and $f$ and $g$ are *nonlinear* scalar functions. Using the transformation $\mathbf{y} = \mathbf{T}\mathbf{x} + \mathbf{t}$, system (21) can be written as

$$\dot{\mathbf{x}} = \tilde{\mathbf{A}}_2\mathbf{x} + \tilde{g}(\mathbf{w}_2^T\mathbf{T}\mathbf{x})\mathbf{T}^{-1}\mathbf{b}_2 + \mathbf{T}^{-1}\mathbf{A}_2\mathbf{t} \tag{22}$$

Then systems (20) and (22) share an equilibrium point $\tilde{\mathbf{x}}$ and the Jacobian matrices at each point share the same eigenvalues. The result follows from

Theorem 3 after using Lemma 1 to remove the term $\mathbf{T}^{-1}\mathbf{A}_2\mathbf{t}$. ■

## 3. Eigenvalue Patterns in the *n*-Dimensional Chua's Oscillator

In this section we extend the three-dimensional Chua's oscillator [Chua, 1993] to higher dimensions by adding additional linear inductors, capacitors and resistors. We will call this the *n-dimensional Chua's oscillator*. We show that the $n$-dimensional Chua's oscillator can synthesize almost every eigenvalue pattern of $n$-dimensional vector fields in $\mathcal{C}$.

For even $n$ the $n$-dimensional Chua's oscillator is shown in Fig. 3(a). For odd $n$ the $n$-dimensional Chua's oscillator is shown in Fig. 3(b). The state equations of the $n$-dimensional Chua's oscillator with an *arbitrary* nonlinearity are given by:

$$
\begin{aligned}
\frac{dv_1}{dt} &= \frac{1}{C_1}\left(\frac{v_2 - v_1}{R_2} - g(v_1)\right)\\
\frac{dv_2}{dt} &= \frac{1}{C_2}\left(\frac{v_1 - v_2}{R_2} + i_3\right)\\
\frac{di_3}{dt} &= \frac{1}{L_3}\left(-v_2 - \frac{R_4 i_3}{1 + G_3 R_4} + \frac{v_4}{1 + G_3 R_4}\right)\\
\frac{dv_4}{dt} &= \frac{1}{C_4}\left(-\frac{G_3 v_4}{1 + G_3 R_4} - \frac{i_3}{1 + G_3 R_4} + i_5\right)\\
&\vdots\\
\frac{di_{2j-1}}{dt} &= \frac{1}{L_{2j-1}}\left(-v_{2j-2} - \frac{R_{2j} i_{2j-1}}{1 + G_{2j-1} R_{2j}} + \frac{v_{2j}}{1 + G_{2j-1} R_{2j}}\right)\\
\frac{dv_{2j}}{dt} &= \frac{1}{C_{2j}}\left(-\frac{G_{2j-1} v_{2j}}{1 + G_{2j-1} R_{2j}} - \frac{i_{2j-1}}{1 + G_{2j-1} R_{2j}} + i_{2j+1}\right)\\
&\vdots\\
\frac{dv_n}{dt} &= \frac{1}{C_n}\left(-\frac{i_{n-1}}{1 + G_{n-1} R_n} - \frac{G_{n-1} v_n}{1 + G_{n-1} R_n}\right)
\end{aligned}
\tag{23}
$$

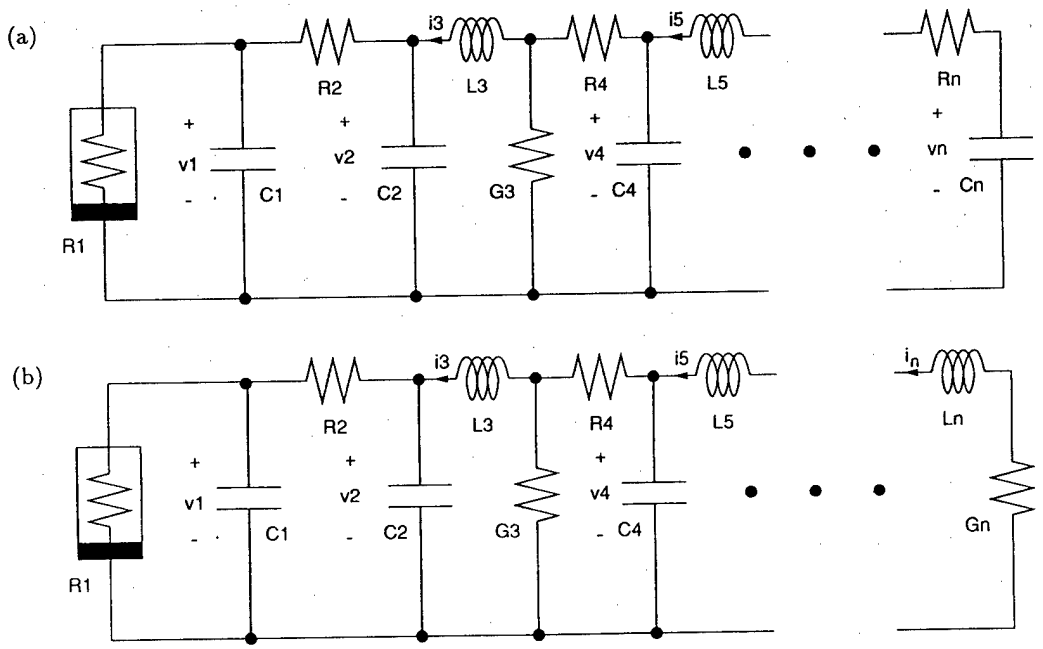


Fig. 3. $n$-dimensional Chua's oscillator. (a) $n$ is even. (b) $n$ is odd.

when $n$ is even, and

$$\begin{aligned}
\frac{dv_1}{dt} &= \frac{1}{C_1}\left(\frac{v_2 - v_1}{R_2} - g(v_1)\right)\\
\frac{dv_2}{dt} &= \frac{1}{C_2}\left(\frac{v_1 - v_2}{R_2} + i_3\right)\\
\frac{di_3}{dt} &= \frac{1}{L_3}\left(-v_2 - \frac{R_4 i_3}{1+G_3R_4} + \frac{v_4}{1+G_3R_4}\right)\\
\frac{dv_4}{dt} &= \frac{1}{C_4}\left(-\frac{G_3 v_4}{1+G_3R_4} - \frac{i_3}{1+G_3R_4} + i_5\right)\\
&\vdots\\
\frac{di_{2j-1}}{dt} &= \frac{1}{L_{2j-1}}\left(-v_{2j-2} - \frac{R_{2j} i_{2j-1}}{1+G_{2j-1}R_{2j}} + \frac{v_{2j}}{1+G_{2j-1}R_{2j}}\right)\\
\frac{dv_{2j}}{dt} &= \frac{1}{C_{2j}}\left(-\frac{G_{2j-1} v_{2j}}{1+G_{2j-1}R_{2j}} - \frac{i_{2j-1}}{1+G_{2j-1}R_{2j}} + i_{2j+1}\right)\\
&\vdots\\
\frac{di_n}{dt} &= \frac{1}{L_n}\left(-v_{n-1} - \frac{i_n}{G_n}\right)
\end{aligned} \tag{24}$$

when $n$ is odd. We define $G_2 = 1/R_2$. For $n$ odd, $\frac{1}{G_n} = 0$ is allowed. The state variable $v_j$ is the voltage across capacitor $C_j$ and the state variable $i_j$ is the current through inductor $L_j$. The function $g(\cdot)$ is a continuous real-valued function describing the $v$-$i$ characteristic of the Chua's diode [R. Madan, Guest Editor, 1993] nonlinear resistor.

By using a state transformation, the following dimensionless form is obtained:

$$\begin{aligned}
\frac{dx_1}{dt} &= k\alpha_1(x_2 - x_1 - h(x_1))\\
\frac{dx_2}{dt} &= k(x_1 - x_2 + x_3)\\
\frac{dx_3}{dt} &= k\alpha_3(-x_2 + \beta_3(-\alpha_4 x_3 + x_4))\\
\frac{dx_4}{dt} &= k\beta_4(\beta_3(-x_3 - \gamma_3 x_4) + x_5)\\
&\vdots\\
\frac{dx_{2i-1}}{dt} &= k\alpha_{2i-1}(-x_{2i-2} + \beta_{2i-1}(-\alpha_{2i} x_{2i-1} + x_{2i}))\\
\frac{dx_{2i}}{dt} &= k\beta_{2i}(\beta_{2i-1}(-x_{2i-1} - \gamma_{2i-1} x_{2i}) + x_{2i+1})\\
&\vdots
\end{aligned} \tag{25}$$

where the last equation is:

$$\frac{dx_n}{dt} = k\beta_n\beta_{n-1}(-x_{n-1} - \gamma_{n-1}x_n)$$

if $n$ is even and

$$\frac{dx_n}{dt} = k\alpha_n\left(-x_{n-1} - \frac{x_n}{\gamma_n}\right)$$

if $n$ is odd. The state transformation is given by:

$$E \triangleq 1V, \quad x_1 = \frac{v_1}{E}, \quad x_{2j} = \frac{v_{2j}}{E}, \quad x_{2j+1} = \frac{i_{2j+1}R_2}{E},$$

$$\text{for } j = 1, 2, \ldots, \left\lfloor \frac{n}{2} \right\rfloor$$

$$k = \frac{1}{C_2R_2}, \quad \alpha_1 = \frac{C_2}{C_1}, \quad h(x) = \frac{R_2 g(xE)}{E}$$

$$\alpha_{2j} = \frac{R_{2j}}{R_2}, \quad \beta_{2j} = \frac{C_2}{C_{2j}},$$

$$\text{for } j = 2, 3, \ldots, \left\lfloor \frac{n}{2} \right\rfloor$$

$$\alpha_{2j-1} = \frac{C_2 R_2^2}{L_{2j-1}},$$

$$\beta_{2j-1} = \frac{1}{1 + G_{2j-1}R_{2j}} = \frac{1}{1 + \gamma_{2j-1}\alpha_{2j}},$$

$$\gamma_{2j-1} = R_2 G_{2j-1},$$

$$\text{for } j = 2, 3, \ldots, \left\lceil \frac{n}{2} \right\rceil$$

where $\lfloor x \rfloor$ is the largest integer less than $x$ and $\lceil x \rceil$ is the smallest integer larger than $x$. If we also rescale time, then we can assume $k = +1$ or $k = -1$ depending on whether $C_2 R_2$ is positive or negative.

We will write [Eqs. (23)–(24)] in the form of Eq. (1) as:

$$\dot{\tilde{\mathbf{x}}} = \tilde{\mathbf{A}}\tilde{\mathbf{x}} + \frac{G_a - G_b}{C_1} f(\mathbf{e}_1^T \tilde{\mathbf{x}})\mathbf{e}_1 \tag{26}$$

where

$$\tilde{\mathbf{x}} = \begin{pmatrix} v_1 \\ v_2 \\ i_3 \\ v_4 \\ i_5 \\ \vdots \\ v_n \end{pmatrix}$$

and

$$\tilde{\mathbf{A}} = \begin{pmatrix} -\frac{G_2+G_a}{C_1} & \frac{G_2}{C_1} & & & & & \\ \frac{G_2}{C_2} & -\frac{G_2}{C_2} & \frac{1}{C_2} & & & & \\ & -\frac{1}{L_3} & -\frac{R_4}{L_3(1+G_3R_4)} & \frac{1}{L_3(1+G_3R_4)} & & & \\ & & -\frac{1}{C_4(1+G_3R_4)} & \frac{-G_3}{C_4(1+G_3R_4)} & \frac{1}{C_4} & & \\ & & & \ddots & \ddots & \ddots & \\ & & & & -\frac{1}{C_n(1+G_{n-1}R_n)} & -\frac{G_{n-1}}{C_n(1+G_{n-1}R_n)} \end{pmatrix} \tag{27}$$

when $n$ is even, and

$$\tilde{\mathbf{x}} = \begin{pmatrix} v_1 \\ v_2 \\ i_3 \\ v_4 \\ i_5 \\ \vdots \\ i_n \end{pmatrix}$$

and

$$\tilde{\mathbf{A}} = \begin{pmatrix} -\frac{G_2+G_a}{C_1} & \frac{G_2}{C_1} & & & & & \\ \frac{G_2}{C_2} & -\frac{G_2}{C_2} & \frac{1}{C_2} & & & & \\ & -\frac{1}{L_3} & -\frac{R_4}{L_3(1+G_3R_4)} & \frac{1}{L_3(1+G_3R_4)} & & & \\ & & -\frac{1}{C_4(1+G_3R_4)} & \frac{-G_3}{C_4(1+G_3R_4)} & \frac{1}{C_4} & & \\ & & & \ddots & \ddots & \ddots & \\ & & & & -\frac{1}{L_n} & -\frac{1}{L_n G_n} \end{pmatrix} \tag{28}$$

when $n$ is odd.

The function $f$ in Eq. (26) is related to the function $g$ in Eqs. (23)–(24) as follows:

$$g(v_1) = G_a v_1 + (G_b - G_a) f(v_1) \tag{29}$$

Consider two tridiagonal matrices $\mathbf{A}_0$ and $\mathbf{A}_1$ defined as follows:

$$\mathbf{A}_0 = \begin{pmatrix} a_{1,1} & a_{1,2} & & & \\ a_{2,1} & a_{2,2} & a_{2,3} & & \\ & \ddots & \ddots & \ddots & \\ & & a_{n-1,n-2} & a_{n-1,n-1} & a_{n-1,n} \\ & & & a_{n,n-1} & a_{n,n} \end{pmatrix} \tag{30}$$

$$\mathbf{A}_1 = \begin{pmatrix} \overline{a}_{1,1} & a_{1,2} & & & \\ a_{2,1} & a_{2,2} & a_{2,3} & & \\ & \ddots & \ddots & \ddots & \\ & & a_{n-1,n-2} & a_{n-1,n-1} & a_{n-1,n} \\ & & & a_{n,n-1} & a_{n,n} \end{pmatrix} \tag{31}$$

Thus $\mathbf{A}_0$ and $\mathbf{A}_1$ only differ in the first entry. Let the characteristic polynomials of $\mathbf{A}_0$ and $\mathbf{A}_1$ be written as:

$$\begin{aligned} \chi(\mathbf{A}_0) &= \lambda^n + r_{n-1}\lambda^{n-1} + \cdots + r_1\lambda + r_0 \\ \chi(\mathbf{A}_1) &= \lambda^n + s_{n-1}\lambda^{n-1} + \cdots + s_1\lambda + s_0 \end{aligned} \tag{32}$$

The following Lemma is proved in Kocarev *et al.* [1993]:

**Lemma 10.** *Define $\kappa_i = a_{i,i}$ for $i = 1, \ldots, n$ and $\rho_i = a_{i,i+1}a_{i+1,i}$ for $i = 1, \ldots, n-1$. Except for a set of measure zero, the values of $\overline{a}_{1,1}$, $\kappa_i$ and $\rho_i$ are uniquely determined by $r_i$ and $s_i$ in (32) and vice versa.*

The following $(n+1)$-step algorithm[2] is given in Kocarev *et al.* [1993] for computing $\overline{a}_{1,1}$, $\kappa_i$ and $\rho_i$ from $r_i$ and $s_i$:

## Algorithm 1

***Step 0.*** Calculate

$$A_{i,1} = (-1)^i r_{n-i} \quad \text{for } i = 1, \ldots, n$$

$$A_{i,2} = (-1)^i \frac{r_{n-i-1} - s_{n-i-1}}{r_{n-1} - s_{n-1}} \quad \text{for } i = 1, \ldots, n-1$$

[2]The algorithm shown here corrects some typographical errors in Kocarev *et al.* [1993].

***Step 1.*** Calculate

$$\kappa_1 = A_{1,1} - A_{1,2}$$

$$\overline{a}_{1,1} = -s_{n-1} - A_{1,2}$$

$$\rho_1 = -A_{2,1} + A_{2,2} + \kappa_1 A_{1,2}$$

$$A_{j,3} = \frac{-A_{j+2,1} + A_{j+2,2} + \kappa_1 A_{j+1,2}}{\rho_1} \quad \text{for } j = 1, \ldots, n-2$$

$$A_{n-2,3} = \frac{-A_{n,1} + \kappa_1 A_{n-1,2}}{\rho_1}$$

***Step 2.*** Calculate

$$\kappa_2 = A_{1,2} - A_{1,3}$$

$$\rho_2 = -A_{2,2} + A_{2,3} + \kappa_2 A_{1,3}$$

$$A_{j,4} = \frac{-A_{j+2,2} + A_{j+2,3} + \kappa_2 A_{j+1,3}}{\rho_2} \quad \text{for } j = 1, \ldots, n-4$$

$$A_{n-3,4} = \frac{-A_{n-1,2} + \kappa_2 A_{n-2,3}}{\rho_2}$$

***Step k, for k = 3, ..., n − 3.*** Calculate

$$\kappa_k = A_{1,k} - A_{1,k+1}$$

$$\rho_k = -A_{2,k} + A_{2,k+1} + \kappa_k A_{1,k+1}$$

$$A_{j,k+2} = \frac{-A_{j+2,k} + A_{j+2,k+1} + \kappa_k A_{j+1,k+1}}{\rho_k} \quad \text{for } j = 1, \ldots, n-k-2$$

$$A_{n-k-1,k+2} = \frac{-A_{n-k+1,k} + \kappa_k A_{n-k,k+1}}{\rho_k}$$

***Step n − 2.*** Calculate

$$\kappa_{n-2} = A_{1,n-2} - A_{1,n-1}$$

$$\rho_{n-2} = -A_{2,n-2} + A_{2,n-1} + \kappa_{n-2} A_{1,n-1}$$

$$A_{1,n} = \frac{-A_{3,n-2} + \kappa_{n-2} A_{2,n-1}}{\rho_{n-2}}$$

***Step n − 1.*** Calculate

$$\kappa_{n-1} = A_{1,n-1} - A_{1,n}$$

$$\rho_{n-1} = -A_{2,n-1} + \kappa_{n-1} A_{1,n}$$

***Step n.*** Calculate

$$\kappa_n = A_{1,n}$$

**End of Algorithm 1**

The matrix $\tilde{\mathbf{A}}$ defined in (27) or (28) is tridiagonal and differs from $\tilde{\mathbf{A}} + \frac{G_a - G_b}{C_1}\mathbf{e}_1\mathbf{e}_1^T$ in only the first entry. Therefore we can apply Lemma 10 to the matrices $\tilde{\mathbf{A}}$ and $\tilde{\mathbf{A}} + \frac{G_a - G_b}{C_1}\mathbf{e}_1\mathbf{e}_1^T$. Applying Algorithm 1 to find $\overline{a}_{1,1}$, $\kappa_i$ and $\rho_i$ and then solving for the circuit parameters in $\tilde{\mathbf{A}}$ and $\tilde{\mathbf{A}} + \frac{G_a - G_b}{C_1}\mathbf{e}_1\mathbf{e}_1^T$, we obtain the following theorem:

**Theorem 5.** *Assume that the parameters $\overline{a}_{1,1}$, $\kappa_i$ and $\rho_i$ are calculated as in Algorithm 1. Suppose that the following inequalities are satisfied:*

$$\overline{a}_{1,1} \neq \kappa_1 \tag{33}$$

$$\kappa_2 \neq 0 \tag{34}$$

$$\rho_i \neq 0 \quad \text{for } i = 1, \ldots, n-1 \tag{35}$$

$$\rho_{2i-1} \neq \kappa_{2i-1}\kappa_{2i} \quad \text{for } i = 1, \ldots, \left\lfloor \frac{n}{2} \right\rfloor \tag{36}$$

*Then the following values for the circuit parameters will give a matrix $\tilde{\mathbf{A}}$ [Eq. (27) or (28)] such that*

$$\chi(\tilde{\mathbf{A}}) = \lambda^n + r_{n-1}\lambda^{n-1} + \cdots + r_1\lambda + r_0$$

$$\chi\left(\tilde{\mathbf{A}} + \frac{G_a - G_b}{C_1}\mathbf{e}_1\mathbf{e}_1^T\right) = \lambda^n + s_{n-1}\lambda^{n-1} + \cdots + s_1\lambda + s_0$$

$$C_1 = 1$$

$$G_2 = -\frac{C_1\rho_1}{\kappa_2}$$

$$G_a = -\kappa_1 C_1 - G_2$$

$$G_b = -\overline{a}_{1,1}C_1 - G_2$$

$$C_2 = -\frac{G_2}{\kappa_2}$$

$$L_3 = -\frac{1}{\rho_2 C_2}$$

$$G_3 = \frac{\kappa_4}{L_3(\rho_3 - \kappa_3\kappa_4)}$$

$$R_4 = -\frac{\kappa_3 L_3(\rho_3 - \kappa_3\kappa_4)}{\rho_3}$$

$$C_4 = -\frac{\rho_3}{L_3(\rho_3 - \kappa_3\kappa_4)^2}$$

$$L_{2i-1} = -\frac{1}{\rho_{2i-2}C_{2i-2}} \qquad \text{for } i = 2, \ldots, \left\lceil \frac{n}{2} \right\rceil$$

$$G_{2i-1} = \frac{\kappa_{2i}}{L_{2i-1}(\rho_{2i-1} - \kappa_{2i-1}\kappa_{2i})} \qquad \text{for } i = 2, \ldots, \left\lfloor \frac{n}{2} \right\rfloor$$

$$R_{2i} = -\frac{\kappa_{2i-1}L_{2i-1}(\rho_{2i-1} - \kappa_{2i-1}\kappa_{2i})}{\rho_{2i-1}} \qquad \text{for } i = 2, \ldots, \left\lfloor \frac{n}{2} \right\rfloor$$

$$C_{2i} = -\frac{\rho_{2i-1}}{L_{2i-1}(\rho_{2i-1} - \kappa_{2i-1}\kappa_{2i})^2} \qquad \text{for } i = 2, \ldots, \left\lfloor \frac{n}{2} \right\rfloor$$

$$G_n = -\frac{1}{L_n\kappa_n} \qquad \text{if } n \text{ is odd} \tag{37}$$

## 4. Topological Conjugacy Between Chua's Oscillator and Vector Fields in $\mathcal{C}$

We are now in a position to combine the results in the previous sections into the main result in this paper which shows that by choosing appropriate parameters the $n$-dimensional Chua's oscillator is topologically conjugate to almost every $n$-dimensional vector field in $\mathcal{C}$. The statement of the next theorem also gives an algorithm for choosing the parameters of Chua's oscillator.

**Theorem 6.** *Consider a proper vector field of $\mathcal{C}$ written in the form (1). Let the characteristic polynomials of $\mathbf{A}$ and $\mathbf{A} + \mathbf{b}\mathbf{w}^T$ be written as Eq. (7). Suppose the inequalities (33)–(36) are satisfied, then the Chua's oscillator defined in (23)–(24) with the parameters specified by (37) and (29) is topologically conjugate to system (1).*

*Proof.* It can easily be shown that given the conditions in the theorem, the matrix $\tilde{\mathbf{A}}$ defined in (27)–(28) together with $\mathbf{e}_1$ satisfies condition $K$. The theorem then follows from Theorem 2 and Theorem 5. ■

*Remark 6.* Lemma 1 implies that almost all vector fields in $\mathcal{C}'$ are topologically conjugate to Chua's oscillator.

*Remark 7.* Lemma 5 implies that the eigenvalues of the Jacobian matrix in Chua's oscillator [Eqs. (23)–(24)] and the vector field in $\mathcal{C}$ [when written as Eq. (2)] will be the same at corresponding points where the Jacobian matrix is defined.

*Remark 8.* The set of vector fields in $\mathcal{C}$ where inequalities (33)–(36) are not satisfied or is not proper is of measure zero. For these vector fields, in general it is possible to perturb the system slightly to obtain a system in $\mathcal{C}$ outside this set which generates similar behavior.

*Remark 9.* In dimensionless form (25), the parameters for Chua's oscillator are given by:

$$
\begin{aligned}
k &= -\kappa_2 \\
\alpha_1 &= \frac{\rho_1}{\kappa_2^2} \\
\alpha_3 &= -\frac{\rho_2}{\kappa_2^2} \\
\gamma_{2i-1} &= -\frac{\kappa_{2i-1}\kappa_{2i}}{\rho_{2i-1}} \qquad \text{for } i = 2, \ldots, \left\lceil \frac{n}{2} \right\rceil \\
\beta_{2i-1} &= \frac{1}{1+\gamma_{2i-1}} \qquad \text{for } i = 2, \ldots, \left\lceil \frac{n}{2} \right\rceil \\
\alpha_{2i+1} &= \frac{\rho_{2i}\rho_{2i-1}\rho_1\alpha_{2i-1}}{(\rho_{2i-1} - \kappa_{2i-1}\kappa_{2i})^2} \qquad \text{for } i = 2, \ldots, \left\lfloor \frac{n}{2} \right\rfloor \\
\beta_{2i} &= -\frac{(\rho_{2i-1} - \kappa_{2i-1}\kappa_{2i})^2}{\kappa_2^2\rho_{2i-1}\alpha_{2i-1}} \qquad \text{for } i = 2, \ldots, \left\lfloor \frac{n}{2} \right\rfloor \\
\alpha_{2i} &= \frac{\kappa_{2i-1}(\rho_{2i-1} - \kappa_{2i-1}\kappa_{2i})}{\kappa_2\rho_{2i-1}\alpha_{2i-1}} \qquad \text{for } i = 2, \ldots, \left\lfloor \frac{n}{2} \right\rfloor \\
h(x) &= \left(\frac{\kappa_1\kappa_2}{\rho_1} - 1\right) x + \frac{\kappa_2}{\rho_1}(\bar{a}_{1,1} - \kappa_1) f(x)
\end{aligned}
\tag{38}
$$

## 5. Continuous Piecewise-Linear Vector Fields

For piecewise-linear vector fields, the Jacobian matrices $\mathbf{J}_1$ and $\mathbf{J}_2$ in neighboring regions must satisfy a consistent variation property $\mathbf{J}_1 - \mathbf{J}_2 = \delta \mathbf{c}\mathbf{a}^T$. Piecewise-linear vector fields in $\mathcal{C}$ are such that the vectors $\mathbf{c}$ and $\mathbf{a}$ are the same at all boundaries. Thus we consider the subclass of piecewise-linear vector fields, where the Jacobian matrix in the different regions differ by a scalar multiple of a fixed rank 1 matrix:

**Definition 8.** The class $\mathcal{P}$ is the class of vector fields which are:

- continuous,
- piecewise-linear with a countable number of regions,
- the boundary planes are parallel planes of the form $\mathbf{w}^T\mathbf{x} = d_i$,
- there is at least one equilibrium point (which can be real or virtual),
- there exists a matrix $\mathbf{A}$ and a vector $\mathbf{b}$ such that the Jacobian matrix in each region is of the form $\mathbf{A} + \mu_i \mathbf{b}\mathbf{w}^T$.

**Lemma 11.** *By a change of coordinates, the vector fields in class $\mathcal{P}$ form a subclass of $\mathcal{C}$ and can be written in the form*

$$\dot{\mathbf{x}} = \mathbf{A}\mathbf{x} + \left( f + e\mathbf{e}_1^T\mathbf{x} + \sum_{i=1}^{\infty} c_i \left| \mathbf{e}_1^T\mathbf{x} - d_i \right| \right) \mathbf{b} \quad (39)$$

*Proof.* The proof is similar to Lemma 1, where an equilibrium point is translated to the origin. Without loss of generality we can assume that $\mathbf{w} = \mathbf{e}_1$. It is clear that vector fields in class $\mathcal{P}$ can be written in the form

$$\dot{\mathbf{x}} = \mathbf{A}_i\mathbf{x} + \mathbf{b}_i\,, \quad \tilde{d}_{i-1} \le \mathbf{e}_1^T\mathbf{x} \le \tilde{d}_i \quad (40)$$

Suppose that there exists an equilibrium point due to the linearization in region $k$, i.e. there exists $\mathbf{f}_k$ such that $\mathbf{A}_k\mathbf{f}_k + \mathbf{b}_k = \mathbf{0}$. The difference between the Jacobian matrices in two different regions are of the form $\delta \mathbf{b}\mathbf{e}_1^T$. If $\tilde{d}_i \neq 0$, by continuity, we must have

$$\mathbf{A}_{i+1} - \mathbf{A}_i = \frac{1}{\tilde{d}_i}(\mathbf{b}_i - \mathbf{b}_{i+1})\mathbf{e}_1^T$$

If $\tilde{d}_i = 0$, by continuity we have $\mathbf{b}_i - \mathbf{b}_{i+1} = \mathbf{0}$. Thus in either case, we have $(\mathbf{b}_i - \mathbf{b}_{i+1}) = \delta \mathbf{b}$ for some constant $\delta$. So we can write Eq. (40) as

$$\dot{\mathbf{x}} = \mathbf{A}_i\mathbf{x} + \mathbf{b}_k + \delta_i\mathbf{b}\,, \quad \tilde{d}_{i-1} \le \mathbf{e}_1^T\mathbf{x} \le \tilde{d}_i \quad (41)$$

where $\delta_i$ are real numbers and $\delta_k = 0$. Using the transformation $\mathbf{y} = \mathbf{x} - \mathbf{f}_k$, we obtain

$$\begin{aligned} \dot{\mathbf{y}} = \dot{\mathbf{x}} &= \mathbf{A}_i\mathbf{y} + \mathbf{A}_i\mathbf{f}_k + \mathbf{b}_k + \delta_i\mathbf{b}\,, \\ \tilde{d}_{i-1} - \mathbf{e}_1^T\mathbf{f}_k &\le \mathbf{e}_1^T\mathbf{y} \le \tilde{d}_i - \mathbf{e}_1^T\mathbf{f}_k \end{aligned} \quad (42)$$

Observing that $\mathbf{A}_i\mathbf{f}_k + \mathbf{b}_k = (\mathbf{A}_i - \mathbf{A}_k)\mathbf{f}_k + \mathbf{A}_k\mathbf{f}_k + \mathbf{b}_k = (\mathbf{A}_i - \mathbf{A}_k)\mathbf{f}_k = \kappa_i \mathbf{b}\mathbf{e}_1^T\mathbf{f}_k = \kappa_i \mathbf{e}_1^T\mathbf{f}_k\mathbf{b}$ for some $\kappa_i$, we see that system (42) is in the form

$$\dot{\mathbf{y}} = \mathbf{A}_i\mathbf{y} + \hat{\delta}_i\mathbf{b}\,, \quad d_{i-1} \le \mathbf{e}_1^T\mathbf{y} \le d_i \quad (43)$$

where $i \in \{0, 1, \ldots, n\}$, $\hat{\delta}_i \in \mathbb{R}$ and $\hat{\delta}_k = 0$ for some $k$. Noting that $\mathbf{A}_i = \mathbf{A} + \mu_i \mathbf{b}\mathbf{e}_1^T$ and by using the canonical piecewise-linear equation [Chua & Kang, 1977], this can be written as Eq. (39). ■

Thus the class $\mathcal{P}$ can be reduced to a subclass of $\mathcal{C}$ and we can apply Theorem 6 to these vector fields. For vector fields in $\mathcal{P}$, Theorem 3 has the following interpretation. If two vector fields in $\mathcal{P}$ have the same boundary planes, and the eigenvalues in corresponding regions are identical, and the equilibrium points are matched, then the two systems with these two vector fields are topologically conjugate (except for a measure zero set in $\mathcal{P}$).

Consider the four-dimensional 3-region piecewise-linear system considered in Matsumoto *et al.* [1986] which exhibits hyperchaos:

$$\begin{aligned} \frac{dv_1}{dt} &= \frac{f(v_2 - v_1) - i_3}{C_1} \\ \frac{dv_2}{dt} &= \frac{-f(v_2 - v_1) - i_4}{C_2} \\ \frac{di_3}{dt} &= \frac{v_1 + Ri_3}{L_3} \\ \frac{di_4}{dt} &= \frac{v_2}{L_4} \end{aligned} \quad (44)$$

where

$$f(x) = m_1 x + \frac{1}{2}(m_0 - m_1)(|x + 1| - |x - 1|)$$

For the parameters $C_1 = \frac{1}{2}$, $C_2 = \frac{1}{20}$, $L_3 = 1$, $L_4 = \frac{2}{3}$, $R = 1$, $m_0 = -0.2$, and $m_1 = 3$, there exists a real equilibrium point in each of the three regions.

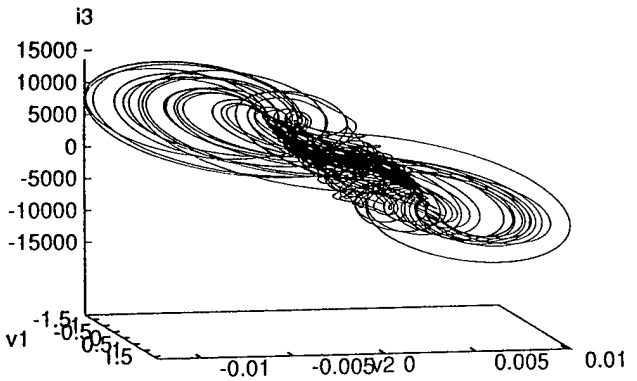


Fig. 4. Attractor from the four-dimensional Chua's oscillator which is topologically conjugate to the system in Eq. (44) with parameters $C_1 = \frac{1}{2}$, $C_2 = \frac{1}{20}$, $L_3 = 1$, $L_4 = \frac{2}{3}$, $R = 1$, $m_0 = -0.2$ and $m_1 = 3$. The attractor is projected onto the $v_1$-$v_2$-$i_3$ plane.

Applying Theorem 5 we obtain the following values for the four-dimensional Chua's oscillator:

$$\begin{aligned} C_1 &= 1 \\ C_2 &= -6.2599109091 \times 10^5 \\ C_4 &= -7.3076305375 \times 10^5 \\ L_3 &= -6.7877793494 \times 10^{-7} \\ R_2 &= 2.4121749046 \times 10^{-4} \\ G_3 &= 7.7704985725 \times 10^5 \\ R_4 &= -9.9757154563 \times 10^{-8} \\ G_a &= -4.1500363636 \times 10^3 \\ G_b &= -4.0796363636 \times 10^3 \end{aligned}$$

with $g(\cdot)$ defined as

$$g(x) = G_b x + \frac{1}{2}(G_a - G_b)(|x+1| - |x-1|)$$

For these parameters, both system (23) and system (44) have an equilibrium point at the origin, both systems are odd-symmetric 3 segment piecewise-linear, and the eigenvalues in corresponding regions are matched. Figure 4 shows a projection of the resulting attractor from Chua's oscillator.

## 6. 2-Segment Continuous Piecewise-Linear Vector Fields

In this section we study the subclass of vector fields in $\mathcal{P}$ which is piecewise-linear with two segments. Thus the system has the form:

$$\dot{\mathbf{x}} = \begin{cases} \mathbf{A}_0\mathbf{x} + \mathbf{b}_0, & \mathbf{e}_1^T\mathbf{x} \le d \\ \mathbf{A}_1\mathbf{x} + \mathbf{b}_1, & \mathbf{e}_1^T\mathbf{x} \ge d \end{cases} \tag{45}$$

Without loss of generality we can assume that there exists a (real or virtual) equilibrium point by linearizing in the region $\mathbf{e}_1^T\mathbf{x} \le d$.[3]

The following corollary to Lemma 11 transforms system (45) into a more simplified form:

**Corollary 2.** *Assume system (45) is in $\mathcal{P}$. System (45) is then topologically conjugate to one of the following systems:*

$$\dot{\mathbf{x}} = \begin{cases} \mathbf{A}_0\mathbf{x}, & \mathbf{e}_1^T\mathbf{x} \le 1 \\ \mathbf{A}_1\mathbf{x} + \mathbf{b}_2, & \mathbf{e}_1^T\mathbf{x} \ge 1 \end{cases} \tag{46}$$

$$\dot{\mathbf{x}} = \begin{cases} \mathbf{A}_1\mathbf{x} + \mathbf{b}_2, & \mathbf{e}_1^T\mathbf{x} \le 1 \\ \mathbf{A}_0\mathbf{x}, & \mathbf{e}_1^T\mathbf{x} \ge 1 \end{cases} \tag{47}$$

$$\dot{\mathbf{x}} = \begin{cases} \mathbf{A}_0\mathbf{x}, & \mathbf{e}_1^T\mathbf{x} \le 0 \\ \mathbf{A}_1\mathbf{x}, & \mathbf{e}_1^T\mathbf{x} \ge 0 \end{cases} \tag{48}$$

*for some vector* $\mathbf{b}_2$.

*Proof.* We will refer to Eqs. (46)-(48) as Form 1 to Form 3, respectively. Consider system (45). Let $\mathbf{f} = (f_1, f_2, \ldots, f_n)^T$ be such that $\mathbf{A}_0\mathbf{f} + \mathbf{b}_0 = \mathbf{0}$. Using the transformation $\mathbf{y} = \mathbf{x} - \mathbf{f}$, we get

$$\dot{\mathbf{y}} = \begin{cases} \mathbf{A}_0\mathbf{y}, & \mathbf{e}_1^T\mathbf{y} \le d - f_1 \\ \mathbf{A}_1\mathbf{y} + \mathbf{b}_1 + \mathbf{A}_1\mathbf{f}, & \mathbf{e}_1^T\mathbf{y} \ge d - f_1 \end{cases}$$

If $d - f_1 \neq 0$, a transformation of the form $\mathbf{z} = \frac{\mathbf{y}}{d-f_1}$ will transform the system into Form 1 [Eq. (46)] if $d - f_1 > 0$ and into Form 2 [Eq. (47)] if $d - f_1 < 0$. If $d - f_1 = 0$, we obtain the system

$$\dot{\mathbf{y}} = \begin{cases} \mathbf{A}_0\mathbf{y}, & \mathbf{e}_1^T\mathbf{y} \le 0 \\ \mathbf{A}_1\mathbf{y} + \mathbf{b}_1 + \mathbf{A}_1\mathbf{f}, & \mathbf{e}_1^T\mathbf{y} \ge 0 \end{cases}$$

which by continuity must be equal to Form 3. ■

This corollary says that one of the equilibrium points, which can be real or virtual, can be translated to the origin. Form 1 and Form 2 correspond to the cases where a real and a virtual equilibrium point, respectively, is translated to the origin. Form 3 corresponds to a real equilibrium point lying on

[3]Thus we assume that there is either a real equilibrium point in the region $\mathbf{e}_1^T\mathbf{x} \le d$ or a virtual equilibrium point in the region $\mathbf{e}_1^T\mathbf{x} > d$. If this assumption is not satisfied, it will be satisfied after the application of the transformation $\mathbf{y} = -\mathbf{x}$ since we assume the existence of at least one equilibrium point for a vector field in $\mathcal{P}$.

the boundary being translated to the origin. When we use $\mathbf{A} = \mathbf{A}_0$ and $\mathbf{A} + \mathbf{b}\mathbf{e}_1^T = \mathbf{A}_1$ in Theorem 5 for calculating the parameters of Chua's oscillator, we only need to deal with Chua's oscillator with one of the following three nonlinearities:

$$g(x) = \frac{1}{2}(G_a - G_b) + \frac{1}{2}(G_a + G_b)x + \frac{1}{2}(G_b - G_a)|x - 1| \quad \text{for Form 1} \quad (49)$$

$$g(x) = \frac{1}{2}(G_a - G_b) + \frac{1}{2}(G_a + G_b)x + \frac{1}{2}(G_a - G_b)|x - 1| \quad \text{for Form 2} \quad (50)$$

$$g(x) = \frac{1}{2}(G_a + G_b)x + \frac{1}{2}(G_b - G_a)|x| \quad \text{for Form 3} \quad (51)$$

Note that using these three forms for $g(\cdot)$ results in Chua's oscillator having the same number of parameters as the 3-segment, odd-symmetric Chua's oscillator.

Let us illustrate the above by transforming two chaotic systems, which have 2-segment piecewise-linear vector fields, into equivalent Chua's oscillators.

Nishio *et al.* [1992] introduced two simple circuits which exhibit hyperchaos. The state equations are given by:

$$\begin{aligned} \dot{x}_1 &= x_3 - f(x_1) \\ \dot{x}_2 &= \gamma_C(x_4 - x_3) \\ \dot{x}_3 &= x_2 - x_1 \\ \dot{x}_4 &= -\gamma_L x_2 + \alpha x_4 \end{aligned} \quad (52)$$

and

$$\begin{aligned} \dot{x}_1 &= x_3 \\ \dot{x}_2 &= \gamma_C(x_4 - x_3 - f(x_2)) \\ \dot{x}_3 &= x_2 - x_1 \\ \dot{x}_4 &= -\gamma_L x_2 + \alpha x_4 \end{aligned} \quad (53)$$

where $f(x) = \frac{1}{2\varepsilon}(|x - 1| + x - 1)$.

Consider Eq. (52) with parameters $\gamma_L = 0.5$, $\gamma_C = 0.5$, $\alpha = 0.18$, $\varepsilon = 0.005$. There exists a real equilibrium point in each of the two regions, so we obtain Form 1. Using Theorem 5, we obtain the following parameters for the four-dimensional Chua's oscillator:

$$\begin{aligned} C_1 &= 1 \\ C_2 &= -1.2980742146337069 \times 10^{33} \\ C_4 &= -2.5961484292674138 \times 10^{33} \\ L_3 &= -1.5407439555097887 \times 10^{-33} \\ R_2 &= -2.7755575615628914 \times 10^{-17} \\ G_3 &= 4.6730671726813447 \times 10^{32} \\ R_4 &= 4.2764235361475130 \times 10^{-50} \\ G_a &= 3.6028797018963968 \times 10^{16} \\ G_b &= 3.6028797018964168 \times 10^{16} \end{aligned}$$

where $g(\cdot)$ is defined by Eq. (49). Note that some ill-conditioning causes $G_a$ to be very close to $G_b$. Figure 5 shows a projection of the resulting attractor from Chua's oscillator.

Consider Eq. (53) with parameters $\gamma_L = 1$, $\gamma_C = 1.545$, $\alpha = 0.26$, $\varepsilon = 0.005$. Again there exists a real equilibrium point in each of the two regions. Using Theorem 5, we obtain the following parameters for the four-dimensional Chua's oscillator:

$$\begin{aligned} C_1 &= 1 \\ C_2 &= -1.8284023669 \times 10^{2} \\ C_4 &= -2.1568595807 \times 10^{2} \\ L_3 &= -1.1321166763 \times 10^{-2} \\ R_2 &= 4.2071197411 \times 10^{-2} \\ G_3 &= 7.1307692308 \times 10^{1} \\ R_4 &= -2.5374219121 \times 10^{-3} \\ G_a &= -2.3769230769 \times 10^{1} \\ G_b &= 2.8523076923 \times 10^{2} \end{aligned}$$

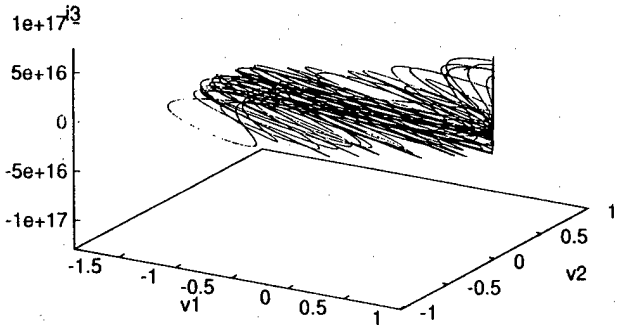


Fig. 5. Attractor from the four-dimensional Chua's oscillator which is topologically conjugate to the system in Eq. (52) with parameters $\gamma_L = 0.5$, $\gamma_C = 0.5$, $\alpha = 0.18$, $\varepsilon = 0.005$. The attractor is projected onto the $v_1$-$v_2$-$i_3$ plane.

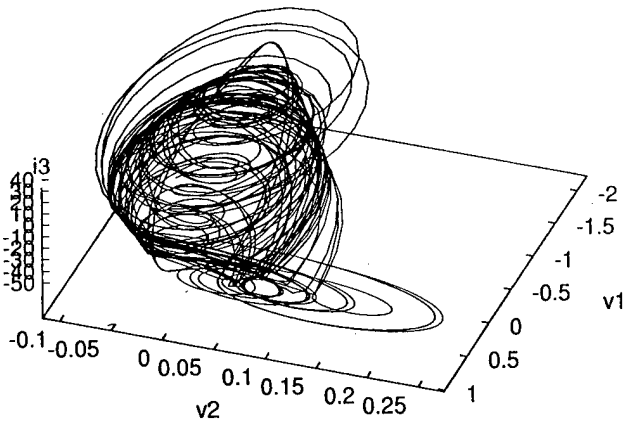


Fig. 6. Attractor from the four-dimensional Chua's oscillator which is topologically conjugate to the system in Eq. (53) with parameters $\gamma_L = 1$, $\gamma_C = 1.545$, $\alpha = 0.26$, $\varepsilon = 0.005$. The attractor is projected onto the $v_1$-$v_2$-$i_3$ plane.

where $g(\cdot)$ is defined by Eq. (49). Figure 6 shows a projection of the resulting attractor from Chua's oscillator.

## 7. Linear Conjugacy of Vector Fields with Multiple Scalar Nonlinearities

We now extend the results in Sec. 2 to vector fields with several scalar nonlinearities. We consider the following class of vector fields:

**Definition 9.** The class $\mathcal{C}_n(\mathbf{w})$ consists of vector fields of the form:

$$\dot{\mathbf{x}} = \mathbf{A}\mathbf{x} + \sum_{i=1}^{\infty} f_i(\mathbf{w}^T\mathbf{x})\mathbf{b}_i \tag{54}$$

where $\mathbf{A}$ is an $n \times n$ matrix, $\mathbf{w}$, $\mathbf{b}_i$ are $n \times 1$ vectors and $f_i(\cdot) : \mathbb{R} \to \mathbb{R}$ are real-valued continuous functions. We define $\mathcal{C}_n = \bigcup_{\mathbf{w}} \mathcal{C}_n(\mathbf{w})$.

If $\mathbf{w} = \mathbf{0}$, this reduces to the class of affine systems. Vector fields in class $\mathcal{C}_n(\mathbf{w})$ can be considered as $n$-dimensional nonlinear vector fields where the nonlinearity occurs only in the direction $\mathbf{w}$. This is stated more precisely in the following lemma.

**Lemma 12.** *For $\mathbf{w} \neq \mathbf{0}$, the class $\mathcal{C}_n(\mathbf{w})$ is equal to the class of continuous vector fields $\dot{\mathbf{x}} = \mathbf{f}(\mathbf{x})$ such that $\mathbf{f}(\mathbf{x}) = \mathbf{A}\mathbf{u} + \mathbf{g}(\mathbf{v})$ for all $\mathbf{x}$ where $\mathbf{x}$ is decomposed as $\mathbf{x} = \mathbf{u} + \mathbf{v}$ and $\mathbf{v} = \frac{\mathbf{w}^T\mathbf{x}}{\mathbf{w}^T\mathbf{w}}\mathbf{w}$ is the orthogonal projection of $\mathbf{x}$ onto $\mathbf{w}$.*

*Proof.* Since $\mathbf{w}^T\mathbf{x} = \mathbf{w}^T\mathbf{v}$, a system in the form (54) can be written as:

$$\dot{\mathbf{x}} = \mathbf{A}\mathbf{u} + \mathbf{A}\mathbf{v} + \sum_{i=1}^{\infty} f_i(\mathbf{w}^T\mathbf{v})\mathbf{b}_i$$

So one direction is clear. Consider a system of the form $\dot{\mathbf{x}} = \mathbf{A}\mathbf{u} + \mathbf{g}(\mathbf{v})$. Since $\mathbf{v} = \left(\frac{\mathbf{w}}{\mathbf{w}^T\mathbf{w}}\right)\mathbf{w}^T\mathbf{x}$, $\mathbf{g}(\mathbf{v})$ can be written as $\tilde{\mathbf{g}}(\mathbf{w}^T\mathbf{x})$. Thus we can write the system as

$$\begin{aligned}\dot{\mathbf{x}} &= \mathbf{A}\mathbf{x} - \mathbf{A}\mathbf{v} + \tilde{\mathbf{g}}(\mathbf{w}^T\mathbf{x}) \\ &= \mathbf{A}\mathbf{x} - \mathbf{A}\frac{\mathbf{w}}{\mathbf{w}^T\mathbf{w}}\mathbf{w}^T\mathbf{x} + \tilde{\mathbf{g}}(\mathbf{w}^T\mathbf{x})\end{aligned}$$

This can be written as (54) if we define $\mathbf{b}_i = \mathbf{e}_i$ and

$$f_i(\mathbf{w}^T\mathbf{x}) = \mathbf{e}_i^T\left(\tilde{\mathbf{g}}(\mathbf{w}^T\mathbf{x}) - \mathbf{A}\frac{\mathbf{w}}{\mathbf{w}^T\mathbf{w}}\mathbf{w}^T\mathbf{x}\right)$$

for $i = 1, \ldots, n$. ■

**Definition 10.** A vector field in $\mathcal{C}_n$ in the form (54) is said to be *proper* if $(\mathbf{A}, \mathbf{w})$ satisfy condition $K$.

The following theorem is the analog of Theorem 2 for the class $\mathcal{C}_n(\mathbf{w})$.

**Theorem 7.** *Consider the systems*

$$\dot{\mathbf{x}} = \mathbf{A}\mathbf{x} + \sum_{i=1}^{\infty} f_i(\mathbf{w}^T\mathbf{x})\mathbf{b}_i \tag{55}$$

*and*

$$\dot{\tilde{\mathbf{x}}} = \tilde{\mathbf{A}}\tilde{\mathbf{x}} + \sum_{i=1}^{\infty} f_i(\tilde{\mathbf{w}}^T\tilde{\mathbf{x}})\tilde{\mathbf{b}}_i \tag{56}$$

*Assume that both systems are proper. Then system (55) and system (56) are linearly conjugate if the eigenvalues of $\mathbf{A}$ and $\tilde{\mathbf{A}}$ are the same and the eigenvalues of $\mathbf{A}+\mathbf{b}_i\mathbf{w}^T$ and $\tilde{\mathbf{A}}+\tilde{\mathbf{b}}_i\tilde{\mathbf{w}}^T$ are the same for each $i$.*

*Proof.* The proof follows the same steps as in Theorem 2. ■

Thus almost all systems in $\mathcal{C}_n$ are determined, up to topological conjugacy, by countable sets of eigenvalues and the scalar nonlinearities $f_i$'s. Given countable arbitrary sets of eigenvalues, is it possible to find a matrix $\mathbf{A}$, and vectors $\mathbf{b}_i$, $\mathbf{w}$ such that $\mathbf{A}$ and $\mathbf{A} + \mathbf{b}_i\mathbf{w}^T$ have these eigenvalues? The answer

is yes and the following $\mathbf{A}$, $\mathbf{b}_i$, $\mathbf{w}$ give characteristic polynomials as described by Eq. (57):

$$\mathbf{A} = \begin{pmatrix} 0 & 0 & & -r_0 \\ 1 & 0 & & -r_1 \\ 0 & 1 & \ddots & \cdots \\ & \ddots & \ddots & -r_{n-1} \end{pmatrix}, \mathbf{w} = \begin{pmatrix} 0 \\ 0 \\ \vdots \\ 1 \end{pmatrix},$$

$$\mathbf{b}_i = \begin{pmatrix} r_0 - s_0^i \\ r_1 - s_1^i \\ \vdots \\ r_{n-1} - s_{n-1}^i \end{pmatrix}$$

$$\chi(\mathbf{A}) = \lambda^n + r_{n-1}\lambda^{n-1} + \cdots + r_1\lambda + r_0$$

$$\chi(\mathbf{A} + \mathbf{b}_i\mathbf{w}^T) = \lambda^n + s_{n-1}^i\lambda^{n-1} + \cdots + s_1^i\lambda + s_0^i \tag{57}$$

The next theorem is the analog of Theorem 3 for the class $C_n$.

**Theorem 8.** *Consider two systems in* $C_n$

$$\dot{\mathbf{x}} = \mathbf{A}\mathbf{x} + \sum_{i=1}^{\infty} f_i(\mathbf{w}^T\mathbf{x})\mathbf{b}_i \tag{58}$$

*and*

$$\dot{\mathbf{x}} = \tilde{\mathbf{A}}\mathbf{x} + \sum_{i=1}^{\infty} g_i(\tilde{\mathbf{w}}^T\mathbf{x})\tilde{\mathbf{b}}_i \tag{59}$$

*where $f_i$ and $g_i$ are differentiable functions for all $i$. Suppose that these two systems are proper and have at least one matched (real or virtual) equilibrium point and their Jacobian matrices at each point have the same eigenvalues, then these systems are linearly conjugate.*

*Proof.* As in Theorem 3 we can assume without loss of generality that $\mathbf{A}$ and $\tilde{\mathbf{A}}$ have the same eigenvalues, that one of the $f_i$'s is not an affine function and that the origin is an equilibrium point for both systems. Consider $\mathbf{K} = \mathbf{K}(\mathbf{A}, \mathbf{w})$ and $\tilde{\mathbf{K}} = \mathbf{K}(\tilde{\mathbf{A}}, \tilde{\mathbf{w}})$ which are nonsingular by hypothesis. Since $\{\mathbf{K}^{-1}\mathbf{e}_i\}_{i=1}^n$ and $\{\tilde{\mathbf{K}}^{-1}\mathbf{e}_i\}_{i=1}^n$ form two bases of $\mathbb{R}^n$, it is easy to see that without loss of generality we can assume that the two systems can be rewritten in the form:

$$\dot{\mathbf{x}} = \mathbf{A}\mathbf{x} + \sum_{i=1}^{n} f_i(\mathbf{w}^T\mathbf{x})\mathbf{K}^{-1}\mathbf{e}_i \tag{60}$$

$$\dot{\mathbf{x}} = \tilde{\mathbf{A}}\mathbf{x} + \sum_{i=1}^{n} g_i(\tilde{\mathbf{w}}^T\mathbf{x})\tilde{\mathbf{K}}^{-1}\mathbf{e}_i \tag{61}$$

The Jacobian matrices of system (58) and system (59) at $\mathbf{x}$ are $\mathbf{A} + \sum_{i=1}^n f_i'(\mathbf{w}^T\mathbf{x})\mathbf{K}^{-1}\mathbf{e}_i\mathbf{w}^T$ and $\tilde{\mathbf{A}} + \sum_{i=1}^n g_i'(\tilde{\mathbf{w}}^T\mathbf{x})\tilde{\mathbf{K}}^{-1}\mathbf{e}_i\tilde{\mathbf{w}}^T$, respectively which are similar to $\hat{\mathbf{A}} + \sum_{i=1}^n f_i'(\mathbf{w}^T\mathbf{x})\mathbf{e}_i\mathbf{e}_1^T$ and $\hat{\mathbf{A}} + \sum_{i=1}^n g_i'(\tilde{\mathbf{w}}^T\mathbf{x})\mathbf{e}_i\mathbf{e}_1^T$. From Corollary 1 it follows that $\sum_{i=1}^n f_i'(\mathbf{w}^T\mathbf{x})\mathbf{e}_i = \sum_{i=1}^n g_i'(\tilde{\mathbf{w}}^T\mathbf{x})\mathbf{e}_i$ for all $\mathbf{x}$. This means that $f_i'(\mathbf{w}^T\mathbf{x}) = g_i'(\tilde{\mathbf{w}}^T\mathbf{x})$ for all $\mathbf{x}$ and for all $i$. Let $\mathbf{x} = \frac{\alpha}{\mathbf{w}^T\mathbf{w}}\mathbf{w}$ for some $\alpha \in \mathbb{R}$ and $\mu = \frac{\tilde{\mathbf{w}}^T\mathbf{w}}{\mathbf{w}^T\mathbf{w}}$. Then $f_i'(\alpha) = g_i'(\mu\alpha)$ for all real $\alpha$ and for all $i$. $\mu \neq 0$ since otherwise all the $f_i$'s are affine. By Lemma 9 this implies that $\mu f_i(\alpha) = g_i(\mu\alpha) + c_i$ for some constants $c_i$.

Similar to the proof of Theorem 3, by using the transformations $\mathbf{y} = \mathbf{K}\mathbf{x}$ and $\mathbf{y} = \frac{1}{\mu}\tilde{\mathbf{K}}\mathbf{x}$ for the two systems, respectively, we get

$$\dot{\mathbf{y}} = \hat{\mathbf{A}}\mathbf{y} + \sum_{i=1}^{n} f_i(\mathbf{e}_1^T\mathbf{y})\mathbf{e}_i$$

$$\dot{\mathbf{y}} = \hat{\mathbf{A}}\mathbf{y} + \frac{1}{\mu}\sum_{i=1}^{n} g_i(\mu\mathbf{e}_1^T\mathbf{y})\mathbf{e}_i$$

Using $\mu f_i(\alpha) = g_i(\mu\alpha) + c_i$ these two systems simplify to

$$\dot{\mathbf{y}} = \hat{\mathbf{A}}\mathbf{y} + \frac{1}{\mu}\sum_{i=1}^{n}(g_i(\mu\mathbf{e}_1^T\mathbf{y}) + c_i)\mathbf{e}_i$$

and

$$\dot{\mathbf{y}} = \hat{\mathbf{A}}\mathbf{y} + \sum_{i=1}^{n} g_i(\mathbf{e}_1^T\mathbf{y})\mathbf{e}_i$$

Now if they share an equilibrium point $\mathbf{y}^* = \mathbf{0}$, then $\hat{\mathbf{A}}\mathbf{y}^* + \frac{1}{\mu}\sum_{i=1}^n (d_i + c_i)\mathbf{e}_i = \mathbf{0}$ for the first system, and $\hat{\mathbf{A}}\mathbf{y}^* + \frac{1}{\mu}\sum_{i=1}^n d_i\mathbf{e}_i = \mathbf{0}$ for the second system, where $d_i = g_i(\mu\mathbf{e}_1^T\mathbf{y}^*)$ if the equilibrium point is real, and $d_i = \mu g_i'(\mu\mathbf{e}_1^T\hat{\mathbf{y}})\mathbf{e}_1^T(\mathbf{y}^* - \hat{\mathbf{y}}) + g_i(\mu\mathbf{e}_1^T\hat{\mathbf{y}})$ if the equilibrium point is virtual due to linearization around $\hat{\mathbf{y}}$. In either case, we see that $c_i = 0$ for all $i$, thus the two systems are linearly conjugate. ■

For completeness, we will state the following analog of Theorem 4 for class $C_n$.

**Theorem 9.** *Consider two systems in* $C_n$

$$\dot{\mathbf{x}} = \mathbf{A}_1\mathbf{x} + \sum_{i=1}^{\infty} f_i(\mathbf{w}_1^T\mathbf{x})\mathbf{b}_{i,1} = \mathbf{h}_1(\mathbf{x}) \tag{62}$$

*and*

$$\dot{\mathbf{y}} = \mathbf{A}_2\mathbf{y} + \sum_{i=1}^{\infty} g_i(\mathbf{w}_2^T\mathbf{y})\mathbf{b}_{i,2} = \mathbf{h}_2(\mathbf{y}) \tag{63}$$

*where $f_i$ and $g_i$ are differentiable functions and $\mathbf{A}_1$ and $\mathbf{A}_2$ are $n \times n$ matrices. Suppose that both systems are proper. Suppose further that $\mathbf{T}$ is an nonsingular matrix and $\mathbf{t}$ is a vector such that $\tilde{\mathbf{x}}$ and $\tilde{\mathbf{y}} = \mathbf{T}\tilde{\mathbf{x}} + \mathbf{t}$ are real equilibrium points of (62) and (63), respectively and $D\mathbf{h}_1(\mathbf{x})$ shares the same eigenvalues as $D\mathbf{h}_2(\mathbf{T}\mathbf{x} + \mathbf{t})$ for all $\mathbf{x}$, then the two systems (62) and (63) are topologically conjugate.*

The simplest case of nonlinear vector fields in $\mathcal{C}_n$ are the continuous piecewise-linear vector fields where the boundary planes are parallel. Parallel boundary planes mean that in the consistent variation property $\mathbf{J}_1 - \mathbf{J}_2 = \mathbf{c}\mathbf{a}^T$ the vector $\mathbf{a}$ is the same at all boundaries. It is easy to show that all piecewise-linear vector fields with parallel boundary planes belong to class $\mathcal{C}_n$. Thus we get the following corollary to Theorem 8:

**Corollary 3.** *Two proper continuous piecewise-linear vector fields with parallel boundary planes are topologically conjugate if the boundary planes and the equilibrium points are matched up and the eigenvalues are the same in corresponding regions.*

In Komuro [1988] it was shown that $n$-dimensional 2-region proper piecewise-linear vector fields are topologically conjugate if the eigenvalues in corresponding regions are the same. In Feldmann & Schwarz [1994] this is shown for all $n$-dimensional 3-region odd-symmetric piecewise-linear vector fields. Corollary 3 extends these results to the class of proper continuous piecewise-linear vector fields with parallel boundary planes.

## 8. A Dual Result

Just as controllability is the dual concept of observability [Chen, 1984], we present here a dual version of Theorem 7. Instead of considering whether $(\mathbf{A}, \mathbf{w})$ satisfy condition $K$, we consider the pair $(\mathbf{A}^T, \mathbf{b})$.

**Theorem 10.** *Consider two systems of the form*

$$\dot{\mathbf{x}} = \mathbf{A}\mathbf{x} + f(\mathbf{w}_1^T\mathbf{x}, \mathbf{w}_2^T\mathbf{x}, \ldots, \mathbf{w}_i^T\mathbf{x}, \ldots)\mathbf{b} \quad (64)$$

*and*

$$\dot{\tilde{\mathbf{x}}} = \tilde{\mathbf{A}}\tilde{\mathbf{x}} + f(\tilde{\mathbf{w}}_1^T\tilde{\mathbf{x}}, \tilde{\mathbf{w}}_2^T\tilde{\mathbf{x}}, \ldots, \tilde{\mathbf{w}}_i^T\tilde{\mathbf{x}}, \ldots)\tilde{\mathbf{b}} \quad (65)$$

*Suppose that $(\mathbf{A}^T, \mathbf{b})$ and $(\tilde{\mathbf{A}}^T, \tilde{\mathbf{b}})$ satisfy condition $K$. Then system (64) and system (65) are linearly conjugate if the eigenvalues of $\mathbf{A}$ and $\tilde{\mathbf{A}}$ are the same and the eigenvalues of $\mathbf{A} + \mathbf{b}\mathbf{w}_i^T$ and $\tilde{\mathbf{A}} + \tilde{\mathbf{b}}\tilde{\mathbf{w}}_i^T$ are the same for each $i$.*

*Proof.* Let $\mathbf{K} = \mathbf{K}(\mathbf{A}^T, \mathbf{b})$ and $\tilde{\mathbf{K}} = \mathbf{K}(\tilde{\mathbf{A}}^T, \tilde{\mathbf{b}})$, which by hypothesis are nonsingular. Using the transformations $\mathbf{x} = \mathbf{K}^T\mathbf{y}$, and $\tilde{\mathbf{x}} = \tilde{\mathbf{K}}^T\tilde{\mathbf{y}}$, we get the following systems:

$$\begin{aligned}
\dot{\mathbf{y}} &= (\mathbf{K}^T)^{-1}\mathbf{A}\mathbf{K}^T\mathbf{y} + f(\mathbf{w}_1^T\mathbf{K}^T\mathbf{y}, \mathbf{w}_2^T\mathbf{K}^T\mathbf{y}, \ldots, \\
&\qquad \mathbf{w}_i^T\mathbf{K}^T\mathbf{y}, \ldots)(\mathbf{K}^T)^{-1}\mathbf{b} \\
&= \hat{\mathbf{A}}^T\mathbf{y} + f(\mathbf{w}_1^T\mathbf{K}^T\mathbf{y}, \mathbf{w}_2^T\mathbf{K}^T\mathbf{y}, \ldots, \mathbf{w}_i^T\mathbf{K}^T\mathbf{y}, \ldots)\mathbf{e}_1 \\
\dot{\tilde{\mathbf{y}}} &= (\tilde{\mathbf{K}}^T)^{-1}\tilde{\mathbf{A}}\tilde{\mathbf{K}}^T\tilde{\mathbf{y}} + f(\tilde{\mathbf{w}}_1^T\tilde{\mathbf{K}}^T\tilde{\mathbf{y}}, \tilde{\mathbf{w}}_2^T\tilde{\mathbf{K}}^T\tilde{\mathbf{y}}, \ldots, \\
&\qquad \tilde{\mathbf{w}}_i^T\tilde{\mathbf{K}}^T\tilde{\mathbf{y}}, \ldots)(\tilde{\mathbf{K}}^T)^{-1}\tilde{\mathbf{b}} \\
&= \hat{\mathbf{A}}^T\tilde{\mathbf{y}} + f(\tilde{\mathbf{w}}_1^T\tilde{\mathbf{K}}^T\tilde{\mathbf{y}}, \tilde{\mathbf{w}}_2^T\tilde{\mathbf{K}}^T\tilde{\mathbf{y}}, \ldots, \tilde{\mathbf{w}}_i^T\tilde{\mathbf{K}}^T\tilde{\mathbf{y}}, \ldots)\mathbf{e}_1
\end{aligned}$$

where $\hat{\mathbf{A}}$ is defined in Eq. (5). By Lemma 6 and the hypothesis, for each $i$, the vectors $\mathbf{K}\mathbf{w}_i$ and $\tilde{\mathbf{K}}\tilde{\mathbf{w}}_i$ are uniquely determined by the eigenvalues of $\mathbf{A}$ and $\mathbf{A} + \mathbf{b}\mathbf{w}_i^T$ and are thus equal to each other. ■

## 9. Conclusions

We have identified a class of vector fields where the members are topologically conjugate whenever the Jacobian matrices have the same eigenvalues at each point and the equilibrium points are matched up. Since Chua's oscillator belongs to this class and can synthesize a large set of eigenvalue patterns, this implies that Chua's oscillator is topologically conjugate to a large class of vector fields. This extends previous results which deal only with three-dimensional odd-symmetric 3-segment piecewise-linear vector fields. The topological conjugacy part of the main result can be extended to systems with multiple scalar nonlinearities and we use that to prove that almost all continuous piecewise-linear vector fields with parallel boundary planes are topologically conjugate if the boundaries and equilibrium points are the same and the eigenvalues in corresponding regions are the same. This result also extends previously known results which are limited to 2-segment and 3-segment odd-symmetric piecewise-linear vector fields.

## Acknowledgments

This work is supported in part by the Office of Naval Research under grant N00014-89-J-1402, and by the

Joint Services Electronics Program under contract number F49620-94-C-0038. The United States Government is authorized to reproduce and distribute reprints for governmental purposes not withstanding any copyright notation hereon.

## References

Arnéodo, A., Coullet, P. & Spiegel, E. A. [1982] "Chaos in a finite macroscopic system," *Phys. Lett.* **A92**(8), 369–373.

Brockett, R. W. [1982] "On conditions leading to chaos in feedback systems," in *Proc. IEEE Conf. on Decision and Control*, 932–936.

Chen, C.-T. [1984] *Linear System Theory and Design* (Holt, Rinehart and Winston, New York).

Chua, L. O. & Kang, S. M. [1977] "Section-wise piecewise-linear functions: Canonical representation, properties, and applications," *Proc. IEEE* **65**(6), 915–929.

Chua, L. O. [1993] "Global unfolding of Chua's circuits," *IEICE Trans. Fundamentals of Electronics, Communications and Computer Sciences* **E76-A**, 704–734.

Feldmann, U. & Schwarz, W. [1994] "Linear conjugacy of $n$-dimensional piecewise-linear systems," *IEEE Trans. Circuits and Systems–I: Fundamental Theory and Applications* **41**(2), 190–192.

Götz, M., Feldmann, U. & Schwarz, W. [1993], "Synthesis of higher-dimensional Chua circuits," *IEEE Trans. Circuits and Systems–I: Fundamental Theory and Applications* **40**(11), 854–860; *Special Issue on Chaos in Electronic Circuits, Part B.*

Huang, A., Pivka, L., Wu, C.-W. & Franz, M. [1996] "Chua's equation with cubic nonlinearity," *Int. J. of Bifurcation and Chaos* **6**(8), (to appear).

Kennedy, M. P. [1994] "Chaos in the Colpitts oscillator," *IEEE Trans. Circuits and Systems–I: Fundamental Theory and Applications* **41**(11), 771–774.

Kocarev, L., Karadzinov, L. & Chua, L. O. [1993] "$n$-dimensional canonical Chua's circuit," *J. Circuits, Syst. Computers* **3**(1), 239–258.

Komuro, M. [1988], "Normal forms of continuous piecewise-linear vector fields and chaotic attractors, Part II: Chaotic attractors," *Jpn. J. Appl. Math.* **5**, 503–549.

Madan, R., Guest Editor [1993] "Special issue on Chua's circuit: A paradigm for chaos, Part I," *J. Circuits, Syst. Computers* **3**(1).

Matsumoto, T., Chua, L. O. & Kobayashi, K. [1986], "Hyperchaos: Laboratory experiment and numerical confirmation," *IEEE Trans. Circuits and Systems* **33**(11), 1143–1147.

Nishio, Y., Inaba, N. & Mori, S. [1990] "Chaotic phenomena in an autonomous circuit with nonlinear inductor," in *ISCAS*, 942–945.

Nishio, Y., Mori, S. & Saito, T. [1992] "Extremely simple hyperchaos generators including one diode," in *Proc. of the 1992 IEEE Int. Symp. on Circuits and Systems*, Vol. 6, 2797–2800.

Ogorzałek, M. J. [1989] "Order and chaos in a third order RC ladder network with nonlinear feedback," *IEEE Trans. Circuits and Systems* **36**(9), 1221–1230.

Rul'kov, N. F., Volkovskii, A. R., Rodríguez-Lozano, A., Río, E. D. & Velarde, M. G. [1992] "Mutual synchronization of chaotic self-oscillators with dissipative coupling," *Int. J. of Bifurcation and Chaos* **2**(3), 669–676.

Shil'nikov, L. P. [1994] "Chua's circuit: Rigorous results and future problems," *Int. J. of Bifurcation and Chaos* **4**(3), 489–519.

Sparrow, C. T. [1981] "Chaos in a three-dimensional single loop feedback system with a piecewise-linear feedback function," *J. Mathematical Analysis and Applications* **83**, 275–291.

Vidyasagar, M. [1978] *Nonlinear Systems Analysis* (Prentice-Hall, New Jersey).

## Appendix 1

In this appendix we present three-dimensional phase projections of attractors from several well-known three-dimensional chaotic systems and their counterparts from the three-dimensional Chua's oscillator by applying Theorem 6. In cases where Eq. (33) is not satisfied, $s_{n-1}$ is decreased by a small amount when applying Algorithm 1.

### *Chaotic Colpitts oscillator*

The state equations of the chaotic Colpitts oscillator [Kennedy, 1994] are given by:

$$C_1\frac{dV_{CE}}{dt} = I_L - I_C$$

$$C_2\frac{dV_{BE}}{dt} = -\frac{V_{EE}+V_{BE}}{R_{EE}} - I_L - I_B$$

$$L\frac{dI_L}{dt} = V_{CC} - V_{CE} + V_{BE} - I_L R_L$$

where

$$I_B = \begin{cases} 0 & V_{BE} \le V_{TH} \\ \dfrac{V_{BE}-V_{TH}}{R_{ON}} & V_{BE} > V_{TH} \end{cases}$$

$$I_C = \beta_F I_B$$

For the parameters $V_{CC} = 5$ V, $R_L = 35\ \Omega$, $L = 98.5\ \mu$H, $C_1 = C_2 = 54$ nF, $R_{EE} = 400\ \Omega$, $V_{EE} = -5$ V, $V_{TH} = 0.75$ V, $R_{ON} = 100\ \Omega$,

$\beta_F = 200$ of this system, the corresponding parameters for Chua's oscillator are given by

$$C_1 = 1$$
$$C_2 = 3.9234278162 \times 10^2$$
$$L_3 = 6.7473529008 \times 10^{-17}$$
$$R_2 = 8.2538319739 \times 10^{-9}$$
$$G_3 = 3.1852491364 \times 10^{11}$$
$$G_a = -1.2092436506 \times 10^8$$
$$G_b = -1.2110955024 \times 10^8$$
$$g(x) = \frac{1}{2}(G_a - G_b) + \frac{1}{2}(G_a + G_b)x + \frac{1}{2}(G_b - G_a)|x - 1|$$

The corresponding attractors from these two systems are shown in Figs. 7(a) and 7(b), respectively.

### *Brockett's system*

The 3rd-order scalar differential equation for Brockett's system [Brockett 1982] is given by:

$$\frac{d^3y}{dt^3} + \frac{d^2y}{dt^2} + 1.25\frac{dy}{dt} + f(y) = 0$$

where $f$ is a 3-segment piecewise-linear function given by:

$$f(y) = \begin{cases} -ky & |y| \le 1 \\ 2ky - 3k\,\mathrm{sgn}(y) & |y| \ge 1 \end{cases}$$

For $k = 1.8$, the corresponding parameters for Chua's oscillator are given by:

$$C_1 = 1$$
$$C_2 = 5.3270141220 \times 10^2$$
$$L_3 = 3.4698425778 \times 10^{-6}$$
$$R_2 = -1.8666566179 \times 10^{-3}$$
$$G_3 = 2.8657513826 \times 10^5$$
$$G_a = 5.3671716962 \times 10^2$$
$$G_b = 5.3672716962 \times 10^2$$
$$g(x) = G_b x + \frac{1}{2}(G_a - G_b)(|x + 1| - |x - 1|)$$

The corresponding attractors from these two systems are shown in Figs. 8(a) and 8(b), respectively.

### *Sparrow's system*

The state equations for Sparrow's system [Sparrow, 1981] are given by:

$$\dot{x}_1 = f(x_3) - x_1$$
$$\dot{x}_2 = x_1 - x_2$$
$$\dot{x}_3 = x_2 - x_3$$

where $f$ is a 3-segment piecewise-linear function given by:

$$f(x_3) = \begin{cases} 8.4rx_3 + 0.96276 + 2.3872r & x_3 \le 0.28419 \\ -8.4x_3 + 3.35 & 0.28419 \le x_3 \le \frac{3}{7} \\ 8.4rx_3 - 0.25 - 3.6r & x_3 \ge \frac{3}{7} \end{cases}$$

For $r = 19.0$, the corresponding parameters for Chua's oscillator are given by:

$$C_1 = 1$$
$$C_2 = -6.2252592698 \times 10^2$$
$$L_3 = 2.8731155811 \times 10^{-7}$$
$$R_2 = 5.3544019103 \times 10^{-4}$$
$$G_3 = 1.1601531225 \times 10^6$$
$$G_a = -1.8646222233 \times 10^3$$
$$G_b = -1.8645922233 \times 10^3$$
$$g(x) = G_b x + \frac{1}{2}(G_a - G_b)(|x + 1| - |x - 1|)$$

The corresponding attractors from these two systems are shown in Figs. 9(a) and 9(b), respectively.

### *Ogorzałek's system*

The state equations for Ogorzałek's system [Ogorzałek, 1989] are given by:

$$\dot{x}_1 = f(x_3) - 2x_1 + x_2$$
$$\dot{x}_2 = x_1 - 2x_2 + x_3$$
$$\dot{x}_3 = x_2 - x_3$$

where $f$ is a 3-segment piecewise-linear function given by:

$$f(x_3) = \begin{cases} m_1x_3 + m_1 - m_0 & x_3 \le -1 \\ m_0x_3 & |x_3| \le 1 \\ m_1x_3 + m_0 - m_1 & x_3 \ge 1 \end{cases}$$

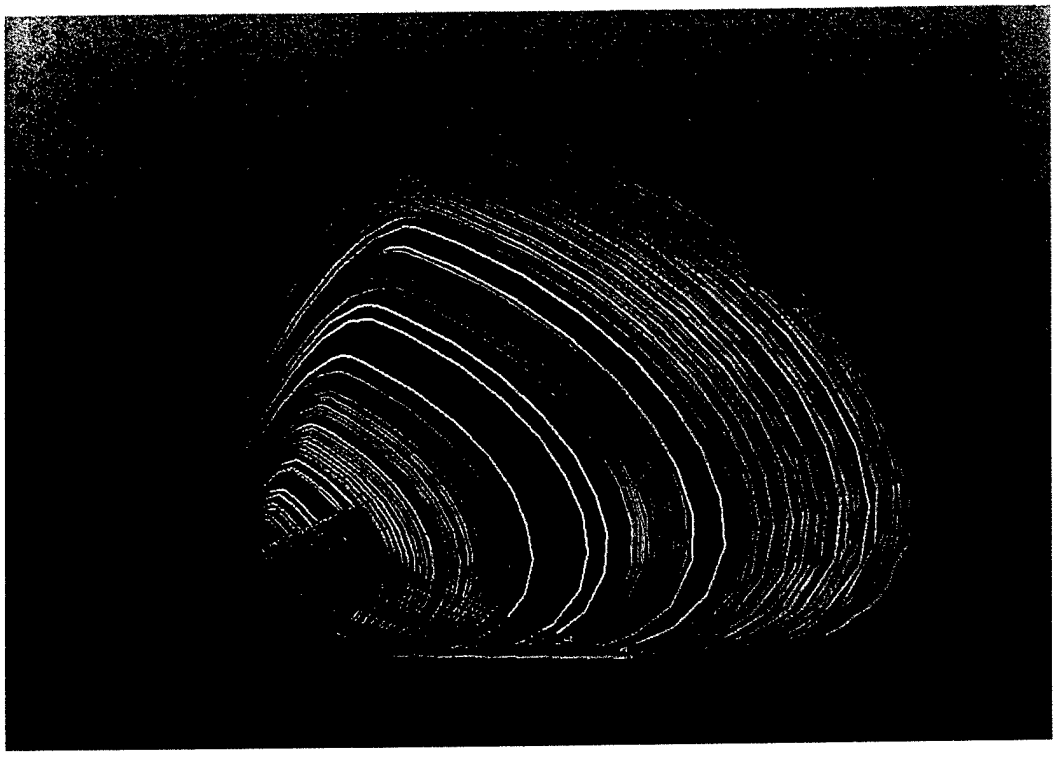

(a)

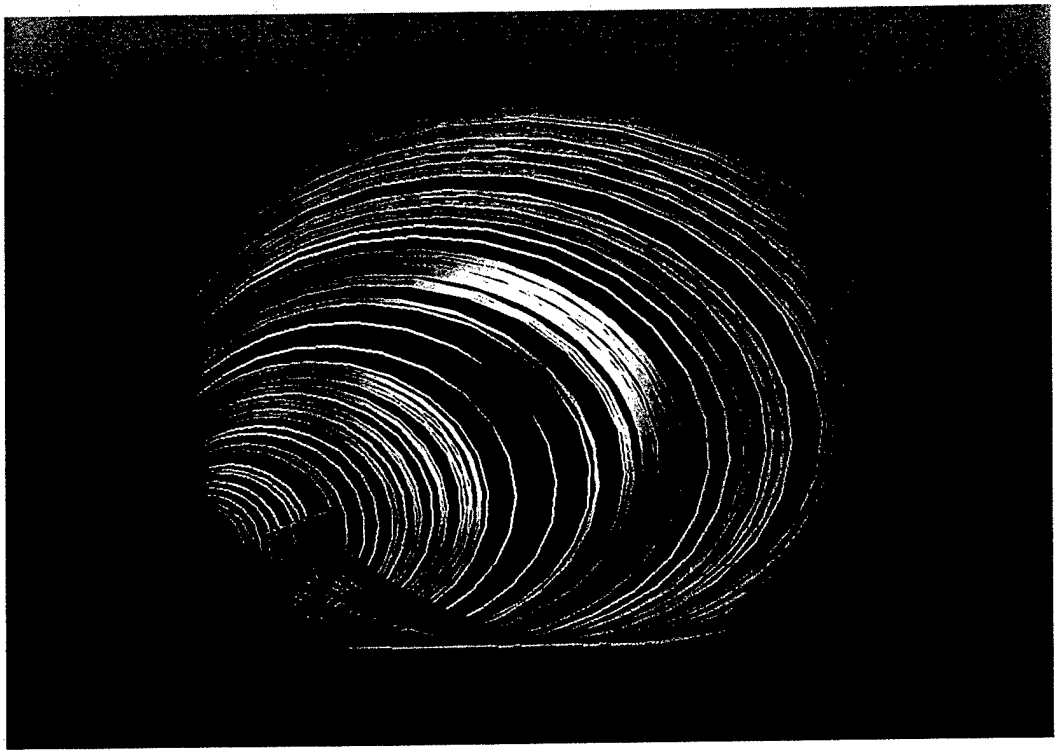

(b)

Fig. 7. (a) Phase portrait projection of a chaotic attractor in the Colpitts oscillator. (b) Phase portrait projection of a chaotic attractor in Chua's oscillator topologically conjugate to Fig. 7(a).

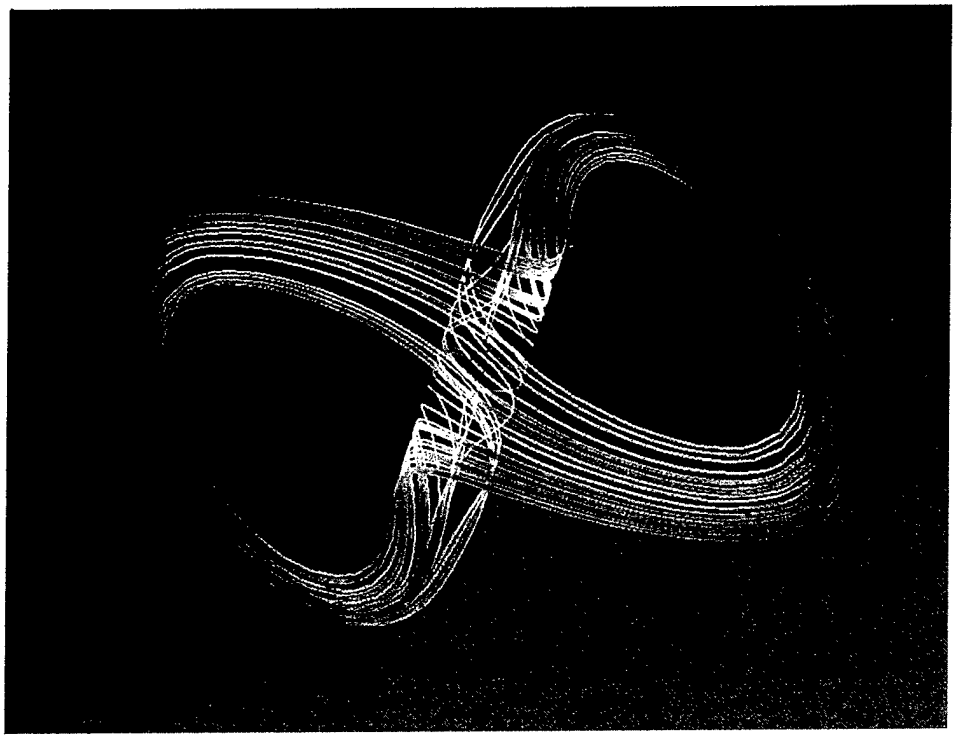

(a)

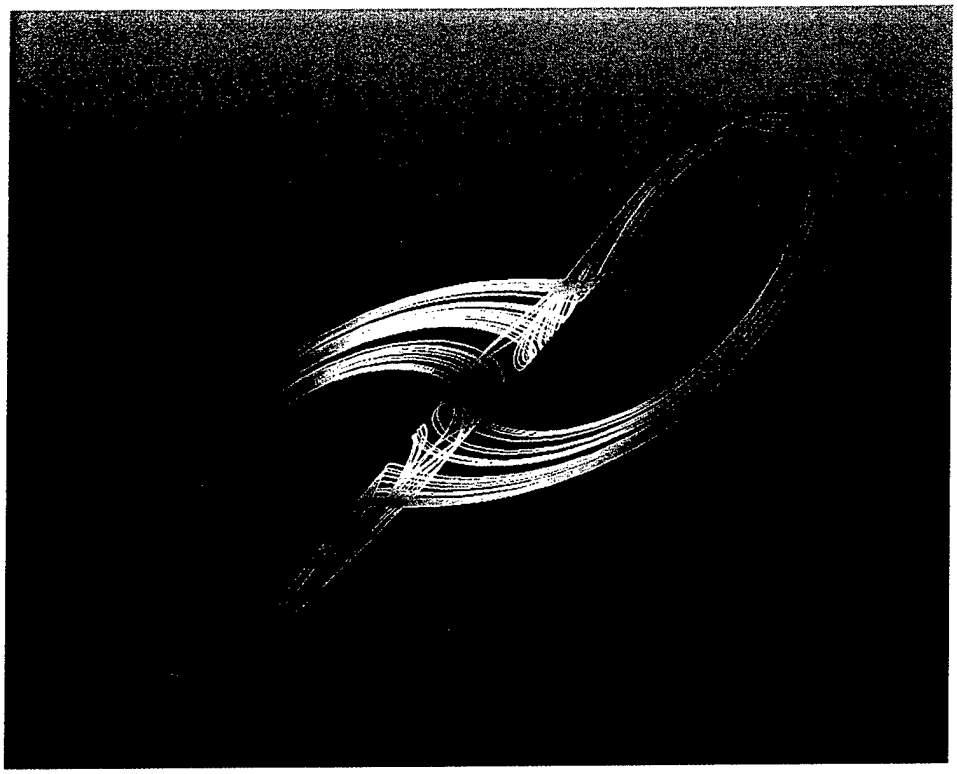

(b)

Fig. 8. (a) Phase portrait projection of a chaotic attractor in Brockett's feedback system. (b) Phase portrait projection of a chaotic attractor in Chua's oscillator similar to Fig. 8(a).

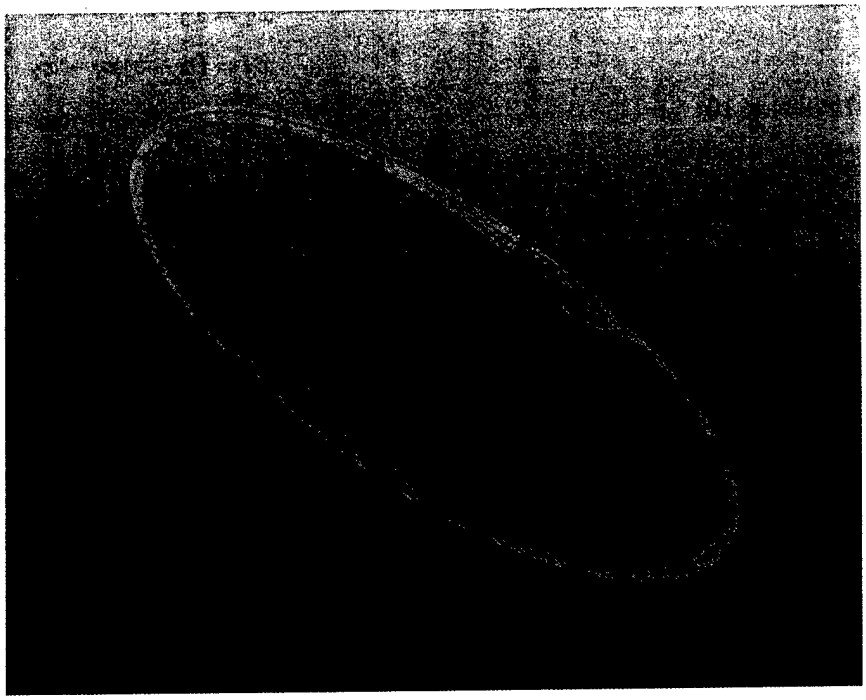

(a)

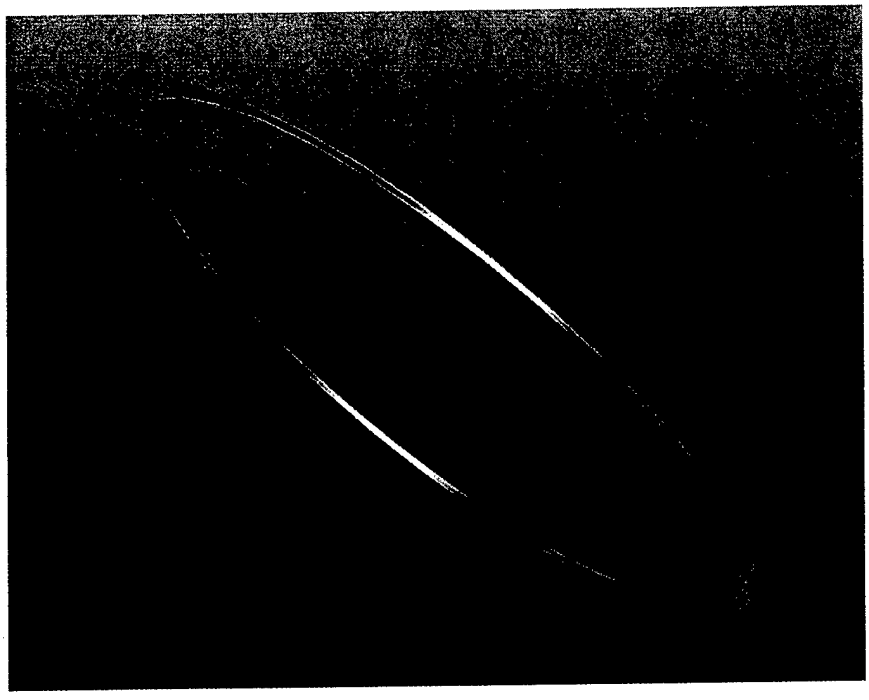

(b)

Fig. 9. (a) Phase portrait projection of a chaotic attractor in Sparrow's system. (b) Phase portrait projection of a chaotic attractor in Chua's oscillator similar to Fig. 9(a).

For $m_0 = -33.03$ and $m_1 = 400$, the corresponding parameters for Chua's oscillator are given by:

$$C_1 = 1$$
$$C_2 = -3.4660736904 \times 10^2$$
$$L_3 = 3.3408722323 \times 10^{-7}$$
$$R_2 = 5.7696798665 \times 10^{-4}$$
$$G_3 = 5.9859025418 \times 10^5$$
$$G_a = -1.7281984151 \times 10^3$$
$$G_b = -1.7281484151 \times 10^3$$
$$g(x) = G_b x + \frac{1}{2}(G_a - G_b)(|x+1| - |x-1|)$$

The corresponding attractors from these two systems are shown in Figs. 10(a) and 10(b), respectively.

### *Arnéodo's system*

The 3rd-order scalar differential equation for Arnéodo's system [Arnéodo *et al.*, 1982] are given by:

$$\frac{d^3y}{dt^3} + \mu_2\frac{d^2y}{dt^2} + \mu_1\frac{dy}{dt} + \mu_0 y = \mu y^3$$

For $\mu = -1$, $\mu_0 = -5.5$, $\mu_1 = 3.5$, $\mu_2 = 1$, the corresponding parameters for Chua's oscillator are given by:

$$C_1 = 1$$
$$C_2 = 8.0737820354 \times 10^1$$
$$L_3 = 1.2239479563 \times 10^{-4}$$
$$R_2 = -1.1329163199 \times 10^{-2}$$
$$G_3 = 7.4732911509 \times 10^3$$
$$G_a = 8.9267772512 \times 10^1$$
$$G_b = 8.9277772512 \times 10^1$$
$$g(x) = G_a x + (G_b - G_a)x^3$$

The corresponding attractors from these two systems are shown in Figs. 11(a) and 11(b), respectively.

### *Nishio's system*

The state equations for Nishio's system [Nishio *et al.*, 1990] are given by:

$$\dot{x}_1 = -b(f(x_1) + x_3)$$
$$\dot{x}_2 = x_3$$
$$\dot{x}_3 = (a-b)x_3 - x_2 - bf(x_1)$$

where $f$ is a 3-segment piecewise-linear function given by:

$$f(x_1) = \begin{cases} m_1 x_1 + m_1 - m_0 & x_1 \le -1 \\ m_0 x_1 & |x_1| \le 1 \\ m_1 x_1 + m_0 - m_1 & x_1 \ge 1 \end{cases}$$

For $m_0 = -0.5$ and $m_1 = 10$, $a = 0.3$, $b = 1$, the corresponding parameters for Chua's oscillator are given by:

$$C_1 = 1$$
$$C_2 = -3.2604757879 \times 10^{-2}$$
$$L_3 = -2.7603333333$$
$$R_2 = -1.0111111111 \times 10^1$$
$$G_3 = 1.0868252626 \times 10^{-1}$$
$$G_a = 5.9890109890 \times 10^{-1}$$
$$G_b = 1.1098901099 \times 10^1$$
$$g(x) = G_b x + \frac{1}{2}(G_a - G_b)(|x+1| - |x-1|)$$

The corresponding attractors from these two systems are shown in Figs. 12(a) and 12(b), respectively.

### *Dmitriev's system*

The state equations for Dmitriev's system [Rul'kov *et al.*, 1992] are given by:

$$\dot{x}_1 = x_2$$
$$\dot{x}_2 = -x_1 - \delta x_2 + x_3$$
$$\dot{x}_3 = \gamma(F(x_1) - x_3) - \sigma x_2$$

where $F$ is given by:

$$F(x_1) = \begin{cases} 0.528\alpha & x_1 < -1.2 \\ \alpha x_1(1 - x_1^2) & |x_1| \le 1.2 \\ -0.528\alpha & x_1 \ge 1.2 \end{cases} \quad (66)$$

For $\alpha = 20$, $\delta = 0.43$, $\sigma = 0.71$, $\gamma = 0.1$, the corresponding parameters for Chua's oscillator are

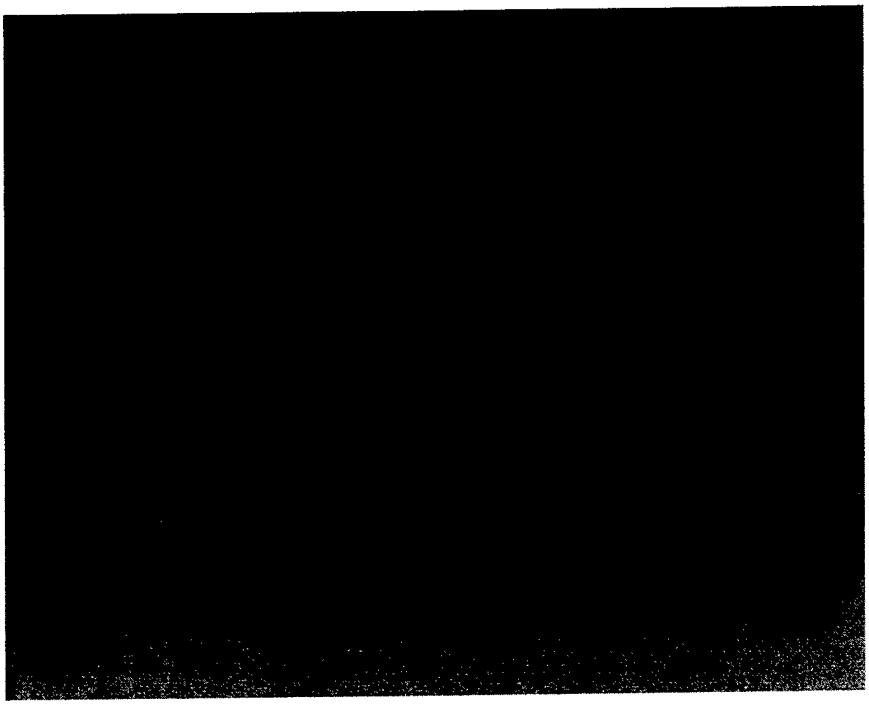

(a)

(b)

Fig. 10. (a) Phase portrait projection of a chaotic attractor in Ogorzalek's system. (b) Phase portrait projection of a chaotic attractor in Chua's oscillator similar to Fig. 10(a).

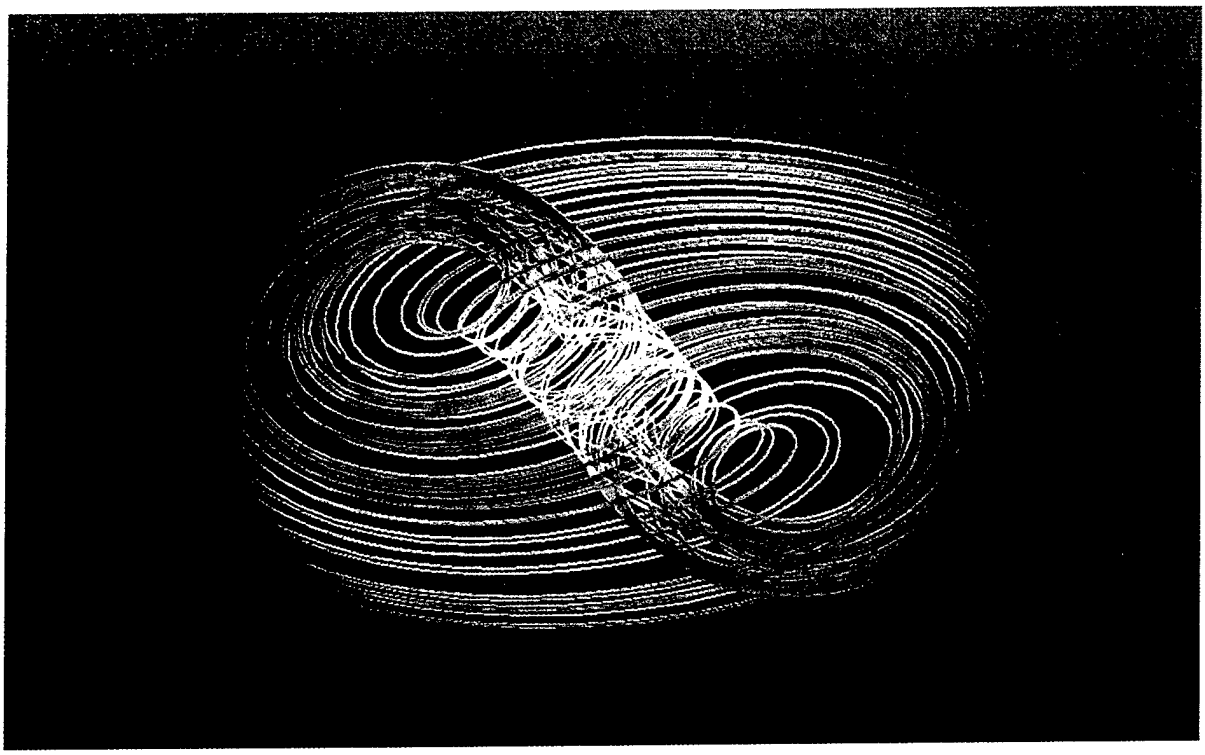

(a)

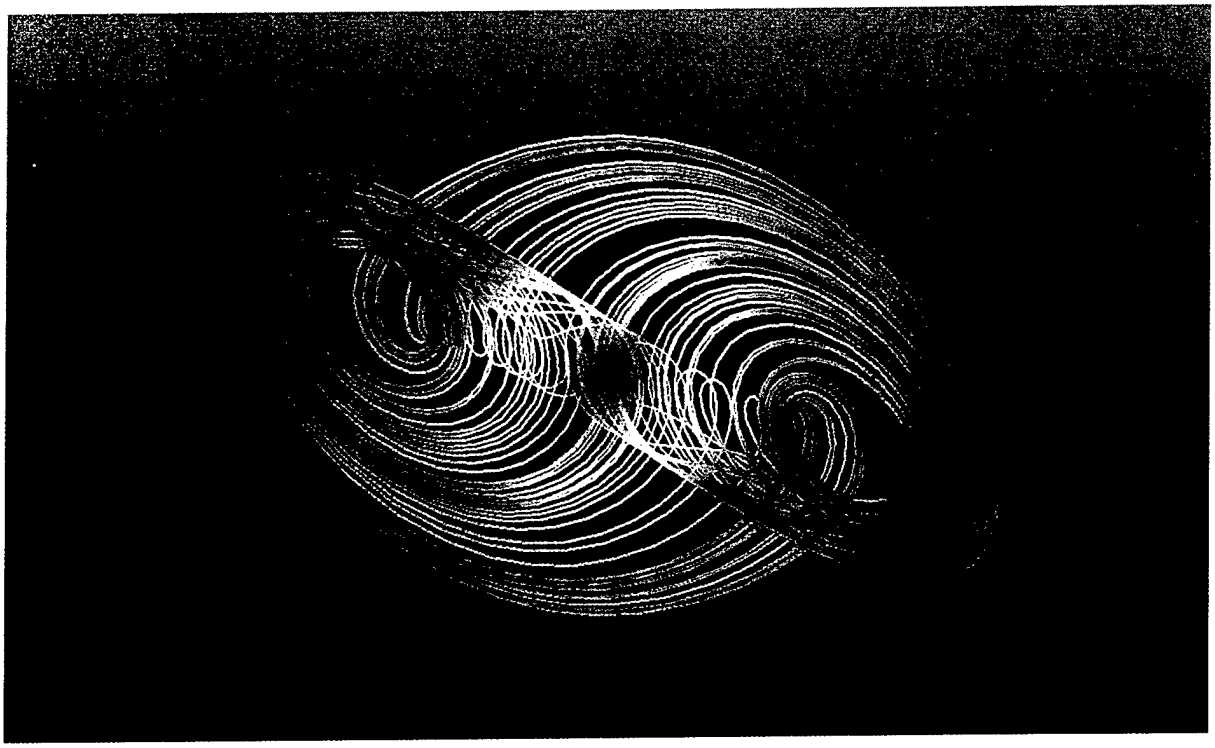

(b)

Fig. 11. (a) Phase portrait projection of a chaotic attractor in Arnéodo's system. (b) Phase portrait projection of a chaotic attractor in Chua's oscillator similar to Fig. 11(a).

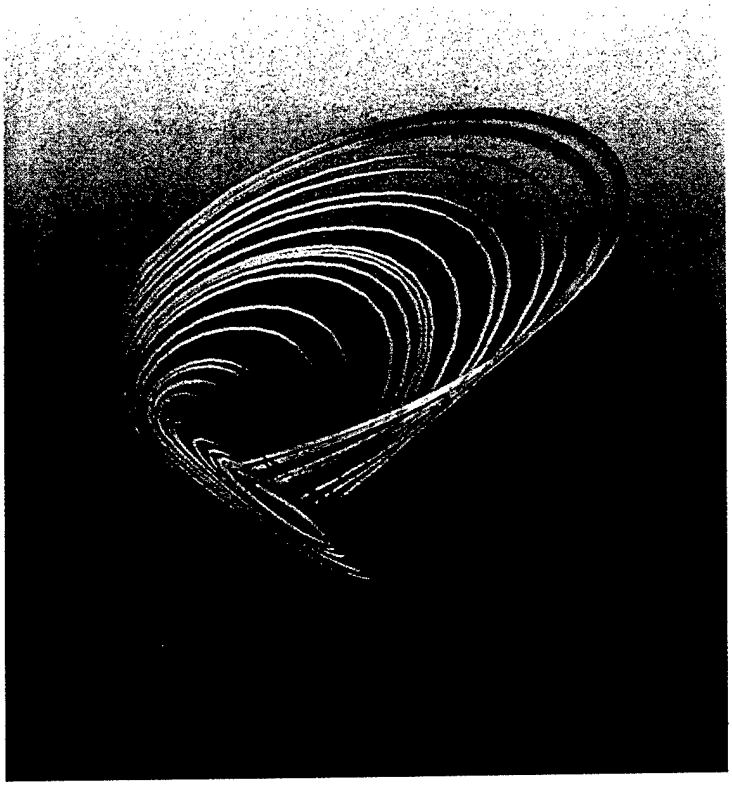

(a)

(b)

Fig. 12. (a) Phase portrait projection of a chaotic attractor in Nishio's system. (b) Phase portrait projection of a chaotic attractor in Chua's oscillator topologically conjugate to Fig. 12(a).

(a)

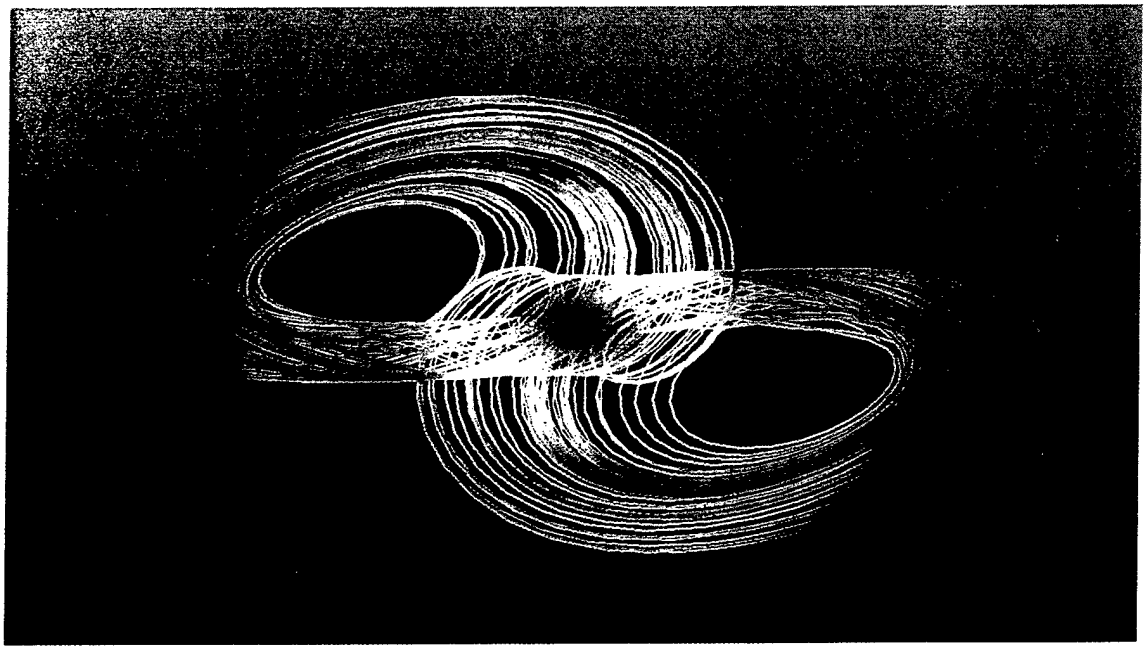

(b)

Fig. 13. (a) Phase portrait projection of a chaotic attractor in Dmitriev's system. (b) Phase portrait projection of a chaotic attractor in Chua's oscillator similar to Fig. 13(a).

given by:

$$\begin{aligned} C_1 &= 1 \\ C_2 &= -8.9906258405 \times 10^1 \\ L_3 &= 5.6294509561 \times 10^{-4} \\ R_2 &= 2.2612337453 \times 10^{-2} \\ G_3 &= 3.6113480161 \times 10^3 \\ G_a &= -4.3693645701 \times 10^1 \\ G_b &= -4.3688645701 \times 10^1 \\ g(x) &= G_a x + (G_b - G_a)F(x) \end{aligned}$$

where $F(\cdot)$ is given by (66). The corresponding attractors from these two systems are shown in Figs. 13(a) and 13(b), respectively.

## Appendix 2

We give in this Appendix a different $n$-dimensional circuit which is presented in Kocarev *et al.* [1993]. This circuit can also synthesize almost all eigenvalue patterns in $\mathcal{C}$. The circuit diagram for $n$ is even and $n$ is odd is shown in Figs. 14(a) and 14(b), respectively.

The state equations are given by:

$$\frac{d\mathbf{x}}{dt} = \mathbf{A}\mathbf{x} - \frac{g(\mathbf{e}_1^T\mathbf{x})}{C_1}\mathbf{e}_1$$

where $g(\cdot)$ is the $v$-$i$ characteristic of the nonlinear resistor and $\mathbf{A}$ is given by:

$$\mathbf{A} = \begin{bmatrix} 0 & \frac{1}{C_1} & 0 & 0 & 0 & \cdots & 0 & 0 & 0 \\ -\frac{1}{L_2} & -\frac{R_2}{L_2} & \frac{1}{L_2} & 0 & 0 & \cdots & 0 & 0 & 0 \\ 0 & -\frac{1}{C_3} & -\frac{G_3}{C_3} & \frac{1}{C_3} & 0 & \cdots & 0 & 0 & 0 \\ \vdots & \vdots & \vdots & & & \vdots & \vdots & \vdots & \\ 0 & 0 & 0 & 0 & \cdots & 0 & -\frac{1}{C_{n-1}} & -\frac{G_{n-1}}{C_{n-1}} & \frac{1}{C_{n-1}} \\ 0 & 0 & 0 & 0 & \cdots & 0 & 0 & -\frac{1}{L_n} & \frac{R_n}{L_n} \end{bmatrix}$$

if $n$ is even and

$$\mathbf{A} = \begin{bmatrix} 0 & \frac{1}{C_1} & 0 & 0 & 0 & \cdots & 0 & 0 & 0 \\ -\frac{1}{L_2} & -\frac{R_2}{L_2} & \frac{1}{L_2} & 0 & 0 & \cdots & 0 & 0 & 0 \\ 0 & -\frac{1}{C_3} & -\frac{G_3}{C_3} & \frac{1}{C_3} & 0 & \cdots & 0 & 0 & 0 \\ \vdots & \vdots & \vdots & & & \vdots & \vdots & \vdots & \\ 0 & 0 & 0 & 0 & \cdots & 0 & -\frac{1}{L_{n-1}} & -\frac{R_{n-1}}{L_{n-1}} & \frac{1}{L_{n-1}} \\ 0 & 0 & 0 & 0 & \cdots & 0 & 0 & -\frac{1}{C_n} & \frac{G_n}{C_n} \end{bmatrix}$$

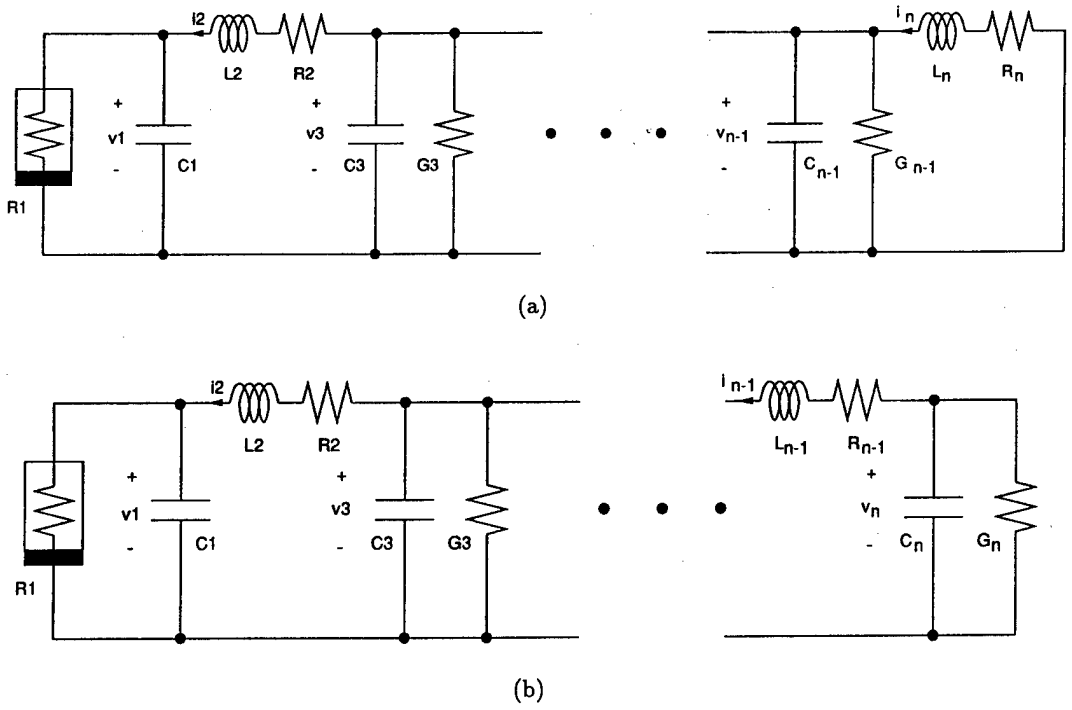


Fig. 14. $n$-dimensional circuit given in Kocarev *et al.* [1993]. (a) $n$ is even. (b) $n$ is odd.

if $n$ is odd. Applying Algorithm 1, the following assignment of circuit parameters will give the desired topologically conjugate system when $g(\cdot)$ is given by (29):

$$
\begin{aligned}
C_1 &= 1 \\
G_a &= -\kappa_1 C_1 \\
G_b &= -\overline{a}_{1,1} C_1 \\
L_2 &= -\frac{1}{\rho_1 C_1} \\
R_2 &= -\kappa_2 L_2 \\
C_3 &= -\frac{1}{\rho_2 L_2} \\
&\vdots \\
G_{2l-1} &= -\kappa_{2l-1} C_{2l-1} \\
L_{2l} &= -\frac{1}{\rho_{2l-1} C_{2l-1}} \\
R_{2l} &= -\kappa_{2l} L_{2l} \\
C_{2l+1} &= -\frac{1}{\rho_{2l} L_{2l}} \\
&\vdots \\
R_n &= -\kappa_n L_n, \quad \text{if } n \text{ is even} \\
G_n &= -\kappa_n C_n, \quad \text{if } n \text{ is odd}
\end{aligned}
$$

Other circuit topologies for synthesizing eigenvalue patterns in $\mathcal{C}$ are given in Götz *et al.* [1993].

Journal of Circuits, Systems, and Computers, Vol. 6, No. 3 (1996) 227–241
© World Scientific Publishing Company

# SYNCHRONIZING NONAUTONOMOUS CHAOTIC SYSTEMS WITHOUT PHASE-LOCKING

CHAI WAH WU, GUO-QUN ZHONG, and LEON O. CHUA
*Electronics Research Laboratory and*
*Department of Electrical Engineering and Computer Sciences,*
*University of California at Berkeley, Berkeley, CA 94720, USA*

Received 17 November 1994
Revised 20 March 1995

Pecora and Carroll[1] have shown how two nonautonomous chaotic circuits driven by periodic forcing can be synchronized using the master-slave driving principle. However, in their scheme, the periodic forcing in both circuits needs to be phase-locked through some additional circuitry for the system to synchronize. In this paper, we show two ways in which this can be avoided.

In the first scheme, the two circuits are connected in a master-slave driving configuration and the periodic forcing is included in the driving signal such that it eliminates the need for the slave circuit to have an external periodic forcing signal. In addition, we can recover the periodic forcing signal at the slave circuit.

In the second scheme, the two circuits are connected in a mutual coupling configuration. The two circuits will synchronize regardless of what the periodic forcing signals of the two circuits are. In particular, the two periodic forcing signals could have different phases, different frequencies, or different shapes.

We discuss two interpretations of these synchronization schemes. First, we consider them as communication systems when the periodic forcing signal is replaced by a properly encoded information signal. We illustrate this in a physical circuit implementation. Second, we consider them as synchronization schemes for nonidentical systems by considering the external forcing signal as an error signal due to the difference between the two systems.

## 1. Introduction

Pecora and Carroll[1] have shown how two nonautonomous chaotic circuits driven by periodic forcing can be synchronized. Since the two circuits need to be identical to synchronize, the periodic forcing in the two circuits must have the same phase. In their implementation, the two periodic forcing signals need to be phase-locked through some additional circuitry for the two circuits to synchronize. In Ref. 2, computer simulations were performed on two nonautonomous chaotic circuits where the periodic forcing signals in both circuits also have the same phase. We show here two cases where such phase-locking is not necessary for synchronization.

First, we show a master-slave driving scheme where the periodic forcing is included in the driving signal, and which eliminates the need for the slave system to

have an external periodic forcing signal. We can then recover the periodic forcing signal from the driving signal.

Second, we show a mutual coupling scheme, where the two systems are synchronized regardless of whether the periodic forcing signals in the two systems are identical or not.

One of the key properties of these synchronization schemes for nonautonomous systems is that the external inputs to the two systems do not need to have the same phase. In fact, they can be arbitrary and completely different. This allows us to use them as communication systems or synchronization schemes for two systems which are not identical. These schemes can be considered as communication systems when the periodic driving signal is replaced by a properly encoded information signal. These schemes are considered as synchronization schemes for two systems which are not identical when the external forcing signal is considered as an error signal due to mismatch between the two systems.

In this paper, we assume that we can write state equations for all the nonlinear circuits that we consider and that for each initial condition, there exists a unique solution for all time.

The organization of this paper is follows. In Sec. 2 we discuss the master-slave synchronization scheme. In Sec. 3 we discuss the possibility of synchronization through linear mutual coupling such that the periodic forcing in both systems can be different. In Sec. 4 we discuss the possibility of using these schemes as communication systems by replacing the periodic driving signals by properly encoded information signals. In Sec. 5 we discuss how we can synchronize two systems which are not identical.

## 2. Master-Slave Synchronization Scheme

In the communication systems proposed in Ref. 3, 4, the slave system is synchronized to the master system, even though the master system has an information signal

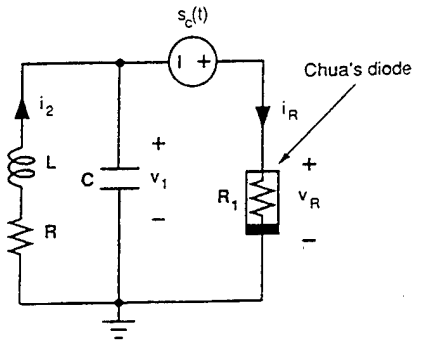


Fig. 1. Nonautonomous chaotic circuit 1. For the circuit to be chaotic, we choose $R$, $C$ and $L$ to be passive and $R_1$ to be active and have a monotone $v$-$i$ characteristic.

injected into it, while the slave system does not. As the information signal is an external source, this can be considered as synchronization of nonautonomous systems. We will use the same principles for our first synchronization scheme.

The chaotic system we use (Fig. 1) is a second order nonautonomous circuit, a modification of the circuit proposed in Ref. 5. In Ref. 5, the periodic forcing is in series with the linear resistor, while in Fig. 1, the periodic forcing is in series with the nonlinear resistor. For the circuit to be chaotic, we choose $R$, $C$ and $L$ to be passive and the nonlinear resistor $R_1$ to be active and have a monotone $v$-$i$ characteristic.

The state equations for this circuit are given by:

$$\begin{aligned} \frac{dv_1}{dt} &= \frac{1}{C}(i_2 - f_c(v_1 + s_c(t))) \\ \frac{di_2}{dt} &= -\frac{1}{L}(v_1 + i_2 R) \end{aligned} \tag{1}$$

where $s_c(t) = A_c \sin(\Omega t)$ is the periodic forcing function and the $v$-$i$ characteristic of the voltage-controlled Chua's diode $f_c(v)$ is a 3-segment piecewise-linear function given by

$$f_c(v) = G_b v + \frac{1}{2}(G_a - G_b)(|v + E| - |v - E|) \tag{2}$$

where $E > 0$.

After normalization using $G = \frac{1}{R}$, $x = \frac{v_1}{E}$, $y = \frac{i_2}{GE}$, $\tau = \frac{t}{|C/G|}$, $a = \frac{G_a}{G}$, $b = \frac{G_b}{G}$, $\omega = \Omega|C/G|$, $\beta = \frac{C}{LG^2}$, $s(t) = \frac{s_c(|C/G|t)}{E}$, $A = \frac{A_c}{E}$, and redefining $\tau$ as $t$, we obtain the following dimensionless equations:

$$\begin{aligned} \frac{dx}{dt} &= k(y - f(x + s(t))) \\ \frac{dy}{dt} &= k\beta(-x - y) \end{aligned} \tag{3}$$

where $k = 1$ if $\frac{C}{G} > 0$ and $k = -1$ if $\frac{C}{G} < 0$, $s(t) = A\sin(\omega t)$ and

$$f(x) = bx + \frac{1}{2}(a - b)(|x + 1| - |x - 1|) \tag{4}$$

We choose the following set of parameters: $a = -1.37$, $b = -0.84$, $\omega = 0.4$, $A = 0.5$, $\beta = 0.895$, and $k = 1$. A chaotic attractor for these parameters is shown in the $x$-$y$ plane in Fig. 2.

We couple two identical chaotic circuits as shown in Fig. 3 which is similar to the scheme proposed for the autonomous Chua's circuit in Ref. 3. It is based on the idea proposed in Ref. 6 that to synchronize two chaotic systems, the parts of the system that are responsible for the instability of the system are used as driving.

The corresponding normalized dimensionless state equations are given by:

$$\begin{aligned}
\frac{dx}{dt} &= k(y - f(x + A\sin(\omega t))) \\
\frac{dy}{dt} &= k\beta(-x - y) \\
\frac{d\tilde{x}}{dt} &= k(\tilde{y} - f(x + A\sin(\omega t))) \\
\frac{d\tilde{y}}{dt} &= k\beta(-\tilde{x} - \tilde{y})
\end{aligned} \tag{5}$$

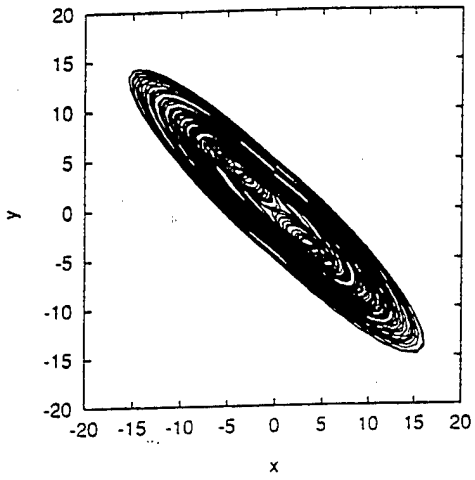


Fig. 2. Chaotic attractor for system (3) in the $x$-$y$ plane. The parameters are $a = -1.37$, $b = -0.84$, $\omega = 0.4$, $A = 0.5$, $\beta = 0.895$, and $k = 1$.

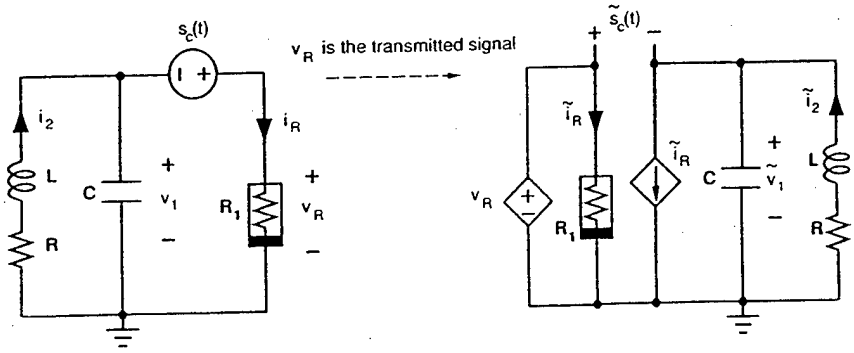


Fig. 3. Two nonautonomous chaotic circuits coupled through unidirectional coupling. This can be viewed as a communication system when the coupling is considered as the transmission of the signal $v_R$. The voltage across the controlled voltage source is $v_R$ and the current through the controlled current source is $\tilde{i}_R$. The recovered signal $\tilde{s}_c(t)$ will asymptotically approach $s_c(t)$ as $t \to \infty$.

When $k, \beta > 0$ (or $R, L, C > 0$) this setup will synchronize, i.e. $x(t) \to \tilde{x}(t)$ as $t \to \infty$. This implies that $\tilde{s}_c(t)$ in Fig. 3 approaches $s_c(t)$ as $t \to \infty$ (in the normalized equations the signal $\tilde{s}(t)$ approaches $s(t)$, where $\tilde{s}(t) = x + s(t) - \tilde{x}$). The proof that this setup will synchronize is similar to that in Ref. 3.

An alternative circuit implementation of Eqs. (5) is to transmit the current $i_R$ to the receiver circuit as shown in Fig. 4. This implementation will also synchronize the two circuits. If we assume that the nonlinear resistor $R_1$ is both current and voltage controlled (i.e., $f_c(v)$ is bijective), then $\tilde{s}_c(t)$ will approach $s_c(t)$ as $t \to \infty$.

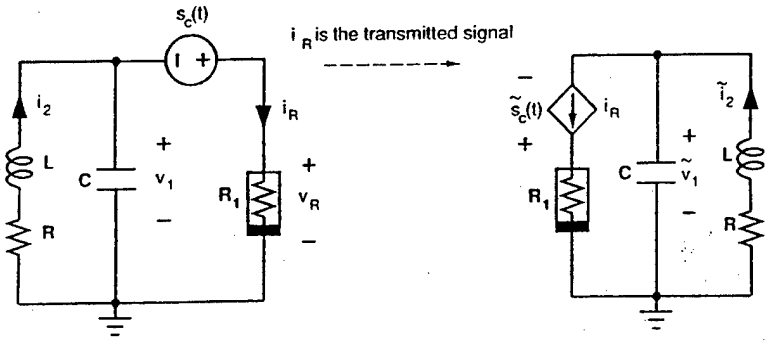


Fig. 4. Alternative way of connecting two nonautonomous chaotic circuits through unidirectional coupling. This can be viewed as a communication system when the coupling is considered as the transmission of the signal $i_R$. The current through the controlled current source is $i_R$. The recovered signal $\tilde{s}_c(t)$ will asymptotically approach $s_c(t)$ as $t \to \infty$ assuming that $R_1$ is both voltage and current controlled.

## 3. Mutual Coupling Synchronization Scheme

The nonautonomous chaotic system that we use for this scheme is similar to the circuit in Fig. 1, except that we interchange the linear resistor and the nonlinear resistor, as shown in Fig. 5. Note that this circuit is the dual circuit of the circuit in Ref. 5 except that we replace the current source in the dual circuit by a Thévenin equivalent voltage source. However, for our synchronization scheme we will use an active linear resistor and a passive nonlinear resistor with a monotone $v$-$i$ characteristic. Note that since the nonlinear resistor has a passive and monotone $v$-$i$ characteristic, the linear resistor must be active for the system to become chaotic (and exhibit sensitive dependence on initial conditions) as otherwise the system will have a unique steady state solution.[7]

The state equations for this circuit are given by:

$$\begin{aligned} \frac{dv_1}{dt} &= \frac{1}{C}\left(i_2 - \frac{1}{R}(v_1 + s_c(t))\right) \\ \frac{di_2}{dt} &= -\frac{1}{L}(v_1 + g_c(i_2)) \end{aligned} \tag{6}$$

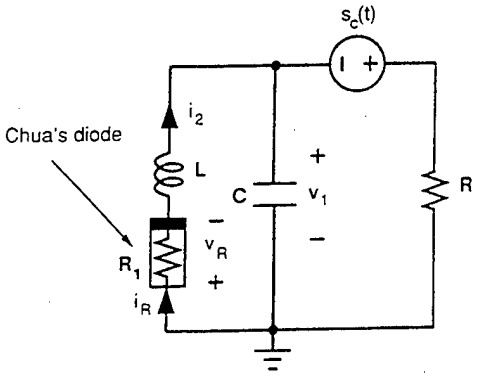


Fig. 5. Nonautonomous chaotic circuit 2. For the system to become chaotic, we use an active linear resistor and a Chua's diode with a passive monotone $v$-$i$ characteristic.

where $s_c(t) = A_c \sin(\Omega t)$ is the periodic forcing function and the $v$-$i$ characteristic of the current-controlled Chua's diode $g_c(i)$ is a 3-segment piecewise-linear function given by

$$g_c(i) = R_b i + \frac{1}{2}(R_a - R_b)(|i + I| - |i - I|) \tag{7}$$

where $I > 0$.

After normalization using $G = \frac{1}{R}$, $x = \frac{v_1 G}{I}$, $y = \frac{i_2}{I}$, $\tau = \frac{t}{|C/G|}$, $a = GR_a$, $b = GR_b$, $\omega = \Omega|C/G|$, $\beta = \frac{C}{LG^2}$, $s(t) = \frac{s_c(|C/G|t)G}{I}$, $A = \frac{A_c G}{I}$, and redefining $\tau$ as $t$, we obtain the following dimensionless equations:

$$\begin{aligned} \frac{dx}{dt} &= k(y - x - s(t)) \\ \frac{dy}{dt} &= k\beta(-x - f(y)) \end{aligned} \tag{8}$$

where $k = 1$ if $\frac{C}{G} > 0$ and $k = -1$ if $\frac{C}{G} < 0$, $s(t) = A \sin(\omega t)$ and $f$ is as defined in Eq. (4).

We choose the following set of parameters: $a = -1.27$, $b = -0.68$, $\omega = 0.5$, $A = 0.2$, $\beta = 1.4$, and $k = -1$. There exists a set of corresponding circuit parameter values such that the inductor and the capacitor are passive, the nonlinear resistor has a passive monotone $v$-$i$ characteristic and the linear resistor is active, i.e. $C$, $L$, $R_a$, $R_b > 0$, $R < 0$. A chaotic attractor for these parameters is shown in the $x$-$y$ plane in Fig. 6.

We will synchronize two such circuits by connecting a linear resistor of resistance $R_c$ across the two linear resistors, as shown in Fig. 7.

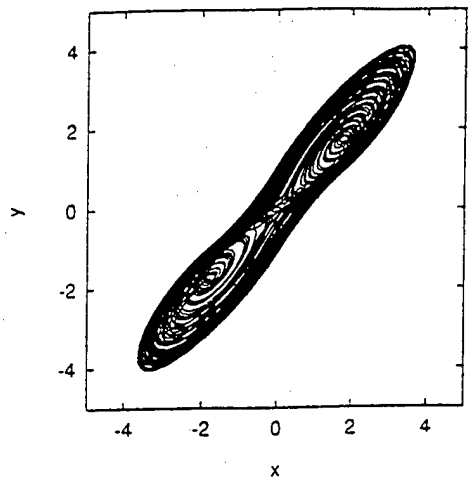


Fig. 6. Chaotic attractor for system (8) in the $x$-$y$ plane. The parameters are $a = -1.27$, $b = -0.68$, $\omega = 0.5$, $A = 0.2$, $\beta = 1.4$, and $k = -1$.

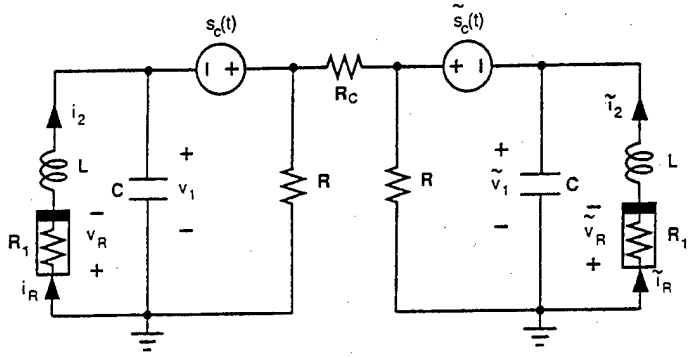


Fig. 7. Two nonautonomous chaotic circuits coupled through a linear resistor. The signal $\tilde{v}_1(t)$ approaches $v_1(t)$ as the system is synchronized.

The normalized state equations of the system in Fig. 7 are:

$$\begin{aligned}
\frac{dx}{dt} &= k(y - x - s(t) + \gamma(\tilde{x} + \tilde{s}(t) - x - s(t))) \\
\frac{dy}{dt} &= k\beta(-x - f(y)) \\
\frac{d\tilde{x}}{dt} &= k(\tilde{y} - \tilde{x} - \tilde{s}(t) + \gamma(x + s(t) - \tilde{x} - \tilde{s}(t))) \\
\frac{d\tilde{y}}{dt} &= k\beta(-\tilde{x} - f(\tilde{y}))
\end{aligned} \tag{9}$$

where $\gamma = \frac{1}{GR_c}$.

We choose $\gamma = -\frac{1}{2}$. This corresponds to $R_c = -2R$, so that if $R < 0$ is an active resistor, $R_c$ will be a passive resistor. Equations (9) can then be rewritten as

$$\begin{aligned}
\frac{dx}{dt} &= k\left(y - \left[\frac{1}{2}(x+\tilde{x}) + \frac{1}{2}(s(t)+\tilde{s}(t))\right]\right)\\
\frac{dy}{dt} &= k\beta(-x - f(y))\\
\frac{d\tilde{x}}{dt} &= k\left(\tilde{y} - \left[\frac{1}{2}(x+\tilde{x}) + \frac{1}{2}(s(t)+\tilde{s}(t))\right]\right)\\
\frac{d\tilde{y}}{dt} &= k\beta(-\tilde{x} - f(\tilde{y}))
\end{aligned} \tag{10}$$

If we set $\eta(t) = -\frac{1}{2}(x+\tilde{x}) - \frac{1}{2}(s(t)+\tilde{s}(t))$, then by Ref. 6. Corollary 1. this system will asymptotically synchronize (i.e. $\tilde{x} \to x$ and $\tilde{y} \to y$ as $t \to \infty$) if the following system is uniformly asymptotically stable for all $\eta(t)$.

$$\begin{aligned}
\begin{pmatrix} \frac{dx}{dt} \\ \frac{dy}{dt} \end{pmatrix} &= k\begin{pmatrix} y \\ \beta(-x - f(y)) \end{pmatrix} + \begin{pmatrix} k\eta(t) \\ 0 \end{pmatrix}\\
&= \frac{k}{\frac{1}{\beta} - c^2}\begin{pmatrix} \frac{1}{\beta} & c \\ c & 1 \end{pmatrix}\begin{pmatrix} 1 & -c \\ -c & \frac{1}{\beta} \end{pmatrix}\begin{pmatrix} y \\ \beta(-x - f(y)) \end{pmatrix} + \begin{pmatrix} k\eta(t) \\ 0 \end{pmatrix}
\end{aligned} \tag{11}$$

where we choose $c$ to be small and positive.

We want the function

$$h(x,y) = \begin{pmatrix} 1 & -c \\ -c & \frac{1}{\beta} \end{pmatrix}\begin{pmatrix} y \\ \beta(-x - f(y)) \end{pmatrix} = \begin{pmatrix} y + c\beta(x + f(y)) \\ -cy - (x + f(y)) \end{pmatrix}$$

to be uniformly increasing for $a < 0$, $b < 0$. Now

$$\begin{aligned}
(x - x', y - y')(h(x,y) - h(x',y')) &= c\beta(x - x')^2 + c\beta(x - x')(f(y) - f(y'))\\
&\quad - c(y - y)^2 - (y - y')(f(y) - f(y'))\\
&= c\beta(x - x')^2 + c\beta s(x - x')(y - y')\\
&\quad + (-c - s)(y - y')^2
\end{aligned}$$

where $s = \frac{f(y) - f(y')}{y - y'}$ which depends on $y$ and $y'$ satisfies $\min(a,b) \le s \le \max(a,b) < 0$ for all $y \neq y'$. Thus

$$\begin{aligned}
(x - x', y - y')(h(x,y) - h(x',y')) &= \left(\sqrt{c\beta}(x - x') + \frac{s\sqrt{c\beta}}{2}(y - y')\right)^2\\
&\quad + \left(\frac{-c\beta s^2}{4} - c - s\right)(y - y')^2
\end{aligned}$$

If we choose $c$ positive and sufficiently small, then $\frac{-c\beta s^2}{4} - c - s$ is positive and $h(x, y)$ is uniformly increasing. Furthermore, when $c$ is sufficiently small and $\beta > 0$, the matrix

$$\frac{1}{\frac{1}{\beta} - c^2} \begin{pmatrix} \frac{1}{\beta} & c \\ c & 1 \end{pmatrix}$$

is symmetric positive definite, so system (11) is uniformly asymptotically stable for all $\eta(t)$ by Theorem 6 in Ref. 6 when $k = -1$. Therefore system (10) will asymptotically synchronize for $a < 0$, $b < 0$, $\beta > 0$ and $k = -1$.

Note that when the two systems are synchronized ($x = \tilde{x}$ and $y = \tilde{y}$), each of the two systems behaves as a single system (8) with the external source replaced by the average of the two sources.

## 4. Communication Systems Based on Chaotic Synchronization

There have been many approaches to implementing communication systems based on chaotic synchronization.[3,4,8–13] In these systems, the input signal is scrambled or converted to a chaotic signal in the transmitter and this chaotic signal is transmitted to the receiver. Nearly all of them utilize an autonomous chaotic system and the information signal does not play a significant role in generating the chaos. We have discussed earlier the relationship between communication systems using chaotic synchronization and synchronizing nonautonomous chaotic systems by considering the information signal as an external input.

Let us now consider the above synchronization schemes in this light. The synchronization schemes in the previous sections can be considered as communication systems if the periodic signal $s_c(t)$ in Fig. 3 (resp. signals $s_c(t)$ or $\tilde{s}_c(t)$ in Fig. 7) is replaced by an encoded information signal that oscillates at the proper rate. Some examples of encoding of binary information signals that could be used are coded PCM (Manchester pulses), FSK or PSK. For FSK and PSK, the frequencies of the keys should be chosen such that system (1) (resp. system (6)) is chaotic.

Consider Fig. 3. The information signal is $s_c(t)$, and this is scrambled by the circuit. The scrambled signal $v_R$ is then transmitted, and in the receiver the signal $\tilde{s}_c(t)$ is recovered which approaches $s_c(t)$. The signal $\tilde{s}_c(t)$ is now an information-bearing signal at the slave circuit (receiver). Some differences between this scheme and the other communication schemes using chaos are:

- The information signal plays a crucial role in generating the chaotic signal to be transmitted which potentially can lead to a secure communication system that is harder to break.
- The minimum number of dimensions needed to generate chaos is less (2 versus 3).

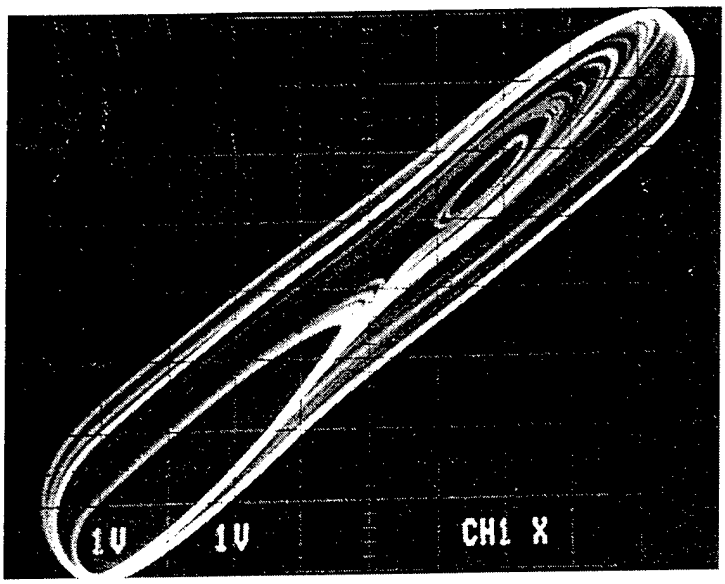


Fig. 8. Phase portrait of a nonautonomous chaotic circuit 1 from a physical implementation. The circuit parameters are $C = 33.65$ nF, $R = 644.7\ \Omega$, $L = 18.71$ mH, $Ga = -1.6$ mS, $Gb = -1.2$ mS, $E = 1.2$ V and $s_c(t) = 0.075$ sgn $(\sin(1380\pi t))$.

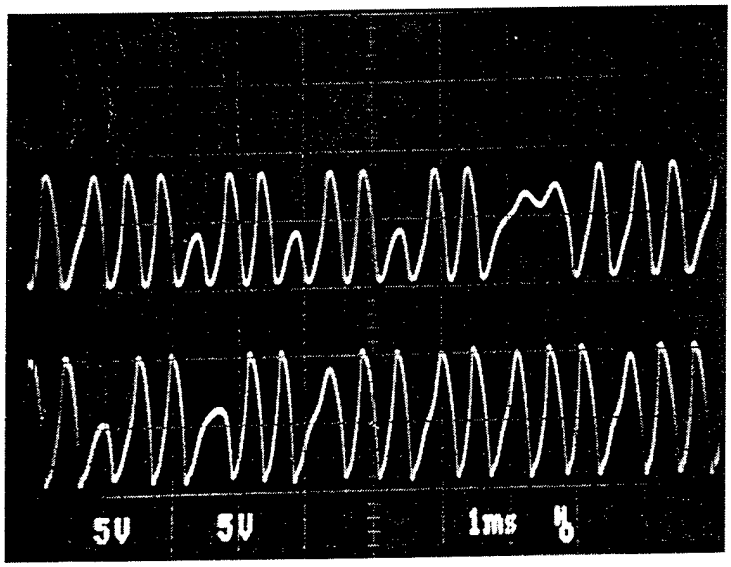


Fig. 9. Time waveforms corresponding to the attractor in Fig. 8. The inductor current $i_2$ is shown in the top trace while the capacitor voltage $v_1$ is shown in the bottom trace.

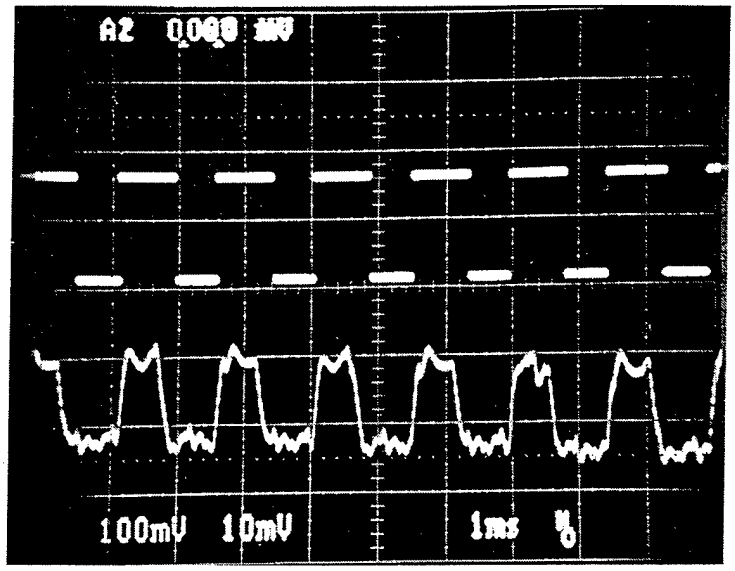


Fig. 10. The input signal $s_c(t)$ and the recovered signal $\tilde{s}_c(t)$. The square wave $s_c(t)$ is shown in the top trace and $\tilde{s}_c(t)$ is shown in the bottom trace.

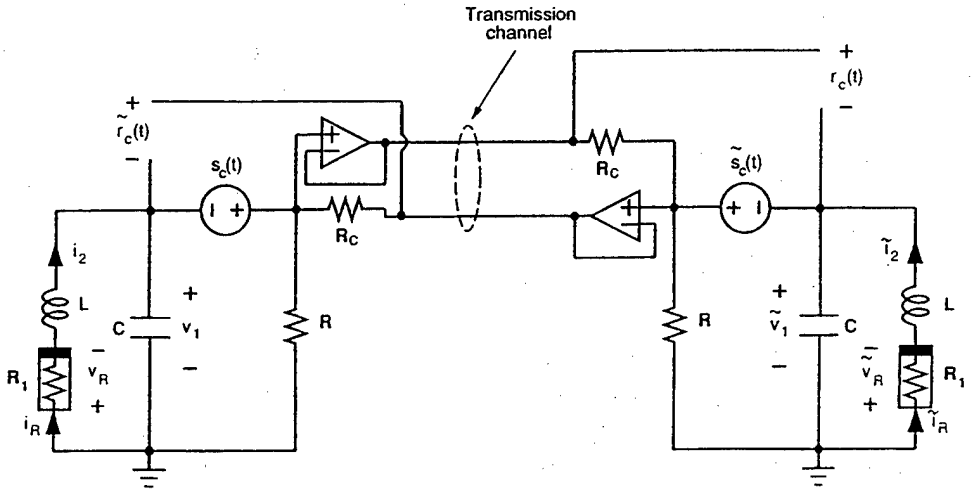


Fig. 11. The system in Fig. 7 redrawn as a bidirectional communication system. The signal $s_c(t)$ is recovered in the second system as $r_c(t)$ ($r_c(t) \to s_c(t)$ as $t \to \infty$) and $\tilde{s}_c(t)$ is recovered in the first system as $\tilde{r}_c(t)$($\tilde{r}_c(t) \to \tilde{s}_c(t)$ as $t \to \infty$).

In Fig. 8 we show an attractor in the $v_1 - i_2$ plane obtained from a physical implementation of Fig. 3. The circuit parameters we used are:

$$C = 33.65 \text{ nF}, \ R = 644.7\ \Omega, \ L = 18.71 \text{ mH},$$

$$Ga = -1.6 \text{ mS}, \ Gb = -1.2 \text{ mS}, \ E = 1.2 \text{ V}$$

and the external periodic signal $s_c(t)$ is a 690 Hz square wave with an amplitude of 75 mV. The time waveforms of $v_1$ and $i_2$ are shown in Fig. 9. In Fig. 10 we show the input square wave $s_c(t)$ and the recovered $\tilde{s}_c(t)$ after filtering.

The scheme in Fig. 7 can be redrawn as a bidirectional communication system, as shown in Fig. 11. Both circuits transmit and receive each other at the same time. The signals $s_c(t)$ and $\tilde{s}_c(t)$ are both information signals. The signal $s_c(t)$ is recovered in the second system as $r_c(t)$ ($r_c(t) \to s_c(t)$ as $t \to \infty$) and $\tilde{s}_c(t)$ is recovered in the first system as $\tilde{r}_c(t)$ ($\tilde{r}_c(t) \to \tilde{s}_c(t)$ as $t \to \infty$).

## 5. Synchronization of Nonidentical Systems

In this section we use the two synchronization schemes to synchronize two systems which are not identical. Since the external forcing voltage source can be arbitrary, we can add a nonlinear (resistive or dynamic) one-port in series with it and the system will still synchronize. Since the two systems are not identical and can have different dimensions, synchronization here means that the state variables in one system which have a corresponding counterpart in the other system will approach each other as $t \to \infty$ (see Definition 8 in Ref. 6).

For the master-slave configuration (Fig. 3) this leads to Fig. 12, where the one-port is shown as $N_2$.

As an example, assume that the one-port $N_2$ consists of a linear capacitor in series with a nonlinear resistor. The resulting system is shown in Fig. 13. We assume that $R_1$ is voltage controlled and the driving point characteristic of $R_1$ in series with $R_2$ is also voltage controlled. Then $\tilde{v}_1 \to v_1$ and $\tilde{i}_2 \to i_2$ as $t \to \infty$.

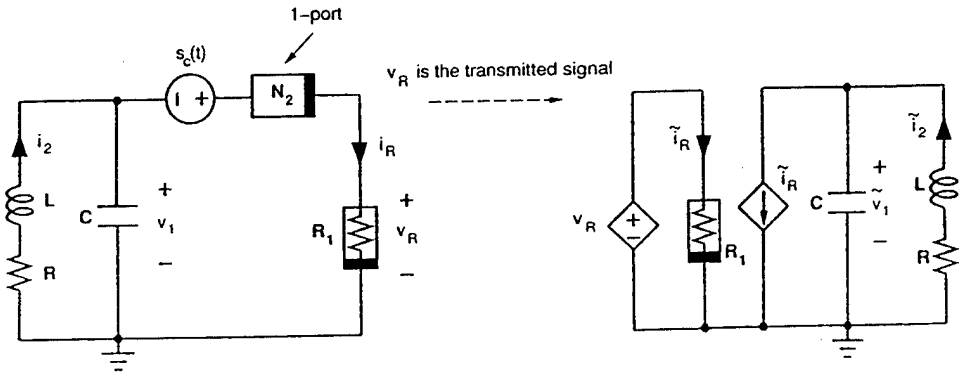


Fig. 12. Synchronization of nonidentical systems. The one-port $N_2$ can be dynamic or resistive.

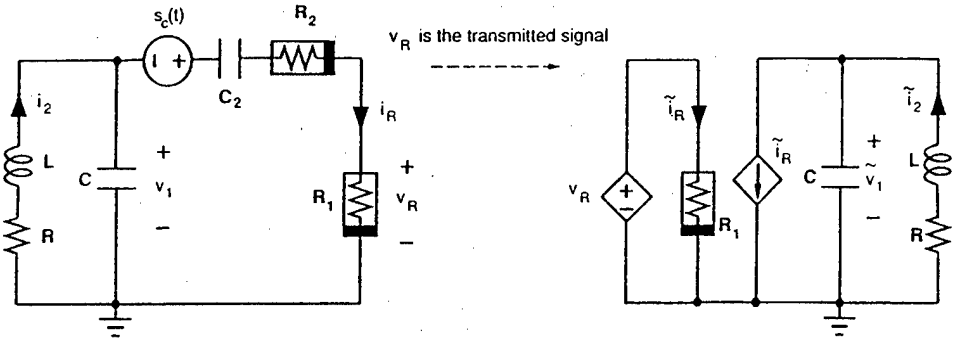


Fig. 13. Figure 12 redrawn when the one-port $N_2$ is a linear capacitor in series with a nonlinear resistor. $\tilde{v}_1 \to v_1$ and $\tilde{i}_2 \to i_2$ as $t \to \infty$.

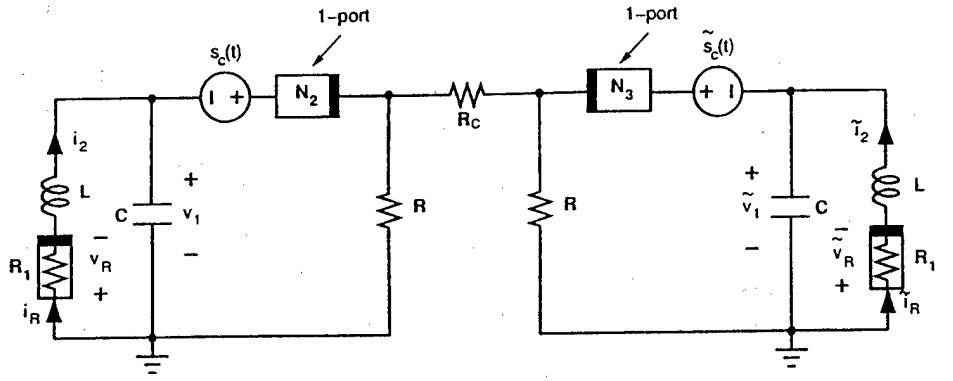


Fig. 14. Figure 7 with two one-ports $N_2$ and $N_3$ inserted in series with the external sources. The system synchronizes in the sense that $\tilde{v}_1 \to v_1$ and $\tilde{i}_2 \to i_2$ as $t \to \infty$.

When the one-port $N_2$ is dynamic, this synchronization scheme is similar to the homogeneous driving scheme of Pecora and Carroll[14] where the driven system is a smaller dimensional system than the driving system (see Ref. 6, Sec. 4.1).

Similarly, two one-ports can be connected in series to the independent sources in Fig. 7 and the system will still synchronize[a] in the sense that $\tilde{v}_1 \to v_1$ and $\tilde{i}_2 \to i_2$ as $t \to \infty$ (Fig. 14).

These exact same approaches can be used to synchronize two nonidentical *autonomous* systems with a similar topology. Examples of such systems are Chua's circuit and Chua's oscillator.[15,16]

## 6. Conclusions

We have shown how two nonautonomous chaotic systems can be synchronized without the need to explicitly phase-lock the periodic forcing in the two systems. The

[a]As long as we can write state equations for the entire system.

key feature of these synchronization schemes is that the external forcing of the two systems can be arbitrary and do not need to be identical. This allows us to consider them as communication systems and synchronization schemes for nonidentical systems.

In particular, in the master-slave configuration the slave system does not need an external periodic forcing and can recover the periodic forcing of the master system. This suggests the possibility of using this as a communication system by replacing the external periodic forcing signal in the master circuit by a properly encoded information signal, which can then be recovered in the slave circuit.

In the mutual coupling scheme, the two periodic forcing signals can be completely different. This suggests the possibility to use this as a bidirectional communication system with the two systems both receiving and transmitting at the same time.

Both schemes can also be considered as synchronization schemes for two systems which are not identical.

The reason these synchronization schemes work is due to the special topology of the circuits being synchronized. It would be interesting to see if synchronization without phase-locking is possible for other circuits.

## Acknowledgements

This work is supported in part by the Office of Naval Research under grant N00014-89-J-1402, by the National Science Foundation under grant MIP 86-14000, by the Josephine de Kármán Fellowship, and by the Joint Services Electronics Program under contract number F49620-94-C-0038. The United States Government is authorized to reproduce and distribute reprints for governmental purposes not withstanding any copyright notation hereon.

## References

1. T. L. Carroll and L. M. Pecora, "Synchronizing nonautonomous chaotic circuits", *IEEE Trans. Circuits and Systems–II: Analog and Digital Signal Processing* **40** (1993) 646–650.
2. K. Murali, M. Lakshmanan, and L. O. Chua, "Controlling and synchronization of chaos in the simplest dissipative non-autonomous circuit", *Int. J. of Bifurcation and Chaos* **5**, 2 (1995) 563–571.
3. C. W. Wu and L. O. Chua, "A simple way to synchronize chaotic systems with applications to secure communication systems", *Int. J. of Bifurcation and Chaos* **3**, 6 (1993) 1619–1627.
4. K. S. Halle, C. W. Wu, M. Itoh, and L. O. Chua, "Spread spectrum communication through modulation of chaos", *Int. J. of Bifurcation and Chaos* **3**, 2 (1993) 469–477.
5. K. Murali, M. Lakshmanan, and L. O. Chua, "The simplest dissipative nonautonomous chaotic circuit", *IEEE Trans. Circuits and Systems–I: Fundamental Theory and Applications* **41** (1994) 462–463.
6. C. W. Wu and L. O. Chua, "A unified framework for synchronization and control of dynamical systems", *Int. J. of Bifurcation and Chaos* **4**, 4 (1994) 979–998.

7. L. O. Chua and D. N. Green, "A qualitative analysis of the behavior of dynamic nonlinear networks: Steady-state solutions of nonautonomous networks", *IEEE Trans. Circuits and Systems* **23** (1976) 530–550.
8. A. V. Oppenheim, G. W. Wornell, S. H. Isabelle, and K. M. Cuomo, "Signal processing in the context of chaotic signals", *Proc. 1992 IEEE ICASSP*, vol. IV, 1992, pp. 117–120.
9. L. Kocarev, K. S. Halle, K. Eckert, L. O. Chua, and U. Parlitz, "Experimental demonstration of secure communications via chaotic synchronization", *Int. J. of Bifurcation and Chaos* **2**, 3 (1992) 709–713.
10. U. Parlitz, L. O. Chua, L. Kocarev, K. S. Halle, and A. Shang, "Transmission of digital signals by chaotic synchronization", *Int. J. of Bifurcation and Chaos* **2**, 4 (1992) 973–977.
11. K. M. Cuomo and A. V. Oppenheim, "Circuit implementation of synchronized chaos with applications to communications", *Phys. Rev. Lett.* **71**, 1 (1993) 65–68.
12. K. M. Cuomo and A. V. Oppenheim, "Chaotic signals and systems for communications", in *Proc. of 1993 IEEE ICASSP III*, 1993, pp. 137–140.
13. H. Dedieu, M. P. Kennedy, and M. Hasler, "Chaos shift keying: Modulation and demodulation of a chaotic carrier using self-synchronizing Chua's circuits", *IEEE Trans. Circuits and Systems–II: Analog and Digital Signal Processing* **40** (1993) 634–642.
14. L. M. Pecora and T. L. Carroll, "Driving systems with chaotic signals", *Phys. Rev.* **A44** (1991) 2374–2383.
15. L. O. Chua, "The genesis of Chua's circuit", *Archiv für Elektronik und Übertragungstechnik* **46**, 4 (1992) 250–257.
16. L. O. Chua, C. W. Wu, A. Huang, and G. Q. Zhong, "A universal circuit for studying and generating chaos, part I: Routes to chaos", *IEEE Trans. Circuits and Systems–I: Fundamental Theory and Applications, Special Issue on Chaos in Electronic Circuits. Part A* **40** (1993) 732–744.

# Impulsive Stabilization for Control and Synchronization of Chaotic Systems: Theory and Application to Secure Communication

Tao Yang, *Member, IEEE,* and Leon O. Chua, *Fellow, IEEE*

***Abstract*— Impulsive control of a chaotic system is ideal for designing digital control schemes where the control laws are generated by digital devices which are discrete in time. In this paper, several theorems on the stability of impulsive control systems are presented. These theorems are then used to find the conditions under which the chaotic systems can be asymptotically controlled to the origin by using impulsive control. Given the parameters of the chaotic system and the impulsive control law, an estimation of the upper bound of the impulse interval is given. We also present a theory of impulsive synchronization of two chaotic systems. A promising application of impulsive synchronization of chaotic systems to a secure communication scheme is presented. In this secure communication scheme, the transmitted signals are divided into small time frames. In each time frame, the synchronization impulses and the scrambled message signal are embedded. Conventional cryptographic methods are used to scramble the message signal. Simulation results based on a typical chaotic system; namely, Chua's oscillator, are provided.**

***Index Terms*— Chaotic secure communication, Chua's oscillator, continuous cryptographic function, impulsive control, impulsive synchronization.**

## I. Introduction

SINCE THE seminal paper of Ott, Grebogi, and Yorke (OGY) [2], several methods for control and stabilization of chaotic motions have recently been presented [3]–[6]. In view of the rich dynamics of chaotic systems, there exists a large variety of approaches for controlling such systems. Some of these approaches include adaptive control [4], [5], error-feedback control [7], time-delay feedback control [7], OGY method [2], predictive Poincaré control [8], occasional proportional feedback control [9], and impulsive control [6], [15]–[20].

In fact, the predictive Poincaré control and the occasional proportional feedback control are two impulsive control schemes with varying impulse intervals. Impulsive control is attractive because it allows the stabilization of a chaotic system using only small control impulses, and it offers a direct method for modulating digital information onto a chaotic carrier signal for spread spectrum applications. However, due to a lack of effective tools for analyzing impulsive differential equations [1], most impulse control schemes had been designed mainly by trial-and-error. The study of the stability of an impulsive differential equation is much more difficult than that of its "corresponding" differential equation [10]. For example, consider the impulsive system

$$\begin{cases} \dot{\mathbf{x}} = A\mathbf{x}, & t \neq \tau_i, \\ \Delta\mathbf{x}|_{t=\tau_i} = B\mathbf{x} \end{cases} \tag{1}$$

where $A$ and $B$ are two constant matrices, and $\Delta\mathbf{x}|_{t=\tau_i} \triangleq \mathbf{x}(\tau_i^+) - \mathbf{x}(\tau_i^-)$, $\mathbf{x}(\tau_i^-)$, and $\mathbf{x}(\tau_i^+)$ being the left and right limit of $\mathbf{x}(t)$ at $t = \tau_i$. The solution of the above system is given by

$$\mathbf{x}(t, \mathbf{x}_0) = \mathbf{X}(t, \mathbf{x}_0)\mathbf{x}_0 \tag{2}$$

where

$$\mathbf{X}(t, \mathbf{x}_0) = e^{A(t-\tau_i)} \prod_{t_0 < \tau_j < t} (I + B)e^{A(\tau_j - \tau_{j-1})} \qquad \tau_0 = t_0, \quad \tau_i < t \leq \tau_{i+1}. \tag{3}$$

As can be seen from this formula, it is not possible in the general case to give necessary and sufficient conditions for stability of solutions of the above system in terms of the eigenvalues of the matrix of this system, which is possible for systems of ordinary differential equations with constant coefficients.

In this paper, we investigate the stability of impulsively controlled chaotic systems. First, the stability of the trivial solution of a kind of impulsive differential equation is studied. Then the theoretical results are used to study the conditions under which an impulsive control of Chua's oscillator is asymptotically stable. An estimate of the upper bound of the impulsive interval is also presented.

Then, an impulsive control theory is used to study the impulsive synchronization of two chaotic systems. We first show that the impulsive synchronization problem is an impulsive control problem. Then a theorem is given for guaranteeing the asymptotic stability of impulsive synchronization. Since only the synchronization impulses are sent to the driven system in

Manuscript received January 30, 1997; revised June 16, 1997. This work was supported by the Office of Naval Research under Grant N00014-96-1-0753. This paper was recommended by Guest Editor M. J. Ogorzałek.

The authors are with the Electronics Research Laboratory, Department of Electrical Engineering and Computer Sciences, University of California, Berkeley, CA 94720 USA.

Publisher Item Identifier S 1057-7122(97)07321-2.

1057–7122/97$10.00 © 1997 IEEE

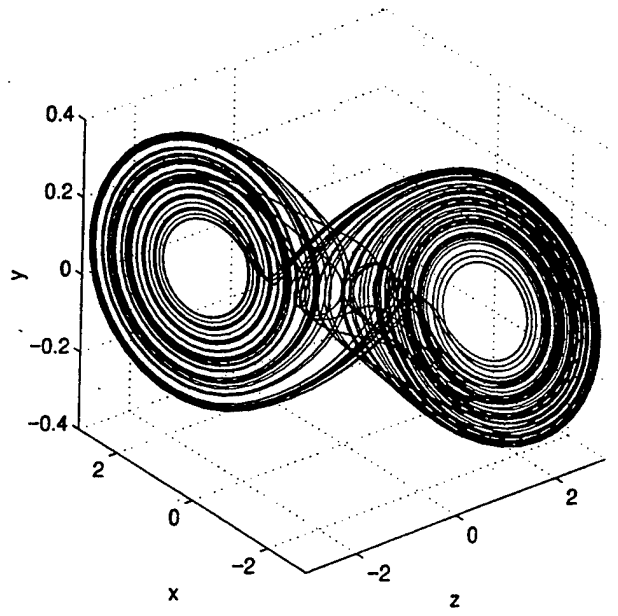


Fig. 1. The Chua's double scroll attractor.

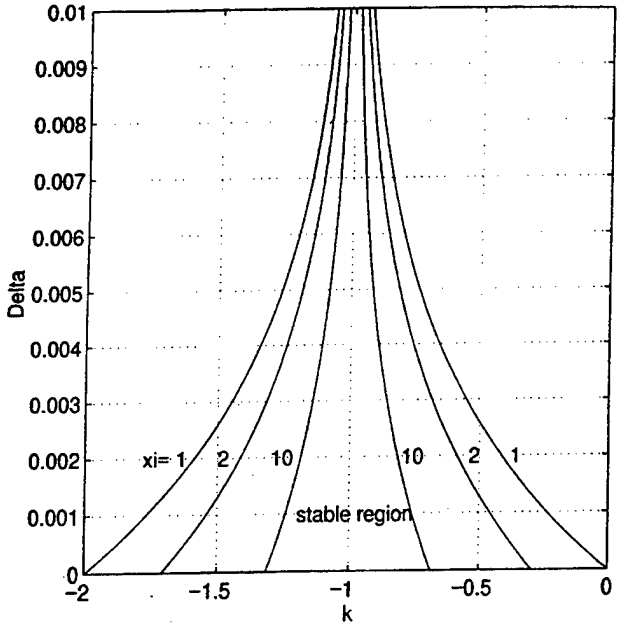


Fig. 2. Estimate of the boundaries of stable regions with different $\xi$'s used in simulation 1.

an impulsive synchronization scheme, the information redundancy in the transmitted signal is reduced. In this sense, even low-dimensional chaotic systems can provide high security. In this paper, we will use impulsive synchronization to develop a new framework for chaotic secure communication.

The organization of this paper is as follows. In Section II, a theory on the stability of impulsive differential equations is given. In Section III, a stability criterion for impulsive control of Chua's oscillator is presented. In Section IV, simulation results on the impulsive control of Chua's oscillator are provided. In Section V, the theory and simulation results of impulsive synchronization of Chua's oscillators are presented. In Section VI, application of impulsive synchronization to secure communication is presented. In Section VII, some concluding remarks are given.

## II. Basic Theory of Impulsive Differential Equations

Consider the general nonlinear system

$$\dot{\mathbf{x}} = \mathbf{f}(t, \mathbf{x}) \tag{4}$$

where $\mathbf{f}: \mathbf{R}_+ \times \mathbf{R}^n \mapsto \mathbf{R}^n$ is continuous, $\mathbf{x} \in \mathbf{R}^n$ is the state variable, and

$$\dot{\mathbf{x}} \triangleq \frac{d\mathbf{x}}{dt}.$$

Consider a discrete set $\{\tau_i\}$ of time instants, where

$$0 < \tau_1 < \tau_2 < \cdots < \tau_i < \tau_{i+1} < \cdots,$$
$$\tau_i \to \infty \text{ as } i \to \infty.$$

Let

$$U(i, \mathbf{x}) = \Delta\mathbf{x}|_{t=\tau_i} \triangleq \mathbf{x}(\tau_i^+) - \mathbf{x}(\tau_i^-) \tag{5}$$

be the "jump" in the state variable at the time instant $\tau_i$. Then this impulsive system is described by

$$\begin{cases} \dot{\mathbf{x}} = \mathbf{f}(t, \mathbf{x}), & t \neq \tau_i \\ \Delta\mathbf{x} = U(i, \mathbf{x}), & t = \tau_i \\ \mathbf{x}(t_0^+) = \mathbf{x}_0, & t_0 \geq 0,\ i = 1, 2, \cdots \end{cases} \tag{6}$$

This is called an impulsive differential equation [1]. To study the stability of the impulsive differential equation (6) we use the following definitions and theorems [1].

*Definition 1:* Let $V: \mathbf{R}_+ \times \mathbf{R}^n \mapsto \mathbf{R}_+$, then $V$ is said to belong to class $\mathcal{V}_0$ if

1) $V$ is continuous in $(\tau_{i-1}, \tau_i] \times \mathbf{R}^n$ and for each $\mathbf{x} \in \mathbf{R}^n$, $i = 1, 2, \cdots$,

$$\lim_{(t, \mathbf{y}) \to (\tau_i^+, \mathbf{x})} V(t, \mathbf{y}) = V(\tau_i^+, \mathbf{x}) \tag{7}$$

exists;

2) $V$ is locally Lipschitzian in $\mathbf{x}$.

*Definition 2:* For $(t, \mathbf{x}) \in (\tau_{i-1}, \tau_i] \times \mathbf{R}^n$, we define

$$D^+V(t, \mathbf{x}) \triangleq \lim_{h \to 0} \sup \frac{1}{h} \{V[t + h, \mathbf{x} + h\mathbf{f}(t, \mathbf{x})] - V(t, \mathbf{x})\}. \tag{8}$$

*Definition 3. Comparison System:* Let $V \in \mathcal{V}_0$ and assume that

$$\begin{cases} D^+V(t, \mathbf{x}) \leq g[t, V(t, \mathbf{x})], & t \neq \tau_i \\ V[t, \mathbf{x} + U(i, \mathbf{x})] \leq \psi_i[V(t, \mathbf{x})], & t = \tau_i \end{cases} \tag{9}$$

where $g: \mathbf{R}_+ \times \mathbf{R}_+ \mapsto \mathbf{R}$ is continuous and $\psi_i: \mathbf{R}_+ \mapsto \mathbf{R}_+$ is nondecreasing. Then the system

$$\begin{cases} \dot{w} = g(t, w), & t \neq \tau_i \\ w(\tau_i^+) = \psi_i[w(\tau_i)] \\ w(t_0^+) = w_0 \geq 0 \end{cases} \tag{10}$$

is called the comparison system of (6).

*Definition 4:*

$$S_\rho = \{\mathbf{x} \in \mathbf{R}^n \,|\, \|\mathbf{x}\| < \rho\} \tag{11}$$

where $\|\cdot\|$ denotes the Euclidean norm on $\mathbf{R}^n$.

*Definition 5:* A function $\alpha$ is said to belong to class $\mathcal{K}$ if $\alpha \in C[R_+, R_+]$, $\alpha(0) = 0$, and $\alpha(x)$ is strictly increasing in $x$.

*Assumptions:* $\mathbf{f}(t, 0) = 0$, $U(i, 0) = 0$, and $g(t, 0) = 0$ for all $i$.

*Remark:* With the above assumptions, we find that the trivial solutions of (6) and (10) are identical for all time except at the discrete set $\{\tau_i\}$.

*Theorem 1. [1, Theorem 3.2.1, p. 139]:* Assume that the following three conditions are satisfied.

1) $V: \mathbf{R}_+ \times S_\rho \mapsto \mathbf{R}_+$, $\rho > 0$, $V \in \mathcal{V}_0$, $D^+V(t, \mathbf{x}) \le g[t, V(t, \mathbf{x})]$, $t \ne \tau_i$.
2) There exists a $\rho_0 > 0$ such that $\mathbf{x} \in S_{\rho_0}$ implies that $\mathbf{x} + U(i, \mathbf{x}) \in S_{\rho_0}$ for all $i$ and $V[t, \mathbf{x} + U(i, \mathbf{x})] \le \psi_i[V(t, \mathbf{x})]$, $t = \tau_i$, $\mathbf{x} \in S_{\rho_0}$.
3) $\beta(\|\mathbf{x}\|) \le V(t, \mathbf{x}) \le \alpha(\|\mathbf{x}\|)$ on $\mathbf{R}_+ \times S_\rho$, where $\alpha(\cdot), \beta(\cdot) \in \mathcal{K}$.

Then the stability properties of the trivial solution of the comparison system (10) imply the corresponding stability properties of the trivial solution of (6).

*Theorem 2. [1, Corollary 3.2.1., p. 142]:* Let $g(t, w) = \dot{\lambda}(t)w$, $\lambda \in C^1[\mathbf{R}_+, \mathbf{R}_+]$, $\psi_i(w) = d_i w$, $d_i \ge 0$ for all $i$. Then the origin of system (6) is asymptotically stable if the conditions

$$\lambda(\tau_{i+1}) + \ln(\gamma d_i) \le \lambda(\tau_i), \quad \text{for all } i, \text{ where } \gamma > 1 \tag{12}$$

and

$$\dot{\lambda}(t) \ge 0 \tag{13}$$

are satisfied.

## III. Stabilization of Chua's Oscillator Using Impulsive Control

In this section, we study the impulsive control of Chua's oscillators [11] by applying the theory presented in the previous section. The dimensionless form of a Chua's oscillator is given by [11]

$$\begin{cases} \dot{x} = \alpha[y - x - f(x)] \\ \dot{y} = x - y + z \\ \dot{z} = -\beta y - \gamma z \end{cases} \tag{14}$$

where $f(x)$ is the piecewise-linear characteristics of the Chua's diode, which is given by

$$f(x) = bx + \tfrac{1}{2}(a - b)(|x + 1| - |x - 1|) \tag{15}$$

where $a < b < 0$ are two constants.

Let $\mathbf{x}^T = (x, y, z)$, then we can rewrite the Chua's oscillator equation into the form

$$\dot{\mathbf{x}} = A\mathbf{x} + \Phi(\mathbf{x}) \tag{16}$$

where

$$A = \begin{pmatrix} -\alpha & \alpha & 0 \\ 1 & -1 & 1 \\ 0 & -\beta & -\gamma \end{pmatrix}, \quad \Phi(\mathbf{x}) = \begin{bmatrix} -\alpha f(x) \\ 0 \\ 0 \end{bmatrix}. \tag{17}$$

The impulsive control of a Chua's oscillator is then given by

$$\begin{cases} \dot{\mathbf{x}} = A\mathbf{x} + \Phi(\mathbf{x}), & t \ne \tau_i \\ \Delta\mathbf{x}|_{t=\tau_i} = B\mathbf{x} \end{cases}. \tag{18}$$

Since the system in (18) has the general form of a kind of nonlinear system, we can give a general result in following lemma.

*Lemma 1:* Let $n \times n$ matrix $\Gamma$ be symmetric and positive definite, and $\lambda_1 > 0$, $\lambda_2 > 0$ are, respectively, the smallest and the largest eigenvalues of $\Gamma$. Let

$$Q = \Gamma A + A^T\Gamma \tag{19}$$

where $A^T$ is the transpose of $A$, and $\lambda_3$ is the largest eigenvalue of $\Gamma^{-1}Q$. $\Phi(\mathbf{x})$ is continuous and $\|\Phi(\mathbf{x})\| \le L\|\mathbf{x}\|$ where $L > 0$ is a constant. $\lambda_4$ is the largest eigenvalue of the matrix

$$\Gamma^{-1}(I + B^T)\Gamma(I + B). \tag{20}$$

$B$ is symmetric and the spectral radius of $I + B$, $\rho(I + B) \le 1$. Then the origin of impulsive control system (18) is asymptotically stable if

$$\left(\lambda_3 + 2L\sqrt{\frac{\lambda_2}{\lambda_1}}\right)(\tau_{k+1} - \tau_k) \le -\ln(\gamma\lambda_4), \qquad \gamma > 1 \tag{21}$$

and

$$\lambda_3 + 2L\sqrt{\frac{\lambda_2}{\lambda_1}} \ge 0. \tag{22}$$

*Proof:* Construct a Lyapunov function $V(\mathbf{x}) = \mathbf{x}^T\Gamma\mathbf{x}$, when $t \ne \tau_k$ we have

$$\begin{aligned} D^+V(\mathbf{x}) &= \mathbf{x}^T(A^T\Gamma + \Gamma A)\mathbf{x} + [\Phi^T(\mathbf{x})\Gamma\mathbf{x} + \mathbf{x}^T\Gamma\Phi(\mathbf{x})] \\ &= \mathbf{x}^TQ\mathbf{x} + [\Phi^T(\mathbf{x})\Gamma\mathbf{x} + \mathbf{x}^T\Gamma\Phi(\mathbf{x})] \\ &\le \left(\lambda_3 + 2L\sqrt{\frac{\lambda_2}{\lambda_1}}\right)V(\mathbf{x}), \qquad t \ne \tau_k. \end{aligned} \tag{23}$$

Hence, condition 1 of Theorem 1 is satisfied with $g(t, w) = (\lambda_3 + 2L\sqrt{\lambda_2/\lambda_1})w$.

Since $B$ is symmetric, we know that $I+B$ is also symmetric. By using Euclidean norm we have

$$\rho(I + B) = \|I + B\|. \tag{24}$$

Given any $\rho_0 > 0$ and $\mathbf{x} \in S_{\rho_0}$, we have

$$\begin{aligned} \|\mathbf{x} + U(k, \mathbf{x})\| &= \|\mathbf{x} + B\mathbf{x}\| \le \|I + B\|\,\|\mathbf{x}\| \\ &= \rho(I + B)\|\mathbf{x}\| \le \|\mathbf{x}\|. \end{aligned} \tag{25}$$

The last inequality is in view of $\rho(I + B) \le 1$. From which we know that $\mathbf{x} + U(k, \mathbf{x}) \in S_{\rho_0}$.

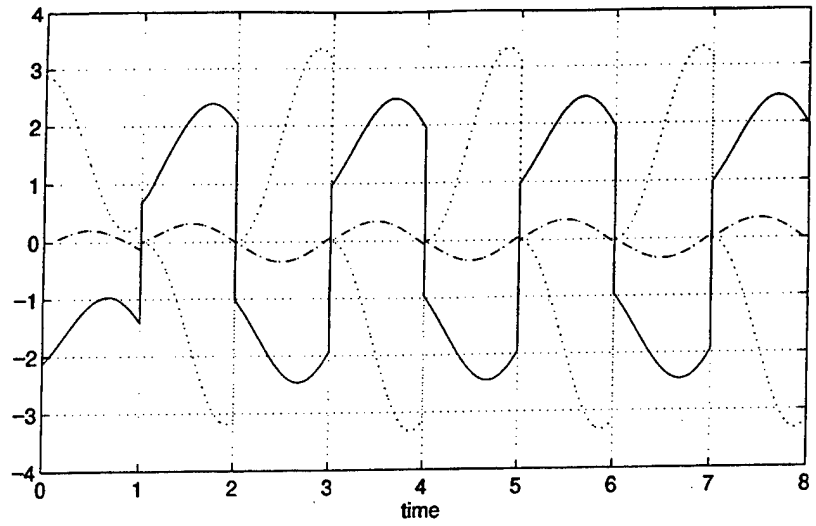


(a)

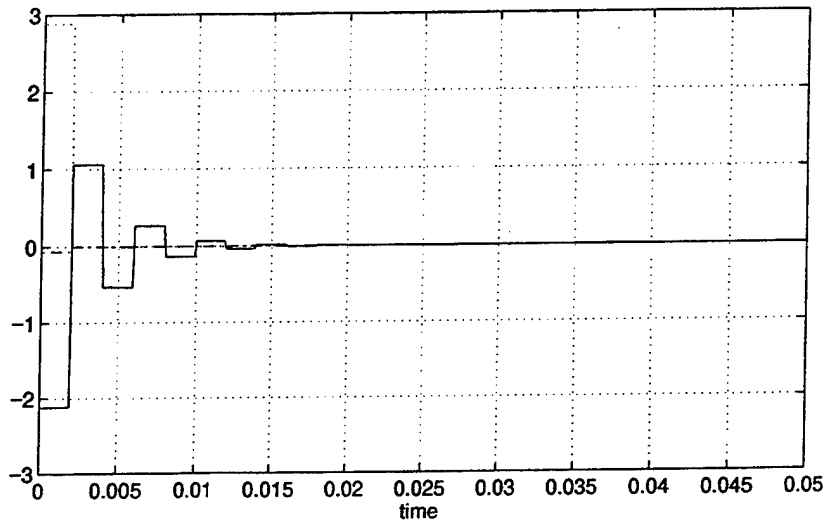


(b)

Fig. 3. Simulation results. (a) Unstable results outside the stable region. (b) Stable results inside the predicted stable region.

When $t = \tau_k$, we have

$$\begin{aligned} V(\mathbf{x}+B\mathbf{x})|_{t=\tau_k} &= (\mathbf{x}+B\mathbf{x})^T\Gamma(\mathbf{x}+B\mathbf{x}) \\ &= \mathbf{x}^T[I+(B)^T]\Gamma(I+B)\mathbf{x} \\ &\le \lambda_4 V(\mathbf{x}). \end{aligned} \tag{26}$$

Hence, condition 2 of Theorem 1 is satisfied with $\psi_k(w) = \lambda_4 w$. And

$$\lambda_1\|\mathbf{x}\|^2 \le V(\mathbf{x}) \le \lambda_2\|\mathbf{x}\|^2. \tag{27}$$

From which one can see that condition 3 of Theorem 1 is also satisfied with $\beta(x) = \lambda_1 x$ and $\alpha(x) = \lambda_2 x$. It follows from Theorem 1 that the asymptotic stability of the impulsive control system in (18) is implied by that of the following comparison system:

$$\begin{cases} \dot{w}(t) = \left(\lambda_3 + 2L\sqrt{\dfrac{\lambda_2}{\lambda_1}}\right)w(t), & t \ne \tau_k \\ w(\tau_k^+) = \lambda_4 w(\tau_k) \\ w(t_0^+) = w_0 \ge 0 \end{cases} \tag{28}$$

It follows from Theorem 2 that if

$$\int_{\tau_k}^{\tau_{k+1}} \left(\lambda_3 + 2L\sqrt{\frac{\lambda_2}{\lambda_1}}\right) dt + \ln(\gamma\lambda_4) \le 0, \qquad \gamma > 1 \tag{29}$$

i.e.,

$$\left(\lambda_3 + 2L\sqrt{\frac{\lambda_2}{\lambda_1}}\right)(\tau_{k+1} - \tau_k) \le -\ln(\gamma\lambda_4), \qquad \gamma > 1 \tag{30}$$

and

$$\lambda_3 + 2L\sqrt{\frac{\lambda_2}{\lambda_1}} \ge 0 \tag{31}$$

are satisfied, then the origin of (18) is asymptotically stable. □

Since this lemma is too general, in practical application, we want to deal with a simple case which is given in the following theorem.

We use the following theorem in order to guarantee the asymptotic stability of the origin of the controlled Chua's oscillator.

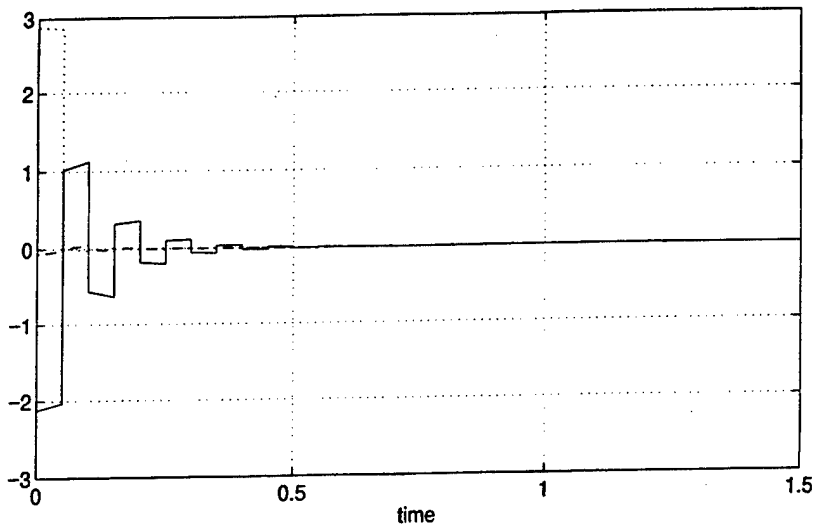


(c)

Fig. 3. (*Continued.*) Simulation results. (c) Stable results outside the predicted stable region.

*Theorem 3:* Let $d_1$ be the largest eigenvalue of $(I + B^T)(I + B)$, where $B$ is a symmetric matrix, $\rho(I + B) \leq 1$, where $\rho(\cdot)$ denotes the spectral radius of $I + B$. Let $q$ be the largest eigenvalue of $(A + A^T)$ and let the impulses be equidistant from each other and separated by interval $\Delta$. If

$$0 \leq q + 2|\alpha a| \leq -\frac{1}{\Delta} \ln(\xi d_1), \qquad \text{where } \xi > 1 \tag{32}$$

then the origin of the impulsively controlled Chua's oscillator is asymptotically stable.

*Proof:* Let us construct the Lyapunov function $V(t, \mathbf{x}) = \mathbf{x}^T\mathbf{x}$. For $t \neq \tau_i$, we have

$$\begin{aligned} D^+V(t, \mathbf{x}) &= \mathbf{x}^T A\mathbf{x} + \mathbf{x}^T A^T\mathbf{x} + \mathbf{x}^T\Phi(\mathbf{x}) + \Phi^T(\mathbf{x})\mathbf{x} \\ &\leq q\mathbf{x}^T\mathbf{x} + 2|\alpha a|\mathbf{x}^T\mathbf{x} \\ &= (q + 2|\alpha a|)V(t, \mathbf{x}). \end{aligned} \tag{33}$$

Hence, condition 1 of Theorem 1 is satisfied with $g(t, w) = (q + 2|\alpha a|)w$.

Since $B$ is symmetric, we know $(I + B)$ is also symmetric. By using Euclidean norm we have

$$\rho(I + B) = \|I + B\|. \tag{34}$$

Given any $\rho_0 > 0$ and $\mathbf{x} \in S_{\rho_0}$, we have

$$\|\mathbf{x} + B\mathbf{x}\| \leq \|I + B\| \, \|\mathbf{x}\| = \rho(I + B)\|\mathbf{x}\| \leq \|\mathbf{x}\|. \tag{35}$$

The last inequality follows from $\rho(I + B) \leq 1$. Consequently, $\mathbf{x} + B\mathbf{x} \in S_{\rho_0}$.

For $t = \tau_i$, we have

$$\begin{aligned} V(\tau_i, \mathbf{x} + B\mathbf{x}) &= (\mathbf{x} + B\mathbf{x})^T(\mathbf{x} + B\mathbf{x}) \\ &= \mathbf{x}^T(I + B^T)(I + B)\mathbf{x} \\ &\leq d_1 V(\tau_i, \mathbf{x}). \end{aligned} \tag{36}$$

Hence, condition 2 of Theorem 1 is satisfied with $\psi_i(w) = d_1 w$. We can see that condition 3 of Theorem 1 is also satisfied. It follows from Theorem 1 that the asymptotic stability of the impulsively controlled Chua's oscillator in (18) is implied by that of the following comparison system

$$\begin{cases} \dot{\omega} = (q + 2|\alpha a|)\omega, & t \neq \tau_i \\ \omega(\tau_i) = d_1\omega(\tau_i) \\ \omega(t_0) = \omega_0 \geq 0 \end{cases} \tag{37}$$

From (32), we have

$$\int_{\tau_i}^{\tau_{i+1}} (q + 2|\alpha a|)\, dt + \ln(\xi d_1) \leq 0, \qquad \xi > 1 \tag{38}$$

and $\dot{\lambda}(t) = q + 2|\alpha a| \geq 0$. It follows from Theorem 2 that the trivial solution of (18) is asymptotically stable. □

Theorem 3 also gives an estimate for the upper bound $\Delta_{\max}$ of $\Delta$; namely,

$$\Delta_{\max} = \left| \frac{\ln(\xi d_1)}{q + 2|\alpha a|} \right|, \qquad \xi \longrightarrow 1^+. \tag{39}$$

Observe that the upper bound given by (39) is sufficient but not necessary. Consequently, we can only say that we have a predicted stable region, which is usually smaller than the actual stable region because we can not assert that all other regions are unstable.

## IV. Simulation Results of Impulsive Control

In the following simulations, we choose the parameters of Chua's oscillator as $\alpha = 15$, $\beta = 20$, $\gamma = 0.5$, $a = \frac{120}{7}$, $b = -\frac{75}{7}$. A fourth-order Runge–Kutta method with step size $10^{-5}$ is used. The initial condition is given by $[x(0), y(0), z(0)] = (-2.121\,304, -0.066\,170, 2.881\,090)$. The uncontrolled trajectories are shown in Fig. 1, which is the Chua's double scroll attractor.

### A. Simulation 1: Strong Control

In this simulation, we choose the matrix $B$ as

$$B = \begin{pmatrix} k & 0 & 0 \\ 0 & -1 & 0 \\ 0 & 0 & -1 \end{pmatrix} \tag{40}$$

where the impulsive control is "strong." It follows from Theorem 3 that $\rho(I+B) \leq 1$ should be satisfied, which implies that $-2 \leq k \leq 0$. By using this $B$ matrix, it is easy to see that

$$d_1 = (k+1)^2. \tag{41}$$

We have

$$A = \begin{pmatrix} -15 & 15 & 0 \\ 1 & -1 & 1 \\ 0 & -20 & -0.5 \end{pmatrix},$$
$$A + A^T = \begin{pmatrix} -30 & 16 & 0 \\ 16 & -2 & -19 \\ 0 & -19 & -1 \end{pmatrix} \tag{42}$$

from which we find $q = 20.162\,180$. Then an estimate of the boundaries of the stable region is given by

$$0 \leq \Delta \leq -\frac{[\ln \xi + \ln (k+1)^2]}{q + 2|\alpha a|}, \qquad -2 \leq k \leq 0. \tag{43}$$

Fig. 2 shows the stable region for different $\xi$'s. The entire region below the curve corresponding to $\xi = 1$ is the predicted stable region. When $\xi \longrightarrow \infty$, the stable region shrinks to a line $k = -1$.

The simulation results are shown in Fig. 3. Fig. 3(a) shows instability for $k = -1.5$ and $\Delta = 1$. The solid waveform, the dash-dotted waveform, and the dotted waveform correspond to $x(t)$, $y(t)$, and $z(t)$, respectively. Fig. 3(b) shows stable results within the stable region for $k = -1.5$ and $\Delta = 0.002$. One can see that the system asymptotically approaches the origin with a settling time of about 0.05. However, the true stable region is larger than that predicted in Fig. 2. In order to demonstrate this fact, we show in Fig. 3(c) the stable results for $k = -1.5$ and $\Delta = 0.05$. We can also see that the system asymptotically approaches the origin with a settling time of about 1.4 which is much larger than that shown in Fig. 3(b).

### *B. Simulation 2: Weak Control*

In this simulation, we choose the matrix $B$ as

$$B = \begin{pmatrix} k & 0 & 0 \\ 0 & -0.1 & 0 \\ 0 & 0 & -0.1 \end{pmatrix} \tag{44}$$

where the impulsive control is much weaker than that chosen in simulation 1.

It is easy to see that

$$d_1 = \begin{cases} (k+1)^2, & (k+1)^2 \geq 0.81 \\ 0.81, & \text{elsewhere.} \end{cases} \tag{45}$$

An estimate of the boundaries of the stable region is given by

$$0 \leq \Delta \leq \begin{cases} -\dfrac{\ln \xi + \ln (k+1)^2}{q + 2|\alpha a|} & (k+1)^2 \geq 0.81 \\ -\dfrac{\ln \xi + \ln (0.81)}{q + 2|\alpha a|} & \text{elsewhere} \end{cases}$$
$$-2 \leq k \leq 0. \tag{46}$$

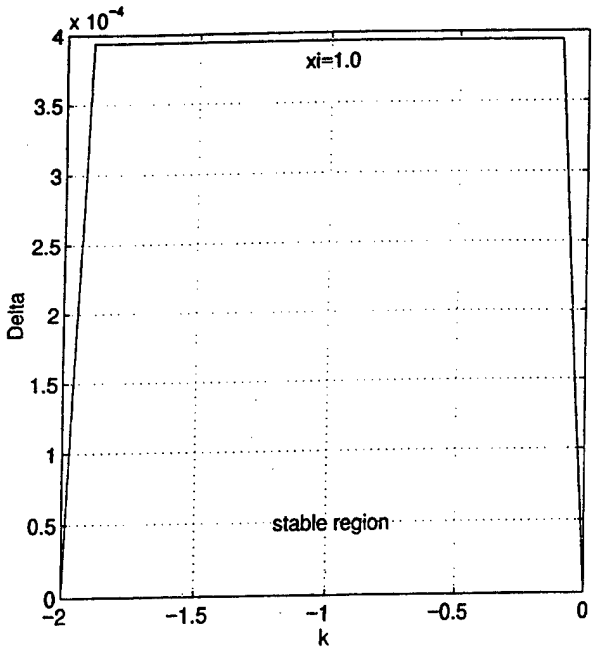


Fig. 4. Estimate of the boundaries of stable region used in simulation 2.

Fig. 4 shows the stable region. The entire region below the curve corresponding to $\xi = 1$ is the predicted stable region. In this case, $\Delta$ is always bounded. It seems that we can't control the system to the origin with an arbitrarily prescribed speed because $\xi$ has to satisfy $1 < \xi < \frac{100}{81}$. This is different from the case shown in Fig. 2, where any value of $\xi > 1$ is possible.

The simulation results are shown in Fig. 5. Again, the solid waveform, the dash–dotted waveform, and the dotted waveform correspond to $x(t)$, $y(t)$, and $z(t)$, respectively. Fig. 5(a) shows the instability results for $k = -1$ and $\Delta = 0.4$. Fig. 5(b) shows the stable results in the stable region for $k = -1$ and $\Delta = 3 \times 10^{-4}$. The control system asymptotically approaches the origin with a settling time of about 0.05. Also, the true stable region is larger than that predicted in Fig. 4. To demonstrate this fact, we show in Fig. 5(c) the stable results for $k = -1$ and $\Delta = 0.01$. We can also see that the system asymptotically approaches the origin with a settling time equal approximately to 1, which is much larger than that shown in Fig. 5(b).

## V. Synchronization of Chua's Oscillators Using Impulsive Control

In this section, we study the impulsive synchronization of two Chua's oscillators. One of the Chua's oscillators is called the *driving system* and the other is called the *driven system*. In an impulsive synchronization configuration, the driving system is given by (14). The driven system is given by

$$\dot{\tilde{\mathbf{x}}} = A\tilde{\mathbf{x}} + \Phi(\tilde{\mathbf{x}}) \tag{47}$$

where $\tilde{\mathbf{x}}^T = (\tilde{x}, \tilde{y}, \tilde{z})$ is the state variables of the driven system.

At discrete instants, $\tau_i$, $i = 1, 2, \cdots$, the state variables of the driving system are transmitted to the driven system and then the state variables of driven system are subject to jumps

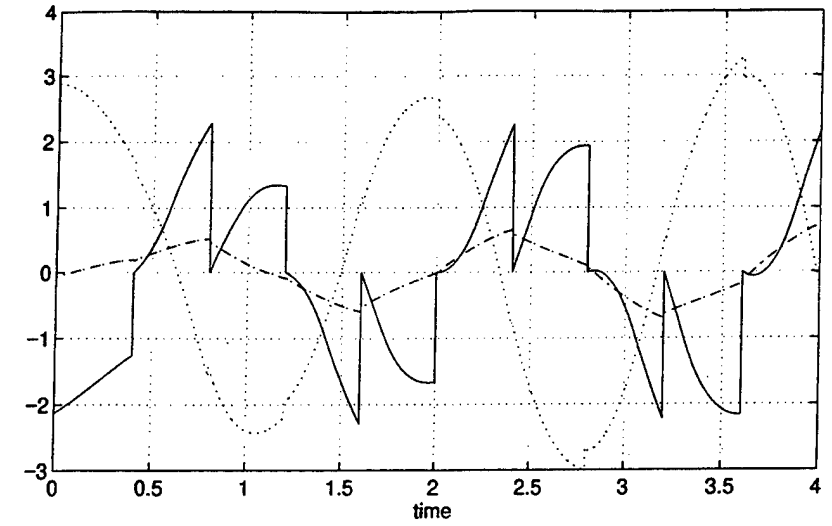


(a)

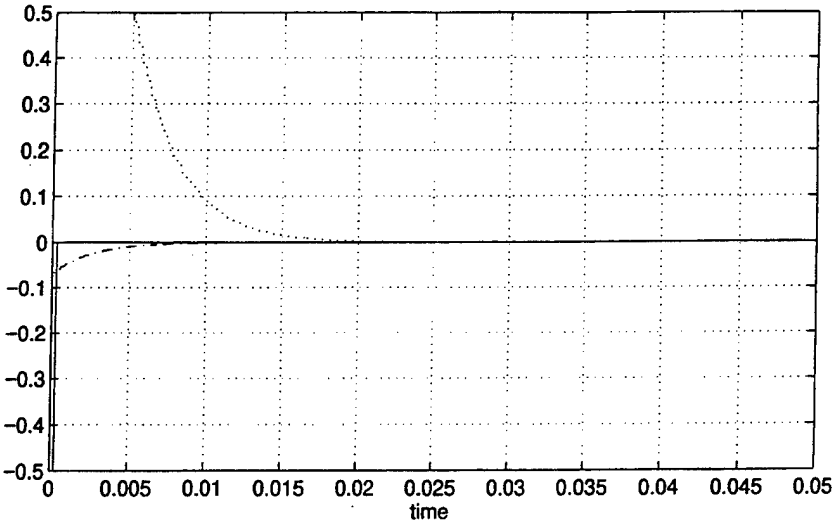


(b)

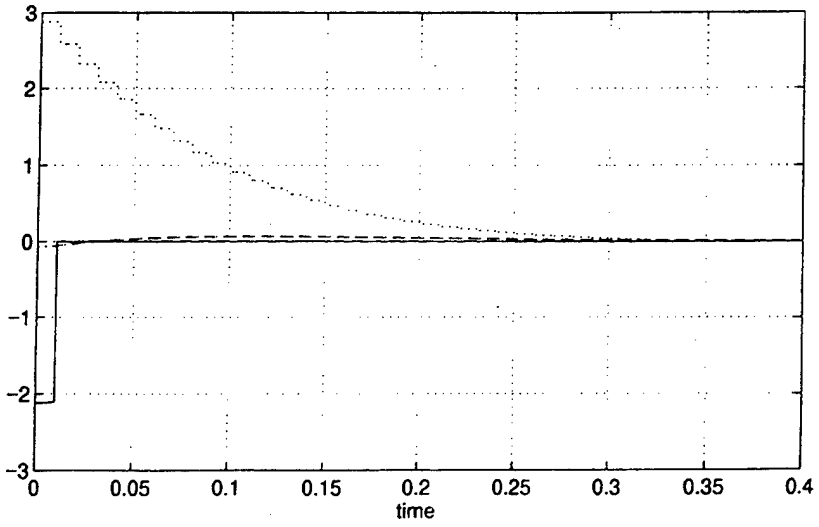


(c)

Fig. 5. Simulation results. (a) Unstable results outside the stable region. (b) Stable results in the stable region. (c) Stable results outside the stable region.

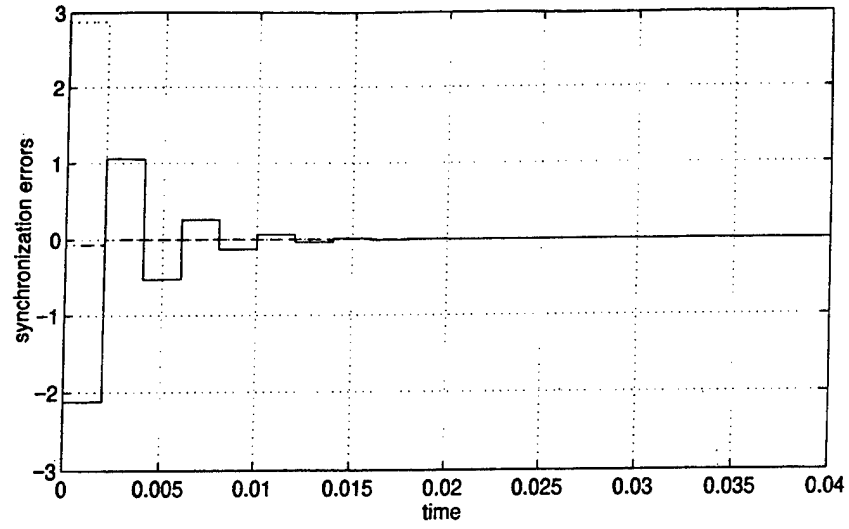


(a)

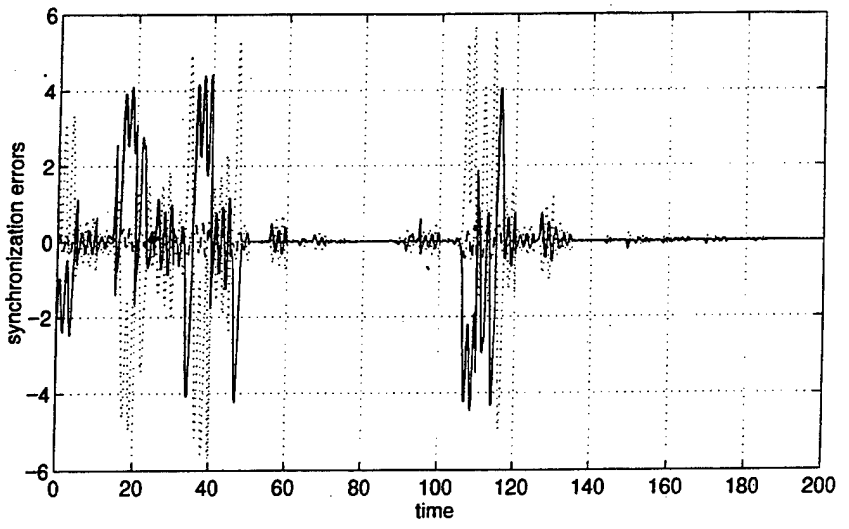


(b)

Fig. 6. Simulation results of impulsive synchronization: (a) stable synchronization results inside our predicted stable region and (b) synchronization can not be achieved when $\Delta$ is too large.

at these instants. In this sense, the driven system is described by the impulsive differential equation

$$\begin{cases} \dot{\tilde{\mathbf{x}}} = A\tilde{\mathbf{x}} + \Phi(\tilde{\mathbf{x}}), & t \neq \tau_i \\ \Delta\tilde{\mathbf{x}}|_{t=\tau_i} = -B\mathbf{e}, & i = 1, 2, \cdots \end{cases} \tag{48}$$

where $B$ is a $3 \times 3$ matrix, and $\mathbf{e}^T = (e_x, e_y, e_z) = (x - \tilde{x}, y - \tilde{y}, z - \tilde{z})$ is the *synchronization error*. If we define

$$\Psi(\mathbf{x}, \tilde{\mathbf{x}}) = \Phi(\mathbf{x}) - \Phi(\tilde{\mathbf{x}}) = \begin{bmatrix} -\alpha f(x) + \alpha f(\tilde{x}) \\ 0 \\ 0 \end{bmatrix} \tag{49}$$

then the error system of the impulsive synchronization is given by

$$\begin{cases} \dot{\mathbf{e}} = A\mathbf{e} + \Psi(\mathbf{x}, \tilde{\mathbf{x}}), & t \neq \tau_i \\ \Delta\mathbf{e}|_{t=\tau_i} = B\mathbf{e}, & i = 1, 2, \cdots \end{cases} \tag{50}$$

We use the following theorem to guarantee that our impulsive synchronization is asymptotically stable.

*Theorem 4:* Let $d_1$ be the largest eigenvalue of $(I + B^T)(I + B)$, where $B$ is a symmetric matrix. Assume the spectral radius $\rho$ of $I + B$ satisfies $\rho(I + B) \leq 1$. Let $q$ be the largest eigenvalue of $(A + A^T)$ and assume the impulses are equidistant from each other and separated by an interval $\Delta$. If

$$0 \leq q + 2|\alpha a|a \leq -\frac{1}{\Delta} \ln(\xi d_1), \qquad \xi > 1 \tag{51}$$

then the impulsive synchronization of two Chua's oscillators is asymptotically stable.

*Proof:* Observe that the error system in (50) is almost the same as the system in (18) except for $\Psi(\mathbf{x}, \tilde{\mathbf{x}})$. Similarly, let us construct the Lyapunov function $V(t, \mathbf{e}) = \mathbf{e}^T\mathbf{e}$. For $t \neq \tau_i$, we have

$$\begin{aligned} D^+V(t, \mathbf{e}) &= \mathbf{e}^T A\mathbf{e} + \mathbf{e}^T A^T\mathbf{e} + \mathbf{e}^T\Psi(\mathbf{e}) + \Psi^T(\mathbf{e})\mathbf{e} \\ &\leq q\mathbf{e}^T\mathbf{e} + 2|\alpha|\,|f(x) - f(\tilde{x})|e_x \\ &\leq q\mathbf{e}^T\mathbf{e} + 2|\alpha a|e_x^2 \end{aligned}$$

$$\leq (q + 2|\alpha a|)\mathbf{e}^T\mathbf{e}$$
$$= (q + 2|\alpha a|)V(t, \mathbf{e}). \quad (52)$$

Hence, condition 1 of Theorem 1 is satisfied with $g(t, w) = (q + 2|\alpha a|)w$. The rest of this proof is the same as that of Theorem 3. □

For the rest of this section, we present our simulation results. We choose the matrix $B$ as

$$B = \begin{pmatrix} -1.5 & 0 & 0 \\ 0 & -1 & 0 \\ 0 & 0 & -1 \end{pmatrix}. \quad (53)$$

The initial conditions are given by $[x(0), y(0), z(0)] = (-2.121\,304, -0.066\,170, 2.881\,090)$ and $[\tilde{x}(0), \tilde{y}(0), \tilde{z}(0)] = (0, 0, 0)$. The other parameters are the same as those used in Section IV. Since the stability boundary estimates are the same as those in Section IV, we do not repeat them here. Fig. 6 shows our simulation results. Fig. 6(a) shows the stable results within our predicted stable region with $k = -1.5$ and $\Delta = 0.002$. The solid line, the dash–dotted line, and the dotted line show $e_x(t)$, $e_y(t)$, and $e_z(t)$, respectively. We can see that impulsive synchronization was achieved rapidly. Fig. 6(b) shows that if $\Delta = 5$ then our impulsive synchronization is unstable.

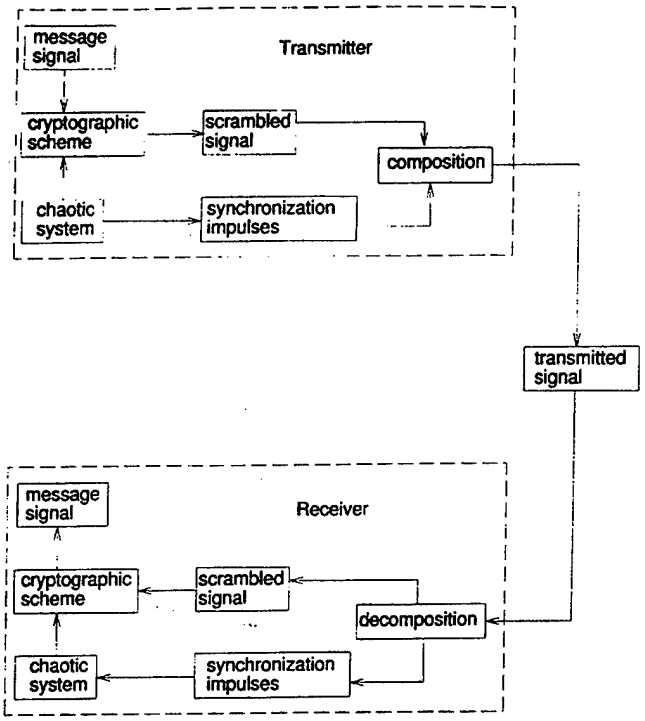


Fig. 7. Block diagram of the impulsive-synchronization based chaotic secure communication system.

## VI. Application of Impulsive Synchronization to Secure Communication

Since the publication of several chaotic cryptanalysis results of *low-dimensional chaos-based* secure communication systems [12], [13], there existed an illusion that such communication schemes were not secure enough. It may be reasonable to exploit hyperchaos based secure communication systems, but such systems may introduce more difficulties to synchronization.

On the other hand, we can enhance the security of low-dimensional chaos-based secure communication schemes by combining conventional cryptographic schemes with a chaotic system [14]. To overcome the low security objections against low-dimensional continuous chaos-based schemes, we should overcome the following problems: 1) make the transmitted signal more complex and 2) reduce the redundancy in the transmitted signal. To achieve the first goal, it is not necessary to use hyper-chaos. In [14], we have presented a method to combine a conventional cryptographic scheme with low-dimensional chaos to obtain a very complex transmitted signal. To achieve the second goal, impulsive synchronization offers a very promising approach.

In this section, we combine the results in [14] and impulsive synchronization to give a new chaotic secure communication scheme. The block diagram of this scheme is shown in Fig. 7.

From Fig. 7, we can see that this chaotic secure communication system consists of a transmitter and a receiver. In both the transmitter and the receiver, there exist two identical chaotic systems. Also, two identical conventional cryptographic schemes are embedded in both the transmitter and the receiver. Let us now consider details of each block in Fig. 7. The transmitted signal consists of a sequence of time frames. Every frame has a length of $T$ seconds and consists of two regions. In Fig. 8, we show the concept of a time frame and its components. The first region of the time frame is a synchronization region consisting of synchronization impulses. The synchronization impulses are used to impulsively synchronize the chaotic systems in both transmitter and receiver. The second region is the scrambled signal region where the scrambled signal is contained. To ensure synchronization, we have $T < \Delta_{\max}$. Within every time frame, the synchronization region has a length of $Q$ and the remaining time interval $T - Q$ is the scrambled signal region.

The composition block in Fig. 7 is used to combine the synchronization impulses and the scrambled signal into the time frame structure shown in Fig. 8. The simplest combination method is to substitute the beginning $Q$ seconds of every time frame with synchronization impulses. Since $Q$ is usually very small compared with $T$, the loss of time for packing a message signal is negligible. The decomposition block is used to separate the synchronization region and the scrambled signal region within each frame at the receiver end. Then the separated synchronization impulses are used to make the chaotic system in the receiver to synchronize with that in the transmitter. The stability of this impulsive synchronization is guaranteed by our results in Section V.

In the transmitter and the receiver, we use the same cryptographic scheme block for purposes of bidirectional communication. In a bidirectional communication scheme, every cellular phone should function both as a receiver and a

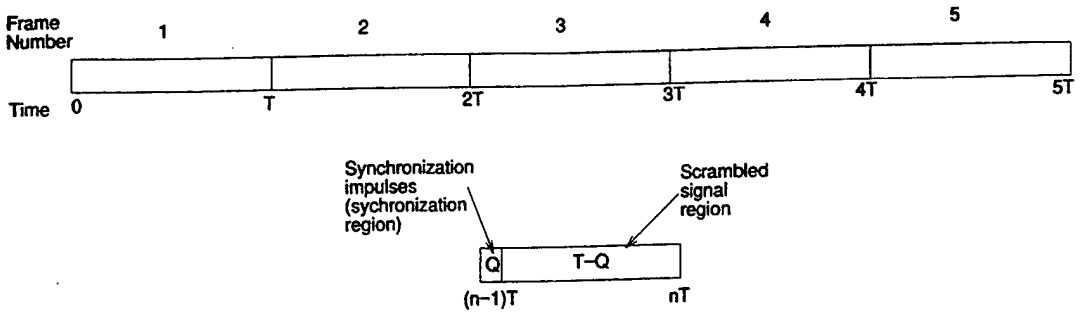


Fig. 8. Illustration of the concept of a time-frame and its components.

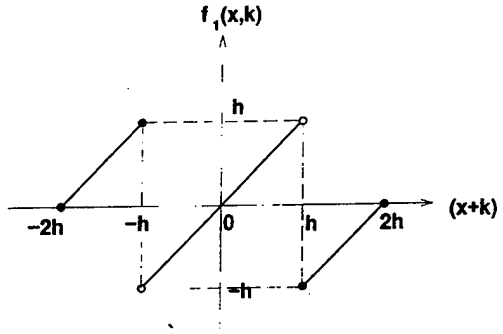


Fig. 9. Nonlinear function used in the continuous shift cipher.

transmitter. Here, the key signal is generated by the chaotic system. The cryptographic scheme is as follows [14]:

We use a continuous $n$-shift cipher to encrypt the plain signal(message signal). The $n$-shift cipher is given by

$$e[p(t)] = \underbrace{f_1(\cdots f_1\{f_1}_{n}[p(t), \underbrace{k(t)], k(t)\}, \cdots, k(t))}_{n} = y(t) \tag{54}$$

where $h$ is chosen such that $p(t)$ and $k(t)$ lie within $(-h, h)$. Here, $p(t)$ and $k(t)$ denote the plain signal and the key signal, respectively, and $y(t)$ denotes the encrypted signal. The key signal $k(t)$ is chosen as a state variable of the chaotic system. The notation $f_1(\cdot, \cdot)$ denotes a scalar nonlinear function of two variables defined as follows:

$$f_1(x, k) = \begin{cases} (x+k) + 2h, & -2h \le (x+k) \le -h \\ (x+k), & -h < (x+k) < h \\ (x+k) - 2h, & h \le (x+k) \le 2h \end{cases} . \tag{55}$$

This function is shown in Fig. 9:

The corresponding decryption rule is the same as the encryption rule

$$p(t) = d[y(t)] = \underbrace{f_1(\cdots f_1\{f_1}_{n}[y(t), \underbrace{-k(t)], -k(t)\}, \cdots, -k(t))}_{n} . \tag{56}$$

To decode the encrypted signal, the same key signal should be used.

The simulation results are as follows. We use an FM scheme to modulate the synchronization impulses such that the synchronization region is located in the initial 1% of every time frame. We choose the frame length as $T = 1$ s. In the synchronization region of every time frame, we transmit the impulses of the three state variables of the Chua's oscillators. The parameter of the encrypted signal is chosen as $h = 0.4$. A continuous 10-shift cipher was used. We choose $x$ and $\tilde{x}$ as the key signals and normalized them to fall within the amplitude range $[-0.4, 0.4]$.

Fig. 10 shows the simulation results of the above proposed secure communication system for transmitting a speech signal. Fig. 10(a) shows the waveforms of the sampled speech of four Chinese digits "NING"(zero)—"YI"(one)—"ER"(two)—"SANG"(three). The sampling rate is 8k. Fig. 10(b) shows the spectrograms of the original speech signal in Fig. 10(a), from which we can see the structure of the speech signal. Fig. 10(c) shows the waveforms of the received scrambled speech signal and the additive channel noise with SNR = 16 dB. This additive noise cannot change the value of the synchronization impulses which are modulated by FM. Fig. 10(d) shows the spectrograms for the scrambled speech signal and the additive channel noise. We can see that the structure of the signal in Fig. 10(b) was totally covered by an almost uniformly distributed noise-like spectrum. Fig. 10(e) shows the waveforms of the descrambled speech signal. Fig. 10(f) shows the spectrograms of the descrambled speech signal. We can see that some noises were introduced into the recovered results due to the channel noise, and that the spectrograms became a little blurry. But the structure of the speech signal was perfectly recovered.

## VII. Concluding Remarks

In this paper, we have presented a theory of impulsive control of chaotic dynamical systems. An estimate of the upper bound of the impulse interval $\Delta$ is also presented. Since all of our results are based on rigorous theoretical analysis and proofs, the results in this paper provide a framework and foundation for future works. We then use this theory to impulsively control and synchronize Chua's oscillators. An application of impulsive chaotic synchronization to secure communication is presented. The chaotic secure communication scheme presented here is a combination of a conventional cryptographic method and impulsive synchronization.

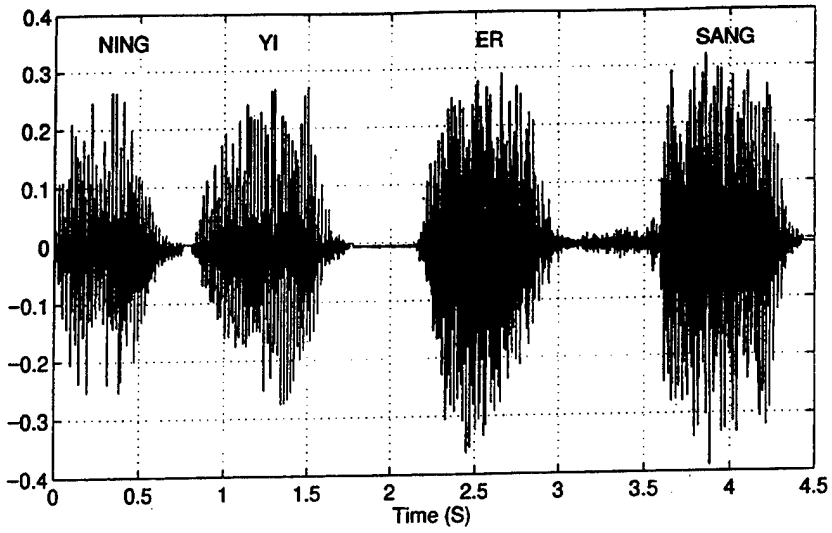


(a)

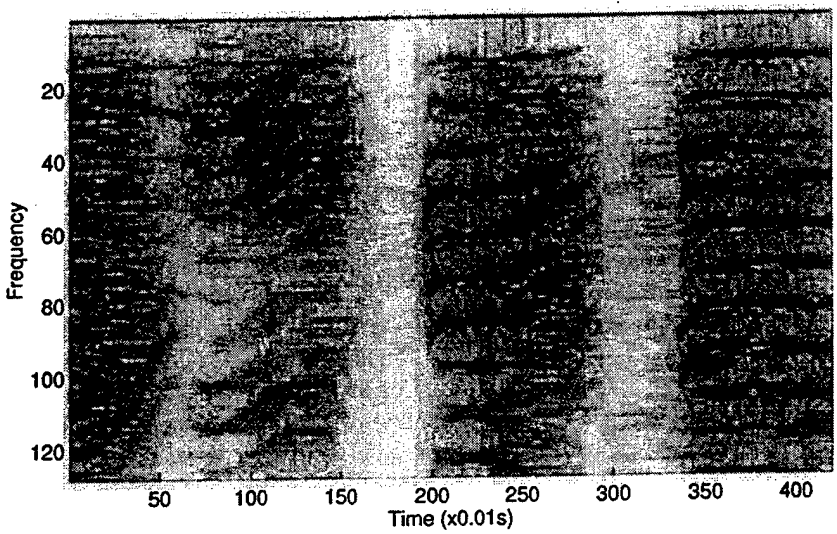


(b)

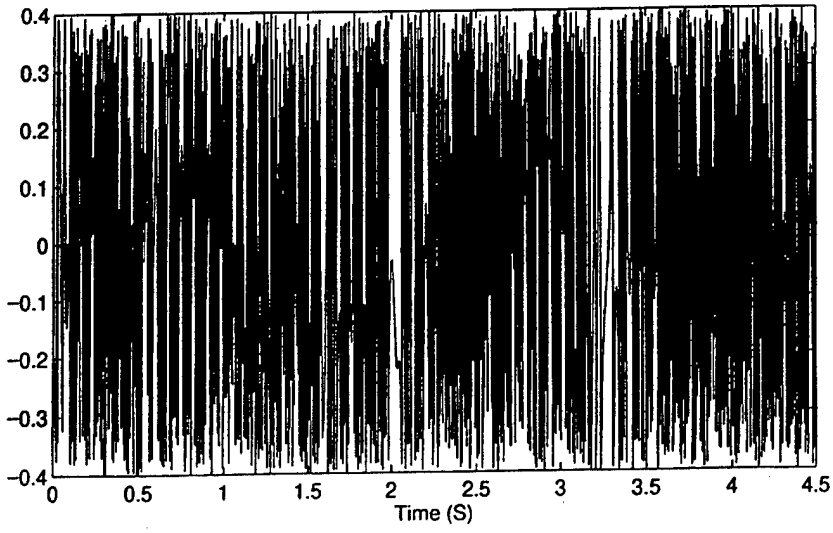


(c)

Fig. 10. The simulation results. (a) The time-domain waveform of the speech signal. (b) The spectrogram for the original speech signal. (c) The time-domain waveform of the scrambled speech signal.

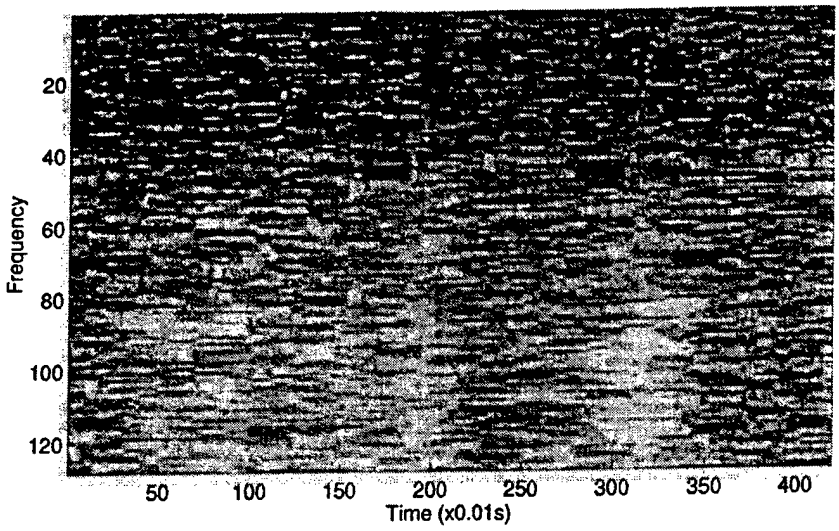


(d)

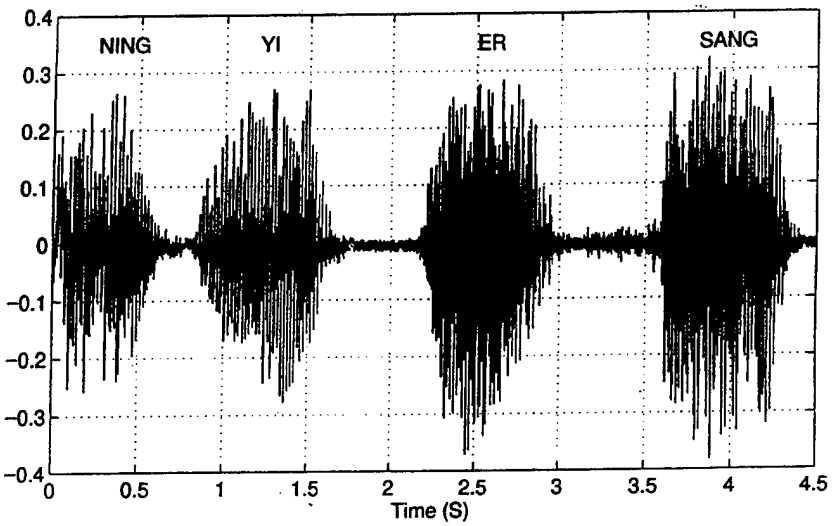


(e)

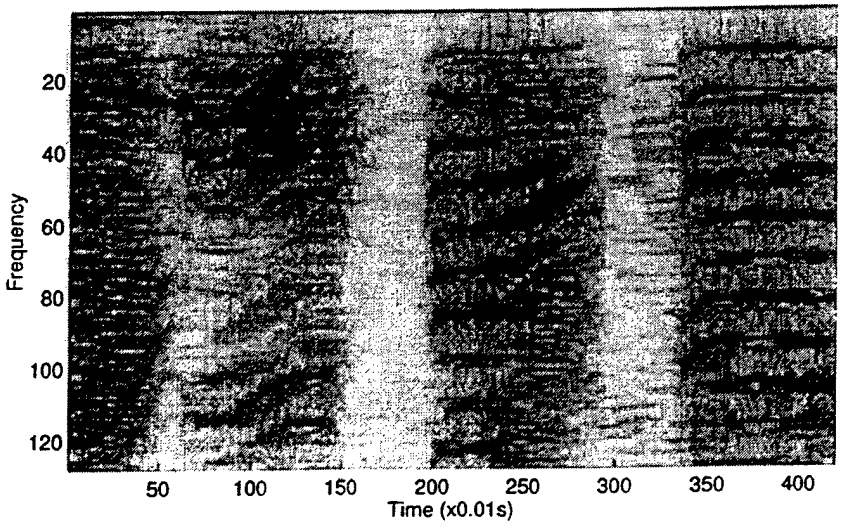


(f)

Fig. 10. (*Continued.*) The simulation results. (d) The spectrogram of the scrambled speech signal. (e) The time-domain waveform of the descrambled speech signal. (f) The spectrogram of the descrambled speech signal.

## REFERENCES


[1] V. Lakshmikantham, D. D. Bainov, and P. S. Simeonov, *Theory of Impulsive Differential Equations.* Singapore: World Scientific, 1989.

[2] E. Ott, C. Grebogi, and J. A. Yorke, "Controlling chaos," *Phys. Rev. Lett.*, vol. 64, pp. 1196–1199, 1990.

[3] G. Chen and X. Dong, "From chaos to order—Perspectives and methodologies in controlling nonlinear dynamical systems," *Int. J. Bifurc. Chaos*, vol. 3, pp. 1363–1409, 1993.

[4] L. O. Chua, T. Yang, G. Q. Zhong, and C. W. Wu, "Adaptive synchronization of Chua's oscillators," *Int. J. Bifurc. Chaos*, vol. 6, no. 1, pp. 189–201, 1996.

[5] C. W. Wu, T. Yang, and L. O. Chua, "On adaptive synchronization and control of nonlinear dynamical systems," *Int. J. Bifurc. Chaos*, vol. 6, no. 3, pp. 455–471, Mar. 1996.

[6] T. Stojanovski, L. Kocarev, and U. Parlitz, "Driving and synchronizing by chaotic impulses," *Phys. Rev. E*, vol. 43, no. 9, pp. 782–785, Sept. 1996.

[7] K. Pyragas, "Continuous control of chaos by self-controlling feedback," *Phys. Lett. A.*, vol. 170, pp. 421–428, 1992.

[8] J. Schweizer and M. P. Kennedy, "Predictive Poincaré control: A control theory for chaotic systems," *Phys. Rev. E*, vol. 52, no. 5, pt. A, pp. 4865–4876, Nov. 1995.

[9] E. R. Hunt and G. Johnson, "Keeping chaos at bay," *IEEE Spectrum*, pp. 32–36, Nov. 1993.

[10] A. M. Samoilenko and N. A. Perestyuk, *Impulsive Differential Equations.* Singapore: World Scientific, 1995.

[11] L. O. Chua, "Global unfolding of Chua's circuit," *IEICE Trans. Fundament.*, vol. E76-A, no. 5, pp. 704–734, May 1993.

[12] T. Yang, "Recovery of digital signals from chaotic switching," *Int. J. Circuit Theory Applicat.*, vol. 23, no. 6, pp. 611–615, Nov./Dec. 1995.

[13] K. M. Short, "Steps toward unmasking secure communications," *Int. J. Bifurc. Chaos*, vol. 4, pp. 957–977, 1994.

[14] T. Yang, C. W. Wu, and L. O. Chua, "Cryptography based on chaotic systems," *IEEE Trans. Circuits Syst. I*, vol. 44, pp. 469–472, May 1997.

[15] T. Yang, L.-B. Yang, and C.-M. Yang, "Impulsive synchronization of Lorenz systems," *Phys. Lett. A*, vol. 226, no. 6, pp. 349–354, Mar. 1997.

[16] R. E. Amritkar and N. Gupte, "Synchronization of chaotic orbits: The effect of a finite time step," *Phys. Rev. E (Statistical Physics, Plasmas, Fluids, and Related Interdisciplinary Topics)*, vol. 47, no. 6, pp. 3889–3895, June 1993.

[17] T. Yang and L. O. Chua, "Impulsive control and synchronization of nonlinear dynamical systems and application to secure communication," *Int. J. Bifurc. Chaos*, vol. 7, no. 3, pp. 645–664, Mar. 1997.

[18] ———, "Impulsive control and synchronization of chaotic systems and secure communication," Electron. Res. Lab., College of Eng., Univ. California, Berkeley, Memo. UCB/ERL M97/12, 29 Jan. 29, 1997.

[19] T. Yang, L.-B. Yang, and C.-M. Yang, "Impulsive control of Lorenz system," *Physica D*, 1997, in press.

[20] T. Yang, C.-M. Yang, and L.-B. Yang, "Control of Rössler system to periodic motions using impulsive control methods," *Phys. Lett. A*, vol. 232, pp. 356–361, Aug. 4, 1997.


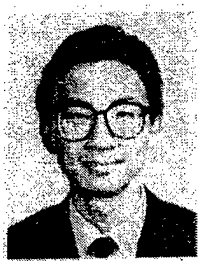

**Tao Yang** (M'96) was born in Wuhan, China, on January 1, 1970. He received the B.E. and M.E. degrees in electrical engineering from Tongji University, Shanghai, China, in 1990 and 1993 with honors, respectively.

From 1993 to 1994, he was with the Department of Automatic Control Engineering, Shanghai University of Technology, Shanghai. Since 1995, he has been a Specialist in the Nonlinear Electronics Laboratory, Department of Electrical Engineering and Computer Sciences, University of California at Berkeley. His research interests include automatic control, nonlinear dynamic systems, neural networks, fuzzy systems, general brain theory, and supernatural phenomena. He has published more than 40 technical papers in different international journals and different proceedings of international conferences.

Prof. Yang serves as a reviewer of several technical journals including: IEEE TRANSACTIONS ON CIRCUITS AND SYSTEMS, *International Journal of Bifurcation and Chaos*, and *SIAM Journal Applied Mathematics*. He received the Overseas Professor Chair of E-Zhou University, China, in 1997. He is the founder and the director of E-Zhou Association of Supernatural Phenomena, China.

**Leon O. Chua** (S'60–M'62–SM'70–F'74), for a biography, see this issue, p. 904.

# Synchronization of Chua's Circuits with Time-Varying Channels and Parameters

Leon O. Chua, Tao Yang, Guo-Qun Zhong, and Chai Wah Wu

*Abstract*—**In this brief, we study the use of adaptive controllers to maintain the synchronization of two Chua's circuits with time-varying channel and time-varying parameters. Both simulation results and experimental results are provided to verify the operation of the designs.**

## I. Introduction

Because of its potential applications to spread spectrum communication, the synchronization of chaotic systems has been studied extensively both in theory and in experiments [1]–[17]. However, in almost all of the previous works, the driving and the driven chaotic systems are assumed to be identical and their parameters are assumed to be time-invariant. The channel through which the transmitted signal is transmitted is also assumed to be time-invariant. The above assumptions limit its applicability in practical systems.

So far, all chaos-based communication systems use chaotic systems both as transmitters and receivers. The transmitter generates a chaotic signal which is used to encode the message signal in different ways, for example: chaotic masking [1]–[3], parameter modulation [8], [9] and state variable modulation [5], [6], [17]. Chaotic masking is not very secure if the message is directly added onto the chaotic masking signal. The authors of [4] and [19] had demonstrated that the smaller the message signal is, the lower the degree of security will be. Chaotic switching is the easiest form of parameter modulation and it was also shown to have a low degree of security [20] if the parameters of the transmitter are not chosen carefully. State variable modulation uses a functional of the message signal to modulate the state variables of the transmitter and hides the message signal, which is usually a narrow-band signal, into the broad-band chaotic signal.

Manuscript received October 4, 1995; revised February 13, 1996. This paper was recommended by Associate Editor T. Endo.

L. O. Chua and C. W. Wu are with the Electronics Research Laboratory and Department of Electrical Engineering and Computer Sciences, University of California, Berkeley, CA 94720 USA.

T. Yang is with the Electronics Research Laboratory and Department of Electrical Engineering and Computer Sciences, University of California, Berkeley, CA 94720 USA, on leave from the Department of Automatic Control Engineering, Shanghai University of Technology, Shanghai 200072, P. R. China.

G.-Q. Zhong is with the Electronics Research Laboratory and Department of Electrical Engineering and Computer Sciences, University of California, Berkeley, CA 94720 USA, on leave from the Guangzhou Institute of Electronic Technology, Academia Sinica, Guangzhou 510070, P. R. China.

Publisher Item Identifier S 1057-7122(96)07600-3.

1057–7122/96$05.00 © 1996 IEEE

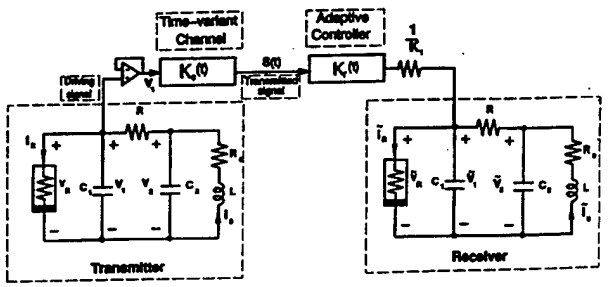


Fig. 1. The synchronization scheme of two Chua's circuits by using $v_1$ in a unidirectional driving configuration.

The transmitted signal is then transmitted to the receiver, which is an identical chaotic system. The transmitted signal will synchronize the receiver to the transmitter to obtain a replica of the chaotic masking signal.

Most of the methods presented so far require that the parameters of the transmitter and the receiver are identical, and the channel is time-invariant. Our experimental results indicate that a time-varying channel can desynchronize the system.

In this brief, we use adaptive controllers to maintain the synchronization between the transmitter and the receiver when the parameters of the transmitter are time-varying or the channel is memoryless and time-varying. We used Chua's circuits as our driving and driven system. The feedback into the adaptive controller is the synchronization error, which measures the degree of de-synchronization between the transmitter and receiver.

The organization of this brief is as follows. In Section II, adaptive controllers are presented which compensate the time-varying channel gain. In Section III, adaptive controllers are presented which compensate the time-varying parameters. In Section IV, experimental results are presented.

## II. Adaptive Controllers for Time-Varying Channel Compensation

In this brief, all the results are based on Chua's circuit [18], [21], which exhibits a family of chaotic attractors and can be easily implemented in hardware. Chua's circuit consists of a linear inductor $L$, a linear resistor $R$, two linear capacitors $C_1$ and $C_2$ and a nonlinear resistor—the Chua's diode $N_R$. The state equations for Chua's circuit are given by

$$\begin{cases} \frac{dv_1}{dt} = \frac{1}{C_1}[G(v_2 - v_1) - f(v_1)] \\ \frac{dv_2}{dt} = \frac{1}{C_2}[G(v_1 - v_2) + i_3] \\ \frac{di_3}{dt} = \frac{1}{L}[-v_2 - R_0 i_3] \end{cases} \tag{1}$$

where $v_1$, $v_2$ and $i_3$ are the voltage across $C_1$, the voltage across $C_2$ and the current through $L$, respectively. We set $G = \frac{1}{R}$. The term $R_0 i_3$ is added to account for the small resistance of the inductor in the physical circuit. $f(v_1)$, the piece-wise linear $v - i$ characteristic of the Chua's diode, is given by

$$f(v_1) = G_b v_1 + \frac{1}{2}(G_a - G_b)(|v_1 + E| - |v_1 - E|) \tag{2}$$

where $E$ is the breakpoint voltage of the Chua's diode.

We use the synchronization scheme shown in Fig. 1 [12]. The state equations are given by

$$\begin{cases} \frac{dv_1}{dt} = \frac{1}{C_1}[G(v_2 - v_1) - f(v_1)] \\ \frac{dv_2}{dt} = \frac{1}{C_2}[G(v_1 - v_2) + i_3] \\ \frac{di_3}{dt} = \frac{1}{L}[-v_2 - R_0 i_3] \end{cases} \tag{3}$$

$$\begin{cases} \frac{d\tilde{v}_1}{dt} = \frac{1}{C_1}[G(\tilde{v}_2 - \tilde{v}_1) - f(\tilde{v}_1) + K_1(s(t) - \tilde{v}_1)] \\ \frac{d\tilde{v}_2}{dt} = \frac{1}{C_2}[G(\tilde{v}_1 - \tilde{v}_2) + \tilde{i}_3] \\ \frac{d\tilde{i}_3}{dt} = \frac{1}{L}[-\tilde{v}_2 - R_0 \tilde{i}_3] \end{cases} \tag{4}$$

where $s(t) = K_c(t)v_1$, and $K_c(t)$ is the time-varying gain of the channel. Constant unity gain channel corresponds to $K_c(t) = 1$.

In this section we study how to compensate for the time-varying channel gain $K_c(t)$. In the driven system, we construct an adaptive gain $K_r(t)$ such that $K_c(t)K_r(t) \to 1$ as $t \to \infty$ to maintain the synchronization. Then the driven system should be rewritten as

$$\begin{cases} \frac{d\tilde{v}_1}{dt} = \frac{1}{C_1}[G(\tilde{v}_2 - \tilde{v}_1) - f(\tilde{v}_1) + K_1(K_r(t)s(t) - \tilde{v}_1)] \\ \frac{d\tilde{v}_2}{dt} = \frac{1}{C_2}[G(\tilde{v}_1 - \tilde{v}_2) + \tilde{i}_3] \\ \frac{d\tilde{i}_3}{dt} = \frac{1}{L}[-\tilde{v}_2 - R_0 \tilde{i}_3] \end{cases} \tag{5}$$

The dynamics of $K_r(t)$ is given by one of the following adaptive controllers:

Controller #1

$$\dot{K}_r(t) = -k_1(K_r(t)|s(t)| - |\tilde{v}_1|) \tag{6}$$

Controller #2

$$\dot{K}_r(t) = -k_1(K_r(t)s^2(t) - s(t)\tilde{v}_1) \tag{7}$$

Controller #3

$$\begin{aligned} \dot{K}_r(t) &= -k_1 \operatorname{sgn}\left(\frac{\partial \dot{\tilde{v}}_1}{\partial K_r}\right)(K_r(t)s(t) - \tilde{v}_1) \\ &= -k_1 \operatorname{sgn}(K_1 s(t))(K_r(t)s(t) - \tilde{v}_1). \end{aligned} \tag{8}$$

Controller #2 is similar to the LMS adaptive controller and controller #3 is a simple form of the adaptive controllers discussed in [22] and [23].

In our simulations, the parameters of Chua's circuit are given by $C_1 = 5.56$ nF, $C_2 = 50$ nF, $G = 0.700\,28$, $L = 7.14$ mH, $R_0 = 0$ $\Omega$, $G_a = -0.8$ mS, $G_b = -0.5$ mS, $E = 1$ V, $K_1 = 0.01$. The Chua's circuit exhibits a double scroll Chua's attractor for these parameters. We choose the synchronization error to be $v_1 - \tilde{v}_1$. In all of our simulations, the initial conditions of the transmitter and the receiver are $(v_1(0),\ v_2(0),\ i_3(0)) = (-0.2$ V, $-0,02$ V, 0.1 mA) and $(\tilde{v}_1(0),\ \tilde{v}_2(0),\ \tilde{i}_3(0)) = (0.02$ V, $-0.12$ V, $-0.1$ mA), respectively. So the transmitter and the receiver are initially desynchronized. The fourth order Runge–Kutta method with fixed step-size $h = 10^{-6}$ s is used to simulate the system.

Fig. 2 shows the simulation results when $K_c(t)$ is a sinusoidal function as follows

$$K_c(t) = 0.5 - 0.1\sin(75\pi t) \tag{9}$$

and controller #1 is used with $k_1 = 10^6$.

Fig. 2(a) shows $K_c(t)$, $K_r(t)$ and $K_c(t)K_r(t)$. We can see that $K_r(t)$ asymptotically approaches $\frac{1}{K_c(t)}$, and the settling time is about 0.6 ms. Fig. 2(b) shows the synchronization error $v_1(t) - \tilde{v}_1(t)$. For comparison, the synchronization error in the case when no adaptive controller is used is shown in Fig. 2(c). One can see that the synchronization error is reduced significantly by using the adaptive controller. When controllers #2 and #3 are used, the simulation results are almost the same.

When the coupling factor $K_1$ becomes too small, the transmitter and he receiver will be desynchronized even when the channel has a unit gain $K_c(t) = 1$ for all times. Fig. 3(a) shows this de-synchronization with $K_1 = 0.0005$. However, we find that the adaptive controllers used can also compensate for this kind of desynchronization. Fig. 3(b) shows the simulation result when $K_c(t) = 1$ and $K_1 = 0.0005$, and controller #1 with $k_1 = 10^6$ is used. We see that the synchronization error approaches 0.

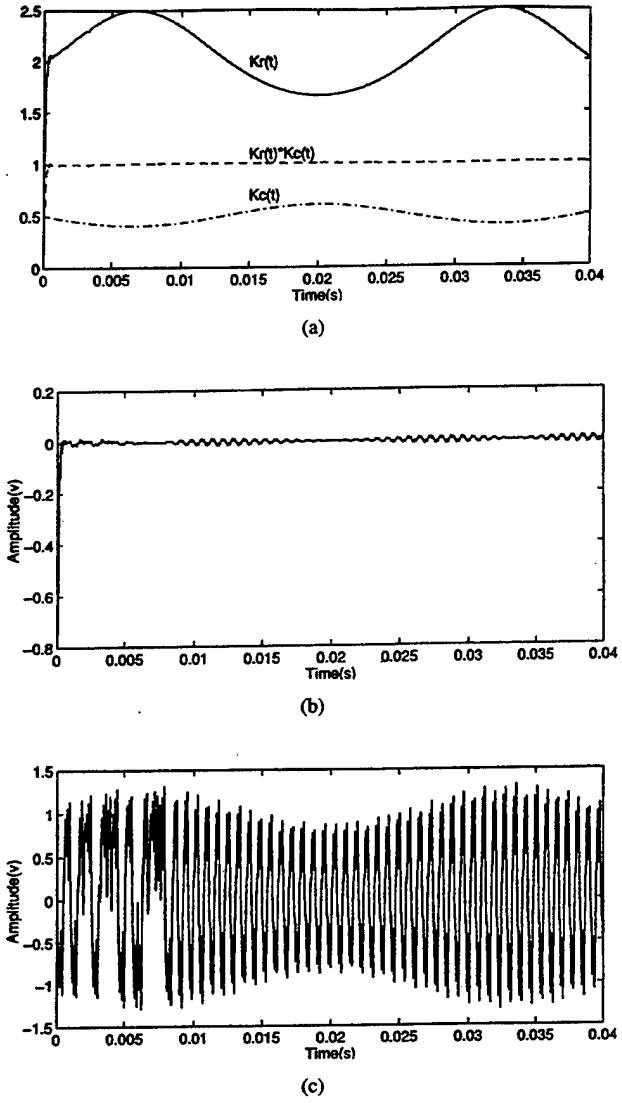


Fig. 2. Synchronization of Chua's circuits when the channel gain $K_c(t)$ is a sinusoidal function and controller #1 is used. (a) The channel gain $K_c(t)$, gain of adaptive controller $K_r(t)$ and the product $K_c(t)K_r(t)$. (b) The synchronization error $(v_1 - \tilde{v}_1)$ when adaptive controller #1 is used. (c) The synchronization error $(v_1 - \tilde{v}_1)$ without using adaptive controller.

## III. Adaptive Controller for Time-Varying Parameter Compensation

Parameter mismatch can also result in the loss of synchronization of the system shown in Fig. 1. Although the synchronization is robust in the sense that it can tolerate some parameter mismatch [10], the authors of [5] gave an experimental example showing that a 1% resistor mismatch can sharply reduce the quality of the received signal.

In this section, we study the synchronization in the cases where the parameters of the transmitter are time-varying. In this case, we rewrite the driving system as follows:

$$\begin{cases} \frac{dv_1}{dt} = \frac{K_{C_1}(t)}{C_1}[K_G(t)G(v_2 - v_1) - f(v_1)] \\ \frac{dv_2}{dt} = \frac{K_{C_2}(t)}{C_2}[K_G(t)G(v_1 - v_2) + i_3] \\ \frac{di_3}{dt} = \frac{K_L(t)}{L}[-v_2 - (K_{R_0}(t) + R_0)i_3] \end{cases} \tag{10}$$

where $K_{C_1}(t)$, $K_{C_2}(t)$, $K_L(t)$, $K_{R_0}(t)$ and $K_G(t)$ are the time-varying factors of the parameters $C_1$, $C_2$, $L$, $R_0$ and $G$, respectively.

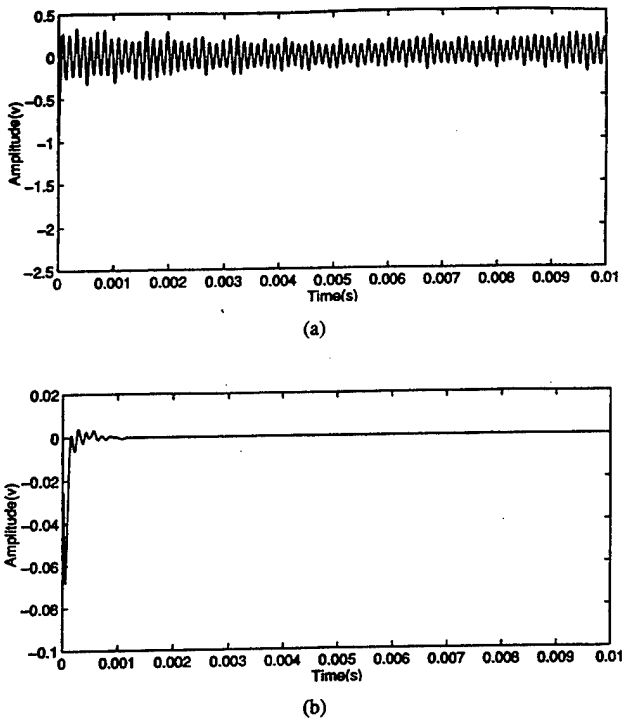


Fig. 3. (a) The synchronization error $(v_1 - \tilde{v}_1)$ when channel gain $K_c(t) = 1$ and a weak coupling factor $K_1 = 0.0005$ is used. No controller is used. (b) The synchronization error $(v_1 - \tilde{v}_1)$ when the channel gain $K_c(t)$ is 1 and a weak coupling factor $K_1 = 0.0005$ is used. Controller #1 is used.

The driven system is as follows:

$$\begin{cases} \frac{d\tilde{v}_1}{dt} = \frac{\tilde{K}_{C_1}(t)}{C_1}[\tilde{K}_G(t)G(\tilde{v}_2 - \tilde{v}_1) - f(\tilde{v}_1) + K_1(v_1 - \tilde{v}_1)] \\ \frac{d\tilde{v}_2}{dt} = \frac{\tilde{K}_{C_2}(t)}{C_2}[\tilde{K}_G(t)G(\tilde{v}_1 - \tilde{v}_2) + \tilde{i}_3 + K_1(v_1 - \tilde{v}_1)] \\ \frac{d\tilde{i}_3}{dt} = \frac{\tilde{K}_L(t)}{L}[-\tilde{v}_2 - (\tilde{K}_{R_0}(t) + R_0)\tilde{i}_3 + K_1(v_1 - \tilde{v}_1)] \end{cases} \tag{11}$$

where $\tilde{K}_{C_1}(t)$, $\tilde{K}_{C_2}(t)$, $\tilde{K}_L(t)$, $\tilde{K}_{R_0}(t)$ and $\tilde{K}_G(t)$ are compensating adjustments of the parameters $C_1$, $C_2$, $L$, $R_0$ and $G$, respectively, which are adaptively modified by using the following adaptive controllers. In this paper, we consider the cases when only one parameter is time-varying at a time. The adaptive controllers used are similar in form to those used in [22] and [23].

### A. Compensating for $K_G$

The controller is chosen as

$$\begin{aligned} \dot{\tilde{K}}_G(t) &= k_1 \operatorname{sgn}\left(\frac{\partial \dot{\tilde{v}}_1}{\partial \tilde{K}_G}\right)(v_1 - \tilde{v}_1) \\ &= k_1 \operatorname{sgn}\left(\frac{1}{C_1}G(\tilde{v}_2 - \tilde{v}_1)\right)(v_1 - \tilde{v}_1) \end{aligned} \tag{12}$$

The simulation results are shown in Fig. 4 with $k_1 = 10^6$. $K_G(t)$ is defined by the following sinusoidal function.

$$1.1 - 0.05 \sin\left(\frac{15\pi}{2}t\right) \tag{13}$$

Fig. 4(a) shows $K_G(t)$(dashed line) and $\tilde{K}_G(t)$(solid line). One can see that $\tilde{K}_G(t)$ asymptotically approaches $K_G(t)$ with a settling time of about 3 ms. Fig. 4(b) shows the synchronization error. Note in Fig. 4(a) that from 45.5 to 63 ms, $\tilde{K}_G(t)$ is almost constant while $K_G(t)$ decreases. This is because in the parameter range corresponding to the waveform of $K_G(t)$ during 45.5 ms to 63 ms, the synchronization is maintained even though $\tilde{K}_G(t) \neq K_G(t)$. In

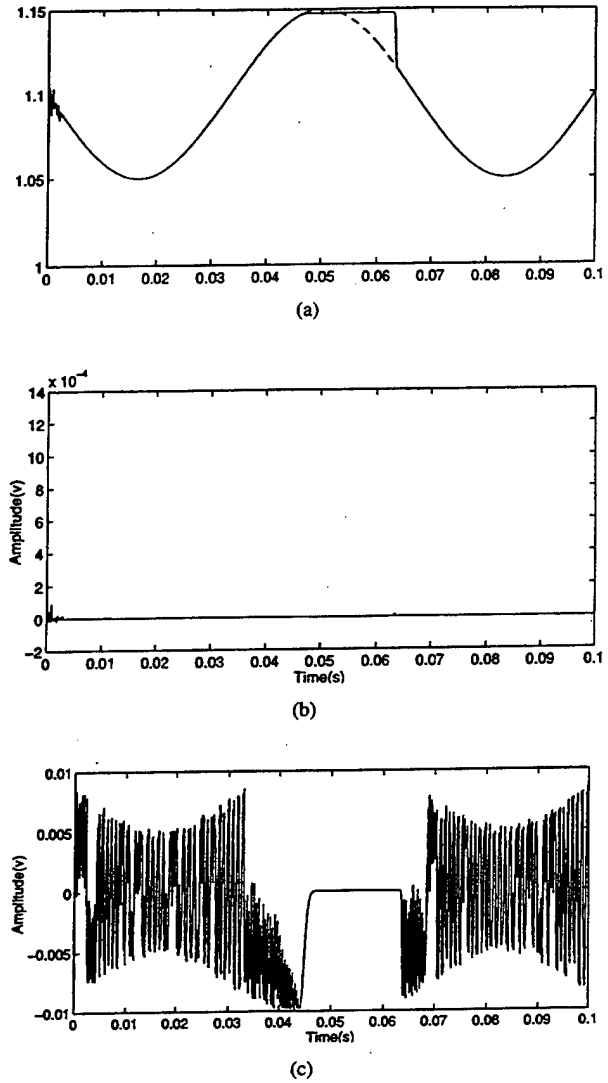


Fig. 4. Synchronization of Chua's circuits when $G$ is a sinusoidal function of time. (a) $K_G(t)$ and $\tilde{K}_G(t)$. (b) The synchronization error $(v_1 - \tilde{v}_1)$ when the adaptive controller is used. (c) The synchronization error $(v_1 - \tilde{v}_1)$ without the adaptive controller.

Fig. 4(c) we show the synchronization error without the adaptive controller and we can see that in the period 45.5 to 63 ms the synchronization error is small.

### B. Compensating for $K_{C_1}$

In this case, the controller used is

$$\dot{\tilde{K}}_{C_1}(t) = k_1 \operatorname{sgn}\left(\frac{\partial \dot{\tilde{v}}_1}{\partial \tilde{K}_{C_1}}\right)(v_1 - \tilde{v}_1)$$
$$= k_1 \operatorname{sgn}\left(\frac{1}{C_1}[G(\tilde{v}_2 - \tilde{v}_1) - f(\tilde{v}_1) + K_1(v_1 - \tilde{v}_1)]\right) \times (v_1 - \tilde{v}_1). \quad (14)$$

The simulation results are shown in Fig. 5 with $k_1 = 2 \times 10^6$. $K_{C_1}(t)$ is the sinusoidal function given in (13). From Fig. 5(a) one can see that $\tilde{K}_{C_1}(t)$ asymptotically approaches $K_{C_1}(t)$ with a settling time of about 1 ms. Fig. 5(b) shows the synchronization error.

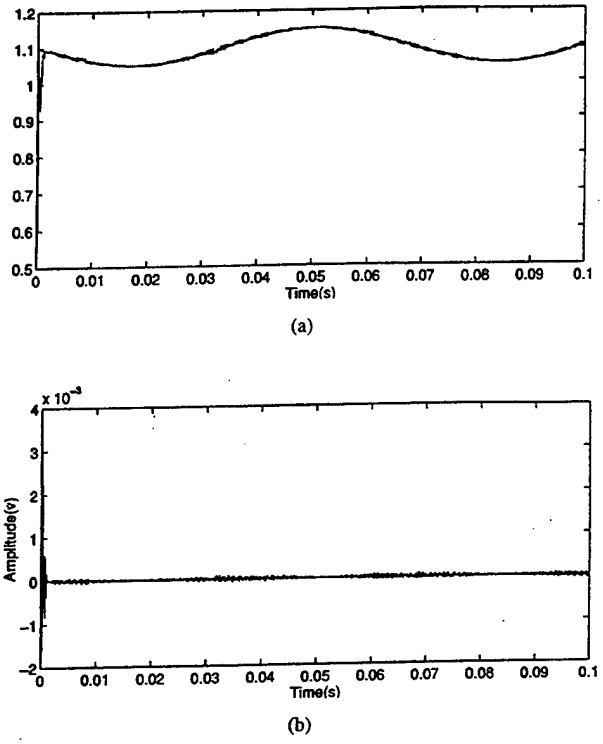


Fig. 5. Synchronization of Chua's circuits when $C_1$ is a sinusoidal function of time. (a) $K_{C_1}(t)$ and $\tilde{K}_{C_1}(t)$. (b) The synchronization error $(v_1 - \tilde{v}_1)$.

### C. Compensating for $K_{C_2}$

In this case, the controller is

$$\dot{\tilde{K}}_{C_2}(t) = k_1 \operatorname{sgn}\left(\frac{\partial \dot{\tilde{v}}_2}{\partial \tilde{K}_{C_2}}\right)(v_1 - \tilde{v}_1)$$
$$= k_1 \operatorname{sgn}\left(\frac{1}{C_2}[G(\tilde{v}_1 - \tilde{v}_2) + \tilde{i}_3 + K_1(v_1 - \tilde{v}_1)]\right) \times (v_1 - \tilde{v}_1). \quad (15)$$

The simulation results are similar to those shown in Fig. 5 with $k_1 = 10^6$ and a settling time of about 2 ms.

### D. Compensating for $K_L$

In this case, the controller is

$$\dot{\tilde{K}}_L(t) = k_1 \operatorname{sgn}\left(\frac{\partial \dot{\tilde{i}}_3}{\partial \tilde{K}_L}\right)(v_1(t) - \tilde{v}_1)$$
$$= k_1 \operatorname{sgn}\left(\frac{1}{L}[-\tilde{v}_2 - R_0\tilde{i}_3 + K_1(v_1 - \tilde{v}_1)]\right) \times (v_1 - \tilde{v}_1). \quad (16)$$

The simulation results are similar to those shown in Fig. 5 with $k_1 = 10^6$ and a settling time of about 2 ms.

### E. Compensating for $K_{R_0}$

In this case, the controller is

$$\dot{\tilde{K}}_{R_0}(t) = k_1 \operatorname{sgn}\left(\frac{\partial \dot{\tilde{i}}_3}{\partial \tilde{K}_{R_0}}\right)(v_1(t) - \tilde{v}_1)$$
$$= k_1 \operatorname{sgn}\left(-\frac{\dot{\tilde{i}}_3}{L}\right)(v_1 - \tilde{v}_1). \quad (17)$$

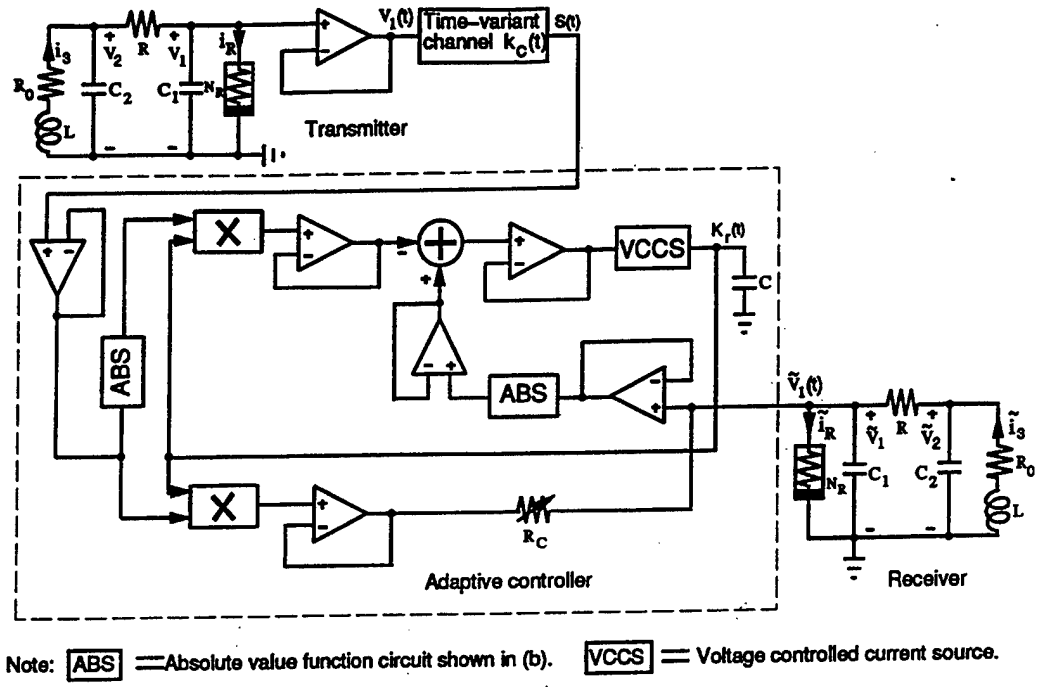


(a)

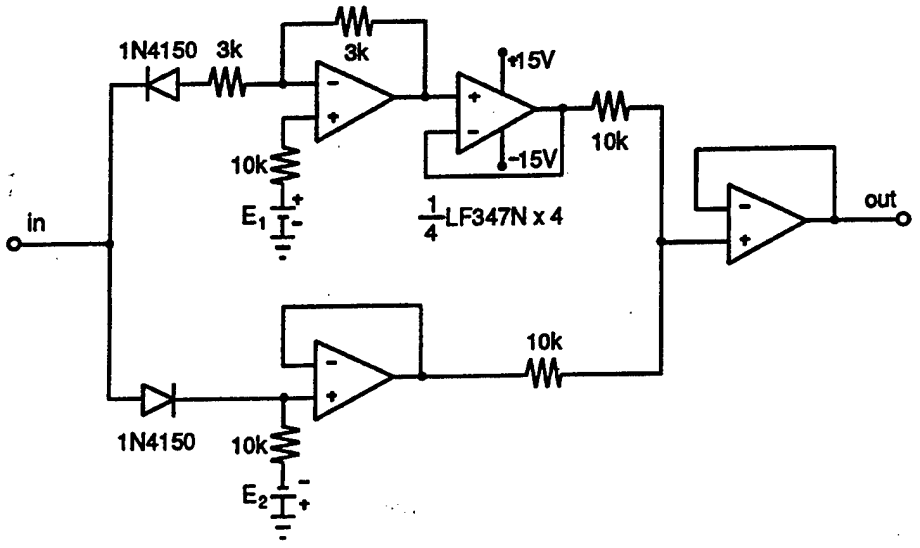


(b)

Fig. 6. (a) Schematic diagram of the experimental circuit for studying the synchronization between two identical Chua's circuits under a time-varying channel. The equations of the adaptive controller is given by (6). (b) Circuit with the absolute value transfer function.

The simulation results are similar to those shown in Fig. 5 with $k_1 = 10^8$ and a settling time of about 1.5 ms.

From the simulation results, we find the frequency of time-varying properties of parameters should be small enough ($\frac{1}{180}$ of the natural frequency of chaotic signal in our simulations), or else the adaptive controllers may not compensate the time-varying parameters.

## IV. Experimental Results

In this section we supplement the computer simulation results with experimental results from a physical circuit implementation. The circuit diagram of the system used to study the synchronization between two Chua's circuits when the channel is time-varying is shown in Fig. 6. In our experiments, both Chua's circuits are identical and have the following parameters: $C_1 = 6.8$ nF, $C_2 = 68$ nF, $L = 18.4$ mH, $R_0 = 12\ \Omega$, $R = 1.98$ k$\Omega$, $G_a = -0.73$ mS, $G_b = -0.4$ mS, $E = 1.8$ V, $R_C = 3.8$ k$\Omega$, where $R_C$ is the coupling resistor, which satisfies $K_1 = \frac{1}{R_C}$.

The circuit parameters we used exhibits the Double Scroll Chua's attractor. When the channel gain is 1, the transmitter and the receiver are synchronized.

When the channel gain drops to $K_c(t) = 0.65$, we find that the transmitter and the receiver are desynchronized. The relation between the voltages $v_2(t)$ and $\tilde{v}_2(t)$ is shown in Fig. 7.

Next we use the the adaptive controller as in (6), which is implemented using the circuit shown in Fig. 6 to compensate for the channel gain which is set at $K_c(t) = 0.65$. The

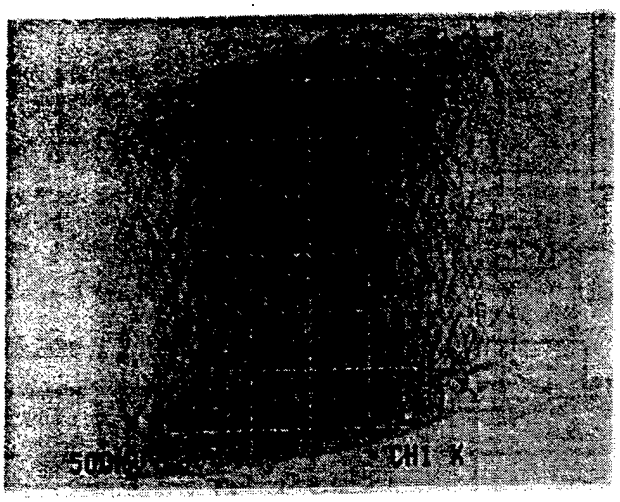


Fig. 7. When the channel gain drops to 0.65, the transmitter and the receiver are desynchronized. No adaptive controller is used. The relationship between $v_2$ and $\tilde{v}_2$.

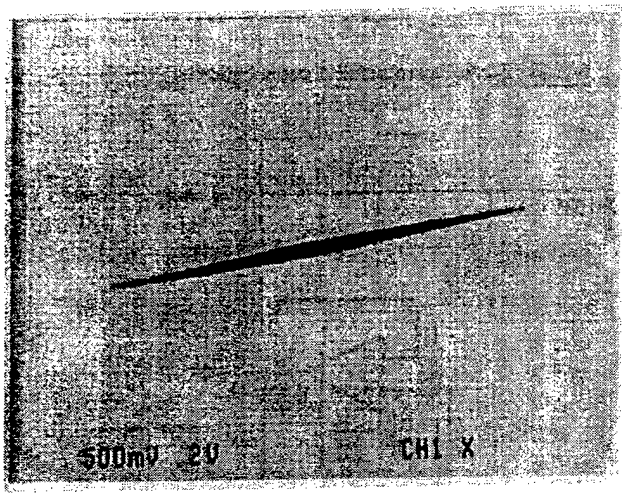


Fig. 8. The adaptive controller in Fig. 6 is used to compensate for the channel gain of 0.65. The relationship between $v_2$ and $\tilde{v}_2$.

relation between voltages $v_2(t)$ and $\tilde{v}_2(t)$ is shown in Fig. 8. One can see that the synchronization is restored. Comparing the results shown in Fig. 8 with those shown in Fig. 7, one can see that the effect of the adaptive controller is very significant.

Next, we study the effect of our controller under a weak coupling condition. In this case, the coupling resistor is 4.46 kΩ, and as shown in Fig. 9(a), this coupling without the aid of the controller is not big enough to synchronize the transmitter and the receiver even when a unity channel gain is used. In Fig. 9(b), we show the synchronization when the channel gain drops to 0.65 and the controller is used.

## V. Conclusion

We have shown how two Chua's circuits can synchronize in the cases where the channel gain and the parameters are time-varying by using adaptive controllers in the receiver to compensate for the time-varying properties of the transmitter and the channel.

Both simulation results and experimental results are presented for the proposed schemes. These results also show that the adaptive controllers can compensate for the weak coupling between the two circuits. These results show that our methods can be useful for developing practical chaotic spread-spectrum communication systems.

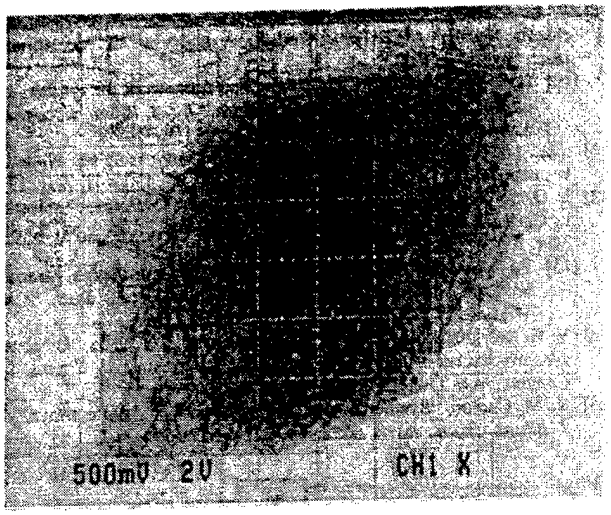


(a)

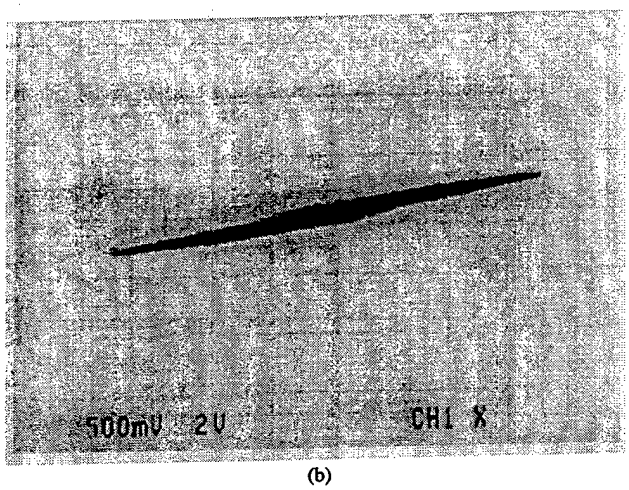


(b)

Fig. 9. The adaptive controller in Fig. 6 can also compensate the de-synchronization caused by weak coupling. (a) The relationship between $v_2$ and $\tilde{v}_2$ shows the de-synchronization when the coupling resistor is 4.46 kΩ with a unity channel gain. No adaptive controller is used. (b) The relationship between $v_2$ and $\tilde{v}_2$ shows synchronization when the adaptive controller is used to compensate for the weak coupling factor with a channel gain of 0.65.

## References

[1] L. Kocarev, K. S. Halle, K. Eckert, L. O. Chua, and U. Parlitz, "Experimental demonstration of secure communications via chaotic synchronization," *Int. J. Bifurc. Chaos*, vol. 2, no. 3, pp. 709–713, 1992.

[2] K. M. Cuomo and A. V. Oppenheim, "Synchronization of Lorenz-based chaotic circuits with applications to communications," *IEEE Trans. Circuits Syst.*, vol. 40, pp. 626–633, Oct. 1993.

[3] R. Lozi and L. O. Chua, "Secure communications via chaotic synchronization II: Noise reduction by cascading two identical receivers," *Int. J. Bifurc. Chaos*, vol. 3, pp. 1319–1325, 1993.

[4] K. M. Short, "Steps toward unmasking secure communications," *Int. J. Bifurc. Chaos*, vol. 4, pp. 959–977, 1994.

[5] K. S. Halle, C. W. Wu, M. Itoh, and L. O. Chua, "Spread spectrum communication through modulation of chaos," *Int. J. Bifurc. Chaos*, vol. 3, no. 2, pp. 469–477, 1993.

[6] C. W. Wu and L. O. Chua, "A simple way to synchronize chaotic systems with applications to secure communication systems," *Int. J. Bifurc. Chaos*, vol. 3, no. 6, pp. 1619–1627, 1993.

[7] M. J. Ogorzalek, "Taming chaos—Part I: Synchronization," *IEEE Trans. Circuits Syst. I*, vol. 40, pp. 693–699, Oct. 1993.

[8] U. Parlitz, L. O. Chua, L. Kocarev, K. S. Halle, and A. Shang, "Transmission of digital signal by chaotic synchronization," *Int. J. Bifurc. Chaos*, vol. 2, no. 4, pp. 973–977, 1992.

[9] T. L. Carroll, "Communicating with use of filtered, synchronized, chaotic signals," *IEEE Trans. Circuits Syst. I*, vol. 42, pp. 105–110, Mar. 1995.

[10] C. W. Wu and L. O. Chua, "A unified framework for synchronization and control of dynamical systems," *Int. J. Bifurc. Chaos*, vol. 4, no. 4, pp. 979–998, 1994.

[11] ——, "Synchronization in an array of linearly coupled dynamical systems," *IEEE Trans. Circuits Syst. I*, vol. 42, pp. 430–447, Aug. 1995.

[12] L. O. Chua, K. Itoh, L. Kocarev, and K. Eckert, "Chaos synchronization in Chua's circuit," *J. Circuit, Syst. Comput.*, vol. 3, no. 1 pp. 93–108, Mar. 1993.

[13] P. Celka, "Synchronization of chaotic systems though parameter adaption," in *Proc. 1995 IEEE Int. Symp. Circuits Syst.*, Seattle, WA, Apr. 1995, pp. 692–695.

[14] V. N. Belykh, N. N. Verichev, L. Kocarev, and L. O. Chua, "On chaotic synchronization in a linear array of Chua's circuits," *J. Circuit, Syst. Comput.*, vol. 3, no. 2, pp. 579–589, 1993.

[15] K. M. Cuomo, "Synthesizing self-synchronization chaotic arrays," *Int. J. Bifurc. Chaos*, vol. 4, no. 3, pp. 727–736, 1994.

[16] ——, "Synthesizing self-synchronization chaotic systems," *Int. J. Bifurc. Chaos*, vol. 3, no. 5, pp. 1327–1337, 1993.

[17] C. W. Wu, G. Q. Zhong, and L. O. Chua, "Synchronizing nonautonomous chaotic systems without phase-locking," to appear in *J. Circuit, Syst. Comput.*

[18] J. M. Cruz and L. O. Chua, "An IC chip of Chua's circuit," *IEEE Trans. Circuits Syst. II*, vol. 40, pp. 614–625, Oct. 1993.

[19] J. Stark and B. V. Arumugam, "Extracting slowly varying signals from a chaotic background," *Int. J. Bifurc. Chaos*, vol. 2, pp. 413–419, 1992.

[20] T. Yang, "Recovery of digital signals from chaotic switching," *J. Circuit Theory Applicat..*, vol. 23, pp. 611–615, Dec. 1995.

[21] L. O. Chua, "Chua's circuit—An overview ten years later," *J. of Circuit, Syst. Comput.*, vol. 4, no. 2, pp. 117–159, June 1994.

[22] B. A. Huberman and E. Lumer, "Dynamics of adaptive systems," *IEEE Trans. Circuits Syst.*, vol. 37, pp. 547–550, Apr. 1990.

[23] J. K. John and R. E. Amritkar, "Synchronization by feedback and adaptive control," *Int. J. Bifurc. Chaos*, vol. 4, no. 6, pp. 1687–1695, 1994.

# Torus-Doubling Bifurcations in Four Mutually Coupled Chua's Circuits

Guo-Qun Zhong, Chai Wah Wu, and Leon O. Chua

*Abstract*— **Coupled oscillators are complicated high-dimensional dynamical systems. They can exhibit a wide variety of rich dynamics which could lead to novel applications in engineering. In this brief we describe a *torus-doubling* phenomenon observed from four mutually coupled Chua's circuits. The qualitative dynamical behavior of the coupled system is robust, yet the exact behavior is very sensitive to the initial conditions and the parameter values of the Chua's circuits. We present numerical simulation results from the system model which are in good qualitative agreement with the experimental measurements.**

*Index Terms*—**Chua's circuits, coupled oscillators, torus-doubling bifurcation.**

## I. Introduction

Coupled oscillators are complicated high-dimensional dynamical systems. They can exhibit a wide variety of dynamics which can be exploited for novel engineering applications, such as secure communication [1], [2], sound synthesis, etc. Torus doubling is an interesting bifurcation phenomenon which can occur in systems having several coupled oscillators. A torus attractor is said to exhibit a torus-doubling phenomenon if at some critical parameter value it loses its normal stability to create a nearby torus attractor having approximately twice its surface area. The torus-doubling bifurcation phenomenon has been observed in numerical investigations [3]–[5] and experiments [5]–[7], [16], [17], respectively. In order to prove the existence of a torus doubling bifurcation, additional technical assumptions must be introduced [8]. To visualize the behavior of four-dimensional dynamical systems, one constructs an associated *Poincaré map* of such systems on a three-dimensional section. Ashwin and Swift utilize a so-called torus unfolder [9] for a system of four weakly coupled van der Pol type oscillators [10]. The four outputs of the oscillators are fed into the torus unfolder which generates a voltage proportional to the phase angle of the $i$th oscillator at the points when the 4th oscillator is defined to have zero phase. This generates a Poincaré section of the dynamics. The output of the unfolder is sampled by an analog-to-digital converter and displayed in color on a computer screen.

In this paper we present a scenario of a torus-doubling phenomenon observed from a system of four mutually coupled Chua's circuits. To observe this complicated behavior visually, we also use a Poincaré return map. However, rather than using the torus unfolder described

Manuscript received August 27, 1996; revised April 17, 1997. This work was supported in part by the Office of Naval Research under Grant N00014-89-J-1402, and by the Joint Services Electronics Program under Contract F49620-94-C-0038. This paper was recommended by Associate Editor T. Endo.

G.-Q. Zhong is with the Electronics Research Laboratory and Department of Electrical Engineering and Computer Sciences, University of California at Berkeley, Berkeley, CA 94720 USA, on leave from Guangzhou Institute of Electronic Technology, Academia Sinica, Guangzhou 510070, China.

C. W. Wu was with the Electronics Research Laboratory and Department of Electrical Engineering and Computer Sciences, University of California at Berkeley, Berkeley, CA 94720 USA. He is now with IBM T. J. Watson Research Center, Yorktown Heights, NY 10598 USA.

L. O. Chua is with the Electronics Research Laboratory and Department of Electrical Engineering and Computer Sciences, University of California at Berkeley, Berkeley, CA 94720 USA.

Publisher Item Identifier S 1057-7122(98)00918-0.

1057–7122/98$10.00 © 1998 IEEE

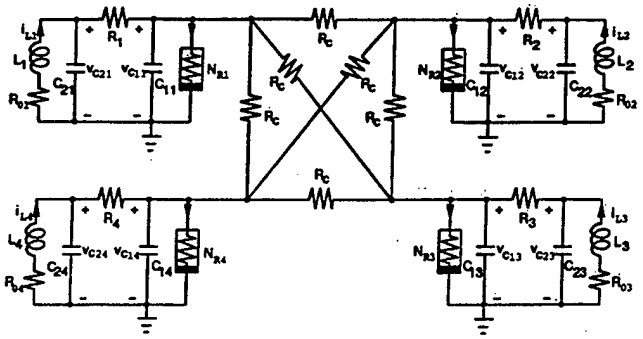

(a)

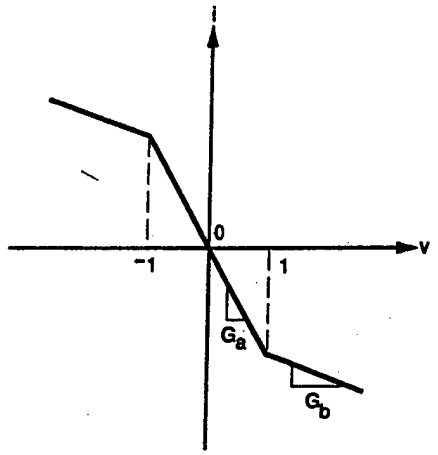


(b)

Fig. 1. (a) Circuit diagram of four mutually coupled Chua's circuits coupled via resistors $R_c$. (b) $v$–$i$ characteristic of Chua's diode $N_R$.

by Ashwin and Swift, we choose the hyperplane of constant $i_L$ as the Poincaré section, where $i_L$ is the current flowing through the inductor $L$ in one of the Chua's circuit. We observe the points where $i_L = I$, for some fixed $I$, and project them onto the $v_{C1}$–$v_{C2}$ plane. Although the state space of the system is 12-D, this projection of the dynamics onto a two-dimensional Poincaré section still reveals the important features of the torus-doubling phenomena. The system of four mutually coupled Chua's circuits we examine in this paper is described in Section II. An interesting landscape of torus-doubling bifurcation phenomenon observed from the system is presented in Section III. Some results numerically simulated via the software INSITE [11] are also presented in this section to illustrate results from the model agreeing qualitatively to the experimental observations.

## II. Description of the System

The system we examine in this paper is shown in Fig. 1(a). Four identical Chua's circuits [12]–[14] are mutually coupled via six linear resistors $R_c$. The parameters in each Chua's circuits are assumed to be identical to those in the other Chua's circuits initially. The dynamics of each uncoupled Chua's circuit is governed by the following state equations:

$$\begin{aligned}
\frac{dv_{C1j}}{dt} &= \frac{1}{C_{1j}}\left[\frac{1}{R_j}(v_{C2j} - v_{C1j}) - f(v_{C1j})\right] \\
\frac{dv_{C2j}}{dt} &= \frac{1}{C_{2j}}\left[\frac{1}{R_j}(v_{C1j} - v_{C2j}) + i_{Lj}\right] \\
\frac{di_{Lj}}{dt} &= -\frac{1}{Lj}[v_{C2j} + R_{0j} i_{Lj}], \qquad j = 1.\ 2.\ 3.\ 4
\end{aligned} \tag{1}$$

where $v_{C1j}$, $v_{C2j}$, $i_{Lj}$ are the voltages across capacitors $C_{1j}$, $C_{2j}$, and the current flowing through the inductor $L_j$, respectively, and

$$f(v_{C1j}) = G_b v_{C1j} + \tfrac{1}{2}(G_a - G_b)[|v_{C1j} + 1| - |v_{C1j} - 1|] \tag{2}$$

is the $v$–$i$ characteristic of the Chua's diode $N_{Rj}$ shown in Fig. 1(b).

Thus the state equations describing the system in Fig. 1(a) are as follows:

$$\begin{aligned}
\frac{dv_{C11}}{dt} &= \frac{1}{C_{11}}\left[\frac{1}{R_1}(v_{C21} - v_{C11}) - f(v_{C11}) + \frac{1}{R_c}(-3v_{C11} + v_{C12} + v_{C13} + v_{C14})\right] \\
\frac{dv_{C21}}{dt} &= \frac{1}{C_{21}}\left[\frac{1}{R_1}(v_{C11} - v_{C21}) + i_{L1}\right] \\
\frac{di_{L1}}{dt} &= -\frac{1}{L1}[v_{C21} + R_0 i_{L1}] \\
\frac{dv_{C12}}{dt} &= \frac{1}{C_{12}}\left[\frac{1}{R_2}(v_{C22} - v_{C12}) - f(v_{C12}) + \frac{1}{R_c}(v_{C11} - 3v_{C12} + v_{C13} + v_{C14})\right] \\
\frac{dv_{C22}}{dt} &= \frac{1}{C_{22}}\left[\frac{1}{R_2}(v_{C12} - v_{C22}) + i_{L2}\right] \\
\frac{di_{L2}}{dt} &= -\frac{1}{L2}[v_{C22} + R_0 i_{L2}] \\
\frac{dv_{C13}}{dt} &= \frac{1}{C_{13}}\left[\frac{1}{R_3}(v_{C23} - v_{C13}) - (v_{C13}) + \frac{1}{R_c}(v_{C11} + v_{C12} - 3v_{C13} + v_{C14})\right] \\
\frac{dv_{C23}}{dt} &= \frac{1}{C_{23}}\left[\frac{1}{R_3}(v_{C13} - v_{C23}) + i_{L3}\right] \\
\frac{di_{L3}}{dt} &= -\frac{1}{L3}[v_{C23} + R_0 i_{L3}] \\
\frac{dv_{C14}}{dt} &= \frac{1}{C_{14}}\left[\frac{1}{R_4}(v_{C24} - v_{C14}) - f(v_{C14}) + \frac{1}{R_c}(v_{C11} + v_{C12} + v_{C13} - 3v_{C14})\right] \\
\frac{dv_{C24}}{dt} &= \frac{1}{C_{24}}\left[\frac{1}{R_4}(v_{C14} - v_{C24}) + i_{L4}\right] \\
\frac{di_{L4}}{dt} &= -\frac{1}{L4}[v_{C24} + R_0 i_{L4}]
\end{aligned} \tag{3}$$

where $R_c$ is the resistance of the linear coupling resistors and $C_{1j} = C_1$, $C_{2j} = C_2$, $L_j = L$, $R_{0j} = R_0$, $R_j = R$, and $N_{Rj} = N_R$, for $j = 1, 2, 3, 4$.

## III. Torus-Doubling Bifurcation in Four Mutually Coupled Chua's Circuits

### 3.1. Poincaré Map for Torus-Doubling Bifurcations

The asymptotic behavior in the $v_{C1}$–$v_{C2}$ phase plane of Chua's circuit is muddled by an infinite tangle of intersections of the trajectory upon itself. An effective method to untangle such a mess of points and extract some useful asymptotic information is to analyze the dynamics of the associated Poincaré map.

In our investigation we use the current $i_L$ flowing through the inductor $L$ of one Chua's circuit to define the Poincaré section and observe the points where the trajectories cross the plane $i_L = I$ and project them onto the corresponding $v_{C1}$–$v_{C2}$. $I$ is a constant current chosen to fix the Poincaré section. In this way, the dynamical behavior of each coupled Chua's circuit can be observed on the Poincaré section on an oscilloscope.

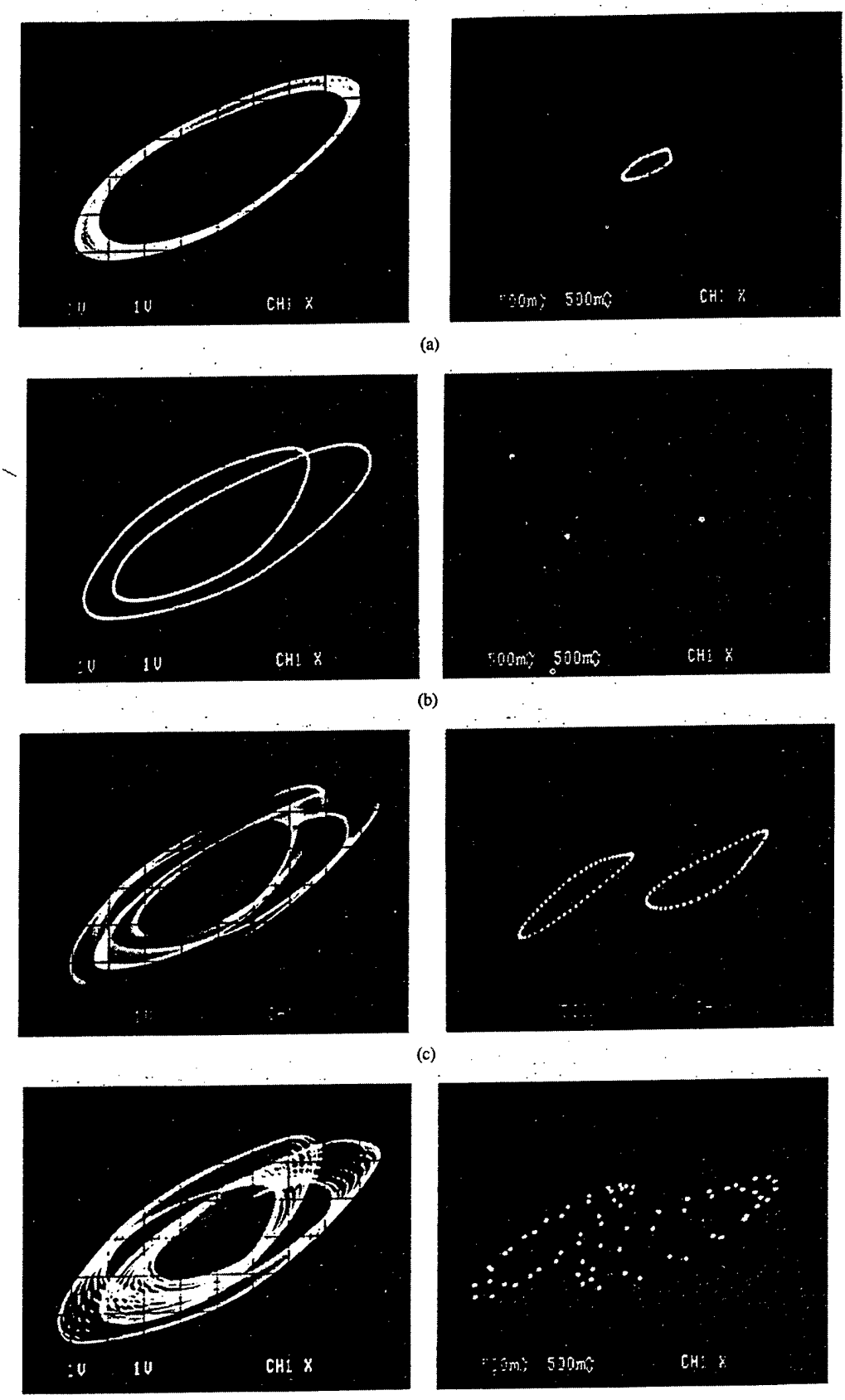


Fig. 2. Trajectory projection (left) and corresponding Poincaré map (right) in the $v_{C1}$–$v_{C2}$ plane of various torus-doubling bifurcation phenomena: Fixed parameter values: $G_a = -0.74$ mS, $G_b = -0.41$ mS, $C_1 = 10$ nF, $C_2 = 100$ nF, $L = 18.68$ mH, $R_0 = 19\Omega$, $R_c = 10$ k$\Omega$. (a) $T_1$ torus attractor; parameter values: $R_1 = 1652\ \Omega$, $R_2 = 1692\ \Omega$, $R_3 = 917\ \Omega$, $R_4 = 3628\ \Omega$. (b) Period-2 limit cycle; parameter values: $R_1 = 801\ \Omega$, $R_2 = 1910\ \Omega$, $R_3 = 917\ \Omega$, $R_4 = 3628\ \Omega$. (c) $T_2$ torus doubling (type-II); parameter values: $R_1 = 724\ \Omega$, $R_2 = 1950\ \Omega$, $R_3 = 917\ \Omega$, $R_4 = 3628\ \Omega$. (d) $T_2$ torus doubling (type-II loci consisting of type-I loci); parameter values: $R_1 = 951\ \Omega$, $R_2 = 1910\ \Omega$, $R_3 = 917\ \Omega$, $R_4 = 3628\ \Omega$.

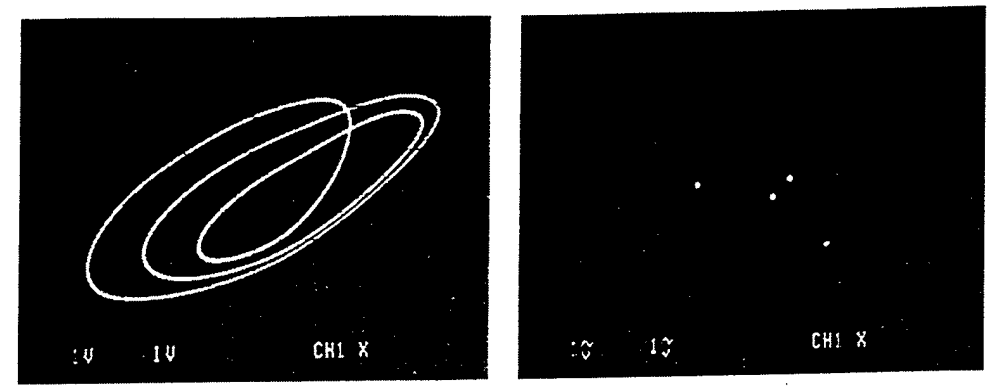


(e)

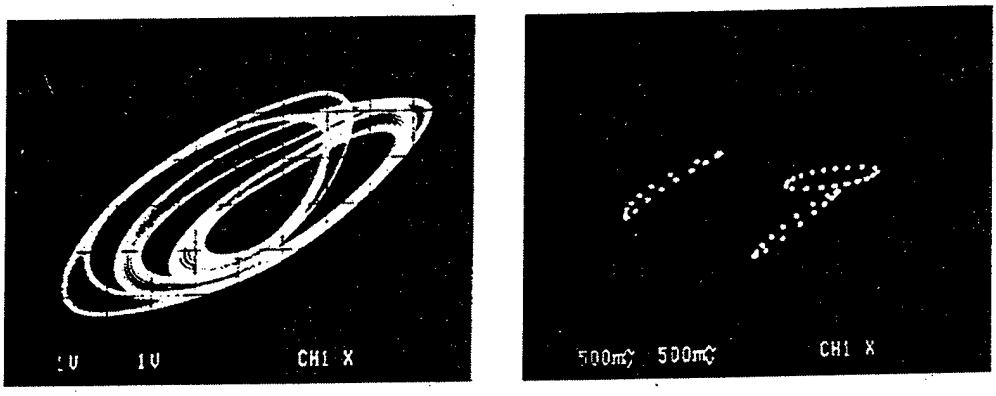


(f)

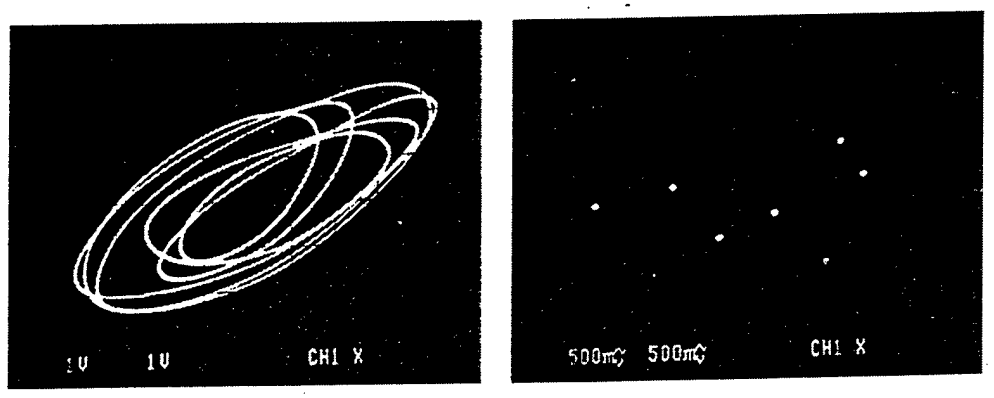


(g)

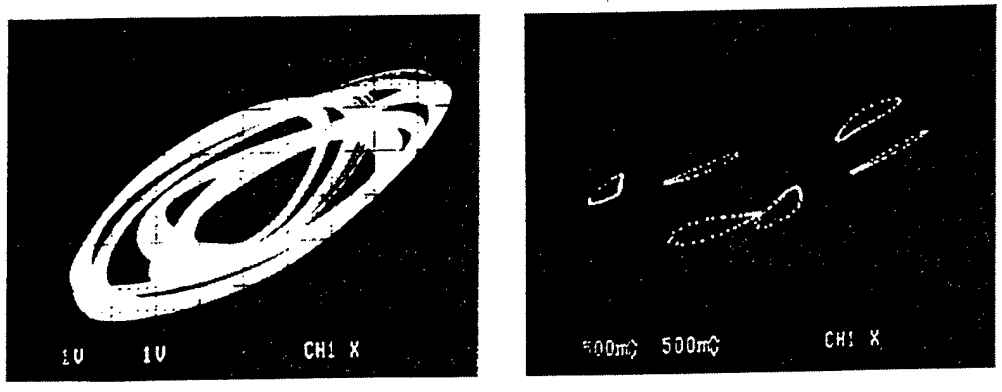


(h)

Fig. 2. *(Continued.)* Trajectory projection (left) and corresponding Poincaré map (right) in the $v_{C1}$–$v_{C2}$ plane of various torus-doubling bifurcation phenomena: Fixed parameter values: $G_a = -0.74$ mS, $G_b = -0.41$ mS, $C_1 = 10$ nF, $C_2 = 100$ nF, $L = 18.68$ mH, $R_0 = 19\Omega$, $R_c = 10$ k$\Omega$. (e) Period-3 limit cycle: parameter values: $R_1 = 1362\ \Omega$, $R_2 = 1715\ \Omega$, $R_3 = 917\ \Omega$, $R_4 = 3628\ \Omega$. (f) $T_3$ torus: parameter values: $R_1 = 1360\ \Omega$, $R_2 = 1696\ \Omega$, $R_3 = 917\ \Omega$, $R_4 = 3628\ \Omega$. (g) Period-6 limit cycle: parameter values: $R_1 = 1300\ \Omega$, $R_2 = 1700\ \Omega$, $R_3 = 917\ \Omega$, $R_4 = 3628\ \Omega$. (h) $T_6$ torus doubling: parameter values: $R_1 = 1328\ \Omega$, $R_2 = 1690\ \Omega$, $R_3 = 917\ \Omega$, $R_4 = 3628\ \Omega$.

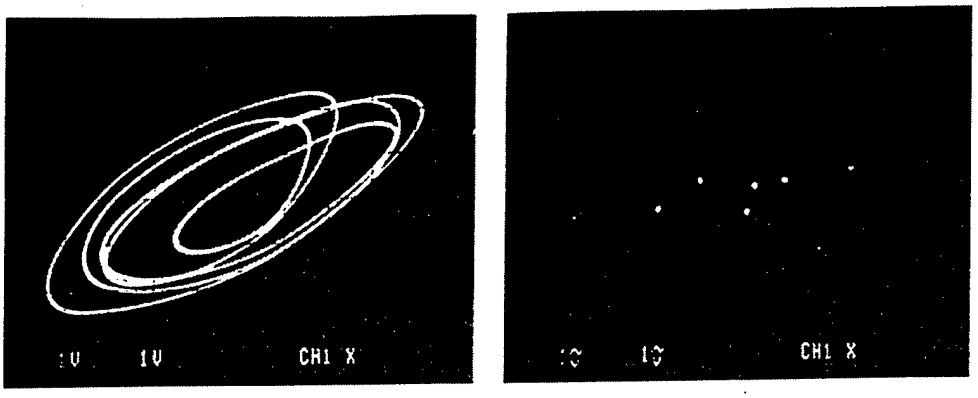


(i)

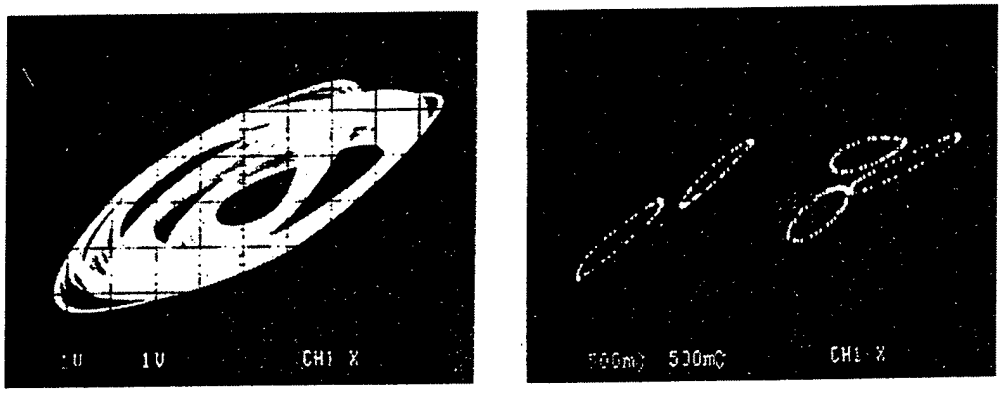


(j)

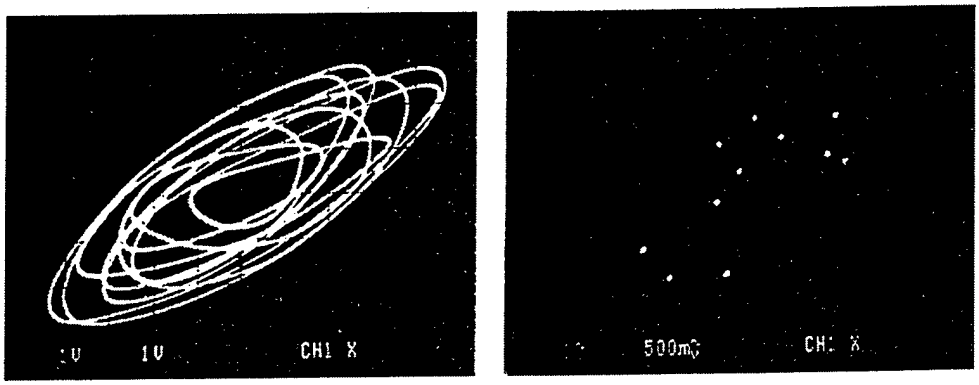


(k)

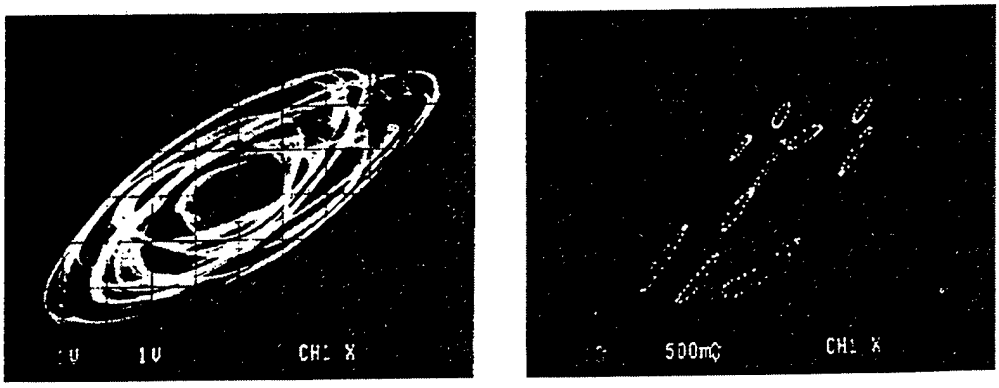


(l)

Fig. 2. *(Continued.)* Trajectory projection (left) and corresponding Poincaré map (right) in the $v_{C1}$–$v_{C2}$ plane of various torus-doubling bifurcation phenomena: Fixed parameter values: $G_a = -0.74$ mS, $G_b = -0.41$ mS, $C_1 = 10$ nF, $C_2 = 100$ nF, $L = 18.68$ mH, $R_0 = 19\Omega$, $R_c = 10$ k$\Omega$. (i) Period-5 limit cycle; parameter values: $R_1 = 1180\ \Omega$, $R_2 = 1690\ \Omega$, $R_3 = 917\ \Omega$, $R_4 = 3628\ \Omega$. (j) $T_5$ torus; parameter values: $R_1 = 1139\ \Omega$, $R_2 = 1910\ \Omega$, $R_3 = 917\ \Omega$, $R_4 = 3628\ \Omega$. (k) Period-10 limit cycle; parameter values: $R_1 = 1090\ \Omega$, $R_2 = 1655\ \Omega$, $R_3 = 917\ \Omega$, $R_4 = 3628\ \Omega$. (l) $T_{10}$ torus doubling; parameter values: $R_1 = 1094\ \Omega$, $R_2 = 1655\ \Omega$, $R_3 = 917\ \Omega$, $R_4 = 3628\ \Omega$.

(m)

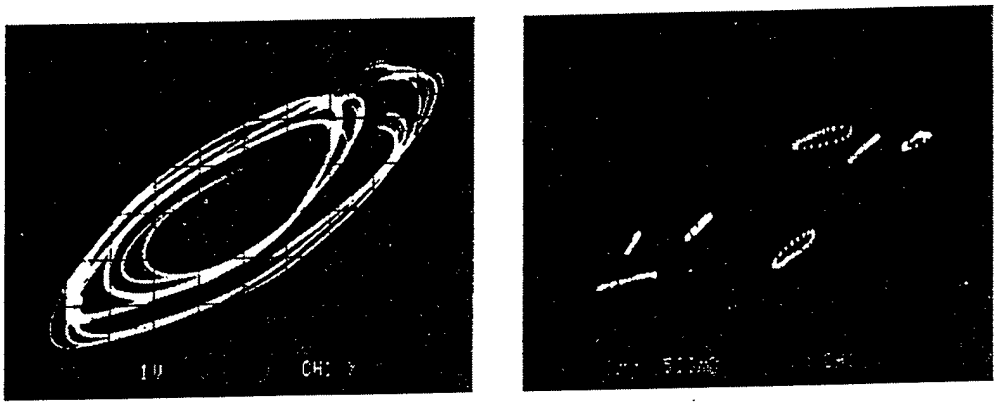

(n)

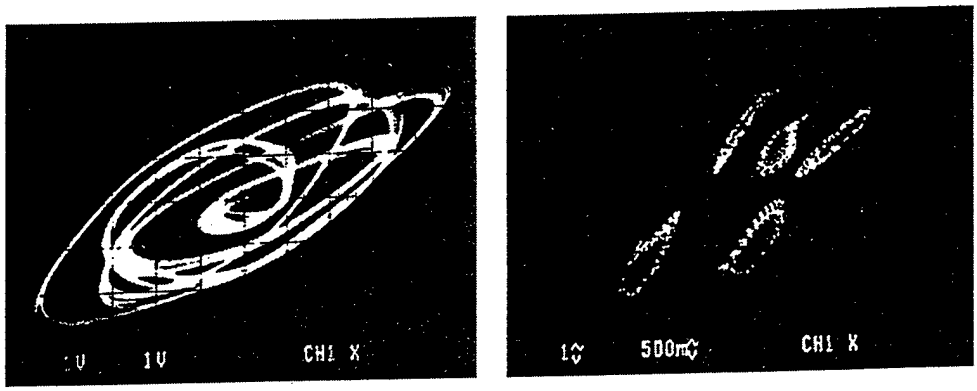


(o)

Fig. 2. *(Continued.)* Trajectory projection (left) and corresponding Poincaré map (right) in the $v_{C1}$–$v_{C2}$ plane of various torus-doubling bifurcation phenomena: Fixed parameter values: $G_a = -0.74$ mS, $G_b = -0.41$ mS, $C_1 = 10$ nF, $C_2 = 100$ nF, $L = 18.68$ mH, $R_0 = 19\Omega$, $R_c = 10$ k$\Omega$. (m) Period-7 limit cycle; parameter values: $R_1 = 345\ \Omega$, $R_2 = 1914\ \Omega$, $R_3 = 917\ \Omega$, $R_4 = 3628\ \Omega$. (n) $T_7$ torus; parameter values: $R_1 = 348\ \Omega$, $R_2 = 1914\ \Omega$, $R_3 = 917\ \Omega$, $R_4 = 3628\ \Omega$. (o) $T_{10}$ torus doubling; parameter values: $R_1 = 1559\ \Omega$, $R_2 = 1228\ \Omega$, $R_3 = 917\ \Omega$, $R_4 = 3628\ \Omega$.

### 3.2. *Torus-Doubling Bifurcation Phenomenon Observed from the System*

The following parameters values for the Chua's circuits of the system shown in Fig. 1(a) are fixed for our study:

$C_1 = 10$ nF, $C_2 = 100$ nF, $L = 18.68$ mH, $R = 1900\ \Omega$, $R_0 = 19\ \Omega$ (which includes the inherent 14.5 &Ohgr; series resistance of the inductor $L$), $G_a = -0.74$ mS, and $G_b = -0.41$ mS.

We first choose $R_c = 10$ k$\Omega$ so that the four Chua's circuits are synchronized with each other in the sense that corresponding voltages and currents in the four Chua's circuits are *identical* functions of time. Then, we adjust the values of the linear resistors $R_j$ $(j = 1, 2, 3, 4)$ of each coupled Chua's circuit and observe a sequence of period-doubling bifurcations of limit cycles. We also find that by changing the parameters, these limit cycles bifurcate into torus attractors. Thus to each limit cycle corresponds a torus attractor and to the period doubling of limit cycles corresponds torus doubling of torus attractors. To describe the torus attractor corresponding to a $n$ periodic orbit. we define $T_n$ as a two-dimensional torus embedded in the phase space which wraps around $n$-times, in correspondence with a period-$n$ periodic orbit. While a $n$-periodic orbit gives us $n$ intersection points with a suitable Poincaré plane, the intersection of $T_n$ with a suitable plane would result in $n$ simple closed curves. In our experiments we only vary $R_1$ and $R_2$ and keep $R_3$ and $R_4$ fixed. Fig. 2(a)–(o) show the trajectories and the corresponding Poincaré map in the $v_{C1}$–$v_{C2}$ plane associated with various period-doubling and torus-doubling bifurcations observed experimentally with a fixed coupling resistor $R_c = 10$ k$\Omega$, while varying the linear resistor $R_1$ of each coupled Chua's circuit. When $R_1 = 1652\ \Omega$, $R_2 = 1692$

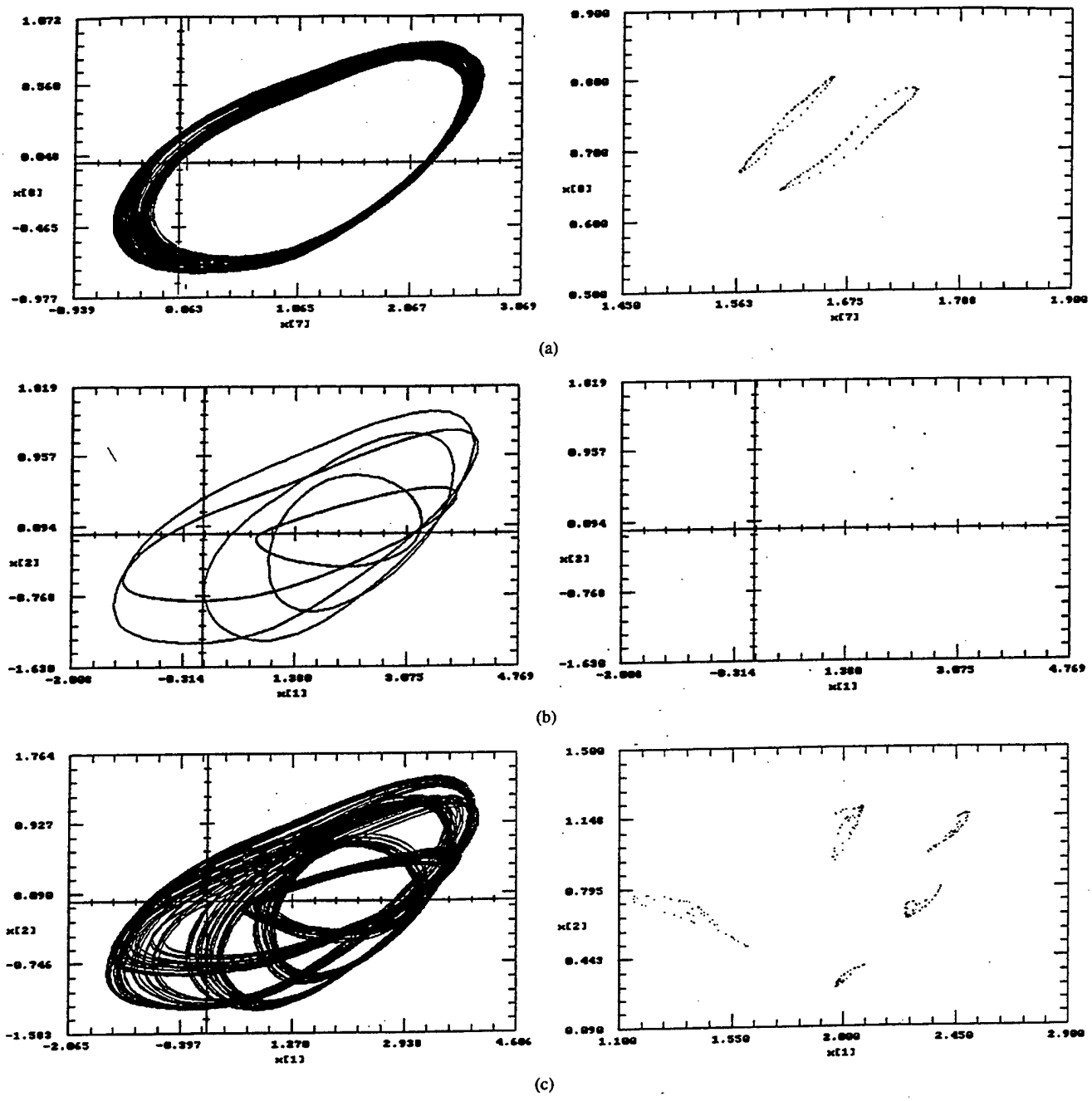

Fig. 3. Coupled Chua's circuits. Trajectory projection (left) and corresponding Poincaré map (right) in the $v_{C1}$–$v_{C2}$ plane of various torus-doubling bifurcation obtained from numerical simulation. Parameter values: $G_a = -0.74$ mS, $G_b = -0.41$ mS, $C_1 = 10$ nF, $C_2 = 100$ nF, $L = 18.68$ mH, $R_0 = 19\ \Omega$, $R_c = 10$ kΩ. (a) $T_2$ torus doubling; parameter values: $R_1 = 1610\ \Omega$, $R_2 = 1840\ \Omega$, $R_3 = 1135\ \Omega$, $R_4 = 2715\ \Omega$. (b) Period-5 limit cycle; parameter values: $R_1 = 1479\ \Omega$, $R_2 = 1800\ \Omega$, $R_3 = 920\ \Omega$, $R_4 = 3380\ \Omega$. (c) $T_5$ torus; parameter values: $R_1 = 1475\ \Omega$, $R_2 = 1788\ \Omega$, $R_3 = 920\ \Omega$, $R_4 = 3380\ \Omega$.

Ω, $R_3 = 917\ \Omega$, and $R_4 = 3628\ \Omega$, the system exhibits a $T_1$ torus as shown in Fig. 2(a). This torus attractor results from a bifurcation of a period-1 limit cycle. When $R_1 = 801\ \Omega$, $R_2 = 1910\ \Omega$, $R_3 = 917\ \Omega$, and $R_4 = 3628\ \Omega$, the period-1 limit cycle bifurcates into a period-2 limit cycle. The projection of this trajectory onto the $v_{C1}$–$v_{C2}$ plane and the corresponding Poincaré map of the output voltages $v_{C1}$ and $v_{C2}$ from the *third* Chua's circuit are shown in Fig. 2(b). Increasing $R_1$ slightly to $R_1 = 934\ \Omega$ while keeping the rest fixed, a bifurcation is observed, resulting in a $T_2$ torus attractor [Fig. 2(c)]. In this case, the loci on the Poincaré section corresponds to the type-II curve doubling phenomenon defined in [5]. However, with $R_1 = 951\ \Omega$ while keeping the other resistors as above, we observed another interesting type of $T_2$ torus doubling bifurcation, as shown in Fig. 2(d). Here, the type-II loci consist of two type-I curves as defined in [5], i.e., the torus lies on a surface generated from a combination of type-I and type-II torus-doubling.[1] Further variation of $R_1$ and $R_2$ while keeping $R_3$ and $R_4$ fixed, we observe period 3 [Fig. 2(e)] and period 6 limit cycles [Fig. 2(g)] and the corresponding $T_3$ torus [Fig. 2(f)] and $T_6$ torus attractors [Fig. 2(h)]. We also find a period 5 [Fig. 2(i)] and its period-doubled period 10 limit cycle [Fig. 2(k)] along with the corresponding $T_5$ [Fig. 2(j)] and $T_{10}$ torus attractors [Fig. 2(l)]. A period-7 and a $T_7$ torus attractor were also

[1] In [5], type-I doubling of a closed curve resulting from a map (in our case the map is the Poincaré map) occurs when a simple curve is transformed into another curve twice its length, but folded to resemble the original curve. Type-II doubling occurs when a simple curve is transformed into two disjoint curves similar to the original curve.

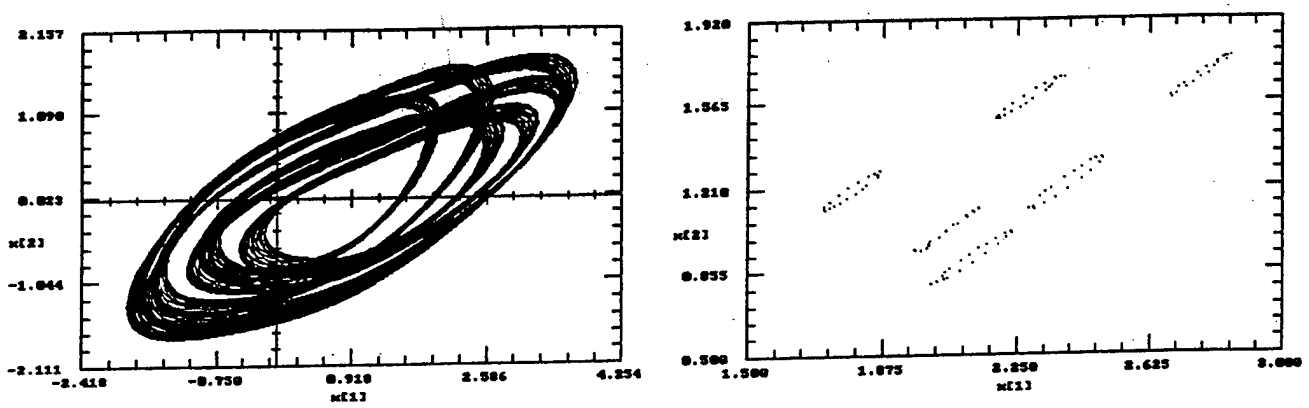


(d)

Fig. 3. *(Continued).* Coupled Chua's circuits. Trajectory projection (left) and corresponding Poincaré map (right) in the $v_{C1}$–$v_{C2}$ plane of various torus-doubling bifurcation obtained from numerical simulation. Parameter values: $G_a = -0.74$ mS, $G_b = -0.41$ mS, $C_1 = 10$ nF, $C_2 = 100$ nF, $L = 18.68$ mH, $R_0 = 19\ \Omega$, $R_c = 10$ k$\Omega$. (d) $T_6$ torus doubling; parameter values: $R_1 = 1000\ \Omega$, $R_2 = 1900\ \Omega$, $R_3 = 880\ \Omega$, $R_4 = 3890\ \Omega$.

found as shown in Fig. 2(m) and (n). In Fig. 2(o) we show that the $T_5$ torus in Fig. 2(j) has doubled via a type-II torus doubling [5], i.e., each circle in Fig. 2(j) has bifurcated into 2 circles close to each other.

It can be concluded, based on our experimental observations from the system shown in Fig. 1(a), that a period-doubling bifurcation precedes the torus-doubling bifurcation of a torus, and a period-$n$ limit cycle bifurcates into a $T_n$ torus; in other words, a period-$n$ period-doubling bifurcation is associated with an $T_n$ torus doubling bifurcation. The torus-doubling bifurcation phenomenon in the system is robust and can be observed from each coupled Chua's circuit of the system for several different combinations of values of $R_j$.

To confirm our experimental measurements, the system was simulated numerically using the system model equations (3) via the software INSITE [11] and the results are shown in Fig. 3(a)–(d). Due to the sensitivity to the initial conditions and parasitics, it is difficult to get exactly the same data set which matches the experimental observations to the numerical observations. Nevertheless, it can be noted from the figures that our simulation results are in good qualitative agreement with those shown in Fig. 2, and hence validating the mathematical model (3) for describing the system in Fig. 1(a). We see in Fig. 3(c) that the Poincaré section has a folding structure, suggesting a nearby torus breakdown route to chaos.

## IV. Concluding Remarks

In this paper we present several torus-doubling bifurcation phenomena observed experimentally and simulated numerically from four mutually coupled Chua's circuits. It is shown from these observations that the torus-doubling bifurcation phenomenon is robust in such a system. It can be observed for several different combinations of parameter values of the linear resistors $R_j (j = 1, 2, 3, 4)$. However the exact behavior is very sensitive to the initial conditions and to changes in the values of the resistors $R_j (j = 1, 2, 3, 4)$. Therefore, special care is needed in order to reproduce the results presented here.

Experiments indicate that the topological structures of the attractors of each coupled Chua's circuit in this system has a torus-like structure, when the values of $R_j (j = 1, 2, 3, 4)$ are properly chosen. The power spectra generated by the system are different from those generated by the uncoupled Chua's circuit, and may find interesting applications in sound synthesis [15].

## References

[1] L. O. Chua and M. Hasler, Guest Eds., special issue on "Chaos in nonlinear electronic circuits," *IEEE Trans. Circuits Syst. I*, vol. 40, Oct. 1993; and *IEEE Trans. Circuits Syst. II*, vol. 40, Nov. 1993.

[2] L. O. Chua, Guest Ed., Special Issue on "Chaos and nonlinear dynamics," *J. Franklin Inst.*, vol. 33, no. 1B, Nov. 1994.

[3] L. R. Keefe, "Dynamics of perturbed wavetrain solutions to the Ginzburg–Landau equation," *Studies Appl. Math.*, vol. 73, pp. 91–153, 1985.

[4] D. Armbruster, "Codimension 2 bifurcation in binary convection with square symmetry," in *Nonlinear Evolution of Spatio-Temporal Structures in Dissipative Continuous Systems*, F. H. Busse and L. Kramer, Eds. New York: Plenum, 1990, NATO ASI Series B: Physics vol. 225, pp. 385–398.

[5] P. Ashwin and J. W. Swift, "Torus doubling in four weakly coupled oscillators," *Int. J. Bifurc. Chaos*, vol. 5, no. 1, pp. 231–241, 1995.

[6] K. E. Mckell, D. S. Broomhead, R. Jones, and D. J. T. Hurle, "Torus doubling in convection molten gallium," *Europhys. Lett.*, vol. 12, p. 513, 1990.

[7] M. R. Bassett and J. L. Hudson, "Experimental evidence of period doubling of tori during an electrochemical reaction," *Physica D*, vol. 35, pp. 289–298, 1989.

[8] L. E. Los, "Nonnormally hyperbolic invariant curves for maps in $\mathbf{R}^3$ and doubling bifurcation," *Nonlinearity*, vol. 2, pp. 149–174, 1989.

[9] P. Ashwin and J. W. Swift, "Unfolding the torus: Oscillator geometry from time delays," *J. Nonlinear Sci.*, vol. 3, pp. 459–475, 1993.

[10] ——, "Measuring rotation sets of weakly coupled oscillators," *Nonlinearity*, vol. 7, pp. 925–942, 1994.

[11] T. Parker and L. O. Chua, *Practical Numerical Algorithms for Chaotic Systems*. New York: Springer-Verlag, 1989.

[12] L. O. Chua, "The genesis of Chua's circuit," *Archiv Elektronik Uebertragungstechnik*, vol. 46, no. 4, pp. 250–257, 1992.

[13] R. N. Madan, *Chua's Circuit: A Paradigm for Chaos*. Singapore: World, 1993.

[14] G. Q. Zhong and F. Ayrom, "Experimental confirmation of chaos from Chua's circuit," *Int. J. Circuit Theory Appl.* vol. 13, no. 1, pp. 93–98, 1985.

[15] I. Choi, "Interactive exploration of a chaotic oscillator for generating musical signals in real-time concert performance," *J. Franklin Inst.*, vol. 331B, no. 6, pp. 785–818, Nov. 1994.

[16] H. Kawakami, "Bifurcation of periodic responses in forced dynamic nonlinear circuits: Computation of bifurcation values of the system parameters," *IEEE Trans. Circuits Syst.*, vol. CAS-31, pp. 248–260, Mar. 1984.

[17] T. Yoshinaga and H. Kawakami, "Bifurcation and chaotic state in forced oscillatory circuits containing saturable inductors," in *Nonlinear Dynamics in Circuits*, L. Pecora and T. Carroll, Eds. Singapore: World, 1995, pp. 89–119.